

Stirling cryogenerators with linear drive

F. Stolfi and A. K. de Jonge

In 1864 Alexander Carnegie Kirk, a Scotsman, built a cryogenerator based on the Stirling cycle. Kirk's machine worked day and night for a period of ten years^[]. The references do not indicate whether worn parts were replaced during that period, but it is probably safe to assume that this was the case. Most mechanical devices, regardless of how ruggedly they are designed, eventually wear out. The Stirling cryogenerator developed by Philips Laboratories at Briarcliff Manor, U.S.A., however, is entirely free of mechanical wear. This special characteristic was achieved with the use of magnetic bearings and a linear drive. There is absolutely no contact between the internal moving parts and the walls of the working space. The miniature cryogenerators developed by Philips USFA B.V. also have a linear drive. In these machines the piston and displacer do come in contact with the walls of the working space via seals made of a special reinforced plastic with good sliding properties.*

Introduction

Philips researchers investigated the use of the Stirling cycle for the generation of cold at cryogenic temperatures as long ago as the fifties^[1]. This research resulted in the well-known Philips cryogenerators, which have been manufactured for many years and are used for the laboratory and factory production of liquid nitrogen, for example. In addition to the need for these industrial machines, there is also a demand for much smaller machines to cool detectors and electronic circuits.

In a Stirling cryogenerator, a piston and a displacer reciprocate in a space filled with a working gas, usually helium. To understand how the piston and displacer have to move with respect to each other, we will first describe the basic operating principles of the Stirling refrigeration cycle. In this process, a quantity of helium in the working space of the machine goes through a thermodynamic cycle with four distinct

stages, see *fig. 1a*: compression at room temperature (*I*), cooling to operating (cold) temperature (*II*), expansion at operating temperature (*III*) and, finally, reheating to room temperature (*IV*). The desired refrigeration occurs during the expansion of the working gas in stage *III*.

The working gas is forced to go through this cycle by the reciprocating movements of the piston *P* and the displacer *D*, as indicated in *fig. 1b*. The piston first compresses the gas and then allows it to expand. The displacer transfers the gas from the compression space — i.e. the room-temperature volume between the piston and the displacer — to the expansion space — the (cold) operating-temperature volume above the displacer. Twice in a cycle the gas is forced through the regenerator, which, in the cryogenerators described in this article, is part of the displacer. The regenerator, often referred to as the 'heart' of the Stirling cycle,

F. Stolfi is with Philips Laboratories, Briarcliff Manor, N.Y., U.S.A. Ing. A. K. de Jonge is with Philips USFA B.V., Eindhoven; he was previously with Philips Research Laboratories, Eindhoven.

[*] R. Thévenot, A history of refrigeration throughout the world, Inst. Int. du Froid, Paris 1979.

[1] J. W. L. Köhler and C. O. Jonkers, Fundamentals of the gas refrigerating machine, Philips Tech. Rev. 16, 69-78, 1954.

consists of porous materials (copper chips or copper gauze, for example) possessing a high heat capacity and a large heat-transferring surface. When flowing through the regenerator, the gas is alternately cooled and reheated by giving off and absorbing the quantity of heat Q_r . The work performed on the gas in the nearly isothermal compression is dissipated to the environment as heat Q_c in a cooler or heat exchanger. The work performed by the gas during the nearly isothermal expansion is drawn from the environment as heat Q_e . As a result, the temperature of the upper wall of the working space — referred to as the 'cold

head' or the 'cold finger' — is lowered significantly. The temperature curve over the longitudinal direction of the working space is shown schematically on the right-hand side of fig. 1b.

The idealized motion of the piston and displacer, illustrated in fig. 1c, is approximated by simple harmonic motion in the cryogenerators discussed in this article. As can be seen from the figure, the motion of the displacer must be approximately a quarter period ahead of the motion of the piston (corresponding to a phase difference of approximately $\pi/2$).

In conventional Stirling cryogenerators the piston and displacer are mechanically driven. A crankshaft mechanism is usually employed, but in special applications a rhombic drive is used [2]; this special form of the crankshaft mechanism had earlier been used in the Stirling engine. The advantage of such mechanical approaches is that the motions of the piston and displacer are accurately determined, so that there is no possibility of collisions. The rhombic drive has the added advantage that the moving-mass forces are balanced. There are several disadvantages: the mechanism is even more complicated than that of a combustion engine; it is difficult to seal the working space hermetically; and, at least in the case of the conventional crankshaft mechanism, side forces are exerted on the walls of the working space. This last effect causes significant wear unless the piston and the displacer are lubricated. Such lubricants are undesirable because their outgassing products mix with the working gas.

These problems can be avoided by driving both the reciprocating piston and the displacer directly, i.e. without having to convert rotary motion into reciprocating motion. To accomplish this, linear electric motors can be used; these are to some extent comparable with the drive of a loudspeaker cone. It is also possible to allow the displacer to move freely and drive only the piston. In this case, the displacer is connected to the housing by a helical spring and the working gas, in passing through the regenerator, produces a small force which drives the displacer. Since there is only a small difference between the resonant frequency of the displacer and the operating frequency of the piston the displacer mass-spring system is driven to large amplitude. The resonant displacer design with one motor is much simpler, but is not as flexible as the double linear-motor approach since it requires careful attention to gas flow, to the displacer mass and to the spring constant of the helical spring. The development work for translating both concepts into practice was carried out at two locations within Philips and has led to two cryogenerator designs; both are discussed in this article.

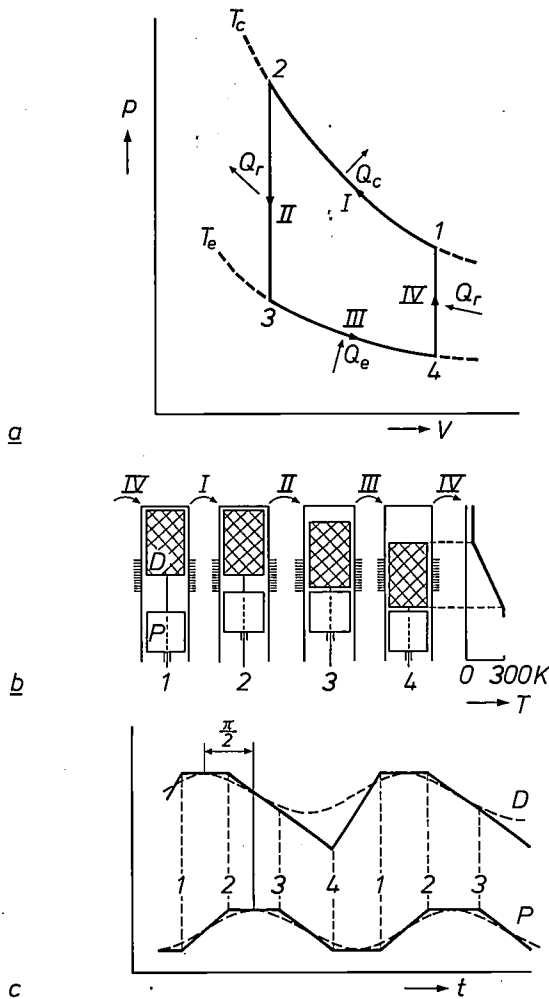


Fig. 1. a) Pressure and volume variations in the ideal Stirling cycle (p - V diagram). In the isothermal compression at temperature T_c (phase I) a quantity of heat Q_c is removed from the working gas; the amount Q_e is absorbed by the gas during the isothermal expansion at temperature T_e in phase III. In the isochorous (equal-volume) cooling phase II the heat Q_r is stored in the regenerator; it is reabsorbed by the gas in the isochorous phase IV. b) Position of the piston P and the displacer D , with integrated regenerator, in the working space at the points 1-4 in (a). The phases I-IV are indicated. The temperature distribution along the working-space wall is shown schematically on the right; the temperature-gradient moves up and down with the regenerator inside the displacer. c) The positions of piston and displacer plotted as a function of time. Their movements can be approximated by simple harmonic motions (dotted lines) that are about $\pi/2$ out of phase.

A Stirling cryogenerator capable of producing 5 W of refrigeration at a temperature of 65 K has been developed at Philips Laboratories at Briarcliff Manor in the United States. This machine, which will henceforth be referred to as the Briarcliff cryogenerator, was designed for NASA (National Aeronautics and Space Administration); its intended use is the cooling of infrared detectors in satellites. To be 'spaceworthy', the cryogenerator must be capable of operating continuously for a minimum of five years without mainte-

The piston and the displacer are each driven by a linear electric motor, so that only electrical power needs to be supplied to the machine, which can therefore be sealed hermetically. The amplitude of both movements, the associated phase difference and the operating frequency are regulated by an electronic control system. The most important operating parameters of the cryogenerator can therefore be varied within a comparatively wide range. This also makes the machine very suitable for experimentally optimizing

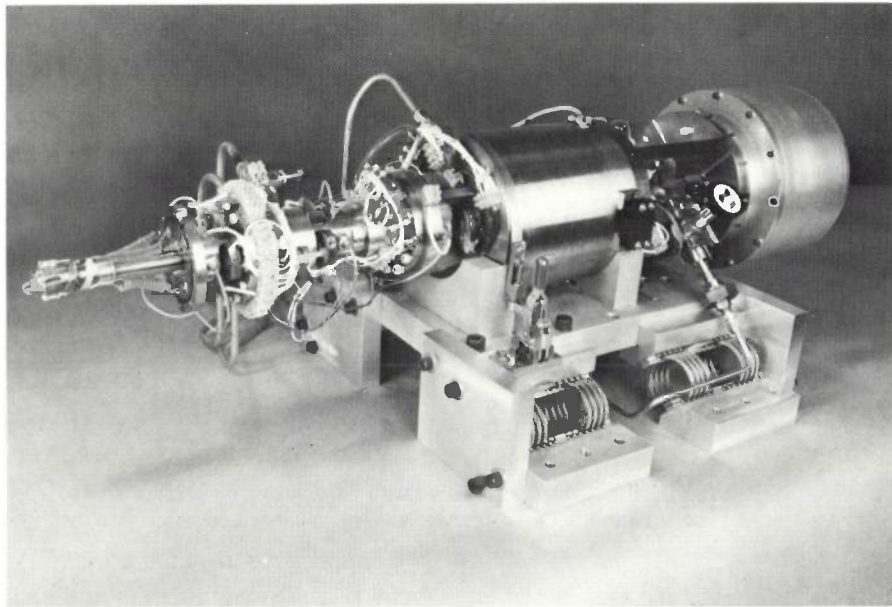


Fig. 2. Prototype of the Stirling cryogenerator that has been developed by Philips Laboratories at Briarcliff Manor, U.S.A. The machine produces 5 W of refrigeration at a temperature of 65 K. It is intended for cooling infrared detectors in satellites. The coldest part of the machine is on the left; the vibration absorber is on the right. The total length of the cryogenerator is about 100 cm.

nance. This requirement appears to have been satisfied by eliminating all mechanical contact between the moving parts of the machine and the adjoining walls of the working space. This contactless operation has been achieved by 'levitating' the piston and the displacer magnetically — to our knowledge the first time magnetic bearings have been used for reciprocating motions in a machine. The bearing system is fully 'active'; i.e. for all degrees of freedom control loops have been used. This configuration, which does not have permanent magnets, is comparatively complex, requiring position sensors, electromagnets, and an electronic control system, but it yields a high stiffness. In addition to providing support, the magnetic bearings allow the annular slits around the displacer and the piston to be extremely narrow. These annular slits form a clearance seal so that no contact seals, i.e. no wearing parts, are needed and lubrication is completely eliminated.

the parameters of motion for the Stirling refrigeration cycle or for operating the cryogenerator at a different cooling power or at different temperatures.

The use of magnetic bearings and the direct-drive linear motors means that the life and reliability of this cryogenerator depend solely on the reliability of electronic circuits. The prototype of this machine, shown in *fig. 2*, has already worked continuously for more than a year and a half without maintenance and without any deterioration in its cooling power or operating temperature. As a result of this project and of associated tasks ^[3], Philips Laboratories in the United States have acquired considerable experience with reciprocating magnetic bearings. Wider application of

- [2] R. J. Meijer, The Philips hot-gas engine with rhombic drive mechanism, *Philips Tech. Rev.* 20, 245-262, 1958/59; A. Daniels and F. K. du Pré, Miniature refrigerators for electronic devices, *Philips Tech. Rev.* 32, 49-56, 1971.
- [3] R. L. Maresca, An integrated magnetic actuator and sensor for use in linear or rotary magnetic bearings, *IEEE Trans. MAG-19*, 2094-2096, 1983.

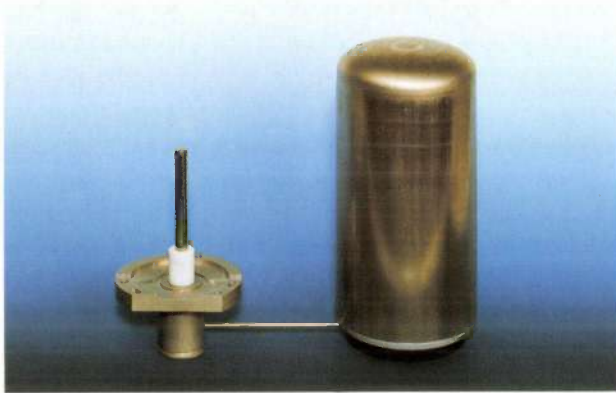


Fig. 3. One of the six different types of miniature Stirling cryogenerators with cooling capacities of 0.25 to 1 W at 80 K, which are in production at Philips USFA B.V. in Eindhoven. The 'cold finger' diameter of the cryogenerator depicted here is about 7 mm; for the smallest machine of the series the diameter is 5 mm, for the largest it is 10 mm. The expansion section (left) and compression section (right) are separated for easy integration in existing installations. The height of the compression section is only 13 cm. The cryogenerators are intended for cooling components such as detectors, lasers or electronic devices, and are hermetically sealed for life (at least 2500 hours). The compression section is provided with a vibration absorber.

these bearings — possibly in projects for third parties — is now practical [4].

The second subject of this article is a cryogenerator for an entirely different field of application. This machine has been developed by Philips USFA B.V. in Eindhoven. A series of six different types is produced, with cooling powers ranging from 0.25 to 1 W, at a cold-finger temperature of 80 K, see fig. 3. The diameter of the smallest displacer is slightly less than 5 mm, that of the largest displacer is about 10 mm. The USFA machine is intended for cooling detectors, lasers and electronic components and for other terrestrial applications. A special feature is that the compression and expansion take place in separate compartments. Both spaces are interconnected by a thin tube, 300 mm long and with a diameter of 2.4 mm. As a result, the cryogenerator can easily be integrated into any existing electronic or physical installation. The machine is hermetically sealed by welding to completely contain the working gas. The piston is driven by a linear electric motor; as noted earlier, the free moving displacer is connected by a helical spring to the wall of the working space. Since the resonant frequency of the displacer system is about 1.25 times the supply frequency, there is a phase difference between the simple harmonic motions of the piston and the displacer. At a phase angle of $\pi/2$, which gives the largest cold production in crank-driven machines, the displacer amplitude would be virtually zero. For this reason a phase difference of approximately $\pi/4$ has been chosen as a compromise.

The support and the sealing of both the piston and displacer are provided by rings of reinforced PTFE (polytetrafluorethene), which combines good sliding properties with low wear and, in addition, requires no lubrication. As a result of this the average life of the machine is approximately 5000 hours, with a guaranteed minimum of 2500 hours. Its simpler design makes it relatively inexpensive to manufacture.

In what follows we shall first deal with the theory of Stirling cryogenerators with simple harmonic linear motions, and then discuss the two cryogenerators in more detail.

Theoretical background

We shall first derive an expression for the theoretical cold production P_c of a Stirling machine assuming simple harmonic piston and displacer motions. This cold production is equal to the work which is transmitted by the gas to the displacer per second in the expansion space and which must be drawn from the environment. We find:

$$P_c = \frac{\omega}{2\pi} \oint p dV_e, \quad (1)$$

where $\omega = 2\pi f$, with f the operating frequency of the linear electric motor for the piston, p the pressure in the expansion and compression spaces and V_e the volume of the expansion space. Disregarding the flow losses, p is only a function of the displacements x of the displacer and y of the piston, so that we have:

$$p = p_m + C_x \hat{x} \cos \omega t + C_y \hat{y} \cos(\omega t - \phi), \quad (2)$$

where p_m is the average pressure of the working gas, C_x and C_y are approximately constant, \hat{x} and \hat{y} the amplitudes of the displacer and piston movements, t time and ϕ is the phase angle between the simple harmonic motions of the piston and the displacer. By substituting (2) in (1) we find:

$$P_c = -\frac{1}{2} \omega C_y \hat{x} \hat{y} S_d \sin \phi, \quad (3)$$

where S_d is the surface area of the displacer perpendicular to the direction of motion. If the parameters of motion of the piston and the displacer can be selected independently, as in the case of mechanically driven machines and in the Briarcliff cryogenerator, then P_c is at a maximum when $\phi = \pi/2$. This has already been demonstrated with the aid of fig. 1.

In the case of the USFA cryogenerator the phase angle ϕ and the displacer amplitude \hat{x} are determined by the dynamic properties of the mass-spring system (the displacer with the helical spring), which is driven by the working gas. Both the phase angle and the amplitude depend on the difference between the reso-

nant frequency of this mass-spring system and the frequency f of the piston. In order to calculate the optimum phase angle for the USFA machine we must first formulate the equation of motion for the displacer [5]:

$$M_d \ddot{x} + \Delta p S_d + C_{hs} x = 0, \quad (4)$$

where M_d is the mass of the displacer, Δp the difference in pressure across the displacer — with flow losses now being taken into account — and C_{hs} the spring constant of the helical spring.

The pressure difference Δp is a function of the velocities \dot{x} and \dot{y} of the displacer and the piston and can be expressed as

$$\Delta p = C_d \dot{x} + C_p \dot{y}, \quad (5)$$

in which C_d and C_p are approximately constant. After substituting (5) into (4), with $x = \hat{x} \cos \omega t$ and $y = \hat{y} \cos(\omega t - \phi)$, we find

$$M_d(\omega^2 - \omega_d^2) \hat{x} \cos \omega t + C_d S_d \omega \hat{x} \sin \omega t - C_p S_d \omega \hat{y} \sin(\omega t - \phi), \quad (6)$$

where $\omega_d = (C_{hs}/M_d)^{0.5}$ is equal to the angular resonant frequency of the displacer mass-spring system. From equation (6) the following expressions for the phase angle and displacer amplitude are derived:

$$\tan \phi = \frac{M_d(\omega_d^2 - \omega^2)}{C_d S_d \omega}, \quad (7)$$

and

$$\hat{x} = -\frac{C_p}{C_d} \hat{y} \cos \phi. \quad (8)$$

From (7) it follows that $\phi = 0$ if $\omega_d = \omega$, i.e. if the resonant frequency of the displacer is equal to the supply frequency. From (3) it follows that the cold production is then equal to zero. Cold production is also zero if $\phi = \pi/2$, since from (8) the amplitude of the displacer is then equal to zero.

If we substitute (8) in (3) we obtain:

$$P_e = -\frac{C}{4} \omega \hat{y}^2 \sin 2\phi,$$

where $C = C_p C_y S_d / C_d$. The theoretical cold production of the USFA machine therefore has a maximum at $\phi = \pi/4$, and is thus equal to

$$P_{e,max} = -\frac{C}{4} \omega \hat{y}^2. \quad (9)$$

The USFA cryogenerator

A cross-section of the USFA cryogenerator is shown in fig. 4. The division of the generator into a compression section and an expansion section can be clearly

seen. The piston is connected to a motor coil; the current to this coil is supplied via flexible copper wires, as in a loudspeaker. The coil is located in a narrow 'air gap', in which a magnetic field is generated by an annular permanent magnet. The piston and the 'gas spring' of compression along with a mechanical spring connected to the housing together form a mass-spring system. (The mechanical spring also centers the piston under gravity.) Calculations show that the highest efficiency of the linear motor is obtained if this mass-spring system is in resonance at the operating frequency, i.e. if there is a phase difference of $\pi/2$ between the alternating current through the motor coil and the simple harmonic motion of the piston. From (3) it follows that the cold production is proportional to the frequency of the supply voltage. The square of the piston resonant frequency, for given parameters

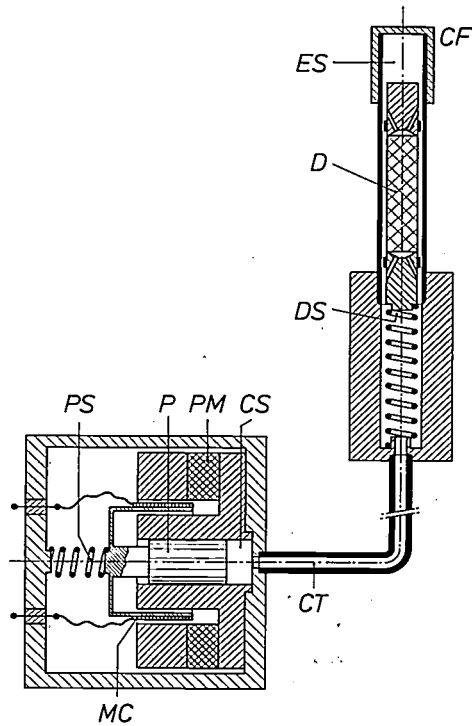


Fig. 4. Longitudinal cross-section of the USFA cryogenerator with compression section on the left and expansion section on the upper right. (The vibration absorber is not shown.) P piston. D displacer with regenerator. PS helical spring for piston. PM annular permanent magnet. MC motor coil. CS compression space. CT connection tube. DS helical spring for displacer. ES expansion space. CF cold finger.

[4] Both the integral design of the cryogenerator and the design of the separate magnetic bearings won an 'IR 100 Award' from the journal Industrial Research and Development; see their issue for October 1983.

[5] A. K. de Jonge, A small free-piston Stirling refrigerator, Proc. 14th Intersoc. Energy Conversion Eng. Conf., Boston 1979, pp. 1136-1141; A. K. de Jonge, Small split Stirling coolers for I.R. detectors, Proc. Int. Conf. on Adv. infrared detectors & systems, London 1981, pp. 55-59.

of the gas spring (swept volume, gas properties, leakage, etc.), is inversely proportional to the piston mass. Since the amount by which the mass of the piston can be reduced is limited, the frequency cannot be increased to an extremely high value. A good compromise is an operating frequency of 50 or 60 Hz [5].

Since the machine is hermetically sealed, the pressure of the working gas behind the piston (i.e. around the coil) is equal to the average pressure in the machine. In the expansion section the helium gas flows through the regenerator, which forms part of the displacer, twice per cycle. The slight pressure drop across the regenerator drives the displacer. For the smallest ver-



Fig. 6. The USFA cryogenerator integrated with an infrared detector in a vacuum vessel (Dewar) on the right. The complete Dewar with detector has the Mullard type number R170.

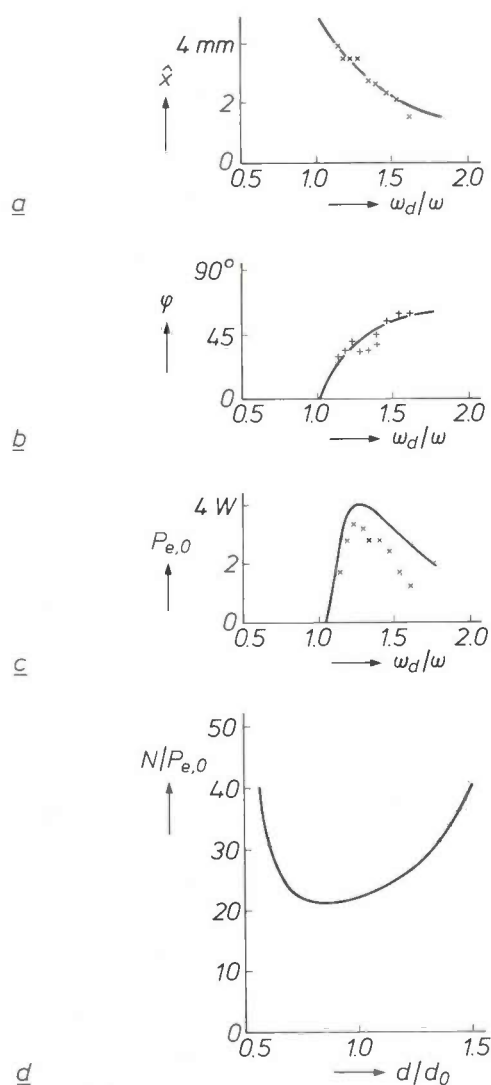


Fig. 5. Results of calculations (lines) and measurements (points) for the USFA cryogenerator. *a*) The displacer amplitude \hat{x} as a function of the ratio of the resonant angular frequency ω_d of the displacer to the operating frequency ω . *b*) The phase angle ϕ as a function of ω_d/ω . *c*) The net cold production $P_{e,0}$ as a function of ω_d/ω . A phase angle of $\phi = 45^\circ$ is obviously a good compromise. *d*) The ratio of input power N to net cold production $P_{e,0}$ as a function of the ratio of the internal tube diameter d (of CT in fig. 4) to a constant tube parameter d_0 in mm.

sions of the machine the regenerator has a diameter of only 4 mm. A temperature difference of approximately 200 K must be bridged over a distance of a few centimeters across the top part of the expansion section, the cold finger. To reduce the 'cold leakage' as much as possible, the cylinder wall of the expansion section is made of stainless steel (with a comparatively low thermal conductivity) with a thickness of only 0.1 mm. Clearly, the fabrication of this component is a challenging manufacturing task.

The results of a number of calculations and measurements on the cryogenerator are presented in *figs 5a-c*. The calculations were made with the aid of a special computer program that has been developed for the Stirling cycle. Fig. 5*a* shows the displacer amplitude \hat{x} , fig. 5*b* the phase angle ϕ between the piston and the displacer motion and fig. 5*c* the net cold production $P_{e,0}$, in each case as a function of the ratio of the resonant frequency of the displacer to the operating frequency. These results clearly show that $\pi/4$ is a good compromise for the phase angle. The net cold production measured is smaller than that calculated, since the calculated losses are about 90% of the theoretical cold production P_e , defined by (3), and a small deviation in the calculated losses affects the net cold production considerably.

One design problem is the choice of the dimensions of the connecting tube between the compression space and the expansion space. If the tube is too long it increases the heat-transfer surface between the two spaces; it also increases the 'dead space' for compression. As already mentioned, a length of 300 mm has been selected. In addition, for the same reasons, a small tube diameter is desirable, but too small a diameter increases the flow resistance. Fig. 5*d* shows the result of calculations for the optimum diameter. The ratio of the incident electrical power to the net cold

production is plotted as a function of the (dimensionless) tube diameter. It is clear that an optimum exists.

A version of the cryogenerator described is also produced with an infrared detector, see *fig. 6*. In this case the cold finger is mounted in a Dewar (vacuum vessel) with detector. The Dewar with integrated infrared detector is produced by Mullard Ltd (type number R170). The Dewar has a polished germanium window which is transparent to infrared radiation with a wavelength of 8 to 12 μm . The only load on the cryogenerator comes from the radiation reaching the

expansion section, and the vibration absorber can be clearly seen. Both the displacer and the piston are driven by linear motors, entirely independent of each other. In the motors of the Briarcliff cryogenerator the permanent magnets move and the coils remain stationary, whereas in the motor of the USFA machine it is the coil that moves. The advantage of the first approach is that there are no flexible power leads, which could break. The disadvantage of the larger mass of the moving parts is not a serious problem since these are driven separately and the operating frequency (typic-

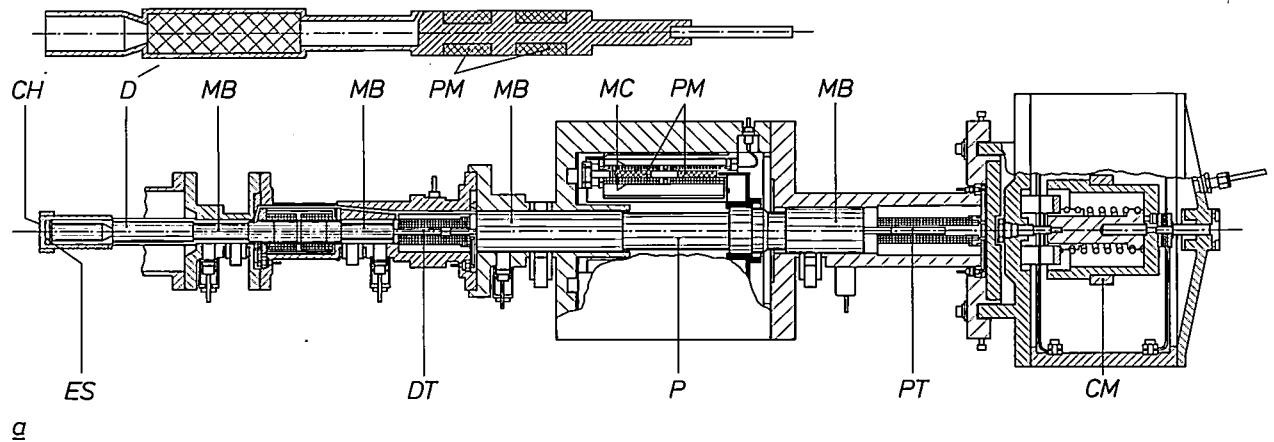


Fig. 7. *a)* Longitudinal cross-section of the prototype of the Briarcliff cryogenerator. CH 'cold head'. DT transducer of displacer axial motion. PT transducer of piston axial motion. MB magnetic bearing. CM counterbalance mass of vibration absorber. See also the caption to *fig. 4.* *b)* Motor-control system. V_{1-4} reference direct voltages proportional to \hat{x} , \hat{y} , ω and ϕ respectively. CE frequency and phase control electronics. V_p alternating voltage proportional to $\hat{y} \cos(\omega t - \phi)$. V_d alternating voltage proportional to $\hat{x} \cos \omega t$. x , y effective displacer and piston position. PCE, DCE piston and displacer motor control electronics. PMD, DMD piston and displacer motor drive. PD, DD system dynamics of piston and displacer.

detector, from the heat conduction via the electrical connections to the detector and from the radiation and conduction in the Dewar itself. Until recently such infrared detectors had to be cooled with liquid nitrogen in Joule-Thomson cooling systems. Liquid nitrogen in these systems is consumed in a few hours. An infrared detector with USFA cryogenerator, however, can operate continuously for at least 2500 hours.

The Briarcliff cryogenerator

The Philips Stirling computer program has also been used extensively to calculate the parameters of the Briarcliff cryogenerator^[6]. *Fig. 7a* shows a longitudinal cross-section of this cryogenerator in which, from left to right, the expansion section, the compres-

sion section, and the vibration absorber can be clearly seen. Both the displacer and the piston are driven by linear motors, entirely independent of each other. In the motors of the Briarcliff cryogenerator the permanent magnets move and the coils remain stationary, whereas in the motor of the USFA machine it is the coil that moves. The advantage of the first approach is that there are no flexible power leads, which could break. The disadvantage of the larger mass of the moving parts is not a serious problem since these are driven separately and the operating frequency (typic-

ally 25 Hz) is lower. The greater side forces that result from the permanent magnets being attracted to the iron stator are easily supported by the magnetic bearings.

A schematic representation of the drive-motor control system is given in *fig. 7b*. The input direct voltages provide a reference for the required values of the amplitudes \hat{x} and \hat{y} of the displacer and piston, the angular frequency ω and the phase angle ϕ . The electronic unit then derives the motor-drive signals, which are proportional to $\hat{x} \cos \omega t$ and $\hat{y} \cos(\omega t - \phi)$. These signals constitute the input references for the servomechanisms (feedback control systems) that regulate

[6] F. Stolfi, M. Goldowsky, J. Ricciardelli and P. Shapiro, A magnetically suspended linearly driven cryogenic refrigerator, Proc. 2nd Biennial Conf. on Refrigeration for cryogenic sensors & electronic systems, Greenbelt, MD, 1982, pp. 263-304.

Ned. Philips Bedrijven B.V.
PHILIPS RESEARCH LABS.
LIBRARY WY - 1
P.O. Box 60.000

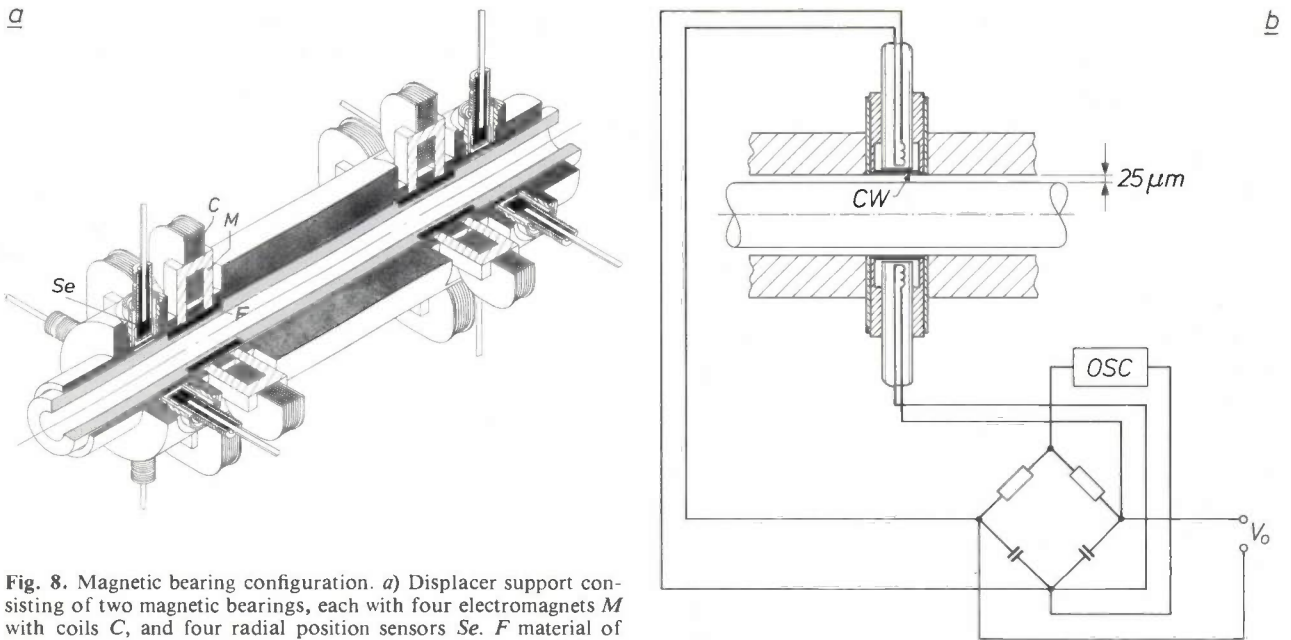
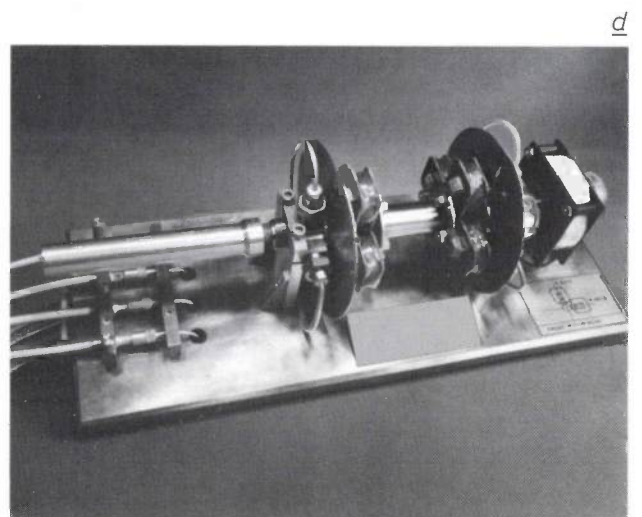
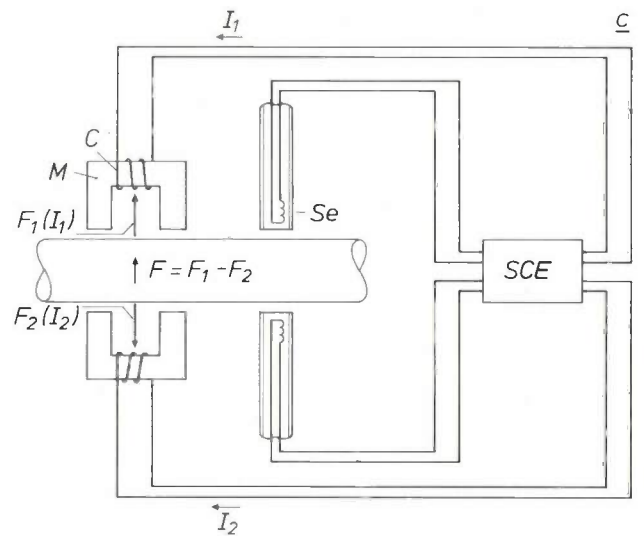


Fig. 8. Magnetic bearing configuration. *a*) Displacer support consisting of two magnetic bearings, each with four electromagnets M with coils C , and four radial position sensors Se . F material of high magnetic permeability. *b*) Two sensors Se in more detail. CW ceramic window. The two sensors for detecting radial displacer motion in one direction are connected into a differential bridge circuit to minimize temperature drift. OSC alternating voltage source. V_o output voltage. The high sensitivity of the displacement measurement system made it possible to reduce the gap width to $25\ \mu\text{m}$. *c*) Forces $F_1(I_1)$ and $F_2(I_2)$ exerted on the displacer by two electromagnets for one direction. $F = F_1 - F_2$ resulting force in equilibrium with external forces. SCE sensor and control electronics. If the equilibrium is perturbed radial movement is detected by the sensors Se . The currents I_1 and I_2 are then adjusted by SCE to find a new equilibrium at the average gap width of $25\ \mu\text{m}$. *d*) First test arrangement for the displacer magnetic bearings.

the motions of the displacer and the piston. Signals from transducers that measure the axial motion of the displacer and the piston are fed back into these control systems and compared to the references. The control system then continuously adjusts the current in the linear motors so that the motions of the piston and displacer accurately follow the reference signals.

As already mentioned, the displacer and the piston do not come into contact with the adjacent walls of the working space. This is achieved by employing magnetic bearings^[7] for guiding the moving parts, as shown in *fig. 8a*. Both the piston and the displacer are provided with two bearings. Each magnetic bearing consists of four electromagnets and four radial displacement sensors. There are two sensors per bearing for the vertical direction and two for the horizontal direction. The two sensors per direction are connected into a differential bridge circuit, which minimizes the effects of temperature drift, see *fig. 8b*. Each bridge is sufficiently sensitive to detect displacements as small as $0.25\ \mu\text{m}$. The measured displacement signals are fed back into control circuits that adjust the currents in the electromagnets to center the piston and displacer in the cylindrical bores, see *fig. 8c*. As a result of the



high sensitivity of the sensors and the high reaction rate of the control circuits, the gaps around both parts have been reduced to 25 μm . This puts tight requirements on the production accuracy of the various cylindrical surfaces that form these gaps. Fig. 8d shows the first test arrangement of a magnetic bearing for the displacer.

The small gaps around the displacer and the piston also function as clearance seals. This means that the cylindrical gaps are sufficiently narrow and long to keep the leakage of the working gas within acceptable limits. For these small gaps the leakage is proportional to the third power of the gap width and inversely proportional to the gap length. A 10% increase in the gap width increases leakage by 33%.

Since absolutely no wear occurs in the cryogenerator, its life is not limited by 'blockage' resulting from wear products. Blockage could, however, occur as a result of gases condensing and solidifying in the cold sections of the machine. The machine is therefore filled with very pure helium. In addition, all parts that come into contact with the working gas are made of metal or ceramic. For this reason, for example, the motor coils are encapsulated in titanium envelopes (the gases from the materials insulating the copper wires cannot therefore reach the working space). Ceramic is used at points where thermal or electrical insulation is needed, as in the displacement sensors of fig. 8b. The parts are carefully cleaned and degreased prior to assembly and are then heated in vacuum to a temperature of 100 °C or more in order to remove any gas that has been absorbed.

Fig. 9a shows a cut-away view and fig. 9b a radial cross-section of the linear motor that drives the piston. The coil volume is split into inner and outer sections each surrounded by iron stators, to minimize the side forces resulting from the attraction between the moving magnet armature and the iron. The circular permanent magnets are connected to the piston by means of a titanium (non-magnetic) yoke. Fig. 9b also shows the lines of force for a non-energized coil; the magnetic field was analysed with the aid of a Philips finite-element magnetic-field computer program. The force on the permanent magnets has been estimated with the computer program and can also be calculated by considering the energy balance [8].

The displacer motor design is similar. The annular permanent magnets here have an external diameter equal to that of the displacer, see fig. 7a. The displacer has an iron core at the center of these magnets, which moves with it.

The passive vibration absorber is also shown in fig. 7a. In the prototype depicted here the vibration absorber consists of a mass suspended on leaf springs

and connected to the housing by a helical spring. This mass-spring system is tuned to resonate at the operating frequency and suppresses the vibrations transmitted to the environment. Since it is a passive system it can only remove vibrations at the operating frequency; higher harmonic vibrations are not suppressed. It suppresses the amplitude of the fundamental operating frequency vibrations in the axial direction by a factor of 1/19.

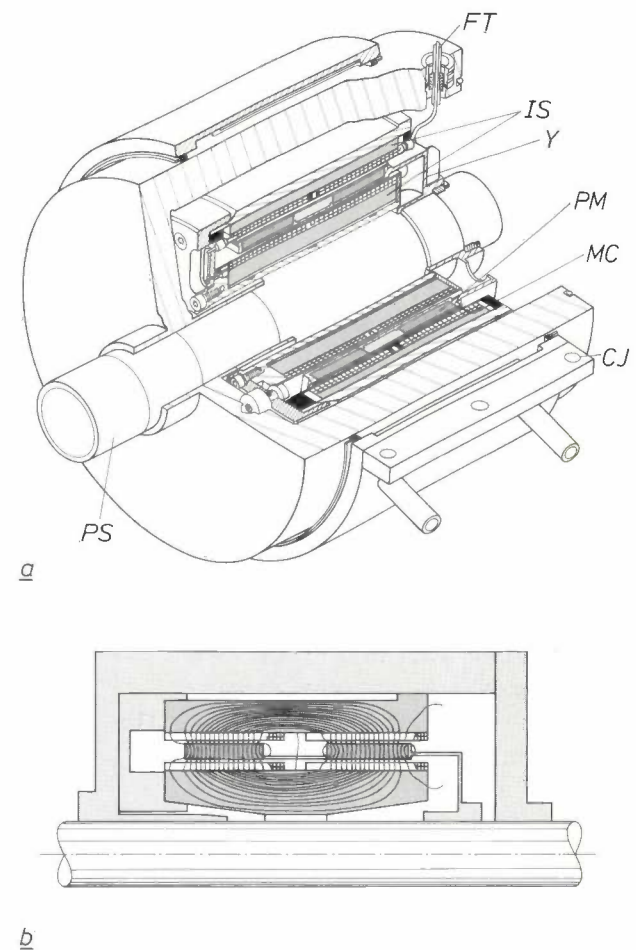


Fig. 9. Piston linear motor. *a*) Cut-away view. *PS* piston shaft. *CJ* water jacket for cooling. *PM* annular permanent magnets. *MC* coil, in two sections. *Y* titanium yoke. *IS* iron stator. *FT* feed-through for motor-current supply. *b*) Radial cross-section with magnetic lines of force for a non-energized coil. The lines of force were calculated with a finite-element field computer program.

[7] The general principles of magnetic bearings are discussed in: E. M. H. Kamerbeek, *Magnetic bearings*, Philips Tech. Rev. 41, 348-361, 1983/84.

[8] L. Hondt and K. H. Meyer, *A linear d.c. motor with permanent magnets*, Philips Tech. Rev. 40, 329-337, 1982; A. K. de Jonge and A. Sereny, *Analysis and optimization of a linear motor for the compressor of a cryogenic refrigerator*, in: R. W. Fast (ed.), *Advances in cryogenic engineering*, Vol. 27, Plenum, New York 1982, pp. 631-640.

At the points of attachment of the leaf springs and helical spring of the vibration absorber in the prototype wear can occur. In the final version of the machine — intended for launching into space — the helical spring has been replaced by gas under pressure (gas spring) and the mass is guided by magnetic bearings. In this version the resonant frequency of the vibration absorber is tuned to the operating frequency by means of a control circuit and a third linear motor. Even better suppression of the vibrations should be obtained with this final version of the absorber, including the suppression of higher harmonics.

As already mentioned, the prototype machine has been in operation for more than a year and a half with no decrease in cold production. The requirement that the cryogenerator produces 5 W of cold at 65 K has been met. Prior to this, extensive tests were made of the variation in performance for changes in various operating parameters such as piston and displacer amplitudes, frequency and phase^[9]. The cryogenerators in the final version will have to operate unattended for five years or longer in space. Design efforts will

^[9] A. Daniels, F. Stolfi, A. Sherman and M. Gasser, Magnetically suspended Stirling cryogenic space refrigerator: test results, in: R. W. Fast (ed.), *Advances in cryogenic engineering*, Vol. 29, Plenum, New York 1984, pp. 639-649.

therefore also be aimed at improving the efficiency and reliability of the electronic circuits so that they can perform their task for the same period of time without any maintenance.

Summary. Stirling cryogenerators that are driven by linear electric motors do not require a complicated mechanism to convert a rotary motion into a linear motion. In these cryogenerators simple harmonic motion is required for the piston and the displacer (with integrated regenerator), with a phase difference between $\pi/4$ and $\pi/2$. The piston is always provided with a linear motor; the displacer can either be driven by a separate linear motor or move freely close to resonance in a mass-spring system. Both schemes have resulted in practical designs. The design with two linear motors is a 5-W 65-K cryogenerator for space applications. This cryogenerator was developed at Philips Laboratories, Briarcliff Manor. A long maintenance-free life has been obtained by using magnetic bearings for the piston and displacer. The magnetic bearings have narrow annular slits that act as gap seals. There is absolutely no contact between the moving parts and the working-space walls, so that mechanical wear has been completely eliminated. A cryogenerator with one linear motor and a free moving displacer was designed by Philips USFA B.V., Eindhoven. The production range consists of a series of six miniature cryogenerators with capacities from 0.25 to 1 W at 80 K for cooling electronic or other components, e.g. infrared detectors. The compression and expansion sections are separated so that the hermetically sealed cryogenerator can easily be included in existing systems. The piston and displacer are supported by seals of reinforced PTFE for a guaranteed life of 2500 hours. Both types of cryogenerator are provided with passive vibration absorbers.

Determining the Von Mises stress from the neck of a tensile-test specimen

H. Galenkamp and H. van Wijngaarden

The tensile test is one of the most widely used methods of testing materials. The interpretation of the result, i.e. the curve giving the relation between force and elongation, causes some difficulties, especially when materials are investigated that have to be subjected to severe plastic deformations. The problems of interpretation are due to the occurrence of a constriction, called the 'neck', in the tensile-test specimen. From the shape of the neck various investigators have derived a correction factor that can be used to correct the mean stress into a quantity known as the Von Mises stress. The authors have used a mathematical model to verify the correction factors given in the literature. They have also designed a method of measurement, with an associated computer program, which will give the Von Mises stress simply and quickly as a function of the strain.

Introduction

Materials testing can be either non-destructive or destructive. In the destructive testing of materials the tensile test is of particular importance. A test specimen, made in the form of a bar or strip of the material to be investigated, is continuously elongated in a tensile-testing machine until fracture occurs. During the test the force on the specimen is recorded as a function of the elongation. To make the result independent of the dimensions of the specimen the tensile force is divided by the original cross-section of the specimen and the elongation is divided by the original length. (The term 'cross-section' as used in this article means the area of the cross-section of the bar perpendicular to the axis of symmetry.) The resultant mean stress σ_0 as a function of the strain ϵ gives the stress-strain curve, as shown in *fig. 1a*.

Fig. 1b shows the test specimen just before the fracture and just after. It can clearly be seen that a marked constriction ('necking') occurs in the specimen before fracture. In the smallest cross-section of the bar the ratio of the force to this cross-section is therefore

much greater than the ratio of the force to the original cross-section. This is why the result of the tensile test is often given as the ratio $\bar{\sigma}$ of the force to the smallest cross-section as a function of the strain ϵ ; see the dashed curve in *fig. 1a*. This ratio is called the 'true mean stress'. For greater elongations the true strain $\bar{\epsilon}$ is plotted along the horizontal axis. This is equal to the integrated relative elongation $d l / l$:

$$\bar{\epsilon} = \int_{L_0}^{L_t} \frac{d l}{l} = \ln \frac{L_t}{L_0}, \quad (1)$$

where L_0 is the original length and L_t is the length of the specimen at the time t .

The components of metal structures such as machines and bridges have to keep their shape when under load. This implies that the material of the components must not be subjected to a heavier load (allowing for a safety factor) than follows from the value of σ_E , the elastic limit; see *fig. 1a*. Up to the point where σ_E is reached the stress-strain curve is a straight line and the material obeys Hooke's law:

$$\bar{\sigma} = \bar{\epsilon} E, \quad (2)$$

where E is Young's modulus.

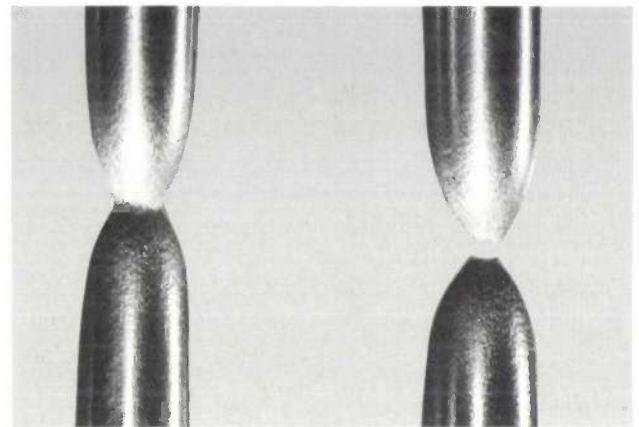
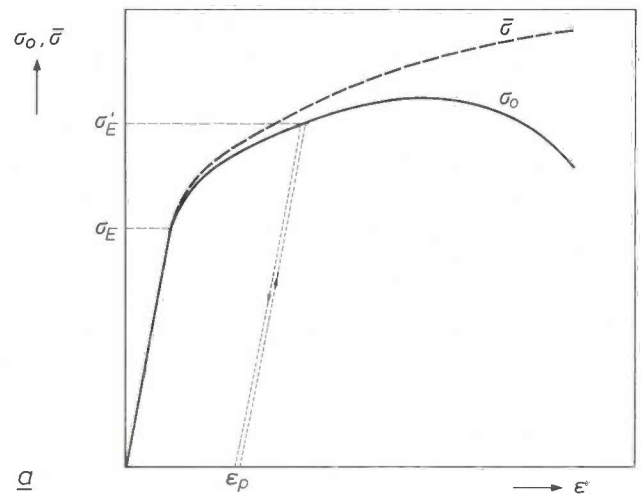
Ing. H. Galenkamp, formerly with Philips Research Laboratories, is now with the Philips Plastics and Metalware Factories, Eindhoven; Ir H. van Wijngaarden is with Philips Research Laboratories, Eindhoven.

If the material is deformed beyond the elastic strain, the strain associated with σ_E , a permanent or plastic deformation occurs: the material has passed the yield point. If the tensile test is now interrupted by relieving the strain temporarily, as indicated by the dotted lines in fig. 1a, the material is then found to be plastically deformed, with the plastic strain ϵ_p . When the load is applied again the stress-strain curve follows approximately the original pattern, as if the test had not been interrupted. The elastic limit is however higher now (σ_E') than during the loading of the 'virgin', undeformed material. This effect is known as strain hardening.

When material is shaped without cutting, the range beyond the elastic limit in the stress-strain curve is extremely important. Examples of operations with no removal of material are deep-drawing and metal spinning — operations in which a three-dimensional product is produced from sheet material — and extrusion and wire drawing — operations in which material is pressed or drawn through a shaped aperture. In such operations the plastic strain in the material can be very high, often much higher than 200%, whereas the elastic strain in steel, say, is no greater than about 2.5×10^{-3} .

A difficulty is encountered in the practical interpretation of the tensile test, because in most deformation processes the stress distribution is more complicated than during this test. Various yield or plastic-flow hypotheses have from time to time been put forward for evaluating the admissibility of practical stress distributions [1]. A common feature of these hypotheses is the mathematical definition of a limiting stress state just before the material yields, i.e. just before the material has become plastically deformed. The oldest yield hypothesis dates from 1773 and was postulated by Charles Augustin Coulomb. In 1871 M. Levy proposed a yield hypothesis that is still widely used today. In 1913 this hypothesis was reformulated mathematically by R. von Mises, who did not know of the work of Levy; since then it has become known as the Levy-Von Mises yield hypothesis. In this hypothesis the 'Von Mises stress' is defined as a mathematical quantity that is a function of the three principal stresses that determine the state of stress.

The problem of interpreting a state of stress also arises in the tensile test when the specimen is 'necked'. Because of the complex state of stress the true mean stress $\bar{\sigma}$ cannot be directly used for evaluating the suitability of the material for processes in which there are substantial plastic deformations. Such an evaluation can however be made, using the Von Mises stress as a function of the true strain $\bar{\epsilon}$. But it is not easy to see how the Von Mises stress can be determined during



b

Fig. 1. a) The stress-strain curve, the mean stress over the specimen cross-section as a function of the strain ϵ , the ratio of the elongation to the original length. The stress-strain curve is the result of a tensile test in which a bar is stretched in a tensile-testing machine until fracture occurs. The solid curve applies for σ_0 , the mean stress related to the original cross-section of the specimen; the dashed curve applies for $\bar{\sigma}$, the true mean stress related to the specimen cross-section at the smallest diameter of the neck. If the test is interrupted before fracture has occurred (the dotted lines) the material is found to be permanently deformed, with a plastic strain ϵ_p . If the specimen is put under load again the original curve continues. The elastic limit σ_E , the stress at the end of the linear part of the curve, is then found however to have a higher value (σ_E'). This effect is known as strain hardening. b) The 'necking' of an aluminium test specimen, on the left just before fracture, on the right just after fracture.

the tensile test, since it is virtually impossible to measure the principal stresses in the material of the specimen during the test.

Several investigators have recognized that a relation must exist between the shape of the neck of the specimen and the Von Mises stress at the centre of the smallest cross-section. Such a relation was formulated as long ago as 1925 by E. Siebel [2]. A similar result was arrived at later by P. W. Bridgman, who considered the radius of curvature over the longitudinal cross-section of the specimen at the position of the

smallest diameter [3]. N. N. Davidenkov and N. I. Spiridonova derived much the same result from the shape of the crystallites in the deformed material, using the second derivative of the curve that describes the neck [4]. We have used a mathematical derivation and have found the same relation as Davidenkov and Spiridonova, although our initial assumptions were slightly different.

By making use of the relation between the shape of the neck and the Von Mises stress (we shall call this stress σ_{VM} from now on) we can recalculate the stress-strain curve. The function $\sigma_{VM}(\bar{\epsilon})$ obtained in this way can be approximated by

$$\sigma_{VM} = C(\bar{\epsilon}_p + \epsilon_0)^n, \quad (3)$$

for example, where $\bar{\epsilon}_p$ is the true plastic strain, ϵ_0 a dimensionless constant, C a constant often referred to as the specific stress, and n is the 'strain-hardening exponent'. The quantities C and n can be used in calculations of processes in which there are substantial plastic deformations.

We have devised a method of measuring the corrected stress-strain curve $\sigma_{VM}(\bar{\epsilon}_p)$, based on continuous measurement of the diameter at different positions along the test specimen. The smallest value from the diameter measurements is selected as a function of time, and hence as a function of the tensile force. From each value of the smallest diameter and closely adjacent diameters, the second derivative with respect to the length of the neck curve is determined at the position of the smallest cross-section. This second derivative is converted into a correction factor for calculating the Von Mises stress from the mean stress in the smallest cross-section. The corrected stress-strain curve $\sigma_{VM}(\bar{\epsilon}_p)$ and the parameters C , ϵ_0 and n can then be obtained as the result of the measurements.

In the rest of the article we shall first recapitulate some concepts of stress theory and then go somewhat deeper into the Levy-Von Mises yield hypothesis. We shall also give the formula for the correction factor, but without any detailed derivation. The method of measurement will then be discussed. Finally we shall show how the procedure for processing the results of the measurements is verified by means of a computer program based on the finite-element method.

Theoretical background

In our treatment we shall assume that the material is homogeneous and isotropic. In a coordinate system (x,y,z) the faces of a block of material of dimensions dx , dy and dz are acted upon by vector stresses defined as force per unit area, which can be resolved into the components indicated in *fig. 2a*. The stress compo-

nents are referred to as σ_{ij} , where the subscript i denotes the plane and the subscript j denotes the direction of the component. The stress component σ_{xz} thus acts in a plane perpendicular to the x -axis in the z -direction. The stress components for which $i \neq j$ act in the plane considered and are called shear stresses.

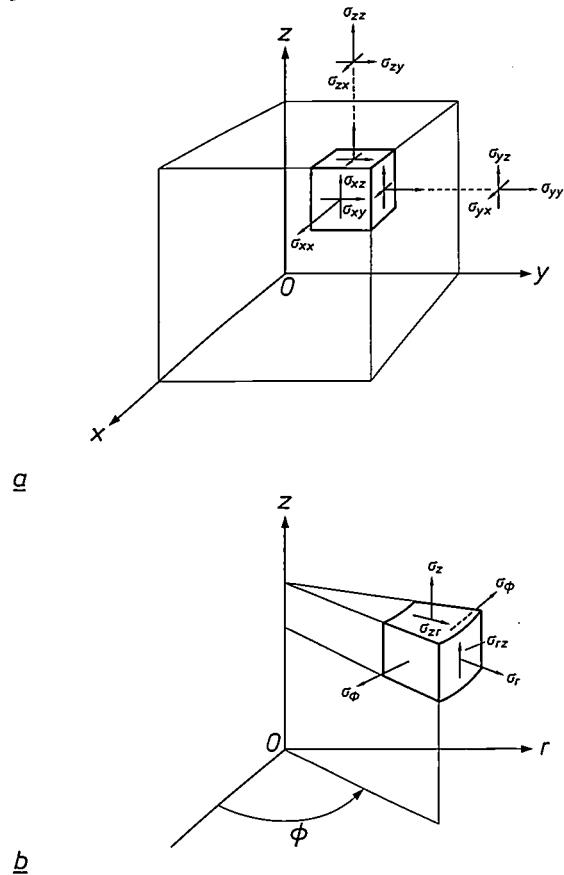


Fig. 2. The components of the stresses at the planes bounding an elementary block of material. *a)* For a block in a rectangular coordinate system (x,y,z) . σ_{xx} , σ_{yy} , σ_{zz} normal stresses, which are perpendicular to the planes perpendicular to the x -, y - and z -axes. σ_{xy} , σ_{xz} shear stresses in the y - and z -directions in the plane perpendicular to the x -axis. σ_{yx} , σ_{yz} , σ_{zx} , σ_{zy} shear stresses in the planes perpendicular to the y - and z -axes. *b)* The stress components for a block in a cylindrical coordinate system (ϕ,r,z) in the case where the stress distribution is symmetrical in relation to the z -axis. σ_ϕ , σ_r , σ_z normal stresses. (The second subscript has been omitted for simplicity.) σ_{rz} , σ_{zr} shear stresses. In view of the necessary equilibrium of forces, these shear stresses are equal in magnitude. Because of symmetry the other shear stresses are equal to zero.

[1] R. Hill, The mathematical theory of plasticity, Clarendon, Oxford 1950;
 I. Szabó, Höhere technische Mechanik, 4th edition, Springer, Berlin 1964;
 W. T. Koiter, Stijfheid en sterkte 1, Scheltema & Holkema, Haarlem 1972.
 [2] E. Siebel, Formänderungsfestigkeit und Spannungsverteilung im eingeschnürten Stabe, Bericht des Werkstoffausschusses des Vereins deutscher Eisenhüttenleute No. 71, 1925.
 [3] P. W. Bridgman, Studies in large plastic flow and fracture, McGraw-Hill, New York 1952.
 [4] N. N. Davidenkov and N. I. Spiridonova, Mechanical methods of testing — analysis of the state of stress in the neck of a tension test specimen, Proc. ASTM 46, 1147-1158, 1946.

The stress components with $i = j$ act at right angles to the plane and are called normal stresses, or tensile or compressive stresses, depending on whether the stress vector is directed away from the plane or towards it. In view of the equilibrium of the moments acting on the block, we have $\sigma_{ij} = \sigma_{ji}$. In the following we shall always indicate the normal stress with one subscript, thus as σ_x , σ_y and σ_z .

It can be shown that at any given point of the material there are always three mutually perpendicular planes in which the shear stresses are equal to zero, so that there will only be normal stresses acting at these planes. These three planes are called the principal planes and the corresponding normal stresses are called the principal stresses. We denote the three principal stresses by σ_1 , σ_2 and σ_3 .

For a small pyramid-shaped piece of material, bounded by three planes perpendicular to the x -, y - and z -axes and one (oblique) principal plane with principal stress σ , we can write the equilibrium equations for the x -, y - and z -directions [1]. The result can be reduced to the following third-degree equation in σ :

$$\sigma^3 - (\sigma_x + \sigma_y + \sigma_z)\sigma^2 + \{(\sigma_x\sigma_y - \sigma_{xy}^2) + (\sigma_y\sigma_z - \sigma_{yz}^2) + (\sigma_z\sigma_x - \sigma_{zx}^2)\}\sigma - \begin{vmatrix} \sigma_x & \sigma_{yx} & \sigma_{zx} \\ \sigma_{xy} & \sigma_y & \sigma_{zy} \\ \sigma_{xz} & \sigma_{yz} & \sigma_z \end{vmatrix} = 0. \quad (4)$$

The three principal stresses σ_1 , σ_2 and σ_3 are the roots of this equation in σ . The coefficients of the terms in σ^2 , σ^1 and σ^0 must be independent of the choice of the coordinate system (x, y, z) and are therefore called the invariants of the stress state. If the coordinate system is chosen such that the axes are perpendicular to the principal planes at the particular point being considered in the material, then in equation (4) σ_x , σ_y and σ_z are equal to the principal stresses σ_1 , σ_2 and σ_3 and the shear stresses are equal to zero. The three invariants can therefore also be written as

$$\sigma_1 + \sigma_2 + \sigma_3, \quad (5a)$$

$$\sigma_1\sigma_2 + \sigma_2\sigma_3 + \sigma_3\sigma_1, \quad (5b)$$

and $\sigma_1\sigma_2\sigma_3. \quad (5c)$

If two of the principal stresses are equal to zero, a uniaxial stress state exists. Both the second invariant (5b) and the third invariant (5c) are then equal to zero. This situation is encountered in the tensile test before the neck begins to form. If one of the principal stresses is equal to zero, a planar stress state exists. Only the third invariant (5c) is then equal to zero. This situation is found for example in the flexure of loaded beams and plates, for small deflections. The general case, in

which none of the principal stresses is equal to zero, is referred to as a three-dimensional stress state.

The limiting stress state as defined by Levy and Von Mises

The plastic flow or yield hypotheses mentioned above define a stress state in which the material is just about to undergo plastic deformation. This limiting stress state thus indicates the transition from the elastic range of the stress-strain curve to the plastic range.

An important experimental fact is that an omnidirectional positive or negative pressure superimposed on an existing stress state has very little effect, if any, on the plastic-flow behaviour of the material. (Extremely large hydrostatic pressures do however affect the plastic-flow behaviour [3].) This means that the first invariant (5a) of the stress state has no effect on the plastic-flow behaviour of the material. The differences between the principal stresses $(\sigma_1 - \sigma_2)$, $(\sigma_2 - \sigma_3)$ and $(\sigma_3 - \sigma_1)$ therefore have a much greater effect on the plastic-flow behaviour than the principal stresses themselves.

With the experimental observation mentioned above as a starting point, both Levy and Von Mises postulated a limiting stress state in which the differences between the principal stresses are all equivalent in the expression $(\sigma_1 - \sigma_2)^2 + (\sigma_2 - \sigma_3)^2 + (\sigma_3 - \sigma_1)^2$. Using (4) and (5) we can convert the limiting stress state thus established into the stress components that appear in a given coordinate system (x, y, z) :

$$\begin{aligned} &(\sigma_1 - \sigma_2)^2 + (\sigma_2 - \sigma_3)^2 + (\sigma_3 - \sigma_1)^2 = \\ &(\sigma_x - \sigma_y)^2 + (\sigma_y - \sigma_z)^2 + (\sigma_z - \sigma_x)^2 + 6(\sigma_{xy}^2 + \sigma_{yz}^2 + \sigma_{zx}^2). \end{aligned} \quad (6)$$

The limiting stress state as defined by Levy and Von Mises is usually expressed in a mathematical quantity σ_{VM} that may be considered as the stress that occurs in a plane perpendicular to the axis of a tensile-test specimen at the moment when the material has just become plastically deformed. Since in this case a uniaxial stress state is present, equation (6) becomes

$$(\sigma_1 - \sigma_2)^2 + (\sigma_2 - \sigma_3)^2 + (\sigma_3 - \sigma_1)^2 = 2\sigma_{VM}^2. \quad (7)$$

This is the most widely used formulation of the above yield hypothesis. The quantity σ_{VM} is called the Von Mises stress.

Equation (7) can thus on the one hand be used for determining whether the limiting stress state has been reached somewhere in the material. If it has not, it is certain that the material has only been elastically deformed. On the other hand the relation between σ_{VM} and the plastic strain in the tensile test can be used to calculate the forces and maximum deformations in

processes where there is plastic deformation, such as deep-drawing, metal spinning and extrusion. We now have to consider how the relation between the Von Mises stress and the plastic strain can be derived from the results of the tensile test.

The stress state in the neck of the tensile specimen

Depending on the material under investigation, the test specimens used in the tensile test are bars of circular or rectangular cross-section. In this article we shall only consider test pieces of circular cross-section. The stress distribution is then symmetrical about the centre-line of the specimen, so that we can use a cylindrical coordinate system (ϕ, r, z) where the z -axis coincides with the centre-line, as shown in fig. 2*b*. The stresses acting on a block of material of magnitude $r d\phi dr dz$ are thus the normal stresses σ_ϕ , σ_r and σ_z , where because of the symmetry σ_ϕ is independent of the angular coordinate ϕ . Also because of the symmetry the shear stresses $\sigma_{\phi r}$ and $\sigma_{\phi z}$ are equal to zero, so that σ_{rz} is the only shear stress remaining. At the smallest cross-section of the neck σ_{rz} is equal to zero if it is assumed that the shape of the neck is symmetrical with respect to this cross-section. With the above simplifications we can derive from (6) and (7) a relation that gives the required Von Mises stress σ_{VM} as a function of the actual stresses in the test specimen:

$$2\sigma_{VM}^2 = (\sigma_\phi - \sigma_r)^2 + (\sigma_r - \sigma_z)^2 + (\sigma_z - \sigma_\phi)^2 + 6\sigma_{rz}^2 \tag{8}$$

If the specimen is not necked, we have, as stated earlier, a uniaxial stress state so that $\sigma_\phi = \sigma_r = \sigma_z = 0$. In this case σ_{VM} would thus be equal to σ_z , which is equal to the mean stress $\bar{\sigma}$ in the cross-section of the specimen.

Since in most materials plastic flow is associated with necking of the tensile specimen, the actual stress distribution is more complex. We ought therefore to calculate σ_{VM} from the actual stresses σ_ϕ , σ_r , σ_z and σ_{rz} occurring in the material at the location of the neck. It is not however very easy to measure the stresses inside the material. As noted earlier, there is a correlation between the shape of the neck and the Von Mises stress. This correlation will be treated later on.

Another problem is the determination of the true plastic strain $\bar{\epsilon}_p$ in the test specimen. Equation (1) for $\bar{\epsilon}$ is also valid for a small piece of the specimen at the centre of the neck. During the plastic flow of the material the volume remains constant. (This is not the case during elastic deformation of the specimen; the change of volume in that stage is accounted for by Poisson's ratio.) Hence for the material at the centre of the neck:

$$A_o \Delta l_o = A_t \Delta l_t, \tag{9}$$

where Δl_o and Δl_t are the lengths of a small region before and after the plastic deformation, and A_o and A_t are the cross-sections before and afterwards. From (9) and (1) we have

$$\bar{\epsilon}_p = \ln \frac{A_o}{A_t} \tag{10}$$

The true plastic strain can thus be calculated simply from the change in diameter at the smallest cross-section.

The correction factor for determining the Von Mises stress

The Von Mises stress corresponding to the stress state at the centre of the smallest cross-section can be written as a function of the quantities measured during the tensile test:

$$\sigma_{VM} = C_1 \frac{F_t}{A_t}, \tag{11}$$

where C_1 is the correction factor mentioned above, F_t is the tensile force exerted on the specimen and A_t is the smallest cross-section. We have derived the following relation for C_1 :

$$C_1 = \frac{4}{4 + R_t R_t''}, \tag{12}$$

where R_t is the external radius and $R_t'' = d^2 R/dz^2$, both at the time t for $z = 0$, i.e. at the location of the smallest cross-section; see fig. 3.

In deriving (12) we have assumed that $u_r = rf(z)$ in the neck, where u_r is the velocity of plastic flow in the material in the r -direction. As a result of symmetry we have $df/dz = 0$ for $z = 0$. It is therefore reasonable to assume that $|df/dz| < |f(z)|$ in the neighbourhood of $z = 0$. Using equation (8), with $\sigma_{rz}(z = 0) = 0$, and the equilibrium equations

$$\frac{\partial \sigma_r}{\partial r} + \frac{\sigma_r - \sigma_\phi}{r} + \frac{\partial \sigma_{rz}}{\partial z} = 0$$

and

$$\frac{\partial \sigma_{rz}}{\partial r} + \frac{\sigma_{rz}}{r} + \frac{\partial \sigma_z}{\partial z} = 0$$

for the block of material in fig. 2*b*, and after some rearrangement, we finally arrive at the expression (12). It also follows from the assumptions that $\sigma_r = \sigma_\phi$ at $z = 0$.

Davidenkov and Spiridonova obtained the same expression for the correction factor by way of an entirely different method [4]. They measured the deformations of the material by determining the dimensions of crystallites before and after the plastic deformation. They did this by microscopic observation of polished and

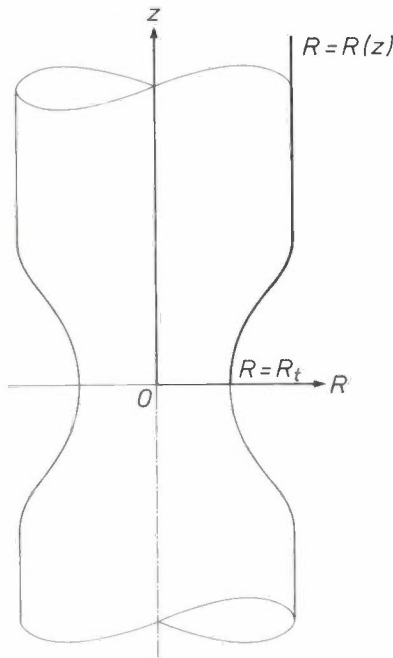


Fig. 3. The shape of the neck as a curve in a planar coordinate system (R, z). The z -axis coincides with the centre-line of the test specimen and the origin is located at the centre of the smallest cross-section. The correction factor for determining the Von Mises stress is a function of the external radius $R = R(z)$, and of its second derivative $R_t'' = d^2R/dz^2$, both at $z = 0$.

a

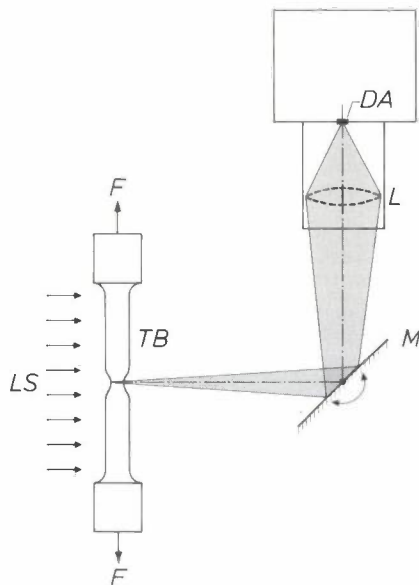


Fig. 4. Measuring the diameters of the test specimen. *a*) Diagram of the experimental arrangement. F forces acting on the test bar TB . LS light from a source consisting of a uniformly illuminated frosted glass window. M mirror that is periodically rotated in steps about an axis perpendicular to the plane of the figure. L positive lens. DA row of 2048 photodiodes; the row is perpendicular to the plane of the figure. The number of non-illuminated photodiodes is a measure of the diameter $2R$ of the test specimen at the position where the optical axis (dot-dashed line) cuts the test specimen. *b*) Photograph of the arrangement. The test specimen, clearly visible against the illuminated window, is located in the jaws of a tensile-testing machine. On the right is a mirror, driven by a stepping motor, and a camera. The camera includes the parts L and DA shown in (*a*).

etched cross-sections that were necked but had not yet fractured. The same formula was also derived in a theoretical approach by Siebel, who made different assumptions^[2]. Bridgman assumed that the shape of the neck in the vicinity of $z = 0$ was part of a toroid, so that the intersection of the neck with a plane through the centre-line was locally an arc of a circle^[3]. With this assumption Bridgman arrived at the following expression for the correction factor:

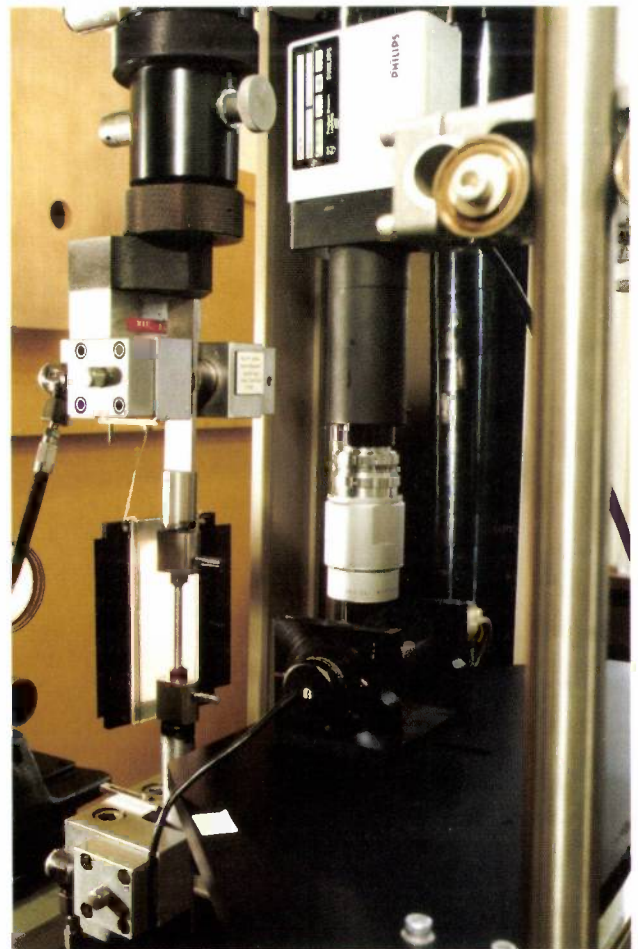
$$C_1 = \frac{1}{\left(1 + \frac{2}{R_t R_t''}\right) \ln\left(1 + \frac{R_t R_t''}{2}\right)}. \quad (13)$$

The correction factors calculated from equations (12) and (13) differ from each other by no more than 3% in practice.

The method of measurement

Fig. 4*a* is a diagram of the measuring arrangement and fig. 4*b* is a photograph. The equipment consists of a standard tensile-testing machine, which we have provided with instruments for measuring the shape of

b



the neck. The system works as follows. A light source, consisting of a uniformly illuminated frosted glass window, illuminates the tensile specimen. A lens and a mirror that can be rotated produce a shadow image of the test bar on a row of 2048 photodiodes, which crosses the axis of the test specimen at right angles. The number of photodiodes that receive no light is a measure of the diameter $2R$ of the specimen at the position of the optical axis. The mirror is rotated in steps, and the total angular displacement of the mirror is a measure of the position z of the diameter being measured. Positioning the mirror takes about 30 ms per step and measuring the bar diameter takes about 20 ms. One hundred diameters are measured over the entire length of the specimen. During the tensile test the entire specimen is measured about 50 to 100 times. A complete test thus takes about 4 to 8 minutes. A microcomputer is used to control the mirror and to process the measurement data.

Processing the data

Measured values R_i as a function of z_i , where $z_{i+1} - z_i$ is equal to a fixed value Δz (see fig. 5), are converted by the computer into approximations for R_t and R_t'' . From these approximations the correction factor C_1 is then determined from (12), and taking the measured tensile force F_t and $A_t = \pi R_t^2$, the Von Mises stress σ_{VM} is calculated from equation (11). The true plastic strain $\bar{\epsilon}_p$ is found from equation (10) so that successive measurements of the specimen give σ_{VM} as a function of $\bar{\epsilon}_p$ — the required result of the

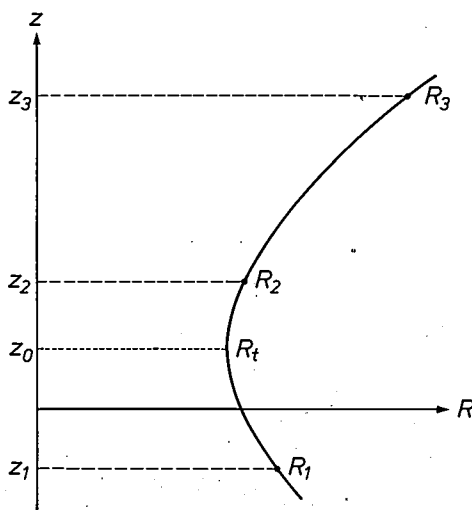


Fig. 5. Determination of R_t and R_t'' from measurements R_1 , R_2 and R_3 of the external radius near the smallest cross-section (see figs 3 and 4). The measurements are performed in such a way that $z_3 - z_2 = z_2 - z_1 = \Delta z$. From the coefficients of the equation of the parabola that contains the points (R_1, z_1) , (R_2, z_2) and (R_3, z_3) , approximations can be derived for $R_t = R(z_0)$ at the minimum of the parabola and $R_t'' = d^2R/dz^2$.

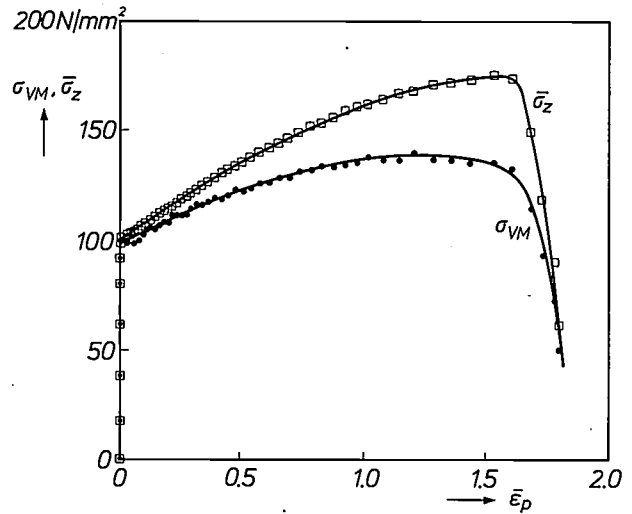


Fig. 6. Results of a tensile test with an aluminium test specimen. The circles relate to the Von Mises stress σ_{VM} , calculated by the method described. The squares relate to the mean tensile stress $\bar{\sigma}_z$ ($C_1 = 1$) over the smallest cross-section. Both quantities are plotted as a function of the true plastic strain $\bar{\epsilon}_p$. At $\bar{\epsilon}_p \approx 1.5$ the stress decreases, because a conical fracture surface forms from inside the specimen outwards.

tensile test. Finally the computer calculates the curve of best fit from equation (3), so that values of C , ϵ_0 and n can be obtained.

The calculation of R_t and R_t'' from the measured diameters of the specimen proceeds as follows (see fig. 5). We assume that R_2 is the smallest value of the measurements of R_i . A parabola $R(z) = a + bz + cz^2$ can be obtained that contains the points (R_1, z_1) , (R_2, z_2) and (R_3, z_3) . The equation for this parabola is:

$$R(z) = R_2 + \frac{R_3 - R_1}{2\Delta z} (z - z_2) + \frac{R_3 - 2R_2 + R_1}{2\Delta z^2} (z - z_2)^2.$$

Differentiating $R(z)$ with respect to z and then equating it to zero, we find the quantity R_t , which is the smallest external diameter of the neck:

$$R_t = R_2 - \frac{(R_3 - R_1)^2}{8(R_3 - 2R_2 + R_1)}$$

The second derivative $R_t'' = d^2R/dz^2$ of the parabola can be calculated from the relation

$$R_t'' = \frac{R_3 - 2R_2 + R_1}{\Delta z^2},$$

which follows from a Taylor series, neglecting the terms of higher order.

Fig. 6 shows the results of a tensile test on a test specimen made from a cylindrical bar of an aluminium alloy containing more than 99.5% of Al (the remainder is mainly Fe and Cu). Both the calculated Von Mises stress and the tensile stress $\bar{\sigma}_z$ ($C_1 = 1$)

averaged over the smallest cross-section are plotted as a function of the true strain. It is clear that the difference between the two curves increases as the strain increases, i.e. as the necking of the bar becomes more pronounced. Beyond a true strain $\bar{\epsilon}_p$ of about 1.5 (ϵ_p

tion). For some time it has also been possible to use this program for large material deformations, by redefining, during the deformation process, the network that divides the material into elements [6]. The input data for this program must include the various

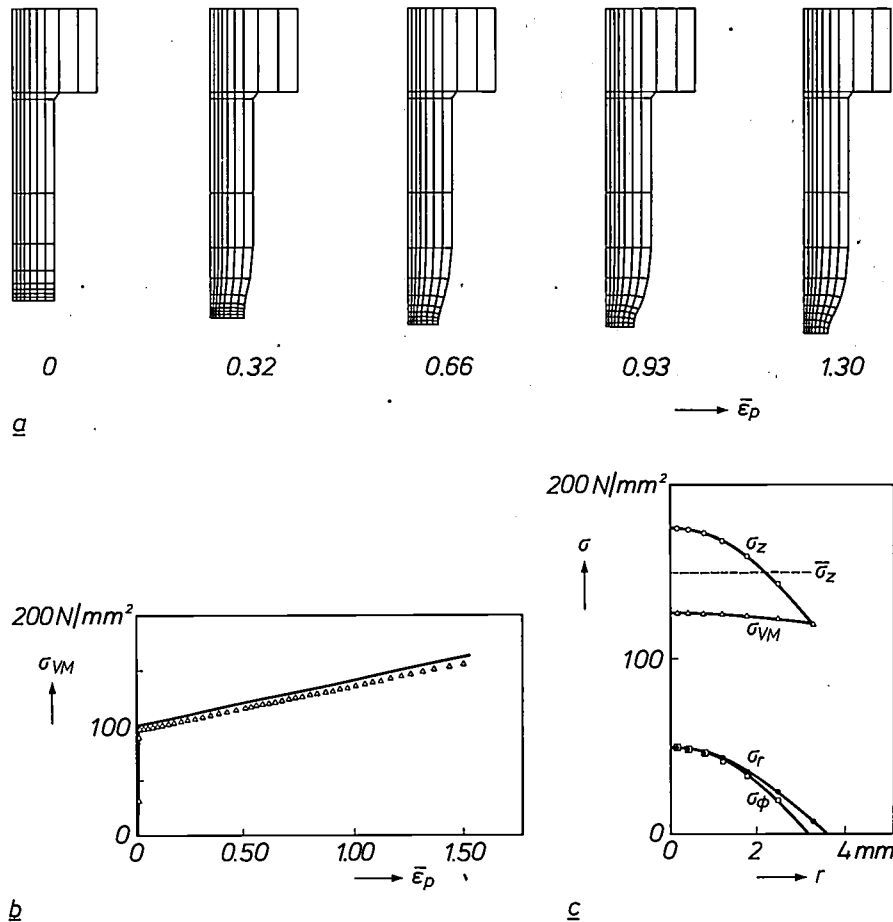


Fig. 7. Results of calculations by the finite-element method using the MARC computer program. a) The MARC networks for different values of the true plastic strain $\bar{\epsilon}_p$. b) The Von Mises stress σ_{VM} as a function of $\bar{\epsilon}_p$. The continuous line served as input for the computer program. The points indicated apply to values of σ_{VM} that have been calculated from the shape of the neck found by MARC (see a). The agreement between the line and the points confirms the correctness of the procedure employed. c) Values, calculated with the computer program, for the normal stresses σ_ϕ , σ_r and σ_z and the Von Mises stress σ_{VM} as a function of the radius r at the smallest cross-section. The mean tensile stress $\bar{\sigma}_z$ is also indicated; this is normally used for giving the result of a tensile test.

is then 450%) the stress shows a marked decrease because of the formation of a conical fracture surface spreading from the inside outwards. In this case no practical significance can therefore be attached to the points measured in the range for $\bar{\epsilon}_p > 1.5$.

Verification by the finite-element method

We have used the finite-element method [6] to verify the procedure for processing the measurement data. We did this with the aid of the well-known MARC computer program (Marc Analysis Research Corpora-

dimensional data for the workpiece under investigation and also the deformation properties of the material. In our case we used an $(\sigma_{VM}, \bar{\epsilon}_p)$ curve measured by our method as input data.

Some results of a MARC calculation performed in this way on a tensile-test specimen are given in fig. 7a. The network for a quarter of the specimen at the start of the test is shown on the far left; the other networks relate to a true plastic strain $\bar{\epsilon}_p$ increasing from left to right. The necking of the bar is clearly visible. From its shape the $(\sigma_{VM}, \bar{\epsilon}_p)$ curve is again calculated. In fig. 7b this curve is shown together with the curve that

was used as input for the program. The two diagrams are virtually identical, which shows that the method used for determining the Von Mises stress is correct.

Fig. 7c gives the stresses σ_ϕ , σ_r and σ_z calculated by the program as a function of the radius at the smallest cross-section of the test specimen in an advanced stage of necking. It also shows the Von Mises stress σ_{VM} calculated from these stresses — and not from the shape of the neck. It is clear that the Von Mises stress differs considerably from the mean stress $\bar{\sigma}_z$ perpendicular to the cross-section, which is normally used in tensile testing. It is also evident that the relation $\sigma_r = \sigma_\phi$ is a good approximation to the actual situa-

tion. The relation $\sigma_{VM} = \sigma_z - \bar{\sigma}_r$, which can be derived from equation (8) with $\sigma_{rz} = 0$ and $\sigma_r = \sigma_\phi$, is also in agreement with the practical situation.

Summary. A consequence of the Levy-Von Mises plastic-flow hypothesis is that the plastic-flow behaviour of a material is determined by the 'Von Mises stress'. In the literature correction factors have been given for calculating the Von Mises stress from the shape of the neck of a specimen during tensile testing. A mathematical model can be used to derive the same formula for the correction factor as the one that Davidenkov and Spiridonova discovered experimentally. A standard tensile-testing machine was modified to allow repeated measurements of the specimen diameter as a function of position along the axis during the tensile test. From these results a computer program calculates the second derivative of the curve describing the neck, at the smallest cross-section. This gives the correction factor for determining the Von Mises stress. The relation between this stress and the true strain is particularly important for calculating metal-working processes in which there are large plastic deformations. The correctness of the method of calculation is demonstrated by means of the program MARC, which is based on the finite-element method.

- [5] D. R. J. Owen and E. Hinton, A simple guide to finite elements, Pineridge Press, Swansea 1980;
O. C. Zienkiewicz, The finite element method, 3rd edition, McGraw-Hill, London 1977.
- [6] C. J. M. Gelten and J. E. de Jong, A method to redefine a finite element mesh and its application to metal forming and crack growth analysis, Proc. Int. FEM Congr., Baden-Baden 1981, pp. 65-85.

Distortion due to spherical aberration

For experimental purposes a fine nickel mesh was applied to the output aperture of one of the electron guns of a colour TV picture tube. By connecting one of the electrodes of this gun to a much lower voltage than usual the focal point of the electron lens is displaced from the screen of the tube towards the position of the mesh. A shadow of the mesh is then projected on to the screen.

If the focal point lies in front of the mesh, the shadow image is relatively faithful (figure *a* on the adjacent page). The situation becomes more complicated if the focal point is made to approach the mesh. This is because the electron lens that focuses the beam introduces spherical aberration, as a spherical

now appear in the other half of the image, opposite to the original shadow; fig. 1 shows the principle of this effect with the aid of a cross-section through the optical axis. *S* is the screen; the image on the screen is 'folded round' through 90° and shown next to it. At a sufficient distance from the optical axis the two new shadows do not appear; in the limiting case they coalesce to form a single shadow. This explains the occurrence of the rings that are so characteristic of the patterns shown.

It is interesting to examine the images of the small defect at the centre of the mesh (*a*) in the successive figures. In *g* the double image of the defect appears in the right-hand half of the picture (see the arrows).

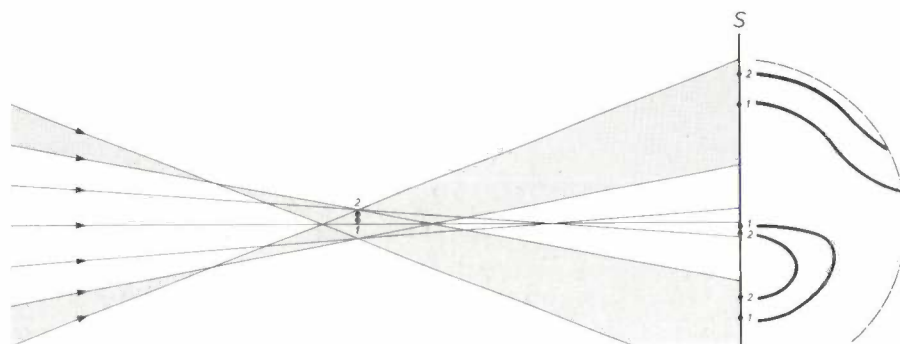


Fig. 1. Ray paths in spherical aberration. Shadow images of two wires 1, 2 in one half of the object plane. The 'normal' shadow images appear on the upper part of the screen *S*, and two rings below.

glass lens does in focusing beams of light rays. The effect arises because the peripheral rays are too strongly refracted; the focal length is not the same for all the rays, but smaller for the rays that pass through the outer zones of the lens (fig. 1).

As the point of smallest cross-section of the beam is gradually moved through the plane of the mesh in the direction of the screen, the shadow images *b-h* are formed successively.

The rays that are focused behind the mesh produce an inverted image of the mesh on the screen. This happens first with the central rays, which only illuminate the wires at the centre of the mesh.

Figure *d* on the following page marks the transition; in *e* the central square of the mesh is shown inverted.

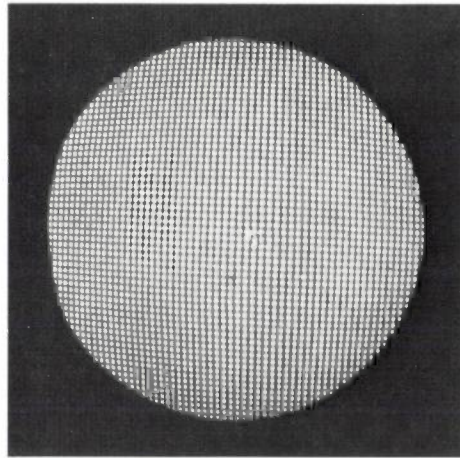
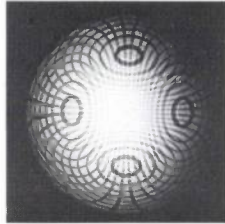
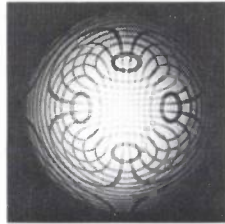
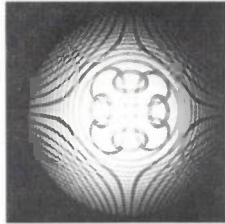
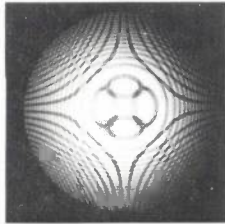
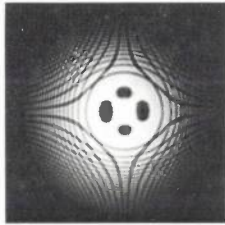
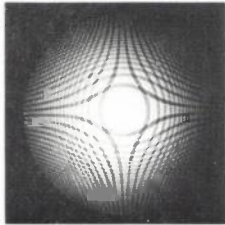
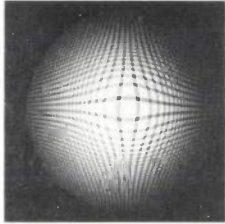
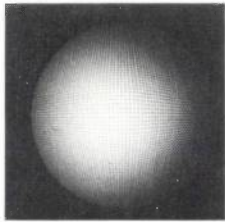
The inversion of the central part of the image is associated with the appearance of three shadows of the central wires rather than one. Two new shadows

As a verification a corresponding optical arrangement was set up with a laser and a simple convex lens. The shadow images obtained are shown on the next page, at a reduced scale. They are symmetrical, unlike the electron-optical images, where the asymmetrical location of the electron gun has caused an asymmetrical limiting of the image.

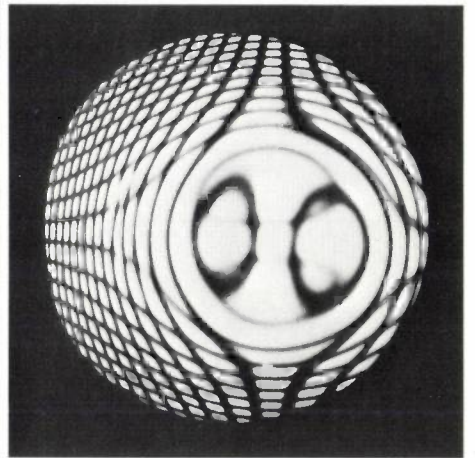
The shadow images shown are not just 'pretty pictures'; they also form a useful aid in the study of spherical aberration in electron optics.

L. C. M. Beirens
A. A. van Gorkum

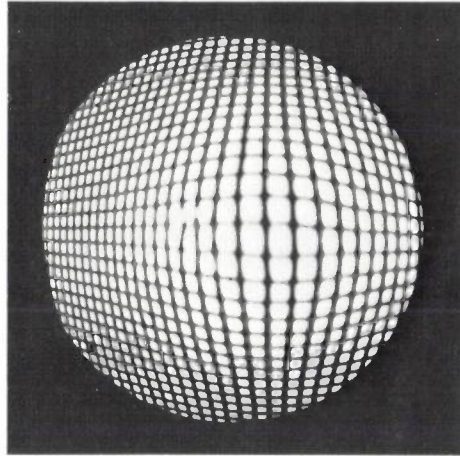
Ing. L. C. M. Beirens, with the Philips Elcoma Division, Eindhoven, was formerly with Philips Research Laboratories, Eindhoven; Dr Ir A. A. van Gorkum is with Philips Research Laboratories.



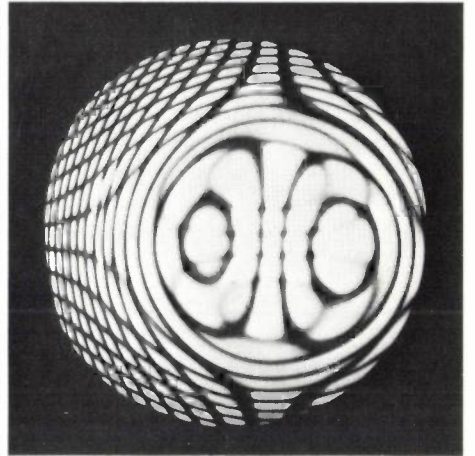
a



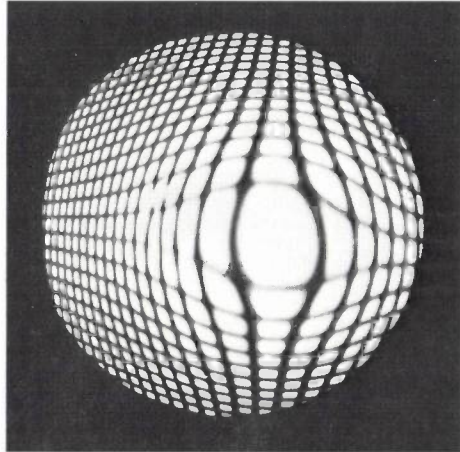
e



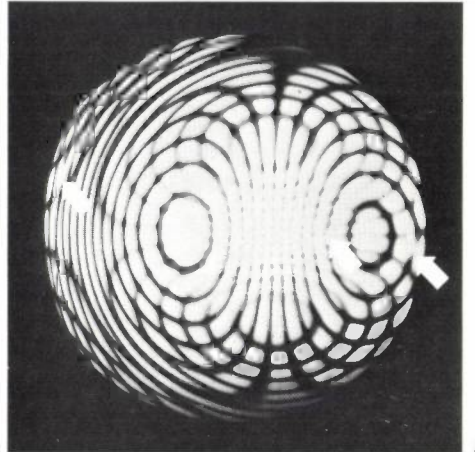
b



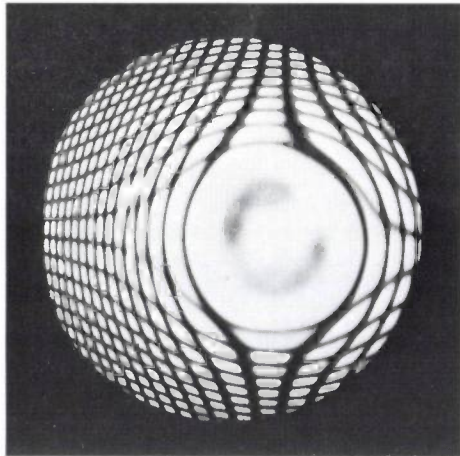
f



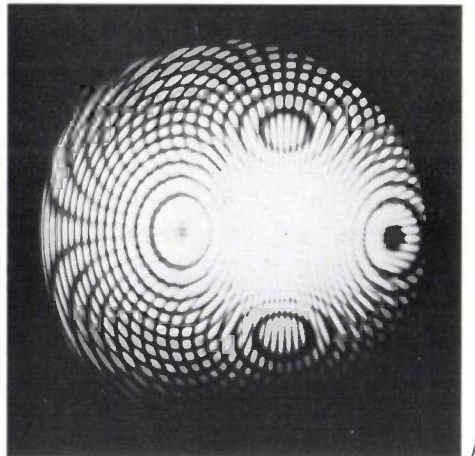
c



g



d



h

Electrochemical micromachining

C. van Osenbruggen and C. de Regt

The anodic dissolution of metals was already known in the previous century, but it was not until the nineteen-sixties that it came into use as a practical machining method. The motivation for the development of electrochemical machining (ECM) was mainly the growing use of extremely hard alloys, which cannot be machined satisfactorily by conventional methods because removal rates are too low and tool wear is excessive. In recent years studies at the Philips Centre for Manufacturing Technology ('CFT') have shown that the ECM method can also be used for high-precision machining. This has considerably widened its field of applications.

Introduction

In electrochemical machining (ECM) the workpiece and the tool are held close together; an electrolyte flows through the machining gap between them^[1]. The workpiece acts as the anode and the tool as the cathode. When an electric current is passed through the electrolyte the metal of the anode dissolves locally, so that the shape of the workpiece becomes complementary to the shape of the tool. To remove the heat generated and the dissolved material the electrolyte is rapidly pumped through the machining gap.

In the ECM method the mechanical properties of the workpiece material play no part. As compared with other machining methods with no direct contact between tool and workpiece, such as spark machining (electro-discharge machining, EDM) as described earlier in this journal^[2], ECM has the advantage that metal can be removed very rapidly, irrespective of the dimensions of the surface to be machined. A further advantage is the absence of tool wear. No burrs are formed during machining and complicated shapes can be produced. Since the workpiece is not subjected to large mechanical loads, there is no introduction of undesirable deformations or internal stresses.

The method does have some limitations, however. The equipment required for ECM is rather complicated. Since the method is still in continuous develop-

ment, the choice of tool shape, current density, electrolyte flow rate and gap width often has to be made empirically. In disposal of the dissolved material precautions have to be taken to prevent environmental pollution. In the aero-engine industry, however, and to a somewhat lesser extent in the automobile industry, the specific advantages of ECM are often more important than the limitations, and this method is therefore widely used for making complex components of hard metal alloys and for deburring conventionally produced parts. In other applications ECM has gained much less acceptance.

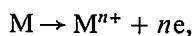
During the last few years the Philips Centre for Manufacturing Technology ('CFT') have developed the method for high-precision (micro)machining. Possible applications within Philips have also been studied in cooperation with other groups. Such applications could include the machining of very small workpiece surfaces (down to about 0.2 mm²), and also the generation of various kinds of profiles in components produced in quantity. This work has resulted in satisfactory control of ECM process parameters to meet the requirements of a micromachining method.

In this article we shall first give a general description of the ECM method. The equipment and operating procedure will then be described, and some problems and proposed solutions will also be discussed. Finally, we shall take a brief look at some of the possible applications.

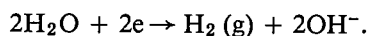
C. van Osenbruggen was formerly with Philips Research Laboratories and the Philips Centre for Manufacturing Technology (CFT), Eindhoven; Ir C. de Regt is with CFT, Eindhoven.

The ECM method

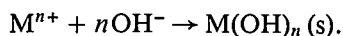
The principle of the ECM method for making a cavity of rectangular cross-section is illustrated diagrammatically in *fig. 1*. An electrolyte is pumped at high pressure through the gap between the tool and the workpiece. A voltage is applied between the workpiece (anode) and the tool (cathode), causing an electric current to flow. This causes a local dissolution of the metal M of the anode by the reaction:



where n^+ is the charge of the metal ion produced. At the cathode there is an electrolytic reduction of water, resulting in the formation of hydrogen gas and hydroxyl ions:



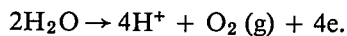
Depending on the metal to be machined and the pH of the solution, metal and hydroxyl ions may combine to form an insoluble hydroxide:



The precipitated hydroxide is removed together with the hydrogen gas by the forced flow of the electrolyte. The flow also removes the heat generated in the gap.

In electrochemical terms the process conditions for ECM are rather extreme. At an operating voltage of 2 to 40 V the current densities in the narrow gap (20 to 200 μm) are very high, ranging from 10 to 1000 A/cm^2 , and the flow rate of the electrolyte is also very high (10 to 50 m/s). Depending on the process conditions, the metal-removal rate generally lies between 0.5 and 10 mm/min .

The current efficiency — the ratio of the amount of dissolved metal to the amount that should be dissolved according to Faraday's Law, for the known current and time — is often lower than 100%. This is because, apart from the dissolution of the metal, other anode reactions can occur such as the oxidation of water, with the release of oxygen gas:



The extent to which this reaction lowers the current efficiency depends greatly on the material of the workpiece, the electrolyte and the current density. With some electrolytes, such as a solution of sodium nitrate (NaNO_3), a passivating oxide or hydroxide film is formed on a steel workpiece. The result is that at low current densities only a fraction of the current is used for dissolving the metal. At high current densities the efficiency is much higher; see *fig. 2*. A passivating film has a beneficial effect on the dimensional accuracy of the workpiece: at places where the metal should not be affected but nevertheless there is a small current

density, no material will dissolve, whereas at places where the current density is high the passivation will have relatively much less effect on the dissolution rate.

Besides the oxidation of water, further oxidation of metal ions can occur at the anode [4]. During the machining of chrome-steel workpieces, for example,

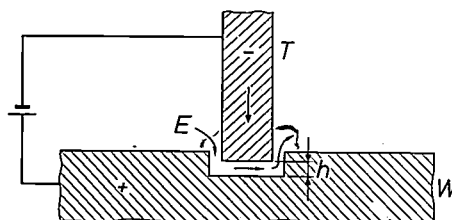


Fig. 1. Diagram illustrating the ECM method for producing a cavity of rectangular cross-section. A tool T , the cathode, is positioned a short distance away from the workpiece W , the anode. An electrolyte E is pumped at high pressure through the space between them (the gap, width h). During the ECM process the workpiece dissolves locally, while the tool is fed towards the workpiece.

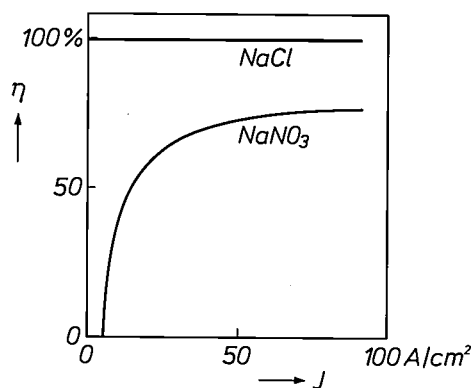


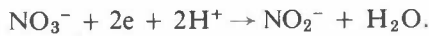
Fig. 2. Current efficiency η as a function of the current density J in the electrochemical machining of a particular type of steel in a solution of NaCl or NaNO_3 [3]. With NaCl the efficiency is independent of the current density and is practically 100%. With NaNO_3 the efficiency is lower; at low current densities there is hardly any metal dissolution.

- [1] Some books on the ECM method are:
A. E. DeBarr and D. A. Oliver, *Electrochemical machining*, Elsevier, New York 1968;
J. F. Wilson, *Practice and theory of electrochemical machining*, Wiley, New York 1971;
J. A. McGeough, *Principles of electrochemical machining*, Chapman & Hall, London 1974.
J. P. Hoare and M. A. Laboda, *Electrochemical machining*, in: J. O'M. Bockris, B. E. Conway, E. Yeager and R. E. White (eds), *Comprehensive treatise of electrochemistry*, Vol. 2, Plenum, New York 1981, chapter 8.
- [2] C. van Osenbruggen, *High-precision spark machining*, Philips Tech. Rev. 30, 195-208, 1969.
J. L. C. Wijers, *Three special applications of the Philips high-speed spark-machining equipment*, Philips Tech. Rev. 40, 199-203, 1982.
- [3] The curves in *fig. 2* are from D. Pahl, *Über die Abbildungsgenauigkeit beim elektrochemischen Senken*, Thesis, Aachen 1969.
- [4] H. Simon, *Werkstatt & Betr.* 112, 19-23, 1979.

the Cr^{3+} ions generated oxidize to form chromate ions (CrO_4^{2-}):



At the cathode a reduction of anions can take place, for example from nitrate to nitrite ions:



The current density J in the solution is determined by the potential difference V_r across the electrolyte, the electrical conductivity κ of the electrolyte and the gap width h :

$$J = \frac{V_r \kappa}{h}. \quad (1)$$

To obtain the required high current density at given values of κ and h , an operating voltage substantially higher than V_r is required. This is due to the activation overvoltage for the transfer of charge at the electrodes, the overvoltage across the passivating film and the concentration overvoltage, required for the transfer of ions; see *fig. 3*. The activation overvoltage at an electrode depends on the current density and the electrochemical potential of the metal with respect to the electrolyte [5]. The concentration overvoltage, the additional voltage that enables the ions to penetrate through the concentration zones near the electrodes, is determined by the movement of the ions in the electric field, the convection in the forced fluid flow and the diffusion under the influence of concentration gradients. The application of a turbulent fluid flow can keep the concentration overvoltage low. The total overvoltage in the ECM process is generally between 2 and 5 V.

The electrolyte in the gap must be a good electrical conductor and should produce a slight passivation of the workpiece surface. A good choice is an NaNO_3 solution (about 4 mol/l) with a conductivity of about 15 S/m. The *pH* of the electrolyte is important too, since it also determines the dissolution behaviour of the metal. The relation between the electrochemical potential E , the *pH* and the solubility of the metal in thermodynamic equilibrium is often presented in a graph called a Pourbaix diagram [6]. This indicates combinations of E and *pH* at which the metal dissolves, is immune (does not dissolve) or is covered with a passivating film. *Fig. 4* shows some diagrams for metals of widely differing dissolution behaviour. Although there is certainly no question of thermodynamic equilibrium in ECM, such diagrams can nevertheless be useful for predicting the behaviour of a particular metal.

When a stationary tool is used, the gap during machining will gradually increase as a result of the

anodic dissolution. The current density will then steadily decrease, so that the profile produced becomes irregular and the machining finally stops. To avoid a decrease in current density the gap must be kept constant. This implies that the tool has to move

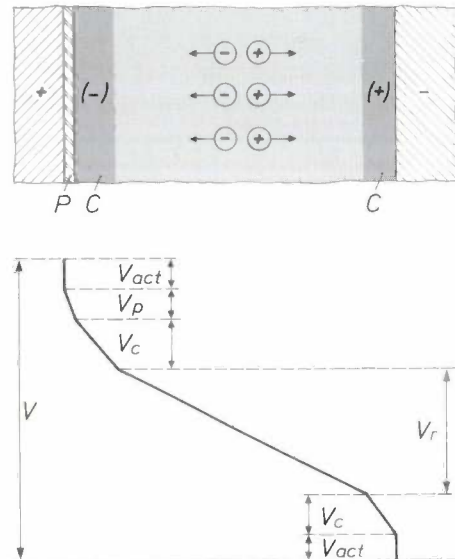


Fig. 3. Voltage profile between the electrodes during the ECM process. It is assumed that a passivating film *P* has settled on the anode. Owing to the migration of ions in the electrolyte a concentration region *C* forms in the neighbourhood of the anode and cathode with an excess of negative and positive ions, respectively. The potential difference V_r across the electrolyte is equal to the operating voltage V less the overvoltages at the two electrodes, i.e. the activation overvoltage V_{act} , the passivation overvoltage V_p and the concentration overvoltage V_c .

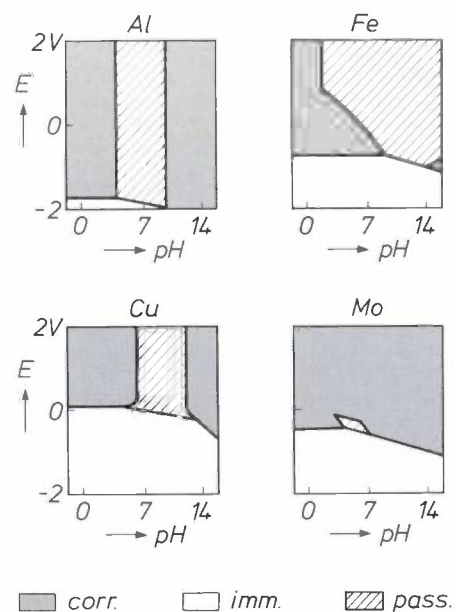


Fig. 4. Pourbaix diagrams for aluminium, iron, copper and molybdenum [6]. These equilibrium diagrams indicate the combinations of electrochemical potential E and *pH* at which the metals dissolve (*corr.*), are immune (*imm.*) or are covered with a passivating film (*pass.*).

towards the workpiece during the machining at a rate equal to the dissolution rate. From Faraday's law the dissolution rate v_d is given by the expression

$$v_d = J\eta V_{sp}, \quad (2)$$

where η is the current efficiency and V_{sp} is the specific soluble volume $A/(nF\rho)$, where A is the atomic weight, F Faraday's constant (9.65×10^4 C/mol) and ρ the density of the anode metal. Substituting eq. (1) in eq. (2) gives:

$$v_d = \frac{V_f \kappa \eta V_{sp}}{h}. \quad (3)$$

In the situation shown in fig. 1 the feed rate v_f of the tool during uniform machining is equal to v_d . The gap width h is then equal to

$$h = \frac{V_f \kappa \eta V_{sp}}{v_f}. \quad (4)$$

As v_f increases, the ECM process will operate with a smaller gap; this improves the machining accuracy. The gap must of course be large enough for effective electrolyte flow.

An important condition for successful machining is the availability of a suitable tool. In general this should consist of a chemically inert material that is a good electrical conductor and can be given the re-

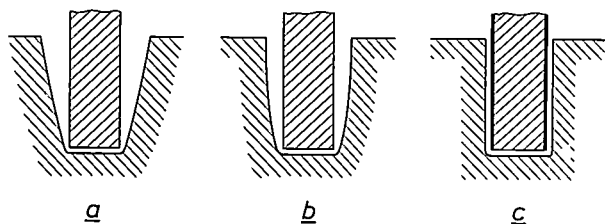


Fig. 5. Diagram showing the effect of passivation and insulation on the accuracy of form of the ECM process in producing a cavity of rectangular cross-section. With a non-passivating electrolyte and an uninsulated tool the workpiece is excessively dissolved opposite the sides of the tool, so that a rectangular profile is not obtained (a). When a passivating film has formed on the workpiece, the deviation is significantly smaller (b). An even better result is obtained if in addition the sides of the tool are coated with an insulating film (c).

quired shape by other machining methods. The parts of the tool that should not pass current but are in contact with the electrolyte are very important. In fig. 1 these are the sides of the tool. It has been found that when a passivating electrolyte is used good dimensional accuracy can be achieved if in addition thin insulating layers are applied at these places; see fig. 5. These layers must be good electrical insulators and must not pass the electrolyte or the ions dissolved in it. They must be uniform, adhere well to the tool and be chemically resistant. They must also be capable of

withstanding the strong fluid flow and the forces that arise if the tool touches the workpiece. The material of the layers must also be readily machinable, of course.

Equipment and working procedure

Fig. 6 shows a diagrammatic representation of an ECM equipment as used in our investigations. The workpiece and the tool are connected as anode and cathode to a d.c. generator. A stepping motor or a linear hydraulic motor is used to feed the tool towards the workpiece at a rate corresponding to a constant gap; see eq. (4). If the feed rate is too high, the tool will come into contact with the workpiece and cause a short-circuit. Foreign metal particles in the electrolyte may also cause short-circuiting due to spark discharges. Since short-circuiting can seriously damage both the tool and the workpiece, a safety system is built into the ECM machine; this switches off the voltage within 5 μ s if a short-circuit is detected.

Electrolyte and pH of the solution are chosen so as to ensure good dissolution of the workpiece material during the ECM process without the tool being attacked. It is usual to work with a neutral NaNO_3 solution ($\text{pH} \approx 7$). The fluid is pumped from a storage tank via a pressure controller (0.2 to 2 MPa) and a filter to the machining gap, e.g. through a duct in the tool. After passing through the gap the fluid goes to a settling tank, where the sludge is removed. The concentration of dissolved impurities can be reduced by the addition of chemicals, e.g. in a parallel system. This is necessary for example during the machining of chrome-steel workpieces, because the chromate ions produced (CrO_4^{2-}) have an adverse effect on the ECM process and are also toxic. The addition of sodium bisulphite (NaHSO_3), for example, reduces CrO_4^{2-} to Cr^{3+} , which can be removed as insoluble $\text{Cr}(\text{OH})_3$ together with $\text{Fe}(\text{OH})_3$. Up to a concentration of about 1 mol/l the addition of NaHSO_3 does not affect the ECM process adversely.

Fig. 7 shows a photograph of an ECM equipment designed at CFT. It contains an elaborate system for circulation and purification of the electrolyte. The combination of tool and workpiece constitutes only a small part of the total system. The equipment also includes extensive measuring and control instrumentation for setting the machining voltage, controlling the tool feed, short-circuit protection and fluid-flow control.

[6] See K. J. Vetter, *Electrochemical kinetics, theoretical and experimental aspects*, Academic Press, New York 1967.

[6] M. Pourbaix, *Atlas of electrochemical equilibria in aqueous solutions*, 2nd edition, Natl. Assoc. Corrosion Eng., Houston 1974.

Tool

The tool must be matched to the required shape of the workpiece. It is necessary to ensure good electrolyte flow through the gap and firm fixture of the tool. Depending on the material and the profile to be produced, conventional machining methods can be used

because H^+ ions can penetrate them. A type of insulation that does meet the requirements consists of two layers of the semiconductor silicon carbide (SiC), one p-type and the other n-type [7]. A good method for applying SiC layers is chemical vapour deposition (CVD) [8]. In this method a gaseous compound,

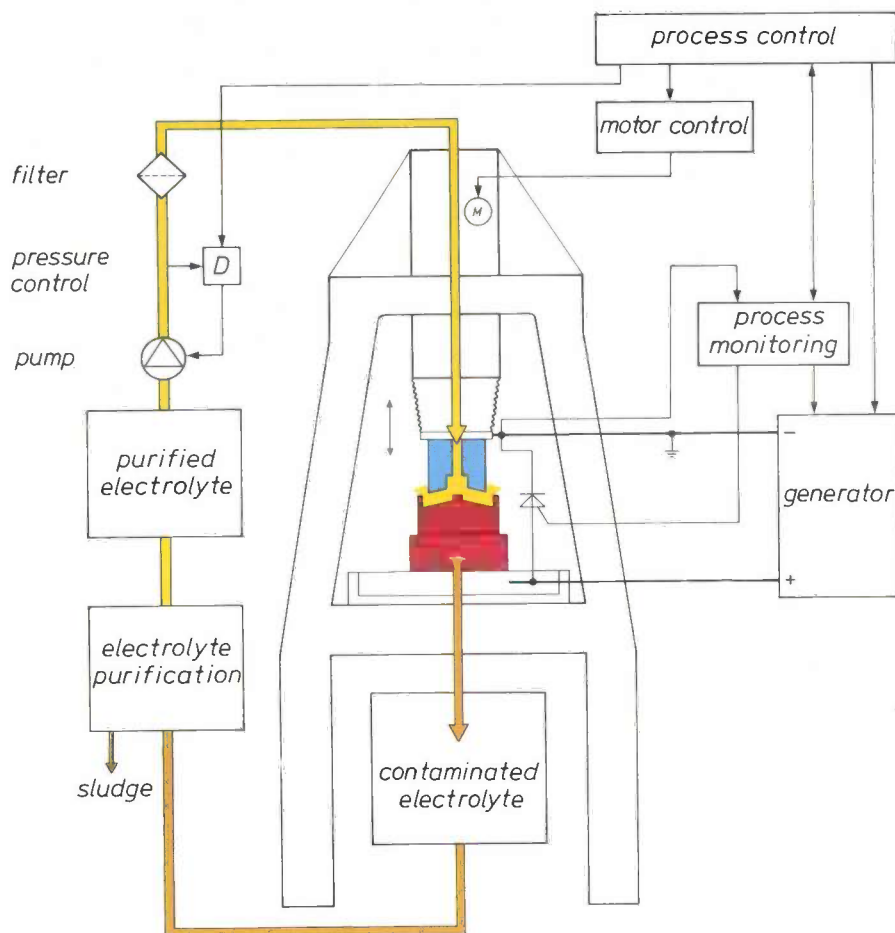
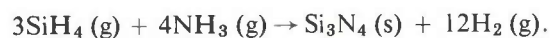


Fig. 6. Diagram of an ECM equipment used at the Philips Centre for Manufacturing Technology. A tool (blue), the cathode, is fed towards the workpiece (red) by a stepping motor or linear hydraulic motor. The tool is positioned by means of a measurement and control system. The system ensures that the correct machining voltage is supplied by the generator, and provides short-circuit protection. The equipment also includes an elaborate system for circulation and purification of the electrolyte (yellow - brown - yellow).

for ECM tools, such as turning, milling and grinding, but special methods like laser cutting and EDM can also be applied [2]. The choice of tool material is determined by the electrochemical and mechanical properties required. Suitable metals for the tools include copper, steel, molybdenum and tungsten. For some types of work the tools have to be locally insulated, for example when deep holes or grooves with flat walls are to be formed at high current densities.

With micro-ECM in mind, we have made a special study of materials and coating techniques for the insulating layers on the tools. It was found that some coatings (e.g. epoxy resins) are not suitable, mainly

e.g. $(CH_3)_2SiCl_2$, decomposes at high temperature ($\geq 1000^\circ C$) at the substrate surface to form a thin compact film of polycrystalline SiC. Another suitable insulation consists of two undoped SiC layers with a highly insulating amorphous layer of silicon nitride (Si_3N_4) sandwiched between them [9]. This intermediate layer can also be applied by CVD, e.g. via the reaction



With the combinations p-SiC/n-SiC and SiC/ Si_3N_4 /SiC the total insulation can be very thin ($< 15 \mu m$), so that the electrolyte flow is not impeded and good

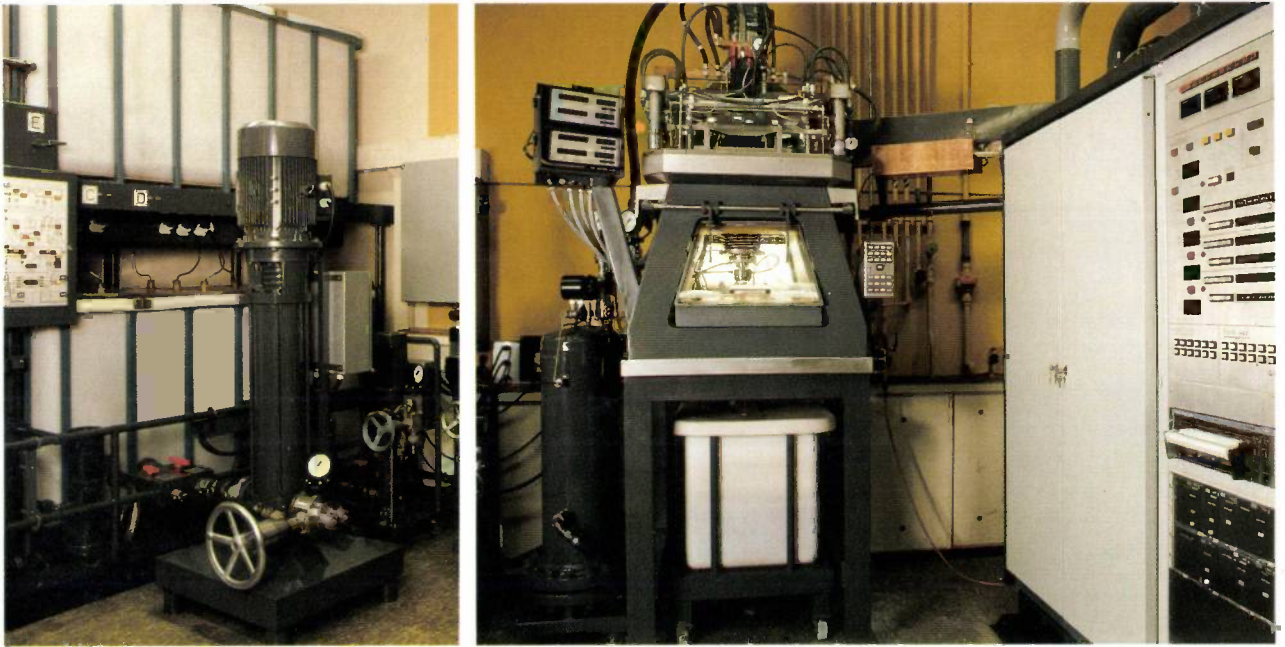


Fig. 7. Experimental ECM equipment. The actual machining takes place in the centre section. The largest part of the equipment is taken up by the electrolyte-circulation system (*left-hand photograph*) and the measurement and control system (*right*).

dimensional accuracy can be achieved. Other advantages are uniform thickness (even with complex profiles), no tool wear and high resistance to chemical corrosion. The use of these types of insulation is limited, however, to metals with a coefficient of expansion fairly close to that of SiC and which an SiC layer will adhere to properly. The tool metal must also be able to withstand the high temperatures of the CVD process. It follows therefore that only metals like molybdenum and tungsten can be insulated in this way. Deposition on these metals has been extensively

investigated^[10]. It is found that SiC adheres particularly well to molybdenum, probably because of the formation of molybdenum carbides and silicides at the interface. Fig. 8 shows an SEM (scanning electron microscope) micrograph of a molybdenum strip on which insulating layers of SiC, Si₃N₄ and SiC have been deposited. The SiC layers are about 6.5 μm thick, while the intermediate Si₃N₄ layer is much thinner, 0.4 μm. The reaction zone between molybdenum and SiC is clearly visible.

Because SiC is brittle there is a danger that the insulation will crumble away during finishing operations on the tool. Experiments with different machining methods have been performed. It was found that no undesirable crumbling occurs during careful grinding of tools insulated with layers of SiC and Si₃N₄.

Correct tool design for ECM is fairly simple when prismatic profiles have to be generated. For die-sinking operations, however, other tool geometries are

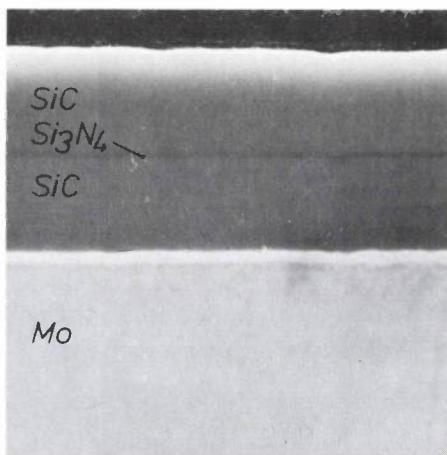


Fig. 8. SEM micrograph of a molybdenum strip coated with two 6.5-μm SiC layers and a 0.4-μm Si₃N₄ intermediate layer. A reaction zone can be seen between the molybdenum and the lower SiC layer.

[7] S. H. Hagen, C. van Osenbruggen, H. A. J. Reemers and G. Verspui, U.S. Patent No. 3972 797 (filed August 1971).

[8] The CVD process has been dealt with in some detail in this journal:

For the application of wear-resistant TiC and TiN coatings on tool steel, see P. J. M. van der Straten and G. Verspui, Philips Tech. Rev. 40, 204-210, 1982;

for the application of silicon films in IC technology, see J. Bloem and W. A. P. Claassen, Philips Tech. Rev. 41, 60-69, 1983/84;

for the manufacture of SiC masks for X-ray lithography, see H. Lühje, Philips Tech. Rev. 41, 150-163, 1983/84.

[9] G. Verspui, Proc. Electrochem. Soc. 79-3, 463-475, 1979.

[10] Research on CVD for application in ECM was started mainly by S. H. Hagen, W. F. Knippenberg and G. Verspui, and was taken up at a later stage by the CVD project group of CFT.

necessary, with faces that are not perpendicular to the direction of tool movement. In such cases local insulation of the tool is difficult and some other way of achieving the required accuracy of form has to be found.

The use of a pulsed voltage

The high current density ($\geq 100 \text{ A/cm}^2$) required for proper operation of the ECM process may give very high concentrations of reaction products, which can only be partly removed by the electrolyte, especially if the gap is narrow. The increasing contamination can cause a deposit to form on the tool, so that the workpiece material no longer dissolves uniformly. Furthermore, changes in the electrolyte composition and the temperature rise and hence in the electrical resistivity can also make the accuracy worse. These problems can be largely avoided by applying a pulsed voltage instead of a continuous one^[11]. When the pulse duration and the intervals between the pulses are properly matched to the current density, the gap can be almost completely swept clean during the current intervals, giving a regular ECM process.

An important difference as compared with the use of continuous voltage is that the current efficiency is much more dependent on the current density. As an example *fig. 9* shows the efficiency for the machining of steel plotted against the current density for continuous voltage and for a pulsed voltage with a pulse duration of 1 ms and an interval of 10 ms. With the continuous voltage the efficiency decreases gradually when the current density is reduced, whereas with the pulsed voltage the decrease is much more rapid.

As noted earlier, a steep fall in efficiency with decreasing current density improves the accuracy of form of the workpiece. This improvement depends on the pulse duration and to a somewhat lesser extent on

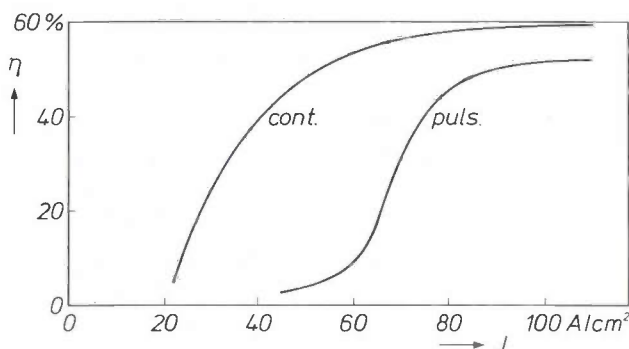


Fig. 9. Current efficiency η of an ECM process as a function of the current density J for continuous voltage and for a pulsed voltage, using pulses of 1 ms duration with an interval of 10 ms between them, under otherwise identical conditions. If the current density is decreased from 100 A/cm^2 a much steeper decrease in efficiency occurs with a pulsed voltage than with a continuous voltage.

the interval. The improved accuracy of form can clearly be seen when cavities are made with a tool of rectangular cross-section. *Fig. 10* shows micrographs of such cavities. Because of the increased side gap the cavity obtained with continuous voltage has walls that slope at an angle of about 17° . The walls generated with pulsed voltage are almost vertical, the deviation

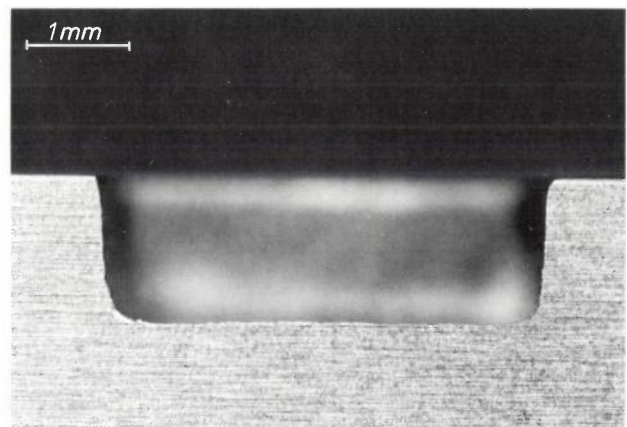
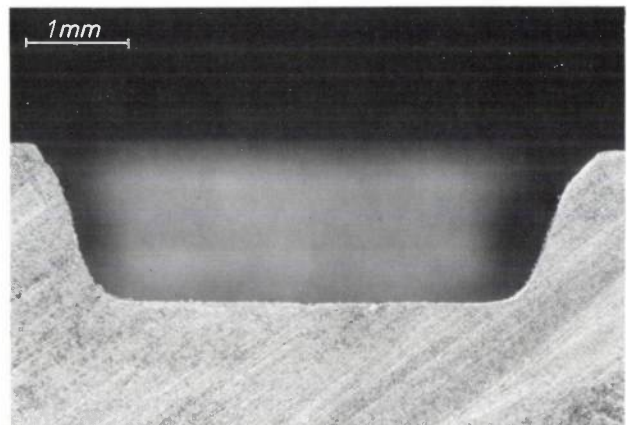


Fig. 10. Micrographs of cavities formed by ECM in a steel workpiece. The tool has a rectangular cross-section. The cavity produced with continuous voltage (*above*) has walls that slope at an angle of about 17° . The deviation from vertical in the cavity made with a pulsed voltage (*below*) is only about 3° .

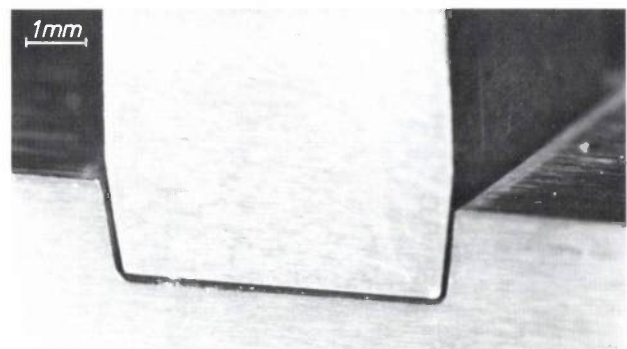


Fig. 11. Micrograph of a steel workpiece in which a cavity has been formed by ECM with a pulsed voltage, and the tool used. Because a pulsed voltage was used, the sloping side walls of the tool are copied accurately in the workpiece.

from the vertical being only about 3° . Another illustration of the accuracy of form attainable is given by the micrograph in *fig. 11*. It can be seen that the sloping side walls of the tool are copied exactly in the workpiece.

The use of a pulsed voltage also improves the surface finish. As a result of the fluid flow there are grooves with a maximum depth of about $1\ \mu\text{m}$ in the surface of a cavity produced with continuous voltage. These probably arise from disturbances of the diffusion boundary layer at the metal surface caused by turbulence in the fluid. When a pulsed voltage is used no such grooves are observed. During the intervals between the voltage pulses the composition of the boundary layer is repeatedly renewed, so that turbulence has far less effect.

Potential applications

The ECM method has many potential applications, especially for the quantity production of precision components for electronic and electromechanical equipment. In recent years CFT have investigated a number of possible applications. The widely different operations studied have ranged from the making of holes with a diameter of $50\ \mu\text{m}$ to the generation of profiles in a surface of area $0.15\ \text{m}^2$. The operations were performed on a wide range of materials, including aluminium, copper, molybdenum, tungsten, steel, 'hard metal' and conducting ceramics. In many cases, at least for small production runs, the machining requirements could be met. Some of the results will be discussed here in more detail.

Profiling with an insulated tool

Fig. 12 shows a cross-section of a tooth profile produced by ECM in a 1.5-mm steel strip. The tool used has the complementary shape to the required profile and is completely insulated except for the ground front face. The insulation is about $15\ \mu\text{m}$ thick and consists of two SiC layers and an intermediate layer of Si_3N_4 .

The operation begins with the tool $50\ \mu\text{m}$ above the surface of the strip. The tool is fed towards the workpiece at a rate of $2.5\ \text{mm}/\text{min}$, with the gap width kept at $50\ \mu\text{m}$. As soon as the tool reaches a preset depth (e.g. $0.72\ \text{mm}$) the operation is stopped. The tooth height is then $0.77\ \text{mm}$. Because of the low gap width during the operation the tooth profile can be generated accurately: the variation in tooth width is less than $20\ \mu\text{m}$.

Since the operation is performed at a high current density ($180\ \text{A}/\text{cm}^2$) and a narrow gap, a relatively high fluid pressure (about $0.8\ \text{MPa}$) is necessary for

pumping sufficient electrolyte through the gap. The direction of fluid flow corresponds to the longitudinal direction of the teeth. Because of the high pressure of the fluid good sealing is required.

Production of calibrated holes

In special cases the ECM method can be used for the accurate production of holes. An example is the making of a diaphragm for an electron-optical system. Metal is removed from the top of a hollow cone, producing a truncated cone whose flat top is the diaphragm. *Fig. 13* shows a diaphragm produced by ECM. The aperture has a diameter of $50 \pm 1\ \mu\text{m}$, well within the required tolerance.

The production of such a diaphragm requires careful control of the hole diameter. The operation is performed with a stationary flat tool about $0.1\ \text{mm}$ above the top of the cone. From the other side a pin of diameter $48\ \mu\text{m}$ is placed against the inside of the top of the cone. This pin, made of an insoluble material (e.g. platinum-rhodium or tantalum) is connected to the generator by a microswitch. During the ECM process the top dissolves first, and then the opening becomes steadily larger. As soon as the required diameter has been reached, the pin gauge starts to move through the hole and the voltage is switched off. Any burrs formed as a result of the movement of the pin can be removed by applying extra pulses. The truncated cone shown in *fig. 13* has a rounded top. The top can be made flat to within $10\ \mu\text{m}$ by fitting a platinum guard ring over the cone.

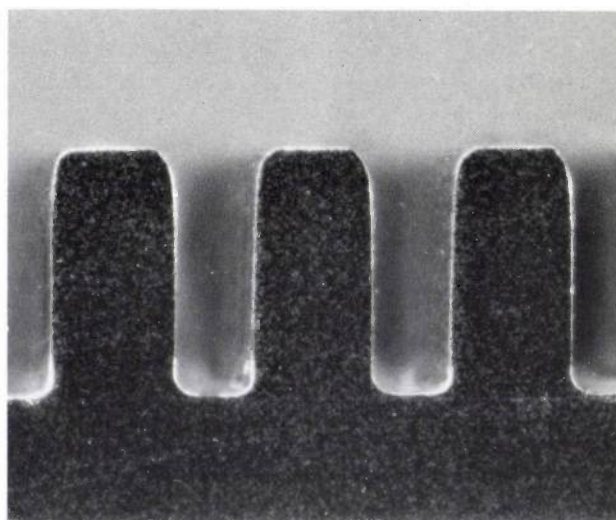


Fig. 12. Micrograph of a cross-section of a tooth profile formed by ECM. The teeth have a width of $0.37\ \text{mm}$ and a height of $0.77\ \text{mm}$.

^[11] See M. Datta and D. Landholt, *Electrochim. Acta* 27, 385-390, 1982.

Deburring

The ECM method is widely used for removing burrs left by previous operations. For Philips the method is mainly of interest for parts that are cut or pressed from thin sheet metal. ECM is a useful method for deburring such products, since it can meet the increasing requirements for accuracy of dimensions and form.

The geometry and dimensions of a burr may vary considerably. Usually, however, it is possible to set up the workpiece and tool in such a way that the current density at the burr is an order of magnitude higher than for the rest of the workpiece. This means that the workpiece itself is hardly affected during the deburring process. The exact dimensions of the burrs are not very important: only the maximum dimensions have to be known, so that the deburring operation can be adjusted to suit. If necessary the current required can be limited by using a tool adapted to the contours of the workpiece.

Electrochemical deburring is very rapid, with virtually no damage to the workpiece. This was found, for example, from the removal of a burr that protruded about 25 μm above a punched hole of 0.4 mm diameter. When the process was correctly set up, the burr was completely removed in about 0.5 s with a flat tool about 0.1 mm above the workpiece. No more than 2 μm of the sheet material was removed and the

diameter of the hole was not made any larger. Because of the short duration of the process the method can easily be integrated in a production line for metal components.

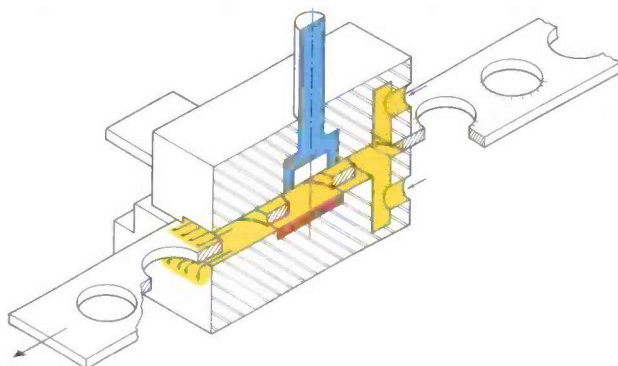


Fig. 14. Diagram of tool and workpiece for deburring by ECM. The workpiece is situated *between* the cathode (*blue*) and the anode (*red*), so that the electrolyte (*yellow*) flows on both sides.

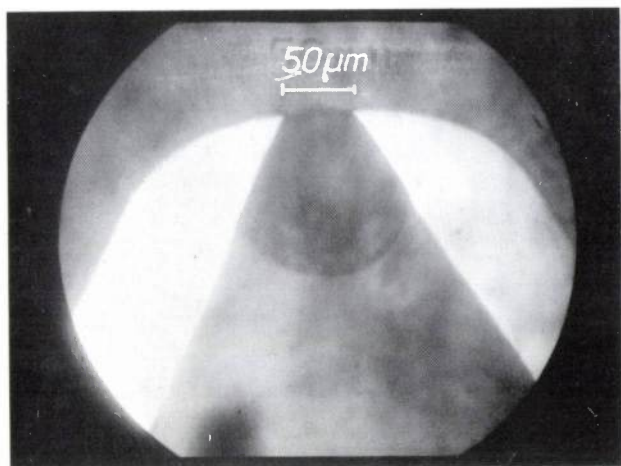
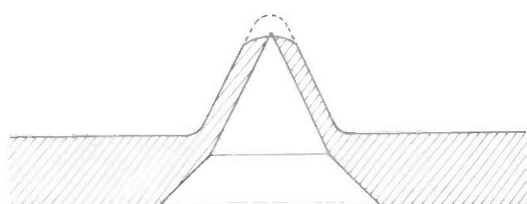


Fig. 13. Micrograph of a cross-section of a truncated cone with diaphragm for an electron-optical system. The calibrated diaphragm aperture, with a diameter of 50 μm , was produced by ECM after dissolving away the top of a hollow cone (*above*).

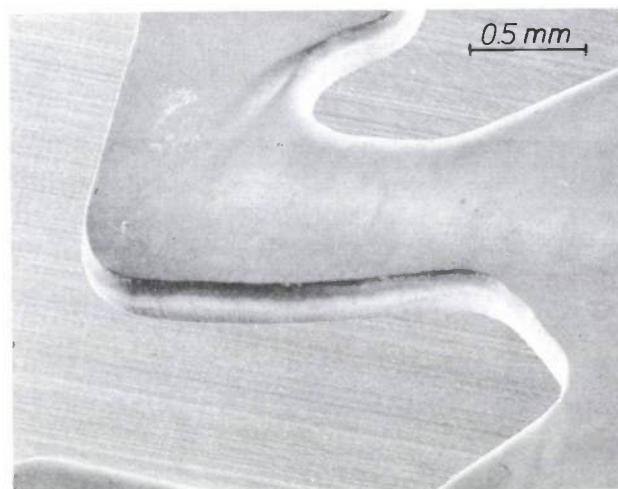
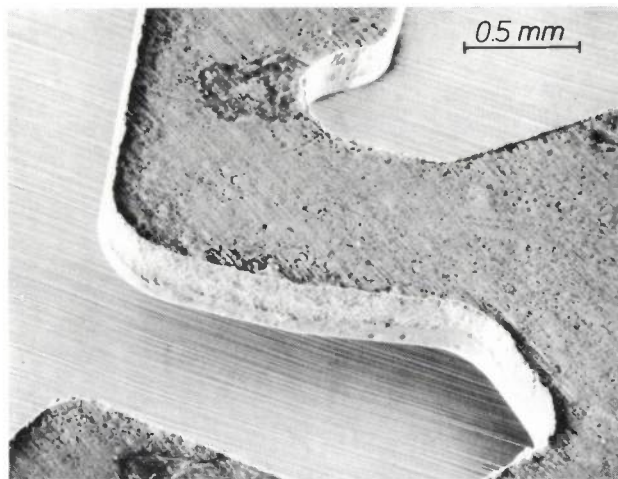


Fig. 15. SEM micrographs of a component before and after deburring by ECM.

Depending on the thickness of the material and the current density required, there are various ways of supplying the electric current. With thick material the current can be supplied directly to the workpiece by means of pressure contacts or sliding contacts. With thin material the current can be conducted through a conductor beneath it, e.g. of platinum. This is only possible, however, for low current densities, since otherwise the conductor may 'burn' at the contact points. If a higher current density is required for deburring, a system can be used in which the workpiece 'floats' with respect to the electrodes, and the current is supplied through the electrolyte. Fig. 14 gives a diagram of a system of this type that was used in our investigation for deburring punched components. With this system the current supply can be made sufficiently uniform for there to be no local overheating of the workpiece. Fig. 15 shows a component before and after deburring by this method. The deburred component is smoothly rounded at the edges.

Edge profiling

The edges of a workpiece can be profiled by setting the tool at a particular angle to the workpiece. As an example we shall consider the generation of a razor-sharp edge with a stationary tool at a particular angle α . As can be seen in fig. 16 the thickness $d(x)$ of the material is determined by the initial thickness d_0 , the

initial gap width h_0 at the edge ($x = 0$), the angle α and the gap width $h(x)$:

$$d(x) = d_0 + h_0 + x \tan \alpha - h(x). \quad (5)$$

For the derivation of $h(x)$ we write eq. (3) as a differential equation:

$$\frac{\partial h(x)}{\partial t} = \frac{V_t \times \eta V_{sp}}{h(x)}, \quad (6)$$

where it is assumed that the dissolution of material takes place only in the vertical direction and that the current efficiency is constant. With the boundary condition that the operation is stopped as soon as the material has dissolved completely at $x = 0$, we can derive an expression for $h(x)$ from eq. (6). Substitution in eq. (5) gives

$$d(x) = d_0 + h_0 + x \tan \alpha - \sqrt{d_0^2 + 2d_0h_0 + (h_0 + x \tan \alpha)^2}. \quad (7)$$

The profile shown in fig. 16 has been calculated for $d_0 = 30 \mu\text{m}$, $h_0 = 30 \mu\text{m}$ and $\alpha = 24^\circ$. At the bottom of the figure the result is shown for an experimentally obtained profile using the same parameter values. Apart from the surface roughness, the profile obtained agrees well with the calculated one.

The above model is no longer valid when the material dissolves in more than one direction and the tool is fed towards the workpiece. In such cases it is possible to use computer programs based on the finite-element method^[12]. Calculations carried out using this method may give a good indication of the possibility of generating a particular profile. Fewer experiments are then necessary for determining the optimum process conditions. Some experiments are still necessary, however, because the computer programs do not take account of effects such as local variations in overvoltage, temperature gradients and effects connected with the fluid flow.

Operations on metal foils

Holes and groove patterns in thin metal foils, which are usually made by punching or photochemical etching, can also be made by ECM. The application of ECM is particularly useful when punching produces excessive burring and internal stresses and when large quantities of components (more than a million) have to be produced. Photochemical etching may then be too expensive owing to the recurring costs of applying and removing photoresist masks.

Various methods can be used for clamping the foils, for the current supply, and for the fluid flow. A profiled tool can be used, which is copied in the workpiece. Another possibility is to use an insulating mask

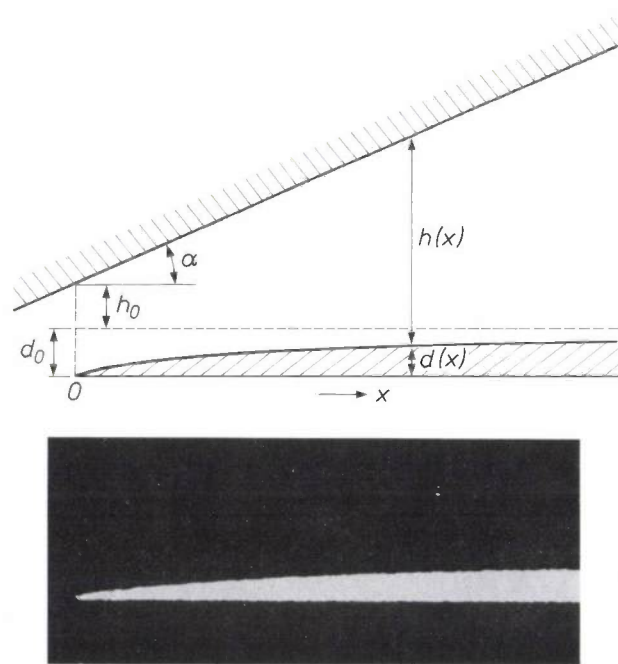


Fig. 16. Above: Parameters for calculating an edge profile to be made by ECM, using equation (7). The thickness $d(x)$ at position x is determined by the initial thickness d_0 , the initial gap width h_0 at $x = 0$, the angle α between workpiece and tool, and the local gap width $h(x)$. The profile shown was calculated for $d_0 = 30 \mu\text{m}$, $h_0 = 30 \mu\text{m}$ and $\alpha = 24^\circ$. Below: Micrograph of the profile obtained experimentally with these values.

^[12] Calculations with the finite-element method have been performed by F. J. du Chatenier and H. J. Eggink.

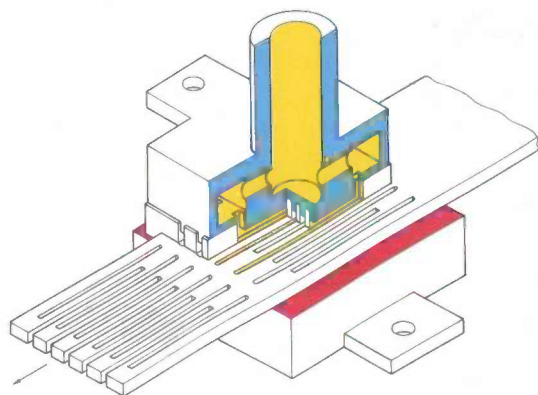


Fig. 17. Diagram of ECM configuration for machining thin metal foils with a profiled stationary tool. Between the conductor plates (blue), acting as cathode, the tool contains insulating plates that press the foil on to the surface below (red). The electrolyte (yellow) flows between the sides of the insulation plates.

that is placed on the foil. The current then flows through the openings in the mask, and the gap with the electrolyte is situated above the mask. The choice of method is primarily determined by the desired rounding of the edges.

An arrangement for generating rectangular patterns is shown in the diagram of *fig. 17*. A profiled tool is used, consisting of alternate conducting and insulating plates. At the surface of the foil the conducting plates are recessed about 0.3 mm with respect to the front face of the insulating plates. The foil is pressed on to the lower face by the insulating plates. The electrolyte

Summary. In electrochemical machining (ECM) metal removal takes place with an electrolyte between workpiece and tool, which are connected as anode and cathode. When an electric current is passed through the electrolyte the workpiece is selectively dissolved and becomes a replica of the shape of the tool. Reaction products and heat are carried away by rapid electrolyte flow through the gap. An elaborate system is necessary for the circulation and purification of the electrolyte and also for adjusting the machining voltage, for tool feed and for protecting the system from short-circuiting. The metal-removal rate and accuracy of form depend on tooling, elec-

trolyte, gap width, current density and electrolyte flow rate. The hardness of the workpiece is of no significance. The accuracy of form can be improved by insulating parts of the tool, e.g. with two SiC layers and an intermediate Si₃N₄ layer, applied by chemical vapour deposition (CVD). The use of a pulsed voltage also gives better results. Complex shapes are produced very rapidly without tool wear, burring and mechanical stresses. The ECM method can be used for high-precision (micro)machining operations such as the formation of tooth profiles and calibrated holes, removal of small burrs, edge profiling and making patterns in foils.

flows through the channel, which is bounded at the top by the conducting plates, underneath by the foil and at the sides by the insulating plates.

Fig. 18 shows a foil with a rectangular pattern that was obtained in this way. With the process correctly set up and with a pulsed voltage the dimensional accuracy is good: 5 μm for a groove width of 0.9 mm. The etch factor is about 2, which means that the metal is dissolved about twice as fast in the vertical direction as in the horizontal direction.

Important contributions to the work described here were made by J. H. de Jongh and W. H. A. Minten.

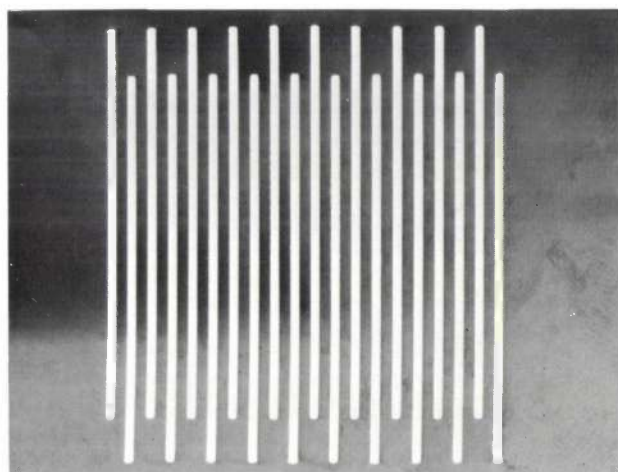


Fig. 18. Rectangular pattern produced by ECM with a profiled stationary tool as in *fig. 17*. The grooves are 0.9 mm wide.

trolyte, gap width, current density and electrolyte flow rate. The hardness of the workpiece is of no significance. The accuracy of form can be improved by insulating parts of the tool, e.g. with two SiC layers and an intermediate Si₃N₄ layer, applied by chemical vapour deposition (CVD). The use of a pulsed voltage also gives better results. Complex shapes are produced very rapidly without tool wear, burring and mechanical stresses. The ECM method can be used for high-precision (micro)machining operations such as the formation of tooth profiles and calibrated holes, removal of small burrs, edge profiling and making patterns in foils.

Scientific publications

These publications are contributed by staff of laboratories and plants that form part of or cooperate with enterprises of the Philips group of companies, particularly by staff of the research laboratories mentioned below. The publications are listed alphabetically by journal title.

Philips GmbH Forschungslaboratorium Aachen, Weißhausstraße, 5100 Aachen, Germany	A
Philips Research Laboratory Brussels, 2 avenue Van Becelaere, 1170 Brussels, Belgium	B
Philips Natuurkundig Laboratorium, Postbus 80 000, 5600 JA Eindhoven, The Netherlands	E
Philips GmbH Forschungslaboratorium Hamburg, Vogt-Kölln-Straße 30, 2000 Hamburg 54, Germany	H
Laboratoires d'Electronique et de Physique Appliquée, 3 avenue Descartes, 94450 Limeil-Brévannes, France	L
Philips Laboratories, N.A.P.C., 345 Scarborough Road, Briarcliff Manor, N.Y. 10510, U.S.A.	N
Philips Research Laboratories, Cross Oak Lane, Redhill, Surrey RH1 5HA, England	R
Philips Research Laboratories Sunnyvale P.O. Box 9052, Sunnyvale, CA 94086, U.S.A.	S

A. Daniels, F. Stolfi, A. Sherman* & M. Gasser* (* NASA, Greenbelt, MD)	N	Magnetically suspended Stirling cryogenic space refrigerator: test results	Adv. Cryogenic Eng. Vol. 29, R. W. Fast (ed.), Plenum, New York 1984	639-649	1984
A. Mitonneau, J.-P. André & A. Brière	L	Fabrication of high frequency Ga _{0.5} Al _{0.5} /GaAs MISFETs	1st Ann. Device Res. Conf., Burlington, VT, 1983	VA5	1983
J. P. Gowers	R	TEM image contrast from antiphase domains in GaAs:Ge(001) grown by MBE	Appl. Phys. A 34	231-236	1984
R. A. A. Kubiak*, E. H. C. Parker*, S. Newstead* (* London Polytechnic) & J. J. Harris	R	The morphology and electrical properties of hetero- epitaxial InAs prepared by MBE	Appl. Phys. A 35	61-66	1984
K. Woodbridge, P. Blood, E. D. Fletcher & P. J. Hulyer	R	Short wavelength (visible) GaAs quantum well laser grown by molecular beam epitaxy	Appl. Phys. Lett. 45	16-18	1984
M. J. Powell & J. W. Orton	R	Characteristics of amorphous silicon staggered-elec- trode thin-film transistors	Appl. Phys. Lett. 45	171-173	1984
J.-P. Hurault	L	La recherche dans les laboratoires d'électronique et de physique appliquée (LEP)	Bull. Soc. Fr. Phys. No. 52	6-9	1984
E. Schnedler	A	The calculation of complex chemical equilibria	CALPHAD 8	265-279	1984
M. Levent-Villegas	L	X-band paraphase amplifier	Electronics Lett. 20	451-453	1984
P. J. van Gerwen, W. A. M. Snijders & N. A. M. Verhoeckx	E	Dual digital transmission system for multipair cables based on 'crank-shaft coding'	Electronics Lett. 20	619-621	1984
L. Fortuin (<i>Philips ISA-CQM, Eind- hoven</i>)		Expected demand for service parts when failure times have a Weibull distribution	Eur. J. Oper. Res. 17	266-270	1984
J. W. Slotboom, M. J. J. Theunissen & A. J. R. de Kock (<i>Philips Elcoma Div., Eindhoven</i>)	E	Impact of silicon substrates on leakage currents	IEEE Electron Device Lett. EDL-4	403-406	1983
R. E. J. van de Grift & R. J. van de Plassche	E	A monolithic 8-bit video A/D converter	IEEE J. SC-19	374-378	1984
P. Delsarte & Y. Kamp	B	Relationship between the Karhunen-Loève trans- form and the Courant-Fischer theorem	IEEE Trans. IT-30	662-664	1984
C. Tsironis, R. Meierer & R. Stahl- mann (<i>Tech. Univ. Aachen</i>)	L	Dual-gate MESFET mixers	IEEE Trans. MTT-32	248-255	1984
W. A. M. Snijders	E	Bedrijfscommunicatie en glasvezel, een symbiose	Inf. & Informatie- beleid No. 7	20-30	1984

M. T. M. Scheffers (<i>Inst. for Perception Res., Eindhoven</i>)		Discrimination of fundamental frequency of synthesized vowel sounds in a noise background	J. Acoust. Soc. Am. 76	428-434	1984
D. Hennings & G. Rosenstein	A	Temperature-stable dielectrics based on chemically inhomogeneous BaTiO ₃	J. Am. Ceram. Soc. 67	249-254	1984
P. F. Fewster	R	Laue orientation and interpretation by microcomputer	J. Appl. Crystallogr. 17	265-268	1984
P. C. Zalm & L. J. Beckers	E	Consequences of sputtering with molecular ions	J. Appl. Phys. 56	220-223	1984
K. H. J. Buschow	E	Effect of short-range order on the thermal stability in amorphous Ti-Ni alloys	J. Appl. Phys. 56	304-306	1984
H. Rau & E. Schnedler	A	Standard molar enthalpy of formation of GeO (g) from flow measurements	J. Chem. Thermodyn. 16	673-682	1984
P. F. Bordui & G. M. Loiacono	N	In-line bulk supersaturation measurement by electrical conductometry in KDP crystal growth from aqueous solution	J. Cryst. Growth 67	168-172	1984
K. H. J. Buschow	E	Research on rare-earth-base metal systems: fundamental and technological aspects	J. Less-Common Met. 100	29-48	1984
A. R. Miedema, A. K. Niessen & K. H. J. Buschow	E	Some notes on diffusion in alloys containing rare earth metals	J. Less-Common Met. 100	71-84	1984
D. B. de Mooij & K. H. J. Buschow	E	Crystal structure and magnetic properties of the ternary compounds Pt ₂ GdSn and Pt ₂ ErSn	J. Less-Common Met. 102	113-117	1984
R. B. Helmholtz (<i>ECN, Petten</i>), R. A. de Groot*, F. M. Mueller* (* <i>Univ. Nijmegen</i>), P. G. van Engen & K. H. J. Buschow	E	Magnetic and crystallographic properties of several C1 ₅ type Heusler compounds	J. Magn. & Magn. Mater. 43	249-255	1984
A. J. E. M. Janssen	E	Positivity properties of phase-plane distribution functions	J. Math. Phys. 25	2240-2252	1984
G. A. C. M. Spierings & T. P. M. Meeuwssen	E	The Rayleigh scattering loss in silicate glasses containing PbO	J. Non-Cryst. Solids 66	489-499	1984
H. A. Post	E	The absolute Hg 6 ¹ P ₁ direct electron impact excitation cross section determined in a low-pressure Hg discharge	J. Phys. B 17	3193-3208	1984
P. C. M. Gubbens*, A. M. van der Kraan* (* <i>Interuniv. Reactor Inst., Delft</i>) & K. H. J. Buschow	E	Quadrupole splitting observed in some cubic Laves-phase compounds by means of ¹⁶⁹ Tm Mössbauer spectroscopy	J. Phys. F 14	2195-2201	1984
M. J. Jongerius & A. J. M. J. Ras	E	Optogalvanic detection of acoustic resonances in a high-pressure sodium discharge	J. Physique 44 (Colloque C7)	C7/377- C7/384	1983
Y. Demay, P. Maurel & S. Gourrier	L	Interactions of Si (111) surface with H ₂ , NH ₃ , SiH ₄ multipolar plasmas studied by in situ ellipsometry	J. Physique 44 (Colloque C10)	C10/253- C10/256	1983
M. Erman, P. Chambon, B. Prévot* & C. Schwab* (* <i>Univ. Strasbourg</i>)	L	Spectroscopic ellipsometry and Raman scattering analysis of Be shallow implantation in GaAs	J. Physique 44 (Colloque C10)	C10/261- C10/265	1983
C. Alibert*, S. Gaillard* (* <i>Univ. Montpellier</i>), M. Erman & P. M. Frijlink	L	Electroreflectance and spectroscopic ellipsometry studies of GaAs/GaAlAs heterojunctions	J. Physique 44 (Colloque C10)	C10/229- C10/233	1983
C. Schiller & M. Duseaux	L	X rays and electron microprobe analysis of III-V semiconductors	J. Physique 45 (Colloque C2)	C2/891- C2/894	1984
K. Woodbridge, P. Dawson, J. P. Gowers & C. T. Foxon	R	Structural and optical properties of GaAs-Al _x Ga _{1-x} As quantum wells	J. Vac. Sci. & Technol. B 2	163-166	1984
M. Iost & P. Baudet	L	TEC millimétrique en GaAs implanté	4èmes Journées Natl. Microondes, Lannion, 1984	66-67	1984
A. Giakoumis*, J. Michel* (* <i>RTC, Limeil-Brévannes</i>), V. Pauker & M. Binet	L	Amplificateurs GaAs monolithiques à large bande et gain élevé	4èmes Journées Natl. Microondes, Lannion, 1984	168-169	1984
C. Kermarrec, J. Faguet, B. Vancon, C. Mayousse, A. Collet, P. Kaikati & D. Beaufort	L	Le premier récepteur microondes entièrement intégré au GaAs. Application à la réception de la TV directe par satellite à 12 GHz	4èmes Journées Natl. Microondes, Lannion, 1984	172-173	1984
W. G. Essers & M. R. M. van Gompel	E	Procesregeling bij synchro-puls-MIG-lassen	Lastechniek 50	174-180	1984

- | | | | | | |
|--|-------------|---|--|---------|------|
| M. H. Verhagen (<i>Univ. Leuven</i>) & P. van Dooren | <i>B</i> | An efficient implementation of square root filtering: error analysis, complexity and simulation on flight-path reconstruction | Lect. Notes Control & Inf. Sci. Vol. 63, A. Bensoussan & J. L. Lions (eds), Springer, Berlin | 250-267 | 1984 |
| W. H. M. Zijm (<i>Philips ISA-CQM, Eindhoven</i>) | | Generalized eigenvectors and sets of nonnegative matrices | Linear Algebra & Appl. 59 | 91-113 | 1984 |
| K. H. J. Buschow | <i>E</i> | Decomposition of metastable ternary hydrides | Mater. Res. Bull. 19 | 935-943 | 1984 |
| R. C. Pond (<i>Univ. Liverpool</i>), J. P. Gowers, D. B. Holt (<i>Imp. College, London</i>), B. A. Joyce, J. H. Neave & P. K. Larsen | <i>R, E</i> | A general treatment of antiphase domain formation and identification at polar-nonpolar semiconductor interfaces | Mater. Res. Soc. Symp. Proc. 25 | 273-278 | 1984 |
| H.-G. Finke*, A. Nicia & D. Rittich* (<i>* Philips Kommun. Ind., Köln</i>) | <i>E</i> | Optischer Kugellinsen-Demultiplexer | Nachrichtentech. Z. 37 | 346-351 | 1984 |
| G. Lütteke & H. C. Raets | <i>A</i> | High-voltage high-frequency class-E converter suitable for miniaturization | PESC '84 Rec., Gaithersburg, MD, 1984 | 54-61 | 1984 |
| J. W. Orton & M. J. Powell | <i>R</i> | The relationship between space-charge-limited current and density of states in amorphous silicon | Phil. Mag. B 50 | 11-21 | 1984 |
| G. G. P. van Gorkom & A. M. E. Hoeberechts | <i>E</i> | An efficient silicon cold cathode for high current densities, I: Experimental data and main results | Philips J. Res. 39 | 51-60 | 1984 |
| P. C. Zalm & L. J. Beckers | <i>E</i> | Secondary electron yields from clean polycrystalline metal surfaces bombarded by 5-20 keV hydrogen or noble gas ions | Philips J. Res. 39 | 61-76 | 1984 |
| J. L. C. Daams & K. H. J. Buschow | <i>E</i> | The crystal structure of LaNiSn | Philips J. Res. 39 | 77-81 | 1984 |
| K. H. J. Buschow & P. G. van Engen | <i>E</i> | Magneto-optical properties of rare earth cobalt compounds and amorphous alloys | Philips J. Res. 39 | 82-93 | 1984 |
| J. J. G. Willems | <i>E</i> | Metal hydride electrodes stability of LaNi ₅ -related compounds (Thesis) | Philips J. Res. 39 (Suppl. No. 1) | 94 pp. | 1984 |
| W. J. W. Kitzen & P. M. Boers | <i>E</i> | Applications of a digital audio-signal processor in T.V. sets | Philips J. Res. 39 | 94-102 | 1984 |
| H. G. R. Maas & J. A. Appels | <i>E</i> | PABLO a versatile VLSI technology | Philips J. Res. 39 | 103-108 | 1984 |
| B. A. Joyce, J. H. Neave, P. J. Dobson (<i>Imp. College, London</i>) & P. K. Larsen | <i>R, E</i> | Analysis of reflection high-energy electron-diffraction data from reconstructed semiconductor surfaces | Phys. Rev. B 29 | 814-819 | 1984 |
| G. F. Neumark, S. P. Herko, T. F. McGee, III & B. J. Fitzpatrick | <i>N</i> | Energy of an interstitial donor in ZnSe from pair spectra | Phys. Rev. Lett. 53 | 604-607 | 1984 |
| L. Minnema & J. M. van der Zande | <i>E</i> | Polymer complex formation of polyamic acids with amines | Polyimides, Vol. 1, K. L. Mittal (ed.), Plenum, New York | 589-598 | 1984 |
| P. Branquart, G. Louis & P. Wodon | <i>B</i> | On the analytical description of CHILL | Proc. CHILL Conf., Lisle, IL, 1983 | 6 pp. | 1983 |
| P. K. Larsen & B. A. Joyce | <i>E, R</i> | Photoemission from semiconductor structures prepared in-situ by molecular beam epitaxy | Proc. Daresbury Study Weekend, Daresbury 1983 | 23-31 | 1983 |
| A. J. E. M. Janssen | <i>E</i> | Gabor representation and Wigner distribution of signals | Proc. ICASSP 84, San Diego 1984 | 4 pp. | 1984 |
| A. J. E. M. Janssen & L. B. Vries | <i>E</i> | Interpolation of band-limited discrete-time signals by minimizing out-of-band energy | Proc. ICASSP 84, San Diego 1984 | 4 pp. | 1984 |
| W. J. W. Kitzen & P. M. Boers | <i>E</i> | Applications of a digital audio-signal processor in T.V. sets | Proc. ICASSP 84, San Diego 1984 | 4 pp. | 1984 |
| M. Lacroix & A. Pirotte | <i>B</i> | Relational model and relational systems | Proc. INRIA Workshop Relat. DBMS on Micro-comput., Toulouse 1983 | 11-25 | 1983 |
| S. L. Tan & R. N. Jackson | <i>E, R</i> | Flexible coding and decoding for extended television | Proc. 10th Int. Broadcasting Conv., Brighton 1984 | 107-110 | 1984 |

D. W. Parker & L. J. van de Polder <i>R, E</i>	Display standards for extended definition component television systems	Proc. 10th Int. Broadcasting Conv., Brighton 1984	120-124	1984
R. E. Horstman, J. Wolter, R. W. van der Heijden*, G. L. J. A. Rikken* & H. Sigg* (* <i>Univ. Nijmegen</i>) <i>E</i>	Infrared transmission and photoconductivity on the 2 DEG in a GaAs/AlGaAs heterojunction	Proc. 17th Int. Conf. on Low temp. phys., Karlsruhe 1984	869-870	1984
C. B. Marshall <i>R</i>	A low-power integrable paging receiver architecture	Proc. Int. Conf. on Mobile radio techniques, York 1984	1-5	1984
R. C. French <i>R</i>	A high technology VHF radio paging receiver	Proc. Int. Conf. on Mobile radio techniques, York 1984	11-15	1984
P. A. Moore <i>R</i>	A high-performance low-power VHF front end	Proc. Int. Conf. on Mobile radio techniques, York 1984	16-20	1984
D. W. H. Calder <i>R</i>	Audio frequency gyrator filters for an integrated radio paging receiver	Proc. Int. Conf. on Mobile radio techniques, York 1984	21-26	1984
W. Rey <i>B</i>	Unifying view in robustness, the scale in M-estimation	Proc. 44th Session Int. Statist. Inst., Madrid 1983	115-118	1983
W. Pollock*, J. Schofield* (* <i>Mullard Central Mater. Lab., Mitcham</i>), R. F. Milsom, R. J. Murray & I. Flinn <i>R</i>	Low-loss saw filter using single-phase IDTs and no external tuning	Proc. Ultrasonics Symp., Atlanta 1983	87-92	1983
R. F. Milsom, J. E. Curran, S. L. Murray, S. Terry-Wood* & M. Redwood* (* <i>London Univ.</i>) <i>R</i>	Effect of mesa-shaping on spurious modes in ZnO/Si bulk-wave composite resonators	Proc. Ultrasonics Symp., Atlanta 1983	498-503	1983
J.-M. Nicolas <i>L</i>	Simulation numérique de la propagation ultrasonore en milieu d'indice variable application à l'imagerie médicale	Rev. Cethedec-Ondes & Signal No. 79	45-53	1984
C. Ronse <i>B</i>	Feedback shift registers (Lect. Notes Comput. Sci. Vol. 169)	Springer, Berlin	144 pp.	1984
J. de Kroon (<i>Philips ISA-CQM, Eindhoven</i>) & P. van der Laan (<i>Agricult. Univ., Wageningen</i>)	A comparison of the powers of a generalized Friedman's rank test and an aligned rank procedure based on simulation	Stat. Neerlandica 38	189-198	1984
J. B. Clegg, A. E. Morgan, H. A. M. de Grefte, F. Simondet, A. Huber (<i>Thomson CSF, Orsay</i>), G. Blackmore (<i>AMTE, Poole</i>), M. G. Dowsett (<i>London Polytechnic</i>), D. E. Sykes (<i>Loughborough Consultants, Loughborough</i>), C. W. Magee (<i>RCA, Princeton, NJ</i>) & V. R. Deline (<i>C. Evans & Assoc., San Mateo, CA</i>) <i>R, S, E, L</i>	A comparative study of SIMS depth profiling of boron in silicon	Surf. & Interface Anal. 6	162-166	1984
W. H. M. Zijm (<i>Philips ISA-CQM, Eindhoven</i>)	Dynamic programming models with general non-negative matrices	Wiss. Z. Tech. Hochsch. Leipzig 8	145-153	1984
A. E. Ronner (<i>Philips ISA-CQM, Eindhoven</i>)	Asymptotic normality of p -norm estimators in multiple regression	Z. Wahrscheinlichkeitstheorie & Verw. Geb. 66	613-620	1984

Contents of Philips Telecommunication Review 42, No. 4, 1984

P. van den Boog & G. C. Groenendaal: The HCS 400 communication terminal (pp. 185-195)

Fifty years ago (pp. 196-197)

C. G. den Hertog & W. J. A. Vonk: Data communication switch type DS-790 (pp. 198-212)

A. Escherle & H. van Kampen: The P3000 office computer system (pp. 214-228)

J. K. Klooster: Non-voice communications in banking (pp. 229-238)

Recent United States Patents

Abstracts from patents that describe inventions from the following research laboratories, which form part of or cooperate with the Philips group of companies:

Philips GmbH Forschungslaboratorium Aachen, Weißhausstraße, 5100 Aachen, Germany	A
Philips Research Laboratory Brussels, 2 avenue Van Becelaere, 1170 Brussels, Belgium	B
Philips Natuurkundig Laboratorium, Postbus 80 000, 5600 JA Eindhoven, The Netherlands	E
Philips GmbH Forschungslaboratorium Hamburg, Vogt-Kölln-Straße 30, 2000 Hamburg 54, Germany	H
Laboratoires d'Electronique et de Physique Appliquée, 3 avenue Descartes, 94450 Limeil-Brévannes, France	L
Philips Laboratories, N.A.P.C., 345 Scarborough Road, Briarcliff Manor, N.Y. 10510, U.S.A.	N
Philips Research Laboratories, Cross Oak Lane, Redhill, Surrey RH1 5HA, England	R
Philips Research Laboratories Sunnyvale, P.O. Box 9052, Sunnyvale, CA 94086, U.S.A.	S

4 449 834

Aerostatic axial thrust bearing

A. Franken

J. L. M. Hagen

An aerostatic axial thrust bearing comprising a movable part and a stationary part, one of said parts being constructed as a cup-shaped member having an upright wall, a closure member and a bottom which faces the other bearing part and which is formed by a diaphragm having a central opening. The side of the diaphragm facing the other bearing part is shaped so that the bearing gap between the two parts becomes narrower from the central opening in the diaphragm towards its outer edge, and the cup-shaped member having an inlet for the admission of a gaseous pressure medium to the space inside the cup-shaped member. The diaphragm is connected to the upright wall of the cup-shaped member at a location which is situated between the central opening and the outer edge of the diaphragm.

E

ichiometric basic compound having the following composition: $Pb(Ti_{1-x-y}Mg_xW_y)O_3$ wherein $0.25 \leq x \leq 0.35$ and $0.25 \leq y \leq 0.35$ and comprising an addition of 0.001 to 0.006 (5PbO + 1WO₃) on an additive molar basis.

4 474 650

Method of manufacturing a mother matrix

A. W. M. de Laat

A method of manufacturing a metal mother matrix in which a master disc, which is a supporting disc, carrying on one side a layer of a positive photoresist in which an information track is provided, is provided with a metal peel, first by electroless deposition and then by electrodeposition, the metal peel is separated from the master disc, the remainders of the photoresist present on the father matrix thus obtained are dissolved and a metal copy, which is a mother matrix, is manufactured by electrodeposition from the father matrix, characterized in that the photoresist is made electrically conductive by means of exposure to light.

E

4 475 032

Plasma spraying of conversion screens

T. J. A. Popma

G. A. te Raa

A. T. Vink

A conversion screen such as is used for X-ray image intensifier screens, X-ray image intensifier tubes, cathode-ray tubes, image pick-up tubes, X-ray electrography, fluorescent lamps and the like is formed by the deposition of a layer of conversion material on a carrier via a melting space which is preferably heated by means of a plasma arc. This method of deposition offers very robust screens with a high density and also allows the filling of recesses in a carrier with conversion material, so that structured conversion screens can be formed.

E

4 474 894

Dielectric on the basis of lead titanates, method of manufacturing same, and a multilayer capacitor comprising the dielectric

K. H. Härdtl

A dielectric having a sintering temperature in the range of from 800 to 1000 °C on the basis of lead titanates, in which at least 50 mol % of the titanium are substituted by Mg and W, the sto-

A

4 475 120

Method of raising the breakdown voltage of an integrated capacitor and capacitor manufactured by this method

M. J. M. Binet

The invention relates to a method suitable for raising the breakdown voltage of a capacitor of the integrated circuit type formed on a semiconductor substrate and characterized in that the lower plate of the capacitor is under etched so that an air wedge is obtained. As a result of the air wedge, the electric current passed through the semiconductor material is lengthened and the breakdown phenomena at the edges of the capacitor are reduced. The invention also relates to capacitors obtained in this manner.

L



PHILIPS

4 475 125

Television pick-up arrangement comprising a solid-state picture pick-up device*L. J. M. Esser**L. J. van de Polder*

E

A television pick-up arrangement comprising a solid-state picture pick-up device rows of picture pick-up elements of which are connectable to parallel inputs of two output shift registers. When the shift registers are read simultaneously they supply at their series outputs picture signals which are associated with each time two pairs of rows of picture pick-up elements. According to the invention, the two picture signals are applied on the one hand separately to a vertical aperture correction circuit having only one delay device with a time delay of one line period and on the other hand combined to a horizontal aperture correction circuit, the corrected signals being combined behind said correction circuits. Advantageous use can then be made of a device in which pick-up information is obtained by both holes and electrons which are caused by photons.

4 476 163

Method of making crucibles for flameless atomic absorption spectroscopy*B. Lersmacher**L. W. J. van Kollenburg*

A, E

A method of making crucibles for flameless atomic spectroscopy comprises the steps of coating carbon crucible preforms with pyrolytic graphite in a reaction vessel by deposition of the graphite from a gas phase wherein the carbon crucible preforms are removed from the reaction vessel after cooling to room temperature and are re-introduced into the reaction vessel orientated in different positions before application of a second or subsequent coating to give a total thickness of the coatings of 20 to 80 μm .

4 476 214

Optical information disc comprising tellurium, selenium and antimony*P. Zalm**B. A. J. Jacobs**A. W. de Poorter*

E

An optical information disc in which information can be written and read optically and which has a substrate plate which on at least one side has a recording layer which satisfies the formula $\text{Te}_x\text{Se}_y\text{Sb}_z\text{S}_q$ wherein $x = 55-85$ at. %, $y = 13-30$ at. %, $z = 1-12$ at. %, $q = 0-10$ at. % and $x + y + z + q = 100$. Suitable recording layers are $\text{Te}_{60}\text{Se}_{26}\text{Sb}_{10}\text{S}_6$ and $\text{Te}_{75}\text{Se}_{15}\text{Sb}_5\text{S}_5$.

4 476 438

Multiplier circuit including amplifier with drift compensation circuit*C. Cantou*

L

An amplifier circuit comprising an amplifier having a first input which receives an electric signal comprising an intermittent useful signal component and an undesired spurious component and a second input of opposite sign to that of the first input. The output signal of a circuit for the compensation of the spurious component is applied to the second amplifier input. The circuit comprises a comparator for comparing the undesired component, taken from the output of the amplifier, with a threshold value, a counter which is incremented or decremented depending on the result of the comparisons and in the rhythm of a clock circuit, and a digital-to-analog converter coupled to the output of the counter to supply the signal for the compensation of the unwanted component to the second input of the amplifier.

4 476 544

Current-controlled magnetic domain memory*N. J. Wiegman*

E

A current-controlled magnetic domain memory comprises a register for propagating magnetic domains in a magnetizable layer. The register comprises a meandering current-conductor pattern. The pattern can be driven by a bipolar current. The current conductors have a width of approximately one domain diameter and a meander period of approximately four domain diameters. The conductor pattern is provided with two control elements per period which generate potential wells in the magnetizable layer of a size of approximately one domain cross-section and which are arranged to center the centers of the domains on the edges of the conductor pattern when the current through the conductor pattern is zero.

4 476 563

Semiconductor laser having at least two radiation beams, and method of manufacturing same*L. J. van Ruyven*

E

A semiconductor laser device has a semiconductor body in which two or more lasers are provided which can generate substantially parallel radiation beams of preferably different frequencies which are situated close together. According to the invention, the semiconductor body has at least one semiconductor laser of the double hetero-junction type (DH-type) comprising a plurality of semiconductor layers with a radiating p-n junction parallel to the semiconductor layers and at least one semiconductor laser of the TJS ("Transverse Junction Stripe") type, the p-n junction surface of which is transverse to that of the DH-laser. The device comprises a layer structure having at least two active layers, each between two passive layers. One laser is formed in a mesa-shaped part of the body which comprises both active layers, the other in an adjacent part in which the uppermost active layer is absent. The TJS-laser is preferably provided in the last-mentioned part. More than two lasers may also be provided.

4 477 401

Method of manufacturing a dielectric*H. J. Hagemann**S. Hüntten**R. Wernicke**C. J. Klomp**W. Noorlander*

A, E

A method of manufacturing a dielectric from ferroelectric ceramic material having a perovskite structure with the basic formula ABO_3 . In the method, the dielectric is sintered in a reducing atmosphere and the sintered body is aftertreated at a temperature in the range of from 500 to 900 $^{\circ}\text{C}$ in an $\text{N}_2\text{-O}_2$ atmosphere. The atmosphere contains a quantity of O_2 corresponding to a partial O_2 -pressure between 10^{-6} bar and 0.2 bar.

4 477 696

Conference system for telephony*A. W. M. van den Enden**J. F. P. van Mil**A. J. Nijman*

E

A conference system comprises a conference circuit to which a plurality of participants are connected via terminals respective connecting circuits having input and output circuits, the signal from the output circuits being fed to the connecting circuit and signals from the conference circuit being fed lines to the input circuits. The conference circuit has summing amplifiers whose inputs are connected to the outputs of the connecting circuits so that the output signals from the connecting circuits are algebraically summed. The signs of the signals to be summed are determined from the relationship $E - S^*S = 0$ where E is the unity matrix and S^* is the transposed complex conjugate matrix of S.

4 477 903

Error correction method for the transfer of blocks of data bits, a device for performing such a method, a decoder for use with such a method, and a device comprising such a decoder

K. A. Schouhamer Immink E
L. B. Vries

For an error correction method for the transfer of word-wise arranged data, two word correction codes are successively used, each code acting on a group of words while therebetween an interleaving step is performed. The actual transfer takes place by means of channel words for which purpose there are provided a modulator and a demodulator. Invalid channel words are provided with an invalidity bit in the demodulator. During the (possibly correcting) reproduction of the data words, the invalidity bits can be used in one of the two error corrections in various ways. When too many words of a group of code words are invalid, all words of the relevant group are invalidated. If a word comprising an invalidity bit is not corrected during correction by means of a syndrome variable, all words of the relevant group are invalidated. If the number of invalidity bits lies within given limits, they act as error locators so that the code is capable of correcting a larger number of words.

4 477 915

Differential pulse code modulation transmission system

J. H. Peters E

Differential pulse code modulation transmission system comprising a transmitter and a receiver. In the transmitter there is subtracted from an information signal to be transmitted, a prediction signal for the purpose of generating a difference signal, which is quantized and converted into a quantized difference signal in a quantizing arrangement. This difference signal is applied to a prediction circuit for generating the prediction signal. It is also transmitted to the associated receiver. In that receiver a similar prediction signal is generated by means of a similar prediction circuit, which prediction signal is now added to the received quantized difference signal. In order to limit the influence of transmission errors in this transmission system, without an excessive increase in equipment, the quantized difference signal is applied in the transmitter and in the receiver to a cascade arrangement of a non-linear network and an auxiliary prediction circuit, which produces an auxiliary prediction signal. Before the quantized difference signal is applied to the prediction circuit, the auxiliary prediction signal is first added thereto.

4 477 916

Transmitter for angle-modulated signals

K. S. Chung E

Transmitter for angle-modulated signals having an input for binary signals, a premodulation filter and a frequency modulation arrangement. In order to improve the error rate of the system of transmitter and receiver a premodulation filter is used having a pulse response

$$h(t): h(t) = g(t) - \sum_{n=1}^N a(n)[g(t - nT) + g(t + nT)], \text{ wherein } g(t)$$

is the pulse response of a Gaussian lowpass filter and T the duration of a binary signal element. The postdemodulation filter has a pulse response of the same general form for optimum results.

4 478 485

Connector for coupling at least one optical fiber to a further optical element

G. D. Khoe E

J. H. F. M. van Leest
L. J. Meuleman

A connector, for coupling pairs of (monomode) optical fibers, comprising a central connection portion, with a V-groove, and two holders. A cylindrical envelope of an optical fiber is arranged in each holder to be resilient in the longitudinal direction. A pin is

secured parallel to each envelope. The envelope is retained in the V-groove by a hold-down spring. When the envelope and the pin are inserted into the central connection portion, the envelope is clamped by a clamping spring which is actuated by the pin after the envelope has reached its ultimate position, e.g. against an abutment pin.

4 478 690

Method of partially metallizing electrically conductive non-metallic patterns

E. Scholtens E

The partial metallization of electrically conductive non-metallic patterns, for example transparent patterns of indium oxide and/or tin oxide or resistance layers of cermet material, on insulating carriers by means of an electroless plating solution. The plating is initiated by applying a potential difference for a short period of time between the patterns and an auxiliary electrode.

4 479 260

Coupling and mixing circuit comprising a dual source transistor

P. Harrop L

A dual-source FET connected in a common gate arrangement for receiving respective input signals at the two-sources and for producing at a drain terminal the sum of the input signals. A circuit is disclosed which combines the dual-source FET with a single-source FET for mixing the input signals.

4 480 229

Amplifier arrangement with parallel-operated amplifier sections

T. J. van Kessel E

N. V. Franssen

By adding the difference between output and input of the one amplifier section to the output signal by means of a subsequent amplifier section a ring of amplifier sections can be formed which compensate for each other's distortion.

4 480 257

Optical printer comprising light switching elements

B. Hill H

An optical printer includes magneto-optical light switching elements formed on a substrate of comparatively small dimensions. The light switching elements are combined so as to form groups which are separated from one another by an equidistant space. Each group is associated with a self-focusing lens so that the distances between all image points of a plurality of groups on a record carrier are equal.

4 480 263

Three-dimensional television system and transmitter suitable therefor

P. C. A. van Merode E

A three-dimensional television system comprising an adapted transmitter, which in further respects does not differ from a colour television system in accordance with the PAL, NTSC or SECAM-standard. A three-dimensional display in a standard receiver is based on the use of two colours, an observer observing a colour picture display screen through differently coloured glasses. In the transmitter, a first picture pick-up device is coupled to an input of a matrix-coding circuit via a low-pass filter. The filter has a bandwidth which is not more than the bandwidth of the colour difference signal channels in the decoding-matrix circuit of the receiver. In order to improve the picture quality, a second picture pick-up device may be coupled via a low-pass filter having a wider bandwidth to a different input of the matrix-coding circuit.

4 480 267

Line standard conversion circuit

P. M. van den Avoort
M. C. W. van Buul

E

The use of a field interpolation circuit which interpolates by means of equal amplitudes of the information from two successive fields results in a television line standard doubler capable of furnishing a very good picture quality.

4 480 332

Apparatus for examination by scattered radiation

H. Strecker

H

The invention relates to an apparatus for imaging a layer of a body to be examined. The body is irradiated by primary radiation, in response to which the layer emits scattered radiation. The apparatus comprises a diaphragm plate which is disposed outside the primary radiation beam. The diaphragm is rotatable about an axis perpendicular to its major surface, and it has at least one aperture which is disposed off of the axis of rotation. A detector or a superposition device is provided for measuring or superimposing the scattered radiation which passes through the diaphragm plate at different aperture settings. The primary radiation is stopped down to form a flat fan-shaped beam. The diaphragm plate is oriented parallel to the fan-shaped beam. Each aperture corresponds to an associated detector, which follows the rotation of the diaphragm plate. The input face of each detector extends parallel to the diaphragm plate. The detector is arranged so as to be rotatable about a detector axis which is perpendicular to an input face and which extends through its center. The detector rotates in a direction opposite to the direction of rotation of the diaphragm plate and with the same angular velocity as this plate.

4 481 340

Photosensitive polyamic acid derivative, compound used in manufacture of derivative, method of manufacturing substrate having polyimide layer, and semiconductor device made from said method

L. Minnema
J. M. van der Zande

E

A photosensitive polyamic acid derivative obtained by treating polyamic acid with a compound of a special formula, method of manufacturing a substrate having a polyimide layer by providing the substrate with a layer of the photosensitive polyamic acid derivative and then exposing, developing and imidizing the layer, as well as a semiconductor device comprising a polyimide layer obtained by using the above-mentioned method.

4 481 385

Arrangement for cancelling echo signals

J. J. W. Kalfs

E

Arrangement for cancelling echo signals in data transmission over a two-wire transmission path. The data signals occurring in the send path are applied to an adjustable signal processing arrangement. From said data signals a synthetic echo signal is derived which is subtracted in a difference producer from the data signal occurring in the receive path. The residual signal is converted into a digital residual signal in an analog-to-digital converter arrangement. An interpolator which increases the sampling rate by a factor L results in the production of a digital control signal from the digital residual signal, for the setting arrangement. The sampling rate of the digital residual signal is M/LT Hz, wherein T is the duration of a data symbol in seconds and M and L represent integers which are relatively prime, L being greater than one.

4 481 447

Power supply for a magnetron

E. H. Stupp
M. W. Fellows

N

A method of controlling the power output of a magnetron tube, and an electric power supply for supplying power to the tube. According to the method, power is continuously supplied to the magnetron heater. At the same time, a voltage is continuously applied across the anode and the cathode of the tube. This voltage across the anode and the cathode varies in cycles between a first value, which is substantially at or below the threshold voltage of the magnetron tube, and a second value, which is above the threshold voltage. The average magnetron power output is determined by the proportion of each cycle during which the voltage across the anode and the cathode is above the threshold voltage.

4 481 477

Method and apparatus for the real-time measurement of the small signal gain of an amplifier

K. R. Wittig

N

A method and apparatus for measuring the small signal gain of an amplifier. Each amplifier responds, in operation, to a small signal input. The small signal input varies substantially linearly over a field time interval. A small bias signal is added to the bias level input of the amplifier during a portion of the field time interval. The output of the amplifier is measured at three or more different times during the field time interval, at least one time when the small bias signal has not been added to the bias level input and at least one time being when the small bias signal has been added to the bias level input. By processing the measured outputs, a signal which is directly proportional to the product of the small bias signal with the small signal gain of the amplifier is obtained. A method and apparatus for actively compensating for differences in the small signal gain among two or more amplifiers is obtained by dividing the small signal output of each amplifier by the signal proportional to the small signal gain of the amplifier.

4 481 540

Television camera comprising a focusing arrangement

F. H. M. Bergen

E

A television camera in which an electronic view-finder is further used for adjusting an optimum focusing. The picture signal is then applied to the view-finder via a switching device, and that during the presence of an aperture correction signal. Outside the occurrence of this aperture correction signal the supply of a picture signal which has been made unsharp may be affected, or the supply thereof may be interrupted. Adjusting the optimum focusing on the basis of the picture on the viewer screen is then facilitated.

4 481 552

Disc unit for information recording and/or reading system

M. J. J. Dona
A. J. J. Franken
P. van der Giessen

E

A system for recording/reading information, comprising interchangeable disc units and a drive unit. Each disc unit comprises a disc pack with at least one information disc which is contained in an enclosure comprising two covers which can move relative to each other and which are interconnected by connecting means. The drive unit comprises means for supporting and driving the information-disc pack and means for recording/reading the information on the information discs, means for releasing the connection between the covers, and means for moving the covers relative to each other.

Erasable magneto-optical recording

M. Hartmann, B. A. J. Jacobs and J. J. M. Braat

Recent articles in this journal described a method of optical recording in which a laser makes holes or pits in a thin layer of material. In magneto-optical recording use is made of a magnetic layer magnetized perpendicular to the surface. A laser is used to reverse the magnetization locally, in the direction of an external magnetic field. Read-out is based on the rotation of the plane of polarization of the laser light, which depends on the local direction of the magnetization. The stored information can also be erased. The erasure is carried out in the same way as the recording, but with the external magnetic field in the same direction as the original magnetization. In a joint study, scientists and engineers at the Philips Research Laboratories in Hamburg and in Eindhoven are looking for suitable magnetic materials, making and evaluating discs and optimizing the magneto-optical recording system. Recent progress suggests that practical applications could soon become a possibility. These could include the storage of alphanumeric data, digital audio signals and even video signals.

Introduction

In magneto-optical recording on a disc, a modulated linearly polarized AlGaAs laser beam is used for storing information in a magnetic layer magnetized perpendicular to the surface, e.g. in the upward direction^[1]. During the recording or 'writing' the focused laser beam (with an effective diameter of about 1 μm) causes local heating. In the presence of a downward-directed magnetic field the direction of magnetization of an irradiated zone is reversed. On cooling to room temperature the new direction is 'frozen in'. In this way a pattern of downward-magnetized domains is created in an upward magnetized matrix. A pattern of this kind forms the basis for the recording of digital signals, with an upward magnetization corresponding to a '0' and a downward magnetization to a '1'.

Read-out takes place with a laser beam of lower intensity. When the linearly polarized light is reflected by the magnetic layer there is a slight rotation of the polarization plane (the Kerr effect). The domains are differentiated from the matrix since the direction of

this rotation depends on the direction of magnetization.

An important difference from digital optical recording (DOR) with tellurium alloys^[2] and optical recording with organic dyes^[3] is that *the recorded information can be erased*. This is done by laser-irradiation of the written domains, but now with an external magnetic field in the same direction as the original magnetization.

Besides possessing a number of specific magnetic and optical properties, the recording layers must be sufficiently stable, not only when the information is being written, read out or erased but also during ageing under various conditions. In the search for suitable materials for recording layers considerable attention was paid to single-crystal garnets^[4] and amorphous alloys of transition metals with heavy rare-

Dr M. Hartmann (formerly M. Urner-Wille) is with Philips GmbH Forschungslaboratorium Hamburg, Hamburg; Ing. B. A. J. Jacobs and Dr Ir J. J. M. Braat are with Philips Research Laboratories, Eindhoven.

^[1] W. K. Unger and R. Rath, IEEE Trans. MAG-7, 885-890, 1971.

^[2] L. Vriens and B. A. J. Jacobs, Philips Tech. Rev. 41, 313-324, 1983/84.

^[3] D. J. Gravesteijn and J. van der Veen, Philips Tech. Rev. 41, 325-333, 1983/84.

^[4] J.-P. Krumme and H. J. Schmitt, IEEE Trans. MAG-11, 1097-1102, 1975.

earth metals (from gadolinium onward). In this article we shall only be concerned with these alloys. The initial results were obtained with alloys of gadolinium with iron or cobalt, deposited by cathode sputtering [5]. Also investigated were alloys of cobalt with holmium and of iron with gadolinium and other rare-earth metals, obtained by vapour deposition in ultra-high vacuum [6].

In the research described in this article alloys of this type were examined to find out how useful they might be for magneto-optical recording. The deposition of the layers and the determination of the relevant magnetic and magneto-optical properties take place mainly at the Philips Forschungslaboratorium in Hamburg. Layers with appropriate properties are used for making different types of discs for magneto-optical recording. Work on evaluating these discs and improving the recording is carried out mainly at Philips Research Laboratories in Eindhoven.

It was found that good discs can be made with an amorphous alloy of gadolinium, terbium and iron [7][8] on a glass substrate coated with a lacquer layer, with a pregrooved structure for tracking by the laser beam [9]. In addition an anti-reflection layer can be sandwiched between the lacquer layer and the recording layer and a protective coating is necessary. With such discs information can be reliably written, read out and erased at a rate of say 4 Mbit/s. No sign of degradation is observed after writing and erasing more than 10^6 times. The attainable signal-to-noise ratio at a bandwidth of 30 kHz and a linear track velocity of 5 m/s is about 50 dB. The life of the discs and the information stored in them is estimated to be longer than five years. This provides good prospects for storing large amounts of information in the form of alphanumeric data and digital audio signals. With a further improvement in the signal-to-noise ratio, video signals could also be recorded.

In this article we shall first describe two magneto-optical recording systems. We shall go into more detail than in the article about the DOR system [2], which referred to the articles about the LaserVision [10] and Compact Disc [11] systems. Besides the various components of the disc and the recorder, some important aspects of writing, read-out and erasure will be covered. We shall then discuss the investigation of materials for the recording layer, testing the discs, especially during ageing, and possible applications.

Magneto-optical recording systems

The principle of magneto-optical recording is shown in *fig. 1*. As in the Philips DOR system described earlier [2][9], the recording layer is applied on a pre-

grooved substrate. The groove is made in a substrate of a material such as polymethyl methacrylate (PMMA) or in a photo-polymerizable lacquer layer (2p layer [10][12]) on a glass substrate. During writing, read-out and erasure, the groove is accurately tracked by the laser beam, incident from the substrate side. The groove may contain pits with address information and a profile for synchronization.

An example of a magneto-optical recording system is shown schematically in *fig. 2*. A modulated AlGaAs laser provides a beam of light at a wavelength of say 850 nm. About 40% of the light emitted is collected by an objective with a numerical aperture (NA) of 0.3. The astigmatism of the laser beam is corrected by means of a cylindrical lens. The parallel beam is focused on the disc by an objective with $NA = 0.6$. At the recording layer the power of the beam is about 20% of the emitted power. Behind the disc there is a coil for generating the magnetic field. A characteristic value for the magnetic field-strength at the 'write' position is 4×10^4 A/m. Some of the light reflected by the disc is used for positioning the laser beam and focusing it on the disc.

For read-out the laser beam first passes through a polarizing beam-splitter before being focused on the disc. This splitter transmits the parallel component of

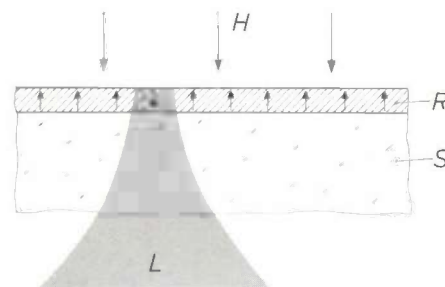


Fig. 1. Schematic representation of magneto-optical recording. The focused laser beam L , which passes through the substrate S to the magnetic recording layer R , produces a local reversal of the magnetization in the direction of the external magnetic field H .

polarization, while the perpendicular component is reflected. The linearly polarized light transmitted is incident on a Faraday rotator, which slightly rotates the plane of polarization. Because of the Kerr effect, the reflection from the recording layer results in a polarization rotation of $\pm \theta_K$, which depends on the local direction of magnetization. The light then passes through the Faraday rotator again and re-enters the beam-splitter. The parallel component is transmitted and used for tracking and focusing, while the perpendicular component is reflected on to an avalanche photodiode. The amplitude fluctuation of this component resulting from the polarization rotation through

$\pm \theta_K$ (fig. 2), provides the read-out signal after squaring.

Now that more powerful AlGaAs lasers are available, the use of a neutral (i.e. polarization-independent) beam-splitter has also become a possibility; see fig. 3. The light reflected for detection then goes through a $\frac{1}{2}\lambda$ plate whose principal axis is at an angle of 22.5° to the original direction of polarization. This causes a rotation of the plane of polarization by 45° , with a modulation of $\pm \theta_K$. A polarizing beam-splitter splits the light into parallel and perpendicular components of almost equal intensity, which are detected by the diodes D_1 and D_2 . In the detection process the

PIN diodes can be used for detection, and the effect of birefringence (e.g. in the substrate) is relatively weak. Furthermore, a pattern of pits (e.g. address information) can easily be read out by detecting the signal sum. The experiments described in this article were mainly carried out with the arrangement shown in fig. 2. We shall now discuss some of the aspects of writing, read-out and erasure in more detail.

Writing

The magneto-optical writing of information can be performed with a pulse duration of 50 ns and a laser power of about 15 mW at the disc. The laser energy

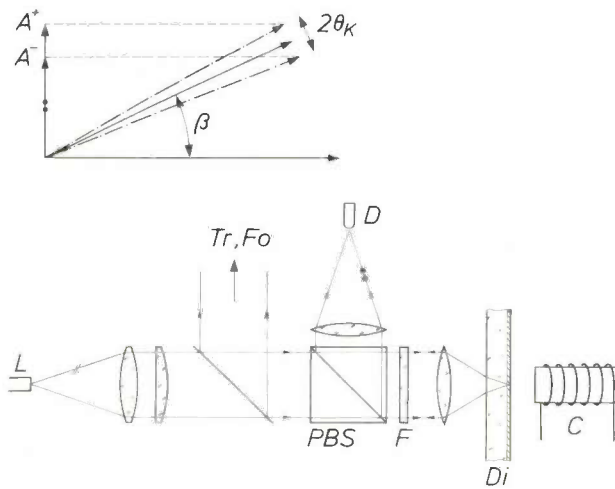


Fig. 2. Schematic arrangement for magneto-optical recording and the light paths during writing, read-out and erasure. The light coming from the laser L is collimated to a parallel beam by an objective ($NA = 0.3$) and a cylindrical lens. The beam is focused by a different objective ($NA = 0.6$) on to the magnetic recording layer of a disc Di , located in a magnetic field produced by a coil C . During writing and erasure the direction of magnetization in the recording layer is reversed locally. A polarizing beam-splitter PBS transmits the parallel polarization component and reflects the perpendicular component. The beam passes through the Faraday rotator F twice, giving a total rotation β of the plane of polarization of the laser light. Read-out is based on the polarization rotation $\pm \theta_K$, which depends on the direction of magnetization in the recording layer. This polarization rotation gives an amplitude fluctuation A^+ , A^- of the perpendicular polarization component reflected on to detector D . Some of the light reflected by the recording layer is used for tracking Tr and focusing Fo .

angular modulation $\pm \theta_K$ is converted into amplitude fluctuations at D_1 and D_2 (fig. 3). Since these are in opposite phase, the signal difference between D_1 and D_2 forms a sensitive read-out signal. Variations in laser intensity and disc reflectance, for example, are compensated by dividing by the signal sum.

This differential detection method results in a signal-to-noise ratio theoretically a little lower, but it does have some important practical advantages. Because of the high intensity of the read-out signal, simple

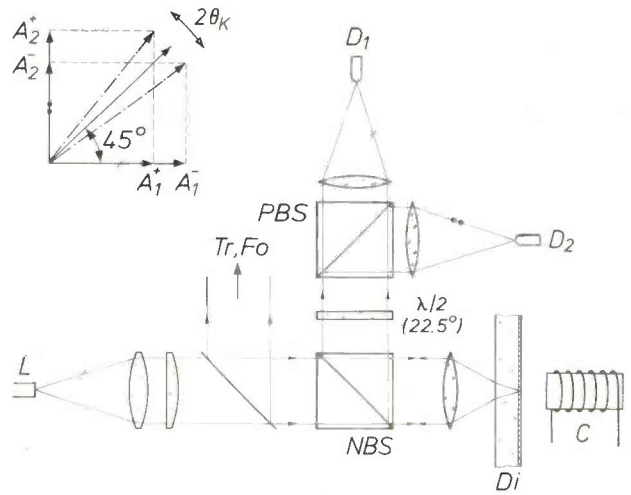


Fig. 3. A different arrangement for magneto-optical recording, and the associated light paths. The arrangement does not contain a Faraday rotator and instead of the polarizing beam-splitter in fig. 2 there is a neutral (i.e. polarization-independent) beam-splitter NBS . On read-out the local reversal of magnetization and a $\frac{1}{2}\lambda$ plate rotate the polarization by $45^\circ \pm \theta_K$. The polarizing beam-splitter PBS splits the light into parallel and perpendicular components, which are detected by D_1 and D_2 . Here the modulation $\pm \theta_K$ produces amplitude fluctuations A_1^+ , A_1^- and A_2^+ , A_2^- . The rest of the arrangement is the same as in fig. 2.

[5] P. Chaudhari, J. J. Cuomo and R. J. Gambino, IBM J. Res. & Dev. 17, 66-68, 1973;
 Y. Mimura, N. Imamura and T. Kobayashi, Jap. J. Appl. Phys. 15, 181-182, 1976.
 [6] This work was done at the Philips Research Laboratories in Eindhoven, by J. W. M. Biesterbos, M. R. de Bont, A. G. Dirks, M. Farla and others. An account of the work on vacuum-deposited amorphous layers of transition metals and rare-earth metals can be found in J. W. M. Biesterbos, J. Physique 40 (Colloque C5), C5/274-C5/279, 1979.
 [7] J. Braat, K. Schouhamer Immink and M. Urner-Wille, Proc. SPIE 420, 206-214, 1983.
 [8] M. Hartmann, J. Braat and B. Jacobs, IEEE Trans. MAG-20, 1013-1018, 1984.
 [9] K. Bulthuis, M. G. Carasso, J. P. J. Heemskerk, P. J. Kivits, W. J. Kleuters and P. Zalm, IEEE Spectrum 16, No. 8 (August), 26-33, 1979.
 [10] H. C. Haverkorn van Rijsewijk, P. E. J. Legierse and G. E. Thomas, Philips Tech. Rev. 40, 287-297, 1982.
 [11] Special issue of Philips Tech. Rev. 40, 149-180, 1982.
 [12] J. G. Kloosterboer, G. J. M. Lippits and H. C. Meinders, Philips Tech. Rev. 40, 298-309, 1982.

locally incident on the recording layer is partly absorbed. This causes an increase in temperature such that the magnetization direction is reversed in the direction of the external magnetic field. After the laser pulse the temperature decreases again, and the energy absorbed is dissipated to the substrate by thermal conduction.

For writing on the disc the data bits to be recorded are first converted into 'channel bits'. Various modulation systems can be used [13]. An important criterion

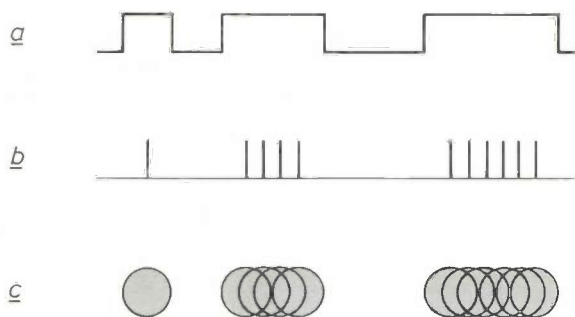


Fig. 4. *a)* Binary Compact Disc signal to be recorded. *b)* Pulse train derived electronically from the Compact Disc signal. The pulse train determines the position of the unit magnetic domains by the laser being switched on and off. *c)* The domain pattern obtained. If unit domains overlap there are variations in the domain length.

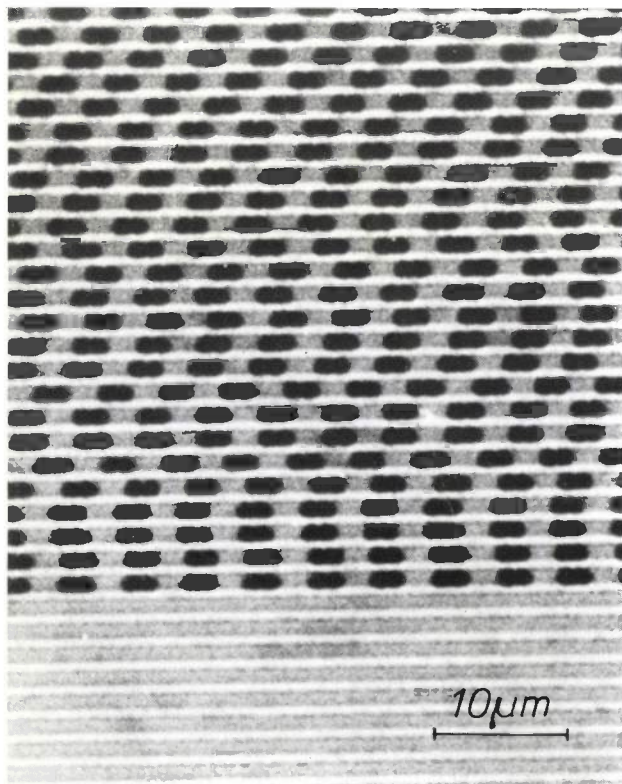


Fig. 5. Magnetic domains written in a pregrooved structure (track spacing $\approx 1.7 \mu\text{m}$) and made visible by a polarization microscope. The domains (dark) are about $2 \mu\text{m}$ long.

for the choice of the modulation system is the attainable information density on the disc. The density is increased if adjacent domains are allowed to overlap. This can be reliably achieved by means of a pulsed laser beam. As an example, *fig. 4* shows the recording process for a binary Compact Disc signal. From the input signal, which has a specific channel bit length, a pulse train is derived electronically. This determines the position of the unit domains in the recording layer by switching the laser on and off. Different overlaps of the unit domains give a pattern with a variable domain length.

The shape and dimensions of the written domains also depend on the diameter of the laser beam and the linear velocity of the disc. The domains are visible under a polarization microscope. *Fig. 5* shows a polarization-microscope photograph of domains written in a pregrooved structure with a track spacing (pitch) of $1.7 \mu\text{m}$. Because of a rapid succession of laser pulses the domains are elongated; the domain length in the direction of the grooves is about $2 \mu\text{m}$.

Read-out

During read-out the laser power is so much lower (e.g. by a factor of 10) than during writing that the stored information is not affected. The laser is pulsed so fast that even the highest frequency in the data stream can be reliably read out. The intensity modulation of the signal resulting from the polarization rotation through $\pm \theta_K$ corresponds to a transition between a '0' and a '1' in the stored information.

One method of assessing the signal quality is by means of an 'eye pattern'. This can be obtained by superimposing the signals from successive periods on an oscilloscope. If a wide eye-opening is obtained it is easy to decide whether a signal corresponds to a '1' or to a '0'. *Fig. 6* shows an eye pattern of a digital signal supplied by an avalanche photodiode during magneto-optical recording. The eye-opening here is wide and high, so that a reliable read-out is possible.

The carrier-to-noise ratio (CNR) increases as the Kerr rotation θ_K of the recording layer increases. Another important factor is the total polarization rotation β (*fig. 2*) produced by the Faraday rotator. The highest value is obtained when β is between 2 and 3° . At a smaller angle the read-out signal is too weak since too little light is incident on the detector, whereas at larger angles the effect of noise is increased. The main sources of noise are photon noise and disc noise. An example of the effect of these noise sources on CNR is shown in *fig. 7*. When β is small ($\approx 3^\circ$), the noise consists almost entirely of photon noise and CNR may be fairly high ($> 50 \text{ dB}$). At larger angles the disc noise causes a considerable drop in CNR.

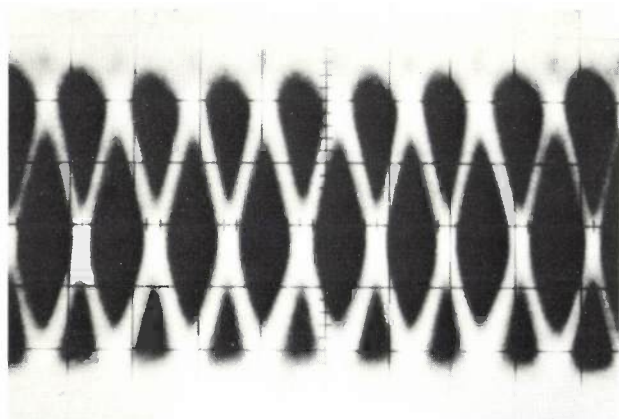


Fig. 6. An oscillogram of the eye pattern of a digital signal from an avalanche photodiode during read-out of information. The linear track velocity is 3 m/s. The width of an eye-opening is about 230 ns.

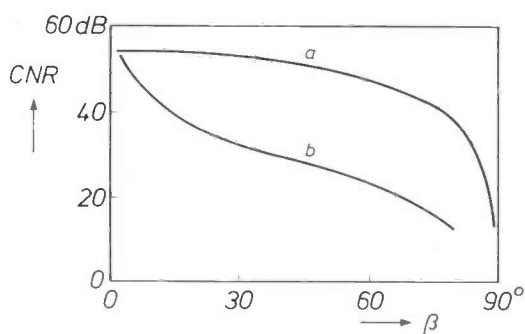


Fig. 7. The carrier-to-noise ratio *CNR* calculated for a bandwidth of 30 kHz during read-out, as a function of the polarization rotation β by the Faraday rotator (fig. 2). In the absence of disc noise (*a*) a high *CNR* is obtained at low β -values. The noise is then made up almost entirely of photon noise. The disc noise introduces a sharp decrease in *CNR* (*b*); this is most noticeable at high values of β . The 'read-out power' at the disc has been taken as 1 mW; the signal period is about 3 μ m.

This problem can be avoided by using differential detection and signal normalization (fig. 3). The polarization rotation β due to the $\frac{1}{2}\lambda$ plate is 45° , so that from curve *a* in fig. 7 the theoretically attainable *CNR* is only 3 dB lower than for detection at low β .

During ageing the disc noise increases because of changes in the structure and the magnetic and optical properties of the recording layer. This is one of the main problems now being studied.

Erasure

During the erasure of recorded information the external magnetic field has the same direction as the original magnetization. Erasure has not been found to have any adverse effect on a later recording: read-out of rewritten information again gives the same signal-to-noise ratio. However, the replacement of old information by new in the two stages of erasure and re-

writing has the disadvantage that it is difficult to carry out in real time, so that high data bit rates cannot be obtained.

In principle the new information can be written over the old by modulating the direction of the magnetic field at a constant laser power. Unfortunately this does not work well at high signal frequencies (> 200 kHz), because the magnetic field cannot be switched so quickly in this configuration. High bit rates can be obtained for example by using an optical system with two light spots, which are focused via a single objective on to two adjacent tracks; see fig. 8. One light spot, the erase spot, is permanently on, so that the magnetization takes the same direction as the external magnetic field along the entire track. The

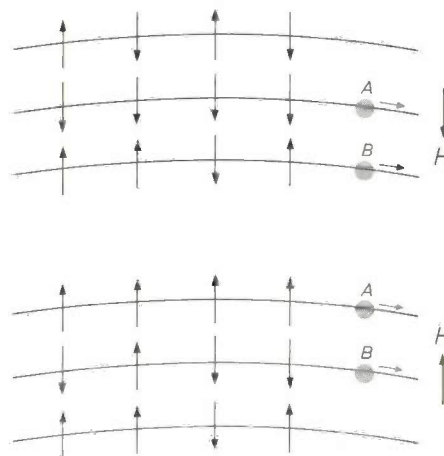


Fig. 8. Simultaneously erasing old information and writing new information with two light spots on adjacent tracks. The erase spot *A* is permanently on so that the direction of magnetization becomes the same as that of the external magnetic field *H* along the entire track. The write spot *B* is modulated by the information to be recorded, so that the direction of magnetization is reversed locally. After one revolution of the disc the direction of the magnetic field is reversed. New information is now written into the track that has just been erased, while the old information is erased from the next track.

other one, the write spot, is modulated by the information to be recorded, so that the direction of magnetization is reversed locally. After one revolution of the disc the direction of the external magnetic field is reversed. The write spot moves to the track that was completely erased during the previous revolution so that its direction of magnetization is now opposite to that of the magnetic field. Meanwhile the erase spot is focused on to the next track so that its magnetization again takes the same direction as the magnetic field. In this way the domains written in successive tracks have a different direction of magnetization.

[13] J. P. J. Heemskerck and K. A. Schouhamer Immink, Philips Tech. Rev. 40, 157-164, 1982.

PHILIPS RESEARCH LABS
 5600 AZ Eindhoven
 THE NETHERLANDS

Materials for the recording layer

In the recording layer magnetic domains should form at places where there are local increases of temperature. These domains must not affect the magnetization in the rest of the layer. They must also be stable at room temperature, which means that they should not become larger or smaller during read-out or erasure elsewhere in the layer. For good magneto-optical contrast during read-out, a large Kerr rotation θ_K is necessary.

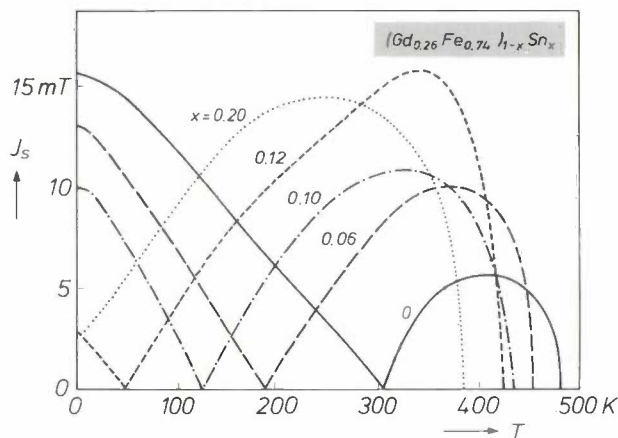


Fig. 9. Magnetic saturation polarization J_s as a function of temperature T , for layers of gadolinium, iron and tin of the composition $(\text{Gd}_{0.26}\text{Fe}_{0.74})_{1-x}\text{Sn}_x$. A change in the tin content x strongly affects J_s as well as the compensation temperature and Curie point.

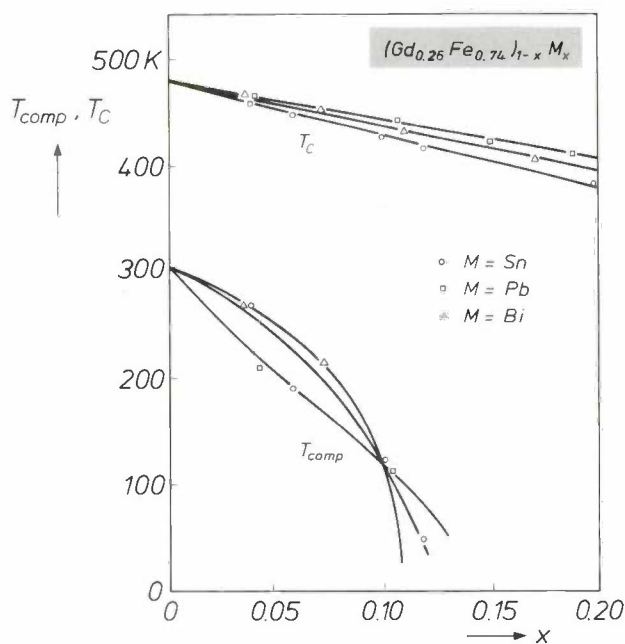


Fig. 10. Effect of the composition on the compensation temperature T_{comp} and the Curie point T_C , for layers of the composition $(\text{Gd}_{0.26}\text{Fe}_{0.74})_{1-x}\text{M}_x$, where $M = \text{Sn}, \text{Pb}, \text{Bi}$. An increase in the M content x causes a sharp decrease in T_{comp} and a slight linear decrease in T_C .

An important parameter for writing and erasing is the magnetic saturation polarization J_s of the layer. As J_s increases, the writing can take place in a weaker external magnetic field, because the demagnetizing energy (proportional to J_s^2) is higher. Erasure, on the other hand, requires a stronger magnetic field, because the demagnetizing energy stabilizes the reversed direction of magnetization. An important factor for the stability of written information is the coercivity H_c , i.e. the minimum external magnetic field-strength to reverse an induced magnetization. A high coercivity at room temperature improves the stability of small domains. A parameter related to the coercivity is the uniaxial magnetic anisotropy constant K_u , i.e. the energy required to bring the direction of magnetization perpendicular to the preferred axis.

There are several methods for magneto-optical writing, depending on the changes in these parameters at higher temperatures [14]. In 'Curie-point writing' the recording material is heated locally to close to its Curie point T_C . Under the influence of the demagnetizing field and an opposing external magnetic field (if necessary), the direction of magnetization becomes opposite to that of the non-irradiated environment. When the material cools to room temperature the new direction is 'frozen in'. With some materials the magnetization direction can be reversed even far below T_C by utilizing the decrease in H_c at higher temperatures. For a magnetic field of field-strength H , magnetization reversal will then occur as soon as $H_c < H$; on cooling this reversal is 'frozen in' again. A special case is 'compensation-point writing' in some ferrimagnetic materials [15]. These have a compensation temperature $T_{\text{comp}} (< T_C)$ at which the magnetic moments of the sublattices completely compensate one another. In the neighbourhood of T_{comp} , H_c has a very high value; above it H_c decreases rapidly with the temperature.

In our investigation we are studying the suitability of different ferrimagnetic alloys for magneto-optical recording. Amorphous layers of these alloys can be applied by vacuum electron-beam deposition, in which the separate elements are deposited simultaneously from the vapour phase on rotating substrates [16]. To produce homogeneous layers with the required composition the partial vaporization rate of each of the elements is carefully controlled. The preparative conditions are adjusted to give layers with a strong uniaxial magnetic anisotropy, with the preferred direction perpendicular to the surface.

The magnetic properties of the layers can be strongly influenced by means of the composition [8][17]. To give an example, *fig. 9* shows the magnetic saturation magnetization J_s plotted against temperature for some alloys of gadolinium, iron and tin. At low tempera-

tures an increase in tin content causes a drastic reduction in J_s , whereas at higher temperatures considerably higher values are obtained. The effect of the composition on T_{comp} and T_C is shown in *fig. 10*. For a higher content of tin, lead or bismuth T_{comp} decreases

relevant properties. The addition of a small amount of terbium produces an increase in K_u and H_c . The combination with cobalt produces an increase in θ_K and T_C , but K_u and H_c become significantly lower. Alloys of terbium with cobalt have good properties,

Table I. Material properties of some vacuum-deposited layers for magneto-optical recording. The table shows the measured room-temperature values of the magnetic saturation polarization J_s , the magnetic uniaxial anisotropy constant K_u , the coercivity H_c and the Kerr rotation θ_K (at a wavelength of 850 nm), as well as the compensation temperature T_{comp} and the Curie point T_C .

Composition	J_s (mT)	K_u ($\times 10^4$ J/m ³)	H_c ($\times 10^5$ A/m)	θ_K (°)	T_{comp} (K)	T_C (K)
Gd _{0.24} Fe _{0.76}	6	2.5	0.4	0.38	300	480
(Gd _{0.95} Tb _{0.05}) _{0.24} Fe _{0.76}	8	5.3	1.6	0.30	230	460
(Gd _{0.95} Tb _{0.05}) _{0.24} (Fe _{0.95} Co _{0.05}) _{0.76}	3	1.2	0.2	0.36	230	580
Tb _{0.18} Co _{0.82}	25	16	1.4	0.45	—	—

sharply, while T_C shows only a slight linear decrease. The decrease in T_{comp} implies a reduction in H_c at room temperature.

Our investigations revealed that good layers for magneto-optical recording can be obtained by combining gadolinium and iron with a little terbium or cobalt or both. *Table I* shows the effects on the

but above 390 K irreversible changes take place. In view of the various requirements for magneto-optical recording, the compound (Gd_{0.95}Tb_{0.05})_{0.24}Fe_{0.76} appears to be a good compromise.

The temperature dependence of the demagnetizing energy E_d , and the uniaxial anisotropy constant K_u of this alloy are given in *fig. 11*. The demagnetizing energy E_d is at its maximum between T_{comp} and T_C , whereas K_u decreases monotonically with the temperature. These temperature dependences, together with that of the magnetic saturation polarization, determine the marked decrease of the coercivity H_c with temperature, also shown in *fig. 11*. With an external magnetic field of say 4×10^4 A/m the recording is achieved not by compensation-point writing but by Curie-point writing. Changes in T_{comp} and H_c , in a slightly modified composition, do not therefore have any marked effect on writing behaviour. The stability of the domains depends on H_c . Owing to the high value of H_c at room temperature, small domains (with a diameter of about 1 μm) can be very stable.

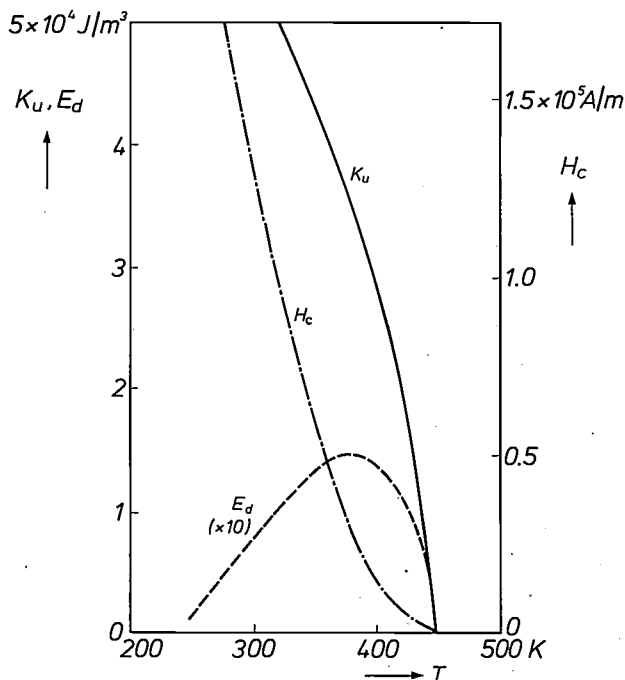


Fig. 11. Uniaxial anisotropy energy K_u , demagnetizing energy E_d and coercivity H_c as a function of the temperature T for a layer of composition (Gd_{0.95}Tb_{0.05})_{0.24}Fe_{0.76}. Between the compensation temperature and the Curie point E_d has a maximum while K_u and H_c decrease sharply with temperature.

[14] See for example P. Dekker, IEEE Trans. MAG-12, 311-327, 1976.

[15] 'Compensation-point writing' has been dealt with earlier in this journal: see:

H. Heitmann, B. Hill, J.-P. Krumme and K. Witter, MOPS, a magneto-optic storage wafer of the discrete-bit type, Philips Tech. Rev. 37, 197-206, 1977;

P. Hansen, B. Hill and W. Tolksdorf, Optical switching with bismuth-substituted iron garnets, Philips Tech. Rev. 41, 33-45, 1983/84.

[16] More information on the preparation and properties of amorphous alloys is given in: K. H. J. Buschow, this issue, pp. 48-57.

[17] P. Hansen and M. Urner-Wille, J. Appl. Phys. 50, 7471-7476, 1979;

M. Urner-Wille, P. Hansen and K. Witter, IEEE Trans. MAG-16, 1188-1193, 1980.

Investigations of discs

Various discs with layers of $(\text{Gd}_{0.95}\text{Tb}_{0.05})_{0.24}\text{Fe}_{0.76}$ were produced in order to study recording characteristics and ageing behaviour. The layers were applied to a glass substrate that had previously been coated with a 2p layer about 10 μm thick. This contained a spiral groove with a pitch of about 1.7 μm . The re-

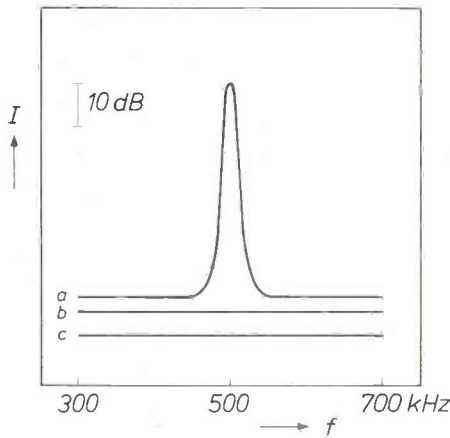


Fig. 12. The signal power I , measured at a bandwidth of 10 kHz, plotted against the frequency f at a linear track velocity of 3 m/s (curve a). The noise level is -50 dB with respect to the signal at 500 kHz. For a stationary disc, the noise level has decreased to -54 dB because of the absence of disc noise (curve b). The noise level due to the dark current and the gain is -60 dB (curve c).

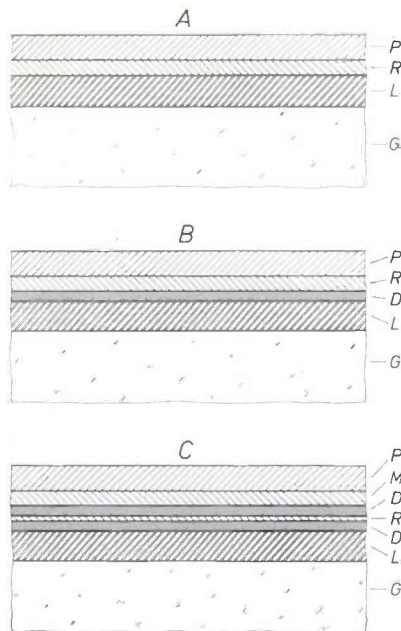


Fig. 13. Schematic sectional view of three layer configurations for a magneto-optical disc. The configurations contain a glass substrate G , a 10- μm 2p lacquer layer L , a recording layer R of $(\text{Gd}_{0.95}\text{Tb}_{0.05})_{0.24}\text{Fe}_{0.76}$ and a protective layer P . Configuration A (the standard design) has no other layers. Configuration B has a dielectric anti-reflection layer D between the 2p layer and the recording layer. Configuration C has a thinner recording layer (15 to 20 nm), two dielectric layers D and a highly reflective layer M .

Table II. Some characteristic values for the reflectance R , the Kerr rotation θ_K and the carrier-to-noise ratio CNR at a bandwidth of 30 kHz and a linear track velocity of 10 m/s, for the three configurations in fig. 13.

Configuration	R (%)	θ_K ($^\circ$)	CNR (dB)
A	46	0.35	47
B	16	1.0	50
C	4	2.8	53

cording layer was covered with a protective layer. For writing and read-out, the experimental recorder shown in fig. 2 is used. To determine the carrier-to-noise ratio (CNR) a carrier signal with a frequency of 500 kHz is recorded while the disc rotates at a constant linear velocity. Writing and read-out take place both before and after the discs have been aged.

In fig. 12, the measured signal power from a disc is plotted against the frequency. At a bandwidth of 10 kHz and a linear track velocity of 3 m/s, a characteristic value of 50 dB is obtained. Some of the noise is due to the surface roughness of the disc. This contribution can be determined by measuring a stationary disc. The level of the remaining noise, primarily photon noise, is -54 dB with respect to the carrier signal. The noise level associated with the dark current and the gain is even lower (-60 dB).

To obtain a high CNR , the reflectance R and the Kerr rotation θ_K must be such that $R\theta_K^2$ is high [7]. To obtain a good compromise between R and θ_K , discs with various layer configurations were examined. The three shown in fig. 13 contain a glass substrate, a 2p lacquer layer, a recording layer and a protective layer. In the 'standard' configuration A there are no other layers. In the configuration B there is a dielectric anti-reflection layer between the 2p lacquer and the recording layer. The configuration C has two dielectric layers on either side of the recording layer and a highly reflective layer of aluminium or gold. The recording layer in C is considerably thinner than the one in A and B (≤ 20 nm as against about 80 nm). Table II shows some characteristic results obtained with these configurations. For B , the reduced reflectance is compensated by an increase in θ_K such that CNR becomes higher. For C this effect is even more pronounced, and results in a further increase in CNR . The poor reflectance of C , however, poses problems in the focusing and tracking.

Ageing behaviour

The optical and magnetic properties of unprotected recording layers are highly sensitive to oxidation and microscopic structural changes. Thin layers with a

thickness of < 50 nm are generally less stable than thicker layers. To study the ageing behaviour, discs are stored under differing conditions: in a standard environment at room temperature, in a dry environment at higher temperatures and in a humid environ-

ment (relative humidity $\approx 93\%$) at temperatures fluctuating between 25 and 65 °C as specified in the cyclic Z/AD test [18]. Properties determined before and after ageing include T_{comp} , H_c , θ_K and CNR.

During ageing oxidation occurs in the recording layers as a result of the diffusion of oxygen. This diffusion increases at higher temperatures. This can be determined by the SIMS analysis method (Secondary Ion Mass Spectrometry) [19], in which the oxygen content of the recording layer is determined as a function of the depth in the material. Fig. 14 shows the depth profiles measured for a layer 150 nm thick immediately after deposition and after being kept for 15 hours in a dry environment at various temperatures. In a fresh layer oxidation is mainly confined to a surface film. At a depth greater than about 50 nm the oxygen content has a low and virtually constant level (0.2% by wt.), which is determined by the residual gas pressure during deposition of the layer. As the heating temperature is increased the oxygen penetrates further into the layer. At 520 K the oxygen content is about 4% by wt. In this case there is a strongly oxidized surface film of about 20 nm.

When chemical or structural changes occur during ageing the coercivity is found to decrease sharply, particularly with thin recording layers [20]. This is the case with configuration C in fig. 13, in which the recording layer is no thicker than 20 nm. Fig. 15 shows the hysteresis loop of the Kerr rotation θ_K , before and after ageing. The hysteresis loop before ageing is fairly wide: $H_c \approx 3 \times 10^5$ A/m. After ageing for 30 days in a standard environment and a one-day Z/AD test, the hysteresis loop has become much narrower: H_c has decreased to $< 8 \times 10^4$ A/m.

The effect on H_c depends not only on the ageing conditions but also to a large extent on the disc configuration; see fig. 16. Configuration B still has a relatively high H_c after a 30-day Z/AD test. Configuration C, on the other hand, with its extremely thin recording layer, gives a sharp decrease in H_c even in a standard environment. This performance could undoubtedly be improved by using dielectric layers that are less rapidly penetrated by oxygen.

For all configurations the Kerr rotation is found to be fairly insensitive to ageing; see fig. 17. Since the Kerr rotation is determined almost entirely by the Fe atoms, we can assume that these are only slightly oxidized during the ageing, and that the decrease in H_c is mainly the consequence of oxidation of the Gd atoms.

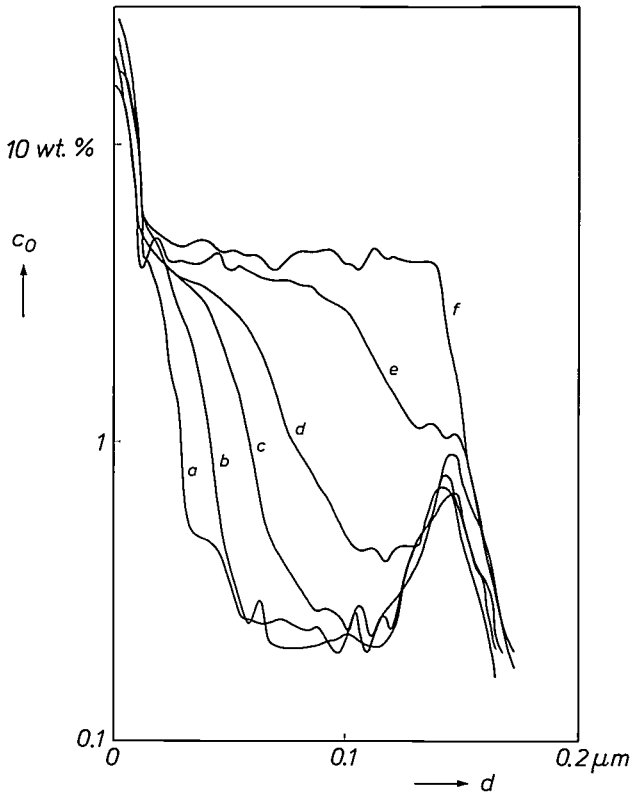


Fig. 14. The oxygen content c_o , determined by SIMS, as a function of the depth d in a 150-nm layer of $(\text{Gd}_{0.95}\text{Tb}_{0.05})_{0.24}\text{Fe}_{0.76}$. The measurements were made immediately after deposition (a) and after heat treatment in a dry atmosphere at 370 K (b), 430 K (c), 475 K (d), 500 K (e) and 520 K (f). At higher temperatures, oxygen penetrates more deeply into the layer.

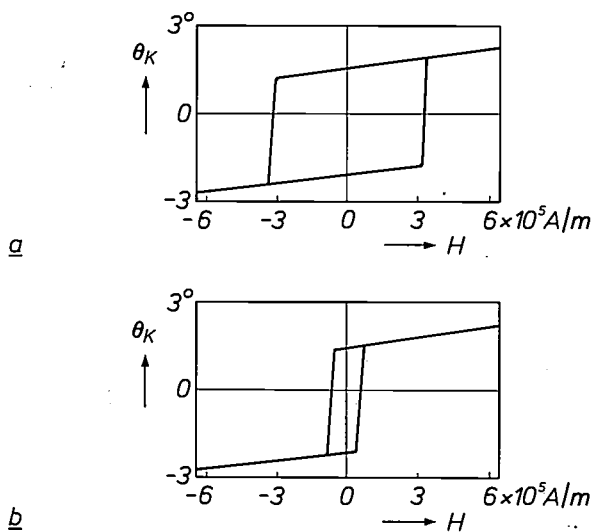


Fig. 15. Hysteresis loops of the Kerr rotation θ_K for the configuration C in fig. 13. a) Before ageing. b) After ageing for 30 days in a standard environment and a one-day Z/AD test. The hysteresis loop becomes considerably narrower with ageing.

[18] IEC Publ. No. 68-2-38, Test Z/AD: Composite temperature/humidity cyclic test, IEC, Geneva 1974.

[19] See for example H. H. Brongersma, F. Meijer and H. W. Werner, Philips Tech. Rev. 34, 357-369, 1974.

[20] B. Jacobs, J. Braat and M. Hartmann, App. Opt. 23, 3979-3982, 1984.

The value of *CNR* is fairly sensitive to ageing. This can be attributed not only to a decrease in H_c , but also to the increase in disc noise. During ageing pin-holes may form in the recording layer and some local crystallization may occur. Configuration *C* soon gives a sharp decrease in *CNR*, even in a standard environment, see *fig. 18*. With *A*, in a hermetically sealed Air Sandwich [21][21], and *B* virtually no decrease in *CNR*

is found in a standard environment. In the Z/AD test *A* and *B* do show a slight decrease as the result of increasing disc noise, as illustrated for *A*.

It can be concluded from the various experiments that with a suitable configuration the discs and the information stored in them will have sufficient life. Discs hermetically sealed as an Air Sandwich [21] should have a life of more than ten years.

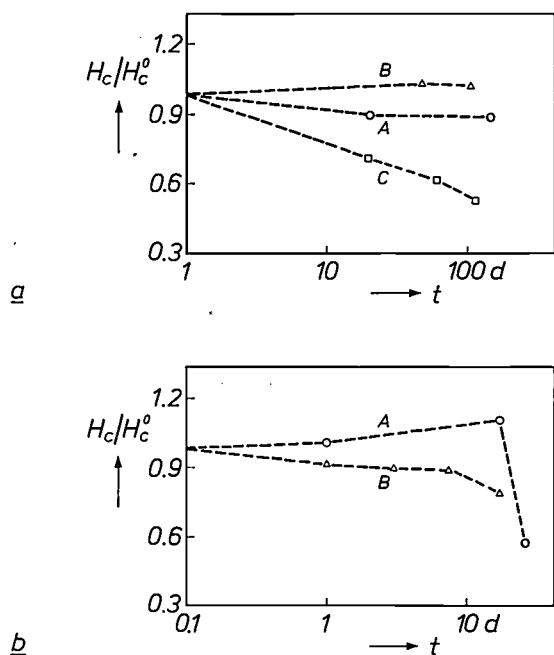


Fig. 16. Effect of ageing upon the coercivity H_c (with initial value H_c^0) for the three configurations in *fig. 13*. The ratio H_c/H_c^0 is plotted against the ageing time t in a standard environment (a) and in a Z/AD test (b). Even in a standard environment configuration *C* gives a sharp decrease. Configuration *B* still has a reasonably high H_c even after a 30-day Z/AD test.

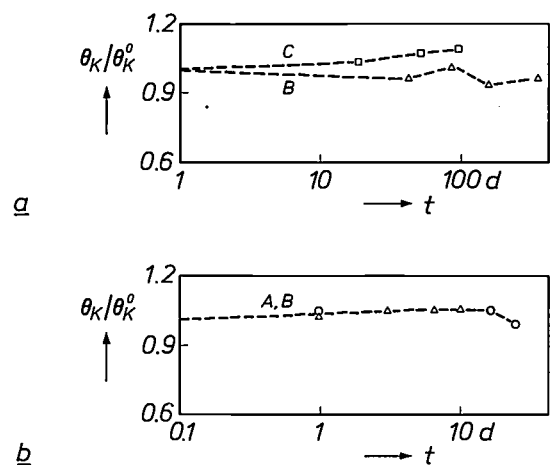


Fig. 17. Comparison between the Kerr rotation after ageing (θ_K) and before ageing (θ_K^0), plotted against the ageing time t in a standard environment (a) and in a Z/AD test (b), for the three configurations in *fig. 13*. The ageing process has little effect on the Kerr rotation.

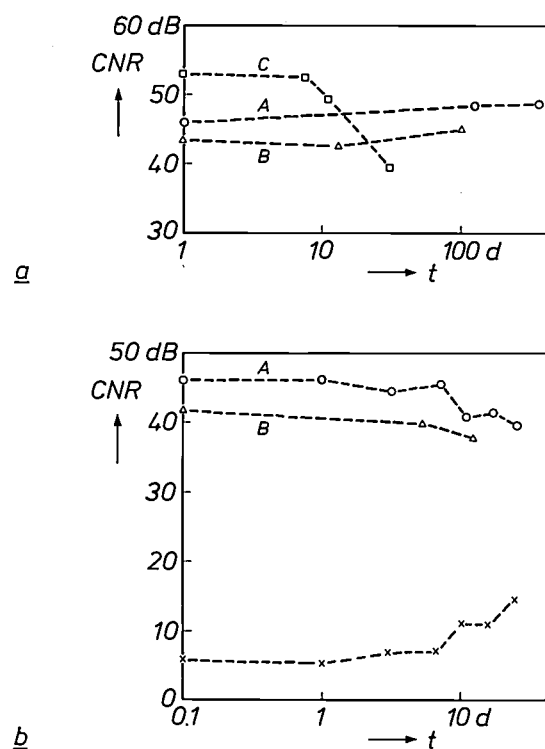


Fig. 18. Carrier-to-noise ratio *CNR* plotted against the ageing time t for the three configurations in *fig. 13*. a) Configuration *C*, unlike *A* (in a hermetically sealed Air Sandwich) and *B*, shows a sharp decrease in *CNR* even in a standard environment. b) In the Z/AD test, *A* and *B* show a slight decrease in *CNR* owing to increasing disc noise. This is indicated for *A* by crosses.

Applications

Applications in various fields can be envisaged for magneto-optical recording on discs. *Table III* mentions a few possibilities and also indicates the specifications for the data bit rate, the bit density, track velocity and *CNR*. In data bit rate, magneto-optical recording can match other optical recording systems. A higher data bit rate can be obtained simply by rotating the disc faster; a linear track velocity of say 20 m/s can be achieved. The bit density is primarily deter-

[21] G. C. Kenney, D. Y. K. Lou, R. McFarlane, A. Y. Chan, J. S. Nadan, T. R. Kohler, J. G. Wagner and F. Zernike, *IEEE Spectrum* 16, No. 2 (February), 33-38, 1979.

mined by the diameter of the laser beam and is at present of the order of 50 Mbit/cm². The main limitation for the moment is that the signal-to-noise ratio is not yet adequate for applications such as high-speed data recording and video recording.

Table III. Possible applications for magneto-optical recording and the specification for the data bit rate, data bit density, linear track velocity and carrier-to-noise ratio *CNR* (at 30 kHz).

Application	Data bit rate (Mbit/s)	Data bit density (Mbit/cm ²)	Track velocity (m/s)	<i>CNR</i> (dB)
Digital optical recording	20	50	20	55
	3	50	3	47
	0.2	5	0.4	35
Compact Disc	2	50	2.0	45
Video	[^a]	—	≥ 10	> 55

[^a] Analog: bandwidth 5 MHz.

In the work described here the authors cooperated with K. Witter (PFH) for the study of the materials, J. Reck (PFH) for the manufacture of the discs and J. Waelpoel (Philips Research Laboratories, Eindhoven) for the recording experiments.

Summary. In magneto-optical recording on discs the direction of magnetization is reversed locally in the recording layer by means of a laser and an external magnetic field. The magnetic domains thus obtained are read out via the change in the rotation of the plane of polarization on reflection of linearly polarized light (the Kerr effect). The recorded information can also be erased, with a domain then again acquiring the same direction of magnetization as its environment. A suitable material for the recording layer is an amorphous alloy with the composition (Gd_{0.95}Tb_{0.05})_{0.24}Fe_{0.76}. Small domains with a diameter of about 1 μm can be written in such a layer. The domains can be read out faithfully and are very stable. The recording layer is vacuum-deposited on a substrate with a pregrooved structure for tracking. Good results have been obtained with discs consisting of a glass substrate, a pregrooved lacquer layer, a recording layer, a protective layer and possibly an anti-reflection layer.

Research on amorphous alloys

K. H. J. Buschow

Alloys usually exist in the crystalline state, but they also occur in a metastable amorphous state in which there is no regular ordering of the atoms. In recent years there has been an immense increase of interest in amorphous alloys, as a consequence of continuous improvements in methods of preparation, and because of their special electrical, magnetic, mechanical and chemical properties. With the wide choice of compositions and the correspondingly wide variation in properties, amorphous alloys provide a rich field of fundamental and applied research in the science of materials.

Introduction

Metal alloys in common use are usually polycrystalline. This means that they are composed of a large number of crystallites that differ from each other in shape, dimensions and orientation and are separated by grain boundaries. Inside a crystallite the atoms are regularly ordered in the same way as in a single crystal. A metal alloy can also occur, however, in an amor-

phous state, the absence of long-range order can give rise to considerable differences in electrical, magnetic, mechanical and chemical properties.

Since the sixties various methods have been developed for obtaining metals in the amorphous state from the liquid or vapour phase. In general this has

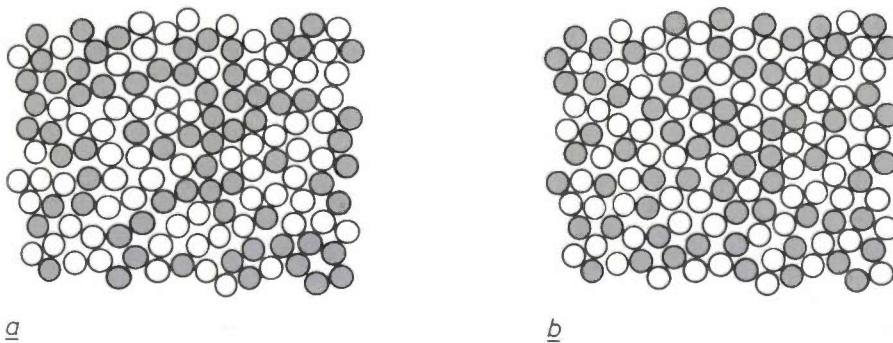


Fig. 1. Schematic two-dimensional representation of atomic structures of amorphous binary metal alloys. The atoms are shown as light and dark circles. *a*) Amorphous state with no atomic ordering. *b*) Amorphous state in which there is some ordering between the two types of atoms extending over short distances (short-range order).

phous state, in which there is no regular ordering of the atoms. The atoms of the different elements in the alloy then have a completely random distribution or some degree of short-range order in relation to one another; see *fig. 1*. Although in the amorphous state the distances between neighbouring atoms differ very

proved to be much easier with metal alloys than with metals in the pure form. It has also been found that amorphous alloys can offer advantages in a number of respects over crystalline alloys^[1]. For instance they are generally more resistant to corrosion and mechanical wear and they are tougher. Magnetic amorphous alloys often have much lower magnetic losses. Many of these advantageous properties stem from the ab-

Dr K. H. J. Buschow is with Philips Research Laboratories, Eindhoven.

sence of grain boundaries. Another advantage of amorphous alloys is that their composition can be varied throughout a wide range, so that certain properties can be optimized more satisfactorily than in crystalline alloys, where the choice is limited to compositions of a homogeneous range of miscibility or to intermetallic compounds.

When amorphous alloys are used it is necessary to take account of their metastable character. This is because the amorphous state of an alloy has a higher free energy than the corresponding crystalline state. This means that an amorphous phase may gradually and irreversibly be transformed into one or more stabler crystalline phases, generally resulting in undesirable changes in properties.

The potential applications of amorphous alloys are many and various [1][2]. Examples are soft-magnetic alloys for transformer cores, mechanically strong alloys as structural materials [3], corrosion-resistant alloys for protective coatings, magnetic alloys for magnetic and magneto-optical recording [4] and readily combustible alloys for flashbulbs [5]. The absence of separate crystallites and grain boundaries is essential for the application in thin films for magneto-optical recording. The reason is that, owing to the different orientation of the crystallites, polycrystalline layers have too little magneto-optical homogeneity, and the grain boundaries introduce additional noise, which decreases the signal-to-noise ratio when the information is read out. During the writing of information amorphous alloys have the additional advantage of a low thermal conductivity, so that the required local reversal of the direction of magnetization can take place at a lower laser power. Elsewhere in this issue a detailed description is given of erasable magneto-optical recording in an amorphous alloy of gadolinium, terbium and iron [6].

In the research described in this article widely diverse amorphous alloys are being made and their properties investigated for a variety of applications. Rules and models developed over the years for alloys [7] are used for interpreting the results. In view of the metastable character of amorphous alloys particular attention is paid to their thermal stability. The electron distribution in the alloys is also of importance in explaining their properties and perhaps improving them. This applies especially to the magnetic behaviour, which has to be readily controlled in certain applications. The research has provided a better understanding of the thermal stability, electron distribution and magnetic properties of amorphous alloys. Before taking a closer look at some results, we shall first briefly describe how amorphous alloys are made and how they can be characterized.

Preparation and characterization

Amorphous alloys can be obtained by means of very rapid cooling (quenching) from the liquid or vapour phase. As a result the atomic disorder prevailing in these phases becomes 'frozen' into the solid alloy. The quenching methods that have been developed differ from each other in the choice of the initial state and in the method of cooling [8]. Other preparative methods are also in use, such as electrochemical deposition and ion implantation, but these will not be dealt with here.

In a commonly used method starting from the liquid phase a piece of alloyed metal is melted by radio-frequency heating. This is done in a silica tube provided with a small orifice. An excess pressure of argon forces the liquid metal through the orifice on to a rotating copper wheel; see *fig. 2*. In many alloys the rapid cooling that then occurs freezes in the disordered liquid state before crystallization can set in. Amorphous alloys obtained by quenching from the melt are often called 'metallic glasses'.

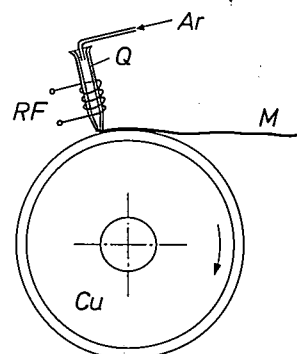


Fig. 2. Producing an amorphous alloy from the liquid phase. A piece of alloyed metal in a silica tube *Q* is melted by radio-frequency heating (*RF*). An excess pressure of argon (*Ar*) then forces the melt through a narrow orifice on to a rotating copper wheel (*Cu*). This quenches the liquid so rapidly that the disordered state of the liquid phase is 'frozen in' and a metallic strip *M* of an amorphous alloy ('metallic glass') is formed.

- [1] K. H. J. Buschow, *Ned. T. Natuurk. A* **47**, 86-90, 1981.
 [2] K. H. J. Buschow, *J. Less-Common Met.* **100**, 29-48, 1984.
 [3] J. W. Drijver and S. Radelaar, *Ned. T. Natuurk. A* **44**, 10-14, 1978.
 [4] A. H. Bobeck and H. E. D. Scovil, *Sci. Am.* **224**, No. 6 (June), 78-90, 1971;
 P. Chaudhari, J. J. Cuomo and R. J. Gambino, *IBM J. Res. & Dev.* **17**, 66-68, 1973;
 R. Hasegawa and R. C. Taylor, *J. Appl. Phys.* **46**, 3606-3608, 1975.
 [5] H. C. M. van den Nieuwenhuizen and K. H. J. Buschow, *High Temp. Sci.* **15**, 301-309, 1982.
 [6] M. Hartmann, B. A. J. Jacobs and J. J. M. Braat, this issue, pp. 37-47.
 [7] Some of these rules and models have been discussed in a number of articles by A. R. Miedema in this journal: *Philips Tech. Rev.* **33**, 149-160, 1973; **33**, 196-202, 1973; **36**, 217-231, 1976 and **38**, 257-268, 1978/79.
 [8] See for example J. W. M. Biesterbos and A. G. Dirks, *Polytech. T. Werktuigbouw* **31**, 145-150, 1976.

The faster the melt is cooled the greater the chance that metallic glasses will form. Quenching rates of 10^6 K/s are nowadays feasible. The composition of the melt is also important. The results of various studies have indicated that there are some general rules for the composition [8][9]. Features favouring the formation of metallic glasses include:

- the presence of different atomic species,
- a large difference in atomic radius and electronegativity,
- a composition corresponding to a 'deep' eutectic in the phase diagram, and
- the presence of non-metallic elements such as B, C, Si, Ge or P.

Known compositions that comply with these rules for metallic glass formation are: $\text{Co}_{0.8}\text{P}_{0.2}$, $\text{Pd}_{0.8}\text{Si}_{0.2}$, $\text{Ni}_{0.8}\text{P}_{0.2}$ and $\text{Fe}_{0.8}\text{P}_{0.14}\text{C}_{0.06}$ [8][10]. Another interesting observation is that the large and small atoms in many metallic glasses occur in a ratio of about 80:20. We shall return to this later on.

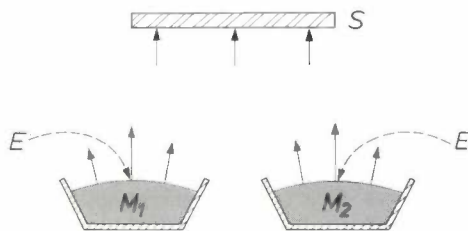


Fig. 3. Producing an amorphous alloy from the vapour phase. The metals M_1 and M_2 contained in the crucibles are separately heated by electron-beam evaporators. The electron beams E , generated by means of a heated filament and a strong electrostatic field, are deflected by magnetic fields into the crucibles containing the metal to be evaporated. From the vapour produced, an amorphous alloy of M_1 and M_2 is deposited on the cold substrate S .

The preparation of amorphous alloys from the vapour phase also takes place at high quenching rates. A widely used method is the deposition of thin amorphous films on a substrate by means of electron-beam evaporation in vacuum; see fig. 3. In this method different electron beams are simultaneously directed into crucibles containing melts of the different pure elements. From the resultant vapour mixture a deposit is formed on the substrate. When the temperature of the substrate is low enough, the vapour mixture cools so quickly that no crystalline ordering can occur, and an amorphous alloy is formed. With careful and rapid control of the partial evaporation rate of each of the elements homogeneous alloys with widely diverse compositions can be obtained.

Amorphous alloys cannot be distinguished from crystalline alloys with the naked eye. They can, how-

ever, when a scanning or transmission electron microscope is used. The difference can also be demonstrated by means of electron diffraction or X-ray diffraction. In the diffraction of X-rays by crystalline materials there is an intensification of the scattered X-ray beam at certain angles because of the regular ordering of the atoms. This produces sharp peaks in the diffraction pattern. Peaks are also observed in the diffraction patterns of amorphous alloys, but owing to the disordered structure they are much smaller and randomly scattered over all the possible angles. This implies that only broad bands appear in the pattern; see fig. 4.

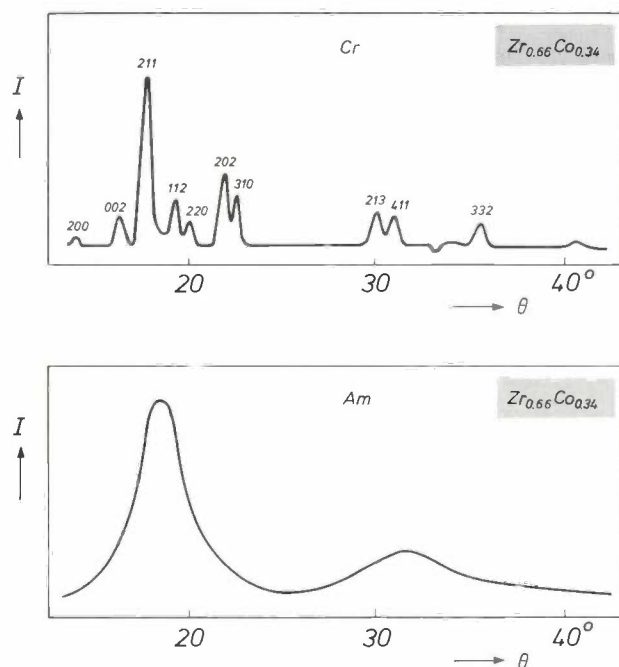


Fig. 4. X-ray diffractogram of a crystalline alloy (Cr) and an amorphous (Am) alloy of the composition $\text{Zr}_{0.66}\text{Co}_{0.34}$. The intensity I of the diffracted radiation is given in arbitrary units as a function of the diffraction angle θ . Because of the regular ordering of the atoms in the crystalline state, very sharp diffraction peaks are produced; the indices indicate the crystal planes from which the various peaks originate. In the amorphous state the absence of long-range order results in relatively broad diffraction peaks.

Stability

Because of their metastable character amorphous alloys can be transformed into the more stable crystalline state. The transition is a function of time and temperature. The heat released in this transition can be measured with a calorimeter. When an amorphous alloy is heated the atoms become so mobile at a particular temperature that crystallization occurs. The temperature at which this takes place is called the crystallization temperature T_{cr} . In a curve of the heat

released against temperature a sharp peak is observed at T_{cr} ; see fig. 5. The crystallization temperature decreases if the alloy is heated more slowly. This implies that there is some probability of crystallization even without heating. A comparison of different amorphous alloys shows that this probability increases as the crystallization temperature at a particular heating rate decreases.

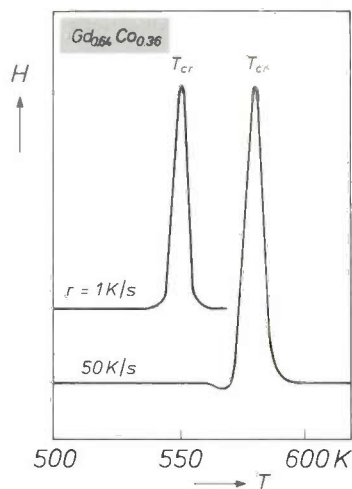


Fig. 5. Heat generated H (arbitrary units) as a function of the temperature T of the amorphous alloy $Gd_{0.64}Co_{0.36}$ at two different heating rates r . The transition to the more stable crystalline state gives a sharp peak. The temperature at which this transition takes place, the crystallization temperature T_{cr} , decreases when the alloy is heated more slowly.

Various models to be found in the literature attempt to explain the thermal stability of amorphous alloys. In one of them large differences in atomic radius and a highly asymmetrical composition are essential for stability [11]. This model is based on the common occurrence of stable amorphous alloys with widely different atomic radii and with the 80/20 ratio mentioned earlier for the large and small atoms in metallic glasses. The basic assumption is that in amorphous alloys $A_{1-x}B_x$ the large A atoms form a dense randomly packed configuration in which the small B atoms occupy the interstices. Since the number of interstices is small only a limited proportion (about 20%) of B atoms can be incorporated. The filling of interstices on an atomic scale results in stronger cohesion and hence a reduction of the free energy of the amorphous state. As the atoms become more closely packed the energy difference $E_{am} - E_{cr}$ between the amorphous and the crystalline states is reduced, and the stability should be greater. In recent years, however, a growing number of alloys have been made which do not answer to

the predictions based on this model. It appears, for example, that stable amorphous alloys exist in which the proportion of small atoms is considerably larger than 20%.

Another model takes account of the redistribution of the electrons in the conduction band that arises when an amorphous alloy is formed [12]. As the kinetic energy of the conduction electrons is lowered during this redistribution the energy of the amorphous alloy decreases, and the stability should be greater. However, this model is also by no means always satisfactory [1].

The main objection to the models mentioned above is that the kinetics of the transition to the crystalline state is not taken into account. While it is true that the energy difference $E_{am} - E_{cr}$ is the driving force behind this transition, a reduction in E_{am} need not necessarily result in a greater stability. A much more important factor is the way in which the mobility of the atoms in the amorphous state changes with temperature. Only when that mobility is sufficiently high can a transition to the crystalline state take place, and this requires an activation energy ΔE .

The value of ΔE can be determined experimentally from the crystallization temperature T_{cr} measured at

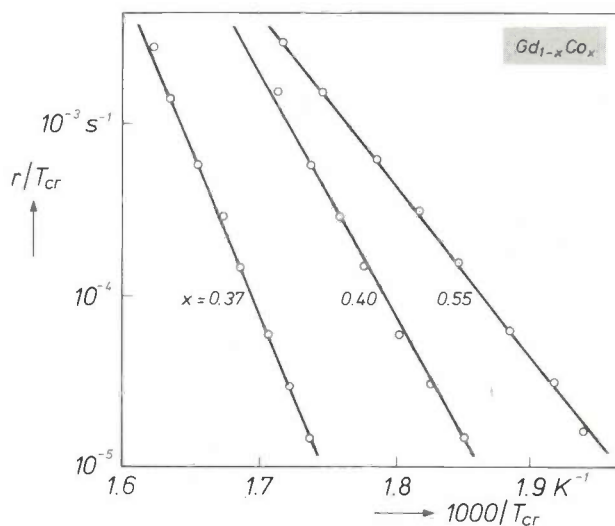


Fig. 6. Ratio of the logarithm of the heating rate r to the crystallization temperature T_{cr} plotted against $1000/T_{cr}$, for amorphous alloys of the composition $Gd_{1-x}Co_x$. The slope of the straight line produced can be used to calculate the activation energy for the transition to the crystalline state.

[9] P. Duwez, *Fizika* 2 (Suppl. No. 2), 1.1-1.15, 1970.

[10] F. J. A. den Broeder, *Chem. Weekbl.* June 1976, pp. m324-m326.

[11] D. E. Polk, *Scr. Metall.* 4, 117-122, 1970; D. E. Polk and H. S. Chen, *J. Non-Cryst. Solids* 15, 165-173, 1974.

[12] S. R. Nagel and J. Tauc, *Phys. Rev. Lett.* 35, 380-383, 1975.

different values of the heating rate r [13]. As *fig. 6* shows, a straight line is obtained for amorphous alloys of gadolinium and cobalt when the logarithm of rT_{cr}^{-1} is plotted against T_{cr}^{-1} . The value of ΔE can be calculated from the slope of this line. During crystallization the energy difference $E_{am} - E_{cr}$ is released as heat. Its value can be derived from the area beneath the peak at T_{cr} in graphs in which the heat released is plotted as a function of temperature (*fig. 5*).

For the composition $Gd_{0.62}Co_{0.38}$ the determination of ΔE and $E_{am} - E_{cr}$ results in the energy diagram shown in *fig. 7*. The activation energy ΔE is seen to be two orders of magnitude greater than the difference between E_{am} and E_{cr} . This means that a reduction in E_{am} (even to $E_{am} \approx E_{cr}$) has only a very small effect on ΔE and therefore has a virtually negligible effect on the stability of the amorphous alloy.

When the composition of certain alloys is varied the crystallization temperature T_{cr} determined at a fixed heating rate is proportional to ΔE . The value of ΔE in this case can be estimated from the heat of formation

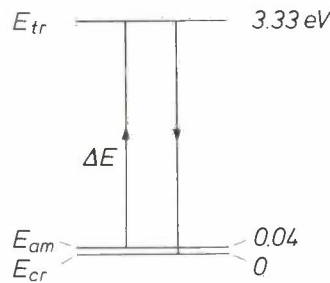


Fig. 7. The energy-level diagram, derived from experiments, for the transition from the amorphous state to the crystalline state of $Gd_{0.62}Co_{0.38}$. The activation energy ΔE , the difference between the energy of the transition state (E_{tr}) and that of the amorphous state (E_{am}), is almost two orders of magnitude greater than the energy difference $E_{am} - E_{cr}$ between the amorphous and crystalline states.

ΔH_h of a 'hole' of the same size as the smaller type of atom in the alloy. It is assumed here that the crystallization starts as soon as the smaller atoms are able to diffuse. This leads to the semi-empirical relation

$$T_{cr}/\Delta H_h = 7.5 \text{ K mol/kJ} \quad (1)$$

In calculating the value of ΔH_h the same kind of approximation can be used as in calculating the monovacancy energy in intermetallic compounds [14]:

$$\Delta H_h = (1 - \bar{x})(V_B/V_A)^{5/6} \Delta H_{1v}^A + \bar{x} \Delta H_{1v}^B \quad (2)$$

where V_A and V_B are the molar volumes and ΔH_{1v}^A and ΔH_{1v}^B are the monovacancy energies of pure metals for the large atom A and the small atom B in the amorphous alloy $A_{1-x}B_x$. The 'effective' concentra-

tion \bar{x} in an amorphous alloy with no short-range order is given by:

$$\bar{x} = xV_B^{2/3} \{ (1-x)V_A^{2/3} + xV_B^{2/3} \}^{-1} \quad (3)$$

With the values of V_A , V_B , ΔH_{1v}^A and ΔH_{1v}^B tabulated in the literature the value of ΔH_h can thus be calculated for a wide range of alloys.

Fig. 8a presents the calculated values of ΔH_h and T_{cr} and the experimental values of T_{cr} as a function of

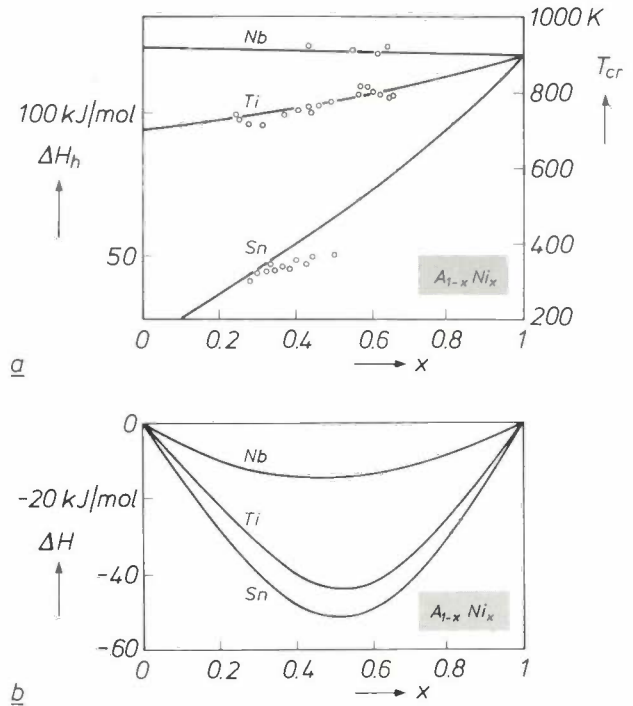


Fig. 8. *a)* Concentration dependence of the required heat for hole formation (ΔH_h) and the crystallization temperature T_{cr} , for alloys of $A_{1-x}Ni_x$ with $A = Ti, Nb, Sn$ [17]. The measured points for T_{cr} agree with the continuous curves, calculated from equations (1), (2) and (3). The scales on the left-hand and right-hand vertical axes correspond to $T_{cr} = 7.5 \Delta H_h$. *b)* Concentration dependence of the heat of formation ΔH for the same alloys. It follows from the difference from the concentration dependence of T_{cr} that there is no direct relationship between ΔH and T_{cr} .

composition for three kinds of amorphous nickel alloys. The calculated variation in T_{cr} with the concentration of the smaller atom (Ni) is also found experimentally in all three cases. The concentration dependence of the heat of formation ΔH of the alloys, on the other hand, is quite different from that of ΔH_h and T_{cr} ; see *fig. 8b*. This clearly shows that no direct relationship exists between the thermal stability of an amorphous alloy and its heat of formation.

The linear relationship between ΔH_h and T_{cr} is found to hold reasonably well for a large number of different alloys; see *fig. 9*. Evidently the occurrence of short-range order, which can differ substantially from

one alloy to another, has relatively little effect on the thermal stability. When such short-range order is present an atom has on average a greater number of dissimilar neighbours surrounding it than would be expected on the basis of a random distribution (fig. 1*b*). This implies that the degree of ordering can be derived from the (negative) heat of formation ΔH . In an amorphous alloy $A_{1-x}B_x$ with no ordering of A and B the concentration dependence of ΔH can be represented to a good approximation as [15]

$$\Delta H = c\bar{x}(1 - \bar{x}), \quad (4)$$

where c is a constant at a given A and B and \bar{x} is the effective concentration of eq. (3). As the experimental value of ΔH becomes more negative with respect to the calculated value the short-range order in the amorphous alloy can be assumed to increase.

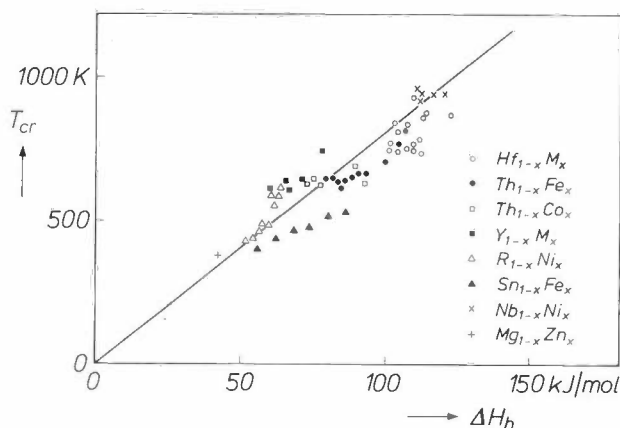


Fig. 9. Crystallization temperature T_{cr} as a function of the heat required for hole formation (ΔH_h), for a large number of binary alloys. M = transition metal; R = rare-earth metal. The measured points differ little from the straight line of eq. (1).

Fig. 10 gives the calculated and measured values of ΔH as a function of x for amorphous $Zr_{1-x}Ni_x$. With increasing nickel content a greater deviation is found, which points to greater short-range order. The ordering is evidently greatest at $x \approx 0.6$. This effect is also found on comparing with the measured concentration dependence of ΔH for the crystalline state. Fig. 10 shows this as well, with an estimated value of 5 kJ/mol [16] for the enthalpy difference between the amorphous and the crystalline state of the pure metals. At $x = 0.1$ it can be seen that ΔH for the amorphous state is about 30% above the curve for the crystalline state, whereas at $x = 0.6$ the relative difference is only about 10%.

A greater ordering in an amorphous alloy will have the effect of reducing the energy difference $E_{am} - E_{cr}$.

Since, however, the activation energy ΔE for the transition to the crystalline state is much greater than $E_{am} - E_{cr}$ (fig. 7), the effect on the thermal stability is negligible. An effect does become noticeable, however, when the ordering influences the kinetics of the transition [21][17].

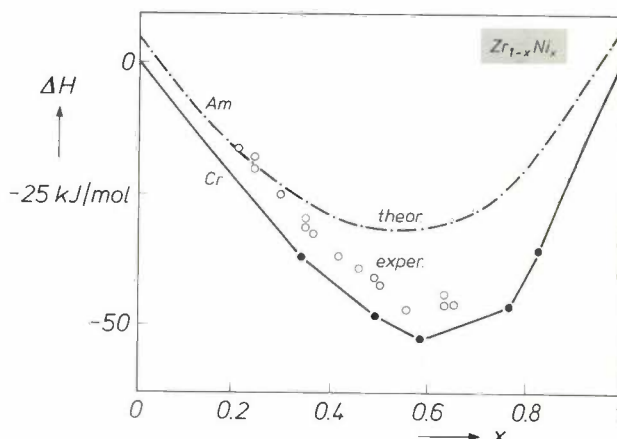


Fig. 10. Heat of formation ΔH of amorphous (Am) and crystalline (Cr) $Zr_{1-x}Ni_x$ as a function of x [17]. For the amorphous alloys the experimental values are clearly lower than those given by the calculated curve, which is attributed to the occurrence of short-range order. This is evidently most pronounced at $x \approx 0.6$. The relative difference in ΔH from the completely ordered crystalline state is then only about 10%.

Electron distribution

Information on the electron distribution in amorphous alloys can be obtained by means of electron-spin resonance (ESR). This technique can be used to study the transitions taking place in a magnetic field between different electron-spin states during the absorption of electromagnetic radiation. The energy of an electron-spin state is affected by the immediate environment. The random arrangement of the atoms in amorphous alloys causes a broadening of ESR signals, which is closely dependent on the composition of the alloys. For instance, at a temperature of 4 K the linewidth of the ESR signal of Gd is about 0.015 T (150 gauss) for $Pd_{0.82}Si_{0.18}:Gd$ and about 0.1 T (1000 gauss) for $Zr_{0.78}Pt_{0.22}:Gd$ [18].

- [13] H. E. Kissinger, *Anal. Chem.* **29**, 1702-1706, 1957;
P. G. Boswell, *J. Therm. Anal.* **18**, 353-358, 1980.
[14] A. R. Miedema, P. F. de Châtel and F. R. de Boer, *Physica* **100B**, 1-28, 1980.
[15] A. K. Niessen, F. R. de Boer, R. Boom, P. F. de Châtel, W. C. M. Mattens and A. R. Miedema, *CALPHAD* **7**, 51-70, 1983.
[16] M. P. Henaff, C. Colinet, A. Pasturel and K. H. J. Buschow, *J. Appl. Phys.* **56**, 307-310, 1984.
[17] K. H. J. Buschow, *Proc. Fifth Int. Conf. on Rapidly quenched metals*, Würzburg 1984 (to be published).
[18] H.-J. Eifert, B. Elschner and K. H. J. Buschow, *Phys. Rev. B* **29**, 2905-2911, 1984;
K. H. J. Buschow, H.-J. Eifert and B. Elschner, *Phys. Stat. Sol. b* **115**, 455-462, 1983.

The line broadening for a given temperature increase is approximately proportional to the square of the density of states of the d electrons at the Fermi energy (i.e. the energy to which the d band is filled with electrons) [18]. In amorphous alloys of Zr with Cu, Ni, Pd, Pt, Co or Rh this density of states is found to be 20 to 40% higher than in pure crystalline Zr. This agrees well with measurements of specific heat capacity [19]. Calculations of the energy-band structures show that this increase is mainly due to a shift of the d band of Zr to a higher energy, with the Fermi energy effectively shifted to a level with a higher density of states [20].

Useful information on the bonding in amorphous alloys is often obtained by means of Mössbauer spectroscopy. In this method the absorption of gamma radiation from a moving radioactive source (e.g. ^{57}Co) is determined for certain nuclei (e.g. ^{57}Fe). Detection is based on the Doppler effect, the velocity of the source determining the incident energy. The differing local surroundings of ^{57}Fe in an alloy as compared with pure iron are characterized by a change in the Mössbauer spectrum. The displacement of the centre of the spectrum, known as the isomer shift δ , is a measure of the density of s electrons at the location of the nucleus. In alloys of the composition $A_{1-x}\text{Fe}_x$ the quantity δ depends closely on A and x. The dependence on A is determined by the difference in electronegativity ($\Delta\phi^*$) between A and Fe and the difference Δn_{WS} in electron density n_{WS}^{A} and $n_{\text{WS}}^{\text{Fe}}$ at the interface of the atomic (Wigner-Seitz) cells [21]. From an analysis of the measured isomer shifts the following relation can be derived [22]:

$$\delta = (1 - \bar{x}) \delta_{\text{m}} \\ \delta_{\text{m}} = 0.75 \Delta\phi^* - 1.65 \Delta n_{\text{WS}} / n_{\text{WS}}^{\text{Fe}}, \quad (5)$$

where \bar{x} is the effective concentration of eq. (3). This relation proves to be valid for various kinds of iron alloys. This is illustrated in fig. 11, where $\delta_{\text{m}}/\Delta\phi^*$ is plotted against $\Delta n_{\text{WS}}/(n_{\text{WS}}^{\text{Fe}} \Delta\phi^*)$ for various alloys. The experimental points correspond well with the straight line of eq. (5).

It follows from these results that the isomer shift is determined by two opposing contributions: the positive one corresponds to a charge transfer from A to Fe, the negative one to a conversion of s into d electrons within the iron atom. In fig. 12 these two contributions are shown separately for $\text{Zr}_{1-x}\text{Fe}_x$ as a function of \bar{x} . If the isomer shift is translated into a change in the number of s, p and d electrons per Fe atom, then for $\bar{x} \rightarrow 0$ there is a charge transfer of 0.7 s,p electrons that corresponds, owing to the intra-atomic electron redistribution, to an effective increase of 0.4 s,p electrons and 0.3 d electrons.

The occurrence of the intra-atomic electron redistribution is connected with the combination of a larger electronegativity and a larger electron density of Fe with respect to Zr. The charge transfer caused by the difference in electronegativity ensures that Fe acquires additional electrons in spite of its higher electron density. This would give an even greater difference in electron density at the boundary of the atomic Fe and Zr cells, which would be energetically unfavourable. However, the electron density is prevented from increasing by the Fe atom becoming larger and by some

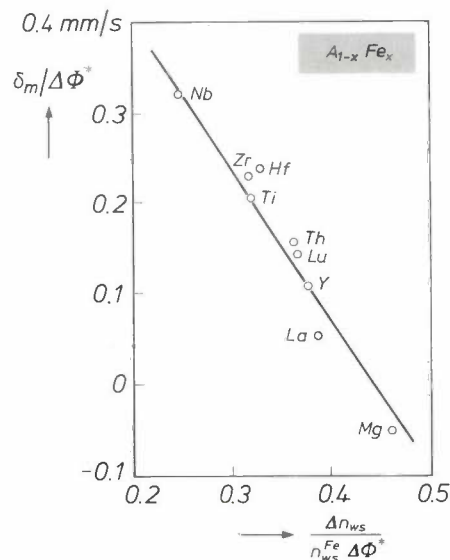


Fig. 11. Ratio of the maximum Mössbauer isomer shift δ_{m} and the electronegativity difference $\Delta\phi^*$ for some alloys of the composition $A_{1-x}\text{Fe}_x$ plotted as a function of $\Delta n_{\text{WS}}/(n_{\text{WS}}^{\text{Fe}} \Delta\phi^*)$, where Δn_{WS} is the difference between the electron densities n_{WS}^{A} and $n_{\text{WS}}^{\text{Fe}}$ at the boundary of the atomic A and Fe cells [21][22]. The continuous line was used to derive the empirical relation of eq. (5).

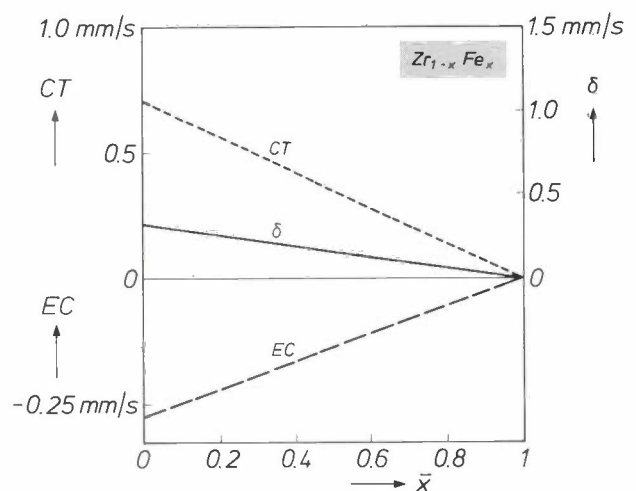


Fig. 12. The experimental isomer shift δ of amorphous $\text{Zr}_{1-x}\text{Fe}_x$ split into a contribution from the charge transfer (CT) and a contribution from the intra-atomic conversion of s into d electrons (EC). The two contributions are plotted against the effective concentration \bar{x} of eq. (3). Since the signs of CT and EC are opposite the value of δ is relatively small even for small \bar{x} .

of the 4s electrons becoming converted into 3d electrons, which lie deeper. Similar effects are expected for other alloys of 3d metals with more strongly electropositive metals, even though these cannot be investigated by Mössbauer spectroscopy.

Magnetic properties

The crystal structure of crystalline alloys and intermetallic compounds has a pronounced effect on their magnetic properties. It is therefore not so surprising that there are also considerable differences in magnetic properties between amorphous and crystalline alloys of the same composition and between amorphous alloys themselves. For instance, in amorphous alloys of a 3d metal the magnetic moment μ per 3d atom is

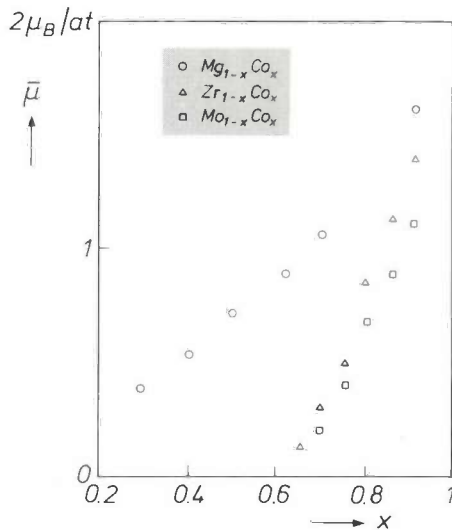


Fig. 13. Concentration dependence of the magnetic moment $\bar{\mu}$ per metal atom for amorphous $A_{1-x}Co_x$, where $A = Mg, Zr, Mo$. The decrease of $\bar{\mu}$ with decreasing x depends on A .

highly sensitive to the presence of electropositive non-magnetic atoms. By way of example *fig. 13* shows the mean magnetic moment $\bar{\mu}$ plotted as a function of x for three cobalt alloys $A_{1-x}Co_x$. A reduction of x gives a marked decrease in $\bar{\mu}$, which depends on the choice of the non-magnetic metal A .

Such decreases in the magnetic moment are usually attributed to the transfer of electrons to the more electronegative 3d atom. This charge transfer results in more paired and fewer unpaired electrons in the 3d band, giving a smaller magnetic moment. Measures frequently used for the charge transfer are the difference in electronegativity and the difference in the number of valence electrons [23]. In qualitative terms this model holds reasonably well for certain classes of

amorphous alloys. It no longer does so, however, when widely different compositions are compared.

One of the main reasons for the deviations found is that the effect of the charge transfer in these alloys is not so pronounced as was originally thought. As described in the previous section, it can be inferred from Mössbauer and other experiments that the effective charge transfer per atom amounts to no more than a few tenths of an electron. This is too small to account for the observed decreases in the magnetic moment.

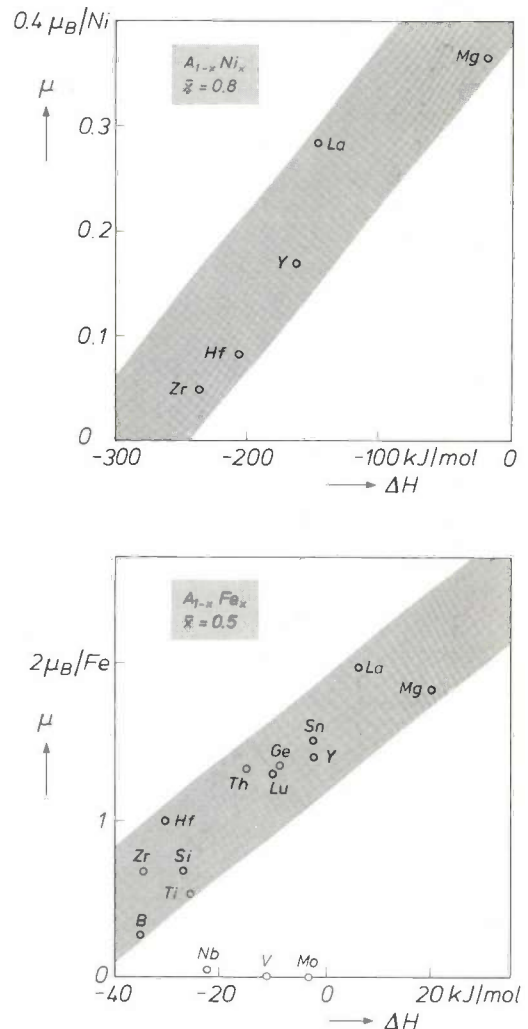


Fig. 14. Magnetic moments μ per nickel and iron atom plotted against the heat of formation ΔH for $A_{1-x}Ni_x$ ($\bar{x} = 0.8$) and $A_{1-x}Fe_x$ ($\bar{x} = 0.5$). Qualitatively there is a linear relation in both cases between μ and ΔH . Exceptions are the Fe alloys of Nb, V and Mo.

[19] J. E. Graebner, B. Golding, R. J. Schutz, F. S. L. Hsu and H. S. Chen, *Phys. Rev. Lett.* **39**, 1480-1483, 1977.

[20] J. Kübler, K. H. Bennemann, R. Lapka, F. Rösel, P. Oelhafen and H.-J. Güntherodt, *Phys. Rev. B* **23**, 5176-5184, 1981.

[21] See the articles by A. R. Miedema given in [7].

[22] A systematic analysis of isomer shifts was first given for alloys and compounds of gold; see A. R. Miedema and F. van der Woude, *Physica* **100B**, 145-156, 1980. The model has also been extended to include iron alloys; see A. M. van der Kraan and K. H. J. Buschow, *Phys. Rev. B* **25**, 3311-3318, 1982.

[23] E. P. Wohlfarth (ed.), *Ferromagnetic materials: a handbook on the properties of magnetically ordered substances*, Vol. 2, North-Holland, Amsterdam 1980, p. 491.

A better explanation is to be found by considering the immediate environment of a 3d atom [24]. In an $A_{1-x}B_x$ alloy the magnetic moment per 3d atom of B increases as it has more B atoms or fewer A atoms as nearest neighbours. With the atoms distributed at random the number of neighbouring B atoms is proportional to the effective concentration \bar{x} of eq. (3). This number changes when short-range order occurs. The degree of ordering can be deduced qualitatively from the sign and the magnitude of the heat of formation ΔH of the alloy. A negative ΔH points to attraction between A and B, so that a B atom will have fewer B atoms as nearest neighbours than would be expected from a random distribution. The opposite applies of course when the heat of formation is positive.

According to this model the magnetic moment for a fixed \bar{x} increases as the heat of formation becomes less negative or more positive. This has been confirmed experimentally for a large number of widely different magnetic alloys. Examples are shown in fig. 14. The magnetic moments per iron or nickel atom in different alloys are seen to be roughly proportional to ΔH . The model can be refined further from the knowledge that

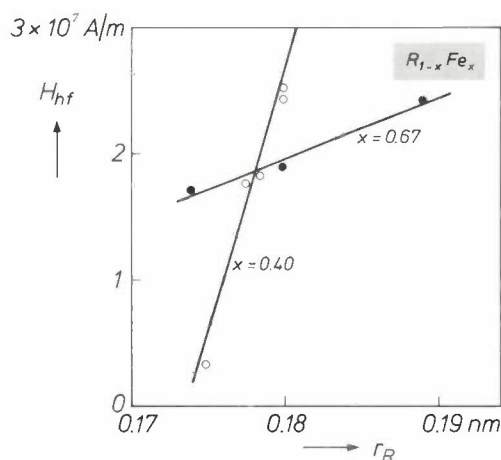


Fig. 15. Hyperfine field H_{hf} of ^{57}Fe in amorphous $R_{1-x}\text{Fe}_x$ (R = rare-earth metal) plotted against the atomic radius r_R for $x = 0.40$ and 0.67 . In both cases, H_{hf} increases linearly with r_R .

a smaller number of B neighbours implies a larger number of A neighbours. According to J. Friedel [25] the extent to which A atoms can reduce the moment of B atoms is not the same for all A elements. The effect of A increases as the columns in which A and B appear occur closer together in the Periodic Table. In alloys of Fe with Nb, V or Mo the effect of the A atoms is very strong, so that a marked deviation

from the linear relationship is found and the magnetic moment is practically zero.

The model described can also be used for explaining other magnetic properties reported in the literature. An example is the variation in the hyperfine field H_{hf} on the ^{57}Fe nucleus as found in Mössbauer measurements on iron alloys. It may be assumed that H_{hf} is proportional to μ . Measurements on $R_{1-x}\text{Fe}_x$ alloys, where R is a rare-earth metal, have shown that H_{hf} increases with the radius r_R of the rare-earth atom [26]; see fig. 15. This effect cannot be attributed to a decrease in the effective concentration \bar{x} , which occurs from eq. (3) at an increasing r_R , because a smaller \bar{x} implies that an Fe atom has fewer Fe neighbouring

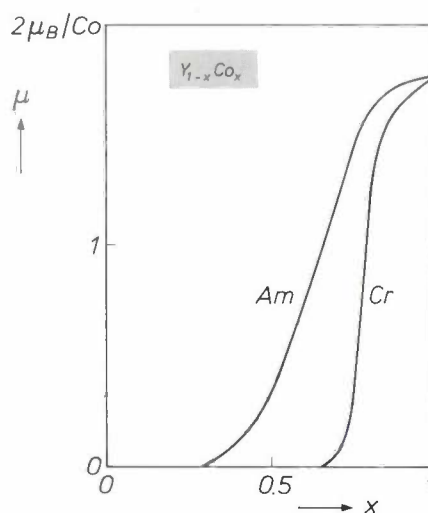


Fig. 16. Concentration dependence of the magnetic moment μ per Co atom for amorphous $Y_{1-x}\text{Co}_x$ (*Am*) and for crystalline intermetallic compounds (*Cr*) with different compositions. The ordered Y environment of Co in the crystalline state causes a greater reduction of μ than in the amorphous alloy of the same composition.

atoms, which would give a decrease in μ and H_{hf} and not an increase. A good explanation does present itself, however, if the variation in the heat of formation ΔH is considered. For we know that an increase in r_R is accompanied by a rise in ΔH [14][15], which points to a decreasing attraction between the iron atom and the rare-earth atoms. The resultant increase in μ is observed as an increase of H_{hf} .

The differences in magnetic properties between amorphous and crystalline alloys can also be explained in terms of this model. It has long been known that the magnetic moment in amorphous alloys decreases less rapidly with decreasing 3d concentration than in corresponding crystalline alloys [27]. As an example fig. 16 shows the situation for amorphous alloys and intermetallic compounds of the type $Y_{1-x}\text{Co}_x$. At first

the more marked decrease in crystalline alloys was attributed to a larger charge transfer [28]. This has not been proved experimentally, however. From Mössbauer experiments [29] and photoemission experiments [30] it can be inferred that the charge transfer in both crystalline and amorphous alloys of 3d metals with more electropositive metals is relatively small and that this effect is certainly not large enough to account for the difference in μ . Something that does imply a distinct difference is the local environment of

the 3d atoms. Whereas in amorphous alloys there is only a limited local order, in intermetallic compounds the local order is at a maximum: the nearest neighbours of each B atom are A atoms. This gives a greater decrease in the value of μ .

- [24] K. H. J. Buschow and P. G. van Engen, *J. Appl. Phys.* **52**, 3557-3561, 1981.
- [25] J. Friedel, *Nuovo Cimento* **7** (Suppl. No. 2), 287-311, 1958.
- [26] N. Heiman and N. Kazama, *Phys. Rev. B* **19**, 1623-1632, 1979; K. H. J. Buschow and A. M. van der Kraan, *J. Magn. & Magn. Mater.* **22**, 220-226, 1981.
- [27] See K. H. J. Buschow, M. Brouha, J. W. M. Biesterbos and A. G. Dirks, *Physica* **91B**, 261-270, 1977.
- [28] L. J. Tao, S. Kirkpatrick, R. J. Gambino and J. J. Cuomo, *Solid State Commun.* **13**, 1491-1494, 1973.
- [29] K. H. J. Buschow, A. M. van Diepen, N. M. Beekmans and J. W. M. Biesterbos, *Solid State Commun.* **28**, 181-185, 1978; P. C. M. Gubbens, A. M. van der Kraan and K. H. J. Buschow, *Phys. Stat. Sol. a* **64**, 657-663, 1981.
- [30] J. Azoulay and L. Ley, *Solid State Commun.* **31**, 131-134, 1979.

Summary. Amorphous alloys, produced by rapid cooling (quenching) from the liquid or vapour phase, have no regular atomic order and are metastable. When the temperature is increased they are transformed into the more stable crystalline state. The kinetics of this transition largely determines the thermal stability. The crystallization temperature rises approximately linearly with the enthalpy theoretically required for making a 'hole' of the same size as the smallest atom. The occurrence of short-range order has little effect on the thermal stability. From determinations of the electron distribution by means of Mössbauer experiments it can be shown that the transfer of electrons to the most electronegative atom in an alloy is relatively small and is partly compensated by an intra-atomic conversion of s into d electrons. The magnetic behaviour of amorphous 3d alloys is therefore not primarily dependent on charge transfer. It is however significantly affected by the occurrence of short-range order.

Reflection reduction on television screens

Reflections on a television screen are annoying. They can make it difficult to see the picture on the screen properly or may even be brighter (see photograph *a*). To reduce the reflection an anti-reflective layer can be applied. This is not so simple, however, as it seems at first sight. An anti-reflective coating only works well for light of one wavelength (λ_0) when the thickness of the coating corresponds to a quarter of that particular wavelength. At all other wavelengths the anti-reflective effect of the coating will be less. The result is colour distortion ('tinting'). Colour distortion also arises when the viewer looks at the anti-reflective coating from an angle. In addition the anti-reflective coating must be hard, resistant to atmospheric action, and unaffected by cleaning agents. What is more, a complete suppression of reflection is only achieved at λ_0 when $n_a = \sqrt{n_b}$, where n_a is the refractive index of the coating and n_b that of the glass of the picture tube.

A suitable anti-reflective material with a low refractive index ($n_a = 1.39$) is magnesium fluoride (MgF_2). This will give an anti-reflective coating that is resistant to scratches, atmospheric influences and cleaning agents. The reflectance decreases from 4.2% for untreated glass to about 1.6%.

Surprisingly, the optical bandwidth can be increased and tinting avoided by first *roughening* the top surface of the picture tube before depositing the anti-reflective coating. This roughening is done with an optical polishing agent, in which the mean value and the distribution of the grain size can be accurately specified. In this way a well-defined surface roughness can be achieved. The MgF_2 layer deposited on it later follows the surface profile of the roughened screen exactly. This results in a superimposition of light scattering and light extinction in the viewing directions from the front and from the sides. This is highly effective for incident light and barely noticeable for transmitted light: the optical bandwidth of the anti-reflective coating increases and there is no tinting.

Photographs *b* and *c* show TV screens whose reflection has been reduced in this manner. (Photo *a* shows an untreated screen.) In comparing the pictures it should be borne in mind that since the screens were mounted one above the other when the photographs were made the position of the reflection on the screen varies. The screen in *b* was less roughened than that in *c*. Reflection diminishes noticeably with increasing roughness, down to less than 0.4%. (A substantial



a



b



c

amount of the remaining reflection in the photographs is attributable to the reflection from the back of the screen.) Although there is a slight decrease in picture sharpness, the colours and the contrast of the picture are clearly unaffected, while the reflection is almost completely suppressed.

On the mechanism of the corrosion of glass by water

B. M. J. Smets

Modern methods of surface analysis such as SIMS and ESCA can help us to obtain a better understanding of the basic processes in the leaching of glass. These studies are of interest because of new applications of glass, such as the DOR disc and glass fibres for optical communication.

Ned. Philips Bedrijven B.V.
PHILIPS RESEARCH LABS
LIBRARY WY - 1
P.O. Box 80.000
5600 JA EINDHOVEN
THE NETHERLANDS

Glass, its structure and its resistance to chemical attack

Window glass or soda-lime glass contains about 10% of sodium, 7% of calcium, 1% of aluminium, and perhaps small quantities of potassium and magnesium as well as silicon and oxygen, of course. In the context of the investigation described in this article we can consider the structure of glass to be represented, as in Zachariassen's theory, by a random three-dimensional network of oxygen tetrahedra, with the centres occupied by the Si^{4+} ions and the Al^{3+} ions, while the Na^+ and the Ca^{2+} ions occupy the interstices of the network (fig. 1a)^[1]. The oxygen atoms can fulfil two functions in the network: they can be bridging oxygen atoms, each forming a covalent bond with two silicon atoms, or non-bridging oxygen atoms, each forming a covalent bond with one silicon atom and an ionic bond with one sodium ion (or with half a calcium ion). At Philips Research Laboratories a study has been made of alkali- and alkali-calcium silicate glasses, as simpler variants of window glass, with the compositions $20\text{Na}_2\text{O} \cdot 80\text{SiO}_2$, $20\text{Na}_2\text{O} \cdot 10\text{CaO} \cdot 70\text{SiO}_2$ etc. (molar ratios), and of aluminosilicate glasses with the composition $20\text{Na}_2\text{O} \cdot x\text{Al}_2\text{O}_3 \cdot (80 - x)\text{SiO}_2$. A typical structural characteristic of aluminosilicate glasses, compared with the glasses mentioned earlier, is the decreasing content of non-bridging oxygen atoms with increasing content of Al_2O_3 ; the alkali ions are then linked by AlO_4^- tetrahedra (fig. 1b).

Glass windows have to be able to withstand atmospheric effects for many years without showing visible

changes. Similarly, household glassware must be resistant to substances such as hot water, fruit juices, dilute acids and alkalis. Laboratory glassware must be resistant to highly concentrated reagents at high temperatures. Special requirements are also necessary for glass used in incandescent lamps, glass insulators, signal lamps and in the various applications of optical glass, to mention only a few examples.

In many cases the way in which glass reacts to water may be regarded as a key property, which could be

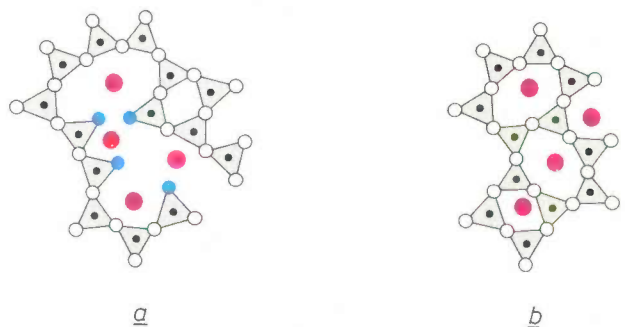


Fig. 1. *a*) Schematic two-dimensional structure of alkali-calcium silicate glasses, from Zachariassen's theory^[1]. O bridging oxygen atom. ● non-bridging oxygen atom. ● network-forming ion, in this case an Si^{4+} ion. ● network-modifying ion, in this case an alkali ion. *b*) The structure of aluminosilicate glasses, in which Al^{3+} ions (●) occur as network-formers. With increasing content of Al^{3+} ions the number of non-bridging oxygen atoms decreases (to zero here) and the network-modifying ions are attached to AlO_4^- tetrahedra. Aluminosilicate glasses therefore have a much less open structure.

Dr B. M. J. Smets, now with the Philips Lighting Division, was formerly with Philips Research Laboratories in Eindhoven. In 1983 he received the W. A. Weyl International Glass Science Award for the work described briefly here.

[1] See for example J. M. Stevels, Philips Tech. Rev. 22, 300-311, 1960/61.

studied for clues to the ability of glass to resist other chemicals.

It has long been known that pure water 'leaches' glass. When the glass comes into contact with water, the alkali ions, which are fairly loosely attached to the network, are especially likely to diffuse in small quantities to the surface and disperse, giving rise to an alkali depletion layer, of a few microns at most, at the surface. In this process OH^- ions are released, which can then take part in a reaction in which covalent Si-O-Si bonds are broken and part of the glass network is dissolved — although extremely slowly.

Significant corrosion rates of a few millimetres a year are only found if the glass is continuously in contact with water and only if the water is not drained away. In most conventional applications of glass this leaching effect is therefore no problem. But it is a problem in some of the recent applications of glass, like optical fibres and DOR discs.

Glass fibres for optical communication are covered with a thin protective coating of a synthetic material [2]. This material, like all plastics, always allows some water to pass through it and the thin film of water that can then form between the glass and the coating may become fairly strongly alkaline, as a result of leaching. The dissolution of the glass network that then starts may cause crazing, ultimately leading to fracture if the glass comes under pressure. (This does not of course apply to optical fibres made of quartz glass, which contains no alkali ions.)

The leaching of glass is also an effect that must be studied if DOR discs of high quality are to be produced (DOR is a digital optical recording system developed by Philips [3]). In the DOR disc the information is contained in a recording layer consisting of a thin film of TeSeSbS applied, with an intermediate layer of lacquer, to a glass substrate. Alkali ions released by leaching due to the penetration of ambient moisture could easily destroy the recorded information.

Applications like this have made it desirable to study such corrosion effects, which extend to only a few microns below the surface of glass. The development some time ago of surface-analysis methods such as SIMS (Secondary-Ion Mass Spectrometry) and ESCA (Electron Spectroscopy for Chemical Analysis) make this possible. In this article the results will be given of an investigation carried out with such methods at Philips Research Laboratories into the mechanism of the corrosion of glass by water. A general description of the methods of analysis that we used has been given in earlier articles in this journal [4], and details of their application to the area of investigation described here have been described elsewhere in the literature [5].

The corrosion of alkali- and alkali-calcium silicate glasses by water: ion exchange?

Fig. 2 gives an example of the sodium profile found on leaching at the surface. The profile was measured with SIMS for glass of the composition $20\text{Na}_2\text{O} \cdot 80\text{SiO}_2$. It was found that the thickness of the depletion layer, defined as the depth at which the sodium concentration has reached half the value in the bulk of the glass, increases linearly with the square

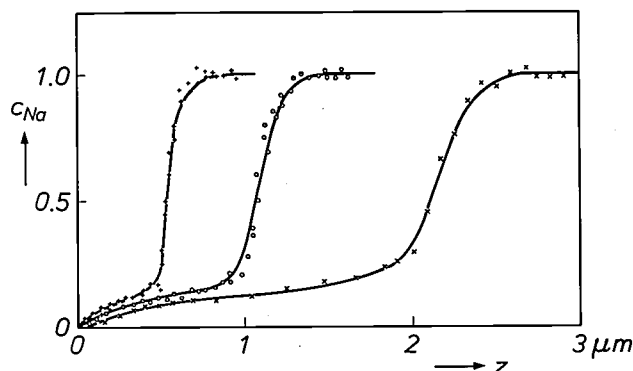


Fig. 2. Sodium profiles measured by SIMS (c_{Na} is the local concentration divided by the bulk concentration and z is the depth beneath the surface) of a glass with composition $20\text{Na}_2\text{O} \cdot 80\text{SiO}_2$ that has been exposed to pure water at 70°C for 5 (left), 15 and 60 minutes.

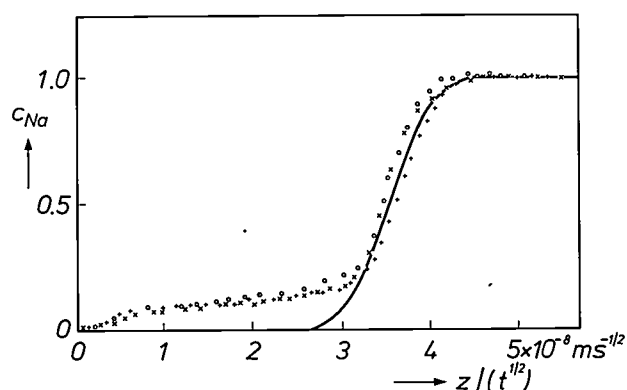
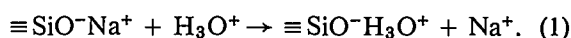


Fig. 3. Results of the same experiments as in fig. 2, represented by plotting the sodium concentration c_{Na} against the depth z divided by the square root of the time t . The theoretical curve, based on ion exchange, is also shown.

root of the time that the glass has been in contact with water. A plot of the sodium concentration against the depth divided by the square root of the contact time, as in fig. 3, shows a neat fit with the experimental profiles for different times.

The variation as the square root of the time is an indication that diffusion is the rate-determining process of leaching, resulting in the S-shaped concentration profiles shown. An obvious assumption is that

diffusion in these glasses causes an exchange between hydronium ions (H_3O^+ , the ionic form in which H^+ usually occurs in water) and sodium ions, in the reaction:



In this reaction the group $\equiv\text{SiO}^-$ represents a silicon plus non-bridging oxygen group.

The ratio of the diffusion coefficients D_{Na} and D_{H} for sodium and hydronium ions then determines the exact shape of the concentration profiles, as calculated in *fig. 4* for a number of values of the diffusion coefficients. By matching these theoretical profiles to those found experimentally the diffusion coefficients can be derived; see *Table I*. It is always found that the value derived for D_{Na} , which in principle applies only at the surface, is much larger than the value measured for

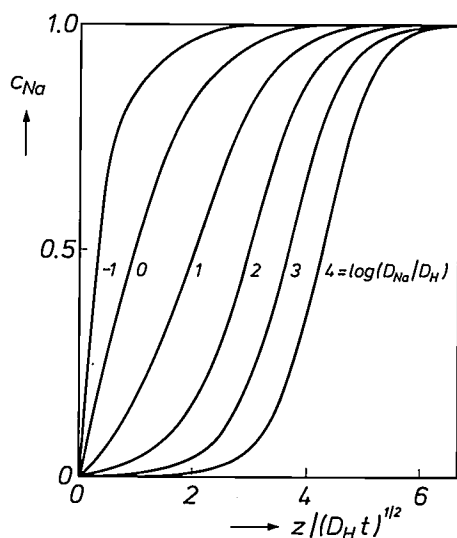


Fig. 4. The calculated variation of the sodium concentration c_{Na} as a function of $z/(D_{\text{H}}t)^{1/2}$, for various values of $\log D_{\text{H}}/D_{\text{Na}}$. In all cases it has been assumed that the leaching was due to ion exchange.

the bulk diffusion of sodium. It is, of course, conceivable that the greater mobility of sodium at the surface found in this way is due to the difference in composition between the surface depletion layer and the bulk of the glass.

However this may be, it must at the very least be accepted from the results of other recent investigations that the mechanism is more complex than has previously been assumed. To start with, it was established some years ago, by measurements of the diffusion of radioactive tracers, that the diffusion coefficient for sodium in a depletion layer is certainly not greater, as the above model suggests, but smaller than

in the bulk of the glass [6]. It is also difficult with the existing theory to explain why the concentration of the sodium ions in the leached layer does not become zero, but 5 to 10% of the initial concentration — as is always found experimentally (*fig. 3*). Also because of measurements by nuclear reaction analysis it has long been assumed that one sodium atom is exchanged for three hydrogen atoms (reaction 1), in accordance with the existing theories: but further experimental investigation has shown that the exchange ratio varies from 1.7 to 3.2, depending on the type of glass [7]. If we wish to explain these values by assuming that protons, and then H_2O molecules, are exchanged and not hydronium ions, we would expect that the use of

Table I. The diffusion coefficients D_{H} and D_{Na} of hydronium and sodium ions for some types of glass, calculated from sodium profiles on the assumption that the leaching takes place by ion exchange. The calculated values of D_{Na} , applicable only at the surface, are in that case much greater than the value D_{Na}^b measured in the bulk of the glass.

Composition	D_{H} (m^2s^{-1})	D_{Na} (m^2s^{-1})	D_{Na}^b (m^2s^{-1})
20Na ₂ O.80SiO ₂	5.10 ⁻¹⁷	5.10 ⁻¹¹	5.10 ⁻¹⁹
20Na ₂ O.10CaO.70SiO ₂	4.10 ⁻¹⁹	4.10 ⁻¹⁵	5.10 ⁻²⁰
10Na ₂ O.10K ₂ O.10CaO.70SiO ₂	5.10 ⁻¹⁹	5.10 ⁻¹⁴	10 ⁻²³

deuterium instead of protons in the water for leaching the glass would result in a 20% smaller depletion layer owing to the larger mass of the deuterium. No such isotopic effect could be demonstrated, however [8]. This can only mean that, if the diffusion of a component containing hydrogen is the rate-determining step, this component must be a relatively heavy compound such as H_3O^+ — after all — or perhaps H_2O . Experimental observations of this kind, which were so difficult to explain, led us to consider another mechanism for the leaching process.

[2] See for example H. M. J. M. van Ass, P. Geittner, R. G. Gossink, D. Küppers and P. J. W. Severin, *Philips Tech. Rev.* **36**, 182-189, 1976, in particular p. 185.

[3] See for example L. Vriens and B. A. J. Jacobs, *Philips Tech. Rev.* **41**, 313-324, 1983/84.

[4] H. H. Brongersma, F. Meijer and H. W. Werner, *Philips Tech. Rev.* **34**, 357-369, 1974.

[5] See for example R. G. Gossink, *Glass Technol.* **21**, 125-133, 1980; B. M. J. Smets and R. G. Gossink, *Fresenius Z. Anal. Chem.* **314**, 285-288, 1983; B. M. J. Smets, M. G. W. Tholen and T. P. A. Lommen, *J. Non-Cryst. Solids* **65**, 319-332, 1984.

[6] M. Takata, J. Acocella, M. Tomozawa and E. B. Watson, *J. Am. Ceram. Soc.* **64**, 719-724, 1981.

[7] I. S. T. Tsong, C. A. Houser, W. B. White, A. L. Wintenberg, P. D. Miller and C. D. Moak, *Appl. Phys. Lett.* **39**, 669-670, 1981.

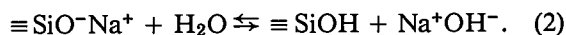
[8] See for example B. M. J. Smets and T. P. A. Lommen, *J. Physique* **43** (Colloque C9), C9/649-C9/652, 1982.

The corrosion of alkali- and alkali-calcium silicate glasses by water: diffusion of H₂O?

If glass leaches more rapidly than might be expected from the measured value of the mobility of the alkali ions, it seems likely that a neutral molecule will be the rate-determining diffusing component. The movements of such a neutral component will encounter little resistance from the presence of negatively charged non-bridging oxygen atoms in the glass structure. The absence of an isotopic effect also led us to conclude that the diffusing entity must be a relatively heavy molecule. The H₂O molecule satisfies both conditions, and it is present in excess.

What happens to the glass network when water diffuses into it? We can answer this question to some extent with the aid of electron spectroscopy (ESCA). Fig. 5a shows part of the ESCA spectrum of a soda-lime glass. Three energy transitions can be identified: one transition at a relatively low kinetic energy, due to sodium, and two transitions attributable to oxygen atoms — and with different charge densities. The difference of about 2.5 eV between the energy of these two transitions corresponds to the difference in charge density between the negatively charged non-bridging oxygen atoms and the non-charged bridging oxygen atoms.

If the sample analysed is immersed in water and then analysed again, the spectrum shown in fig. 5b is obtained. The peak attributable to sodium has almost disappeared, as also has the peak due to the non-bridging oxygen atoms. The disappearance of the sodium ions is seen to be accompanied by the disappearance of the negative groups to which they were attached. The most obvious explanation for this is that, under the influence of the inward-diffusing water, non-bridging oxygen atoms are converted into silanol groups ($\equiv\text{SiOH}$), in which the oxygen atom has virtually the same charge density as the bridging oxygen atom:



This reaction enables the sodium ions — no longer attached to the glass network — to diffuse to the surface, with OH⁻ ions as co-ions.

If the diffusion of water is the rate-determining step in this process, it follows anyway that S-shaped sodium profiles ought to be obtained (fig. 6). The forward tilt of the S of the profile then depends on the equilibrium constant K of reaction (2) and on the local concentration of H₂O at the glass surface.

But this hypothesis contains even more that fits in with the facts. It was mentioned earlier that it was originally thought that Na and H atoms were exchanged in the ratio 3:1 for all types of glass. For the

concentrations of Na and H atoms found in the depletion layer this should give a ratio of $(i - a)/3a$, where i is the initial concentration of Na atoms and a is the proportion of them exchanged. However, now it has been established that the exchange ratio varies from 1.7 to 3.2, depending on the type of glass used, this must of course mean that the concentration ratio of Na and H atoms found in the depletion layer must have a spread of $(i - a)/1.7a$ to $(i - a)/3.2a$.

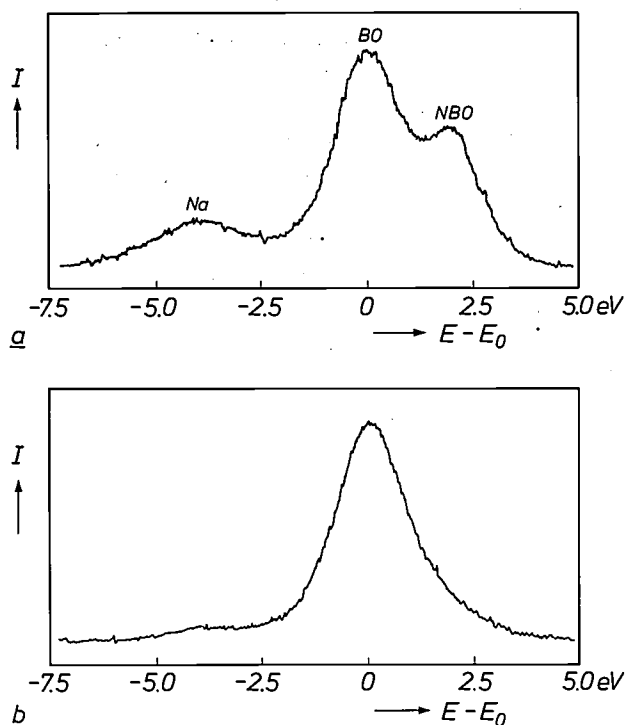


Fig. 5. ESCA spectra of a) a sample of the composition $20\text{Na}_2\text{O} \cdot 10\text{CaO} \cdot 70\text{SiO}_2$, and b) the same part of the sample after 10 minutes in water at 20 °C. The peak Na corresponds to a sodium-Auger transition, the peak BO is due to bridging oxygen atoms and the peak NBO to non-bridging oxygen atoms.

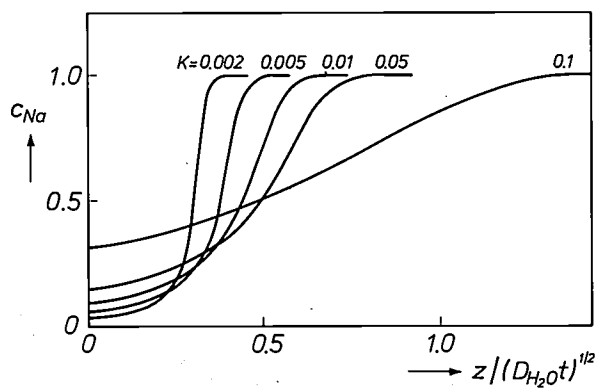


Fig. 6. Calculated curve of the sodium concentration c_{Na} as a function of $z/(D_{\text{H}_2\text{O}t})^{1/2}$, for different values of the equilibrium constant K of reaction (2). It has been assumed that the leaching was due to diffusion of H₂O.

This scatter in values can be more easily explained with the diffusion of H_2O as the rate-determining step rather than ion exchange, since the number of H atoms in the depletion layer will then be determined by the number of silanol groups formed in the glass and also by the concentration of H_2O in the glass. Depending on the equilibrium constant K , the concentration of H_2O in different types of glass, with the number of silanol groups remaining unchanged, may differ, and the ratio of Na and H atoms could have a corresponding spread of values (figs 7 and 8).

The theoretically calculated and experimentally determined Na and H profiles shown in these figures are *not* complementary — and they do not need to be for the model we are now considering. But they would have to be complementary if they were due to ion exchange.

Another point in agreement with the experimental data of fig. 8 is that in our hypothesis some of the Na ions will always remain behind in the leached layer: the equilibrium of reaction (2) is never completely shifted to one side.

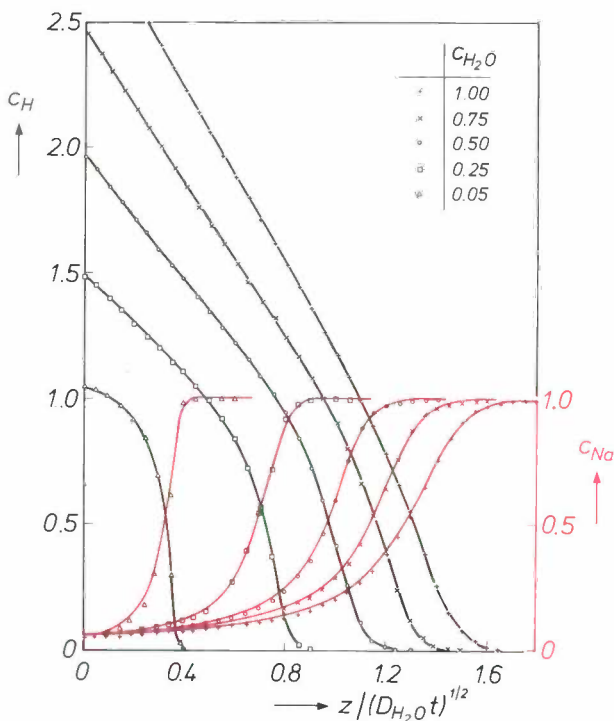


Fig. 7. H and Na profiles (red) calculated from the H_2O diffusion model for different values of the water concentration c_{H_2O} (local concentration at the surface divided by the bulk Na concentration). The equilibrium constant K of reaction (2) is taken such that the residual concentration of sodium is 5% of the sodium concentration in the bulk of the glass (this is usually so in practice). In the new model the hydrogen concentration can assume smaller values than three times the concentration of outward-diffusing sodium ions; this would be impossible with the model discussed earlier of ion exchange between hydronium and sodium ions.

A final remark about this part of the investigation: the experimentally determined profiles can always be 'translated back' into an equilibrium constant of reaction (2) and a diffusion coefficient for H_2O , applicable at the surface. Since they relate only to a very thin layer at the surface, both quantities are difficult to measure experimentally, if at all; nor has it yet proved possible to bring them into relationship with other experimental data, and they cannot therefore be

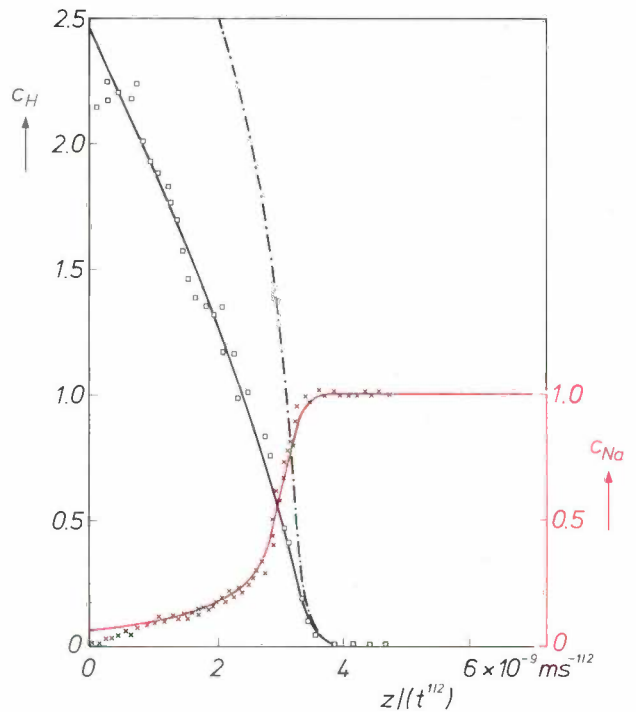


Fig. 8. H and Na profiles (squares and crosses respectively) determined experimentally by SIMS in $20Na_2O.10CaO.70SiO_2$ after treatment with water at $70^\circ C$. The continuous curves (black for H and red for Na) were calculated with the values 0.75 for c_{H_2O} , 3.9×10^{-2} for K and 7.3×10^{-18} for D_{H_2O} . The profiles are clearly not complementary, as they should be for the ion-exchange model (the dot-dash line gives the calculated complementary H profile).

checked against reality. On the basis of the data used so far it is therefore not yet possible to make a definitive statement about the validity of the proposed mechanism.

However, the usefulness of this model also became apparent when we extended the investigation to aluminosilicate glasses.

The corrosion of aluminosilicate glasses by water: ion exchange or diffusion of H_2O ?

The mechanism that we have proposed, with the diffusion of H_2O as the rate-determining step, depends essentially on the presence of non-bridging

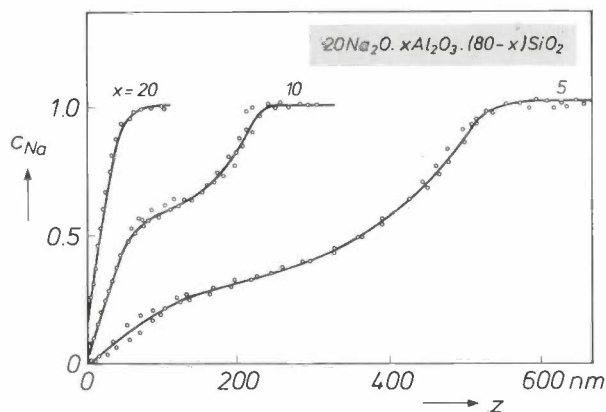


Fig. 9. Na profiles of aluminosilicate glasses of the composition $20\text{Na}_2\text{O} \cdot x\text{Al}_2\text{O}_3 \cdot (80-x)\text{SiO}_2$, determined experimentally with SIMS, for different values of x and after being in contact with water at 70°C for 16 hours.

oxygen atoms in the glass. Aluminosilicate glasses with an Al content higher than the Na content contain no non-bridging oxygen atoms and all the sodium ions are bonded to AlO_4^- groups. In these glasses, therefore, reaction (2) is impossible and in this case the sodium ion would only be removed by an ion exchange process, which is slower.

From fig. 9 it does indeed appear that the presence of Al_2O_3 in glasses of the composition $20\text{Na}_2\text{O} \cdot x\text{Al}_2\text{O}_3 \cdot (80-x)\text{SiO}_2$ has a pronounced effect on the action of water on the glass. The larger the value of x , the slower the leaching. It is also noteworthy that glasses with $x = 5$ and 10 have a distinct plateau in the sodium profile. We know for example that in the glass with 5 mol% of Al_2O_3 one quarter of the sodium ions will be attached to AlO_4^- groups, and three quarters to non-bridging oxygen atoms. It is clear from the measured profile that in this glass three quarters of the ions diffuse rapidly while the other

quarter diffuses much more slowly to the surface. For the glass with 10 mol% of Al_2O_3 half of the sodium ions are attached to AlO_4^- groups and the other half to non-bridging oxygen atoms. We see here that the plateau does indeed occur at 50% of the initial Na concentration. It has been demonstrated that glasses with 20 mol% of Al_2O_3 contain no non-bridging oxygen atoms, and here the whole leaching process does in fact take place very slowly. For the sodium ions thus exchanged we find a diffusion coefficient D_{Na} equal to $2 \times 10^{-19} \text{ m}^2\text{s}^{-1}$, corresponding in order of magnitude to the diffusion coefficient of sodium ions in the bulk of the glass (Table I). All this is in complete accord with the expected behaviour, as described in the foregoing.

On the basis of the mechanism we have found for the corrosion of glass by pure water we also performed experiments in which the pH of the water was varied. The measured corrosion behaviour could also be satisfactorily explained in terms of our model.

Summary. The use of modern methods of surface analysis has led to a new hypothesis for the mechanism of the leaching of alkali-calcium silicate glasses. The distribution of the sodium ions at the surface upon leaching, determined by SIMS, and the associated changes in the content of non-bridging oxygen atoms, measured by ESCA, as well as the resulting ratio of H and Na atoms in the depletion layer, can now be more satisfactorily explained if it is assumed that the rate-determining step is not ion exchange but the diffusion of H_2O . These H_2O molecules enter into a reaction with non-bridging oxygen atoms in the glass, forming silanol groups and releasing OH^- ions. As a result of this reaction the neighbouring Na ions are no longer attached to the glass network and can easily diffuse to the surface, together with OH^- ions as co-ions. In aluminosilicate glasses the Na ions attached to AlO_4^- tetrahedra cannot be released by such a reaction. This then takes place by ion exchange, and much more slowly.

Scientific publications

These publications are contributed by staff of laboratories and plants that form part of or cooperate with enterprises of the Philips group of companies, particularly by staff of the research laboratories mentioned below. The publications are listed alphabetically by journal title.

Philips GmbH Forschungslaboratorium Aachen, Weißhausstraße, 5100 Aachen, Germany	A
Philips Research Laboratory Brussels, 2 avenue Van Becelaere, 1170 Brussels, Belgium	B
Philips Natuurkundig Laboratorium, Postbus 80000, 5600 JA Eindhoven, The Netherlands	E
Philips GmbH Forschungslaboratorium Hamburg, Vogt-Kölln-Straße 30, 2000 Hamburg 54, Germany	H
Laboratoires d'Electronique et de Physique Appliquée, 3 avenue Descartes, 94450 Limeil-Brévannes, France	L
Philips Laboratories, N.A.P.C., 345 Scarborough Road, Briarcliff Manor, N.Y. 10510, U.S.A.	N
Philips Research Laboratories, Cross Oak Lane, Redhill, Surrey RH1 5HA, England	R
Philips Research Laboratories Sunnyvale P.O. Box 9052, Sunnyvale, CA 94086, U.S.A.	S

V. Doormann, J.-P. Krumme, C.-P. Klages & M. Erman <i>H, L</i>	Measurement of the refractive index and optical absorption spectra of epitaxial bismuth substituted yttrium iron garnet films at uv to near-ir wavelengths	Appl. Phys. A 34	223-230	1984
P. Chambon, M. Erman, J. B. Theeten, B. Prévot* & C. Schwab* (* <i>Univ. Louis Pasteur, Strasbourg</i>) <i>L</i>	Spectroscopic ellipsometry and Raman scattering study of the annealing behavior of Be-implanted GaAs	Appl. Phys. Lett. 45	390-392	1984
P. Delsarte, Y. Genin & Y. Kamp <i>B</i>	Parametric Toeplitz systems	Circuits Syst. & Signal Process. 3	207-224	1984
D. Meyer-Ebrecht & T. Wendler <i>H</i>	An architectural route through PACS	Computer 16 (No. 8)	19-28	1983
W. G. Essers & G. A. M. Willems <i>E</i>	Plasma-MIG-Schweißen — Schweißen von Aluminium, Auftragschweißen und Zweielektroden-schweißen von Baustahl	DVS-Berichte 90	9-14	1984
J. H. Waszink & M. J. Piena <i>E</i>	Erzeugung und Transport von Wärme beim Schweißen mit Stabelektroden	DVS-Berichte 90	45-48	1984
A. E. Ronner (<i>Philips ISA-CQM, Eindhoven</i>) & E. Sterken (<i>Univ. Groningen</i>)	Generalization of $M(x)$ -matrices	Econ. Lett. 16	321-326	1984
F. Hottier & M. Fink <i>L</i>	Characterisation of biological tissue by ultrasound	Europhysics News 15 (No. 8/9)	12-16	1984
B. Hill & K. P. Schmidt <i>H</i>	Optischer Bildmuster-generator in Festkörpertechnik für elektrophotografische Drucker	Feinwerktech. & Messtech. 92	189-192	1984
H. U. Ulmer*, K. Würthner* (* <i>Univ.-Frauenklinik, Hamburg</i>) & K. M. Lüdeke <i>H</i>	Vergleich von Mikrowellen- und Infrarotthermographie bei der Entdeckung von malignen Brusttumoren	Fortschr. Röntgenstr. 141	208-211	1984
G. Kersuzan (<i>TRT, Le Plessis-Robinson</i>) & A. G. van Nie <i>E</i>	Modèles de calcul précis pour la détermination de l'augmentation de température de sources de chaleur rectangulaires dans les circuits hybrides	Hybrid Circuits No. 5	4-11	1984
F. L. H. M. Stumpers <i>E</i>	The history, development, and future of telecommunications in Europe	IEEE Commun. Mag. 22 (No. 5)	84-95	1984
K. S. Chung <i>E</i>	Generalized tamed frequency modulation and its application for mobile radio communications	IEEE J. SAC-2	487-497	1984
H. J. M. Veendrick <i>E</i>	Short-circuit dissipation of static CMOS circuitry and its impact on the design of buffer circuits	IEEE J. SC-19	468-473	1984
A. Thayse <i>B</i>	A matrix formalism for asynchronous implementation of algorithms	IEEE Trans. C-33	289-300	1984
P. Piret <i>B</i>	Multiple-word correcting convolutional codes	IEEE Trans. IT-30	637-644	1984

P. Röschmann	<i>H</i>	Intrinsic relaxation of the ferromagnetic resonance in substituted yttrium iron garnets	IEEE Trans. MAG-20	1213-1215	1984
P. Blood & J. J. Harris	<i>R</i>	Deep states in GaAs grown by molecular beam epitaxy	J. Appl. Phys. 56	993-1007	1984
P. Blood & A. D. C. Grassie (<i>Univ. Sussex, Brighton</i>)	<i>R</i>	Influence of clustering on the mobility of III-V semiconductor alloys	J. Appl. Phys. 56	1866-1868	1984
P. C. M. Gubbens*, A. M. van der Kraan* (* <i>Interuniv. Reactor Inst., Delft</i>) & K. H. J. Buschow	<i>E</i>	⁵⁷ Fe Mössbauer effect in ThFe ₅ hydride	J. Appl. Phys. 56	2547-2552	1984
C. P. Janse & A. J. M. Kaizer	<i>E</i>	Time-frequency distributions of loudspeakers: the application of the Wigner distribution	J. Audio Eng. Soc. 31	198-223	1983
E. Stikvoort	<i>E</i>	Digital distortion analyzer	J. Audio Eng. Soc. 32	539-541	1984
A. M. J. G. van Run	<i>E</i>	An optimum time step length for convergence to steady-state solution in compressible-flow calculations	J. Comput. Phys. 56	356-360	1984
M. R. Czerniak & B. C. Easton	<i>R</i>	An investigation of the pyrolysis of dimethylcadmium and diethyltelluride by in-situ gas sampling and analysis	J. Cryst. Growth 68	128-135	1984
M. R. Leys, C. van Opdorp, M. P. A. Viegiers & H. J. Talen-van der Mheen	<i>E</i>	Growth of multiple thin layer structures in the GaAs-AlAs system using a novel VPE reactor	J. Cryst. Growth 68	431-436	1984
J. P. André, A. Brière, M. Rocchi & M. Riet	<i>L</i>	Growth of (Al,Ga)As/GaAs heterostructures for HEMT devices	J. Cryst. Growth 68	445-449	1984
P. J. Roksnoer	<i>E</i>	The mechanism of formation of microdefects in silicon	J. Cryst. Growth 68	596-612	1984
C. J. Werkhoven, C. W. T. Bulle-Lieuwma, B. J. H. Leunissen & M. P. A. Viegiers	<i>S, E</i>	Characterization of metallic precipitates in epitaxial Si by means of preferential etching and TEM	J. Electrochem. Soc. 131	1388-1391	1984
K. H. J. Buschow	<i>E</i>	Influence of short-range order on the thermal stability in amorphous Hf-Ni alloys	J. Non-Cryst. Solids 68	43-51	1984
D. M. Krol & J. G. van Lierop	<i>E</i>	Raman study of the water adsorption on monolithic silica gels	J. Non-Cryst. Solids 68	163-166	1984
K. de Kort	<i>E</i>	Interactions and localisation effects in sputtered Ru and RuO ₂ films	J. Phys. C 17	5237-5260	1984
A. J. M. van den Broek, H. C. Haverkorn van Rijsewijk, P. E. J. Legierse, G. J. M. Lippits & G. E. Thomas	<i>E</i>	Manufacture of LaserVision discs by a photopolymerization video process	J. Radiat. Curing 11 (No. 1)	2-9	1984
J. G. Kloosterboer & G. J. M. Lippits	<i>E</i>	Photopolymerizable coatings for LaserVision video discs	J. Radiat. Curing 11 (No. 1)	10-21	1984
L. D. Knox	<i>N</i>	Squeeze film forces in a magnetic shaft suspension system	J. Tribol. 106	473-476	1984
P. R. Prud'homme van Reine (<i>Philips Lighting Div., Eindhoven</i>) & G. de With	<i>E</i>	De toepassing van Al ₂ O ₃ als keramisch lampomhulmingsmateriaal	Klei/Glas/Keramiek 5	210-215	1984
C.-P. Klages	<i>H</i>	Site selectivity in praseodymium- and bismuth-substituted gadolinium gallium garnet epilayers	Mater. Res. Bull. 19	633-642	1984
C.-P. Klages	<i>H</i>	Dissolution of iron garnet LPE layers in acidic solutions containing reducing agents	Mater. Res. Bull. 19	1329-1336	1984
H. Baumgart, E. Arnold, J. Petruzzello, T. F. McGee & M. H. Frommer	<i>N</i>	Structural properties of dielectric layers following CO ₂ laser irradiation of SOI structures	Mater. Res. Soc. Symp. Proc. 33	87-92	1984
P. Saraga, C. V. Newcomb, P. R. Lloyd, D. R. Humphreys & D. J. Burnett	<i>R</i>	Visually controlled robots for unpacking and mounting television deflection units	Opt. Eng. 23	512-517	1984
A. R. Calderbank (<i>AT&T Bell Labs, Murray Hill, NJ</i>) & J.-M. Goethals	<i>B</i>	Three-weight codes and association schemes	Philips J. Res. 39	143-152	1984
P. Branquart	<i>B</i>	A method of code generation for algorithmic languages	Philips J. Res. 39	153-177	1984
P. J. Courtois & P. Semal	<i>B</i>	Block decomposition and iteration in stochastic matrices	Philips J. Res. 39	178-194	1984

C. Couvreur & P. Piret	B	Codes between BCH and RS codes	Philips J. Res. 39	195-205	1984
M. Davio	B	Algorithmic aspects of digital system design	Philips J. Res. 39	206-225	1984
P. Delsarte, Y. Genin & Y. Kamp	B	Application of the index theory of pseudo-lossless functions to the Bistritz stability test	Philips J. Res. 39	226-241	1984
C. Dierieck & F. Crowet	B	Helmholtz decomposition on multiply connected domains	Philips J. Res. 39	242-253	1984
B. M. J. Smets & D. M. Krol	E	Group III ions in sodium silicate glass. Part 1. X-ray photoelectron spectroscopy study	Phys. & Chem. Glasses 25	113-118	1984
D. M. Krol & B. M. J. Smets	E	Group III ions in sodium silicate glass. Part 2. Raman study	Phys. & Chem. Glasses 25	119-125	1984
M. Davio & J.-J. Quisquater	B	Contemporary evolution in cryptographic techniques	Phys. Technol. 15	191-196	1984
P. Röschmann	H	Ringresonator RF-probes for proton imaging above 1 Tesla	Proc. 3rd Ann. Meeting Soc. Mag. Resonance Med., New York 1984	634-635	1984
P. I. Kuindersma, A. Valster & W. Baks	E	1.3 μm buried heterojunction laser diodes under high electrical stress: leakage currents and aging behavior	Proc. 10th ECOC, Stuttgart 1984	64-65	1984
P. I. Kuindersma & A. H. E. Willekes	E	On the CW multimode behavior of 1.3 μm buried heterojunction laser diodes	Proc. 10th ECOC, Stuttgart 1984	66-67	1984
G. D. Khoe, L. J. Meuleman & J. Poulissen	E	Laser diode devices for coherent fibre optics and special applications	Proc. 10th ECOC, Stuttgart 1984	134-135	1984
C. Kermarrec, J. Faguet, B. Vancon, C. Mayousse, A. Collet, P. Kaikati & D. Beaufort	L	The first GaAs fully integrated microwave receiver for DBS applications at 12 GHz	Proc. 14th Eur. Microwave Conf., Liège 1984	749-754	1984
R. Meierer & C. Tsironis	L	Optimum design of dual gate MESFET amplitude modulators	Proc. 14th Eur. Microwave Conf., Liège 1984	767-772	1984
V. Pauker, B. Bru & M. Binet	L	High real estate efficiency, wideband monolithic GaAs amplifiers	Proc. 14th Eur. Microwave Conf., Liège 1984	773-776	1984
A. Mitonneau, M. Rocchi, I. Talmud, J. C. Mauduit & M. Henry (CNET, Lannion)	L	Direct experimental comparison of submicron GaAs and Si NMOS MSI digital ICs	Proc. GaAs IC Symp., Boston 1984	3-6	1984
H. Sari	L	Baseband equalizer performance in the presence of selective fading	Proc. GLOBECOM '83, San Diego 1983	7 pp.	1983
H. Bourlard, C. J. Wellekens & H. Ney	B, H	Connected digit recognition using vector quantization	Proc. ICASSP 84, San Diego 1984	4 pp.	1984
H. K. Kuiken	E	Etching through a slit	Proc. R. Soc. London A 396	95-117	1984
D. Guyomar, M. Fink & R. H. Coursant	L	Acoustical displacement reconstruction of axisymmetric transducers	Proc. Ultrasonics Symp., Atlanta 1983	766-769	1983
M. Naillon, F. Besnier (CISI, Paris) & R. H. Coursant	L	Finite element analysis of narrow piezoelectric parallelpiped vibrations; energetical coupling modeling	Proc. Ultrasonics Symp., Atlanta 1983	773-777	1983
J. L. Bernatets & F. Hottier	L	Estimation of frequency dependent attenuation in biological tissue by a time-frequency representation of the echographic A-lines	Proc. Ultrasonics Symp., Atlanta 1983	835-840	1983
J. F. Cardoso & M. Fink (Univ. Louis Pasteur, Strasbourg)	L	Diffraction correction in pulse-echo attenuation measurements	Proc. Ultrasonics Symp., Atlanta 1983	841-846	1983
B. Strocka, P. Hansen & H. Heitmann	H	The annealing behavior of ion-irradiated garnet crystals	Radiat. Eff. 72	219-227	1983
P. C. Zalm	E	A critique of semiempirical formulae for the sputtering yield near threshold energy	Radiat. Eff. Lett. 86	29-34	1984
R. L. Bronnes & R. C. Sweet	N	Sputter-sealed IR windows resist thermal effects	Res. & Dev. (November 1984)	130-133	1984
G. F. Neumark & K. Kosai (Santa Barbara Res. Center, Goleta, CA)	N	Deep levels in wide band-gap III-V semiconductors	Semiconductors and semimetals, Vol. 19, R. K. Willardson & A. C. Beer (eds), Academic Press, New York	1-74	1983

C. Loty	L	A 7 GHz CRT for realtime digital oscilloscopy	SID 83 Digest, Philadelphia 1983	126-127	1983
C. Loty	L	Improved simulation of electron beams	SID 84 Digest, San Francisco 1984	262-263	1984
J. S. Nadan & R. N. Jackson	N, R	Signal processing for wide-screen television: the smart receiver	SMPTE J. 93	726-729	1984
S. G. Einstein (<i>Philips Medical Systems, Shelton, CT</i>), A. A. Maudsley*, S. K. Mun*, H. E. Simon*, S. K. Hilal* (<i>* Columbia Presbyterian Med. Center, New York</i>), R. M. Sano (<i>Advanced NMR, Woburn, MA</i>) & P. Röschmann	H	Installation of high-field NMR systems into existing clinical facilities: special considerations	Technology of Nuclear Magnetic Resonance, P. D. Esser & R. E. Johnston (eds), Soc. Nucl. Med., New York	217-231	1984
H. W. Werner	E	The application of beam and diffraction techniques to thin film and surface micro-analysis	Thin film and depth profile analysis, H. Oechsner (ed.), Springer, Berlin	5-38	1984

Contents of Philips Telecommunication Review 43, No. 1, 1985

- J. H. Buijs & J. H. Wolken: Field trial of a 565 Mb/s coaxial line system (pp. 1-11)
 K. Brokkelkamp & F. W. J. Veerman: Electro-magnetic compatibility in Design 400-slim (pp. 12-16)
 C. J. den Hollander: Third-generation higher-order digital multiplex equipment (pp. 17-30)
 J. Drupsteen: A high-capacity 565 Mb/s optical system bridges long distances (pp. 31-42)
 A. Wismeier: Long-distance single-mode fibre transmission (pp. 43-49)
 H. P. J. M. de Wert, V. van der Hulst, G. Kuyt & J. G. J. Peelen: Production of single-mode fibres by the PCVD process (pp. 50-56)
 F. L. van den Berg: An earth station for the EUTELSAT Multi-service System (pp. 57-68)

Contents of Electronic Components & Applications 6, No. 3, 1984

- B. Vernooij: An architectural contrast — 68 000 versus iAPX 286 (pp. 130-140)
 J. Seltzer & N. Siddique: Interfacing different local area networks (pp. 141-148)
 G. Keitel: The KP100A monolithic pressure sensor (pp. 149-154)
 G. Hine: New implosion technology to meet explosion in diode demand (pp. 155-158)
 J. Exalto: HCMOS — fast but cool logic ICs (pp. 159-165)
 R. E. F. Bugg: EUROM — a single-chip colour c.r.t. controller (pp. 166-177)
 C. Mackenna, R. Main & J. Black: Backup support gives VMEbus powerful multiprocessing architecture (pp. 178-185)
 A. Woodworth: Epitaxial diodes — rectifiers compatible with today's fast switches (pp. 186-189)

Contents of Electronic Components & Applications 6, No. 4, 1984

- G. Thomsen: Disk controller supports both rigid and floppy drives (pp. 194-201)
 E. Loward & P. Streit: Liquid-crystal displays for automotive applications (pp. 202-208)
 J. Nijhof: An integrated approach to CD players; Part 1: The optical pickup (pp. 209-215)
 J. Nijhof: An integrated approach to CD players; Part 2: The decoding electronics (pp. 216-222)
 U. Feddern & S. Zur Verth: The frame-transfer sensor — an attractive alternative to the tv camera tube (pp. 223-229)
 G. Thomsen & B. Vernooij: DMA Interface for 68 000 systems (pp. 230-238)
 J. P. Exalto: Interfacing HCMOS with other logic families (pp. 239-245)
 G. Hine: High-voltage rectifier stacks for diode-split transformer (pp. 246-252)

Recent United States Patents

Abstracts from patents that describe inventions from the following research laboratories, which form part of or cooperate with the Philips group of companies:

Philips GmbH Forschungslaboratorium Aachen, Weißhausstraße, 5100 Aachen, Germany	A
Philips Research Laboratory Brussels, 2 avenue Van Becelaere, 1170 Brussels, Belgium	B
Philips Natuurkundig Laboratorium, Postbus 80 000, 5600 JA Eindhoven, The Netherlands	E
Philips GmbH Forschungslaboratorium Hamburg, Vogt-Kölln-Straße 30, 2000 Hamburg 54, Germany	H
Laboratoires d'Électronique et de Physique Appliquée, 3 avenue Descartes, 94450 Limeil-Brévannes, France	L
Philips Laboratories, N.A.P.C., 345 Scarborough Road, Briarcliff Manor, N.Y. 10510, U.S.A.	N
Philips Research Laboratories, Cross Oak Lane, Redhill, Surrey RH1 5HA, England	R
Philips Research Laboratories Sunnyvale, P.O. Box 9052, Sunnyvale, CA 94086, U.S.A.	S

4 458 174

Colour display tube

A. A. de Keijzer

E

A colour display tube comprises, in an evacuated envelope, means for generating a number of electron beams, a display screen comprising a large number of regions luminescing in different colours when struck by the beams, and colour selection means for associating each electron beam with luminescent regions of one colour. The colour selection means includes a plurality of conductive strips and a metal plate having a plurality of parallel apertured rows. The plate, between the apertured rows, and the strips, in the sides facing the plate, have grooves extending in the longitudinal direction of the strips. The strips are accurately positioned between the rows by insulating carriers secured in respective grooves by adhesive materials. Each carrier engages its respective grooves in only two locations per groove. The adhesive material, at least in the grooves of the strips, is an electrically conductive adhesive.

4 481 576

Method of storing data in a memory of a data processing system

J. Bicknell

R

When addressing a store comprising a plurality of low speed memory blocks each of which can be accessed through a high speed buffer having a limited number of memory elements, in accordance with a pattern which is more flexible than sequential then conflicts can occur due to overloading of the memory elements. In order to avoid this, prior to storing data, the address parameters are calculated taking into account the read/write sequence, depth of buffer and access times and a check is made to see if there are any conflicts among the simulated addresses. If so then a number of alternative measures can be tried in order to resolve the conflicts. Such measures include the use of a small capacity, high speed vestigial memory, adding an offset to the addresses or skipping a number of addresses. Once acceptable address parameters have been calculated then a hardware address generator can be instructed to address data accordingly.

4 481 644

Differential pulse code modulation transmission system

J. H. Peters

E

Differential pulse code modulation transmission system in which the transmitter and the receiver each comprise a prediction circuit for generating a prediction signal from the transmitted DPCM-signal. This prediction circuit is in the form of two or more prediction channels each consisting of a non-linear network followed by a leaky integrator circuit. The inputs of these prediction channels are connected to a common input and the output of each prediction channel is connected to an input of a summing device, which produces the desired prediction signal.

4 482 214

Device for applying light to a linear array of magneto-optical light switches, notably for optical printers

B. Hill

H

G. Much

A device for illuminating a line-shaped light switching mask having a plurality of magneto-optical light modulation elements and which is arranged between polarizers, comprising a light source, an optical transmission system for transmitting as large as possible part of the light emitted by the light source to the light switching mask, and at least one optical body which is arranged in the light path between the light source and the light switching mask in order to homogenize the light distribution. The optical transmission system comprises an adapter whose entrance surface corresponds to the geometry of the light source and whose exit surface corresponds to the geometry of the line-shaped light switching mask and a thin light conductor plate. The line direction of the exit surface of the adapter as well as that of the light switching mask extends in the plane of said plate.

4 482 954

Signal processor device with conditional interrupt module and multiprocessor system employing such devices

H. Vrieling

E

E. M. A. M. van der Ouderaa

A. Willemse

Signal processor device having a processor module and a conditional interrupt module for use in a multiprocessor system emp-



PHILIPS

loying these signal processor devices. The processor module has address, data and control inputs and outputs, including an interrupt signal input for receiving an incoming interrupt request signal. The signal processor device has at least one conditional interrupt module in which the identity address of the signal processor is present, said interrupt module having inputs for receiving an incoming external interrupt request signal with corresponding destination address. The conditional interrupt module also has comparators in which its identity address is compared with the destination address. If the addresses agree, an interrupt signal is fed to the interrupt signal input of the processor module. The processor module may also have an interrupt signal output and be provided with an arbitration module to prevent conflicts between several interrupt requests. The provision of the conditional interrupt module enables interrupts to be processed in a multiprocessor system employing a plurality of such devices without all the devices being initially interrupted and without it being necessary to provide a multiplicity of interrupt lines.

4 483 425

Vibration control system

W. S. Newman N

A vibration compensation system for actively attenuating the vibration of a machine. The machine has a housing, with respect to which vibration is to be damped, and at least one body moving within the housing. The vibration compensation system includes a counter-mass capable of being linearly reciprocated relative to the housing in a direction parallel to the motion of the moving body within the machine. A motor, coupled to the housing, drives the counter-mass. Elements are provided for sensing the position, or any time derivative or time integral thereof, relative to the housing of the moving body and the counter-mass. Control elements supply power to the motor in response to the signal outputs from all of the sensors so that the acceleration of the counter-mass is in a direction opposite the acceleration of the moving body. The magnitude of the acceleration of the counter-mass is equal to the product of the acceleration of the moving body multiplied by its mass divided by the mass of the counter-mass.

4 484 037

Ribbon-type electro-acoustic transducer with low distortion and improved sensitivity

J. A. M. Nieuwendijk E
W. D. A. M. van Gijssel

A ribbon-type electro-acoustic transducer has a magnet system which comprises an upper plate and a center pole between which an air gap is formed. A diaphragm on which conductors are arranged is disposed in the air gap. The upper plate comprises two plate-shaped parts between which a space is formed in which an edge portion of the diaphragm is located. This results in a more homogeneous magnetic field so that the transducer distortion may be reduced. Moreover, the transducer sensitivity is improved and is suitable for handling signals in the mid-range audio frequency spectrum. A cavity enclosed by the magnet system and the diaphragm can be acoustically coupled via an additional cavity to a (bass-reflex) duct or an additional (passive radiator) diaphragm.

4 484 108

High frequency ballast-ignition system for discharge lamps

E. H. Stupp N
M. W. Fellows
L. R. Guarnera

A high frequency oscillator-inverter ballast-ignition system for a discharge lamp includes a leakage reactance transformer that forms a part of the oscillator-inverter and also couples same to the discharge lamp. An impedance element electrically couples the primary and secondary windings of the transformer in additive phase to provide more reliable lamp ignition over a wide range of voltage and temperature than was heretofore possible. The preheat time period of the lamp cathodes can be better controlled by a proper choice of the transformer heater windings turns.

4 484 151

Amplifier circuit

A. J. Nijman E
F. A. C. M. Schoofs
J. F. P. van Mil

An amplifier circuit for supplying output voltages which are much higher than the breakdown voltage of the individual components forming the amplifier comprises a control circuit and an amplifier stage. The amplifier stage comprises $2n$ transistors where n is an integer greater than one, having their main current paths serially connected between two supply terminals. The bases of the transistors are connected to tapping points on a series chain of diodes in the control circuit. Further supply sources apply an incrementally decreasing sequence of voltages to the transistors so that the voltage across any of the transistors is limited to one increment of the sequence of voltages.

4 484 163

Arrangement for biasing high-frequency active components

F. C. de Ronde L

An arrangement for applying a DC bias current to an RF active component, such as a field effect transistor, serially-connected with an RF transmission line. The biasing current is supplied by a transmission line section connected at a junction to the transmission line. Two conductive strips, connected in parallel with the transmission line, on opposite sides of the junction, form a band-pass filter. Each of these strips is situated at a distance from the junction which is equal to approximately one-eighth of the wavelength of the signal frequency transmitted on the transmission line.

4 485 315

Blooming suppression in a CCD imaging device

M. G. Collet E
J. G. van Santen

A CCD solid state image sensor device. During the integration period the surface in the image pick-up section is switched alternately into inversion and into accumulation. Any excess of charge carriers which results from possible overexposure can thus be drained by means of recombination via surface states.

4 485 357

Circuit for amplitude and phase modulation of a carrier signal by two respective input signals

J. O. Voorman E

An electronic arrangement for generating an amplitude and phase-modulated carrier signal having a phase modulation stage with two inputs for receiving two modulation signals, which modulation stage generates two different phase-modulated signals having the same carrier frequency and substantially the same amplitude, and an output stage to which the phase-modulated signals are applied for assembling by means of summation of the phase-modulated signals to produce the amplitude and phase-modulated carrier, the amplitude of which is modulated in dependence on the phase difference of the phase-modulated signals and the phase of which is modulated in dependence on the sum of the phases of the phase-modulated signals.

4 485 392

Lateral junction field effect transistor device

B. M. Singer N

A lateral junction field effect transistor device includes both a surface semiconductor layer located between the gate and drain contact regions of the device and a buried semiconductor layer which extends beneath at least the drain contact region and the surface semiconductor layer of the device. The buried layer may be in the form of a continuous layer extending beneath the gate, source, and drain contact regions of the device as well as the surface semicon-

ductor layer, or it may be provided in annular form with an aperture beneath the source and gate regions. The annular central buried layer configuration may further include an additional buried layer portion extending beneath the source region of the device. Devices having buried and surface layers in accordance with the invention feature improved high-voltage breakdown characteristics, enhanced conductivity in the 'on' state, and the ability to operate in the source-follower mode.

4 485 401

Television system for high-definition television and a television transmitter and receiver suitable therefore

S. L. Tan

E

L. J. van de Polder

T. M. M. Kremers

A compatible television system for high-definition and for standardized low-definition television. In a transmitter in the system, a high-definition video signal is generated which is split into a contour signal which on display shows details in the horizontal and vertical directions, and a low-definition video signal. The low-definition video signal is converted into a low-definition video signal in conformity with the standard. The contour signal is also converted, but is transmitted periodically over several picture periods. Both these converted signals are transmitted or stored, respectively, in two separate signal channels, each suitable for standard low-definition television. In a receiver the standard video signal can be utilized directly for low-definition display by a standard display device. In addition, a receiver comprises a high-definition display device in which the converted signals are reconverted and, after having been combined result in a high definition video signal suitable for high-definition display by a picture display apparatus. As high-definition in the region of movement in the picture may disturb the picture quality, the contour signal may be locally suppressed on display.

4 486 697

Reversing device for a two-pole single-phase synchronous motor

G. Diefenbach

A

E. Krainer

A reversing device for a two-pole single-phase synchronous motor without a starting coil. The motor comprises a diametrically magnetized permanent-magnet rotor having a shaft that runs against elastic stops for reversing the direction of rotation, and a capacitor arranged in series with the stator exciter coil. The capacitor serves for improving the reversing operation and is dimensioned so that its reactance at the AC supply frequency is greater than the reactance of the exciter coil of the synchronous motor.

4 486 716

Digital FM demodulator using delay circuits

G. le Floch

L

A digital circuit for demodulating a signal which was modulated in accordance with the relation

$$X = A \sin\left(\omega_0 t + \int_0^t f(t) \cdot dt + \phi_0\right),$$

wherein ω_0 is the carrier and $f(t)$ the modulating signal. This circuit comprises first of all two distinct paths which are arranged in parallel and are formed by two digital value determining stages, the first stage being intended to determine the values of the function

$$M = (1/A) \cos\left(\omega_0 t + \int_0^t f(t) \cdot dt + \phi_0\right),$$

which correspond to the values of the input signal of the two paths and the second stage being intended to determine the derivative of the input signal for said same values of the input signal. The circuit also comprises, at the output of these two paths, a multiplying circuit for corresponding signals supplied by the first and second stages, intended to recover a digital signal which is proportional to the instantaneous frequency of the input signal. A clock circuit determines the rate of operation of the first and second stages and of the multiplying circuit.

4 486 758

Antenna element for circularly polarized high-frequency signals

F. C. de Ronde

L

An antenna element for coupling circularly-polarized radiation to a feedline. The element includes a pair of superposed planar dielectric layers. An outer surface of each layer is covered with an electrically-conductive layer forming a ground plane and having a circular opening defining respective cavities. Orthogonally-crossed dipoles are disposed between the dielectric layers and adjacent the openings for coupling radiation to the feedline through striplines also disposed between the dielectric layers.

4 486 878

Digital telephone exchange with means for processing packet-switched data

G. M. J. Havermans

E

Digital telephone exchange comprising a plurality of peripheral control domains which are either connected to a digital trunk network or are directly interconnected. Each domain comprises several digital subscriber interface units, a group of digital subscriber sets being connected to each interface unit. The transmission of information over the subscriber line is effected in a b-channel for speech (64 kb/s) a b'-channel for circuit-switched data (0/8/64 kb/s) and a Δ -channel for packet-switched data (8/16 kb/s). The subscriber line interface circuits comprise means for identifying the packet-switched data signals and to apply them to a packet processing unit. In this unit the packets are distinguished as firstly signalling information and secondly telemetry and slow data. The separately applied signalling information and telemetry data and slow data intended for a subscriber line are combined by the packet processing unit to form one packet-switched data signal for the subscriber line. In a data unit connected to the trunk network the signals combined into messages are exchanged between the subscribers without loading the central control unit of the telephone exchange.

4 486 882

System for transmitting binary data via a plurality of channels by means of a convolutional code

P. M. O. A. Piret

B, E

T. Krol

A system for correcting multiple simultaneously erroneous channels within a plurality of parallel data channels including redundant channels. At the receiving side a group of syndrome generators each applies a secondary parity check matrix for producing corresponding groups of syndrome bit streams. If the error is correctable, one or more of the syndrome bit streams is added to corresponding code bit streams. If a syndrome bit stream indicates an error in a non-applicable code bit channel, or otherwise indicates too many errors, it remains unused. Decoders with feedback (restoration of syndromes after correction) and feedback-free decoders are possible.

4 487 817

Electrochemical cell comprising stable hydride-forming material

J. J. G. S. A. Willems

E

J. R. G. C. M. van Beek

K. H. J. Buschow

An electrochemical cell having a negative electrode comprising a compound derived from LaNi_5 , in which La is optionally substituted by a plateau pressure-increasing element and in which Ni is substituted entirely or partly by a plateau pressure-reducing element, for example, Co and/or Cu, with the object of considerably reducing volume steps and hence crack formation of the intermetallic compound during charging and discharging. Moreover, the corrosion of the intermetallic compound is counteracted by adding small quantities of Al, Cr and/or Si, which metals enhance the formation of a protecting oxide layer.

4 488 277

Control system for an optical data recording apparatus

R. McFarlane N
G. C. Kenney

A closed loop control system for an optical recording apparatus of the read after write type comprises a comparator for comparing the input data signal with a playback signal derived from the read beam which trails the write beam and is modulated by the data pattern inscribed on the recording medium by the write beam. The error signal generated by the comparator is applied to a controller which varies the modulation of the read beam in dependence on the error signal, for example, by modifying the data signal used to drive the write beam modulator. In this way, the control system compensates for nonuniformities in the recording medium and the like so as to ensure that the pattern inscribed by the write beam accurately represents the data to be stored.

4 488 789

Electromagnetically deflectable device

G. C. Kenney N

An electromagnetically deflectable device includes a mirror pivotally mounted to a support by means of a silicone based resilient element. An electromagnetic deflection coil is fixed to the mirror underside. The coil lead wires are embedded in the resilient element and pass through the element to the support.

4 489 050

Method of preparing a hydrogen-absorbing alloy

R. M. van Essen E
K. H. J. Buschow

Alloys consisting of from 64 to 77 atomic percent of manganese with the remainder zirconium are not suitable without further processing as a material for storing hydrogen at technically desired pressures. This property can be advantageously influenced by a heat treatment until a homogeneous C14 type of Laves phase has been obtained.

4 489 338

Memory cell with thick oxide at least as deep as channel stop

W. G. Voncken E

In a dynamic memory cell, the mutual cross-talk is considerably reduced by providing a diffused selection line below a layer of thick oxide (for example, LOCOS). As a result of this the capacitive coupling with other selection lines is considerably reduced, as is the capacity of the selection line with respect to channel stopping regions provided between the memory cells.

4 489 357

Magnetic sensor having multilayered flux conductors

J. A. C. van Ooijen E
R. D. J. Verhaar

A magnetic sensor includes a magneto-resistive element which magnetically bridges a gap between two magnetic flux conductors. In order to reduce the noise level and higher harmonic distortion of the sensor, each of the flux conductors includes at least two layers of magnetically permeable materials having substantially the same composition between which a layer is present which has a different composition.

4 489 480

Method of manufacturing field effect transistors of GaAs by ion implantation

G. M. Martin L
S. Makram-Ebeid
C. Venger

The invention relates to a method of manufacturing field effect transistors of gallium arsenide obtained by ion implantation of light

donors, such as silicon or selenium, in a semi-insulating substrate of gallium arsenide. In order to reduce out-diffusion of the deep level responsible for parasitic phenomena in the operation of the transistors, the method is characterized in that in addition oxygen ions are implanted in at least the region of the substrate intended to form the channel region of the field effect transistor. After implantation, the substrate is sintered at a temperature between 600 and 900 °C in either an enveloping substance or uncovered, and/or in an atmosphere of arsine.

4 490 163

Method of manufacturing a fiber-optical coupling element

C. M. G. Jochem E
G. D. Khoe
A. J. A. Nicia

A method of manufacturing a fiber-optical coupling element by fusion of two monomode fibers. The fiber cores are made of a core glass, the American softening temperature of which is at least 80 °C higher than that of the cladding glass. The fibers are heated to a temperature between 520 and 560 °C. By the method, fibers can be fused to form a coupling element without undesirable deformation of the fiber cores.

4 490 264

Device incorporating a bearing

J. Gerkema E
A. R. Miedema

Bearings can be lubricated with ductile metal films. It has been found that the service life of such lubricating films can be improved by the use of metals which are alloyed with a component having a higher surface tension than the metal.

4 490 605

Photoelectric detection structure

P. Dolizy L
F. Grolière

The photoelectric device comprises a photosensitive layer on a substrate which is transparent to incident radiation. An intermediate layer for optically adapting the photosensitive layer to the substrate is provided therebetween. The respective thicknesses of the intermediate layer and the photosensitive layer are proportioned so that photon absorption takes place in the photosensitive layer near the output of the layer within a distance on the order of magnitude of the escaping depth of the electrons. Photon absorption takes place in such manner that the efficiency of the photoemission of the structure is optimum taking into account the nature of the materials of the layers.

4 490 695

Wideband power adder-divider for high-frequency circuits and impedance transformer realized on the basis of the adder-divider

F. C. de Ronde L

A wideband power adder-divider for high-frequency circuits including a first conductive transmission line for passing a high-frequency current, second and third conductive transmission lines over which this high-frequency current is distributed, and a conductive wedge-shaped transition section joining the first to the second and third lines. This section has two arc-shaped outer edges which are tangentially connected at one end of the section to the first line and at the other end to the second and third lines. The section includes parallel slots extending transversely to the direction of propagation of the current. The parallel slots have ends which are separated from the arc-shaped edges by a distance which is less than the width of the second and third transmission lines.

4 490 714

Digital-to-analog converter for bipolar signals

R. J. van de Plassche

E. C. Dijkmans

E

In a digital-to-analog converter for bipolar signals all the bits change when the signals pass through the zero level. This results in a poor signal-to-noise ratio owing to the small signal and the large noise contribution by the switching transients. The invention proposes to add a digital number to or subtract it from the digital input signal as an offset. As a result of this, the switching point is shifted towards a higher amplitude, which improves the signal-to-noise ratio and the distortion in the case of digital audio signals.

4 490 839

Method and arrangement for sound analysis

E. Bunge

H

For sound analysis, especially for speaker identification, a long-term spectrum is often formed from the recorded signal and compared to a long-term spectrum of a previously recorded signal. When the signal is, for example, received over telephone lines the transfer function thereof may distort the received signal to such an extent that identification is impossible. It is now proposed not to use the long-term spectrum for identification but rather its change, that is to say to accumulate the difference between two consecutive short-term spectra or the difference between such short-term spectrum and the long-term spectrum and to divide this accumulated value by the long-term spectrum in a Divider. Since the numerator and denominator each contain the frequency-weighting factor of the telephone line transfer function, this factor is effectively cancelled out by virtue of the division operation performed in the Divider thereby eliminating the effect of the unknown transfer function. As a result the influence of the transfer function of the transmission path disappears almost completely.

4 490 906

Shaving apparatus

F. Haes

C. M. Reynhout

E

A shaving apparatus is provided with a shear plate having hair-entry apertures and formed with an inner surface, and a cutting unit associated with and drivable relative to the shear plate. The cutting unit comprises cutting elements extending towards the shear plate, each cutting element having an end surface facing the inner surface of the shear plate and being formed with a cutting edge, and hair-pulling elements respectively associated with the cutting elements and positioned in front of the cutting elements in the direction of driving, each hair-cutting element being rigidly connected to its associated cutting element and having a first end surface portion facing the inner surface of the shear plate and being formed with a contact edge. Each contact edge is situated at a greater distance than its associated cutting edge from the inner surface of the shear plate. Each hair-pulling element also has a second end surface portion adjoining the first end surface portion but situated at a greater distance than the first end surface portion from the inner surface of the shear plate to thereby provide a recess between the end surface of each cutting element and the first end surface portion of its associated hair-pulling element.

4 491 529

Heat accumulating agent

V. Piel

J. Schröder

A

The use of calcium chloride hexahydrate as a heat accumulating agent for latent heat accumulators is improved when as a nucleating agent (so as to avoid supercooling) special caesium salts, bismuth salts and/or lead salts are used.

4 491 743

Voltage translator

D. D. Smith

S

A bipolar voltage translator contains a pair of differentially coupled transistors for converting an input voltage supplied to one of the pair into an output voltage taken between the other and a first resistor. A further transistor coupled through a second resistor to a voltage supply V_{EE} provides current for the differential pair. A voltage reference circuit containing at least three serially coupled diodes with a resistive voltage divider across an intermediate one of the diodes provides the current-source transistor with a reference voltage that equals $V_{EE} + (1 + \alpha)V_{BE}$ where α is 0.2-3.0. The ratio of the first resistor to the second is desirably β/α where β is the output voltage swing divided by V_{BE} . If β is 1 and the transistors are NPN devices, the output voltage level is suitable for current tree logic.

4 491 860

TiW₂N fusible links in semiconductor integrated circuits

S. C. P. Lim

S

A film of titanium-tungsten nitride is used to provide the dual function of a fuse link between a semiconductive device and an interconnect line in a memory array and of a barrier metal between another metal and a semiconductor region.

4 492 426

Optical branch coupler

A. J. A. Nicia

C. J. T. Potters

E

An optical branch coupler comprising a semi-transparent mirror which is tiltable about an axis which is situated substantially in the plane of the mirror and substantially parallel to the plane determined by the directions of the transmitted and the reflected light beams. A wall toward which the reflected beam is directed is adjustable about an axis which is at right angles to the plane of the light beams.

4 492 721

Method of providing magnesium fluoride layers

P. H. Joosten

T. J. A. Popma

H. J. P. Nabben

H. A. M. van Hal

J. Haisma

E

Magnesium fluoride layers are obtained by disproportionation of fluorine-containing organic magnesium compounds, notably magnesium trifluoroacetate, magnesium trifluoroacetylacetonate and magnesium hexafluoroacetylacetonate. A solution of such a compound is provided on the substrate in an organic solvent by spinning or dipping at room temperature after which the layer is heated to 500 °C. The solution may also be atomized and sprayed on the substrate which is maintained at a temperature of 600 °C. It is possible by means of this method to provide pure magnesium fluoride layers at a comparatively low temperature in air and without using film forming vehicles. The MgF₂ layers obtained according to said method are useful as antireflective layers on display screens, on optical elements and as components in a multilayer packet, for example a dichroic mirror.

4 492 967

Optical recording disc

D. J. Broer

A. W. de Poorter

E

Optical recording disc having a supporting plate of synthetic resin or being coated with a layer of synthetic resin, an ablative recording layer on the synthetic resin or the layer of synthetic resin and a phosphorus derivative having at least one organic radical in the interface of the synthetic resin or layer of synthetic resin on the side of the recording layer.

4 492 976

Line standard conversion circuit for a television signal

M. C. W. van Buul

J. G. Raven

W. H. C. A. van de Ven

E

A television receiving system for converting a video signal of one line standard to a video signal of another line standard. A field delay circuit is provided which separates the video signal of the one line standard into a high frequency and low frequency portion. The low frequency portion of the signal is processed to have a delay during one field different from the delay of a subsequent field. Independent processing means for the high frequency portion of the separated signal is provided. The processed high frequency and low frequency signals are combined to provide a video signal for converting to a different line standard. By processing the high frequency and low frequency portions of the video signal differently, a savings in hardware components is realized without material degradation in performance.

4 493 099

FM broadcasting system with transmitter identification

J. M. Schmidt

E

An FM broadcasting system comprises an FM transmitter for transmitting a multiplex signal which is frequency-modulated on a main carrier wave and an FM receiver for cooperation with said FM transmitter. The multiplex signal comprises: an audio-frequency first information signal and, in the case of a stereo transmission, a second information signal modulated on a suppressed stereo subcarrier, a stereo pilot signal whose frequency (f_p) is situated between the frequency spectra of the two information signals, a first binary-code signal ($f_p - f_c$) which is phase-modulated on a first code subcarrier situated outside the frequency spectra, which code subcarrier is a harmonic of a subharmonic of the stereo pilot (f_p) which harmonic does not coincide with a harmonic of said pilot (f_p), the multiplex signal, in order to extend the transmission capacity, comprising a second binary-code signal which is phase-modulated on a second code subcarrier ($f_p + f_c$). The carrier wave information of the two code subcarrier waves can be identified in a simple way by selecting their frequencies to be symmetrical about the stereo pilot signal or its harmonic ($3f_p$) and by selecting the phase angle between the sum of the two code subcarriers and the stereo pilot or the relevant harmonic thereof to be situated at preferably an integral multiple of $\pi/4$.

4 493 365

Heating device with heat storage

F. Ortega

L

A heat storage device comprises a hermetically sealed metallic container having one or more molten alkali metal fluorides and/or alkaline earth metal fluorides included therein. A material having a carbon basis is also included in the metallic container to react with any oxygen present in the metallic container and thereby prevent corrosion of the metallic container by the molten fluorides.

4 493 887

Optical recording element

W. L. Peeters

J. J. Ponjé

J. W. D. Martens

E

Optical recording element comprising a transparent supporting plate which on one side has successively a recording layer of preferably a ferrite, an optional transparent intermediate layer and a reflecting optical structure of reflection areas which are situated alternately at a high level and at a lower level and which can be read optically.

4 494 031

High power acoustic wave arrangements with N^2 parallel-series connected acoustic wave devices

C. S. Barnes

P. A. Moore

P. D. White

R

N^2 acoustic wave devices with substantially the same electrical impedance and transfer characteristics at a given operating frequency are electrically connected in a parallel-series arrangement which has substantially the same electrical impedance and transfer characteristics as any one of the individual N^2 devices, but an increased active device area. The increased active area reduces stress and alleviates acoustically-induced migration in the metal of, for example, transducer electrode fingers of resonators at high power levels. The parallel-series arrangement consists of N groups, each of which comprises N devices, the corresponding pairs of terminals of which are connected in series. Some terminals may be common to two or more devices and some devices may have merged transducers in which the electrode fingers of one transducer are a longitudinal extension of the fingers of a parallel transducer. In the case of multiport devices the input and output terminal pairs may be differently grouped as regards the individual devices to which they belong.

4 495 221

Variable rate semiconductor deposition process

E. K. Broadbent

S

A layer of a conductive material consisting of aluminium alone or in combination with a small percentage of copper and/or silicon is formed on a semiconductor surface in a two-step deposition process in such a manner as to largely avoid serious continuity defects in the layer.

4 495 412

Device for the optical scanning of a document

M. L. G. Thoone

G. D. Khoe

D. Küppers

P. A. G. J. Gustin

E, A, B

The device comprises a transducer comprising a row of photoelectric elements, and a coupling member with an entrance which is to be directed towards the document and an exit which is coupled to the transducer. The coupling member is constructed as an integrated optical waveguide circuit comprising a glass substrate in which there are provided grooves which, in order to form optical conductors, are filled with a glass having a refractive index which is higher than that of the glass of the substrate. The width of each groove gradually decreases from the entrance of the coupling member towards the exit and over the entire length of the grooves the distance between every two adjacent grooves is substantially constant and substantially smaller than the width of the grooves, so that substantially all light originating from a scanned line of the document is supplied to the transducer.

4 496 202

Device for high voltage transfer between two parts which are rotatable relative to each other

F. K. Beckmann

T. Helzel

H. Peemöller

H

The invention relates to a high voltage transfer device comprising two insulator bodies which are rotatable with respect to each other. In each insulator body there is embedded an electrode arrangement which horizontally encloses the axis of rotation. The two electrode arrangements together form a kind of Faraday cage, so that the field between the two electrode arrangements and in their vicinity is corrected and reduced.

4 497 699

Method of treating foil for electrolytic capacitors*H. J. de Wit**A. W. M. van Berlo**C. Crevecoeur*

A method of treating foil for use in electrolytic capacitors in which the foil moves in one direction through a treatment liquid and in which the capacitance is measured continuously by means of at least one current-carrying electrode from which alternating current is conveyed and at least one voltage electrode at a small distance from the foil. The foil capacitance is measured by means of a phase-sensitive voltmeter. The measured capacitance is used to control the treatment method, etching or forming. In a preferred embodiment two current-carrying electrodes are present on either side of the foil and two voltage electrodes are present between the current-carrying electrodes and the foil on either side thereof. This avoids contacting of the foil.

4 498 111

Method and apparatus for recording or reproducing stereophonic information in a magnetic record carrier*A. M. A. Rijckaert**A. Walraven*

In accordance with a method of recording and/or reproducing stereophonic information in two adjacent tracks of a magnetic record carrier, an auxiliary signal whose frequency content is situated outside the frequency spectrum of the stereophonic information is recorded in the tracks and in the magnetic record-carrier area between the tracks during recording. During reproduction, the auxiliary signals read from the record carrier by the two transducers are used to control the gain of a pair of variable amplifiers so as to ensure that the amplitudes of the stereophonic information signals thus reproduced are independent of tracking errors.

4 498 296

Thermodynamic oscillator with average pressure control*K. Dijkstra**A. J. Garenfield*

A thermodynamic oscillator having a displacer and a piston (further displacer) movable due to pressure fluctuations at the resonance frequency of the oscillator. The displacer and the piston are located in a working space which is filled with working medium and can be connected through a release valve and a supply valve, respectively, to a simple reservoir filled upon working medium with an increase and a decrease, respectively, of the ambient temperature with respect to a nominal temperature. The valves have an opening pressure which is a function of the ambient temperature. The average pressure and the resonance frequency of the oscillator can thus be stabilized at a variable ambient temperature. The oscillator can be operated as a cold-gas engine, a hot-gas engine (motor), a heat pump or a current generator.

4 499 011

Resistance paste for a resistor body*A. H. Boonstra**C. A. H. A. Mutsaers**F. N. G. R. van der Kruijs*

A resistance paste for the manufacture of a resistor body, for example, by silk-screening and the resistance body manufactured herewith, which paste comprises a mixture of $Pb_2Rh_xRu_{2-x}O_{7-y}$, a permanent binder and a temporary fireable binder. In the formula $0.15 \leq x \leq 0.95$ and $0 \leq y \leq \frac{1}{2}$. The resulting resistor body in the temperature range of from -55 to $+150^\circ C$ has a temperature coefficient of the resistance between $-10 \times 10^{-6}/^\circ C$ and $+10 \times 10^{-6}/^\circ C$ and is very stable. The resistance variation during the life of the resistor is smaller than $\pm 0.5\%$.

4 499 177

Method of manufacturing a semiconductor device*F. A. Vollenbroek**E. J. Spiertz*

A method of manufacturing a semiconductor device in which a photosensitive lacquer layer is developed in a lye solution, and comprises a polymeric material and a sensitizer with a diazo group and a ketone group. This lacquer layer is formed on a substrate surface. After a patterning irradiation, but before development, the lacquer layer is subjected to an intermediate treatment comprising two irradiations. These irradiations result in that differences in solubility in lye are obtained in the direction of thickness in the parts of the lacquer layer which were not exposed during the patterning irradiation. In this manner, it is possible to realize lacquer patterns with different profiles.

4 499 521

Low-fire ceramic dielectric compositions for multilayer ceramic capacitors*R. T. McSweeney**S. A. Long*

A low fire ceramic dielectric composition, a multilayer capacitor made from such a ceramic dielectric composition provided with silver/palladium electrodes having at least 65 atomic percent silver, and a method of manufacturing such a multilayer capacitor. The ceramic is barium titanate-based and includes Bi_2O_3 , Nb_2O_5 and TiO_2 to improve sinterability. $MnCO_3$ is added to increase the insulation resistance. The multilayer capacitor includes high silver-content electrodes to reduce the quantity of expensive noble metals. The multilayer part may be fired at a temperature of $1150^\circ C$ or less to yield a capacitor meeting EIA specification X7R. The low firing temperature also inhibits a chemical reaction between bismuth and palladium.

4 499 524

High value surface mounted capacitor*L. J. Shiolen*

A high value surface mounted capacitor assembled from a ganged assembly of multilayer ceramic capacitors adapted to fit within a package which may be either surface mounted or pin mounted, said package being shaped for handling by automatic insertion equipment.

4 499 540

Device for the testing of bodies comprising periodic structures*G. Kowalski*

The invention relates to a device for testing a body which comprises periodic structures. The device includes an image forming device for determining measurement signals representing the periodic structures, and a further electronic device. This electronic device forms the frequency spectrum from neighbouring measurement values in the direction of the periodic body structures, suppresses the fundamental and higher harmonics of the periodic structures in the relevant spectrum, and retransforms the spectrums thus modified for application to an image evaluation device.

4 499 570

Dropout circuit arrangement for converting an information signal into a rectangular signal*K. A. Schouhamer Immink**R. M. Aarts*

For the conversion of a signal read from a record carrier into a rectangular signal, a threshold-value circuit is used, whose threshold value is determined by a reference signal. The reference signal is derived from a d.c. component in the converted signal. During a dropout in the signal being read, the reference signal is maintained at the level which it had before the occurrence of the dropout.

4 499 574

Record carrier with an optically readable information structure

J. J. M. Braat

E

A record carrier is described having an optically readable information structure comprising trackwise arranged information areas which, in the track direction, alternate with intermediate areas, the information being contained in at least the local length of the information areas, of which information structure the average length of the information areas varies. It is demonstrated that by adapting the track period to the average length of the information areas in the tracks, the cross-talk between the tracks may be reduced without essentially reducing the information density.

4 500 825

Self-starting single-phase synchronous motor

H. Schemmann

H

L. Bertram

A self-starting single-phase synchronous motor without an auxiliary coil comprises a diametrically magnetized permanent-magnet rotor and a two-pole stator provided with exciter coils. A PTC resistor is arranged in the circuit of the exciter coils. The PTC resistor is proportioned so that its resistance will increase to a continuously permissible load resistance value after approximately 0.5 to 1 sec.

4 501 016

Device for the dynamic adjustment of a black/white discrimination threshold for the processing of images containing grey values

E. H. J. Persoon

E

R. M. S. S. Abeysekera

A device for binarizing an image consisting of grey values by means of a dynamically adjusted black/white discrimination threshold comprises: a. a generator for determining a discrimination threshold each time for a first local sub-set of pixels; b. an edge detector for determining a local edge between darker and lighter pixels from a second local sub-set of pixels, associated with a first local sub-set of pixels, in order to form an accept signal, and otherwise a reject signal; and c. a discriminator for presenting, on the basis of a grey value and the relevant discrimination threshold, alternatively a black or a white signal.

4 501 967

Broad band pyroelectric infrared detector

A. Shaulov

N

An infrared thermal detector includes an infrared thermal sensing element, a load resistor, and a voltage supply means. The infrared thermal sensing element is a pyroelectric material whose electrical conductivity changes with temperature. The circuit and device parameters are chosen such that the detector will have a frequency response over a broad band from dc to a high frequency determined by the electronic time constant of the circuit. The detector thus has all the advantages of either a pyroelectric detector without a chopper, or a thermistor bolometer having a fast response time.

4 502 017

Operational amplifier having frequency compensation

R. J. van de Plassche

E

E. C. Dijkmans

An operational amplifier with frequency compensation is described. The amplifier includes a first amplifier with a low-impedance output followed by a transconductance amplifier with a capacitive feed-forward. The transconductance amplifier is followed by a Miller integrator.

4 502 019

Dynamic amplifier circuit

A. H. M. van Roermund

E

A dynamic amplifier circuit, specifically for switched-capacitor filters, having a current source which supplies an exponentially-decreasing bias current. In addition, a current source is included for supplying an additional bias current in order to define the minimum bias current in the amplifier circuit.

4 503 346

Electric motor having a stator iron of a bent shape

L. Bertram

H

H. Schemmann

Electric motor, in particular series-, split-pole- and single-phase synchronous motor, having a bent stator iron, pole shoe shanks formed by the stator iron which form pole shoes at their free ends. Induction coils are provided on the pole shoe limbs. A rotatable, radially magnetized permanent magnetic rotor is present between the pole shoes. In this electric motor the oppositely located pole shoes are formed at the end faces of the pole shoe shanks. The rotor shaft intersects the central longitudinal line of the two pole shoe shanks. Finally, the parts of the pole shoe shanks facing away from the pole shoes are bent and interconnected in the form of a bridge.

4 503 482

Ceramic dielectric based on bismuth-containing BaTiO₃

D. Hennings

A

H. Schreinemacher

Ceramic dielectric based on bismuth-containing BaTiO₃ in the form of a monophase mixed crystal-ceramic in which 0.02 to 0.12 mol of the layer perovskite PbBi₄Ti₄O₁₅ or SrBi₄Ti₄O₁₅ per mol of BaTiO₃ are provided. On account of its comparatively low sintering temperature and in particular on account of the very small change of the value of the relative dielectric constant with applied direct voltage fields, the ceramic is particularly suitable for the manufacture of multilayer capacitors.

4 504 111

Method of multiplexing transmission channels in a step-index optical fibre and device for carrying out the method

J. J. Hunzinger

L

An optical multiplexer wherein a plurality of channels are formed in a step index optical fibre by groups of light rays which propagate along the fibre by consecutive total reflections at the core/cladding interface. The rays are grouped depending on their angle with the fibre axis so that for each channel, at any point of the fibre, the rays of a given group are situated between two cones whose common apex is formed by that point and which are rotationally symmetrical about a common axis parallel to the fibre axis. The cones define the portion of the angular aperture relating to each channel. The aperture portions relating to all the channels are moreover juxtaposed. A multi-axial optical system directs each of a plurality of light signals along a region defined by the cones so as to inject the light signal into the aperture portion of the associated channel for each channel at the fibre input and reception means which are specific of the aperture portion of said channel at the output.

4 504 574

Method of forming a resist mask resistant to plasma etching

J. Meyer

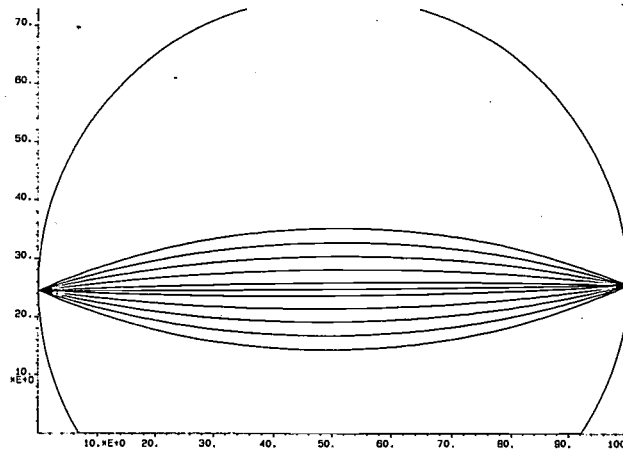
R

D. J. Vinton

A mask which is resistant to a plasma etching treatment is formed by lithographically patterning a radiation sensitive film present on a substrate. The etch resistance of the mask is enhanced by exposure to a carbon monoxide plasma which forms a region with an enhanced etch resistance over the surface of the patterned film. This method may be used, for example, to manufacture a photomask using a chromium coated glass substrate, or during the manufacture of semiconductor devices on a semiconductor wafer substrate.

CAD in light optics and electron optics

K. J. van Oostrum



In 1854 J. C. Maxwell devised his fish-eye lens — a sphere with a radially diminishing refractive index []. The optical characteristics of this lens, which can produce a perfect image of an object, as the computer plot above suggests, are fairly easy to calculate analytically. This is not generally the case with optical elements of varying refractive index as used today for data transmission. The refractive index distribution for light-optical elements can be more or less freely chosen, but for electron-optical elements the Laplace equation or Maxwell's equations have to be taken into account when determining the corresponding distribution. In the absence of analytical solutions it is necessary to resort to numerical methods of approximation. Light optics and electron optics have developed quite independently, so it is somewhat surprising to find that the same software is now being used at Philips Research Laboratories in Eindhoven for solving problems in both fields. Different designs can thus be optimized in a short time by CAD (Computer-Aided Design). Hypothetical experiments can be performed on the monitor screen in the first stage of development, so that there is no need for the time-consuming and expensive construction of experimental models.*

Introduction

The Laplace equation is of great use in various branches of physics: in hydrodynamics, mechanics and more especially in electrical field theory. In a rectangular coordinate system the Laplace equation for an electrostatic field with no space charge may be written:

$$\frac{\partial^2 V}{\partial x^2} + \frac{\partial^2 V}{\partial y^2} + \frac{\partial^2 V}{\partial z^2} = 0$$

or briefly

$$\Delta V = 0, \quad (1)$$

where V is the electrical potential and Δ the Laplacian operator. The solution of this important equation was long a scientific challenge. Since an analytical solution only exists for simple cases, various methods of ap-

[*] See page 76 of W. D. Niven (ed.), The scientific papers of James Clerk Maxwell, Hermann, Paris 1890; E. W. Marchand, Gradient index optics, Academic Press, New York 1978.

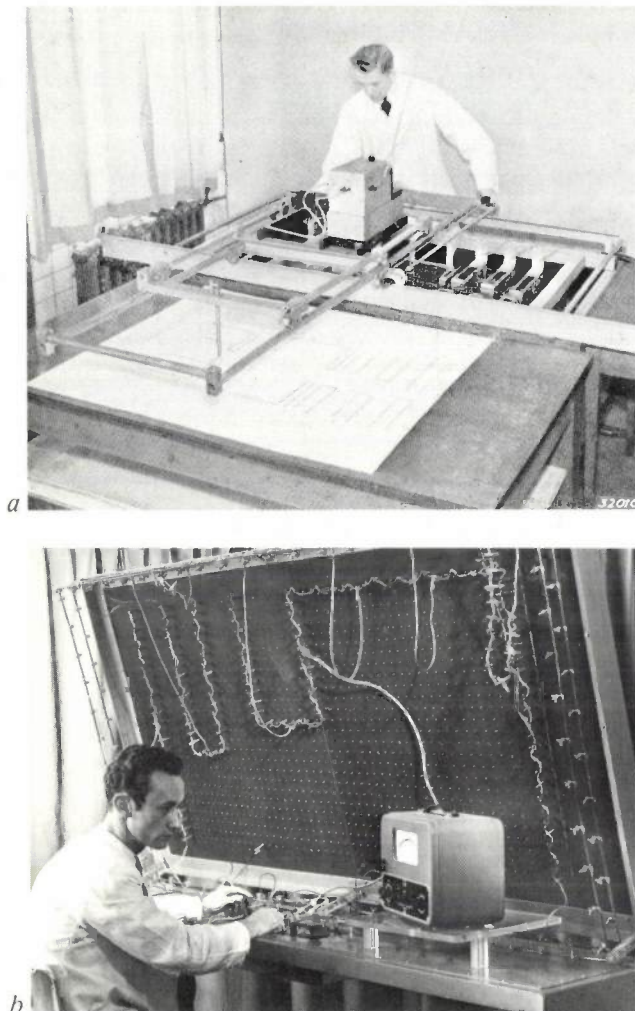


Fig. 1. Examples of classical methods of solving the Laplace equation. *a)* The electrolytic tank. *b)* The resistance network.

proximation have been devised, some of them showing considerable ingenuity. A few of these methods will be briefly reviewed here, in the same chronological sequence in which they appeared in the pages of this journal [1].

The form of a stretched membrane (such as a soap film) is also described by the Laplace equation. The vertical deflection of the membrane is equivalent to the potential V in equation (1). The boundary conditions, which are given by direct voltages on electrodes, can be taken into account by local deflections of the membrane. In experiments the membrane is usually a rubber sheet; steel balls rolling on it simulate the electrons and the force of gravity simulates the electrostatic force. Only two-dimensional problems can be solved with this model. The familiar electrolytic tank, illustrated in *fig. 1a*, can be used to solve two-dimensional problems and three-dimensional problems with rotational symmetry. The solutions obtained are equipotential surfaces; the electron trajectories have to be

constructed from equipotential lines. The use of the electrolytic tank for two-dimensional problems is roughly comparable with the use of conducting paper, which was widely used for such problems.

Resistance networks, as a method of solving two-dimensional problems, give a transition to the numerical methods of solution used today; see *fig. 1b*. The correspondence with the numerical methods is that a network divides the area under investigation into elements; the nodes of the network are connected by resistances. The equipotential lines are found by measuring the voltages at the nodes. The method is improved by combining the resistance network with an analog computer, which can simulate differential equations by means of circuits including operational amplifiers. The resistance network then gives the equipotential lines, and from these the analog computer calculates the electron trajectories, which are traced on an XY recorder.

An advantage of these classical methods of solving the Laplace equation and determining the electron trajectories is that the geometry and the electrode voltages can fairly easily be changed. These classical methods do however have the disadvantage that their accuracy is limited. Another disadvantage is that it is extremely difficult or impossible to take account of the space-charge effects of the electrons in their trajectories. The presence of space charge requires a correction of the Laplace equation, transforming it to the Poisson equation:

$$\frac{\partial^2 V}{\partial x^2} + \frac{\partial^2 V}{\partial y^2} + \frac{\partial^2 V}{\partial z^2} = -\frac{\rho}{\epsilon_0}, \quad (2)$$

where ρ is the charge density (in C/m^3) and ϵ_0 is the permittivity of free space. Using the Laplace equation for the calculation thus introduces an additional error in the electron trajectories.

It was largely due to C. Weber that the foundations for the ELOP (electron optics) software package for calculating electron trajectories in electrostatic fields [2] were laid at Philips Research Laboratories in Eindhoven in the sixties. The first such calculations were made at the time on the PASCAL computer [3] developed at Philips, which succeeded an experimental computer built in 1954 at Philips Research Laboratories. The mathematical foundation of Weber's program for determining potentials at the nodes of a network is formed by the iterative solution of a set of difference equations that approximate to the Laplace equation. The convergence of the iteration is improved by applying the method known as successive over-relaxation. The associated program for calculating the electron trajectories is based on the solution of the equations of motion of an electron, for a series of successive

points in time, and makes use of a Runge-Kutta third-order integration process proposed by J. A. Zonneveld^[4]. The special feature here is that the program determines the size of each 'time interval' in such a way that the residual error in position and velocity per

and the results are shown on a graphic display in the form of equipotential lines and electron trajectories. Successive programs in the package can be called as required. The user can move crossed wires over the graphic display to indicate the electrodes whose geom-



Fig. 2. The GELOP terminal. Left, the graphic display, right, the alphanumeric screen. 'Menus' displayed on the alphanumeric screen enable the user to make his wishes known to the computer system. The results of the calculations are displayed on the graphic display.

calculation step always has the same (predetermined) value. The interval length thus increases with increasing radius of curvature of the trajectory.

The ELOP software package can be used to calculate two-dimensional, rotationally-symmetrical three-dimensional and general three-dimensional potential distributions, as well as the associated electron trajectories. Space charge can be taken into account if there is rotational symmetry. The increase in the storage capacity and speed of computers through the years has resulted in greater accuracy and shorter computer times. Until recently, however, the difficulty with these programs was that they were not so convenient to use as the classical methods of solution. Varying the problem parameters took a relatively long time, as the data had to be fed into the computer on punched cards. Nor was the presentation of the results very convenient: the output was first obtained as series of numbers and later in the form of diagrams traced by a plotter.

The addition of the GELOP ('graphics for electron optics') software package has made the programs much easier to use. The user can now input the data to the system from his own terminal; see *fig. 2*. 'Menus' presented on the alphanumeric screen enable the user to make his wishes known to the computer system,

etry or potential he wishes to change. If required, the modulation transfer functions, intensity distributions in the image plane or geometrical aberrations can be calculated. The user thus performs hypothetical experiments, which would be very difficult to carry out

- [1] P. H. J. A. Kleynen, The motion of an electron in two-dimensional electrostatic fields, *Philips Tech. Rev.* **2**, 338-345, 1937; G. Hepp, Measurements of potential by means of the electrolytic tank, *Philips Tech. Rev.* **4**, 223-230, 1939; G. Alma, G. Diemer and H. Groendijk, A rubber membrane model for tracing electron paths in space charge fields, *Philips Tech. Rev.* **14**, 336-344, 1953; J. C. Francken, The resistance network, a simple and accurate aid to the solution of potential problems, *Philips Tech. Rev.* **21**, 10-23, 1959/60; J. L. Verster, An apparatus for automatically plotting electron trajectories, *Philips Tech. Rev.* **22**, 245-259, 1960/61; A. J. F. de Beer, H. Groendijk and J. L. Verster, The plotting of electron trajectories with the aid of a resistance network and an analogue computer, *Philips Tech. Rev.* **23**, 352-362, 1961/62.
- [2] C. Weber, Calculation of potential fields and electron trajectories using an electronic computer, *Philips Tech. Rev.* **24**, 130-143, 1962/63; C. Weber, Analogue and digital methods for investigating electron-optical systems, Thesis, Eindhoven 1967.
- [3] W. Nijenhuis, The "PASCAL", a fast digital electronic computer for the Philips Computing Centre, *Philips Tech. Rev.* **23**, 1-18, 1961/62.
- [4] J. A. Zonneveld, Automatic numerical integration, Thesis, Amsterdam 1964; C.-E. Fröberg, Introduction to numerical analysis, Addison-Wesley, Reading, MA, 1966; M. Abramowitz and I. A. Stegun (eds), Handbook of mathematical functions, 10th edition, National Bureau of Standards, Washington 1972.

or perhaps impossible in an actual experiment in the real world. Once reasonably definitive values for the design parameters have been decided on, the user can obtain a definitive plot of the geometry on the graphic display, with the equipotential lines and the electron beams. With all these facilities available an electron-optical design can be optimized in an hour or two. This used to take many months, because of the time-consuming construction of experimental models, and the results were far less reliable.

The practical scope of the ELOP and GELOP software packages has recently been considerably extended. The facilities for solving general three-dimensional problems have been increased and extra software packages are now available for calculating magnetic fields and for solving problems of light optics. The calculation of electron trajectories in a combined electrostatic *and* magnetic field has special relevance to the design of Plumbicon camera tubes and television picture tubes. (In both types of tube the electron beam is deflected horizontally and vertically by magnetic fields.) The program for light-optical problems can calculate the path of light rays in media of varying refractive index. This is especially important for the design of data transmission lines with graded-index optical fibres.

In the following we shall first look at the theoretical background of the programs for the potential calculations, the trajectory calculations and the light-optical calculations. We shall then consider the software and a number of applications.

Theoretical background

Calculating the potential distribution

The space for which we wish to calculate the potential distribution is divided into elements by a rectangular grid or network. The solution of the Laplace equation (1) is based on the solution of as many difference equations as there are nodes in the grid. For each node a difference equation gives the relation between the potential at the node and the potential at the surrounding nodes. A unique solution of the set of difference equations is possible if the potential at the contours of the space considered is specified in the form of boundary conditions. As the number of nodes increases, i.e. as the grid becomes finer, the set of difference equations approximates more closely to the Laplace equation, though the computer time required becomes longer.

We shall derive the difference equation for one point for the two-dimensional case ($\partial V/\partial z = 0$). The equation gives the relation between the potential $V(P_0)$ at the point P_0 and the potential at the

surrounding points P_1 to point P_4 ; see *fig. 3a*. We expand the potentials $V(P_1)$ to $V(P_4)$ in a Taylor series, neglecting terms of third and higher order:

$$V(P_1) = V(P_0) + h_x \left(\frac{\partial V}{\partial x} \right)_{P_0} + \frac{1}{2} h_x^2 \left(\frac{\partial^2 V}{\partial x^2} \right)_{P_0}, \quad (3a)$$

$$V(P_3) = V(P_0) - h_x \left(\frac{\partial V}{\partial x} \right)_{P_0} + \frac{1}{2} h_x^2 \left(\frac{\partial^2 V}{\partial x^2} \right)_{P_0}, \quad (3b)$$

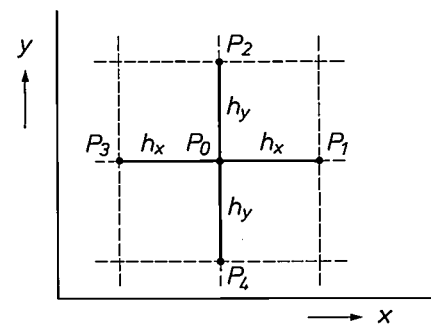
$$V(P_2) = V(P_0) + h_y \left(\frac{\partial V}{\partial y} \right)_{P_0} + \frac{1}{2} h_y^2 \left(\frac{\partial^2 V}{\partial y^2} \right)_{P_0}, \quad (3c)$$

$$V(P_4) = V(P_0) - h_y \left(\frac{\partial V}{\partial y} \right)_{P_0} + \frac{1}{2} h_y^2 \left(\frac{\partial^2 V}{\partial y^2} \right)_{P_0}. \quad (3d)$$

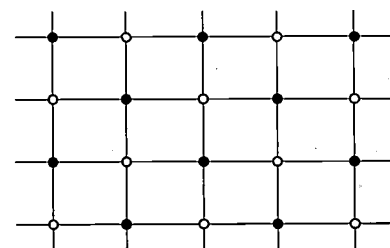
From these equations we derive the expressions for $(\partial^2 V/\partial x^2)_{P_0}$ and $(\partial^2 V/\partial y^2)_{P_0}$. The Laplace equation gives a relation between these two derivatives, from which in turn the required difference equation for the point P_0 can be obtained:

$$V(P_0) = \frac{h_y^2 \{V(P_1) + V(P_3)\} + h_x^2 \{V(P_2) + V(P_4)\}}{2(h_x^2 + h_y^2)}. \quad (4)$$

For N nodes of the grid there are thus N difference equations. At a number of the nodes the potentials are known because of the boundary conditions.



a



b

Fig. 3. The rectangular grid for the numerical solution of the Laplace differential equation. *a*) The quantities that can be used to express the potential at a point P_0 in terms of those at the points P_1 to P_4 . The mesh widths in the x - and y -directions are h_x and h_y . *b*) The 'checker-board' distribution of the points of the grid. The potentials at the 'white points' are calculated from those at the 'black points' and vice versa.

Proceeding from the boundary conditions and a first estimate of the potential at the points inside the boundaries, we calculate a new value for the potentials with the aid of the difference equations. With these values and the boundary conditions we can repeat the

calculation. In the resulting iterative process the calculated values give a steadily improving approximation to the true solution as the number of iterations increases. During the process we thus have to keep replacing the potentials at all the points by new potential values. This means that for every two successive computing steps the potentials at all the points should be stored in the computer memory. In fact half this amount of storage is sufficient if we adopt a procedure in which the potential at one point is always replaced by a better approximation, and all the points are then worked through in succession. D. Young has shown that the order in which this is done for the various points of the grid is very important [5]. He demonstrated that the nodes should be grouped in such a way that for calculating the potentials in one group it is only necessary to have the potentials of the previous group. A distribution of points that satisfies this requirement is known as the checker-board distribution; see fig. 3b.

In the procedure described the potential at a point gradually converges towards the true value. The convergence of the iterative process can be improved by extrapolating in the direction of the change every time a potential is replaced. Thus, in step $k+1$ we do not replace the potential V_k by V_{k+1} but by $V_k + \omega(V_{k+1} - V_k)$, where ω is the over-relaxation factor. This procedure is known as the method of successive over-relaxation. Convergence is only obtained when $0 < \omega < 2$. The convergence is improved when the range for the over-relaxation factor is $1 < \omega < 2$. Our program calculates the optimum value of ω for every step in the iteration process [6], after the user has entered an initial value, which is usually 1.5.

Calculating the electron trajectories

The three equations that describe the motion of an electron in a combined electrostatic and magnetic field for the general three-dimensional case are:

$$\frac{d^2x}{dt^2} = \frac{e}{m} \left\{ \frac{\partial V}{\partial x} + \mu_0 \left(\frac{dz}{dt} H_y - \frac{dy}{dt} H_z \right) \right\}, \quad (5a)$$

$$\frac{d^2y}{dt^2} = \frac{e}{m} \left\{ \frac{\partial V}{\partial y} + \mu_0 \left(\frac{dx}{dt} H_z - \frac{dz}{dt} H_x \right) \right\}, \quad (5b)$$

$$\frac{d^2z}{dt^2} = \frac{e}{m} \left\{ \frac{\partial V}{\partial z} + \mu_0 \left(\frac{dy}{dt} H_x - \frac{dx}{dt} H_y \right) \right\}, \quad (5c)$$

where H_x , H_y and H_z are the three components of the magnetic field-strength, t is the time, μ_0 is the magnetic permeability of free space, and e and m are the charge and mass of an electron. In this article the treatment will be limited to calculations of electron trajectories in purely electrostatic fields, although the

software package can also be combined with other programs to allow calculation of trajectories in a combination of electrostatic and magnetic fields.

The numerical method of approximation used, based on a Runge-Kutta integration process of the third order, will be described here for the one-dimensional equation of motion:

$$\ddot{x} = f(x), \quad (6)$$

where

$$f(x) = \frac{e}{m} \frac{\partial V}{\partial x}.$$

The initial values for x and dx/dt at the starting time $t = t_0$ are:

$$x(t_0) = x_0, \quad (7a)$$

and

$$\dot{x}(t_0) = \dot{x}_0, \quad (7b)$$

where x_0 and \dot{x}_0 represent given numbers.

The successive phases in the algorithm will be given, resulting in estimates $\tilde{x}(t_0 + \tau)$ and $\tilde{\dot{x}}(t_0 + \tau)$ for the position and the velocity of the electron at the time $t = t_0 + \tau$, where τ represents a small time interval. It will then be shown that the error introduced is of the order of magnitude of τ^4 . It must therefore be shown that:

$$\tilde{x}(t_0 + \tau) - x(t_0 + \tau) = O(\tau^4), \quad (8a)$$

and

$$\tilde{\dot{x}}(t_0 + \tau) - \dot{x}(t_0 + \tau) = O(\tau^4). \quad (8b)$$

First of all, equation (6) can be used to calculate two ancillary quantities k_0 and k_1 from the data (7a,b) and the time interval τ . These quantities k_0 and k_1 are defined as:

$$k_0 = \tau f(x_0), \quad (9a)$$

and

$$k_1 = \tau f(x_0 + \frac{2}{3}\tau \dot{x}_0 + \frac{2}{9}\tau k_0). \quad (9b)$$

The algorithm gives estimates for the position and the velocity that depend on the initial values and the ancillary quantities in the following way:

$$\tilde{x}(t_0 + \tau) = x_0 + \tau \dot{x}_0 + \frac{1}{4}k_0 + \frac{1}{4}k_1, \quad (10a)$$

and

$$\tilde{\dot{x}}(t_0 + \tau) = \dot{x}_0 + \frac{1}{4}k_0 + \frac{3}{4}k_1. \quad (10b)$$

To prove the relations (8a,b) equation (6) is differentiated twice with respect to time:

$$\ddot{x} = \dot{x}f'(x),$$

$$\dddot{x} = \ddot{x}f'(x) + \dot{x}^2 f''(x).$$

From this, using (6) expressions can be obtained for the second, third and fourth derivatives of position at time t_0 :

$$\ddot{x}(t_0) = f(x_0), \quad (11a)$$

$$\ddot{x}(t_0) = \dot{x}_0 f'(x_0), \quad (11b)$$

and

$$\ddot{x}(t_0) = f(x_0)f'(x_0) + \dot{x}_0^2 f''(x_0). \quad (11c)$$

Expanding (9b) in a Taylor series, we have:

$$k_1 = \tau f(x_0) + \frac{2}{3}\tau^2 \dot{x}_0 f'(x_0) + \frac{2}{9}\tau^2 k_0 f'(x_0) + \frac{2}{9}\tau^3 \dot{x}_0^2 f''(x_0) + O(\tau^4),$$

in which the residual term is thus of the order of magnitude of τ^4 .

[5] D. Young, Iterative methods for solving partial difference equations of elliptic type, Trans. Am. Math. Soc. 76, 92-111, 1954.

[6] B. A. Carré, The determination of the optimum accelerating factor for successive over-relaxation, Computer J. 4, 73-78, 1961.

Substituting equations (11a,b,c) in this equation and in (9a) gives the result:

$$k_0 = \tau \ddot{x}(t_0), \quad (12a)$$

and

$$k_1 = \tau \ddot{x}(t_0) + \frac{2}{3} \tau^2 \dddot{x}(t_0) + \frac{2}{9} \tau^3 \ddot{\ddot{x}}(t_0) + O(\tau^4). \quad (12b)$$

The ancillary quantity k_1 is thus an approximation for $\tau \ddot{x}(t_0 + \frac{2}{3}\tau)$. Substituting (12a,b) in (10a,b) now gives the equations (8a,b), which we wished to prove.

When terms in τ^4 and higher are neglected the term in τ^3 , just found in the substitution in the equations for the estimates $\tilde{x}(t_0 + \tau)$ and $\tilde{\dot{x}}(t_0 + \tau)$, gives some idea of the errors made in a single step. The errors ε_1 in position and ε_2 in velocity are then found to be approximately equal to:

$$\varepsilon_1 = \frac{1}{6} \tau^3 \ddot{\ddot{x}}(t_0),$$

and

$$\varepsilon_2 = \frac{1}{6} \tau^3 \ddot{\ddot{x}}(t_0).$$

The quantities ε_1 and ε_2 can be calculated for each step with the aid of a third ancillary quantity k_2 , defined as:

$$k_2 = \tau f\{\tilde{x}(t_0 + \tau)\}.$$

Estimates of the errors in each step can be expressed as follows in terms of the ancillary quantities:

$$\tilde{\varepsilon}_1 = -\frac{1}{4} \tau k_0 + \frac{1}{4} \tau k_1,$$

and

$$\tilde{\varepsilon}_2 = \frac{1}{2} k_0 - \frac{3}{2} k_1 + k_2.$$

These expressions can be derived in the same way as equations (8a,b).

The calculation procedure is as follows. Limiting values, which must not be exceeded in any iteration step, are set for the residual errors of position and velocity. In addition an initial value is chosen for the time interval τ . From the equations given above in the small print, estimates are made of the position and velocity at the end of the interval. The residual errors of position and velocity are also determined, and a check is then made to see whether both residual errors are smaller than the specified values. If they are, a new step in the calculation is started, with the calculated position and velocity as the initial conditions. The interval is now increased such that the estimate for the error in position amounts to 0.9 of the specified limiting value. In this way, using variable interval lengths, estimates are calculated for the position and velocity of the entire trajectory until the boundaries of the region for the electrostatic field are passed.

Light-optical calculations

The program used for calculating electron trajectories can also be used for light-optical calculations. Since the Laplace equation does not have to be taken into account in light-optical problems we usually have a refractive-index variation that can be chosen more or less freely. The freedom of choice is limited only by

the ability to make optical components with such a varying refractive index.

A particular distribution of the optical refractive index n can be converted into a hypothetical electrostatic field by means of the equation

$$n = \sqrt{\frac{V}{V_0}}. \quad (13)$$

In this equation the constant voltage V_0 is set equal to 1 V, so that light rays in free space are equivalent to electrons with a kinetic energy of 1 eV. The path of the light rays is thus equivalent to the paths of electrons in the hypothetical field, and we have assumed that the electrons are at rest when $V = 0$. As noted earlier, we are no longer concerned with the Laplace equation in converting the refractive index into an electrostatic field, so that a completely different program is required for the conversion.

Electron optics differs from light optics in that the variation of the 'refractive index' is much greater. A potential difference of 100 kV (which is not exceptional) results in a 300-fold variation in the refractive index. In light optics, on the other hand, a refractive index of 2 is exceptionally high. Another difference is that in conventional optics the refractive index in the various components is assumed to be constant, so that the index makes discontinuous transitions from component to component. In electron optics, on the other hand the refractive index is usually continuously variable. A system of two parallel mesh electrodes, situated at an infinitely small distance apart and carrying different direct voltages, constitutes the electron-optical analogue of a discontinuous transition in the refractive index.

Equation (13) thus forms the basis for light-optical calculations with the software package for the calculation of electron trajectories. For calculations on graded-index optical fibres it is important to have a good understanding of the velocity of propagation of light-optical signals. We shall therefore take a closer look at the significance of the refractive index concept in connection with the velocity of electrons and light waves.

In a medium of variable refractive index the refractive index can be defined as a scalar field quantity, which is a function of the position vector r . From Snell's law (a special case of Fermat's principle) the path of an electron or of a light quantum can in general be described by

$$\frac{d}{ds} \left(n \frac{dr}{ds} \right) = \nabla n, \quad (14)$$

where s is a variable that gives the position along the path.

With the aid of *fig. 4* it will be shown that equation (14) is the general formulation of Snell's Law. An electron or light wavefront moves from point 1 to point 2, which are separated by a distance ds . The change in the refractive index is represented as a discontinuous change from n_1 to n_2 , while e_n is the unit vector perpendicular to a hypothetical boundary plane between the spaces with refractive indices n_1 and n_2 . The vectors $(dr/ds)_1$ and $(dr/ds)_2$ are unit vectors that are tangential to the path at the points 1 and 2.

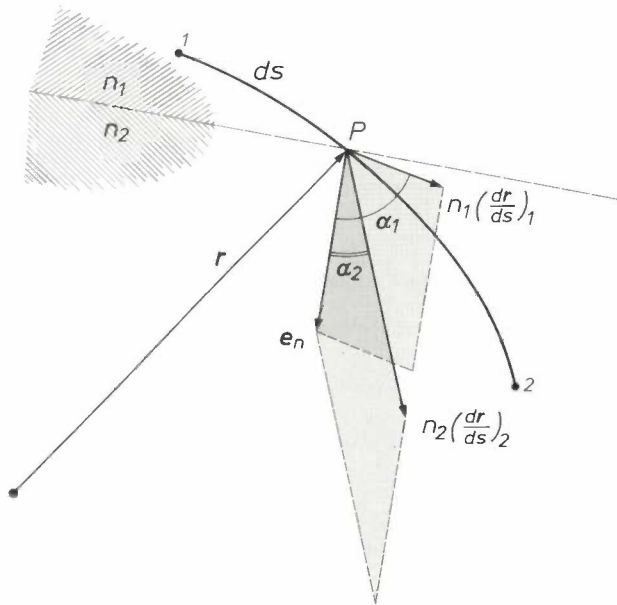


Fig. 4. The quantities used in the generalized statement of Snell's law for a continuous change in the refractive index. An electron or light wavefront moves from point 1 to point 2, separated by a distance ds along the path. The dashed line is the intersection of an imaginary boundary plane between media of refractive indices n_1 and n_2 with the plane of the drawing. r position vector. e_n unit vector perpendicular to the boundary plane. $(dr/ds)_1$ unit vector tangential to the path at 1; $(dr/ds)_2$ unit vector tangential to the path at 2. α_1 and α_2 angles that these vectors make with e_n . Snell's law for a discontinuous change in the refractive index states that the areas of the two parallelograms shown shaded are identical.

Snell's Law for a discontinuous change in the refractive index is:

$$n_1 \sin \alpha_1 = n_2 \sin \alpha_2, \tag{15}$$

where α_1 and α_2 are the angles between the vector e_n and the vectors $(dr/ds)_1$ and $(dr/ds)_2$ respectively. In *fig. 4* both of these vectors are shown at a point P situated between points 1 and 2 on the path, with their lengths multiplied by n_1 or n_2 , as appropriate. The parallelograms shown shaded in the figure have the same area from equation (15). In vector notation this equation becomes:

$$e_n \times \left[n_1 \left(\frac{dr}{ds} \right)_1 \right] = e_n \times \left[n_2 \left(\frac{dr}{ds} \right)_2 \right]. \tag{16}$$

For an infinitely small change in the refractive index eq. (16) becomes:

$$e_n \times \left[d \left(n \frac{dr}{ds} \right) \right] = 0.$$

This equation can now be manipulated to give equation (14), the generalized Snell's Law [7].

Equation (14) has a general validity in electron optics and in light optics. In the first case the refractive index is proportional to the velocity of the electrons; in the second case the refractive index is proportional to the reciprocal of the velocity of the light wavefronts. It must be borne in mind here that the velocity of the electrons should be regarded as the group velocity of the wave packet that according to De Broglie is equivalent to an electron. The velocity of light should be regarded as the phase velocity of the wavefronts, after Huygens. The product of the phase velocity and the group velocity of a wave packet is equal to the square of the velocity of light [8]. To calculate the propagation velocity of light wavefronts with the program packages for electron-optical calculations we use equation (13) and the following two equations:

$$eV = \frac{1}{2} m v_{el}^2, \tag{17}$$

and

$$n = \frac{c}{v_1}, \tag{18}$$

where c is the velocity of light, v_{el} the velocity of an electron and v_1 the phase velocity of a light wavefront. To convert electron-optical to light-optical calculations a path trajectory $v_{el}\tau_{el}$ must be set equal to a path trajectory $v_1\tau_1$, where τ_{el} and τ_1 are the time intervals for an electron and a light wavefront respectively. From (13), (17) and (18) it follows that:

$$\tau_1 = \frac{\tau_{el}}{c} \sqrt{\frac{2eV^2}{mV_0}}$$

When $V_0 = 1$ V this equation becomes:

$$\tau_1 = \frac{\tau_{el}V}{c} \sqrt{\frac{2e}{m}}. \tag{19}$$

Equation (19) permits an interval τ_{el} used in the Runge-Kutta procedure to be converted into an interval τ_1 for a light wavefront, so that the time of transit of light signals can be calculated.

The software

The ELOP software package

ELOP contains the individual programs for the actual calculations, which are based on the mathematical and physical principles described earlier. The procedures for the calculations are largely comparable with those described earlier by C. Weber in this journal and elsewhere [2]. The present software package ELOP contains the following programs:

[7] W. Glaser, Grundlagen der Elektronenoptik, Springer, Vienna 1952.
 [8] O. Klemperer, Electron optics, University Press, Cambridge 1953.

- RELA. This calculates the voltages at the nodes of a rectangular grid by solving a large number of difference equations.
- BAAN. This program calculates the trajectories of electrons in an electrostatic field, described by data supplied by RELA. The BAAN program can at the same time make use of data provided by programs for calculating magnetic fields [9].
- CODE. This program calculates the position of the boundary of the electrostatic field region with respect to the nodes of the rectangular grid.

The GELOP software package

GELOP is used to input the data for a problem to the ELOP software package. After a computation cycle GELOP presents the results to the user via various output peripherals. If required, several CAD cycles can be run one after the other (CAD = Computer-Aided Design) see *fig. 5*. The user 'talks' to GELOP by using 30 menus, each offering him 13 choices. Data input and job control in the various programs are performed by means of EXEC commands in the VM/CMS operating system used in the IBM 3081 computer. GELOP contains the following programs, which we shall discuss in more detail shortly.

- CONTOUR. This program is used to give a geometrical description of the boundaries enclosing the space for which the problem is to be solved. The user also states the boundary conditions, i.e. the voltages for the different parts of the boundary. The program also defines the grid for the electrostatic field.
- BEAM GENERATION. The user uses this program to input initial conditions for the individual electrons of the beam.
- DIAGNOST. This program shows beam cross-sections at locations selected by the user. It also supplies him with information about aberrations.
- PLOT. This program operates a digital plotter to draw the boundaries, the grid, a number of equipotential lines and the electron trajectories.

The GRINOP software package

GRINOP consists of somewhat modified versions of ELOP and GELOP and is designed for solving light-optical problems in media of varying refractive index. In the RELA program the subroutines for solving the Laplace equation are replaced by subroutines for calculating a hypothetical voltage from the refractive index from equation (13).

The CONTOUR program

When defining the boundaries of the problem a distinction must be made between geometries with two-dimensional symmetry and rotational symmetry on

the one hand and three-dimensional geometries on the other. In the following the rotationally symmetric and two-dimensional cases will be lumped together, since there is no difference between them in practice.

The boundary of the problem region forms a barrier for the moving electrons (no account is taken of effects such as reflection or secondary emission). The voltage distribution at the boundary is also specified as a boundary condition for the Laplace equation. Finally, the boundary limits the number of nodes for which the voltage must be calculated. For two-dimensional problems the maximum number of nodes is 20000, for three-dimensional problems it is 30000.

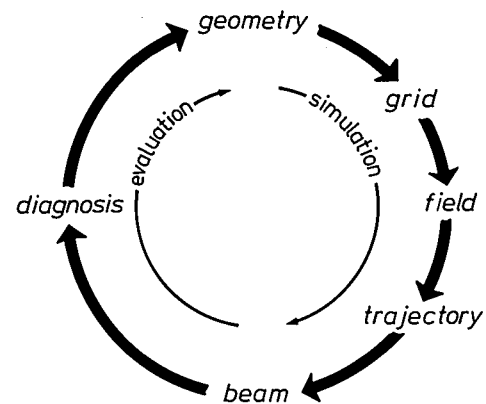


Fig. 5. Schematic representation of a CAD cycle produced with the GELOP software package.

For two-dimensional cases a boundary consists of a number of closed curves that must not intersect. The closed curves represent intersections of the problem plane with surfaces in which the voltage distribution is given as a boundary condition. For each subregion within the outer boundary it is necessary to state whether it is 'full' or 'empty', the statement 'empty' meaning that electrons can move freely. By definition the region outside the outer boundary is 'full'. The program is designed so that every crossing of a closed curve represents a transition from 'full' to 'empty' or vice versa. Each closed curve is built up from straight or circular line segments. The user must state the radius of curvature and end-point for each circular line segment. He must also indicate whether the curvature is concave or convex on the outside. In this manner any two-dimensional curve can be defined unambiguously.

For three-dimensional cases the problem region must be built up from a number of volume elements. There are five basic shapes for these volume elements: cylinder, cone, spherical sector, rectangular block and irregular hexahedron. To each of these volume ele-

ments the user assigns the statement 'full' or 'empty'. Also, for regions in which two or more basic shapes have been defined, the user must indicate by priority numbers 1, 2 etc. which basic form is applicable.

The user also uses the CONTOUR program to relate the grid for the potential distribution to the problem region. The grid can be refined locally if required. The user specifies symmetry planes if possible, thus reducing the number of nodes and the computer time. Fig. 6 gives an example of a problem — a calculation

cedure the user can vary the design parameters even more simply than was possible with the classical simulation methods.

The BEAM GENERATION program

In GELOP the position and velocity of a moving electron at a specified time are determined by the quantities $X, Y, Z, E, QX/Q$ and QY/Q . X, Y and Z are the coordinates of position; E is the kinetic energy of the electron; Q is the length of the velocity vector;

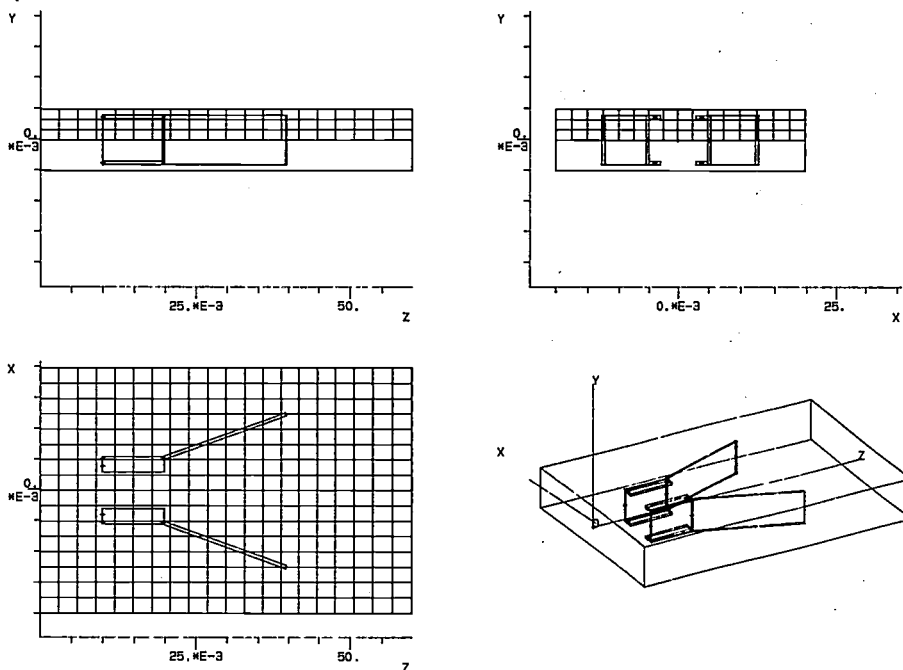


Fig. 6. Statement of the geometry of the problem by means of the CONTOUR program. The problem represents the calculation of a set of deflection plates. The program gives the projections of the problem region in the ZX-, ZY- and XY-planes. It also produces a 'wire-frame model' in oblique projection. In this case there is one plane of symmetry, so that the user only has to define a mesh network for half of the problem region. All boundaries are planes. The actual problem region has the shape of a rectangular block and is 'empty'. The regions defined inside it are 'full' and form the two electrodes.

on a set of deflection plates — with one plane of symmetry. The figure also shows that the CONTOUR program presents the problem boundaries in three orthogonal projections perpendicular to the X-, Y- and Z-axes and also as a 'wire-frame model' shown in oblique projection. The Z-axis usually corresponds to the direction in which the electrons are moving, so that in general the object plane and the image plane are perpendicular to the Z-axis.

The user also uses CONTOUR to assign electrode reference numbers to the various parts of the boundary surfaces of the problem space. During the various design runs the reference numbers can be assigned to a direct voltage, a voltage distribution (linear or logarithmic) or a value for the first derivative of the voltage (the field-strength). With this pro-

QX and QY are the components of this vector in the X- and Y-directions. The magnitude of the velocity vector thus follows from the value of E . The direction of the velocity vector is completely determined by QX/Q and QY/Q , since the cosine of the angle γ between the velocity vector and the Z-coordinate is given by

$$\cos^2 \alpha + \cos^2 \beta + \cos^2 \gamma = 1,$$

where $\cos \alpha = QX/Q$ and $\cos \beta = QY/Q$.

[9] S. J. Polak, A. de Beer, A. Wachtters and J. S. van Welij, MAGGY2, a program package for two-dimensional magnetostatic problems, Int. J. Numer. Methods Eng. 15, 113-127, 1980; W. A. L. Heijnemans, J. A. M. Nieuwendijk and N. G. Vink, The deflection coils of the 30AX colour-picture system, Philips Tech. Rev. 39, 154-171, 1980.

In the BEAM GENERATION program moving electrons are represented for a particular value of the Z-coordinate by points in the four coordinate systems (X, Y), (X, QX/Q), (Y, QY/Q) and (QX/Q, QY/Q). The user also gives the initial conditions for an electron beam as points in these coordinate systems. The points in the coordinate system (X,Y) form an 'electron cloud'. The propagation of this electron cloud as a function of time and hence of the Z-coordinate determines the dimensions of an electron beam.

The initial conditions for an electron cloud may be a uniform distribution of position, velocity and direction, or a random distribution of these quantities. The user may decide to choose the same starting point for all electrons (indicating it on the graphic display by means of the crossed wires). The end-points of the velocity vectors may be situated on a hemisphere, for example, with the end-points of the projections $\sqrt{(QX^2 + QY^2)}$ of the velocities at the nodes of a rectangular grid; see fig. 7. If a random distribution is chosen for the various quantities, the program operates with uniform distribution functions. The sets of initial conditions for position, direction and velocity can if required be multiplied by one another. At each of the various starting points the electrons then start their movement from different angles. Different velocities are then associated with each angle and with each starting point. In addition to these facilities it is also possible to assign to each electron trajectory a relative intensity number with a value between 0 and 1. This number gives the probability that an electron with the specified initial conditions will actually be generated.

The DIAGNOST program

The DIAGNOST program can be used to determine the extent of the geometrical aberrations and the parts of the electrostatic field that are responsible for them. DIAGNOST thus provides the user with various ways of evaluating the characteristics of an electron beam, and hence of the imaging system.

In the first place DIAGNOST can present the position and velocity of individual electrons in a beam at various locations in the object under investigation, either for different values of the Z-coordinate, or for different equipotential surfaces (i.e. for different voltage values). In addition the program can calculate the modulation transfer functions of the imaging system for the X- and Y-directions. (The quality of an imaging system can be characterized more satisfactorily by the modulation transfer function than by a value for the resolution ^[10]).

The DIAGNOST program can also display intensity distributions in the image plane. The program supplies

these distributions by integrating the number of electrons for each mesh of a grid to be defined in the image plane. It does this on the basis of the stated relative intensity distribution of the electrons generated in the object plane. The program presents the intensity dis-

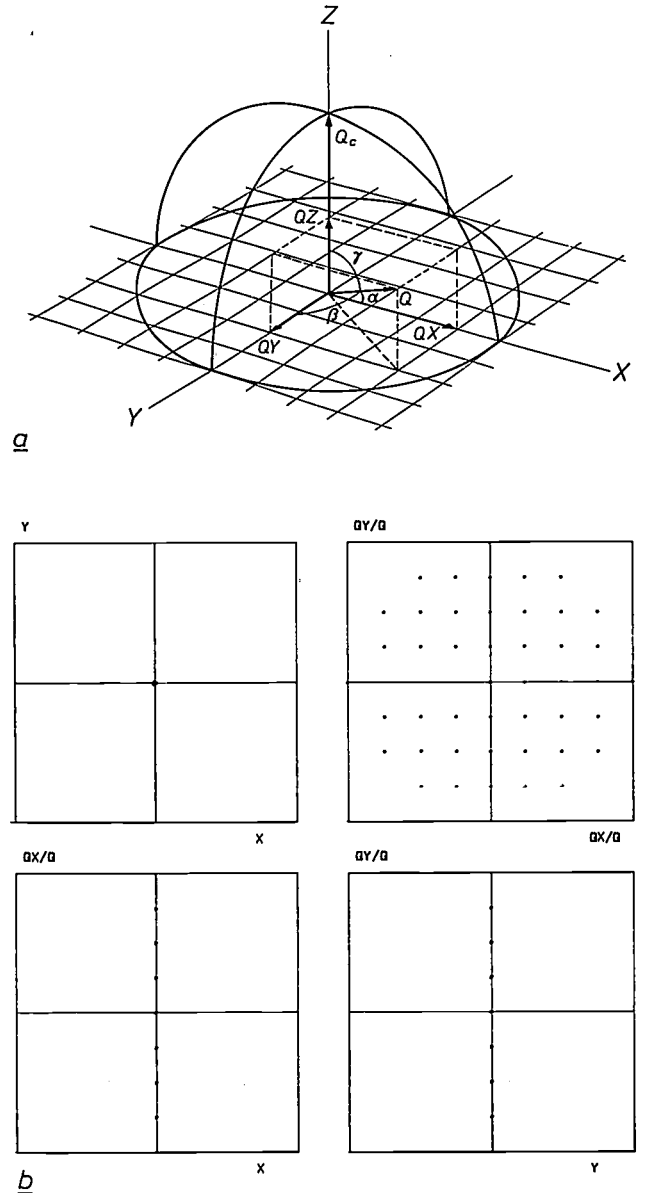


Fig. 7. Example of the statement of the initial conditions for an electron cloud, using the BEAM GENERATION program. The same starting point and the same velocity have been chosen for all the electrons. The end-points of the projections in the XY-plane of the velocity vectors are situated at the nodes of a rectangular grid, defined by the user. a) Schematic representation of the initial conditions. Q velocity vector with components QX, QY and QZ along the X-, Y- and Z-coordinates. α , β and γ angles made by the velocity vector with these projections. Q_c velocity vector for the central trajectory. The arcs are the cross-sections of the spherical surface on which the end-points of the velocity vectors are located with the three planes of the coordinate system. b) Presentation of the initial conditions by the program. The starting points of the velocity vectors are represented as points (here at the origin) in the coordinate system (X,Y), the directions of the velocity vectors are represented as points in the coordinate systems (X,QX/Q), (Y,QY/Q) and (QX/Q,QY/Q).

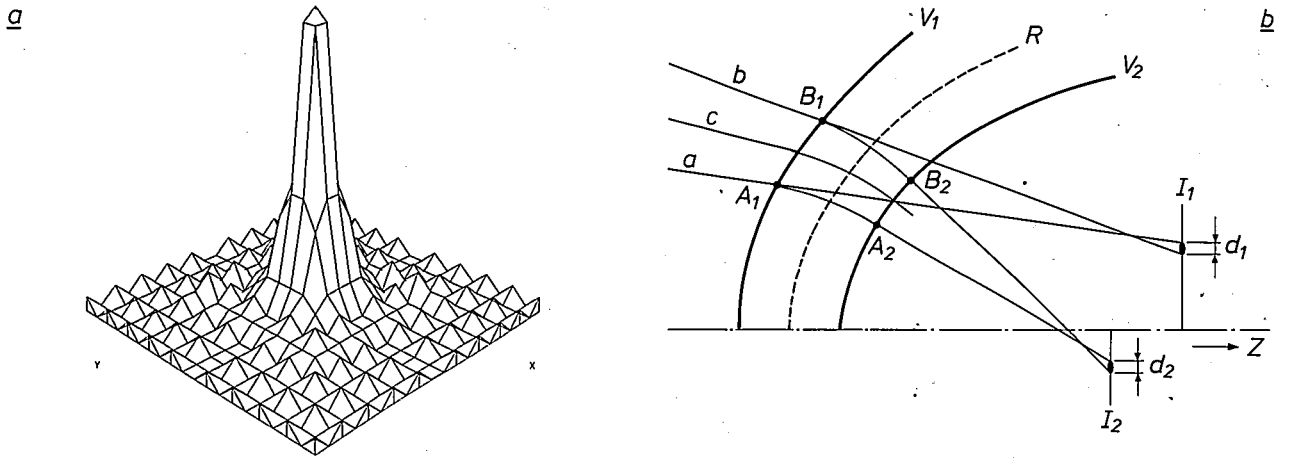


Fig. 8. Some of the facilities offered by the DIAGNOST program. *a*) Presentation of an electron-intensity distribution. The lines connect points that represent the number of electrons, integrated for each mesh of a grid defined by the user. *b*) Schematic representation of the construction of intermediate images. *a, b* electron trajectories, *c* central electron trajectory. The optical properties of the refracting surface *R* follow from the change in the intermediate images associated with the neighbouring equipotential surfaces V_1 and V_2 . The intermediate image I_1 is obtained from the extrapolation of *a* and *b* at the points A_1 and B_1 . Similarly, I_2 is obtained from the extrapolation of *a* and *b* at A_2 and B_2 . The position of the intermediate images is obtained from the point of intersection of the extrapolation of *c* with the extrapolation of a reference trajectory (not shown) of an electron that leaves the object point at an angle to *c*. The magnifications of the intermediate images follow from a second reference trajectory (not shown) of an electron that leaves the object plane at some distance from the object point. The dimensions d_1 and d_2 of the intermediate images in the *X*- or *Y*-directions are corrected by the magnifications thus determined. *c*) Presentation of the corrected dimensions in the *X*-direction of the intermediate images as a function of a sequential number for the equipotential planes. The computer also prints out a list of voltages corresponding to the numbers of the equipotential planes. The values along the vertical axis are a measure of the relative aberration in the *X*-direction. If the imaging system produces no aberration, regions *P* with increasing aberration must be compensated completely by regions *N* with decreasing aberration.

tributions as 'contour lines' for fixed intensity values, as a two-dimensional curve along a line in the *X*- or *Y*-direction, or as a three-dimensional distribution; see fig. 8*a*.

DIAGNOST can also transform the position coordinates of an electron cloud, without any change in the original velocities, by displacing it through a specified distance to another plane perpendicular to the *Z*-axis. In cases with rotational symmetry an electron cloud can be moved to the *Z*-coordinate where the beam cross-section is at a minimum. In this way beam cross-sections at different positions can be compared and the origin of aberrations such as astigmatism and coma can be established.

The principal facility that DIAGNOST offers is the construction of a virtual intermediate image for a stated potential surface by extrapolation of the electron trajectories of the beam; see fig. 8*b*. The figure

caption explains how the program determines the position of the intermediate images and how it calculates the magnification of the intermediate images. Each intermediate image is corrected by the calculated magnification factor, so that the various intermediate images are comparable with one another.

DIAGNOST can display the aberrations in the *X*- and *Y*-directions, obtained from the dimensions of the corrected intermediate images, as a function of a number corresponding to the sequence of the equipotential surfaces; see fig. 8*c*. At the same time the program prints out a list of the potentials associated with these numbers. In fig. 8*c* the region of the field in which the aberrations increase is denoted by *P*; the region in which the aberrations decrease is denoted by *N*. The resulting aberration is zero when the con-

[10] B. van der Eijk and W. K uhl, An X-ray image intensifier with large input format, Philips Tech. Rev. 41, 137-148, 1983/84.

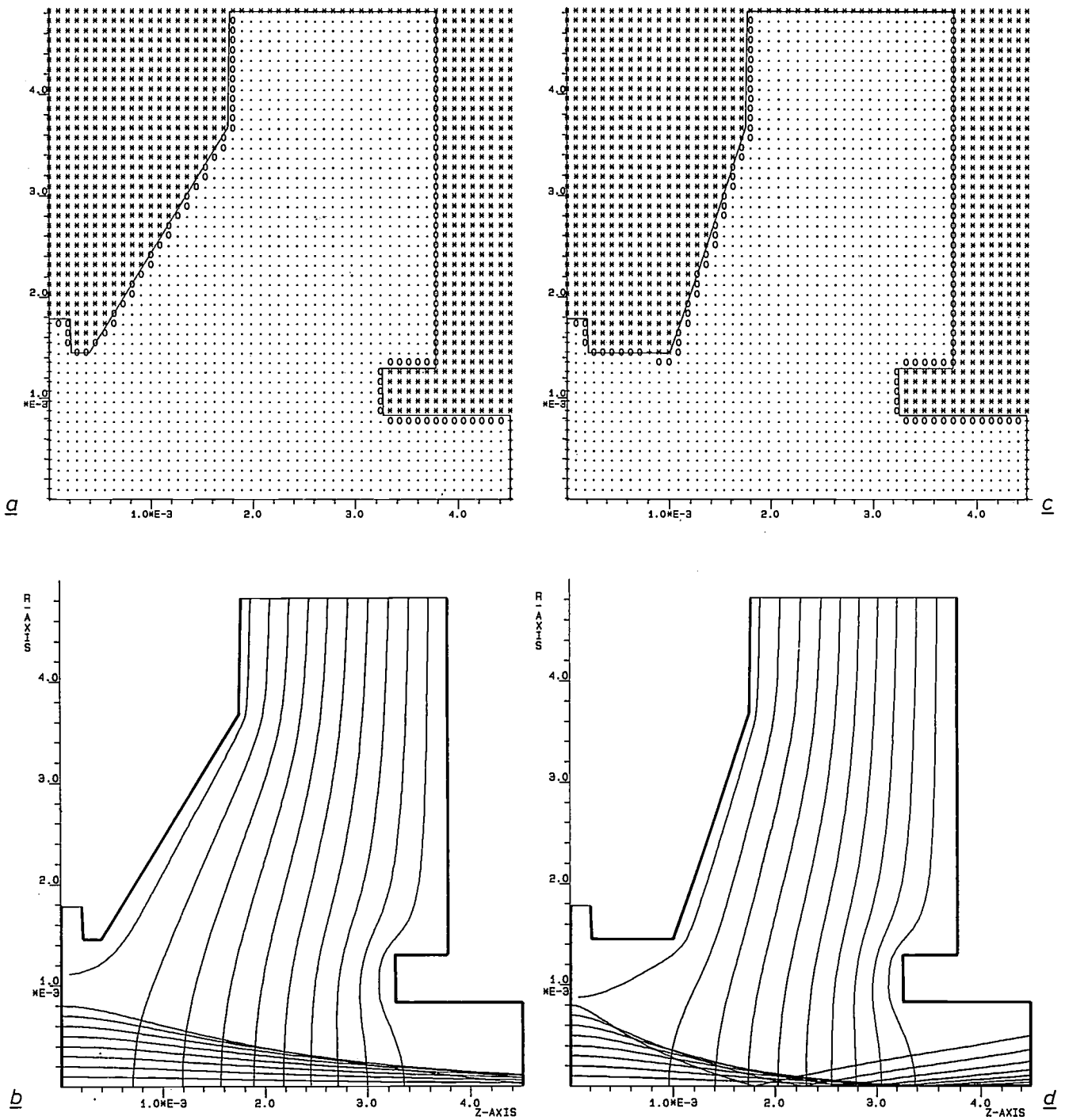


Fig. 9. Modification of the characteristics of a triode electron gun, e.g. of a picture tube. a) Geometry of the original gun. The horizontal axis, which is the Z-axis, is the axis of rotational symmetry. The asterisks and points indicate nodes of the grid defined by the CONTOUR program. The points lie in the region stated to be 'empty'; the asterisks lie in the region stated to be 'full'. The nodes denoted by '+' lie exactly on the boundary of the problem region; the nodes denoted by '0' are separated from the boundary by less than one mesh width. b) A number of equipotential lines and electron trajectories for the original gun. The electrodes are indicated by thickening of the lines traced by the plotter. The cathode is on the left, the grid is at the centre and the anode is on the right. (In reality the anode has a centre hole aligned with the Z-axis.) The potentials on the electrodes are 0, -200 and 4000 V; between the electrodes the voltage changes linearly along the boundary. The beam crossover — which is also the object point for the picture tube — is on the right outside the diagram. The problem was to shift the crossover towards the cathode. c) Geometry of the gun with modified grid-electrode dimensions. d) The corresponding equipotential lines and electron trajectories (with the same electrode voltages). It can be seen that the equipotential lines are more curved, so that the gun converges the electron trajectories more strongly. The crossover is therefore about half-way between the cathode and the anode.

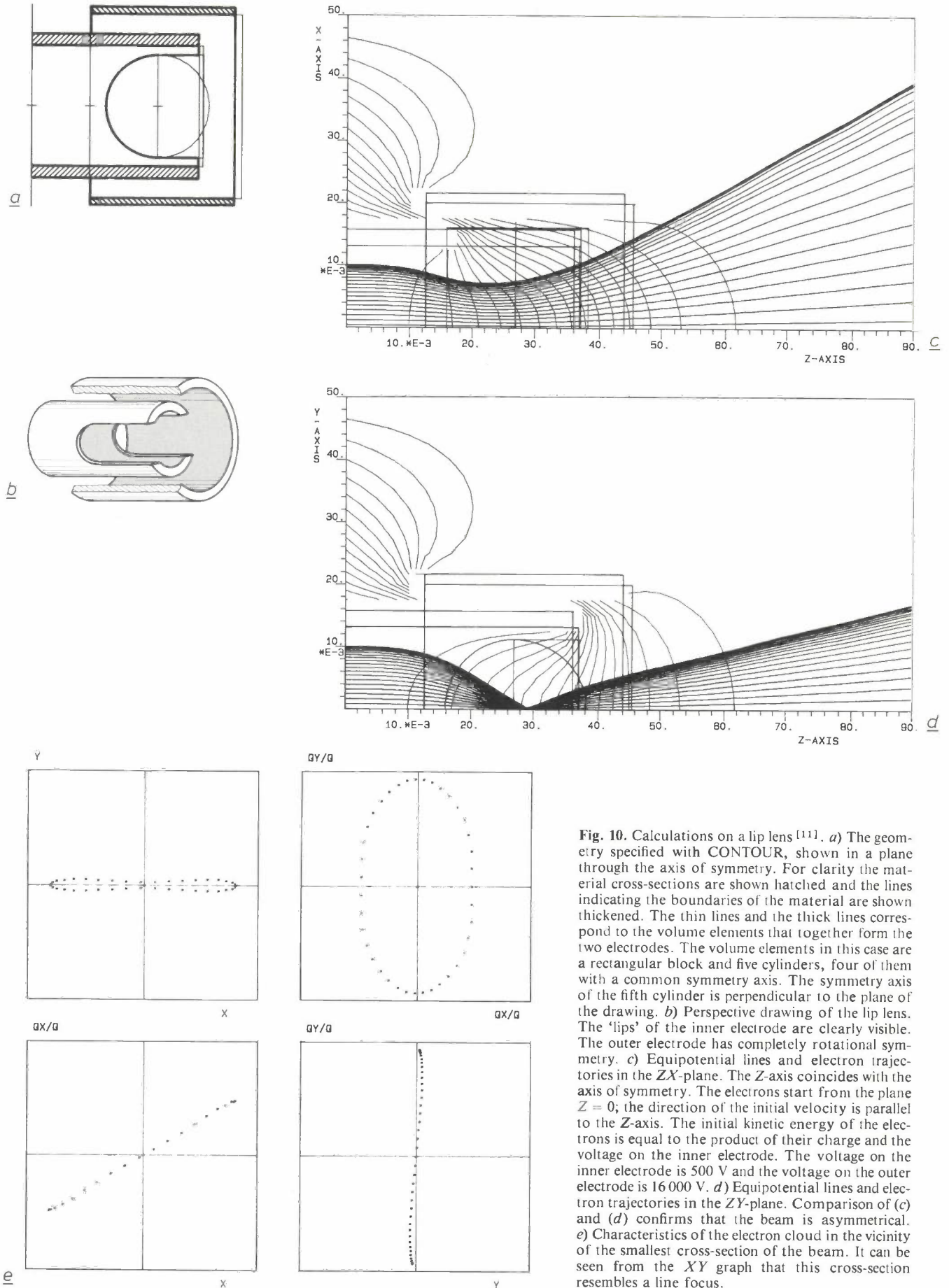


Fig. 10. Calculations on a lip lens^[11]. *a)* The geometry specified with CONTOUR, shown in a plane through the axis of symmetry. For clarity the material cross-sections are shown hatched and the lines indicating the boundaries of the material are shown thickened. The thin lines and the thick lines correspond to the volume elements that together form the two electrodes. The volume elements in this case are a rectangular block and five cylinders, four of them with a common symmetry axis. The symmetry axis of the fifth cylinder is perpendicular to the plane of the drawing. *b)* Perspective drawing of the lip lens. The 'lips' of the inner electrode are clearly visible. The outer electrode has completely rotational symmetry. *c)* Equipotential lines and electron trajectories in the ZX-plane. The Z-axis coincides with the axis of symmetry. The electrons start from the plane $Z = 0$; the direction of the initial velocity is parallel to the Z-axis. The initial kinetic energy of the electrons is equal to the product of their charge and the voltage on the inner electrode. The voltage on the inner electrode is 500 V and the voltage on the outer electrode is 16 000 V. *d)* Equipotential lines and electron trajectories in the ZY-plane. Comparison of (c) and (d) confirms that the beam is asymmetrical. *e)* Characteristics of the electron cloud in the vicinity of the smallest cross-section of the beam. It can be seen from the XY graph that this cross-section resembles a line focus.

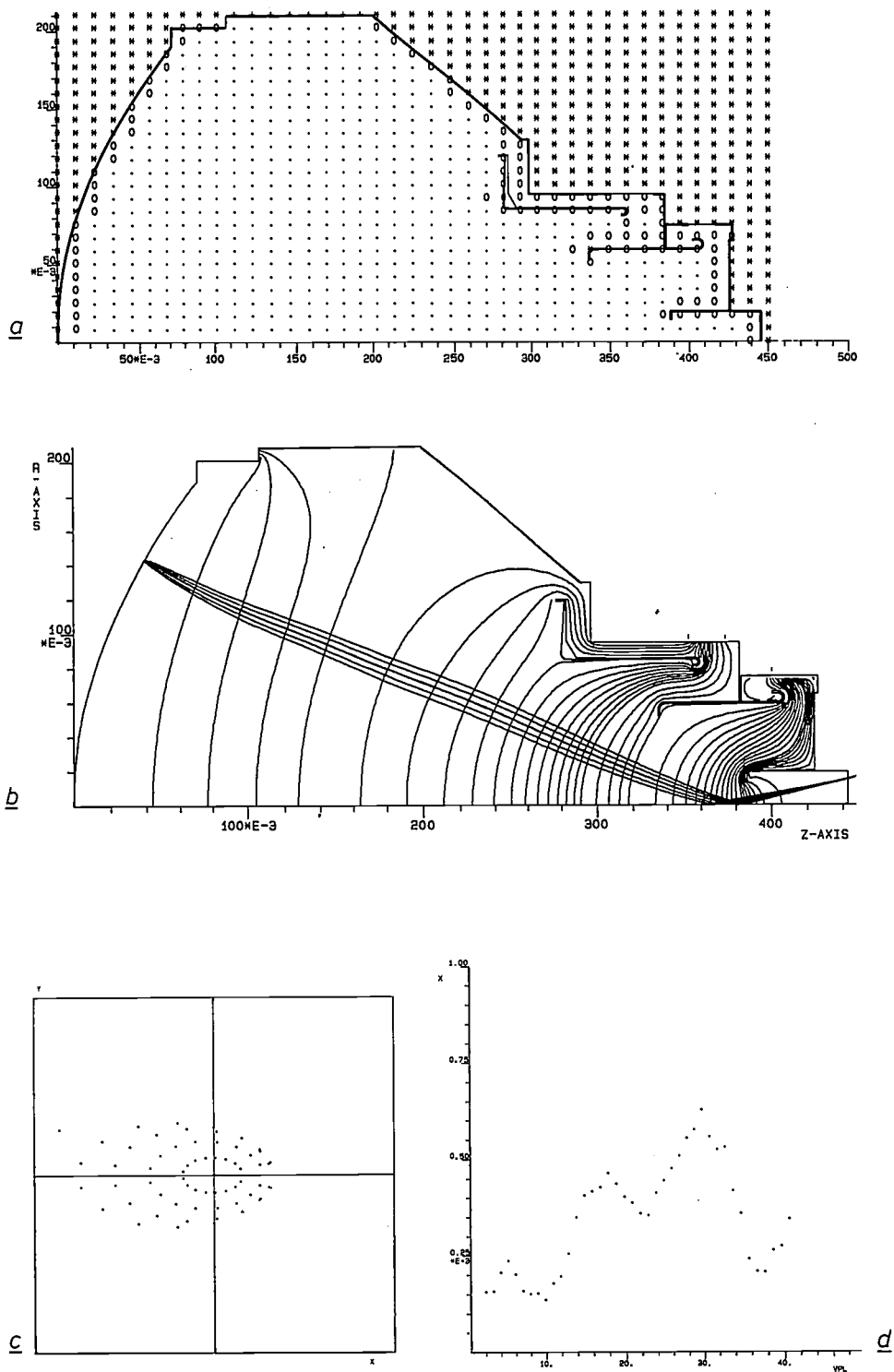


Fig. 11. Calculations on an X-ray image intensifier with large input format^[10]. *a*) Geometry of the image intensifier with five electrodes; the electrodes are indicated by thick lines. The X-ray screen (object plane), which acts as the cathode, is on the left; the output screen (image plane), which acts as the anode, is on the right. *b*) The equipotential lines and the trajectories of electrons that start from a point situated well off-center in the object plane. *c*) *XY* plot of the cross-section of the beam in (*b*) near to the smallest cross-section. This cross-section is close to the output screen. The asymmetry of the beam shows that the aberrations of astigmatism and coma are present; they are relatively minor, however. *d*) Computer-calculated radial dimensions of the intermediate images, constructed by extrapolation and subsequently corrected, as a function of the sequential number of the equipotential surfaces. The increase in the aberrations at the location of the two inner electrodes is compensated by a decrease in the vicinity of the anode so that the resultant aberration is relatively small.

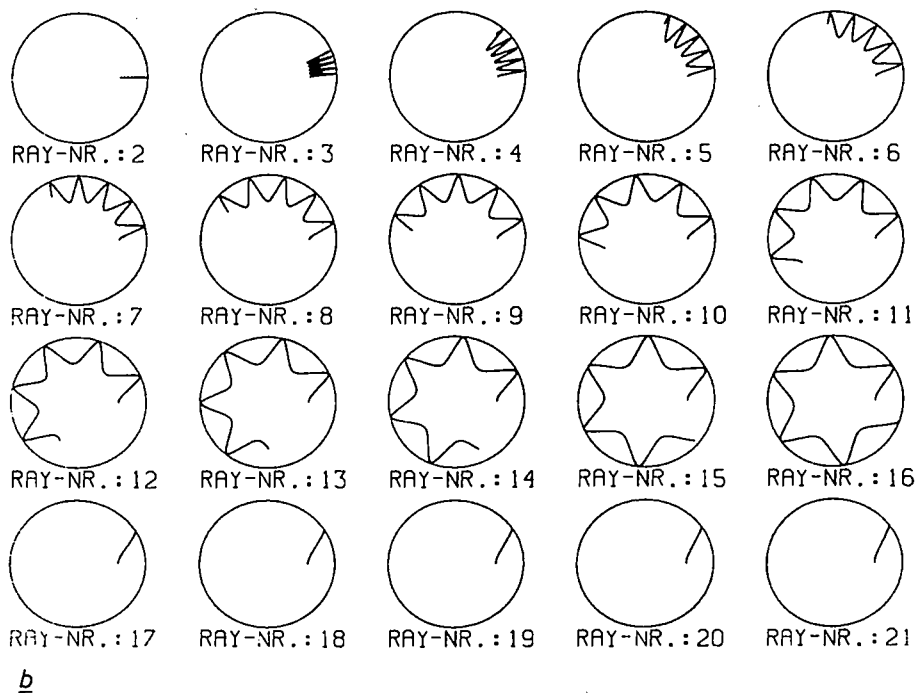
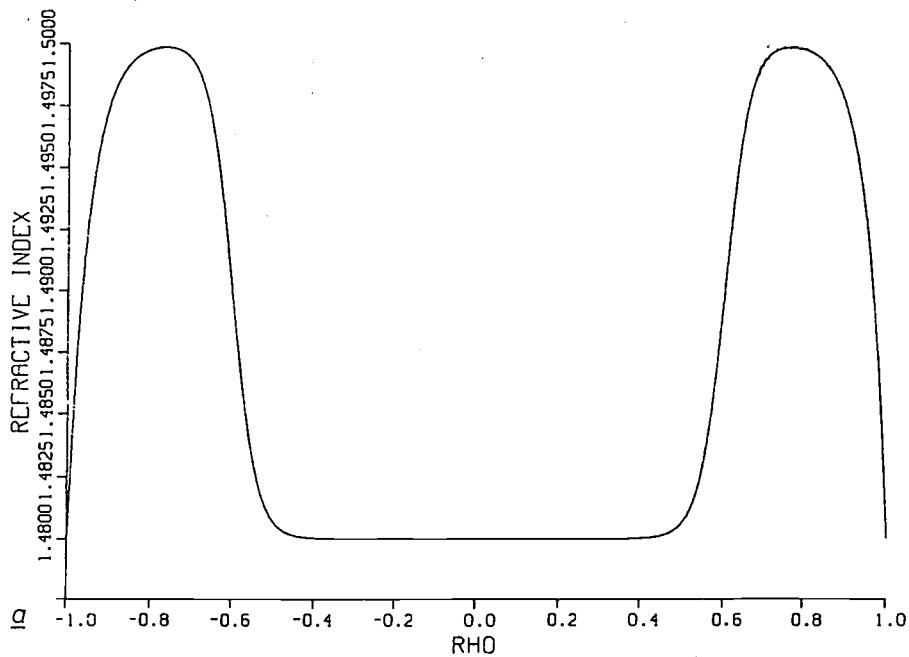


Fig. 12. Calculations on an optical fibre with the GRINOP software package. *a)* The refractive index profile: the refractive index as a function of the ratio *RHO*, equal to the distance from the symmetry axis divided by the outer radius of the fibre. An unusual refractive index profile has been chosen. *b)* Paths of the light rays in the fibre, seen in the direction of its length. The rays are numbered from 2 to 21. All the rays start at the position where *RHO* = 0.6; all the light rays have the same initial velocity. The radial component of the velocity is zero for all rays; the tangential component, starting from zero for ray 2, increases in proportion to the number of the light ray; the axial component thus decreases correspondingly. Ray 2 propagates in a plane through the axis of symmetry. The rays 2 to 16 travel more or less along the circumference of the fibre, but because of total internal reflection they do not leave the 'skin' of *RHO* = 0.6 to *RHO* = 1.0. The tangential component of the velocity of the rays 17 to 21, has become so large that these rays are not totally internally reflected, and therefore leave the fibre.

tributions of regions P and N compensate one another in the image plane.

Examples of applications

Fig. 9 shows calculations on an electron gun, e.g. for a television picture tube. From left to right the gun consists of a cathode, a grid and an anode, at constant potentials of 0, -200 and 4000 V. We wanted to find how to change the position of the beam 'crossover' without altering the voltages on the electrodes. (Changing the position of the crossover changes the magnitude of the spot on the tube screen.)

Fig. 10 shows calculations on a 'lip lens'. A lip lens is a classical example of a line-focus lens [11]. By using an approximation to a line-focus electron source astigmatism in an imaging system can be compensated.

Fig. 11 gives an idea of the calculations for the aberrations (they are only small) of the large-format X-ray image intensifier described in an earlier article in this journal [10]. For a beam issuing from a point on the X-ray screen the DIAGNOST program calculates the shape of the beam cross-section close to the output screen. It also calculates the magnitude of the extrapolated and corrected intermediate images as a function of the sequential number of the equipotential planes, thus indicating where the aberrations arise.

[11] See page 298 of [8].

Fig. 12 shows calculations made with the GRINOP software package for light rays in a graded-index optical fibre.

Important contributions to the research that resulted in the software packages described here were made by J. W. Ero, B. Kallenkoot, W. C. J. Peperkamp, H. J. A. M. Sandkuyl, H. M. M. van de Schoot and A. H. M. Smeets.

Summary. The Laplace equation determines the potential distribution in an electrostatic field. If a space charge is taken into account, this equation becomes the Poisson equation. From either equation the potential distribution can be calculated by solving as many difference equations as there are nodes in a network extending throughout the region under investigation. The equations of motion can be solved by applying a Runge-Kutta integration method; the electron trajectories can then be determined from the calculated potential distribution. The paths of light rays in media of varying refractive index can be calculated from an imaginary electrostatic field in which the potential is proportional to the square of the refractive index. The calculations are performed with a software package called ELOP (Electron Optics), provided with extensions for solving problems in light optics and for calculating electron trajectories in a magnetic field. The user transfers his problem definitions to ELOP with the GELOP software package; this software package also presents the results of the calculations. Besides equipotential lines and electron trajectories the user can also obtain results that quantify the geometrical aberrations. He can thus optimize his design in a number of CAD cycles. This saves a great deal of time since experimental models are not usually necessary. The article concludes with illustrative examples.

Indentation measurements on thin films

P. E. Wierenga and A. J. J. Franken

Thin films have an important part to play in modern technology. It is difficult to characterize the mechanical properties of thin films because the films cannot usually be investigated separately from the substrate. One of the few methods that can be used for such investigations consists in making an indentation in the film by applying an extremely small and accurately controlled force while at the same time measuring the depth of indentation. The indentation-test machine that has been designed at Philips Research Laboratories in Eindhoven is capable of applying forces between 10 μN and 50 mN. It can be used for measuring the ultramicrohardness of thin metal films and also for determining the visco-elastic properties of polymer films. Both quasi-static and dynamic measurements can be performed.

Introduction

Thin films are used today to an increasing extent in high-technology products. Thin metal films are used for example to improve the wearing properties or corrosion resistance of metal components. Thin polymer films are used as protective coatings for optical fibres for data transmission. In applications of this kind the mechanical properties are crucial, and the mechanical characterization of the film by measurements is therefore essential.

Tensile tests and hardness measurements, the classical methods of materials testing [1], are inadequate for determining the mechanical properties of films only a few microns thick or less. Where it is possible to separate the film from the substrate, handling and clamping problems add to the difficulties of making reliable measurements. When the film and substrate are measured together, the result of the measurement is usually affected by the properties of the substrate.

One of the few methods suitable for the mechanical characterization of thin films consists in measuring the depth of an indentation produced by a lightly loaded pointed object. The effect of the substrate is negligible if the depth of the indentation is no more than 10 to 20% of the film thickness, and the substrate is not much softer than the film. The object, usually called an indenter, must have a well-defined shape and the applied force must be very low. In practice this means that, depending on the deformability of the

film, the force must lie in the range from 10 μN to 50 mN. The mechanical properties then follow from the depth of the indentation as a function of time or load. For the characterization of films about one micron thick it is necessary to be able to observe displacements of 10 nm or less. Measurements of the indentation depth in thin metal films are referred to as ultramicrohardness tests. Various ultramicrohardness testers have been described in the literature [2]. Results of hardness measurements made with different instruments are not usually comparable because they depend so much on the test conditions, such as the shape of the indenter and the applied force. They are certainly not comparable with the results of 'conventional' hardness tests, such as Vickers hardness measurements.

We have designed an ultramicroindentation-test machine that not only measures the ultramicrohardness of thin metal films, but can also determine the mechanical properties of other types of films, such as polymer coatings. These coatings generally have a visco-elastic behaviour, which means that the response

[1] M. M. Eisenstadt, Introduction to mechanical properties of materials, Macmillan, New York 1971.

[2] M. Nishibori and K. Kinoshita, Ultra-microhardness of vacuum-deposited films, I: Ultra-microhardness tester, Thin Solid Films 48, 325-331, 1978;

D. Newey, M. A. Wilkins and H. M. Pollock, An ultra-low-load penetration hardness tester, J. Phys. E 15, 119-122, 1982; J. B. Pethica, Microhardness tests with penetration depths less than ion implanted layer thickness, in: V. Ashworth, W. A. Grant and R. P. M. Procter (eds), Ion implantation into metals, Pergamon, Oxford 1982, pp. 147-156.

of the indentation to a step-function change in the load is not instantaneous but gradual. Our machine can be used to measure this step-function response. The visco-elastic properties can also be characterized by the complex modulus of elasticity. This quantity is particularly important in processes with a short characteristic time. The complex modulus of elasticity can be determined in our machine by measuring the indentation dynamically instead of quasi-statically. This is done by superimposing a sinusoidally alternating force on the force for the quasi-static indentation. The required complex modulus of elasticity can then be obtained from the amplitude ratio and phase shift of

ing in particular with quasi-static indentation measurements on protective coatings for glass optical fibres and on binary metal-alloy films. Finally we shall discuss dynamic indentation measurements on pigmented polymer films on magnetic tape.

The ultramicroindentation machine

The ultramicroindentation machine is shown schematically in *fig. 2a*. The sample is held by suction to a sample holder, which can be moved vertically and horizontally. The indenter holder, supported by an air bearing, has virtually frictionless movement along a

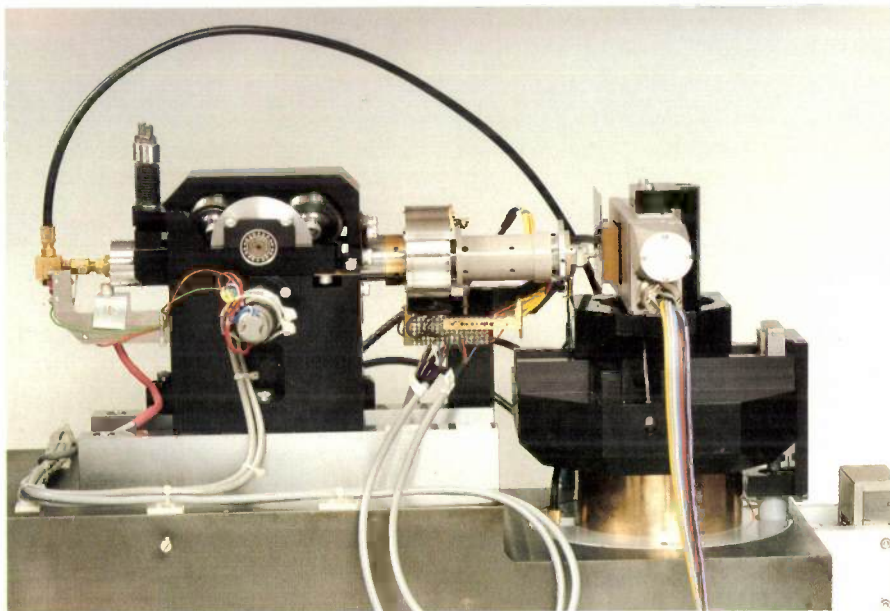


Fig. 1. The machine designed at Philips Research Laboratories, Eindhoven, for ultramicroindentation measurements on thin films.

the alternating indentation relative to the alternating load. The machine is also suitable for surface-scratch experiments, for example to quantify the adhesion of films to their substrates, and it can be used for measuring the roughness of soft materials. These two applications will not be dealt with in this article.

A photograph of our ultramicroindentation machine for the mechanical characterization of thin films^[3] is shown in *fig. 1*. In developing the machine we used several special techniques that have been initiated and refined over the years at Philips Research Laboratories. These techniques have provided sharp diamond indenters with a tip radius smaller than $0.1 \mu\text{m}$, a precision air-bearing^[4] to carry the indenter holder, and a hysteresis-free friction-wheel drive mechanism^[5] for the slow uniform motion of the indenter holder.

We shall next describe the operation of the machine. Then we shall look at a number of applications, deal-

horizontal shaft. The shaft itself can be moved very slowly towards the sample by friction wheels and guide wheels; the principle of a friction-wheel transmission is illustrated in *fig. 2b*. A coil fixed to the indenter holder is located in the air gap of an electromagnet, which is mounted on the shaft. When the coil is energized with direct current, a force is exerted on the indenter; this force can be varied from $10 \mu\text{N}$ to 50mN . Two inductive displacement transducers measure the displacement of the indenter with respect to the shaft and the displacement of the shaft with respect to the surroundings. Two stops attached to the

[3] P. E. Wierenga and A. J. J. Franken, Ultramicroindentation apparatus for the mechanical characterization of thin films, *J. Appl. Phys.* **55**, 4244-4247, 1984.

[4] A. F. Foederer, J. L. M. Hagen and A. G. van Nie, An instrument for measuring the curvature of reflecting surfaces, *Philips Tech. Rev.* **40**, 338-341, 1982.

[5] M. J. J. Dona, Constructie-elementen ten behoeve van microverplaatsingen, *Mikroniek* **21**, No. 6, 7-10, 1981 (in Dutch).

shaft limit the movement of the indenter holder. Isolation from building vibrations is provided by mounting the entire machine on a table top supported on air springs. The resonant frequency of the sprung table

fig. 2a) is adjusted to give a zero signal when the indenter holder is somewhere between the two stops. A small current is then passed through the coil, so that the holder is gently pushed against the front stop (St_1),

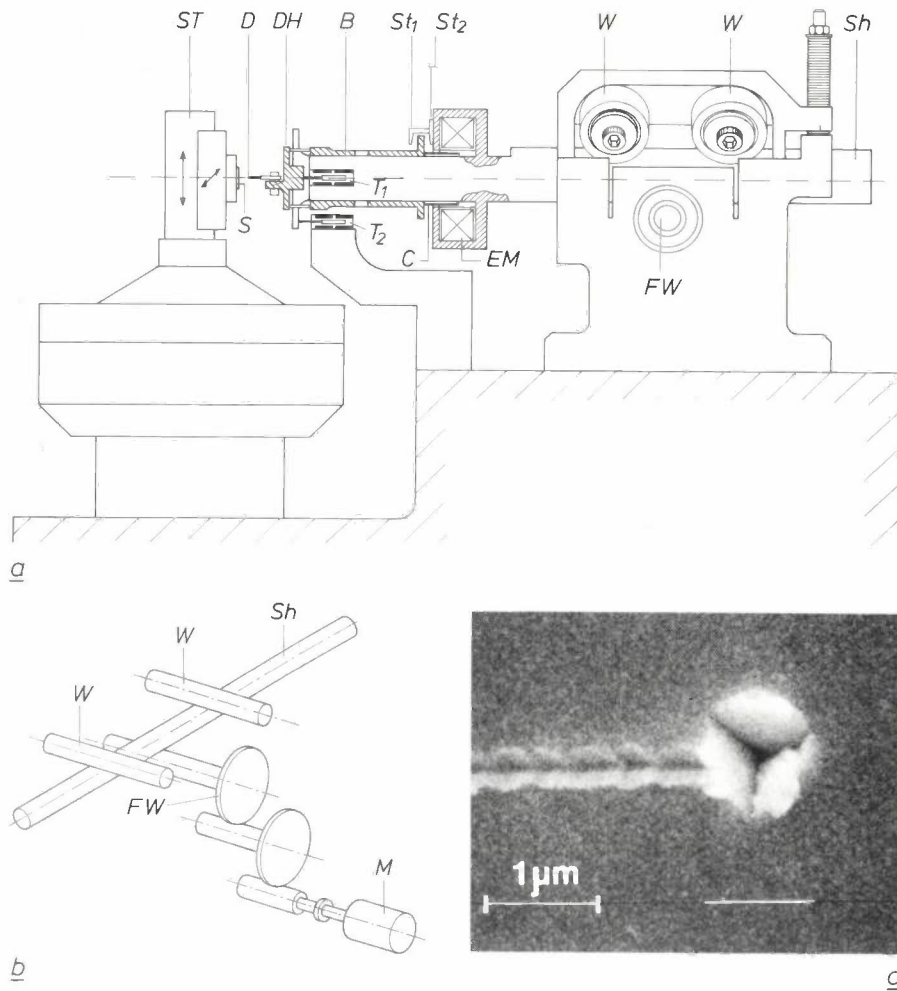


Fig. 2. a) Schematic diagram of the indentation-test machine, partly in cross-section. *S* sample. *ST* sample table. *D* diamond indenter. *DH* indenter holder, fixed to the bush of air-bearing *B*. *Sh* shaft. T_1 transducer for measuring the displacement of *D* with respect to *Sh*. T_2 transducer for measuring the displacement of *Sh* with respect to the surroundings. St_1 , St_2 stops limiting the movement of *DH* with respect to *Sh*. *C* coil fixed to *DH*. *C* is located in the air gap of the electromagnet *EM*, which is mounted on *Sh* and is energized by direct current. *W* guide wheels for the linear movement of *Sh*. *FW* friction wheel for the drive of *Sh*. b) Principle of the hysteresis-free uniform drive of *Sh* by means of friction wheels. In reality there are four guide wheels *W*, arranged in pairs at an angle of 90° to one another. *M* motor. c) A track and the actual indentation produced by a triangular pyramidal indenter *D* in a gold film vacuum-evaporated on silicon. The track is caused by the sideways movement of the sample *S* with respect to the indenter *D* at a minimum force of $10 \mu\text{N}$. The actual indentation is the result of increasing the force to 0.5 mN .

top is about 2 Hz. A pneumatic control system for the air springs keeps the table top horizontal to within 0.001° . To minimize the effect of air currents the measuring system is enclosed in a box of transparent polymethyl methacrylate.

An indentation experiment proceeds as follows. The displacement transducer that measures the position of the indenter holder relative to the shaft (T_1 in

with a force of say $10 \mu\text{N}$. The motor of the linear drive mechanism is now switched on, causing the shaft to move slowly in the direction of the sample. After some time the indenter touches the sample. A control system stops the movement of the shaft when the signal from the displacement transducer T_1 falls to zero. The indenter then presses against the sample with a force of $10 \mu\text{N}$, leaving a slight indentation in it. To

provide a 'virgin' surface the sample is moved a short distance sideways at the same small force between indenter and sample, and then the force is increased. At the same time the control system makes the shaft move so that the signal from the displacement transducer T_1 remains equal to zero. The indentation depth of the indenter in the sample is then given by the displacement measured by transducer T_2 . The smallest observable displacement is 1 nm. The signal from T_2 is automatically corrected for changes in the ambient temperature during the measurement. The temperature-sensing element is a platinum resistor, mounted around the displacement transducer T_2 . The degree of correction is determined by calibration.

Fig. 2c shows an example of the track made by the indenter during the sideways movement with the minimum indenter force of 10 μN . The actual indentation produced by a force of 0.5 mN can also be seen. The figure relates to indentation measurements on a soft gold film vacuum-evaporated on silicon; in harder films the track produced by the sideways movement is far less deep. The imprint is that of a triangular pyramidal diamond, ground with an angle of 97° between the edges. The radius of the tip is less than 0.1 μm . This is the indenter we use in our ultramicrohardness measurements [6]. The projected area of the indentation can be calculated from the measured penetration depth at a given load. The ratio of the applied force to this area is then the ultramicrohardness as in our definition. The measurement information is digitally processed and stored in a microcomputer.

Applications

Quasi-static indentation measurements on protective coatings for optical fibres

Protective coatings for optical fibres have to satisfy a number of optical and mechanical requirements. First of all the refractive index of the transparent material of the coating must be higher than that of the glass cladding of the fibre. Another requirement is that the fibre must be 'embedded' in the protective coating in such a way that the fibre cannot 'kink' if the fibre-optic cable is bent, which would make the radius of curvature of the fibre too small. (Deformation of the optical fibre with an unduly small radius of curvature is called 'microbending'.) This requirement can be met by using two polymer layers: a relatively hard outer layer and a soft inner layer, the buffer layer. Both layers should give little creep, i.e. they should keep their shape under permanent load and not become further deformed. Finally the layers must protect the fibre from external mechanical and chemical effects, to prevent damage and the penetration of

water. The coating must retain all these properties over a long period of time, without the material becoming cracked or otherwise degraded.

The indentation machine described here is particularly suitable for measuring the mechanical properties of protective polymer coatings *in situ*. The tip radius of the indenter is much smaller than the outer radius of the protective film, which can therefore be regarded as a planar layer and no correction is necessary. As the depth of the indentation is small compared with the thickness of the film, the result of the measurement is not affected by the mechanical properties of the intermediate layer or the glass.

If at time $t = 0$ an indenter of radius R is pressed with force F into the plane surface of a visco-elastic material occupying a semi-infinite space, the depth ε of the indentation follows from a generalized form [7] of Hertz's equation [8]:

$$\{\varepsilon(t)\}^{3/2} = \frac{3(1-\nu)}{8\sqrt{R}} J(t) F H(t). \quad (1)$$

Here ν is the lateral contraction coefficient (Poisson's ratio) and $J(t)$ is the (time-dependent) creep-compliance function (in m^2/N), characterizing the mechanical properties of the visco-elastic material. $H(t)$ is the unit-step function (or Heaviside function): $H(t) = 1$ for $t \geq 0$ and $H(t) = 0$ for $t < 0$.

The creep compliance of a perfectly elastic material (i.e. one with no viscous properties) is not time-dependent, and is then equal to the reciprocal of the shear modulus of elasticity G . On applying the well-known relation

$$G = \frac{E}{2(1+\nu)},$$

where E is the modulus of elasticity, equation (1) reduces to:

$$\varepsilon^{3/2} = \frac{3(1-\nu^2)}{4E\sqrt{R}} F. \quad (2)$$

This is Hertz's equation for an infinitely rigid sphere of radius R pressed into the plane surface of an elastic material with modulus of elasticity E occupying a semi-infinite space.

For relatively soft materials it is not permissible to neglect the indentation at the minimum load F_0 (equal to 10 μN in our case). The modulus of elasticity is then given by an expression derived from equation (2):

$$E = \frac{3(1-\nu^2)}{4\sqrt{R}} \left(\frac{F^{2/3} - F_0^{2/3}}{\Delta\varepsilon} \right)^{3/2}, \quad (3)$$

where $\Delta\varepsilon$ is the difference between the indentations at normal load F and minimum load F_0 .

In selecting polymers for protective coatings on glass fibres certain conditions must be taken into account: the modulus of elasticity of the buffer layer must be small compared with that of the outer layer, and the creep and plastic deformation of both layers must be small. We shall now describe a number of measurements on protective coating materials in which these aspects are important [9].

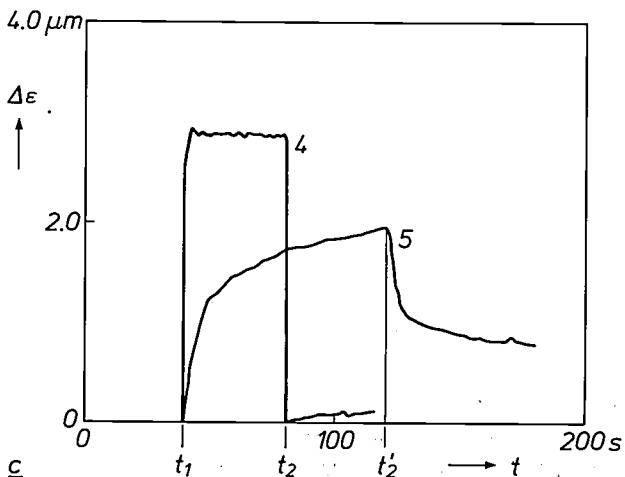
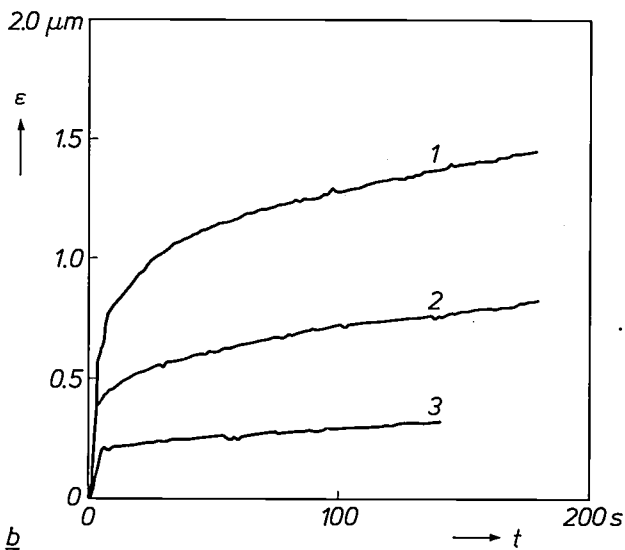
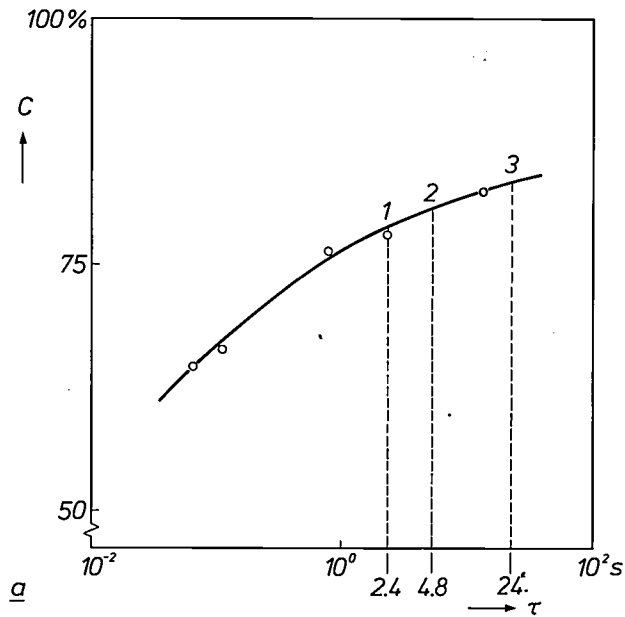


Fig. 3. Results of measurements on polymer coatings for optical fibres. a) The degree of polymerization C — measured with a differential scanning calorimeter — as a function of the time τ during which a UV-cured acrylate resin is irradiated. b) The penetration depth ϵ as a function of the time t — measured with the indentation machine of figs 1 and 2 — for the three differently exposed acrylates indicated in (a) by 1, 2 and 3. At the time $t = 0$ the minimum indentation force of $10 \mu\text{N}$ is suddenly increased to 0.5 mN . c) The difference $\Delta\epsilon$ between the indentation depth at a load of $50 \mu\text{N}$ and the indentation depth at the minimum load of $10 \mu\text{N}$ as a function of time t for a silicone rubber (4) and a polyurethane acrylate (5). At time t_1 the load was suddenly increased; at times t_2 and t_2' it was brought back to the minimum value.

First of all we studied the effect of the UV curing time on a commercially available polymerizable acrylate, to be applied as a hard outer layer. Fig. 3a shows the effect of the curing time on the degree of polymerization of this material. It was determined by means of a differential scanning calorimeter, which measures the heat liberated during the polymerization of the as yet uncombined oligomers — the ‘building blocks’ of the acrylic resin. Next we measured indentation curves of samples of the same acrylic resin that had been exposed for 2.4, 4.8 and 24 seconds to ultraviolet irradiation at a wavelength of 365 nm and an intensity of 0.6 W/cm^2 . In these measurements we used an indenter with a radius of $7 \mu\text{m}$ and a ‘jig’ with a V-groove in which the fibre with the protective coating is held by suction. Fig. 3b shows the curves of indentation depth as a function of time; the numbers on the curves correspond to the numbers in fig. 3a. It can be seen that as the exposure increases, and hence the degree of polymerization, the initial deformation decreases and with it the creep. Our indentation machine can thus also be used for monitoring the curing conditions during the production process.

Fig. 3c illustrates some measurements on soft materials for buffer layers, where the difference $\Delta\epsilon$ between the depth of penetration at normal load and minimum load is plotted as a function of time. The radius of the indenter used for these measurements was $4 \mu\text{m}$. Curve 4 relates to a commercially available thermohardening silicone rubber. The material is per-

[6] This indenter differs from the four-sided pyramidal indenter used for Vickers hardness measurements. It is simpler, however, to give a sharp point to a diamond indenter shaped like a triangular pyramid than to one shaped like a four-sided pyramid.
 [7] E. H. Lee and J. R. M. Radok, The contact problem for viscoelastic bodies, *Trans. ASME E* 27, 438-444, 1960; T. C. T. Ting, The contact stresses between a rigid indenter and a viscoelastic half-space, *Trans. ASME E* 33, 845-854, 1966.
 [8] I. Szabó, *Höhere technische Mechanik*, 4th edition, Springer, Berlin 1964; S. P. Timoshenko and J. N. Goodier, *Theory of elasticity*, 3rd edition, McGraw-Hill, New York 1970.
 [9] P. E. Wierenga, D. J. Broer and J. H. M. van der Linden, Mechanical characterization of optical-fiber coatings by ultramicroindentation measurements, *Appl. Opt.* 24, 960-963, 1985.

fectly elastic in its behaviour: there are no creep effects, and after removal of the load the residual deformation is virtually zero. Curve 5 relates to a commercially available UV-polymerizable polyurethane acrylate. As can be seen, this material does show creep effects, and after removal of the load some plastic deformation remains.

A polyurethane acrylate for buffer layers, which has better mechanical properties than the material of curve 5, has been developed in our own laboratory. In the indentation measurement the layer behaves in virtually the same way mechanically as the silicone rubber of curve 4. Advantages of polyurethane acrylate compared with silicone rubber are that it has a higher refractive index and is easier to apply as a protective coating on the glass fibre. The modulus of elasticity of our polyurethane acrylate is calculated from the measurements as 1.7 MPa; for the silicone rubber the value is 1.6 MPa. (In the calculations Poisson's ratio was taken as 0.5.)

Ultramicrohardness measurements on thin metal films

It is important to measure the hardness of thin metal films primarily because there is usually a correlation between hardness and resistance to wear. The mechanical properties of vacuum-evaporated binary metal-alloy films have been investigated at our Laboratories^[10]. The ultramicrohardness of the films was measured with our indentation machine with the triangular pyramidal indenter whose imprint is shown in fig. 2c. The force applied to the indenter was 0.5 mN; the indentation depths were only read off if they had not changed for 10 seconds. Some results of measurements were checked with a scanning electron microscope.

Many thin metal films were investigated; we shall only discuss here the measurements on cobalt/nickel and silver/gold films. At room temperature silver and gold are completely soluble in one another; evaporated silver/gold films are therefore found to be single-phase in practice. Cobalt and nickel are only partly soluble in one another, and for this reason cobalt/nickel films are two-phase in a large range of miscibility. The phases consist of mixed crystals with more than 95% cobalt and mixed crystals with more than 70% nickel. The silver/gold mixed crystals and the cobalt/nickel mixed crystals consisting mostly of nickel are both face-centred cubic (fcc), that is to say the atoms form a cubic close packing. The cobalt/nickel mixed crystals that are largely cobalt form a hexagonal close packing (hcp).

We have evaporated metal films about 1 μm thick on to silicon substrates, successively increasing the relative proportions of the elements from 0% to 100%

in steps of 10%. We then determined the phase diagrams (metastable for $\text{Co}_{1-x}\text{Ni}_x$) of the films at room temperature by X-ray diffraction and transmission electron microscopy. The results for the two alloys are shown in the top row of fig. 4. The two-phase region of the cobalt/nickel alloys is indicated by the horizontal hatching.

The second row in fig. 4 gives the results of the ultramicrohardness measurements. In general the hardness of metals increases when the propagation of dislocations encounters obstacles, such as foreign atoms in the crystal structure. This effect increases with the difference in size between the foreign atoms and the atoms of the metal itself. There is not much difference, however, between the radii of cobalt and nickel atoms and those of silver and gold atoms. The increase in the hardness of silver films alloyed with gold or of gold films alloyed with silver must clearly be due to some other effect.

The propagation of dislocations in the crystal structure is also obstructed by grain boundaries. A fine-grained metal is therefore in general harder than a similar coarse-grained metal. The TEM micrographs in the bottom two rows, made with a Philips transmission electron microscope, demonstrate that this effect is the cause of the increased hardness. The micrographs of the $\text{Co}_{1-x}\text{Ni}_x$ films with $x = 0.4$ and 0.9 show an almost identical grain size. The micrographs of the $\text{Ag}_{1-x}\text{Au}_x$ films with $x = 0$ and $x = 0.4$ show a distinctly different grain size. The difference in grain structure also appears from the corresponding electron-diffraction patterns, made with the same electron microscope. In the diffraction pattern of the pure silver film there are breaks in the rings. This points to the presence of texture (preferred orientation of the crystallites), presumably due to recrystallization after vacuum evaporation. The regularity of the rings in the other diffraction patterns indicates random orientation of a large number of crystallites.

Dynamic indentation measurements on magnetic tape

The methods of measurement we have been discussing are quasi-static, i.e. the sample is subjected for some time to the load exerted by the indenter during the measurement. Quasi-static measurements are appropriate when the processes to which the material of the sample is subjected in its application have

[10] A. G. Dirks, J. J. van den Broek and P. E. Wierenga, Mechanical properties of thin alloy films: ultramicrohardness and internal stress, *J. Appl. Phys.* 55, 4248-4256, 1984; P. E. Wierenga, A. G. Dirks and J. J. van den Broek, Ultramicrohardness experiments on vapour-deposited films of pure metals and alloys, *Thin Solid Films* 119, 375-382, 1984.

[11] H. F. Huisman and C. J. F. M. Rasenberg, Porosimeter measurements on magnetic tape, *Philips Tech. Rev.* 41, 260-266, 1983/84.

a long characteristic time. This is the case with fibre-optic telecommunication cables, which are wound on reels during manufacture, so that the fibres in the cable are bent to a certain radius of curvature.

At Philips Research Laboratories the running characteristics of magnetic tape for video and audio cassette recorders are also a topic of investigation. Magnetic tape consists of carrier material 10 μm thick and a coating of about 5 μm of visco-elastic polymer containing the magnetic particles [11]. Since the friction is associated with the actual contact surface between the tape and the magnetic heads and guide pins, we expect

that the coefficient of friction will depend on the deformability of the magnetic coating. Clearly, the characteristic times associated with the friction that occurs as the magnetic layer passes along the heads and pins will be short. A quasi-static measurement of the visco-elastic properties is therefore not suitable for determining the deformability of the polymer layer.

We have recently started experiments with magnetic tape in which the visco-elastic properties of the magnetic layer are measured with our indentation machine in a dynamic method. In the configuration shown schematically in fig. 5 a diamond indenter with a

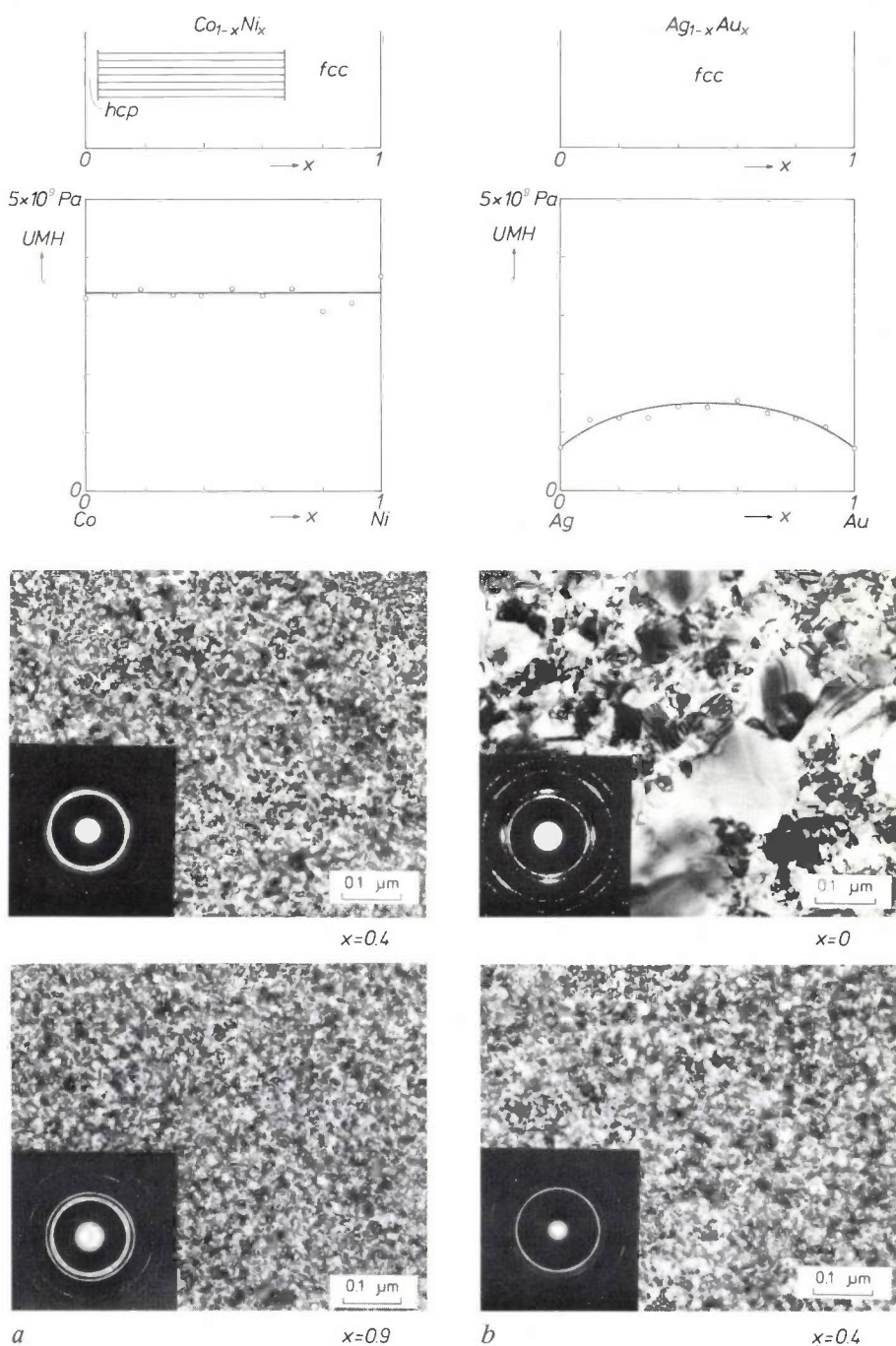


Fig. 4. Results of measurements on a) cobalt/nickel alloys and b) silver/gold alloys. The first row gives the phase diagrams for vacuum-evaporated films at room temperature. The second row gives the results of measurements of the ultramicrohardness *UMH* of the films. The horizontal axes show the content *x* of Ni or Au, in atomic fractions. The horizontal hatching refers to a two-phase region. *fcc* phase of face-centred cubic mixed crystals. *hcp* phase of mixed crystals with hexagonal close packing. The micrographs in the bottom two rows are TEM micrographs of $\text{Co}_{1-x}\text{Ni}_x$ and $\text{Ag}_{1-x}\text{Au}_x$ films for different values of *x*. The corresponding electron-diffraction patterns are shown at the bottom left of each picture.

radius of about 5 μm is pressed against the magnetic tape with a well-defined force. The tape is stretched tight over a smooth cylinder of hardened steel. The magnetic layer on the tape is subjected to a static indentation, which must not be greater than about 0.2 μm or the results would be distorted by the carrier material. Next a sinusoidally alternating force at a frequency of up to 100 Hz is superimposed on the static force. The static force and the dynamic force

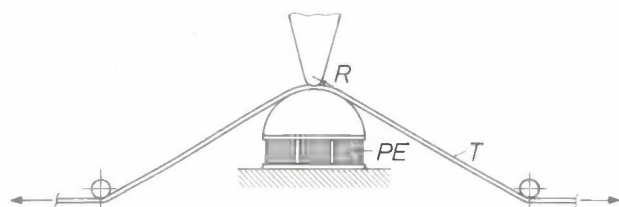


Fig. 5. Configuration for the dynamic indentation measurements on magnetic tape. The tape T is stretched tight over a half-cylinder. R indenter radius. PE Peltier element for heating or cooling the tape during the measurements.

are produced by a direct current and an alternating current in coil C (see fig. 2). The sum of the static and dynamic indentations is measured by displacement transducer T_1 (fig. 2). During the dynamic measurements the control system for the linear drive mechanism is switched off. The temperature in the magnetic tape can be made locally higher or lower than the ambient temperature by the Peltier element shown in fig. 5.

The microcomputer determines the amplitude ratio of the alternating force to the dynamic indentation during the measurement. The corresponding phase difference is measured as well. The values for the real and imaginary parts of the complex (frequency-dependent) modulus of elasticity E^* can now easily be derived from the amplitude ratio and phase angle, provided that the amplitude of the dynamic indenta-

tion does not exceed about 20 nm. The complex modulus of elasticity is defined as

$$E^* = E' + iE''$$

where E' is a measure of the elastic properties and E'' is a measure of the damping properties of the material. E''/E' represents the loss factor of the material, and the corresponding arc tangent is indicated as the loss angle. For the visco-elastic polymer coating on magnetic tape typical values for E' are in the range from 2.5 to 4 GPa and the loss factor is in the range from 0.02 to 0.10.

We intend to carry out a series of measurements of the complex modulus of elasticity for tapes of simplified composition in the near future, to gain a better understanding of the running characteristics of magnetic tape.

In the design and building of the ultramicroindentation machine important contributions were made by R. M. van Bree, K. W. de Graaf, F. G. A. Homburg and A. C. Jacobs. The studies on protective coatings for optical fibres were made in cooperation with D. J. Broer, and the investigations of metal films were carried out in cooperation with J. J. van den Broek and A. G. Dirks.

Summary. In an ultramicroindentation machine very low forces — 10 μN to 50 mN — are exerted on a diamond indenter to produce small indentations in thin films. For thin metal films the ratio of the applied force to the projected area of the indentation is a measure of the ultramicrohardness. The indenter used in these measurements is shaped like a triangular pyramid with a tip radius of less than 0.1 μm . The visco-elastic properties of protective polymer coatings on optical fibres for data transmission are measured with an indenter of radius about 5 μm . When the force is suddenly increased the curve of the depth of indentation as a function of time gives information about the creep and other deformation properties of the polymer film. For short characteristic times the visco-elastic properties can be characterized by the complex modulus of elasticity. This can be determined by superimposing an alternating force on a constant indentation force and then measuring the phase and amplitude ratio of the dynamic force and the dynamic indentation depth.

Continuous skull-melting of glass

In the manufacture of pure and homogeneous soft glass, e.g. as used for glass fibres in data transmission, the conventional method of batch production in a crucible or in a tank furnace — for large quantities — is unsuitable. This is because glass produced in this way always contains impurities originating from the wall material, and these effects increase with the reactivity of the molten glass and the wall material. Nor is the batch production of glass compatible with continuous production processes such as the double-crucible method used in the manufacture of optical fibres [1]. Philips Research Laboratories in Eindhoven now have an experimental arrangement, based on the 'skull-melting' method, which can produce pure and homogeneous glass with no inclusions or gas bubbles in a continuous process.

'Skull melting' [2] is an established method of manufacturing pure refractory materials. The melt is contained in a shell or 'skull' of the cooled unmolten material. Since the melt is not in contact with a crucible wall there is no risk of it becoming contaminated. Another advantage, compared with the production of glass in a tank furnace, is that the type of glass being made can be changed quickly. The material is heated by r.f. heating, a method in which eddy currents are induced in the material by a rapidly alternating magnetic field, so that energy is transferred to it.

The principle used in the skull-melting method is that the electrical conductivity of molten oxides is much greater than that of oxides in the solid state, partly because of higher ion mobility. The resistivity of pure crystalline oxides as a function of temperature has a step near their melting point. Glass, which behaves as a supercooled liquid during cooling, does not have a melting point, but a melting range. The curve of the resistivity of glass as a function of temperature is therefore more gradual; this is illustrated in *fig. 1* for a silicate glass with 26.5% by weight of Na₂O [3]. The discontinuity in the curve is near the transition temperature, the temperature at which a discontinuity also appears in the curves for other physical quantities. The viscosity changes from about 10¹⁹ Pa s at 20 °C to about 10² Pa s at 1200 °C; at the transition temperature the viscosity of all types of glass is 10¹² Pa s [4].

In the r.f. heating of molten oxides in a skull of unmelted material the skull is 'transparent' to the energy in the magnetic field. The field can however deliver energy to the molten material. Sufficient energy can only be transferred if the resistivity, for particular

skull dimensions, is lower than a threshold value proportional to the frequency of the r.f. field. At 2.6 MHz, the frequency that we use, this threshold value is about 100 ohm cm. Starting the melting process is thus a problem, and we shall return to this presently.

Until now the skull-melting method has been used only in batch production. This is done in a 'cold crucible' formed by free-standing water-cooled axial copper fingers inside the r.f. heating coil [2]. The coil has always taken the form of a copper tube with cooling water flowing through it. The distance between coil and crucible must be relatively large, otherwise ionization of the air could cause voltage breakdown (flashover). In such an arrangement flashovers can also

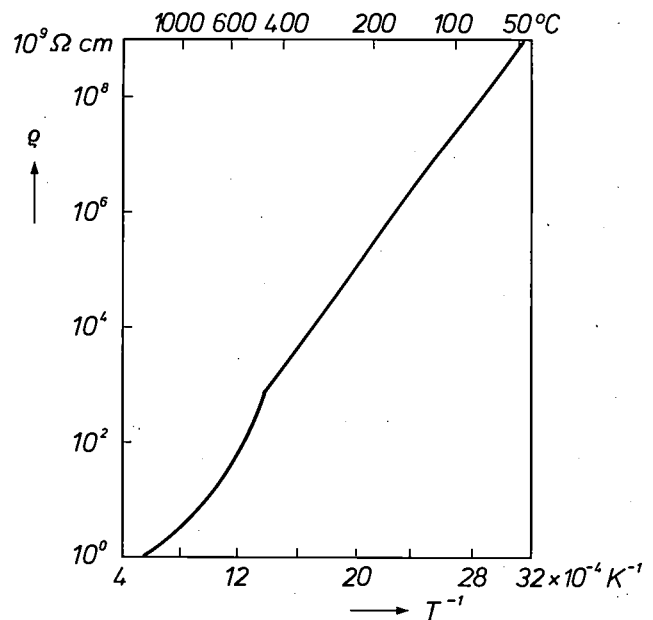


Fig. 1. The electrical resistivity ρ of glass with 26.5% by weight of Na₂O, the rest SiO₂, as a function of the reciprocal of the absolute temperature [3]. (A scale in °C is given at the top.) The transition temperature of the glass is near the discontinuity in the curve at 430 °C. In the low-temperature range the curve corresponds to the function $\rho = \rho_0 \exp(Q/RT)$, where ρ_0 is a constant, Q is the activation energy and R the gas constant, so that with the scale divisions used a straight line is found in this range.

- [1] H. M. J. M. van Ass, P. Geittner, R. G. Gossink, D. Küppers and P. J. W. Severin, The manufacture of glass fibres for optical communication, Philips Tech. Rev. 36, 182-189, 1976.
 [2] V. I. Aleksandrov, V. V. Osiko, A. M. Prokhorov and V. M. Tatarintsev, Synthesis and crystal growth of refractory materials by RF melting in a cold container, in: E. Kaldis (ed.), Current topics in materials science, Vol. 1, North-Holland, Amsterdam 1978, pp. 421-480.
 [3] R. H. Doremus, Glass science, Wiley, New York 1973.
 [4] H. Scholze, Glas, 2nd edition, Springer, Berlin 1977.

occur between the turns of the coil, since the voltage between turns can rise to 1000 V. The risk of flashovers also increases with the frequency. The energy transfer is proportional to the fourth power of the ratio of the outside diameter of the molten glass to the inside diameter of the coil [5]. For efficient energy transfer this ratio should be as large as possible, but this conflicts with the need to have large air gaps to avoid voltage breakdown. At Philips Research Laboratories a continuous skull-melting process was there-

There are three distinct zones in the glass mass in the inner tube during the process:

- The outer, ring-shaped 'skull' of cooled, unmelted material, which absorbs no energy from the r.f. field because of the high resistivity; the radial temperature gradient in this zone can be as high as 500 °C/mm.
- A hot outer liquid zone in which the resistivity is lower than 100 ohm cm; the eddy currents are concentrated here, because of the skin effect; the maximum temperature in this zone is 1650 °C.

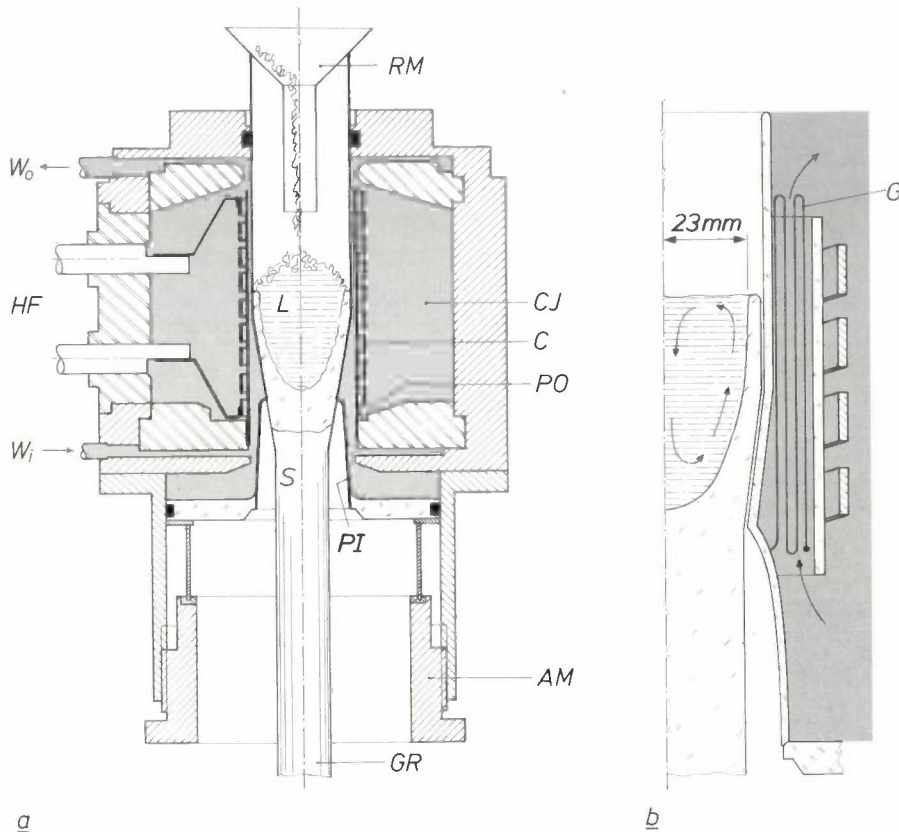


Fig. 2. *a*) The experimental arrangement for producing pure glass rods. *PI* inner tube of silica glass. *PO* outer tube of silica glass. *C* r.f. coil. *CJ* cooling jacket with deionized water. *RM* feed of raw mix. *L* liquid glass. *S* solidified glass. (In reality the transition from *S* to *L* is much more gradual than shown here.) *HF* connections to r.f. generator. *W_i*, *W_o* inlet and outlet for cooling water. *GR* the glass rod produced. *AM* mechanism for adjusting the inner tube. *b*) Interior on a larger scale. (For clarity the distance between the two tubes is exaggerated.) *G* earthed screen of vertical copper wires, extending over the whole circumference between the inner and outer tube.

fore developed from completely different principles, with the risk of dangerous flashovers now completely eliminated.

The new arrangement is shown in *fig. 2*. The coil is surrounded by cooling water, deionized to ensure high resistivity. The 'mix' of raw materials for the glass is fed into a tapering silica-glass inner tube. This tube, in which the actual process takes place, is surrounded by a silica-glass outer tube. Between these concentric tubes there is a strong flow of deionized cooling water.

- A colder inner liquid zone in which, although the resistivity is sufficiently low, there are no eddy currents, because of the skin effect; the temperature in this zone is about 1550 °C.

The heat transfer from the outer liquid zone to the inner one takes place by convection and radiation. *Fig. 2b* shows the flow pattern produced in the molten glass. This flow is maintained by density differences resulting from the temperature gradient in the melt. Because of the intensive circulation and the low vis-

cosity of the hot glass, large gas bubbles can easily escape at the outside. The small gas bubbles concentrate in the upper liquid region, so that the lower region is free of impurities. (This is comparable with the situation in zone melting.)

where material is fed in. The heat transfer from the molten zone to the cooling water takes place mainly by radiation. The silica of the inner tube is almost completely transparent to radiation at a wavelength of less than $4\ \mu\text{m}$, so that this heat radiation is directly

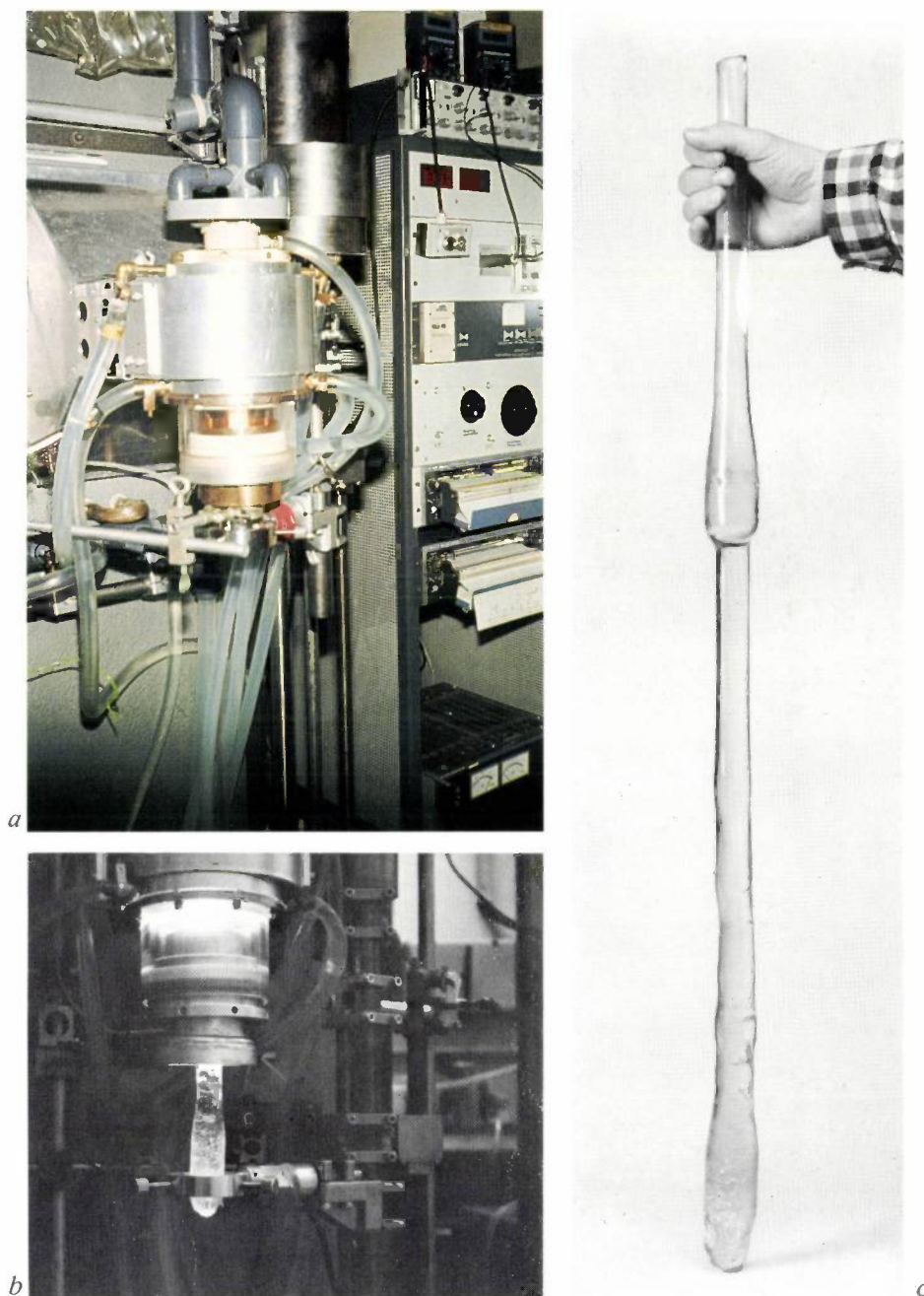


Fig. 3. *a*) The arrangement with the control equipment. *b*) The process in operation; the white-hot glass rod is clearly visible. *c*) The product. (The changes in diameter are due to changes in process parameters.)

Overheating of the molten glass cannot cause volatile components (e.g. B_2O_3 or ZnO) to escape, because these components condense in the colder zone

absorbed by the cooling water without causing any increase in the temperature of the silica. (In the conventional crucible with fingers, the heat has to be transferred to the cooling water through the copper.)

At the start of the process the passage through the tapering part of the inner tube is closed off by a glass

^[5] J. F. Wenckus and W. P. Menashi, Growth of high purity oxygen-free silicon by cold crucible techniques, Report RADC-TR-82-171 (NTIS Order No. AD-A118992), 1982.

rod. The mix is then poured into the inner tube. The process is started by inserting a silica tube containing a carbon rod surrounded by a shielding gas into the mix. Because of its low resistivity the carbon rod absorbs energy from the r.f. field, so that it heats up and melts the surrounding mix. When sufficient liquid glass has formed, the silica tube with the carbon rod is removed. The mass is then heated further, and a bath of molten glass forms inside the mix. Once the right temperature distribution has been reached inside the tapered constriction, a rod of clear glass can be drawn from it with very little force.

The viscosity of the molten glass at the constriction determines the mass flow. This viscosity depends on the temperature and hence on the transferred power. The mass flow can therefore be varied by changing the position of the constriction in relation to the r.f. coil, using a mechanism for adjusting the inner tube as illustrated in fig. 2*a*. The rate at which the rod is withdrawn from the inner tube determines the diameter. The present arrangement can produce 75 to 100 grams of glass per hour with 10 to 15 kW of continuous-wave power from the r.f. generator and a rated power of 25 kW.

The capacitive coupling of the r.f. coil to the electrostatic field could cause plasma discharges in the gases escaping from the mix. (The gas has a lower dielectric constant than the surrounding material.) An earthed screen is therefore mounted in the cooling water between the coil and the inner tube. The screen consists of vertical copper wires, see fig. 2*b*; it passes the magnetic field and screens off the electrostatic field.

The transferred power is controlled by keeping the anode current of the output valve of the r.f. generator constant by means of a PID controller. Since almost the entire transferred power enters the cooling water, the product of the volume flow and the increase in temperature of the cooling water is a measure of this power. Both quantities are therefore continuously measured and monitored. Control of the anode voltage of the generator is not practical, since a very small increase in the voltage causes an almost explosive in-

crease in the transferred power. The reason for this is that changes in the transferred power are accompanied by changes in other process parameters, such as the resistivity and the thickness of the skull, and hence the ratio of diameters mentioned above, so that the transferred power rises even more.

As we mentioned earlier, the glass production depends on the temperature of the liquid glass at the location of the constriction in the inner tube, and is consequently determined by the heat economy in the inner tube. The level of the glass bath is therefore continuously monitored, and adjusted if necessary by changing the amount of mix fed in per unit time. The level of the mix is measured by radiation detectors around the circumference of the inner tube.

In the conventional method of glass production the glass remains in the tank furnace for many hours, sometimes longer than a week. In the method described here the glass remains in the hot zone for no longer than two hours. Assuming a 'classical' mix consisting of a dry mixture of crystalline raw materials, the composition of the initial charge will not usually be sufficiently homogeneous. Since there is insufficient time for diffusion of the constituents in the glass bath, it is better to prepare the constituents so that the charge will have the correct composition right from the start. This is often done by wet granulation or pelletization of the mix.

With the arrangement described here we have made glass rods with a diameter of about 4 cm that are free from gas inclusions and are of pure composition. Fig. 3 shows photographs of the experimental arrangement and a rod produced in it.

W. C. P. M. Meerman
T. L. van Rooy
M. C. M. Voss

W. C. P. M. Meerman and Ing. T. L. van Rooy are with Philips Research Laboratories, Eindhoven; Ing. M. C. M. Voss, formerly with Philips Research Laboratories, is now with the Philips Lighting Division, Maarheeze.

Scientific publications

These publications are contributed by staff of laboratories and plants that form part of or cooperate with enterprises of the Philips group of companies, particularly by staff of the research laboratories mentioned below. The publications are listed alphabetically by journal title.

Philips GmbH Forschungslaboratorium Aachen, Weißhausstraße, 5100 Aachen, Germany	A
Philips Research Laboratory Brussels, 2 avenue Van Becelaere, 1170 Brussels, Belgium	B
Philips Natuurkundig Laboratorium, Postbus 80 000, 5600 JA Eindhoven, The Netherlands	E
Philips GmbH Forschungslaboratorium Hamburg, Vogt-Kölln-Straße 30, 2000 Hamburg 54, Germany	H
Laboratoires d'Electronique et de Physique Appliquée, 3 avenue Descartes, 94450 Limeil-Brevannes, France	L
Philips Laboratories, N.A.P.C., 345 Scarborough Road, Briarcliff Manor, N.Y. 10510, U.S.A.	N
Philips Research Laboratories, Cross Oak Lane, Redhill, Surrey RH1 5HA, England	R
Philips Research Laboratories Sunnyvale P.O. Box 9052, Sunnyvale, CA 94086, U.S.A.	S

J. Donjon	L	The place of ultrasonics in medical imaging	Acta Electronica 25	293-300	1983
P. J. 't Hoen (<i>Philips Ultrasound, Santa Ana, CA</i>)		Design of ultrasonographic linear arrays	Acta Electronica 25	301-310	1983
C. Méquio, R. H. Coursant & P. Pesqué	L	Simulation of the acousto-electric response of piezoelectric structures by means of a Fast Fourier-Transform algorithm	Acta Electronica 25	311-323	1983
P. Pesqué, R. H. Coursant & C. Méquio	L	Methodology for the characterization and design of linear arrays of ultrasonic transducers	Acta Electronica 25	325-340	1983
M. Naillon, R. H. Coursant & F. Besnier (<i>CISI, Paris</i>)	L	Analysis of piezoelectric structures by a finite element method	Acta Electronica 25	341-362	1983
F. Hottier & J.-L. Bernatets	L	Estimation of ultrasonic attenuation in biological tissues	Acta Electronica 26	33-58	1984
M. Fink, J.-F. Cardoso & P. Laugier (<i>UER Cochon Port-Royal, Paris</i>)	L	Diffraction effect analysis in medical echography	Acta Electronica 26	59-80	1984
F. Towfiq*, C. W. Barnes (<i>Univ. California, Irvine, CA</i>) & E. J. Pisa* (* <i>Philips Ultrasound, Santa Ana, CA</i>)		Tissue classification based on autoregressive models for ultrasound pulse echo data	Acta Electronica 26	95-110	1984
H. Schomberg, W. Beil, G. C. McKinnon, R. Proksa & O. Tschendel	H	Ultrasound computerized tomography	Acta Electronica 26	121-128	1984
B. Jacobs, J. Braat & M. Hartmann	E, H	Aging characteristics of amorphous magneto-optic recording media	Appl. Opt. 23	3979-3982	1984
G. B. McMillan (<i>INMOS, Newport</i>), D. J. Smith*, J. P. Gowers & H. Ahmed* (* <i>Univ. Cambridge</i>)	R	Transmission electron microscopy and high resolution electron microscopy studies of shallow ($R_p \sim 20$ nm) As and B implanted and electron beam annealed silicon	Appl. Phys. Lett. 44	1081-1083	1984
J. M. Woodcock & J. M. Shannon	R	Thermionic emission in bulk unipolar camel diodes	Appl. Phys. Lett. 45	876-878	1984
G. J. van Gurp, P. J. de Waard & F. J. du Chatenier	E	Thermomigration in indium films	Appl. Phys. Lett. 45	1054-1056	1984
P. Dawson & K. Woodbridge	R	Effects of prelayers on minority-carrier lifetime in GaAs/AlGaAs double heterostructures grown by molecular beam epitaxy	Appl. Phys. Lett. 45	1227-1229	1984
J. S. Nadan	N	A glimpse into future television	Byte 10	135-150	1985
J. M. Goldstein*, Y. Z. Efe* (* <i>Cooper Union School of Eng., New York</i>) & J. J. Bernitt	N	A fast compositional modeling system for computer graphics	Control & Comput. 12	34-38	1984

- G. B. McMillan*, J. M. Shannon & H. Ahmed* (* *Univ. Cambridge*) R Processing of unipolar diodes with electron beams Electronics Lett. 20 863-865 1984
- A. Thayse B Synthesis and asynchronous implementation of algorithms using a generalized *P*-function concept IEEE Trans. C-33 861-868 1984
- J. L. W. Kessels E Two designs of a fault-tolerant clocking system IEEE Trans. C-33 912-919 1984
- S. B. Luitjens, J. W. Smits & V. Zieren E The write field of a ring head for a double layer perpendicular medium IEEE Trans. MAG-20 724-726 1984
- J. J. M. Ruigrok E Analysis of metal-in-gap heads IEEE Trans. MAG-20 872-874 1984
- J. J. M. Ruigrok E Cross measurements in magnetic recording: a new way of determining head performance IEEE Trans. MAG-20 875-877 1984
- J. W. D. Martens & A. B. Voermans E Cobalt ferrite thin films for magneto-optical recording IEEE Trans. MAG-20 1007-1012 1984
- A. M. van der Kraan (*Interuniv. Reactor Inst., Delft*) & K. H. J. Buschow E Magnetism and ^{57}Fe Mössbauer effect in amorphous Fe-base alloys: significance of charge transfer and short-range atomic ordering IEEE Trans. MAG-20 1284-1289 1984
- G. A. C. M. Spierings (*Philips Glass Div., Eindhoven*), C. M. G. Jochem, T.P.M. Meeuwsen & G.E. Thomas E A new class of glasses for double-crucible optical fibers with high numerical apertures J. Am. Ceram. Soc. 67 657-663 1984
- A. H. van Ommen E Diffusion of ion-implanted As in SiO_2 J. Appl. Phys. 56 2708-2715 1984
- H. A. van Sprang & J. L. M. van de Venne E Influence of the surface interaction on threshold values in the cholesteric-nematic phase transition J. Appl. Phys. 57 175-179 1985
- C. P. Janse & A. J. M. Kaizer E The Wigner distribution: a valuable tool for investigating transient distortion J. Audio Eng. Soc. 32 868-882 1984
- P. J. Schoenmakers E Thermodynamic model for supercritical fluid chromatography J. Chromatogr. 315 1-18 1984
- T. F. McGee III, C. Werkhoven & J. Jansen N, E Segregation coefficients of selected impurities in ZnSe grown by LPE J. Cryst. Growth 59 649-650 1982
- W. H. de Roode (*Philips Lighting Div., Eindhoven*) & C. A. P. W. van de Pavert E Incorporation of manganese in LPE-grown Mn,YIG films in the presence of Ca^{2+} and Ge^{4+} ions J. Cryst. Growth 69 173-181 1984
- W. J. M. J. Josquin & M. J. E. Ule-naers E Oxidation-induced defects at the poly/mono silicon interface J. Electrochem. Soc. 131 2380-2386 1984
- J. Boersma*, J. J. E. Indenkleeft* (* *Univ. of Technol., Eindhoven*) & H. K. Kuiken E A diffusion problem in semiconductor technology J. Eng. Math. 18 315-333 1984
- D. B. M. Klaassen, D. M. de Leeuw & T. Welker E, A Systematic analysis of phosphor degradation under cathode-ray excitation J. Lumin. 31 & 32 687-689 1984
- P. Schobinger-Papamantellos (*ETH-Zentrum, Zürich*) & K.H.J. Buschow E Magnetic structure and incommensurate phase transition in HoGe J. Magn. & Magn. Mater. 44 149-157 1984
- S. Sinnema*, R. J. Radwanski*, J. J. M. Franse* (* *Univ. Amsterdam*), D. B. de Mooij & K. H. J. Buschow E Magnetic properties of ternary rare-earth compounds of the type $\text{R}_2\text{Fe}_{14}\text{B}$ J. Magn. & Magn. Mater. 44 333-341 1984
- E. Dormann*, U. Dressel* (* *Univ. Bayreuth*), H. Kropp (*TH Darmstadt*) & K. H. J. Buschow E Quadrupolar interaction of gadolinium nuclei at the cubic sites of ferromagnetic GdAl_2 J. Magn. & Magn. Mater. 45 207-218 1984
- V. Weissenberger*, B. Elschner* (* *TH Darmstadt*) & K.H.J. Buschow E Ferromagnetic resonance in amorphous $\text{Y}_{1-x}\text{Co}_x$ J. Magn. & Magn. Mater. 46 19-28 1984
- G. de With E Note on the use of the diametral compression test for the strength measurement of ceramics J. Mater. Sci. Lett. 3 1000-1002 1984
- B. Nienhuis, H.J. Hilhorst* & H.W.J. Blöte* (* *Univ. of Technol., Delft*) E Triangular SOS models and cubic-crystal shapes J. Phys. A 17 3559-3581 1984
- J. C. M. Henning, J. P. M. Ansems & A. G. M. de Nijs E Photoluminescence excitation of Saxena's deep donor in AlGaAs J. Phys. C 17 L915-L921 1984

- | | | | | | |
|---|-------------|--|--|---------|------|
| P. Friedel, P. K. Larsen, S. Gourrier, J. P. Cabanie & W. M. Gerits | <i>L, E</i> | Photoemission studies of the interaction of hydrogen plasmas with GaAs (001) | J. Vac. Sci. & Technol. B 2 | 675-680 | 1984 |
| J. M. B. Terken (<i>Inst. for Perception Res., Eindhoven</i>) | | The distribution of pitch accents in instructions as a function of discourse structure | Lang. & Speech 27 | 269-289 | 1984 |
| P. Delsarte & Y. Genin | <i>B</i> | Spectral properties of finite Toeplitz matrices | Lect. Notes Control & Inf. Sci., Vol. 58, P. A. Fuhrmann (ed.), Springer, Berlin | 194-213 | 1984 |
| P. van Dooren | <i>B</i> | A unitary method for deadbeat control | Lect. Notes Control & Inf. Sci., Vol. 58, P. A. Fuhrmann (ed.), Springer, Berlin | 864-881 | 1984 |
| F. L. van Nes (<i>Inst. for Perception Res., Eindhoven</i>) | | Perceptual limits in man-machine communication | Limits in perception, A. J. van Doorn, W. A. van de Grind & J. J. Koenderink (eds), VNU Science Press, Utrecht | 173-197 | 1984 |
| C. M. J. van Uijen & J. H. den Boef | <i>E</i> | Driven-equilibrium radiofrequency pulses in NMR imaging | Magn. Resonance Med. 1 | 502-507 | 1984 |
| M. J. Powell | <i>R</i> | Material properties controlling the performance of amorphous silicon thin film transistors | Mater. Res. Soc. Symp. Proc. 33 | 259-273 | 1984 |
| P. Branquart | <i>B</i> | A high-level intermediate code | Methods and tools for compiler construction, B. Lorho (ed.), Cambridge Univ. Press, Cambridge | 317-344 | 1984 |
| K. H. J. Buschow | <i>E</i> | Formation, thermal stability and physical properties of amorphous 3d-based alloys | Philips J. Res. 39 | 255-274 | 1984 |
| J. L. C. Daams & J. H. N. van Vucht | <i>E</i> | Contribution to the system Mg-Au-Hg | Philips J. Res. 39 | 275-292 | 1984 |
| W. J. van Gils | <i>E</i> | Some constructions of optimal binary linear unequal error protection codes | Philips J. Res. 39 | 293-304 | 1984 |
| C. Ronse | <i>B</i> | Networks for sorting with fusion | Philips J. Res. 39 | 305-316 | 1984 |
| H. W. A. M. Rompa, M. F. H. Schuurmans & F. Williams (<i>Univ. Delaware, Newark, DE</i>) | <i>E</i> | Predicted modifications in the direct and indirect gaps of tetrahedral semiconductors | Phys. Rev. Lett. 52 | 675-678 | 1984 |
| H. M. van Noort, D. B. de Mooij & K. H. J. Buschow | <i>E</i> | Crystal structure, magnetic properties, and ⁵⁷ Fe Mössbauer effect of PtFeSn | Phys. Stat. Sol. a 86 | 655-662 | 1984 |
| A. Huijser | <i>E</i> | Optical recording | Physica 127B | 90-94 | 1984 |
| G. de With & J. E. D. Parren | <i>E</i> | Surface stresses in modified BaTiO ₃ ceramics | Proc. Br. Ceram. Soc. No. 34 | 99-108 | 1984 |
| J. T. Klomp | <i>E</i> | Ceramic and metal surfaces in ceramic-to-metal bonding | Proc. Br. Ceram. Soc. No. 34 | 249-259 | 1984 |
| R. Cuppens, C. D. Hartgring, J. F. Verwey & H. L. Peek | <i>E</i> | An EEPROM for microprocessors and custom logic | Proc. ISSCC 84, San Francisco 1984 | 3 pp. | 1984 |
| H. J. M. Veendrick, L. C. Pfennings, M. J. J. C. Annegarn, H. A. Harwig, M. J. M. Pelgrom, H. J. F. Peuscher, J. G. Raven, A. Slob & J. W. Slotboom | <i>E</i> | A 40MHz 308Kb CCD video memory | Proc. ISSCC 84, San Francisco 1984 | 3 pp. | 1984 |
| F. P. J. M. Welten, J. Lohstroh & A. J. Linssen (<i>La Radiotechnique-Compelec, Caen</i>) | <i>E</i> | A 25/50MHz dual-mode parallel multiplier/accumulator | Proc. ISSCC 84, San Francisco 1984 | 3 pp. | 1984 |
| G. de With & J. E. D. Parren | <i>E</i> | Fracture of modified BaTiO ₃ ceramics | Silicates Ind. 49 | 179-183 | 1984 |
| G. de With | <i>E</i> | Anisotropy in mechanical properties of sintered Sr-hexaferrite | Silicates Ind. 49 | 185-189 | 1984 |
| F. Berz, J. Pritchard & A. B. Crowley (<i>R. Mil. College Sci., Shrivenham</i>) | <i>R</i> | Modelling pin diode switch off with the enthalpy method | Solid-State Electron. 27 | 769-774 | 1984 |

- P. W. J. M. Boumans & J. J. A. M. Vrakking *E* High-resolution spectroscopy using an echelle spectrometer with predisperser — I. Characteristics of the instrument and approach for measuring physical line widths in an inductively coupled plasma *Spectrochim. Acta* **39B** 1239-1260 1984
- P. W. J. M. Boumans & J. J. A. M. Vrakking *E* High-resolution spectroscopy using an echelle spectrometer with predisperser — II. Analytical optimization for inductively coupled plasma atomic emission spectrometry *Spectrochim. Acta* **39B** 126-1290 1984
- P. W. J. M. Boumans & J. J. A. M. Vrakking *E* High-resolution spectroscopy using an echelle spectrometer with predisperser — III. A study of line wings as a major contribution to the background in line-rich spectra emitted by an inductively coupled plasma *Spectrochim. Acta* **39B** 1291-1305 1984
- P. R. Boudewijn, H. W. P. Akeroom & M. N. C. Kempeners *E* Profile distortion in SIMS *Spectrochim. Acta* **39B** 1567-1571 1984
- A. Thayse *B* P-functions and Boolean matrix factorization (Lect. Notes Comput. Sci., Vol. 175) Springer, Berlin 248 pp 1984
- P. R. Boudewijn, H. W. P. Akeroom, C. W. T. Bulle-Lieuwma & J. Haisma *E* Ion-bombardment-induced changes in the surface topography of MBE-grown silicon on gallium phosphide *Surf. & Interface Anal.* **7** 49-52 1985
- P. N. T. van Velzen *E* An IETS study of the reaction of 5-bromo-2-hydroxybenzaldehyde with monomolecular layers of 3-aminopropyltriethoxysilane and 3-(2-aminoethyl)aminopropyltrimethoxysilane immobilized on aluminium oxide *Surf. Sci.* **146** 319-328 1984
- P. van Dooren *B* Reduced order observers: a new algorithm and proof *Syst. & Control Lett.* **4** 243-251 1984
- P. J. Severin & E. A. Dirven *E* Optische fiber sensor werking, een doel en een middel *T. Ned. Elektron. & Radiogenoot.* **49** 169-183 1984
- J. S. Nadan & R. N. Jackson *N, R* Signal processing for wide screen television: the smart receiver *Television image quality*, J. B. Friedman (ed.), SMPTE, Scarsdale, NY 301-314 1984
- P. E. Wierenga, A. G. Dirks & J. J. van den Broek *E* Ultramicrohardness experiments on vapour-deposited films of pure metals and alloys *Thin Solid Films* **119** 375-382 1984
- A. van Oostrom *E* Characterization of semiconductor materials and devices by surface analysis techniques *Vacuum* **34** 881-892 1984
- A. G. Tangena, H. van Wijngaarden & J. G. Fijnvandraat *E* A comment on "An energy-based model of friction and its application to coated systems" *Wear* **97** 303-306 1984
- G. M. Baudet (*Brown Univ., Providence, RI*), M. Cutler (*Aerospace Corp., Los Angeles*), M. Davio, A. M. Peskin (*Brookhaven Natl. Lab., Upton, NY*) & F. J. Rammig (*Univ. Dortmund*) *B* The relationship between HDLs and programming languages *Workshop Rep. VLSI & Software Eng. Workshop, Port Chester, NY, 1983* 64-69 1984

Contents of Philips Telecommunication Review **43**, No. 2, 1985

- H. van Kampen & R. T. van der Schaaf: Office communication (pp. 75-82)
- R. T. van der Schaaf: The SOPHO S family (pp. 83-91)
- M. B. Geelhoed & M. J. Jordaan: SOPHO S2500, the high-range communication switch (pp. 92-113)
- R. J. Mulder & A. C. Zwinkels: SOPHO S250/1000, a proven concept (pp. 115-128)
- R. J. Mulder: SOPHO S100, a small but powerful junior (pp. 129-136)
- W. J. A. Pasman: SOPHO S data facilities (pp. 137-149)
- P. B. Hesdahl: Digital voice/data terminals and data-terminal adapters (pp. 150-163)
- H. van Kampen: SOPHO-TEXT, the text server for SOPHO S (pp. 164-171)
- C. M. Smits: Telephone management functions (pp. 172-181)
- G. G. Maks & R. J. Parsons: Analogue voice terminals (pp. 182-188)

Recent United States Patents

Abstracts from patents that describe inventions from the following research laboratories, which form part of or cooperate with the Philips group of companies:

Philips GmbH Forschungslaboratorium Aachen, Weißhausstraße, 5100 Aachen, Germany	A
Philips Research Laboratory Brussels, 2 avenue Van Becelaere, 1170 Brussels, Belgium	B
Philips Natuurkundig Laboratorium, Postbus 80 000, 5600 JA Eindhoven, The Netherlands	E
Philips GmbH Forschungslaboratorium Hamburg, Vogt-Kölln-Straße 30, 2000 Hamburg 54, Germany	H
Laboratoires d'Electronique et de Physique Appliquée, 3 avenue Descartes, 94450 Limeil-Brévannes, France	L
Philips Laboratories, N.A.P.C., 345 Scarborough Road, Briarcliff Manor, N.Y. 10510, U.S.A.	N
Philips Research Laboratories, Cross Oak Lane, Redhill, Surrey RH1 5HA, England	R
Philips Research Laboratories Sunnyvale, P.O. Box 9052, Sunnyvale, CA 94086, U.S.A.	S

4 504 930

Charge-coupled device

H. A. Harwig

J. W. Slotboom

M. J. M. Pelgrom

E

The invention relates to a charge-coupled SPS memory comprising a series input register, a parallel section and a series output register. In order to increase the retention time leakage current drain regions are provided beside the memory. Since the charge collected as a result of leakage current is largest during the transport through the outermost registers of the parallel section, only the sides of the parallel section are screened by the said draining regions which preferably consist of dummy registers.

4 504 936

Modular data storage system

J. W. Faber

J. A. de Vos

E

A modular data storage system for a plurality of identical data carriers includes at least one recorder apparatus and at least one storage module. The storage module includes an internal transport device. An external transport device is associated with the outside of the storage module, which external transport device can transport data carriers between the recorder apparatus and the storage module. The recorder apparatus includes a recorder module comprising a module frame having outer dimensions which are substantially equal to those of a module frame of the storage module so that all of these modules can be arranged successively adjacent to form optional configurations adapted to suit specific requirements. The external transport device cooperates with the recorder and storage modules at their backs and is located inside a cabinet of the modular data storage system.

4 507 619

Amplifier with signal-dependent voltage supply source

J. Dijkstra

E. Roza

E

In a combination of an amplifier and a signal-dependent voltage supply source coupled thereto, a portion of the signal from a signal source is applied by an amplifier to a comparator, the output signal

of which controls a limiter. A portion of the output signal thereof is applied as a feedback signal to a second input of the comparator by means of a low-pass filter and a feedback network in series. The feedback loop thus formed is arranged so that it oscillates at a comparatively high frequency. A signal-dependent modulation of the pulse width and/or the pulse density then occurs at the limiter output. A supply voltage for the amplifier is derived from the output of the filter. Owing to the high feedback factor of the feedback loop at the signal frequencies the supply voltage can adequately follow the output signal of the amplifier independently of component tolerances and any load variations.

4 508 811

Recording element having a pyrylium or thiopyrylium-squarylium dye layer and new pyrylium or thiopyrylium-squarylium compounds

D. J. Gravesteijn

C. Steenbergen

J. van der Veen

W. P. M. Nijssen

E

An optical recording element having a recording layer which comprises an alkyppyrylium-squarylium dye, as well as novel alkyppyrylium-squarylium compounds.

4 509 020

Push-pull amplifier

R. J. van de Plassche

E. C. Dijkmans

E

For a satisfactory cross-over behaviour of the transistors T_1 and T_2 of a push-pull amplifier, it is necessary that the sum of the base-emitter voltages of the transistors T_1 and T_2 remains substantially constant. For this purpose a first voltage-current converter is coupled between the base and the emitter of transistor T_1 , the inverting input of this converter being coupled to the base of transistor T_1 via a first reference-voltage source and the non-inverting input to the emitter of transistor T_1 . Similarly, a second voltage-current converter and a second reference-voltage source are arranged between the base and the emitter of transistor T_2 . The output currents of the first and the second voltage-current converters are compared with each other in a combining circuit which drives a control ampli-



fier, which in its turn controls the base-emitter voltage of transistor T_2 in such a way that the sum of the base-emitter voltages of transistors T_1 and T_2 remains constant. The push-pull amplifier exhibits a minimal amount of second-harmonic distortion, because only the difference of the errors introduced by the first and the second voltage-current converters is of importance in this respect and these errors are substantially equal to each other due to the method of fabrication of the voltage-current converters.

4 509 021

Circuit for amplifying and/or attenuating a signal

A. J. P. M. van Uden

E

In a circuit for amplifying and/or attenuating a signal, which circuit comprises an amplifier stage having an inverting input and a non-inverting input and an output, a first voltage divider having n taps is arranged between an input terminal and ultimately a point of constant potential. The taps are connected to a first controllable switching unit for switching individual ones of the taps to the non-inverting input of the amplifier stage. Further, a second voltage divider having m taps is connected between an output terminal, which is the output of the amplifier stage, and (ultimately) the point of constant potential. The taps are connected to a second controllable switching unit for switching individual ones of the taps to the inverting input of the amplifier stage.

4 509 205

Radio receiver comprising a frequency-locked loop with audio frequency feedback, and a muting circuit

W. G. Kasperkovitz

E

Radio-receiver having a frequency-locked loop which comprises, arranged one after the other, a tunable voltage-controlled oscillator, a mixer stage, a filtering element, as well as a frequency-voltage converter which is connected to the tunable voltage-controlled oscillator, several stable tunings being possible for each transmitter. An unambiguous selection is made from these stable tunings of a tuning to a desired station by muting the radio receiver in the other stable tuning frequency ranges. To this end the radio receiver according to the invention comprises a muting circuit as well as a control circuit for the muting circuit in which use is made of a further frequency-voltage converter comprising an allpass frequency-dependent 180° phase shifting network, a phase detector and a limiter. By adjusting the muting circuit of the radio receiver to the quiescent condition only in the desired tuning range and by activating it outside this range, a suppression of interstation noise is obtained at the same time.

4 510 471

Acoustic surface wave device including a reflective multistrip coupler

I. Flin

R

R. Murray

An acoustic surface wave device comprising a piezoelectric substrate provided with an input transducer an output transducer and a compact reflective multistrip coupler in which the strips of each pair of comparatively widely spaced strips in one array of mutually parallel strips are connected to respective strips of a pair of comparatively narrowly spaced strips in the other array. The wide and narrow spacings alternate along each array. The improvement provides further electrodes located in the relatively wide spaces in each array and electrically interconnected so as to effect a transfer of signal currents along each array and from one array to the other. The device improves efficiency, reduces insertion loss and improves the shape of the pass band.

4 510 520

Television transmission system

D. W. Parker

R

L. J. van de Polder

E

A high definition colour television transmission system in which wide band luminance information is divided to produce a first luminance information portion (below 3.8 MHz) and a second lumi-

nance information portion (between 3.8 and 8.8 MHz). The first luminance information portion is transmitted by way of a first transmission path together with a colour subcarrier modulated by colour information. The bandwidth of the colour information is such that the modulation components lie outside the bandwidth of the first luminance information portion. The second and higher frequency luminance information portion is frequency shifted to lie within 0 and 5 MHz and is transmitted by way of a second transmission path. The two transmissions may also carry sound signals. The two transmissions may be jointly received for the provision of a high definition display but the invention has the distinct advantage that the signal of the first transmission path may be received alone by currently manufactured television receivers for reproduction of a display of a quality which is currently acceptable.

4 510 528

Smear reduction for a television pick-up

F. H. M. Bergen

E

A television pick-up arrangement comprises a solid state pick-up device which is read by field transfer. The pick-up produces a picture signal which on display shows information smear. It is known to perform a correction by obtaining signal smear information from under an opaque, masking strip on the picture pick-up portion of the pick-up device. The smear picture signal is stored once in every field period in a memory device which is repeatedly readable at line frequency. The smear picture signal is subtracted from the picture signal to be corrected. If there is movement in the scene in the horizontal direction, an unacceptable smear is, however, still observable. According to the invention, a correction may be effected, using a second memory device. The second memory device may be used for performing a signal averaging operation over several field periods or for storing a smear picture signal so that different smear corrections can be effected in the upper and lower picture halves. In both cases the smear is reduced to an acceptable level.

4 510 612

System comprising mutually synchronizing first and second active functional units

C. S. Scholten

E

A. Slob

P. G. Jansen

A synchronization system for two active functional units which are interconnected by means of a synchronization connection. In order to obtain reliable synchronization without using an untoward number of wires in the connection, at least one of the two functional units has a generator which is capable of generating three successive discrete signal levels on a single connection wire of the synchronization connection. This function unit also has a detector for detecting a signal transition which is produced by a generator in the other active functional unit and for generating an activation signal in reaction thereto. In response to this activation signal, the generator of the same functional unit produces a succession of two signal transitions from one prevailing extreme signal level to the other extreme signal level of the three successive signal levels. The other functional unit has a detector which produces, in response to the second signal transition of the succession, an activation signal for the generator of the other functional unit in order to produce a synchronized signal transition or transitions. Such successions of signal transitions can be transmitted in one or both directions; the synchronization connection may even consist of a single connection wire on which a total of five different signals levels may then occur.

4 511 601

Copper metallization for dielectric materials

J. R. Akse

N

S. A. Long

A method of providing a copper metallization on a dielectric or semiconductive body, and a dielectric or semiconductive body having a metallization consisting essentially of copper. According to the method, a mixture of copper oxide powder and 0 to 15 weight percent reduction-resistant glass frit is dispersed in an organic vehicle and a solvent to produce a paste. The paste is applied to the body to provide a coating thereon. The coating is dried to remove

the solvent, and then the coated body is fired in an oxidizing atmosphere at a temperature below the melting temperature of the glass frit to remove the organic vehicle. Finally, the coated body is fired a second time in an atmosphere which is reducing to the copper oxide but substantially nonreducing to the glass frit. The second firing is at a temperature from 700 to 1050 °C for from 120 to 15 minutes to convert the copper oxide to copper metal. The metallized body may comprise a reduction-resistant dielectric body and a metallization consisting essentially of copper, with no glass frit.

4 511 855

Compensation for differences in gain among amplifiers

K. R. Wittig

N

A method and apparatus for measuring the small signal gain of an amplifier. Each amplifier responds, in operation, to a small signal input. The small signal input varies substantially linearly over a field time interval. A small bias signal is added to the bias level input of the amplifier during a portion of the field time interval. The output of the amplifier is measured at three or more different times during the field time interval, at least one time when the small bias signal has not been added to the bias level input and at least one time being when the small bias signal has been added to the bias level input. By processing the measured outputs, a signal which is directly proportional to the product of the small bias signal with the small signal gain of the amplifier is obtained. A method and apparatus for actively compensating for differences in the small signal gain among two or more amplifiers is obtained by dividing the small signal output of each amplifier by the signal proportional to the small signal gain of the amplifier.

4 511 933

Method and apparatus for recording a digital information signal

M. H. H. Höfelt

E. de Niet

A. M. A. Rijckaert

E

For a controlled positioning of a read element relative to a track to be read during the read-out of such a record carrier, low-frequency tracking signals may be recorded in the tracks. Instead of adding separate tracking signals to the information signal, these tracking signals are represented by the d.c. content of the information signal. During conversion of the information words of the information signal into channel words steps are therefore taken to provide two channel words whose d.c. content is equal but opposite for each information word. The choice between these two channel words is made depending on a control signal which depends on the desired tracking signal.

4 512 020

Data processing device for processing multiple-symbol data-words based on a symbol-correcting code and having multiple operating modes

T. Krol

B. J. Vonk

E

A computer system based on a symbol-correcting code. The code words consist of a number of code symbols. In the normal operating mode of the error correction members, correction is possible of all errors which are either limited to one code symbol or which concern only two arbitrarily situated code bits. During operation in the erasure mode, a predetermined code symbol within the code word is not taken into account; therefore, it may contain an arbitrary, unknown error. An error can be corrected which concerns only one arbitrarily situated code bit. In the selection mode, two predetermined code symbols within the code word are not taken into account. The data words can be reconstructed from the others. The mode is controlled by the content of the mode register. The mode register is controlled by the output signals of syndrome generators.

4 513 262

Acoustic surface wave device

J. Schofield

R. F. Milsom

R

An acoustic surface wave device using an interdigital electrode array to launch and receive surface waves overcomes problems of diffraction by making the arrays approximately $3\lambda_c$ wide between the outer boundaries of the bus bars. As a result, the arrays can each only propagate and transduce a single acoustic surface waveguide mode which is symmetrical about the axis of the array.

4 513 263

Bandpass filters

B. J. Minnis

R

The specification describes four classes of microwave bandpass filters formed in triple plate stripline with portions of line having a commensurate length equal to a quarter-wavelength at the center of the stopband, enabling the widths of the pass and stop bands to be specified independently; lumped capacitors are also used to assist in providing elements with high series capacitance. The four classes together cover a wide range of electrical specifications, and enable wide pass and stop bands and high selectivity to be obtained. Each class corresponds to a bandpass S-plane prototype network configuration derived using exact synthesis procedures from a specification of transmission zero locations. The filters can be manufactured using photolithographic technology to have consistently accurate performance.

4 513 272

Devices for manufacturing a magnetic quadrupole post-focusing mask

J. Verweel

H. Zijlstra

E

In a first method, a meander-shaped coil is provided on each side of a mask having apertures. The coils are oriented perpendicularly relative to each other. If a current flows through the coils in the correct direction, a magnetic quadrupole is formed along the circumference of each aperture. In a second method, a holder with permanent magnetic strips is provided on each side of the mask. The strips in the one holder are oriented perpendicularly relative to the strips in the other holder. A coil is provided around the holders with which a decaying magnetic alternating field is generated which initially drives the material of the mask on both sides of the hysteresis curve into saturation. After the decay of said alternating field a magnetic quadrupole is present along the circumference of each aperture.

4 513 315

Community antenna television arrangement for the reception and distribution of TV signals and digital audio signals

C. B. Dekker

L. B. Vries

E

Community antenna television arrangement for the reception and distribution of TV signals and digital audio signals, in particular signals which are transmitted per satellite, including a head-end connected to a receiving antenna and a signal distribution network, a time-division multiplex signal which comprises the digital audio signals in a time-multiplex distribution, being applied to the head-end, which time-division multiplex signal is modulated on a sound carrier, the bit rate of the digital audio signals to be distributed being reduced in the head-end of the community antenna television arrangement by a TDM/FDM conversion in order to reduce signal echoes.

4 513 388

Electronic device for the execution of a mathematical operation on sets of three digital variables

H. J. M. Veendrick
L. C. M. G. Pfenning
J. G. Raven
A. H. H. J. Nillesen

E

A device is described for electronically executing a mathematical operation, being $Z = KA + (1 - K)B$. It is also described how this device or how several of such devices can be used for the design of a number of realizations, such as a recursive filter, a digital mixer etc. The basic idea is the electronic implementation of a mathematical function for binary variables.

4 513 433

Fluoroscopy apparatus for forming layer images of a three-dimensional object

H. Weiss
R. Linde
U. Tiemens
E. Klotz

H

Apparatus for the layer-wise imaging of an object by means of a large number of radiation sources which are situated in a radiation source plane and whose radiation beams intersect one another so that the approximately equally large radiation beam cross-sections which are situated in one irradiation plane almost completely cover one another. A record carrier is arranged on the other side of the object in order to record perspective images produced by the radiation beams. An imaging matrix which comprises imaging elements for the superposition of the perspective images on an image display device is disposed behind the record carrier. Displacement means are provided in order to realize a relative movement between the irradiation plane and the object or an object table carrying the object.

4 514 251

Method of manufacturing a semiconductor device, in which patterns are formed in a layer of silicon nitride by means of ion implantation

A. H. van Ommen
H. G. R. Maas
J. A. Appels
W. J. M. J. Josquin

E

In a method of manufacturing a semiconductor device, ions are implanted into a layer of silicon nitride over a part of its surface, and the layer is then subjected to an etching treatment. According to the present invention, before the etching treatment takes place, but after the ion implantation, the layer is subjected to a heat treatment in which the implanted part of the layer obtains a higher resistance to etching than the non-implanted part. The heat treatment occurs at temperatures above 750 °C. Thus, a negative image of a patterned ion irradiation can be formed in the silicon nitride layer. As a result, the number of cases in which an etching or oxidation mask can be formed in a silicon nitride layer without using additional mask is considerably increased.

4 514 754

Digital colour television signal processing circuit

A. H. H. J. Nillesen
P. W. G. Welles

E

In a phase control loop for the A/D converter of a digital colour television signal processing circuit an input and an output of a delay circuit are connected to a comparator to derive a control signal from the inequality of the signals at said input and output.

4 514 837

Apparatus for optically reading and/or recording information

G. E. van Rosmalen

E

An apparatus for optically reading and/or recording information on a rotary optical disc, such as a videodisc player or an optical recorder, comprises an objective carrier for an objective which is radially moved to and fro over a frame by a drive unit. Driving is effected by means of two electric motors which rotate in opposite directions and which move the objective carrier to and fro and, simultaneously but in an opposite direction, move two balancing masses in paths on each side of the path of movement of the objective carrier, so that during accelerations and decelerations of the to-and-fro movements of the objective carrier no reactive forces or reaction moments are transmitted to the frame.

4 516 146

Electron sources and equipment having electron sources

J. M. Shannon
A. M. E. Hoeberechts
G. G. P. van Gorkom

E

An electron source having a rapid response time comprises at least one n-p-n structure (and possibly an array of said n-p-n structure) formed in a silicon or other semiconductor body by a p-type first region between n-type second and third regions. Electrons are generated in the n-p-n structure for emission into free space from a surface area of the body after flowing from the second region through the first and third regions. The n-p-n structure has electrode connections only to the n-type second and third regions. The first region provides a barrier region restricting the flow of electrons from the second region to the third region until a potential difference is applied between the electrode connections to bias the third region positive with respect to the second region and to establish a supply of hot electrons injected into the third region with sufficient energy to overcome the potential barrier present between the surface area and free space. The barrier region forms depletion layers with both the n-type second and third regions and is depleted of holes by the merging together of these depletion layers at least when the potential difference is applied to establish said supply of hot electrons. The n-p-n structure can be provided in a mesa portion of the body at a window in an insulating layer so as to form a compact arrangement having very low associated capacitances. The electron sources may be used in cathode-ray tubes, display devices and even electron lithography equipment.

4 516 252

Device for imaging layers of a body

R. Linde
E. Klotz

H

In a short-time tomosynthesis apparatus for imaging layers of a body to be examined, the body is irradiated by radiation beams from a large number of different directions in order to form perspective images. The radiation beams are detected by a detector which is arranged underneath the body. The perspective images appearing on the exit of the detector will overlap when the radiation beams have a comparatively large angle of aperture. For separating the perspective images, an image separating system is provided at the exit of the detector. The image separating system may comprise a fiber-optical system or an electron-optical deflection unit.

4 516 261

Device for reducing faults in layer images of a three-dimensional object formed by means of penetrating radiation

G. Harding
E. Klotz

H

A device for reducing artefacts in layer images. Several layer images are formed of an object layer by irradiation from different directions. The same points of these layer images are compared in order to obtain a corrected layer image: when corresponding image information is present in all images points compared, the image information is transferred to corresponding layer image points in a corrected layer image; when the image information in the compared image points is not the same, that information is at least partly suppressed.

Digital signal processing I Background

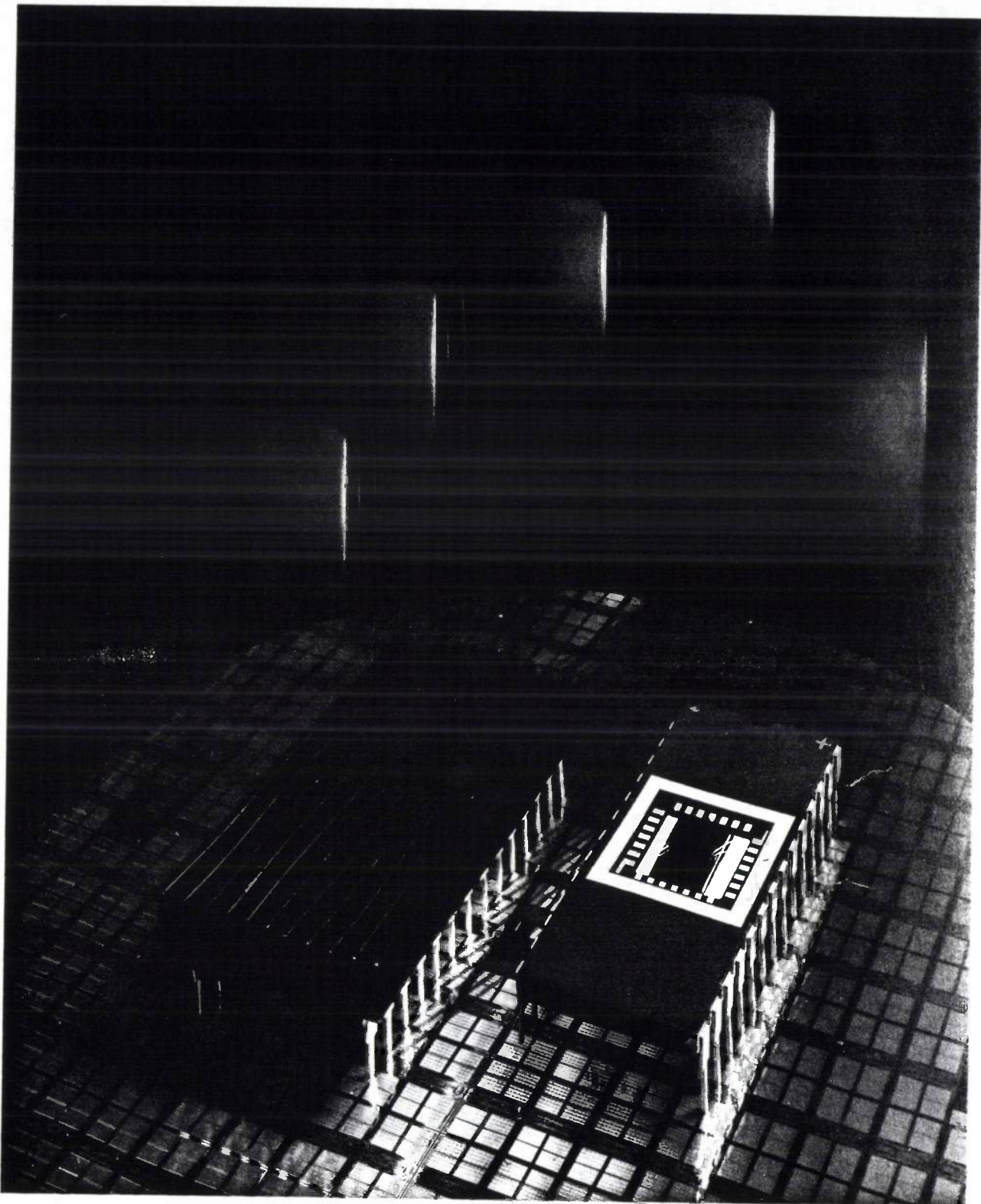
'00000000 00000011 00000000 00000011 00000000 00000011 00000000 00000011 00000000
00000011 00000000 00000010 01101000 11010000 11001110 11001110 00000000 00000001
00000000 00000001 00000000 00000001 11111111 11111101 11111111 11111101 11111111
11111100 00101100 01000111 01110011 10000110 00000000 00000011 00000000 00000011
00000000 00000011 00000000 00000100 00000000 ...' This is the start of Tchaikovsky's
1812 Overture. The pattern represents the first few binary digits of the digital recording on a
Compact Disc. However, we cannot tell much from this about the male-voice choir whose
singing starts the overture. Apart from the fact that such a digital signal is virtually unreadable
in itself, the portion represented here contains an ingenious but complicated interweaving of
the left-hand and right-hand components of the stereo audio signal with one another and with
the parity bits for automatic error correction. Moreover, this represents less than 200 micro-
seconds from the start of the opening chorus and cannot therefore represent much more than
the singers' intake of breath before they start!

Before the listener can obtain any impression of the sound at all, the Compact Disc signal
must be subjected to an extensive series of operations that can be lumped together as 'digital
signal processing' (DSP). In a continuous succession of many, yet each extremely simple,
'computer-like' operations, a perfection in quality of reproduction and faithfulness to the
original is reached that could not be obtained by analog methods. In many professional appli-
cations DSP has therefore established itself already. In the life of the 'ordinary' consumer the
Compact Disc heralds the widespread introduction of DSP in many fields; first for audio sig-
nals, later for video signals, telephone signals, and so on.

For a good understanding of the pros and cons of DSP in comparison with conventional
signal processing a number of concepts are required that are by no means generally familiar.
These include the concepts of 'discrete time', 'discrete amplitude' and their implications.
A greater familiarity with this material should therefore lead to an even better appreciation
of DSP.

For these reasons this issue of our journal and a later one are entirely given over to this sub-
ject. The two articles in this issue are mainly intended to throw some light on the background.
The first one is about the historical development that enabled DSP to grow to a practical pos-
sibility — the arrival of microelectronics was a key factor here. It also gives a general picture
of the advantages, disadvantages and applications. The second article fills most of this issue.
It offers an introduction to the theory of DSP and is based on an internal Philips series of
tutorial lectures. This article was written to propagate the basic knowledge necessary for a
good understanding of DSP. It also forms the foundation for the future articles about DSP in
this journal, starting with our next special issue, 'Digital signal processing II, applications'.
This will describe a number of interesting examples of DSP, with particular reference to audio
and television.

PHILIPS RESEARCH LABS
LIBRARY
P.O. BOX 1000
5600 JA Eindhoven
THE NETHERLANDS



The quality of television receivers can be improved by using digital signal processing. This requires image-storage devices that can be produced economically. An important step in that direction is the Charge-Coupled Device (CCD) shown here, which can store 308 kbit of picture information with sufficiently high input and output rates. The photograph shows a 28-pin package complete with cooling fins, alongside a partly unpackaged unit. The substrate is a 'slice' or 'wafer' from an earlier phase in the production process. A large number of unmounted chips of the same type can be seen on the substrate.

Digital signal processing — growth of a technology

J. B. H. Peek

Introduction

It is hard to imagine a life without numbers. All un-awares, we have gradually become used to using numbers in dealing with all the various commonplaces of everyday living. For many people the day begins with a look at the clock, and much depends on whether it says 'ten to six' or 'five past eleven'. During the rest of the day we are bombarded with numerical data, from the prices in the shops to ages of traffic accident victims in the newspapers, from the latest quotations of stock-market prices to the quantities in a recipe.

In about 500 B.C. the Greek philosopher and mathematician Pythagoras and his followers based a complete philosophy of life on the conviction that 'number is the essence of all'. Although not everyone would agree with such a sweeping generalization, it is an aphorism that might well apply to some modern technological developments. It seems very relevant to microelectronics: electronic circuits with components of extremely small dimensions. One of the keywords in this subject today is 'digitization', derived by way of 'digit' (figure), from the Latin 'digitus' (finger). The complicated circuits — called integrated circuits, ICs or chips — that can be made by microelectronics technology are by their nature eminently suitable for manipulating numbers (*Table I*). This has had two important consequences.

In the first place there is an almost exponential growth in the use of the computer in all kinds of applications where numbers have traditionally been used, as in bookkeeping, stock control, numerical computation and statistics. These applications come under the general heading of *data processing*.

In the second place there is a tendency to use numbers in situations where they would not have been used before. Here too there are often advantages to be gained from microelectronics. One of the best known examples is the digital wristwatch, which has largely taken the place of the mechanical spring-driven watch with hands and a dial. An even more recent example is the Compact Disc player, replacing the conventional

record player. In this example the music information is recorded on the disc in digital form, that is to say as a series of numbers. On playback the numbers are processed and converted back to music. This is referred to as *digital signal processing*.

The electronic equipment used for digital signal processing has many features in common with the electronic equipment used for data processing, because both are essentially concerned with the manipulation of numbers. The individual elementary components are the same 'logic circuits' — such as gates, adders and storage or memory cells. The aim pursued, however, and the manner of attaining it (the algorithm) are completely different. Sometimes it is the similarities between the two fields that are striking, sometimes the dissimilarities. It is quite possible that a computer in a scientific institution might at one moment be occupied in processing the payroll, and at another moment it might be processing signals received from interplanetary space probes. The computer programs or software necessary for the two activities are completely different. In most cases, however, we see that the hardware is also tailored to specific applications. Although built up from the same elementary compo-

Table I. Some of the techniques that have facilitated the manipulation of numbers, and their dates. The last column gives a figure for the number of elementary arithmetic operations (additions) per second. The term VLSI (Very-Large-Scale Integration) indicates that a large number (more than 50 000 to 100 000) of components are integrated on a single chip.

Technique	Characteristic component	Dates	Number of additions per second
Mechanical	gearwheel	1650-1900	1
Electromechanical	relay, switch	1900-1945	10
Electronics	thermionic valve	1945-1955	10 ⁴
Semiconductor electronics	transistor	1955-1965	10 ⁵
Microelectronics	integrated circuit	1965-1975	10 ⁶
VLSI micro-electronics	microprocessor	1975-	10 ⁷

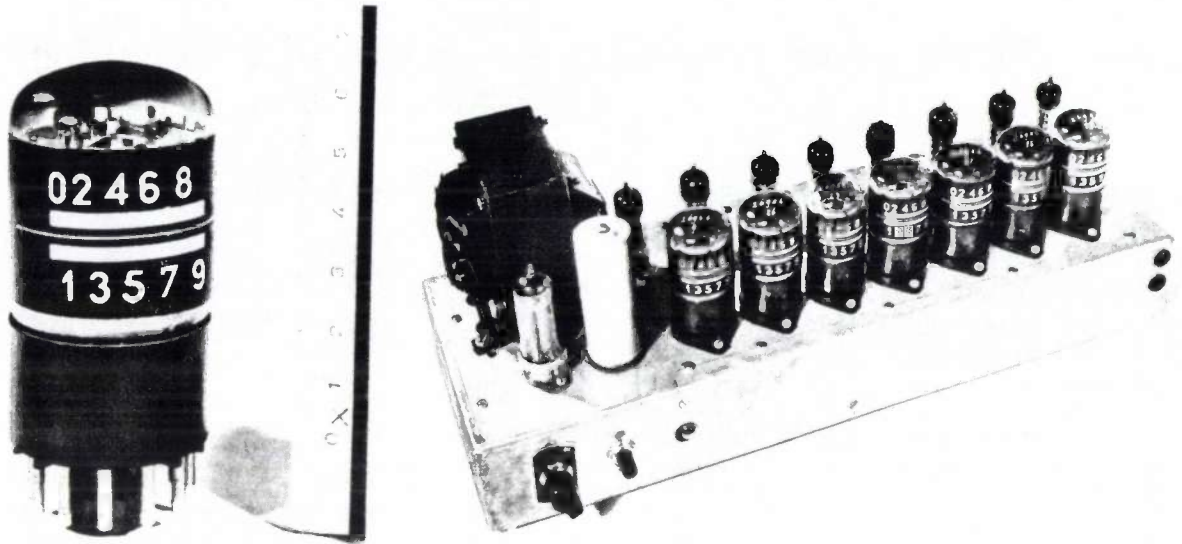


Fig. 1. With thermionic valves, numbers could be manipulated by electronics for the first time. *a)* Counter tube from the late forties; it counted from 0 to 9. The count could be read from a light spot on the front of the tube. *b)* Decimal counter that could count from 0 to $10^7 - 1$ at a maximum rate of 30 000 units per second.

nents, there are quite different digital chips for watches, pocket calculators, video games, Compact Disc players and digital TVs. To a large extent these differences stem from the totally different algorithms required for signal processing as opposed to data processing.

The general opinion is that neither data processing nor digital signal processing have yet developed to their full extent. So much more is to be gained (improved quality, or lower costs, or both — and much more) through this continuing digitization of technology (*figs 1* and *2*). This article outlines the background to the development of digital signal processing.

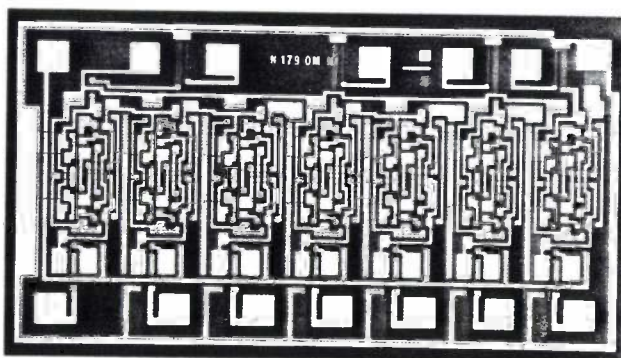


Fig. 2. Integrated circuit (binary divider) from the late sixties. The dimensions of this chip are only 2 mm × 1.1 mm. Although this circuit does not fulfil exactly the same function as the one in *fig. 1*, a general comparison demonstrates the radical changes that have taken place during the first 20 years in the development of electronic digital techniques. And this was only the beginning...

Signals and signal processing

Man has long used signals. These include all natural and artificial phenomena that vary as a function of some independent variable. The independent variable is usually time, and for simplicity we shall confine ourselves to this for the moment. Simple examples of signals are the variation of the temperature of an object or the changes in air pressure caused by a sound source. Such effects are often 'translated' by a converter into an electrical quantity, such as a current or a voltage, which also varies as a function of time. This produces an electrical signal, which characterizes the original effect and can be used for recording, transmission or other manipulations.

In many cases (as in the two examples just mentioned) time, acting as an independent variable, is a continuous variable t , i.e. the signal occurs at every real value of t ; it is then referred to as a continuous-time signal (*fig. 3a*). In other cases the signal only occurs at discrete values nT of the time; we then have a discrete-time signal. This would happen, for example, when we take the temperature of a sick person at fixed intervals during the day, or when we note a particular share price on the stock exchange at the end of each working day (*fig. 3b*).

The required information cannot always be read directly from the signals and it may be that the signals are not free from disturbances such as noise. The usefulness of the signals can then be increased by means of signal processing. Familiar concepts encountered

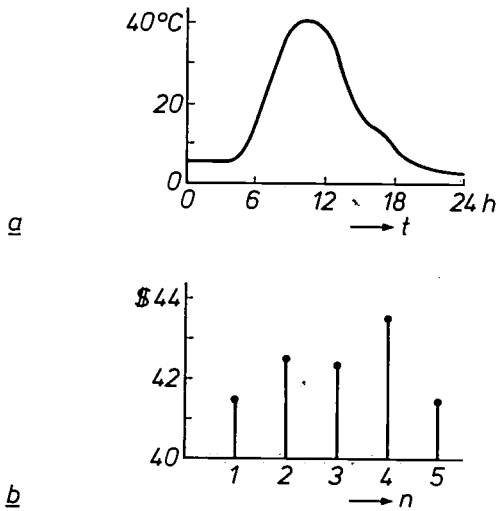


Fig. 3. a) Continuous-time signal giving the variation of temperature as a function of time t during a period of 24 hours. b) Discrete-time signal showing the price of an imaginary share on the stock exchange at the end of a number of successive days n .

the samples $x[n]$ can also take all real values, so that the instantaneous values of $x(t)$ can be reproduced exactly. Here we come to the fundamental difference, between a general discrete-time signal $x[n]$ and a digital signal $x_Q[n]$: although both consist of a series of samples or numbers, with a digital signal the number of possible different values is essentially limited, although arbitrarily large (fig. 4). The transition from a discrete-time signal of the general type to a digital signal always implies a form of approximation ('quantization'), and although the quantization may be arbitrarily fine, it is irreversible.

This brings us up against a major discrepancy that is typical of digital signal processing in the present state of the art. On the one hand the use of digital signals is attractive from the practical viewpoint because the signals can be processed by standard circuits used in computers. Each sample or number is then represented as a group (a 'word') of zeros and ones ('bits').

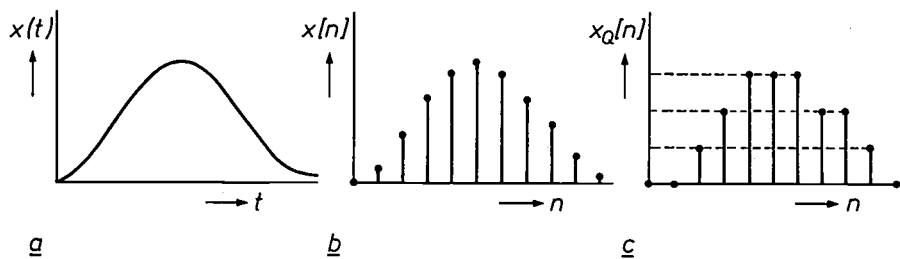


Fig. 4. a) A continuous-time signal $x(t)$ whose amplitude can assume any value. This is an analog signal. b) A discrete-time signal $x[n]$ of the general type; its amplitude can also assume any value. Such a signal is sometimes referred to as a sampled-data signal. c) A discrete-time signal $x_Q[n]$ whose amplitude can assume only a finite number of different values. This is a digital signal.

here are interpolation, extrapolation, smoothing, filtering and prediction [1]. A historic example of signal processing is to be found in the work of Sir Arthur Schuster in the eighteen-nineties; he investigated the occurrence of periodicities in certain meteorological phenomena [2].

Formerly, continuous-time and discrete-time signals were always treated as two separate worlds. All this changed in 1949, when C. E. Shannon introduced his sampling theorem [3]. This showed that any continuous-time signal $x(t)$ whose frequency spectrum is limited in bandwidth can be represented without loss of information as a series of samples (denoted as $x[nT]$ or $x[n]$) of the original signal, or, in other words, as a discrete-time signal.

The instantaneous amplitude of most continuous-time signals $x(t)$ can in principle assume any real value; they are referred to as analog signals. In the derivation of the sampling theorem it is assumed that

To minimize the complexity of the circuits the word lengths are kept small and so therefore is the number of possible different values. On the other hand, most of the theoretical tools available (described in a number of excellent text books [4]-[6]) are based on the properties of discrete-time signals of the general type, with no limiting conditions imposed on the possible signal values.

- [1] N. Wiener, Extrapolation, interpolation and smoothing of stationary time series, Wiley, New York 1949;
- E. A. Robinson, A historical perspective of spectrum estimation, Proc. IEEE 70, 885-907, 1982.
- [2] A. Schuster, On the investigation of hidden periodicities with application to a supposed 26-day period of meteorological phenomena, Terr. Magn. 3, 13-41, 1898.
- [3] A. J. Jerri, The Shannon sampling theorem — its various extensions and applications: a tutorial review, Proc. IEEE 65, 1565-1596, 1977.
- [4] L. R. Rabiner and B. Gold, Theory and application of digital signal processing, Prentice-Hall, Englewood Cliffs, NJ, 1975.
- [5] A. V. Oppenheim and R. W. Schaffer, Digital signal processing, Prentice-Hall, Englewood Cliffs, NJ, 1975.
- [6] A. V. Oppenheim, A. S. Willsky with I. T. Young, Signals and systems, Prentice-Hall, Englewood Cliffs, NJ, 1983.

In the historical sense this discrepancy is not surprising, since the interest in digital signals is of much more recent date than the interest in general discrete-time signals. Another point is that the theory of quantization operations is more difficult than the theory of sampling operations, for example, because it is nonlinear. This can lead to a variety of undesired effects, such as instabilities.

The usual approach to the application of digital signal processing is therefore to complete the analysis and design first, without paying any attention to the quantization. Then the effects of the quantization are considered to see if they are negligible or if they need to be taken into account separately.

Much of what is written about digital signal processing really refers to general discrete-time signal processing, since — for convenience — little attention is paid to the quantization effects. The articles in the two special issues of our journal on digital signal processing will be no exception to the rule.

Finally, it should be emphasized that not all digital signals are derived by sampling and quantization from an analog signal; some electrical signals are digital right from the outset. A simple example is a digital tone generator that supplies directly a series of numbers of sinusoidally varying value. Here again the successive signal values are referred to as 'samples'.

Advantages and disadvantages of digital signal processing

The advantages of digital signal processing fall into three categories: those that are fundamental in nature, those that come about through the use of microelectronics, and those that are most evident from a comparison with conventional analog signal processing.

The first category consists mainly of advantageous effects that are a direct consequence of using a limited number of discrete sample values. If the electrical representation of a sample value is unambiguously recognizable (i.e. each bit is uniquely recognizable as a 'zero' or a 'one'), small errors in the representation are not important. This has the following positive consequences:

- the tolerances on the value of the components used to build the circuits do not need to be very close;
- the sensitivity to external effects (temperature and interfering signals) and internal effects (ageing and drift) is low;
- the accuracy of operation can be precisely controlled by selecting the number of different possible sample values (directly related to the word length);
- the circuits are completely reproducible (i.e. identical circuits behave identically), so that no trimming is required during manufacture, for example;
- the number of successive operations that can be per-

formed on a signal is theoretically unlimited, since undesired accumulation of interfering effects such as noise can be avoided.

Another advantage that we would like to put in this category is the flexibility that can be achieved by making a circuit or system programmable. This makes it possible to modify a particular processing function without having to make radical changes in the hardware.

Making digital signal processing equipment in the form of chips gives the following advantages in the second category:

- small dimensions,
- high reliability,
- capability of complex processing,
- low price.

In a comparison with analog signal processing the advantages of the third category are very obvious. Some processing functions are too complex for practical analog execution, or may for fundamental reasons be difficult or impossible in an analog system, or only possible by approximation. On the other hand, digital implementation of the same functions may often be quite straightforward. Some examples are:

- the 'ideal memory', whose contents can in principle remain completely uncorrupted for an indefinite period; with such a memory a digital 'ideal integrator' can be made and very-low-frequency signals can be processed digitally;
- phase-linear filters, which are important in data transmission and TV applications;
- circuits in which certain processing operations have to be exactly equivalent, e.g. for the compensation of two effects;
- self-regulating ('adaptive') systems;
- signal transformations, e.g. from the time domain to the frequency domain and vice-versa, as in the Discrete Fourier Transform (DFT). Working with numbers allows various special mathematical techniques to be used (the most familiar is the Fast Fourier Transform or FFT technique, which considerably reduces the number of calculations required);
- the processing of two-dimensional signals, such as images;
- new ways of suppressing the effects of interference by error correction, and of improving security.

This is a fairly long list of advantages; however, there are some disadvantages. The principal ones are:

- in the present state of the technology, digital signal processing always requires a certain amount of electrical power: passive digital circuits do not yet exist. (But note that in modern analog systems as well active circuits are definitely going to outnumber passive circuits);

- digital signal processing cannot be applied to signals at the higher frequencies, although the upper limit is steadily rising;
- when digital signal processing is used in an analog environment analog-to-digital and digital-to-analog converters are necessary, and these may be fairly complex;
- in the present state of the technology there can be difficulties in the analog-to-digital or digital-to-analog conversion of very weak or very strong signals. The digital processing of very weak signals (e.g. antenna signals) and strong signals (e.g. for driving a loud-speaker or a television picture tube) must therefore still be accompanied by analog preamplification or post-treatment, as appropriate;
- the same information (e.g. music) requires a larger bandwidth as a digital signal than it does as an analog signal;
- the design and manufacture of digital chips is a highly specialized technology, often requiring large quantities of manpower, money, specialized knowledge and special equipment, which increase as chips become more complex (fig. 5).

equipment. An example already mentioned is the Compact Disc player. Now wide-ranging applications in the television field also seem to be becoming an economic proposition.

Modules for digital signal processing

The theoretical principles of digital signal processing apply just as much to the execution of a particular algorithm in the form of software for a general-purpose computer as to an implementation in the form of a specific piece of hardware. The great practical and economic significance of digital signal processing is especially apparent in the second of these two forms. We shall therefore take a look now at the modules used here.

The most elementary components are the electrical circuits (gates) that perform logic functions such as AND, OR, NAND, NOR and NOT. Each only requires a few electronic components, such as transistors. An assembly of gates results in somewhat more complex components, such as parts of counters (half-adders) and memory cells (bistables or flip-flops). From these in turn larger modules can be formed, such as adders, multipliers and serial memories (shift registers). In principle we then have all the elements we need for making any of the circuits belonging to the very important class of linear time-invariant digital systems^{[7][8]}. The only functions required for such systems are addition, multiplication and delay (or temporary storage in a memory). Systems of this class include most digital filters in common use.

As well as shift registers, some other types of electronic memory have been developed that have characteristics that in some respects are significantly different. Two such memories are the 'Random-Access Memory', or RAM, whose name emphasizes the difference from shift registers with their serial access, and the permanent 'Read-Only Memory', or ROM, whose contents can be read as often as required but not rewritten.

Complete digital systems can be built with the modules mentioned above used as separate components. Sometimes a ready-made microprocessor chip — really a small computer in itself — is used for controlling the interaction between the different components. From this point two further steps can be taken in the development towards components of higher

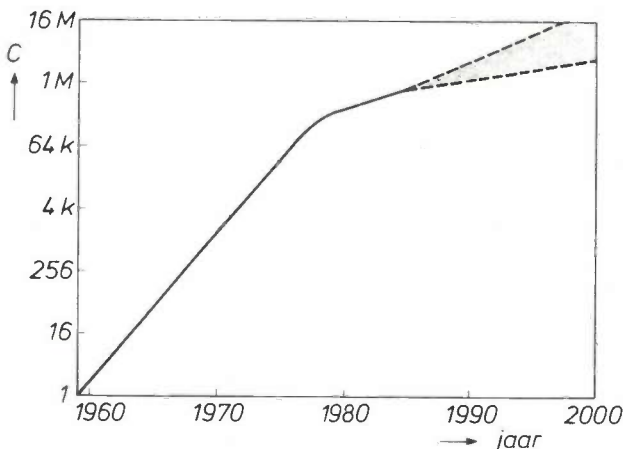


Fig. 5. The highest degree of complexity C of integrated circuits, expressed in terms of the number of components (e.g. transistors) per chip, has increased approximately exponentially. C has doubled every year from 1959 to the late seventies; since then the rate of increase has decreased slightly, and now doubles every two years. In the near future chips with a million components will probably not be exceptional. The trend follows 'Moore's law'; in 1964 and in 1975 G. E. Moore produced the forecasts confirmed by the development shown here. On the vertical axis k represents 2^{10} ($= 1024$) and M represents 2^{20} ($= 1\,048\,576$).

In each practical case it will be necessary to consider the pros and cons very carefully to decide whether digital signal processing will provide the best results. Originally it was mainly in the professional applications (see later) that the balance first moved towards the digital side. Recently, however, we have seen the same development in much more ordinary consumer

[7] Because the word lengths are finite, leading to quantization and overflow effects^[8], digital systems are never *strictly speaking* linear. The combination here of the two concepts 'linear' and 'digital' indicates that *in practice* these effects are negligible and that there are no other nonlinear operations.

[8] A. W. M. van den Enden and N. A. M. Verhoeckx, Digital signal processing: theoretical background, this issue, pages 110-144.

complexity. These are the 'signal processor' and the 'custom IC'. The signal processor is a more elaborate type of microprocessor with provision for more efficient implementation of typical signal-processing functions, such as large numbers of multiplications (fig. 6). Since the signal processor is programmable, it can be used for a variety of applications [9][10]. In mass production it may be cheaper to use digital signal processing based on custom ICs; see fig. 7. As the name implies, these are 'custom-made' for one specific application.

Here again it is important to emphasize the importance of digital memories in the growing application of digital signal processing. In audio applications, for example, developments were greatly stimulated by the appearance of the Compact Disc [11]. In essence, every individual optical disc is simply a huge permanent digital memory with an effective storage capacity of the order of 5 gigabits (5 000 000 000 bits), with 1.4 megabits representing one second of stereo sound. Digital signal processing in colour television receivers will only really become interesting when an inexpensive digital memory is available that can record and play back the information in a complete television field (about 2 megabits) 50 or 60 times a second. It now seems that this is economically feasible. (See photograph on page 102.)

One category of components that should not be left out here is that of analog-to-digital and digital-to-analog converters (A/D and D/A converters for short). In considering digital signal processing in an analog

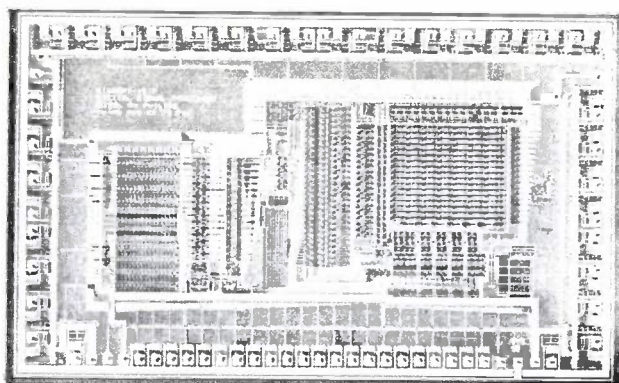


Fig. 6. Photograph of a 'number cruncher' for use in a digital signal processor. This circuit has been optimized in certain respects. For example, the minimum of time is lost on internal transfer of signal samples, and little time is taken up by the most common signal operations, such as addition of multiplication results. The circuit is primarily intended for processing 16-bit signals, but its modular design readily permits extension to larger word lengths. When memories and input-output circuits are added on the same chip, the result is a complete programmable integrated digital signal processor. The IC shown here is a product of CMOS technology. It contains about 19 000 transistors on an area of 15.5 mm^2 . The smallest dimensions are $2 \mu\text{m}$ and the cycle time for the calculations is only $0.1 \mu\text{s}$ [10].

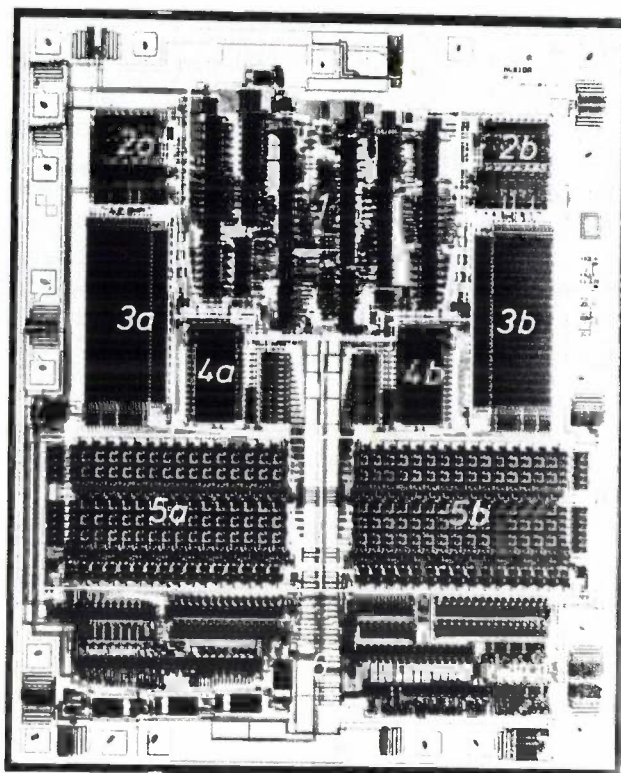


Fig. 7. A custom-made chip for digital signal processing in Compact Disc players. The circuits on this chip are designed specifically for certain tasks. One important task is the replacement of fragments of 'mutilated' sound (linear interpolation for 'error concealment'); this should not be confused with error correction, already performed on the digital signal). The other main task is the calculation of three audio samples between each two successive values stored on the Compact Disc (interpolation for increasing the sampling rate by a factor of four). Digital filtering is of vital significance in both tasks. Because of the stereo nature of the system, all major circuits are duplicated on the chip: one half of the chip processes the left sound signal, the other the right sound signal. 1 clock and control circuits. 2a, 2b input registers. 3a, 3b random-access memories (RAMs) for storing the filter input signals. 4a, 4b read-only memories (ROMs) for storing filter coefficients. 5a, 5b multipliers/accumulators for performing the filter calculations. 6 output circuits. This chip is a product of $2.5\text{-}\mu\text{m}$ NMOS technology. It contains about 17 000 transistors on an area of about 16 mm^2 .

environment these are often assumed to be ideal components. But since they are — literally — the link between the analog world and the digital world, any errors either in amplitude or in time that are made in the conversions are usually directly reflected in the ultimate quality of the processed signal. When such converters are included in a digital system the designer should therefore give full attention to their performance [12].

Applications of digital signal processing

As far as is known, the first applications of digital signal processing for civil purposes were in geophysics (soil research for oil and gas exploration), and then in radio astronomy and radar astronomy. Digital correlation techniques [13] have been used in these fields

since the end of the fifties. The calculations were usually made on general-purpose computers. Since then the possible uses have increased very considerably in number and versatility, largely because of the introduction of special signal-processing hardware. Significant examples are to be found in telecommunications, for instance in modems^[14] for data transmission to and from computers — one of the first commercial applications of adaptive digital signal processing (automatic equalization). Digital techniques are also used in telephony, for example in vocoders^[15] and transmultiplexers^[16], mostly for long-distance communications. It looks as if in the long run telephone signals will be digitized at source (i.e. at the subscriber's location) and transmitted all the way to their destination in digital form.

Another important field is that of medical applications; this applies not only to investigations of the functioning of heart and brain, but also to examinations of other organs and even of the unborn child. Image processing is becoming increasingly important here, and can be used in combination with X-ray and NMR techniques^[17]. Professional digital image processing is also applied to photographs received from weather satellites or from space vehicles at an even greater distance from the Earth. This began in about 1964 with space flights to the moon (Ranger VII) and to the planet Mars (Mariner 4)^[18]. Television studios are also making increasing use of digital techniques for manipulating picture signals^[19].

There are interesting applications in instruments based on digital signal transforms (DFT, FFT) for spectrum analysis and other analytical purposes, and also for industrial process control, especially in the chemical industry.

Most of the examples of applications mentioned here are of a professional nature. Digital signal processing has been brought within the reach of the ordinary consumer with the introduction of the Compact Disc. In the near future this will be followed by applications in the television receiver^[20], the radio receiver and the telephone set. It seems to be a natural and inevitable development. Perhaps the day will come when people will ask: 'Analog signal processing, now what's that?'

- [9] E. H. J. Persoon and C. J. B. Vandenbulcke, Digital audio: examples of the application of the ASP integrated signal processor. Forthcoming article in the special issue of this journal, 'Digital signal processing II, applications'.
- [10] F. P. J. M. Welten, A. Delaruelle, F. J. A. van Wijk, J. L. van Meerbergen, J. Schmid, K. Rinner, K. J. E. van Eerdewijk and J. H. Wittek, A 2- μ m CMOS 10-MHz microprogrammable signal processing core with an on-chip multiport memory bank, IEEE J. SC-20, 754-760, 1985.
- [11] Special issue, 'Compact Disc Digital Audio', Philips Tech. Rev. 40, 149-180, 1982.
- [12] J. J. van der Kam, A digital 'decimating' filter for analog-to-digital conversion of hi-fi audio signals. Forthcoming article in the special issue of this journal, 'Digital signal processing II, applications'.
D. Goedhart, R. J. van de Plassche and E. F. Stikvoort, Digital-to-analog conversion in playing a Compact Disc, Philips Tech. Rev. 40, 174-179, 1982.
- [13] J. B. H. Peek, The measurement of correlation functions in correlators using 'shift-invariant independent' functions (Thesis, Eindhoven 1967), Philips Res. Rep. Suppl. 1968, No. 1 (76 pp.).
- [14] R. A. van Doorn and N. A. M. Verhoeckx, An I²L digital modulation stage for data transmission, Philips Tech. Rev. 37, 291-301, 1977;
P. J. van Gerwen, W. A. M. Sniijders and N. A. M. Verhoeckx, An integrated echo canceller for baseband data transmission, Philips Tech. Rev. 39, 102-117, 1980.
- [15] R. J. Sluyter, Digitization of speech, Philips Tech. Rev. 41, 201-223, 1983/84.
- [16] T. A. C. M. Claasen and W. F. G. Mecklenbräuer, A generalized scheme for an all-digital time-division multiplex to frequency-division multiplex translator, IEEE Trans. CAS-25, 252-259, 1978.
- [17] P. R. Locher, Proton NMR tomography, Philips Tech. Rev. 41, 73-88, 1983/84.
- [18] K. R. Castleman, Digital image processing, Prentice-Hall, Englewood Cliffs, NJ, 1979.
- [19] J. H. Peters and J. T. Kanters, CAROT: a digital method of increasing the 'robustness' of an analog colour television signal. Forthcoming article in the special issue of this journal, 'Digital signal processing II, applications'.
- [20] M. J. J. C. Annegarn, A. H. H. J. Nillesen and J. G. Raven, Digital signal processing in television receivers. Forthcoming article in the special issue of this journal, 'Digital signal processing II, applications'.

Summary. The rapid development of microelectronics has resulted in an exponential growth of data processing in all the administrative activities (such as clerical work) where numbers have been processed since time immemorial. Moreover, it can be seen that the same elementary electronic building blocks are being used to an increasing extent in circuits and systems for digital signal processing. This happened first in professional applications, e.g. geophysics, astronomy and space flight, and now, with the Compact Disc player, these techniques have entered the consumer field. In the near future digital TV applications will undoubtedly follow. This article outlines a number of the developments behind the advancing 'digitization' of modern technology. The article also considers the main advantages and disadvantages of digital signal processing, the main modules now used and some common applications.

Contents

INTRODUCTION	111
I. DISCRETE SIGNALS	112
Description in the time domain	112
Description in the frequency domain	114
The Fourier transform for discrete signals (FTD)	114
The z-transform (ZT)	115
The relation between FTD and ZT	117
The discrete Fourier transform (DFT)	117
The fast Fourier transform (FFT)	119
II. DISCRETE SYSTEMS	120
System descriptions	121
Difference equations	121
Impulse response	121
Frequency response	122
System function	123
Poles and zeros	124
III. DISCRETE FILTERS	125
Discrete filter structures	126
NRDFs (non-recursive discrete filters)	127
RDFs (recursive discrete filters)	127
Special filter structures	128
Comb filters	128
Ladder and lattice filters	128
Wave digital filters	130
Transposed filters	130
Adaptive filters	130
IV. METHODS OF DESIGNING DISCRETE FILTERS	130
FIR filter design	131
Using IFTD and time window	131
Equiripple design	132
IIR filter design	133
Impulse invariance	133
Bilinear transformation	134
Transformation of elements	135
Optimization by computer	135
V. PRACTICAL ASPECTS OF DIGITAL SYSTEMS	135
From continuous time to discrete time and vice versa	135
Change of sampling rate	136
From continuous amplitude to discrete amplitude	140
Quantization	140
Overflow	140
Number representation	140
Finite-word-length effects	141
A/D conversion	141
Digital filter design	141
Digital computations	142
SUMMARY	144

Digital signal processing: theoretical background

A. W. M. van den Enden and N. A. M. Verhoeckx

INTRODUCTION

Signals exist in many and various forms, ranging from drum signals in the bush to the stop signal from the traffic policeman or the combined radio/television signal received through a central antenna system. The typical common characteristic of all these signals is that they represent a message, or information. The message does not depend greatly on the nature of the signal. The acoustic drum signal can be converted by a microphone into an electrical signal for transmission to the other end of the world. There it can be converted into an optical signal for recording on a Compact Disc. Then the opposite route can be followed, from optical signal via electrical signal to acoustic signal, without any degradation of the original drum message.

In the present state of the technology, electrical signals offer the widest scope for transmission, storage and manipulation ('signal processing'). In signal transmission, however, the arrival of the fibre-optic cable has considerably increased the significance of optical signals. In theoretical considerations the physical nature of a signal is irrelevant. Every signal is 'abstracted' to a function of one or more independent variables, representing for example time or position in space.

In this article we shall confine ourselves to signals that can be represented as a function of a single variable, which we generally take to be 'time', while the value of the function itself is denoted as 'the (instantaneous) amplitude'. The signals fall into different categories. Time can be either a continuous variable t , which may assume any arbitrary real value, or a discrete variable n , which can only represent integers. We can also distinguish between signals that have a continuous amplitude, which may assume any value (between two extremes), and signals that have a discrete amplitude, which only has a limited number of different values. In this way we have signals of four kinds, which are shown schematically in *fig. 1* and which will be denoted as $x(t)$, $x_Q(t)$, $x[n]$ and $x_Q[n]$. The most familiar type of signal is undoubtedly $x(t)$, usually referred to as an analog signal. In the past this type of signal has received the most attention, since

the components and circuits available were most suitable for processing such signals. But the situation has changed greatly in the last twenty years or so. Technological developments have given much greater significance to both types of discrete-time signals. This applies both to the digital signal $x_Q[n]$ and to the sampled-data signal $x[n]$.

Digital signals can be represented as series of numbers with a limited range of possible different values, and it is therefore easy to process them with the same logic circuits as those from which digital computers are formed [1].

Sampled-data signals have become so important mainly because of the considerable progress in electrical circuits in which signals are represented as electric charges that are transferred from one point to another at regular intervals and thus processed. Typical devices of this kind are charged-coupled devices (CCDs), charge-transfer devices (CTDs) [2] and switched-capacitor filters (SCFs) [3].

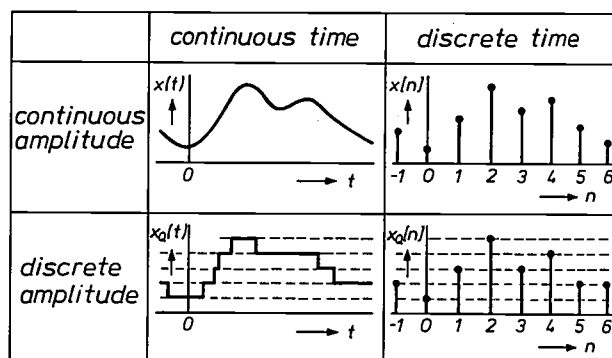


Fig. 1. Signals can be either continuous or discrete in both time and amplitude. They can therefore be subdivided into four types, as illustrated here. The signal $x(t)$ is analog and $x_Q[n]$ digital. The discrete-time signal of continuous amplitude $x[n]$ is generally referred to as a sampled-data signal. The signals of type $x[n]$ and $x_Q[n]$ are both frequently referred to simply as discrete signals. The continuous-time signal of discrete amplitude $x_Q(t)$ is not commonly known by any alternative name.

[1] J. B. H. Peek, Digital signal processing — growth of a technology, this issue, pp. 103-109.

[2] H. Dollekamp, L. J. M. Esser and H. de Jong, P²CCD in 60 MHz oscilloscope with digital image storage, Philips Tech. Rev. 40, 55-68, 1982.

[3] A. H. M. van Roermond and P. M. C. Coppelmans, An integrated switched-capacitor filter for viewdata, Philips Tech. Rev. 41, 105-123, 1983/4.

Signals of the type $x_Q(t)$, where the transition from one discrete amplitude to another can take place at random times, are the least commonly used. If they are used, the number of possible amplitudes is often limited to two. Examples of such signals are to be found in certain forms of pulse modulation, e.g. in the LaserVision video-disc system [4].

In general a signal-processing system is referred to by the same name as the signal being processed: an analog system processes analog signals; a discrete-time system processes discrete-time signals.

In this article we shall examine the theoretical fundamentals of digital signal processing. In doing so we must however bear in mind that the particular part of the theory that deals with the discrete-amplitude nature of the signals is in fact the least suitable for a systematic description and is therefore generally the least accessible. To some extent this is because the resultant 'finite-word-length effects' appear as non-linear effects, which can be responsible for undesirable behaviour of the system, such as oscillations. Also the discrete-amplitude nature of the signals and the operations often results in an apparent addition of noise-like disturbances, called 'quantization noise', whose consequences can only be properly described in statistical terms.

In the design or analysis of digital signal-processing systems the discrete amplitudes are really a serious complication. The usual practice is therefore to deliberately ignore this aspect at first and only consider the discrete-time aspect. The consequences of the discrete amplitude are then considered separately and taken into account if necessary. This is why much of the literature on digital signal processing [5][6] really belongs to the wider category of general discrete-time signal processing [7]. In this article from now on we shall limit the term 'digital' as far as possible to those situations in which we do in fact take the finite word length into account. We shall also use the terms 'continuous' and 'discrete' without further qualification, tacitly referring to the time aspect and not to the amplitude aspect.

In the sections that follow we shall first give some examples of discrete signals and their main characteristics. We shall then give an appropriate representation of the Fourier transform and the associated z-transform. Next we shall turn our attention to discrete systems and describe a number of analytical methods. We shall look in particular at the many possible kinds of discrete filters and at some of the principal methods used to design them. Where it seems useful, we shall mention similarities to or differences from continuous signals and systems. We shall also deal with the transition from continuous time to discrete time and vice

versa, and with the possibility of changing the sampling rate. Finally we shall look at the transition from continuous amplitude to discrete amplitude and at some finite-word-length effects in digital systems.

I. DISCRETE SIGNALS

Description in the time domain

A discrete signal consists of a series of signal values, which we call 'samples', whatever the exact origin of the signal. Some typical examples are given in fig. 2 to illustrate the different kinds of discrete signals that can be encountered. In fig. 2a we see a signal $x_1[n]$, which is defined by:

$$x_1[n] = \begin{cases} n & \text{for } 1 \leq n \leq 3 \\ 0 & \text{elsewhere.} \end{cases} \quad (1)$$

Although this signal is defined for every value of n between $-\infty$ and $+\infty$, it differs from zero for only a finite number of values of n ; we call this a discrete signal of finite duration. Other examples of discrete signals of this type are the discrete unit pulse $\delta[n]$ and the version of it shifted by i places, $\delta[n - i]$; see fig. 2b and c. They can be written formally as:

$$\delta[n] = \begin{cases} 1 & \text{for } n = 0 \\ 0 & \text{elsewhere} \end{cases} \quad (2)$$

and

$$\delta[n - i] = \begin{cases} 1 & \text{for } n = i \\ 0 & \text{elsewhere.} \end{cases} \quad (3)$$

Fig. 2d shows a signal $x_2[n]$ for which:

$$x_2[n] = \begin{cases} 0.8^n & \text{for } n \geq 0 \\ 0 & \text{elsewhere.} \end{cases} \quad (4)$$

This is a discrete signal of infinite duration. Other examples of such signals are the discrete unit-step function $u[n]$ that (see fig. 2e) is defined as:

$$u[n] = \begin{cases} 1 & \text{for } n \geq 0 \\ 0 & \text{elsewhere} \end{cases} \quad (5)$$

and the discrete sine function

$$x[n] = A \sin(n\theta + \phi), \quad (6)$$

where A is the (maximum) amplitude, θ the (relative)

[4] See pp. 332-335 of F. W. de Vrijer, Modulation, Philips Tech. Rev. 36, 305-362, 1976.

[5] L. R. Rabiner and B. Gold, Theory and application of digital signal processing, Prentice-Hall, Englewood Cliffs, NJ, 1975.

[6] A. V. Oppenheim and R. W. Schaffer, Digital signal processing, Prentice-Hall, Englewood Cliffs, NJ, 1975.

[7] In some modern textbooks discrete-time and continuous-time signal processing are treated as a combined subject; see for example:

A. Papoulis, Circuits and systems: a modern approach, Holt, Rinehart & Winston, New York 1980;

A. V. Oppenheim and A. S. Willsky, with I. T. Young, Signals and systems, Prentice-Hall, Englewood Cliffs, NJ, 1983.

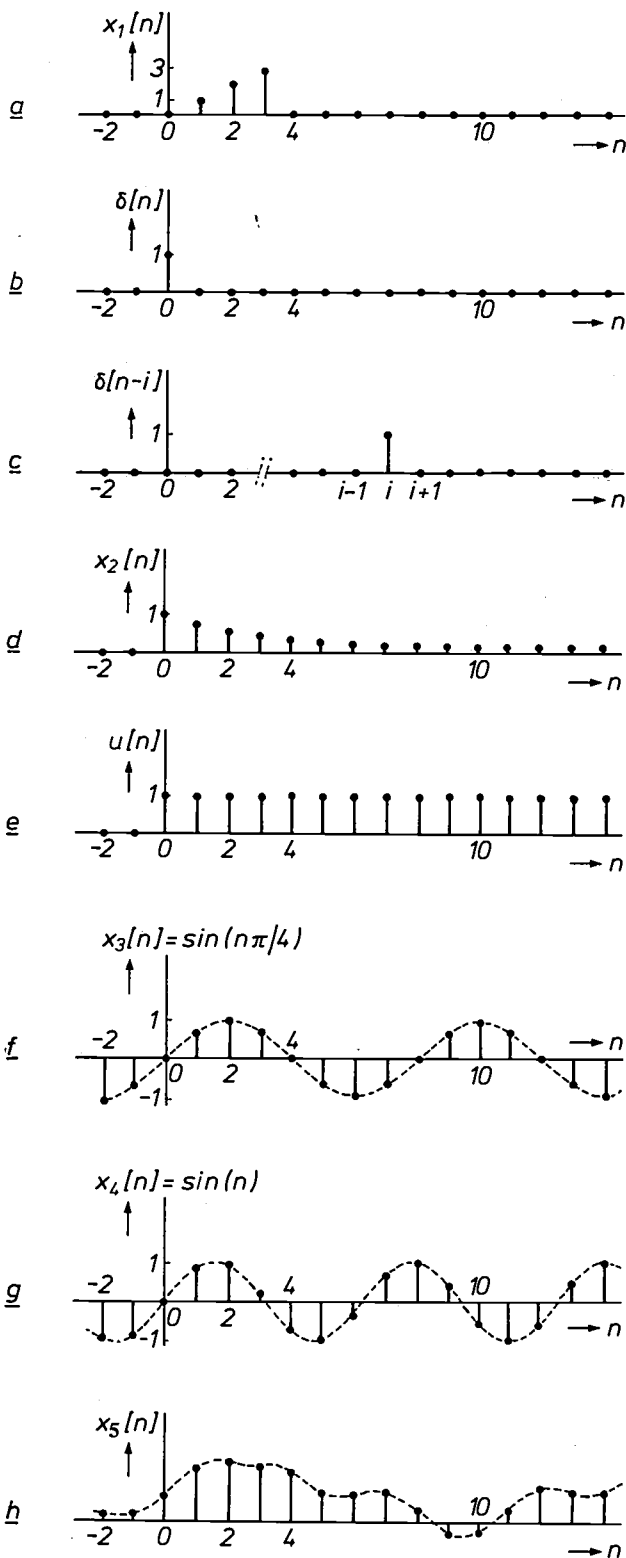


Fig. 2. a)-c) Examples of discrete signals of finite duration; $x_1[n]$ is an arbitrarily chosen signal, $\delta[n]$ and $\delta[n - i]$ represent the frequently used discrete unit pulse and the discrete unit pulse shifted by i places. d)-h) Examples of discrete signals of infinite duration; $x_2[n]$ is a signal decreasing as a power function, and $u[n]$ is the discrete unit-step function. Both $x_3[n]$ and $x_4[n]$ are discrete sine functions. It can be seen that $x_3[n]$ is periodic and $x_4[n]$ is not. The signal $x_5[n]$ cannot easily be expressed by a mathematical expression, but could represent a discrete noise signal or a speech signal in discrete form.

frequency and ϕ the phase. In fig. 2f and g two discrete sine functions $x_3[n]$ and $x_4[n]$ are shown, with

$$x_3[n] = \sin(n\pi/4) \tag{7}$$

and

$$x_4[n] = \sin(n). \tag{8}$$

From $x_3[n]$ and $x_4[n]$ we can indicate for the first time distinct similarities and differences between discrete and continuous signals. The signal $x_3[n]$ is periodic in n with period 8, since

$$x_3[n] = \sin(n\pi/4) = \sin\{(n + 8)\pi/4\} = x_3[n + 8] \tag{9}$$

for all values of n . This agrees with our experience that the continuous sine function $x(t) = \sin(\omega t)$ is periodic in t . For $x_4[n]$, however, no integer N_0 can be found for which

$$x_4[n] = x_4[n + N_0]. \tag{10}$$

A discrete sine function need not therefore be periodic at all.

It is also interesting that two discrete sine functions with relative frequencies θ_1 and θ_2 , where

$$\theta_2 = \theta_1 + 2\pi i \quad (i = \text{integer}), \tag{11}$$

have exactly the same sequence of signal values ('samples') and are thus identical, since

$$\begin{aligned} \sin(\theta_2 n) &= \sin\{(\theta_1 + 2\pi i)n\} \\ &= \sin(\theta_1 n + 2\pi i n) \\ &= \sin(\theta_1 n). \end{aligned} \tag{12}$$

The signal $x_5[n]$ in fig. 2h represents a stochastic discrete signal: it cannot be directly expressed by a mathematical expression and can only be described in statistical terms. It might be part of a discrete noise signal or a sequence of samples taken from an analog speech signal (dashed line), now representing a discrete version of it.

In all the examples of discrete signals given so far we have been concerned with *real* samples, corresponding with our practical experience. In theoretical considerations it is very useful — as in the continuous case — to use complex signals as well, i.e. signals that consist of a sequence of *complex* samples. For our purposes the most important is the complex exponential function

$$x[n] = z^n, \tag{13}$$

where $z = Ae^{j\phi} = \text{Re}z + j\text{Im}z$ can be any arbitrary complex number. An important subcategory of complex discrete signals is obtained if z in eq. (13) is limited to the complex numbers of modulus 1, i.e. to $z = e^{j\phi}$. Using Euler's relation we then have:

$$x[n] = e^{j\phi n} = \cos(n\phi) + j \sin(n\phi). \tag{14}$$

The discrete unit pulse $\delta[n]$ in eq. (2) makes it possible to write any discrete signal $x[n]$ explicitly as a sequence of samples of value $x[i]$:

$$x[n] = \sum_{i=-\infty}^{\infty} x[i] \delta[n - i]. \quad (15)$$

At this point the usefulness of this alternative mode of expression is not very clear; we shall return to it later.

We conclude this section with a remark on the notation. Until now we have denoted discrete signals as $x[n]$, where n represents an integer. There is thus no clear reference to absolute time (expressed in seconds, say). This may sometimes be a disadvantage, for example if the discrete signal has been obtained by sampling a continuous signal at a sampling interval of T seconds and we want to give a frequency description in terms of absolute frequency (i.e. in Hz or rad/s). This simple notation may also have its disadvantages in situations where signals with different sampling intervals T_1 and T_2 (in other words, with different sampling frequencies) are to be treated simultaneously. In all these cases [8] we shall use the equivalent notation $x[nT]$, $x[nT_1]$, $x[nT_2]$, etc. for $x[n]$.

Description in the frequency domain

The Fourier transform for discrete signals (FTD)

By analogy with the theory for continuous signals a (frequency) spectrum for the discrete signal $x[nT]$ can

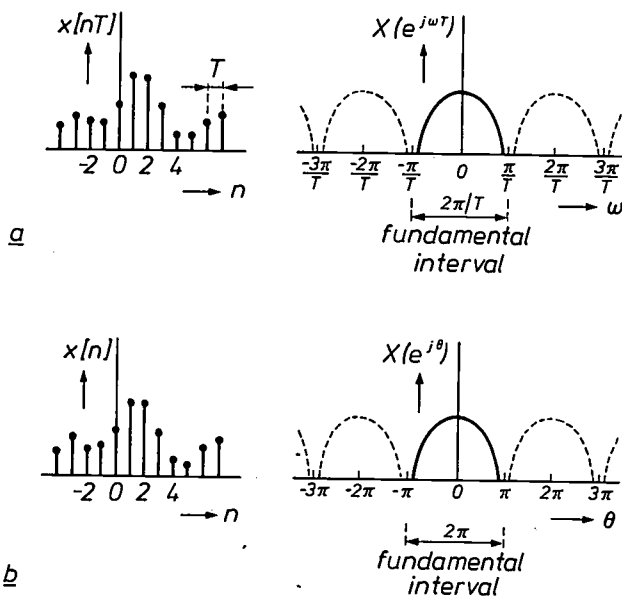


Fig. 3. a) Schematic representation of the spectrum $X(e^{j\omega T})$ of a signal $x[nT]$, obtained with the Fourier transform for discrete signals (FTD) from eq. (16). The spectrum is completely characterized by its behaviour in the fundamental interval $-\pi/T \leq \omega < \pi/T$. b) The same result when the FTD is applied in normalized form as given by eq. (19). The fundamental interval is now 2π . ω absolute frequency, θ relative frequency.

be derived by means of the Fourier transform for discrete signals (FTD). This is defined as follows:

$$\text{FTD: } X(e^{j\omega T}) = \sum_{n=-\infty}^{\infty} x[nT] e^{-jn\omega T}. \quad (16)$$

A schematic example of this transform is given in fig. 3a. In this figure the periodicity of $X(e^{j\omega T})$ with the period $2\pi/T$ is at once apparent. This is one of the most typical features of the spectrum of any discrete signal. A single period is all we need to fully define $X(e^{j\omega T})$ and hence $x[nT]$. It is usual to take the interval $-\pi/T \leq \omega < \pi/T$ and to call it the fundamental interval. (Sometimes the interval $0 \leq \omega < 2\pi/T$ may be taken.) From the variation of $X(e^{j\omega T})$ in the fundamental interval we can find $x[nT]$ by means of the inverse Fourier transform for discrete signals (IFTD):

$$\text{IFTD: } x[nT] = \frac{T}{2\pi} \int_{-\pi/T}^{\pi/T} X(e^{j\omega T}) e^{jn\omega T} d\omega. \quad (17)$$

The functions $x[nT]$ and $X(e^{j\omega T})$ constitute a pair of transforms (or Fourier pair), which we can represent symbolically by

$$x[nT] \underset{\circ}{\overset{\circ}{\text{FTD}}}\ X(e^{j\omega T}). \quad (18)$$

The analogy of the FTD and the Fourier transform for continuous signals (FTC) appears most directly from a comparison of the relevant equations. The FTC and the corresponding IFTC are given by

$$\text{FTC: } X(j\omega) = \int_{-\infty}^{\infty} x(t) e^{-j\omega t} dt,$$

$$\text{IFTC: } x(t) = \frac{1}{2\pi} \int_{-\infty}^{\infty} X(j\omega) e^{j\omega t} d\omega.$$

The greatest differences are found in the replacement of the integral by a summation for the transformation from time to frequency and in the change of the integration interval for the inverse transformation.

The fact that we use the notation $X(e^{j\omega T})$ for the FTD and not, for example, $X(j\omega)$ is due to the connection between the FTD and the z-transform, which we shall deal with later. It has the incidental advantage that the use of $e^{j\omega T}$ as a variable gives explicit expression to the periodicity in ω .

[8] Sometimes the opposite is true: little use is then made of the fact that $x[n]$ is a function of the variable n , and one only wishes to make a clear distinction between discrete signals and continuous signals. The more compact notation x_n can then be used, as in [9].
 [9] M. J. J. C. Annegarn, A. H. H. J. Nillesen and J. G. Raven, Digital signal processing in television receivers. Forthcoming article in the special issue of this journal on 'Digital signal processing II, applications'.

Besides the forms of equations (16) and (17), the FTD and IFTD also have the (more usual) normalized forms. These are obtained by substituting n for nT and θ for ωT . We then obtain (see fig. 3b):

$$\text{FTD: } X(e^{j\theta}) = \sum_{n=-\infty}^{\infty} x[n] e^{-jn\theta}, \quad (19)$$

$$\text{IFTD: } x[n] = \frac{1}{2\pi} \int_{-\pi}^{\pi} X(e^{j\theta}) e^{jn\theta} d\theta. \quad (20)$$

The quantity θ is called the relative frequency. There is also a fundamental interval for $X(e^{j\theta})$, of magnitude 2π . This interval is usually taken as $-\pi \leq \theta < \pi$. Since $x[n]$ and $X(e^{j\theta})$ form a Fourier pair, we can write:

$$x[n] \underset{\text{FTD}}{\circlearrowleft} X(e^{j\theta}). \quad (21)$$

We should realize that $X(e^{j\theta})$ is a complex function; when making graphical representations we have to split $X(e^{j\theta})$ into a real part $R = \text{Re} X(e^{j\theta})$ and an imaginary part $I = \text{Im} X(e^{j\theta})$ or into a modulus $A = |X(e^{j\theta})|$ and an argument $\phi = \arg X(e^{j\theta})$, giving

$$X(e^{j\theta}) = R + jI = A e^{j\phi}, \quad (22)$$

where R, I, A and ϕ are functions of the frequency, so that we really ought to write $R(e^{j\theta}), I(e^{j\theta}), A(e^{j\theta})$ and $\phi(e^{j\theta})$. The same considerations also apply of course to $X(e^{j\omega T})$. In fig. 3 it has been assumed for convenience that the spectra are purely real. A more realistic example is given in fig. 4, where the actual FTD is shown in the two ways just mentioned for the signal $x[n] = 0.8^n u[n]$.

The FTD has a large number of properties that correspond to those of the Fourier transform for continuous signals. For illustration we shall state here the most important properties that we shall be using in the rest of this article. We start out from the two Fourier pairs:

$$x[n] \underset{\text{FTD}}{\circlearrowleft} X(e^{j\theta}) \text{ and } y[n] \underset{\text{FTD}}{\circlearrowleft} Y(e^{j\theta}).$$

I. *Linearity.* For all values of the constants a and b :

$$ax[n] + by[n] \underset{\text{FTD}}{\circlearrowleft} aX(e^{j\theta}) + bY(e^{j\theta}).$$

II. *Shift.* For every integer i :

$$x[n - i] \underset{\text{FTD}}{\circlearrowleft} e^{-ij\theta} X(e^{j\theta}).$$

III. *Convolution.* Although we shall not be dealing in detail with the convolution operation (indicated by $*$) until we get to page 122, we should mention one extremely important property here: the convolution of two signals in the time domain corresponds to multiplication of their Fourier transforms in the frequency domain. Expressed formally:

$$x[n] * y[n] \underset{\text{FTD}}{\circlearrowleft} X(e^{j\theta}) Y(e^{j\theta}).$$

IV. *For real signals* $x[n]$, the real part of the Fourier transform is even and the imaginary part odd, i.e.:

$$R(e^{j\theta}) = R(e^{-j\theta}) \text{ and } I(e^{j\theta}) = -I(e^{-j\theta})$$

or, expressed in terms of modulus and argument:

$$A(e^{j\theta}) = A(e^{-j\theta}) \text{ and } \phi(e^{j\theta}) = -\phi(e^{-j\theta}).$$

To describe real signals, it is therefore sufficient to use the spectrum in a half fundamental interval.

The z-transform (ZT)

Besides the FTD described above there are other very useful related signal transforms for discrete signals. An extremely important one is the (bilateral)

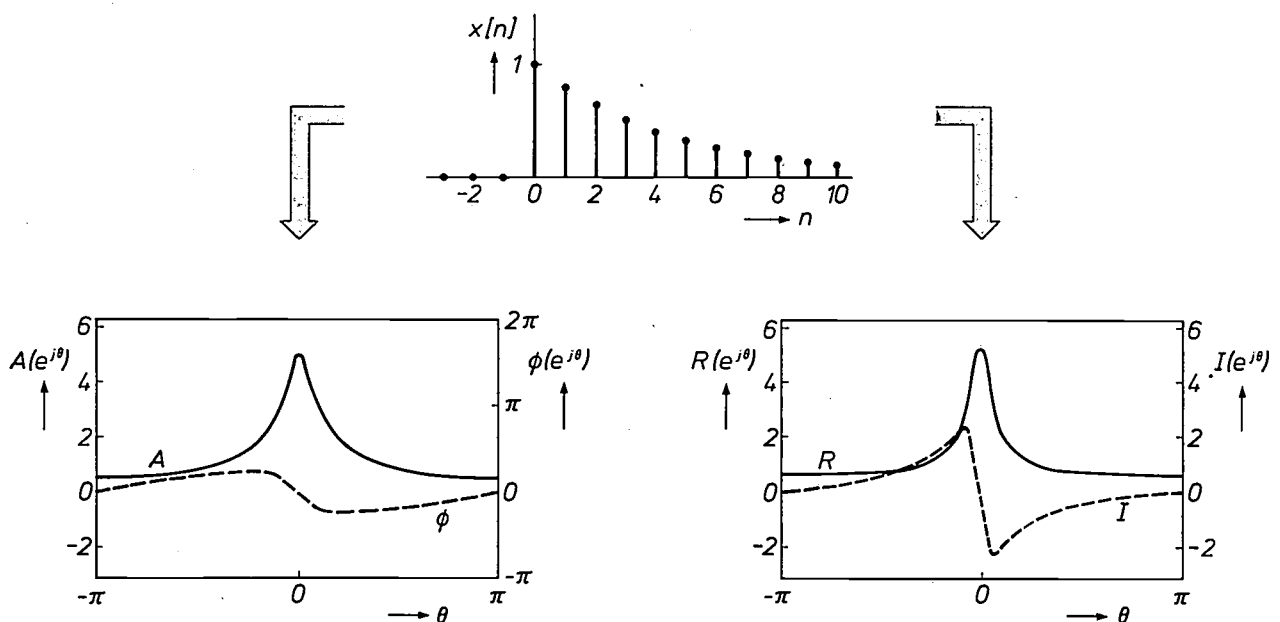


Fig. 4. Applying the FTD to a discrete signal generally results in a complex spectrum, so that two frequency functions have to be shown. The combination usually chosen is modulus $A(e^{j\theta})$ and argument $\phi(e^{j\theta})$ or the combination of real part $R(e^{j\theta})$ and imaginary part $I(e^{j\theta})$. Both alternatives are shown here for the case $x[n] = 0.8^n u[n]$.

z-transform (ZT). The z-transform $X(z)$ of a discrete signal $x[n]$ is defined as:

$$\text{ZT: } X(z) = \sum_{n=-\infty}^{\infty} x[n] z^{-n}. \quad (23)$$

We see how use is made here of the complex exponential function z^{-n} , where z can assume any arbitrary complex value. $X(z)$ is thus a complex function of the complex variable z . This means that we cannot easily produce a direct graphical representation of all values of the function $X(z)$. This would require two 3-dimensional figures ('hill-and-valley landscapes'), one of which would for example give $\text{Re } X(z)$ as a function of $\text{Re } z$ and $\text{Im } z$, and the other would do the same for $\text{Im } X(z)$ (fig. 5). We shall see later, however, that there is another very different, but effective, graphical method of obtaining an understanding of the properties of $X(z)$ and $x[n]$ (the 'poles-and-zeros plot').

The z-transform plays the same role for discrete signals as the Laplace transform (LT) for continuous signals. The (bilateral) Laplace transform is given by:

$$\text{LT: } X(p) = \int_{-\infty}^{\infty} x(t) e^{-pt} dt.$$

The most important difference is the replacement of the integral by a summation. The fact that the base of the natural logarithm e can be recognized in the LT but not in the ZT is a mere detail, since any complex number z can be written as:

$$z = a + jb = Ae^{j\phi} = e^{\ln(A) + j\phi} = e^{\sigma}.$$

With the ZT, as with the LT, the question of convergence arises. For a given function $x[n]$ the infinite sum of eq. (23) will not 'converge' for every value of z to yield a finite value. For every $X(z)$ we should therefore, strictly speaking, mention the relevant region of convergence. This is particularly important from the theoretical point of view, because under different convergence conditions the same $X(z)$ corresponds to different functions $x[n]$. In practical systems, however, there is never any doubt about which $x[n]$ is being dealt with. In this article we therefore do not usually consider convergence.

Let us now look at the ZT of the signal

$$x_1[n] = A \delta[n - i]. \quad (24)$$

This represents a discrete pulse of amplitude A at the time $n = i$. From eq. (23) we find:

$$X_1(z) = \sum_{n=-\infty}^{\infty} A \delta[n - i] z^{-n} = A z^{-i}. \quad (25)$$

Similarly we find for

$$x_2[n] = 2 \delta[n - 1] + 3 \delta[n - 2] \quad (26)$$

that

$$X_2(z) = 2 z^{-1} + 3 z^{-2}. \quad (27)$$

On these two examples we can base an interpretation

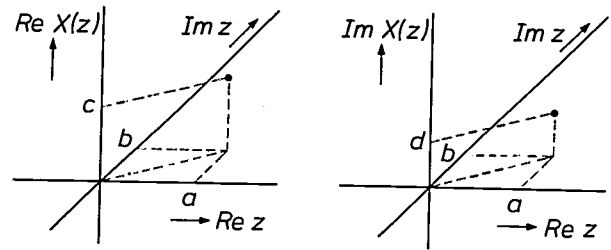


Fig. 5. Applying the z-transform to a discrete signal $x[n]$ generally results in a complex function $X(z) = \text{Re } X(z) + j \text{Im } X(z)$ of the complex variable $z = \text{Re } z + j \text{Im } z$. In a graphical representation we should need two 3-dimensional figures ('hill-and-valley landscapes'). To indicate this the figure gives $X(a + jb) = c + jd$ corresponding to a single value of $z = a + jb$.

of $X(z)$ that can often be very useful: if $X(z)$ has the form of a polynomial in z^{-1} , then the factor associated with the term z^{-i} corresponds exactly to the value of $x[n]$ at the time $n = i$.

The formal counterpart of the ZT as given by eq. (23) is the inverse z-transform (IZT):

$$\text{IZT: } x[n] = \frac{1}{2\pi j} \oint X(z) z^{n-1} dz. \quad (28)$$

This expression represents a contour integral in the z-plane. In practical applications it is seldom used, however, because the required inverse transform from $X(z)$ to $x[n]$ can often be achieved much more simply: e.g. by using general properties of the ZT (such as linearity) or reduction to known z-transforms. Some frequently occurring pairs of transforms have been collected in Table I.

Table I. Some common pairs of bilateral z-transforms

$x[n]$	$X(z)$
$\delta[n]$	1
$\delta[n - i]$	z^{-i}
$u[n]$	$\frac{z}{z - 1}$
$a^n u[n]$	$\frac{z}{z - a}$
$a^{n-1} u[n - 1]$	$\frac{1}{z - a}$
$n u[n]$	$\frac{z}{(z - 1)^2}$
$n^2 u[n]$	$\frac{z(z + 1)}{(z - 1)^3}$
$\cos(n\xi) u[n]$	$\frac{z^2 - z \cos \xi}{z^2 - 2z \cos \xi + 1}$
$\sin(n\xi) u[n]$	$\frac{z \sin \xi}{z^2 - 2z \cos \xi + 1}$
$a^n \sin(n\xi + \psi) u[n]$	$\frac{z^2 \sin(\psi) + az \sin(\xi - \psi)}{z^2 - 2az \cos \xi + a^2}$

The fact that $x[n]$ and $X(z)$ constitute a pair of transforms is indicated in the following way:

$$x[n] \xrightarrow{\text{ZT}} X(z). \tag{29}$$

The most frequently used properties of the ZT relate to linearity, shift and convolution. Proceeding from the pairs of transforms

$$x[n] \xrightarrow{\text{ZT}} X(z) \text{ and } y[n] \xrightarrow{\text{ZT}} Y(z)$$

these properties are as follows:

I. *Linearity.* For all values of the constants a and b :

$$ax[n] + by[n] \xrightarrow{\text{ZT}} aX(z) + bY(z).$$

II. *Shift.* For every integer i :

$$x[n - i] \xrightarrow{\text{ZT}} z^{-i} X(z).$$

III. *Convolution.* Although the convolution operation (indicated by $*$) will not be treated until page 122, we mention the convolution property in advance because it is so extremely important:

$$x[n] * y[n] \xrightarrow{\text{ZT}} X(z) Y(z).$$

In the inverse transformation of a given $X_0(z)$, which is a ratio of two polynomials in z , to the corresponding $x_0[n]$ it is common practice to use the technique of expansion in partial fractions. This is best explained by an example. Suppose that

$$X_0(z) = \frac{z}{(z - \alpha)(z - \beta)}, \tag{30}$$

where α and β are constants. In Table I we find no $X(z)$ that immediately resembles this. We now try to rewrite $X_0(z)$ with as yet unknown constants A and B , as:

$$X_0(z) = \frac{Az}{z - \alpha} + \frac{Bz}{z - \beta}. \tag{31}$$

Next we reduce everything to a common denominator:

$$\begin{aligned} X_0(z) &= \frac{Az(z - \beta) + Bz(z - \alpha)}{(z - \alpha)(z - \beta)} \\ &= \frac{(A + B)z^2 - (\beta A + \alpha B)z}{(z - \alpha)(z - \beta)}. \end{aligned} \tag{32}$$

We now see that equations (30) and (32) are identical when

$$A + B = 0 \quad \text{and} \quad \beta A + \alpha B = -1 \tag{33}$$

or

$$A = \frac{1}{\alpha - \beta} \quad \text{and} \quad B = \frac{-1}{\alpha - \beta}. \tag{34}$$

We can therefore rewrite eq. (31) as:

$$X_0(z) = \frac{1}{\alpha - \beta} \left(\frac{z}{z - \alpha} - \frac{z}{z - \beta} \right). \tag{35}$$

Writing the equation in this way we see two terms of the form $z/(z - a)$, which occurs in Table I. Using the linearity of the ZT we then find:

$$x_0[n] = \frac{1}{\alpha - \beta} (\alpha^n - \beta^n) u[n]. \tag{36}$$

The relation between FTD and ZT

Between the z -transform and the Fourier transform for discrete signals a direct relationship exists: when $z = e^{j\theta}$ the ZT of eq. (23) becomes identical with the FTD of eq. (19). How can we best interpret this? With $z = e^{j\theta}$ and $-\pi \leq \theta < \pi$ we describe exactly all the points for which $|z| = 1$, that is to say all the points on the unit circle in the z -plane. This brings us to an important statement: the FTD of a discrete signal corresponds to the ZT on the unit circle in the z -plane. This relationship can be represented graphically (fig. 6). For convenience we have chosen an $X(z)$ that is purely real on the unit circle, so that both for $X(z)$ and for $X(e^{j\theta})$ a single diagram is sufficient.

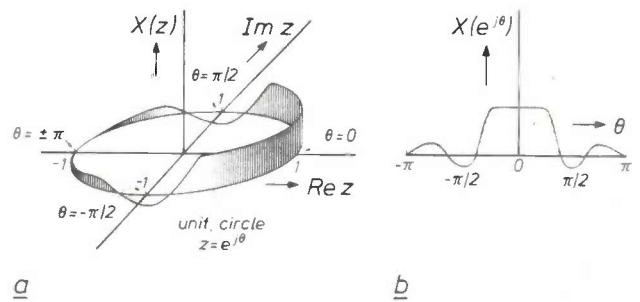


Fig. 6. Plot of the relation between a) the ZT on the unit circle in the z -plane (i.e. $z = e^{j\theta}$) and b) $X(e^{j\theta})$ obtained from the FTD. For convenience it is assumed that $X(e^{j\theta})$ is purely real.

The above relationship only applies of course when the z -transform exists (in other words, when $X(z)$ converges) on the unit circle. In most practical situations this is in fact the case. But signals that correspond to the impulse response of an unstable system (see the section 'Discrete systems') form a notorious exception. These have a z -transform that does not converge on the unit circle and therefore no FTD exists.

The relations discussed so far between a discrete signal $x[n]$, its Fourier transform $X(e^{j\theta})$ and its z -transform $X(z)$ are summarized in fig. 7.

The discrete Fourier transform (DFT)

The Fourier transform for discrete signals (FTD), which we have described earlier in this article, is a powerful analytical tool for determining the frequency spectrum of discrete signals. But it has its limitations. We shall now look at these with the aid of the FTD in the normalized form, as given in equations (19) and

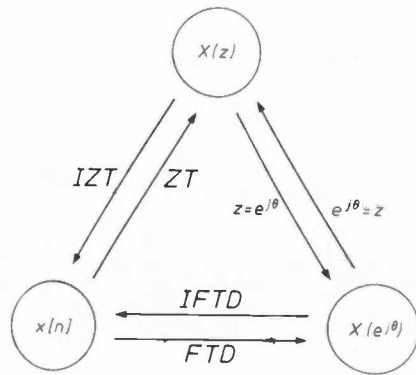


Fig. 7. Relations between a discrete signal $x[n]$, its Fourier transform $X(e^{j\theta})$ and its z-transform $X(z)$. ZT z-transform, IZT inverse z-transform, FTD Fourier transform for discrete signals, IFTD inverse Fourier transform for discrete signals. The transition from $X(z)$ to $X(e^{j\theta})$ and vice versa is a simple substitution: $z = e^{j\theta}$. (It is assumed that the relevant transforms do really exist.)

precisely, the N -point discrete Fourier transform (N -point DFT). This is defined as follows:

$$N\text{-point DFT: } X_N[k] = \sum_{n=0}^{N-1} x_N[n] e^{-j(2\pi/N)kn} \quad (37)$$

The corresponding inverse transform is:

$$N\text{-point IDFT: } x_N[n] = \frac{1}{N} \sum_{k=0}^{N-1} X_N[k] e^{j(2\pi/N)kn} \quad (38)$$

Using the DFT we can thus calculate N values of the discrete frequency function $X_N[k]$ from the signal $x_N[n]$. From this, using the corresponding IDFT, we can then retrieve the original N values of $x_N[n]$ exactly. The two functions $x_N[n]$ and $X_N[k]$ thus constitute a regular pair of transforms, which is represented symbolically by:

$$x_N[n] \underset{\text{DFT}}{\circlearrowright} X_N[k] \quad (39)$$

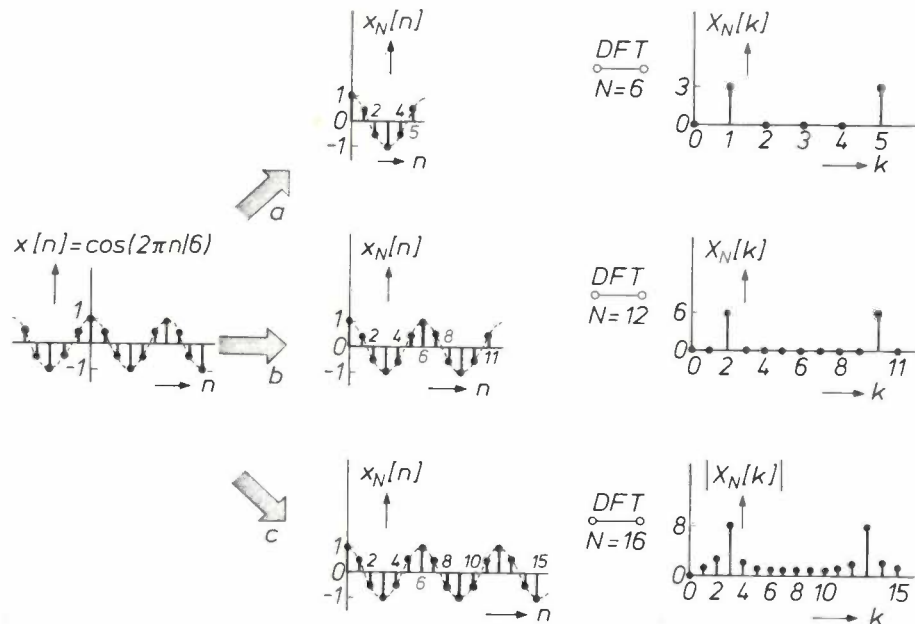


Fig. 8. Example of the application of an N -point DFT for different values of N to the periodic signal $x[n] = \cos(2\pi n/6)$. It is advisable to choose N equal to an integral number of periods of $x[n]$, for example $N = 6$ (case a) or $N = 12$ (case b). Otherwise there is 'leakage' of the spectral components (case c). For $N = 6$ and $N = 12$ a purely real spectrum is found. For $N = 16$ the spectrum is complex and only the modulus $|X_N[k]|$ is shown.

(20). In the first place we may note that eq. (19) is not directly applicable to periodic signals $x[n]$; the summation of an infinite number of terms will then present difficulties. Nor is such an infinite summation very meaningful if $x[n]$ is of finite duration and therefore differs from zero only for a finite number of values of n . In addition, computer calculation of the IFTD from eq. (20) requires a numerical calculation (hence: approximating) of the relevant integral. It has therefore been helpful to introduce another aid, in the form of the discrete Fourier transform (DFT), or, more

To illustrate the application of the DFT we shall first take a simple periodic function. Let us choose $x[n] = \cos(2\pi n/6)$, with three different values of N : 6, 12 and 16 (fig. 8). The function $x[n]$ is periodic with the period $N_0 = 6$, since $x[n] = x[n + 6]$ for all n .

We now see in fig. 8 that it is important when applying the DFT to periodic signals of period N_0 to take the length N equal to N_0 or an integral multiple of N_0 (cases a and b). If this is not so (case c), the discrete spectrum $X_N[k]$ does not contain the 'right' frequency positions for representing the original periodic signal

$x[n]$. We then find contributions at all values of k , an effect known as 'leakage'.

From a comparison of cases *a* and *b* we also see that a larger N gives greater spectral resolution. The spectrum $X_N[k]$ shows a high degree of symmetry because $x_N[n]$ is a real function; in Fourier transformation this always results in such properties (see for example what was said in small print on page 115 on the properties of the FTD).

At the beginning of this subsection we suggested that the N -point DFT can be used to calculate the spectrum $X_N[k]$ of a discrete signal of finite duration ($\leq N$). This leads us to ask whether there is a relation between $X_N[k]$ and the spectrum $X(e^{j\theta})$ that can be calculated for the same signal with the FTD in eq. (19). This is in fact the case. A direct comparison of equations (37) and (19) shows that the following simple relation exists between these two spectra:

$$X_N[k] = X(e^{j(2\pi/N)k}). \quad (40)$$

Expressed in words: for a discrete signal of finite duration N_1 , the N -point DFT is a sampled version of the FTD, provided that $N_1 \leq N$. To illustrate this relation *fig. 9* shows the FTD and the 8-point DFT for a discrete signal $x[n]$ of finite duration $N_1 = 4$.

We have assumed above that we are considering both $x_N[n]$ and $X_N[k]$ for n and k between 0 and $N - 1$. However, the complex exponential functions $e^{-j(2\pi/N)kn}$ and $e^{j(2\pi/N)kn}$ are periodic in k and in n with period N . If we calculate $X_N[k]$ in eq. (37) for $k < 0$ or $k > N - 1$, we therefore find the same values as we found for $0 \leq k \leq N - 1$. Similar considerations apply to $x_N[n]$ in eq. (38). We can therefore say that $x_N[n]$ and $X_N[k]$ are periodic functions of period N , and only the fundamental interval between 0 and $N - 1$ is of significance in the transformation process.

The fast Fourier transform (FFT)

In addition to the transforms described so far, the term FFT (for 'fast Fourier transform') is often encountered in the literature on discrete signal processing. This is not another type of transformation, however, but refers simply to a very effective manner of calculating the DFT. The name FFT is really a collective name for various interrelated calculation methods and stratagems.

If we again look at equations (37) and (38) for the DFT and the IDFT, we see that for each result (each 'point') of the transformation we have to perform N complex multiplications and $N - 1$ complex additions. For a complete N -point transformation this amounts to N^2 and $N(N - 1)$ respectively. A direct calculation of an N -point DFT thus requires a number of complex operations of the order of magnitude of N^2 . For $N = 4$ this is 16, but for $N = 2048$ we are already at $N^2 = 4194304$. In the practical application

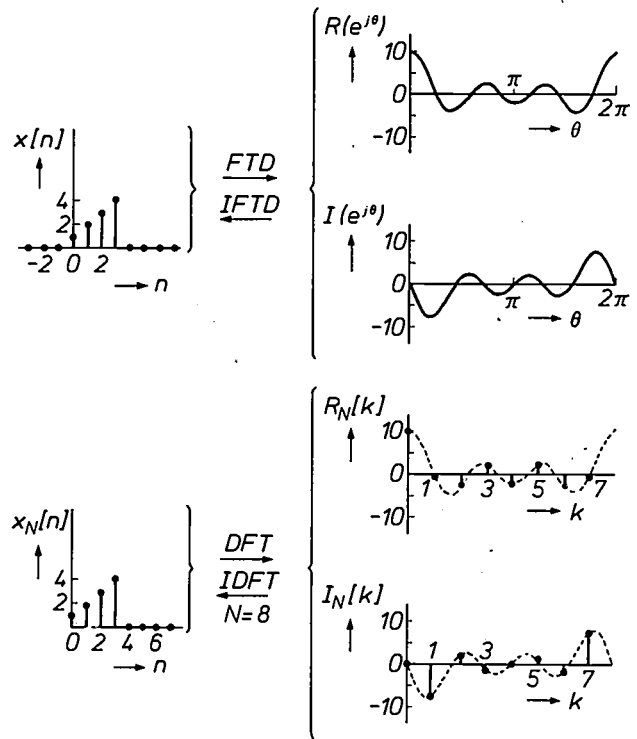


Fig. 9. Comparison of the FTD and the 8-point DFT of a discrete signal $x[n]$ of finite duration $N_1 = 4$. It is clear that the DFT spectrum $X_N[k] = R_N[k] + jI_N[k]$ is a sampled version of the FTD spectrum $X(e^{j\theta}) = R(e^{j\theta}) + jI(e^{j\theta})$.

of the DFT this number of operations is of considerable importance, since it determines the time and the type of equipment we need. For nearly 200 years, and especially in the last twenty or thirty years [10], there has therefore been keen interest in methods that make it possible to calculate an N -point DFT with fewer operations. The procedure always followed is first to calculate a number of DFTs of smaller length and then to combine the results in an appropriate way. If N is even, an $N/2$ -point DFT can be performed first on all the even-numbered samples of $x_N[n]$ and then on all the odd-numbered samples. Next, the required N -point DFT can be calculated from the results of these two smaller DFTs. Altogether this requires fewer calculations than a direct procedure. If $N/2$ itself is also an even number, this procedure can be repeated. The most familiar are therefore the FFT algorithms, in which N is an integral power of two, so that $N = 2^M$. The same procedure can then be repeated as many as M times. In this way the total number of operations is of the order of $N \times M$, which is a reduction by a factor of N/M . The very substantial effect of the FFT compared with a direct calculation of the DFT, especially for large N , is evident from *fig. 10*.

[10] M. T. Heideman, D. H. Johnson and C. S. Burrus, Gauss and the history of the fast Fourier transform, IEEE ASSP Mag. 1, No. 4 (October), 14-21, 1984.

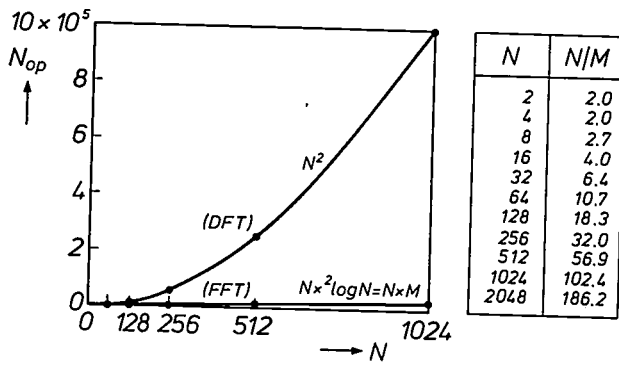


Fig. 10. Comparison of the number of operations N_{op} required for a direct calculation of the N -point DFT and for a calculation made with the FFT. Only values of N that are an integral power of 2 are considered; $N = 2^M$. The number of operations is then reduced by a factor of N/M . This is indicated for a number of values of N in a separate table.

II. DISCRETE SYSTEMS

Now that we have dealt with a number of fundamental theoretical aspects of discrete signals, we can turn our attention to discrete systems. Quite generally, a discrete system is defined as a system that converts one or more discrete input signals $x[n]$ into one or more discrete output signals $y[n]$ in accordance with certain discrete rules. In the following we shall be concerned mainly with systems with one real input signal $x[n]$ and one real output signal $y[n]$. For the time being we shall also confine our considerations to the very important category of linear time-invariant discrete systems (LTD systems). For practical purposes these include most discrete (and hence digital) filters.

A discrete system is *linear* when the input signal $ax_1[n] + bx_2[n]$ produces an output signal $ay_1[n] + by_2[n]$, where a and b are arbitrary constants. Here, $x_1[n]$ and $x_2[n]$ are arbitrary input signals and $y_1[n]$ and $y_2[n]$ are the corresponding output signals.

A discrete system is *time-invariant* if the input signal $x[n - i]$ produces an output signal $y[n - i]$, where i is an arbitrary integer, $x[n]$ an arbitrary input signal and $y[n]$ the corresponding output signal.

For practical purposes, discrete systems should also possess the following two properties: stability and causality.

A discrete system is *stable* if any arbitrary input signal of finite amplitude (i.e. $|x[n]|_{max} \leq A$) produces an output signal of finite amplitude (i.e. $|y[n]|_{max} \leq B$).

A discrete system is *causal* if at any instant $n = n_0$ the output signal corresponding to any arbitrary input signal is independent of the values of the input signal later than n_0 . (Loosely formulated: there can be no output signal before there has been an input signal.) In the rest of this article the term 'practical' implies the concept 'causal'.

LTD systems have a number of particularly attractive properties. The first is that all feasible systems of this type can be composed of only three basic elements (fig. 11):

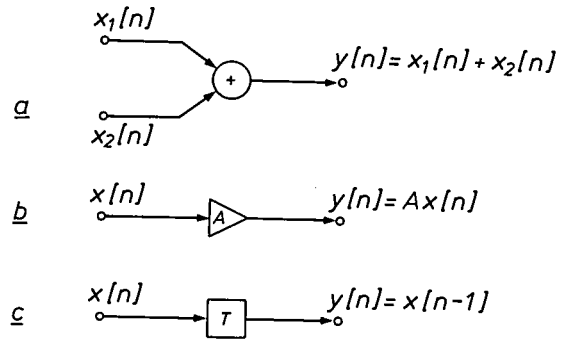


Fig. 11. The three basic elements from which all realizable linear time-invariant discrete systems (LTD systems) can be built up. a) Adder. b) Multiplier by a constant factor A . c) Unit-delay element. T unit delay or sampling interval.

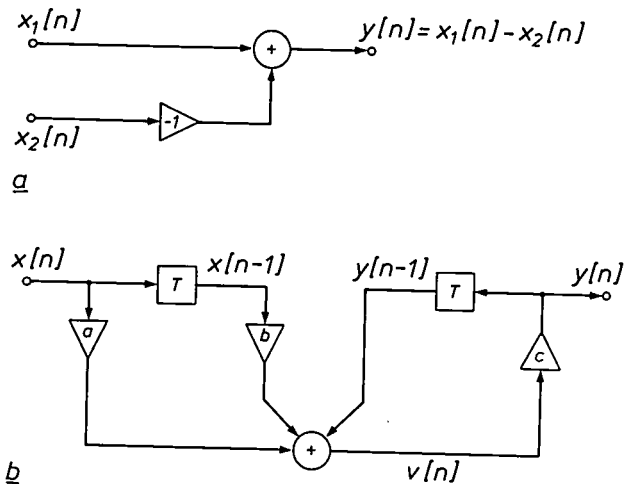


Fig. 12. a) The combination of an adder with a multiplier by a factor of -1 results in a subtractor. b) Example of a simple LTD system containing all the basic elements. In addition to the input and output signals a number of internal signals ('intermediate results') are indicated.

- the adder, in which two input signals are added to form one output signal,
- the multiplier, in which a signal is multiplied by a constant, and
- the unit-delay element, in which the input signal is delayed by one discrete time unit (sampling interval).

By combining these elements we can make other functions, for example a subtractor (fig. 12a). Another simple but realistic LTD system is shown in fig. 12b. Later we shall analyse the filter properties of this circuit.

A close relation exists between the theory of discrete signals, which we have dealt with in the foregoing, and the theory of LTD systems. There is a good explanation for this, since the most important properties of an LTD system can be derived from only one discrete signal — the output signal that is obtained when the input signal is the discrete unit pulse $\delta[n]$. We call this output signal the impulse response $h[n]$ of the LTD system (fig. 13).

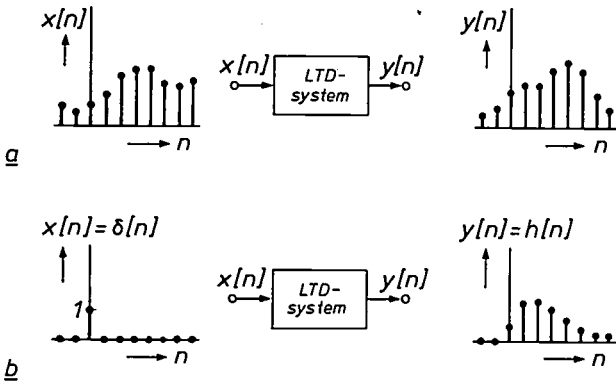


Fig. 13. a) Like any other discrete system an LTD system converts an input signal $x[n]$ into an output signal $y[n]$. b) The special feature of an LTD system is that it can be characterized by its impulse response $h[n]$; this is the output signal $y[n] = h[n]$ corresponding to the input signal $x[n] = \delta[n]$.

Signal transforms such as the FTD or the ZT can be applied to the impulse response $h[n]$. We then obtain alternative descriptions of the LTD system for which we use separate names. Applying the FTD to $h[n]$ we obtain the frequency response $H(e^{j\theta})$. Applying the ZT to $h[n]$ we get the system function $H(z)$. We know from the foregoing that:

$$H(e^{j\theta}) = H(z)|_{z=e^{j\theta}} \tag{41}$$

The frequency response and the system function constitute descriptions of the system in the frequency domain. The impulse response, on the other hand, gives a description of the system in the time domain, as do also the difference equations. We shall consider all these four modes of description in somewhat more detail, starting with the last.

System descriptions

Difference equations

Let us look again at the system of fig. 12b. We can describe this system by the following simple equations:

$$v[n] = ax[n] + bx[n - 1] + y[n - 1] \tag{42a}$$

$$y[n] = cv[n]. \tag{42b}$$

Eliminating $v[n]$:

$$y[n] = acx[n] + bcx[n - 1] + cy[n - 1]. \tag{43}$$

This equation will give us the present value of the output signal if we know the present input signal and the previous values of the input and output signal. Quite generally, a practical LTD system can be described by:

$$y[n] = \sum_{i=0}^N b_i x[n - i] + \sum_{i=1}^M a_i y[n - i], \tag{44}$$

where a_i and b_i are real constants. Equation (44) is called a linear difference equation (of the M th order) with constant coefficients.

Equation (44) is the discrete counterpart of the linear differential equation with constant coefficients that can be used to describe practical linear time-invariant continuous systems, which is written as follows:

$$y(t) = \sum_{k=0}^N b_k \frac{d^k x(t)}{dt^k} + \sum_{k=1}^M a_k \frac{d^k y(t)}{dt^k}.$$

The description of a discrete system by a difference equation is important for two main reasons. In the first place it is a good starting point for deriving other system descriptions, such as the system function. In this case the difference equations are replaced by algebraic equations. Calculation with these is much simpler, as we shall see. In the second place a difference equation gives a direct indication of a possible structure for a system. For instance, a system that is described by the difference equation

$$y[n] = \sum_{i=0}^3 b_i x[n - i] + \sum_{i=1}^3 a_i y[n - i], \tag{45}$$

can be realized with the circuit shown in fig. 14. It will appear later that there are many other structures with the same difference equation.

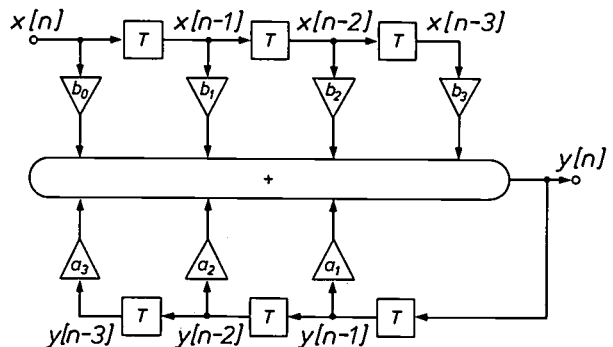


Fig. 14. LTD system described by the difference equation given in eq. (45).

Impulse response

Sometimes the impulse response of a discrete system can be derived directly from the block diagram; sometimes it is more complicated. This will become clear from a few examples. For fig. 15a it is fairly easy to see that:

$$h_A[n] = 2\delta[n] - \frac{1}{2}\delta[n - 1], \tag{46}$$

and for fig. 15b

$$h_B[n] = (-\frac{3}{4})^{n+1} u[n]. \tag{47}$$

Although fig. 15c is only the cascade arrangement of (a) and (b), it is perhaps less obvious at this point that its impulse response is given by:

$$h_C[n] = \frac{1}{2}\delta[n] - 2(-\frac{3}{4})^n u[n]. \tag{48}$$

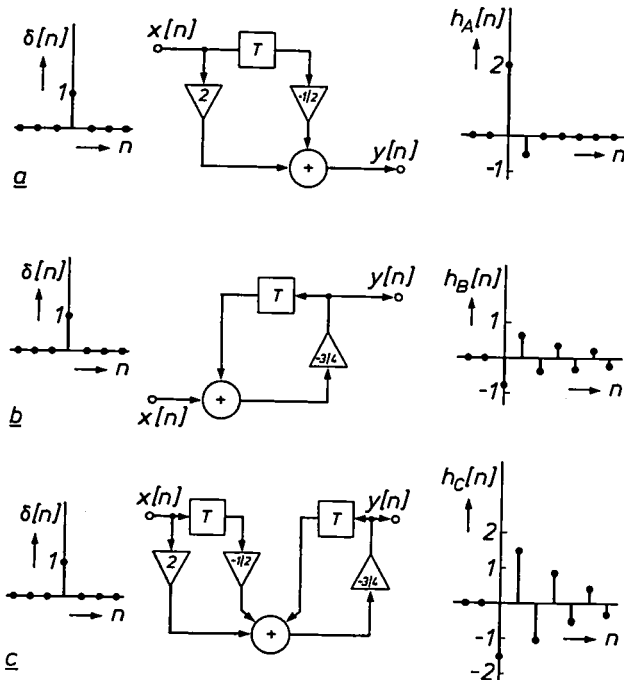


Fig. 15. Simple LTD systems with corresponding impulse response. The system in c) corresponds to the cascade arrangement of (a) and (b).

In principle it is not difficult to see that we can use the impulse response of an LTD system to calculate the output signal for any arbitrary input signal. To do this we return to eq. (15), which we now recapitulate:

$$x[n] = \sum_{i=-\infty}^{\infty} x[i] \delta[n - i]. \quad (49)$$

In this equation $x[n]$ is expressed as a series of weighted unit pulses, where the i th pulse has the weight $x[i]$. Since we are dealing with a linear time-invariant system, this i th pulse produces an output signal $x[i]h[n - i]$. Therefore

$$x[i]\delta[n - i] \rightarrow x[i]h[n - i] \quad (50)$$

and

$$\sum_{i=-\infty}^{\infty} x[i]\delta[n - i] \rightarrow \sum_{i=-\infty}^{\infty} x[i]h[n - i]. \quad (51)$$

In this way, then, we have found the exact output signal $y[n]$ corresponding to $x[n]$ as given by eq. (49):

$$y[n] = \sum_{i=-\infty}^{\infty} x[i]h[n - i] \quad (52a)$$

or

$$y[n] = \sum_{i=-\infty}^{\infty} x[n - i]h[i]. \quad (52b)$$

(Equation (52b) is obtained from (52a) by substituting $j = n - i$ in the right-hand side and then replacing j

by i .) Equations (52a) and (52b) represent the convolution of $x[n]$ and $h[n]$. We can abbreviate this to:

$$y[n] = x[n] * h[n] = h[n] * x[n]. \quad (52c)$$

Summarizing: the output signal of an LTD system can be obtained from the convolution of the input signal and the impulse response.

It is very easy to see whether an LTD system is stable or causal (or both) from its impulse response $h[n]$. For a stable LTD system we have:

$$\sum_{n=-\infty}^{\infty} |h[n]| = C < \infty.$$

For a causal LTD system we have: $h[n] = 0$ for $n < 0$.

Frequency response

Instead of the impulse response $h[n]$ we often consider the corresponding FTD, i.e. the frequency response $H(e^{j\theta})$. One of the main reasons for doing this is the convolution property of the FTD: the convolution of two discrete signals $x[n]$ and $h[n]$ corresponds to the multiplication of their FTDs. This provides us with a second means of calculating the output signal $y[n]$ from an input signal $x[n]$.

- We first determine $X(e^{j\theta})$ and $H(e^{j\theta})$.
- We multiply $X(e^{j\theta})$ by $H(e^{j\theta})$; this gives the FTD of $y[n]$:

$$Y(e^{j\theta}) = X(e^{j\theta}) H(e^{j\theta}). \quad (53)$$

- We apply the IFTD to $Y(e^{j\theta})$ and thus find $y[n]$. Both methods of calculating $y[n]$ are shown schematically in fig. 16. The method using the FTD is often preferable because it requires the least calculation.

The second important virtue of the frequency response as a system description is the intuitive ease with which it is often possible to analyse discrete systems, especially filters, from their amplitude and phase characteristics, which are merely the modulus and argument of the FTD. A simple LTD system is shown as an example in fig. 17. The impulse response $h[n]$ is given by:

$$h[n] = a^n u[n]. \quad (54)$$

For the frequency response $H(e^{j\theta})$ we then find from eq. (19):

$$H(e^{j\theta}) = \sum_{n=-\infty}^{\infty} h[n]e^{-jn\theta} = \sum_{n=0}^{\infty} a^n e^{-jn\theta} = \sum_{n=0}^{\infty} (ae^{-j\theta})^n. \quad (55a)$$

If $|a| < 1$, we can then write:

$$H(e^{j\theta}) = \frac{1}{1 - ae^{-j\theta}} = \frac{1}{1 - a \cos \theta + aj \sin \theta}. \quad (55b)$$

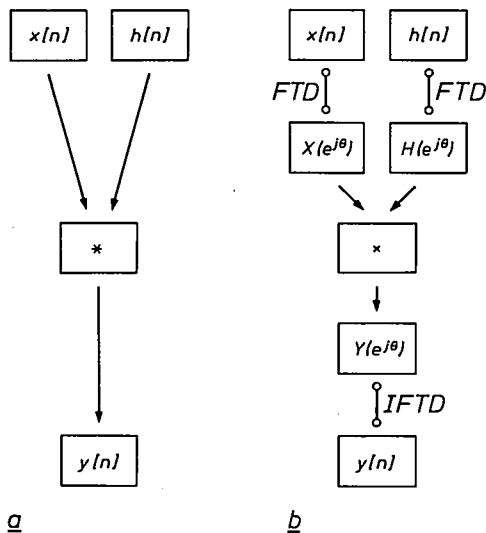


Fig. 16. With a given input signal $x[n]$ and impulse response $h[n]$ of an LTD system there are two different methods of calculating the output signal $y[n]$. a) Direct calculation using the convolution operation. b) Calculation by a succession of two FTDs, multiplication and IFTD.

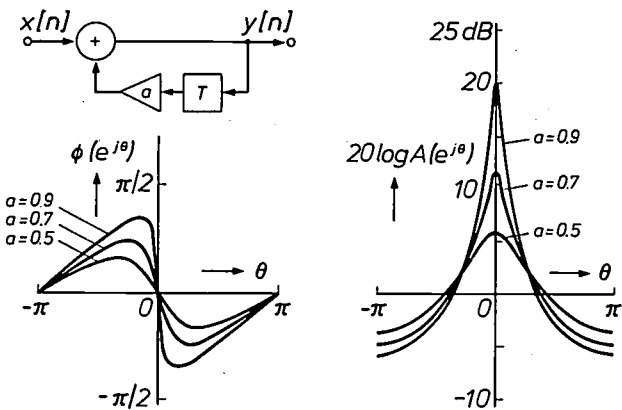


Fig. 17. Simple LTD system with impulse response $h[n] = a^n u[n]$ and corresponding amplitude characteristic $A(e^{j\theta})$, on a dB scale, and phase characteristic $\phi(e^{j\theta})$ for different values of a .

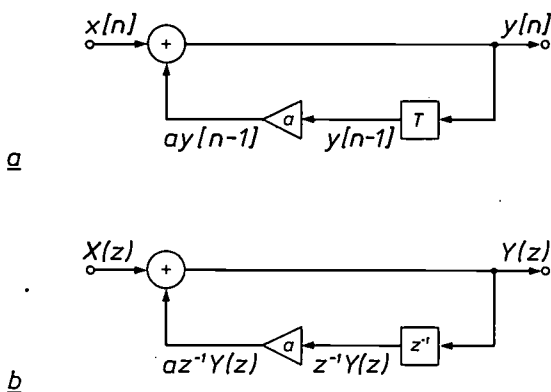


Fig. 18. Direct determination of $H(z) = Y(z)/X(z)$ from the block diagram of an LTD system. a) Original block diagram in the time domain. b) Corresponding block diagram in the z-domain.

If we also use eq. (22) we find for the amplitude and phase characteristic:

$$A(e^{j\theta}) = \frac{1}{\sqrt{1 + a^2 - 2a \cos\theta}} \quad (56)$$

and

$$\phi(e^{j\theta}) = \arctan\left(\frac{-a \sin\theta}{1 - a \cos\theta}\right). \quad (57)$$

These characteristics are shown in fig. 17 for various values $0 < a < 1$.

System function

The most abstract but at the same time the most versatile description of an LTD system is given by the system function $H(z)$, which we can obtain as the z-transform of the impulse response $h[n]$. In the first place we can use the convolution property of the ZT, which states that convolution of two discrete signals (see eq. 52) corresponds to multiplication of the associated z-transforms. If $x[n]$ is the input signal and $y[n]$ the output signal of an LTD system with impulse response $h[n]$, then:

$$Y(z) = X(z)H(z). \quad (58)$$

We can rearrange this as:

$$H(z) = Y(z)/X(z). \quad (59)$$

Here we have a second, often very effective, manner of determining $H(z)$, since the ratio on the right-hand side of eq. (59) can easily be derived from the difference equation of an LTD system. As an example let us take the difference equation of eq. (43). If we apply the ZT term by term (this is permissible because of the linearity of the ZT), we find

$$Y(z) = ac X(z) + bcz^{-1} X(z) + cz^{-1} Y(z). \quad (60)$$

This gives:

$$H(z) = \frac{Y(z)}{X(z)} = \frac{ac + bcz^{-1}}{1 - cz^{-1}}. \quad (61)$$

In the same way we find from the general difference equation of a practical LTD system (eq. 44):

$$H(z) = \frac{Y(z)}{X(z)} = \frac{\sum_{i=0}^N b_i z^{-i}}{1 - \sum_{i=1}^M a_i z^{-i}}. \quad (62)$$

In practice the analysis of an LTD system is often based on a block diagram. To determine the system function the difference equation is usually omitted as a separate intermediate step and a direct description is made by means of z-transforms. Considerable use is

made here of the property that a delay of one sampling interval in the time domain corresponds to multiplication by z^{-1} in the z -domain. This procedure is illustrated in *fig. 18* for the system of *fig. 17*. It is easily seen from *fig. 18b* that:

$$Y(z) = X(z) + az^{-1}Y(z), \tag{63}$$

so that

$$H(z) = \frac{Y(z)}{X(z)} = \frac{1}{1 - az^{-1}}. \tag{64}$$

By substituting $z = e^{j\theta}$ we also find the frequency response determined earlier, though more laboriously, in eq. (55).

Poles and zeros

In eq. (62) we have already found that the system function $H(z)$ of practical LTD systems takes the form of a ratio of two polynomials in z^{-1} , i.e.:

$$H(z) = \frac{b_0 + b_1z^{-1} + b_2z^{-2} + \dots + b_Nz^{-N}}{1 - a_1z^{-1} - a_2z^{-2} - \dots - a_Mz^{-M}}. \tag{65}$$

We can always rewrite the numerator and denominator as a product of factors:

$$H(z) = b_0 \frac{(z - z_1)(z - z_2) \dots (z - z_N)}{(z - p_1)(z - p_2) \dots (z - p_M)} z^{M-N}. \tag{66}$$

The precise (complex) values z_1, z_2, \dots, z_N and p_1, p_2, \dots, p_M depend on the (real) coefficients $b_0, b_1, b_2, \dots, b_N, a_1, a_2, \dots, a_M$ in eq. (65). For $z = z_1, z_2, \dots, z_N$ the value of $H(z)$ is zero and for $z = p_1, p_2, \dots, p_M$ the value of $H(z)$ is infinite. We therefore speak of the zeros z_i ($i = 1, \dots, N$) and the poles p_i ($i = 1, \dots, M$) of the system function $H(z)$. If some z_i (or p_i) are equal to each other, we speak of multiple zeros (or multiple poles). The factor z^{M-N} in eq. (66) corresponds formally to an $(M-N)$ -fold zero (if $M > N$) or to an $(N-M)$ -fold pole (if $N > M$) at $z = 0$. On the other hand, we know that this factor only represents a simple shift of $h[n]$ in time and therefore generally neglect it. We see that the poles and zeros fully determine the function $H(z)$ and hence the corresponding LTD system, except for a constant factor b_0 . The positions of poles and zeros are easily visualized in the complex z -plane. This gives the poles-and-zeros plot of $H(z)$, which is a very useful graphic aid. *Fig. 19* gives an example for an arbitrary LTD system. We shall now use this figure and the following, to make some remarks of general validity for practically feasible systems, but we shall offer no derivations or proofs.

• With real coefficients $b_0, \dots, b_N, a_1, \dots, a_M$, poles and zeros can only be real or occur in complex conjugate pairs (the poles-and-zeros plot is therefore al-

ways symmetrical with respect to the horizontal axis).

• Since the frequency response corresponds to the system function on the unit circle in the z -plane, each pole and each zero has the most effect on the frequency range associated with the nearest part of the unit circle. Furthermore, the effect of a pole or zero on the frequency response increases the closer it is to the unit circle. In the extreme case of a zero actually on the unit circle, e.g. at $z = e^{j\theta_1}$, the amplitude of the frequency response is zero at $\theta = \theta_1$ and there is a jump of π radians in phase at that point. On the other hand, a pole on the unit circle, e.g. at $z = e^{j\theta_2}$, gives an infinite amplitude at $\theta = \theta_2$, again with a phase jump of π radians.

• In a stable system all the poles are inside the unit circle; zeros may lie inside it, on it, or outside it.

• If all the zeros are inside the unit circle, we have a 'minimum-phase network' (*fig. 20a*), if they do not we have a 'non-minimum-phase network' (*fig. 20b*). The systems in *fig. 20a* and *b* have the same amplitude characteristics, because the zeros of one case are the exact 'reflections' of the zeros of the other case in the unit circle (i.e. the zero $z_i = r_i e^{j\theta_i}$ is replaced by the zero $z_i = (1/r_i) e^{j\theta_i}$).

• If all the poles are inside the unit circle and all the zeros are outside it, and if poles and zeros are always reflections of one another in the unit circle, we have a constant-amplitude system (a phase-shifter or allpass network); see *fig. 20c*.

• If a system (except for the origin) has poles only, we call it an 'all-pole' system (*fig. 20d*).

• If a system (except for the origin) has zeros only, and these are reflected in pairs in the unit circle (possibly also with zeros on the unit circle) then the phase characteristic is strictly linear and we have a linear-phase system (*fig. 20e*).

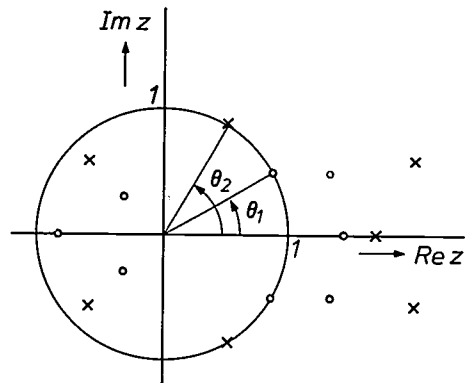


Fig. 19. Poles-and-zeros plot for an arbitrary LTD system. x pole. o zero. The poles are real or form complex conjugate pairs. The same applies to the zeros. The diagram is therefore symmetrical with respect to the horizontal axis. (In a realizable stable system all the poles must lie inside the unit circle.)

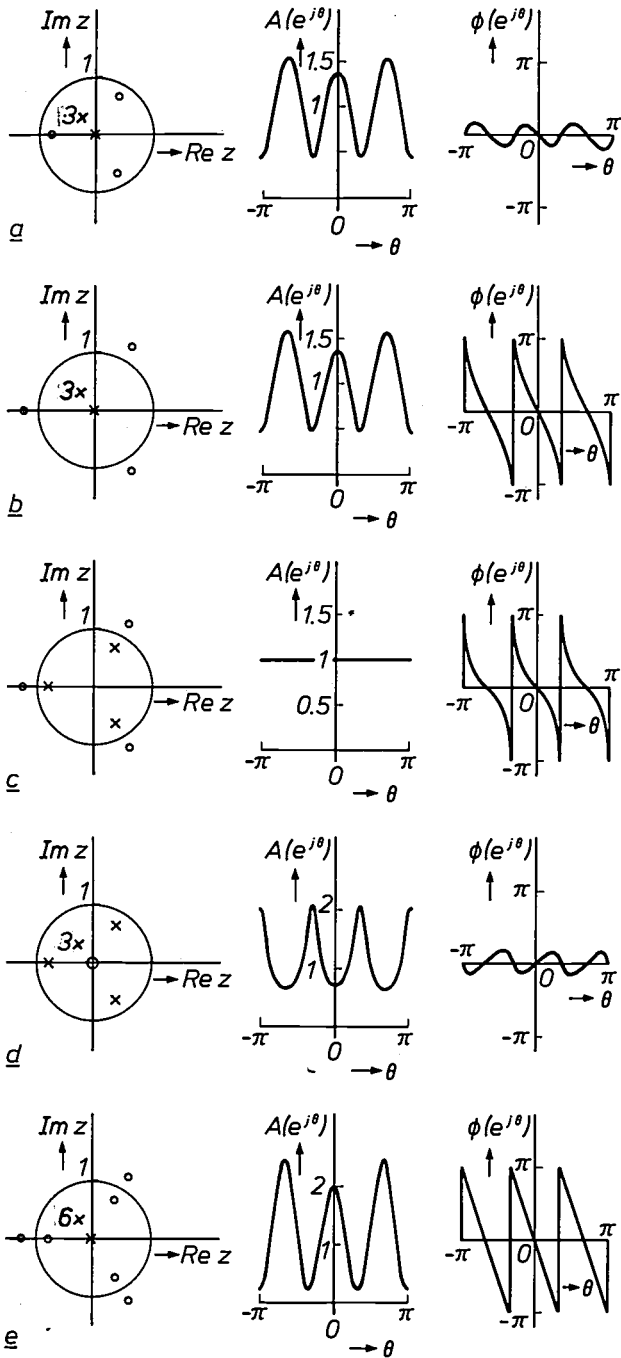


Fig. 20. Poles-and-zeros plots of some realizable types of LTD systems with corresponding amplitude and phase characteristics. a) Minimum-phase system. b) Non-minimum-phase system. c) All-pass system or phase shifter. d) All-pole system. e) Linear-phase system.

III. DISCRETE FILTERS

By far the most important representatives of the LTD systems are the LTD filters, which we shall just call discrete filters from now on. We define a filter here as a circuit (or an algorithm) that converts an input signal into an output signal whose spectrum is related to the spectrum of the input signal in a speci-

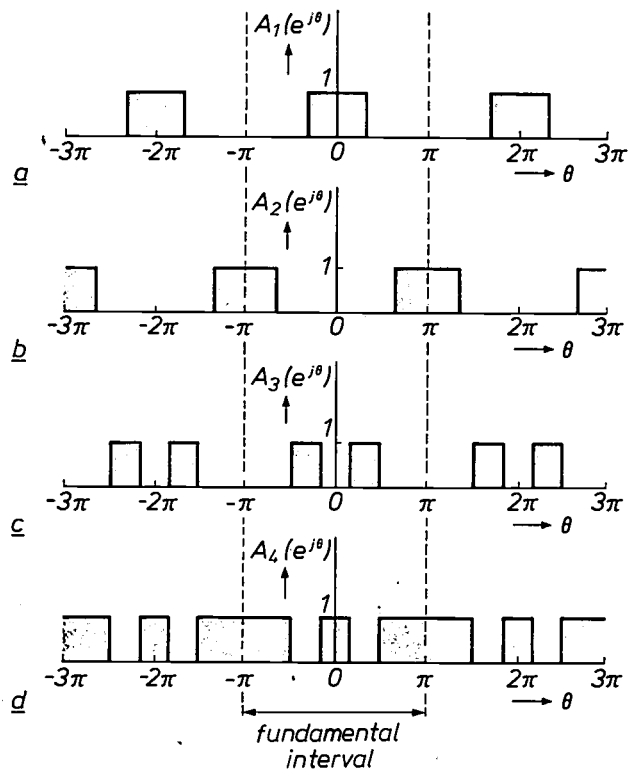


Fig. 21. Examples of the amplitude characteristic of ideal discrete filters: a) lowpass, b) highpass, c) bandpass, d) bandstop. (To emphasize the periodic nature of the frequency response the frequency interval shown here is larger than the fundamental interval $-\pi \leq \theta < \pi$.)

fied way (e.g. certain frequency components may be attenuated or completely suppressed).

The different ways in which a filter can be characterized lead to different kinds of categorization. As with the continuous filters, we can classify discrete filters by the type of frequency response (i.e. by amplitude and phase characteristics). The filters whose amplitude characteristic is the main feature can be subdivided into

- lowpass filters,
- highpass filters,
- bandpass filters and
- bandstop filters.

Examples of idealized filters are given in *fig. 21*.

Just as in the case of continuous filters, transformation rules that convert a filter of one type into a filter of one of the other types also exist in the discrete case.

In addition to the types of filter mentioned above, there are filters whose phase characteristic and amplitude characteristic both have to meet exact specifications. Two examples have already been encountered: the phase-shifter (allpass network) with a constant amplitude characteristic and a precisely defined phase characteristic. This filter can be used in combination with any type of filter in *fig. 21* to obtain not only a specified amplitude characteristic but a required phase

characteristic as well. The other example relates to filters with accurately linear phase characteristics. These filters are useful in applications such as TV and data transmission. The impulse responses of linear-phase filters have considerable symmetry, as we shall see.

Other examples of special filters are:

- the differentiator

$$H_D(e^{j\theta}) = j\theta, \quad -\pi \leq \theta < \pi;$$

- the integrator

$$H_I(e^{j\theta}) = 1/j\theta, \quad -\pi \leq \theta < \pi;$$

- the Hilbert transformer

$$H_H(e^{j\theta}) = \begin{cases} -j, & -\pi \leq \theta < 0 \\ +j, & 0 \leq \theta < \pi. \end{cases}$$

It can also be very useful to classify discrete filters by the duration of the impulse response:

- if it is finite, the filter is known as a Finite Impulse Response (FIR) filter;
- if it is infinite, the filter is called an Infinite Impulse Response (IIR) filter.

These two types differ in many respects, and some of the principal differences are mentioned below.

- System function: away from the origin, an FIR filter can only possess zeros, an IIR filter can have both zeros and poles.
- Phase characteristic: an FIR filter can have an exactly linear phase; an IIR filter can be a phase shifter.
- Stability: an FIR filter is always stable, an IIR filter is unstable if for some reason or other one or more poles lie on the unit circle or outside it.

A few other differences will be encountered later under the headings 'Discrete filter structures' and 'Methods of designing discrete filters'.

Discrete filter structures

Besides the more fundamental classifications touched on in the previous section, we can also classify discrete filters by structure, as indicated by their block diagram. This alone is sometimes sufficient to permit certain general conclusions to be drawn about the characteristics of a particular filter. In addition, we have to remember that a particular structure is rarely unique: a particular specified filter characteristic can usually be achieved with different structures — often very many.

Significant differences in characteristics between structures may also be found when the finite-word-length effects of digital filters are taken into account. We shall return to this point later on (pages 128 and 141).

The first aspect of filter structures to be considered is the combination of simple filters or 'filter sections' to form complex filters. This is done mainly by connecting the filters in cascade or in parallel (fig. 22). In

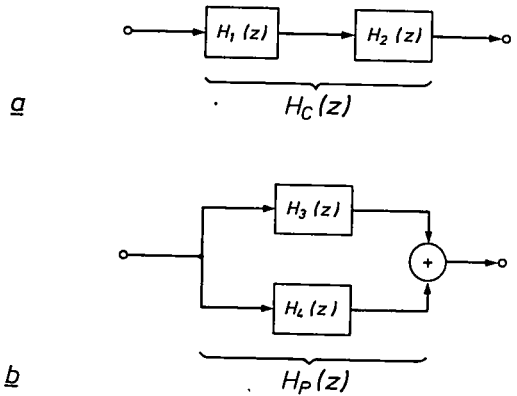


Fig. 22. Composite filters can be obtained by a) cascading: $H_c(z) = H_1(z)H_2(z)$, and b) parallel connection: $H_p(z) = H_3(z) + H_4(z)$.

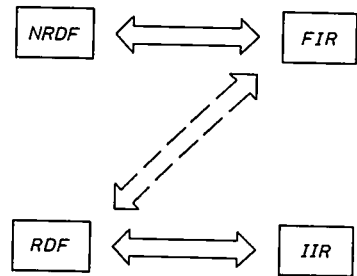


Fig. 23. Usually an FIR filter has an NRDF structure and an RDF structure gives an IIR filter. In rare cases the combination of the RDF structure and an FIR filter is found (if all the poles coincide with zeros).

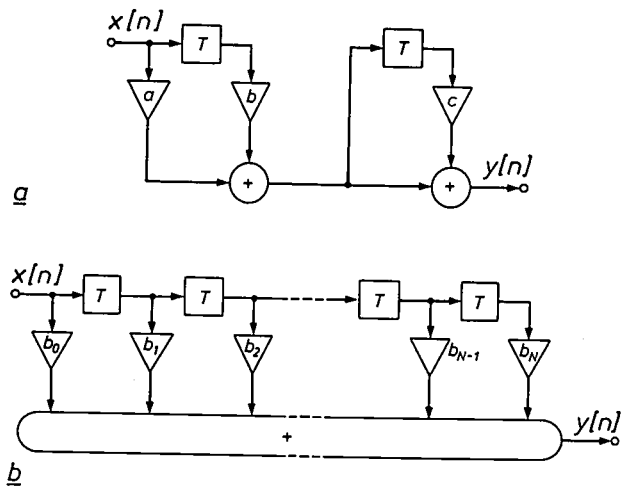


Fig. 24. a) Arbitrary example of a discrete filter with a non-recursive structure (NRDF). b) A transversal filter is an NRDF in which only the input signal is stored in the delay elements. In this case the successive samples of the impulse response have the exact values of the successive coefficients.

a cascade arrangement we obtain the overall system function by multiplying the individual system functions:

$$H_C(z) = H_1(z)H_2(z). \tag{67}$$

The zeros of $H_C(z)$ are therefore the zeros of $H_1(z)$ plus the zeros of $H_2(z)$, and the poles of $H_C(z)$ are the poles of $H_1(z)$ plus the poles of $H_2(z)$. If a zero of $H_1(z)$ coincides with a pole of $H_2(z)$ (or vice versa), they compensate each other and cannot then be found separately in $H_C(z)$. In a parallel arrangement the individual system functions have to be added together:

$$H_P(z) = H_3(z) + H_4(z). \tag{68}$$

The poles of $H_P(z)$ here again consist of the sum of the poles of the subsystems, but it is not easy to make any general comment about the relation between the zeros.

From their structure, discrete filters can be simply classified as:

- recursive discrete filters (RDFs), in which there is at least one feedback path (e.g. fig. 15b, c), and
- non-recursive discrete filters (NRDFs), in which there is no feedback at all (e.g. fig. 15a).

It is often wrongly assumed that an RDF structure always gives an IIR filter and that an FIR filter always has an NRDF structure. Although this is usually the case, it is not necessarily so. The opposite is however true. An IIR filter requires an RDF structure and an NRDF structure always yields an FIR filter (fig. 23).

A discrete filter is said to be *canonical* when it contains the minimum number of delay elements theoretically necessary to give the system function.

The feedback paths that characterize RDFs introduce closed loops. Each closed loop must contain at least one delay element, otherwise the resultant system will not be realizable because of the paradoxical requirement that the value of a signal sample must be known before it can be calculated.

NRDFs

A filter with a non-recursive structure is shown in fig. 24a. The system function $H(z)$ and the impulse response $h[n]$ of this filter are:

$$H(z) = (a + bz^{-1})(1 + cz^{-1}) = a + (b + ac)z^{-1} + bcz^{-2} \tag{69a}$$

$$h[n] = a\delta[n] + (b + ac)\delta[n - 1] + bc\delta[n - 2]. \tag{69b}$$

It is easily seen that the impulse response of an NRDF can never be longer than the number of unit-delay elements that the filter contains, plus one. A common type of NRDF is the *transversal* discrete filter (fig. 24b).

It is characterized by the fact that the only signal that is stored in the delay elements is the original input signal $x[n]$. The system function $H(z)$ and the impulse response $h[n]$ of this filter are

$$H(z) = b_0 + b_1z^{-1} + \dots + b_Nz^{-N} \tag{70a}$$

$$h[n] = b_0\delta[n] + b_1\delta[n - 1] + \dots + b_N\delta[n - N]. \tag{70b}$$

In this case we immediately recognize the impulse response in the filter coefficients. With a transversal filter we can therefore see almost at a glance whether we have a linear phase characteristic, the requirement being a symmetric or antisymmetric impulse response of arbitrary length N , i.e. $h[i] = h[N - i]$ or $h[i] = -h[N - i]$ for $i = 0, \dots, N$.

Although only FIR filters can be made with an NRDF, which means for instance that the relevant system function can contain no poles (except for the origin), a good approximation to almost any frequency response can be obtained by making the length N sufficiently large. In practice we can have NRDFs with an impulse response comprising hundreds or thousands of samples [11]. (The system function in such a case also contains hundreds or thousands of zeros.)

RDFs

One possible structure for recursive discrete filters follows directly from the general description of discrete filters in eq. (44). This is shown in fig. 25a and is simply named the 'direct-form-I structure'. We can

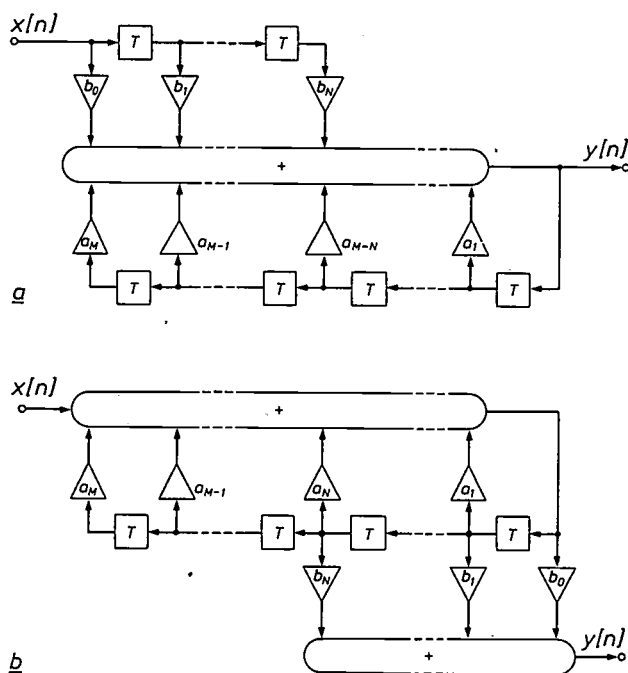


Fig. 25. Two examples of general structures for recursive discrete filters (RDFs). a) Direct-form-I structure. This comprises $M + N$ unit-delay elements. b) Direct-form-II structure. In the example given here ($M > N$) this only requires M unit-delay elements.

[11] J. J. van der Kam, A digital 'decimating' filter for analog-to-digital-conversion in hi-fi audio signals. Forthcoming article in the special issue of this journal on 'Digital signal processing II, applications'.

think of it as split up into a transversal part with filter coefficients b_0, b_1, \dots, b_N followed by a purely recursive part with filter coefficients a_1, a_2, \dots, a_M . This structure requires a total of $M + N$ unit-delay elements. If the recursive part and the transversal part are made to change places (this is permissible because each part is an LTD system in itself), the result is the 'direct-form-II structure' (fig. 25b). This only contains M unit-delay elements if $M > N$ (or N if $N > M$). The system function is the same in both cases; the zeros are determined by the coefficients b_i and the poles by

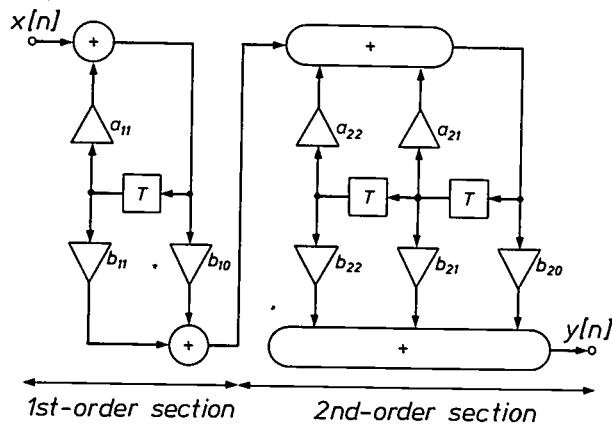


Fig. 26. Third-order filter produced by cascading a 1st-order section and a 2nd-order section. Filters of arbitrarily high order can be made by cascading such sections, without the high sensitivity to coefficient variation which characterizes the direct-form structures.

the coefficients a_i . A disadvantage here is that each coefficient b_i affects all of the zeros. The same thing applies for each a_i and all of the poles. This means that even small changes in the coefficients can have a considerable effect on the frequency response of the filter. This is a less desirable feature: it is a serious drawback if for example we have to use quantized (i.e. slightly modified) coefficient values in a digital filter. A solution to this problem can be found by building up the total filter from smaller units (see fig. 22) in which each pole and each zero is determined by a smaller number of coefficients. A very advantageous and widely used arrangement is a cascade of 1st-order and 2nd-order filter sections. With a 1st-order section one pole and one zero that are both real can be determined. With a 2nd-order section two poles and two zeros can be determined, which can be either real or complex (fig. 26).

Special filter structures

Comb filters

An interesting type of filter, known as a comb filter, is obtained from any given discrete filter with the sys-

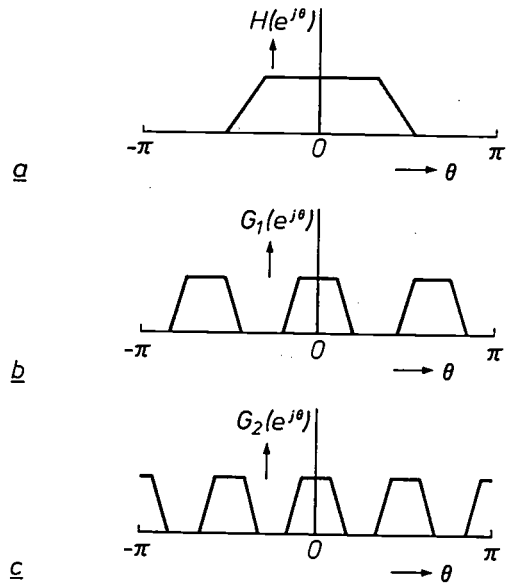


Fig. 27. Schematic representation of the frequency responses $H(e^{j\theta})$, $G_1(e^{j\theta})$ and $G_2(e^{j\theta})$. a) Original filter. b) Comb filter obtained from (a) with $N = 3$; c) as (b) but with $N = 4$.

tem function $H(z)$ by replacing each unit-delay element by a cascade arrangement of N unit-delay elements. This results in a new filter with the system function $G(z)$:

$$G(z) = H(z^N). \tag{71}$$

This means that the frequency response in the fundamental interval $(-\pi \leq \theta < \pi)$ is periodically repeated N times, as illustrated schematically in fig. 27 for $N = 3$ and $N = 4$. An interesting type of comb filter, which is also one of the oldest, is shown in fig. 28. In some applications N can be 100, 1000 or even more [9].

Ladder and lattice filters

In recent years there has been a marked growth of interest in the filter structures known as ladder filters and lattice filters. Some typical examples are given in figs 29 and 30. There are, however, a large number of variations. The common feature of these filters is that they are built up from basic units (see the shaded parts of the figures), each with two inputs and two outputs. Lattice filters, as the name suggests, are typified by a crossover structure within the basic unit. These filters are interesting mainly because of the following features:

- the stability of the filter can be expressed in terms of specifications for each coefficient separately, and
- the frequency response is not very sensitive to variations in the precise value of the coefficients.

These filters are often used for processing of discrete speech signals [12].

[12] L. R. Rabiner and R. W. Schafer, Digital processing of speech signals, Prentice-Hall, Englewood Cliffs, NJ, 1978.

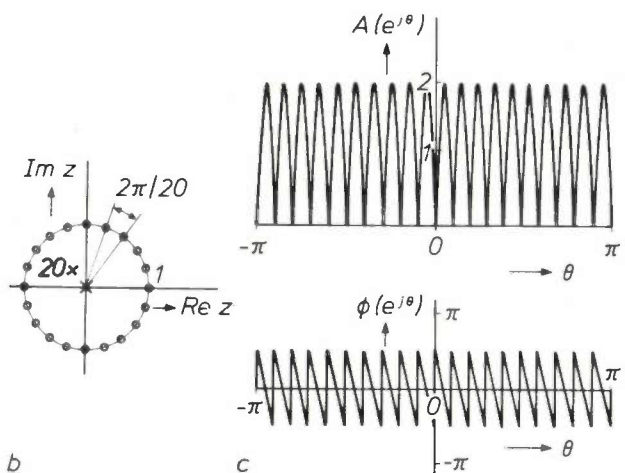
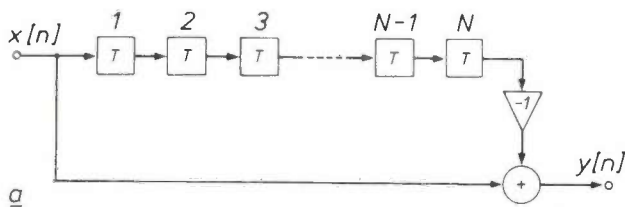


Fig. 28. a) Block diagram of one of the oldest types of comb filter, which is particularly useful for colour-TV applications. b) Corresponding poles-and-zeros plot for $N = 20$. c) Corresponding amplitude and phase characteristic for $N = 20$.

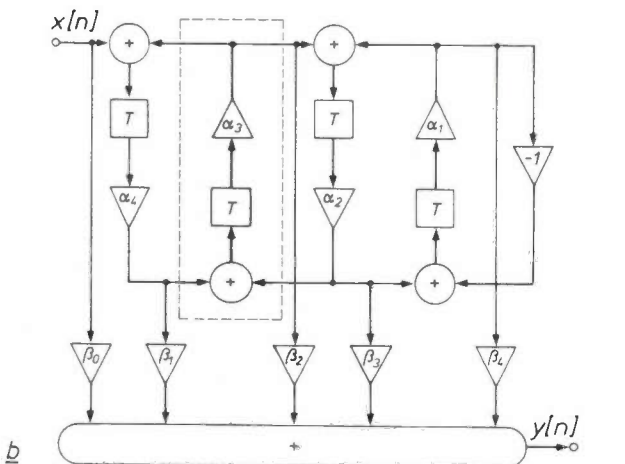
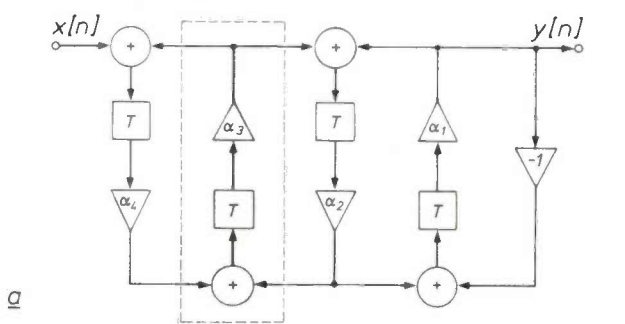


Fig. 29. a) Ladder filter with a system function $H(z)$ that only contains poles. b) Ladder filter with poles determined by the α 's, and zeros determined by the β 's. (The shaded area indicates a basic unit which is regularly repeated.)

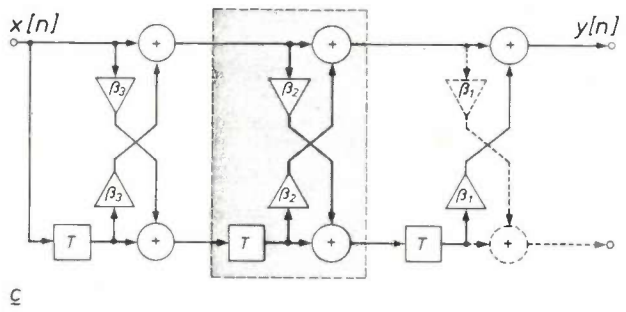
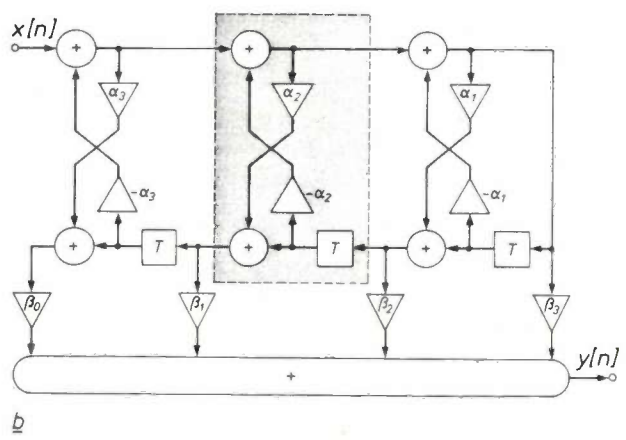
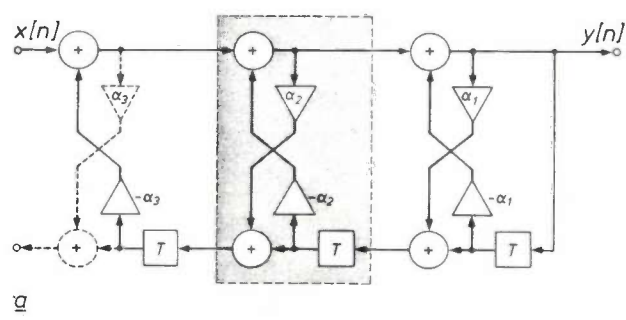


Fig. 30. a) Lattice filter with a system function that only contains poles. b) Lattice filter with poles determined by the α 's, and zeros determined by the β 's. c) Lattice filter containing only zeros in the system function.

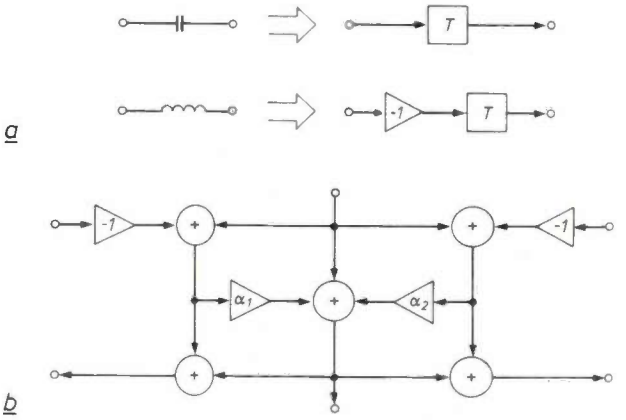


Fig. 31. a) Wave digital filters are obtained by 'translating' the components of analog filters into discrete components on the basis of wave equations. This is indicated here for a capacitance and an inductance. b) The discrete components thus obtained are connected by adaptors, which only contain adders and multipliers. The example shown here is one of many possible types of adaptor.

Wave digital filters

Wave digital filters, or WDFs, are a category apart. They can be obtained from a direct 'translation' of a given analog filter on the basis of wave equations. A capacitance is translated into a simple unit-delay element, and an inductance is translated into the cascade arrangement of a unit-delay element and an inverter (multiplier by -1). These components are interconnected by series or parallel adaptors, which contain a combination of adders and multipliers (fig. 31). These filters also have low sensitivity to coefficient variations and have good stability [13].

Transposed filters

A very general method of deriving from a given filter a second filter with a different structure but with the same system function is based on the application of the transposition theorem. This theorem states that the system function of an LTD system remains unchanged if:

- the signal flows reverse direction (implying that the input is made the output and vice versa), and
 - adders are replaced by nodes, and nodes by adders.
- This is illustrated in fig. 32, which shows a 2nd-order filter section before and after transposition. We can apply transposition to all the LTD systems that we have encountered so far; the same principle can however be extended to a much larger class of discrete systems [14].

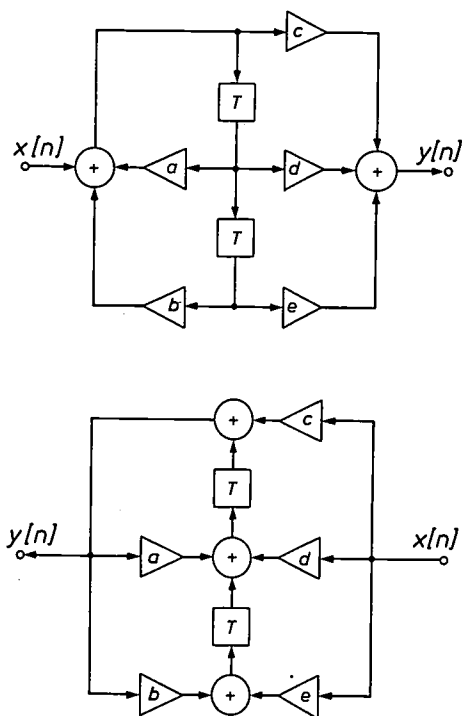


Fig. 32. Transposition of an LTD system gives a different structure with exactly the same system function. (Reversing the signal flows exchanges input and output.)

Adaptive filters

Another useful type of filter for signal processing, especially with digital signals, is the adaptive filter [15]. The filter coefficients do not have a fixed predetermined value, but are calculated during use. An adaptive filter consists of two distinct parts (fig. 33): the filter proper, which in principle can have any of the structures described earlier with time-dependent filter coefficients $c_0[n], c_1[n], \dots, c_N[n]$, and a control unit. The values of the coefficients are automatically calculated in the control unit from a control criterion, which is usually based on minimizing the difference $\epsilon[n]$ between the actual output signal $y[n]$ and a reference signal $g[n]$. By far the most commonly used structures for adaptive filters are the transversal structure and certain lattice and ladder structures [16].

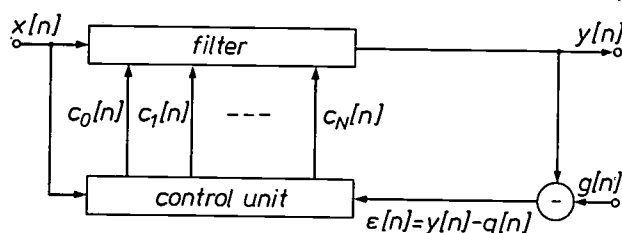


Fig. 33. In an adaptive filter the filter coefficients $c_0[n], \dots, c_N[n]$ do not have fixed values but are calculated in a control unit. Usually the aim is to minimize the difference $\epsilon[n]$ between the actual output signal $y[n]$ and a reference signal $g[n]$.

IV. METHODS OF DESIGNING DISCRETE FILTERS

The design of a discrete filter usually starts with a specification of the frequency behaviour required. As a rule the specification states the limits for the required amplitude and phase characteristic. The shape of the phase characteristic is sometimes left completely unspecified. In other cases the phase is required to be linear. The specifications usually take the form of a tolerance diagram, as shown in fig. 34 for the amplitude characteristic of a lowpass filter. The characteristic to be achieved must not pass through the hatched areas. (Since we are almost invariably concerned with real impulse responses, the specifications need only be indicated in the interval $0 \leq \theta < \pi$; see property IV in the small print on page 115.) We see three frequency ranges: a passband, a stopband and a transition band. In this example the maximum deviation of the amplitude in the passband ($0 \leq \theta < \theta_1$) must not be more than δ_1 ; in the stopband ($\theta_h \leq \theta < \pi$) it must not be more than δ_2 . In the transition band ($\theta_1 \leq \theta < \theta_h$) there is a gradual unspecified transition in the amplitude characteristics. Curve A in fig. 34 represents an

amplitude characteristic that meets the specifications exactly.

A common procedure in the design of a discrete filter is as follows:

- We decide whether we want to approximate to the required frequency characteristic with an FIR filter or with an IIR filter and we select the order of the filter.
- We calculate a set of coefficients that will approximate the corresponding system function as closely as possible.
- We decide on the filter structure, bearing in mind possible finite-word-length effects (for digital filters).
- We check whether the resultant filter meets the original specifications and if it does not, we repeat the design procedure, adopting a different type of filter or structure or a different order or form of quantization, or combinations of these alternatives.

In the design of discrete filters certain steps in the design process are usually repeated several times. The process may therefore be described as iterative.

In this section we are mainly concerned with the second of these steps, which may be regarded as the crucial step in the design process. We shall only consider a limited number of the many possible alternatives. It will be noted that this step does not always have exactly the form described above; the reason is that the design procedure does not always give first place to the system function, but may place more

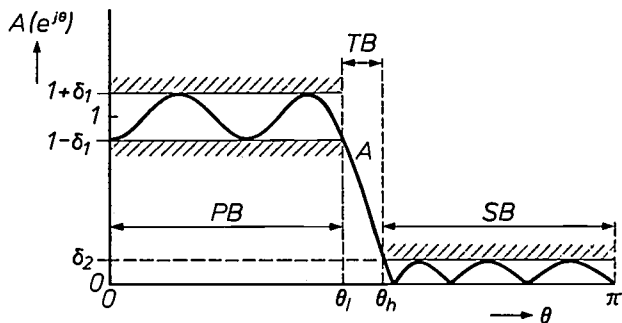


Fig. 34. Specification of the characteristics of a discrete filter by a tolerance diagram. The amplitude characteristic $A(e^{j\theta})$ of the filter to be designed must not pass through the hatched area. The characteristic A given here satisfies this requirement. The filter is a lowpass filter with a passband PB , a transition band TB and a stopband SB .

[13] A. Fettweis, Digital circuits and systems, IEEE Trans. CAS-31, 31-48, 1984.
 [14] T. A. C. M. Claasen and W. F. G. Mecklenbräuker, On the transposition of linear time-varying discrete-time networks and its application to multirate digital systems, Philips J. Res. 33, 78-102, 1978.
 [15] T. A. C. M. Claasen and W. F. G. Mecklenbräuker, Overview of adaptive techniques in signal processing, in: H. W. Schüssler (ed.), Signal processing II: theories and applications, Elsevier Science, Amsterdam 1983.
 [16] M. L. Honig and D. G. Messerschmitt, Adaptive filters: structures, algorithms and applications, Kluwer Academic, Boston 1984.

emphasis on for example the impulse response, or the fully specified circuit diagram of the continuous filter that must be translated into an equivalent discrete system.

FIR filter design

Using IFTD and time window

The starting point in this design method is the frequency response $H_d(e^{j\theta})$, to be realized as well as possible with an FIR filter. By applying the IFTD to $H_d(e^{j\theta})$ we find directly the 'ideal' impulse response $h_d[n]$. For most purposes, however, this will not be used because $h_d[n]$ is of very great or even infinite length and because $h_d[n]$ is not causal (that is to say $h_d[n] = 0$ for some negative values of n) — or both. We therefore have to limit the length of $h_d[n]$ to N samples and shift the impulse response sufficiently to guarantee causality. This is made clear in fig. 35. The lowpass filter characteristic $H_d(e^{j\theta})$ gives an $h_d[n]$ of

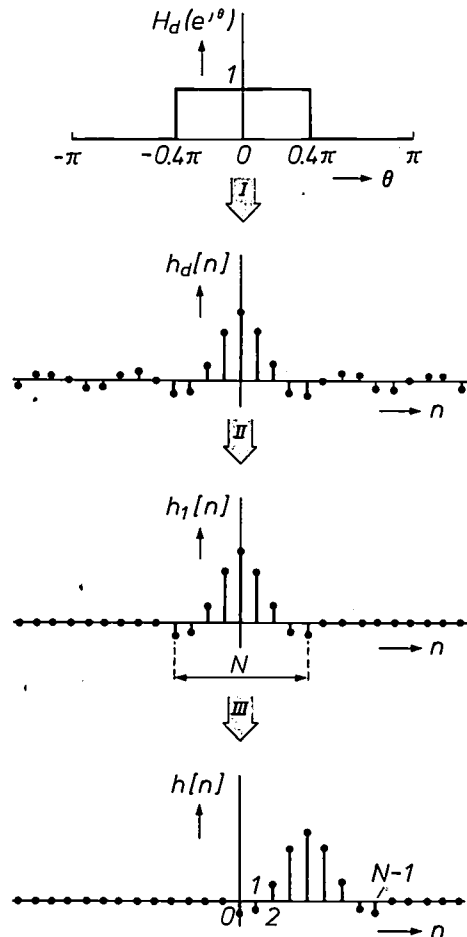


Fig. 35. Transformation in three steps of a filter specification in the frequency domain to a realizable impulse response of finite duration by IFTD (I), truncation (II) and shifting (III).

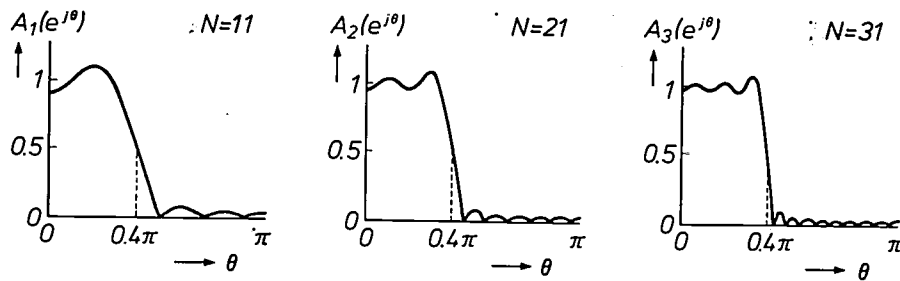


Fig. 36. The quality of the filter produced by the design method in fig. 35 depends on the length N of the impulse response. The resultant amplitude characteristic $A(e^{j\theta})$ is shown here for three different values of N .

infinite duration via the IFTD. Limiting this duration to N gives $h_1[n]$ and a shift to the right results in the required impulse response $h[n]$. This can be realized directly in the form of a transversal filter, for example.

Truncation of $h_d[n]$ results in deviations in the frequency response that depend on the value of N . Fig. 36 shows the differences in the amplitude characteristic for $N = 11, 21$ and 31 . Truncation of the impulse response causes an abrupt transition from samples in $h_d[n]$ that do count in $h_1[n]$ to samples that do not count at all in $h_1[n]$. It is always better to make this a gradual transition by means of a window function $w[n]$, such that:

$$h_1[n] = h_d[n] w[n], \quad (72)$$

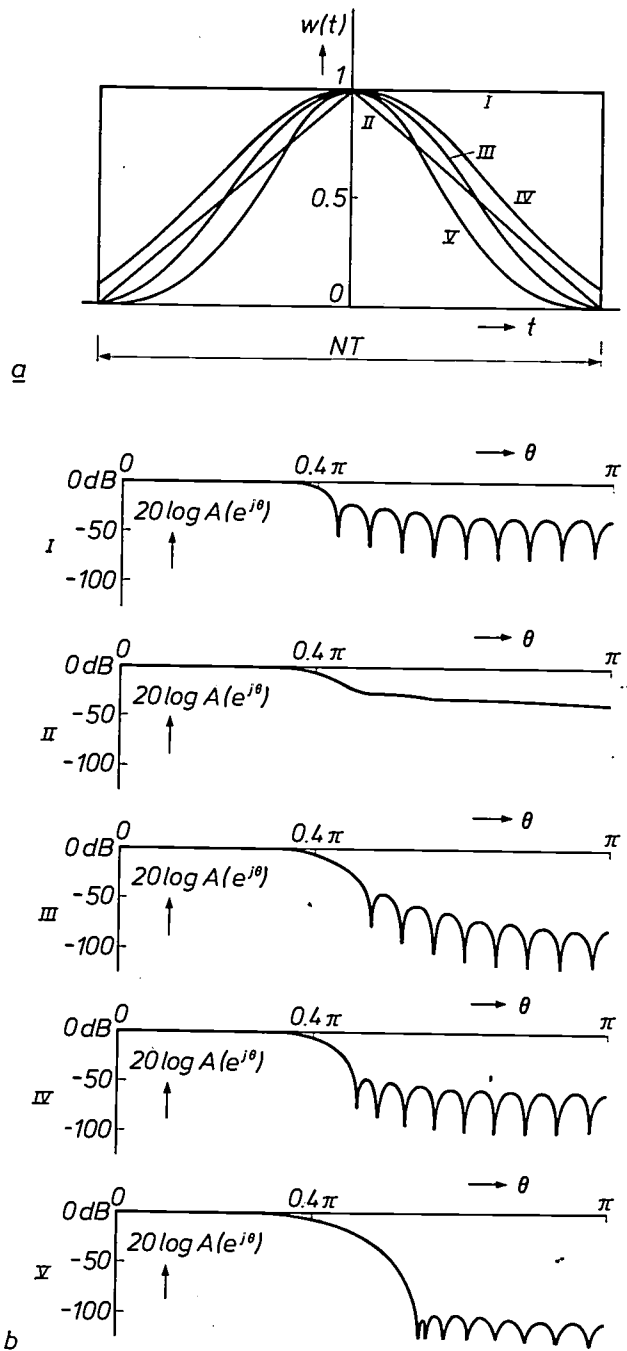
where $w[n]$ has the required length N . Some possible window functions [5]-[7] are given in fig. 37a, and the resultant amplitude characteristics for the example in fig. 35 are shown in fig. 37b. These figures demonstrate how important the choice of the window can be. (Incidentally, straightforward truncation of the impulse response is the same as using a rectangular window.)

We should mention in passing that window functions are also used for calculating an N -point DFT for a discrete signal of excessive or infinite length. Here again it is important to choose the right type of window, for one thing to reduce leakage.

Equiripple design

In the examples with the previous design method we saw that the approximations made during the design

Fig. 37. a) Window functions that can be used in the transition from $h_d[n]$ to $h_1[n]$ in fig. 35. Although the window functions are discrete functions of length N , they are shown here for clarity as continuous functions $w(t)$. I Rectangular window. II Bartlett window. III Hanning window. IV Kaiser window ($\beta = 4$). V Kaiser window ($\beta = 10$). The Kaiser windows form a complete family with β as parameter. Two actual values of β are taken here by way of illustration. b) Each of the window functions gives a filter with a different amplitude characteristic. Results obtained when filters are designed as illustrated in fig. 35 using windows of types I, ..., V (in all cases $N = 31$) are shown. The amplitude $A(e^{j\theta})$ is given on a dB scale.



process introduced 'ripples' in the ideal characteristic. It is often found that optimum filter behaviour is obtained when the ripples in the passband or bands all have the same magnitude. The same applies for ripples in the stopband or bands. Such filters are known as

Various rules of thumb have been given in the literature for obtaining a general idea of the values required for different parameters before making the computer calculations. For example, a rough estimate of the length of the impulse response N of an FIR equiripple

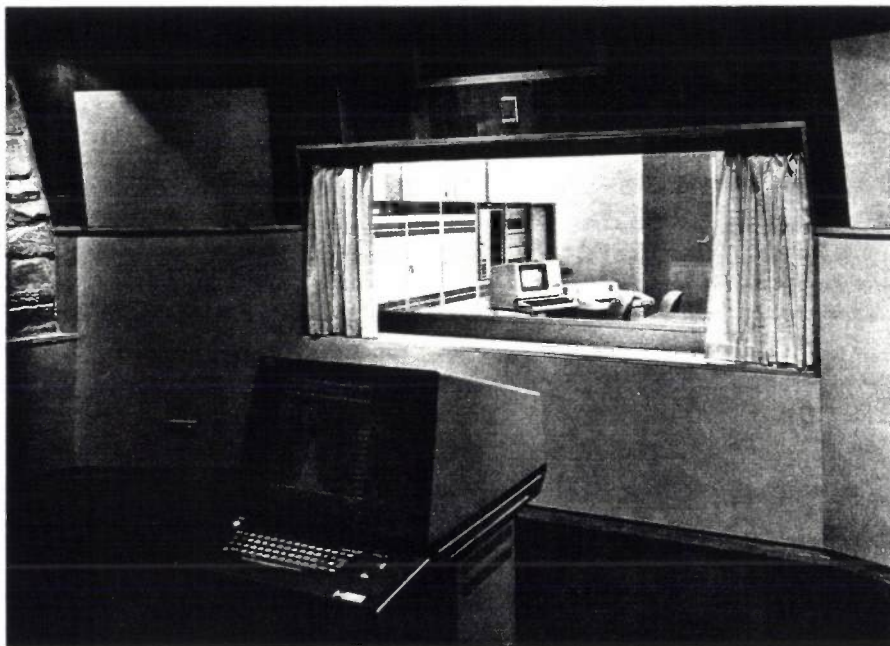


Fig. 38. The computer (visible through the window) can perform various functions in designing digital filters. Besides making all kinds of design calculations and displaying the resultant filter characteristics on a screen (foreground) the computer can immediately simulate the result that a particular filter would give in practice. The foreground in this photograph is a 'listening room', which is almost completely isolated acoustically from the environment. The effects of digital signal processing on audio signals can be assessed in this room by using simulated signals.

'equiripple' filters. The amplitude characteristic A in fig. 34 represents an equiripple filter.

Calculating the filter coefficients of an equiripple filter is a laborious task. It generally requires iterative optimization, and the computer is almost indispensable.

Various programs for designing filters of this type, and with linear phase, have been described [17]. They can be used not only for designing lowpass filters but also for designing bandpass and bandstop filters (with one or more pass- or stopbands) and differentiators. The method can also be extended for designing filters with much more general characteristics.

By way of illustration let us look for a moment at the design of a lowpass equiripple filter with the specifications given in fig. 34. This design is characterized by five parameters: the length of the impulse response N , the maximum deviations in the passband δ_1 and in the stopband δ_2 , and the limits θ_1 and θ_h of the transition band. After we have decided on the value of four of these parameters, the fifth is fixed. The program used determines which four parameters are the freely chosen ones.

filter that meets the specifications in fig. 34 is given for large values of N from the rule:

$$N \approx - \frac{10 \log_{10}(\delta_1 \delta_2) + 15}{14(\theta_h - \theta_1)/2\pi} + 1 \quad (73)$$

An example of the use of a computer for digital signal-processing design [18] is shown in fig. 38.

IIR filter design

Impulse invariance

In this method we start with an analog filter with impulse response $h_a(t)$, and we wish to make an IIR filter with impulse response $h_d[n]$, such that:

$$h_d[n] = h_a(nT), \quad (74)$$

i.e. $h_d[n]$ is to be identical with a sampled version of $h_a(t)$. It can be shown that the discrete frequency response $H_d(e^{j\theta})$ is found by periodically repeating the

[17] Programs for digital signal processing, IEEE Press, New York 1979.

[18] L. D. J. Eggermont and P. J. Berkhout, Digital audio circuits: computer simulations and listening tests, Philips Tech. Rev. 41, 99-103, 1983/84.

frequency response of the original analog filter at intervals of $\theta = \omega T = 2\pi$ (see also the section headed 'From continuous time to discrete time and vice versa'). If the sampling interval T is chosen sufficiently small, then $H_d(e^{j\theta})$ in the fundamental interval will closely resemble $H_a(j\omega)$; see fig. 39.

The calculations required for this design method are fairly simple. Let us assume that the original analog filter has a system function $H_a(p)$ with only single poles. This can then always be written in the form:

$$H_a(p) = \sum_{k=1}^M \frac{A_k}{p - q_k}$$

The system function $H_d(z)$ of the discrete filter expressed in terms of A_k , q_k and T is then given by:

$$H_d(z) = \sum_{k=1}^M \frac{A_k}{1 - e^{q_k T} z^{-1}}$$

Various block diagrams can be constructed with the aid of this system function.

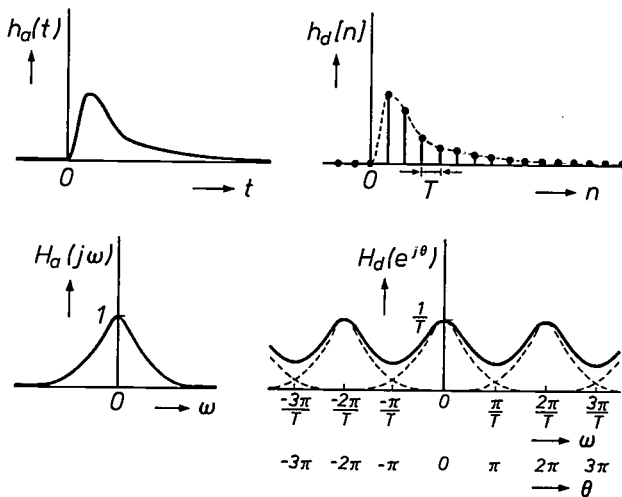


Fig. 39. Relation between the impulse responses $h_a(t)$ and $h_d[n]$ and between the corresponding frequency responses $H_a(j\omega)$ and $H_d(e^{j\theta})$ in the method of discrete-filter design based on impulse invariance.

Bilinear transformation

The starting point for this method is the system function $H_a(p)$ of an analog filter. Substituting the expression

$$p = \frac{2}{T} \frac{1 - z^{-1}}{1 + z^{-1}} \tag{75}$$

in $H_a(p)$ we obtain the system function $H_d(z)$ of a discrete filter whose frequency response $H_d(e^{j\theta})$ has a direct relation with the frequency response $H_a(j\omega)$ of the original filter: this is because the complete curve of

$H_a(j\omega)$ for $-\infty < \omega < \infty$ is 'compressed' into the fundamental interval $-\pi \leq \theta < \pi$ of $H_d(e^{j\theta})$. This applies to both the amplitude characteristic and the phase characteristic. Proceeding for example from

$$H_a(p) = \frac{a}{p + a}, \tag{76}$$

and substituting eq. (75) in this expression, we find after some calculation:

$$H_d(z) = \frac{aT(1 + z^{-1})}{aT + 2 + (aT - 2)z^{-1}} \tag{77}$$

The amplitude characteristics $|H_a(j\omega)|$ and $|H_d(e^{j\theta})|$ of the two corresponding frequency responses for $a = 1000$ and $T = 1/1000$ are shown in fig. 40. The 'frequency compression' is not in fact linear but has the form of a tangent function: the compression is greatest at higher frequencies. This can clearly be seen in fig. 41, where the bilinear transformation is applied to an analog equiripple filter. Although there is obvious nonlinear 'warping' of the frequency axis, it can also be seen that the ripple is kept constant. This is one of the great advantages of this method in the design of filters that can be fully specified in terms of passbands and stopbands. To ensure that the resultant discrete filter will have transition bands around certain specified frequencies (ω_4, ω_5), it is necessary to base the design on a continuous filter with transition bands around quite different frequencies (ω_1, ω_2), which are however easy to calculate. This is called 'prewarping'.

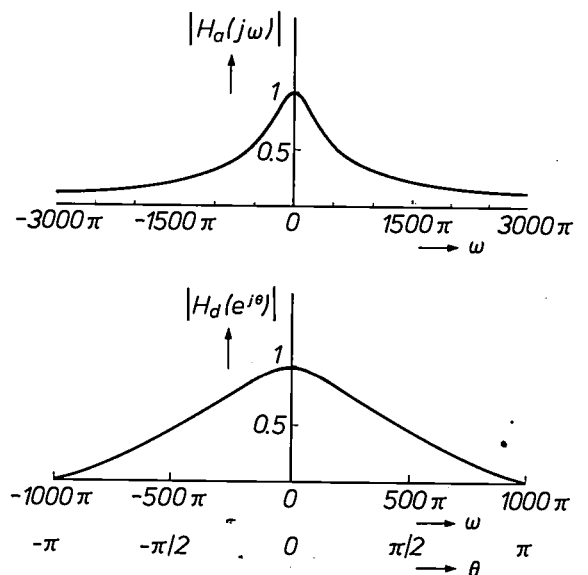


Fig. 40. Example of the application of the bilinear transformation with $T = 1/1000$ to an analog filter with the frequency response $H_a(j\omega) = 1000/(j\omega + 1000)$. The resultant discrete filter has an amplitude characteristic $|H_d(e^{j\theta})|$, which is like $|H_a(j\omega)|$ but compressed along the frequency axis. The value reached by $H_a(j\omega)$ for $\omega = \infty$ is already attained by $H_d(e^{j\theta})$ at $\omega = \pi/T = 1000\pi$.

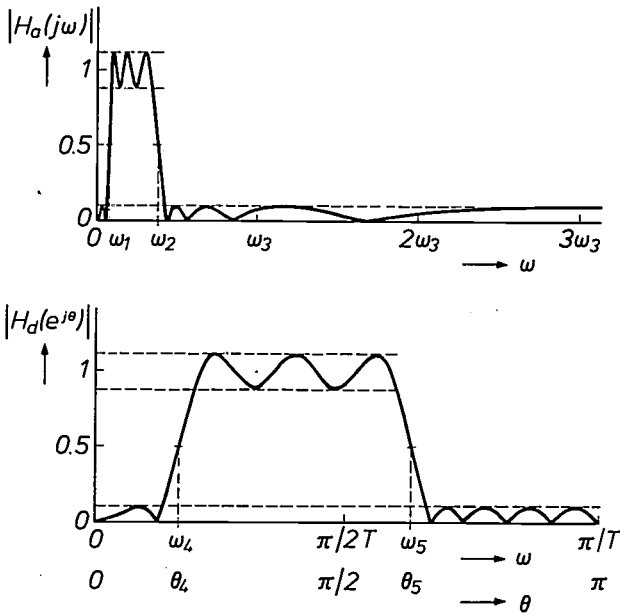


Fig. 41. Example of the application of the bilinear transformation to an analog bandpass filter. It can be seen from the ripples in the filter characteristics that the compression of the frequency axis is not constant in this design method, but increases with frequency. It is also clear, however, that the equiripple property is retained.

Transformation of elements

In this method we also start from an analog filter, often an LC filter. Each component in the block diagram of this filter is separately translated into a discrete-time equivalent, and in principle these equivalents are connected together in the same way as in the analog filter. This is a method of design that retains some of the desirable features of LC filters, such as low sensitivity to component variations. As we noted earlier, the method is used for wave digital filters (fig. 31). It is also used for designing certain

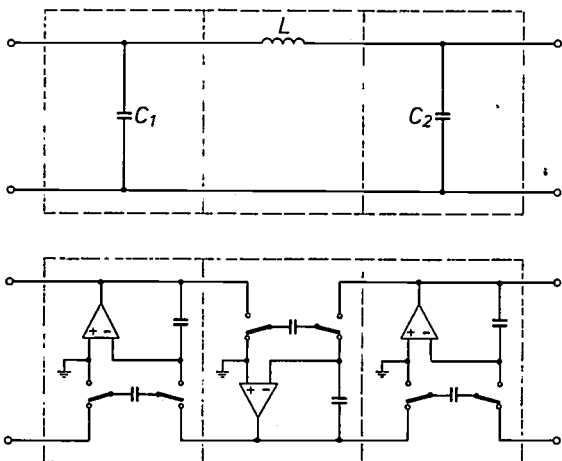


Fig. 42. a) Continuous LC filter of third order and b) switched-capacitor filter obtained from it using the design method based on element transformation.

types of digital ladder filters and discrete filters based on switched capacitors [3]. A simple example of the latter is shown in fig. 42.

Optimization by computer

In the fourth and final method we shall mention here for the design of IIR filters the optimization is done on the computer. There are special programs for this [17]. The starting point is the specification of a required frequency response, with rough estimates of the coefficients a_i and b_i of the final system function (eq. 62). The computer then modifies a_i and b_i in steps in such a way as to minimize the difference between the final frequency response and the required frequency response. Some programs only take deviations in the amplitude into account; others also include deviations in the phase characteristic (mainly in connection with group delay, which is directly related to the derivative of the phase characteristic).

V. PRACTICAL ASPECTS OF DIGITAL SYSTEMS

From continuous time to discrete time and vice versa

If we want to process a continuous-time, say analog, signal $x_a(t)$ in a discrete-time system, we must first convert $x_a(t)$ into a discrete-time signal $x[n]$ without loss of information (or at least as little as possible). But is this always possible? The answer is to be found in the sampling theorem [19]:

If a signal $x_a(t)$ contains no frequency components at frequencies above $\omega_{max} = 2\pi f_{max}$ rad/s, all the information about $x_a(t)$ is entirely contained in the values $x_a(nT)$ provided that $T \leq 1/(2f_{max})$.

The values $x_a(nT)$ can be obtained from $x_a(t)$ by sampling at the sampling rate $f_s = 1/T$. By now defining a discrete-time signal such that

$$x[n] = x_a(nT) \tag{78}$$

we have completed the entire transition from continuous time (CT) to discrete time (DT); see fig. 43. The form in which the samples of $x[n]$ are represented, whether as a series of numbers in a computer or a series of charge packets in a switched-capacitor filter, is irrelevant.

Now what is the relation between the spectrum $X_a(j\omega)$ of $x_a(t)$ and the spectrum $X(e^{j\omega T})$ of $x[n]$? It

[19] The sampling theorem is usually attributed to C. E. Shannon, who introduced it in information theory at the end of the forties. The same was done almost simultaneously in Russia by V. A. Kotelnikov. A few decades earlier, however, the actual theoretical foundation had already been laid by E. T. and J. M. Whittaker. It is probably better to follow A. J. Jerri's example and to refer to 'the WKS sampling theorem', using the first letters of all three names:

A. J. Jerri, The Shannon sampling theorem — its various extensions and applications: a tutorial review, Proc. IEEE 65, 1565-1596, 1977.

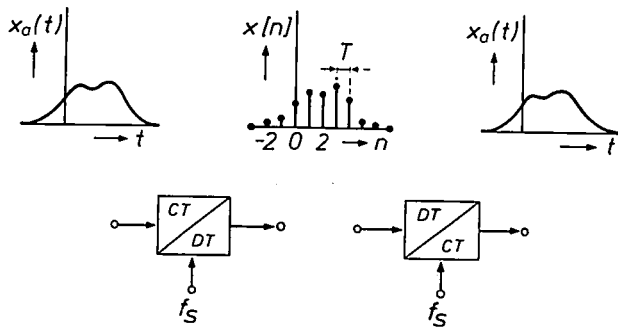


Fig. 43. To convert a continuous-time signal into a discrete-time signal a CT/DT converter is used; the inverse operation is performed in a DT/CT converter. CT continuous time. DT discrete time. f_s sampling rate. $T (= 1/f_s)$ sampling interval.

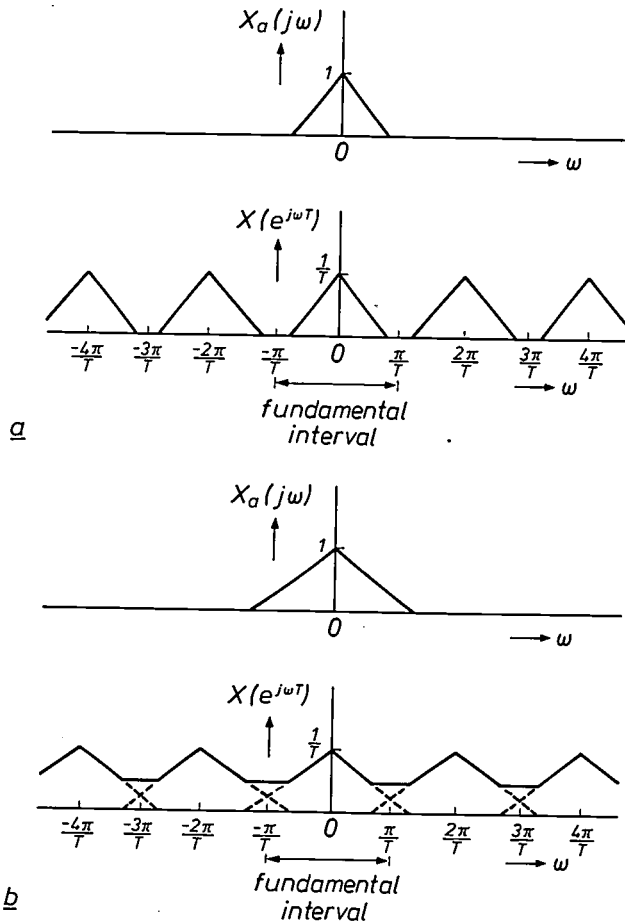


Fig. 44. a) If the sampling theorem is satisfied in the CT/DT conversion in fig. 43, the spectrum $X(e^{j\omega T})$ of $x[n]$ is simply a repeated and scaled version of the spectrum $X_a(j\omega)$ of $x_a(t)$. b) If it is not satisfied, the repetitions overlap and aliasing occurs. Then $x_a(t)$ can never be recovered from $x[n]$ in its exact original form.

can be shown that $X(e^{j\omega T})$ is simply a periodically repeated version of $X_a(j\omega)$ multiplied by $1/T$:

$$X(e^{j\omega T}) = \frac{1}{T} \sum_{n=-\infty}^{\infty} X_a \left(j\omega - j \frac{2\pi n}{T} \right). \quad (79)$$

Fig. 44 shows the spectra for two cases; in one case the

condition of the sampling theorem is satisfied and in the other it is not. In fig. 44b the periodic repetitions of $X_a(j\omega)$ in $X(e^{j\omega T})$ partly overlap, a situation known as 'aliasing'. Because of this, $X_a(j\omega)$ and therefore also $x_a(t)$ can never be recovered in their exact original form. From fig. 44a on the other hand, we can show in principle how we can recover $X_a(j\omega)$ from the corresponding $X(e^{j\omega T})$: we have to derive from $X(e^{j\omega T})$ a continuous-time signal with a spectrum that is identical in the fundamental interval and is zero elsewhere. The DT/CT converter in fig. 43 should therefore contain an ideal lowpass continuous-time filter that gives a gain T for $|\omega| < \pi/T$ and zero gain elsewhere. Such a filter cannot be realized in practice, however, since its impulse response extends from $t = -\infty$ to $t = \infty$.

A more practical system for conversion from CT to DT and vice versa is outlined in fig. 45. The actual CT/DT converter is preceded by a lowpass prefilter with a passband extending to half the sampling frequency. This prevents aliasing that might be caused by unwanted high frequencies (noise for example). The figure also indicates that practical DT/CT converters often employ a stepwise approximation $\hat{x}_a(t)$ to the signal $\bar{x}_a(t)$. This approximation introduces some distortion, however, referred to as $(\sin x)/x$ distortion, at frequencies in the fundamental interval of $x[n]$, and also causes incomplete attenuation outside it. This attenuation can be increased to any desired value by including a subsequent lowpass filter that gives a smooth approximation $\tilde{x}_a(t)$.

The signal $\hat{x}_a(t)$ in fig. 45 consists of a succession of rectangular pulses of width T . Each separate pulse has a Fourier transform which has the form of a $(\sin x)/x$ function. This determines the distortion of the spectrum of $\hat{x}_a(t)$. The same type of distortion is still present in the spectrum $\tilde{X}_a(j\omega)$ of $\tilde{x}_a(t)$ for $|\omega| < \pi/T$. This can be eliminated, however, in the discrete-time operations normally carried out between point 2 and point 3 by discounting as pre-distortion the complementary $x/(\sin x)$ distortion in the fundamental interval [20].

Change of sampling rate

Until now we have always been concerned with discrete-time systems in which only one sampling rate was used. Input signals, output signals and all the other signals occurring in a system always had the same sampling rate $f_s = 1/T$. In the previous section we have seen that f_s can be freely chosen in CT/DT conversion as long as we satisfy the condition of the sampling theorem ($f_s \geq 2f_{max}$) — for every discrete-time signal in that case gives a complete representation of the original continuous-time signal, irrespective of f_s (fig. 46).

In discrete-time signal processing the number of calculations that have to be performed per second is directly related to the sampling rate f_s of the signals. The higher the sampling rate the more calculations have to be performed per second. There are thus ob-

vious advantages in keeping f_s as low as possible, preferably close to $2f_{max}$. Now it is not unusual for f_{max} to differ considerably at different points in a system. In a lowpass filter, for example, f_{max} is lower, sometimes very much lower, at the output than at the input.

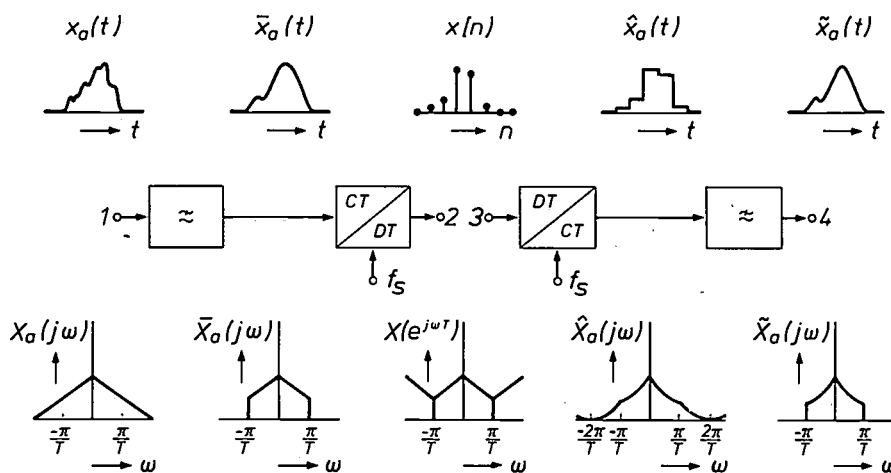


Fig. 45. In a practical situation the signal $x_a(t)$ is first processed in a lowpass prefilter before CT/DT conversion to ensure that it will satisfy the condition of the sampling theorem. After DT/CT conversion the initial result is usually a stepwise approximation $\hat{x}_a(t)$ of $\bar{x}_a(t)$. With an extra postfilter the steep transitions can be removed. This gives $\tilde{x}_a(t)$. The corresponding spectrum of each signal is also shown.

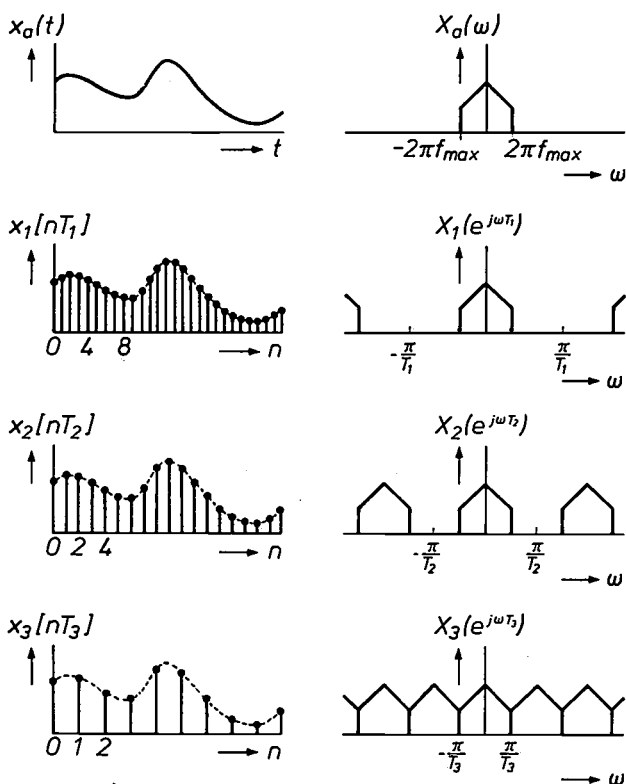


Fig. 46. Continuous-time signal $x_a(t)$ and three discrete-time signals $x_1[nT_1]$, $x_2[nT_2]$, $x_3[nT_3]$ obtained from $x_a(t)$ by CT/DT conversion, with the corresponding spectra. Since the sampling theorem is satisfied in all cases, the discrete-time signals are all a complete representation of $x_a(t)$.

In a modulator circuit exactly the opposite usually applies: f_{max} at the output is higher than f_{max} at the input. In such systems it may be better to use different sampling rates at different points (fig. 47). To do this, however, we have to provide some means of changing from one value of f_s to the other, and this is what is

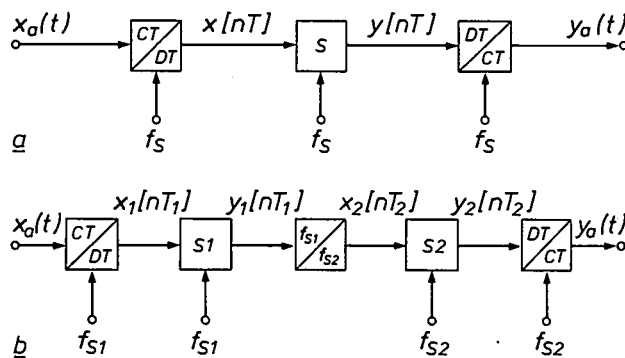


Fig. 47. a) Processing a continuous-time signal $x_a(t)$ in a discrete-time system S with CT/DT and DT/CT converters. Only one sampling rate f_s is used, made high enough to ensure that the sampling theorem is satisfied at all points in the system. b) If the highest frequency occurring at different points in the system does not always have the same value, it may be better to use different sampling rates (f_{s1} , f_{s2}) in different parts of the system. The sampling rate will then have to be adapted appropriately by an f_{s1}/f_{s2} converter.

[20] See pp. 174-179 in: special issue 'Compact Disc Digital Audio', Philips Tech. Rev. 40, 149-180, 1982. See also: J. Nijhof, An integrated approach to CD players, Electronic Components & Appl. 6, 209-222, 1984.

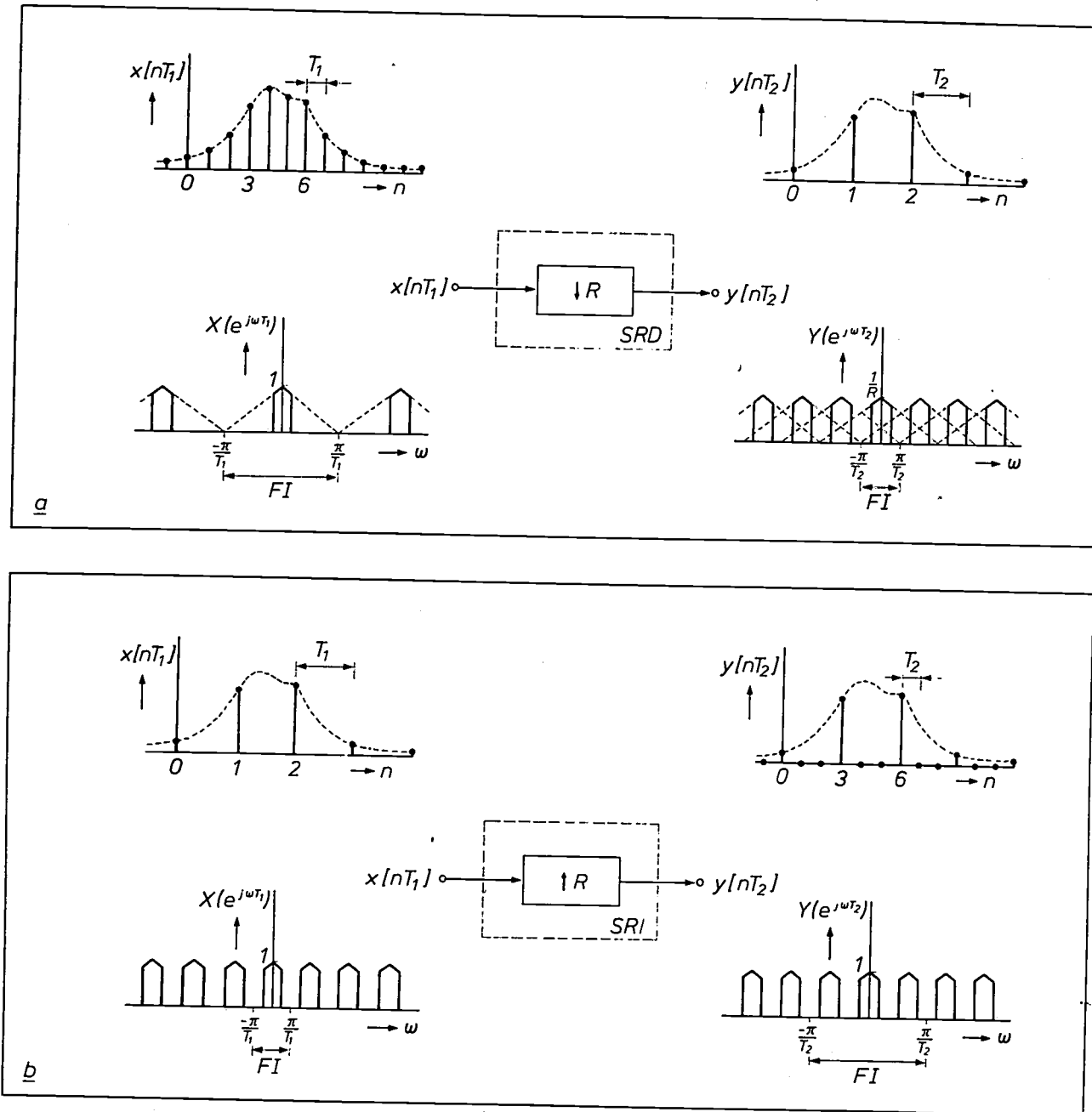


Fig. 48. a) A circuit that decreases the sampling rate (SRD) by an integral factor $f_{s1}/f_{s2} = T_2/T_1 = R$ eliminates $R - 1$ samples from every R input samples (here $R = 3$). b) A circuit that increases the sampling rate (SRI) by an integral factor $f_{s2}/f_{s1} = T_1/T_2 = R$ adds $R - 1$ samples with the value 0 between every two input samples (here $R = 3$). A schematic spectrum is shown for each signal. FI fundamental interval.

done in an f_{s1}/f_{s2} converter. We shall confine our attention now to the cases in which the ratio f_{s1}/f_{s2} or f_{s2}/f_{s1} is an integer R . If $f_{s2} < f_{s1}$ we have a circuit that decreases the sampling rate (SRD, for Sampling Rate Decreaser) by a factor R , and if $f_{s2} > f_{s1}$ we have a circuit that increases the sampling rate (SRI, for Sampling Rate Increaser) by a factor R . We indicate these circuits by the two special block-diagram symbols given in fig. 48. The operation of an SRD or an SRI can easily be pictured from the input and output

signals shown in this figure. With the SRD for every R successive input samples only one sample appears at the output. All the SRI does is to add $R - 1$ samples with the value 0 between every two input samples. In practice operations of this kind can be implemented very easily. But what happens to the overall operation of a discrete-time system when SRIs and SRDs are used? In answering here we must be careful to take the following 'complication' into account: SRIs and SRDs do *not* come under the category of LTD sys-

tems, because they are *time-varying* (although otherwise linear). For this reason they themselves and the discrete-time systems in which they are used cannot simply be described in terms of impulse response, frequency response or system function.

This does not mean, however, that we are left completely powerless; it is perfectly possible to describe the relation between input and output signals in a different manner. To illustrate this fig. 48 shows for $R = 3$ the input and output signals of an SRD and of an SRI together with the corresponding spectra. In the case of the SRD in fig. 48a we see first of all that the fundamental interval of the output signal is a factor of R smaller than that of the input signal. The dashed lines indicate that aliasing can occur in $Y(e^{j\omega T_2})$ if the input spectrum $X(e^{j\omega T_1})$ is not narrow enough. Distinct parallels can be recognized here with the sampling theorem of the previous section. In the case of the SRI in fig. 48b all that happens is that the fundamental interval is increased by a factor of R . The spectrum of $Y(e^{j\omega T_2})$ repeats itself exactly R times within that interval.

To ensure that no aliasing will occur when an SRD is used, an ideal lowpass discrete-time filter with a passband for $|\omega| < \pi/T_2$ and sampling rate $1/T_2$ could be inserted in front of it. This combination is known as a 'decimator'; the required ideal filter cannot be realized, however.

With the SRI the periodic repetitions in the spectrum of $Y(e^{j\omega T_2})$ could theoretically be removed within the fundamental interval by filtering $y[nT_2]$ with an ideal lowpass discrete-time filter with a passband $|\omega| < \pi/T_1$ and sampling rate $1/T_2$. This combination is known as an 'interpolator'. Its output signal is a sequence of samples whose value changes smoothly without the many zero samples of $y[nT_2]$. Strictly speaking the interpolator remains a theoretical circuit, however, because of the ideal filter it requires.

In practice an SRD will often be found at the output of a discrete-time filter. This combination of networks is called a *decimating filter*, because the sampling rate at the output is lower than at the input. We must remember, however, that a filter of this type is not an LTD system.

With a decimating filter it is not very sensible to first calculate samples in the filter part and then disregard them later in the SRD. It is better to 'interweave' the operations of filter and SRD as closely as possible (fig. 49) during the design.

In the cascade arrangement of an SRI and a discrete-time filter, called an *interpolating filter*, it is possible to benefit from the prior knowledge that many input samples of the actual filter have the value zero. This can be taken into account in the design (fig. 50). An interpolating filter is also a system that does not come into the LTD category, of course.

A very interesting application of decimating and interpolating filters is to be found in CT/DT and DT/CT conversions that are shown in fig. 45. If an increase in the sampling rates of the actual converters is permissible, the specifications for the continuous-time pre- and post-filters can be greatly relaxed by using decimating and interpolating filters [20].

With a carefully chosen sequence of interpolating and decimating filters the sampling rate can also be changed by rational factors [21].

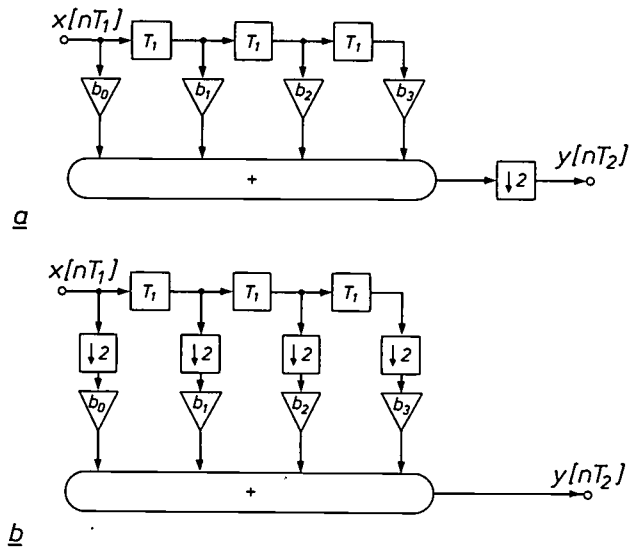


Fig. 49. Decimating filter. a) Combination of a discrete-time filter and an SRD with $R = 2$. In this circuit four multiplications are carried out in every sampling interval T_1 . b) With better 'interweaving' of the operations exactly the same output signal $y[nT_2]$ can be obtained with only four multiplications per interval $T_2 = 2T_1$.

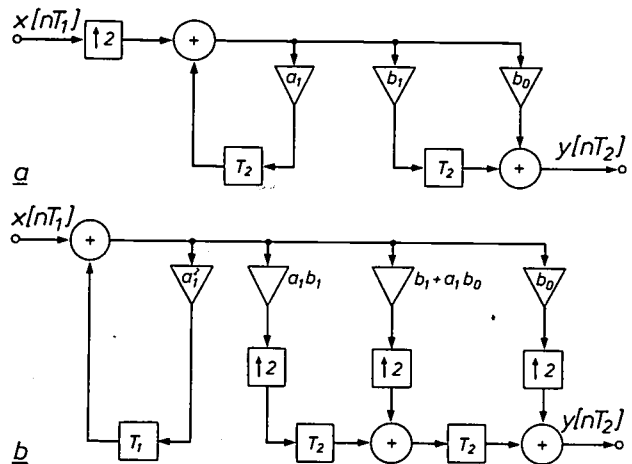


Fig. 50. Interpolating filter. a) Example of the combination of an SRI with $R = 2$ and a discrete-time filter. This structure requires six multiplications per interval T_1 . b) Filter that yields exactly the same output signal as (a). With this improved design, only four multiplications per interval $T_1 = 2T_2$ are necessary.

[21] R. E. Crochiere and L. R. Rabiner, Multirate digital signal processing, Prentice-Hall, Englewood Cliffs, NJ, 1983.

From continuous amplitude to discrete amplitude

As we saw at the beginning of this article, the samples from which digital signals are built up can only have discrete values. Indeed, the same is true of all the other quantities (such as filter coefficients) that occur in digital systems.

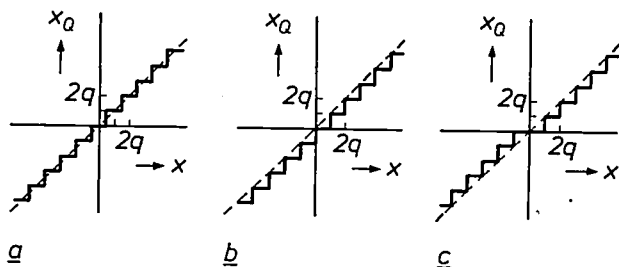


Fig. 51. Three different quantization characteristics: a) rounding off, b) value truncation, c) magnitude truncation. q quantization step.

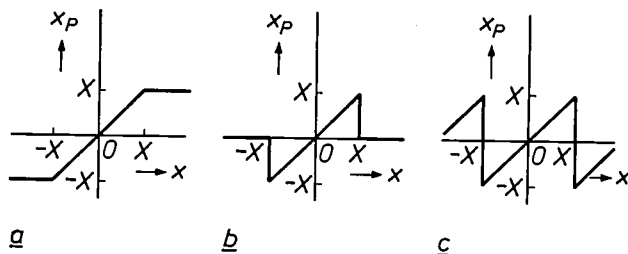


Fig. 52. Three different overflow characteristics: a) saturation, b) zeroing, c) sawtooth overflow.

Table II. Four examples of number representations commonly used in digital signal processing. The word length B is put equal to 3 in all cases.

Decimal value	Sign and magnitude	One's-complement	Two's-complement	Offset binary
+4	—	—	—	111
+3	011	011	011	110
+2	010	010	010	101
+1	001	001	001	100
+0	000	000	000	—
-0	100	111	—	011
-1	101	110	111	010
-2	110	101	110	001
-3	111	100	101	000
-4	—	—	100	—

In practical applications of digital systems, however, we often start with analog signals which, by definition, are continuous in amplitude. In dealing with the theory of discrete-time systems so far we have always assumed a continuous amplitude.

The transition from continuous amplitude to discrete amplitude is in principle never completely reversible, since the number of permitted values unavoid-

ably decreases. This means that there is always a loss of information, however slight. In this transition three concepts are crucial: quantization, overflow and number representation. Let us first consider these three concepts.

Quantization

Quantization is the process in which a quantity x is converted into a quantity x_Q that is approximately equal to x but can assume fewer different values than x . The relation between x and x_Q is called the quantization characteristic. The most widely used forms of quantization in digital processing are (fig. 51): rounding off, value truncation and magnitude truncation. In these examples there is always a fixed distance q , the quantization step, between the successive discrete values of x_Q .

Overflow

Overflow is what happens when a quantity x seeks to assume a value outside the limits $(-X, +X)$ that must be observed. In formal terms we can describe this as a conversion of x into x_P , where

$$x_P \begin{cases} = x & |x| \leq X \\ \leq X & |x| > X. \end{cases} \quad (80)$$

The relation between x and x_P is called the overflow characteristic. Three examples are given in fig. 52: saturation, zeroing and sawtooth overflow. In theory, any form of quantization can be combined with any form of overflow; we can always form a combined overflow/quantization characteristic.

Number representation

Usually the value of a quantity in a digital system is expressed as a group (a 'word') of a specified number (say B) of bits. The corresponding overflow/quantization characteristic then has a maximum of 2^B different values. Each of these values corresponds to one particular group of B bits. Which particular group it is depends on the number representation used. There is considerable variety in this. By way of illustration, four common number representations for $B = 3$ are given in Table II. Some forms of quantization or overflow go better with one form of representation than with another. In practice there are distinct preferences for particular combinations.

The fact that binary words in digital systems always have a finite length results in a number of effects that we shall look at in more detail in the next section.

Before going on we should perhaps note that the common concept of analog-to-digital conversion (often abbreviated to A/D conversion) includes the combination of the CT/DT conversion from the sec-

tion headed 'From continuous time to discrete time and vice versa' and the conversion from continuous amplitude to discrete amplitude dealt with in this section.

Finite-word-length effects

In this section we shall look at three situations in which the finite word length is a significant factor. These are A/D conversion, digital filter design and the execution of digital computations.

A/D conversion

In converting a signal of continuous amplitude $x[n]$ into a signal of discrete amplitude $x_Q[n]$, we can proceed as if $x_Q[n]$ were obtained by adding the noisy signal $e[n] = x_Q[n] - x[n]$ to $x[n]$ (fig. 53). In this way we arrive at the useful concept of quantization noise. If we now consider specifically the case of quantization by rounding off with step size q , the power P_e of this noise is given by:

$$P_e = \frac{q^2}{12} \tag{81}$$

If we then also assume that the samples of $x_Q[n]$ are represented as words of B bits and that $x[n]$ is a sinusoidal signal with the largest possible amplitude before overflow can occur, we then find a signal/quantization noise ratio of

$$\frac{P_x}{P_e} = 6B + 1.76 \text{ (dB)} \tag{82}$$

in $x_Q[n]$. An important conclusion of generally validity can be drawn from this equation: any increase of the word length B by one bit improves the maximum achievable signal/quantization noise ratio by 6 dB.

Digital filter design

The procedures described earlier for designing discrete filters generally give very accurate values for the filter coefficients. In a practical digital filter, however, the number of bits used for representing the coefficients must be as small as possible, largely for reasons of cost. The values found must therefore be quantized. But this alters the characteristics of the filter [22], i.e. it changes the locations of the poles and zeros. These changes can be very substantial (fig. 54). It may happen that, after quantization, the filter no longer satisfies the design specifications that were used in calculating the unquantized coefficients. In extreme cases a stable filter may even become unstable, because a pole moves from a position inside the unit circle in the z -plane to a position outside it. However, the quantization of filter coefficients introduces no changes

in the linear operation of a circuit, nor does it cause any effects that depend on the input signal or that vary with time. It introduces no more than a once-only calculable change in the characteristics of the filter.

Some filter structures are much more sensitive to quantization of the coefficients than others. In general a filter structure becomes *less* sensitive as the location of each pole and each zero becomes dependent on *fewer* coefficients. This point has been mentioned briefly in the section 'Discrete filter structures'.

Another significant effect is that the possible positions for poles and zeros with quantized coefficients do not have to be uniformly distributed over the z -plane. This can vary considerably with the structure of the filter. If poles and zeros are required in regions where there are few, the quantization effects will be more pronounced. This is illustrated in fig. 55, which shows two simple purely recursive filters of the 2nd order, with the possible pole positions when the coefficients are quantized to four bits (one of them for the sign). Because of the symmetry only one quadrant of the z -plane is shown.

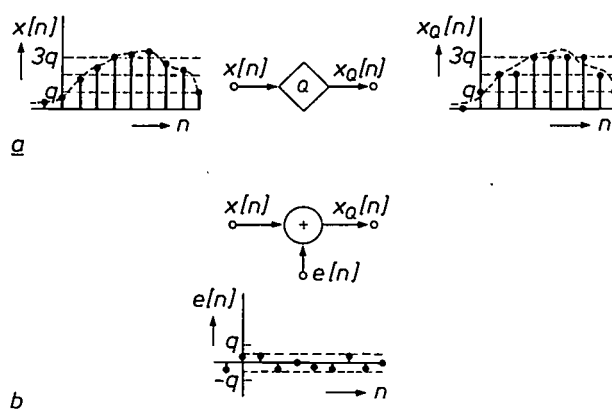


Fig. 53. a) Conversion of a signal of continuous amplitude $x[n]$ into a signal of discrete amplitude $x_Q[n]$ can be regarded as the addition of a noisy signal $e[n] = x_Q[n] - x[n]$. b) Equivalent circuit based on this.

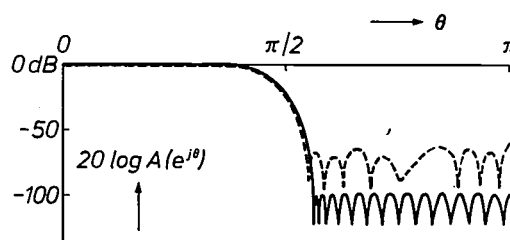


Fig. 54. Amplitude characteristic of a transversal filter (of length $N = 49$) with unquantized coefficients (continuous line) and coefficients rounded off to 12 bits (dashed line).

[22] V. B. Lawrence and A. C. Salazar, Finite precision design of linear-phase FIR filters, Bell Syst. Tech. J. 59, 1575-1598, 1980.

Digital computations

The most complicated consequences of working with a finite word length are found when limiting the word length of intermediate results in digital systems [23]. Just as in everyday calculations in the decimal system, addition and multiplication in the binary system often increase the number of digits required, i.e. the word length. With recursive filters, however, this inevitably introduces problems because the result of one calculation is the starting point of the next. See for example fig. 55a: if $y[n]$ and the coefficient a_2 both have a word length of 4 bits, this can give a result of 7 bits after multiplication. Calculation of the next input sample

speaking the filter is not linear. The most troublesome effects are usually due to overflow: signal distortion can then be very serious, and with recursive structures there may even be 'overflow oscillations' of very large amplitude. Filters are therefore generally designed so that this cannot happen or only happens very rarely. A widely used aid in this context is 'scaling', particularly for filters consisting of cascaded sections. In the design a multiplier by a constant factor (< 1) is inserted between the sections, to prevent the occurrence of overflow in the following section. If this factor is an integral negative power of 2, the multiplication only means a shift of the sample value by one or more

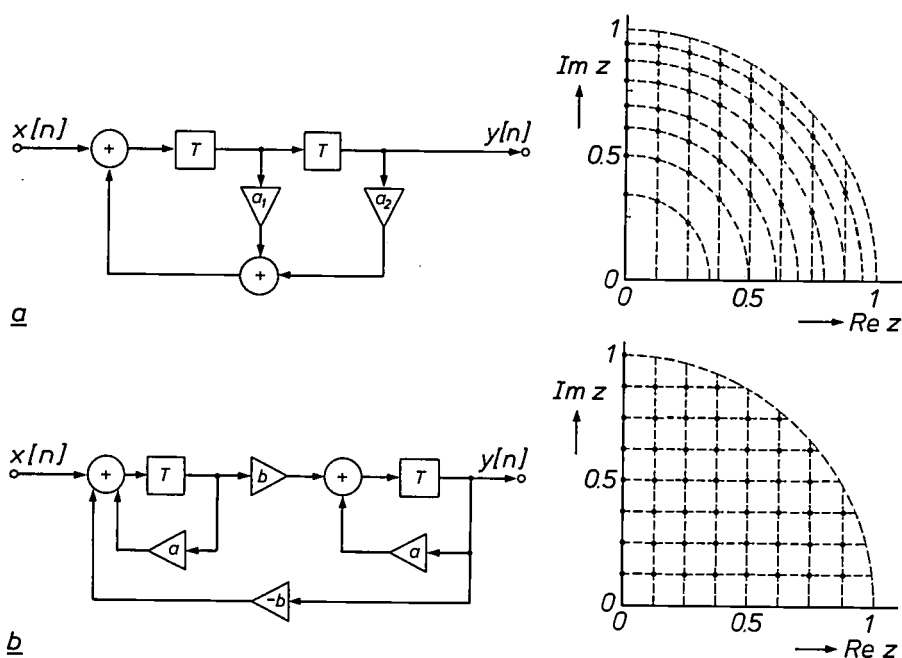


Fig. 55. a) Purely recursive 2nd-order filter with direct-form structure and realizable complex poles when the value of the filter coefficients a_1 and a_2 is expressed in terms of four bits (one bit is for the sign). Because of the symmetry, only one quadrant of the z -plane is shown. b) Purely recursive 2nd-order filter with coupled structure. In this structure the positions of the realizable complex poles are distributed quite differently over the z -plane for the same quantized coefficient values.

can then give an intermediate result of more bits again, then more again, and so on.

With recursive structures we are therefore forced to limit the word length of intermediate results. With non-recursive filters the increase in the word length is always finite, but even then some limitation may often be necessary. In principle we can still choose the form of quantization and overflow (or both) to be used, and whether it should be used at one or more places in the filter. This can have completely different effects on the operation of the filter.

The great problem in analysing word-length limitation of intermediate results rests in the fact that strictly

binary places. (In some cases scaling by a constant > 1 will be used, if it appears during the design that the most significant bits in the following section would otherwise remain unused.) After such measures have been taken, overflow does not have to be considered further. Then an attempt is usually made to get some idea of the effects due to quantization of the intermediate results in the filter output signal.

In the first place this gives rise to an unwanted 'noisy' signal, rather like the quantization noise in A/D conversion. This noise is generated at the quantizers and is filtered ('coloured') on its way to the output of the filter. To obtain quantitative results the

occurrence of this quantization noise is modelled in the same way as with A/D conversion: each quantizer is replaced by an additive noise source (fig. 56). The assumption is made that each source produces noise with a particular frequency spectrum (in the case of

we assume that $x[n] = 0$ for $n > 0$ and $y[0] = 7q$, we see that oscillations of period $N = 2$ and amplitude $5q$ appear in the output signal.

In recursive filter sections of higher order, limit cycles are a familiar problem, and they have to be

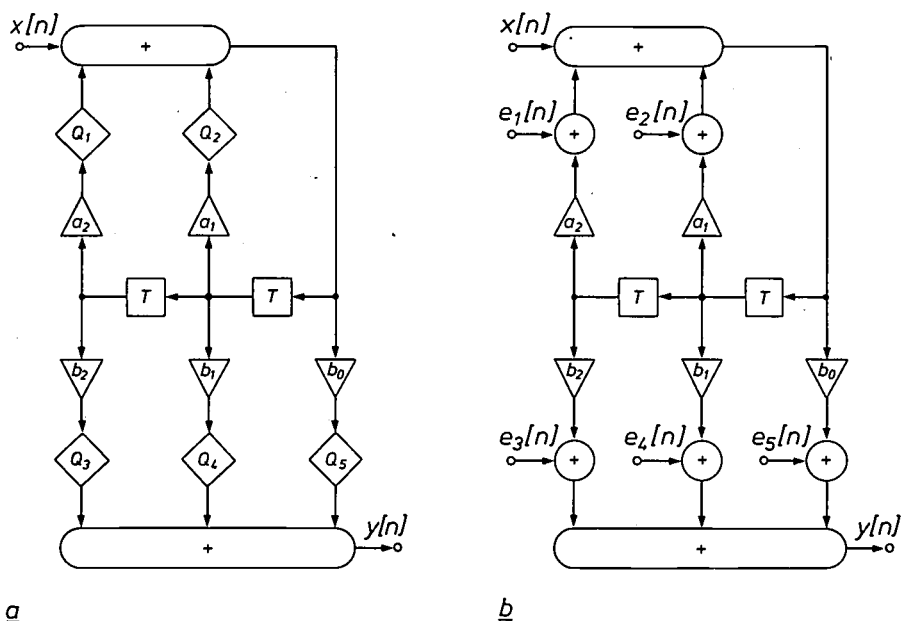
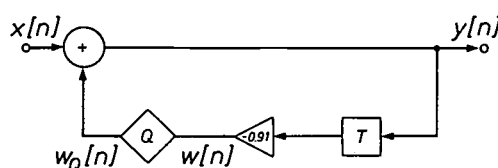


Fig. 56. a) Example of a digital filter in which the word length of the intermediate results is limited by the quantizers Q_1, \dots, Q_6 after each multiplication. b) To obtain an idea of the noise then produced in the output signal $y[n]$, a noise-source model is used: each quantizer is replaced by an imaginary additive noise source $e_1[n], \dots, e_6[n]$. If quantization is by rounding off with step size q , each source has a noise power of $q^2/12$ and a flat ('white') spectrum. The noise is then filtered with the frequency response encountered between a particular source and the output. In the filter shown here the noise contributions of $e_3[n], e_4[n]$ and $e_5[n]$ appear unfiltered at the output. The contributions from $e_1[n]$ and $e_2[n]$, on the other hand, are filtered in the same way as the input signal $x[n]$.

rounding off, the noise has a flat spectrum and a total power of $q^2/12$). The noise contribution at the output of the filter from each source can then be calculated.

Although this analysis with noise sources can produce very useful results, it is based on a number of assumptions that are usually not entirely correct and can sometimes even be quite wrong. This applies for example to the assumption that the noise contributions are independent of each other and independent of the useful signals in the filter. Provided the waveform of the input signal $x[n]$ is sufficiently irregular, the assumption is not unreasonable. This situation changes, however, if the value of the input signal is constant (or zero) over a longer period of time or is periodic. Periodic interference signals ('limit cycles') may then appear at the output. If for example $x[n]$ is a digitized speech signal, this may happen in the pauses in the conversation. But this is where periodic interfering signals, even at a very low level, are most annoying. A very simple example is shown in fig. 57, where the intermediate result is quantized by rounding off. If



n	$w[n] = -0.91 y[n-1]$	$y[n] = w_Q[n]$
0	...	$7q$
1	$-6.37q$	$-6q$
2	$5.46q$	$5q$
3	$-4.55q$	$-5q$
4	$4.55q$	$5q$
5	$-4.55q$	$-5q$
...
...

Fig. 57. In this simple model a limit cycle of period $N = 2$ and amplitude $5q$ arises when $x[n] = 0$ for $n > 0$ and $y[0] = 7q$. In quantizer Q there is rounding off with step size q .

[23] T. A. C. M. Claassen, W. F. G. Mecklenbräuer and J. B. H. Peek, Effects of quantization and overflow in recursive digital filters, IEEE Trans. ASSP-24, 517-529, 1976.

taken into account. It is found that quantization by means of magnitude truncation is not so liable to cause oscillation of this type as other forms of quantization. It is also useful to know that limit cycles are always confined to a number of the least significant bits. If we reduce the quantization step q of all the quantizers in a filter in which these cycles occur by increasing all the word lengths, then the amplitude of the limit cycle expressed in an absolute sense (e.g. as a voltage and not as a number of quantization steps) will also decrease. By then quantizing the output signal $y[n]$ we can make a filter that is *apparently* free from limit cycles.

Summary. In the theoretical aspects digital signal processing has two essential characteristics: all the processes take place in discrete time and all the quantities occurring in the processes are discrete in amplitude, i.e. they can only assume discrete values. Theoretical analyses relating to discrete time require special techniques, such as the Fourier transform for discrete signals (FTD), the z-transform (ZT), the discrete Fourier transform (DFT), the fast Fourier transform (FFT) and the use of difference equations, where the discrete-amplitude aspect is deliberately left out of consideration. With this approach, many parallels can be found between analog signal and system theory on the one hand and digital signal and system theory on the other. This means that existing analog design techniques (e.g. for filters) can be used as the starting point for the design of digital filters and systems. The transition from continuous time to discrete time and from continuous amplitude to discrete amplitude has much to offer (new system structures, changing of sampling rate) but also raises new problems (aliasing, instabilities, quantization noise). These problems form a separate branch of the theory of digital signal processing.

Polymer chemistry in the electrical industry

L. K. H. van Beek

From 1976 until his retirement in 1985 Dr L. K. H. van Beek was in charge of polymer research at Philips Research Laboratories in Eindhoven. In the article below he takes a number of illustrative examples to demonstrate the effectiveness of his chemical credo: 'Never be content with empiricism but keep on investigating until the reaction mechanism is completely explained'.

Introduction

Making polymer material insoluble

The electrical industry is one of the world's largest users of polymer materials. In Europe alone the consumption of polystyrene, polyvinyl chloride, polyethylene, polypropylene, etc., runs into billions of dollars. Vast quantities are used in the manufacture of protective casings for all kinds of equipment, not just for consumer products such as refrigerators, television sets and record players, but also for professional equipment such as computers and medical instruments. Polymer material is also used in large quantities for the sheathing of cables. The chemical industry can supply all these materials 'custom-made' to the specifications of the electrical industry.

In addition to these large-scale uses the electrical industry has innumerable other applications for polymer materials. The quantities may be often relatively small, so that the chemical industry will be disinclined to spend too heavily on research into these materials. Often, however, these are the very applications where the specifications for the materials are the most stringent. Important factors are chemical and thermal resistance in use and during manufacture ('pot life'), dimensional stability, modulus of elasticity and permeability to gases and liquids.

A recent example of an application of polymers where the research was carried out in the electrical industry is the LaserVision video disc [1][2]. Here the polymer disc must replicate faithfully from the matrix thousands of millions of pits 0.4 μm wide, 0.12 μm deep and between 0.5 and 2.0 μm long. Other examples are coatings for optical fibres [3] which are applied while the fibre is being drawn, and photoresist patterns on semiconductor surfaces [4].

In applications like these the initial material must be easy to process, whereas in its final form it often has to meet quite different and sometimes conflicting requirements.

In the range of specifications that polymer material in its final state must satisfy for all its various applications, there will usually be one that is regarded as fundamental: the material will be required to be highly resistant to external influences. Expressing this funda-

[1] See H. C. Haverkorn van Rijsewijk, P. E. J. Legierse and G. E. Thomas, *Philips Tech. Rev.* **40**, 287-297, 1982.

[2] See J. G. Kloosterboer, G. J. M. Lippits and H. C. Meinders, *Philips Tech. Rev.* **40**, 298-309, 1982.

[3] See H. M. J. M. van Ass, P. Geittner, R. G. Gossink, D. Küppers and P. J. W. Severin, *Philips Tech. Rev.* **36**, 182-189, 1976.

[4] See E. D. Roberts, *Philips Tech. Rev.* **35**, 41-52, 1975; J. C. Jagt and P. W. Whipps, *Philips Tech. Rev.* **39**, 346-352, 1980;

H. Lüthje, *Philips Tech. Rev.* **41**, 150-163, 1983/84.

mental requirement more in terms of manufacturing technology, the polymer material should at the least be made insoluble after the preliminary processing stages [5].

The principal ways of making a polymer insoluble are 'modification', 'physical cross-linking' and 'chemical cross-linking'.

Modification is usually achieved by using a suitable reagent to increase the size of the molecule or to change its chemical character in such a way as to radically reduce its solubility in certain solvents. A reaction of this kind can be initiated by heat or by radiation. Another approach is to make the surface of the polymer material inaccessible to certain solvents by 'grafting' a suitable reagent.

Physical cross-linking is an effect on which no consensus yet exists; we shall consider it briefly. We define physical cross-linking of polymer molecules as an effect that is brought about by intermolecular forces, such as electrostatic and Van der Waals forces or hydrogen bonds. This definition includes the physical cross-linking that occurs in branched polyethylene on crystallite formation, in thermoplastic elastomers, which are reversibly converted from a physically cross-linked elastic state into a plastic state on changing the temperature, and in polymer 'blends' that are stabilized by physical forces between side groups. A separate category is that of the polymer-polymer complex-formers, where two different polymers form a network because groups of physical bonds in 'ladder' blocks provide stable cross-linkage points. We shall later consider an example of the latter mode of physical cross-linking in the form of a negative photoresist.

Chemical cross-linking can be achieved by two methods, usually depending on heat or radiation. The first method is based on *monomers* or *oligomers* (consisting of a few monomers), which possess various reactive groups. The photo-initiated radical polymerization of acrylates described earlier in this journal [2] provides an example. The second method is based on linear *polymer* molecules possessing reactive positions along the chain. These positions can react with a substance, usually one of low molecular weight that has more than one reactive group (cross-linking agents). These agents have the effect of linking the separate polymer chains. In the rubber industry the method is called 'vulcanization'.

It is obvious that these methods of making polymers insoluble require a thorough knowledge of the reaction mechanism. In practice, chemical cross-linking is often accelerated by the addition of catalysts. Their operation needs to be thoroughly understood. Because of the demands that will be made on the end-product it is also necessary to understand how the

properties of the end-product will be affected by the molecular structure of the 'building blocks' — monomers, oligomers, polymers, cross-linking agents or other additives — and by the way they are linked together. For example, flexible building blocks will result in a rubbery end-product, a high degree of cross-linking will make it more brittle, and the introduction of aromatic groups into the building blocks will give a higher refractive index. Only by taking account of effects such as these can material with the required properties be produced.

In the four sections that follow the various methods of making a polymer insoluble will be discussed, with reference to new applications in the electrical industry, especially at Philips. In all four examples the application only became possible through a good understanding of the reaction mechanism.

We begin with two examples of a category of materials whose function depends essentially on the extent to which their solubility (or 'developability') can be varied: photoresists.

A negative photoresist must be less soluble after exposure, a positive photoresist must be more soluble [6]. The solubility can be *reduced* by enlarging the molecular structure of the original material to form linear chains or three-dimensional networks. It can be *increased* by the opposite process: breaking the bonds by exposure to illumination; but this is not the only method, nor even the most widely used one. The positive photoresist most frequently used today has a special low-molecular-weight compound added to the polymer material (the binder) whose chemical nature can be changed by illumination — e.g. from hydrophobic to hydrophilic. We shall first consider the example where use is made of the reactions of the polymer in a *positive* photoresist, and in the section that follows we shall give an example of a polymer material acting as a *negative* resist.

A photolithographic method for varying the profile of the patterns

An example of modification

Integrated circuits are made by lithographic processes [4][7], usually in a succession of stages, with each successive stage on a substrate on which a pattern is already present. Since the projected illumination generally used produces a conical exposure profile in the layer of resist, the patterns formed after development will usually have side walls that are not perpendicular but slope so that lines broaden towards the base (*fig. 1a*). This broadening is an unwanted effect, of course, which becomes more inconvenient as the number of lithographic process stages required in-

creases. It also becomes more inconvenient as the spacings in the patterns become smaller, as is indeed required in advanced integrated circuits.

F. A. Vollenbroek, E. J. Spiertz and H. J. J. Kroon of Philips Research Laboratories have developed a photolithographic method in which the slope in the profile of the pattern can be varied as required [8]. This method will not only give vertical profiles if desired but can also provide the overhanging profiles required when the patterns are removed later by the 'lift-off' method.

The positive photoresist most commonly used nowadays is based on a novolac (a linear cresol-formaldehyde polymer) combined with an *o*-naphthoquinone diazide (fig. 1*b*). These two substances are dissolved in a volatile solvent. Additives are sometimes introduced

in an aqueous alkaline developer the exposed areas are dissolved faster than the unexposed areas.

Let us now take a closer look at the reaction mechanism responsible for the positive action of the resist. The photochemical reaction, shown in fig. 1*c*, in which the *o*-naphthoquinone diazide is converted into an indenecarboxylic acid, was discovered by O. Süss [9] in 1944. The hypothesis that a ketene was an intermediate product had also been put forward at that time, but Süss was unable to isolate this ketene, and thus prove the hypothesis. It was not until later that the correct chemical structure of the acid (3-indenecarboxylic acid) was established.

Some time ago J. Pacanski and J. R. Lyerla made a new study of the reaction mechanism of this lithographic process with the aid of infrared and nuclear-

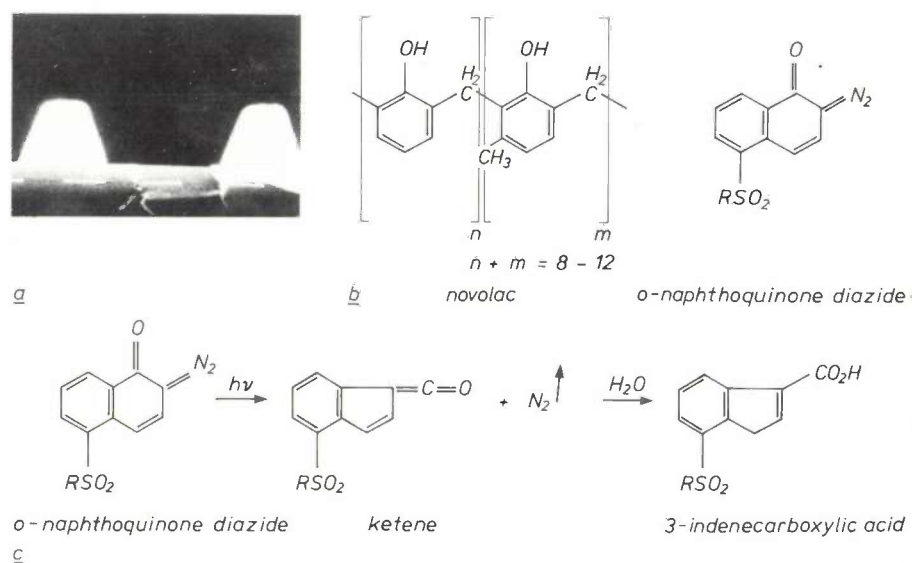


Fig. 1. *a*) SEM photographs of a resist pattern produced by a standard procedure with a polymer novolac as binder and an *o*-naphthoquinone diazide (or — IUPAC-approved name — 1-oxo-2-diazo-naphthalene) as the photosensitive agent [8]. The dashes are 1 μm long. *b*) The chemical formulae of the constituents used: novolac (left) and *o*-naphthoquinone diazide (R is usually a derivative of hydroxybenzophenone). *c*) The photochemical reaction for the positive action of this photoresist. The polymer binder in combination with the 3-indenecarboxylic acid formed is more readily soluble in an alkaline developer than in combination with the photosensitive component *o*-naphthoquinone diazide.

to improve properties such as the adhesion to the silicon substrate.

The photoresist solution is distributed over the silicon wafer by spinning and gently heated until a thin dry film is formed. For the spinning operation to be successful the novolac must not have a high molecular weight, or the solution may be too viscous.

The exposure can be made with illumination from a high-pressure mercury-vapour lamp in the wavelength range between 360 and 435 nm. The positive action of the resultant resist depends on the conversion of the hydrophobic *o*-naphthoquinone diazide into a hydrophilic acid during the exposure, so that after treat-

[8] More general information on polymer chemistry can be found in:

P. J. Flory, Principles of polymer chemistry, 9th printing, Cornell University Press, Ithaca, NY, 1975;

D. J. Williams, Polymer science and engineering, Prentice-Hall, Englewood Cliffs, NJ, 1971;

F. W. Billmeyer, Jr., Textbook of polymer science, 3rd edition, Wiley, New York 1984;

G. Odian, Principles of polymerization, 2nd edition, Wiley, New York 1981.

[9] In fact it is really the rate of solution that is increased in a positive photoresist.

[7] The fabrication of integrated circuits is discussed in: H. Bosma and W. G. Gelling, Philips Tech. Rev. 37, 267-277, 1977;

A. N. Broers, IEEE Trans. ED-28, 1268-1278, 1981.

[8] F. A. Vollenbroek, E. J. Spiertz and H. J. J. Kroon, Polymer Eng. & Sci. 23, 925-930, 1983.

[9] O. Süss, Ann. Chem. 556, 65-84, 1944.

magnetic-resonance spectroscopy^[10]. They also varied the reaction environment. In a water-free environment (vacuum) it was found that the 3-indenecarboxylic acid did not occur. In the absence of water, and at the relatively low temperature of 77 K, it was possible for the first time to isolate and identify the hypothetical intermediate product (the ketene in fig. 1c). The 3-indenecarboxylic acid is formed — in a fast reaction — only after a little water is admitted into the reaction environment. In a subsequent series of experiments, in which the polymer novolac itself was added, it was found that, if the temperature is allowed to rise to room temperature in water-free conditions, the ketene forms ester bonds with the hydroxyl groups of the novolac (fig. 2).

The improved understanding of the reaction mechanism for this lithographic process gave the researchers the idea that it might be possible to use it to improve the quality of the patterns. For if the 'image' exposure in normal atmospheric conditions is followed by a uniform 'flood' exposure in vacuum, the less-soluble area of resist will become even less soluble in the alkaline developer as a consequence of the esterification of the novolac with the ketene. (The second, uniform exposure does not have such an effect in the part of the resist exposed earlier since all the ketene has then already been converted into 3-indenecarboxylic acid, which is not capable of such esterification.)

It is not such an easy task to expose a silicon wafer in vacuum. Vollenbroek, Spiertz and Kroon therefore

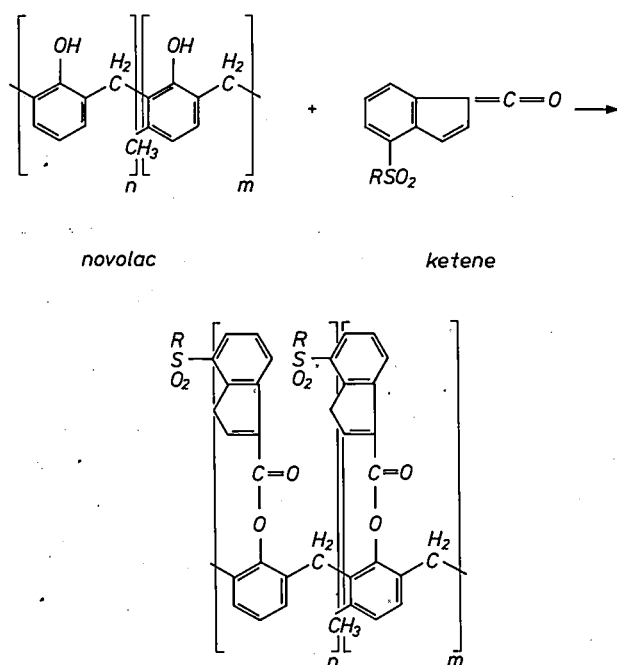


Fig. 2. Reaction of the photoresist system in fig. 1 in water-free conditions.

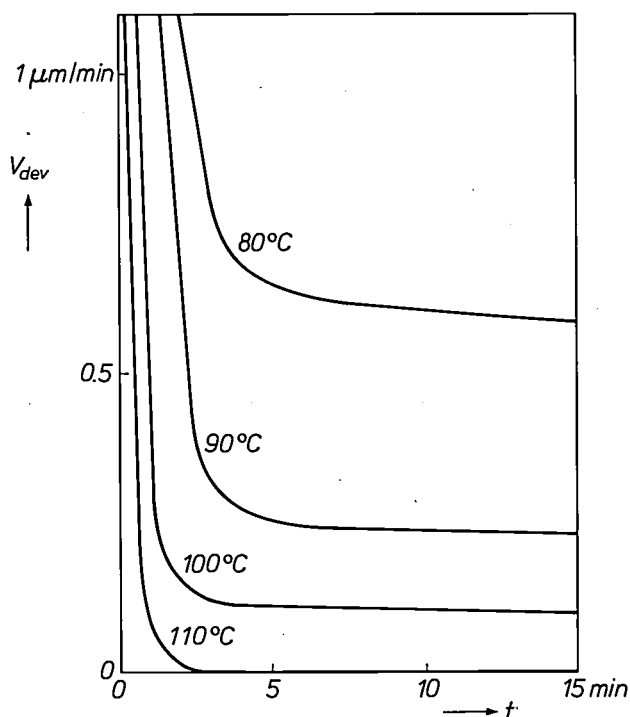


Fig. 3. 'Developability' V_{dev} of the photoresist system in fig. 1 as a function of time t after illumination at 1 atm pressure and at the temperatures 80, 90, 100 and 110 °C.

wondered, when they started investigating this process at our Laboratories, whether it might not be easier to obtain the required water-free conditions in other ways, e.g. by subjecting the wafer to a high temperature, above 100 °C, during the exposure^[8].

They therefore first investigated the behaviour at this high temperature of the least stable compound of the system, the *o*-naphthoquinone diazide. Within the short time that this substance was subjected to this high temperature, it was found to dissociate to only a slight extent: after 30 min at 110 °C its action was 75% unaffected, and after 5 min at this temperature its action was 98% unaffected.

The simplification of the process that Vollenbroek, Spiertz and Kroon were trying to achieve gave excellent results. As can be seen in fig. 3, operation at a temperature of 110 °C — instead of in vacuum — produces the desired reduction in the developability of the exposed areas of resist within two minutes. At this temperature the developability may even fall to zero: this is attributable to the ester bonds between the ketene and the novolac. It can also be seen in fig. 3 that if temperatures lower than 110 °C are applied, a certain degree of solubility remains. It seems that in these conditions small quantities of 3-indenecarboxylic acid are formed as a consequence of residual small concentrations of water.

Vollenbroek, Spiertz and Kroon now came upon the idea, following on from this method of varying the

solubility, of using a second means of varying it, i.e. the wavelength of the radiation. With these two means of variation — and this is the new feature of their method — they can adjust the profile angle of the patterns.

In their method, following the pattern exposure at room temperature, they subjected the wafer to *two*

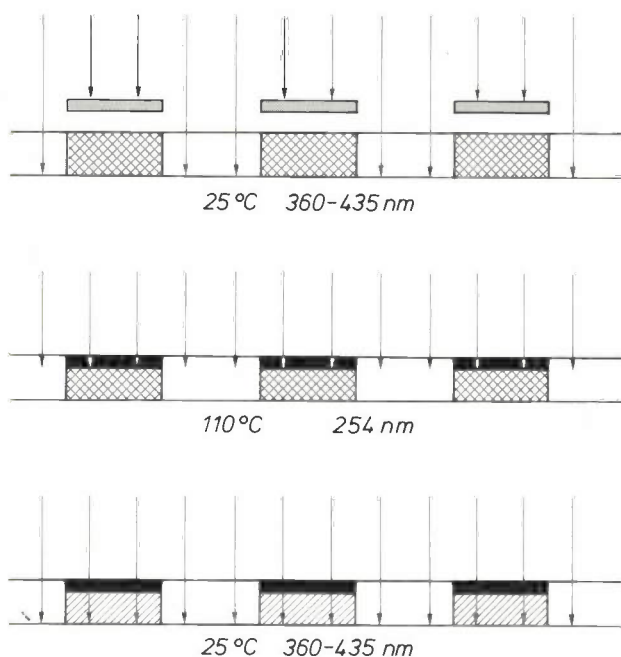


Fig. 4. Schematic illustration of the three exposures in our method of profile modification. Grey: mask. White: readily soluble owing to complete conversion of *o*-naphthoquinone diazide into 3-indenecarboxylic acid. Double hatching: not readily soluble because this conversion has not taken place. Single hatching: moderate solubility owing to partial conversion. Black: insoluble owing to esterification.

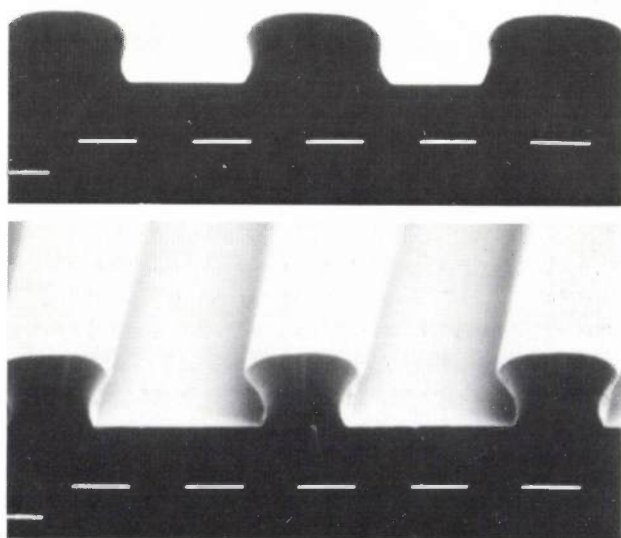


Fig. 5. SEM photographs of resist patterns with vertical (*above*) and overhanging profiles. Experimental details are given in [8].

flood exposures, the first at a temperature of 110 °C using a wavelength of 254 nm, in the near ultraviolet, and the second of variable duration at room temperature with the usual wavelengths (much longer) of the high-pressure mercury-vapour lamp (*fig. 4*) [8].

The wavelength of 254 nm was chosen because light at this wavelength (which is also capable of converting *o*-naphthoquinone diazide into ketene) is strongly absorbed by the novolac. Consequently, during the first flood exposure, all the *o*-naphthoquinone diazide is converted into ketene only in a thin upper layer of the pattern, and therefore it is only here that an insoluble ester is formed. The second flood exposure only has an effect in the layer *beneath* this insoluble upper layer, where of course intact *o*-naphthoquinone diazide is still present. Since the second exposure is also made at room temperature, and hence in the presence of moisture, 3-indenecarboxylic acid is again formed here, and in proportion to the length of the second flood exposure.

In this way the developability of the resist can be varied over the depth of the pattern, and hence the slope of the profile.

Fig. 5 shows some of the results obtained with our method.

A photolithographic method for obtaining permanent stable patterns

An example of physical cross-linking

Whereas the patterns produced by means of photoresists only have to give temporary protection and must be easily removable, for many other applications permanent stable patterns are required.

Materials that appear suitable for such applications are polyimides (*fig. 6*); these are thermally stable heterocyclic polymers that can be used in continuous exposure to air at 250 °C and even for a short time at 500 °C. They have exceptionally constant mechanical and electrical properties in a very wide temperature range (from -150 °C to +300 °C). They are also resistant to organic solvents and radiation.

Another interesting feature of polyimides is that, as a prepolymer, the polyamic acid, they can be applied from a solution by the usual methods, and the insoluble polyimide is then formed by heating (*fig. 6*). This means of course that they are applied in uniform layers and not as various patterns.

This material could perhaps be made suitable for photolithographic methods by reacting photosensitive compounds with the carboxyl groups of the polyamic acid. For example, a methacrylate might be chemically

[10] J. Pacansky and J. R. Lyerla, IBM J. Res. & Dev. 23, 42-55, 1979.

bonded to the polyamic acid in this way, since methacrylates are polymerized after the exposure of an added photo-initiator as described previously in this journal [2]. After the exposure an insoluble product is indeed attained — and hence a developable pattern —

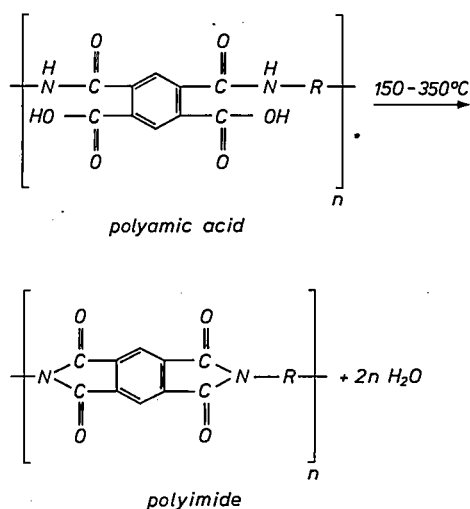


Fig. 6. Reaction for the formation of the insoluble polyimide from the soluble polyamic acid.

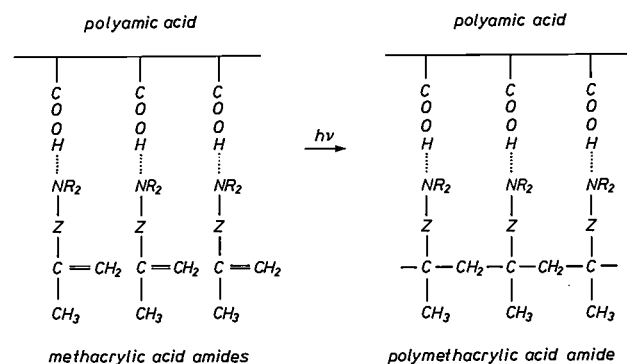


Fig. 7. Methacrylic acid amides, forming a complex with the polyamic acid, undergo a polymerization reaction on exposure. (R is an alkyl group; Z is CONHR', where R' is an alkylene group.) The physical bonds are indicated by dotted lines. See also fig. 10.

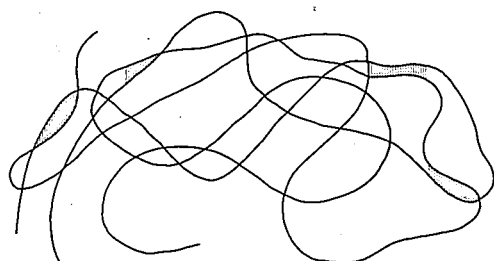


Fig. 8. Illustrating the formation of complexes between different polymer molecules via complex bonds formed by hydrogen bonds, electrostatic forces etc., in ladder blocks.

but it does not appear to be possible to convert this product into the required stable polymer by heating it; under these conditions the main chain of the polyamic acid degrades before the attached groups split off.

This fact therefore seems to point the way to a different approach, in which no groups are attached to the polyamic acid and an attempt is made to use light to generate a second polymer in addition to and distinct from the polyamic acid. The original material here could be methyl methacrylate. This approach does not however give an exposure product that differs sufficiently in solubility from the unexposed product to permit the development of the exposed pattern.

These findings prompted L. Minnema and J. M. van der Zande of our Laboratories to see whether the second polymer, formed by the exposure, might be linked to the polyamic acid by electrostatic forces between side groups of both polymers, as in the formation of polymer-polymer complexes mentioned in the introduction [11].

The method used by Minnema and Van der Zande consists in generating this polymer-polymer complex by exposure and polymerization, producing a great difference in solubility between the exposed and unexposed parts of the material — so that the pattern becomes developable — and subsequently removing the linking electrostatic interaction by increasing the temperature.

A typical monomer chosen for their method was N-(dimethylaminopropyl)-methacrylamide (DMAPMA). This was added to the polyamic acid in a quantity corresponding to the concentration of carboxyl groups in the polyamic acid. The desired electrostatic interaction now occurs between the carboxyl groups of the polyamic acid and the dimethylamino groups of DMAPMA (fig. 7). When the monomer is polymerized by photo-initiation, a second polymer forms (a polymethacrylamide) that is separate from the neighbouring polyamic-acid chains at many locations because of its own thermal motion. Where groups of neighbouring bonds are clustered together, however, they reinforce one another in 'ladder' blocks, which are the polymer-polymer complex formers referred to (fig. 8). A characteristic of polymer-polymer complex formation is that the ladder blocks disintegrate upon heating within a small temperature interval, e.g. between 120 and 150 °C [12].

After development of the layer of resist the pattern is baked at 350 °C. In the process the two polymers become detached from each other as described above. Between 200 and 250 °C the polymethacrylamide dissociates into its monomer building blocks by a mechanism known as 'unzipping' (fig. 9) [13]; this feature of methacrylates was of course one of the reasons why

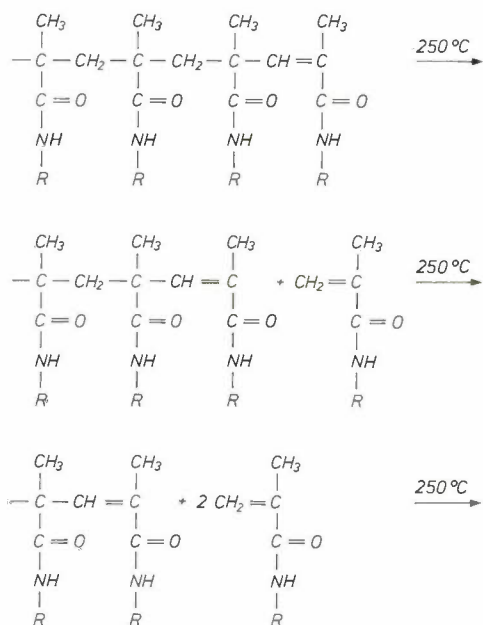


Fig. 9. Progress of the depolymerization, a kind of 'unzipping', of a polymethacrylamide^[13]. R is hydrogen or a substituted or unsubstituted alkyl group.

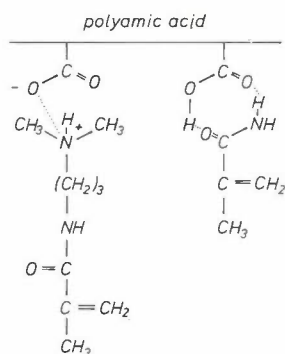


Fig. 10. Two possible complex bonds of polyamic acid: by salt formation with N,N'-dimethylaminopropylmethacrylic acid amide (left: see also fig. 7) and by the formation of hydrogen bonds with methacrylic acid amide.

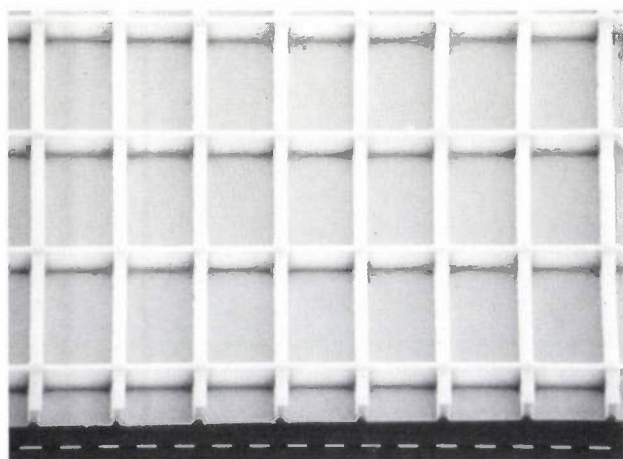


Fig. 11. Raster of polyimide for a display panel^[11] made by the Minnema and Van der Zande method. The dashes represent a length of 10 μm .

they were chosen for this purpose. These monomer building blocks evaporate and the polyamic acid left behind is converted into polyimide by the reaction of fig. 6.

A disadvantage of the photoresist in the composition described here is that the thickness of the layer of resist decreases by about 50% during the baking. Some of the DMAPMA was therefore replaced by a smaller monomer, such as methacrylamide. This monomer is not combined electrostatically to the carboxyl groups, but much more loosely, by hydrogen bonds (fig. 10). The reduction in volume after baking is indeed less. It is surprising that as much as 75% of the DMAPMA can be replaced by methacrylamide without causing any deterioration in the properties of the photoresist. The volume reduction during baking can therefore be limited to 30%.

The polyimide resist described here has the further advantage that it can be prepared from commercial polyamic acids, so that the resist can be modified for different applications. Further modification of the resist is available from the choice of the monomers used.

Fig. 11 shows a grid pattern obtained by applying the above method in a display panel^[14]. The grid consists of a crossbar arrangement in which the bars are 6 μm wide and 12 μm high.

Catalysis of the vulcanization of silicone rubbers

An example of chemical cross-linking by heat

Silicone rubbers are very useful for the encapsulation of solar cells. They are applied as low-viscosity fluids and then vulcanized at room temperature. The resultant chemical cross-linking gives the material good heat resistance as well as the required optical and mechanical properties over a wide temperature range.

In practice, however, the manufacturing process is not always entirely reproducible. The reason for this was discovered by F. W. van der Weij from an investigation of the catalysis of the vulcanization reaction^[15].

The silicone rubbers used for this purpose consist of two main components: α -hydrogen- ω -hydroxy-poly(dimethyl siloxane) and a polyfunctional alkoxy silane, such as tetra-ethoxy silane (fig. 12). In the vulcanization reaction, during which ethanol is released,

[11] L. Minnema and J. M. van der Zande, 30th IUPAC Int. Symp. on Macromolecules, The Hague 1985 (to be published).
 [12] L. Minnema and J. M. van der Zande, in: K. L. Mittal (ed.), Polyimides, Vol. 1, Plenum, New York 1984, pp. 589-598.
 [13] See H. I. Bolker, Natural and synthetic polymers, Dekker, New York 1974.
 [14] P. Mürrau and B. Singer, J. Appl. Phys. 49, 4820-4829, 1978.
 [15] F. W. van der Weij, Makromol. Chem. 181, 2541-2548, 1980.

In view of this chain of partial reactions it is clear that fluctuations in atmospheric moisture can cause variations in the concentration of the catalyst, which is formed only in the presence of water, as can be seen from the equation in fig. 14a. This effect becomes worse as thicker layers of rubber have to be cured. The better understanding thus obtained of the reaction mechanism of the catalysis made it possible to propose improvements in the manufacturing process that ensured reproducibility of the production.

Polysiloxane acrylates for protective coatings for optical fibres

An example of chemical cross-linking by radiation

Optical fibres are drawn at rates of between 60 and 90 m/min, but trials are already being carried out at rates of 300-600 m/min. Immediately after drawing, and before it is removed from the production line, the fibre is coated as quickly as possible with a primary protective layer to keep out harmful atmospheric effects. The fibres are then given other protective coatings, of the kind usually applied to cables that are required to give trouble-free operation for many years.

In this section we shall confine ourselves to the primary protective coating and we shall assume that it has to be applied at a drawing rate of 300 m/min. This means that the coating must be applied and cured within 0.1 s.

There are various other requirements to be met by such a protective coating. For example, the layer should have the properties of a relatively soft rubber, with a modulus of elasticity less than 5 MPa. A rubber as soft as this can reduce the optical losses caused by microbending of the fibre due to lateral forces. The coating must also remain rubbery over the entire temperature interval to which the fibre is exposed during operation, which is from -50 to $+80$ °C. This means that the rubbery material should not reach the glass-rubber transition point, where it becomes glass-like, until the temperature goes below -50 °C. Other requirements are that the layer must be capable of withstanding the extrusion of a secondary protective coating around it, and that the refractive index must be higher than 1.48 (higher than that of the outermost layers of the glass fibre, so that light scattered from the fibre can be dispersed via the primary protective coating [31][18]).

The requirement for curing within 0.1 s can in fact only be met by the acrylates mentioned earlier, which are very rapidly polymerized under ultraviolet light with the use of a photo-initiator [2]. The elasticity modulus of conventional acrylates, however, rises too rapidly below room temperature. This prompted

Table I. Comparison of the advantages and disadvantages of three different polymer coatings for optical fibres.

	Epoxy and urethane acrylates	Poly(dimethyl siloxane) rubbers	Poly(methylphenyl siloxane) rubbers
Ease of application (e.g. wetting behaviour)	-	+	-
Pot life and curing rate	+	-	-
Elasticity modulus at room temp.	+ -	+	+
Glass-rubber transition temperature	-	++	-
Strength & abrasion resistance	+	+ -	?
Thermo-stability	+ -	++	++
Refractive index	+ -	-	+
Ease of removal	-	+	+
Absorption of short-wave UV	+	-	+

D. J. Broer and G. N. Mol of Philips Research Laboratories to work on new types of acrylates that are more capable of fulfilling the requirements [19].

In Table I the properties of the widely used epoxy and urethane acrylates are compared with those of two rubbery materials, poly(dimethyl siloxane) rubber and poly(methylphenyl siloxane) rubber, which are of interest here because of properties other than the curing rate. Most of the criteria in the table speak for themselves, except perhaps the last two. The ease of removal is connected with the later operations on the glass fibres, such as splicing the ends after local removal of the protective coating [20]. The absorption of short-wave UV (below 300 nm) should be sufficiently high to avoid radiation damage to the silica of the fibre.

Table I shows that the properties of these three types of polymer complement one another ideally for this application. This led to the idea of trying to com-

[16] V. V. Severnyi, R. M. Minas'yan, I. A. Makarenko and N. M. Bizyukova, *Polymer Sci. USSR* **18**, 1464-1471, 1976.

[17] See J. March, *Advanced organic chemistry: reactions, mechanisms, and structure*, 2nd edition, McGraw-Hill Kogakusha, Tokyo 1977, pp. 485 and 488.

[18] See K. Mouthaan, *Philips Tech. Rev.* **36**, 178-182, 1976.

[19] D. J. Broer and G. N. Mol, *Conf. Proc. Integration of fundamental polymer science and technology*, Rolduc 1985 (to be published).

[20] See A. J. J. Franken, G. D. Khoe, J. Renkens and C. J. G. Verwer, *Philips Tech. Rev.* **38**, 158-159, 1978/79.

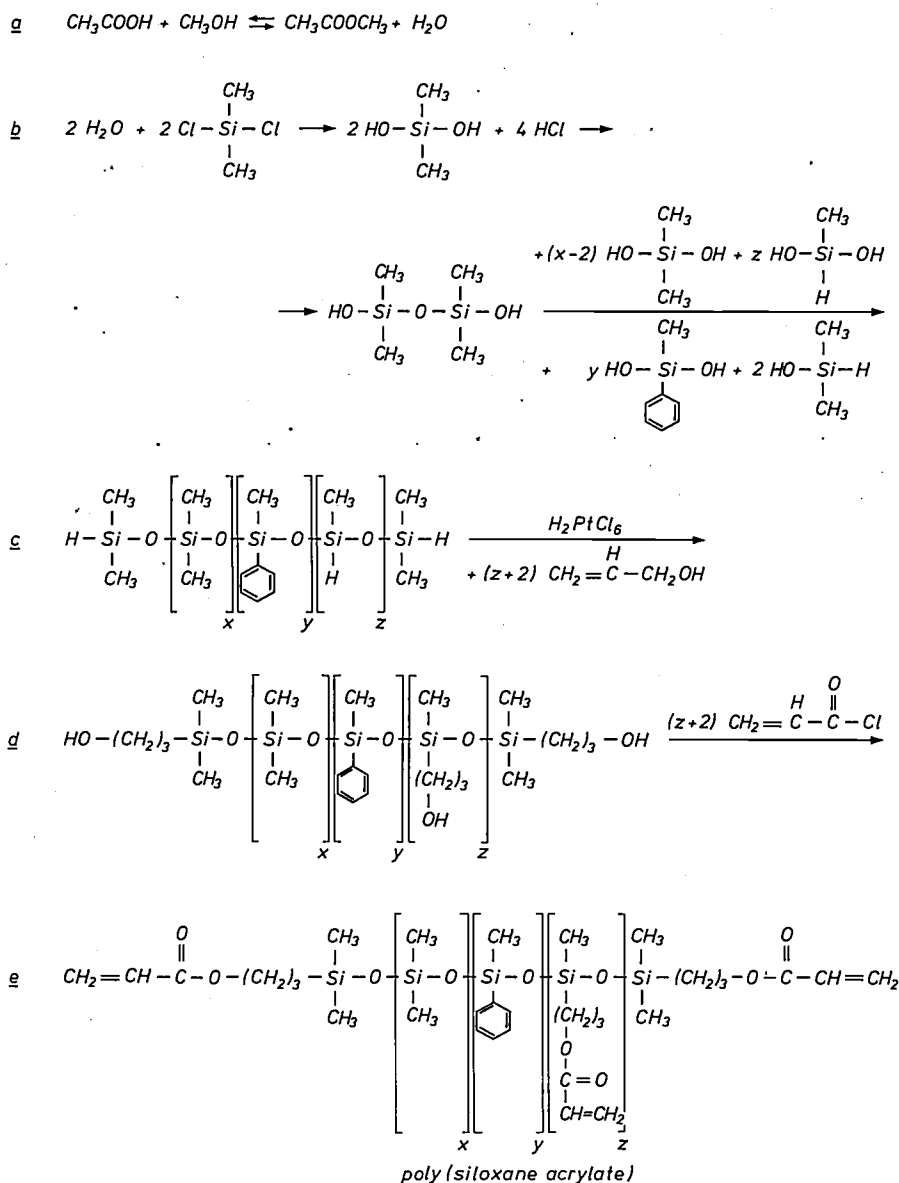


Fig. 15. The synthesis of poly(siloxane acrylate).

bine the properties of the three types of polymer in a single copolymer, in which the various building blocks would be arbitrarily distributed among the chain molecules.

Putting this idea into practice was not so easy. It was necessary to depart from the usual methods of synthesis to start with chlorine-substituted alkyl and phenyl silanes, which had to be hydrolysed and then linked together to form polysiloxane rubbers (fig. 15).

The dimer product of fig. 15b can grow into a polymer through continuous reactions with other monomers or with oligomers that have formed in the meantime. The building blocks selected for this purpose are the hydrolysis products of $Cl_2Si(CH_3)_2$, $Cl_2Si(C_6H_5)CH_3$ and $Cl_2Si(CH_3)H$, and for the end groups the hydrol-

ysis product of $ClSi(CH_3)_2H$. Incorporation of the first two compounds results in the combined properties of poly(dimethyl siloxane) and poly(methylphenyl siloxane) rubbers (see the two last columns of Table I). This is because the first building block, with its two methyl groups, helps to lower the glass-rubber transition temperature, while the aromatic phenyl group of the second building block contributes towards an increase in the refractive index. The hydrolysis products of $Cl_2Si(CH_3)H$ and $ClSi(CH_3)_2H$, with their H atom, provide points of attachment for vinyl groups to be added later. With this method of synthesis the different building blocks are not distributed along the chain in groups or blocks but presumably more or less at random.

The reaction is controlled by introducing the water into the reaction mixture in carefully controlled doses, achieved by releasing the water during the esterification reaction between acetic acid and methanol (fig. 15*a*). The initial ingredients are first dissolved in acetic acid, and methanol is then added gradually.

The polysiloxane chain formed in this way, shown in fig. 15*c*, is next prepared for photo-initiated radical polymerization by the substitution of a few vinyl groups. This is done in two stages, which have been known for some time. In the first stage the H atoms directly linked to Si are replaced by $\text{HO}(\text{CH}_2)_3$ groups in a reaction with $\text{CH}_2=\text{CHCH}_2\text{OH}$ catalysed by H_2PtCl_6 (fig. 15*d*). In the second stage the $\text{HO}(\text{CH}_2)_3$ groups are converted into $\text{CH}_2=\text{CHCOO}(\text{CH}_2)_3$ by a reaction with $\text{CH}_2=\text{CHCOCl}$ (fig. 15*e*). The resultant poly(siloxane acrylate) has the property mentioned earlier that when a photo-initiator is added chemical cross-linking takes place very rapidly under UV irradiation through the polymerization of radicals.

By varying the ratio x/y in fig. 15*e* (dimethyl siloxane/methylphenyl siloxane) it is possible to control the optical, thermal and rheological properties of the copolymer. To achieve the optimum rheological behaviour and the lowest possible glass-rubber transition temperature the factor x/y should have a high value. On the other hand a fairly high refractive index of 1.50 is required, which implies that x/y cannot be higher than 1. The x/y ratio must also be reduced further to make the solubility of the photo-initiator sufficiently high. After all this was taken into consideration, a poly(siloxane acrylate) was obtained that

possessed good properties with $x/y = 0.63$, where $x + y = 96$. The glass-rubber transition temperature of the protective coating made with this product is -60°C .

The factor z , which indicates the fraction of the attached vinyl groups, is used for controlling the rate of polymerization and the mechanical properties. A higher z obviously gives a higher degree of cross-linking and hence greater mechanical strength, but it also increases the modulus of elasticity, which is undesirable. The optimum lies at $z/(x + y + z) = 0.04$. The time of exposure for curing with a high-intensity mercury lamp is then less than 0.1 s. The modulus of elasticity of the cured protective coating is 1 MPa, which is well below the specified maximum value (less than 5 MPa).

Summary. In the electrical industry polymer materials are used for many highly specialized applications, such as protective photoresist patterns in IC production and coatings on optical fibres. A basic requirement for the end-product is that it must be resistant to external influences, which at the very least implies insolubility. To achieve this, the chain molecules are modified by a reaction with groups that are not readily soluble and especially by physical and chemical cross-linking. Four applications are discussed in which four different ways of making polymer material insoluble were used and in which success came from a good understanding of the reaction mechanism: a photolithographic method in which the profile can be varied, a photolithographic method for making stable patterns from polyimides, a reproducible method of manufacturing a particular silicone rubber, and the synthesis of a new material for a primary protective coating on optical fibres.

Introducing a new feature: '50 years ago'

On 1st January 1986 this journal was 50 years old, and the 50th birthday made the editors think of the idea of a feature based on excerpts from the early articles. Is this a nostalgia for a simpler age? Let us not delude ourselves about that simplicity: the latest results of science and technology seemed just as complicated in those days as they do now, if only because unfamiliar subjects and phenomena have always been perceived as complicated. Perhaps this is why the progress of science and technology has always gone hand in hand with both anxiety and fascination.

If indeed we are not so very different from the people of those days, we shall be able to reflect in this new feature on their attempts to master new technology, and we can share in scientific adventures that led to inventions such as television, synthetic resins, the Philips-Müller system, optical telephony, and so on.

The editors would also like to mark the fact that Philips Technical Review is 50 years old by bringing out an anniversary issue. This issue will treat a number of subjects from fields in which Philips has been active during this period, making a not insignificant contribution to science and technology. We intend to publish this issue in the summer of 1986.

Philips Technical Review 50 years ago

INTRODUCTION

With the appearance of the first issue of this new periodical, the policy and aims should be outlined which will be pursued in these pages. The Philips Research Laboratories are continually receiving an ever-increasing number of enquiries and requests from many quarters for more detailed data and particulars of the extensive range of Philips products, and especially for information as to their specific characteristics and practical applications. A large proportion of these enquiries comes from the engineering world and it is hoped by means of this periodical to establish permanent contact with these circles.

Each contribution to this periodical will be, as far as possible, complete in itself. Owing to the wide range of products manufactured by Philips every article cannot be expected to command the same measure of interest from every reader. Nevertheless, it may be expected that many readers will find matter of interest also in those contributions which do not concern their own immediate activities.

This periodical therefore will be not merely a journal embracing the activities of the Philips organisation nor a technical journal on popular lines, but a source of information of value and interest to the whole engineering profession. Our hope is that this publication will prove of practical interest and use to many, and in consequence merit a wide circle of readers.

JANUARI 1936

G. HOLST.

THE LOUDSPEAKER AND SOUND-AMPLIFYING INSTALLATION ON THE T.S.S. "NORMANDIE"

With the steady perfection in the efficiency of microphones, amplifiers and loudspeakers in recent years, sound-amplifying installations have come more and more into favour for the transmission of speech and music and their amplified reproduction without loss of naturalness.

Installations of this type have recently also been carried out in ships. For the T.S.S. "Normandie", Philips has evolved and constructed a very comprehensive loudspeaker and sound-amplifying installation, a description of which will give some idea of what has already been achieved in this direction.

Seventy-four loudspeakers are distributed throughout the vessel. These are of watertight construction where necessary being protected against sea-water and rain by the addition of weatherboards which in no way affect the radiation of sound.

In the passenger saloons the loudspeakers are installed as inconspicuously as possible; in fact



Fig. 2. 1st Class saloon, with loudspeaker built in over the entrance.

Principle of Television

The human eye is a very complex and sensitive organ, whose optical mechanism functions briefly as follows: The crystalline lens of the eye produces an image of the field of view on the retina which is made up of a very large number of minute lightsensitive cells. Each of these cells through its own nerve filament communicates to the brain the stimulus it receives from the amount of light falling on it, and from the sum-total of the stimuli received by it the brain builds up the image seen by the eye.

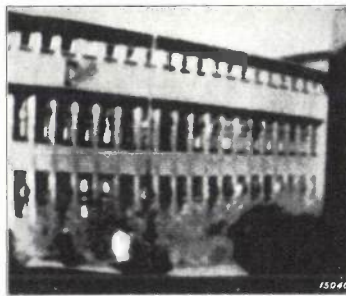


Fig. 7. Two television pictures (180 lines) produced with the new television plant at this laboratory.

In the human eye Nature has provided us with the basic principles of television fully worked out; also in televising the area of the picture to be



Fig. 1. Principle of television. The surface of the picture to be televised is resolved into a number of small elements which are numbered in succession. The brightness of each individual element is telegraphed. At the receiver where the picture surface is subdivided into similar elements each element is given the brightness transmitted for its respective number, so that the received picture exactly reproduces the original.

transmitted is resolved into a large number of small elements or cells (fig. 1). Each of these elements is given a number and the light value



of each element is telegraphed to the receiver in sequential order. Exactly as at the transmitter, the picture surface at the receiver is also resolved into elements which are numbered in the same way, and each element is given the light value telegraphed for its particular number. In this way the picture reproduced at the receiver is the same as that transmitted by the sender.

In the eye every element of the picture in the transmitter (cell of retina) has its own conductor (optic nerve filament) to the receiver (brain), and the light values of all elements are telegraphed simultaneously. In television this simultaneity naturally cannot be effected, as only one conductor (a single carrier wave) is available for all picture elements, so that the separate light values must be telegraphed in succession. In consequence television technique is rather complex, as may be exemplified by a simple calculation. To obtain a picture of satisfactory quality, the area of a picture measuring 4x4.8 in. must be resolved into about 40000 elements. In televising moving pictures, it is necessary, as in cinematography, to send a sufficient number of pictures per second, at least 25, in order to produce a connective image on spectator's eye. Thus, only 1/25th of a second is available for the transmission of each picture, in other words each second the light values of 25x40000 = 1,000,000 elements of the picture must be telegraphed¹⁾.

Receivers constructed on these principles were evolved some time ago in this laboratory and have operated with complete satisfaction. Fig. 7 reproduces two photographs of televised pictures (180 lines) which show the quality of reproduction already here attained.

¹⁾ This is aptly brought out by the following example: For some years facsimile and picture telegraphy has enabled pictures to be transmitted by telegraphy, the transmission of a single picture taking from 10 to 20 seconds or even longer. In the Melbourne Air Race in October, 1934, a film was made of the arrival of the winners at Melbourne and was transmitted to London. This short film, which was on exhibition at London cinemas on the same day already, took a 3/4 minute to project, while the time of transmission from Australia was about 6 hours. In television the same transmission must be completed in a 3/4 minute.

in the 1st Class saloon it is almost impossible to detect that the gilt rosette over the escutcheon at the entrance hides a loudspeaker horn (fig. 2).

For the transmission of music and speech, microphones are installed in the chapel, the 1st Class dining saloon, the large 1st Class saloon, the theatre, in the grill room and on the bridge. The bridge microphone has precedence over all other microphones, the captain being always in a position to address every one of the 2000 passengers from the bridge. Oral communications regarding landing arrangements, explanations of delays, notices of festivities, etc., can now be transmitted to all passengers from the bridge much quicker than by the method employed hitherto of posting up notices at various points in the vessel. Loudspeakers are also provided on the boat deck, so that orders and instructions can similarly be issued during boat drill.

Should the space available in the chapel be insufficient to accommodate the whole of the congregation, arrangements can be made for the Tourist Class passengers to remain in their saloon and receive the service through the medium of the loudspeakers installed there. These speakers are connected to the microphone in the chapel through one of the amplifiers.

The theatre which has 400 seats is not large enough to accommodate all the First Class passengers, but with the aid of the loudspeaker installation it is possible to transmit theatrical productions, musical recitals and other stage productions to all those passengers unprovided with seats.

The ship's orchestra plays alternatively in the dining room and in the grill room, both of which are provided with microphones; the grill room can moreover be converted for dancing.

Electron-probe microanalysis of thin films

P. Willich and D. Obertop

In electron-probe microanalysis the local composition of a solid is determined from the characteristic X-radiation generated by bombardment with a fine electron beam. Since the first analyses, some 35 years ago, the electron probe has undergone considerable development. Applications are found in widely different fields including metallurgy, mineralogy, geology and biology. There is also considerable interest in electron-probe microanalysis in the electrical industry. In recent years, attention has mainly concentrated on thin films, which are now used increasingly for a wide variety of advanced applications. In the article below the authors show that electron-probe microanalysis can be a useful aid in the further development of thin-film technology.

Introduction

Films thinner than 5 μm are widely used in the electrical industry. They are applied to substrates such as silicon, gallium arsenide, glass, plastic, metal and ceramics. Various methods are used for applying these thin films: liquid-phase and gas-phase epitaxy, electron-beam vacuum evaporation and sputtering. The composition and the thickness of the films can be accurately matched to the requirements for a particular application. Several examples have already been given in this journal; for example in articles on semiconductor lasers^[1], thin-film strain-gauge transducers^[2], magneto-optical switching^[3], low-friction wear-resistant thin solid films^[4], optical recording^[5] and erasable magneto-optical recording^[6].

The methods used for the chemical analysis of thin films have to meet some special requirements. The analysis must in general be non-destructive and capable of being used for all possible combinations of elements, without being affected by the composition of the substrate. The volume of the samples may be less than 1 μm^3 , the concentrations less than 0.5 wt.% or the films thinner than 0.3 μm . In addition there are the general requirements for short analysis times (for batch analyses) and small systematic deviations (< 5%).

A method that can meet these requirements is electron-probe microanalysis. In this method the composition of a small area of the film is derived from the characteristic X-radiation generated when the film is bombarded by a fine electron beam^[7]. A detailed description of this method of analysis has been given in an earlier article in this journal^[8], with some examples illustrating the broad field of application.

In the study described in the present article we use an electron microprobe to analyse thin films of technological importance. Among the films we have investigated are garnet films of complex composition, amorphous metal films thinner than 1 μm , films with light elements and incorporated gases, and films thinner than 0.3 μm . In all these cases electron-probe microanalysis gives good results, which can be used advantageously for optimizing the method of applying the films, their composition and their thickness. Before going into these aspects, we shall first briefly describe the principle, the equipment and the operating procedure.

Principle of the electron microprobe

The operating principle of the electron microprobe used in our investigations is shown schematically in fig. 1. A fine electron beam with an energy between 1

Dr P. Willich and Ing. D. Obertop are with Philips GmbH Forschungslaboratorium Hamburg, Hamburg, West Germany.

and 50 keV strikes the sample to be analysed. Some of the characteristic X-radiation thus excited goes to a crystal spectrometer. There it is spectrally analysed by X-ray diffraction (wavelength-dispersive spectrometry) in accordance with Bragg's law:

$$2d \sin \theta = n\lambda, \quad (1)$$

where d is the distance between the lattice planes of the crystal, θ is the angle of incidence at which the reflection occurs, n is an integer and λ is the X-ray wavelength. The reflected X-radiation is detected by a proportional gas counter, which is connected to a data-processing system (a minicomputer). Fig. 2 shows photographs of an arrangement with three crystal spectrometers. The electron microprobe can be used for analysing both electrically conducting and non-conducting films; the non-conducting films are first coated with a thin layer of a conducting material, such as carbon or aluminium.

The excitation of a characteristic X-ray line spectrum is related to the shell structure of the distribution of electrons in atoms. If an electron with sufficient kinetic energy penetrates an atom it can eject an electron from an inner shell (e.g. the K shell) of the atom. An electron from one of the outer shells (e.g. the M shell) can then fall back to the K shell. The bond energy of an electron is higher in the K shell than in the M shell. The increase in bond energy, $E_K - E_M$, is emitted as a photon whose wavelength is

$$\lambda = \frac{hc}{E_K - E_M}, \quad (2)$$

where h is Planck's constant and c is the velocity of light. The values of E_K and E_M depend to a great extent on the atom. Consequently the wavelength of the emitted X-radiation corresponding to the electron

transition from the M shell to the K shell has a value that is characteristic of the atom. The same applies to other transitions to the K shell and to transitions to the L and M shells. The characteristic X-ray lines are denoted by a capital letter corresponding to the shell to which the electron drops back, and a subscript indicating the shell from which the electron originates. The occurrence of characteristic lines in the X-radiation emitted from a sample forms the basis for a chemical analysis.

Besides the method described here, there are other ways in which chemical analysis can be performed by detection of characteristic X-rays excited by electrons. Chemical analyses can be performed for example with a scanning electron microscope, and using an energy-dispersive Si(Li) detector instead of a wavelength-dispersive crystal spectrometer [8][9]. In principle this method can also be used to determine the concentrations of light elements such as carbon, nitrogen and oxygen, using window-less detectors to increase the detection efficiency for long-wave X-rays. The sensitivity is low, however, and contamination makes the detectors difficult to maintain. Since the signal-to-background ratio is small, it is difficult to perform trace analyses. The poor spectral resolution can also cause problems in the analysis of films that have complex compositions.

Another method uses a modification of the X-ray-fluorescence analytical equipment described earlier in this journal [9]. Here a relatively large area (e.g. 7 cm²) of the sample surface is irradiated with a broad beam of low-energy electrons (≤ 15 keV) [10]. Such a beam excites long-wave radiation much more efficiently than a short-wave X-ray beam in the conven-

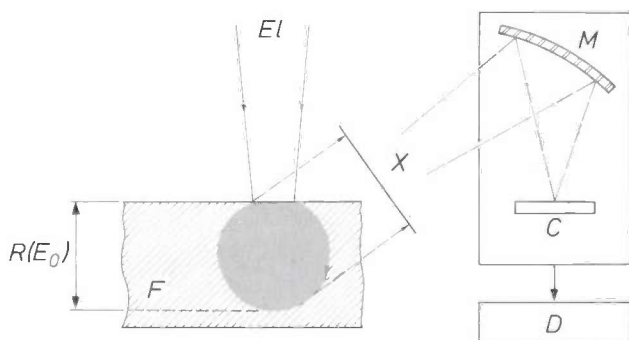


Fig. 1. Schematic representation of thin-film analysis with an electron microprobe. Bombardment with a fine electron beam EI of energy E_0 excites characteristic X-radiation X in a part (shown hatched) of the thin film F . The escape depth R of this radiation depends on E_0 . A crystal monochromator M (wavelength dispersion) discriminates between the various characteristic X-ray lines. The intensities are measured with a proportional counter tube C . D data-processing system (minicomputer).

- [1] G. A. Acket, J. J. Daniele, W. Nijman, R. P. Tjburg and P. J. de Waard, Semiconductor lasers for optical communication, Philips Tech. Rev. 36, 190-200, 1976;
- J. C. J. Finck, H. J. M. van der Laak and J. T. Schrama, A semiconductor laser for information read-out, Philips Tech. Rev. 39, 37-47, 1980.
- [2] K. Bethe and D. Schön, Philips Tech. Rev. 39, 94-101, 1980.
- [3] P. Hansen, B. Hill and W. Tolksdorf, Philips Tech. Rev. 41, 33-45, 1983/84.
- [4] H. Dimigen and H. Hübsch, Philips Tech. Rev. 41, 186-197, 1983/84.
- [5] L. Vriens and B. A. J. Jacobs, Digital optical recording with tellurium alloys, Philips Tech. Rev. 41, 313-324, 1983/84;
- D. J. Gravesteyn and J. van der Veen, Organic-dye films for optical recording, Philips Tech. Rev. 41, 325-333, 1983/84.
- [6] M. Hartmann, B. A. J. Jacobs and J. J. M. Braat, Philips Tech. Rev. 42, 37-47, 1985.
- [7] R. Castaing and A. Guinier, Proc. 1st Int. Conf. on Electron microscopy, Delft 1949, pp. 60-63;
- R. Castaing, in W. K. Mueller (ed.), Advances in X-ray analysis, Vol. 4, Plenum, New York 1961, pp. 351-369;
- K. F. J. Heinrich, Electron beam X-ray microanalysis, Van Nostrand Reinhold, New York 1981.
- [8] M. Klerk, Philips Tech. Rev. 34, 370-374, 1974.
- [9] M. L. Verheijke and A. W. Witmer, Philips Tech. Rev. 34, 339-343, 1974.
- [10] A. W. Witmer and E. W. J. M. van Meijl, Spectrochim. Acta 34B, 415-422, 1979.

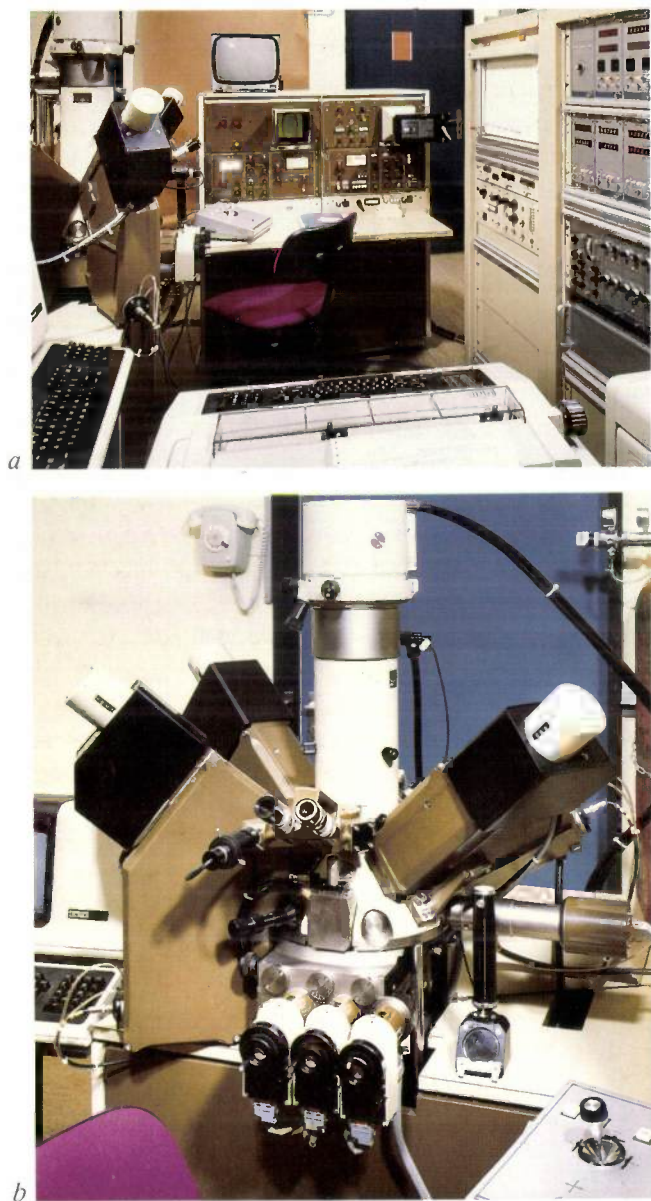


Fig. 2. Electron-probe microanalysis equipment (a) with three crystal spectrometers (b).

tional equipment for X-ray fluorescence analysis. It thus provides a better method for determining concentrations of light elements and for analysing thin films. A limitation compared with the electron microprobe, however, is its low lateral resolution.

The method we are using requires a larger investment in equipment than the others, but it offers distinctly better prospects for the microanalysis of thin films. We shall now indicate in general terms how a quantitative chemical analysis can be made.

Quantitative analysis procedure

The measured intensity I of a characteristic X-ray line cannot simply be translated into a concentration by weight c of the element in the sample. This is because the relationship between I and c is not linear, on

account of the presence of other elements (the 'matrix effect'). Three distinct effects are found:

- Atomic-number effect: the energy available for excitation depends on the other elements in the sample because of elastic and inelastic collision and scattering processes.
- Fluorescence effect: the intensity of a characteristic X-ray line can be enhanced by fluorescence excited by short-wave X-radiation from other elements in the sample.
- Absorption effect: some of the excited X-radiation is absorbed on its way to the surface.

One way to arrive at a quantitative analysis is to make a direct comparison of the measured intensity I with the intensity I_s of a standard with a known concentration by weight c_s . If the films are not too thin, so that the penetration depth of the electrons is less than the film thickness, the intensity ratio I/I_s may be expressed as

$$I/I_s = (k/k_s)c/c_s, \quad (3)$$

where k and k_s are parameters representing the effects mentioned above. A particular advantage of electron-probe microanalysis is that k and k_s can be calculated with the aid of a number of fundamental parameters: the mean atomic number Z and the mean atomic weight A of the sample, the mean mass-absorption coefficient μ of the excited characteristic X-radiation, the electron energy E_0 , the critical excitation energy E_c and the X-ray take-off angle as an instrumental parameter. Since Z , A and μ depend on the (as yet unknown) composition of the sample, an iterative procedure is necessary. The parameter k can be derived from ^[11]:

$$k = \int_0^{\infty} \phi(\rho z) d(\rho z), \quad (4)$$

where ρ is the density of the material, z the depth in the film and $\phi(\rho z)$ the depth-distribution function of the emitted characteristic X-radiation, neglecting the fluorescence effect. In principle equation (4) is valid for any electron energy and an 'infinitely thick' film (bulk material). In thin-film practice the maximum electron penetration depth should be within the film thickness provided.

In the classical ZAF correction methods (Z = atomic-number effect, A = absorption and F = fluorescence) a simple approximation is taken for the distribution function and empirical parameters are used for calculating the concentration. If the matrix effects are not too pronounced and the electron energy is about 15 keV, this produces reliable results. In modern correction methods the exact distribution function is calculated with the aid of fundamental parameters, and

the agreement with the experimental curves is surprisingly good^[12]. These methods are used with strong matrix effects, light elements and low electron energies (< 10 keV). The analysis of extremely thin films requires a special procedure, and we shall return to this later.

Analysis of thin films

We shall discuss electron-probe microanalysis for two practical examples, one relating to epitaxial iron-garnet films at least 2 μm thick, the other to amorphous metal films thinner than 1 μm .

Iron-garnet films

Thin films of single-crystal iron garnets can be used in magnetic-bubble memories^[13], magneto-optical memories^[14] and switching devices^[3]. The films are grown on a garnet substrate by liquid-phase epitaxy^[13]. The crystal structure of iron garnets contains Fe^{3+} and O^{2-} ions and relatively large R^{3+} ions (e.g. Y^{3+} , Gd^{3+}). The general formula is $\text{R}_3\text{Fe}_5\text{O}_{12}$. For certain applications it may be advantageous to substitute other elements for some of the R and Fe. An example is to be found in $\text{Gd}_{3-x}\text{Bi}_x\text{Fe}_{5-y-z}\text{Ga}_y\text{Al}_z\text{O}_{12}$ films, which have properties that are particularly suitable for magneto-optical switching^[3]. At least six elements have to be analysed in order to establish the exact composition of such films. In practice there are more, because of possible impurities. For example, the films always contain a trace of Pb^{2+} from the lead in the melt used in liquid-phase epitaxy^[13], and a trace of Pt^{4+} from the platinum present in the crucible and stirrer.

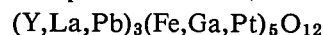
Because there may be so many elements in a film, the spectral resolution of the crystal spectrometers must be very good. This applies especially to the resolution of the characteristic lines of the lead and platinum traces and those of a major element such as bismuth^[15]. It is also necessary to ensure that the incident electrons do not excite the substrate. If they did, X-rays from the substrate would cause a distorted image. It follows therefore that there is a minimum film thickness for a reliable analysis.

An important parameter for the minimum film thickness and the attainable accuracy of an analysis is the energy E_0 of the incident electrons. At lower values of E_0 the electrons do not penetrate so far into the film, which can therefore be thinner. When there is strong absorption of the excited X-rays in the film the accuracy of the analysis increases with decreasing E_0 : since this radiation then has to cover a shorter path in the film, the absorption effect becomes less important. In general, however, E_0 should not be

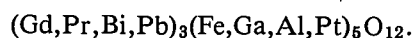
lower than about one and a half times the critical excitation energy E_c of the X-ray line to be used, otherwise its intensity will be too low. For the garnet films investigated this means that E_0 must be between 12 and 15 keV, with a minimum film thickness of about 1.5 μm .

The electrical and thermal conduction required for electron bombardment is achieved by evaporating a conducting carbon film about 30 nm thick on to the garnet film and the standard. A characteristic value for the beam current during the electron bombardment is 50-100 nA. At $E_0 = 12$ keV this corresponds to a minimum beam diameter of about 0.8 μm . The diameter of the region in which X-radiation is excited is about 2 μm under these conditions. The standard used is the pure element or an oxide. The characteristic X-ray lines are each detected for 30 seconds and the corresponding background for 10 seconds. With a computer the measured intensities are converted into concentrations by weight automatically, with the matrix effect taken into account 'on line' through a ZAF correction procedure^[16]. When three crystal spectrometers are used (fig. 2) the total analysis time for nine elements is only two minutes, which is short enough for routine analyses.

Table I gives some results of analyses on films with two different compositions:



and



The concentrations determined are given in percentages by weight and in the number of atoms per formula unit. The oxygen content was calculated with the assumption of the nominal valency of the cations. Also given are the standard deviations of the different determinations, and a comparison is made with the results for bulk material of comparable composition. These were obtained with X-ray fluorescence analysis for high concentrations and atomic absorption spectrometry for low concentrations, both established methods for the analysis of bulk material^[16].

The reproducibility of the analyses with the electron microprobe in these cases is found to be reasonably high. The standard deviation for high concentrations is less than 2%; for low concentrations it is of the

[11] R. Castaing, Thesis, Paris 1951.

[12] J. D. Brown and R. H. Packwood, X-ray Spectrom. 11, 187-193, 1982.

J. L. Pouchou and F. Pichoir, Rech. Aérop. 3, 167-192, 1984.

[13] J. A. Pistorius, J. M. Robertson and W. T. Stacy, Philips Tech. Rev. 35, 1-10, 1975.

[14] H. Heitmann, B. Hill, J.-P. Krumme and K. Witter, Philips Tech. Rev. 37, 197-206, 1977.

[15] P. Willich, W. Tolksdorf and D. Obertop, J. Cryst. Growth 53, 483-489, 1981.

[16] See for example W. F. Knippenberg, Inorganic chemical analysis, Philips Tech. Rev. 34, 298-304, 1974.

Table I. Concentrations (wt.% and number of atoms per formula unit), standard deviation s and relative difference δ compared with results of X-ray fluorescence analysis (XFA) and atomic absorption spectrometry (AAS), obtained by electron-probe microanalysis of two iron-garnet films (see text).

Element	wt. %	at.	s (%)	δ (%)	
				XFA	AAS
Y	34.2	2.91	0.7	-0.5	
La	1.72	0.093	3.2	-3.2	
Pb	0.20	0.007	9.6		-5.2
Fe	32.2	4.35	0.8	-0.8	
Ga	5.94	0.645	0.4	+1.7	
Pt	0.10	0.004	14.5		+8.2
O	25.4[*]	12[*]			
Gd	29.5	1.83	0.8	-1.0	
Pr	8.2	0.56	1.8	-1.0	
Bi	12.9	0.60	1.8		+2.0
Pb	1.13	0.053	6.2		-6.8
Fe	24.5	4.27	0.8	-0.8	
Ga	1.11	0.155	0.9		-1.8
Al	1.37	0.50	0.5		+1.3
Pt	0.88	0.044	12.5		+7.8
O	19.8[*]	12[*]			

[*] On the basis of the stoichiometric composition.

order of 10%. The results differ only very slightly from those obtained by other analytical methods: about 1% for high concentrations and less than 10% for low concentrations.

Amorphous metal films thinner than 1 μm

Thin amorphous metal films can be used in many applications. An example is the use of amorphous alloy films consisting of gadolinium, terbium and iron for magneto-optical recording [6]. Such films can be deposited on a glass or plastic substrate by electron-beam vacuum evaporation. The composition and thickness of the films largely determine the magnetic and magneto-optical properties. Here again, electron-probe microanalysis can produce useful information in a very short time.

In films thinner than 1 μm the penetration depth of the electrons is of the same order as the film thickness. This means that a proper choice of the electron energy E_0 requires a knowledge of the exact relationship between E_0 and the depth R from which the excited X-radiation escapes from the sample (fig. 1). To determine this relationship experimentally we evaporated very thin metal films of different thickness (from 0.05 to 0.5 μm) on to a conducting carbon substrate [17]. From the amount of deposited material, determined by chemical analysis, we calculated the thickness of the different films. For all the films the intensity of a few characteristic X-ray lines relative to a bulk-elemental standard was measured as a function of E_0 . The materials and the characteristic lines were chosen so that the critical excitation energy E_c varied between 0.7 and 12 keV.

In a film of a given thickness (e.g. 0.2 μm) it is found that the intensity decreases from a certain value of E_0 , since some of the electrons enter the substrate. At this electron energy the escape depth of the X-radiation is equal to the film thickness. The required relation between E_0 and R is obtained by performing this determination on films of different thickness. Some results obtained with pure iron and gold films are shown by way of example in fig. 3. Here R is plotted against E_0 for two characteristic X-ray lines of iron and two of gold. The increase in the escape depth at a higher electron energy is much greater in an iron film than in a gold film. The values of R are within 10 nm of those obtained from calculations based on R. Castaing's equation [18],

$$R = 0.033(E_0^{1.7} - E_c^{1.7}) \frac{A}{Z_0}, \quad (5)$$

and with calculations of the depth-distribution function $\phi(\rho z)$ [19].

To obtain an escape depth between 0.3 and 1 μm the electron energy for most elements has to be between 5 and 12 keV. The advantage of an escape depth smaller than the film thickness is that the substrate composition has no effect on the analysis. Working with a lower electron energy, however, has the disadvantage that the intensity of the detected X-radiation decreases, and this reduces the sensitivity.

In fig. 4 the relation between the ratio E_0/E_c and the intensity I of the excited X-radiation is given for a large number of binary iron alloys. The values of E_0/E_c and I are plotted against the atomic number of the other element. The values of E_0 were chosen so that the X-ray escape depth was 0.3 μm for all the alloys. When $E_0/E_c \leq 2$ the intensity is generally much lower than when $E_0/E_c \gg 2$. If the most sensitive X-ray line is chosen and the measurement time is increased, typically by a factor between 5 and 10, a detection limit of at least 0.5 wt.% can nevertheless be achieved. This was established by analysis of thin amorphous alloy films consisting of gadolinium, iron and lead [20].

The correction for the matrix effect is less accurate for thinner films, especially if the atomic number of the element to be analysed differs considerably from the mean atomic number of the film. This was found in the analysis of gold-copper alloy films in which the difference ΔZ in atomic number is very large [17]. In fig. 5 the relative analysis error is plotted against the electron energy E_0 for gold in a copper-rich alloy and for copper in a gold-rich alloy; in both cases $\Delta Z = 40$. At a low electron energy the inaccuracy is larger. At the electron energies required for a film thickness of about 0.5 μm the errors found range from 3 to 5%.

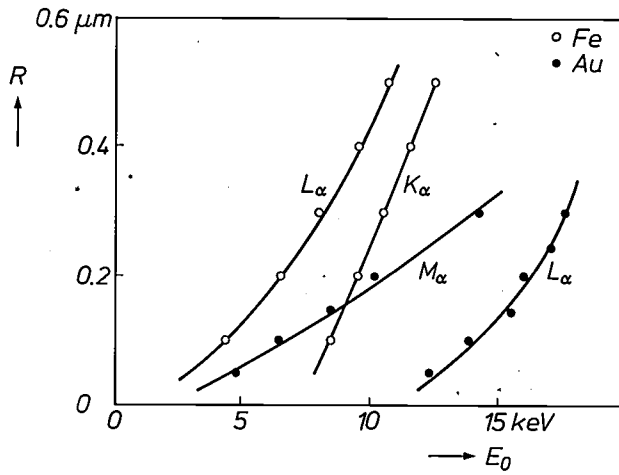


Fig. 3. Escape depth R of the excited K_α and L_α radiation in an iron film and L_α and M_α radiation in a gold film, as a function of the electron energy E_0 . The values of R were determined experimentally from the variations in the detected X-ray intensity with the electron energy at different film thicknesses. In the iron film R increases very rapidly with E_0 .

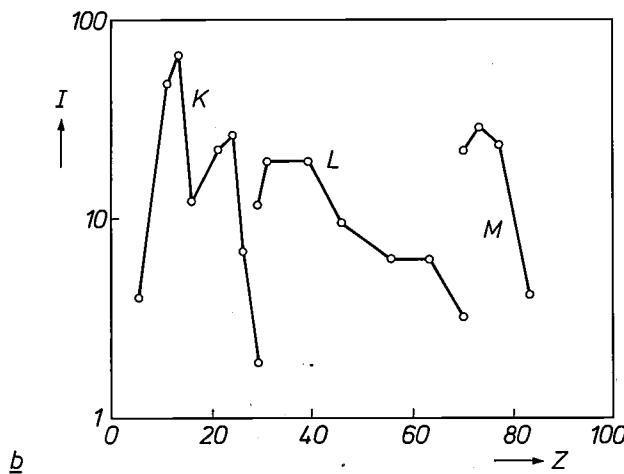
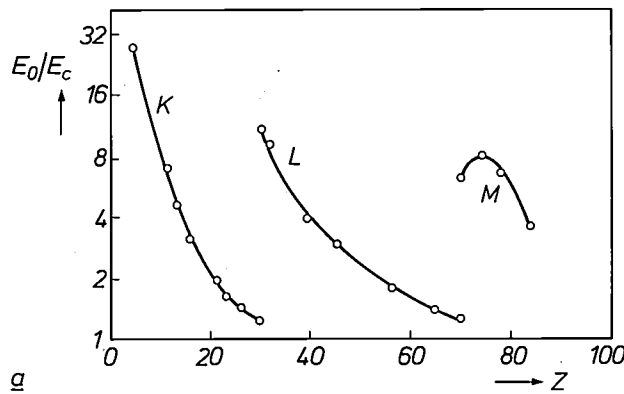


Fig. 4. a) Ratio of the electron energy E_0 at which the escape depth of the excited X-radiation is 0.3 μm to the critical excitation energy E_c of the K, L or M lines used, for thin films of binary alloys with 70 wt.% iron and 30 wt.% of another element (varying from carbon to bismuth). The value of E_0/E_c is plotted against the atomic number Z of the other element. b) Intensity I (in relative units) of the detected X-ray line as a function of Z . Alloys where $E_0/E_c \leq 2$ generally give a much lower intensity than those with $E_0/E_c > 2$.

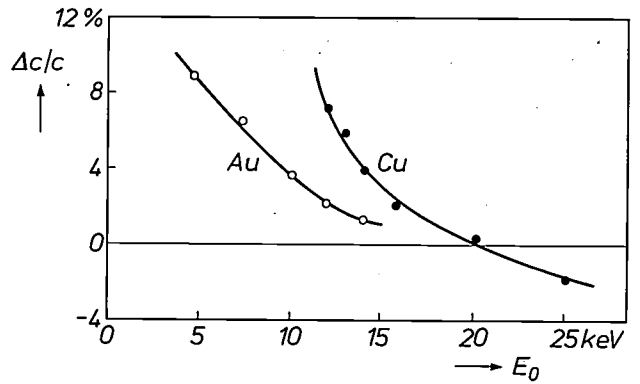


Fig. 5. Relative error $\Delta c/c$ in a determination of the gold concentration (M_α radiation) in a film with 80 wt.% Cu and 20 wt.% Au, and of the copper concentration (K_α radiation) in a film with 80 wt.% Au and 20 wt.% Cu, as a function of the electron energy E_0 . In both cases the analysis is less accurate at low values of E_0 .

For analyses with $\Delta Z \leq 30$, however, the error is no greater than 2%.

Some special cases

Sometimes it is not so easy to process the results from an electron microprobe to obtain a quantitative analysis. Examples are the analysis of light elements and of elements for which no suitable standard is available, and the determination of the thickness and composition of films thinner than 0.3 μm . However, reliable analyses can also be made in these special cases if appropriate analysis parameters and correction methods are adopted.

Light elements

An advantage of the electron microprobe with wavelength dispersion is that it can also be used for determining concentrations of light elements such as carbon, nitrogen and oxygen ($Z < 9$). The position and the shape of the characteristic X-ray lines from these elements depend on the chemical state in the sample. Compared with the heavier elements ($Z > 9$) both the excitation probability and the detection sensitivity are low. Since the energy of the excited X-radiation is low ($< 1 \text{ keV}$), absorption in the sample is relatively high. When the electron energy is high ($E_0 > 10 \text{ keV}$) the correction factor k/k_s in eq. (3) can differ appreciably from 1 (< 0.5 or > 1.5). It is difficult to determine k/k_s because the mass-absorption coefficients are not precisely known.

[17] P. Willich, J. Physique 45 (Colloque C2), C2/621-C2/624, 1984.
 [18] R. Castaing, in: L. Marton (ed.), Advances in electronics and electron physics, Vol. XIII, Academic Press, New York 1960, pp. 317-386.
 [19] L. Parobek and J. D. Brown, X-ray Spectrom. 7, 26-30, 1978.
 [20] M. Hartmann, P. Hansen and P. Willich, J. Appl. Phys. 56, 2870-2873, 1984.

We have studied the problems of measuring light elements by analysis of sputtered metal-carbon films 0.5 μm thick [21]. The properties of such films make them particularly suitable for the dry lubrication of moving parts [4]. In view of the changes in the shape and position of the X-ray lines we took the area under the lines rather than the height as a measure of the intensity. The electron energies were between 5 and 10 keV. In this range of energies there is not such a marked variation in k/k_s (between 0.8 and 1.2) and conventional ZAF correction methods can be used. The accuracy of the carbon-content determination is then about 5%. With correction procedures based on an exact calculation of the distribution $\phi(\rho z)$ [12], an even higher accuracy can be achieved, even for $k/k_s < 0.8$ and > 1.2 .

Fig. 6 shows some results of analyses of ruthenium-carbon films applied by reactive sputtering of a ruthenium target in an ethyne-containing argon atmosphere. The measured content of ruthenium, carbon, argon and oxygen in the film is plotted against the ethyne content during the sputtering. As expected, a higher ethyne content results in a film with more carbon and less ruthenium. A striking feature is the incorporation of argon at a low ethyne content and oxygen at a high ethyne content. We shall now take a closer look at the analysis of these elements.

Argon in sputtered films

When a thin film is applied to a substrate by sputtering in argon, it is often found to contain a small amount of argon. This can have a marked effect on the mechanical and electrical properties of the film. A quantitative determination of the argon content can then be useful for establishing the optimum process conditions.

A problem in determining the argon content of thin films is that there is no suitable standard available. It is customary to interpolate between the intensities of corresponding X-ray lines (K_α) of chlorine and potassium [22], the two nearest neighbours in the periodic system. However, when a proportional gas counter tube is used, with argon flowing through it, this can lead to considerable errors. The K_α energy E_{K_α} of a lighter element (e.g. chlorine with $E_{K_\alpha} = 2.62$ keV) is lower than the critical energy E_c for excitation of the K_α radiation of argon (3.20 keV), whereas E_{K_α} of a heavier element (e.g. potassium with $E_{K_\alpha} = 3.31$ keV) is higher. This affects the mechanism of the interaction between the X-radiation and the argon in the counter tube.

To determine the effect of the interaction mechanism, we measured the intensity of the K_α radiation of a series of neighbouring elements (silicon to chrom-

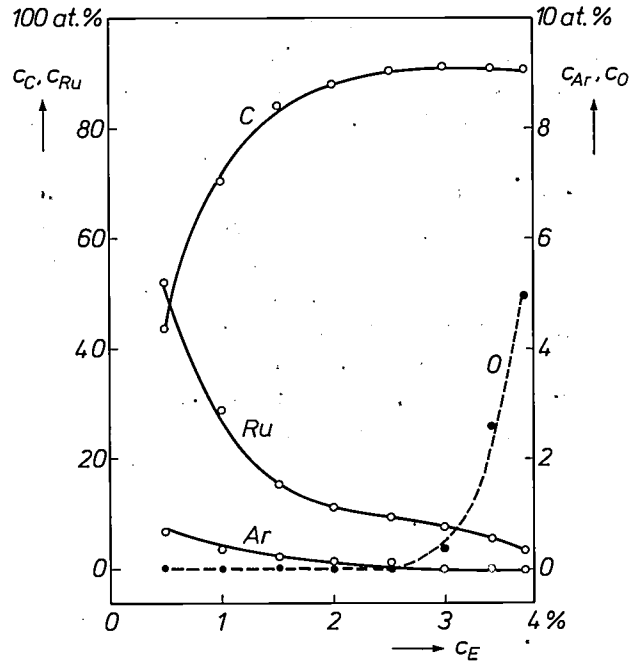


Fig. 6. The concentrations, determined with an electron microprobe, of carbon (c_C), ruthenium (c_{Ru}), argon (c_{Ar}) and oxygen (c_O) in films deposited by reactive sputtering of a ruthenium target in an atmosphere of ethyne (C_2H_2) and argon. With increasing ethyne content c_E films with more carbon and less ruthenium are obtained, and less argon and more oxygen is incorporated in the films.

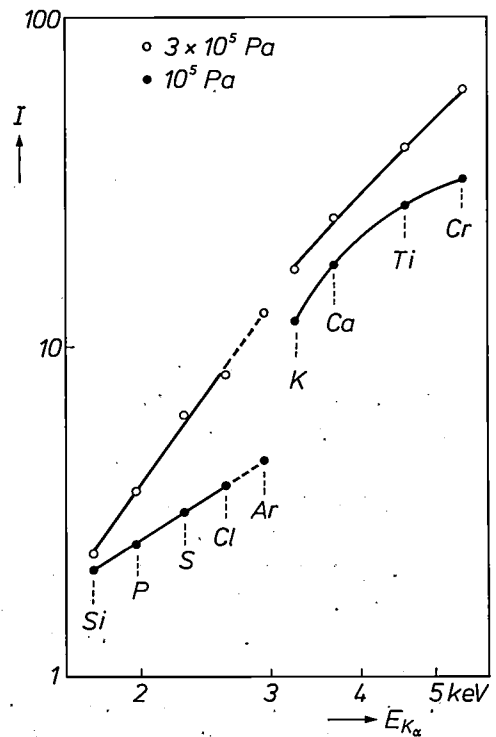


Fig. 7. Relative intensity I (at $E_0/E_c = 2$) for two argon pressures in the counter tube, as a function of the K_α energy E_{K_α} , for elements close to argon in the periodic system. The K_α intensities for argon have been extrapolated from the values for the lighter elements (Si to Cl). Interpolation between the K_α intensities of Cl and K would give an unreliable value at an argon pressure of 10^5 Pa.

ium) for different conditions in the counter tube [23]. In fig. 7 the intensity of the K_{α} radiation excited at $E_0/E_c = 2$ is plotted against $E_{K_{\alpha}}$ for two argon pressures. At 3×10^5 Pa (3 atm) the effect of the K_{α} absorption edge of argon is negligible, so that interpolation between the intensities of potassium and chlorine gives a reasonably good value for the intensity of argon. At 10^5 Pa (1 atm), however, the K_{α} absorption edge of argon does have a noticeable effect: from chlorine to potassium there is a sharp increase in the measured K_{α} intensity. On the other hand, extrapolation from the K_{α} intensities of the lighter elements (silicon to chlorine) gives a reliable value for the K_{α} intensity of argon in both cases.

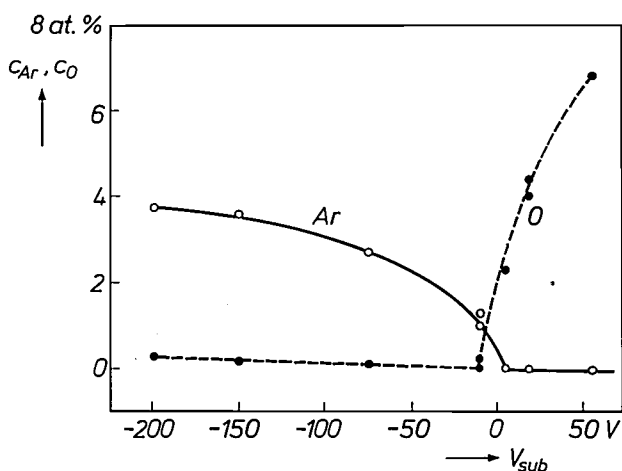


Fig. 8. The concentrations of argon (c_{Ar}) and oxygen (c_O) in iron-carbon films, determined with an electron microprobe, as a function of the substrate potential V_{sub} during deposition of the film by reactive sputtering of an iron target in an ethyne and argon atmosphere. As the substrate potential becomes more negative more argon is incorporated in the films. With a more positive substrate potential the incorporation of oxygen increases.

Using the standard derived from this (10.4 wt. % Ar in 89.6 wt. % Si) we carried out analyses on a large number of films with an argon content varying from 0.1 to 10 wt. %. The detection limit was 0.01 wt. %, which is more than enough for most cases. The analyses showed that the argon content depends closely on the gas composition and on the process conditions during the sputtering. As can be seen in fig. 6, in the presence of a larger amount of reactive gas (ethyne) less argon is incorporated. More argon is incorporated if a more negative substrate potential is used. An example is shown in fig. 8, where the measured argon content in iron-carbon films is plotted against the substrate potential during the sputtering. At 0 V hardly any argon is incorporated in the films, whereas at -200 V the argon incorporation is almost 4 at. %. The increasing incorporation of argon at a more negative substrate potential is related to the larger numbers of positive argon ions landing on the substrate.

Table II. Oxygen content c_O in differently treated iron films and the mass depth ϱz of an oxidized surface film (Fe_2O_3), determined by measurements of I/I_s at two values of the electron energy E_0 (see text). One iron film was not annealed, the other was annealed for 1 hour at temperature T_a .

T_a (°C)	I/I_s		c_O (wt. %)	ϱz ($\mu g/cm^2$)
	$E_0 = 5$ keV	$E_0 = 10$ keV		
[*]	0.138	0.095	2.2	2.8
100	0.143	0.094	2.1	3.2
150	0.181	0.109	2.2	4.8
200	0.289	0.145	2.3	9.6
250	0.472	0.206	2.4	17.9

[*] Not annealed.

Oxygen

When thin films are sputtered there is almost invariably some incorporation of oxygen as well. The oxygen concentration in the films is also dependent on the gas composition (fig. 6) and on the process conditions (fig. 8) during the sputtering. Some oxygen is also incorporated when the films are deposited by electron-beam evaporation in high vacuum (10^{-5} - 10^{-3} Pa). The presence of oxygen in thin films can have a marked effect on their mechanical, electrical, magnetic and chemical properties.

When determining low oxygen concentrations (< 5 wt. %) it is often necessary to take into account a thin oxide film that has formed on the surface [24]. The relative intensity I/I_s of the X-ray line of oxygen, is then given by

$$I/I_s = ac_O + b(\varrho z)_{ox}, \quad (6)$$

where c_O is the oxygen concentration and $(\varrho z)_{ox}$ is the mass thickness of the oxide film. The constants a and b depend on the electron energy and can be derived from calculated depth-distribution functions. The values of c_O and $(\varrho z)_{ox}$ can be determined by measuring the intensity ratio I/I_s at two different values of E_0 . This gives two equations with c_O and $(\varrho z)_{ox}$ as the unknowns, so that these can be determined simultaneously and independently. The analysis errors here are no larger than 5%.

Table II presents by way of example some results of determinations of the oxygen content in thin iron films, showing the effect of annealing at different temperatures. Annealing at a higher temperature has little effect on the oxygen content in the iron films here, but the oxide film (Fe_2O_3) on the surface becomes appreciably thicker.

[21] P. Willich, A. P. von Rosenstiel and N. Drost, Mikrochim. Acta Suppl. 10, 211-216, 1983.

[22] W. Hoffmeister and M. Zuegel, Thin Solid Films 3, 35-40, 1969;

M. A. Short, J. Tabock and D. W. Hoffman, in: D. B. Wittry (ed.), Microbeam analysis 1980, San Francisco Press, San Francisco 1980, pp. 97-100.

[23] P. Willich and D. Obertop, X-ray Spectrom. 11, 32-34, 1982.

[24] P. Willich, D. Obertop and H. J. Tolle, X-ray Spectrom. 14, 84-88, 1985.

Films thinner than 0.3 μm

The electron microprobe can also be used for determining the thickness and composition of layers thinner than 0.3 μm. The procedure for a quantitative analysis, however, is quite different from the procedure described earlier for 'conventional' electron-probe microanalyses of films that are not so thin. If a film is thinner than 0.3 μm the minimum electron penetration depth that will give a sufficiently high X-ray intensity (high sensitivity) is greater than the thickness of the film. This means that some of the incident electrons enter the substrate.

In the simplest case of a film containing only one element the ratio of the measured intensity *I* of a particular X-ray line to the intensity *I_s* of a thick-film standard is a function of the film thickness:

$$I/I_s = f(\rho z). \tag{7}$$

The ratio *I/I_s* can be calculated using $\phi(\rho z)$ and $\phi_s(\rho z)$, the depth-distribution function of the combination of film and substrate and that of the standard [25]:

$$I/I_s = \int_0^{\rho z} \phi(\rho z) d(\rho z) / \int_0^{\infty} \phi_s(\rho z) d(\rho z). \tag{8}$$

The distribution functions are dependent on the electron energy *E₀*, while $\phi(\rho z)$ also depends on the mean atomic number of the substrate. For films with a mass thickness up to 250 μg/cm² this simple approximation holds for high values of *E₀* (20-40 keV). The interaction with the incident electrons is then mainly determined by the mean atomic number of the substrate, since $R(E_0) \gg \rho z$.

Fig. 9 shows how the ratio *I/I_s* can be determined from the distribution functions for the K_α line of iron

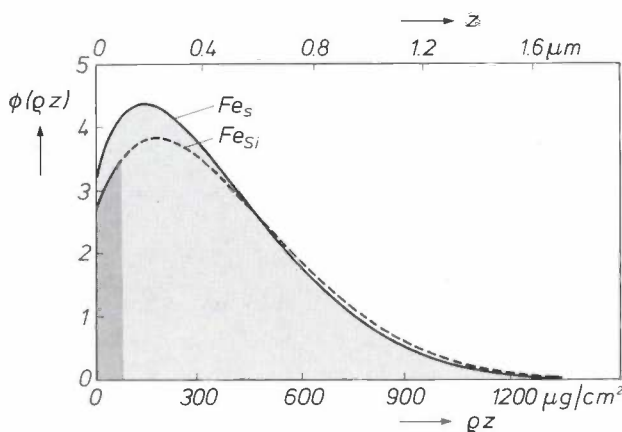


Fig. 9. Depth-distribution function $\phi(\rho z)$ (arbitrary units) of the K_α radiation of iron (at *E₀* = 25 keV) in an iron film about 0.1 μm thick on a silicon substrate (*Fe_{s_i}*) and in a thick iron film (*Fe_s*) used as a standard. Eq. (8) shows that the intensity ratio *I/I_s* is equal to the ratio of the area of the dark-shaded region to that of the entire shaded region. Calculation of *I/I_s* at different values of ρz gives a calibration curve for determining film thicknesses less than 0.3 μm.

that is present as a thin film on a silicon substrate. The calculated relation between *I/I_s* and ρz can be used as calibration curve for determining the film thickness from the experimentally determined value of *I/I_s*. Some examples of calibration curves are given in

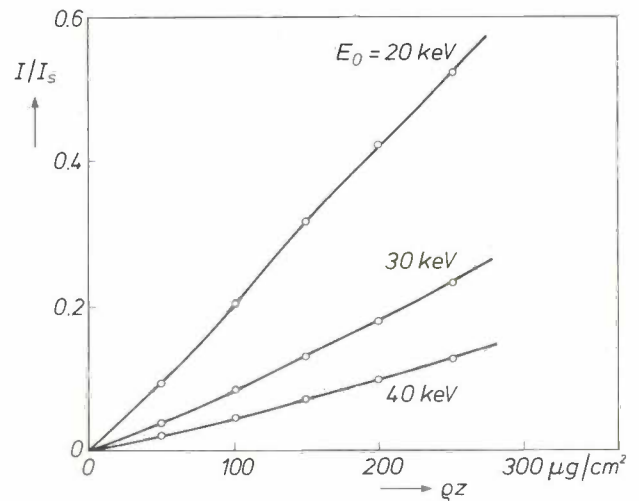


Fig. 10. Calculated calibration curves for determining the thickness *z* of very thin iron films on a silicon substrate, for different values of the electron energy *E₀*. From the measured intensity ratio *I/I_s* at a given *E₀* the mass thickness ρz can be determined.

Table III. X-ray line used (*X*), mean atomic number of the substrate (*Z_{sub}*), electron energy *E₀*, measured intensity ratio *I/I_s*, the mass thickness ρz derived from this and the value obtained by wet-chemical analysis, for a number of very thin metal films, containing only one element.

Element	<i>X</i>	<i>Z_{sub}</i>	<i>E₀</i> (keV)	<i>I/I_s</i>	ρz (μg/cm ²)					
					[a]	[b]				
Al	K _α	5	12	0.0324	13.3	14.5				
				0.0166	6.9	7.3				
				0.0098	4.2	4.4				
				0.0075	3.2	3.4				
Fe	K _α	14	30	0.046	79	73				
				0.0314	40	40				
				0.0677	82	79				
				0.1406	163	158				
				0.0178	39	40				
				0.0377	81	79				
Ni	K _α	10	22	0.035	25	26				
				0.017	24	26				
				Cu	M _α	10	30	0.063	83	83
								Gd	L _α	14
0.0571	71	71								
0.1324	156	142								
0.0172	36	36								
Au	L _α	14	35	0.0342	70	71				
				0.0767	153	142				
				0.067	73	77				
				0.182	197	193				

[a] Determined by electron-probe microanalysis by the method described here.
 [b] Determined by wet-chemical analysis.

fig. 10. The advantage of this method is that no separate thin-film standard is required. The detection limit for most elements is about $0.5 \mu\text{g}/\text{cm}^2$, corresponding to the thickness of a few atomic layers. Systematic errors are generally smaller than 5%.

Table III gives the measured ratio I/I_s for a number of very thin metal films and characteristic X-ray lines, with the value of ρz derived from them. This value is compared with the value obtained by wet-chemical analysis. Reasonably good agreement is found for the majority of films.

The procedure described here can also be used for determining the thickness and composition of very thin films consisting of more elements [26]. As an example Table IV gives the results of an analysis of three amorphous alloy films applied in the same composition but with different thicknesses to a silicon substrate. Here again the measured thicknesses agree well with the values obtained in other ways.

The composition of such films is determined by calculating the 'apparent' film thickness for each element. Dividing by the sum of the 'apparent' film thicknesses for all elements present then gives the different concentrations. As can be seen from Table IV, the film thickness has hardly any effect on this determination. For films of thickness from $0.25 \mu\text{m}$ to $0.35 \mu\text{m}$ very good agreement is found with the composition determined by conventional electron-probe microanalysis. Table IV gives an example of this as well.

This method could be very useful for determining the thickness and composition of magneto-optical recording films thinner than $0.1 \mu\text{m}$ [6]. It could also be used for analysing very thin metal films that have been given a protective coating of aluminium or silicon oxide with a mass thickness of up to $30 \mu\text{g}/\text{cm}^2$.

Depth analysis

In the methods of thin-film analysis described here it is usually assumed that the composition is constant over the entire thickness of the film. Proof of constant composition can be obtained by means of secondary-ion mass spectrometry [27]. Recently it has been shown that electron-probe microanalysis can also be used for samples whose composition varies in depth [28], as in multilayer structures. The procedure is similar to that

Table IV. Electron energy E_0 with the corresponding composition and thickness z , determined by the procedure described, using Gaussian depth-distribution functions, for three amorphous films of an alloy consisting of gadolinium, terbium, iron and cobalt on a silicon substrate.

E_0 (keV)	Composition (wt.%)				z (nm)	
	Gd	Tb	Fe	Co	[a]	[b]
30	34.3	12.3	1.3	52.1	74	80 ± 5
40	34.3	12.5	1.5	51.7	75	
30	34.1	12.3	1.4	52.2	157	160 ± 10
40	34.7	12.5	1.4	51.4	156	
30	33.6	11.9	1.4	53.1	359	350 ± 20
40	34.5	12.1	1.5	51.9	348	
11 [c]	34.2	12.2	1.4	52.2		

[a] Derived from the mass thickness; a value of 7.5 was obtained for the density by wet-chemical analysis.

[b] Measured by optical interference and/or mechanical scanning.

[c] 'Conventional' electron-probe microanalysis.

used for oxygen determination in the presence of an oxidized surface layer. This implies that measurements at different electron-energy values and calculations of the depth-distribution functions are necessary. With further improvements of the correction methods, reliable analysis will also be possible in this case.

[26] W. Reuter, in: G. Shinoda, K. Kohra and T. Ichinokawa (eds), Proc. Sixth Int. Conf. on X-ray optics and microanalysis (Osaka 1971), Univ. of Tokyo Press, Tokyo 1972, pp. 121-130.

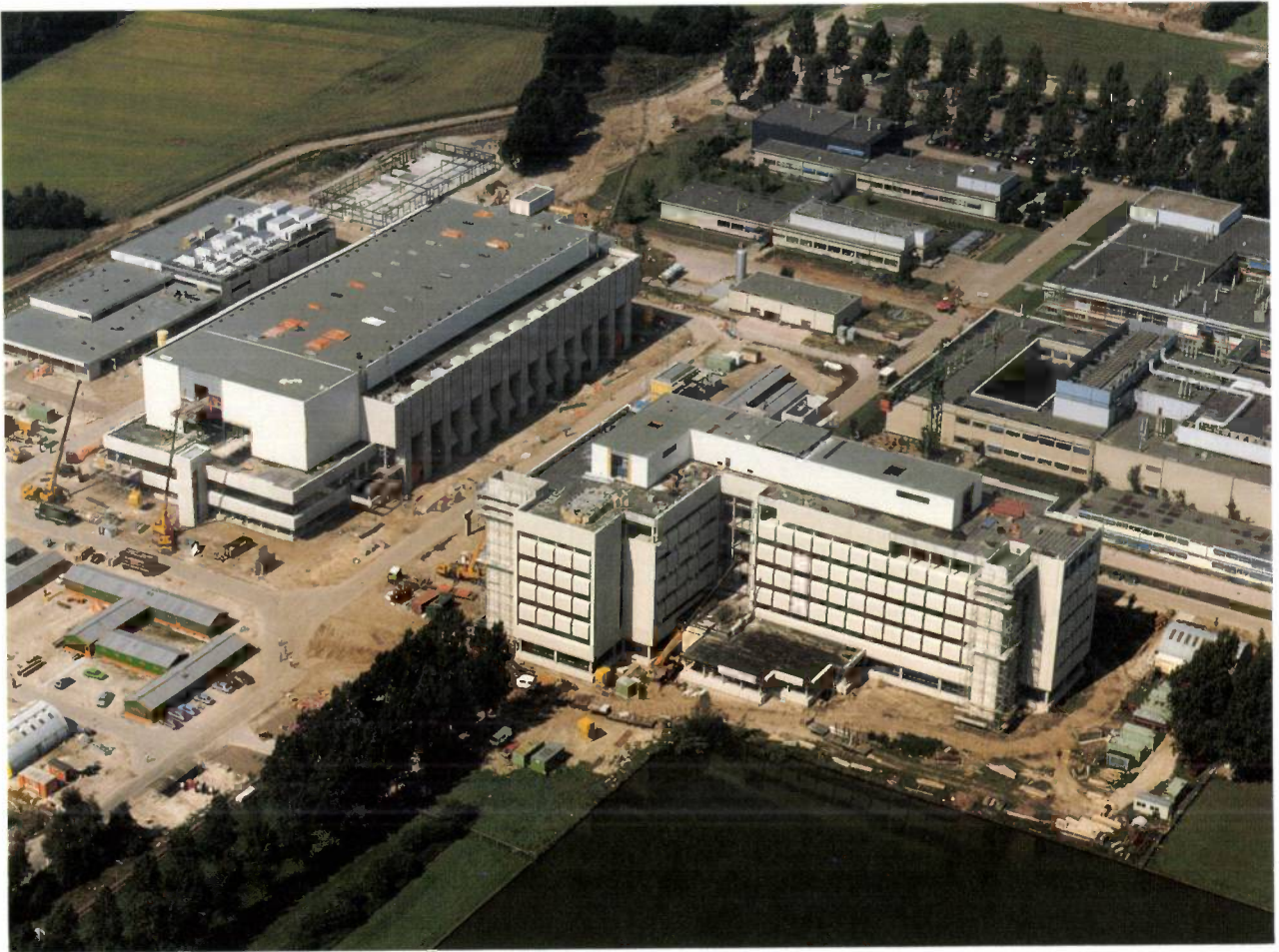
[26] P. Willich, J. Microsc. & Spectrosc. Electronics (to be published).

[27] H. H. Brongersma, F. Meijer and H. W. Werner, Philips Tech. Rev. 34, 357-369, 1974.

[28] J. L. Pouchou and F. Pichoir, Rech. Aérosp. 5, 349-367, 1984.

Summary. Electron-probe microanalysis is based on the detection of characteristic X-radiation generated by local bombardment with electrons. When differences in sample and standard are taken into account, the corresponding concentration by weight can be derived from the intensity of a characteristic X-ray line. In this way concentrations of nine elements in epitaxial iron-garnet films can be determined in a time of only two minutes. In amorphous metal alloys thinner than $1 \mu\text{m}$ the effect of the electron energy on the X-ray escape depth is particularly important. Analyses of light elements are also possible with an appropriate electron energy and the appropriate data processing. In sputtered films the quantity of incorporated argon can be determined by comparison with a standard obtained by extrapolation of data for lighter elements. Oxygen analyses provide information about the incorporated quantity of oxygen and the thickness of an oxidized surface layer. The thickness and composition of films thinner than $0.3 \mu\text{m}$ can be derived from the measured intensities, using calculated calibration curves.

Expansion of IC activities



Photograph: Flying Camera, Eindhoven Airport.

In connection with the expansion of the Philips activities in VLSI (Very-Large-Scale Integration) new buildings have appeared at the Philips Research Laboratories site in Eindhoven. The tendency to increase the size of ICs and reduce the details leads to 'submicron technology'. At the top left is the laboratory for research and development work on this process technology; this building will also house the pilot production of ICs. The special architectural feature of the building is that some of the floors are almost unaffected by vibration. The air-treatment plant is designed to bring the dust content of the air to a very low level, much lower than has normally been used previously in IC production. The building at the lower right will house the IC design centre. At the heart of this building there are areas for computers and measuring equipment, which will be used for designing, simulating and testing the VLSI circuits.

An article on the new IC activities will appear shortly.

Weighing and sorting machine

In many industrial processes the dosage of small quantities of raw materials (in milligrams or in parts of milligrams) plays an important role, as it does at Philips. Examples are to be found in the manufacture of certain lamps. In some types of fluorescent lamps minute quantities of alloys are used to control the mercury pressure in the lamp; in high-pressure gas-discharge lamps tiny amounts of iodides and sodium amalgams are used. If the additive consists of small units of exactly known mass, weighing during production is unnecessary, and it is sufficient to add a specific number of these units.

This is why methods for making spherical particles of an additive are being studied at Philips Research Laboratories in Eindhoven. The particles are obtained by solidification of spherical droplets of molten material. Since the ratio of area to mass is lowest for spherical particles, contaminating influences can be minimized. This is extremely important for the applications mentioned above. Spherical particles with a mass of less than a few milligrams are obtained from droplets which are produced by interrupting a jet of the molten material by means of an applied vibration. Since the spherical particles obtained in this way have too large a spread in weight, they have to be sorted. We have therefore developed a weighing and sorting machine, based on a prototype that was designed and made for us by B. J. Mulder of our Laboratories [1]. Our new machine is capable of weighing spherical particles of mass from 0.1 to 20 mg and can make 7000 measurements an hour. The weighed particles are sorted into three categories ('too light', 'correct', 'too heavy'), with continuously variable limits between them. The sorting limits usually contain a mass interval of a few hundred micrograms.

We shall first explain the operation of the weighing element, and then we shall describe the machine itself.

The weighing element (see *fig. 1*) consists of two commercially available piezoelectric flexure elements, which are connected in series electrically. The two elements are connected in parallel mechanically, with a small collector plate. The connection between the elements and the plate consists of a light and stiff frame of glass tubing. The spherical particles fall on to the plate from a fixed height, with zero initial velocity. The plate is covered with a thin layer of rubber selected for its high mechanical damping, so that the orientation

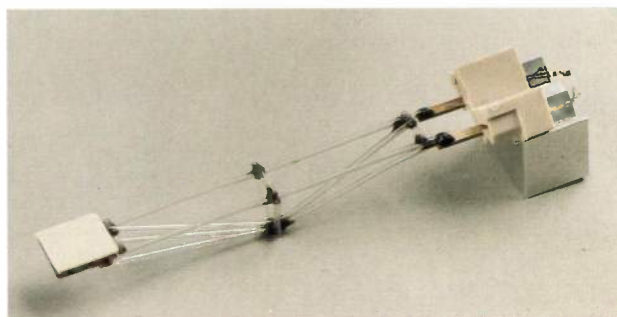


Fig. 1. Photograph of the weighing element. On the right two piezoelectric flexure elements can be seen. These are clamped in two tilted rubber blocks, which in turn are fixed to an aluminium block. The particles fall on the plate on the left. The 'framework' of glass tubing is very light and stiff.

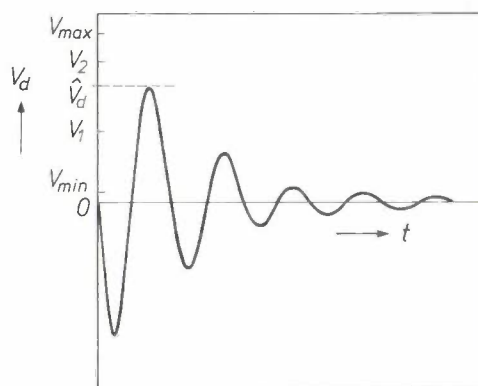


Fig. 2. The signal V_d from the weighing element, generated by a particle falling on it, as a function of time t . The height of the first maximum (\hat{V}_d) is a measure of the mass of the particle. The period of the damped vibration is about 12 ms. V_1 , V_2 lower and upper limits of the sorting mechanism. V_{min} , V_{max} extreme limits of V_1 and V_2 for the operation of the electronic circuits. In the model described, $V_{min} = 2$ V and $V_{max} = 10$ V.

of an imperfectly spherical particle has little effect on the transfer of momentum from the particle to the plate. The electrical signal generated in the piezoelectric elements by the transfer of momentum is shown in *fig. 2*. The waveform of the signal represents the damped vibration of the weighing element. The height of the first maximum, corresponding to the first upward movement of the plate, was found to be the best measure of the mass of the particle, since it is proportional to the mass. *Fig. 3* shows a calibration chart for

[1] B. J. Mulder, Dynamic weight detector for milligram particles, *J. Phys. E* 15, 501-503, 1982.

different values of the signal gain. Each point of the chart was obtained by determining the signal maximum \hat{V}_d for a number of particles (e.g. 8) of about the same mass ($\pm 10\%$) at different values of gain. The mean signal for each group of particles was then plotted against the mean mass, with the gain as parameter.

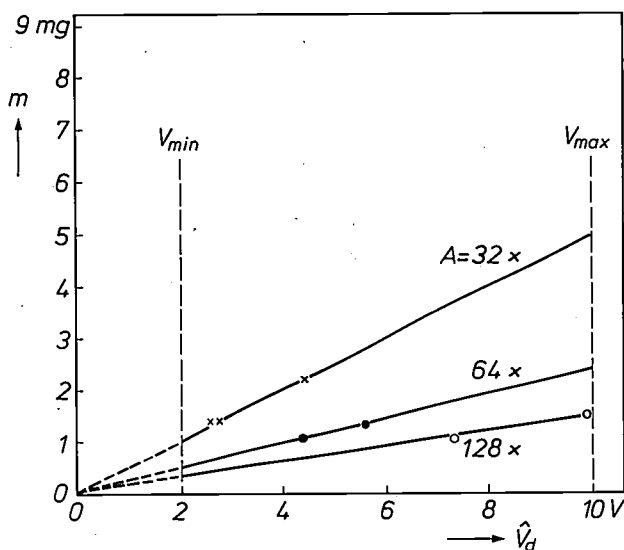


Fig. 3. Calibration chart for the weighing element. The mass m is plotted against \hat{V}_d for different values of the signal gain A . This can be varied between $1\times$ and $256\times$ by doubling.

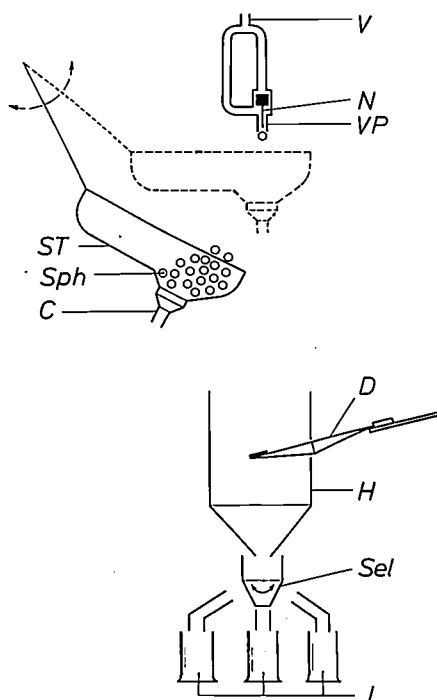


Fig. 4. Diagram of the weighing and sorting machine. V connection for vacuum lead. VP vacuum pipette. N needle. ST mobile stock tray. Sph spherical particles. C compressed air feed. H hopper. D weighing element (detector). Sel selector. J collector jars.

By varying the gain of the signal, a desired difference in mass can be converted into a voltage difference that can be processed by the electronic measuring equipment.

The weighing and sorting machine is shown schematically in *fig. 4*, with photographs in *fig. 5*. A mobile stock tray contains a quantity of spherical particles that must be weighed and sorted. Compressed air blown in from underneath the tray creates a 'fluid bed' of the particles. (Instead of compressed air a pure inert gas may be used, e.g. if particles sensitive to water or oxygen have to be sorted.) The pressure in a vacuum pipette is adjusted so that a particle is drawn against the pipette whenever the stock tray moves underneath it.

The pipette can easily be changed to adapt the size of the suction opening to the size of the particles. The tip of the pipette is made of aluminium and coated with a layer of platinum or hafnium nitride. Aluminium was chosen because it can be machined accurately, while the platinum or hafnium nitride prevents static charge, contamination and chemical reactions with the material of the particles. Inside the pipette there is a small steel needle, which is also coated with a layer of platinum or hafnium nitride (see also *fig. 6*). In its lowest position this needle only projects a few tenths of a millimetre from the pipette opening. If the vacuum is cut off, the needle drops through a distance of a few millimetres. Any particle that might have remained stuck to the pipette is then given a very small initial momentum. Although this does give the particle a small initial velocity, the contribution to the measured result is negligible.

As soon as a particle has been picked up by the pipette, the stock tray moves downwards and to one side, and the vacuum in the pipette is temporarily cut off, so that the particle is released. It falls exactly on to the centre of the plate of the weighing element, which is located in a hopper. After the particle has bounced off the plate (and thus been weighed) it continues its way downwards. It only takes a fraction of the time of descent for the electronic circuits to decide whether the signal generated lies inside or outside the preset limits V_1 and V_2 , and a selector is then set to the appropriate position to ensure that the particle arrives in the appropriate collector jar ('too light', 'correct', 'too heavy'). The selector is moved by two electrically controlled rotary magnets. For the position of the selector to be adjusted quickly and without hesitation, the positions are fixed by phosphor-bronze leaf springs damped with silicone rubber. Electronic counters indicate the numbers of particles that are too light, correct and too heavy. If a microcomputer is used to control the machine and to process the measured data for

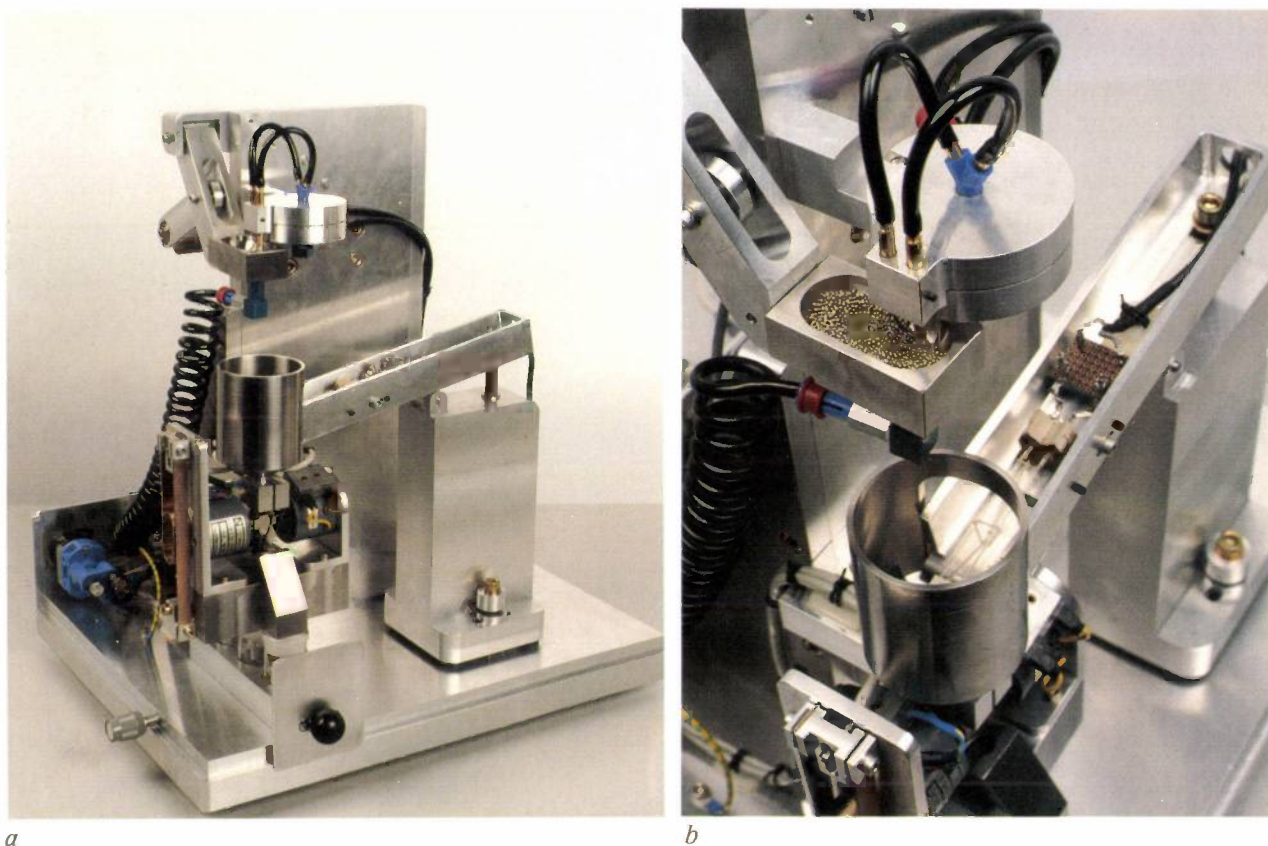


Fig. 5. The weighing and sorting machine (see also fig. 4). Its operation is described in the text. The control equipment for compressed air and vacuum and the equipment for measurement and data processing are not shown. *a)* This photograph shows the stock tray just below the vacuum pipette. The compressed gas is fed through the spiral tube. The supporting bar carrying the weighing element can be seen protruding from the right of the hopper. The selector mechanism can be seen between the two rotary magnets. Below these there is a drawer with three collector jars. The plastic cover normally fitted over the machine has been removed for making this photograph. *b)* Detail of the machine. The vacuum pipette is at the top, with the stock tray containing the spherical particles beneath it. The weighing element can easily be seen in the supporting bar that projects through the opening at the back of the hopper.

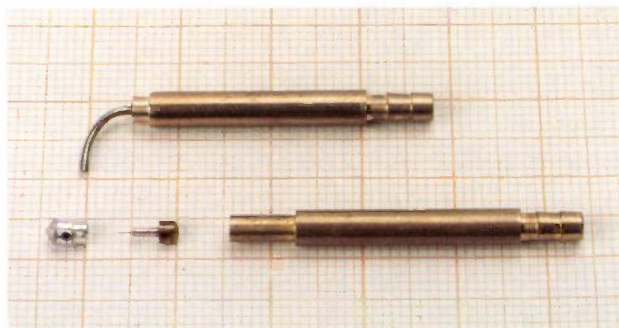


Fig. 6. Components of the vacuum pipette. Particles are drawn against the point on the left. The needle that removes any particles that stick to the pipette is on the right. The upper tube draws up the particle, the lower tube draws the needle back. The scale division in the background is in millimetres.

each particle, it is possible to make a statistical distribution of the mass of the particles in each of the collector jars, since the mass of each particle is known and therefore the jar it goes into. It is then easy to determine the mass fraction that can be selected from the rejected particles for some other application.

A. Huizing
A. H. T. Sanders
J. F. K. Thijssen

A. Huizing, A. H. T. Sanders and J. F. K. Thijssen are with Philips Research Laboratories, Eindhoven.

Scientific publications

These publications are contributed by staff of laboratories and plants that form part of or cooperate with enterprises of the Philips group of companies, particularly by staff of the research laboratories mentioned below. The publications are listed alphabetically by journal title.

Philips GmbH Forschungslaboratorium Aachen, Weißhausstraße, 5100 Aachen, Germany	A
Philips Research Laboratory, Brussels, 2 avenue Van Becelaere, 1170 Brussels, Belgium	B
Philips Natuurkundig Laboratorium, Postbus 80 000, 5600 JA Eindhoven, The Netherlands	E
Philips GmbH Forschungslaboratorium Hamburg, Vogt-Kölln-Straße 30, 2000 Hamburg 54, Germany	H
Laboratoires d'Electronique et de Physique Appliquée, 3 avenue Descartes, 94450 Limeil-Brévannes, France	L
Philips Laboratories, N.A.P.C., 345 Scarborough Road, Briarcliff Manor, N.Y. 10510, U.S.A.	N
Philips Research Laboratories, Cross Oak Lane, Redhill, Surrey RH1 5HA, England	R
Philips Research Laboratories, Sunnyvale P.O. Box 9052, Sunnyvale, CA 94086, U.S.A.	S

D. Küppers, K. H. Schelhas, U. Biermann, G. D. Khoe & H. G. Kock	A, E	Microlenses prepared by the plasma-activated chemical vapor deposition technique	Adv. Low-Temp. Plasma Chem. Technol. Appl. 1	92-107	1984
H. Ihrig	A	Physics and technology of PTC-type BaTiO ₃ ceramics	Advances in Ceramics, Vol. 7, American Ceramic Society, Columbus, OH	117-127	1984
P. E. Wierenga, D. J. Broer & J. H. M. van de Linden	E	Mechanical characterization of optical-fiber coatings by ultramicroindentation measurements	Appl. Opt. 24	960-963	1985
P. C. Zalm, P. M. J. Marée* & R. I. J. Olthof* (* FOM, Amsterdam)	E	Silicon molecular beam epitaxy on gallium arsenide	Appl. Phys. Lett. 46	597-599	1985
F. L. van Nes (<i>Inst. for Perception Res., Eindhoven</i>)		Limits of visual perception in the technology of visual display terminals	Behav. & Inf. Technol. 3	371-377	1984
W. Hermann, H. Rau & J. Ungelenk	A	Solubility and diffusion of chlorine in silica glass	Ber. Bunsenges. Phys. Chem. 89	423-426	1985
S. M. Marcus (<i>Inst. for Perception Res., Eindhoven</i>)		Associative models and the time course of speech	Biblioth. Phonet. 12	36-52	1985
J. E. A. M. van den Meerakker	E	The reduction of iodine at GaAs: the role of potential-redistribution at the semiconductor/electrolyte interface	Electrochim. Acta 30	435-440	1985
D. H. Evans	R	High-efficiency Ka- and Ku-band MESFET oscillators	Electron. Lett. 21	254-255	1985
P. K. Larsen & B. A. Joyce	E, R	Surface studies of MBE-grown semiconductor films	Europhys. News 16 (No. 4)	12-15	1985
J. L. van Meerbergen & F. J. van Wijk	E	A 256-point discrete Fourier transform processor using 2µm ED-NMOS technology	Fachtagung Gross Integration, Baden-Baden 1983	44-48	1984
P. A. Devijver, C. Ronse, P. Haaker, E. Klotz, R. Koppe & R. Linde	B, H	Pseudomask technique for digital subtraction angiography (DSA)	Inf.-Fachber. 87	230-236	1984
W. J. van Gils	E	How to cope with faulty processors in a completely connected network of communicating processors	Inf. Process. Lett. 20	207-213	1985
F. E. J. Kruseman Aretz	E	Aard en wezen van software	Informatie 27	245-332	1985
F. E. J. Kruseman Aretz	E	Software-educatie voor management	Informatie 27	549-644	1985
D. M. Krol & R. K. Janssen	E	Raman study of grain size effects in the melting behavior of 15Na ₂ CO ₃ -10BaCO ₃ -75SiO ₂ batches	J. Am. Ceram. Soc. 67	796-799	1984
A. H. van Ommen	E	Diffusion of ion-implanted Ga in SiO ₂	J. Appl. Phys. 57	1872-1879	1985

- | | | | | | |
|---|------|--|--|---------------|------|
| H. K. Kuiken & C. van Opdorp | E | Evaluation of diffusion length and surface-recombination velocity from a planar-collector-geometry electron-beam-induced current scan | J. Appl. Phys. 57 | 2077-2090 | 1985 |
| R. Schäfer & H. P. Stormberg | A | Time-dependent behavior of the contraction regions of high-pressure mercury arcs | J. Appl. Phys. 57 | 2512-2518 | 1985 |
| H. J. de Wit & M. Brouha | E | Domain patterns and high-frequency magnetic properties of amorphous metal ribbons | J. Appl. Phys. 57 | 3560-3562 | 1985 |
| C. A. M. de Vries, A. J. van Roosmalen & G. C. C. Puylaert | E | Microwave spectroscopic measurement of the electron density in a planar discharge: relation to reactive-ion etching of silicon oxide | J. Appl. Phys. 57 | 4386-4390 | 1985 |
| F. Weling | A | A model for the plasma-activated chemical vapor deposition process | J. Appl. Phys. 57 | 4441-4446 | 1985 |
| A. H. van Ommen | E | Diffusion of ion-implanted In and Tl in SiO ₂ | J. Appl. Phys. 57 | 5220-5225 | 1985 |
| H. M. van Noort, D. B. de Mooij & K. H. J. Buschow | E | ⁵⁷ Fe Mössbauer spectroscopy study of the magnetic properties of R ₂ Fe ₁₄ B compounds (R = Ce, Nd, Gd, Y) | J. Appl. Phys. 57 | 5414-5419 | 1985 |
| W. F. van der Weg (<i>Univ. Utrecht</i>), Th. J. A. Popma (<i>Tech. Univ., Enschede</i>) & A. T. Vink | E | Concentration dependence of UV and electron-excited Tb ³⁺ luminescence in Y ₃ Al ₅ O ₁₂ | J. Appl. Phys. 57 | 5450-5456 | 1985 |
| E. P. Honig | E | The nature of the surface charge on ionic crystals | J. Chem. Soc. Faraday Trans. 1 81 | 703-711 | 1985 |
| J. C. Jacco, G. M. Loiacono, M. Jaso, G. Mizell & B. Greenberg | N | Flux growth and properties of KTiOPO ₄ | J. Cryst. Growth 70 | 484-488 | 1984 |
| P. F. Bordui, J. J. Zola, G. Kostecky & G. M. Loiacono | N | Aqueous solution growth of KDP from "spliced" seeds | J. Cryst. Growth 71 | 269-272 | 1985 |
| J. E. A. M. van den Meerakker, J. J. Kelly & P. H. L. Notten | E | The minority carrier recombination resistance: a useful concept in semiconductor electrochemistry | J. Electrochem. Soc. 132 | 638-642 | 1985 |
| A. Molenaar & B. C. M. Meenderink | E | Electrochemical study of the autocatalytic deposition of gold-copper alloys | J. Electrochem. Soc. 132 | 574-576 | 1985 |
| W. A. P. Claassen, W. G. J. N. Valkenburg, M. F. C. Willemsen & W. M. van de Wijgert | E | Influence of deposition temperature, gas pressure, gas phase composition and RF frequency on composition and mechanical stress of plasma silicon nitride layers | J. Electrochem. Soc. 132 | 893-898 | 1985 |
| M. W. M. Graef | E | The mechanism of aluminum electrodeposition from solutions of AlCl ₃ and LiAlH ₄ in THF | J. Electrochem. Soc. 132 | 1038-1046 | 1985 |
| L. J. van Ruyven (<i>Nederlandse Philips Bedrijven, Eindhoven</i>) | | Double heterojunction lasers and quantum well lasers | J. Lumin. 29 | 123-161 | 1984 |
| P. Schobinger-Papamantellos (<i>ETH, Zürich</i>) & K. H. J. Buschow | E | Magnetic properties of Nd ₅ Ge ₃ studied by neutron diffraction and magnetic measurements | J. Magn. & Magn. Mater. 49 | 349-356 | 1985 |
| G. de With, P. J. Vrugt & A. J. C. van de Ven | E | Sodium corrosion resistance of translucent alumina: effect of additives and sintering conditions | J. Mater. Sci. 20 | 1215-1221 | 1985 |
| J. W. C. de Vries*, R. C. Thiel* (* <i>Univ. Leiden</i>) & K. H. J. Buschow | E | Volume effects on the Mössbauer isomer shift in intermetallic compounds containing gadolinium | J. Phys. F 15 | 1413-1426 | 1985 |
| J. W. D. Martens, W. L. Peeters, H. M. van Noort & M. Erman | E, L | Optical, magneto-optical and Mössbauer spectroscopy on Co ³⁺ substituted cobalt ferrite Co ²⁺ Fe _{2-x} Co _x ³⁺ O ₄ (0 ≤ x ≤ 2) | J. Phys. & Chem. Solids 46 | 411-416 | 1985 |
| C. A. M. Mulder & J. T. Klomp | E | On the internal structure of Cu- and Pt-sapphire-interfaces | J. Physique 46 (Colloque C4) | C4/111-C4/116 | 1985 |
| H.-P. Stormberg & R. Schäfer | A | Determination of temperature profiles from optically thick lines | J. Quant. Spectrosc. & Radiat. Transfer 33 | 27-33 | 1985 |
| R. C. Ellwanger (<i>Signetics Corp., Orem, UT</i>), A. E. Morgan, W. T. Stacy & Y. Tamminga | S, E | The Schottky barrier height of platinum nickel silicide | J. Vac. Sci. & Technol. B 1 | 533-539 | 1983 |
| B. A. Joyce, J. H. Neave, P. J. Dobson, P. K. Larsen & J. Zhang (<i>Imp. College, London</i>) | R, E | A RHEED/ARPES/CORE level spectroscopic evaluation of the structure of MBE-grown GaAs(001)-2×4 surfaces | J. Vac. Sci. & Technol. B 3 | 562 | 1985 |
| C. T. Foxon, J. B. Clegg, K. Woodbridge, D. Hilton, P. Dawson & P. Blood | R | The effect of the oxygen concentration on the electrical and optical properties of AlGaAs films grown by MBE | J. Vac. Sci. & Technol. B 3 | 703 | 1985 |

A. E. T. Kuiper, G. C. J. van der Ligt, W. M. van de Wijgert, M. F. C. Willemsen & F. H. P. M. Habraken	E	Surface segregation and initial oxidation of titanium silicide films	J. Vac. Sci. & Technol. B 3	830-835	1985
B. Smets	E	De aantasting van glas door water: ionenuitwisseling of diffusie van H ₂ O?	Klei/Glas/Keramiek 4	89-92	1983
C. M. J. van Uijen, J. H. den Boef & F. J. J. Verschuren	E	Fast Fourier imaging	Magn. Resonance Med. 2	203-217	1985
H. M. van Noort, J. W. D. Martens & W. L. Peeters	E	The cation distribution of CoFe _{2-x} Al _x O ₄ as determined by conversion electron Mössbauer spectroscopy	Mater. Res. Bull. 20	41-47	1985
L. A. H. van Hoof & W. J. Bartels	E	The perfection of Bridgman-grown Bi ₄ Ge ₃ O ₁₂ crystals	Mater. Res. Bull. 20	79-83	1985
S. D. Brotherton, P. Bradley & A. Gill	R	Low temperature interactions between gold and iron in silicon	Mater. Res. Soc. Symp. Proc. 36	31-36	1985
M. P. A. Vieggers, C. W. T. Bulle-Lieuwma, P. C. Zalm & P. M. J. Marée (FOM-Amsterdam)	E	Misfit dislocations in epitaxial layers of Si on GaP (001) substrates	Mater. Res. Soc. Symp. Proc. 37	331-342	1985
A. W. Kolfshoten	E	Effects of the combined exposure of silicon to beams of low-energy argon ions and halogen containing molecules	Mater. Res. Soc. Symp. Proc. 38	143-153	1985
J. T. Klomp	E	Ceramic-metal interactions	Mater. Res. Soc. Symp. Proc. 40	381-391	1985
W. J. A. Goossens	E	Bulk, interfacial and anchoring energies of liquid crystals	Mol. Cryst. & Liq. Cryst. 124	305-331	1985
E. Aarts & P. van Laarhoven	E	Statistische fysica en optimalisatie bij IC-ontwerp	Ned. T. Natuurk. B 51	67-68	1985
J. Dieleman, F. H. M. Sanders & P. C. Zalm	E	Experimental evidence for the absence of local thermal equilibrium in chemical sputtering	Nucl. Instrum. & Methods Phys. Res. B7/8	809-813	1985
G. Dittmer & U. Niemann	A	Heterogeneous reactions and chemical transport of tantalum with chlorine and bromine	Philips J. Res. 40	55-71	1985
J. G. Dil, J. W. Bartsen, R. D. J. Verhaar & A. E. T. Kuiper	E	LOCOS with thick and thin nitride masking	Philips J. Res. 40	72-87	1985
J. J. H. van den Biesen	E	P-N junction capacitances. Part I: the depletion capacitance	Philips J. Res. 40	88-102	1985
J. J. H. van den Biesen	E	P-N junction capacitances. Part II: the neutral capacitance	Philips J. Res. 40	103-113	1985
D. R. Wolters & J. J. van der Schoot	E	Dielectric breakdown in MOS devices. Part I: defect-related and intrinsic breakdown	Philips J. Res. 40	115-136	1985
D. R. Wolters & J. J. van der Schoot	E	Dielectric breakdown in MOS devices. Part II: conditions for the intrinsic breakdown	Philips J. Res. 40	137-163	1985
D. R. Wolters & J. J. van der Schoot	E	Dielectric breakdown in MOS devices. Part III: the damage leading to breakdown	Philips J. Res. 40	164-192	1985
T. T. M. Palstra*, G. J. Nieuwenhuys*, J. A. Mydosh* (* Univ. Leiden) & K. H. J. Buschow	E	Mictomagnetic, ferromagnetic, and antiferromagnetic transitions in La(Fe _x Al _{1-x}) ₁₃ intermetallic compounds	Phys. Rev. B 31	4622-4632	1985
H. Höchst*, E. Colavita* (* Univ. Wisconsin, Madison, WI) & K. H. J. Buschow	E	Photoemission study of the hydrogenation of the intermetallic compounds YFe ₃ and YFe ₂	Phys. Rev. B 31	6167-6171	1985
J. W. C. de Vries*, R. C. Thiel* (* Univ. Leiden) & K. H. J. Buschow	E	Magnetic properties and ¹⁵¹ Eu Mössbauer effect studied in Eu-Ga and Eu-Sn intermetallic compounds	Physica 128B	265-272	1985
J. W. C. de Vries*, R. C. Thiel* (* Univ. Leiden) & K. H. J. Buschow	E	The hybridization contribution to the Mössbauer isomer shift in intermetallic compounds containing ¹⁵¹ Eu	Physica 128B	309-312	1985
M. Rocchi	L	Status of the surface and bulk parasitic effects limiting the performances of GaAs IC's	Physica 129B	119-138	1985
A. H. van Ommen, H. G. R. Maas & J. A. Appels	E	Bombardment induced strengthening of nitride (BISON) a novel effect in the etch properties of ion implanted LPCVD - Si ₃ N ₄	Physica 129B	220-223	1985

- Y. Crosnier*, G. Salmer*, H. Gérard*, J. Wyrwinski* (* *Univ. Sci. & Tech. Lille, Villeneuve d'Ascq*) & P. Baudet
L
New aspects of the power limitations in the GaAs MESFETs
Physica **129B** 395-398 1985
- B. Gabillard, C. Rocher & M. Rocchi
L
Theoretical and experimental temperature dependence of GaAs N-OFF IC's over 120 K to 400 K
Physica **129B** 403-407 1985
- K. E. Knol*, L. W. van Horssen, G. Challa* (* *Univ. Groningen*) & E. E. Havinga
E
Synthesis, crosslinking and electrical conductivity of poly-1,8-nonadiyne
Polym. Commun. **26** 71-73 1985
- A. J. M. van Gorp* & J. H. C. van Mourik* (* *Philips Centre for Manufacturing Technol., Eindhoven*)
Development of a multilayer/overglaze system
Proc. 5th Eur. Hybrid Microelectronics Conf., Stresa 1985 2-9 1985
- P. de Groot (*AT&T and Philips Telecommun., Hilversum*), A. G. van Nie & W. Rey
E
An extrapolation method for estimating the long-term drift of (thick) film resistors
Proc. 5th Eur. Hybrid Microelectronics Conf., Stresa 1985 66-76 1985
- H. H. M. van Roij* & J. W. van Dalen* (* *AT&T and Philips Telecommun., Hilversum*)
A hybrid integrated micropackage with a fiber coupling to a PIN-FET receiver front-end
Proc. 5th Eur. Hybrid Microelectronics Conf., Stresa 1985 439-445 1985
- R. Kersten & B. Vitt
A
A simplified solar domestic hot water and heating system with evacuated tubular heat pipe collectors
Proc. IEC Conf. on Solar heating, 1985 7 pp. 1985
- A. J. P. Theuwissen, C. H. L. Weijtens, L. J. M. Esser, J. N. G. Cox, H. T. A. R. Duyvelaar & W. C. Keur
E
The accordion imager: an ultra high density frame transfer CCD
Proc. IEDM 84, San Francisco 1984 40-43 1984
- T. Poorter & P. Zoestbergen
E
Hot carrier effects in MOS transistors
Proc. IEDM 84, San Francisco 1984 100-103 1984
- R. Jayaraman, V. Rumennik, B. Singer & E. H. Stupp
N
Comparison of high voltage devices for power integrated circuits
Proc. IEDM 84, San Francisco 1984 258-261 1984
- J. W. Slotboom, J. W. Bartsen, J. G. Dil, M. J. J. Pelgrom, J. J. M. J. de Klerk, R. D. J. Verhaar, C. A. H. Juffermans, D. J. Vinton & J. P. Swetman
E, R
Submicron CCD memory structures fabricated by electron-beam lithography
Proc. IEDM 84, San Francisco 1984 308-311 1984
- F. M. Klaassen, J. J. Bastiaens, W. Hes & M. Sprokel
E
Scaling of compensated MOSFETs towards submicron dimensions
Proc. IEDM 84, San Francisco 1984 613-616 1984
- F. Manola & A. Pirotte
B
An approach to multi-model database systems
Proc. 2nd Int. Conf. on Databases, Cambridge 1983 53-57 1983
- L. F. Feiner
E
Transition metal impurities in silicon: substitutional on interstitial?
Proc. 13th Int. Conf. on Defects in semiconductors, Coronado, CA, 1984 877-883 1984
- P. Dawson, S. Duggan, H. I. Ralph & K. Woodbridge
R
Photoluminescence decay times in multiple quantum well heterostructures prepared by molecular beam epitaxy
Proc. 17th Int. Conf. on the Physics of semiconductors, San Francisco 1984 551-554 1985
- R. N. Bhargava
N
II-VI semiconductor materials and devices — recent progress
Proc. 17th Int. Conf. on the Physics of semiconductors, San Francisco 1984 1531-1536 1985
- S. Colak, G. M. Loiacono, G. Mizell, W. K. Zwicker & R. C. Powell (*Oklahoma State Univ., Stillwater, OK*)
N
Spectroscopic survey of some new transition metal ion-host structures
Proc. Int. Conf. on Lasers, 1983 179-184 1983
- P.-J. Courtois & P. Semal
B
Error bounds for the analysis by decomposition of non-negative matrices
Proc. Int. Workshop on Applied mathematics and performance reliability, Pisa 1983 253-268 1983
- J. L. van Meerbergen & F. J. van Wijk
E
A 2 μ NMOS 256-point discrete Fourier transform processor
Proc. ISSCC'83, New York 1983 3 pp. 1983
- K. H. J. Buschow
E
Magnetic and electronic properties of amorphous alloys based on 3d transition metals
Proc. MRS Conf., Strasbourg 1984 313-323 1984

J. Wijdenes & M. J. H. J. Geomini	E	Effect of photoresist composition on the origin of the interfacial layer in the bilevel system	Proc. SPIE 539	97-102	1985
E. D. Roberts	R	Improvements to the dry-etch resistance of sensitive positive-working electron resists	Proc. SPIE 539	124-130	1985
R. Brehm & J. Haisma	E	Verspanen van glas met een beitel is realiseerbaar	PT/Werktuigbouw 40 (No. 5)	36-39	1985
J. M. Robertson, M. Brouha, H. H. Stel & A. J. C. van der Borst	E	Surface quality and thickness effects of amorphous ribbons for recording head applications	Rapidly quenched metals, S. Steeb & H. Warlimont (eds), Elsevier Science, Amsterdam	79-82	1985
K. H. J. Buschow	E	Formation, thermal stability and magnetic properties of amorphous Ni-base alloys	Rapidly quenched metals, S. Steeb & H. Warlimont (eds), Elsevier Science, Amsterdam	163-170	1985
C. Ronse & P. Devijver	B	Connected components in binary images: the detection problem	Research Studies Press, Letchworth	165 pp.	1984
P. Q. J. Nederpel & J. W. D. Martens	E	Magneto-optical ellipsometer	Rev. Sci. Instrum. 56	687-690	1985
J. F. Dijkstra & E. P. W. Savenije	E	The flow of Newtonian and non-Newtonian liquids through annular converging regions	Rheol. Acta 24	105-118	1985
M. Davio & J.-M. Goethals	B	Elements of cryptology	Secure digital communication, G. Longo (ed.), Springer, Wien	1-59	1983
P. Severin	E	Optische actieve en passieve sensoren, fase en amplitude metingen	Seminar optische fibertechniek en opto-elektronica, PBNA, Arnhem	8 pp.	1984
P. Severin	E	Materialen, typen, definities, gebruik van optische vezels voor niet-datacommunicatie doeleinden	Seminar optische fibertechniek en opto-elektronica, PBNA, Arnhem	16 pp.	1984
P. Murau	N	Characteristics of an X-Y addressed electrophoretic image display (EPID)	SID 84 Digest, San Francisco 1984	141	1984
D. Cammack, R. Dalby, D. Walz & R. N. Bhargava	N	Performance of ZnS _x Se _{1-x} dc and ac TFEL devices	SID 84 Digest, San Francisco 1984	34-36	1984
M. J. J. Theunissen & F. J. List	E	Analysis of the soft reverse characteristics of n ⁺ p drain diodes	Solid-State Electron. 28	417-425	1985
H. van Doveren	E	Laser mass spectroscopy	Spectrochim. Acta 39B	1513-1516	1984
J. Gerkema & A. R. Miedema	E	Adhesion between solid metals: observations of interfacial segregation effects in metal film lubrication experiments	Surf. Sci. 124	351-371	1983
P. C. Zalm & L. J. Beckers	E	Ion-induced secondary electron emission from copper and zinc	Surf. Sci. 152/153	135-141	1985
M. J. Sparnaay	E	Thermodynamics (with an emphasis on surface problems)	Surf. Sci. Rep. 4	101-270	1984
L. Gillott*, P. N. Guile*, N. Cowlam* (* Univ. Sheffield) & K. H. J. Buschow	E	A structural investigation of hafnium-based transition metal glasses	The structure of non-crystalline materials 1982, P. H. Gaskell <i>et al.</i> (eds), Taylor & Francis, London	455-464	1983
D. R. Wolters	E	Growth, conduction, trapping and breakdown of SiO ₂ layers on silicon	Thesis, Groningen	163 pp.	1985
F. J. A. den Broeder	E	Diffusion-induced grain boundary migration and recrystallization, exemplified by the system Cu-Zn	Thin Solid Films 124	135-148	1985
J. Visser & J. E. Crombeen	E	D. C. planar magnetron sputtering source for video disc metallization	Vak. Tech. 34	67-77	1985
F. P. Welten, A. Delaruelle, F. J. van Wijk, J. L. van Meerbergen, J. Schmid* & K. Rinner* (* TEKADE, Nürnberg)	E	A 2 micron CMOS, 10 MHz, microprogrammable vector processing unit with on-chip 3-port register file for incorporation in single chip general purpose digital signal processors	VLSI signal processing, P. R. Capello <i>et al.</i> (eds), IEEE Press, New York	76-87	1984
J. Gerkema	E	Lead thin film lubrication	Wear 102	241-252	1985

Recent United States Patents

Abstracts from patents that describe inventions from the following research laboratories, which form part of or cooperate with the Philips group of companies:

Philips GmbH Forschungslaboratorium Aachen, Weißhausstraße, 5100 Aachen, Germany	A
Philips Research Laboratory Brussels, 2 avenue Van Becelaere, 1170 Brussels, Belgium	B
Philips Natuurkundig Laboratorium, Postbus 80 000, 5600 JA Eindhoven, The Netherlands	E
Philips GmbH Forschungslaboratorium Hamburg, Vogt-Kölln-Straße 30, 2000 Hamburg 54, Germany	H
Laboratoires d'Electronique et de Physique Appliquée, 3 avenue Descartes, 94450 Limeil-Brévannes, France	L
Philips Laboratories, N.A.P.C., 345 Scarborough Road, Briarcliff Manor, N.Y. 10510, U.S.A.	N
Philips Research Laboratories, Cross Oak Lane, Redhill, Surrey RH1 5HA, England	R
Philips Research Laboratories Sunnyvale, P.O. Box 9052, Sunnyvale, CA 94086, U.S.A.	S

4 527 124

Method of and device for determining a nuclear magnetization distribution in a part of a body

C. M. J. van Uijen

E

The invention proposes a method and a device in which resonance signals (generated for NMR imaging) are sampled in the presence of a (semi-) static and a time modulated gradient magnetic field, the gradient direction of the fields applied being mutually perpendicular. The resonance signal is conditioned prior to the start of sampling. The sampled signals are associated with spatial frequencies (i.e. points in a spatial frequency space (k_x, k_y) which is the (2-D) Fourier transform of the actual (x, y) space), which are determined by the applied gradient fields. The (semi-) static gradient field always produces an increase (for example, in k_x), while the time modulated gradient field always produces an image frequency which lies between two limits (k_y and $k_y + k_y$). Consequently, the invention enables the determination of data in an entire band in the (k_x, k_y) space; this is in contrast with the present state of the art where data can be collected only along a straight line (k_x or k_y is constant), or on the entire region of interest (the total k_x, k_y space). The method and device according to the invention are also applicable for 3-D imaging of 3-D objects.

4 527 165

Miniature horn antenna array for circular polarization

F. C. de Ronde

L

An antenna for circularly polarized high-frequency signals comprising a succession of layers. A first insulating layer includes openings defined by metal plated walls forming miniature horns, each having a square cross-section. A first dielectric layer adjacent the first insulating layer supports a first supply network for signals whose direction of polarization is of a first type of linear polarization. A second insulating layer adjacent the first dielectric layer includes openings defined by metal plated walls forming miniature waveguides each having the same square cross-section as a respective horn, at the side facing the first supply network, and having a rectangular cross-section at the other side. A second dielectric layer adjacent the second insulating layer supports a second supply network for signals whose direction of polarization is perpendicular to the polarization of the signals of the first network. A third insulating layer adjacent the second dielectric layer includes openings defined by metal plated walls forming miniature waveguides each having the same rectangular cross-section as a respective waveguide in the second insulating layer, at the side facing the second network, and which has a depth smaller than the thickness of the third insulating layer.

4 527 130

Push-pull microwave oscillator with fundamental and second harmonic outputs

G. Lütteke

A

A push-pull microwave oscillator circuit, including two transistors, for producing the second harmonic of a fundamental frequency at a symmetry point of the circuit which is connected to the bases of the transistors through identical arrangements of circuit elements. The circuit includes tuning means coupled to at least one of the transistors, an output and an input. The output, which is utilized to provide to a phase comparison means an output signal at the fundamental of the second harmonic frequency, is coupled to the base of at least one of the transistors by a capacitive impedance. The input, which is utilized to receive a tuning signal produced by the phase comparison means in response to the output signal, is coupled to the tuning means.

4 527 255

Non-volatile static random-access memory cell

P. Keshtbod

S

A non-volatile memory cell contains a pair of cross-coupled like-polarity FET's that serve as a volatile location for storing a data bit and a like-polarity variable-threshold insulated-gate FET that serves as a non-volatile storage location. The variable-threshold FET has its source coupled to the drain of one of the cross-coupled FET's, its insulated-gate electrode coupled to the drain of the other of the cross-coupled FET's, and its drain coupled to a power supply. A pair of impedance elements are coupled between the drains of the cross-coupled FET's, respectively, on one hand and the power supply on the other hand. Just before a power shutdown which causes the data bit to evaporate, the power supply is pulsed to a suitable level to cause the bit to be transferred to the non-volatile location. When power is restored to the normal level, the original data bit automatically returns to the volatile location.



4 528 558

Door-open alarm device for a refrigerating appliance

M. Steers

L

J.-P. Hazan

M. Courdille

A door-open alarm device comprises alarm means connected to an electric circuit which comprises, arranged on the stationary part, a voltage source, a switch having two positions in which the circuit is interrupted and closed respectively, electrical time delay means responsive to a current flow in the circuit to produce a voltage variation across said alarm means after a time delay, thereby triggering said alarm means. Arranged on the door is a mechanical actuating element for said switch, which opens said switch when the door is wide open or closed, and which closes said switch when the door is ajar.

4 528 583

Programmable semiconductor device and method of manufacturing same

T. S. te Velde

E

A. Slob

A programmable semiconductor device having a microswitch which over a part of its length is provided separately from a bridging conductor, for example, a word line and a supporting element. Since the dimensions of the switch and the conductor are independent of each other, the resistance of the conductor may be low so that programmable memories having a high read-in and read-out rate are obtained. In addition the circuit element, for example a Schottky diode can be realized below the bridging part of the conductor, which results in a high bit density. Since the switch is present below the conductor the assembly can be passivated in the unprogrammed state by means of a protective layer, so that the switch is encapsulated in a hollow space.

4 528 695

Distribution system for a local fibre network

G. D. Khoe

E

A transparent optical distribution system which is tolerant to system variations and extension in future, such as the choice of analogue or digital signals, bandwidth, bit rate, the number of services and connections per subscriber comprises a common terminal unit provided at each subscriber's premises. The common terminal unit comprises an input connected via a power splitter to a distribution box which has a plurality of outputs each connected to a respective wall socket. A second distribution box has a plurality of inputs to which the wall sockets are connected and outputs which are connected via a power splitter to the input of the terminal unit. A third distribution box has a plurality of terminals connected to the wall sockets and a further plurality of terminals connected to a power splitter whose output is connected to a mirror. Intercommunication between terminals takes place via the third distribution box and is independent of incoming and outgoing signals.

4 529 027

Method of preparing a plurality of castings having a predetermined composition

J. C. Brice

R

C. R. Brough

A method is set forth for simultaneously preparing a plurality of castings of a solution of an element, or compound, in a solvent, which solvent may also be an element and/or a compound. The solution is saturated at a temperature T_s . A problem in liquid epitaxy growth processes is the simple preparation of growth charges of sufficient reproducible composition and size to produce epitaxial layers of reproducible composition and thickness. The present invention provides a melt consisting of the solvent, of the solvent together with at least one constituent of the solution, or of a solution which is unsaturated at the temperature T_s which melt is prepared in a boat body of a liquid-tight boat assembly. An equilibrium is established at T_s between the melt and a solid body having an excess of any constituent in which the melt is deficient with respect to the saturated solution so as to form the saturated solution.

The saturated solution is transferred into a plurality of moulds in which the solution is allowed to solidify to form the castings. The solid body is contained in a solid-retaining portion of a trough of the board body, which portion is separated from the remainder of the trough by an apertured partition.

4 529 445

Invar alloy on the basis of iron having a crystal structure of the cubic NaZn_{13} type

K. H. J. Buschow

E

An invar alloy on the basis of iron is formed by an intermetallic compound having a cubic crystal structure of the NaZn_{13} type having nominal composition $\text{La}(\text{FeCoX})_{13}$, wherein X is Si or Al. By subjecting the present intermetallic compound after melting to a tempering treatment at 800-1000 °C and cooling it in an accelerated manner, a brittle material is obtained which can be ground to form a powder. From this powder, articles having any desired (optionally complicated) shape can be produced by means of powder metallurgy. By mixing powders of two different intermetallic compounds, a material can be obtained having a substantially negligible coefficient of linear thermal expansion in the temperature range of from 0 to 200 °C.

4 529 618

Method of photolithographically treating a substrate

J. J. Ponjé

E

F. J. B. Smolders

C. J. A. Verwijlen

The invention relates to a method of photolithographically treating a substrate, in which a surface of the substrate is treated at least at the area at which it consists of an inorganic material with an organosilicon compound. In order to improve the adhesion of a photo-lacquer layer to be applied, the organosilicon compound used is a 3-aminopropyl-trialkoxysilane in the form of an aqueous solution.

4 531 221

Premodulation filter for generating a generalized tamed frequency modulated signal

K.-S. Chung

E

L. E. Zegers

A transmitter for transmitting a carrier whose frequency is modulated by pseudo five-level signals. In order to obtain a simple receiver and an improved signal-to-noise ratio, a substantially three-level signal is generated in the transmitter at the detection instants by means of a pre-modulation filter.

4 533 429

Method of manufacturing a semiconductor device

W. J. M. J. Josquin

E

In a LOCOS process, depressions are formed in a semiconductor body, and are filled by means of oxidation. The bottom and side walls of the depressions are coated with a double layer including an oxide and an oxidation-resistant material. This double layer is removed from the bottom of the depression and under-etching below the sidewalls under the oxidation-resistant layer is carried out to form cavities. As a result the remaining portions of the oxidation-resistant material are lifted along the surfaces of the side walls. With oblique walls for the depression, a high accuracy as to the size of active semiconductor regions can then be obtained with respect to an original mask.

4 533 849

Ceramic bistable deflection element

A. Schnell

A

A bistable ceramic deflection element includes an assembly of two ceramic plates of a ferroelectric ceramic material which can be easily polarized and which has a low coercive field strength, one plate thereof being polarized so that the deflection element is de-

flected. The other plate is not polarized. The depolarization of the polarized plate can be performed simultaneously with the polarization of the plate non-polarized thus far, because the interchanging of the polarization condition can be simply performed by briefly applying a direct voltage via two extreme electrodes, provided on the plates. The direct voltage causes polarization of the plate not polarized thus far.

4 533 852

Method of manufacturing a thermionic cathode and thermionic cathode manufactured by means of said method

B. Frank
G. Gärtner
H. Lydtin

A

The cathode the material of which is substantially high-melting metal such as W, Mo, Ta, Nb, Re and/or C, consists of a very fine-grained mechanically stable support layer, a series of layers considerably enriched with emissive material, in general from the scandium group especially from the group of rare earth metals, preferably with Th or compounds thereof and a thermally stable preferentially oriented coating layer. All the layers are provided via the gaseous phase, for example, CVD methods, on a substrate formed according to the desired cathode geometry. The substrate is removed after termination of the deposition.

4 533 873

RF phase shift control system

R. N. Alcock

R

A system for amplifying RF signals with a selectable substantially constant phase at the output port relative to the input port comprises a phase shifter and an amplifier, a phase discriminator and a video processor which controls the phase shifter in accordance with the output of the phase discriminator and a phase selection signal. This signal selects a bias voltage to cause the phase shifter to introduce a phase shift such that the relative phase at the output port is approximately equal to a desired value and also to select a monotonically varying error function which is derived from the phase discriminator and which is representative of the difference between the desired value and the actual value of the relative phase.

4 534 929

Matrix and method of using an aliphatic alcohol coated silica glass matrix

J. J. Ponjé
C. J. A. Verwijlen

E

A matrix having a surface of silica glass which is suitable for the manufacture of articles of synthetic resin in which the surface of the matrix comprises a monolayer of an aliphatic alcohol, as well as a method of manufacturing articles having a surface of synthetic resin while using the matrix.

4 535 303

Driver circuit

F. A. C. M. Schoofs
A. J. Nijman

E

In a driver circuit including at least one integrated circuit amplifier, adapted to be interconnected with a subscriber's line of a telephone system, the operating supply for the amplifier includes a pair of series connected voltage supplies having a maximum sum voltage that exceeds the breakdown voltage of the amplifier. The junction of the voltage supplies is connected to a reference, and the amplitudes of the output voltages of the two supplies are controlled in opposite directions with variations in the amplifier input signal to maintain the effective sum voltages of the supplies below the breakdown voltage of the amplifier. The series connected supplies may be employed to supply the input of a similarly connected second amplifier, with the controlled voltage supply of the second amplifier serving to supply the input of the first amplifier. In this latter arrangement, the amplitudes of the supplies of the two amplifiers are commonly controlled.

4 535 449

Time-locking method for stations which form part of a local loop network, and local loop network for performing this time-locking method

J.-P. Arragon

L

A method for use in a local loop network comprising a plurality of stations which are distributed along a bus, each station being connected to the bus via a coupler which is inserted in the bus. The time-locking method for these stations comprises a transmission phase during which a looping unit which is also inserted in the bus transmits a frame (transmission frame) which consists of a synchronization word and one or more slots which initially do not contain data and which correspond to the time position occupied by each of the stations, a receiving phase during which the demodulation of the transmission frame by the master clock of the looping unit is performed after the retransmission in the form of a frame which is referred to as the receiving frame, of this frame to the coupler of each of the successive stations and, after the receiving phase, new transmission and receiving phases until the insertion of the data on the bus by each station during a transmission phase takes place with the desired accuracy.

4 535 529

Method of making semiconductor devices by forming an impurity adjusted epitaxial layer over out diffused buried layers having different lateral conductivity types

P. J. W. Jochems

E

A method of manufacturing a semiconductor device is provided in which semiconductor circuit elements are provided in regions formed by diffusion from one or more buried layers into an epitaxial layer. The diffusion is carried out such that a surface layer having substantially the same doping as the original epitaxial layer is left above the diffused into epitaxial layer above the buried layer. The surface layer serves as a reference doping for insulated gate field effect transistors to be formed. This is of a particular importance for threshold voltage determinations in CMOS circuits having adjoining "twin tub" regions diffused from buried layers of opposite conductivity types.

4 535 720

Liquid phase epitaxy apparatus

J. C. Brice
J. L. Page
P. A. C. Whiffin

R

In a sliding boat liquid phase epitaxy apparatus a base structure, a support substrate disposed on the base and being horizontally fixed with respect to the base, and a slidable well member disposed above the substrate in an abutting relationship are included. The slidable well member has at least one well capable of holding a growth solution for growing epitaxial layers on substrates. A significant problem in growth of layers by liquid phase epitaxy when using a sliding boat apparatus occurs by the inability to achieve a sufficiently good wipe-off so as to produce a layer having a smooth surface. The apparatus of the present invention includes in the structure of a sliding boat apparatus a substrate support structure including a block provided with a flat-bottom recess in part of the top surface of the block and between the ends of the blocks, and a plate is fitted into the recess so that the top surface of the plate is level with the top surface of the block outside of the recess. The plate is provided with an aperture capable of containing a substrate on which an epitaxial layer is to be grown, and can be disposed under one well of the slidable well member. The plate and well member are made of different materials.

4 536 059

Liquid crystal display device with ridges

T. H. M. van den Berk

E

In a matrix display device using the bistability effect of cholesteric liquid crystals, two supporting plates are provided with first and second pluralities of ridges. The electrodes of the liquid crystal ex-

tend across the second ridges onto the first ridges on which a separation strip separates the electrodes from one another. Liquid crystal orienting layers are provided over the entire surface of the supporting plate. The second ridges lying between the first ridges divide each picture element of the display into many sub-elements. Accordingly, the formation of focal-conical texture because of surface inhomogeneities in the picture element display will be restricted to a single sub-element as a result of the homeotropic-nematic texture at the edges of the sub-element.

4 536 227

Method of and apparatus for producing a controlled unsaturated vapour pressure of a volatile liquid in a heat treatment chamber

J. C. Brice R
C. R. Brough

It is necessary in many heat treatment processes conducted in open systems to maintain a given partial pressure of a volatile component of a material being treated, and it is desirable to conserve this volatile component, both on account of cost and in the case of components such as mercury, toxicity. A controlled unsaturated vapour pressure of a volatile liquid may be produced in a tube by passing a stream of a carrier gas through a vapourizer containing the liquid at a temperature T_s , passing the mixture of the carrier gas and vapour of the liquid through a tube containing material to be treated, which material is at a temperature T_t . The mixture of the carrier gas and vapour of the liquid is then passed to a condenser from which the carrier gas is vented to waste, and the vapour of the liquid is condensed at a temperature T_c in a condenser. $T_t > T_s > T_c$. The condensate passes from the condenser to the vapourizer through a tube, and the liquid fills a cross-section of a length of the tube.

4 536 415

Method of manufacturing an optically readable information disc

T. H. G. Martens E
F. H. M. Sanders

A method of manufacturing an optically readable information disc in which a disc-shaped substrate of a synthetic resin which comprises an optically readable structure on at least one side is treated with an oxidizing gas of reactive, electrically neutral particles and is then provided on the side of the structure with a non-electrolytic deposited reflection layer.

4 536 416

Matrix and method of manufacturing articles of a synthetic resin by the matrix

J. J. Ponjeé E
F. B. Melgert

A matrix having a surface which is manufactured from metal and which comprises a monolayer of an alkylmercaptan or a fluoro-alkylmercaptan, as well as a method of manufacturing copies of synthetic resin from the matrix or copies comprising a coating layer of synthetic resin.

4 536 679

Photocathode

P. Guittard L
B. Guillemet
C. Piaget

The photocathode is of the type which comprises a photo-emissive layer consisting of at least an active layer of the P-type, a solid support for said semiconductor of a material which is transparent to radiation, a layer having a bonding glass for the photo-emissive layer on the support. The invention is characterized in that the sup-

port comprises two parts situated one on top of the other and which are bonded together, namely a thick second part (thickness for example 5 mm) of a type of glass having properties of thermal expansion which are substantially identical to those of the bonding glass and a part in the form of a disc-shaped first part (thickness for example 1 mm) of a material having softening and transition points which are much higher than those of the bonding glass and of the glass of the thick part.

4 536 742

Method of encoding a stream of data bits, device for carrying out the method, and device for decoding a stream of data bits

K. A. Schouhamer Immink E

The invention relates to a method of encoding a stream of data bits of a binary source signal into a stream of data bits of a binary channel signal. The stream of data bits of the source signal is divided into a sequence of five permissible source words of variable length. Each of these five permissible source words is converted into a channel word with twice the number of data bits. This conversion has been selected in such a way that the error propagation is very small and the electronics can be very simple.

4 536 857

Device for the serial merging of two ordered lists in order to form a single ordered list

W. J. Schoenmakers E

A merging device is used for combining a first list and a second list in order to form a result list. All lists satisfy a linear ordering criterion. At the beginning of the actual merging operation, the second list is stored in a random access memory. This memory is divided into (k_{\max}) memory blocks, the second list filling at the most the ($k_{\max} - 2$) non-largest memory blocks thereof. Efficient book-keeping is achieved by means of two block list updating devices.

4 536 864

Apparatus for reading an optically coded disc-shaped record carrier

G. E. van Rosmalen E

The invention relates to an apparatus for reading a disc-shaped record carrier with a spiral information track in which an optically readable digitally coded information signal is recorded with a spatial bit frequency which is independent of the radius of the track turn. The scanning speed of the information track is selected to be a factor n higher than the scanning speed normally employed of the reproduction for the recorded information. By means of a memory device, information blocks being read and comprising a fixed number of data bits are time-expanded to restore the customary time relationship. A control unit determines the read-in cycles of the memory device for the storage of the information blocks being read and, via the radial positioning system for the read spot, it determines the scanning pattern of the record carrier so that the ultimately recorded information blocks are reproduced in the same sequence and at the desired rate.

4 536 948

Method of manufacturing programmable semiconductor device

T. S. te Velde E
A. Slob

A blowable fuse is provided over a part of its length separately from the walls of an enveloping cavity and separated from a supporting member. As a result of this the fuse is readily thermally isolated so that it fuses more rapidly and with less energy. In addition, a semiconductor circuit element, for example a Schottky diode, can be realized below a bridging part of a conductor which serves as an upper wall of the cavity, which results in a high bit density.

Digital signal processing II Applications

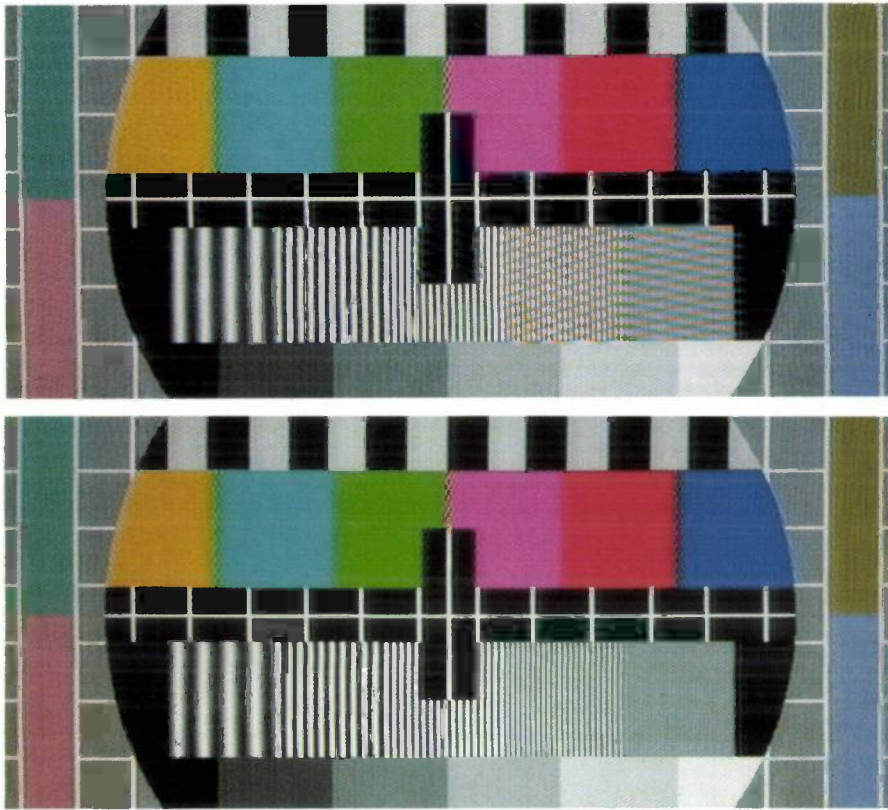
After the general treatment in our recent special issue 'Digital signal processing I, background' we now wish to examine more closely a number of actual applications in this young but vigorous subject. We have therefore chosen a number of examples in fields where Philips has long been active: video and audio technology.

In the opening article we look at digital signal processing in television receivers. Because of the relatively large bandwidth of television signals, a high sampling rate, many digital operations per second and relatively large memories are required. But once these barriers are overcome, a number of important advantages can be gained, including improved image reproduction, reduction of noise and elimination of flicker. In addition new features can be obtained, such as 'freeze-frame', 'picture-in-picture', 'zoom' and teletext background memory.

The second article, which is devoted to hi-fi audio, first describes how digital methods can provide compression (or expansion) of the dynamic range, artificial reverberation and equalization of the frequency characteristic of a room. For these and other kinds of audio operations a programmable 'custom-made' IC with the name 'ASP' has been designed.

The third and fourth articles from this special issue to some extent complement one another. The article about the CAROT method shows how digital signal processing (in this case in the video field) can sometimes offer features that are essentially new: a kind of matrix manipulation of digital signal samples can convert a standard analog television signal into a new analog television signal with different and in some ways improved properties.

The fourth article, about a digital 'decimating' filter for hi-fi audio, gives an example of a trade-off between analog and digital filter operations. In such cases an accurate cost comparison will eventually decide the choice between the two alternatives.

*Cross-colour reduction*

Conventional analog signal processing in television receivers is associated with cross-colour effects: closely spaced vertical lines tend to introduce unintended colour patterns (upper test card). In practice these effects are often observed in scenes where people are wearing clothes with finely detailed patterns. In addition noise signals may show up as a confetti-like disturbance of the picture (left-hand half of the test portrait). Digital signal processing in which use is made of field or frame memories can largely suppress these two undesirable effects, considerably improving the image quality (lower test card and right-hand half of the test portrait).

*Noise reduction*

Digital signal processing in television receivers

M. J. J. C. Annegarn, A. H. H. J. Nillesen and J. G. Raven

Introduction

To convert a scene into electrical signals all conventional television systems employ periodic image scanning in a line pattern. The scan is made in much the same way as our eyes follow the lines on the pages of a book when reading. Little has changed here in the hundred years or more since the very first ideas about television were put forward. The German patent filed by P. Nipkow in 1884, in which he proposed a form of mechanical scanning using a rotating disc perforated with a spiral pattern of holes (the 'Nipkow disc'), is of course well known.

Since that time there has really only been one fundamental change in the scanning pattern used. This is 'interlacing', the system in which all the even lines are scanned first and then all the odd lines, producing two alternate 'fields' of even and odd lines, which combine to make up a complete picture, or frame. This is done to prevent flicker in the display.

Television first began to make real headway when a completely electronic system became possible. The first broadcasts (in monochrome) took place at the end of the thirties, e.g. in the United Kingdom and the United States. In 1936 in Germany there was even an experimental television broadcast with a portable transmitter from the Olympic Games in Berlin^[1]. Since that time there has been a continuous development, yielding steady improvements of quality and additional features, such as large-screen displays, colour reproduction, improved image and sound quality, stereo sound, teletext and remote control.

Fig. 1 shows the block diagram of a modern television receiver. With the exception of parts of the remote control unit, the remote-control receiver and the teletext decoder, most receivers are still based entirely on analog circuits. There is however a distinct trend towards the application of digital circuits in other parts of the sets^[2]. This applies in the first place to the decoders for image, sound and teletext and to

the processors for image^[3], sound and synchronization. For technical reasons digitization will not for the time being extend to the circuits for tuning, mixing, i.f. amplification, demodulation, output amplification and deflection, owing to the high frequencies, high powers or high voltages in these circuits.

The advantages to be expected from this advancing digitization of television receivers are to be found in three main fields:

- new features,
- improved quality, and
- greater economy.

The new features that digitization will generate are closely connected with the use of digital field or picture memories. Some examples of these are still pictures ('freeze-frame'), combined pictures ('picture-in-picture') and teletext background memory. We shall deal with these later in more detail.

The second category of advantages arising from the digitization of television receivers comes about because present-day colour TV systems can really provide a better picture quality than analog methods now give^[4]. To some extent this is due to undesirable interaction between chrominance and luminance signals and to the relatively crude methods used for correction. In addition there may be noise, and buildings and mountains can give signal reflections (echoes). There can also be negative effects due to the scanning pattern used, such as flickering pictures (large-area flicker) or jittering lines (line flicker). With larger and brighter television screens, effects of this kind have become more of a nuisance. Digital signal processing, however, can do much to improve this situation.

Ir M. J. J. C. Annegarn is with Philips Research Laboratories, Eindhoven, Ing. A. H. J. J. Nillesen is with the Elcoma Division, Philips NPB, Eindhoven, and Ir J. G. Raven is with the Consumer Electronics Division, Philips NPB, Eindhoven.

^[1] Radio progress during 1936, part IV: Report by the technical committee on television and facsimile, Proc. IRE 25, 199-210, 1937.

^[2] E. J. Lerner, Digital TV: makers bet on VLSI, IEEE Spectrum 20, No. 2 (February), 39-43, 1983.

^[3] Existing analog receivers either do not contain a video processor, or contain only a very rudimentary form of video processor. In digital receivers, on the other hand, this processor plays an extremely important role, as will appear in this article.

^[4] R. N. Jackson and M. J. J. C. Annegarn, Compatible systems for high-quality television, SMPTE J. 92, 719-723, 1983.

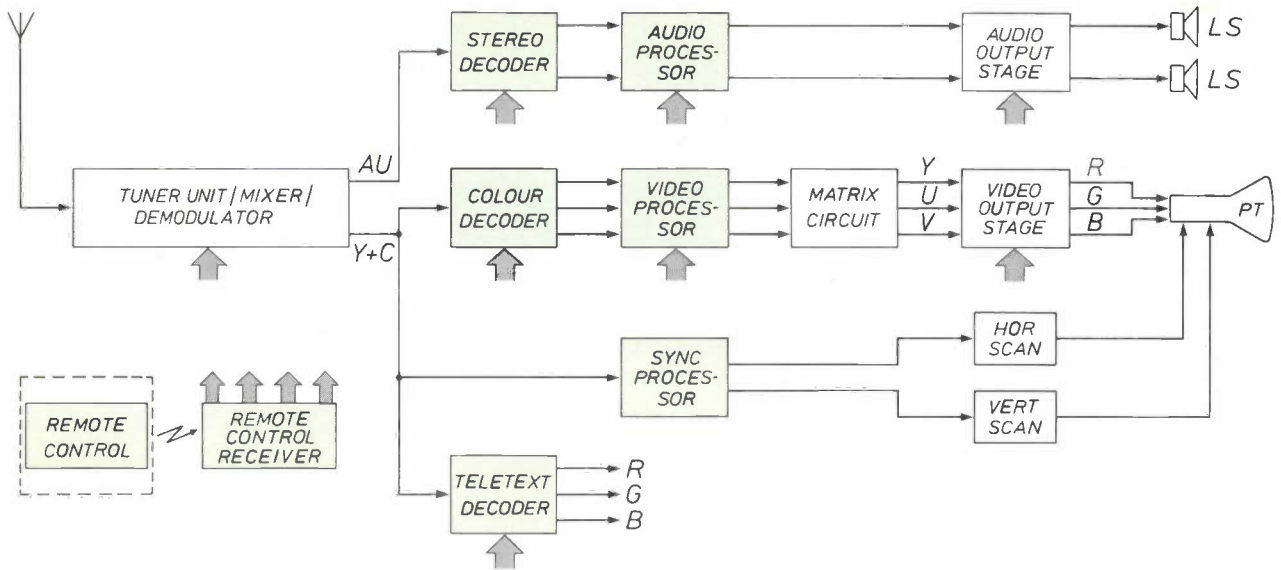


Fig. 1. General block diagram of a modern colour television receiver. The incoming signal, after tuning, mixing, amplification and demodulation, is split into a sound signal AU and a composite picture signal $Y + C$. The sound signal is separately decoded, processed and reproduced via the loudspeakers LS . The signal $Y + C$ is processed in several stages to provide the colour signals R , G and B (for red, green and blue) for producing a picture on the picture tube PT . Horizontal and vertical deflection signals are required for the formation of the picture. These are generated by means of a sync processor and the horizontal and vertical scanning circuits $HOR\ SCAN$ and $VERT\ SCAN$. In most present-day receivers digital circuits are only used for the remote control, the remote-control receiver and the teletext decoder. In the near future, however, the other green blocks will increasingly be digitized. At present this does not apply to the other units because analog circuits still have certain advantages, connected with the high frequencies, high voltages or high powers in these circuits.

The economic advantages can be summarized under 'lower price' or 'lower costs'. To some extent these stem from the reduced number of components and the replacement of relatively expensive components (for example analog glass delay lines) by inexpensive ones (digital memories). Production costs have been brought down by better trimming procedures and better stock control, and also by the increased reliability of the products.

In this article we shall confine our attention to the digital processing of the composite signal $Y + C$ (see fig. 1), which contains the actual picture information and consists of the luminance signal Y and the modulated colour subcarrier signal C , referred to in this article as the 'chroma' signal. We shall start by describing in some detail the characteristics of the frequency spectrum of this composite signal as defined by the PAL and NTSC system standards and we shall also describe the operations performed on it in the receiver. From this information we shall show how important the choice of sampling rate is here. We shall also show that certain filters that are particularly well suited to digital implementation, such as comb filters, are eminently useful for television applications. We shall then explain how digital signal processing can be used to obtain pictures of better quality and to add new features to the television receiver.

Background

Colour television is based on the fact that a colour picture can be formed from three basic colours: red, green and blue. In the television camera a scene is therefore converted into three electrical signals R , G and B , each representing one basic colour. A replica of the original picture is recovered from these signals in the picture tube of the receiver. The colour signals R , G and B are not, however, sent directly from transmitter to receiver. This would require three TV channels, and in any case none of these three signals would be suitable for reproduction as a monochrome picture on a monochrome screen. In the studio, therefore, a matrix circuit is used for deriving from R , G and B a brightness or luminance signal Y and two colour-difference or chrominance signals U and V . (Y , U and V are sometimes referred to as component signals.) The signal Y now contains all the monochrome information and the signals U and V can be combined by modulation to produce a single chroma signal C , which can be added to Y relatively easily. This results in the composite signal $Y + C$, which can be sent via a single television channel to the receivers^[6]. The composite signal also contains the signals required for synchronization in the receiver, but these do not really come within the scope of this article.

Major differences between the three colour television systems PAL (Phase Alternation Line), NTSC (National Television System Committee) and SECAM (SEquential Couleur A Mémoire), which are world standards [6], are to be found in the modulation process used in generating the chroma signal *C*. PAL and NTSC use a combined form of phase and amplitude modulation (quadrature modulation), and SECAM uses frequency modulation. The PAL system is mainly used in Western Europe (except in France), the NTSC system is the standard in the United States of America and Japan, and the SECAM system is used in Eastern Europe and France.

Frequency spectra in NTSC and PAL

In dealing with the composite signals we shall confine our attention in this article to the two standardized colour television systems known as NTSC and PAL. However, much of the digital processing performed after colour decoding is in principle also suitable for signals in the SECAM system.

Table 1. The principal frequencies and frequency relationships in two standardized NTSC and PAL colour television systems.

	NTSC	PAL
Picture frequency f_p	29.97 (≈ 30) Hz	25 Hz
Field frequency f_t	59.94 (≈ 60) Hz = $2f_p$	50 Hz = $2f_p$
Line frequency f_l	15 734 Hz = $525f_p$	15 625 Hz = $625f_p$
Colour subcarrier frequency f_{sc}	3 579 545 Hz = $227\frac{1}{2}f_l$	4 433 618 Hz = $283\frac{3}{4}f_l + f_p$

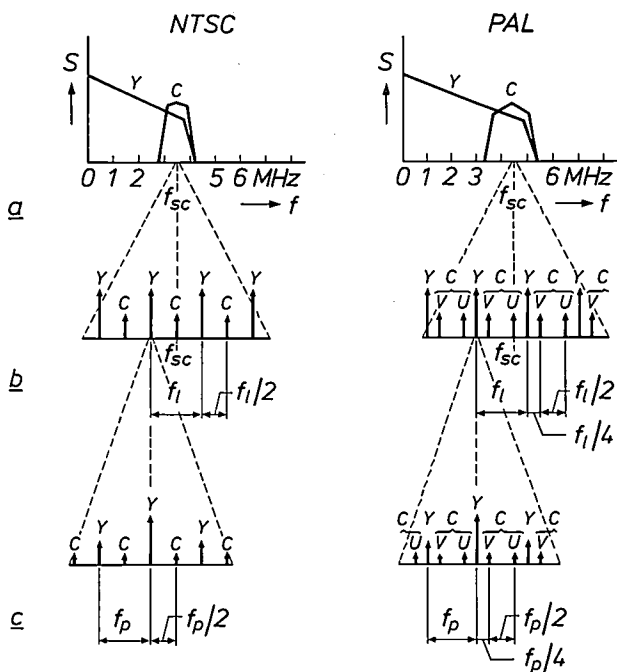


Fig. 2. Frequency spectra of the composite signals $Y + C$ in the standardized NTSC and PAL colour-television systems. *S* signal power per Hz bandwidth. Some distinct similarities and differences can be seen. *a*) In general terms it can be seen that in both cases the colour information, in the form of the chroma signal *C*, lies in the same frequency band as the highest frequencies of the luminance signal *Y*. This is produced by modulating a subcarrier of frequency f_{sc} with the colour information. *b*) If the frequency scale is expanded it can be seen that *Y* and *C* consist of separate frequency components spaced by an amount corresponding to the line frequency f_l . In the PAL system it is in fact possible to distinguish between the *U* and *V* information in the spectrum. Strictly speaking, these spectra are applicable only to stationary pictures in which all the television lines are identical. *c*) If there are differences between the lines, a further expansion of the frequency scale shows an even finer spectral structure, which is associated with the picture frequency f_p . (In this figure the important aspect is the relative locations of the different frequency components, rather than the exact representation of their relative amplitudes. Since the expansions in *c*) are made around a *Y* component from *b*), this component is clearly stronger than the other ones. At other places in the spectrum other components will dominate. The frequency positions are classified in the same way throughout the complete spectrum, however.)

Fig. 2 shows the spectra [7] of composite signals in NTSC and PAL. From the general diagram of fig. 2*a* it is clear that the chroma signal *C* and the luminance signal *Y* share the upper part of the frequency band, around the subcarrier frequency f_{sc} . The more detailed view on an expanded frequency scale (fig. 2*b*) shows that *Y* consists of separate frequency components situated at multiples of the line frequency f_l . With appropriate modulation of the *U* and *V* signals, however, the frequency components of *C* can be made to appear at different locations, which makes it possible to separate *Y* and *C* in the receiver. The PAL system even uses different frequencies for the *U* and the *V* information.

The spectral structures of fig. 2*b* are strictly speaking only applicable to stationary pictures in which all the successive lines are identical. This would be very unusual, of course. When differences do exist between the lines (but there is still no movement) then a second expansion of the frequency scale gives the spectra shown in fig. 2*c*. Around each frequency component from fig. 2*b* there are other *Y*, *U*, *V* or *C* components at frequency spacings that are related to the picture frequency f_p . If we also wish to take randomly moving images into consideration, we then find that the elementary line structure of the spectra remains, but that the lines, depending on the movement, become broader or 'spread out'. The values of the principal frequencies that occur in standard signals of the NTSC or PAL type and the relations between them [6] are summarized in Table 1.

In the receiver the composite signal $Y + C$ is recovered from the antenna signal after a number of operations such as tuning, mixing, amplification and demodulation (fig. 1). This composite signal must be

[5] P. S. Carnt and G. B. Townsend, *Colour television*, Vol. 2, PAL, SECAM and other systems, Iliffe, London 1969.
 [6] D. H. Pritchard and J. J. Gibson, *Worldwide color television standards — similarities and differences*, SMPTE J. 89, 111-120, 1980.
 [7] J. O. Drewery, *The filtering of luminance and chrominance signals to avoid cross-colour in a PAL colour system*, BBC Eng. No. 104 (September), 8-39, 1976.

subjected to a second demodulation or decoding (at least in a colour television receiver) to recover the individual Y , U and V signals, which are then converted, by a matrix circuit, into the R , G and B signals ultimately required.

Digital TV signal processing

The analog processing of TV signals is mainly based on the characteristics of the overall spectrum (fig. 2a). The separation of Y and C is then achieved by using, say, a bandpass filter and a bandstop filter ('notch filter'), both centred on f_{sc} . It is assumed that the first filter suppresses the Y signal sufficiently and the second filter suppresses the C signal sufficiently. However, this is only partly true, and in fact high frequencies of the Y signal interfere with the C signal, causing the coloured streaks referred to as 'cross-colour' (see photograph on page 182). Conversely, upon closer examination some of the C signal may be observed as a variation in luminance in the form of fine dots ('cross-luminance'), especially at the edges of coloured transitions. In this form of analog filtering only successive signal values are combined, corres-

ponding to closely adjacent picture elements (pixels) in the same line, so it is therefore called *horizontal filtering*. If line memories are used it is possible to combine signals separated by exactly one or more lines, and therefore corresponding to pixels above and below one another in the picture. This is referred to as *vertical filtering*; it is seldom used in analog processing. The filters employed have frequency characteristics with a fine structure of the order of magnitude of f_1 . In digital technology it is possible to make filter characteristics with a fine structure of the order of f_p . This requires delays of a field period or a picture period, which can be achieved by means of a field memory or a picture memory. This is referred to as *temporal filtering* since corresponding pixels occurring in successive fields or pictures are combined [8][9].

In the rest of this article we shall base our treatment of the processing of $Y + C$ to R , G and B on the diagram in fig. 3. First, the signal $Y + C$ is converted into the signal $y_n + c_n$ (n is the discrete-time variable [10]) in an analog-to-digital converter with sampling rate $f_s = 1/T_s$. In the digital colour decoder the 'crude' component signals y_n^* , u_n^* and v_n^* are obtained as an intermediate result; after further digital processing they give y_n , u_n and v_n . These are applied to digital-to-analog converters to give the required analog component signals Y , U and V , from which the R , G and B signals are derived with a matrix circuit.

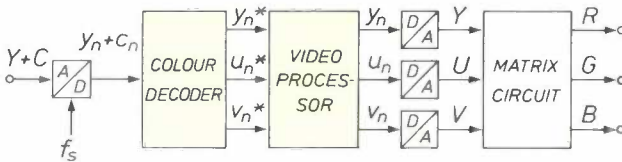


Fig. 3. Diagram illustrating the digital conversion of the analog composite signal $Y + C$ into the analog colour signals R , G and B . A/D analog-to-digital converter. f_s sampling rate. The digital circuit *COLOUR DECODER* produces the 'raw' component signals y_n^* , u_n^* and v_n^* from the digital composite signal $y_n + c_n$ as an intermediate result. These raw component signals are processed in the digital circuit *VIDEO PROCESSOR* to provide the 'pure' digital component signals y_n , u_n and v_n . The digital-to-analog converters D/A produce the analog component signals Y , U and V .

The R , G and B signals are simple linear combinations of the Y , U and V signals and vice versa. The R signal, for example, is given by:

$$R = aY + bU + cV,$$

where a , b and c are constants, which are different in every colour television system. In principle it would also be easy to design the matrix circuit as a digital circuit. The D/A converters would then be located *after* this circuit instead of *in front of* it. This has deliberately not been done in the diagram shown in fig. 3, because the signals U and V have a much smaller bandwidth than Y . Use is made of this in digital processing by applying a lower sampling rate for u_n^* and v_n^* than for y_n^* . The same applies for the corresponding D/A converters. The signals R , G and B , on the other hand, all have the same wide bandwidth as Y . The solution of fig. 3 therefore offers a number of advantages.

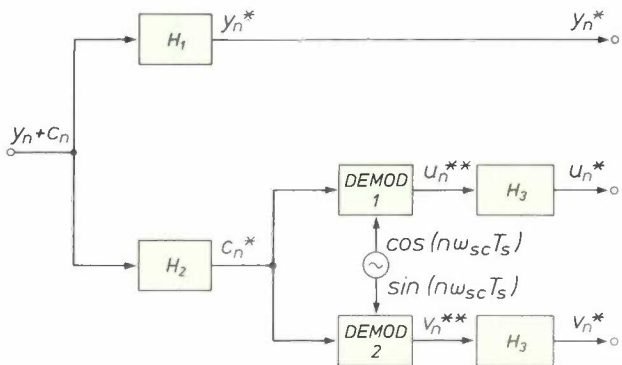


Fig. 4. Block diagram of a digital colour decoder. H_1 bandpass filter, centred on the subcarrier frequency $f_{sc} = \omega_{sc}/2\pi$. H_2 bandpass filter, also centred on f_{sc} . *DEMOD1*, *DEMOD2* demodulators. H_3 lowpass filter. $y_n + c_n$ digital composite signal. y_n^* , u_n^* , v_n^* digital component signals. c_n^* , u_n^{**} , v_n^{**} digital intermediate results. T_s sampling interval.

A more detailed block diagram of a possible digital colour decoder is given in fig. 4. The digital composite signal $y_n + c_n$ is first split into y_n^* and c_n^* by a band-

[8] H.-P. Richter, Verfahren zur digitalen Decodierung des PAL-signals, Fernseh- & Kino-Tech. 37, 511-519, 1983.
 [9] W. Weltersbach and M. Jacobsen, Digitale Videosignalverarbeitung im Farbfernsehempfänger, 1. Teil: PAL-Farbdecoder, Fernseh- & Kino-Tech. 35, 317-323, 1981, and 2. Teil: Maßnahmen zur Verbesserung der Bildqualität, *ibid.*, 371-379.
 [10] A. W. M. van den Enden and N. A. M. Verhoeckx, Digital signal processing: theoretical background, pp. 110-144 in the special issue 'Digital signal processing I, background', Philips-Tech. Rev. 42, 101-148, 1985.

stop filter H_1 and a bandpass filter H_2 . Next, the signals u_n^* and v_n^* are obtained from c_n^* by demodulating it with two carriers in quadrature at a frequency $f_{sc} = \omega_{sc}/2\pi$ and using two lowpass filters H_3 . In fig. 4 there is only horizontal filtering. All the vertical and temporal filtering takes place in the next block, the video processor (fig. 3).

Although fig. 4 gives the essential functions of the colour decoder, some important simplifications have been made. The generation of the colour subcarrier, for example, is not shown explicitly; it must in some way be brought into synchronism with the received signal. Also, a practical circuit includes operations such as amplitude control of the chroma signal, 'colour killing' for monochrome transmissions, and periodic phase-switching for one of the sub-carrier signals in PAL (PAL switch).

Digital filters for television applications

Filters play a very important part in digital signal processing [10]. In television applications we can list three categories:

- Filters in which the length of the individual delays amounts to only one or a few sampling intervals $T_s = 1/f_s$ and which are characterized by 'simple' coefficients (e.g. 1/4, 1/2, 1, 2, 4).
- Transversal comb filters in which the individual delays correspond to a line period or a field period.
- First-order recursive comb filters in which the individual delays also correspond to a line period or a field period.

With non-recursive filters it is possible to achieve an exactly linear phase characteristic. This is often im-

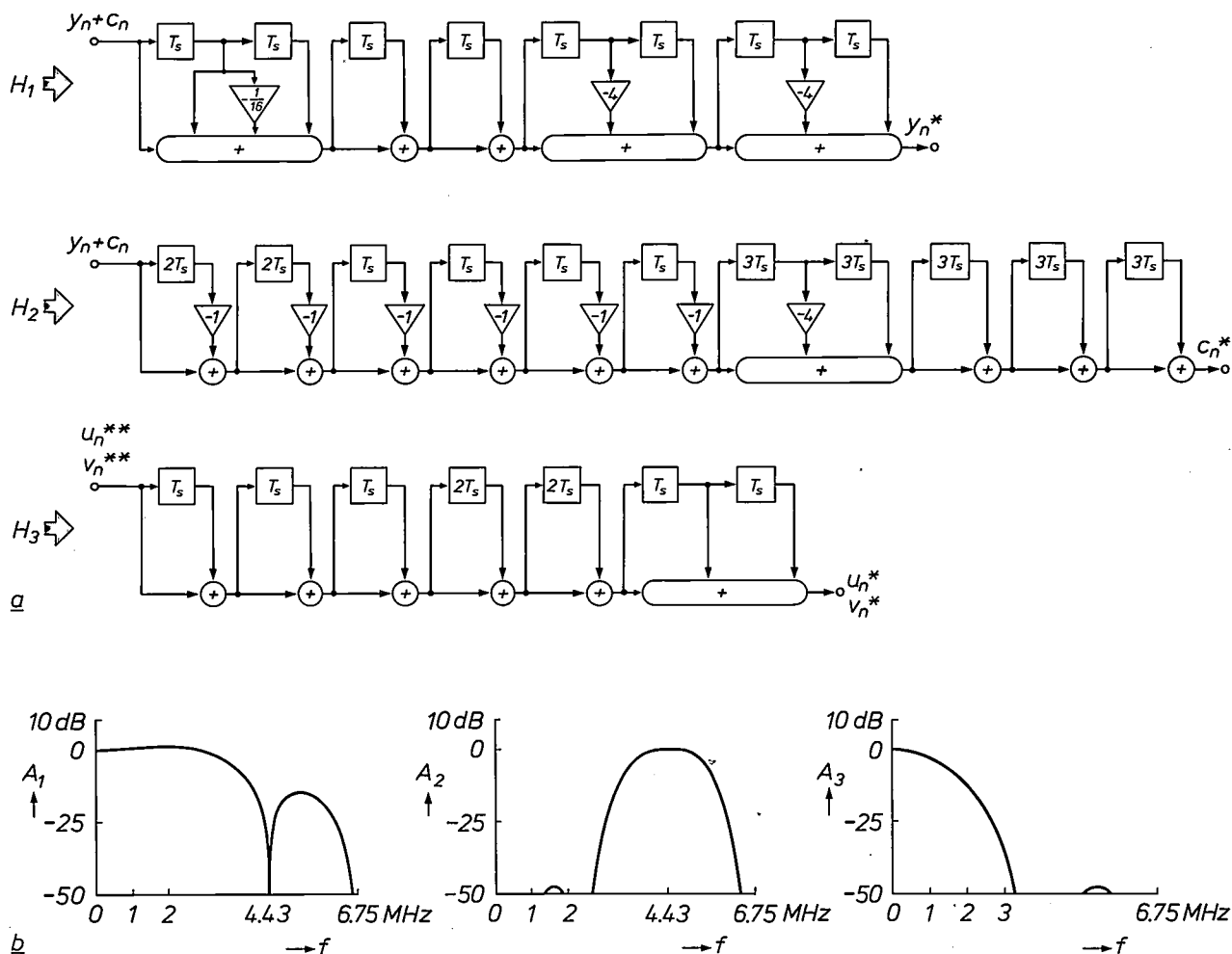


Fig. 5. a) Some examples of digital filters H_1 , H_2 and H_3 with simple coefficients, which can be used in the block diagram of fig. 4. These filters have the following system functions:
 $H_1(z) = (1 + \frac{1}{16}z^{-1} + z^{-2})(1 + z^{-1})^2(1 - 4z^{-1} + z^{-2})^2$,
 $H_2(z) = (1 - z^{-2})^2(1 - z^{-1})^4(1 - 4z^{-3} + z^{-6})(1 + z^{-3})^3$ and
 $H_3(z) = (1 + z^{-1})^3(1 + z^{-2})^2(1 + z^{-1} + z^{-2})$.
 b) Amplitude characteristics A_1 , A_2 and A_3 of the filters H_1 , H_2 and H_3 . The sampling rate here is $f_s = 1/T_s = 13.5$ MHz. These filters have a linear phase characteristic. The bandstop and bandpass characteristics of H_1 and H_2 are clearly seen around $f_{sc} = 4.43$ MHz [11].

portant in television applications and is one of the advantages of digital solutions compared with analog ones. We shall now take a closer look at all three categories and discuss some examples.

Filters with simple coefficients

Because of the relatively high sampling rate (10 to 20 MHz) digital filters for television should perform as few multiplications as possible, since these require relatively complex circuits and considerable electrical power. One way of accomplishing this is to use filter coefficients that as far as possible are integer (positive and negative) powers of 2. Multiplication then

amounts to no more than shifting the bits of a binary number by an integer number of bit places, with a change of sign if necessary (for negative coefficients). Fig. 5a shows how the filters H_1 , H_2 and H_3 of the colour decoder in fig. 4 can be realized. They consist of a cascade arrangement of simple transversal filters [11]. A linear phase characteristic is obtained by ensuring that the filter coefficients always satisfy the appropriate rules of symmetry. Fig. 5b shows the corresponding amplitude characteristics A_1 , A_2 and A_3 , based on $f_s = 1/T_s = 13.5$ MHz.

Fig. 6a gives an example of a recursive filter with simple coefficients. Filters of this type can be used in digital synchronization circuits (phase-locked loops or PLLs). Finally, fig. 7 shows an integrated circuit of a simple digital transversal filter made a few years ago for an application in colour television [12].

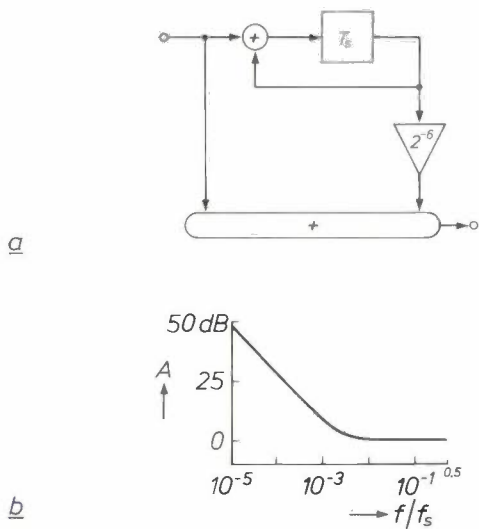


Fig. 6. a) Simple filter, suitable for application in a digital phase-locked loop in synchronization circuits. Its system function is $H(z) = \{1 - (1 - 2^{-6})z^{-1}\}/(1 - z^{-1})$. b) Amplitude characteristic A of this filter. For clarity the frequency is shown on a logarithmic scale [11].

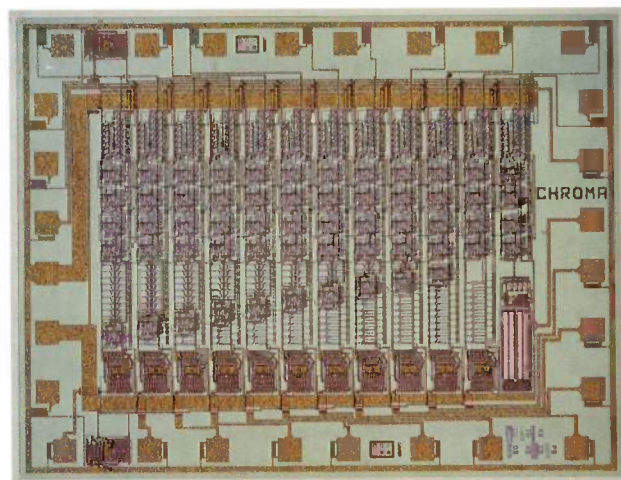


Fig. 7. Integrated circuit that can be used to make a digital transversal filter with the system function $H(z) = -1 + 2z^{-2} + 6z^{-4} + 2z^{-6} - z^{-8}$ or $H(z) = 1 + 2z^{-2} + z^{-4}$. The area of this chip is about 10 mm^2 . Made in two-phase NMOS technology, it operates at a maximum sampling rate of 40 MHz. The input signal consists of 9-bit samples and the output signal of 11-bit samples [12].

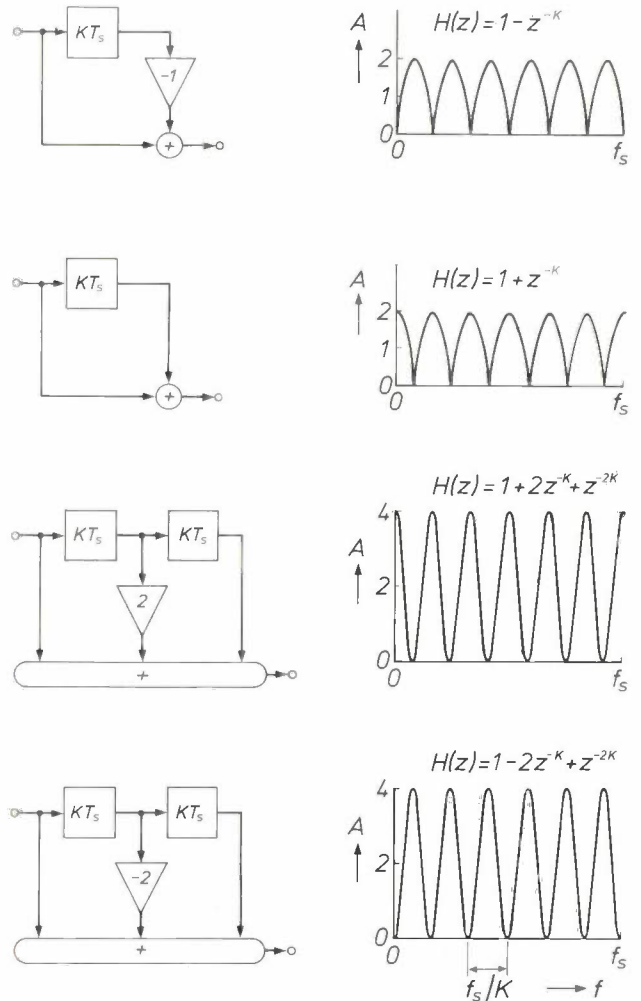


Fig. 8. Transversal comb filters that are particularly suitable for separating the frequency components of colour-television signals (see fig. 2). In addition to a block diagram for each filter, the system function $H(z)$ and the amplitude characteristic A are also shown. For the amplitude characteristics shown here $K = 6$, so the characteristics have only six 'teeth'. In reality KT_s corresponds to a line period T_l or a field period T_f . At a sampling rate of about 13.5 MHz the characteristics then contain nearly 900 or 250 000 teeth in the fundamental frequency interval from 0 to $f_s = 1/T_s$.

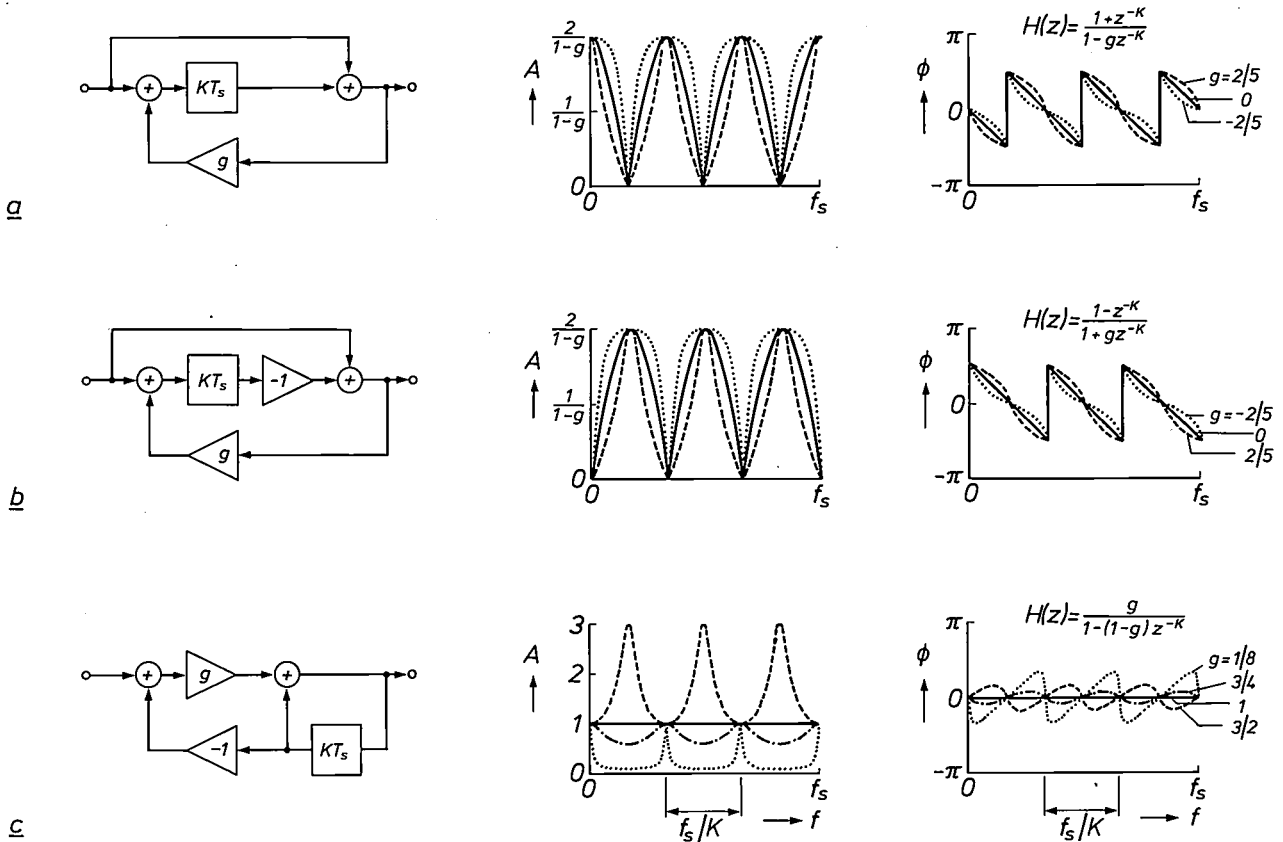


Fig. 9. Some examples of first-order recursive comb filters that are very suitable for the digital processing of colour-television signals. The system function $H(z)$ and the corresponding amplitude characteristic A and phase characteristic ϕ can be changed by varying the values of the coefficients g . A few examples are given for each filter. The values chosen for the upper two filters are $g = -\frac{2}{5}, 0$ and $\frac{2}{5}$. Those for the lower filter are $g = \frac{3}{8}, 1, \frac{3}{4}$ and $\frac{1}{8}$. Owing to their recursive structure, these filters do not in general have a linear phase characteristic, although the deviations are not necessarily large. A linear phase characteristic is found only for $g = 0$ in (a) and (b) and for $g = 1$ in (c). (In these three special cases, however, the filter is not really recursive.) For clarity the value $K = 3$ has been taken in this figure, so that the comb filter characteristics have only three 'teeth'.

Transversal comb filters

The characteristic line structure of the frequency spectrum of PAL and NTSC can be used for separating the different signal components. Comb filters [10] are particularly useful for this. Some widely used types of comb filter are shown in fig. 8. The length of the delay KT_s of the digital delay elements is deliberately not specified here ($K = \text{constant}, T_s = 1/f_s$) because it depends on the exact application; we shall give some examples shortly. We can make a rough distinction between delays of a line period T_l (vertical comb filters or line comb filters), delays of a field period T_f (temporal comb filters or field comb filters) and possible combinations of both. It is also quite common for the comb characteristic to apply to only a part of the spectrum when a comb filter is combined with 'ordinary' filters [13].

Comb filters are particularly useful for improving the separation of the signals y_n^*, u_n^* and v_n^* to reduce cross-colour and cross-luminance.

First-order recursive comb filters

Interesting filters for video applications can also be realized with simple first-order recursive structures. A few examples are shown in fig. 9. The filters in fig. 9a and 9b with $KT_s = T_l$ have been proposed earlier [6] in analog form for splitting the composite signal into its luminance and chroma components. The amplitude characteristics of these filters resemble those of the comb filters discussed in the previous subsection; by varying the one filter coefficient g the shape of the characteristic can be modified slightly. These filters, however, do not have a linear phase characteristic and are stable only for $-1 < g < 1$.

[11]. The filters in figs 5 and 6 form part of the digital multi-standard decoder developed at VALVO, Philips GmbH, Hamburg, West Germany.
 [12]. H. J. M. Veendrick, An NMOS dual-mode digital low-pass filter for color TV, IEEE J. SC-16, 179-182, 1981.
 [13]. J. H. Peters and J. T. Kanters, CAROT: a digital method of increasing the robustness of an analog colour television signal, this issue, pp. 217-229.

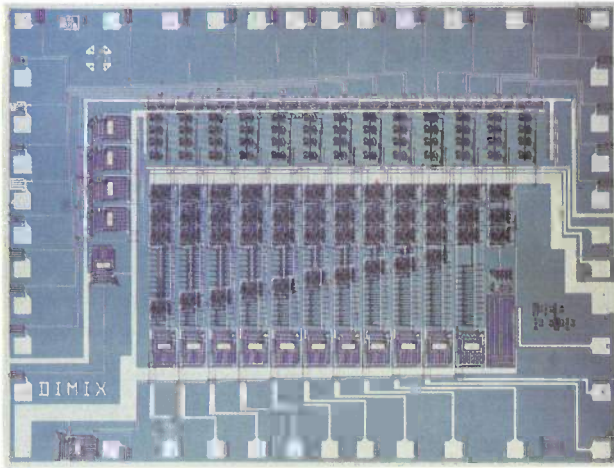


Fig. 10. Integrated digital circuit that takes two 10-bit input signals a_n and b_n to form an 11-bit signal $c_n = ga_n + (1-g)b_n$, where $g = 0, \frac{1}{8}, \frac{2}{8}, \dots, \frac{7}{8}, 1$. The addition of a delay KT_s results in the filter shown in fig. 9c, but this integrated circuit has many other applications. Made in two-phase NMOS technology, the chip has an area of 15 mm^2 . The maximum sampling rate is 40 MHz [14].

Another recursive filter, which we shall deal with at some length later, is shown in fig. 9c. Completely different frequency characteristics can be obtained by taking the value of g between 0 and 2; for other values of g the filter is unstable. It is also possible to switch g between two fixed values, e.g. $g = 1$ and $g = 1/8$. In one case ($g = 1$) there is apparently only a direct connection between input and output. In the other case ($g = 1/8$) the circuit acts as a comb filter (fig. 10).

These recursive filters are especially useful for reducing cross-colour, cross-luminance and noise.

The sampling rate

In the digital processing of television signals the choice of the sampling rate f_s is more significant than in the digital processing of other types of signal, such as speech or music. A relatively small change in the value of f_s can have considerable consequences. This is closely related to the special features of TV signals such as the breakdown of a scene into lines and fields and the way in which the colour information is coded.

Table I shows the main frequencies that occur in a composite signal in the NTSC or PAL systems. If the interrelationships shown are satisfied, the signals are referred to as 'standard signals'. In television broadcasts these are virtually the only types of signal used.

After recording and playback of such a signal, e.g. with a video cassette recorder, there may be considerable departures from these frequencies. The same applies to certain video signal sources such as video games or home computers. We then refer to 'non-standard signals'.

The ratio f_1/f_p , even if it deviates from the standard value of 625 or 525, will often be a fixed integer number. In general, however, there will be no connection at all between f_{sc} and f_1 or f_p . Since the digital processing of video signals must also include non-standard signals, it has to be accepted that no fixed relation exists between f_1 and f_{sc} . That is really a great pity, as we shall show.

The great difference between standard signals and non-standard signals appears most clearly from a comparison of the tolerances applicable to certain important parameters. In standard PAL, for example, where the number of lines per frame is $N = f_1/f_p = 625$, the line frequency f_1 has a tolerance of 0.0001% , and $f_{sc} = 283\frac{3}{4}f_1 + f_p$. For non-standard PAL, however, we find $607 \leq N \leq 643$, f_1 has a tolerance of 4% and f_{sc} is given by $f_{sc} = 4433\ 618 \pm 200 \text{ Hz}$.

Locking f_s to f_{sc}

A very simple decoder can be designed if the sampling rate f_s is in a fixed ratio to (is 'locked' to) f_{sc} . If $f_s = 4f_{sc}$, demodulating with say $d_n = \cos(n\omega_{sc}T_s)$ and $e_n = \sin(n\omega_{sc}T_s)$ amounts to multiplying by -1 , 0 and $+1$. These operations can be performed *without* a true multiplier circuit, which usually requires a fair number of basic digital elements. Attractive solutions for the multiplying operation can also be found for some other rational ratios of f_s to f_{sc} . A further advantage of such a ratio, which we mention here in passing, is that the linearity of the A/D converter preceding the colour decoder (fig. 3) is not so critical.

Locking f_s to f_1

It is necessary to lock the sampling rate f_s to the line frequency f_1 of a television signal (so that $f_s = Mf_1$, where M is an integer) if digital memories are to be used in the signal processing to obtain delays of exactly one line period, one field period or multiples of these. We have seen some examples of this with the filters of figs 8 and 9. Other examples will be encountered in the section 'New features'.

Choice of f_s

Since, as noted, we must assume that no fixed relation exists between f_1 and f_{sc} , we have to opt for locking f_s to either f_1 or f_{sc} . But which is best?

Locking f_s to f_{sc} with a fixed ratio is the optimum choice for the colour decoder. However, the signals y_n^{**} , u_n^{**} and v_n^{**} obtained in this way, especially if they are non-standard signals, cannot easily be processed with digital memories. This first requires a change ('conversion') of the sampling rate [10] to lock to the line frequency (fig. 11a). For non-standard signals, however, there is not necessarily any fixed common multiple of f_1 and f_{sc} , and this makes the conver-

sion complicated and unattractive. Such a solution does not therefore seem a good choice if digital signal operations have to be performed on the output signals of the colour decoder.

On the other hand, a fixed ratio of f_s to f_l in the decoding of colour information requires 'real' multiplications because the carrier samples d_n and e_n are now no longer limited to the values 0 and ± 1 , but may

PLL1. This sampling rate should be accurately known and because of its relationship to f_r the magnitude of any error can be determined and expressed as a correction signal. This signal is applied to a second digital phase-locked loop *PLL2* in which the carrier for the colour decoder is generated. Here the errors in the sampling rate are exactly compensated. This is done to ensure that in spite of the variations in the sampling

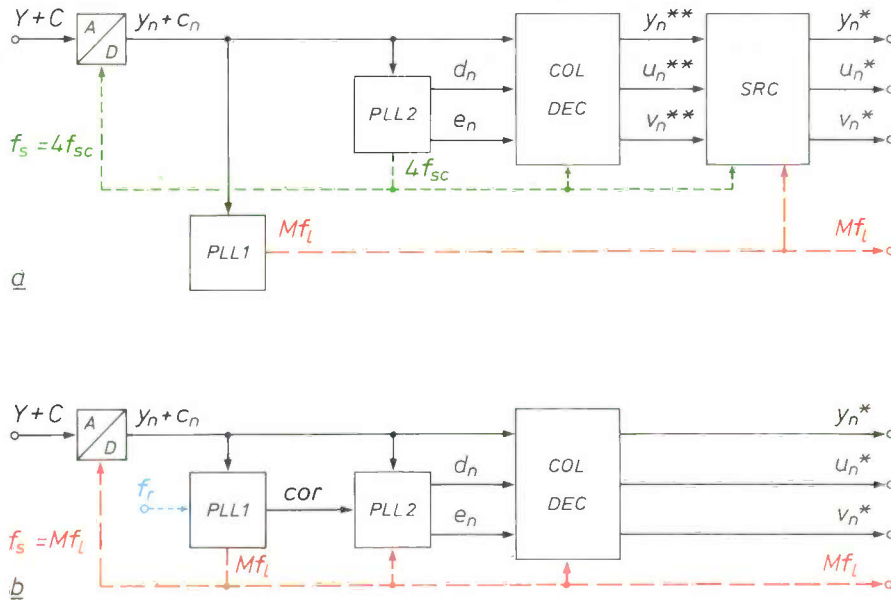


Fig. 11. a) Locking the sampling rate f_s to the subcarrier frequency f_{sc} (here $f_s = 4f_{sc}$) considerably simplifies the colour decoding, since demodulation only requires simple multiplication factors. (The carrier samples d_n and e_n only need to have the values $-1, 0$ and $+1$ here). For a large number of other digital operations, however, it is necessary to couple f_s to f_l . In this arrangement a fairly complicated sampling-rate converter *SRC* is therefore necessary for changing the sampling rate from $4f_{sc}$ to Mf_l . b) Locking f_s directly to the line frequency f_l of the incident signal (so that $f_s = Mf_l$) requires special precautions to ensure that the carrier samples $d_n = \cos(n\omega_{sc}T_s)$ and $e_n = \sin(n\omega_{sc}T_s)$ are generated with sufficient accuracy. This is done by synthesizing f_s from a stable reference frequency f_r and generating a correction signal *cor*. *A/D* analog-to-digital converter. *PLL1*, *PLL2* digital phase-locked loops. *COL DEC* colour decoder. *M* constant factor (≈ 900). y_n^{**} , u_n^{**} , v_n^{**} digital signals that are only significant as intermediate results; the other signals have the same significance as in the other figures.

assume any value. A further and more serious complication arises from the very high accuracy required of the colour subcarrier samples to ensure high-quality colour decoding. (In an analog version the carrier must therefore possess 'crystal stability'.) Locking f_s to f_l , however, gives the sampling rate f_s (and hence $T_s = 1/f_s$) the same relative inaccuracy as the line frequency f_l of the incident composite signal. This inaccuracy may be unacceptably large, especially for non-standard signals. The required accuracy of d_n and e_n can then only be achieved by taking special measures (fig. 11b). Starting with a stable reference frequency f_r , a sampling rate f_s locked to the incident f_l (i.e. $f_s = Mf_l$) is derived in a phase-locked

loop. At certain times, the carrier samples d_n and e_n always have the exact value corresponding to each actual sampling time.

In principle there is considerable freedom in the choice of the constant factor $M = f_s/f_l$, but in practice several factors have to be considered. In the first place it will usually be desirable to satisfy the sampling theorem [15], which gives a lower limit for the value of M . While an increase in M relaxes the specifications for the analog prefilter in analog-to-digital conver-

[14] H. J. M. Veendrick and L. C. Pfennings, A 40 MHz multi-applicable digital signal processing chip, IEEE J. SC-17, 40-43, 1982.

[15] Sometimes the theorem is *not* satisfied, by deliberate choice. Reference is then made to 'sub-Nyquist sampling'; see [13].

sion and for the analog post-filter in digital-to-analog conversion^[10], it also increases the number of digital operations required per second as well as the memory capacity necessary for storing the signals. The sampling theorem indicates that a minimum value between 10 and 12 MHz is required for the frequency f_s , depending on the television system being considered (so that $M > 650$ to 750). A good choice for both NTSC and PAL seems to be $f_s = Mf_1 = 13.5$ MHz. Looking at the systems of Table I, this means that $M = 858$ for NTSC and $M = 864$ for PAL. An additional argument favouring this choice is that the standard sampling rate for studio applications is also 13.5 MHz. Keeping to this value can have certain advantages, especially if transmission from studio to receiver is to be entirely digital in the future.

In the SECAM system the methods of coding and decoding the colour information do *not* indicate any preference for locking f_s to f_{sc} . This leaves only the preference for locking to f_1 , particularly if field or picture memories are used for the signal processing. In spite of the larger bandwidth of the luminance signal (6 MHz) than in NTSC and PAL, a good choice for SECAM will probably also be a line-locked f_s of 13.5 MHz.

At the present time the digitization of video equipment is still in its infancy. The choice we now make for the sampling rate f_s will have a long-term impact, however: the first sets will contain a number of different digital ICs that operate at f_s . In addition, we may expect a gradual but sustained progress towards new and improved chips. But since we shall require compatibility with the existing chips, these will have to be based on the same f_s . It therefore seems likely that the 'life span' of f_s will be much longer than that of a single generation of chips. This emphasizes yet again the importance of a well-considered choice of f_s in the present initial phase.

Improving the picture quality

There are many ways in which the picture quality can be improved with the digital filters in figs 5, 8 and 9, primarily by reducing cross-colour, cross-luminance and noise. The wide variety of possible methods is connected with the existence of the following alternatives:

- The colour coding system used (NTSC or PAL).
- The type of digital filter (recursive or not).
- The amount of delay (one or more line periods, one or more field periods).

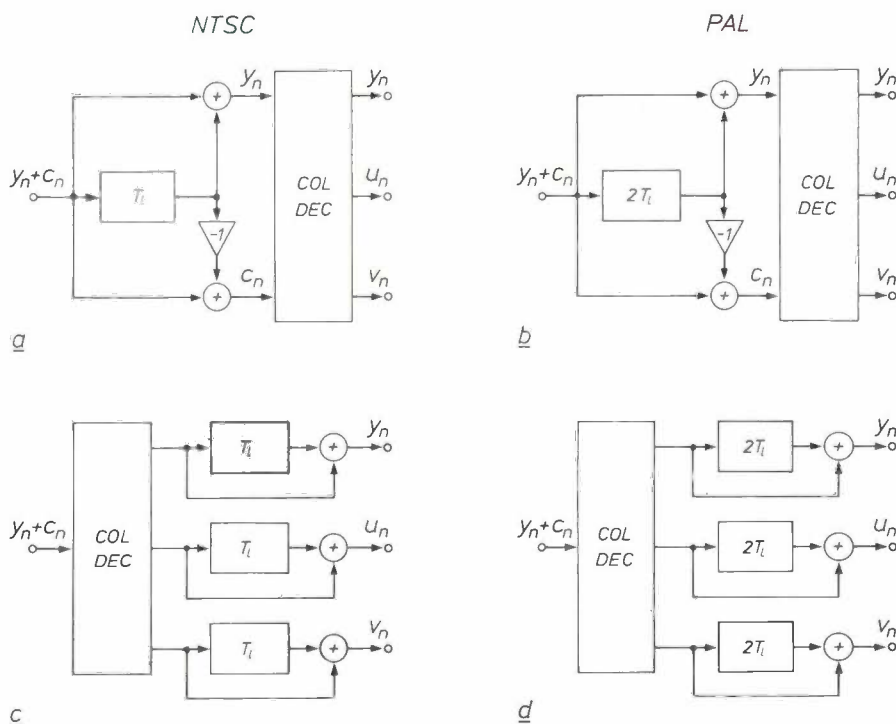


Fig. 12. Some examples of possible applications of transversal line comb filters for reducing cross-effects in NTSC and PAL. In principle the filters can be placed either before the colour decoder *COL DEC* (a and b) or after it (c and d). In the first case different filters are used for reducing cross-colour and cross-luminance; in the other case the filters are the same, but three are necessary instead of two. With the actual spectral relationships (fig. 2) delays of T_l are required for NTSC and $2T_l$ for PAL, where T_l is the period of one TV line.

- The location of the filters (before or after colour decoding).

Complete coverage in this article is not really possible, so we shall confine ourselves to giving a few outstanding examples of vertical filtering and temporal filtering.

Vertical filtering

Fig. 12 shows a number of comb filters based on vertical filtering, with which cross-colour and cross-luminance can be reduced. With NTSC a delay of one line duration T_l in the composite signal is sufficient to produce an improvement (fig. 12a). This is because the frequency of the colour subcarrier is exactly an odd multiple of half the line frequency; see fig. 2b. With PAL this is not the case and for the same improvement a minimum delay of two line periods would be necessary (fig. 12b).

In principle, cross-effects can also be reduced after colour decoding, both for NTSC and for PAL. This requires separate operations on the three component signals, however. In each of these signals the required frequency components are always concentrated around integer multiples of the line frequency. The unwanted (cross-colour or cross-luminance) frequency components lie in between. The same type of comb filter can therefore be used for all three signals, for NTSC again with a delay of T_l and for PAL with a delay of $2T_l$ (fig. 12c and d and fig. 13).

The operation of the two comb filters for PAL signals given here is not ideal. The required delays of two line periods cause a perceptible reduction of the definition of the picture in the vertical direction because the signals corresponding to relatively widely spaced lines are combined. In addition the cross-effects are only strongly reduced if the combined picture lines are identical, that is to say if the picture has a distinct vertical structure. Both for NTSC and for PAL a loss of picture definition occurs in the diagonal direction because diagonal picture structures give rise to frequency components that are strongly attenuated by line comb filters. This can be improved somewhat by using a rather more complicated comb filter structure, where the actual 'combing' of the luminance signal does not take place at low frequencies but is limited to the frequency range in which the chroma signal is situated (see for example [13]).

The comb filter in fig. 12a has long been used in *analog* systems, mainly for reducing cross-colour. All that is required is a delay line whose performance is not critical except in the frequency band of the chroma signal (on account of the bandpass characteristic). Conventional analog glass delay lines give adequate results here.

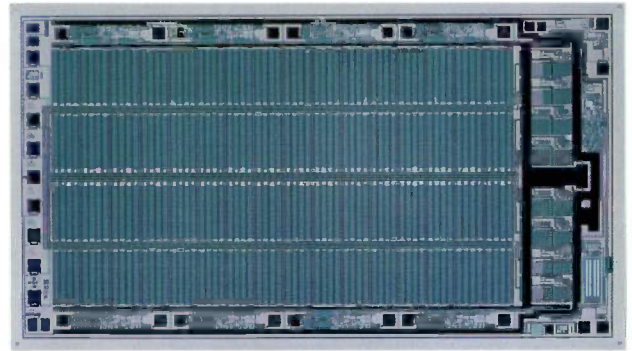


Fig. 13. Integrated digital line memory. This memory can serve as an elementary module in the construction of circuits for vertical filters in which delays of a line period or multiples of this are required. It has a capacity of 8×1024 bits, is a product of dynamic NMOS technology and has an area of almost 13 mm^2 . This chip is suitable for sampling rates up to 40 MHz.

Temporal filtering

Completely new ways of improving the picture quality can be obtained by basing filters on delays of about one field period T_f or multiples of T_f . Until now this has hardly been possible with analog methods, but recently the use of integrated digital memories has made such delays an economic proposition (fig. 14) [16]–[18]. Temporal filtering is best implemented after colour decoding. First of all, there is no longer any need to take account then of the exact value of f_{sc} . In the second place the signal operations are then largely independent of the colour television standard in use. We shall therefore confine ourselves to signal operations performed after colour decoding.

As we have seen, vertical filtering combines the information from pixels that are closely adjacent to each other in successive lines of the same field. Temporal filtering, on the other hand, combines the information from pixels that are close together in successive fields or even exactly coincident in successive pictures. In the main, vertical filtering depends on properties of the signal spectrum on the scale of fig. 2b and temporal filtering depends on those on the scale of fig. 2c.

The greatest advantage of temporal filtering is that the degree of cross-effect reduction is not so strongly dependent on the structure of the picture, and is therefore not so very different for sharp vertical, horizontal or diagonal colour transitions. We shall now present some actual examples of temporal filtering.

[16] M. J. M. Pelgrom *et al.*, A digital field memory for television receivers, IEEE Trans. CE-29, 242-250, 1983.

[17] E. J. Berkhoff, U. E. Kraus and J. G. Raven, Applications of picture memories in television receivers, IEEE Trans. CE-29, 251-258, 1983.

[18] W. Conrads, Integrated feature TV concept with serial I²C-bus-control and field memory, IEEE Trans. CE-29, 469-474, 1983.

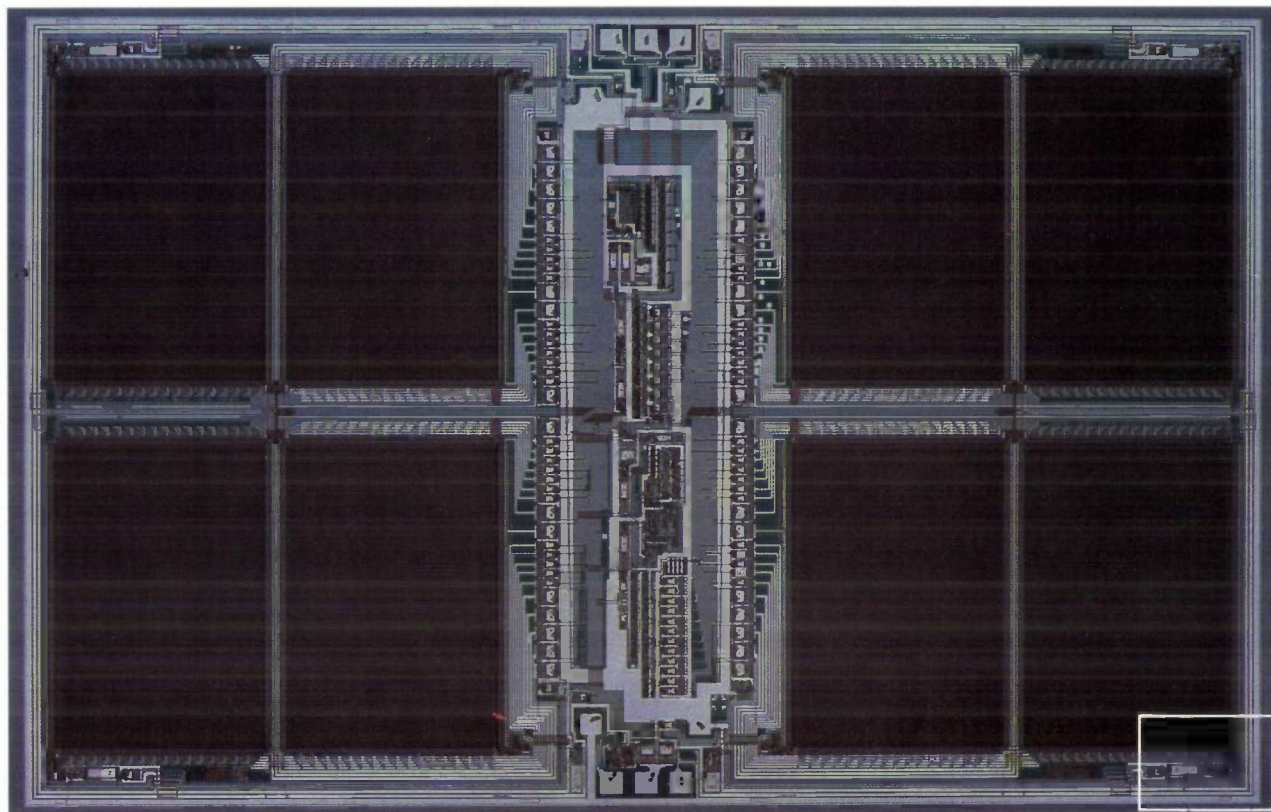


Fig. 14. Advancing technological developments have recently opened up the prospect of relatively low-cost fully integrated digital field and picture memories. The use of such memories is essential if the many potential advantages of the digital processing of television signals are to be fully realized. The upper photograph shows an integrated memory of the CCD type (charge-coupled device) with a capacity of 308 kbit. The chip is a product of 2- μ m NMOS technology. The chip is shown at actual size (about 35 mm²) at the top right-hand corner of this text. Seven such chips can be combined to make a complete field memory for the component signals of all current television systems. To make the fine details visible, the part of the upper photograph in the white rectangle is shown on the right on a greatly enlarged scale [16].

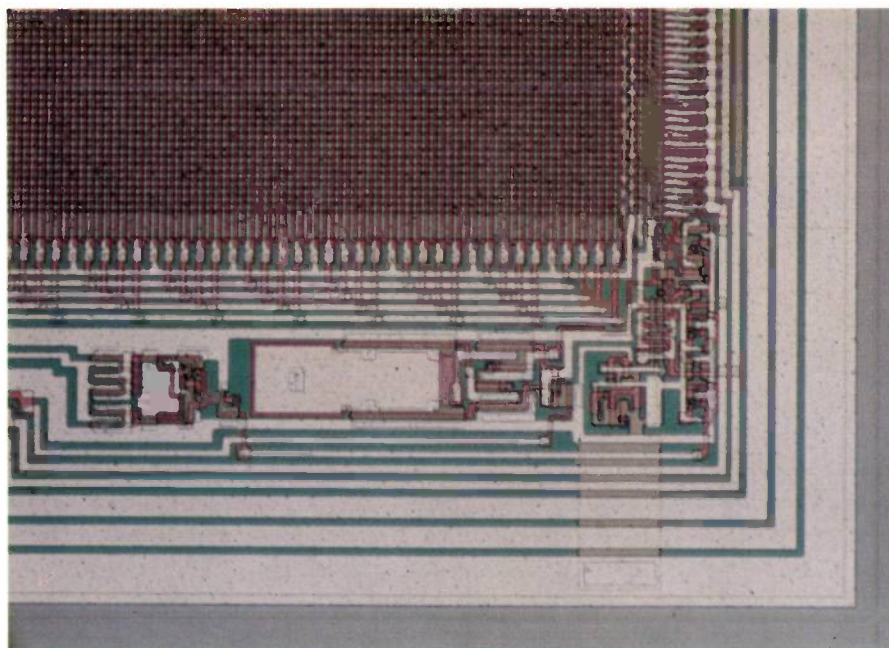


Fig. 15a shows a filter that removes cross-effects from the component signals in the NTSC system (with 525 lines) and *fig. 15b* shows a similar filter for the PAL system with 625 lines. An effect of the $312T_l$ delay for the PAL system is that two pixels directly one above the other in two successive fields are combined in the adder. If f_{sc} were equal to $283\frac{3}{4}f_1$, then (because 312 is a multiple of 4) the cross-effects in the adder would be in phase and would reinforce each

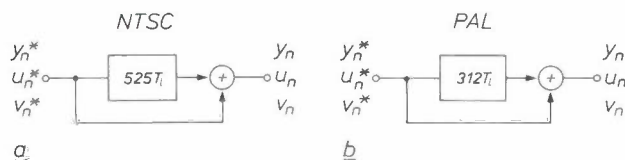


Fig. 15. Temporal transversal filter for reducing cross-effects in *a*) NTSC signals and *b*) PAL signals. These filters are designed for insertion after the colour decoder. The delay in both cases is such that cross-colour or cross-luminance can be reduced by the adding operation.

other — exactly what we do *not* want. But since, at least with standard signals, f_{sc} also has a frequency-offset of 25 Hz (see Table I), a delay of $312T_1$ represents an effective additional phase shift of 180° for f_{sc} , and the cross-effects in the adder will in fact be reduced.

The exact phase shift is $(312/312.5) \times 180^\circ$. In principle the delay of $312T_1$ for the PAL system can be replaced by a delay of $1250T_1$ (corresponding to the duration of four fields, or two complete pictures). Since 1250 is two plus a multiple of four, the subcarrier phase is shifted by an integer number of periods *plus* a half period, while the 25-Hz offset now gives no extra phase shift. Once again the result is therefore the extinction of cross-effects. The advantage is that in this case we combine coincident pixels in the adder (whereas with the delay of $312T_1$ there is a slight difference in the vertical position). A disadvantage, however, is the time difference of two complete pictures, which can cause blurring effects with moving scenes.

In the circuit for the NTSC system (fig. 15a) the delay of $525T_1$ corresponds to one picture (two fields). The odd number of line periods means that there is a delay for f_{sc} of an integer number of subcarrier periods *plus* a half period. Here again cross-effects are reduced in the addition.

Temporal filters can also be obtained with the recursive structures in fig. 9 by giving the delay an appropriate value. If we make KT_s equal to one picture period (i.e. $625T_1$ for PAL and $525T_1$ for NTSC) we can for example use the filter in fig. 9c for reducing cross-colour or cross-luminance in the component signals.

Movement detection

In all temporal filters the values of certain pixels are combined that were recorded in the camera with rather long intervals between them ($312T_1$, $625T_1$, etc.). For stationary pictures this has no consequences, of course, but if the picture moves, the movements cause changes in the signal value that have nothing to do with cross-colour or cross-luminance, although they are treated as if they had. This can lead to movement blur that completely negates the positive result of the reduction of cross-effects and can even make matters worse.

In this respect recursive filter structures are inferior to non-recursive types; the effects of picture delays will be worse than those of field delays, and for purely perceptive reasons the luminance signal will be more vulnerable than the colour-difference signals. Experiments have shown that one of the few cases in which there is virtually no perceptible movement blur with temporal filtering is when the filter in fig. 15b is used for cross-colour reduction in the PAL system.

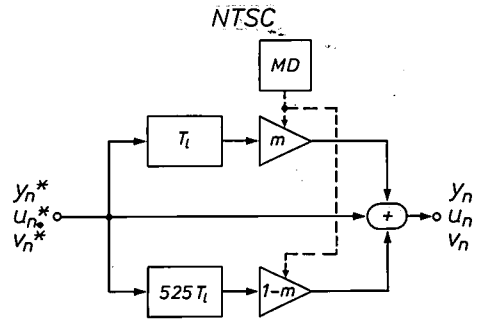


Fig. 16. Reduction of cross-effects in NTSC signals with a movement detector MD. When there is movement in the picture, $m = 1$ and there is vertical filtering; with no movement, $m = 0$ and there is temporal filtering.

When temporal filters are used, it is therefore usual to add a movement detector, which decides for each pixel whether there has been a movement with respect to the preceding field or picture. Temporal filtering is only applied for those parts of the picture in which there is no movement; the other parts are not processed in this way. In the structure of fig. 9c a movement detector can ensure that $g = 1$ for moving-parts of the picture (it is not a recursive filter then but a direct connection). All other temporal filters can be similarly extended with a movement detector. A second example is given in fig. 16, which shows a circuit for cross-colour reduction in the NTSC system. Here we can recognize a combination of reduction by vertical filtering (fig. 12c) and reduction using temporal filtering (fig. 15a). Under the control of a movement detector a decision is made between $m = 0$ and $m = 1$ for each pixel and thus between the two methods of filtering.

We shall not go into the details of movement-detector design in this article; in principle they all make use of the fact that the frequency spectrum of a truly stationary picture consists of lines at known positions (see fig. 2). If the spectrum contains energy at other positions, this must be the result of movement. Various types of comb filters are again used for detecting this.

Noise reduction

Any form of cross-colour or cross-luminance reduction based on filtering out unwanted frequency components will usually be associated with a reduction in the noise originating from external sources of interference, and therefore with an improvement in the signal-to-noise ratio (although this does not necessarily imply a subjective improvement in picture quality). The extent of this improvement, however, will differ

from one type of filter to the other. Let us for convenience assume that the noise has a flat power spectrum (i.e. white noise). Comb filters of the upper two types in fig. 8 then give an improvement of 3 dB. Comb filters of the lower two types in fig. 8 give as much as 4.3 dB. An even greater improvement in signal-to-noise ratio can be achieved with some recursive filter structures. With the filter of fig. 9c a gain of 2.2 dB is obtained for $g = \frac{3}{4}$ and 11.8 dB for $g = \frac{1}{8}$.

For stationary pictures it is easy to see how the noise can be reduced with this type of recursive filter, if KT_1 is a delay of an entire *picture period* (i.e. $625T_1$ or $525T_1$). The signal values corresponding to one particular pixel are constant and are simply added together, whereas the noise contributions vary and are therefore averaged out (see also the lower photograph on p. 182).

A noise reduction can also be achieved, however, by using a memory that gives a delay of only about one *field period*. Here use is made of the fact that the signal values for every two pixels lying immediately one above the other in successive fields do not as a rule change very much. Owing to the recursive structure, the averaging takes place over a large number of

fields. If in PAL a fixed field memory of $312T_1$ or $313T_1$ were to be taken, pixels on lines increasingly far apart would then gradually be combined (fig. 17). To avoid this, the delay must be made to alternate between $312T_1$ and $313T_1$ in this case. This can be done with a field memory of $312T_1$ to which an extra line delay T_1 is periodically added; during the successive fields the switch S is alternately in the upper and lower positions.

It is possible to use the same picture or field memory simultaneously for reducing cross-effects and for additional improvement of the signal-to-noise ratio. We shall give two examples of this. Fig. 18 shows a possible solution for NTSC and is in fact a combination of fig. 9c and fig. 16. A complete *picture* memory is used in this case. Fig. 19 shows a solution for PAL that only needs one *field* memory. This is in fact a combination of the circuits in fig. 15b and fig. 17.

As we have seen, most circuits in which temporal filtering is used include a movement detector. One result of this is that there is no noise reduction at the pixels where movement is detected. This is not so serious as it may seem, however, since the noise at these pixels is perceptually less of a nuisance.

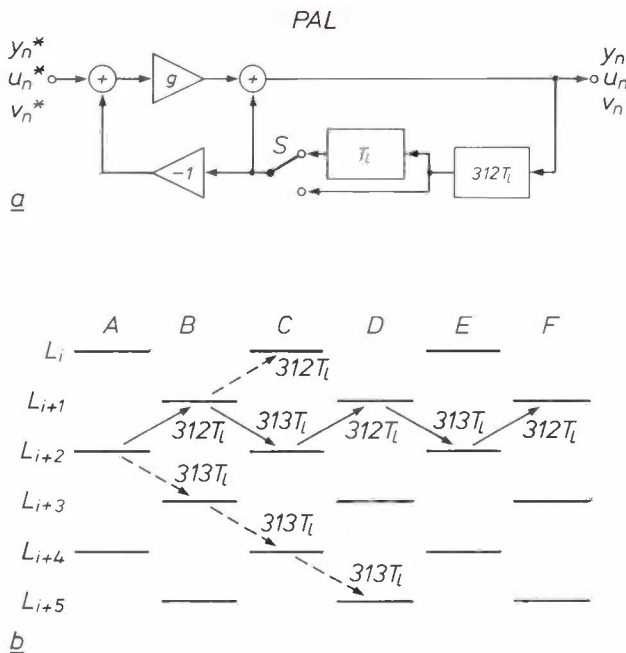


Fig. 17. a) Noise reduction for each of the PAL component signals y_n^* , u_n^* and v_n^* , by using a first-order recursive comb filter with only one *field* memory ($312T_1$ or $313T_1$). b) Half of the successive lines $L_i, L_{i+1}, L_{i+2}, \dots$ of a television picture occur during the odd fields A, C, E, ... and the other half occur during the even fields B, D, F, ... With a fixed delay of either $312T_1$ or $313T_1$ the result with this circuit would be that lines more and more distant from each other would be combined (dashed arrows), causing an unacceptable deterioration of definition in the vertical direction. This is corrected by making the delay during the successive fields alternately equal to $312T_1$ and $313T_1$ (solid arrows). This is done by means of the switch S .

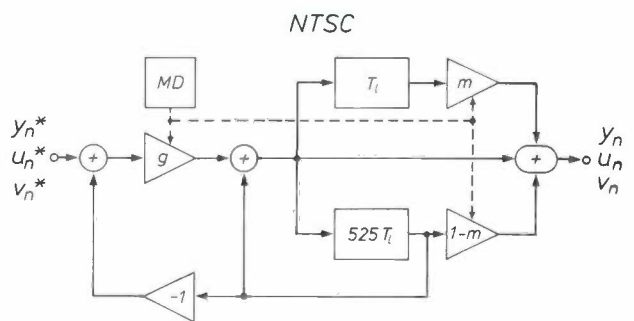


Fig. 18. Reduction of cross-effects and noise for each of the NTSC component signals y_n^* , u_n^* and v_n^* , with a *picture* memory and a movement detector MD . If there is movement in the picture, $g = m = 1$. If there is no movement, $0 < g < 1$ and $m = 0$.

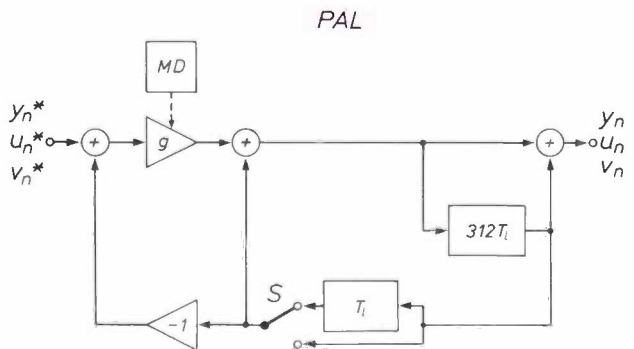


Fig. 19. Reduction of cross-effects and noise for each of the PAL component signals y_n^* , u_n^* and v_n^* , with a *field* memory and a movement detector MD . If there is movement, $g = 1$; otherwise $0 < g < 1$.

Reduction of large-area flicker

One of the imperfections of present-day television receivers is most clearly observed on uniform picture areas in the TV systems operating at 25 pictures per second. These areas show a visible periodic variation in luminance, referred to here as 'large-area flicker', even though its frequency is doubled to 50 Hz by using interlaced fields. The higher luminous output of modern picture tubes, which enables us to watch television with more background lighting and in daylight, does make this effect much more troublesome. The reason is that faster variations can be observed when the luminance is higher. A solution to this problem is to display each field twice, giving a field repetition rate of 100 Hz, which is much more acceptable to the human eye. This field doubling can be obtained by using a memory that stores only one field (half a picture). The control of such a memory is rather complicated, however. It becomes much simpler if two field memories are used in which, alternately, the fields are written in slowly and read out quickly (fig. 20). Denoting the successive original fields by A, B, C, D, \dots we obtain with this circuit a signal with successive fields $A, A, B, B, C, C, D, D, \dots$. To display the signal properly, the receiver unit has to be modified so that:

- the signal bandwidth is doubled;
- each picture line lasts for only $32 \mu\text{s}$ instead of $64 \mu\text{s}$ and the duration of each field is only 10 ms instead of 20 ms; the field scan is thus twice as fast in both the horizontal and the vertical directions;
- The successive fields are displayed *in pairs* (instead of alternately) at the same position in the frame.

The effect of large-area flicker can be completely suppressed in this way.

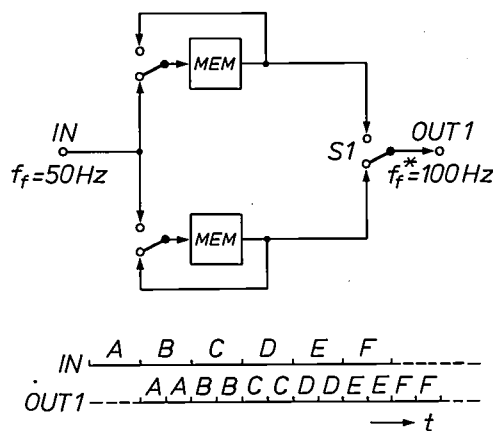


Fig. 20. Large-area flicker can be reduced by doubling the field frequency (from $f_t = 50 \text{ Hz}$ to $f_t^* = 100 \text{ Hz}$ here). This can be done by using two field memories *MEM*, in which the signals are alternately written in slowly and then read out twice at double speed. The original field sequence A, B, C, D, E, \dots is thus changed to $A, A, B, B, C, C, D, D, \dots$. This is known as 'field doubling'.

Reduction of line flicker

In addition to large-area flicker there is also *line flicker*. This also results from the kind of scanning pattern, and especially from the interlacing. A sharp image transition that is exactly parallel to the lines of the picture occurs at different heights in consecutive fields and therefore seems to dance up and down at a frequency of 25 Hz. With the circuit in fig. 20 nothing has been done about this; so it still has a line flicker at 25 Hz. By adding a third field memory (fig. 21) we can have a 100-Hz field frequency in which the sequence of the fields is $A, B, A, B, C, D, C, D, E, F, E, F, \dots$. We then have, just as in fig. 20, a field frequency of 100 Hz, but any line flicker now occurs at 50 Hz and is therefore barely perceptible, if at all. However, this circuit gives undesirable effects with moving pictures, since the original sequence of the fields has been altered so that the older field A , say, appears again after the display of the newer field B . In essence we would like to combine the advantages of one 100-Hz field sequence (*OUT1*) with that of the other 100-Hz field sequence (*OUT2*). However, the signals *OUT1* and *OUT2* have become relatively displaced in time, so that direct switching between them is not possible. This problem has been solved in the circuit of fig. 22. The signal *OUT3* is a delayed version of *OUT1*. The switch *SM*, controlled by a movement detector, can now be switched at any instant between *OUT2* and *OUT3*, depending on whether there is any movement or not in the picture.

In switching between *OUT2* and *OUT3* even fields are repeatedly replaced by odd fields and vice versa. Since the even and odd fields correspond to slightly different positions on the television screen, some means of correction is required. The problem can be solved by the simple expedient of inserting a line memory and an adder. We shall not pursue the matter further here, however.

Also shown in fig. 22 is a switch *S4* that can provide the signal *OUT4*, which is delayed by exactly one *picture* period with respect to the original input signal *IN*. This signal *OUT4* is used to good effect in the *VIDEO PROCESSOR* block for temporal filtering, as dealt with in the previous sections. The circuit in fig. 22 can therefore improve the quality of the picture in five respects: large-area flicker, line flicker, cross-colour, cross-luminance and noise.

The methods described here for reducing large-area flicker and line flicker leave the interlaced structure of the picture essentially unchanged: each field received is displayed without modifications. With the availability of field memories, however, the lines of each two successive fields can be interwoven ('field addition'), so that all the lines of one picture (two fields) are displayed consecutively from top to bottom. Then interlacing is eliminated, and we have obtained another method of reducing the two types of flicker.

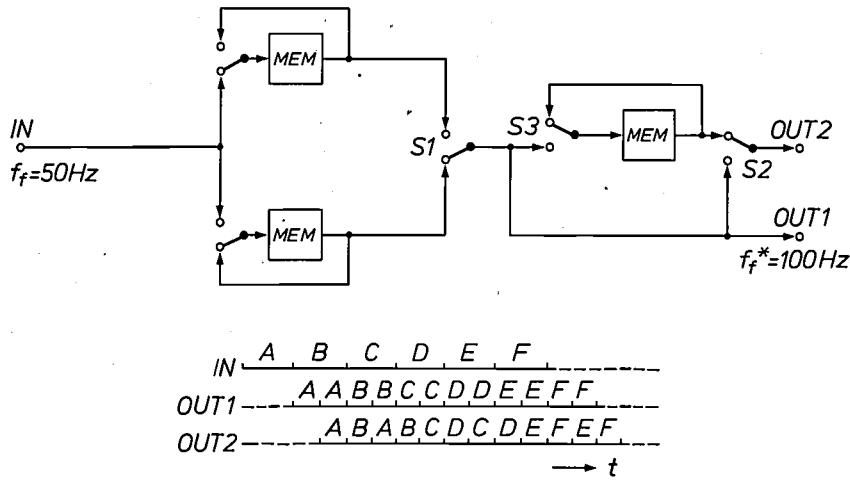


Fig. 21. The addition of a third field memory MEM to the circuit in the previous figure gives a signal OUT2 with twice the field frequency and a field sequence A, B, A, B, C, D, C, D, This is known as 'frame doubling'. In this way both line flicker and large-area flicker are reduced. This circuit has some adverse effects, however, if the picture contains movement. (The OUT1 signal is not used here.)

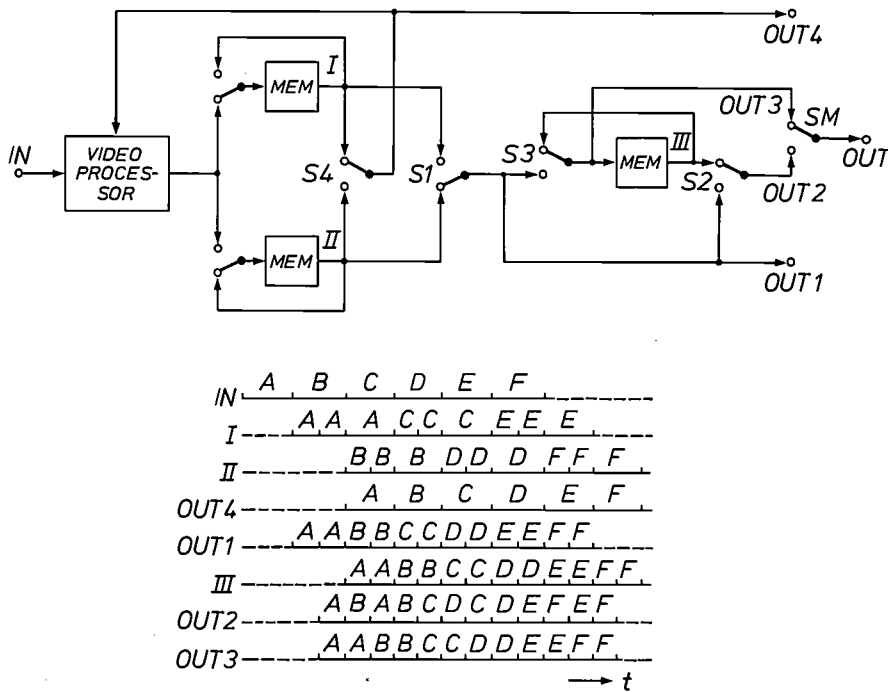


Fig. 22. By adding a switch SM, operated by a movement detector (not shown), the advantages of the circuits in fig. 20 and fig. 21 can be combined. The signal OUT has the field sequence A, A, B, B, C, C, D, D, . . . or A, B, A, B, C, D, C, D, . . . , depending whether there is movement or not. The sequence can be chosen separately for each pixel. The addition of a switch S4 makes the signal OUT4 available. This is a version of the input signal delayed by a complete picture period. It can be used as the starting point for any desired form of temporal filtering in the circuit VIDEO PROCESSOR. In all, the circuit in this figure can be used for the combined reduction of large-area flicker, line flicker, cross-colour, cross-luminance and noise.

Other improvements

The improvements discussed above are just a few of those offered by the introduction of digital signal processing in television receivers. We shall now briefly mention two other cases in which digital filters play an

important part. In the first place, picture definition in the horizontal and vertical directions can be increased by horizontal and vertical filtering with the appropriate filters. This is referred to as 'aperture correction', because it corrects some of the blurring due

to certain optical and electrical limitations in the receiver ^{[19][20]}. In this kind of aperture correction it is often of great importance that digital filters can have a perfectly linear phase characteristic.

A second example of more advanced digital signal processing is echo cancellation. Because of multiple reception of reflected signals, e.g. from high buildings or mountains, a television picture may contain annoying echoes or 'ghost images'. In principle these echoes can be removed by echo cancellation with adaptive filters ^[21].

of (say) 9 pictures ('multi-picture-in-picture'). This latter facility is particularly convenient for making a choice from a large number of programmes (*fig. 23*).

If digital signal processing is used, it becomes simpler and therefore cheaper to make a receiver designed to receive television signals that have been coded in different standards (PAL, NTSC, SECAM).

With a field or picture memory 'slow-scan TV' operation can be obtained, so that signals from a telephone line, for example, can be displayed on a conventional television screen as a series of slowly chan-



Fig. 23. The use of field memories also makes it possible to combine parts of pictures. The example given here is 'multi-picture-in-picture', where the signals originating from several different transmitters are displayed simultaneously. This can be a very useful facility when making a selection from a large number of programmes.

New features

Now that it is becoming an economic proposition to digitize television pictures and to store them in a memory in a television receiver, a number of new features can be introduced. Some of these are fairly obvious but are still a welcome addition to the existing features. In the first place there is of course the facility of stopping ('freezing') a particular picture, so that a stationary picture can be observed. A picture can also be stored for shorter or longer periods of time for later display or for printing out on paper (hard copy). A part of a stored picture can be displayed as a complete picture (i.e. magnified), by a process referred to as 'zooming'. The memory can also be used for simultaneously displaying a second picture in the corner of the screen ('picture-in-picture') or even a combination

of pictures. One application of this facility is found in remote visual monitoring. In combination with a video cassette recorder, video disc player or video camera, countless other applications come to mind. If

^[19] H. Schönfelder and M. Jacobsen, Qualitätsverbesserung einer PAL-Farbfernsehübertragung durch digitale Filtertechnik, *Frequenz* 37, 324-333, 1983.

^[20] H. Schönfelder, Möglichkeiten der Qualitätsverbesserung beim heutigen Fernsehsystem, *Fernseh- & Kino-Tech.* 37, 187-196, 1983.

^[21] Adaptive echo cancellation is not only applied to video signals. An analog integrated circuit for adaptive echo reduction in Teletext is described in [22]. A digital integrated circuit for adaptive echo reduction in data transmission is described in [23].

^[22] J. O. Voorman, P. J. Snijder, J. S. Vromans and P. J. Barth, An automatic equalizer for echo reduction in Teletext on a single chip, *Philips Tech. Rev.* 40, 319-328, 1982.

^[23] P. J. van Gerwen, W. A. M. Snijders and N. A. M. Verhoeckx, An integrated echo canceller for baseband data transmission, *Philips Tech. Rev.* 39, 102-117, 1980.

memories are used, signals originating from non-standard sources can be synchronized with each other, or with standard signals, permitting simple switching between them ('editing').

A very useful application is the background memory for teletext. In teletext [22] all the available pictures ('pages') are transmitted in a continuously repeated sequence as a small part of an ordinary broadcast television signal. At the present time only the page actually being displayed on the screen is stored in a memory of limited capacity in the receiver. This means that, after selecting a new page, the viewer has to wait until that particular page is received again before he can see it displayed. In a cycle of 300 pages this can take as long as a minute. If the user wants to change pages frequently, i.e. to browse through them as in an information search, this can be a long time to wait. Since one complete teletext page in coded form only occupies a fraction (about 0.3%) of a television field, many hundreds of teletext pages can be stored in only one field memory. All these pages can be displayed with a delay of half a second at most — almost instantaneously [24].

Economic digital field and picture memories ultimately open up the prospect of fundamental changes in the signal standards for colour television. By virtue of these memories, chrominance and luminance signals, which must be *simultaneously* available for display, can nevertheless be transmitted and received

consecutively. This can provide a fundamental solution to the existing problems of cross-colour and cross-luminance. In addition, each component signal can have exactly the right amount of the total transmission capacity allocated to it to give the optimum overall result. Systems of this kind, known as MAC ('Multiplexed Analog Component') [20][25], are the subject of steadily growing interest.

[24] H. J. R. Schmitz, M. J. J. C. Annegarn and W. F. Fekkes, A CCD memory controller for instant access to teletext, IEEE Trans. CE-30, 442-446, 1984.

[25] H. Mertens and D. Wood, The C-MAC/packet system for direct satellite television, EBU Rev. Tech. No. 200, 172-185, 1983.

Summary. The modern trend of replacing analog electronic circuits by digital ones is now starting to take effect in colour television receivers. Besides bringing economic advantages, digitization can substantially improve the quality of the present television picture. The improvements include a better separation of chrominance and luminance information (reduction of cross-colour and cross-luminance), noise reduction and the reduction of large-area flicker and line flicker. New features such as 'freeze-frame', combined pictures ('picture-in-picture'), the magnification of parts of a picture (zoom) and teletext memory also appear. This article describes the background and present capabilities of digital television signal processing. Some characteristic filter operations are discussed, including vertical filtering and temporal filtering, as well as characteristic types of filter, such as comb filters. It is found that in very many cases there is a need for economic field or picture memories. The importance of making the right choice of sampling rate is underlined. This article is concerned mainly with the NTSC system (America, Japan) and the PAL system (Europe).

Digital audio: examples of the application of the ASP integrated signal processor

E. H. J. Persoon and C. J. B. Vandenbulcke

Ned. Philips Bedrijven B.V.
PHILIPS RESEARCH LABS.
LIBRARY WY - 1
P.O. Box 80.000
5600 JA EINDHOVEN
THE NETHERLANDS

Introduction

Electronic processing of audio signals is not new. Tone control by means of one or more analog filter stages is a well-known example from hi-fi technology — the technology of the faithful reproduction of speech and music. Another example is the improvement of audio quality by altering spatial perception with the aid of stereo effects and reverberation. The basic knowledge of acoustics and perception required here has long been available, but until now many practical applications have been restricted to professional use in the studio, e.g. for records, radio, TV and film.

However, great changes are on the way, for we are now in the digital age of audio technology, and this includes equipment for the 'ordinary' consumer. For the best results, sound is now recorded in digital form on tape or disc (the Compact Disc^[1]). This can be done virtually without distortion and with signal-to-noise ratios previously thought impossible. From digital recording to digital processing is but a single step. All the advantages of digital signal processing^[2] are then assured.

With digital methods it is easy to make an ideal memory. This is of primary importance for audio technology, for signals can then be delayed as desired. Another important feature is that processing, once selected, remains fixed and immutable — for example, feedforward controls always remain stable, even in the long term. On the other hand, various settings of the equipment are easy to change automatically by digital methods ('adaptive control'), so that an optimum result is always obtained by an appropriate self-adjustment.

For the listener, the introduction of digital signal processing in audio^[3] provides a number of new facilities that were previously too expensive or technically too difficult, such as:

- Dynamic-range compression or expansion — reducing or increasing the difference between the levels of loud and soft passages as required.

- Reverberation — adding delayed versions of the audio signal.
- Equalization — detailed adaptation of the frequency characteristics of the reproducing equipment to the acoustics of the room.

The above operations can be performed digitally and with high quality by circuits that can be incorporated in one or more ICs. The filters in these circuits can be completely free of undesirable phase distortion, something that is not really possible with conventional filter circuits.

Digital circuits can be designed for external programming, so that the same circuit can perform different operations. This has led us to develop a programmable integrated circuit for processing audio signals: We call it ASP (Audio Signal Processor). A system consisting of a few of these ASPs will perform operations such as those described above.

In this article we describe the architecture of the ASP. In the context of the special issue in which this article appears, however, we should first like to give more attention to the background, the characteristics and some practical implementations of the examples of advanced audio signal processing mentioned above.

Compression and expansion of the dynamic range

Necessity for adapting the dynamic range

The human ear has a formidable dynamic range. It is so sensitive that it can almost detect the Brownian motion of the air molecules against the eardrum (the threshold of hearing, 0 dB), but it is not overloaded until the sound intensity level is 10^{12} times higher (the threshold of pain, 120 dB). These extreme limits are reproduced in *fig. 1*.

Dr E. H. J. Persoon is with Philips Research Laboratories, Eindhoven, and Dr Ir C. J. B. Vandenbulcke is with the Philips Consumer Electronics Division, Eindhoven.

[1] Special issue 'Compact Disc Digital Audio', Philips Tech. Rev. 40, 149-180, 1982.

[2] J. B. H. Peek, Digital signal processing — growth of a technology, pp. 103-109 in the special issue 'Digital signal processing I, background', Philips Tech. Rev. 42, 101-148, 1985.

[3] See also: W. J. W. Kitzen and P. M. Boers, Applications of a digital audio-signal processor in T.V. sets, Philips J. Res. 39, 94-102, 1984.

In everyday life there is always a background of sound. Music or speech that we want to listen to must stand out above it. In a quiet concert hall the sound background is very low (30 dB above the threshold of hearing). The quietest musical passages are also on that level. On the other hand, the *fortissimo* of a symphony orchestra reaches about 110 dB, so that the dynamic range is 80 dB.

In a domestic setting the background is usually louder. In a living room a level of 40 dB is typical. Reproduction of the original dynamic range of the symphony orchestra would give levels of 120 dB in the room, which is not acceptable. In general levels above 100 dB seem unpleasantly loud, particularly in a small room. The difference in volume between the loudest and quietest passages must therefore be reduced: this is called compression of the dynamic range.

Even greater compression is desirable if the music is only to be used as background. In this case people must be able to speak to one another, at a conversational level of about 65 dB; the loudest passages of music must not exceed this level. Very large compression is also desirable in a car, where the background level can be 80 dB.

The new Compact Disc has an unprecedentedly large dynamic range; in principle it can record music with the large dynamic range of a concert hall extremely faithfully. However, each listening environment requires its own dynamic range for the optimum final reproduction (fig. 1). Now that the Compact Disc is here, the desirability of adapting the dynamic range to the listening conditions has become even greater. In most cases dynamic range *compression* is required.

Under certain conditions it may be preferable to have a greater dynamic range than that offered by, say, a particular conventional record. In such cases the opposite of compression — *expansion* — of the dynamic range is useful.

How can the dynamic range be compressed (or expanded)?

There are analog circuits for dynamic range compression (or expansion). These include a peak detector that provides a control signal $r(t)$, that reduces or increases the gain A in the signal path (fig. 2a). We shall be mainly concerned with compression here.

The typical reaction of a compression system to a varying signal $x(t)$ is represented in fig. 2b. After an increase in the amplitude of $x(t)$ the gain falls very rapidly and after a reduction in the amplitude the gain gradually returns to the initial value (the release effect).

Some 'sluggishness' is desirable so that the gain does not follow the fine structure of the audio signal

too closely and thus eliminate all of the dynamic variation. For the best result, the start of the control action should be somewhat delayed, so that the reaction to the signal $x(t)$ becomes like that shown in fig. 2c.

All this can also be carried out by digital methods. The rectification, which forms a part of the peak detection, is then replaced by for example one or more simple operations on the binary representation of the signal. A digital filter delays the start of the control and also limits the control bandwidth to a few hertz. In dynamic-range compression and expansion with the ASP the delayed start, the release effect and the compression/expansion ratio can in principle be set independently.

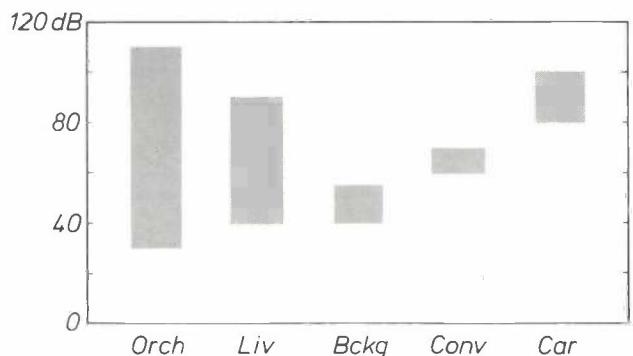


Fig. 1. Schematic presentation of the dynamic range of sound under various listening conditions. *Orch* the dynamic range of a symphony orchestra in a concert hall. *Liv* the desirable dynamic range for quality reproduction in a living room. *Bckg* the desirable dynamic range for background music in a living room; it should not swamp the conversation *Conv*. *Car* the desirable dynamic range in a moving car.

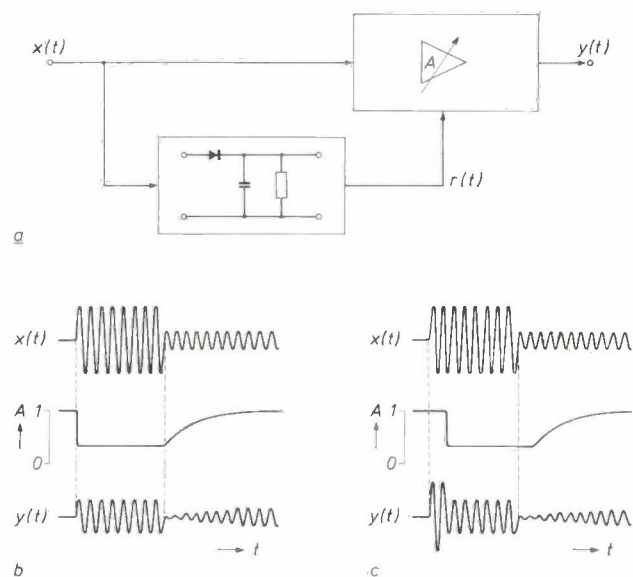


Fig. 2. Dynamic-range control. a) A control signal $r(t)$ is derived from the applied signal $x(t)$ by peak detection and used to vary the gain A . If the gain increases with increasing $r(t)$ we obtain expansion, in the opposite case compression. $y(t)$ is the resulting signal. b) Example of dynamic-range compression with instant response. t time. c) Example of dynamic-range compression with delayed response.

Artificial reverberation

When recordings are made in the studio, artificial reverberation is usually added. This is obtained with the aid of a reverberation chamber, a reverberation plate (a fairly large metal plate in which an electrically excited oscillation is allowed to die away) or — nowadays — an electronic reverberation circuit. Home-recording enthusiasts would also like to have reverberation for their recordings, which are usually made in rooms with not enough reverberation, if they could afford it. And in reproducing music recorded elsewhere, it is sometimes desirable to liven up dead acoustics with artificial reverberation. (In this way the special character of a live performance can be enhanced.)

Reverberation occurs because of the combination of long delays and sound reflections in some enclosed spaces (concert halls, churches, bathrooms). The sound reaches the listener with different delays from different directions. These delayed presentations of the sound can now be achieved with electronic equipment of acceptable size, because of the miniaturization of semiconductor memories. Electronic reverberation is thus becoming available to the consumer and is also one of the applications of the ASP.

We are especially interested in artificial reverberation that sounds natural. Therefore we should examine the phenomenon of reverberation more closely.

The characteristics of reverberation

If someone in a hall is listening to a source of sound on the stage, the sound coming directly from the source reaches him first. A little while later this is followed by the early reflections, reflected once by walls, ceiling and floor around the proscenium. In a large hall these early reflections take longer to arrive than in a small hall and a listener, influenced by experience, unconsciously connects their delay with the dimensions of the hall. This initial delay is generally smaller, and usually much smaller, than 150 ms.

The sound spreads out into the hall and is reflected many more times there. After the first, early reflections the listener hears multiple reflections from all sides. These reach him at irregular times. Their density increases continuously (fig. 3), on average as the square of the time. In view of the attenuation at each reflection their amplitude decays exponentially with time. The rate of decay increases with the attenuation at each reflection, i.e. as the reflecting surface absorbs more energy from the sound.

The time in which the level of the reverberation falls by 60 dB is called the reverberation time T_{60} . The reverberation time is not the same for all audio frequencies, because the absorption characteristics of the

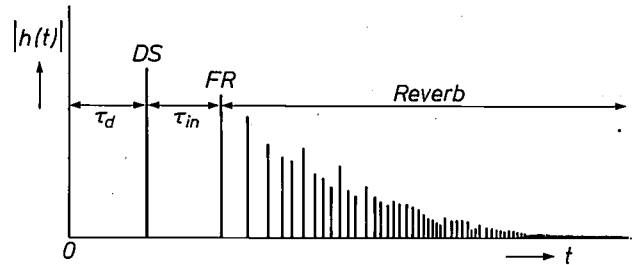


Fig. 3. Schematic rendering of the impulse response $h(t)$ of a concert hall (absolute value), as observed at an arbitrary location in the hall. The original impulse occurs at time $t = 0$. The direct sound DS arrives after a time τ_d , the first reflection FR arrives after a second period τ_{in} followed by a series of reflections of exponentially decreasing amplitude and spaced more and more closely together (Reverb).

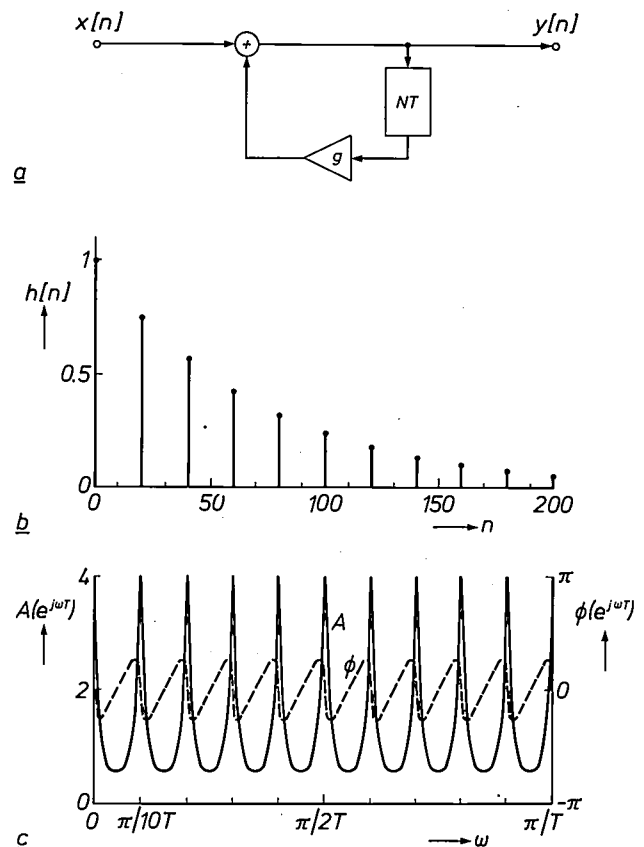


Fig. 4. Recursive digital comb filter of the N th order with one filter coefficient g . a) Block diagram. The output of a delay line (delay NT) is attenuated ($|g| < 1$) and fed back to the input. b) Impulse response $h[n]$. A pulse presented to the input is repeated at the output after every N sampling intervals (here $N = 20$); each repetition is weaker than the previous one by a factor g (here $g = 0.75$). (Output samples of value 0 are not explicitly reproduced in this and following figures because there are very many. Also $h[n]$ in principle lasts for an infinite time.) c) Associated amplitude characteristic $A(e^{j\omega T})$ and phase characteristic $\phi(e^{j\omega T})$. These characteristics are periodic with a period $2\pi/NT$. There are therefore exactly N periods in the fundamental interval $0 \leq \omega < 2\pi/T$. Here we have only shown half of the fundamental interval, i.e. $0 \leq \omega \leq \pi/T$.

different materials are not the same at all frequencies. In general the absorption is higher at high frequencies — so that the reverberation time is shorter — than at low frequencies.

Electronic excitation of reverberation

A suitable aid for the excitation of artificial reverberation is the recursive digital comb filter of the N th order ^[4] (fig. 4a). This consists of a series of N unit-delay elements whose output is fed back to the input (via an attenuation $|g| < 1$). A pulse presented to the input will therefore appear regularly at the output, with intervals equal to N sampling intervals (fig. 4b). The attenuation in the feedback loop ensures that the pulse grows weaker at each reappearance. The amplitude characteristic of the filter has N peaks spaced regularly throughout the fundamental interval $0 \leq \omega < 2\pi/T$ (fig. 4c). This explains the name of the filter.

The behaviour of this comb filter is similar to that of reverberation in a hall. In both cases there is continuous repetition of a single pulse with a gradually decreasing amplitude. The rate of decrease of this amplitude can be altered by means of the attenuation factor in the feedback path. If it is desirable for the higher-frequency components to die off more rapidly,

as is usual in natural reverberation, the frequency-independent attenuation in the feedback path can be replaced by a lowpass filter, e.g. that of fig. 5. We shall call the result a 'modified comb filter' (fig. 6). Examples of the associated impulse response and phase and amplitude characteristics are also given in fig. 6.

One difference from 'natural' reverberation is the regularity with which the pulses recur. This gives the periodicity in the frequency characteristic. The frequency interval between successive peaks in this characteristic is constant, just like the frequency interval between the components of a musical tone. This means that our hearing interprets a series of pulses with such a frequency characteristic as a 'tone'. Somewhat incorrectly it is said that the reverberation produced with a comb filter suffers from 'colouring'. In fact this is not a matter of sound colour but of pitch. If a complex of different tones is presented, the tone that is 'in tune with' the comb filter is strongly enhanced.

Such regular impulse responses are often met when metal objects, e.g. metal springs, are acoustically ex-

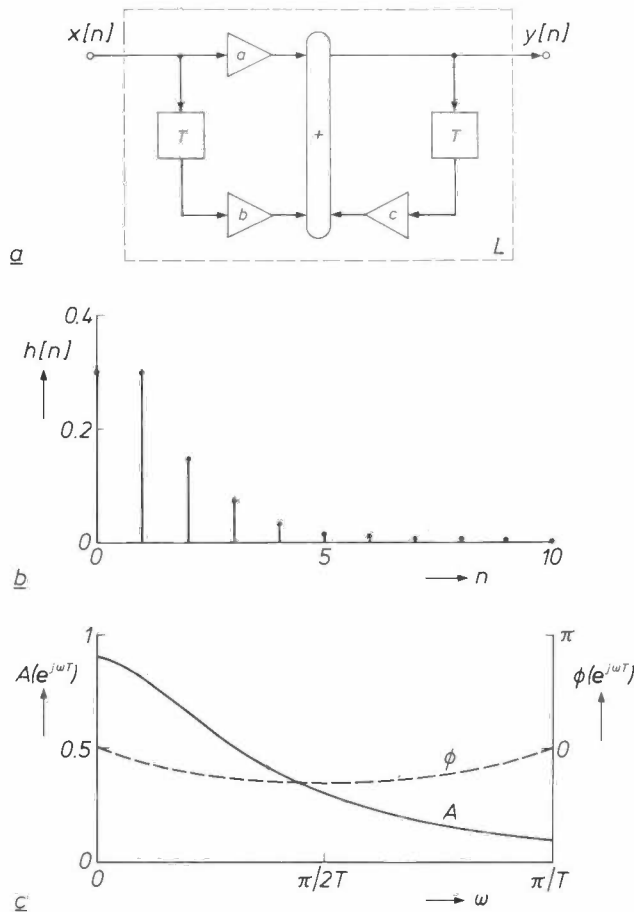


Fig. 5. Simple digital filter L of the 1st order. a) Block diagram. b) Impulse response $h[n]$ for $a = 0.3$, $b = 0.15$ and $c = 0.5$. c) Associated amplitude characteristic $A(e^{j\omega T})$ and phase characteristic $\phi(e^{j\omega T})$.

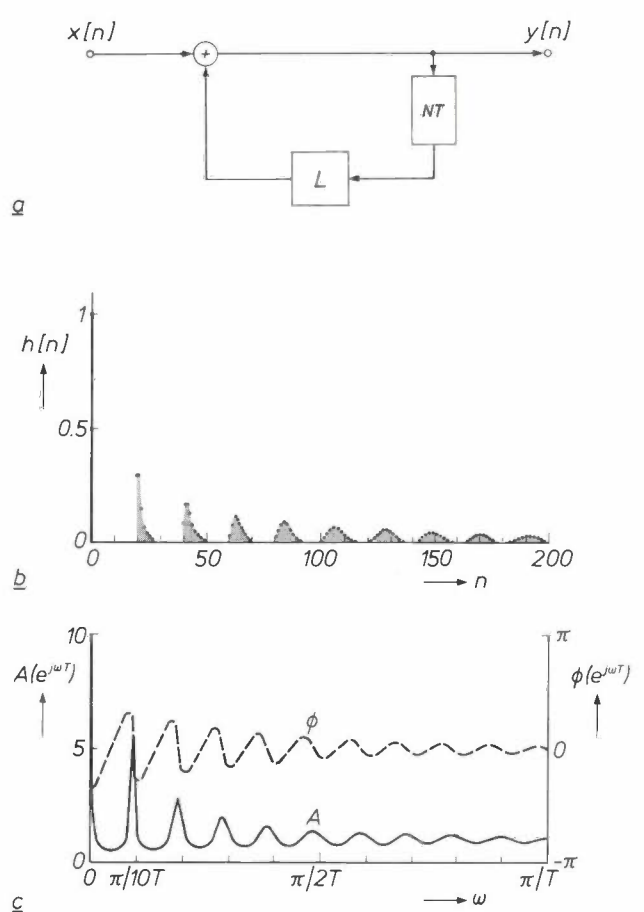


Fig. 6. Modified recursive digital comb filter. a) Block diagram; the constant attenuation g in the feedback loop of fig. 4 has now been replaced by the filter L from fig. 5. b) Impulse response $h[n]$ for $N = 20$. c) Associated amplitude characteristic $A(e^{j\omega T})$ and phase characteristic $\phi(e^{j\omega T})$.

cited. Our hearing makes associations with what is familiar from experience, so that the reverberation produced by a comb filter is often said to be 'metallic'. This is undesirable, of course. If the delay in the filter is very large the individual pulses can be detected. The rapid rattling sounds then heard are called 'flutter echoes'. These are also undesirable.

One way of correcting these difficulties is to connect several comb filters in parallel, each with a different delay. This increases the density of the 'reflections' and masks the regularity of each individual comb filter. Another way is to add phase-shifters ('allpass filters') [5][6].

A phase-shifter is a filter that introduces a frequency-dependent phase shift and has a flat amplitude characteristic. An example of a digital phase-shifter of the N th order is given in fig. 7a. For $N = 20$ and $g = 0.75$ the associated impulse response and frequency characteristics are shown in figs 7b and c. It can be seen that this type of network also creates a whole series of pulses of decreasing amplitude from a

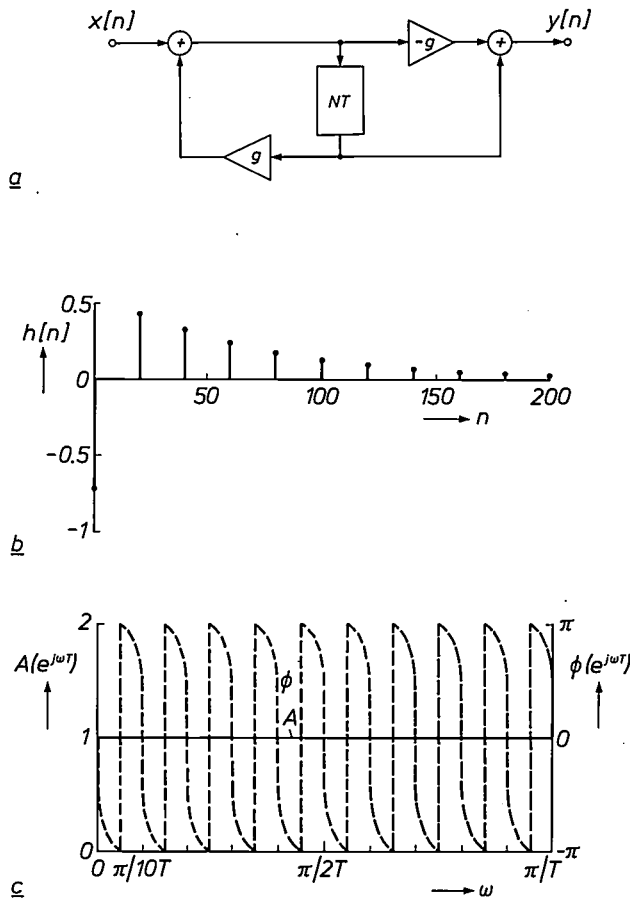


Fig. 7. Digital phase-shifter of the N th order with only two filter coefficients ($|g| < 1$). a) Block diagram. b) Impulse response $h[n]$ for $N = 20$ and $g = 0.75$. It can be seen that the 'main pulse' $h[0]$ is the only sample with a negative value. c) Associated phase and amplitude characteristics.

single incident pulse. On this basis the density of the 'reflections' in the artificial reverberation can be increased further without colouring.

By appropriate use of several delay elements and filter coefficients a more general type of phase-shifter is obtained (fig. 8). This gives more scope for defining

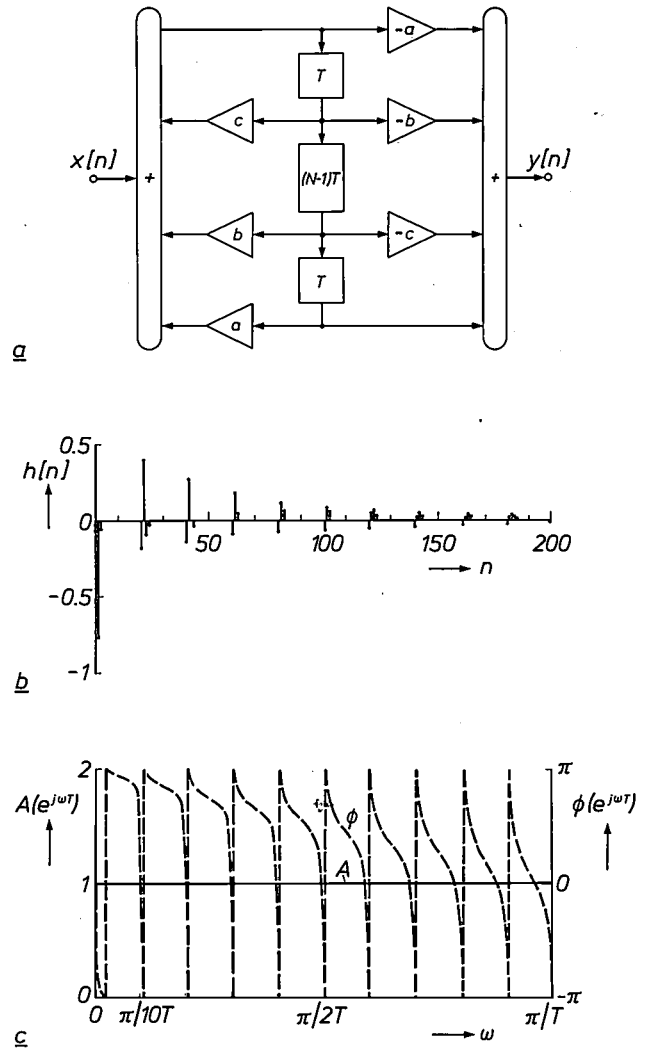


Fig. 8. Digital phase-shifter of the $(N + 1)$ th order with six filter coefficients. If a , b and c are selected appropriately, this network will give the desired variation of phase shift and hence decay time with frequency; the high-frequency components could for example be made to decay faster than low-frequency components. a) Block diagram. b) Impulse response $h[n]$ for $N = 20$, $a = 0.1$, $b = 0.75$ and $c = 0.1$. c) Associated phase and amplitude characteristics.

[4] A. W. M. van den Eenden and N. A. M. Verhoeckx, Digital signal processing: theoretical background, pp. 110-144 in the special issue 'Digital signal processing I, background', Philips Tech. Rev. 42, 101-148, 1985.
 [5] M. R. Schroeder, Natural sounding artificial reverberation, J. Audio Eng. Soc. 10, 219-223, 1962.
 [6] N. V. Franssen, Artificial reverberation apparatus for audio frequency signals, U.S. Patent No. 4352954 (5th October 1982); N. V. Franssen, K. A. Immink, E. C. Dijkmans and M. H. Geelen, Arrangement for the transmission of audio signals, U.S. Patent No. 4375623 (1st March 1983).

the frequency dependence of the phase shift, and hence also the decay of each individual frequency component.

The system function $H(z)$ of the comb filter shown in fig. 4a is given by

$$H(z) = \frac{1}{1 - gz^{-N}} \quad (1)$$

and hence the associated frequency response is given by

$$H(e^{j\omega T}) = \frac{1}{1 - ge^{-j\omega TN}} \quad (2)$$

It can easily be seen that this frequency response is a periodic function of ω with a period $2\pi/NT$, because it gives exactly the same value for ω and $(\omega + i2\pi/NT)$ for any integer number i .

The system function of the digital filter of fig. 5 is:

$$H(z) = \frac{a + bz^{-1}}{1 - cz^{-1}} \quad (3)$$

with the associated frequency response

$$H(e^{j\omega T}) = \frac{a + be^{-j\omega T}}{1 - ce^{-j\omega T}} \quad (4)$$

This function is also periodic in ω ; now, however, the period is exactly equal to the sampling rate $\omega_s = 2\pi/T$, as indeed it is for any digital filter. With appropriate choice of a , b and c equation (4) represents a lowpass filter; with other choices it can be a highpass filter.

The system function and frequency response of the phase-shifter in fig. 7 are given by ($|g| < 1$):

$$H(z) = \frac{-g + z^{-N}}{1 - gz^{-N}} \quad (5)$$

and

$$H(e^{j\omega T}) = \frac{-g + e^{-j\omega TN}}{1 - ge^{-j\omega TN}} \quad (6)$$

or

$$H(e^{j\omega T}) = e^{-j\omega TN} \cdot \frac{1 - ge^{j\omega TN}}{1 - ge^{-j\omega TN}} \quad (7)$$

From this last expression we can easily see that we are concerned with a pure phase-shifter, because the modulus of the first factor is 1, while the numerator and denominator of the fraction are complex conjugates. We can reach the same conclusion by determining the poles and zeros of $H(z)$ in the z -plane in equation (5). It then turns out that poles and zeros appear in pairs that are reflected in the unit circle $|z| = 1$. (In this case there are N zeros on the circle $|z| = g^{-1/N}$ and N poles on the circle $|z| = g^{1/N}$.) This reflection property is characteristic of phase-shifters. It can be shown that this property always applies if the coefficients of the denominator of $H(z)$ have the opposite order to those of the numerator^[7], i.e.

$$H(z) = \frac{a_0 + a_1z^{-1} + a_2z^{-2} + \dots + a_{M-1}z^{-M+1} + a_Mz^{-M}}{a_M + a_{M-1}z^{-1} + a_{M-2}z^{-2} + \dots + a_1z^{-M+1} + a_0z^{-M}} \quad (8)$$

Taking this as the starting point it can easily be seen that the system function $H(z)$ of fig. 8, which is

$$H(z) = \frac{-a - bz^{-1} - cz^{-N} + z^{-N-1}}{1 - cz^{-1} - bz^{-N} - az^{-N-1}} \quad (9)$$

also represents a phase-shifter.

Both comb filters and phase-shifters carry out linear processing on the signal. This means that the designer of an electronic reverberation system can select the order of these processes arbitrarily.

Fig. 9 shows the block diagram of a (stereo) reverberation system that can be produced with the ASP. It includes two phase-shifters F_1 and F_2 in cascade and six modified comb filters K_1, \dots, K_6 in parallel. In this system two *different* (uncorrelated) reverberation signals for the left-hand and right-hand sound channels can be formed from a single mono signal equal to the sum of the two original stereo subsignals. This approach gives a considerable saving in the number of operations required per unit time and in the amount of memory required to effect the different delays. The input signal IN of the reverberation system is first filtered in a digital highpass filter H_h that suppresses frequencies below 55 Hz. This filter has the same structure as that in fig. 5a, but its coefficients are modified. The delay circuit with a delay of N_iT provides the initial delay of the first reflections with respect to the direct sound (τ_{in} in fig. 3). At various points in the circuit gains d and e and scaling factors sc are incorporated. The gains determine the relative magnitudes of the subsignals, the scaling factors ensure that the signals occurring 'match' the numerical values allowed in the system as well as possible. Without scaling there might be overflow, or alternatively it could happen that some of the most-significant bits were never used at all^[4].

All six modified comb filters have the same structure K (fig. 9b), but the values of N_k and the filter coefficients vary. In addition each comb filter has two outputs, one contributing to the left-hand reverberation signal L and the other to the right-hand reverberation signal R . The signals L and R are ultimately added to the two original stereo subsignals that formed the starting point.

During the design of this reverberation system extensive use was made of listening tests (see also [8]), which in this case were largely carried out with the help of prototypes ('breadboard' models). This was done both for selecting the number of phase-shifters and comb filters and also for determining the delays and coefficients. These tests showed that a set of four comb filters could not provide a sufficiently colour-free reverberation. They also showed that the bandwidth of the reverberation signals can be limited to 10 kHz, for example, without reducing the subjective quality. This makes it possible to operate the whole reverberation system at a lower sampling rate than the original stereo signal (e.g. 22.05 kHz instead of 44.1 kHz). To do this it is necessary that the reverberation circuit is preceded and followed by sampling-

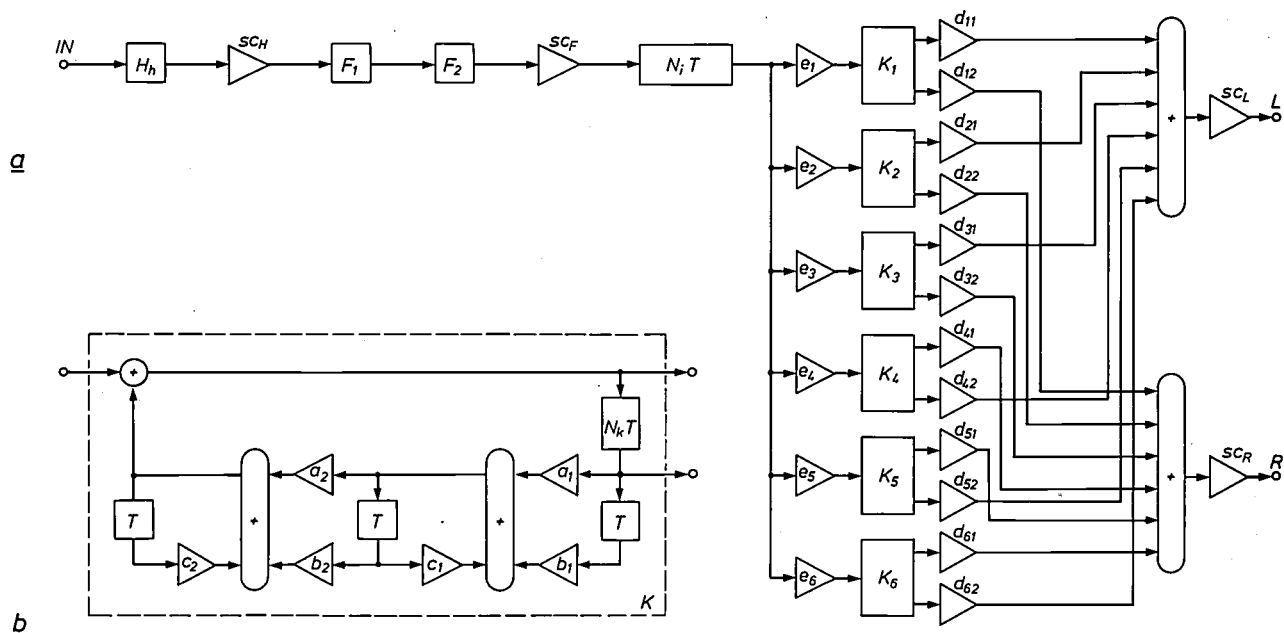


Fig. 9. a) Block diagram of a complete digital stereo reverberation system. *IN* mono input. *L*, *R* stereo outputs for left-hand and right-hand channels. The most important components are: a highpass filter H_h for suppressing frequencies below 55 Hz, two phase-shifters F of the type shown in fig. 8, a delay $N_i T$ and a parallel arrangement of six modified comb filter $K_1 \dots K_6$. The delay $N_i T$ corresponds to the initial delay τ_{in} between the direct sound and the first 'reflection'. sc scaling factor. d , e , gains. b) Detailed block diagram of one of the modified comb filters K . The feedback loop includes a combination of two lowpass filters as in fig. 5a. This makes the reverberation time frequency-dependent. a , b , c , filter coefficients.

rate converters, which decrease or increase the sampling rate [4]. A further considerable saving in the number of operations and memory capacity is achieved in this way.

To give an impression of the operation of the reverberation system described above, fig. 10 shows its impulse response and amplitude characteristic as obtained after digital-to-analog conversion. Both the curves shown have the desired irregular structure and are free from periodicity. The impulse response also reproduces the initial delay τ_{in} of the first reflection with respect to the direct sound. This quantity will in general be made adjustable, so that the listener can simulate the reverberation of a small room or of a large one.

The length of the delay incorporated in the filters is related to the volume of the room being simulated: the larger the room, the longer the time between two reflections of a sound signal from the walls. In the same way the coefficients in the feedback circuits represent the absorption of sound at a reflection. By making the delay periods and coefficients adjustable, the reverberation of enclosures of very different size and nature can be simulated — from a bathroom to a sports hall!

Equalization of the frequency characteristic

In quality reproduction the audio equipment is required to reproduce all audio frequencies, both low and high, at equal strength. This is a flat frequency

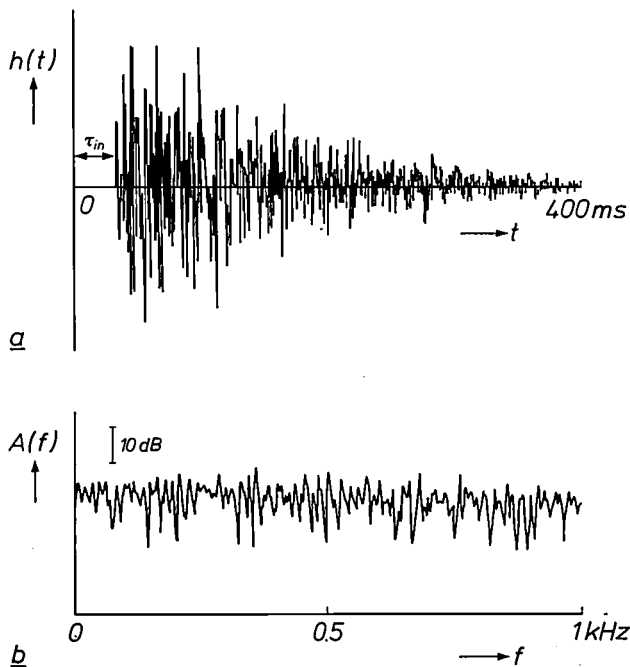


Fig. 10. a) Impulse response $h(t)$ (over 400 ms), and b) amplitude characteristic $A(f)$ of a reverberation system made with the ASP. Both curves were obtained after digital-to-analog conversion and relate to a frequency band deliberately limited to 1000 Hz to avoid too much detail in the figures. They are largely free from regularity or periodicity, giving reverberation without 'colouring'.

[7] E. C. Dijkmans and N. V. Franssen, Artificial reverberation apparatus, U.S. Patent No. 4366346 (28th December 1982).
 [8] L. D. J. Eggermont and P. J. Berkhout, Digital audio circuits: computer simulations and listening tests, Philips Tech. Rev. 41, 99-103, 1983/84.

response. Audio frequencies are usually considered as the band from 20 Hz to 20 000 Hz.

The components that require most attention in such applications are the transducers: the microphone, the pick-up stylus and the loudspeaker. The design of the loudspeaker is usually based on measurements carried out in an anechoic chamber. In such an enclosure there are no sound reflections at all from the walls or other surfaces, so that there is an unambiguous result that is the same for every anechoic chamber.

In ordinary use the situation is quite different. The room where the loudspeaker is used does not have completely absorbing walls, and standing waves (resonances) occur in it. The same applies to sound reproduction in a car. These resonances have a considerable effect on the final result, particularly at low frequencies where their ratios are fairly widely spaced, and they enhance certain notes and suppress others. In spite of efforts to approach the desired flat characteristic of loudspeakers as closely as possible in the anechoic chamber, in a practical 'listening situation' differences in level of more than 10 dB can easily occur. However, by adjusting the gain as a function of the frequency and depending on the actual situation ('equalization') it is nevertheless possible to obtain a flat characteristic.

For this purpose we have used adjustable octave-band filters, i.e. a series of filters whose centre frequencies and bandwidths increase regularly by a fac-

tor of 2. Octave-band filters are therefore suitable for correcting them. The location of the centre frequency of the octave-band filters is not always optimum, of course. The digital audio system in which the ASP is used is therefore programmed in such a way that the centre frequency for the octave-band filters below 1000 Hz can be raised or lowered by a third of an octave. This can be done independently in each stereo channel.

Filter structure

In the design of the digital octave-band filters it was not possible to use the same filter structure^[4] in all cases. The normal direct-form-I recursive filters (fig. 14), for example, are less suitable for the lower frequency ranges. This is because only a limited number of bits (in our case 12) are available for each coefficient. This means that only a limited number of frequency responses are obtainable for each filter, and also that they are dependent on the filter structure selected. In the case of the adjustable octave-band filters which we wanted, the requirements with 12-bit coefficients were satisfied best by using the direct-form-I structure (fig. 14) for the higher octaves (centred on 1, 2, 4, 8 and 16 kHz) and the coupled form (fig. 15) for the lower octaves (centred on 31.5, 63, 125, 250 and 500 Hz). Furthermore, the desired filter curves can be approached more closely by quantizing the coefficients in each filter in a well-considered

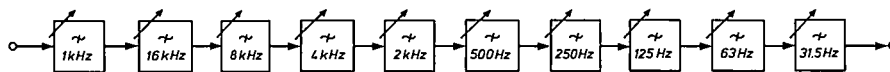


Fig. 11. Cascade arrangement of 10 octave-band filters for equalization of a frequency characteristic. The gain at the centre of each octave band can be adjusted in steps of 1 dB between -12 dB and +12 dB. For the realization with the ASP the sequence of octave bands was chosen so that the noise caused by the finite precision of the digital processing was kept to a minimum at the end of the chain (see p. 210).

tor of 2. The complete frequency range is therefore divided into 10 octave bands. Each octave band can be amplified or attenuated separately. The 10 octave-band filters are connected in cascade (fig. 11). The transmission at the midpoint of each octave can be adjusted between +12 dB and -12 dB in steps of 1 dB. See fig. 12.

Fig. 13a shows how the sound level in different frequency bands can vary on reproduction in a room. Correction with the 10 octave-band filters gives a much more even distribution of the sound level over the frequency scale (fig. 13b).

The peaks and troughs that appear in the frequency characteristic because of the characteristics of the room are about an octave wide at low frequencies.

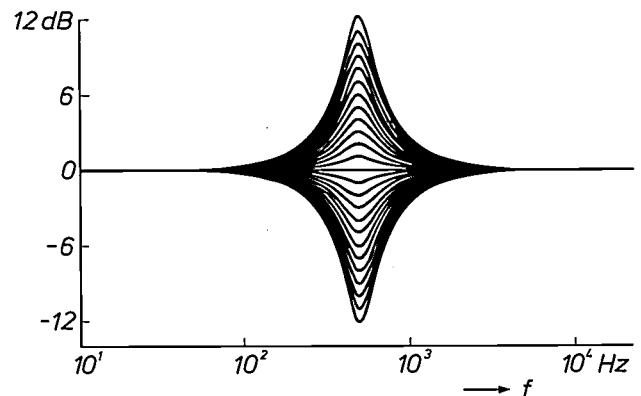


Fig. 12. The 25 possible response curves of one of the octave-band filters (the filter centred on 500 Hz).

coordinated manner during the design. In realizing the two coefficients a in fig. 15, which would have exactly the same value without quantization, as 12-bit numbers it might for example be advantageous to round one of them up and the other one down.

If we neglect the quantizers Q , for a direct-form-I filter (fig. 14) we find the system function

$$H(z) = \frac{b_0 + b_1z^{-1} + b_2z^{-2}}{1 - a_1z^{-1} - a_2z^{-2}}, \quad (10)$$

and for a filter of the coupled form (fig. 15)

$$H(z) = z^{-2} \left\{ 1 + cb \frac{1 - z^{-2}}{1 - 2az^{-1} + (a^2 + b^2)z^{-2}} \right\}. \quad (11)$$

The octave-band filters that we require can be realized with both types of system function. The most important differences only become apparent if we limit the word lengths of filter coefficients and intermediate results, particularly if attention is paid to limit cycles, quantization noise and realizability of certain frequency responses.

Quite different problems (which nevertheless fall under the same general heading of 'finite-word-length effects') arise because results of calculations in the fil-

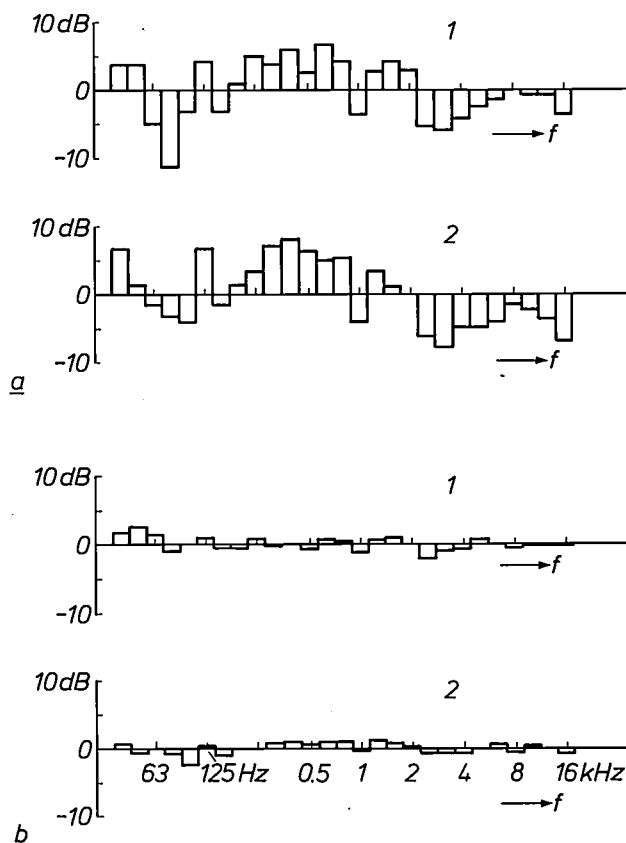


Fig. 13. Variation of the power density in the sound field as a function of the frequency f at a certain point in a room on reproduction of an electrical noise signal with a uniform power spectral density, a) before and b) after equalization with the aid of octave-band filters. Recordings 1 and 2 were made by driving the two channels of a stereo system separately. In the figure the frequency is divided into bands of one-third of an octave.

ter must constantly be quantized, because the number of bits available for storing the signal obtained (the word length) is limited. Thus fig. 14 includes a quantizer Q that limits the word length of the sum of the five products (in our case to 24 bits).

This is necessary because the delay elements in the feedback loops only have a fixed number of bit places available. However, the execution of operations (mainly multiplications) generally causes an increase in the word length. The required quantization of intermediate results has two main undesirable consequences: the possible occurrence of 'limit cycles' and degradation of the signal-to-noise ratio [4]. We shall now look more closely at these effects.

Limit cycles

Limit cycles are oscillations of small amplitude that can be maintained by the filter if the input signal has a constant value (including zero) for some time, or is periodic. In spite of their low level these oscillations can be particularly troublesome in audio systems. The first countermeasure that can be used here is to use 'magnitude truncation' in all the filters as a method of quantizing the intermediate results [4]. This was sufficient for all our octave-band filters except the 1-kHz filter, in which limit cycles could still occur. A double

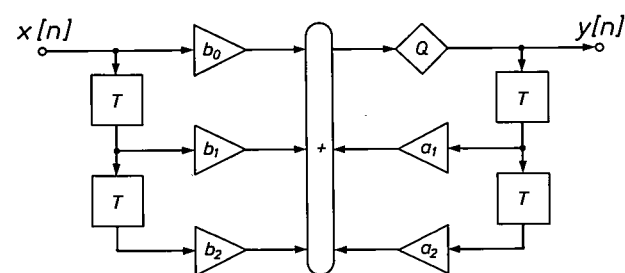


Fig. 14. Recursive digital filter of the second order (direct-form-I structure). a_1, a_2, b_0, b_1, b_2 filter coefficients. Q quantizer, in which the word length of the signal samples is reduced to 24 bits.

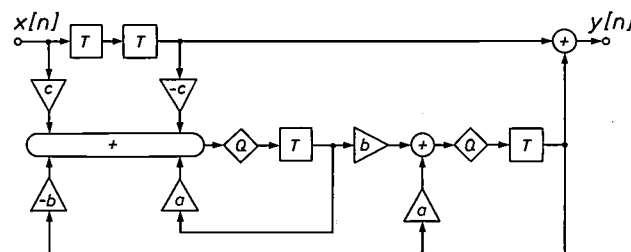


Fig. 15. Recursive digital filter of the second order (coupled-form structure). This type has been selected for the 500-Hz, 250-Hz, 125-Hz, 63-Hz and 31.5-Hz octave-band filters, because the desired filter curves can be obtained more accurately with it for these lower frequencies, in spite of the quantization of the filter coefficients to no more than 12 bits. a, b, c filter coefficients. Q quantizer in which the word length of the signal samples is reduced to 24 bits.

word length was therefore used for the signals in this filter (i.e. 46 bits instead of 24 bits), making the quantization step smaller by a factor of 2^{22} . This meant that any limit cycles also had an amplitude that was 2^{22} times smaller than before. Subsequent limitation of the output signal of the filter to 24 (most-significant) bits makes these oscillations undetectable outside the filter.

Signal-to-noise ratio

If the input signal varies sufficiently the quantization of intermediate results has about the same effect as adding some noise to the useful signal. This could degrade the signal-to-noise ratio, which is of course undesirable. To analyse these effects it is assumed that each quantizer can be considered as an additional noise source of noise with a flat frequency spectrum, located at the quantizer.

Quantization by rounding off with a quantization step q is accompanied by a rounding-off error between $-q/2$ and $q/2$; the corresponding noise source has a total noise power of $q^2/12$. Magnitude truncation with the same quantization step gives a quantization error between $-q$ and 0 for positive signal values and between 0 and q for negative signal values. The power of the corresponding noise source can be taken to be $q^2/3$. The direct-form-I filter (fig. 14) only requires one quantizer, but the coupled form (fig. 15) requires two. This alone gives different noise characteristics, although it is not apparent beforehand which structure produces most noise.

As the quantizers are located inside the filter sections, the noise no longer has a flat spectrum at the output of the section in which it arises. Before the noise finally reaches the output of the complete equalizer it must first pass through all the following sections and acquire further 'colouring'. Meanwhile new noise contributions are constantly added by the successive quantization operations. The important feature is the total amount of noise power that appears at the output and the shape of its spectrum (as a result of colouring). In view of this the sequence chosen for the cascade arrangement of octave-band filters is the one shown in fig. 11. The smallest noise contribution comes from the 1-kHz filter because it is the only one with a double word length for its internal operation. This filter is therefore made the first one. Next come the sections with the direct-form-I structure and then the coupled-form sections, in order of descending centre frequency. The coupled-form sections make the largest contributions to the total noise. To illustrate this fig. 16 shows the different noise contributions from four octave-band filters as they appear at the output of each of these filters and as calculated by a computer. The level of 0 dB corresponds to the noise

level at the quantizer; the noise spectrum is initially assumed to be flat there. For frequencies below about 6 kHz the internal noise in most of the sections is therefore amplified. The dashed line indicates the sum of the noise contributions from all ten filter sections as it appears at the output of the equalizer if each filter is set to maximum gain (+12 dB). Averaged over the whole audio band from 0 to 20 kHz the total noise level is about 31 dB higher than the level of each individual noise source. To ensure that the equalizer does not noticeably degrade the original good signal-to-noise ratio (maximum value about 96 dB) of the 16-bit input signal, the internal noise sources must each be at least 31 dB below the input noise. This requires a smaller internal quantization step and hence a greater word length than that of the input signal. Each 6 dB requires 1 additional bit. We have therefore added 6 bits.

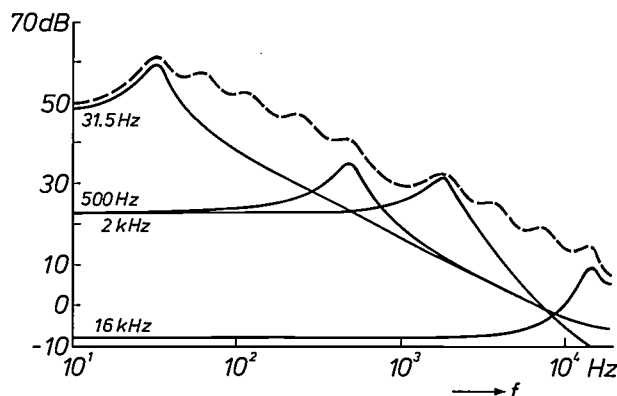


Fig. 16. Continuous curves: frequency spectra of the individual noise contributions from four octave-band filters from fig. 11 as they appear at the outputs of each of these filters. The 16-kHz filter and the 2-kHz filter have the structure of fig. 14. The 500-Hz filter and the 31.5-Hz filter have the structure of fig. 15. Dashed line: spectrum of the total noise from all ten octave-band filters together measured at the output of the equalizer. These curves are for the worst case, i.e. for the gain of all the filters set to +12 dB. 0 dB on the vertical axis corresponds to the level at which quantization noise arises in each quantizer. It can also be seen from the dashed line that the 1-kHz filter contributes hardly any noise itself (as a consequence of the 'double precision').

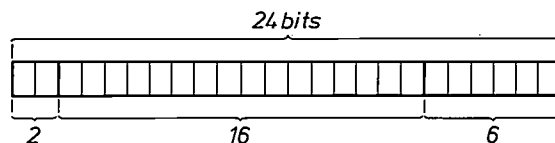


Fig. 17. The word length of the original input signal is normally 16 bits. In the internal processing, however, the signals consist of words with a length of 24 bits. This can be explained as follows. The possible gain of +12 dB (a factor of 4 in amplitude) in the equalization filters requires an extension of 2 bits at the most-significant value end, to prevent overflow. On the other hand an internal refinement of the quantization by 6 bits relative to the input signal is necessary to prevent the equalizer from degrading the signal-to-noise ratio of the input signal.

With a maximum gain of 12 dB for each octave-band filter there may be appreciable amplification for certain input signals. To prevent this from causing overflow the internal word length must again be increased. We therefore added 2 more bits, so that our total internal word length is $16 + 6 + 2 = 24$ bits (fig. 17).

The architecture of the ASP

The ASP is an integrated digital signal processor that can perform all the operations arising in the applications described above, and more. It is used either alone or with other ASPs, and with ancillary circuits such as standard microprocessors. It is highly suitable for the processing of 44 100 discrete signal samples per second (the sampling rate of 44.1 kHz is then the same as for the Compact Disc). The input and output signals take the form of words with a maximum length of 24 bits.

In one sampling period the ASP can execute 128 machine instructions, which brings the maximum repetition rate of these instructions to about 6 MHz.

There are two versions of the ASP, a ROM version and a RAM version. The difference relates to the program memory. If this is a random-access memory (RAM), the same ASP can be programmed for all sorts of different operations, which makes it very versatile. If the program memory is a read-only memory (ROM) then the program is fixed permanently in the IC. This also fixes the application. This version is simpler than the other; it requires a smaller area of silicon and is intended for use in the applications such as the digital audio system that we shall describe later.

In the first part of this article on digital audio signal processing we frequently encountered the three basic operations: multiplication, addition and delay. Probably the most common operation is the addition of a number of multiplication results. There are also operations such as rectification and the quantization of intermediate results. High-precision computation also occupies a special place. In a practical system the transfer of signal samples (which we shall call 'data' from now on for brevity), coefficients and results plays an important part. The ASP is designed to carry out all these operations as efficiently as possible.

Block diagram of the ASP

Fig. 18 is a block diagram of the ASP. Many of the blocks are interconnected. Some connections are common to several blocks; these are the 'buses'. There are three buses: the data bus, the coefficient bus and the control bus ('C Bus'). The most important blocks are the multiplier *Mpy* and the *ALU* (Arithmetic Logic

Unit). The multiplier is asymmetrical: it multiplies words of 12 bits by words of 24 bits. The 24-bit words represent signal samples, the 12-bit words represent filter coefficients when an ASP is used to carry out filtering processes. The result of the multiplication is given as 36 bits.

If the task being carried out by the ASP is one of automatic control, as in dynamic-range compression, the 12-bit words include control information derived from the signal itself. For dynamic range compression quantization to 12 bits is too coarse; the steps in the adjustment of the sound level would be audible. Therefore two words of 12 bits are always taken together to represent one control value ('double precision'). The signals can also be handled with 'double precision', which is used in the 1000-Hz octave-band filter in the equalizer mentioned above.

The ASP can in fact operate at better than double precision. However, this facility has not been used in the audio signal processing described so far.

For the multiplication of a signal value at double precision by a coefficient at double precision, four consecutive multiplications are performed as shown in the diagram of fig. 19. The signal value is represented by two words of 24 bits. The first word, which we will call d , contains the 24 most-significant bits; the second word d' contains two zeros in the first two places and then the 22 least-significant bits. The signal value, which is thus represented by 46 bits, takes up two memory locations; it can be expressed as $d + d' \times 2^{-22}$. In a similar way a 12-bit coefficient acquires double precision by the addition of 11 less-significant bits; we can then write the coefficient as $c + c' \times 2^{-11}$. In the execution of the product

$$(d + d' \times 2^{-22})(c + c' \times 2^{-11}) \approx p + p' \times 2^{-22} \quad (12)$$

the least-significant parts are first multiplied together. The resulting product $c' \times d'$ is then shifted by 11 places. The product $c \times d'$ is then formed and added to it. The sum is again shifted by 11 places, and then $c' \times d$ is added to it. After a further shift $c \times d$ is finally added. Of the total thus obtained the 24 most-significant bits (the word p) are stored in a 'high' register, the following 22 bits (the word p') in a 'low' register. Both registers transfer their contents to a selector, a wide register, which transfers parts of the long words stored in it to the data bus when it receives a control signal. These registers are collectively indicated by *Res Reg* in the block diagram (fig. 18).

The unit *ALU* is an adder with a width of 40 bits. This adds the results of multiplications carried out in the multiplier *Mpy* to earlier results stored in the accumulator register *Accu*, which also has a width of 40 bits. The output of this register is therefore connected to a second input of *ALU*.

The results of the addition in *ALU* are sent back to the data bus via the *Res Reg* register. They are in fact too long for this bus and are therefore quantized to 24 bits in the circuit *Ovf Clip*. Various types of quantization and overflow are possible here^[4]. In cases

where calculations must be made with double precision the least-significant bits and the most-significant bits are handled separately.

The coefficients are supplied via the coefficient bus *Coef Bus*. They come from the memory *Coef RAM*, which is loaded from outside the ASP with the coeffi-

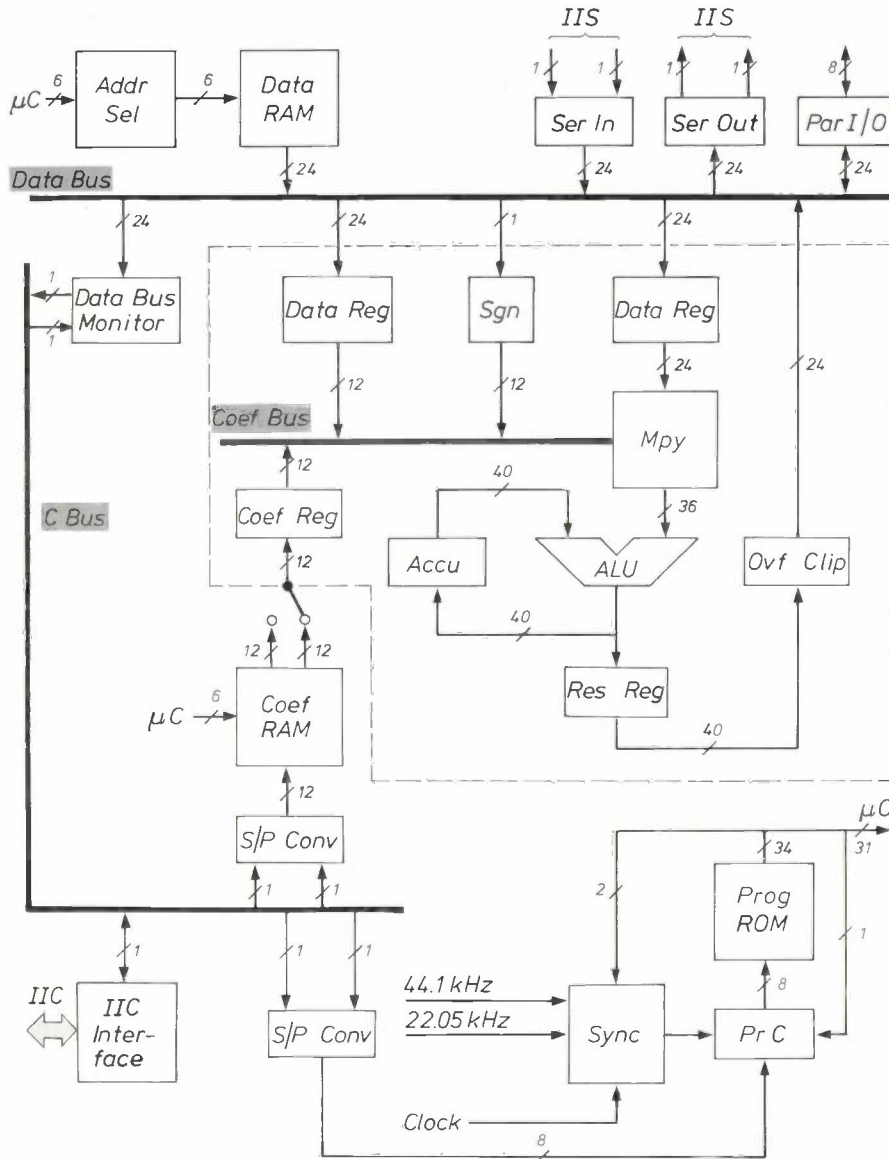


Fig. 18. Block diagram of the ASP. The central section surrounded by a dashed line is the arithmetic unit in which the actual calculations take place. The multiplier *Mpy* multiplies a 24-bit word (data) by a 12-bit word (often a filter coefficient), if desired the product can be added in the arithmetic logic unit *ALU* to the sum obtained from the previous calculation and stored in the accumulator register *Accu*. The data is brought from the random-access memory *Data RAM* via the data bus (*Data Bus*), the coefficients are brought via the coefficient bus (*Coef Bus*) from a memory *Coef RAM*, which has been supplied with the appropriate coefficients, e.g. via the connection unit *IIC Interface* from an external microprocessor; the latter is the link between the controls that are set by the user and the ASP. The significance of the abbreviations is as follows:

- Accu* accumulator register for intermediate results
- Addr Sel* address control for data memory
- ALU* arithmetic logic unit
- C Bus* control bus
- Clock* clock signal
- Coef Bus* coefficient bus
- Coef RAM* random access memory for coefficients
- Coef Reg* coefficient register

- Data Bus* data bus
- Data Bus Monitor* unit that monitors the traffic on the data bus for control purposes
- Data RAM* random-access memory for data
- Data Reg* data register
- IC* integrated circuit
- IIC* standardized control signal ('Inter-IC Control')
- IIC Interface* connection with the (external) IIC bus that carries the signals to and from other ICs in accordance with a standard protocol
- IIS* standardized digital signal ('Inter-IC Signal')
- Mpy* multiplier (24 × 12 bits)
- Ovf Clip* quantization and overflow circuit
- Par I/O* parallel input and output unit
- Pr C* program counter
- Prog ROM* read-only memory containing the program
- Res Reg* results register
- Ser In, Out* serial input and output units
- Sgn* register for the sign bit
- S/P Conv* serial/parallel converter
- Sync* synchronization circuit
- μC microcode

coefficients appropriate to the task in hand (e.g. by a micro-processor via the IIC circuit). When the task changes the reloading requires some time; this may introduce undesirable signals in the audio output. To prevent this the coefficient memory is duplicated; while one half is being reloaded, the other half retains the old coefficients. When reloading is completed the system switches over to the newly loaded half-memory, so that the transition is inaudible.

tion is a regular part of the filtering process, for which the signals are held temporarily in *Data RAM*. Once they arrive there they are not shifted along (as they would have to be if a shift register was used as the delay element) but put in fixed memory locations. The unit *Addr Sel* records this and computes the addresses from which the signals must be fetched when required.

If a series of second-order filters are to be realized with an ASP, then a large number of multiplications

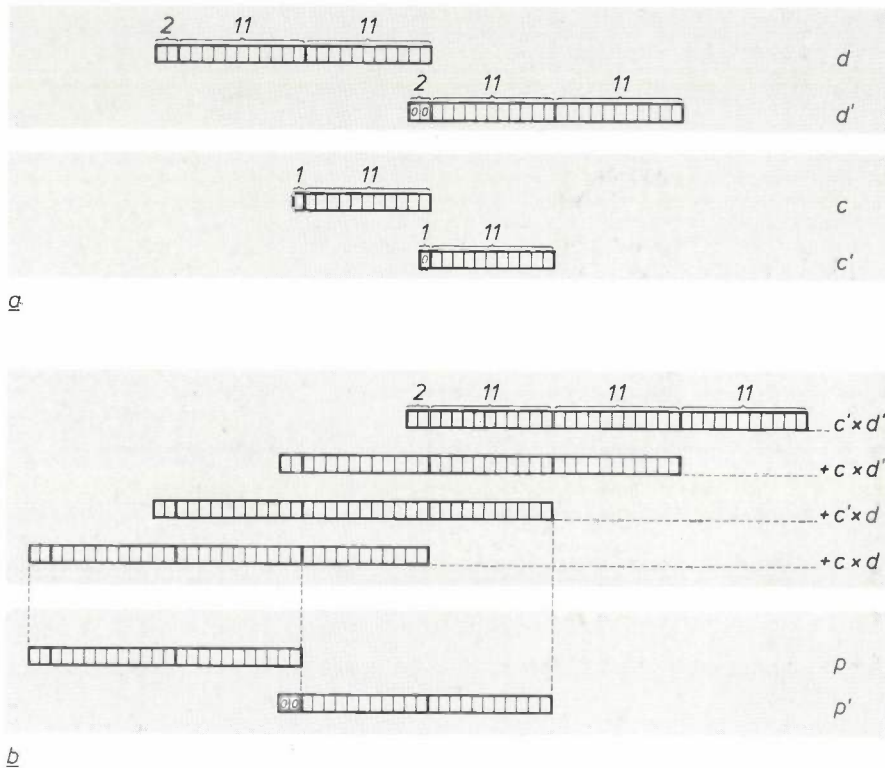


Fig. 19. Calculation with 'double precision'. *a)* Obtaining a data word of 46 bits from 24 most-significant bits d and 22 least-significant bits d' , and a coefficient word of 23 bits from a most-significant part of 12 bits c and a least-significant part c' . *b)* The creation of the product in double precision from four partial products that are given the right weight by shifting by 11 bits after each part of the operation. The product consists of 46 bits, which are split into 24 most-significant bits p and 22 least-significant bits p' . Thus $p + p' \times 2^{-22} = (d + d' \times 2^{-22})(c + c' \times 2^{-11})$, apart from quantization effects.

With the aid of one of the two data registers *Data Reg* (capacity 24 bits) the 24-bit signals are obtained from the data bus. Both parallel and series input and output units are connected to the data bus, as well as the data memory *Data RAM* (capacity 64 words of 24 bits). This memory is used for temporary storage of received data and intermediate results and final results that are awaiting further processing or transfer to the output.

The data memory *Data RAM* therefore also performs the elementary delay operation, i.e. delaying a signal by a sampling period (at the usual audio sampling rate of 44.1 kHz this is 22.7 μ sec). This opera-

tion must be performed in each sampling period rather than a single multiplication. These multiplications occur in sequence. Acceleration of the process is obtained by 'pipelining': the operations are prepared by bringing in the necessary data and feeding it through any intermediate registers at the same time as the operations on previous data are completed. To make this possible intermediate registers are necessary.

Routing the data streams and addressing the memories correctly require extensive control facilities, of course. An important part is played by the program read-only memory *Prog ROM*, which contains the complete program of consecutive operations that the

ASP must perform. *Prog ROM* is directly connected to all the appropriate subsidiary units and controls them via 'microcode μC '. For clarity only a few of the μC connections are shown in fig. 18. For the control of the ASP the control bus *C Bus* is also available, with a number of special components such as a program counter, a synchronization and clock-signal unit and an IIC unit for connection to an external IIC bus that can carry data traffic with other ICs to a standard protocol ('IIC' stands for 'Inter-IC Control').

Let us now consider the input and output units for a moment. The parallel input/output unit *Par I/O*

selection signal is provided to indicate the start of each new word ('IIS' stands for 'Inter-IC Signal'). This protocol is also used in all kinds of other modern ICs for digital audio, such as digital filters and digital-to-analog converters.

It is characteristic of the ASP that many operations run in parallel; the term 'pipelining' has already been mentioned. This means that the control is complicated. The complete IC was therefore simulated on a computer in the design phase. A full set of software was written for this simulation. An assembler language was defined in which the commands could be expressed,

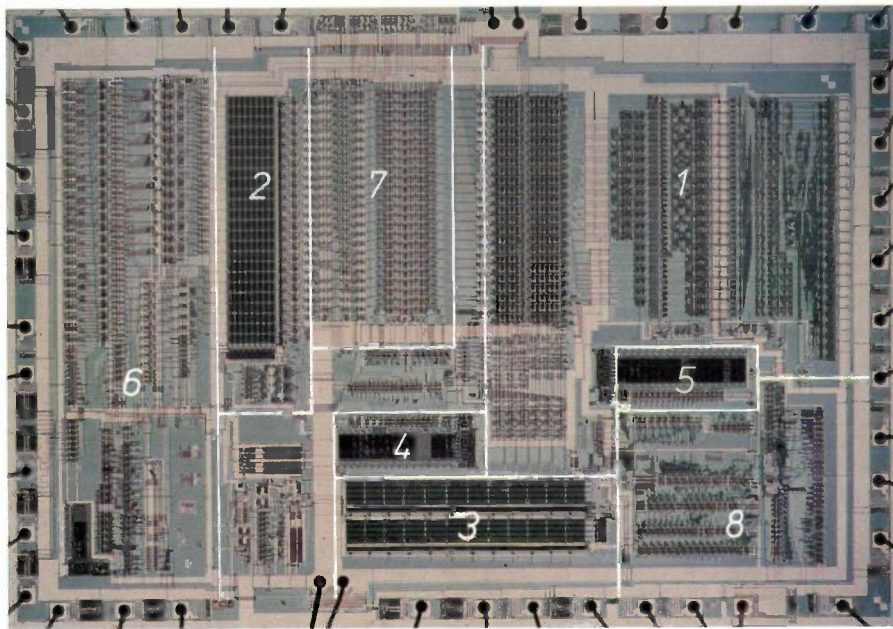


Fig. 20. Photomicrograph of the ASP. This integrated circuit is intended for digital audio signal processing. It is made in 2.5- μm NMOS technology, with a chip area of 46 mm². The most important components are: 1 the part of fig. 18 inside the dashed line; 2 data RAM; 3 coefficient RAM; 4, 5 program ROM; 6 parallel input and output units; 7 serial input and output units; 8 IIC circuit.

consists of a whole complex of registers, one of whose tasks is to separate the internal synchronization of the ASP from that of the incident signals. In addition, *Par I/O* does not just transfer data but is also used in addressing the external memories that are used in dynamic-range compression and the excitation of reverberation. (The internal memories of the ASP are much too small for these applications.) The external memory addresses required are computed by *Par I/O*.

The serial input and output units are not simple shift registers but separately controllable 'latches' in which the most significant bit of the received word always arrives at the same place whatever the length of the word. This means that traffic with other ICs can follow the IIS protocol, a standard in which a word-

and an assembler program was written to translate these commands into machine instructions for the ASP. In addition a simulation program was written, and during the design phase prototypes ('breadboard' models) were used for carrying out listening tests.

Finally, we should mention that the current ASP is an integrated NMOS circuit with an area of 46 mm² (see fig. 20). It has 40 connection pins.

A digital audio system made up of ASPs

As mentioned earlier the ASP IC does not carry out the tasks we have described on its own. Fig. 21 represents the block diagram of a digital audio system that contains five ASPs, two standard microprocessors and

a number of ancillary ICs. These are used mainly as input and output circuits and memories.

One of the microprocessors ($\mu P1$) provides the main control for the system. All the ASPs are connected to this microprocessor via the IIC bus, and the instructions resulting from the commands that the user gives are supplied to the ASP in this way. The second microprocessor ($\mu P2$) is provided to control the display panel, which shows information such as the equalizer setting. (The same panel can also display the frequency spectrum of the sound, split into ten octave bands.) To simplify the application of the system, the prac-

tical version is combined with two power amplifiers ($2 \times 100\text{ W}$) in a single unit.

Serial transfer of signals between the different ICs follows the IIS standard protocol. This requires three lines. One of these is for the serial clock signal, which tells the receiving IC how fast the bits are arriving; this rate is independent of the internal operating rate of the IC. A second line carries a word-selection signal. This is a symmetrical square wave whose edges indicate the start of a new data word (a trailing edge indicates a word for the left-hand audio channel, a rising edge indicates a word for the right-hand chan-

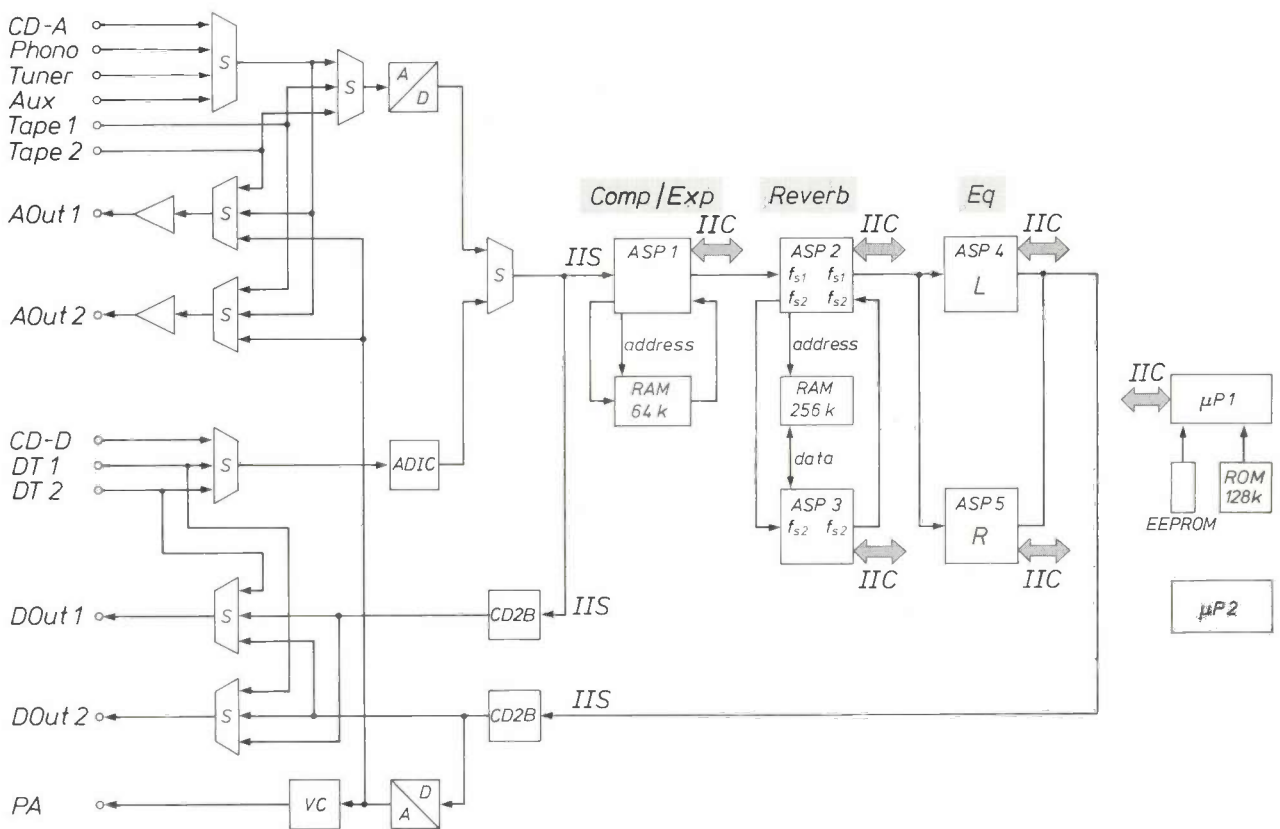


Fig. 21. Block diagram of a digital signal-processing system for audio, based on ASPs. There are analog inputs for various signal sources and analog outputs for the processed or unprocessed signals; there are also digital inputs and outputs. Five ASP ICs perform the operations. The significance of the abbreviations is as follows:

- A/D* analog-to-digital converter
- ADIC* converter to IIS format (for incoming digital signal)
- ASP* audio signal processor
- AOut* analog output
- Aux* auxiliary analog input
- CD-A* Compact Disc player (analog signal)
- CD-D* Compact Disc player (digital signal)
- CD2B* converter to external signal format (for outgoing IIS signal)
- Comp/Exp* compression/expansion
- D/A* digital-to-analog converter
- DOut* digital output

- DT* digital tape player
- EEPROM* electrically erasable programmable read-only memory for preset states and for final state on switching off
- Eq* equalization
- f_s sampling rate ($f_{s1} = 44.1\text{ kHz}$, $f_{s2} = 22.05\text{ kHz}$) (see fig. 18)
- IIC, IIS* (see fig. 18)
- L* left-hand channel
- PA* power amplifier
- Phono* record player
- R* right-hand channel
- RAM* random-access memory
- Reverb* reverberation generation
- ROM* read-only memory for program and filter coefficients
- S* digitally-controlled selector
- Tape* tape player
- Tuner* radio tuner
- VC* volume control
- μP microprocessor

nel), so that the length of the words does not need to be known in advance by the receiving IC. The third line carries the actual signals (in 'two's complement' representation^[4], with the most significant bit first).

The digital audio system works almost exclusively (see below) with a sampling rate of $f_{s1} = 44.1$ kHz. Either analog sources (record player, radio tuner, tape player) or digital sources can be connected to it. With analog sources analog-to-digital conversion of both the stereo channels is necessary. Digital sources would include the Compact Disc player, a digital cassette player, a video recorder adapted for digital audio or a receiver for the proposed digital radio broadcast from future broadcasting satellites. The signals from the digital sources must be put into the required serial form, this is done in the IC *ADIC*.

First the dynamic range is compressed or expanded in *ASP1*. The time required for preparing this process after peak detection is obtained by temporarily storing the signal in a 64-kbit memory. This time is not inconsiderable, because of the slow nature of the control signals. After processing in the first ASP the signal words have the standard length of 24 bits. They are sent to *ASP2*.

To introduce reverberation *ASP2* splits off a mono signal with half the bandwidth (up to 10 kHz), which is sampled at $f_{s2} = 22.05$ kHz and used as the starting point (see also page 206). This signal is applied to *ASP3*, which is also connected by the parallel input/output unit to a 256-kbit memory consisting of 4 ICs each with a capacity of 64 kbits. The addresses of these memories are sent via the parallel input/output lines of *ASP2*. The storage time in these memories gives the signals the delay necessary for the operation of the reverberation circuits. In *ASP3* a reverberation signal with a sampling rate of 22.05 kHz is calculated for each of the two stereo channels as indicated in fig. 9. These signals are fed back to *ASP2*. In *ASP2* new reverberation signals are then calculated at twice the sampling rate and these are finally added to the two original stereo subsignals.

So much processing is required for the equalization of the frequency characteristic by adjusting the 10 octave-band filters that a separate ASP has to be used for each of the two stereo channels (*ASP4* and *ASP5*). For the moment the equalization is set up by hand.

After the processing the 24-bit audio signal is scaled in such a way that it does not overload the digital-to-analog converter. The converter is intended for 16-bit signals and where possible it is driven to full scale to obtain the best possible signal-to-noise ratio. It supplies an analog signal to the gain control of the power amplifier. Two 16-bit output signals are also available at two digital outputs.

Retrospect and prospect

The ASP is one of the first ICs to be 'custom-made' for digital processing in hi-fi audio. It is nevertheless very versatile and can be used for a number of applications with appropriate programming. Three examples have been given above; these are by no means the only ones. For instance, we have not discussed the suppression of the 'tick' produced by a scratch on a gramophone record, or of similar defects of different origin. This application has already been proved in the laboratory. Another possible use is 'physiological volume control': the enhancement of low and high frequencies when the total volume is reduced, to take account of the variable frequency characteristic of the human ear^[8]. This has also been put into practice. A third possibility now close at hand is the automation of the equalization function. By means of the signal from a microphone, incorporated for example in the remote-control unit, the frequency characteristic of the reproduced sound can be corrected automatically. In a similar way the compression or expansion of the dynamic range can in principle also be controlled automatically as a function of the background noise.

The digital audio system described here shows how such complicated operations can be carried out with equipment that the 'ordinary' consumer can afford and use, through the application of digital techniques.

The ASP IC and the digital signal-processing system for audio based on it originated in the Digital Audio Signal Processor Project Group led by the two authors. The other members of this group were H. W. A. Begas, P. J. Berkhout, M. H. Geelen, W. J. W. Kitzen, E. A. M. Odijk, A. C. A. M. van der Steen, E. F. Stikvoort, R. A. H. van Twist (all with Philips Research Laboratories), P. Bakker, F. J. Op de Beek, J. M. Rijnsburger and J. J. H. Verspay (all with the Consumer Electronics Division, Philips NPB).

Summary. The ASP integrated circuit has been developed for the digital processing of hi-fi audio signals. The heart of the IC is a multiplier (24×12 bits) followed by an adder of width 40 bits that can add the result of a multiplication to earlier results. About 6 million instructions per second can be executed. With external programming the ASP can perform various digital filter processes. In a digital audio system described as an example, five ASPs are combined with ancillary circuits to perform three tasks: dynamic-range compression or expansion, the excitation of reverberation and the equalization of the frequency characteristic with the aid of 10 octave-band filters, which are adjustable between +12 dB and -12 dB. The first part of this article deals with the practical and theoretical background to these tasks and with the implications of their digital execution.

CAROT: a digital method of increasing the robustness of an analog colour television signal

J. H. Peters and J. T. Kanters

Introduction

Colour pictures can be optically resolved into three component pictures R , G and B , each containing only one basic colour (red, green or blue). In colour television this resolving process takes place in the camera, and the three component pictures are recombined in

This comes about because of two important conditions that were made when colour television was introduced: the colour signal was to produce a monochrome picture on unmodified existing monochrome receivers, and the addition of colour information was

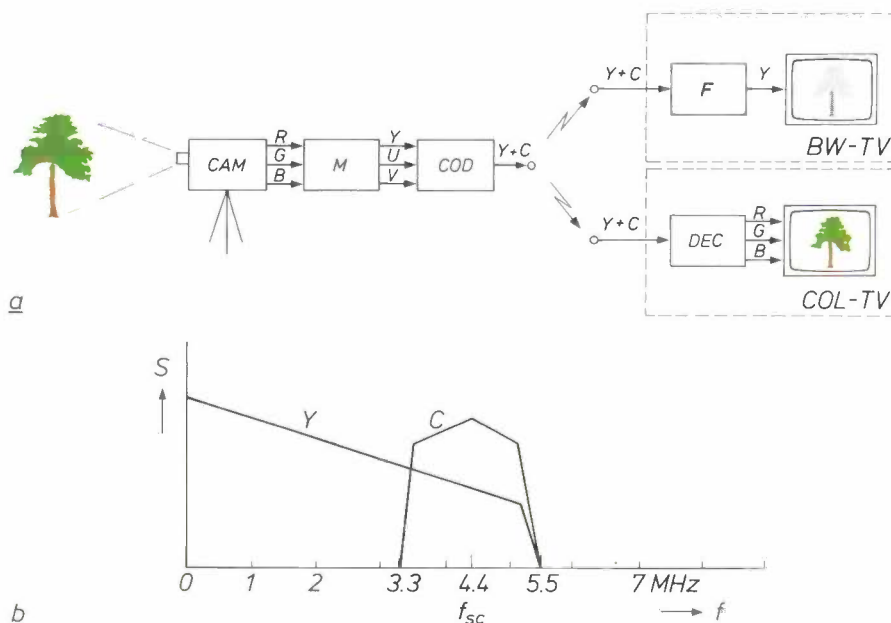


Fig. 1. a) A complete colour television signal $Y + C$ (the composite signal) is generated in three stages. First, three basic colour signals R , G and B are derived from a scene in the camera CAM . They are converted into the luminance signal Y and the colour-difference signals U and V in the matrix circuit M . The signals U and V are combined by modulation in the coder COD to form the 'chroma' signal C , which is added to Y . In a monochrome receiver $BW-TV$ only the subsignal Y is used for display, after the signal C has been suppressed by a filter F (in modern receivers). In a colour receiver $COL-TV$ the signals R , G and B are recovered in a colour decoder DEC . b) Schematic representation of the frequency spectrum of a composite signal $Y + C$ for the PAL system, which is the one most commonly used in Western Europe. S signal power per unit bandwidth. The power of the chroma signal is concentrated around $f_{sc} \approx 4.4$ MHz, the frequency of the subcarrier used in the coder COD . The bandwidth of C is considerably narrower than that of Y , because fine details in the luminance information are more important to the human eye than fine details in the colour information.

the colour receiver to form a single complete picture containing all the original colours. In the camera the RGB pictures are converted into three RGB signals, but these are not transmitted to the receiver directly.

Ir J. H. Peters, now with the Medical Systems Division, Philips NPB, Best, was formerly with Philips Research Laboratories, Eindhoven. Ing. J. T. Kanters is with Philips Research Laboratories, Eindhoven.

not to cause any increase in the bandwidth of the television signal. These requirements were ingeniously met^[1] by converting the RGB signals into three other signals Y , U and V (fig. 1a). The luminance signal Y represents the monochrome information, and the

[1] F. W. de Vrijer, Colour television transmission systems, Philips Tech. Rev. 27, 33-45, 1966.

signals U and V represent the colour information or *chrominance*. The presence of the Y signal permits the first requirement to be met. To meet the second requirement as well, the signals U and V are combined with the Y signal to form one complete colour television signal or *composite signal* $Y + C$. This is done by using the signals U and V to modulate a subcarrier of relatively high frequency f_{sc} (about 4 MHz); see fig. 1*b*. When an appropriate value is chosen for f_{sc} and certain special measures are taken, including filtering in the camera and receiver, there is virtually no interaction between the signals Y and C .

There are various methods of converting the two chrominance (colour-difference) signals U and V into one 'chroma' signal C . This has resulted in three different colour television systems: NTSC (United States, Japan), SECAM (Eastern Europe and France) and PAL (Western Europe outside France). The CAROT principle in this article will be described in relation to PAL coding (hence the use of the letters U and V for the chrominance signals; in the other systems other letters are generally used). CAROT can in principle be adapted to NTSC, but not directly to SECAM.

conversion the signal could be recoded by fairly simple digital operations. After converting back again to analog this gives a new analog composite signal $(Y + C)^*$ that is considerably more robust in certain respects than the original signal $Y + C$. We have called this recoding 'CAROT', an acronym for Composite Analog Recoding by Orthogonal Transform. Before display on a conventional colour television receiver, $(Y + C)^*$ is recoded again to $Y + C$. Both types of recoding closely resemble each other. If we need to distinguish between the two we can refer to CAROT1 and CAROT2; see fig. 2.

In this article we describe the principle of CAROT, taking a PAL colour television signal as our starting point. With the aid of a few examples, sometimes simplified, we shall attempt to provide an understanding of the operation of CAROT. We shall use a number of specialized, but established, techniques such as sub-Nyquist sampling, filtering by comb filters, and analysis with two-dimensional spectra. In conclusion we shall give some practical results as illustrated by colour photographs.

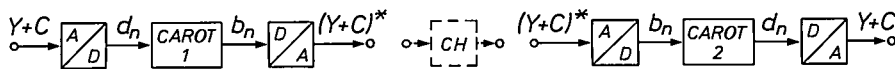


Fig. 2. An analog composite signal $Y + C$ can be recoded by CAROT to form a new analog composite signal $(Y + C)^*$ that is more 'robust', i.e. it is less susceptible to certain types of interference and distortion that can occur in the transmission channel CH — not specified here. If CH can be replaced by a direct connection, the CAROT operation is completely reversible and the original signal $Y + C$ can be recovered in full from $(Y + C)^*$. The blocks CAROT1 and CAROT2 represent the two recoders. Since these are digital, each is preceded by an analog-to-digital converter A/D and followed by a digital-to-analog converter D/A .

The composite signal $Y + C$ is very suitable for the amplitude modulation of a carrier to be transmitted by a television transmitter^[2]. For some other applications, however, this signal has certain disadvantages, mainly because the colour information is primarily represented by the higher signal frequencies. This means that the first effect of any loss or distortion of these frequency components of the signal will be to impair the colours. Another disadvantage arises when frequency modulation (FM) and the corresponding demodulation are applied in succession, e.g. before and after recording on magnetic tape. This is accompanied by the characteristic 'FM triangular noise', whose power increases with the frequency. Here again the colour information suffers disproportionately. The conventional composite colour television signal is therefore not very 'robust' with respect to bandwidth limitation and certain types of noise interference. However, we have found that after analog-to-digital

The CAROT principle

The principle of CAROT will be explained with reference to fig. 3, which shows a number of signals from fig. 2. First of all we have a part of a composite signal $Y + C$ that corresponds to a scene of constant colour and constant luminance. Here we can clearly see a relatively fast sinusoidal variation, which is due to the modulated colour subcarrier. After analog-to-digital conversion we obtain a digital signal d_n , in which the fast signal variations are still evident. The CAROT1 operation gives the digital signal b_n which gives the signal $(Y + C)^*$ after digital-to-analog conversion. We see that the fast signal variations have now been replaced by slower ones, which indicates that the colour information is now represented by lower frequencies and is therefore coded in a more robust manner. It can easily be shown that A/D conversion, CAROT2 operation and D/A conversion will completely recover the signals b_n , d_n and $Y + C$ from

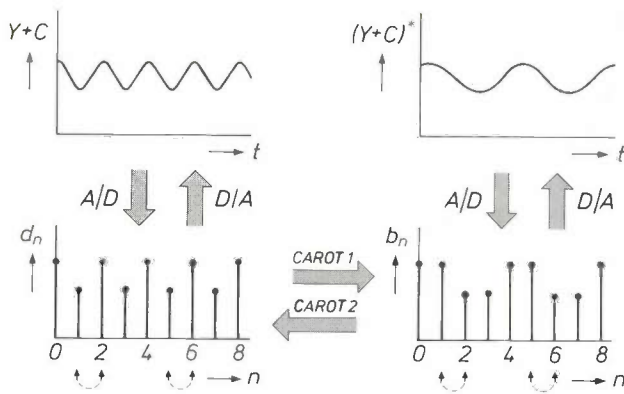


Fig. 3. The principle of CAROT can be understood from a closer consideration of the signals that can occur in the configuration shown in fig. 2. This highly simplified example shows that certain changes in neighbouring samples (see dashed arrows at the bottom of the drawing) can convert the digital signal d_n into b_n and vice versa. The corresponding analog signals $Y + C$ and $(Y + C)^*$ have very different characteristics; in particular the sinusoidal signal waveform, which carries the colour information for a patch of the scene of constant colour, has a lower frequency in $(Y + C)^*$ than in $Y + C$. CAROT1, CAROT2 recoding operations. A/D analog-to-digital conversion. D/A digital-to-analog conversion.

the signal $(Y + C)^*$. In this simple example the two operations CAROT1 and CAROT2 are identical. They amount to no more than the exchange of certain neighbouring samples (for example with $n = 1$ and $n = 2$), as indicated by the dashed arrows. In the CAROT system whose practical results we shall describe later in this article the operations are somewhat more complex, but the principle is the same. To describe this system properly, however, we must consider a few other matters first.

Sub-Nyquist sampling

As shown in fig. 1b, the spectrum of a PAL colour television signal extends to about 5.5 MHz. According to the sampling theorem we should therefore take a minimum sampling rate of 2×5.5 MHz for A/D conversion, to avoid aliasing. But the composite signal $Y + C$ is a rather special case, and it is in fact possible to sample at only twice the subcarrier frequency, i.e. at 2×4.4 MHz = 8.8 MHz, without serious signal distortion. To indicate that we are not meeting the conventional 'Nyquist condition', this is called sub-Nyquist sampling [3][4]. The fundamental interval of the spectrum of the discrete-time signal obtained in this way is shown in fig. 4. At first sight it looks as if there will be unacceptable aliasing in the frequency range between 3.3 and 5.5 MHz, for both the luminance signal Y and the chroma signal C . This is not so, however. There are three important factors here:

- A television signal is obtained by scanning a scene in a horizontal line pattern (just as our eyes scan the lines of a page as we read). In the PAL system

the number of lines is $625 \times 25 = 15625$ lines per second. This means that stationary pictures in which all the lines are exactly the same give Y , U and V signals that have frequency components only at multiples of $f_1 = 15625$ Hz (for most other pictures the signal energy remains strongly concentrated around these frequencies [5]).

- The frequency of the subcarrier f_{sc} has been taken equal to $283\frac{3}{4}f_1$ [6]. The effect of this is that the frequency components of the chroma signal C come between the signal frequencies of Y . Because the signals U and V are processed differently they arrive at different frequencies after modulation. Both U and V are subjected to double-sideband modulation, so that the resultant chroma spectrum has a certain degree of symmetry with respect to f_{sc} .

- The sampling rate f_s has been taken exactly equal to $2f_{sc}$.

The consequences of all this for the spectrum of the composite signal before and after sub-Nyquist sampling can be seen in fig. 5. This shows parts of the spectra of fig. 1b and fig. 4 on an expanded frequency scale. In fig. 5b we see that aliasing effects do in fact occur around f_{sc} . For the luminance signal Y the aliasing components (shown dashed) lie exactly between the original luminance components and can therefore in principle still be removed. For the signals U and V , on the other hand, they lie exactly on top of the ori-

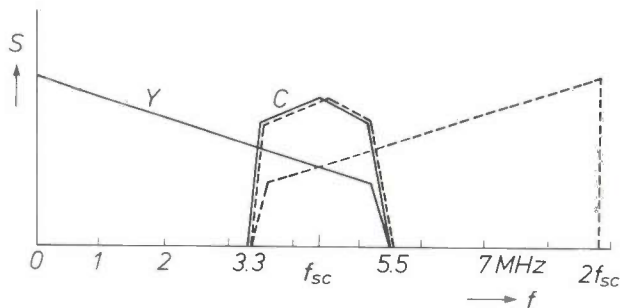


Fig. 4. When the composite signal $Y + C$ is sampled at a rate $f = 2f_{sc}$ it looks as if a part of Y and the whole spectrum of C will suffer unacceptable interference from aliasing, indicated here by dashed lines.

[2] F. W. de Vrijer, Modulation, Philips Tech. Rev. 36, 305-362, 1976.
 [3] V. G. Devereux, Digital video: sub-Nyquist sampling of PAL colour signals, BBC Res. Dep. Rep. No. 1975/4.
 [4] K. H. Barratt and K. Lucas, An introduction to sub-Nyquist sampling, IBA Tech. Rev. No. 12, 3-15, 1979.
 [5] M. J. J. C. Annegarn, A. H. H. J. Nillesen and J. G. Raven, Digital signal processing in television receivers, this issue, pp. 183-200.
 [6] In fact, the value is $f_{sc} = 283\frac{3}{4}f_1 + 25$ Hz; see [5] and [7]. This small deliberate offset of 25 Hz does not affect the validity of the reasoning in this article and can therefore be safely disregarded. This simplifies the presentation here in some respects.
 [7] P. S. Carnt and G. B. Townsend, Colour television, Vol. 2, PAL, SECAM and other systems, Iliffe, London 1969.

ginal components, and invariably in such a way that upper and lower sidebands of the modulation process that belong together (e.g. U_1 and U_{-1} or V_1 and V_{-1}) coincide; this is referred to as 'constructive aliasing', because it is well-defined and can in principle be compensated.

Sub-Nyquist sampling does not, by definition, give rise to signal distortion if we can recover the spectrum of fig. 5a from the spectrum of fig. 5b. This can be done with a filter [8] with the frequency characteristic H as shown in fig. 6. This filter has:

- A flat frequency response of value 1 below 3.3 MHz.
- A sinusoidal frequency response ('comb-filter characteristic') in the chroma-signal band (3.3-5.5 MHz).
- A flat frequency response of value 0 above 5.5 MHz.

The characteristic H can easily be realized with two cascaded filters with the frequency characteristic G

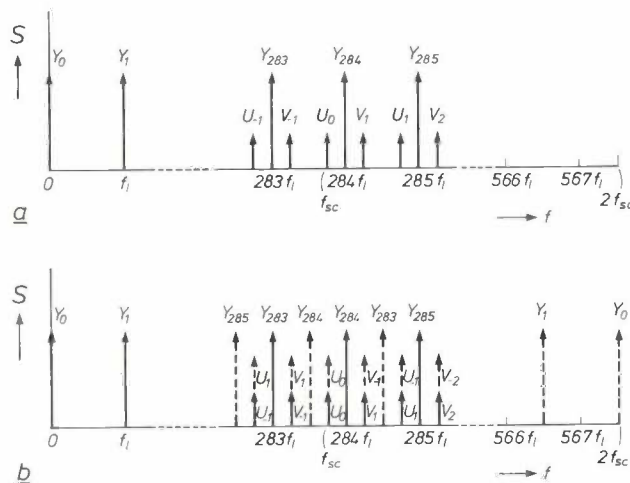


Fig. 5. a) Representation of some parts of the spectrum S of $Y + C$ on an expanded frequency scale. To a first approximation, the luminance signal consists of discrete frequency components Y_0, Y_1, \dots at a spacing of f_1 (the line frequency). The chroma signal also consists of discrete components. Because the subcarrier frequency f_{sc} has been given an appropriate value and the right type of modulation is used, none of the components originating from the signals Y, U and V coincide. The components associated with U and V are numbered starting from the subcarrier frequency. b) Sub-Nyquist sampling of the composite signal at exactly $2f_{sc}$ results in aliasing products (shown here by dashed lines) that appear in a very specific pattern and are therefore not so damaging as they seem from fig. 4.

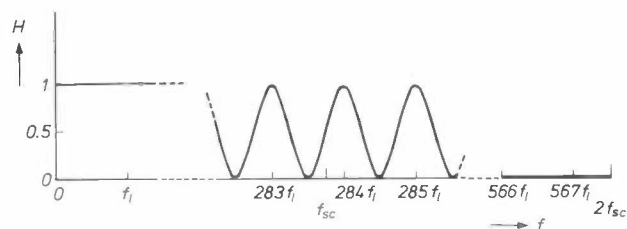


Fig. 6. Frequency characteristic H of a filter that will remove all aliasing from the spectrum of fig. 5b, thus enabling the spectrum of fig. 5a to be recovered. (The frequency axis is shown in the same way as in fig. 5.)

(such that $H = G^2$) as shown in fig. 7. If one of these filters is used at the input and the other at the output of a system operating with sub-Nyquist sampling (fig. 8a) it turns out in practice that this too-low sampling rate only gives an extremely small loss of quality, which is scarcely perceptible [9]. We are then in a position, however, to perform all the digital operations on the composite signal with the low sampling rate $2f_{sc}$, with all the technical advantages that this implies [10].

In fig. 8a a system is shown in which G represents an analog filter. However, G can also be realized as a digital filter [11]. Since the characteristics of H (and hence those of G) are precisely specified for frequencies to far above f_{sc} , a digital version must operate with a sampling rate higher than $2f_{sc}$. The most convenient course is then to take the value of $4f_{sc}$. The transition to and from sub-Nyquist-sampled signals can be made by decreasing or increasing the sampling rate, as the case may be, by a factor of 2 [10]. This is illustrated in fig. 8b.

Two-dimensional spectra

The usual spectral representations of signals and filter characteristics in television engineering, as used so far in this article, contain only one frequency variable (ω or f). We therefore refer to them as one-dimensional spectra or 1D spectra. Sometimes with this representation it is difficult to get a proper idea of the consequences of certain signal operations. For example, it is fairly easy to see that

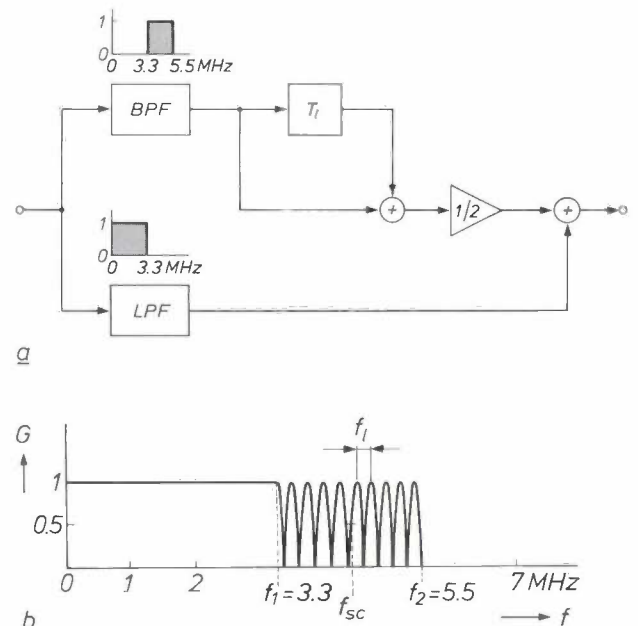


Fig. 7. a) Block diagram of a filter and b) the corresponding frequency characteristic G . When two such filters are cascaded the frequency characteristic H of fig. 6 is obtained. The most striking feature of G is the comb-filter behaviour in the chroma-signal band (3.3-5.5 MHz). For clarity, far fewer comb-filter 'teeth' are shown here than are really present. The true line frequency $f_1 = 1/T_1$ is 15.625 kHz. BPF bandpass filter. LPF lowpass filter.

limiting the bandwidth of the luminance signal Y will result in a loss of resolution (picture sharpness) in the horizontal direction of the television picture. However, if during filtering (or during any other operation on a signal) information originating from more than one picture line is used at the same time, effects can also occur in the

vertical direction, and in fact in any direction between horizontal and vertical. This is most apparent from a two-dimensional or 2D analysis [12]. We shall first confine our attention here to the luminance information (corresponding to the luminance signal); we shall return later to composite signals.

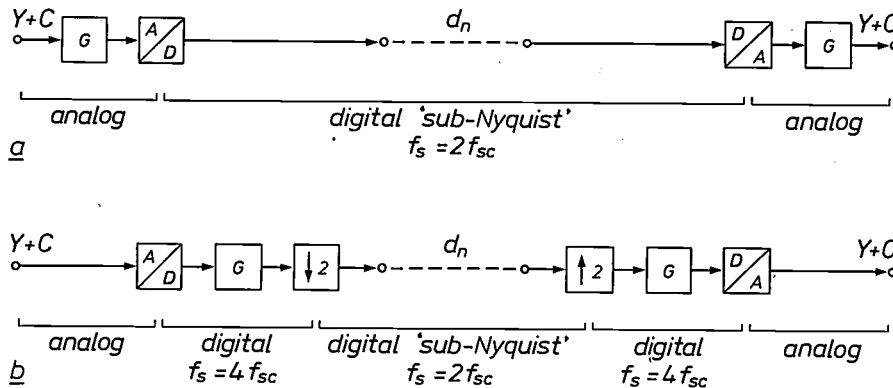


Fig. 8. a) The use of analog filters with frequency characteristic G before A/D and after D/A conversion makes it possible to process the composite signal $Y + C$ as a sub-Nyquist-sampled digital signal d_n without any significant loss of quality. b) The filters can also be designed as digital circuits. However, the A/D and D/A conversions must then take place at a sampling rate $f_s = 4f_{sc}$. The transition to or from sub-Nyquist-sampled operations is made by decreasing or increasing the sampling rate by a factor of two.

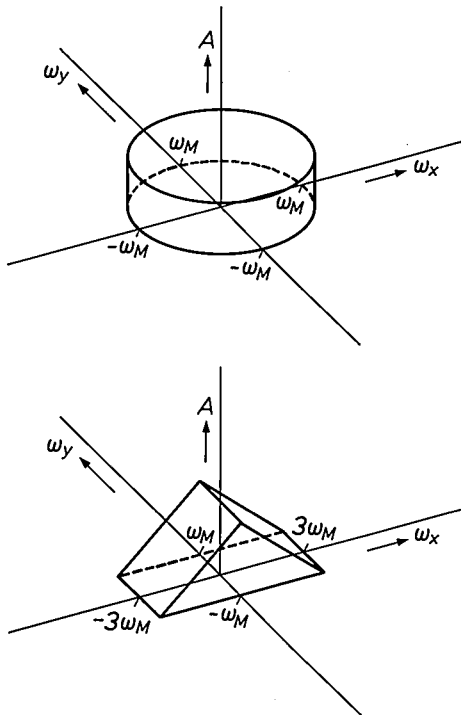


Fig. 9. 2D spectra of two different scenes. The spectra are functions of the spatial angular frequencies ω_x and ω_y . Fine details in the x -direction (horizontal) correspond to high values of ω_x ; the same relation exists between details in the y -direction (vertical) and ω_y . We consider both positive and negative frequencies, as is often done with 1D spectra. In fact the spectra are complex and can only be fully represented by separate curves for the real and imaginary parts or for the amplitude and phase. Here only the amplitude A is shown. a) Spectrum of a scene in which the frequencies between 0 and ω_M are equally represented in all directions and no higher frequencies are present. b) Spectrum of a scene in which frequencies with a decreasing amplitude occur in the x -direction up to $3\omega_M$ and with a constant amplitude in the y -direction up to ω_M .

The luminance information of any stationary scene can be expressed in terms of the luminance function I , whose value varies with the position (x, y) in the area of the picture:

$$I = f(x, y).$$

The 2D Fourier integral of I is defined as

$$\mathcal{F}(I) = F(\omega_x, \omega_y) = \iint f(x, y) e^{-jx\omega_x - jy\omega_y} dx dy,$$

where ω_x and ω_y are spatial angular frequencies in the x -direction (horizontal) and y -direction (vertical). (The quantities $\omega_x/2\pi$ and $\omega_y/2\pi$ are dimensioned in terms of the number of periods per unit of picture width and the number of periods per unit of picture height, respectively.) Fine details in the picture correspond to high frequencies and coarse details to low frequencies. As an example fig. 9 shows the 2D amplitude spectrum $A = |F(\omega_x, \omega_y)|$ of two different hypothetical scenes.

In the generation of a television signal a scene is scanned in a pattern of horizontal lines; this is really sampling in the vertical direction, with all the known consequences of such an operation [10]. The two principal effects involved are the following:

- [8] From now on it will be assumed that all filters considered have a linear phase characteristic unless stated otherwise. The filter characteristic will thus be adequately specified by only giving the amplitude characteristic, which we shall generally refer to as the 'frequency characteristic'.
- [9] Optimum results are in fact achieved if H is divided into two characteristics G_1 and G_2 (with $H = G_1 G_2$) that have a small difference deliberately introduced between them [8].
- [10] A. W. M. van den Enden and N. A. M. Verhoeckx, Digital signal processing: theoretical background, pp. 110-144, in the special issue 'Digital signal processing I, background', Philips Tech. Rev. 42, 101-148, 1985.
- [11] J. H. Taylor, Digital sub-Nyquist filters, IBA Tech. Rev. No. 12, 21-26, 1979.
- [12] A publication on this subject appeared over 50 years ago: P. Mertz and F. Gray, A theory of scanning and its relation to the characteristics of the transmitted signal in telephotography and television, Bell Syst. Tech. J. 13, 464-515, 1934.

- Spectral periodic repetition (in this case along the ω_y -axis; see fig. 10), so that we only need to consider a fundamental interval in the ω_y -direction. The length of this interval is $2\pi/D_y$, where D_y is a measure of the distance between the picture lines^[13].
- Aliasing, if the distance between the lines is taken too large so that the periodic spectral repetitions overlap. Pictures that are too finely detailed in the vertical direction cannot then be distinguished from certain less-finely detailed pictures.

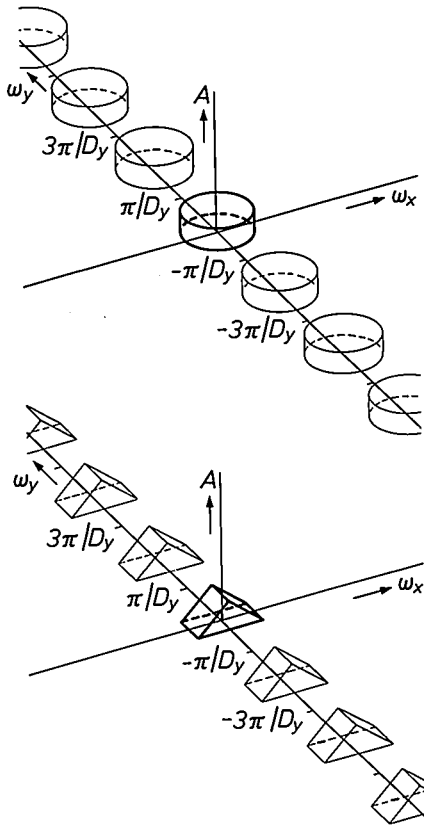


Fig. 10. Scanning of a scene in the usual horizontal television line pattern gives a periodic repetition of the 2D spectrum along the ω_y -axis. This is shown here by way of example for the spectra in fig. 9. The ω_y -axis can now be limited to the fundamental interval $(-\pi/D_y, \pi/D_y)$, where D_y is a measure of the distance between the lines of the scan. The parts outside this interval are therefore shown here by thin lines.

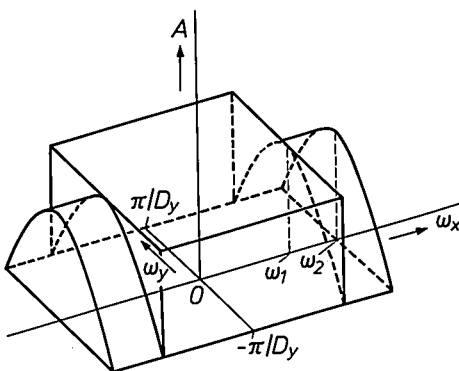


Fig. 11. 2D amplitude characteristic of the filter in fig. 7. The magnitude $2\pi/D_y$ of the fundamental interval corresponds to the line frequency in fig. 7. The quantities ω_1 and ω_2 correspond to f_1 and f_2 .

A 2D frequency characteristic can also be derived in a similar way for filters designed to handle television signals. As an example fig. 11 gives the results for the filter of fig. 7. The ω_y -axis is limited to the fundamental interval $(-\pi/D_y, \pi/D_y)$. We can immediately recognize the following filtering properties:

- Purely horizontal frequencies ($\omega_y = 0$) with $|\omega_x| < \omega_2$ are not attenuated, whereas purely horizontal frequencies with $|\omega_x| > \omega_2$ are completely rejected.
- Purely vertical frequencies ($\omega_x = 0$) are not attenuated throughout the entire fundamental interval.
- The comb filter gives a pronounced attenuation only for combinations of high horizontal and high vertical frequencies (that is to say for pictures with fine detail in the diagonal directions).

In principle we can proceed in the same way with 2D signal spectra and 2D filter characteristics as is customary in the 1D case: the output spectrum $T(\omega_x, \omega_y)$ of a linear filter with filter characteristic $G(\omega_x, \omega_y)$ and input spectrum $S(\omega_x, \omega_y)$ is given by

$$T(\omega_x, \omega_y) = G(\omega_x, \omega_y) S(\omega_x, \omega_y).$$

The CAROT method

We shall now take a closer look at the operations that constitute the essence of the CAROT method. We start with a small patch of uniformly coloured television picture (fig. 12). When this patch is strongly magnified we see clearly the line structure $L_i, L_{i+1}, L_{i+2}, \dots$. Since all the even lines and all the odd lines are scanned alternately (shown as solid and dashed lines respectively), two fields of lines are obtained, one even and one odd. We shall only consider the field with the solid lines, since we treat both fields individually but in the same way. The crosses indicate the points in the picture (pixels) that are sampled in sub-Nyquist sampling at twice the subcarrier frequency. The result is a highly regular pattern of pixels. Even more remarkable is the fact that the samples of the composite signal within any arbitrary though uniformly coloured area can assume only four different values, indicated symbolically here by a, b, c and d . In the CAROT operations we always take two groups of four adjacent samples from two lines L_j and L_{j+4} together (for the two lines that we examine more closely in fig. 12, $j = i + 2$). These samples can be given the general designation of k_1, k_2, \dots, k_8 . The actual recoding now takes place on the basis of these octuples: we use them to calculate eight new samples l_1, l_2, \dots, l_8 and we substitute these for the old signal samples. For a uniformly coloured area the new values correspond exactly to a, b, c and d , but they now occur at other places. It must not be concluded from this, however, that the recoding of k samples to l samples is no more than a rearrangement of sample values. This is not the case, because it would not give the desired 'robustness' of the signals for arbitrarily composed pictures; it appears that there would still be relatively too much colour information represented by high signal fre-

quencies. The real secret of the CAROT method lies in the appropriate choice of the recoding algorithm. We have based this on an *orthogonal transform*. This means that we use an orthogonal matrix for deriving a new vector with the elements l_1, l_2, \dots, l_8 from a vector with the elements k_1, k_2, \dots, k_8 . This can be done in the following way:

$$\begin{bmatrix} l_1 \\ l_2 \\ l_3 \\ l_4 \\ l_5 \\ l_6 \\ l_7 \\ l_8 \end{bmatrix} = \frac{1}{2} \begin{bmatrix} 1 & 1 & 0 & 0 & 1 & -1 & 0 & 0 \\ -1 & 1 & 0 & 0 & 1 & 1 & 0 & 0 \\ 0 & 0 & 0 & 0 & 0 & 0 & 2 & 0 \\ 0 & 0 & 0 & 2 & 0 & 0 & 0 & 0 \\ 1 & -1 & 0 & 0 & 1 & 1 & 0 & 0 \\ 1 & 1 & 0 & 0 & -1 & 1 & 0 & 0 \\ 0 & 0 & 2 & 0 & 0 & 0 & 0 & 0 \\ 0 & 0 & 0 & 0 & 0 & 0 & 0 & 2 \end{bmatrix} \begin{bmatrix} k_1 \\ k_2 \\ k_3 \\ k_4 \\ k_5 \\ k_6 \\ k_7 \\ k_8 \end{bmatrix} \quad (1)$$

It can easily be shown that with this matrix we can make the CAROT1 transition in fig. 12.

What we have done so far is to give a full *description* of a CAROT operation that gives good results in practical experiments — but we have not formally *proved* that it works. A conclusive theoretical proof would certainly be beyond the scope of this article. We can, however, explain the operation to some extent by making use of *basic pictures*. For present purposes we refer to eight pictures B_1, B_2, \dots, B_8 consisting of 2×4 pixels k_1, k_2, \dots, k_8 , each of which can assume only one of two possible standard values (for example $+1$, indicated by a black square and -1 , represented by a white square) (fig. 13). The basic pictures are chosen in such a way that any possible picture K of 2×4 pixels can be formed by weighting and superimposing basic pictures. By determining how the CAROT operation turns out for all eight basic pictures individually we can draw some general conclusions. Fig. 13 indicates how the orthogonal transform

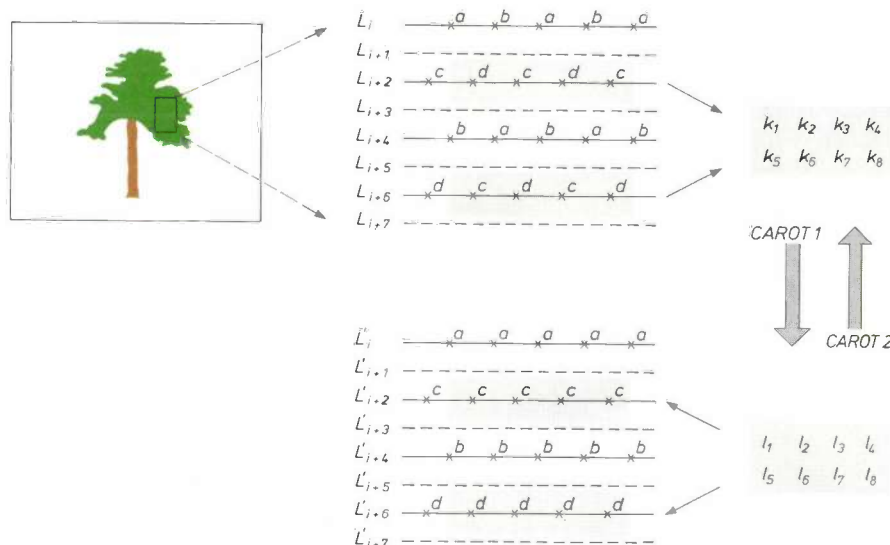


Fig. 12. The CAROT method in more detail. Each television picture is built up from lines $L_i, L_{i+1}, L_{i+2}, \dots$, which are shared between an even field (solid lines) and an odd field (dashed lines). These are processed separately. The television signal is sampled at the positions indicated by crosses. The samples are processed in groups of eight (denoted by k_1, k_2, \dots, k_8) in accordance with the algorithm *CAROT1*. This results in eight samples l_1, l_2, \dots, l_8 , and from these a new television signal can be formed in which the new samples are given the places formerly occupied by the original samples. In a uniformly coloured patch of the picture the samples k_1, k_2, \dots, k_8 have only two pairs of possible values (a and b or c and d). In this case the values of the samples have not been changed by the CAROT operation but only grouped in a better way. In general, however, there will be some change in the sample values for a given patch of the picture. The transition from k_1, k_2, \dots, k_8 to l_1, l_2, \dots, l_8 is completely reversible by means of the inverse operation *CAROT2*.

In an orthogonal matrix all the rows form orthogonal vectors, that is to say the scalar product of each two vectors is zero, unless a vector is multiplied by itself. An orthogonal matrix has many interesting properties. One of them is the fact that matrix inversion amounts to transposition (exchanging rows and columns) and gives another orthogonal matrix. In using an orthogonal matrix for the CAROT1 operation we therefore immediately know the matrix for the inverse operation CAROT2. Another consequence of this property is that there will be a close relationship between the software (or hardware) required for both operations.

[13] If all the TV lines are successively scanned from top to bottom, D_y is associated with the distance between two lines that are visible one directly under the other in the picture. In most current TV systems, however, interlacing is used: all the odd lines are scanned first (producing the odd field) and then all the even lines (producing the even field). The quantity D_y is then associated with the distance between the lines within one of the fields, i.e. with twice the distance between the lines of the picture. It will be shown later that in the CAROT method the even and odd lines of each field are treated separately. This means that D_y is then associated with four times the distance between the lines of the picture.

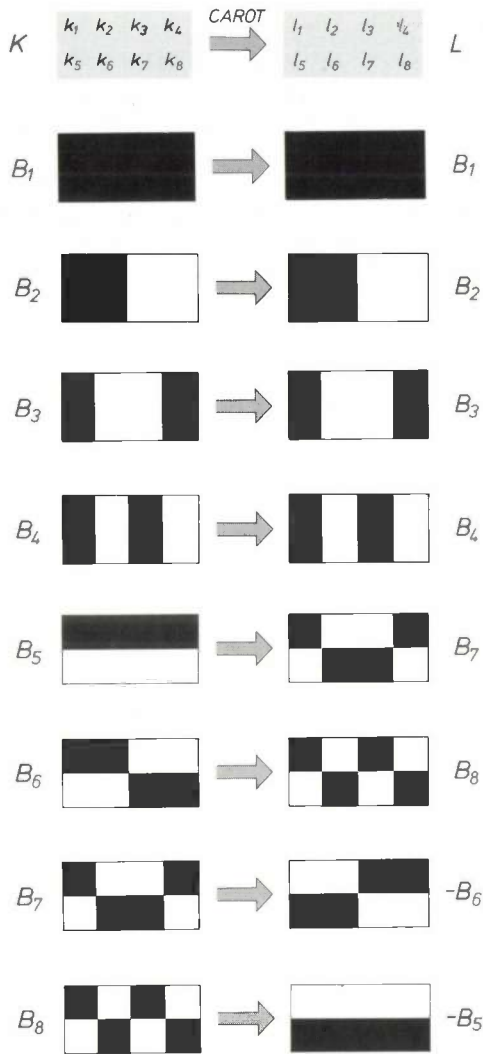


Fig. 13. Any given picture K consisting of 2×4 samples ('pixels') k_1, k_2, \dots, k_8 can be formed from a weighted combination of eight basic pictures B_1, B_2, \dots, B_8 in which each pixel can assume only two standard values (indicated here as black and white squares). The CAROT operation on picture K gives the picture L , which can also be found by superimposition of separately processed basic pictures. For each basic picture the transformed version from eq. (1) is given.

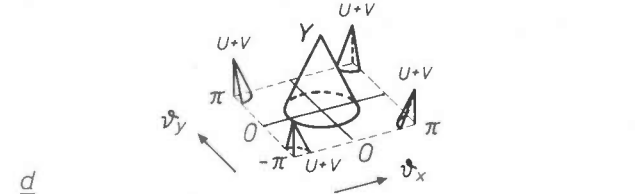
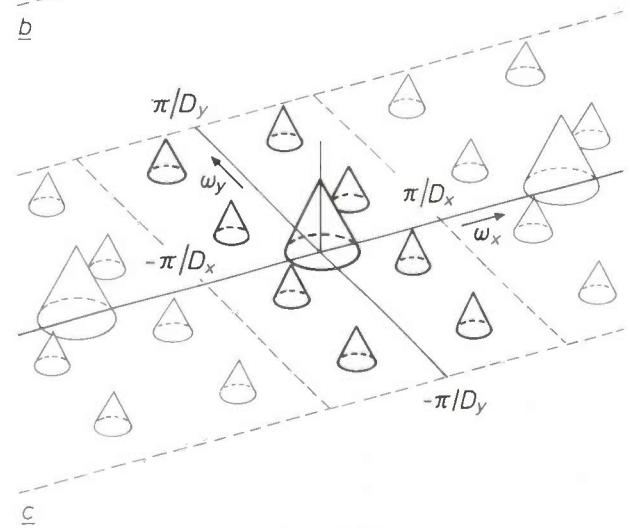
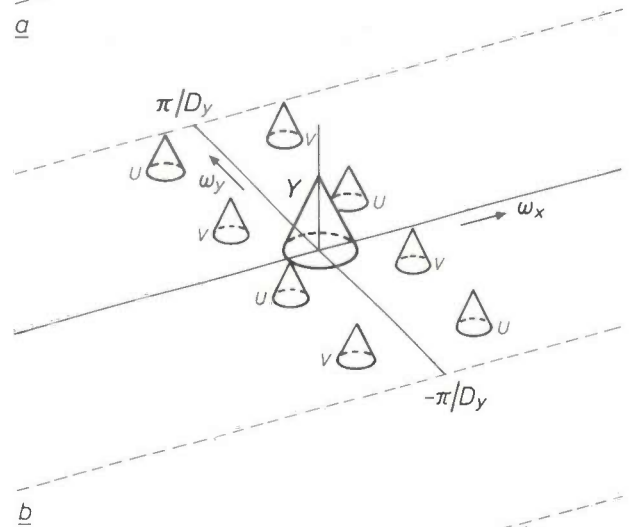
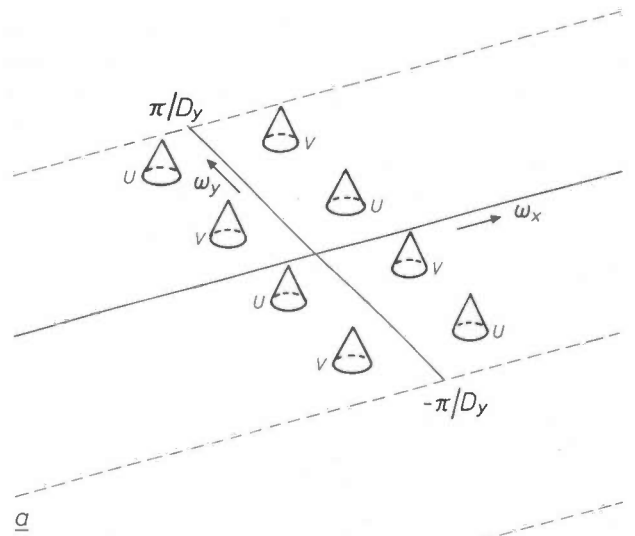


Fig. 14. a) 2D spectrum of the chroma signal C as specified in the PAL colour television standard. It consists of eight contributions, represented here as small cones. These indicate approximately where the power corresponding to the U and V information is concentrated. The exact location of the cones is determined by the frequency f_{sc} of the subcarrier and the method of modulation. b) 2D spectrum of an analog PAL composite signal $Y + C$. The luminance is represented by the cone Y , which indicates that the centre of the luminance spectrum is at $\omega_x = \omega_y = 0$. For clarity in the diagram, the base of the cone Y has been made relatively small. In reality Y usually contains higher frequencies both in the ω_x -direction and the ω_y -direction. c) After A/D conversion of the composite signal the 2D spectrum is periodically repeated along the ω_x -axis (here shown in thin lines). In this direction it is sufficient to take a fundamental interval $(-\pi/D_x, \pi/D_x)$, where D_x is a measure of the distance between the samples. In the case illustrated the sampling rate is an exact integer multiple of the line frequency, since otherwise the repetitions in the ω_x -direction would be accompanied by a simultaneous shift in the ω_y -direction. d) The starting point in the CAROT operation is a 2D spectrum $K(\theta_x, \theta_y)$ as illustrated here schematically with $\theta_x = D_x \omega_x$ and $\theta_y = D_y \omega_y$. In the θ_x -direction

we have a fundamental interval that corresponds to $2f_{sc}$. In the θ_y -direction the fundamental interval is determined by the fact that three lines are always missed out in the operations, so that the distance between the lines has apparently been increased by a factor of four [13].

of eq. (1) transforms the basic pictures. Some remain unchanged and others change into one of the other basic pictures. The example in fig. 12 (uniformly coloured patch of picture) corresponds to a weighted combination of the basic pictures B_1 and B_8 . We see that these are transformed into B_1 and $-B_5$ respectively, neither of which contains changes in the horizontal direction. The corresponding signal will there-

2D interpretation of CAROT

The characteristics of the CAROT operation can best be analysed with the aid of two-dimensional spectral representations, as introduced earlier in this article (figs 9-11). It is possible to derive for each CAROT transformation matrix an equation in which the 2D spectrum of the new composite signal is given as a function of the 2D spectrum of the original composite signal. Without going into detailed theoretical considerations we shall now briefly examine this aspect.

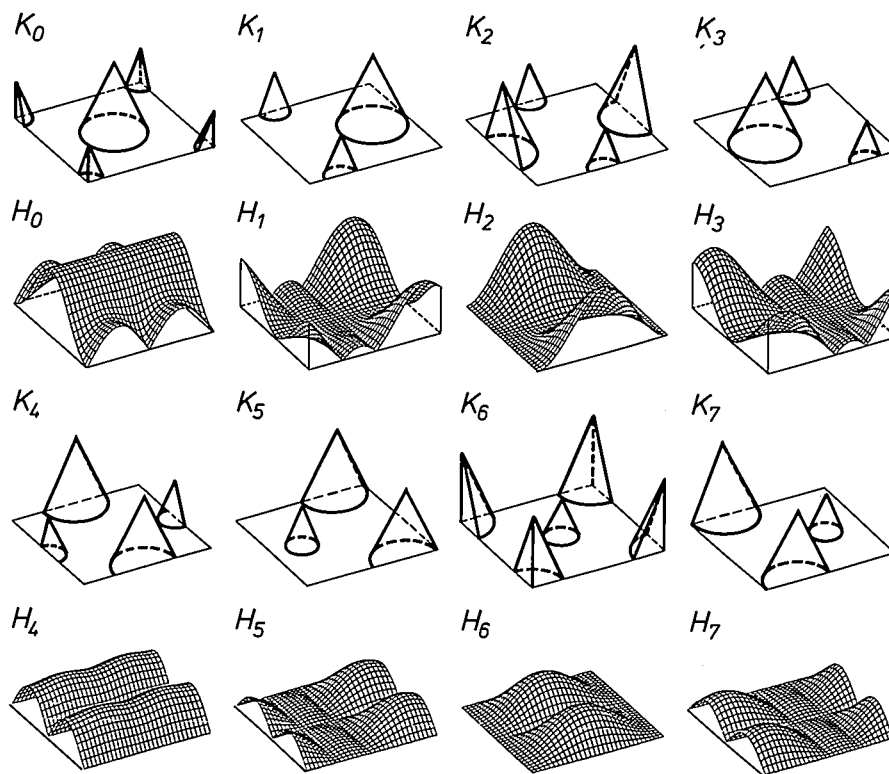


Fig. 15. The 2D spectrum of the composite signal resulting from the CAROT operation consists of the sum of eight contributions. Each individual contribution is formed by the product of a 2D signal spectrum K_i and a 2D filter characteristic H_i . K_0 is the original input spectrum, K_1, K_2, \dots, K_7 are shifted versions. H_0, H_1, \dots, H_7 are determined by the CAROT transform matrix used.

fore contain fewer high frequencies and will thus possess the required increased robustness. The opposite applies to the basic picture B_6 , whose robustness will have decreased after the transform.

Because of the characteristics of the PAL colour-coding process and the sub-Nyquist sampling, by no means all eight basic pictures occur to the same extent. They are therefore not all equally important. This applies all the more when certain perceptual rules relating to the human eye are taken into consideration. In this way with the right choice of transform matrix, the robustness of the final signal can be increased.

The chroma signal C is obtained by modulating the subcarrier with the signals U and V . The 2D spectrum of C ^[14] can be represented schematically as in fig. 14a. The ω_y -axis here is again limited to the fundamental interval $(-\pi/D_y, \pi/D_y)$. The spectrum consists of eight contributions that are concentrated around eight different positions determined by the subcarrier frequency f_{sc} . Since f_{sc} in the PAL colour television system is deliberately *not* made an integer multiple of the line frequency, these contributions do not lie on the ω_x -axis and they do not represent pure horizontal frequencies, which could be perceptually very disturbing.

The 2D spectrum of an analog composite signal $Y + C$ can be represented as in fig. 14b. The cone around $\omega_x = \omega_y = 0$ represents

[14] J. O. Drewery, The filtering of luminance and chrominance signals to avoid cross-colour in a PAL colour system, BBC Eng. No. 104 (September), 8-39, 1976.

symbolically the spectrum of Y , or really its 'centre of mass', because the spectrum will in general extend far beyond the base of the cone (the same applies to the eight small cones that make up the spectrum of C).

After A/D conversion of the composite signal the 2D spectrum is periodically repeated in the ω_x -direction, so that again we only need to consider a fundamental interval $(-\pi/D_x, \pi/D_x)$ along the ω_x -axis; see fig. 14c. Here D_x is a measure of the distance between two consecutive samples of the digitized composite signal.

In the CAROT method described here we use sub-Nyquist sampling with $2f_{sc}$; this determines the fundamental interval in the ω_x -direction. In addition, the picture lines are in fact divided into four groups (fig. 12) that are treated separately. Each of these four groups has its own 2D spectrum whose fundamental interval in the ω_y -direction is limited to $(-\pi/D_y, \pi/D_y)$ where D_y is now associated with four times the distance between the TV lines [13]. By introducing $\theta_x = D_x\omega_x$ and $\theta_y = D_y\omega_y$ we can refer to a 2D input spectrum $K(\theta_x, \theta_y)$ for the CAROT operation, where $|\theta_x| < \pi$ and $|\theta_y| < \pi$. This is illustrated in fig. 14d. The U and V contributions of C now seem to coincide completely; we know however from the earlier 1D spectra that 'constructive aliasing' occurs here.

It can be shown that the spectrum $L(\theta_x, \theta_y)$ of the new composite signal resulting from the CAROT operation is given by

$$L(\theta_x, \theta_y) = \sum_{i=0}^7 K_i(\theta_x, \theta_y) H_i(\theta_x, \theta_y).$$

K_1, K_2, \dots, K_7 are shifted versions of the original 2D input spectrum K_0 . H_0, H_1, \dots, H_7 are 2D filter characteristics that are determined by the transform matrix employed.

Fig. 15 shows the functions K_i and the characteristics H_i associated with equation (1). We see that H_0 suppresses the original chroma signal at $(\theta_x, \theta_y) = (\pm\pi, \pm\pi)$, whereas H_2 passes the shifted chroma information at $(\theta_x, \theta_y) = (0, \pm\pi)$. With the aid of the 2D spectra many more conclusions can be drawn in a similar way about the effects of the CAROT operation as described by equation (1).

The improved CAROT method

Although good results can be achieved with the CAROT method described in the previous section, experiments have shown that even better robustness can be obtained by arranging for an orthogonal transform of 2×4 pixels to be followed by a second operation that we have called 'vertical shift'. The orthogonal transform is then described by the following matrix multiplication:

$$\begin{bmatrix} l_1 \\ l_2 \\ l_3 \\ l_4 \\ l_5 \\ l_6 \\ l_7 \\ l_8 \end{bmatrix} = \frac{1}{2} \begin{bmatrix} 1 & 1 & 0 & 0 & 1 & -1 & 0 & 0 \\ 1 & 1 & 0 & 0 & -1 & 1 & 0 & 0 \\ 0 & 0 & 2 & 0 & 0 & 0 & 0 & 0 \\ 0 & 0 & 0 & 2 & 0 & 0 & 0 & 0 \\ 1 & -1 & 0 & 0 & 1 & 1 & 0 & 0 \\ -1 & 1 & 0 & 0 & 1 & 1 & 0 & 0 \\ 0 & 0 & 0 & 0 & 0 & 0 & 2 & 0 \\ 0 & 0 & 0 & 0 & 0 & 0 & 0 & 2 \end{bmatrix} \begin{bmatrix} k_1 \\ k_2 \\ k_3 \\ k_4 \\ k_5 \\ k_6 \\ k_7 \\ k_8 \end{bmatrix} \quad (2)$$

In this operation the samples that correspond to k_3, k_4, k_7, k_8 remain unchanged. The result for a uniformly coloured picture with sample values a and b is

shown schematically in the left-hand part of fig. 16. Both sample values still occur on each horizontal line; however, if we follow the guidelines shown, we find only one value. In the vertical-shift operation we delay alternate pairs of horizontally adjacent samples by one line duration; the other pairs are not delayed. This causes a partial vertical shift of one line; for evenly coloured areas, this gives the same result as described in the previous section by equation (1). For other types of picture the result is generally found to be better (i.e. it is more robust). It is evident that vertical shift is a reversible operation, which can be completely negated by the inverse CAROT operation.

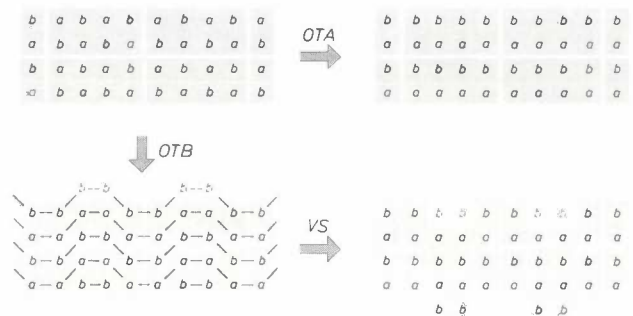


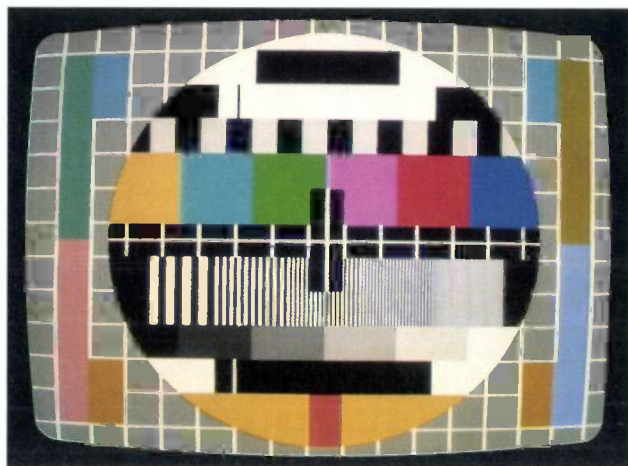
Fig. 16. In the method of eq. (1) the CAROT operation is a single step in which an orthogonal transform OTA is applied to groups of eight pixels. In the improved method an orthogonal transform OTB as described by eq. (2) is followed by a second 'vertical shift' operation VS . Because of this vertical shift the newly calculated samples are no longer at the same place as the original ones; half of them have been shifted in the vertical direction (note the grey backgrounds). For uniformly coloured pictures (as indicated here by the sample values a and b) the final result is the same with both methods; for other pictures it is generally not the same.

Practical results

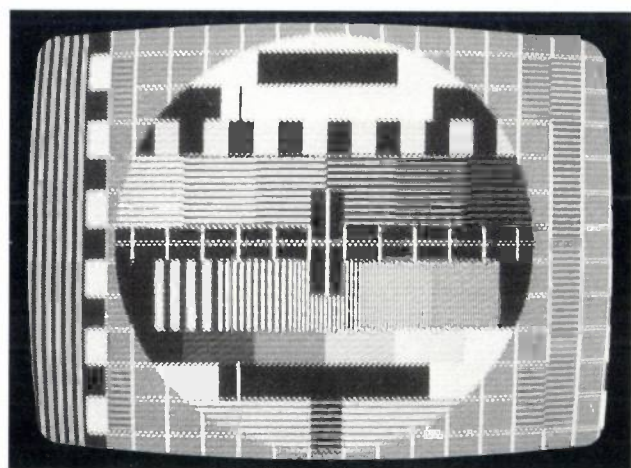
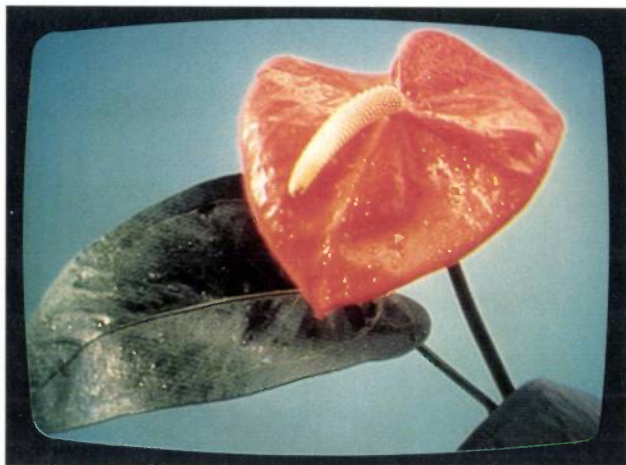
The characteristic features of the CAROT method, and particularly those of the improved CAROT method, can be illustrated with a number of photographs. We place the emphasis here on two aspects, the *reversibility* of the CAROT operation and the *increased robustness* of the composite signal. Fig. 17 shows, in two adjacent columns, the following displays for a test chart and an ordinary scene:

- a) The original colour picture.
- b) Display of the composite signal as a monochrome picture after a CAROT operation.
- c) The resultant colour picture after a CAROT operation and an inverse CAROT operation.

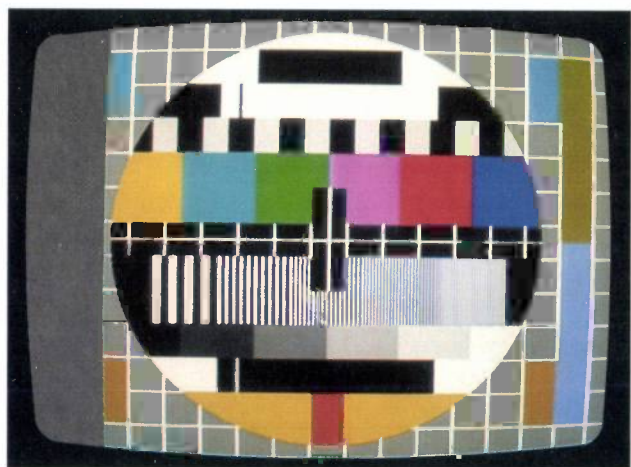
In these pictures there is no question of any interfering external influences such as noise or bandwidth limitation. We see that in this case there is no essential difference between (a) and (c) and that the CAROT operation is thus completely reversible. (We can also



a



b



c

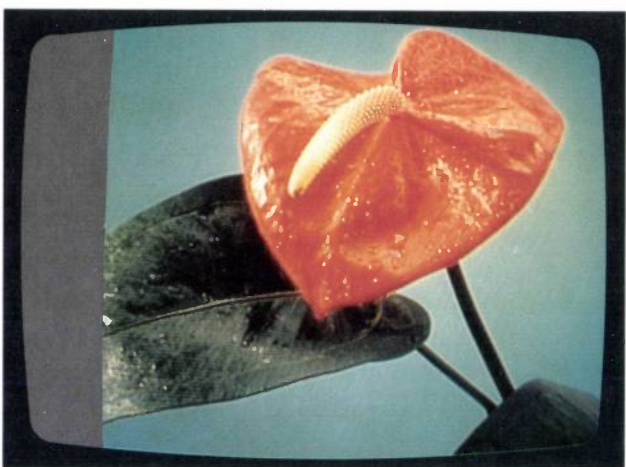
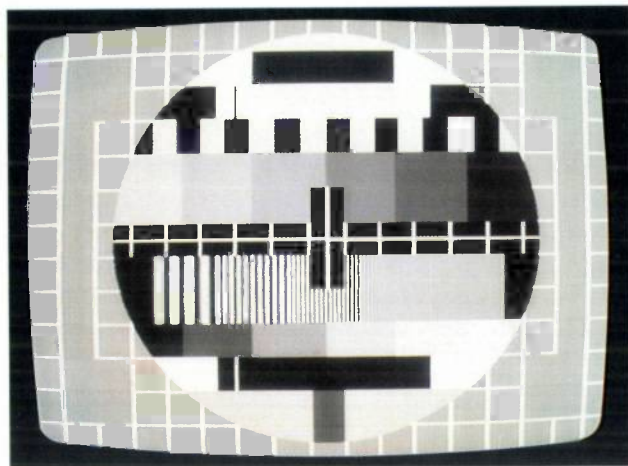
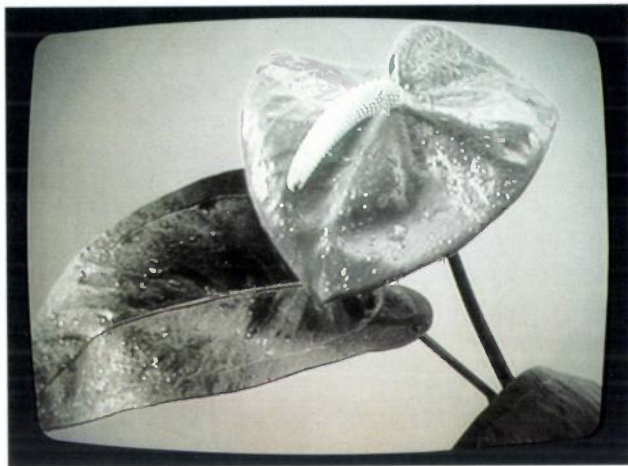


Fig. 17. a) Original colour pictures. b) Monochrome display of these pictures after the CAROT operation. The photographs show that the colour information has been 'translated' into low-frequency signals, which appear as horizontal bar patterns. c) Final result of a CAROT operation and an inverse CAROT operation. The photographs show the complete reversibility of the CAROT operation in the absence of interfering external effects such as noise or bandwidth limitation. (The left-hand part of the pictures in (b) and (c) is missing as a result of the particular experimental arrangement we used for making these photographs; it has nothing to do with CAROT. The same applies to figs 18b and 19b.)



a



b

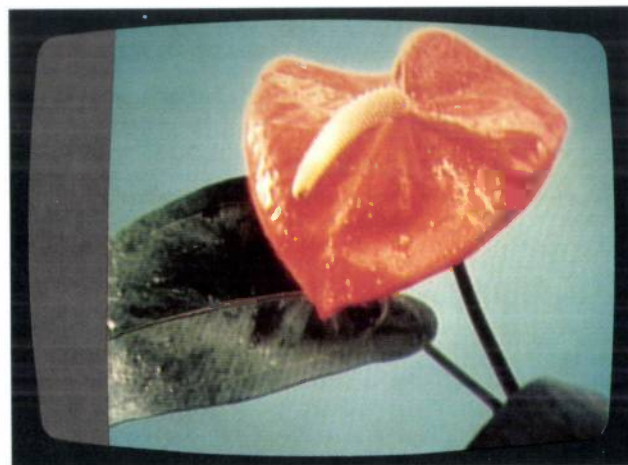


Fig. 18. *a*) The original colour pictures of fig. 17*a* after bandwidth limitation of the composite signal to 3 MHz. *b*) Result after a CAROT operation on the original pictures, followed by bandwidth limitation of the new composite signal to 3 MHz and an inverse CAROT operation.

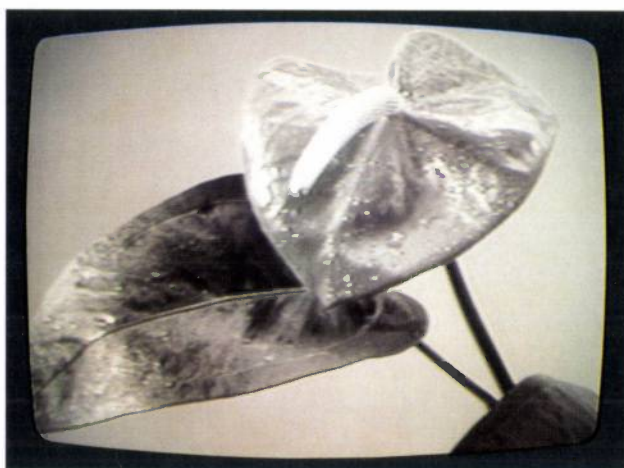
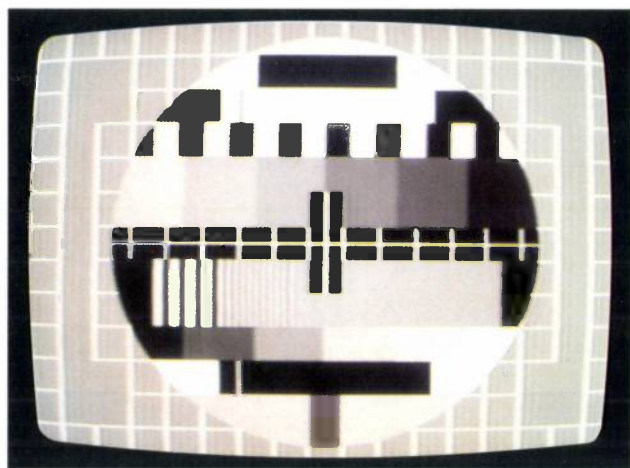
see from this how well sub-Nyquist sampling works in practice.) The pictures in fig. 17*b* do perhaps require some further explanation. The new composite signal $(Y + C)^*$ resulting from the CAROT operation cannot give a colour picture without an inverse operation. We can, however, simply display it as a monochrome picture. We then get some idea of how the colour information is represented by particular horizontal line patterns that correspond to much lower frequencies than the original colour subcarrier. In essence we have here a macroscopic version of the kind of effect we considered on a microscopic scale in figs 12, 13 and 16.

In fig. 18 the effects can be seen of limiting the bandwidth of the composite signal to 3 MHz. Fig. 18*a* shows what the pictures in fig. 17*a* look like when no CAROT operations have been applied. Fig. 18*b* gives the results after the application of CAROT operations. Fig. 19 shows the same picture with bandwidth limitation to 1 MHz. The photographs make it unequivocally clear that when the CAROT method is

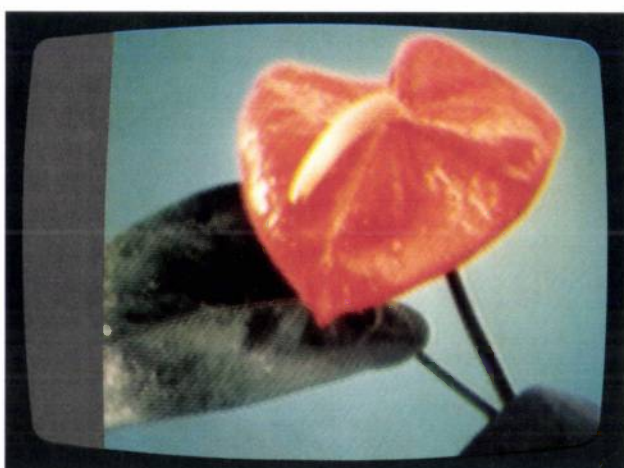
applied, bandwidth limitation of a composite signal no longer impairs the colour information disproportionately. The robustness in this respect is therefore clearly increased.

Finally, a few marginal notes. If the CAROT method is to work properly, strict accuracy is essential for the times at which the new composite signal $(Y + C)^*$ is sampled at the start of the inverse operation. This is particularly significant if there are time variations in $(Y + C)^*$, introduced perhaps by a video recorder. Each sampling should therefore occur within about 20 nanoseconds of its optimum position. In our experiments, however, this was not an insoluble problem.

In this article we have confined ourselves to PAL-system colour television signals and we have used sub-Nyquist sampling. However, it is relatively easy to adapt the CAROT method to the NTSC standard or to extend it for ratios of sampling rate to subcarrier frequency other than two.



a



b

Fig. 19. As in fig. 18, but now with bandwidth limitation to 1 MHz.

Summary. In the current colour television systems (PAL, NTSC, SECAM) a colour scene is converted into a single combined analog electrical signal (the composite signal); the quality is usually good. In this signal the colour information is mainly represented by the higher frequencies. Undesirable external effects such as bandwidth limitation and certain types of noise (in particular FM triangular noise) will therefore impair the colours disproportionately. In this respect the standard composite signal is consequently not very

'robust'. The CAROT method (Composite Analog Recoding by Orthogonal Transform) can effect a considerable improvement. By means of fairly simple digital operations this method produces a new and more robust analog composite signal. The method is described in this article for signals in the PAL system. Sub-Nyquist sampling is used; this has certain advantages but does not exclude other solutions. The CAROT method can also be adapted to the NTSC system.

A digital 'decimating' filter for analog-to-digital conversion of hi-fi audio signals

J. J. van der Kam

Introduction

The digital processing of audio signals offers many new prospects. Transmission, recording, adaptation of the frequency response to the characteristics of the human ear, compression and expansion of the dynamic range, the addition of reverberation to music^[1] — all this can be done by digital methods with less distortion, with a better signal-to-noise ratio and often more cheaply than by analog methods.

In 'professional' applications there is nothing new about this. In telephony, speech signals in digital form have been transmitted over long distances for many years. Now, however, digital techniques are increasingly penetrating the more consumer-oriented areas of hi-fi audio technology; a typical example is the Compact Disc^[2].

Before audio signals can be processed digitally they have to be converted from the analog form, in which they originated, into a digital form, by means of an analog-to-digital (A/D) converter. This conversion must not introduce any distortion or noise. The specifications for hi-fi audio here are stricter than for telephony, since the frequency bandwidth for hi-fi audio is much larger: 20 kHz as compared with only 3.4 kHz in telephony, and the signal-to-noise ratio required is very much higher than the 33 dB that is sufficient for telephony.

It was only with the advent of fast and very complex integrated circuits that it became possible to meet the special requirements that audio imposes on A/D conversion at an economic price. However, it is still necessary to select the best technique. This article gives prominence to one of the many different choices. It deals with the application to hi-fi audio of a concept that has already been applied successfully in telephony: A/D conversion via the intermediate stage of 1-bit coding^{[3]-[5]} at a very high sampling rate. The

1-bit coding stage is followed by a complex digital filtering operation in which the 1-bit coding is replaced, in our case, by a 16-bit coding and in which the sampling rate is reduced to a more manageable lower value.

Digital filters in which the sampling rate is reduced are known as 'decimating filters', even if the reduction factor has no clear relation to the number ten. The design of such a filter for hi-fi audio is the particular subject of this article. However, we should first look at the requirements to be met by an A/D converter and at the arguments in favour of the intermediate stage of a 1-bit coding.

Analog-to-digital conversion

Any form of A/D conversion consists of at least two operations:

- sampling, i.e. taking samples of the analog signal at regular intervals, and
- quantization, i.e. limiting the number of different values that the samples can assume so that each sample can be expressed in a digital word of a finite number of bits.

In sampling, the sampling theorem has an important part to play. This theorem states that the minimum sampling rate is equal to twice the highest frequency present in the analog signal. Conversely, at a given sampling rate the signal frequencies may not exceed half the sampling frequency to prevent the formation of distortion products ('aliasing').

Pulse-code modulation

The kind of digital signal most commonly encountered in audio technology is 16-bit pulse-code modulation (16-bit PCM). An audio signal then consists of a series of words (or pairs of words in the case of stereo) with each word consisting of 16 bits. This means that $2^{16} = 65\,536$ different signal values are available,

Ir J. J. van der Kam, formerly with Philips Research Laboratories, Eindhoven, is now with the Elcoma Division, Philips NPB, Eindhoven.

making high-quality audio possible. The highest signal frequency to be reproduced is usually 20 kHz. For the Compact Disc a sampling rate of 44.1 kHz was accordingly adopted, and in this article we shall adopt the same value.

The conversion of an analog audio signal into a PCM signal usually takes place in a circuit as represented in *fig. 1*. First, the bandwidth of the input signal is limited to about half the sampling rate. This is followed by sampling and quantization. The quantization circuit calculates the 16-bit word that most closely reproduces the value of each sample, e.g. by comparing each sample value with a set of reference voltages.

The three successive steps of the operations in *fig. 1* seem simple in principle, but are far more difficult in practice. For a start let us consider the lowpass input filter. If, as is usual in digital technology, the audio band is allowed to extend to 20 kHz at the usual sampling rate of 44.1 kHz, then the filter must have a flat characteristic up to 20 kHz and it must attenuate strongly above 24.1 kHz to prevent aliasing^[6]. (An original frequency component of say 24.5 kHz is 'aliased' as a result of sampling to $44.1 - 24.5 = 19.6$ kHz, i.e. to a position within the audio band where it appears as distortion.) This filter characteristic has to be realized with a filter for analog signals, i.e. in analog technology. This implies a high-order filter that requires accurate trimming, which will make it relatively expensive. A further difficulty is that such a filter will inevitably cause considerable phase shifts at some frequencies in the audio signal, so that certain waveforms will be distorted.

Very high precision is also required for the operations in the quantizer in *fig. 1*. Reproducible discrimination between the 65 536 voltage levels mentioned above, in a range of say -5 volts to $+5$ volts (corresponding to a quantization-step size of $153 \mu\text{V}$) requires an exceptionally stable circuit and very high precision in the voltage dividers.

An analog-to-digital converter of the kind we have described is very largely an *analog* circuit, and very complex. It would be much better if more of the operations required could be performed *digitally*.

The need for an input filter with a sharp cut-off (i.e. a narrow transition band) can be avoided by using a higher sampling rate. If, however, a digital signal at a given sampling rate is ultimately required — perhaps at 44.1 kHz as mentioned above — then an extra digital conversion must be provided to give this lower sampling rate. This then requires a filter that meets much the same specifications as the original analog input filter. Now, however, we are dealing with a digital filter, so that completely different rules apply:

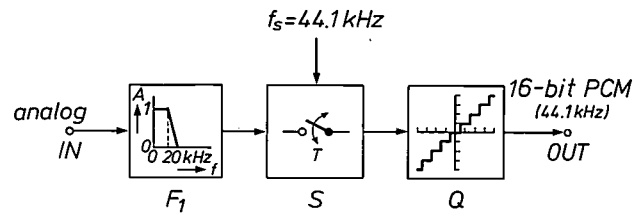


Fig. 1. Schematic diagram illustrating analog-to-digital conversion by 16-bit pulse-code modulation (16-bit PCM) with a sampling rate of $f_s = 44.1$ kHz. In the analog prefilter F_1 with amplitude characteristic A the frequency spectrum of the input signal is limited to about half the sampling rate, leaving the audio band, which extends up to 20 kHz, largely unaffected. In the sampling circuit S one sample is taken in every sampling interval $T = 1/f_s$. This sample is then quantized in the quantization circuit Q and translated into a 16-bit word.

the high precision required can now be obtained without accurate trimming of the filter. What is more, a digital filter can have a linear phase characteristic, so that there is no signal distortion, and it can be made as an integrated circuit.

1-bit coding

Another advantage of using a higher sampling rate is that fewer bits per sample are necessary in the quantization, especially in a circuit arrangement where the quantizer is included in a feedback loop^[7]. Indeed, it is even possible for each sample to be represented by only 1 bit. This is referred to as 1-bit coding: the most familiar example of this is delta modulation. The basic circuit diagram of a delta modulator is shown in *fig. 2*. Here the 1-bit coder consists simply of a subtracter, a clocked two-level quantizer (a 'decision circuit') and an integrator. The operation of the circuit can be understood in general terms from the signals a , d and \hat{a} shown in the diagram. The attraction of this coding is mainly due to its simplicity and the small number of critical components.

With 1-bit coding as an intermediate step an analog audio signal can be converted into a 16-bit PCM signal with a sampling rate of 44.1 kHz in a circuit as

- [1] E. H. J. Persoon and C. J. B. Vandenbulcke, Digital audio: examples of the application of the ASP integrated signal processor, this issue, pp. 201-216.
- [2] Special issue 'Compact Disc Digital Audio', Philips Tech. Rev. 40, 149-180, 1982.
- [3] L. D. J. Eggermont, M. H. H. Höfelt and R. H. W. Salters, A delta-modulation to PCM converter, Philips Tech. Rev. 37, 313-329, 1977.
- [4] D. J. G. Janssen and L. van de Meeberg, PCM codec with on-chip digital filters, Electron. Components & Appl. 2, 242-250, 1980.
- [5] J. J. van der Kam, A telephony codec using sigma-delta modulation and digital filtering, Proc. Conf. on Communications equipment and systems (IEE Conf. Publ. No. 209), Birmingham 1982, pp. 49-53.
- [6] See pages 135-136 in: A. W. M. van den Enden and N. A. M. Verhoeckx, Digital signal processing: theoretical background, Philips Tech. Rev. 42, 110-144, 1985.
- [7] R. J. Sluyter, Digitization of speech, Philips Tech. Rev. 41, 201-223, 1983/84.

shown in fig. 3. The analog prefilter F_2 is very much simpler than F_1 in fig. 1, since the filter specification is now far less strict, mainly because the transition band can now be much wider. The 1-bit coding with a sampling rate of $R \times 44.1$ kHz is followed by a digital filter F_3 and a 'sampling-rate decreaser' SRD . F_3 and

SRD form a decimating digital filter^[8] that supplies the required PCM signal. In this article we shall confine ourselves to the case $R = 72$, which means that the 1-bit coding takes place at a sampling rate of 72×44.1 kHz = 3175.2 kHz.

Sigma-delta modulation

Depending on the situation, the 1-bit coding in fig. 2 can be improved in various respects. In our application an important aspect is the inevitable quantization noise that is always produced in any A/D conversion, including 1-bit coding. We would prefer the quantization noise to be least in the audio band and immediately above it, because such noise cannot be removed, while quantization noise at higher frequencies (up to $0.5 \times 3.1752 = 1.5876$ MHz) can in principle be filtered out by F_3 (fig. 3). This 'noise shaping' can be achieved by sigma-delta modulation ($\Sigma\Delta M$ or $\Sigma\Delta M$)^[9].

A block diagram of a sigma-delta modulator is shown in fig. 4a. As can be seen, it closely resembles the 1-bit coder of fig. 2, but its exact operation is rather more difficult to illustrate. The noise shaping is determined by the integrating filter LF . In the choice of this filter care must be taken to ensure the stability of the complete circuit. To illustrate the noise shaping fig. 4b shows the amplitude characteristic of a possible filter LF and fig. 4c gives the frequency spectrum of the resultant quantization noise. The lowpass characteristic of LF gives the noise a 'highpass' character.

Further details of the sigma-delta modulator will not be given here. It is merely assumed that it delivers a series of bits at the repetition rate mentioned above. We now have to consider how a digital decimating filter uses it to produce a series of 16-bit words with a repetition rate of 44.1 kHz, yet without adding impermissible noise or causing distortion during the transformation process.

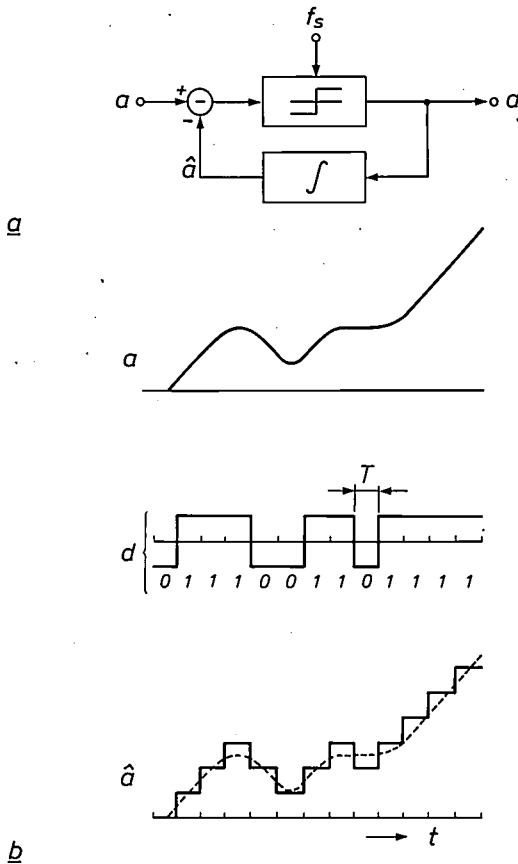


Fig. 2. a) Schematic diagram of a delta modulator, consisting of a subtracter, decision circuit and integrator. b) The analog signal a is converted into a bit stream d in the delta modulator; d represents a digital signal consisting of 1-bit words with a sampling rate of $f_s = 1/T$. Integrating d gives a stepped signal \hat{a} that is a good approximation to a . The decision circuit operates on the difference signal $a - \hat{a}$.

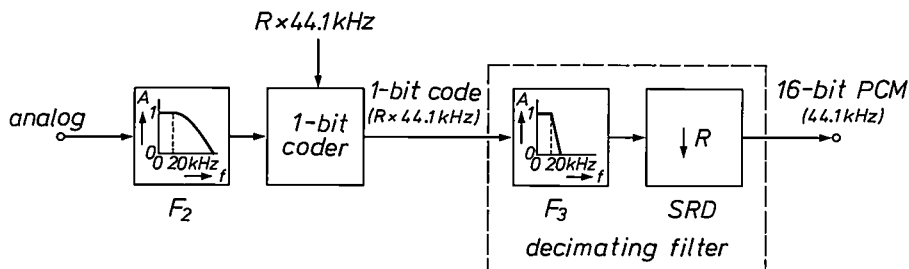


Fig. 3. Schematic diagram illustrating analog-to-digital conversion with 1-bit coding at a high sampling rate as an intermediate stage. The specification for the analog prefilter F_2 is far less strict than that for F_1 in fig. 1. The output signal of the 1-bit coder can now be converted by digital methods alone into a 16-bit PCM signal with a sampling rate of 44.1 kHz. This is done by means of a decimating filter, which consists in principle of a lowpass digital filter F_3 and a sampling-rate decreaser SRD .

The decimating filter

The first task of the digital decimating filter, which follows the sigma-delta modulator, is to suppress frequencies above the audio band, i.e. higher than 20 kHz. In the context of fig. 1 we have already discussed the necessity of suppressing these frequencies in direct A/D conversion. It is just as necessary in the present arrangement, where the ultimate sampling rate of 44.1 kHz is achieved in a roundabout way. Ideally, the digital filter F_3 should have the amplitude

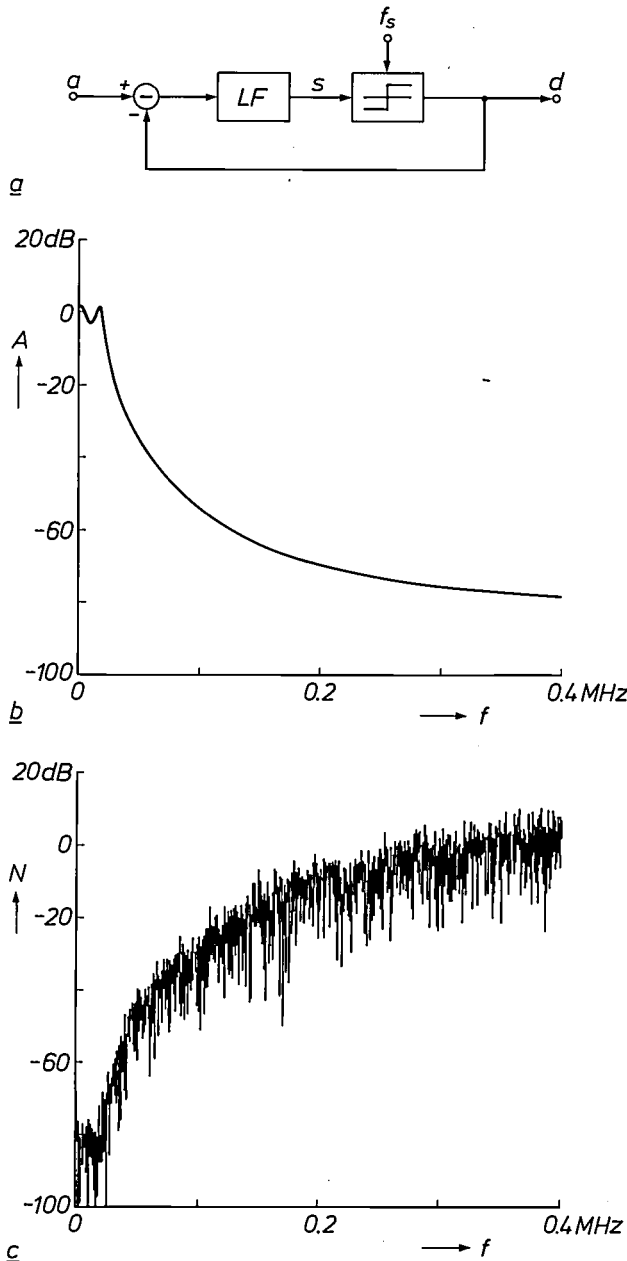


Fig. 4. a) Schematic diagram of a sigma-delta modulator consisting of a subtracter, a lowpass filter LF and a decision circuit. The rectangular output signal d is now directly subtracted from the analog input signal a (see fig. 2). s input signal of the decision circuit. b) Typical amplitude characteristic A of the filter LF . c) Corresponding power-density spectrum N of the quantization noise in the signal d , when a is a sinusoidal signal at 990 Hz and the sampling rate f_s is 3.1752 MHz. (For clarity the frequency scale is only shown from 0 to 0.4 MHz.)

characteristic shown in fig. 5: a passband with a gain of 1 from 0 Hz to 20 kHz, an infinitely narrow transition band at 20 kHz and complete suppression in the stopband between 20 kHz and 1.5876 MHz (half the sampling rate).

The stopband

Apart from the fact that the filter in fig. 5 cannot be realized (since it would require an infinitely large number of filter coefficients and infinitely high accuracy for the coefficient values), we do not strictly speaking need it, since the measure for the required quality of the ultimate 16-bit PCM signal is the direct conversion in fig. 1. This means for one thing that the maximum signal-to-noise ratio for a digitized sinusoidal signal need never be more than 98 dB. From this we may deduce a specification for the attenuation in the stopband of the digital filter F_3 . To start with we shall use a number of approximations. In the first place we assume that the noise shaping of the 1-bit coding is perfect, i.e. all the quantization noise is located in the frequency range above the audio band. In the second place we consider the largest sinusoidal input signal that does not saturate the decision circuit in the sigma-delta modulator (fig. 4), so that the peak value of the input signal s is equal to the peak value of the signal d (fig. 6). For the time being we put both at 1 volt. Ap-

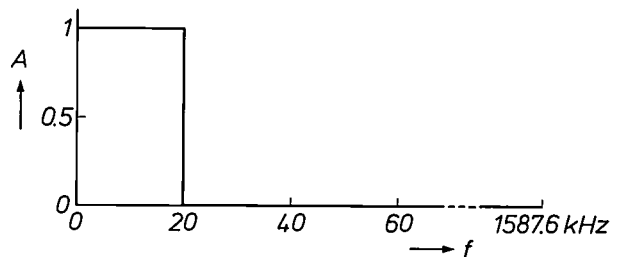


Fig. 5. Ideal amplitude characteristic A of the lowpass digital filter F_3 in fig. 3.

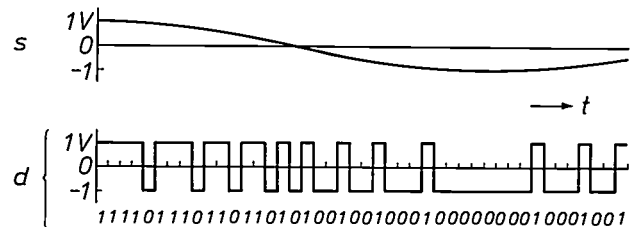


Fig. 6. Determining the signal-to-noise ratio in the output signal of a sigma-delta modulator with the decision circuit just below saturation. The sinusoidal input signal s of the decision circuit then has the same peak value as the output signal d . The total power of d is twice that of s . This means that the signal power and the noise power in d are identical. The signal-to-noise ratio is thus 0 dB.

[8] See pages 136-139 in [6].
 [9] B. P. Agrawal and K. Shenoi, Design methodology for $\Sigma\Delta M$, IEEE Trans. COM-31, 360-369, 1983.

plied across a hypothetical load resistance of 1 ohm the signal s then represents a power of 0.5 watt and the signal d a power of 1 watt. Of this 1 watt, 0.5 watt represents signal power and 0.5 watt represents noise power. The signal d therefore now has a signal-to-noise ratio of 0 dB (where the noise in the full frequency band up to half the sampling rate is taken into account).

With these simplifying assumptions we can achieve the ultimately required maximum signal-to-noise ratio of 98 dB by specifying for the filter F_3 a stopband attenuation of 98 dB over the complete bandwidth of 20 kHz up to 1.5876 MHz (fig. 7a).

The transition band

The filter characteristic in fig. 7a also cannot be realized because of the sharp transition from passband to stopband. In a practical filter a certain bandwidth will always have to be reserved for this. This has two consequences for the 16-bit PCM output signal:

- the quantization noise in the transition band is less strongly attenuated, and
- frequency components of the input signal of the A/D converter that fall within the part of the transition band above 22.05 kHz will be aliased to frequencies below 22.05 kHz.

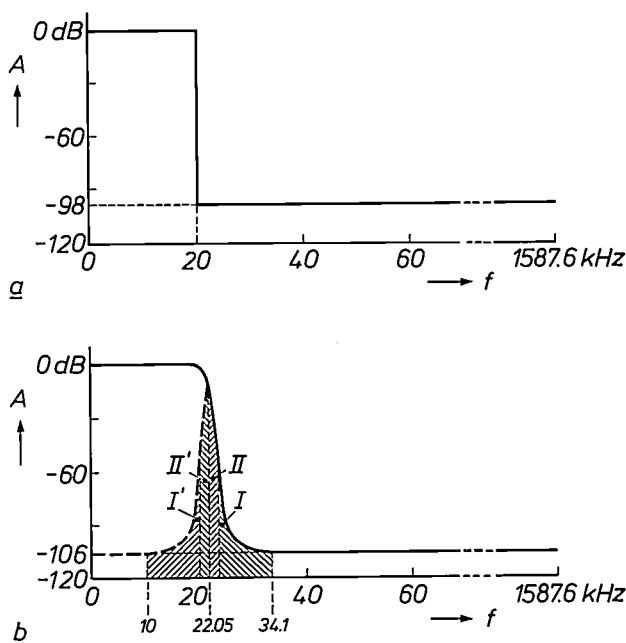


Fig. 7. a) The attenuation in the stopband of the filter F_3 in fig. 3 does not have to be infinite. With an infinitely narrow transition band and 'perfect' noise shaping an attenuation of 98 dB is sufficient. b) Amplitude characteristic used for our filter F_3 . The transition band extends from 20 kHz to 34.1 kHz, so that aliasing can occur in the 16-bit PCM signal, which has a sampling rate of 44.1 kHz. This is indicated by the hatching. A distinction is made here between aliasing products that appear in the audio band ($I-I'$) and aliasing products that are outside it ($II-II'$). To avoid an increase in the total noise power, the required stopband attenuation is increased to 106 dB.

Input frequencies between 22.05 kHz and 24.1 kHz are aliased to between 22.05 kHz and 20 kHz, i.e. above the audio band (fig. 7b). As long as they are not too strong they will cause no interference. But even a cut-off band of 20 kHz to 24.1 kHz would give an impractically complicated filter, since both the number of filter coefficients and the accuracy required (i.e. the number of bits) would be excessively high. To obtain a realizable filter (although still a very complex one) yet another concession to the original specification is required: input frequencies above 24.1 kHz are indeed aliased into the audio band, but to a limited extent this is acceptable because the sensitivity of the ear to frequencies between 10 kHz and 20 kHz is weak at low levels.

On the basis of all these considerations we opted for a filter with a transition band from 20 kHz to 34.1 kHz (fig. 7b). Above about 22 kHz the attenuation first increases rapidly and then rather less rapidly up to 106 dB. The increased stopband attenuation compared with fig. 7a serves to compensate for the quantization noise in the transition band and for the noise shaping, assumed to be perfect, in the 1-bit coding. Another factor that we have not yet taken into account is that the necessary limitation of the word length of the output signal of the decimating filter to 16 bits itself limits the maximum signal-to-noise ratio to 98 dB. For this reason also a greater attenuation is required in the stopband than is suggested in fig. 7a.

The passband

In the passband from 0 Hz to 20 kHz some ripple in the amplitude characteristic is acceptable; this is also a relaxation of the filter specifications. We decided to limit the ripple to ± 0.2 dB. To make the phase characteristic linear as well we decided to use a transversal digital filter (we shall return to this in the next section). In view of all the requirements that the filter characteristic had to satisfy, as many as 2304 filter coefficients were required. It was mainly because we represented the input signal by a 1-bit code and used a decimating filter that we were able to realize this digital filter with only two ICs, as will appear later.

Practical design of the filter

Structure of the filter

In the practical design of a digital filter it is always necessary to choose between a recursive structure and a non-recursive structure. In a recursive filter the signal samples are fed back from at least one point in the filter, via delays and possible multiplications, to a point closer to the input. In our case the input samples consist of only one bit. All that is necessary to delay

them are 1-bit memory cells (bistables or flip-flops). However, the signal samples that appear as intermediate results and at the output of our filter have a much greater word length (16 bits and more) and therefore require much more elaborate memory cells for producing delays. It is therefore better to choose a filter structure in which only input samples are delayed. Such a structure is found in non-recursive filters of the transversal type. With filters of this type it is also easy to take advantage of the fact that the output samples have a lower sampling rate than the input samples.

The structure that our digital filter took will be explained in a number of steps, which are illustrated in *fig. 8*. *Fig. 8a* shows a transversal filter in its most familiar form. After each unit-delay element T , which corresponds to one sampling interval for the input signal, the delayed signal sample is tapped off and applied to a multiplier, where it is multiplied by a coefficient. The products are then added to form a total sum. In our case, however, each input sample is only 1 bit long and represents either $+1$ or -1 . The multiplication is therefore simplified to an operation on the sign and the total sum is arrived at by the addition and subtraction of coefficients. It will be obvious that this speeds up the processing procedure very considerably and that it is a definite advantage of using the 1-bit code as the first phase of the A/D conversion.

All the possible combinations that can be obtained by adding together N coefficients or subtracting them from each other in a transversal filter together form a finite set of numbers with at most 2^N different values. Each output sample of the filter is an element of this set, but always a different one, depending on the last N input samples. The filter can now be arranged in such a way that this sum does not have to be recalculated every time, because all the possible results are already stored in a read-only memory (ROM). The last N bits of the input signal are then treated as the address of the memory location where the relevant result is stored (*fig. 8b*).

It is of course also possible to make combined forms of *fig. 8a* and *b*, drastically reducing the number of additions, although not to zero, while at the same time substantially reducing the number of memory locations required in the ROM. *Fig. 8c* shows such an arrangement, which requires two ROMs each with $2^{N/2}$ memory locations (instead of 2^N in *fig. 8b*) and one addition per output sample.

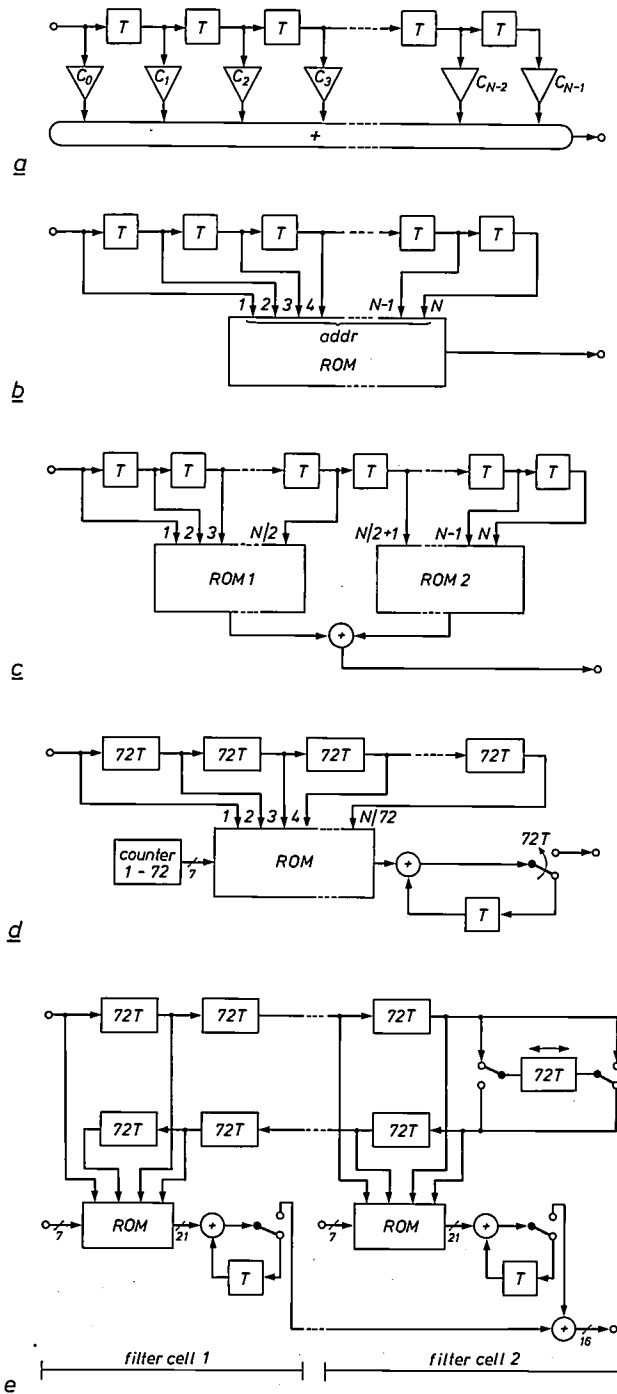


Fig. 8. Derivation of the structure of the decimating filter. *a*) Transversal filter in its basic form. T unit-delay element. c_0, c_1, \dots, c_{N-1} filter coefficients. *b*) The 1-bit words at the taps of the delay elements can be treated as one large N -bit address word *addr*. This can be used to address a read-only memory (ROM) in which all the possible (i.e. 2^N) values of the output signal are already preprogrammed and stored. No further calculation is therefore required. *c*) Combination of the two previous structures: the total number of ROM addresses is $2 \times 2^{N/2}$, and one addition is required per output sample. *d*) Since the sampling rate has been decreased by a factor of 72, the calculation of each output sample can take place in 72 successive steps. These are counted by a '72-counter'; the 72 results are added together in an adder circuit with a feedback loop. The number of ROM addresses is now $72 \times 2^{N/72}$. *e*) The filter has a symmetrical impulse response and hence a symmetrical set of coefficients. By 'folding in two' the row of delay elements, the 1-bit words that have to be multiplied by the same coefficient come close to one another. In this diagram the sampling rate is reduced by a factor of 72 and the ROM is divided into smaller units that are each addressed by only four 1-bit words. This produces filter cells, two of which are shown here.

The transversal structures outlined are not the complete answer, however. We have still taken no advantage of the fact that what we are finally aiming at is a decimating filter with a decimation factor of 72. This means that we do not have to generate a new output sample after every input bit, but only after every 72 input bits. We can use this for calculating the output sample in 72 steps and then adding the 72 results together successively.

This can be done in the way shown in fig. 8d. We now have delay circuits (shift registers) that can contain 72 input bits. The number of taps has been reduced from N to $N/72$. With a '72-counter' a cycle of 72 subsets of ROM addresses is counted. The counter uses a 7-bit address for this. The total number of ROM addresses is $72 \times 2^{N/72}$. An adder with a feedback loop and a switch that substitutes a connection to the output instead of the feedback once every $72T$ provide the output samples at the reduced sampling rate. But even with the arrangement in fig. 8d we have still not arrived at our final structure.

We have already mentioned that the transversal digital filter can have a linear phase characteristic — a feature that gives it an advantage over a conventional filter in analog technology. It can be shown that a transversal filter with a linear phase characteristic and a lowpass amplitude characteristic has a symmetrical impulse response (fig. 9). This implies that the row of coefficients c_0, c_1, \dots, c_{N-1} is symmetrical: the first coefficient and the last are identical, the second and the next-to-last are identical, and so on. Consequently the number of coefficients with a different value is halved. We take advantage of this feature to obtain a further improvement in the design of our filter. We do this by 'folding the filter in two'. This is illustrated in fig. 8e, which also shows the division into sub-ROMs in accordance with fig. 8c and the decimation as in fig. 8d. The two input bits, which always have to be multiplied by the same coefficient,

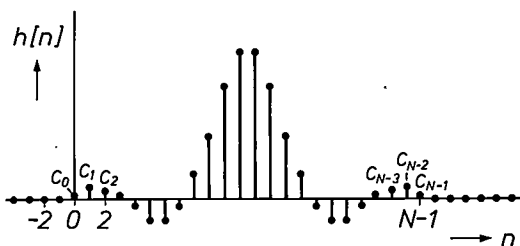


Fig. 9. Example of a symmetrical impulse response $h[n]$ of a digital lowpass filter with a linear phase characteristic. Since the successive coefficients of a transversal filter correspond exactly to the successive sample values of the impulse response, the coefficients are also symmetrical, i.e. $c_i = c_{N-1-i}$ for $i = 0, 1, 2, \dots, N-1$.

therefore come close together and serve as address bits for the same sub-ROM.

Halfway through the filter, i.e. 'on the fold', a special step has to be taken. The groups of 72 bits have to reverse direction at this point to preserve the symmetry of the operation. They are therefore entered into a shift register and extracted backwards ('last in, first out'), like a train reversing out of a terminus. In the final version of our filter we use eight sub-ROMs, which together with four shift registers each with a delay of $72T$, and a few other subsidiary circuits, form a unit or 'filter cell'. Seven of these filter cells are identical, and the eighth is slightly different because of the 'last in, first out' effect. We shall now describe one filter cell in rather more detail.

The filter cell

The operations in a filter cell (fig. 10) involve four input bits b_1, b_2, b_3, b_4 , each of which may represent the value +1 or -1. There can therefore be a total of $2^4 = 16$ different combinations of bits. The four bits address the ROM, which is required to give the output signal $r = c_1(b_1 + b_2) + c_2(b_3 + b_4)$; c_1 and c_2 are two filter coefficients from a linear-phase filter. The remarkable thing here is that there are only nine possible different results for r . If we look at its absolute value, we are concerned with only four numbers, different from zero, which must be available to sufficient accuracy and must therefore be present in the memory. These have the values $|2c_1|, |2c_2|, |2c_1 + 2c_2|$ and $|2c_1 - 2c_2|$. In this way valuable memory space can be saved. Each of the numbers still has to be given the correct sign, and it is also possible for the result to be

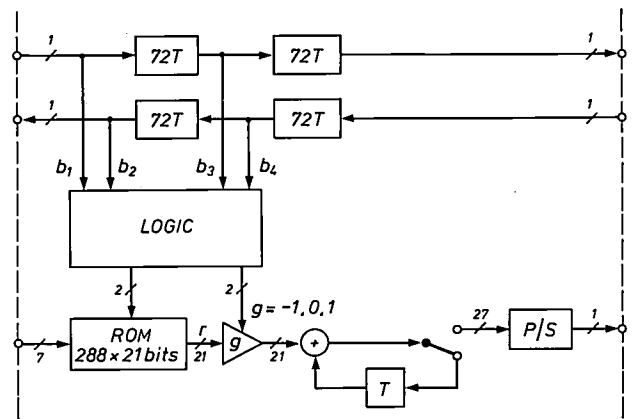


Fig. 10. More detailed diagram of a filter cell. Although the four bits b_1, b_2, b_3, b_4 can form sixteen different combinations, the corresponding ROM contents r can assume only nine different values. One of these is zero and the others are in pairs differing only in sign. For every 4-bit combination the LOGIC circuit therefore calculates a 2-bit address for the ROM plus a multiplication constant $g = -1, 0$ or 1. P/S parallel/series converter.

zero. This can all be taken as an extra multiplication by $g = -1, 0$ or 1 . The value of g is separately derived from the four bits b_1, b_2, b_3, b_4 by a logic circuit.

As we have seen in fig. 8d, our decimating filter uses a 72-counter that selects one of the 72 subsets in the ROM by means of a 7-bit address. Altogether the ROM of each filter cell must therefore contain

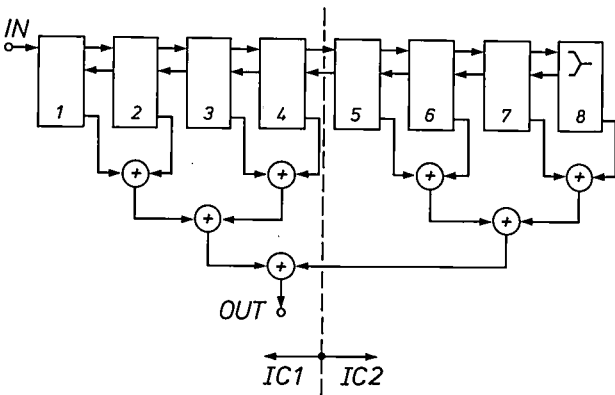


Fig. 11. Our decimating filter consists of eight filter cells arranged on two chips IC1 and IC2. The outputs of the filter cells are added in pairs to give a final result OUT.

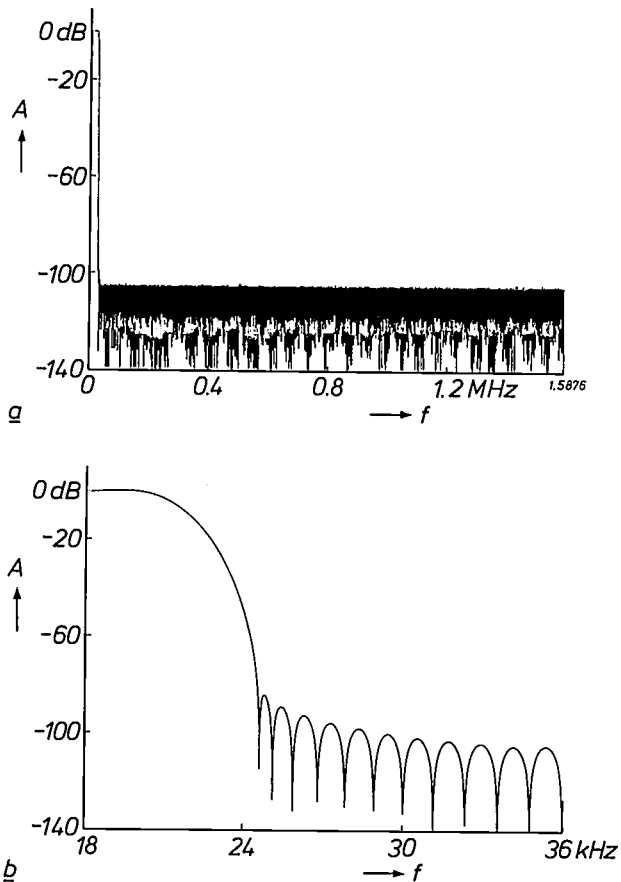


Fig. 12. Computer-calculated amplitude characteristic of the filter F_3 from fig. 3, with 2304 coefficients and the coefficient values rounded off to 21 bits, a) between 0 Hz and 1.5876 MHz, and b) on an expanded scale between 18 kHz and 36 kHz. (See also fig. 7b.)

$72 \times 4 = 288$ numbers r . Each number r in the ROM consists of a word of 21 bits. The ROM of the filter cell therefore has a capacity of $288 \times 21 = 6048$ bits. In the calculation of each output sample 72 of the 21-bit words are always added together in an adder circuit with a feedback loop, which, in this case, makes an extra addition width of 6 bits necessary to prevent overflow. The adder is thus 27 bits wide. After every period of $72T$ the total is passed in parallel to a shift register and the adder is reset to zero. The same signal also resets the memory counter to its initial state, and a new cycle starts. Meanwhile the output register is read out serially.

The same thing happens in the other cells of the filter and the results are added up two by two (fig. 11). Because of the serial read-out serial adders can be used, which require relatively little hardware. In three steps of addition a final result is thus obtained, which is then rounded off to 16 bits.

Use of the computer for design and simulation

After the choice of the filter structure — in our case the transversal filter — an important task is to calculate the coefficients. Computer programs for this are available^[10]. We have made use of these and we have also written some supplementary programs for showing the impulse response of a filter that has been calculated and for determining the frequency response. A special program does the same thing for decimating filters, with choice of value for the decimation factor.

The resulting filter-software package would not have been complete without a program that calculates the effect of the finite word length of the coefficients on the filter characteristics. We have added such a program; the number of bits in which the coefficients are expressed can be input as required.

Fig. 12 shows the amplitude characteristic of the filter F_3 in fig. 3 as calculated by the computer; fig. 12a shows the entire frequency range up to half the sampling rate, and fig. 12b shows the transition band and the closely adjacent range with an expanded frequency scale. The 2304 coefficient values are rounded off to 21 bits here.

Integration of the complete filter on two chips

Experimental ICs of the decimating filter were made. Because of its size, the filter divided between two integrated circuits (chips). Each chip contains four of the eight filter cells. The signal goes from chip 1 to

[10] J. H. McClellan, T. W. Parks and L. R. Rabiner, A computer program for designing optimum FIR linear phase digital filters, IEEE Trans. AU-21, 506-526, 1973.

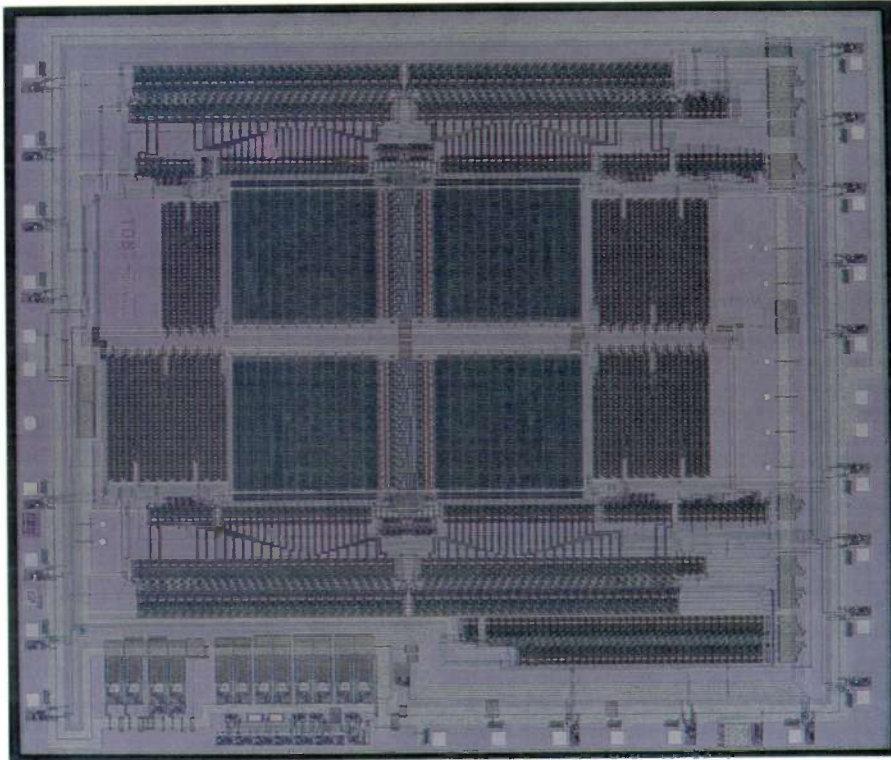


Fig. 13. Experimental chip of the decimating filter in NMOS technology. The chip shown here contains the second half of the filter (the second four filter cells, including the reversal cell). The four central fields are the ROMs in which the required combinations of filter coefficients are stored. The first half is contained on another chip; each chip has an area of 50 mm^2 . They were made by the 'N 700' process. The minimum detail size is $4 \mu\text{m}$.

chip 2, changes direction, goes through chip 2 again and then on to chip 1. Fig. 13 shows a photograph of chip 2, which contains the reversal stage. The four fields in the middle are four ROMs.

The area of each chip is about 50 mm^2 . They are produced in NMOS technology with smallest details of $4 \mu\text{m}$ in a process in which the thickness of the oxide beneath the gate electrode of the transistors is 70 nm .

Summary. For analog-to-digital conversion of audio signals with no loss of hi-fi quality, it can be advantageous to first use sigma-delta modulation to convert the audio signal into a 1-bit signal with a high sampling rate, and then to convert the result into the required 16-bit signal by means of a 'decimating' transversal digital filter. The requirements for the analog prefiltering of the audio signal then become far less stringent and the problems are mainly shifted to the digital domain. A large digital filter that meets the requirements has been integrated on two chips; it has 2304 coefficients and decreases the sampling rate from 3.1752 MHz to 44.1 kHz . Computer programs were used for calculating the filter coefficients, the resulting frequency response and the irregularities that occur on rounding off the coefficients to a limited number of bits (21).

Scientific publications

These publications are contributed by staff of laboratories and plants that form part of or cooperate with enterprises of the Philips group of companies; particularly by staff of the research laboratories mentioned below. The publications are listed alphabetically by journal title.

Philips GmbH Forschungslaboratorium Aachen, Weißhausstraße, 5100 Aachen, Germany		A		
Philips Research Laboratory, Brussels, 2 avenue Van Becelaere, 1170 Brussels, Belgium		B		
Philips Natuurkundig Laboratorium, Postbus 80 000, 5600 JA Eindhoven, The Netherlands		E		
Philips GmbH Forschungslaboratorium Hamburg, Vogt-Kölln-Straße 30, 2000 Hamburg 54, Germany		H		
Laboratoires d'Electronique et de Physique Appliquée, 3 avenue Descartes, 94450 Limeil-Brévannes, France		L		
Philips Laboratories, N.A.P.C., 345 Scarborough Road, Briarcliff Manor, N.Y. 10510, U.S.A.		N		
Philips Research Laboratories, Cross Oak Lane, Redhill, Surrey RH1 5HA, England		R		
Philips Research Laboratories, Sunnyvale P.O. Box 9052, Sunnyvale, CA 94086, U.S.A.		S		
E. Roaux, J. C. Richard & C. Piaget L	Third-generation image intensifier	Adv. Electron. & Electron Phys. 64A	71-75	1985
D. Washington, A. J. Guest & A. G. Knapp R	A large-area electron image multiplier	Adv. Electron. & Electron Phys. 64A	101-110	1985
J. P. Boutot (<i>Hyperelec, Brive</i>), R. Goret, M. Jatteau, J. Paulin & J. C. Richard L	Diode intensifier tube with fast phosphor screen	Adv. Electron. & Electron Phys. 64A	113-122	1985
M. Lemonier, C. Piaget & M. Petit L	Thinned backside-bombarded RGS-CCD for electron imaging	Adv. Electron. & Electron Phys. 64A	257-265	1985
B. Jean*, J. P. Boutot* (* <i>Hyperelec, Brive</i>), V. Duchenois & R. Polaert L	High-resolution and large size wafer microchannel image intensifier	Adv. Electron. & Electron Phys. 64B	315-322	1985
V. Duchenois, M. Fouassier & C. Piaget L	High-resolution luminescent screens for image intensifier tubes	Adv. Electron. & Electron Phys. 64B	365-371	1985
W. Schreiner & T. Fawcett (<i>Dow Chemical, Midland, MI</i>) N	Results of a round robin study of systematic errors found in routine X-ray diffraction raw data	Adv. X-ray Anal., Vol. 28, C. S. Barret <i>et al.</i> (eds), Plenum, New York	309-314	1985
A. Giakoumis*, J. Michel* (* <i>RTC, Limeil-Brévannes</i>), V. Pauker & M. Binet L	Amplificateurs GaAs monolithiques à large bande et gain élevé	Ann. Télécommun. 40	127-134	1985
D. Visser, T. G. Gijsbers & R. A. M. Jorna E	Molds and measurements for replicated aspheric lenses for optical recording	Appl. Opt. 24	1848-1852	1985
J. J. M. Braat, A. Smid & M. M. B. Wijnakker E	Design and production technology of replicated aspheric objective lenses for optical disk systems	Appl. Opt. 24	1853-1855	1985
J. H. Neave, P. J. Dobson, B. A. Joyce & J. Zhang (<i>Imp. College, London</i>) R	Reflection high-energy electron diffraction oscillations from vicinal surfaces — a new approach to surface diffusion measurements	Appl. Phys. Lett. 47	100-102	1985
P. Blood, E. D. Fletcher & K. Woodbridge R	Dependence of threshold current on the number of wells in AlGaAs-GaAs quantum well lasers	Appl. Phys. Lett. 47	193-195	1985
P. R. Locher E	NMR imaging methods seen as trajectories in the reciprocal space	Bull. Magn. Resonance 6	140-141	1984
P.-J. Courtois B	On time and space decomposition of complex structures	Commun. ACM 28	590-603	1985
W. Tolksdorf H	Flux growth technology	Crystal growth of electronic materials, E. Kaldis (ed.), Elsevier Science, Amsterdam	175-182	1985

D. Mateika	H	Substrates for epitaxial garnet layers: crystal growth and quality	Curr. Top. Mater. Sci., Vol. 11, E. Kaldis (ed., Elsevier Science, Amsterdam)	151-239	1984
P. Delsarte & P. Piret	B	An extension of an inequality by Ahlswede, El Gamal and Pang for pairs of binary codes	Discrete Math. 55	313-315	1985
C. Venet & P. Baudet	L	2-20 GHz hybrid GaAs MESFET distributed amplifier	Electron. Lett. 21	376-377	1985
M. J. M. Pelgrom, J. Herrmann, H. P. van Gijn & F. W. P. Vreeswijk	E	Compact noise-reduction system for quasistatic TV pictures	Electron. Lett. 21	766-768	1985
R. Woltjer, J. Mooren, J.-P. André & G. Weimann (<i>Deutsche Bundespost, Darmstadt</i>)	E, L	Four-terminal Quantum Hall and Shubnikov-De Haas measurements with pulsed electric fields	Festkörperprobleme 25	419-427	1985
A. Comberg	A	Bessere Katodenstrahlröhren in Sicht	Funkschau 57 (No. 11)	43-46	1985
P. C. M. Gubbens*, A. M. van der Kraan* (* <i>Interuniv. Reactor Inst., Delft</i>) & K. H. J. Buschow	E	Quadrupole splitting observed in some cubic Tm compounds by ^{169}Tm Mössbauer spectroscopy	Hyperfine Interactions 15/16	721-724	1983
R. S. Soin & P. J. Rankin	R	Efficient tolerance analysis using control variates	IEE Proc. G 132	131-142	1985
T. N. Saadawi & M. Schwartz	N	Distributed switching for data transmission over two-way CATV	IEEE J. SAC-3	323-329	1985
V. Rumennik	N	Power devices are in the chips	IEEE Spectrum 20 (No. 7)	42-48	1985
E. Bolte	A	Current displacement of a solid cylindrical conductor placed in a semiclosed slot, taking into account the leakage field in the gap	IEEE Trans. MAG-20	2150-2156	1984
M. Jatteau	L	ASIT gamma-ray camera: a new camera head provided with an array of scintillation intensifier tubes	IEEE Trans. NS-32	1225-1231	1985
M. Hartmann, P. Hansen & P. Willich	H	Magnetic and magneto-optical properties of amorphous GdFePb films	J. Appl. Phys. 56	2870-2873	1984
J.-P. Krumme, V. Doormann & P. Willich	H	Bismuth iron garnet films prepared by rf magnetron sputtering	J. Appl. Phys. 57	3885-3887	1985
H. Yokoyama (<i>Electrotech. Lab., Sakura-mura, Ibaraki</i>) & H. A. van Sprang	E	A novel method for determining the anchoring energy function at a nematic liquid crystal-wall interface from director distortions at high fields	J. Appl. Phys. 57	4520-4526	1985
A. J. van Roosmalen, W. G. M. van den Hoek & H. Kalter	E	Electrical properties of planar rf discharges for dry etching	J. Appl. Phys. 58	653-658	1985
G. J. van Gorp, P. J. de Waard & F. J. du Chatenier	E	Thermomigration in indium and indium alloy films	J. Appl. Phys. 58	728-735	1985
D. R. Wolters & J. J. van der Schoot	E	Kinetics of charge trapping in dielectrics	J. Appl. Phys. 58	831-837	1985
C. A. M. de Vries & W. G. M. van den Hoek	E	Validity of self-bias voltage measurements on insulating electrodes in radio-frequency dry etching systems	J. Appl. Phys. 58	2074-2076	1985
C. Ronse	B	An isomorphism for digital images	J. Comb. Theory A 39	132-159	1985
P. M. Frijlink, J. P. André & J. L. Gentner	L	Very narrow interface multilayer III-V heterostructures by organometallic vapor phase epitaxy	J. Cryst. Growth 70	435-443	1985
P. Capper*, J. J. G. Gosney*, C. L. Jones*, I. Kenworthy* (* <i>Mullard, Southampton</i>) & J. A. Roberts	R	Acceptor doping of Bridgman-grown $\text{Cd}_x\text{Hg}_{1-x}\text{Te}$	J. Cryst. Growth 71	57-65	1985
N. Vodjdani, M. Erman & J. B. Theeten	L	Structural analysis and optical characterization of low loss GaAs waveguides fabricated by selective epitaxy	J. Cryst. Growth 71	141-148	1985
J. H. N. van Vucht	E	On the crystal structures of some compounds of gallium with potassium, rubidium and caesium	J. Less-Common Met. 108	163-175	1985
K. H. J. Buschow, H. M. van Noort & D. B. de Mooij	E	Magnetic and structural properties of $\text{Nd}_2\text{Fe}_{14}\text{B}$, $\text{Th}_2\text{Fe}_{14}\text{B}$, $\text{Nd}_2\text{Co}_{14}\text{B}$ and related materials	J. Less-Common Met. 109	79-91	1985
D. B. de Mooij & K. H. J. Buschow	E	The crystal structure of Eu_3Ga_8	J. Less-Common Met. 109	117-122	1985

K. H. J. Buschow	E	Amorphous alloys	J. Less-Common Met. 110	205-223	1985
P. C. M. Gubbens*, A. M. van der Kraan* (* Interuniv. Reactor Inst., Delft) & K. H. J. Buschow	E	Spin lattice relaxation in TmNi ₅ above its Curie temperature	J. Magn. & Magn. Mater. 50	199-204	1985
A. J. E. M. Janssen	E	Bilinear phase-plane distribution functions and positivity	J. Math. Phys. 26	1986-1994	1985
C. A. M. Mulder, R. K. Janssen, P. Bachmann & D. Leers	E, A	Micro-Raman spectroscopy of fluorine-doped PCVD silica fibre preforms	J. Non-Cryst. Solids 72	243-248	1985
H. J. Cornelissen	E	Measurement of the diffusion coefficient of sodium in neon at 530 K	J. Phys. B 18	3445-3455	1985
J. Woodhead (Toshiba Res. & Dev. Centre, Kawasaki City), R. C. Newman*, A. K. Tipping* (* Univ. Reading), J. B. Clegg, J. A. Roberts & I. Gale	R	Calibration of the infrared absorption due to silicon in gallium arsenide	J. Phys. D 18	1575-1583	1985
W. J. A. Goossens	E	The smectic A — smectic C phase transition: sense and nonsense	J. Physique 46	1411-1415	1985
B. Knör & W. Tolksdorf	H	Lattice parameters and misfits of gallium garnets and iron garnet epitaxial layers at temperatures between 294 and 1300 K	Mater. Res. Bull. 19	1507-1513	1984
J. B. Theeten, S. Gourrier, P. Friedel, M. Taillepied, D. Arnoult & D. Benarroche	L	Plasma passivation scheme for III-V compound semiconductor surfaces	Mater. Res. Soc. Symp. Proc. 38	499-510	1985
H. Baumgart & F. Philipp (Max Planck Inst., Stuttgart)	N	High-voltage electron microscopy investigation of subgrain boundaries in recrystallized silicon-on-insulator structures	Mater. Res. Soc. Symp. Proc. 35	593-598	1985
K. A. Vissers	E	MILSIM: A high level digital simulator	Microcomputers, usage and design, K. Waldschmidt & B. Myrhaug (eds), Elsevier Science, Amsterdam	201-210	1985
H. A. van Sprang & R. G. Aartsen	E	Torsional anchoring of 5CB and 5PCH on various substrates	Mol. Cryst. & Liq. Cryst. 123	355-368	1985
P. van de Weijer & R. M. M. Cremers	E	The pulsed optogalvanic effect in a low-pressure mercury discharge induced by optical pumping on the 408 nm line	Opt. Commun. 54	273-276	1985
E. H. L. Aarts & P. J. M. van Laarhoven	E	Statistical cooling: a general approach to combinatorial optimization problems	Philips J. Res. 40	193-226	1985
K. H. J. Buschow, D. B. de Mooij & H. M. van Noort	E	The Fe-rich isothermal section of Nd-Fe-B at 900 °C	Philips J. Res. 40	227-238	1985
J. M. Shannon	R	A comparison between bulk unipolar diodes and Schottky barriers	Philips J. Res. 40	239-258	1985
R. Memming	H	Kinetic aspects in photoelectrochemical solar cells	Photoelectrochemistry, photocatalysis and photoreactors, M. Schiavello (ed.), Reidel, Dordrecht	107-153	1985
P. Hansen, C.-P. Klages, J. Schuldt & K. Witter	H	Magnetic and magneto-optical properties of bismuth-substituted lutetium iron garnet films	Phys. Rev. B 31	5858-5864	1985
M. F. H. Schuurmans & G. W. 't Hooff	E	Simple calculations of confinement states in a quantum well	Phys. Rev. B 31	8041-8048	1985
G. Martens, P. Rabe (Univ. Kiel) & P. Wenck (URW, Hamburg)	H	Destructive interference and multiple scattering effects observed in Ca K-edge EXAFS spectra	Phys. Stat. Sol. a 88	103-111	1985
P. C. M. Gubbens*, A. M. van der Kraan* (* Interuniv. Reactor Inst., Delft) & K. H. J. Buschow	E	¹⁶¹ Dy Mössbauer effect in Dy ₂ Fe ₁₄ B	Phys. Stat. Sol. b 130	575-580	1985
P. C. M. Gubbens*, A. M. van der Kraan* (* Interuniv. Reactor Inst., Delft) & K. H. J. Buschow	E	Dynamic lattice distortions in cubic TmCu ₅ at low temperatures?	Physica 130B	415-417	1985

P. C. M. Gubbens*, A. M. van der Kraan* (* <i>Interuniv. Reactor Inst., Delft</i>) & K. H. J. Buschow <i>E</i>	TmB ₁₂ : another singlet-triplet induced moment system	Physica 130B	412-414	1985
K. H. J. Buschow, J. W. C. de Vries* & R. C. Thiel* (* <i>Univ. Leiden</i>) <i>E</i>	Note on the crystal field induced magnetic anisotropy in several permanent magnet materials	Physica 132B	13-16	1985
U. Enz <i>E</i>	The sine-Gordon breather as a moving oscillator in the sense of De Broglie	Physica 17D	116-119	1985
G. M. X. Fernando, D. W. Parker & P. Saraga <i>R</i>	Investigations on raster conversion for HDTV display	Proc. 2nd Colloquium on New television systems: HDTV '85, Ottawa 1985	1-11	1985
P. J. M. van Laarhoven, E. H. L. Aarts & M. Davio <i>E, B</i>	PHIPLA — a new algorithm for logic minimization	Proc. 22nd Design Automation Conf., Las Vegas 1985	739-743	1985
J. P. Jensma*, A. P. G. Jacobs*, W. E. Hendriks* & G. Verspui* (* <i>Philips Centre for Manufact. Technol., Eindhoven</i>)	LPCVD for silicon carbide at moderate temperatures	Proc. 5th Eur. Conf. on Chemical vapour deposition, Uppsala 1985	405-412	1985
M. W. M. Graef, B. J. H. Leunissen & J. Soeteman (<i>Philips Elcoma Div., Eindhoven</i>) <i>E</i>	Selective epitaxy: the filling of deep grooves	Proc. 5th Eur. Conf. on Chemical vapour deposition, Uppsala 1985	465-470	1985
P. Huguet, P. Baudet, J. Maluenda, J. Bellaiche & M. Pertus <i>L</i>	A fully implanted 1 W, 18 GHz FET	Proc. 15th Eur. Microwave Conf., Paris 1985	251-255	1985
P. Gamand <i>L</i>	A 0.1 to 25 GHz HMIC distributed amplifier on Al ₂ O ₃ substrate	Proc. 15th Eur. Microwave Conf., Paris 1985	541-546	1985
M. Soulard, M. Levent-Villegas, C. Tsironis, A. Blanchard* & G. Floury* (* <i>TRT, Brive-la-Gaillarde</i>) <i>L</i>	Linear phase modulator for digital microwave links using dual gate FETs	Proc. 15th Eur. Microwave Conf., Paris 1985	955-960	1985
N. M. Marinovic & G. Eichmann (<i>City Univ. New York</i>) <i>N</i>	An expansion of Wigner distribution and its applications	Proc. ICASSP 85, Tampa, FL, 1985	1021-1024	1985
R. G. Gossink <i>E</i>	Photosensitive coatings for electronic applications: IC technology, optical discs and lenses, and glass fiber waveguides	Proc. 11th Int. Conf. on Organic coatings, science and technology, Athens 1985	63-73	1985
R. E. Horstman, E. J. van den Broek, J. Wolter, A. P. J. van Deursen (<i>Univ. Nijmegen</i>) & J. P. André <i>E, L</i>	Fractional quantum Hall effect in MOCVD-grown GaAs/AlGaAs heterostructures at pulsed high magnetic fields	Proc. 17th Int. Conf. on the Physics of semiconductors, San Francisco 1984	295-298	1985
J. M. Mercy*, C. Bousquet*, A. Raymond*, J. L. Robert* (* <i>G.E.S.-USTL, Montpellier</i>), G. Gregoris*, J. Beerens*, J. C. Portal* (* <i>L.P.S. INSA, Toulouse</i>) & P. M. Frijlink <i>L</i>	Magnetic field induced metal-non metal transition in Ga _{0.7} Al _{0.3} As/GaAs heterojunctions under hydrostatic pressure	Proc. 17th Int. Conf. on the Physics of semiconductors, San Francisco 1984	1099-1102	1985
G.-M. Martin, M. Duseaux & J. Maluenda <i>L</i>	The preparation of active layers for GaAs ICs: is there any problem left?	Proc. Int. Symp. on GaAs and related compounds, Biarritz 1984	13-21	1985
S. Martin, M. Duseaux & M. Erman <i>L</i>	Distribution of EL2 concentration in dislocated and dislocation-free GaAs substrates before and after annealing	Proc. Int. Symp. on GaAs and related compounds, Biarritz 1984	53-58	1985
J.-P. Cornier, M. Duseaux & J.-P. Chevalier (<i>C.E.C.M.-C.N.R.S., Vitry</i>) <i>L</i>	Evidence for polycrystalline insulators in dislocated undoped GaAs single crystals; comparison with near dislocation free crystals	Proc. Int. Symp. on GaAs and related compounds, Biarritz 1984	95-100	1985
N. Vodjdani, M. Erman, J. B. Theeten & M. Ketata <i>L</i>	Growth and optical assessment of low loss GaAs waveguides fabricated by localized vapor phase epitaxy	Proc. Int. Symp. on GaAs and related compounds, Biarritz 1984	151-156	1985
P. Langlade & S. Makram-Ebeid <i>L</i>	Defect clustering phenomena and related hopping type conduction in GaAs and near its surface	Proc. Int. Symp. on GaAs and related compounds, Biarritz 1984	281-286	1985
M. Erman, P. Frijlink, J. B. Theeten, C. Alibert* & S. Gaillard* (* <i>USTL, Montpellier</i>) <i>L</i>	Electronic properties of MOVPE grown GaAs/GaAlAs heterostructures and quantum wells using electroreflectance and spectroscopic ellipsometry	Proc. Int. Symp. on GaAs and related compounds, Biarritz 1984	327-332	1985

- | | | | | | |
|---|------|--|---|-----------|------|
| P. Dawson, G. Duggan, H. I. Ralph & K. Woodbridge | R | Energies of sub-band minima in GaAs-(AlGa)As quantum well heterostructures | Proc. Int. Symp. on GaAs and related compounds, Biarritz 1984 | 391-396 | 1985 |
| P. Blood, E. D. Fletcher, K. Woodbridge, P. Dawson & P. J. Hulyer | R | Short wavelength quantum well lasers grown by molecular beam epitaxy | Proc. Int. Symp. on GaAs and related compounds, Biarritz 1984 | 427-432 | 1985 |
| F. P. J. Kuijpers, G. A. Acket & H. G. Kock | E | Ga _{1-x} Al _x As power lasers made by MO-VPE | Proc. Int. Symp. on GaAs and related compounds, Biarritz 1984 | 433-438 | 1985 |
| J. N. Patillon, S. Makram-Ebeid, J. P. Chane, B. G. Martin & G. M. Martin | L | Analysis of electrical performance of GaInAs PIN photodiodes for telecommunication applications | Proc. Int. Symp. on GaAs and related compounds, Biarritz 1984 | 475-478 | 1985 |
| C. Tsironis, J. Graffeuil*, F. Henze (Univ. Braunschweig) & Z. Hadjoub* (* Univ. Paul Sabatier, Toulouse) | L | Low frequency noise in GaAs MESFETs | Proc. Int. Symp. on GaAs and related compounds, Biarritz 1984 | 611-616 | 1985 |
| T. Ducourant, D. Meignant & M. Binet | L | N-on versus N-off GaAs MESFETs for an ultra high speed comparator | Proc. Int. Symp. on GaAs and related compounds, Biarritz 1984 | 659-664 | 1985 |
| C. W. T. Bulle-Lieuwma, P. C. Zalm & M. P. A. Viegiers | E | Characterization of MBE grown Si on (001) GaAs by transmission electron microscopy | Proc. Microscopy of Semiconductor Materials Conf., Oxford 1985 | 123-128 | 1985 |
| M. J. Powell & J. W. Orton | R | Bulk and interface densities of states from measurements on amorphous silicon thin film transistors | Proc. MRS Conf., Strasbourg 1984 | 539-543 | 1984 |
| M. J. Powell, J. A. Chapman & M. V. C. Stroomer | R, E | Amorphous-silicon TFT matrix for large-area liquid-crystal displays | Proc SID 25 | 269-273 | 1984 |
| A. Girard, C. Loty, J. P. Roux, J. Noel*, J. C. Rebuffie & J. L. Allamargot* (* Hyperelec, Brive) | L | P700: a new high speed streak tube with lamellar electron optics | Proc. SPIE 491 | 58-62 | 1985 |
| D. Lenstra (Univ. of Technol., Delft), G. A. Acket, A. J. den Boef & B. H. Verbeek | E | Optical-feedback effects in single-mode semiconductor lasers: multistability, hysteresis, fluctuations and optical chaos | Proc. SPIE 492 | 59-67 | 1985 |
| C. M. J. van Uijen | E | Reversible optical recording: phase-change media and magneto optics | Proc. SPIE 529 | 2-5 | 1985 |
| J. L. Bernatets & J. Pergrale | L | New capabilities of ultrasonic imaging for tissue characterization and medical diagnosis | Proc. SPIE 535 | 230-239 | 1985 |
| W. A. Smith, A. A. Shaulov & B. M. Singer | N | Properties of composite piezoelectric materials for ultrasonic transducers | Proc. Ultrasonics Symp., Dallas 1984 | 539-544 | 1984 |
| A. A. Shaulov, W. A. Smith & B. M. Singer | N | Performance of ultrasonic transducers made from composite piezoelectric materials | Proc. Ultrasonics Symp., Dallas 1984 | 545-548 | 1984 |
| N. M. Marinovic & W. A. Smith | N | Use of the Wigner distribution to analyze the time-frequency response of ultrasonic transducers | Proc. Ultrasonics Symp., Dallas 1984 | 1023-1028 | 1984 |
| P. C. Zalm | E | Elementary processes in plasma-surface interactions with emphasis on ions | Pure & Appl. Chem. 57 | 1253-1264 | 1985 |
| W. Hoving*, F. van der Woude* (* Univ. Groningen) & K. H. J. Buschow | E | Structural investigations in the amorphous iron-boron system | Rapidly quenched metals, S. Steeb & H. Warlimont (eds), Elsevier Science, Amsterdam | 549-552 | 1985 |
| M. Duseaux & S. Martin | L | Growth and characterization of large dislocation-free GaAs crystals for integrated circuits applications | Semi-insulating III-V materials (Kah-nee-ta, OR, 1984), D. C. Look & J. S. Blakemore (eds), Shiva, Nantwich | 118-125 | 1984 |
| S. Makram-Ebeid, P. Langlade & G. M. Martin | L | Nature of EL2: the main native midgap electron trap in VPE and bulk GaAs | Semi-insulating III-V materials (Kah-nee-ta, OR, 1984), D. C. Look & J. S. Blakemore (eds), Shiva, Nantwich | 184-203 | 1984 |

G. Martens	<i>H</i>	Measurement of pressure by photoelastic effects	Sensors & Actuators 6	181-190	1984
P. Delsarte, A. J. E. M. Janssen & L. B. Vries	<i>B, E</i>	Discrete prolate spheroidal wave functions and interpolation	SIAM J. Appl. Math. 45	641-650	1985
D. Washington, J. R. Mansell, D. L. Lamport, A. G. Knapp & A. W. Woodhead	<i>R</i>	Progress of the flat channel multiplier CRT	SID 85 Digest, Orlando, FL, 1985	166-169	1985
H. M. van Noort & T. J. A. Popma (<i>Univ. of Technol., Enschede</i>)	<i>E</i>	Concentration-dependent site occupancy in europium-doped Y_2WO_6 as studied by ^{161}Eu Mössbauer spectroscopy	Solid State Commun. 55	77-79	1985
C. A. M. Mulder & G. de With	<i>E</i>	Translucent $Y_3Al_5O_{12}$ ceramics: electron microscopy characterization	Solid State Ionics 16	81-86	1985
G. de With & J. E. D. Parren	<i>E</i>	Translucent $Y_3Al_5O_{12}$ ceramics: mechanical properties	Solid State Ionics 16	87-94	1985
M. P. A. Vieggers	<i>E</i>	TEM observations of grain boundary phenomena	Solid State Ionics 16	115-124	1985
C. M. P. M. Saris (<i>Univ. of Technol., Eindhoven</i>) & H. Verweij	<i>E</i>	Formation of sodium aluminates at high temperatures under the influence of Mg and Ca	Solid State Ionics 16	185-194	1985
F. J. C. M. Toolenaar	<i>E</i>	Effects of presintering on densification phenomena of ferrites	Solid State Ionics 16	267-274	1985
M. P. A. Vieggers, A. F. de Jong & M. R. Leys	<i>E</i>	Characterization of structural features in thin layers of GaAs, $Al(x)Ga(1-x)As$ and AlAs by means of structure factor imaging and high resolution electron microscopy	Spectrochim. Acta 40B	835-845	1985
P. K. Larsen, B. A. Joyce & P. J. Dobson	<i>E, R</i>	RHEED and photoemission studies of semiconductors grown in-situ by MBE	Springer Ser. Surf. Sci., Vol. 3, F. Nizzoli <i>et al.</i> (eds), Springer, Berlin	196-219	1984
S. Gourrier, P. Friedel & P. K. Larsen	<i>L, E</i>	Core level photoemission study of the interaction of plasmas with real GaAs(100) surfaces	Surf. Sci. 152/153	1147-1152	1985
H. A. Post	<i>E</i>	Excitation and radiative decay of the 184.9 nm Hg resonance line in low-pressure mercury noble-gas discharges	Thesis, Eindhoven	84 pp.	1985
M. J. Verkerk & I. J. M. M. Raaijmakers	<i>E</i>	Topographic characterization of vacuum-deposited films by optical methods	Thin Solid Films 124	271-275	1985
I. J. M. M. Raaijmakers & J. L. C. Daams	<i>E</i>	The interaction of hafnium and aluminium thin films on silicon substrates	Thin Solid Films 125	335-340	1985
A. G. Tangena & P. J. M. Wijnhoven	<i>E</i>	Finite element calculations on the influence of surface roughness on friction	Wear 103	345-354	1985

Contents of Philips Telecommunication Review 43, No. 4, 1985

- J. van Gelder & R. J. Mulder: Private networking with SOPHO-TBX and SOPHO S systems (pp. 237-252)
 A. A. J. M. van Heck: Economising a private voice/data network (pp. 253-261)
 G. Toes: A new public message switching system for the Dutch PTT (pp. 262-274)
 J. M. Preston: New Media Systems and the computer (pp. 275-282)

Contents of Valvo Berichte, October 1985

- K. Ruschmeyer: Permanentmagnete und ihre Weiterentwicklung (pp. 1-12)
 H. J. H. van Heffen: Keramische Permanentmagnete für Gleichstrommotoren (pp. 13-28)
 J. Koch: Dimensionierung permanentmagnetisch erregter Gleichstrommotoren unter Berücksichtigung der Ankerrückwirkung (pp. 29-36)
 G. Kramp & H. J. Plaumann: Einfache, überschlägige Dimensionierung von Gleichstrom-Kollektormotoren mit permanentmagnetischer Erregung durch Ferroxdure-Magnetsegmente (pp. 37-48)

Recent United States Patents

Abstracts from patents that describe inventions from the following research laboratories, which form part of or cooperate with the Philips group of companies:

Philips GmbH Forschungslaboratorium Aachen, Weißhausstraße, 5100 Aachen, Germany	A
Philips Research Laboratory Brussels, 2 avenue Van Becelaere, 1170 Brussels, Belgium	B
Philips Natuurkundig Laboratorium, Postbus 80 000, 5600 JA Eindhoven, The Netherlands	E
Philips GmbH Forschungslaboratorium Hamburg, Vogt-Kölln-Straße 30, 2000 Hamburg 54, Germany	H
Laboratoires d'Electronique et de Physique Appliquée, 3 avenue Descartes, 94450 Limeil-Brévannes, France	L
Philips Laboratories, N.A.P.C., 345 Scarborough Road, Briarcliff Manor, N.Y. 10510, U.S.A.	N
Philips Research Laboratories, Cross Oak Lane, Redhill, Surrey RH1 5HA, England	R
Philips Research Laboratories Sunnyvale, P.O. Box 9052, Sunnyvale, CA 94086, U.S.A.	S

4 538 125

Device for microwave transmission between two bodies which are rotatable relative to each other

F. K. Beckmann
W. Hoppe
W. Meyer

H

The invention relates to a device for transmitting microwaves between two bodies which are rotatable relative to each other. Two annular waveguides are arranged on a common axis. Each waveguide has a coupling slot along its circumference. A transmitting aerial projects into each coupling slot and is moveable relative to the associated waveguide. The electromagnetic waves generated by the transmitting aerials are received by receiving aerials at the ends of the waveguides, respectively. The outputs of the receiving aerials are prepared for further processing.

4 538 285

FM-receiver for receiving FM-signals with transmission identification

G. C. M. Gielis
A. M. M. van Kessel

E

FM-receiver for receiving an FM-signal with transmission identification. An aerial input is connected to a tuning unit to which there are connected, in succession, an IF-unit, an FM-detection circuit, a pilot regeneration circuit for regenerating a pilot, a demodulation arrangement for demodulating the code signal which contains transmission identification information, and a clock regeneration circuit which is connected to both the pilot regeneration circuit and the demodulation arrangement. The clock regeneration circuit comprises a resettable phase search circuit for producing a clock signal whose frequency is derived from the regenerated pilot and whose phase is derived from the demodulated code signal, a clock-controlled decoding circuit for decoding the code signal and a clock-controlled signal processing unit. For the purpose of stabilizing the processing, for example, for the reproduction of the transmission identification information, more specifically with mobile reception, use is made, in the event of disturbances of the code signal, of correctly decoded bits which were stored during undisturbed reception in a memory circuit. Only in the event of extreme interferences the phase search circuit of the clock regeneration circuit and also the other clock-controlled circuits are reset to correct a possible phase slip of the clock signal.

4 539 508

Method of producing a low-pressure mercury vapour discharge lamp

B. J. Mulder
S. van Heusden

E

A method of producing a low-pressure mercury vapour discharge lamp which includes positioning a container in the lamp vessel of the lamp between the electrodes. The container holds a quantity of mercury required for operation of the lamp and is attached to a supporting element (wire). The supporting element is connected to a lead-in wire of a first electrode by a metal connecting wire. A direct current discharge is generated between the container and the second electrode, the mercury escapes from the container, thereafter the connection between the supporting element and the lead-in wire is interrupted.

4 539 513

Circuit arrangement for starting and operating a high-pressure gas discharge lamp

H. G. Ganser
R. Schäfer
H. P. Stormberg

A

A circuit arrangement for starting and operating a high-pressure gas discharge lamp having an outer starting electrode connected to an igniter. A full-wave rectifier is connected to an alternating voltage supply, and has an output shunted by a series arrangement of a diode and a capacitor. The capacitor is discharged in part through the lamp after each half period of the alternating voltage. A resistor, which is high-ohmic with respect to a current limiter, is connected in the current circuit between the end of the capacitor facing the diode and the lamp. Thus, starting of the lamp is facilitated.

4 539 646

Tone detection arrangement

P. J. Stein
R. W. Gibson

R

A multi-tone sequential call signal detector in which a microcomputer is used to detect the tones of a received signal by simulating digitally the response of analogue tuned circuits. The detector in-



cludes a limiter for producing a square wave signal from a tone signal, a differentiator for producing interrupt pulses, and a micro-computer which responds to the interrupt pulses to activate a visual display and a call lamp of an output circuit when it detects all the received tones of the signal. The microcomputer performs an algorithm by which it measures the period between successive interrupt pulses, determines which tone frequency has this period, starts a number count which represents the 'rise' response of a tuned circuit for that tone frequency, and determines when the number count reaches a threshold number which represents the resonant condition of the tuned circuit.

4 540 876

Furnace suitable for heat-treating semiconductor bodies

G. K. McGinty

R

A furnace according to the present invention includes a rectangular chamber for receiving a semiconductor wafer or other body to be heated. The chamber has six plane reflecting walls. A bank of mutually parallel, equally spaced elongated heat radiation lamps extend between two opposite sidewalls inside the chamber. The distance between the outermost lamps and two opposite sidewalls extending at the sides of the lamps is less than one and one half times, and preferably equal to one half times, the spacing between adjacent lamps. The lamps are so arranged with respect to the walls that the configuration of lamps and their images formed by reflection approximate an array of infinite size which, at least in the plane of the lamps, is approximately continuous. A semiconductor body can be heated very rapidly and uniformly in this furnace, and as such, it is particularly suitable for rapidly annealing ion-implanted semiconductor wafers.

4 541 095

System for communication by way of repeatedly transmitted messages, and stations for use in such a system

L. B. Vries

E

A description is given of a system for communication between a transmitting station and a receiving station by way of a message which consists of a direct succession of a number of identical code words. Each message uses only a comparatively small part of the capacity of the message channel. Each code word has at least a pre-determined minimum Hamming distance with respect to any other code word, including the cyclic transpositions of the latter code word. Therefore, for the detection and reproduction of a code word it is not necessary to realize word synchronization and a given category of errors can still be detected and/or corrected. The code words may concern, for example, a transmitter or program identification in a broadcasting system or a paging code for a receiving station in a system comprising selectively addressable receiving stations as in a paging system.

4 541 279

Method of determining the time-of-flight of an ultrasonic pulse

H. Schomberg

H

For the correction of the time-of-flight of an ultrasonic signal, the measurement signal produced by an ultrasonic transducer is digitized, stored and compared with a reference signal. The comparison is performed by way of different relative shifts between the measurement signal and the reference signal. The value of the shift where both signals correspond best is used for the correction.

4 541 811

Method of manufacturing a low-pressure mercury vapour discharge lamp and low-pressure mercury vapour discharge lamp manufactured by this method

B. J. Mulder

E

S. van Heusden

Method of manufacturing a low-pressure mercury vapour discharge lamp comprising a discharge envelope, the glass wall of which comprises at least an (alkaline earth) alkali constituent, a silicon di-

oxide-containing transparent layer being produced on the inner wall of the discharge envelope. In the method, such a direct current is maintained through the glass that the (positive) (alkaline earth) alkali ions move away from the inner wall and upon heating the said silicon dioxide-containing transparent layer is produced.

4 542 305

Impedance buffer with reduced settling time

R. A. Blauschild

S

A bipolar impedance buffer contains an input transistor whose emitter is coupled to that of a like-polarity intermediate transistor. Its collector is coupled to the base of a like-polarity output transistor, while its base is coupled to the collector of an opposite-polarity transistor. A resistor coupled between the base and collector of the intermediate transistor significantly reduces the output settling time.

4 542 331

Low-impedance voltage reference

R. M. Boyer

S

A voltage reference for providing a reference voltage between a pair of terminals contains a diode and a bipolar transistor whose base is coupled to one electrode of the diode. The collector of the transistor is coupled to a node between one of the terminals and the other electrode of the diode. The emitter of the transistor is coupled to the other terminal.

4 542 332

Precision current-source arrangement

R. J. van de Plassche

E

A current-distribution circuit supplies a plurality of substantially equal currents to a permutation circuit, which transfers these currents to outputs in accordance with a cyclic permutation. The currents in these outputs exhibit a ripple caused by the inequality of the currents. A detection circuit detects the ripple component of the currents and applies this ripple component to an associated control circuit of a block of control circuits. The relevant control circuit supplies a control current for correcting the relevant current in such way that the ripple component is substantially eliminated.

4 542 405

Method and apparatus for displaying and reading out an image

E. Arnold

N

B. M. Singer

An apparatus and technique are described for storing a latent radiation image on a photoconductor by way of charge produced on the photoconductor and absorption of light from an object transmitted onto the photoconductor. Read out is provided by scanning a light source over the photoconductor to create a photocurrent which activates a CRT read out device or is stored in an image recording system.

4 542 425

Apparatus for reading a record carrier

E. de Niet

E

The invention relates to apparatus for reading a record carrier on which digital information and tracking signals of comparatively low frequency have been recorded. The apparatus comprises a correction circuit to which the regenerated digital signal is applied, which correction circuit has a transfer characteristic which at least within the frequency band of the tracking signals corresponds to the transfer characteristic of the chain comprising the recording element, the record carrier and the read element. The correction-signal supplied by the correction circuit is subtracted from the signal that is read and the tracking signals are derived from the signal thus obtained. In this way cross-talk components produced in the tracking signals by the digital signal are compensated for.

4 542 512

Semiconductor laser having a metal-filled groove for improved cooling and stability

J. A. C. van den Beemt

E

A semiconductor laser of the DH-type has a first and a second passive layer, an interposed active layer and a top layer which may be disposed on the second passive layer. In the surface, a preferably V-shaped groove is provided on the side of the second passive layer, which groove extends at most over only part of the thickness of the second passive layer. According to the invention, the groove is filled selectively with a metal, preferably gold, up to the level of the surface, while on both sides of the groove there is present an insulating region, which is preferably obtained by proton implantation and does not extend up to the active layer. The invention also relates to a method in which the insulating region is provided in a self-aligned manner by ion implantation while using the metal as a mask. The groove is preferably filled with gold by an electroless method.

4 542 535

RF balanced mixer

R. N. Bates

P. M. Ballard

R

An RF balanced mixer comprises on an insulating substrate with opposed major surfaces a balanced first transmission line having a pair of conductors on a first major surface and an unbalanced second transmission line having a strip conductor on one major surface and a ground conductor on the side of the substrate remote from the strip conductor. Two diodes are electrically connected between the pair of conductors of the first line and the strip conductor of the second line to form an arrangement operable as a 180° hybrid junction, the first line coupling an RF signal to the diodes and the second line coupling an LO signal to and an IF signal from the diodes. To reduce the impedance of the IF signal ground return path and inhibit resonant effects, the pair of conductors of the first line to which the diodes are respectively connected are on the same major surface as the strip conductor of the second line and are coupled to the ground conductor of the second line by means which include conductive connections through the substrate and which present a low impedance to the LO and IF signals.

4 543 537

Method of and arrangement for controlling the gain of an amplifier

M. H. Kuhn

H. Piotrowski

R. Geppert

H

For processing a signal applied to an input of audio signal processing devices, for example a speech signal received via a microphone in a speaker-identification or speech recognition system, the signal must have a specific level. For this purpose the signal is applied via an amplifier with variable gain. Before processing begins, the gain is set to an initial value. During processing of the speech signal, it is checked, at regular time intervals, in which range of a plurality of predetermined amplitude ranges the amplified signal is situated, and whether overloading takes place and the frequency which the amplitude of the signal occurs in each of the amplitude ranges is counted. When the signal ends, the optimum gain setting is determined from the histogram of frequencies. In the case of a signal which is specific of an individual speaker and which must be processed in speech recognition or speaker identification systems, this optimum gain setting may be stored in a memory at a location assigned to the speaker, and when the system is subsequently used by the same speaker this value is used as the initial setting of the amplifier gain. In this way the gain is set to an optimum value during the first time that the system is used by a specific speaker and it is corrected continuously when the system is used again by the same speaker.

4 543 831

Optical pressure transducer

W. Meyer

H

Optical pressure transducers are used in devices for the measurement of the pressure of explosive gasses and liquids. In order to increase the sensitivity of the optical pressure transducer, a diaphragm is made to be reflective on both sides. Two pairs of light conductors, each comprising a first light conductor for a light emission and a second light conductor for intercepting the light reflected by the diaphragm, are arranged on opposite sides of the diaphragm.

4 544 806

Ribbon-type transducer with a multi-layer diaphragm

J. A. M. Nieuwendijk

W. D. A. M. van Gijsel

G. B. J. Sanders

E

A ribbon-type electro-acoustic transducer comprising a magnet system having a pole plate and a center pole between which at least one air gap is formed with a diaphragm arranged in the air gap. The diaphragm comprises at least two foils which extend substantially parallel to each other in the diaphragm plane, every two adjacent foils being joined to each other at their circumference in an air-tight manner so that a volume is enclosed. A conductor is arranged on each of the foils. Preferably the volume enclosed between two foils contains a damping material.

4 544 918

Analog-to-digital conversion circuit

G. de Haan

E

An analog-to-digital conversion circuit, in which the coarse bits are produced by a counter, is made suitable for processing a video signal by having, in the event of fast large amplitude variations, an analog-to-digital converter, connected to the input of the conversion circuit, write into the counter in response to a threshold-crossing signal produced by a difference threshold circuit, while slow and small amplitude variations are followed by a correction circuit coupled to an output of a digital-to-analog converter which is connected to the outputs of the conversion circuit, the correction circuit also being coupled to the input of the conversion circuit, which correction circuit corrects the counting position, while the fine bits are obtained from a fine analog-to-digital converter which is responsive to the difference between the signal at the input of the conversion circuit and the signal at the output of the digital-to-analog converter.

4 545 110

Method of manufacturing an insulated gate field effect device

H. G. R. Maas

F. M. Klaassen

J. A. Appels

E

A method of manufacturing a field effect device is set forth where the source and drain zones have extensions of an accurately and reproducibly determined length adjoining the gate electrode. According to the present invention, an oxygen-preventing insulating layer is formed on a first silicon layer forming the gate electrode, and a second silicon layer is provided on the oxygen-preventing layer. A part of the second silicon layer is removed and the edges substantially coincide with the edges of the gate electrode to be formed. The edges of the remaining part of the second silicon layer are oxidized. Through successive maskless selective etching steps, the first silicon layer is exposed and etched away at the area of the oxidized etched portions. The extensions of the source and drain zones are implanted through the openings thus obtained.

4 546 258

Charged particle beam apparatus

T. Chisholm

R

The apparatus, which may be an electron beam column, has a lens system for coarse- and fine-focus adjustments of the beam. The coarse-focus is effected by a magnetic lens and the fine-focus by an

electric lens in parallel with the magnetic lens. The electric lens may comprise a plurality of electrically conductive cylinders inside the magnetic lens. The cylinders are so arranged that, by applying appropriate potentials to them, fine-focus adjustments can be carried out without causing the beam to rotate.

4 546 384

Test method for workpieces

G. Kowalski

H

The invention relates to a method for the testing of a workpiece which is moved past a stationary camera in order to record a sequence of images, the images being subsequently superposed so that the movement of the workpiece is compensated for low-noise images of the workpiece are thus obtained.

4 546 463

Apparatus for recording and reading information tracks on an optical record carrier with a beam of radiation

W. G. Opheij

E

G. E. van Rosmalen

An apparatus is described for writing and reading information tracks in an information surface of a record carrier by optical radiation. The apparatus comprises two diode lasers, one of which produces the write beam and the other a read beam. By means of polarization sensitive device the write spot and the read spot formed on the information layer are projected at a very small and stable distance from each other and the beams reflected by the information layer are spatially separated. The separated beams are routed to separate detectors with residual cross-talk between the beams being eliminated by wavelength-selective filters.

4 546 484

Device for the continuous manufacture of elongated bodies starting from unmolten solid starting material

W. C. P. M. Meerman

E

A device for continuously making elongated bodies, particularly rods of glass or optical fibers, includes a melting tube for containing molten material and surrounded by a cooling jacket. Within the cooling jacket exists a high frequency electromagnetic coil for heating and melting the starting material in the melting tube. A plurality of metal wires extending parallel to the axis of the melting tube and being grounded as well as a tube of insulating material are located between the wall of the melting tube and the coil. The melt traverses a heating zone and a refining zone so that a solid elongated body is withdrawn from the bottom of the melting tube.

4 546 534

Semiconductor device manufacture

K. H. Nicholas

R

A first masking layer on a semiconductor body is defined by exposing a layer of negative acting radiation sensitive resist to a radiation pattern through a mask. Doped regions are then formed at unmasked surface areas of the body. A layer of positive acting resist is provided on an insulating layer at the surface of the body, and a second masking layer is defined in this layer by exposure to the pattern radiation beam through the same mask. An insulating layer pattern which is accurately aligned above the doping region is then formed by etching the exposed parts of the layer. Alternatively, the same type of resist is used at both exposure stages. By adjusting the resist processing, the second masking layer is made larger than the first masking layer. In this case, the second masking layer is used to define an oxygen mask before oxidizing the exposed surface of the body to form an accurately aligned oxide layer pattern.

4 547 069

Tubular cuvette for atomic absorption spectrometry

B. Lersmacher

A

W. F. Knippenberg

E

A cuvette having a thin-walled basic member of pyrolytic graphite is provided with annular graphite components in proximity to its ends. These parts are connected to form a unit which is further coated by an enveloping pyrolytic graphite coating. This cuvette having flanged parts is simpler to electrically contact and is mechanically stable.

4 547 631

Large-excursion electroacoustic transducer

J. A. M. Nieuwendijk

E

G. B. J. Sanders

C. D. van Dijk

A. J. M. Kaizer

An electroacoustic transducer comprises a diaphragm, a magnet system and a voice coil arranged on a voice-coil former in an air gap of the magnet system. The movement is transmitted between the voice-coil former and the diaphragm via a lever mechanism comprising n lever devices arranged at an angle relative to each other ($n \geq 2$). A lever device comprises a lever arm coupled to a fulcrum at the location of a first position on the lever arm, to the voice-coil former at the location of a second position, and to the diaphragm at the location of a third position. The lever mechanism multiplies the excursion of the voice-coil former by a factor greater than unity. This results in an electroacoustic transducer with a long stroke which provides large excursions of the diaphragm. The lever mechanism may also be employed in other types of transducer, such as piezoceramic transducers. A compliant element formed as a zigzag bellows secured both to the outer circumference of the diaphragm and to the chassis to permit the large excursion of the diaphragm, is constructed so as to reduce the acoustic contribution of the compliant element to the transducer output signal, which contribution forms a distortion component in the output signal.

4 547 699

Green luminescing cathode-ray tube device

B. J. Fitzpatrick

N

A CRT device for generating a bright green light spot is shown. The device employs a terbium activated phosphor. Troublesome radiations emitted by the phosphor particularly in the 586 nm region are significantly decreased without significant decrease of the desired 544 nm radiation by use of a concentrated solution of a soluble praseodymium salt.

4 547 744

Integrated amplifier arrangement

W. G. Kasperkovitz

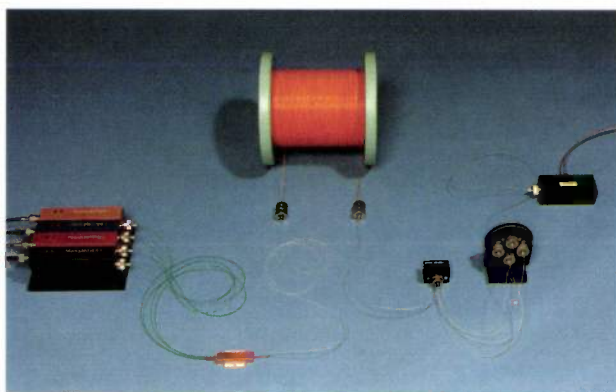
E

An integrated amplifier arrangement in which the dc voltage gain is suppressed, which includes two transistors arranged as a differential pair with an output between the collectors of these transistors. In order to improve the high-frequency properties of the amplifier arrangement, the collector circuit of the transistors includes two load transistors in cascade with the two transistors arranged as a differential pair, each load transistor including an impedance in its base circuit in order to obtain an inductive input impedance on the emitter side of the transistor. In order to obtain direct-current and low-frequency negative feedback for eliminating the dc gain, the base electrodes are cross-coupled to the collector electrodes of the load transistors.

An optical communication system with wavelength-division multiplexing and minimized insertion losses

I. System and coupling efficiency

A. J. A. Nicia



Somewhere in the north-east of the United States there lies a rather strange 'vessel' for land-based training. It is a simulation of a cable-laying ship bearing the appropriate name 'Fantastic'. Before the year 1990 the 'Fantastic', sailing at eight knots, will have the task of laying the first optical-fibre cable to cross the Atlantic Ocean. This information can be found in Jeremy Bernstein's book 'Three degrees above zero — Bell Labs in the Information Age' (Charles Scribner's Sons, New York 1984). A voyage as unusual as this will undoubtedly attract much more attention than the 'journeyings' of the flashes of light themselves inside the cores of the glass fibres ever could, even though they will travel beneath the Atlantic at a rate of 400 million knots, not eight knots. The present detailed study, to be published in two parts^[*], of an optical communication system using wavelength-division (or colour) multiplexing demonstrates yet again how fascinating the physical background of guided light transmission for communications becomes when the main consideration is to minimize optical losses in transmission. Part II deals with the components developed for wavelength-division multiplexing and demultiplexing. These will eventually be used to increase the capacity of existing optical links in a relatively simple way.

Breakthrough

If the information society of the future is to function properly optical digital communication will almost certainly be required, and it looks as if the installation of a single optical fibre for each subscriber is a practical goal. Cable television and telephone can

then become part of an integrated system, with various other services in the broad field of information and communication. Possibilities already envisaged include video lending libraries, video telephony, and pay-TV (where viewers select television programmes

Dr Ir A. J. A. Nicia is with Philips Research Laboratories, Eindhoven.

[*] Part II, 'Wavelength-division multiplexing', will appear in our next volume.

themselves, with payment per channel), local television broadcasts, newspapers by cable, and so on [1].

This projected integration of information streams is the factor that could eventually make a subscriber network of this kind, built up from optical-fibre cables, economically feasible and profitable in a country such as the Netherlands. Since as many as 90% of all dwellings have a telephone and more than 70% already have cable television — with virtually separate distribution centres and links at present — the cable costs per connection in such an integrated subscriber network could remain comparable with those of the present telephone network.

Very large amounts of information can already be transmitted by optical-fibre cables more economically than by the conventional coaxial cable, and furthermore the price advantage is steadily shifting towards smaller transmission capacities. Optical-fibre cables therefore certainly qualify for use in situations such as the interconnection of new telephone exchanges.

In a cooperative venture between the Netherlands PTT (Postal and Telecommunications Service), the Delft and Eindhoven Universities of Technology and N.V. Philips it was decided to set up a small experimental local optical-fibre network at Philips Research Laboratories, Geldrop. The experimental system, known as DIVAC (an acronym for the Dutch words for digital connection between subscriber and exchange), has since been used to test the actual integration of different information and communication services [2]. The German PTT is also investigating such experimental networks, with about 30 to 50 connections, in some six cities.

It has been clear for some years that the technical aspects of this integration will have to be mainly concentrated in the transmission parts of the projected system, i.e. in the optical-fibre links [3]. An important argument for combining signals in a single fibre is the saving in cable costs thus obtained. This applies particularly to long-distance links, where plans to provide as many fibres as there are optical channels can hardly be considered realistic because of the excessive costs. For the local-area networks (LANs), the enormous expansion of communication facilities makes this combining of signals absolutely necessary. The installation of these LANs could pioneer the way for 'consumer optics' as an extension of consumer electronics. The aim is for all information streams to be combined in digital form and transmitted simultaneously along links of this type; at the receiving end they then have to be separated as required. The possibility of simultaneous signal transfers is also essential for two-way links via the same optical fibre, as for example in video telephony.

Colour multiplexing and demultiplexing, a main topic of this article, is a method that allows a number of optical signals to be combined at the input end of a

fibre and separated at the output end. In the method described here the separate signals are identified by the colour, or, to be more exact, the carrier wavelength: the method is therefore more generally known as 'wavelength-division multiplexing'. A good example of an element that can produce wavelength-division multiplexing is the familiar colour-dispersing prism. When the path of rays through such a prism is *reversed* a group of separate beams of light of different colour (red, green, blue, *fig. 1*) is seen to be combined by the prism to form a single beam of white light (the multiplexing operation). When the combined signals arrive at their destination, a second prism can be used to separate the original beams of different colour from the white beam (the demultiplexing operation).

In all optical-fibre cables so far installed for trunk (inter-city) links each fibre still needs its own light source and detector. This means that the combination and separation of the many types of information envisaged would really only be possible by electronic methods. Cost studies have meanwhile shown that these electronic combination and separation processes would be at a disadvantage, in view of the cost of new hardware, compared with the purely optical method of wavelength-division multiplexing and demultiplexing. Combined systems, partly electronic and partly optical, are also being considered [2]. In the rather

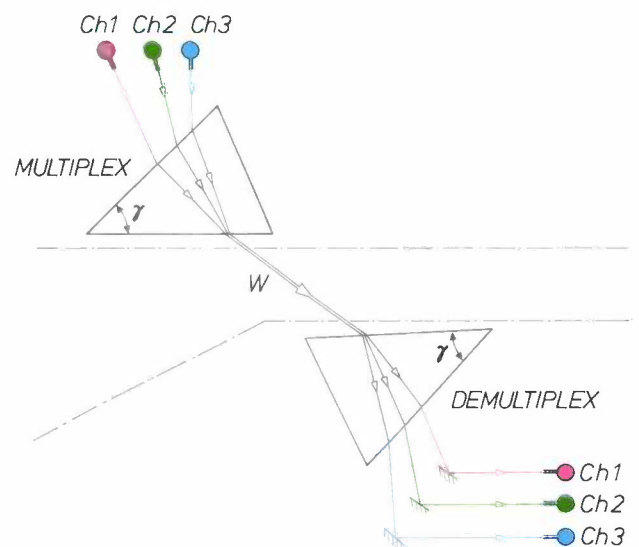
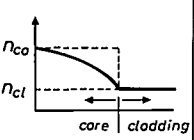
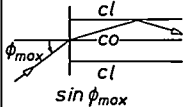


Fig. 1. An elementary example of a three-channel optical communication system in which signals are combined by wavelength-division multiplexing. Two prisms with a refracting angle γ are required. In the first (*MULTIPLEX*) the three signals are combined for long-distance transmission (*W*). At the receiving end is the second prism (*DEMULPLEX*), which restores the separate signals. Each signal is characterized by its own wavelength (or colour). This figure illustrates the principle of the WDM (Wavelength-Division Multiplexing) system dealt with in this article (see title photograph and fig. 3a). *Ch1,2,3* input and output of the three communication channels.

longer term it will be better if most or all of these processes are carried out optically. The various optical 'communication channels' would then have to be accommodated in a single optical fibre: these channels would have to be 'invisible' to one another; i.e. there would be no crosstalk between the separate channels.

fibres the bandwidth is not a practical limitation for optical communication, since there is no 'intermodal dispersion' by definition. The optical carrier wave has such a high frequency (about 2×10^{14} Hz) that the digital signal rates required by the PTT, such as 140 Mbit, or even 560 Mbit per second, are easily attainable. A

Table I. Numerical data characteristic of three generations of optical fibre cables. The attenuation, measured at three commonly used wavelengths, and the product of bandwidth and corresponding cable length, also determined experimentally, are the principal performance figures (grey background), 'Length' here is the maximum distance along the cable to the next repeater. The figures given are unlikely to be much improved in the near future. Theoretically, however, there is still room for improvement, since it can be shown that the 'absolutely best' profile of the refractive index for the multimode fibres of the second-generation cable would raise the maximum of 2000 MHz \times km by a factor of five to seven (see the chapter on 'Transmission system design' in the book by S. E. Miller and A. G. Chynoweth (eds) [9]). A MHz \times km product of 2000 corresponds to a broadening of the pulse signals of about 0.5 ns per km. Such pulses can be detected with good resolution after transmission over a distance of 1 km, provided that the repetition rate is less than 2000-MHz. The first four columns give the principal structural data of the fibres. The waveguide effect is based on total internal reflection, as indicated above the column for the numerical aperture of an optical fibre. The small radial decrease in the refractive index $n_{co} - n_{cl}$ is the physical reason for the confinement of the radiation within the fibre cores; in the axial direction the refractive index does not normally vary at all. *co* core. *cl* cladding. *n.a.* not applicable.

cable generation	refractive index 	radius (μm)		fibre volume (cm^3/km)	numerical aperture 	attenuation (dB/km)			bandwidth \times length (MHz \times km)
		core	core + cladding			$\lambda = 1300 \text{ nm}$	$\lambda = 1550 \text{ nm}$	$\lambda = 830 \text{ nm}$	
3 single-mode fibres	step-index $n_{co} - n_{cl} \approx 0.0034$	4.5	62.5	12.3	0.1	0.40	0.25	n.a.	> 100 000
2 multimode fibres	parabolic $n_{co} - n_{cl} \approx 0.014$	25	62.5	12.3	0.2	0.60	n.a.	2.1	1000 to 2000
1 multimode fibres	step-index $n_{co} - n_{cl} \approx 0.030$	50	70	15.4	0.3	n.a.	n.a.	2.1	50

The breakthrough of transmission by optical fibre has now reached the point where designers are already familiar with the idea of being able to base their plans for new systems on optical-fibre cables of the second or even third generation (Table I). Since 1976, when an issue of this journal was entirely devoted to optical communication [4], the development of the various types of fibre has certainly not stood still. The most significant advance is probably the reduction of the optical attenuation per km, achieved through the production of extremely pure glass (fig. 2). This high purity is now attainable on an industrial scale [5]; single-mode fibres (for third-generation cables) are now being produced in which the optical attenuation is less than 0.5 dB/km, which means that a telephone conversation can be transmitted by such a fibre over a distance of about 40 km without significant loss of quality and without any regeneration. In single-mode

single-mode fibre, with a core diameter of 9 μm (about one tenth that of a human hair), can therefore carry thousands of telephone conversations simultaneously, with no crosstalk.

In the multimode fibres for second-generation cables the situation is different. As the maximum repeater spacing is increased, the permissible bandwidth for telecommunication decreases correspondingly. With these fibres, therefore, the maximum repeater spacing

[1] This subject is under consideration by the European Community in its 'RACE Initiative'. RACE (Research for Advanced Communications technologies for Europe) is a telecommunications programme now in the definition phase.

[2] J. van der Heijden, DIVAC — an experimental optical-fibre communications network, Philips Tech. Rev. 41, 253-259, 1983/84.

[3] W. J. Tomlinson, Wavelength multiplexing in multimode optical fibers, Appl. Opt. 16, 2180-2194, 1977.

[4] Philips Tech. Rev. 36, 177-216, 1976.

[5] In November 1983 Philips opened a new optical-fibre factory in Eindhoven; both multimode and single-mode fibres are manufactured here on a commercial scale.

has a clear correlation with the bandwidth, and is far less limited by attenuation.

It will be clear that any work, including research, on components for wavelength-division multiplexing and demultiplexing is most effective within the context of a complete system study. A complete communication system contains both the transmitting and receiving ends as well as the central section for the new method of optical signal transmission.

Part I of the article, following this introduction, will therefore deal in general terms with the system that has been designed, a WDM ('Wavelength-Division Multiplexing') system giving maximum coupling efficiency. The propagation of the (infrared) 'light' will be described with the aid of a block diagram, and subjects that will be dealt with are the various optical interfaces, the boundary conditions and ways and means of manipulating the radiation, with the primary object of minimizing the insertion losses in the system.

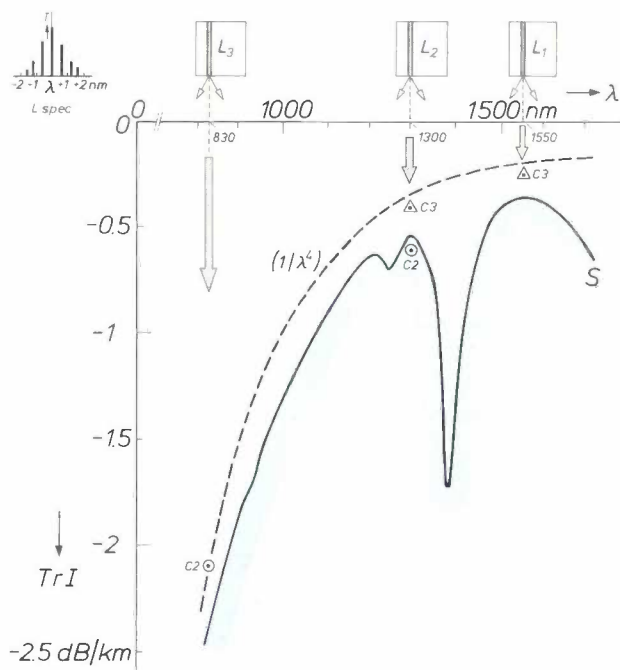


Fig. 2. Example of a transmission spectrum (S) measured on an optical fibre more than 2 km long, of the type mounted in the second-generation cables (Table I). This type is now in regular production [6]. Vertical: TrI , the transmission of radiation, in decibels per kilometre. Horizontal: the wavelength λ of the infrared test radiation, in nm. The wavelengths of three lasers (L_1 , L_2 , L_3) that can be used in optical communication systems are displayed on the horizontal axis. Near the origin of the coordinate system the extremely narrow emission spectrum (L_{spec}) of one of the many types of diode laser is shown. The nature of the material of the fibre core and its impurities determine the material dispersion; this unwanted effect decreases as the spectrum of the light guided through the core becomes narrower. In practice the effect is not large enough to be troublesome. The dashed curve ($1/\lambda^4$) shows the calculated transmission spectrum when Rayleigh scattering is the only source of attenuation. C_2 and C_3 irradiances derived from the maximum performance figures in Table I, found in cables of the second and third generations. The sharp dip in S at about 1380 nm is caused by resonances (valence vibrations) of free OH groups, which are present as traces in the core material.

Part II of the article will chiefly be concerned with the multiplexing and demultiplexing components of our WDM system. Considerable emphasis will be placed on the choice of design and construction. The operation of these components will be briefly explained, and some theoretical principles and background will be discussed.

Principles of system design

The general block diagram of a WDM system is shown in fig. 3. As in any communication system, the diagram can be divided into three main parts: (I) the transmitter section, where in this case three independent electrical signals are converted into infrared signals with the wavelengths λ_1 , λ_2 , and λ_3 ; (II) the transmission section proper with — in our case — a second-generation optical cable, which therefore contains one multimode fibre (F) with a parabolic refractive-index profile (see Table I); (III) the receiver section for the composite optical signal, where finally the three original signals, each in their own channel, reappear at the outputs as digital electrical signals. Although compatible with current ideas, our choice of *digital* signals is not essential, and indeed the system is 'transparent' in this respect, since the laser injection currents could equally well be modulated by *analog* signals.

As we shall see in part II, the number of parallel optical channels used in F will be limited to three or four. (The title photograph shows our experimental system with *four* input channels.) Given the known designs for multiplexing and demultiplexing units, the use of more channels would soon introduce considerable practical difficulties. The *demultiplexing* unit seems to give fewer problems here, and indeed a demultiplexing unit for *six* parallel channels has now been developed [6].

The main principle behind the design of our WDM system is the achievement of maximum efficiency, i.e. minimizing the insertion losses. In the design of such a system certain more or less fixed conditions have to be observed, but a number of variables can be freely chosen so as to comply with the main principle. The main conditions are set by the characteristics of the multimode fibre (F in fig. 3) in the second-generation cables, as shown in Table I. Major factors in the design are the core radius and the numerical aperture, the first two of the fixed parameters.

[6] H. G. Finke, A. J. A. Nicia and D. Rittich, Diffraction efficiency limited grating demultiplexer suitable for up to six channels with arbitrary central wavelengths, Proc. 4th Int. Conf. on Integrated optics and optical fibre communication (IOOC), Tokyo 1983, pp. 376-377.

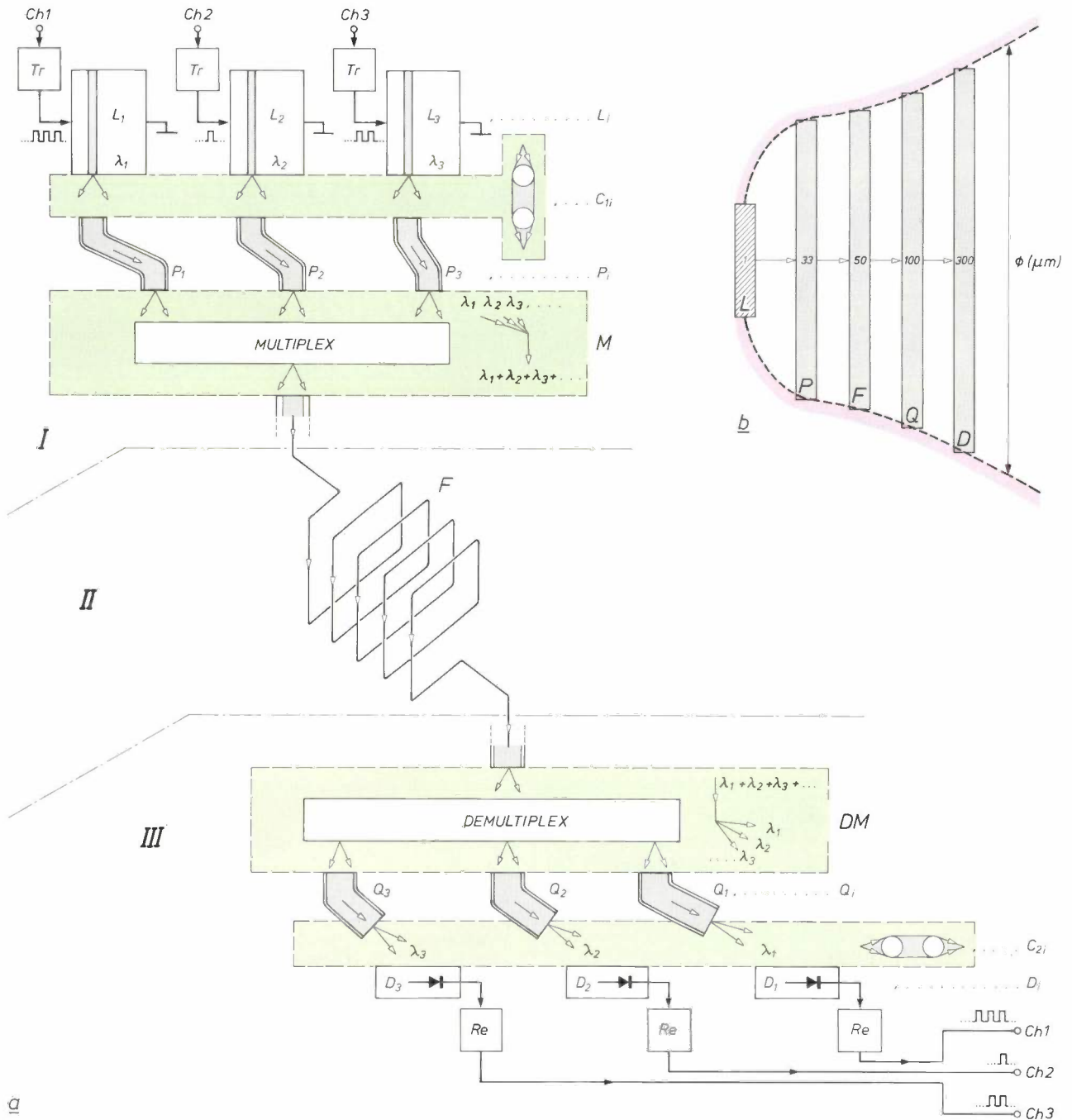


Fig. 3. a) A wavelength-division multiplexing system for optical communication. The multiplex component (*M*) is in the transmitter section (*I*), the demultiplex component (*DM*) in the receiver section (*III*). As an example, three separate communication channels are shown, indicated by *Ch1*, *Ch2* and *Ch3* at the input and output terminals. (As can be seen in the title photograph, four parallel channels are also a practical proposition.) The three combined signals propagate through one optical fibre (*F*) of the multimode type in second-generation cables, in the region (*II*) for long-distance transmission. *Tr* transmitter, which modulates the injection current of the diode laser connected to it (L_1 ($\text{In}_\mu\text{Ga}_{1-\mu}\text{As}_\nu\text{P}_{1-\nu}$), L_2 ($\text{In}_\mu'\text{Ga}_{1-\mu}'\text{As}_\nu'\text{P}_{1-\nu}'$) and L_3 ($\text{Al}_\chi\text{Ga}_{1-\chi}\text{As}$), see also fig. 4) in accordance with the required digital input signal. *Re* receiver, which restores the appropriate digital input signal from the photocurrent of the detector (D_1 , D_2 , D_3) and feeds it to the output terminals. P_1 , P_2 , P_3 pigtails with a parabolic refractive-index profile for the core. Q_1 , Q_2 , Q_3 pigtails with step-index core material (multimode). Green blocks: interface zones containing optical coupling elements, often very simple (C_{1i} , C_{2i} , $i = 1, 2, 3$; symbolically represented by a pair of ball collimator lenses). **b)** The 'trumpet geometry' chosen for the system (the red dashed-line contour). *L* laser. *P* pigtail for input signal. *F* long-distance fibre. *Q* pigtail for output signal. *D* detector. ϕ characteristic diameter, available for signal guidance. Because of the increase in ϕ in the direction of propagation of the guided signal the various couplings between the components *L*, *P*, *F*, *Q*, *D* are easy to arrange mechanically. The value quoted for *L* (1 μm) is only an order of magnitude; there is also no rotational symmetry.

The numerical aperture (NA) is a measure of the ability of the fibre core to capture radiation and guide it, by repeated total internal reflection. For the radiation originating from a point source outside the fibre core on the optical axis, it can be shown that NA is equal to $(n_{co}^2 - n_{cl}^2)^{1/2}$, the maximum possible value of the numerical aperture for the fibre core.

The third standardized parameter, the thickness of the cladding, is not so important. Another major con-

final fixed condition is the detector (D_i in fig. 3). The type of photodiode chosen has a radiation-sensitive surface of about $300 \mu\text{m}$ diameter. This dimension, which determines the capacity of the photodiodes, sets a limit of about 500 MHz to the rate of response. Signals in which significantly higher frequencies occur would require photodiodes of smaller diameter. This, however, would require tighter tolerances for the

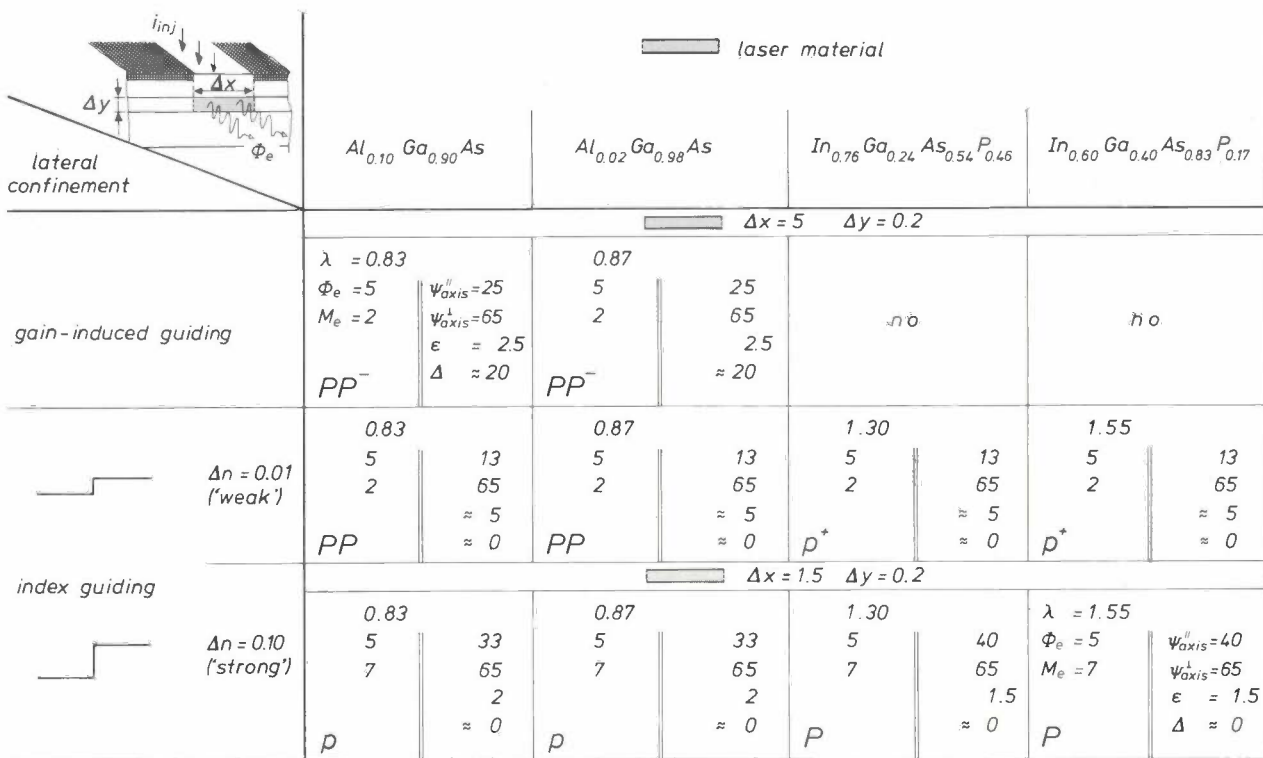


Fig. 4. Ten types of diode laser arranged in a matrix of characteristics with the choices of active material and lateral confinement mechanism as inputs^[7]. The active 'stripe' has the lateral dimension Δx in its principal plane of symmetry, and perpendicular to it the dimension Δy , both in μm . In the y -direction the confinement of the radiation in all ten cases is the consequence of an abrupt step in the refractive index at the position of the two 'horizontal' boundary planes of the active stripe. λ , in μm , wavelength of the laser radiation. Φ_e , in mW, the radiant power. M_e , in $\text{mW}/(\mu\text{m})^2$, the radiant exitance. ψ_{axis}^{\parallel} , ψ_{axis}^{\perp} , in degrees, the far-field beam divergence angle, in the principal plane of symmetry and in the plane of symmetry perpendicular to it. ϵ the ellipticity, the ratio of the smallest beam diameter (or 'waist') in the laser in the principal plane of symmetry, to the waist in the longitudinal plane of symmetry perpendicular to it. Δ the astigmatism, in μm : the distance between the two waists within the laser (one waist is situated exactly at a reflective end face of the laser, see fig. 5). *no* type of no practical use. *PP* very common type. *P* common type. *p* uncommon type. - use on the decline, + use on the increase. i_{inj} injection current, which effects the population inversion required for laser action. The development of new types of diode laser certainly does not seem to have run its course yet^[8]. 'Distributed feedback', introduced by making a longitudinal periodic discontinuity in the refractive index, will not only help to make the emission spectrum narrower but will also make it easier for the system designer to choose the appropriate wavelengths, which will of course facilitate the introduction of wavelength-division multiplexing.

dition is the choice of the laser light source (L_i in fig. 3). The different types of diode laser that seem at present to be most suitable for optical communications (fig. 4) produce a light spot about one μm square at their output with a radiation pattern like an elliptical cone. The

dimensions and alignment of the optical coupling (C_{2i} in fig. 3).

The more or less free variables here are the short pieces of fibre, P_i and Q_i in fig. 3, referred to as 'pig-tails', and the multiplexing and demultiplexing units

(M and DM in fig. 3). In the pigtailed, whose core material has a parabolic or stepped refractive-index profile (the Q_i 's only), the variables are the numerical aperture and the core radius. The values chosen for the P_i 's must be large enough to ensure that the radiation pattern from the laser matches them properly and for the coupling elements C_{1i} to be kept simple. The insertion loss due to the interfaces should be kept as small as possible. The interfaces between the end of the P_i 's and the M unit are less critical in this respect. The explanation lies in the 'trumpet' geometry used for the system (fig. 3b): the signals are guided inside a 'characteristic diameter' that either increases along the axis of propagation or remains constant (and therefore never decreases). For the pigtailed at the output of the optical parts, the Q_i 's, the situation as a whole is thus easier. It is fortunate that there is considerable scope for variation in the DM unit and also in the M unit, especially because the range of possible variations is based on a choice between different operating principles here (see Table III, in part II of this article [1]).

In the rest of the discussion of the block diagram we shall follow the 'natural' sequence step by step, as the radiation propagates through the system, although there is one exception right at the start. We begin in fact with the four green blocks in fig. 3a, the optical interface zones. This is because an accurate analysis of the interface components and their possible radiation leaks becomes relatively more important for maximizing the *total* system efficiency as the performance of the main components such as lasers and fibres improves. First we shall look at the interface zone immediately following the lasers; analysis of this zone was the one that presented most of the difficulties, which were mathematical. The treatment of the second and third interface zones, which was much simpler, will be given in part II of this article, since their characteristics are closely connected with the structure of the M or DM units that they contain. The fourth interface zone, between pigtailed and photodiodes, will however be treated in this part. In view of the strongly pronounced trumpet geometry of the system, it should not be too difficult to estimate the efficiency of the fourth zone once the efficiency of the first zone has been properly calculated.

The interface zones

In the first interface zone (C_{1i} in fig. 3a) a laser and a pigtail for an input signal are coupled together. The efficiency of this coupling interface is in the region of 50 to 80 per cent, as will appear later. The radiation leaves the laser directly through a partly transmitting 'mirror', one of the two end faces perpendicular to

the active stripe of the laser [8]. The radiation next passes through the actual coupling element to reach the front face of the appropriate pigtail (P_i) and is then guided through the fibre core. A small single ball lens has proved satisfactory as a coupling element, in the form of a glass bead with a radius of 0.1 mm. The bead is provided with an antireflection coating.

The ball lens corrects the divergence of the beam. The cross-section of the beam at this front face is therefore given dimensions that correspond reasonably well with the diameter of the central region in the core, the region where the energy of the fundamental mode of a guided electromagnetic wave pattern in the core is concentrated. As will be seen below from the approximate description given here the fundamental mode, compared with higher-order modes also excited, is mathematically the simplest wave pattern — and it also remains the most strongly concentrated one — to ensure that the energy of the beam is transferred through the full length of the fibre [9].

The efficiency of the first interface zone does not only depend on the ball lens, of course. It is also strongly dependent on the properties of the wave pattern that can be excited inside the next element (P_i), starting at its front face. In our examination of the interface zones we shall therefore first take a closer look at the propagation modes inside a fibre core.

Modes

Inside a fibre core types of resonant electromagnetic wave patterns can be excited, called modes. They are important because a general solution for the guided-radiation field inside the fibre core can always be obtained as a sum of a complete set of modes (the superposition principle), which can be calculated relatively easily. The radiation is propagated longitudinally, in the z -direction. A mode is characterized by a well-defined phase velocity and an energy velocity (or group velocity), a state of polarization, and its transverse distribution functions, which are expressed

[7] The editors are indebted to Prof. Dr G. A. Acket of Philips Research Laboratories, and a Visiting Professor of Delft University of Technology, for his detailed help in drawing up this matrix.

[8] G. A. Acket, J. J. Daniele, W. Nijman, R. P. Tjburg and P. J. de Waard, Semiconductor lasers for optical communication, Philips Tech. Rev. 36, 190-200, 1976. See also G. D. Khoe and L. J. Meuleman, Light modulation and injection in optical-fibre transmission systems with semiconductor lasers, Philips Tech. Rev. 36, 201-204, 1976. Various other developments are described in L. J. van Ruyven, Double heterojunction lasers and quantum well lasers, J. Lumin. 29, 123-161, 1984.

[9] M. J. Adams, An introduction to optical waveguides, Wiley, Chichester 1981; D. Marcuse, Light transmission optics, Van Nostrand Reinhold, New York 1972; S. E. Miller and A. G. Chynoweth (eds), Optical fiber telecommunications, Academic Press, New York 1979.

in terms of the coordinates (x, y) . Since the refractive-index profile in the core is independent of z , the transverse distribution functions are independent of the value of z . This means that the components of the field vectors E and H of a given mode all have the same fixed, functional dependence on both x and y . However, depending on the appropriate boundary conditions, there can be differences in amplitude and phase between the various components of the field vectors. The two coordinates are *separated* variables here; this rather unusual feature is due to the choice of the refractive-index profile.

The modes are of two kinds: 'bound' or guided modes and 'leaky' modes. In the first kind the value of the transverse distribution functions decreases rapidly to zero as the distance from the z -axis increases, so that outside the core the field energy is practically zero. If the energy were predominantly transported by leaky modes, the fibre would be not so much a waveguide as an antenna emitting radiation.

In describing radiation fields it is customary to assign the well-known time-dependence $\exp(j\omega t)$ of the harmonic oscillator to the bound modes, while the z -dependence, because of the longitudinal propagation, appears only in the phase factor $\exp(-j\beta z)$. The modes can then be expressed as a function of the four variables (x, y, z, t) by

$$M(x, y, z, t) = X(x)Y(y)\exp\{j(\omega t - \beta z)\}. \quad (1)$$

Their wavefronts are planar; they will travel a distance λ_0/n_{co} in the z -direction inside the fibre core in the time $(2\pi/\omega)$ for one oscillation. The propagation constant β , which has the dimension of a wave number, is approximately equal to $2\pi n_{co}/\lambda_0$. In this approximation the difference $\omega t - \beta z$ therefore remains *constant* during the propagation of the radiation; in this case the guidance of the radiation is said to be 'ideal'. A hypothetical observer of the constancy of the difference will therefore move with the light waves at the 'phase velocity'.

The dielectric constant does not vary at all in the z -direction inside the fibre core. We can assume that its variation in the lateral direction is slow enough for its gradient to be negligible. This has the advantage that Maxwell's equations — which in principle will give a complete solution for the modes for given boundary conditions — then reduce to a Helmholtz equation, which is much more manageable. It is also known as the reduced scalar wave equation for the modes:

$$\frac{\partial^2 M}{\partial x^2} + \frac{\partial^2 M}{\partial y^2} + \{n^2(x, y)k_0^2 - \beta^2\}M = 0. \quad (2)$$

This equation applies to all the components of the electric and magnetic field-strengths. The function $n(x, y)$ is the refractive index of the core material; k_0 is a constant (the wave number in free space, $2\pi/\lambda_0$). In the parabolic material preferred here, also referred to as a square-law guiding medium, the following relation applies:

$$\begin{aligned} n(x, y) &= n_{co}\{1 - g^2(x^2 + y^2)\}^{1/2} \\ &\approx n_{co}\{1 - \frac{1}{2}g^2(x^2 + y^2)\}, \end{aligned} \quad (3)$$

provided, of course, that $(x^2 + y^2)^{1/2}$ remains smaller than the core

radius; g is a focusing constant. It can be seen in equation (3) that the coordinates x and y occur as separated variables.

As noted, certain boundary conditions have to be observed when finding the modes. It is fairly evident, for example, that both $X(x)$ and $Y(y)$ in eq. (1) must tend to zero when x and y tend to infinity. The rate at which they do so must also be fast enough to ensure that there is no divergence of the integral of the field energy. It is also assumed that $\frac{1}{2}g^2(x^2 + y^2) \ll 1$, at least within the core — because of this inequality said to be 'weakly guiding' — and that the change in the refractive index in distances of a wavelength or less is negligibly small. The latter condition is always met in practice.

Equation (2) can now be solved after some mathematical manipulation to transform it into two ordinary differential equations, one for $X(x)$ and the other for $Y(y)$. Both differential equations are of the type used in quantum mechanics for describing the bound states of the one-dimensional harmonic oscillator mentioned above. The known solutions, which contain the function of the Gaussian distribution and a Hermite polynomial, are therefore applicable to the present case.

On the basis of the formal equivalence between a general radiation field and a number of harmonic oscillators (here both in the x -direction and in the y -direction, the two transverse directions within the fibre core) the following mathematical expressions can be found for the propagation modes in a core of the type with a parabolic refractive-index profile (Table I) as a function of the four coordinates (x, y, z, t) :

$$\begin{aligned} M(x, y, z, t) &= (\pi 2^{m+n-1} m! n! w_0^2)^{-1/2} H_m\left(2^{1/2} \frac{x}{w_0}\right) \times \\ &\times H_n\left(2^{1/2} \frac{y}{w_0}\right) \exp\{-(x^2 + y^2)/w_0^2\} \times \\ &\times \exp\{j(\omega t - \beta_m z)\}, \end{aligned} \quad (4)$$

where m and n , independently of each other, may assume all values in the sequence 0, 1, 2, 3, 4, The z -coordinate used here is calculated along the optical axis of the core. The functions H_m and H_n are Hermite polynomials^[10] of order m and n ; together with $\exp\{-(x^2 + y^2)/w_0^2\}$, a (two-dimensional) Gaussian distribution function, they determine the transverse dependence of the various modes — which are therefore often referred to as Hermite-Gauss field distributions. In eq. (4) the propagation constant β is also 'labelled' by the mode numbers, m and n , to indicate that it cannot represent a continuum of values, just as in quantum mechanics the energy of a harmonic oscillator can only assume discrete values. The constant w_0 , a parameter of the core, will be dealt with separately later.

The modes can be divided into 'groups'. Within each group the *sum* of the mode numbers m and n is the same for all modes — which, as we shall see, implies that the propagation constant has the same value for all modes in the group, and thus characterizes a particular group (see eq. (6) below).

The expressions (4) may be used as modes for the formation of all components of both the electric and the magnetic field. In the case of a fundamental mode we use the expression for which $m = n = 0$; the relevant polynomials are then equal to 1 and the transverse dependence is completely determined by the Gaussian distribution function. The field distribution associated with the fundamental mode in the core is very important for the coupling, since more than 99% of the laser radiation itself is present in the field distribution corresponding to the *laser* fundamental mode, which is also purely Gaussian (or normal). The coupling is of course improved by this correspondence.

A fibre core with zero loss of radiation energy is an unattainable ideal. In an actual material bound modes have losses that increase with their mode numbers (m and n). Because of these losses, any given mode pattern in the core tends to degenerate into the fundamental mode as z increases. Since it is more concentrated about the axis, this mode will continue to exist longest and therefore propagate farthest. Also, a coupling between a fundamental mode and a higher-order mode always gives higher losses than a coupling between one fundamental mode and another [11].

Maximum matching

The art of coupling consists mainly in producing the best match between the near-field pattern of the laser radiation and the fundamental mode of the radiation field that can be excited in the fibre core — which may be considered as a dielectric waveguide inside a sheath or cladding, both with local cylindrical symmetry. The interface zone and the core of the fibre that follows it must also be 'matched' to ensure a continuous concentration of the optical energy along the axis — this is of course an essential contribution to the optical efficiency of the complete system.

Unfortunately, two of the characteristics of the available lasers are not very helpful here: their astigmatism and their ellipticity. Two of the AlGaAs types have both (fig. 4), with the result that more than 60% of the laser radiation will excite groups of higher-order modes inside the core. The excitation of higher orders will in any case cause an extra loss of concentration, compared with the fundamental mode. The first ten of these groups, with the bound modes, do make some contribution to the guidance of the electromagnetic energy; but with the leaky modes serious losses occur in guidance over distances of more than say 1000 wavelengths.

Two constants in eq. (4), the 'characteristic spot parameter' (w_0) and the propagation constant ($\beta_{m,n}$) mentioned earlier, should be treated separately here since they help to determine the concentration of the energy at the axis.

Characteristic spot parameter and propagation constant

In the derivation of eq. (4) dimensionless spatial coordinates are necessary. The unit of length adopted here is the characteristic spot parameter, w_0 . This is defined by:

$$\frac{1}{2} NA \times \frac{w_0^2}{a} = \frac{\lambda}{2\pi}, \quad (5)$$

where NA is the (maximum) numerical aperture of the core and a its radius.

We can see from eq. (5) that the quantities a and NA , which are of importance for the system design, therefore determine the characteristic spot parameter of the core at a given wavelength. Thinking mainly of guidance in the fundamental mode, we see from eq. (4) that at the distance w_0 away from the optical axis (this distance is about 7 μm for the pigtailed P_i) the amplitude of the field will have fallen to about $1/e$ of the maximum value. The irradiance there will therefore be as much as e^2 times smaller than on the axis. The length w_0 consequently functions as the radius of a circle (the 'spot'). As the characteristic spot parameter decreases, the electromagnetic energy becomes more concentrated around the axis of the core; this effect is strongest for the fundamental mode.

The propagation constant $\beta_{m,n}$ in eq. (4) derives its importance from the fact that it determines the magnitude of the velocity of energy transfer — or, more directly: of the velocity of power transfer — for the various groups of modes. The interesting thing is that it is only in core material with a parabolic refractive-index profile that these velocities are to a good approximation equal for the various groups. In practice this has the consequence that the intermodal dispersion — which broadens the signal pulses along the axis in proportion to the propagation time, and which can cause unacceptable intersymbol interference — remains two orders of magnitude smaller in this core material than in fibres where the refractive index has a stepped profile. This improves the transmission capacity of the parabolic material correspondingly.

Like the characteristic spot parameter of the core, the propagation constant also appears as the square in the mathematical manipulations used for the derivation of (4):

$$\beta_{m,n}^2 = \frac{1}{c^2} n_{co}^2 \omega^2 \left\{ 1 - 2(m+n+1) \frac{cNA}{\omega n_{co}^2 a} \right\}, \quad (6)$$

[10] L. Pauling and E. B. Wilson Jr., Introduction to quantum mechanics, McGraw-Hill, New York 1935.

[11] H. Kogelnik, Coupling and conversion coefficients for optical modes, in: J. Fox (ed.), Proc. Symp. on Quasi-optics (New York 1964), Polytechnic Press, Brooklyn, NY, 1964, pp. 333-347.

where again $m, n = 0, 1, 2, 3, 4, \dots$; c is the velocity of light and ω the angular frequency. From eq. (6), after taking the square root and expanding as a series:

$$\beta_{m,n} \approx \frac{1}{c} n_{co} \omega - (m+n+1) \frac{NA}{n_{co} a}. \quad (7)$$

From this result it can be seen that the energy-transfer velocity, which is equal to the group velocity ($= 1/(d\beta_{m,n}/d\omega)$), does not to a first approximation depend on the mode numbers m and n . If an exact calculation is made, a dependence on the mode numbers does emerge, with the restriction that they always appear as a sum $(m+n)$ — typical of the various *groups* of modes.

The approximate values for $\beta_{m,n}$ found in eq. (7) are valid only when the modes are of such low order that $2(m+n+1)cNA/(\omega n_{co}^2 a)$ is sufficiently small, in relation to 1, for the series to be terminated after two terms. An even greater restriction on the useful modes arises from the fact that the parabolic material does not of course fill the entire space; it extends only a distance a from the axis of the fibre. The higher the mode numbers, the further the mode pattern extends from the axis (this reflects the behaviour of the Hermite polynomials). Beyond a certain mode number the power contained in the modes will tend to lie in the zone of the cylindrical interface. In this situation such modes will rapidly lose power and, as leaky modes, will then contribute little if anything to the *guidance*.

The theory shows that the wave equation for the modes gives an oscillatory behaviour — in the lateral direction, corresponding to 'leakage' — at positions where $n^2(x,y)k_0^2$ exceeds $\beta_{m,n}^2$, and an exponentially decaying behaviour (i.e. 'guidance') at positions where $n(x,y)k_0^2$ is smaller than $\beta_{m,n}^2$. With D. Marcuse^[12] we may therefore locate the 'cut-off' for the guidance in our core at the largest value L of the sum $m+n+1$, for which the propagation constant is still dominant:

$$n^2(a)k_0^2 \leq \beta_{m,n}^2, \quad (8)$$

where $a = (x^2 + y^2)^{1/2}$ and $m+n+1 = L$. From equations (6) and (8) it can be shown that L is the largest integer that satisfies

$$L \leq \frac{1}{2} \frac{\omega}{c} a NA. \quad (9)$$

On substituting the appropriate data from Table I in eq. (9), we find confirmation that the first ten groups in the multimode fibres of second-generation cables do indeed include these bound modes. Modes of still higher order do not, as we have seen, make any significant contribution to the efficiency of the first interface zone, or may even reduce it. Fortunately, however, they are only weakly excited.

Free space and Gaussian beams

Before a pigtail can be reached, the laser beam must first travel two short distances in 'free space' (air in fact) in the interface zone, in front of the ball lens and

after it; the ball lens is the coupling element in this zone, as mentioned earlier. Since it was necessary to match the two fundamental modes as well as possible, we first established how exactly the excited laser fundamental mode would propagate as a radiation field directly linked to the end face of the laser.

The mathematical treatment again contains considerable simplification because the two spatial variables (x, y) occur separately. In such a region of free space the irradiance on the z -axis always has the maximum value, as would be expected in view of the existing symmetries in the laser. The calculations showed that at right-angles to the optical axis the irradiance decreases in a pure Gaussian curve as a function of x , the coordinate in the major plane of symmetry — assumed to be horizontal — of the active 'stripe' in the laser^[13]. As a function of y , i.e. in the vertical plane of symmetry, the decrease is also purely Gaussian, although at a different rate.

The two two-dimensional beams, whose field distributions give the total fundamental-mode field after multiplication, differ only in their 'effective' widths — which of course must always be compared at the *same* value of z . The cause of these differences lies in the different mechanisms for the 'confinement' (or guidance) of the radiation inside the laser in the related horizontal and vertical directions. The 'effective' widths of the two beams are established by means of the $1/e$ contour points, in other words the values of x and y at which the irradiance has fallen to $(1/e)^2$ of the value on the axis, taken at the same z .

The two beams, which are called 'Gaussian beams' to indicate their type, each originate from an initial constriction or 'waist', where their wavefront can be represented by a straight line. The initial waist of the beam is real in the vertical symmetry plane and located exactly at one of the end faces of the laser; the initial waist of the other beam is virtual and located towards the front, inside the laser. The distance between them varies from about 1 μm or less (denoted in fig. 4 by ' $\Delta \approx 0$ ') to 15 μm or even more (' $\Delta \approx 20$ ' in fig. 4). The longitudinal dimension of the two waists has a maximum value of a few μm ; the exact values depend on the type of laser used, of course. Since the waists do not coincide, the exit beam from the laser has the undesirable feature, mentioned earlier, that it is strongly astigmatic. When the radiation propagates in free space the two (planar) Gaussian beams will start to fan out (fig. 5). As the initial waist decreases the

[12] D. Marcuse, The impulse response of an optical fiber with parabolic index profile, Bell Syst. Tech. J. 52, 1169-1174, 1973.

[13] The calculations for the whole of the first interface zone are most simply performed when the coordinates x and y for equation (4), treated earlier, are the same as the coordinates here, chosen to suit the structure of the laser (fig. 4).

angle in free space in which rays of the beams can be encountered becomes larger. The emergent wavefront approximates to an arc of a circle.

In the paraxial approximation the radius of curvature of such a circular wavefront is equal to:

$$R(z) = z \left\{ 1 + \left(\frac{\pi w_{in}^2}{\lambda_0 z} \right)^2 \right\}, \tag{10}$$

where w_{in} is a measure equal to *half* the appropriate initial waist. The coordinate z is measured from the initial waist. It can be seen from eq. (10) that the wavefront can be approximated by a straight line for both small and large values of z (the curvature, $1/R(z)$, is then zero). The wavefront has its greatest curvature at the value z_m of z , given by:

$$\frac{1}{2} \frac{1}{z_m} \times w_{in}^2 = \frac{\lambda_0}{2\pi}. \tag{11}$$

The corresponding minimum radius of curvature, R_{min} , is given by:

$$\frac{1}{R_{min}} \times w_{in}^2 = \frac{\lambda_0}{2\pi}. \tag{12}$$

From equations (11) and (12) it also follows that R_{min} is equal to $2z_m$.

To characterize the Gaussian beams completely we need in addition to their radii of curvature their effective widths, of course. In the paraxial approximation these are given by:

$$w(z) = w_{in} \left\{ 1 + \left(\frac{\lambda_0 z}{\pi w_{in}^2} \right)^2 \right\}^{1/2} \tag{13}$$

where $w(z)$ is a dimension equal to *half* the effective width at the position z (again measured from the initial waist). The effective width is chosen so that along the z -axis it corresponds to four times the standard deviation of the local distribution of the irradiance. In mathematical terms, this local distribution is simply a normal probability distribution. It may be seen from eq. (13) that as they spread out in free space the Gaussian beams follow hyperbolic branches as boundary contours. The asymptotes intersect exactly at the centre of the initial waist, and their angle of inclination $\frac{1}{2} \psi_{axis}$ to the optical axis — a kind of far-field value of half the beam divergence — satisfies the equation:

$$\frac{1}{2} w_{in} \times \tan \left(\frac{1}{2} \psi_{axis} \right) = \frac{\lambda_0}{2\pi}. \tag{14a}$$

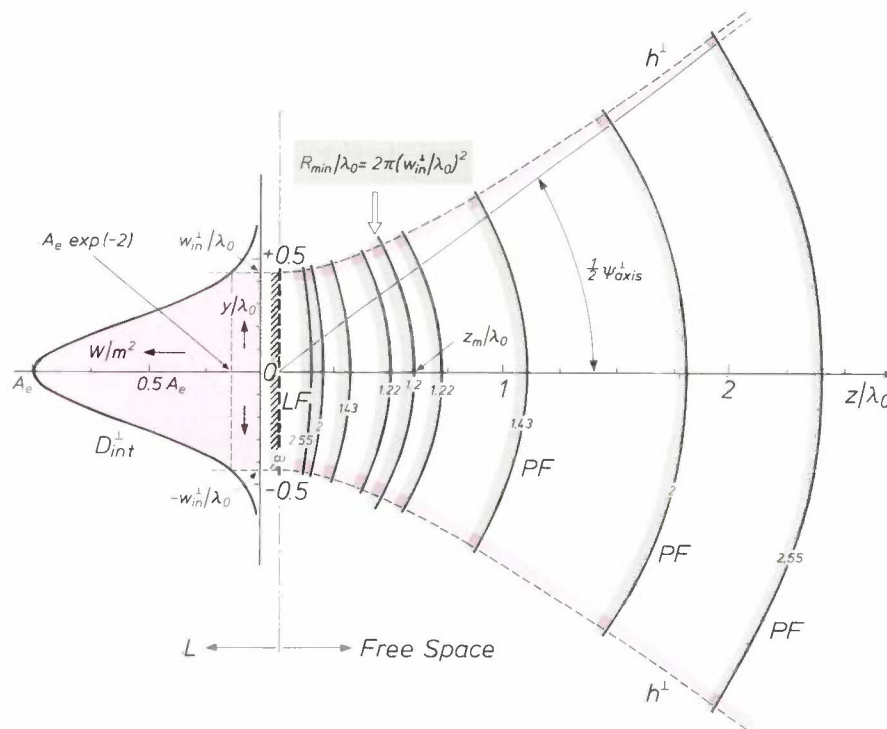


Fig. 5. Calculated example of a Gaussian beam emerging from a laser (L) and fanning out in free space. This situation exists just in front of the ball lens of a coupling element C_{1i} (fig. 3a). The circular arcs, considered to be in the vertical plane (some are marked PF) represent eight wavefronts. The radius of curvature is indicated on each wavefront in terms of λ_0 , the laser wavelength: two wavefronts are shown for each curvature. The ninth wavefront, at the dimensionless coordinate $z_m/\lambda_0 = 0.6$, has the smallest possible radius of curvature (R_{min}), determined by λ_0 and w_{in}^{\perp} , half the width of the initial waist of the beam taken as an example, in the (y, z) -plane. The waist is located in LF , the partly transmitting end face of L ; its radius of curvature is of course ∞ . The corresponding normal distribution function D_{int}^{\perp} for the irradiance in LF is plotted against y/λ_0 , the dimensionless vertical coordinate. The maximum value (A_e) of D_{int}^{\perp} is found exactly at the origin (O) of the z -axis, the optical axis of the laser. h^{\perp} hyperbolic branches; at each point the intensity is equal to the local maximum (i.e. the maximum on the optical axis for the same z) multiplied by $\exp(-2)$. These hyperbolic branches are widely used in practice for mathematically defining the boundaries of Gaussian beams — about 95% of the energy is contained within these boundaries. The laser parameters taken for this example are: $\lambda_0 = 1.3 \mu\text{m}$ and $w_{in}^{\perp} = 0.568 \mu\text{m}$ (see also fig. 6).

Substituting eq. (11) in eq. (14a) we find:

$$\tan\left(\frac{1}{2}\psi_{\text{axis}}\right) = \frac{w_{\text{in}}}{z_m} \quad (14b)$$

If the astigmatism of the laser were negligible, the hyperbolic branches in fig. 5 could be considered as a longitudinal cross-section, in free space, of a complete hyperboloid with rotational symmetry.

The possible spread in the angle of inclination of the light rays, given by the angle ψ_{axis} in eq. (14a), and the possible spread in the spatial coordinate of the light rays, given by w_{in} , are related to one another in a way that makes eq. (14a) the analogue of a Heisenberg uncertainty relation. The wavelength λ_0 then represents the analogue of Planck's constant.

w_{in}^{\perp} in the vertical plane (red contour) and secondly for the beam from $w_{\text{in}}^{\parallel}$ in the horizontal plane (blue contour, partly virtual). In minimizing the insertion losses the greatest difficulty here is not so much that w_{in}^{\perp} and $w_{\text{in}}^{\parallel}$ are about an order of magnitude smaller than the characteristic spot parameter (w_0) of the given fibre, but rather the reality that the laser beams are often strongly astigmatic (Δ , in this case put at $15 \mu\text{m}$). A lens that functioned theoretically in the best possible way would at least get rid of the astigmatism and could consequently have no rotational symmetry. To avoid fabrication difficulties (and ex-

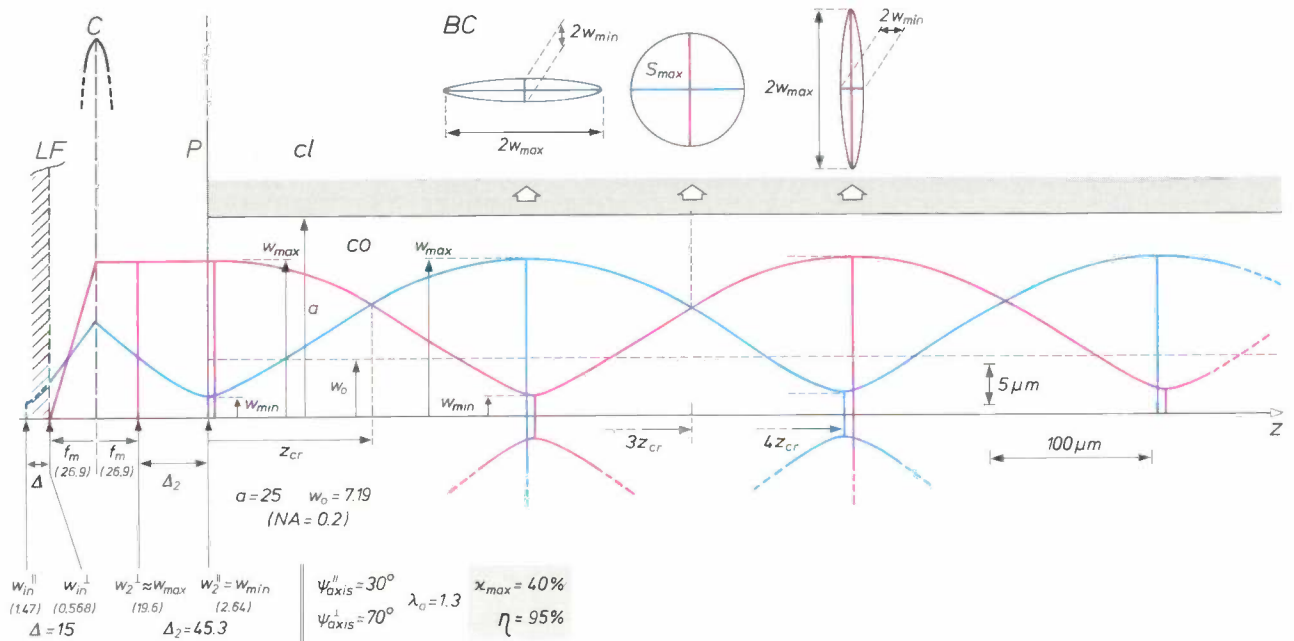


Fig. 6. Calculated example of an optimized optical interface with matching beam guidance along an optical axis (z), obtained by the collimator action of a single lens (C) and repetitive focusing in a fibre core (co) of a pigtail (P). The actual rays are *not* shown, but two bounding contours are shown in part (red: in the vertical plane, blue: in the horizontal plane). The rays are assumed to start from a real waist (w_{in}^{\perp}) at the partly transmitting end face (LF) of a laser, or a virtual waist ($w_{\text{in}}^{\parallel}$) inside the laser. The wavelength (λ_0) of the laser and its two beam divergence angles ($\psi_{\text{axis}}^{\perp}$ and $\psi_{\text{axis}}^{\parallel}$) are given; the two input waists can be calculated from equation (14a). The laser has an astigmatism (Δ) which is also shown. f_m focal length of C . a , NA , w_0 characteristic parameters of the core. All quantities are expressed in μm (except NA , which is dimensionless). Particulars of the image waists (w_2^{\perp} and w_2^{\parallel}), the astigmatism Δ_2 , the coordinate of position z_{cr} and the extremes (w_{min} and w_{max}) will be found in the text. Three typical beam cross-sections are illustrated in BC . The centre one (S_{max}) represents the largest beam cross-section in the fibre core (see also fig. 7). η maximum coupling efficiency, calculated ratio of the power of the guided beam, at the start inside co , to the power of the input beam on leaving the laser, as a percentage. χ_{max} calculated fraction of the power of the input beam that receives the fundamental mode in the core of the fibre as transfer medium, also as a percentage. cl cladding of the pigtail.

The ball lens: strength and position of the coupling element

The left-hand side of fig. 6 illustrates how an 'ideal', i.e. aberration-free, single lens (C) in our communication system pinches a Gaussian beam fanning out from a waist (see fig. 5) to form a converging Gaussian beam. This correcting action of C has been calculated and depicted twice, first for the beam from the waist

(pense) we have confined ourselves to simple lenses, which do have such symmetry [14]. As already mentioned, beads of high-grade optical glass are satisfactory for this purpose; they need to have a diameter of only a fraction of a millimetre.

In the pinching of the Gaussian beams in the 'free space' beyond C the waists w_2^{\perp} and w_2^{\parallel} are formed; they can be considered to be the images of w_{in}^{\perp} and

w_{in}^{\parallel} . These two images can be said to be ‘ideal’, since the field distributions on either side of C match one another perfectly, the reflection and absorption losses caused by C are negligible, and, as assumed, there are no aberrations. Of course, the astigmatism is still there, and consequently w_2^{\perp} and w_2^{\parallel} are spaced by Δ_2 instead of being coincident. After passing C the beam formed there brings all the rays contained in it, via the consecutive waists w_2^{\perp} and w_2^{\parallel} , into the fibre core (co) ‘matched as well as possible’. This matching requirement implies that the largest lateral cross-section of the radiation field within co should be minimized; this is done by making a suitable choice for the strength of C and its position. Particular attention is paid to finding the optimum position for the entrance plane of P , which should of course theoretically lie somewhere on the section of path (Δ_2) defined by the two waists w_2^{\perp} and w_2^{\parallel} .

At the centre of fig. 6 it can be seen how a continuous concentration of the optical energy along the axis (z) is ensured by the alternate ‘expansion and contraction’ of the field in co . The photograph (fig. 7) shows a three-dimensional model of such a field, made in plastic on a numerically controlled lathe.

A guided field of this type — the resultant of all the modes excited in co — can always be based in a mathematical sense on the *spatially oscillating* contours (red and blue in fig. 6) of two planar Gaussian beams at right angles to one another. This is illustrated in fig. 6 by the beam cross-sections (BC). The two elliptical cross-sections have the same area, $\pi w_{max} \times w_{min}$. This value is equal to the area of the characteristic spot, πw_0^2 , a property which is connected with the self-focusing character of the parabolic medium [15]. The circular cross-section (S_{max}), which occurs at the location of the points of intersection of the two contours, is the largest lateral section of the entire radiation field inside co . Calculations show that it is given by:

$$S_{max} = \frac{1}{2} \pi w_0^2 \left(\frac{w_{max}}{w_{min}} + \frac{w_{min}}{w_{max}} \right), \quad (15)$$

where w_{max} is half the maximum width of the two oscillating contours, and w_{min} is half the minimum width, again of the two contours.

The half-width, $w^{\parallel}(z)$, of the blue contour satisfies the equation [15]:

$$(w^{\parallel}(z))^2 = w_{min}^2 \cos^2 \left(\frac{\lambda_0 z}{\pi w_0^2} \right) + w_{max}^2 \sin^2 \left(\frac{\lambda_0 z}{\pi w_0^2} \right). \quad (16a)$$

The half-width, $w^{\perp}(z)$, of the red contour satisfies the equation:

$$(w^{\perp}(z))^2 = w_{max}^2 \cos^2 \left(\frac{\lambda_0 z}{\pi w_0^2} \right) + w_{min}^2 \sin^2 \left(\frac{\lambda_0 z}{\pi w_0^2} \right). \quad (16b)$$

In both equations the z -coordinate should be taken from the first extreme value inside the core. In the case of the blue contour that extreme value is the minimum ‘exactly’ at the front plane of co ; in the case of the red contour, on the other hand, it is the maximum that occurs at a finite distance, although negligible in practice (less than 5 μm), from that same front plane. Half-way between the first minimum and the first maximum of the blue contour is the point of intersection of the two contours; its z -coordinate (z_{cr}) is found to be equal to $\frac{1}{4} \pi a/NA$. The period of spatial oscillation for both contours, as can be seen from fig. 6, is equal to four times the distance z_{cr} .

The different rays that can exist, in terms of geometrical optics, within such oscillatory envelopes include ‘straight’ rays that follow the optical axis, and *curved* rays that start at acute angles to the optical axis and then continually return to the axis to intersect the straight rays repeatedly, forming a row of regularly distributed image points along this axis (‘repetitive focusing’, characteristic of the guidance of rays by a parabolic refractive-index profile). In view of the formation of such a row of axial image points, the mean pro-

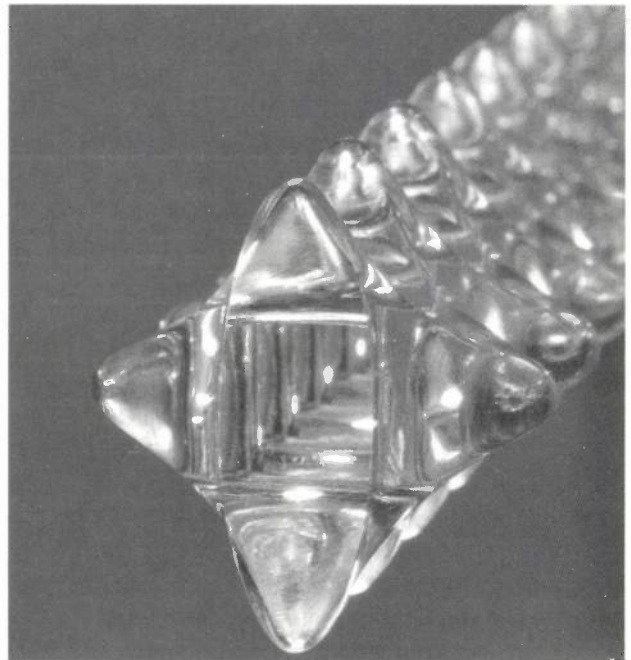


Fig. 7. Model of a stationary field distribution for a guided beam of rays inside a fibre core. The bounding surface of the field distribution is so defined that about 95% of the radiant energy is contained within it. In the direction of the optical axis it can be seen that the bounding surface has a row of maxima in both the vertical plane and the horizontal plane, and also on both sides (the maxima are the zones where the surface is furthest from the axis). Alternating with the maxima are minima — hence the guiding effect. The minima are barely visible in the photograph. The distance of the minima from the axis can however be estimated from the vertical ellipse at the front of the model. Half the minor axis of the ellipse is approximately equal to this minimum distance (w_{min} in fig. 6). Half the major axis of the ellipse is of course equal to the maximum distance (w_{max} in fig. 6). In this model the ratio w_{max}/w_{min} is about half the value of that used in fig. 6. Although there is this difference, the two ellipses in the group of three beam cross-sections shown in fig. 6 (BC) can easily be traced in this photograph.

[14] A. J. A. Nicia, Loss analysis of laser-fiber coupling and fiber combiner, and its application to wavelength division multiplexing, *Appl. Opt.* 21, 4280-4289, 1982. See also: errata, *Appl. Opt.* 22, 1801, 1983.

[15] J. A. Arnaud, *Beam and fiber optics*, Academic Press, New York 1976.

pagation velocity along the axis must be the same for rays of both kinds. The equality of these two mean velocities is indeed made possible by the two principal properties of the core material: the rotational symmetry and the parabolic decrease of the refractive index in the radial direction (eq. 3). The curved rays, which are not shown in fig. 6, have a spatial variation that resembles the corresponding oscillatory envelope, with the restriction that the oscillation period of an envelope is exactly half that of an enclosed individual curved ray [16].

Clearly, when the wavefronts pass through the ball lens (C) their curvature changes more or less abruptly. The further development of these modified wavefronts determines the 'image waists' (w_2^\perp and w_2^\parallel), as mentioned earlier, and in their turn these determine the w_{\max} and w_{\min} occurring inside the core (co). One more parameter that plays a role, and is in principle variable, is the position of the front plane of co .

Calculations of this 'waist-on-waist' image formation have shown that the lens strength we are looking for has an upper limit, D_m [16]:

$$D_m = \frac{\lambda_0}{\pi} \text{minimum} \left(\frac{1}{w_{in}^\perp w_2^\perp}, \frac{1}{w_{in}^\parallel w_2^\parallel} \right). \quad (17)$$

With a stronger lens the image waists could no longer be correctly dimensioned, which would impair the coupling efficiency unnecessarily. The focal length of the ball lens must therefore be no smaller than f_m ($\equiv 1/D_m$). The marginal value for the focal length, $1/D_m$, is a choice that is only just possible. The case illustrated in fig. 6 was in fact based on that choice.

There are three practical reasons for adopting this marginal coupling geometry. The marginal (i.e. minimum) value of the focal length goes with the smallest possible value for the spherical aberration of the ball lens, which is the first advantage [17]. Reducing the focal length obviously implies reducing the dimensions of the coupling element: the second advantage. The third advantage is that the alignment of the lens with respect to the laser is greatly simplified. The partly transmitting end face (LF) of the laser should coincide with a focus; the lens is therefore displaced axially in such a way that the divergence of the beam in the vertical plane reaches a minimum well past the lens, as can easily be ascertained, at least before the pigtail (P) has been mounted. A coupling geometry as shown in fig. 6, with an 'object waist' (LF) at the focal point of the lens, might be called a 'collimator geometry' or, to be somewhat more exact (because of the astigmatism Δ on the object side) a *semi-collimator geometry*. At this stage of the treatment, however, D_m cannot be derived from eq. (17) since the image waists (w_2^\perp and w_2^\parallel) are as yet unknown.

It can be seen from eq. (15) that optimizing the coupling element certainly implies making S_{\max}

smaller, because the field distribution will then become more concentrated around the axis. On referring to fig. 7 and eq. (15) it can be seen that to achieve maximum coupling efficiency — which corresponds to optimum matching — the largest beamwidth within the core ($2w_{\max}$ in fig. 6) must have the same value in both the horizontal and vertical planes; this value must also be minimized. In other words, the circumscribed circle of the field distribution perpendicular to the z -axis must be as small as possible. For this double minimization two independent variables are required: the ones chosen are the strength of the ball lens C and the ratio of the line sections into which the transformed astigmatism Δ_2 is divided by the front plane of the pigtail (P). (In fig. 6 this ratio has the marginal value 0, which is connected with the choice of the *marginal* variable, D_m , for the lens strength.)

The first result of the mathematical determination of the double minimization is that the best match with a coupling element with a semi-collimator geometry, as in fig. 6, will be obtained when the strength of the ball lens (C) is equal to:

$$D_m = \left(\frac{\varepsilon}{\Delta} \frac{NA}{a} \right)^{1/2}, \quad (18)$$

where ε is the ellipticity ($= w_{in}^\parallel/w_{in}^\perp$, see fig. 4) of the laser.

The lens strength required is therefore, from equation (18), the geometric mean of two quantities, the first (ε/Δ) originating from the laser, the second (NA/a) originating from the pigtail. The second result of the double minimization is the location of the front plane of P on Δ_2 .

The calculations show that the best distance (δs) to the image waist w_2^\parallel is equal to:

$$\delta s \approx \left(\frac{\pi}{\lambda_0} \frac{w_{in}^\parallel w_{in}^\perp}{\Delta} \right)^2 \left\{ 1 - \left(\frac{\pi}{\lambda_0} \right)^2 \frac{(w_{in}^\parallel)^4}{\Delta^2} \right\} \Delta_2, \quad (19)$$

where Δ_2 , the astigmatism in the image space, is equal to:

$$\Delta_2 \approx \frac{a}{NA} \frac{w_{in}^\perp}{w_{in}^\parallel} \left\{ 1 - \frac{1}{2} \left(\frac{\pi}{\lambda_0} \right)^2 \frac{(w_{in}^\parallel)^4}{\Delta^2} \right\}. \quad (20)$$

The condition for the validity of equations (19) and (20) is that $\pi^2 (w_{in}^\parallel)^4 / (\lambda_0 \Delta)^2 \ll 1$. The relatively large value for the astigmatism Δ in the laser explains why $\delta s/\Delta_2$ remains negligibly small — about 0.016 in the example given in fig. 6.

The two image waists, w_2^\perp and w_2^\parallel , in the case of the semi-collimator geometry, are given by:

$$w_2^\perp \approx \frac{\lambda_0}{\pi} \left(\frac{a}{NA} \frac{\Delta}{w_{in}^\perp w_{in}^\parallel} \right)^{1/2}, \quad (21)$$

and

$$w_2^\parallel \approx \left(\frac{a}{NA} \frac{w_{in}^\perp w_{in}^\parallel}{\Delta} \right)^{1/2}. \quad (22)$$

Using eq. (5) we easily find from this pair of equations that:

$$w_2^\perp w_2^\parallel = w_0^2, \quad (23)$$

which is a further illustration of the attainment of (or better: good approximation to) the best possible match using the arrangement described for the interface zone between laser and pigtail.

In the case of the semi-collimator geometry it is found to be a good approximation to let the position of the front plane of the connecting pigtail coincide with the end of the transformed astigmatism in the image space of the lens — i.e. at w_2^\parallel . The magnitude of Δ_2 itself is immaterial since, of course, with the semi-collimator geometry w_{in}^\perp will be magnified much more than w_{in}^\parallel . (In the example of fig. 6 the magnifications are $34\times$ and $1.8\times$ respectively.) The beam divergence in the vertical plane is therefore almost zero (the red contour between C and P , fig. 6).

Coupling efficiency

Further calculations on the double-minimization conditions mentioned in the previous section, at the coupling interface with the semi-collimator geometry (fig. 6), have enabled us to find the maximum possible efficiency (κ_{max}) for energy transfer via the fundamental mode. The expression found is ^{[14][17]}:

$$\kappa_{max} = \frac{2}{1 + \frac{1}{2} \left\{ \left(\varepsilon + \frac{1}{\varepsilon} \right)^2 + b^2 \right\}^{1/2}}, \quad (24)$$

where κ_{max} is the maximum ratio of the power in the guided beam that acquires the fundamental mode in the core as transfer field to the total power in the input beam (i.e. the total power emitted as a laser signal); ε is the ellipticity $w_{in}^\parallel/w_{in}^\perp$, as stated, of the laser. The astigmatism of the laser is accounted for here by the parameter b , with the astigmatism Δ taken equal to $(\pi/\lambda_0)w_{in}^\parallel w_{in}^\perp \times b$. When the ellipticity has its smallest value (1) and if also the laser is 'ideal', with absolutely no astigmatism, the efficiency κ_{max} will be exactly equal to 1 (or 100%), the maximum possible value for the coupling of one fundamental mode (that of the laser) to another. We note here that eq. (24) can also be used for estimating the maximum attainable efficiency for the coupling between a laser and a *single-mode* fibre.

To establish the *total* efficiency (η in fig. 6), characterizing the coupling interface, it is of course necessary to include in the calculation the amounts of power that are *not* transferred by the fundamental mode in the core but by the groups of bound modes of higher order. The desired expression for the best total coupling efficiency is:

$$\eta = \kappa_{max} \{ 1 + (1 - \kappa_{max}) + (1 - \kappa_{max})^2 + \dots \\ \dots + (1 - \kappa_{max})^{II-1} + (1 - \kappa_{max})^{II} \}, \quad (25)$$

where η is the maximum possible ratio of the total power of the guided beam — at the start inside the core — to the total power of the input beam calculated as the beam leaves the laser. The quantity II , the highest exponent of the geometric progression in eq. (25), is the *number* of groups of bound modes. Taking into account the cut-off point for guided modes (eq. 9) and the fact that only the groups of modes for which the sum $m + n + 1$ is *even* can be excited, we find for II as an integer the value (rounded downwards) of the expression $\frac{1}{2} \{ (\pi/\lambda_0) a NA - 1 \}$. From eq. (25) it is also easily shown that η will, at least theoretically, approach the maximum 1 (or 100%) when κ_{max} itself approaches the value of 100% or when II is very large.

Modes for which $m + n + 1$ is odd cannot be excited, essentially because of the occurrence of the Hermite polynomials. These polynomials are even or odd functions of the appropriate transverse coordinate, depending on whether the mode number is even or odd. The expression for a coupling coefficient ^[11] contains a product of two Hermite polynomials. For our system one polynomial cannot be other than H_0 , i.e. equal to 1, since the laser emits its radiation only in the fundamental mode. Integration over the transverse coordinate from $-\infty$ to $+\infty$, stemming from the requirement to match the two field distributions on either side of the 'coupling plane', gives zero for the coupling coefficient, unless the two polynomials in the product have the same parity. In the present case of the coupling to the laser the parity is thus *even*.

The equations (24) and (25) therefore make it possible for the designer to calculate the maximized coupling efficiency of such an optical interface, using the characteristic data of the laser and the pigtail as more or less free parameters.

The value of 95% calculated for η by way of example from eq. (25) as shown in fig. 6 is typical of the efficiency that the coupling elements C_{1i} (fig. 3a) should theoretically be able to attain if reflection and absorption are neglected. The values that can be obtained with coupling elements corresponding to our system are somewhat lower; as mentioned earlier, the practical values were found to be between 50 and 80%.

The efficiencies of the coupling elements C_{2i} , between the pigtails at the output of the optical section and the photodiodes, will certainly be no lower, because of the strongly pronounced local 'trumpet geometry' mentioned earlier (the 'characteristic diameter'

^[16] See for example the book by D. Marcuse mentioned in [9] or H. Kogelnik and T. Li, Appl. Opt. 5, 1550-1567, 1966.

^[17] A. J. A. Nicia, Micro-optical devices for fiber communication, Thesis, Eindhoven 1983.

increases from 100 μm to 300 μm ; see fig. 3b). The value for η should really be 100%, apart from minor reflection losses, and a short piece of 'light-pipe' is an adequate coupling element. For the last of the four green blocks in fig. 3a no 'real' coupling lens is therefore necessary.

To obtain an estimate for the total coupling efficiency for the four interface zones in fig. 3a it is also necessary to take into account the two green blocks containing the multiplexing and demultiplexing units. Anticipating results in part II of the article, we should think here in terms of an efficiency of 50% for the multiplexing and demultiplexing units together. A reasonable estimate of the total coupling efficiency for the four interface zones in our system would therefore seem to be 25%, which corresponds to a loss of 6 dB.

Finally, we should note that the parameters of the pigtail in the calculation of η are expressed directly in the exponent Π alone. This once more emphasizes that the higher-order bound modes in the core can also make a very important contribution to the coupling efficiency.

The efficiency equations (24) and (25) have a wider validity than might perhaps be supposed from the marginal coupling geometry on which fig. 6 is based. As long as the lens strength remains below the upper limit indicated in eq. (17), the double minimization described always gives the same pair of expressions for κ_{max} and η as equations (24) and (25); the lens strength does not therefore appear as an explicit parameter in these equations. The reason for this is the assumption that the lens, as an 'ideal' coupling element, introduces no optical losses, i.e. no reflection or absorption losses. The required 'matching' of the electromagnetic field from the laser to the field that

can exist inside the fibre core — and the associated enlargement on imaging the initial waists — is apparently so simple an optical transformation that it does *not* uniquely determine the strength of the lens (which it does, however, once the interface zone has to meet geometrical requirements as well, as in the example in fig. 6).

The curves plotted in fig. 8 for constant κ_{max} values show how very much the astigmatism of the laser

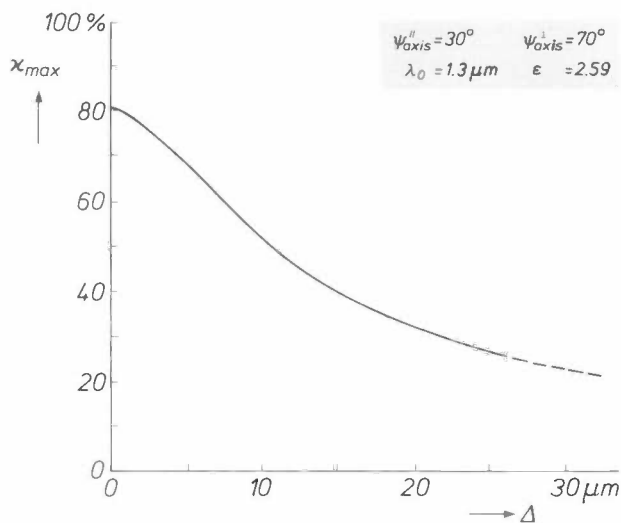


Fig. 9. The maximum coupling efficiency κ_{max} for power transfer to the fundamental mode in the fibre core, from equation (24). The independent variable Δ is the astigmatism (in μm) in the laser. The other laser parameters (λ_0 , ϵ , $\psi_{\text{axis}}^{\parallel}$, $\psi_{\text{axis}}^{\perp}$) are made equal to those of the laser used in the example in fig. 6.

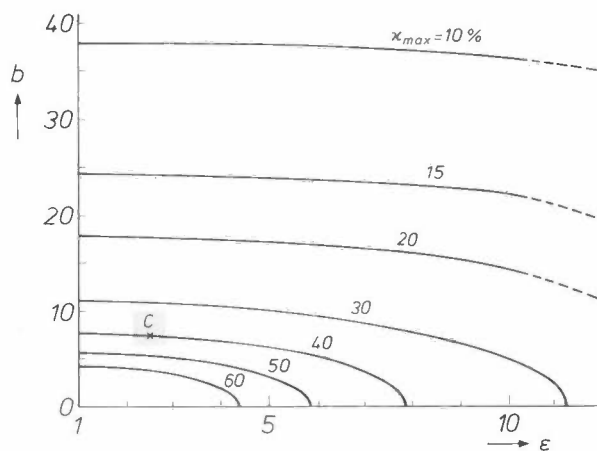


Fig. 8. Family of curves for κ_{max} values, in percentages, calculated from equation (24), with the ellipticity ϵ and the astigmatism parameter b of the laser as dimensionless input variables. C the example from fig. 6 (the laser-fibre coupling with semi-collimator geometry).

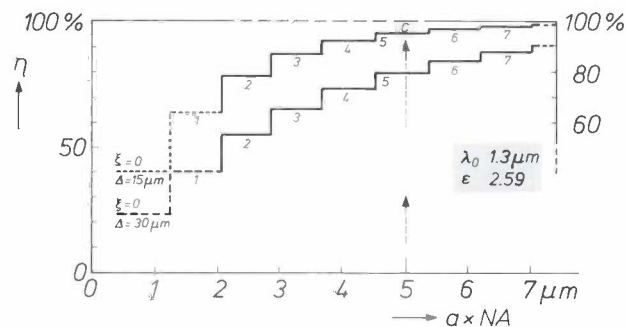


Fig. 10. Two calculated curves for the best total coupling efficiency η , in percentages, at optical interfaces via a coupling lens, from a laser to a pigtail, as given by equation (25). The independent variable is $a \times NA$, in μm , the product of the core radius and the maximum numerical aperture of the pigtail. λ_0 , ϵ , Δ are the wavelength, ellipticity and astigmatism of the laser. ξ positive integer, which identifies a group of higher-order modes (see text). The total coupling efficiency, as indicated by the stepped shape, is the sum of the contributions of the separate groups of guided modes. For the dashed part of the curves the theory used does not seem entirely adequate [14][17]. C the example from fig. 6 ($a = 25 \mu\text{m}$, $NA = 0.2$). If the contribution to η from a group of modes vanishes on reduction of the independent variable, the term cut-off is used, although that group is — and continues to be — excited.

weakens the coupling to the fundamental mode of the fibre core. The effect of the ellipticity seems relatively small, as appears from the rather horizontal nature of the curves. Mathematically, this behaviour is understandable, since the quantity $\varepsilon + 1/\varepsilon$ in eq. (24) varies more slowly than b , the variable that represents the astigmatism.

Fig. 9 shows κ_{\max} as a function of the astigmatism for lasers that correspond in all other characteristics (λ_0 , ε , $\psi_{\text{axis}}^{\parallel}$, $\psi_{\text{axis}}^{\perp}$) to the laser in fig. 6. An astigmatism of even only a few μm — which can also occur in some index-guiding lasers (fig. 4) — has a distinctly reducing effect on κ_{\max} .

Fig. 10, finally, illustrates the multimode nature of the guidance of the radiation. The independent variable plotted horizontally is the product of the radius of the core and its numerical aperture. The efficiency, as given by eq. (25), follows a rising 'staircase' curve. Whenever the product $a \times NA$ exceeds a value of $(\lambda_0/\pi)(2\xi + 1)$ when the curve is followed — where ξ is a positive integer — a group of modes of higher order 'join in', and consequently this accounts for a contribution of $\kappa_{\max}(1 - \kappa_{\max})^\xi$ to the efficiency. If the astigmatism (Δ) of the laser were zero, then the

variation of $a \times NA$ would have hardly any effect, since η would have been about 100% right from the start and the groups of higher-order modes would make no significant contribution to the total coupling efficiency.

Summary. A study of an optical communication system for digital or analog signals is described. Wavelength-division multiplexing is used with minimized insertion losses. The design provides for three to four channels in parallel operation in a multimode optical fibre (with a square-law core, radius 25 μm , numerical aperture 0.2, $\text{MHz} \times \text{km}$ product about 2000) in a second-generation cable for optical telecommunication. The light sources are diode lasers operating at wavelengths of 0.83 μm , 0.87 μm , 1.30 μm and 1.55 μm . The detectors are photodiodes of about 300 μm diameter and a maximum rate of response of 500 MHz. The multiplexing and demultiplexing components are the main subject of part II of the article. Part I deals with the maximization of the total system efficiency. There are four interface zones, accounting for a total insertion loss of about 6 dB. The first interface (laser to fibre via a ball lens) is analysed using Hermitian-Gaussian modal field distributions. The astigmatism and ellipticity of the lasers, and the cut-off of the higher-order modes (because of the finite radius of the fibre core) are accounted for in the optimized efficiency equations. An astigmatism of only a few μm reduces the efficiency noticeably. The optimum strength and the location of the ball lens (between laser and fibre) are derived for the case of the semi-collimator geometry. The behaviour of two-dimensional Gaussian beams in free space and inside the core is also calculated.

Beam manipulation with optical fibres in laser welding

At the Centre for Manufacturing Technology (CFT) in Eindhoven a method for beam manipulation in laser welding has been developed in which the laser beam is conducted from the laser to the workpiece by optical fibres. Before we look more closely at this new method, we shall first compare resistance spot-welding with laser spot-welding, and then we shall say something about the conventional method for beam manipulation.

For welding light metal components together in large numbers, considerable use is made of resistance spot-welding^[1]. In this method the components are pressed together by two pointed electrodes, and then the material is heated by passing a current. Because of the higher contact resistance the heating effect is greatest at the places where the parts to be welded touch: the metal melts, and a strong weld results after cooling. A disadvantage of spot-welding is that the fairly large compression forces can cause distortion of the components. This can lead to complications, particularly in light components that have to be welded together very accurately. This is the case for example in assembling the electron guns for television picture tubes or the heads for tape-recording equipment.

A welding method that does not have this disadvantage is laser spot-welding. In this method the heating of the material is produced by a focused laser beam (we shall return to this later).

Laser welding has a number of advantages over resistance spot-welding:

- The components to be welded are not pressed together during the welding and therefore do not become distorted because of this.
- There is no need for welding electrodes, which wear very easily, so that far less maintenance is usually necessary, and the machine is out of action for much less time. (Welding electrodes can be used for about 5000 welds before they have to be replaced; a laser spot-welder can make about 10^6 welds without maintenance.)
- The quality of the weld is better than in resistance welding.
- The laser beam can reach places that welding electrodes cannot reach.
- The materials to be welded do not have to be electrically conducting. Laser welding does however have some disadvantages: the capital investment required is high, and the components have to be positioned accurately in relation to one another and to the laser beam.

For laser spot-welding an Nd:YAG laser is frequently used; this has a wavelength of $1.06 \mu\text{m}$. The emitted beam consists of light pulses whose energy content, pulse duration and repetition rate can be controlled. The pulses used generally have a duration from 3 to 10 ms and a repetition rate of up to 100 Hz. Their energy content is in the range 2 to 15 J.

For efficient mass production the way in which the laser beam is directed to the weld location is of great importance. The simplest solution is shown in *fig. 1a*. Here the laser beam is focused directly on to the workpiece by a lens. A small displacement of the focus (the weld point) can be obtained by moving the lens perpendicularly with respect to the beam; this possibility is indicated in *fig. 1a* by the dotted line. If more than one weld per workpiece is required, there are various possibilities. The workpiece can be displaced after each weld in such a way that the next weld can be made. This can however give a complicated arrangement — since there are six degrees of freedom for the movement. Moreover, the continual displacement of

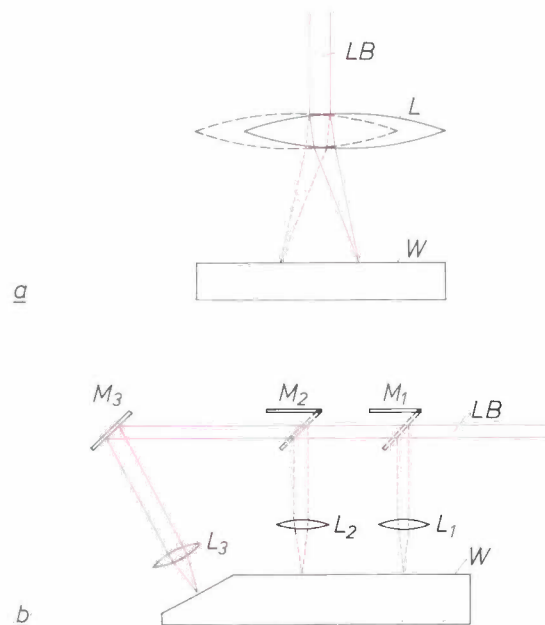


Fig. 1. Focusing the laser beam on to the workpiece. *a*) The simplest case. *LB* laser beam. *L* lens. *W* workpiece. A small displacement of the focus can be obtained by displacing the lens (dashed line). *b*) Making more than one weld on the workpiece. *M*₁₋₃ mirrors, which may be pivoted. The other symbols are as in (*a*). This arrangement is not easily modified to suit another product, however.

[1] See for example pages 333-335 of R. L. Little, *Metalworking technology*, McGraw-Hill, New York 1977.

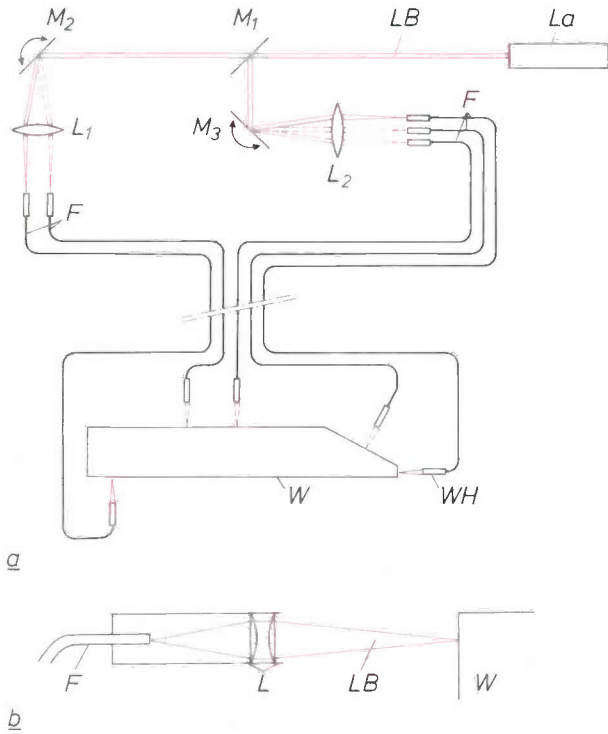


Fig. 2. a) Diagram of beam manipulation with optical fibres. L_a Nd:YAG laser. M_1 half-silvered mirror. M_2, M_3 numerically controlled mirrors; in the case shown M_2 has 2 different positions and M_3 has 3. L_1, L_2 lenses that focus the split laser beam on to the optical fibres F . WH welding heads attached to the optical fibres, to focus the laser beam on to the workpiece W . Because the fibres are flexible it is easy to reach the workpiece from all sides. b) Diagram of the welding head. The laser beam LB emitted from the fibre F is collimated by the pair of lenses L and focused on to the workpiece W .

the workpiece is rather time-consuming. Another solution is the installation of as many lasers as the number of welds that have to be made on each workpiece. This requires a very high capital investment, however. Another disadvantage of these two possible solutions is that the arrangement cannot be altered quickly for another product.

Another solution is to manipulate the laser beam in such a way that various weld locations on the workpiece can be reached with a single laser beam. It would for example be possible to use various combinations of pivoted or half-silvered mirrors (see fig. 1b). However, these arrangements are also not easy to alter to suit a new product.

At CFT work is now in progress on a better solution in which optical fibres are used. With the aid of numerically controlled mirrors and several lenses the laser beam is divided and focused on to a number of optical fibres; see fig. 2a. These optical fibres consist of a core of quartz glass (with a diameter of 600 μm) surrounded by cladding with a lower refractive index and a plastic protective coating. The laser beam can propagate along the core by total internal reflection at the cladding. In these optical fibres the laser beam can be transmitted over considerable distances (up to 100 m) with no significant losses. At the far end of each optical fibre there is a 'welding head' with a lens that focuses the beam emitted from the fibre on to the workpiece; see fig. 2b. The total optical losses amount

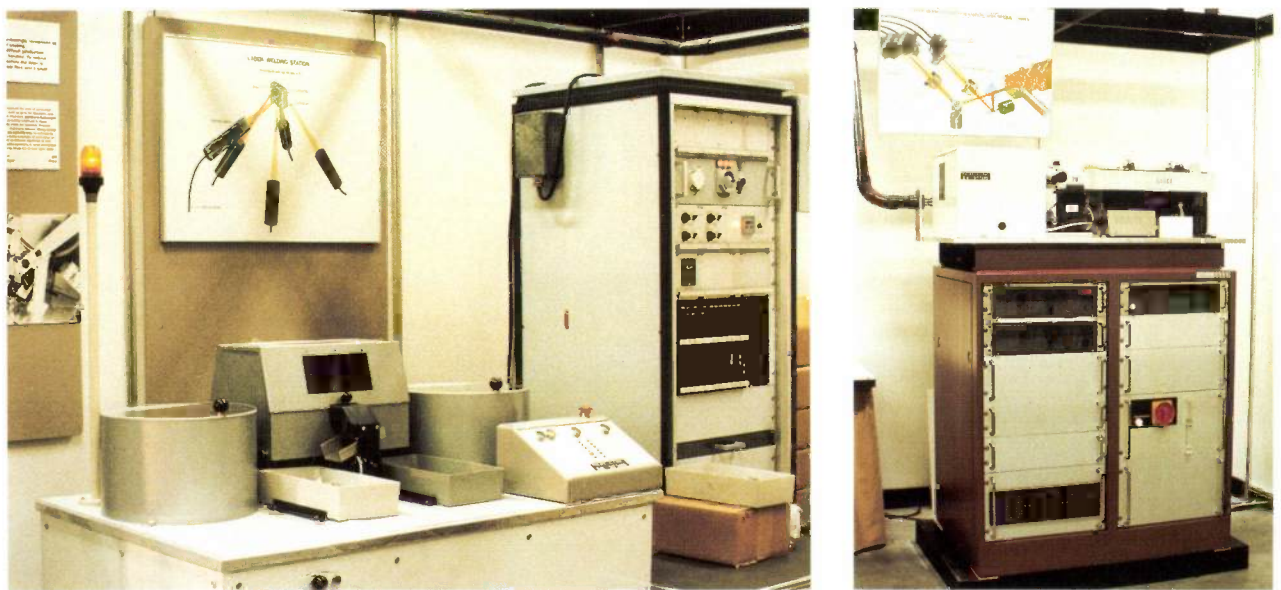


Fig. 3. Industrial version of a laser spot-welder. In the right-hand photograph there is a large cabinet for supply and cooling of the laser, which is on the right on top of the cabinet. To the left of the laser there is a large white 'box' in which the beam is split and focused on to the optical fibres, which continue through the black tube on the left in the photograph. In the left-hand photograph the cabinet on the right contains the control electronics for the system. The welding takes place inside the approximately rectangular light-tight shield at the centre of the table. The cylinders on either side of the shield contain the feed mechanism and the working stock of components to be welded.

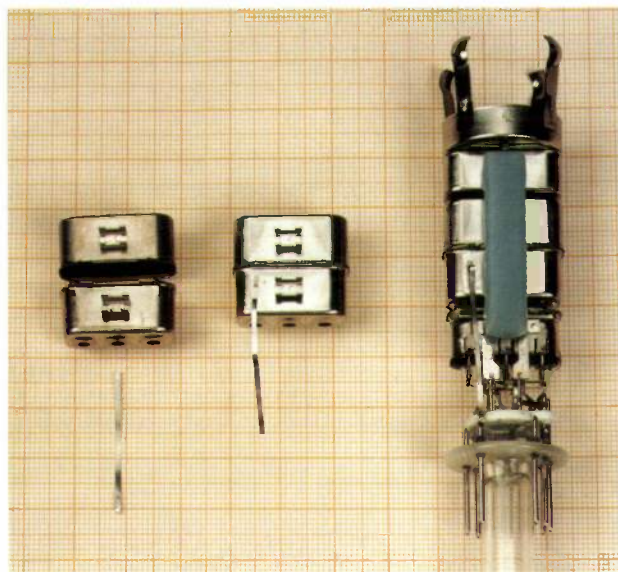


Fig. 4. A product made with the laser spot-welder. Left: two grids ('grids 3a and 3b') and a contact strip for a gun for a colour television picture tube. Centre: the two grids and the contact strip welded together by 5 spot-welds. Right: the complete gun, which contains about 80 spot-welds.

to about 15%; of this, 8% is accounted for by the input and output losses of the optical fibre (two glass/air interfaces). The remaining 7% of losses can be attributed to undesired reflections and absorption at the other optical components. Since the welding head is small (about 150 mm long, with a diameter of about 25 mm) and the optical fibres are long and flexible, the arrangement is very versatile and can easily be altered to suit new products.

Fig. 3 shows an industrial version of the welder, which is now set up in the Philips establishment at Sittard. In the right-hand photograph there is a large white 'box', in which the laser beam is split and distributed among the optical fibres, which continue through the black tube on the left in the photograph. The actual laser spot-welding takes place inside the approximately rectangular shield that can be seen at the centre of the table in the left-hand photograph.

An example of a product that has been made with the welder can be seen in fig. 4. On the left in the photograph are two grids (grids '3a' and '3b') and a contact strip for a gun for a colour television picture tube, which are welded together with the laser spot-welder (centre). On the right is the complete gun, which is assembled with about 80 spot-welds.

Laser spot-welding is a technology of increasing importance at Philips: at the moment there are more than 200 laser spot-welders in use and the number is still growing. More than ten of these machines employ the method described above for beam manipulation by means of optical fibres.

C. J. Nonhof
G. J. A. M. Notenboom

Dr C. J. Nonhof and Ing. G. J. A. M. Notenboom are with the Philips Centre for Manufacturing Technology (CFT), Eindhoven.

Philips Technical Review 50 years ago

OPTICAL MODEL EXPERIMENTS FOR STUDYING THE ACOUSTICS OF THEATRES

FEBRUARY 1936

By R. VERMEULEN and J. DE BOER.

Summary. In the auditoriums of theatres where one of the primary considerations is the perfect audibility and intelligibility of the spoken word, a short period of reverberation is essential; this, however, should not cause too great a reduction in the "useful sound intensity". The distribution of loudness is examined in this paper with the aid of optical model experiments, in which the source of sound is replaced by a small lamp and the walls of the theatre simulated in a three-dimensional model by walls with a suitable coefficient of reflection. This method was applied on the occasion of the rebuilding of the assembly hall in Philips "Ontspanningsgebouw" (Philips Theatre).

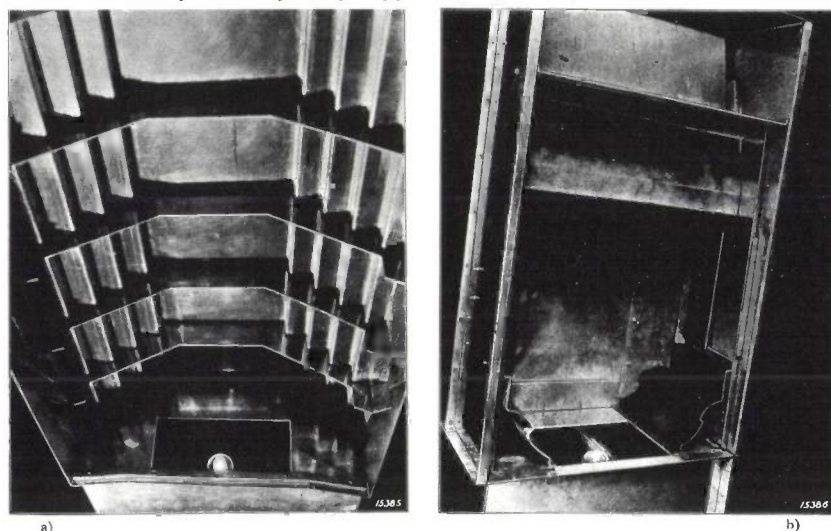


Fig. 1. Models for examining the "useful" intensity of sound in a hall. The source of sound is represented by a small lamp, shown at the bottom of the photograph. The walls of the model are made of aluminium which reflects about 50 per cent of the light-rays falling on it, so that, in accordance with the definition of the "useful" intensity, a ray after only a few reflections can just contribute to the illumination of the opal glass representing the audience. (In the pictures this glass has been removed in order to show the interior; in the upper half of fig. 1b, however, the opal glass representing the seating on the balcony is visible. Sound-absorbing surfaces in the hall are blackened in the model, e.g. the right-hand wall in fig. 1b. The brightness of the opal glass (see figs. 4, 8 and 11) represents the distribution of the useful intensity of sound.

- a) Model of hall of Philips "Ontspanningsgebouw" (Theatre) before reconstruction.
- b) Model of the same hall after reconstruction on the plans of Prof. Witzmann, Vienna.

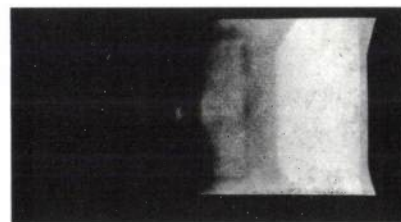


Fig. 4. Photograph of the opal glass in the model of the old hall (fig. 1a). The stage is on the right-hand side. The rapid diminution in illumination intensity towards the left may be noted; at the rear of the hall the useful sound intensity was far too small. The bright trapezoidal spot near the stage is due to reflection at the forefront of the ceiling which was not screened by the transverse roof trusses.

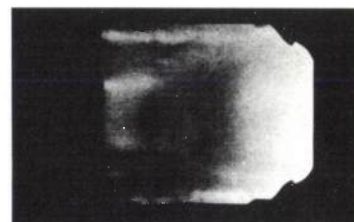


Fig. 8. Photograph of the opal glass in the model of the new hall (fig. 1b). The stage is again on the right-hand side. The distribution of illumination (useful sound intensity) is much more uniform than in fig. 4. The rear part of the hall under the balcony is still fairly dark (see fig. 11).

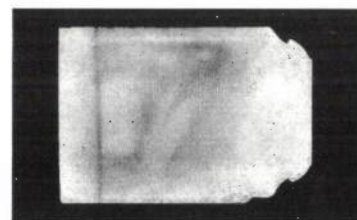


Fig. 11. Photograph of the opal glass in the model, as in fig. 8, but now with the rear wall under the balcony sloping slightly forward. The space under the balcony now also receives a satisfactory intensity of sound.

PRACTICAL APPLICATIONS OF X-RAYS FOR THE EXAMINATION OF MATERIALS

By W. G. BURGERS.

3. Quality Tests on Soapstone before Firing

Soapstone is a soft material which can be worked to exact dimensions. After suitable shaping it can be converted by firing (heating to about 1200 deg. C, during which about 6 per cent of water is given off) into a compact, hard and heat-resisting stone. During firing it frequently happens that certain places swell and as a result cracks appear which make the product useless. It is desirable to be able to detect and reject these pieces before firing, and as it appeared probable that the cracking was associated in some way with certain structural characteristics, examination by means of X-rays was indicated as offering a possible solution.

Fig. 1a shows a radiograph of that part of the raw material which did not swell on subsequent firing, while fig. 1b is a similar exposure of another part where swelling actually took place later.

An examination of these exposures reveals the same system of interference rings in both. But there is a fundamental difference in that the intensity distribution is uniform round the periphery of the rings in exposure 1a, but varying in 1b, where

certain intensity maxima appear round the circumference. This enables us to conclude that while there is no essential difference in composition at swelling and non-swelling places (identical systems of rings are obtained) there is yet a difference in texture: the places swelling on subsequent firing reveal that the crystallites favour a pronounced directional configuration (fibro-crystalline structure). Thus without entering into an analysis why this difference in structure causes a swelling during firing, we have evolved a method for testing the quality of soapstone before the firing process.

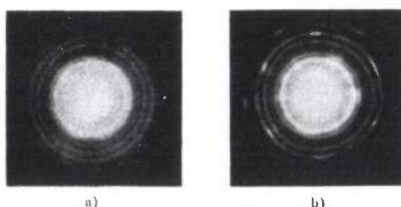


Fig. 1. Radiographs of steatite before firing: a) of a place which did not swell on subsequent firing, and b) of a place which later swelled on firing.

SHORT NOTICE

Brightness greater than on the sun

Brightnesses greater than those on the sun were recently produced in the Philips Laboratory by further increasing the wattage of the water-cooled super-high-pressure mercury vapour lamp described by Bol (De Ingenieur 50, E 91, 1935). Theoretical considerations of Elenbaas indicated that by reducing the diameter the brightness would be increased, and a lamp was therefore constructed with an internal diameter of 1 mm and an external diameter of 3 1/2 mm, which with electrodes 10 mm apart and an 805-volt alternating current took a load of 1400 watts. The luminous intensity with this load was 11,000 candle-power and the pressure about 200 atmos. Along the axis of the discharge the brightness was 1,160,000 candle-power per sq. in.; this was measured by passing a photo-electric cell with a small slit parallel to the axis of the discharge tube across an enlarged image of the lamp.

Seen from the earth, the brightness at the surface of the sun is only 1,065,000 candle-power per sq. in. (according to the International Critical Tables).

The new centre for submicron IC technology

W. G. Gelling and F. Valster

Taking part in the race to produce integrated circuits with diminishing details and expanding areas calls for enormous investment in people and buildings, not to mention computers and production equipment. People are necessary for their knowledge of processes such as plasma etching, chemical vapour deposition, implantation, oxidation and diffusion, and for combining these processes to produce patterns that form useful electronic circuits on a silicon slice. The equipment is necessary for projecting these patterns in minute detail on to the slice and creating the right conditions for the processes. Computers are needed for calculating and simulating the integrated circuits and for evaluating test data. Buildings are necessary to accommodate the people and hardware. In the new centre for submicron IC technology, now virtually completed at the Philips Research Laboratories site in Eindhoven, these buildings include areas where vibration and the dust content of the air are held to extremely low levels.

Introduction

In the sixties Philips brought out a hearing aid, for behind-the-ear wear, which contained an integrated circuit [1]. This IC consisted of an amplifier with three transistors. The 1-Mbit static RAM (RAM = random-access memory), which will go into pilot production in a few years in the new centre for IC submicron technology, will contain nearly ten million transistors. The hearing aid circuit was produced on a silicon chip with an area of about 0.6 mm², the static RAM will be produced on an area of about 90 mm². The old circuit was used for processing analog information, the new one will be used for storing immense amounts of digital information. These two examples typify the developments in electronics: integrated circuits are growing and contain more and more functions, the area required for each function continues to decrease, and digital technology is becoming firmly established.

If we look at the developments in the IC industry over a number of years, we see that the manufacturing cost per electronic function has decreased by a factor of ten in every five or six years. And this trend appears to be continuing. So it is more than likely that the number of applications of electronics in our daily life will continue to increase. We have digital electronics

very much in mind here. The digitization of audio and video equipment, for example, is already under way, and the computer in all its manifestations will occupy an increasingly important place.

Keeping up with all of these developments requires much effort from a company such as ours. To meet this challenge, Philips decided to build a new centre for IC technology at the Research Laboratories site in Eindhoven. In this centre staff from the research laboratories will cooperate closely with development engineers from the Elcoma division, who are the producers of integrated circuits in the Philips group.

The new IC centre will mainly be housed in two buildings; see *fig. 1* and *2*. In one building there will be research and development on submicron technology — the technology that will give us integrated circuits with details smaller than 1 μm. This building will also contain the pilot production of advanced ICs before the Elcoma division take over the technology and start to manufacture the circuits. The design of this building is very largely determined by the requirements for dust-free production and insensitivity to vibration — vital conditions for the manufacture of high-technology integrated circuits. In the other building, now completed, the electronic circuits are designed. The layout of this building is mainly determined by the



Fig. 1. The building for submicron-technology research and development at the new IC centre. This is where advanced ICs will go into pilot production.

large computers and the test equipment it will have to accommodate: advanced ICs can only be designed and simulated with the help of computers (CAD, or Computer-Aided Design). For example, the computers in use at the moment require about ten hours to calculate how a large IC will respond to a signal at the input; the computers to be installed in the new building will perform calculations of this type in less than an hour.

The mastery of modern IC technology can be assessed by the ability to produce large memory circuits with a high yield. The largest integrated circuits now being made are RAMs. Since 1971, when the first IC memory with a capacity of 1 kbit ($2^{10} = 1024 \approx 10^3$ bit) was introduced, the capacity per IC has increased roughly sixfold every five years. Philips, for example, are well on the way with the design of a static RAM with a capacity of 256 kbit; see fig. 3. Philips plan to start pilot production of this memory, on 6-inch silicon slices, at the new centre in about a year. Samples

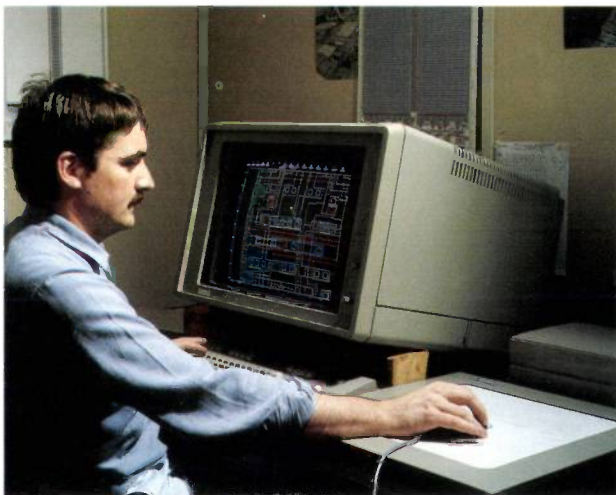


Fig. 3. CAD of the static-RAM semiconductor memory with a capacity of 256 kbit, which Philips will put into pilot production in about a year's time.



Fig. 2. The building where the circuits will be designed with the help of computers (CAD, Computer-Aided Design).

of a 1-Mbit static RAM will be available in 1988. (1 Mbit = $2^{20} = 1048576 \approx 10^6$ bits.)

The 1-Mbit memory will be made in CMOS technology, and the individual transistors will have a channel length of $0.7 \mu\text{m}$. The extremely detailed patterns required for these circuits will be projected on the silicon slice by photolithography. For this work a new high-resolution wafer stepper (or repeater projector) will be developed as a successor to the well-known Silicon Repeater [2]. The submicron technology required for manufacturing the static 1-Mbit memory will be used later for a wide variety of other types of integrated circuit. The advanced memory will thus act as the 'locomotive' that will provide the motive power for other Philips IC technology in the coming years.

In the following pages we shall explain why CMOS technology, photolithography and a static RAM have been chosen for the new centre. We shall also look at some of the technical aspects of the new buildings.

IC technology

CMOS

Large digital ICs are now more and more likely to be made in MOS technology (MOS: metal-oxide semiconductor). Bipolar technology is mainly used in analog circuits and in high-speed digital circuits. Bipolar ICs are built up from npn transistors and in many cases pnp transistors. Bipolar transistors derive their name from the fact that both electrons and holes contribute to the conduction. In MOS transistors, on the other hand, the conduction is due to the transport

[1] B. de Boer, Behind-the-ear hearing aids, Philips Tech. Rev. 27, 258-263, 1966.

[2] A. G. Bouwer, G. Bouwhuis, H. F. van Heek and S. Wittekoek, The Silicon Repeater, Philips Tech. Rev. 37, 330-333, 1977;

S. Wittekoek, Optical aspects of the Silicon Repeater, Philips Tech. Rev. 41, 268-278, 1983/84.

of holes or electrons: there is only one type of charge carrier.

The operation of a MOS transistor is based on the capacitive coupling of a conductor (the 'gate') to a p-doped or n-doped semiconducting material via a thin insulating oxide layer. A silicon NMOS transistor (on the left in fig. 4) contains two islands of heavily doped n-type silicon in a p-type silicon substrate. The two islands are called the source and drain respectively. The transistor operation is based on the conduction of electrons in the p-type silicon. These electrons are drawn from the source by a positive voltage on the gate to a thin layer of the p-type silicon (the 'channel') immediately below the insulating oxide. The gate may consist of metal or of heavily doped polycrystalline silicon. In a PMOS transistor (on the right in fig. 4) the source and drain take the form of islands of heavily doped p-type silicon in a larger island of n-type silicon. In this type of transistor a negative voltage on the gate produces hole conduction at the surface of the n-type silicon. The operation briefly described above applies to PMOS and NMOS transistors of the enhancement type. Transistors of the depletion type, on the other hand, conduct when there is no voltage applied to the gate.

In CMOS technology (CMOS: complementary metal-oxide semiconductor) PMOS and NMOS transistors are combined. As an example a diagram of a logic inverter made in CMOS technology is shown in fig. 4. With a positive supply voltage the output voltage V_o is 0 when there is a positive input voltage V_i . If on the other hand V_i is 0, then V_o is equal to the supply voltage. As we shall presently see, similar transistor combinations are also found in static RAMs.

Compared with bipolar transistors, MOS transistors have a simple structure and make ideal switches. Another advantage is that simpler techniques are ade-

quate for insulating MOS transistors from each other. The 'packing density' of MOS ICs is therefore about four times that of bipolar ICs. This high packing density and their operation as switches make MOS transistors particularly suitable for large digital integrated circuits. The first MOS circuits were produced in PMOS technology. It was the introduction of ion implantation in IC manufacture that made circuits in NMOS technology a possibility. ICs in NMOS technology are faster than those in PMOS technology, because electrons have a higher mobility than holes.

Raising the packing density in integrated circuits has increased the problem of heat removal. It is therefore a considerable advantage that the heat dissipation of ICs in CMOS technology is low. This is because the elements of logic circuits and memories in CMOS technology only conduct when there is a change in the information content of a switching element. The only currents flowing in the circuit in fig. 4, for example, in the steady state are the leakage current of the non-conducting transistor and the leakage currents in the reverse-biased p-n junctions. A disadvantage of CMOS technology is that the packing density is lower than in PMOS or NMOS technology, since n-type silicon islands are required. The problem of the lower packing density can be compensated to a considerable extent by ingenious design.

The level of 'sophistication' of the technology used to produce an integrated circuit can be characterized by the channel length (l in fig. 4). In recent years this parameter has been dramatically reduced, and in the static 256-kbit memory we mentioned it is 1.2 μm . The transistors to be made in the new centre for IC submicron technology will have a channel length of 0.7 μm . This sharp reduction in scale will create new problems, of course, and we shall look at some of them here.

To produce a smaller MOS transistor with a useful characteristic it is necessary to satisfy certain rules for scaling. A smaller channel area, the product of the length and width of the channel, implies that the thickness of the channel oxide must also be proportionately smaller. At the same time, the implantation dose of boron or arsenic must be larger to achieve the required threshold voltage. The diffusion depth must also be proportionately smaller if the lateral source and drain diffusion is to be limited during the diffusion of boron or arsenic at high temperature. Shallow diffusion, however, increases the resistances in the transistor, and this can reduce its speed of response.

The dimensions can also be scaled down by means of 'three-dimensional' cell structures. Research in the new centre will therefore include work on techniques such as the 'stacking' of elements and the fabrication

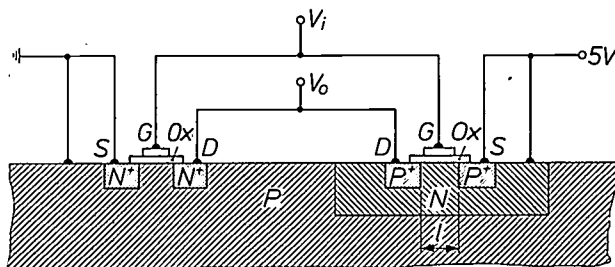


Fig. 4. Principle of a logic inverter in CMOS technology. An NMOS transistor is shown on the left, a PMOS transistor on the right. The supply voltage is 5 V. V_i input voltage. V_o output voltage. S source. D drain. G gate. Ox insulating layer of SiO_2 (channel oxide). P silicon with a surplus of free holes. P⁺ silicon with an extra surplus of free holes. N silicon with a surplus of free electrons. N⁺ silicon with an extra surplus of free electrons. l channel length.

of 'vertical' structures in a groove in the slice. This introduces the additional difficulty of restoring the surface flatness of the slices during the production.

With smaller details it is obvious that the alignment should be more accurate and the resolution better when the mask patterns are projected on the slice. The accuracy of the application and partial removal of the various layers must also be improved. These are problems of lithography, and we shall now consider them more closely.

Lithography

It might seem obvious that X-ray lithography or electron lithography would be used in the new IC centre. It has been decided, however, to use photolithography, although this does not exclude the possibility of other techniques in the future, and there is research on new lithographic techniques in Philips laboratories [3][4].

X-ray and electron lithography have the advantage of a higher resolution because the radiation has a shorter wavelength (0.5 to 3 nm for X-rays, 0.05 nm for electron lithography and about 400 nm for photolithography). The disadvantage of X-ray lithography is that the masks are as yet very difficult to produce and it is necessary to use synchrotron radiation [4]. At present the large and expensive storage ring that is required as an X-ray source is not suitable for use in an IC factory. The disadvantage of electron lithography is that it takes a long time to write a pattern — about an hour for a complete 6-inch silicon slice. Although a more ingenious method of scanning the pattern saves time, the method would still not be economic even if the scanning duration were reduced by a factor of ten (if such a reduction were possible). Electron-optical pattern generators are however used for producing accurate masks for photolithography.

The wafer stepper that was developed at Philips Research Laboratories (the Silicon Repeater [2]) has a highly refined alignment system, with a sensitivity of 0.02 μm , which makes it suitable in principle for sub-

micron technology. It is necessary, however, to improve the resolution of the projection optics, and a new optical system is therefore now being developed in cooperation with a specialist manufacturer.

The etching operations following exposure in the repeater projector in the new IC centre will in general be 'dry'. With conventional wet-etching techniques the highly detailed patterns cannot be transferred with the required accuracy and not all materials can be etched. The dry-etching techniques of plasma etching and (reactive) ion etching are less subject to these difficulties [5].

Memory circuits

As noted earlier, semiconductor memories may be regarded as the 'locomotive' of submicron IC technology, since the most advanced techniques are required in order to accommodate as many memory cells as possible in unit area. With good test procedures faults can be traced and localized very accurately in many cases. Minute examination of the faults then provides the vital clues that enable the technology to be improved. Logic circuits are not very suitable for our 'locomotive' function here, since it is much more difficult to localize the faults in a logic circuit. Memories are thus an important link in the learning process for an optimum mastery of IC technology, whether in research and development or in actual production. In turn, mastering the technology of standardized memories generates the skills required for the economic manufacture of other types of custom-made integrated circuit.

Semiconductor memories fall into various categories. Research on the applications of analog and digital CCD memories (CCD: charge-coupled device) has long been in progress at Philips [6]. Memories of this type work serially, on the shift-register principle, and the individual memory cells do not have addresses. The cells in ROM and RAM memories (ROM: read-only memory, RAM: random-access memory) do have addresses. A ROM can only be read. The contents are fixed and have already been entered into it during manufacture. A RAM can be 'read from' and 'written to', so that its contents can be changed.

RAMs are 'volatile' memories: the information is lost if the supply voltage fails. RAMs can be subdivided into dynamic and static types. A cell of a dynamic RAM consists in principle of a capacitor and a transistor; see *fig. 5a*. The gate of the transistor is connected to the 'word line' (for addressing the rows of the memory matrix) and the source is connected to the 'bit line' (for addressing the columns). The capacitor of a memory cell is charged by applying a relatively high voltage to the word line and bit line correspon-

[3] J. P. Beasley and D. G. Squire, Electron-beam pattern generator, Philips Tech. Rev. 37, 334-346, 1977;

J. P. Scott, Electron-image projector, Philips Tech. Rev. 37, 347-356, 1977.

[4] H. Lütjhe, X-ray lithography for VLSI, Philips Tech. Rev. 41, 150-163, 1983/84.

[5] H. Dimigen and H. Lütjhe, An investigation of ion etching, Philips Tech. Rev. 35, 199-208, 1975;

H. Kalter and E. P. G. T. van de Ven, Plasma etching in IC technology, Philips Tech. Rev. 38, 200-210, 1978/79.

[6] H. Heyns, H. L. Peek and J. G. van Santen, Image sensor with resistive electrodes, Philips Tech. Rev. 37, 303-311, 1977;

H. Dollekamp, L. J. M. Esser and H. de Jong, P²CCD in 60 MHz oscilloscope with digital image storage, Philips Tech. Rev. 40, 55-68, 1982;

H. J. M. Veendrick *et al.*, A 40MHz 308 Kb CCD video memory, Proc. ISSCC 84, San Francisco 1984, pp. 206-207.

A forthcoming article in this journal will deal with a new CCD image sensor.

ding to the address of the cell. The charge of the capacitor slowly leaks away to earth. The contents of the cell must therefore be 'refreshed' periodically, (e.g. every 2 ms), by supplying sufficient charge to restore the voltage to its original value. A disadvantage of a dynamic RAM is therefore that it requires extra elec-

tors are required to connect the cell to the two bit lines in this case; see fig. 5*b*. The word line is connected to the gates of these coupling transistors, and each bit line is connected to a source. The contents of a cell are changed by applying the higher voltage to a bit line and the word line, and the lower voltage to the other

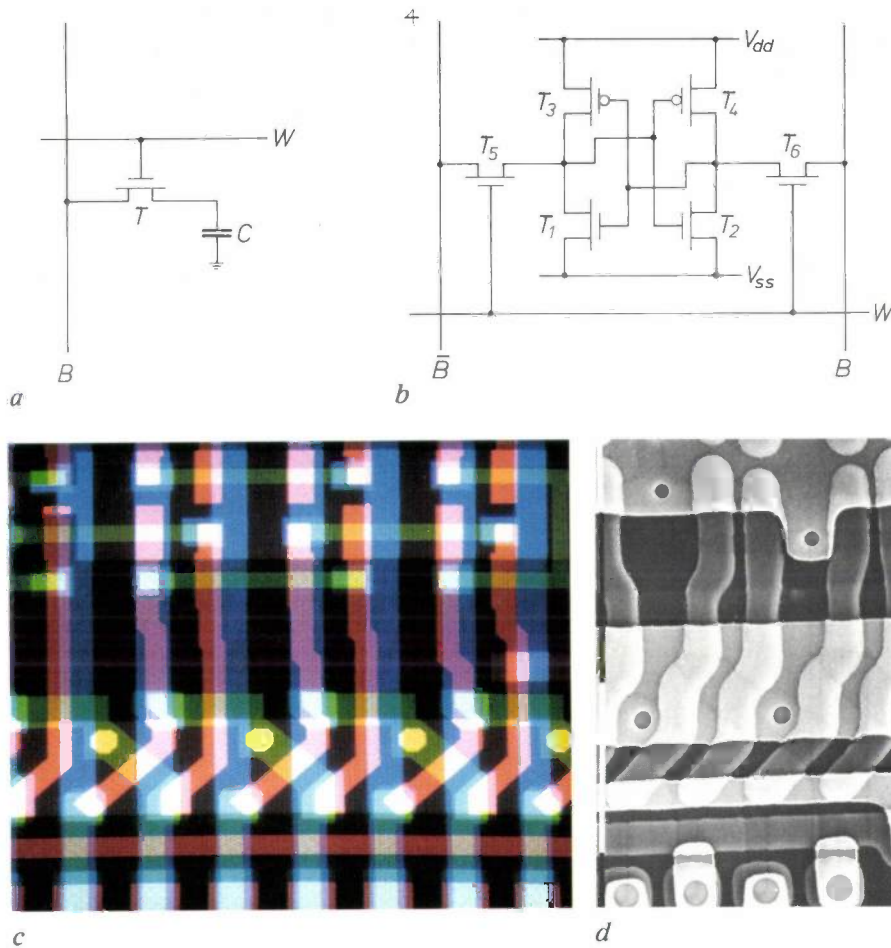


Fig. 5. *a*) Diagram of a cell in a dynamic RAM. *T* MOS transistor. *W* word line. *B* bit line. *C* capacitor. *b*) Diagram of a cell in a static RAM. T_{1-4} MOS transistors that form a flip-flop. (The upper two transistors are PMOS transistors, the lower two are NMOS transistors.) $T_{5,6}$ coupling transistors. \bar{B} inverse bit line. V_{dd} voltage on drain electrodes. V_{ss} voltage on source electrodes. *c*) Photograph of some memory cells on the graphic display during CAD of the 256-kbit SRAM; see also fig. 3. The various coloured areas represent masks used in the fabrication process. For clarity not all of the masks have been shown. The vertical blue stripes are bit lines (*B* and \bar{B} in *b*); the horizontal red stripe is a word line (*W* in *b*). *d*) Scanning electron micrograph of a few cells from a very similar memory at an intermediate stage of the fabrication process: the first metal conductor lines have been applied, but not the bit lines. One 'dash' on the scale on the left corresponds to 10 μm on the slice. The minimum pitch of the lines is 2.6 μm . The linewidth is 1.2 μm . The actual lines are obscured by layers above them, so that the lines seem to be wider. The circular patterns at the bottom of the picture correspond to the squares that can be seen at the bottom of the screen in (*c*). These patterns are the bit-line contacts on the extreme left and right in (*b*).

tronics for the refresh operation and that the contents of the memory are not available during this operation. An advantage is that a dynamic-RAM cell takes up extremely little space.

A memory cell of a static RAM needs much more space, because each cell consists of a flip-flop with four transistors. Furthermore, two additional transis-

bit line. Designing the four transistors in pairs as NMOS and PMOS types in CMOS technology considerably reduces the dissipation of a cell. Cells of the 256-kbit SRAM mentioned earlier are shown in figs 5*c* and *d*.

The 256-kbit SRAM is provided with spare memory cells (future memories will be similarly equipped). If

faults are found in one or more cells, they can be disconnected. This is done by interrupting conductor lines with a focused laser beam. Some of the spare cells then take over the function of the failed cells. This is done by interrupting lines to the gates of depletion-type transistors, so that these transistors then conduct.

A memory cell of a dynamic RAM takes up about a quarter of the space occupied by a cell of a static RAM. However, the control electronics of a static RAM occupies far less space and the stored information is continuously available at all times. Because of their specific advantages and disadvantages, both types of memory have their preferred areas of application. As we mentioned earlier, Philips will devote a substantial part of the effort in the new IC centre to the development of a 1-Mbit SRAM. In terms of packing density a 1-Mbit SRAM is comparable with a 4-Mbit DRAM.

Some technical aspects of the buildings

As more and more transistors of ever smaller dimensions are accommodated on a chip, the chance of an error occurring in any transistor will have to diminish correspondingly. Otherwise the probability of a fault-free circuit will become so small that a satisfactory production yield will no longer be possible. It is found that dust is one of the most common causes of faults. One of the principal requirements to be met by the processing rooms in the submicron-technology building (fig. 1) is therefore an extremely low dust content in the air.

Fig. 6 is a diagram showing the connection between the number of bits of a dynamic RAM, the width of the lines in it and the required minimum dust concentration in the air as specified by extrapolation of the American Federal Standard 209B [7]. In this standard the highest degree of cleanliness is referred to as class 100. In a class-100 clean room the air must contain no more than 3500 particles of 0.5 μm diameter or larger per m^3 (100 such particles per cubic foot). The corresponding line in the figure relates to cumulative values for other particle sizes. It is now normal practice to extrapolate standards for classes 10 and 1 from this standard; lines for these classes are also shown in the figure. These degrees of cleanliness will probably be standardized as well. With the initial assumption that

particles whose diameter is 10% of the linewidth will not cause chip rejects, it is further assumed that for manufacture of 64-kbit DRAMs the air must be cleaner than air of class 10. For 256-kbit DRAMs the air cleanliness should be class 1; see fig. 6.

As mentioned earlier, the new 1-Mbit SRAM has a packing density comparable to that of a 4-Mbit DRAM. Further extrapolation of Federal Standard 209B shows that the air in the clean room for fabricating memories of this type must contain no more than 350 particles of 0.1 μm diameter or larger per m^3 (10 per cubic foot). This is a much more difficult require-

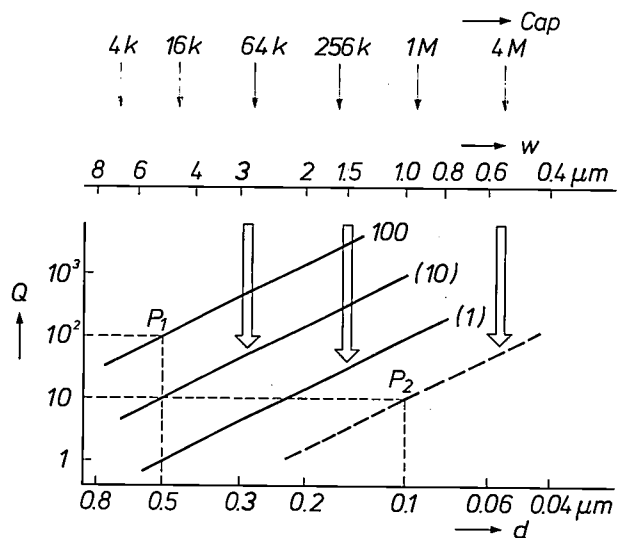


Fig. 6. The connection between the detail of a memory circuit and the required degree of cleanliness of the air [7]. Cap number of bits of dynamic RAMs. w corresponding linewidth. d diameter of dust particles. Q number of particles permitted in American Federal Standard 209B, per cubic foot and with diameter d or larger. The number 100 on the upper line (based on the coordinates of the point P_1) gives the class of air cleanliness defined in this standard. The other lines (numbers in brackets) correspond to an extrapolation of this standard. The dashed line gives the degree of cleanliness (based on the coordinates of the point P_2) for the cleanest process tunnels in the new technology building. The arrows indicate the connection between linewidth and maximum particle size.

ment than those conventionally used in IC manufacturing centres. It can only be met by installing very large and expensive air-treatment plants and by the personnel following the strictest 'cleanliness discipline'.

Only 7% of the total volume of the building is taken up by the space used for the actual manufacturing. This consists of a number of adjacent 'tunnels' for the various stages of the process. 'Superclean' tunnels, which meet the cleanliness requirement specified above, alternate with tunnels that are relatively less clean. The superclean tunnels are designed for the

[7] R. P. Donovan, B. R. Locke, D. S. Ensor and C. M. Osburn, The case for incorporating condensation nuclei counters into a standard for air quality, *Microcontamination* 2, No. 6 (December), 39-44, 1984; K. Takahashi and K. Yagi, Development of clean tunnels for semiconductor manufacturing, Proc. 6th Int. Symp. on Contamination control, Tokyo 1982, pp. 165-168.

actual processes. The less-clean tunnels contain equipment requiring regular maintenance. For example, the ion-implantation equipment will be accommodated in a less-clean tunnel that opens into a superclean tunnel. To avoid manipulations with bottles or containers in the superclean tunnels, all liquids and gases are transported along pipelines. Containers for liquids and gases are kept in separate compartments on the outside of the building. Alongside the actual technology

building, adding 10% of outside air. The Sankey flow diagram in *fig. 7* shows the extent to which particles are trapped by the mechanical filters in the superclean tunnels [8]. The air entering from outside passes through a filter that traps 99.8% of the particles of diameter 0.1 μm or larger. The air then passes through a 73% prefilter and then, before entering the tunnel, it goes through a 99.99995% filter — clearly a filter of very special design.

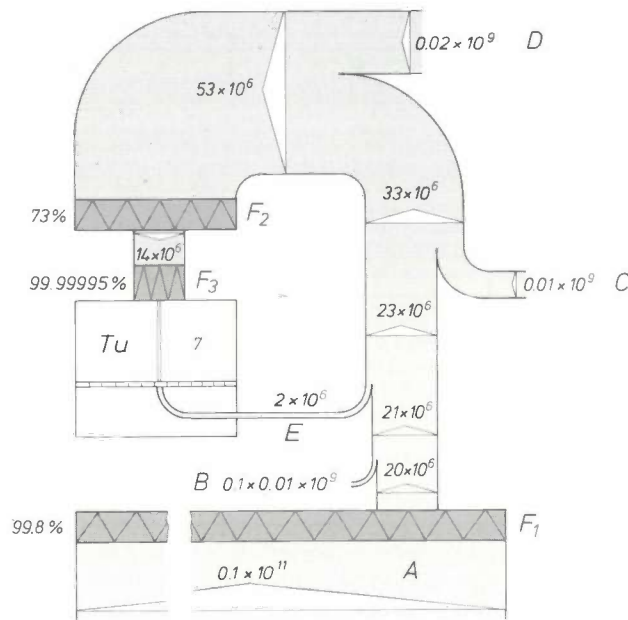


Fig. 7. Sankey flow diagram [8] for the dust content of the air flowing through the technology building. *Tu* (superclean) tunnel. The numbers in the 'flow paths' indicate the number of particles larger than 0.1 μm per m^3 volume; the width of the flow paths is approximately proportional to this number. The filters are indicated by a zig-zag line; the percentages give the degree of filtering for particles of 0.1 μm and larger. *F*₁ outside air filter. *F*₂ prefilter for the superclean process tunnels. *F*₃ final filter for these tunnels. *A* air drawn in from outside. The outside air contains 10^{11} particles per m^3 . The fresh air amounts to 10% of the circulating air. *B* 1% of leakage air in the outside-air suction line; this leakage air contains 10^9 particles per m^3 . *C* 1% of leakage air in the channels of the circulation system, with the same particle content. *D* 2% of leakage air in the fans of the circulation system, also with the same particle content. *E* exit air from the process rooms; a content of 2×10^6 particles per m^3 is assumed for *E*. This diagram shows that the air in the cleanest process tunnels contains 7 particles of 0.1 μm diameter or more per m^3 . In calculating the filters a safety factor of 50 was applied to the specification of a maximum of 350 of these particles per m^3 .

building there are three service buildings for supplying materials used in the production such as decontaminated deionized water and various process gases.

In the technology building each tunnel will have its own 'down-flow' air-circulation system, with a vertical flow from ceiling to floor. There is no possibility of interaction between the different circulation systems. Powerful fans circulate a total of about 2.2×10^6 cubic metres of air per hour through the

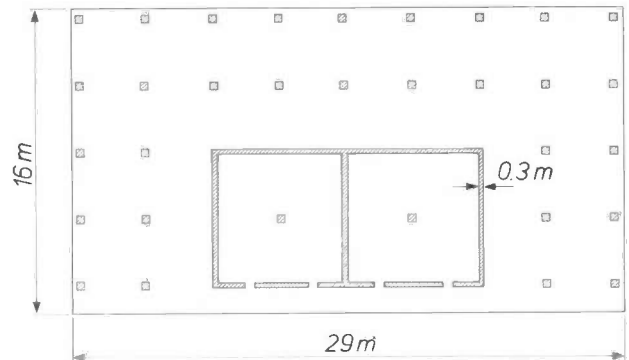


Fig. 8. Horizontal cross-section through the columns and walls that connect the foundation floor and the floor for the wafer steppers. The two floors and the walls form a stiff concrete box construction.

Other important aspects of the design of the technology building are the precautions for suppressing vibration at certain locations. The wafer steppers are the units most sensitive to vibration, so that these precautions relate mainly to the floor on which they stand. These instruments always have their own vibration isolation in the form of weak undamped springs. It can be shown theoretically [9] that the spring-mounted instrument should have a low natural frequency, since floor vibrations with a frequency of at least $\sqrt{2}$ times the natural frequency are attenuated in amplitude. The natural frequency of our wafer steppers on their weak springs is low: 2 to 4 Hz.

The floor and foundations for the wafer steppers are designed to give the whole structure the highest possible natural frequency, in any case higher than $4\sqrt{2}$ Hz. In addition the combined mass of floor and foundations must be high, so that the impacts of collisions with moving objects will only produce vibrations of low amplitude. A large mass in combination with a high natural frequency results in a high stiffness. In the design of low-vibration buildings it is generally only the stiffness in the vertical direction that is kept

[8] This diagram is based on calculations made by Meissner & Wurst GmbH, Stuttgart, the firm that supplied the air-conditioning equipment.

[9] J. P. den Hartog, Mechanical vibrations, 4th edition, McGraw-Hill, New York 1956.

high. Since impact can also operate in the horizontal direction, the floors for the repeater projectors also have a high stiffness in the horizontal direction.

Calculations have been made for two models of the combined construction of concrete piles, foundation floor and the actual floor for the wafer steppers. In one model both floors are connected by columns, in the other by walls *and* columns, giving a sort of box construction. The calculations on the box-construction model showed that this design had the highest natural frequency in the horizontal direction. *Fig. 8* shows a horizontal cross-section through the concrete construction that has been used. The upper floor is 45 cm thick and supports the wafer steppers. The meas-

ured natural frequency in the horizontal direction is 55 Hz — much higher than the natural frequency of the repeater projectors.

Summary. The pilot production of 256-kbit static RAMs will start in about a year at the new centre for submicron technology. Use will be made of CMOS technology and photolithography with wafer steppers. In certain parts of the technology building the dust content of the air will be extremely low and the floors will be extremely insensitive to vibration. The low dust content will be achieved by using separate air-circulation systems for each 'process tunnel' with filters that trap 99.99995% of particles down to a diameter of 0.1 μm . The vibration insensitivity of the floors that support the wafer steppers will be obtained by using a concrete box construction with high vertical and horizontal stiffness.

Dual-energy X-ray diagnostics

J. J. H. Coumans

In about 1960 the well-known Dutch radiologist B. G. Ziedses des Plantes Sr succeeded in 'subtracting' radiographs produced by hard and soft X-rays. He had described the principle of the subtraction method many years before, in 1934, in his thesis 'Planigraphy and subtraction'. By using hard and soft X-rays he could substantially increase the contrast due to heavy elements such as calcium. However, the method did not become widely used until digital technology and computers were available for rapid image processing. A difficulty with dual-energy imaging in computed tomography until now has been the occurrence of artefacts caused by movement of the object. At Philips it has now been found that these artefacts can be avoided by supplying the X-ray tube with alternate high-voltage and low-voltage pulses during tomography with a Philips CT scanner. The contrast between tissue structures can be varied by carefully processing high-energy and low-energy images. Tissues can also be analysed quantitatively by assigning values for the electron density and atomic number to the individual picture elements (pixels).

Introduction

The different grey levels in an X-ray image correspond to different attenuations of the X-ray beam in tissue structures. The attenuation is due to the removal of X-ray quanta from the beam by photoelectric absorption, Compton scattering and Rayleigh scattering. In photoelectric absorption X-ray quanta are absorbed by energy transitions of bound electrons. In Compton scattering X-ray quanta collide non-elastically with free electrons; this process is associated with energy loss and hence with an increase in wavelength. In Rayleigh scattering X-ray quanta collide elastically with free electrons, so that there is no change in wavelength. In X-ray diagnostics the most important effects are photoelectric absorption and Compton scattering. In the rest of this article it will therefore be assumed that the slight attenuation due to Rayleigh scattering is included in the photoelectric absorption, so that we shall attribute two physical effects here instead of three to X-ray attenuation.

The contributions of photoelectric absorption and Compton scattering to the total X-ray attenuation are both dependent on the energy of the X-radiation and

on the properties of the tissue. For the same tissue, hard X-radiation — i.e. radiation with a high energy and hence a short wavelength — is more scattered than absorbed; the opposite is the case with soft X-radiation. For the same energy, soft tissue, consisting of light atoms such as oxygen, carbon and hydrogen, gives a great deal of scattering and little absorption of the X-rays. Bone tissue, containing heavy atoms such as calcium, gives a great deal of absorption and little scattering.

This is illustrated in *fig. 1*. In *fig. 1a* the X-ray attenuation coefficient μ of polymethyl methacrylate and aluminium is plotted as a function of the X-ray energy. In X-ray attenuation, polymethyl methacrylate is comparable with soft tissue and aluminium is comparable with bone. *Fig. 1b* shows the relative contribution of photoelectric absorption in the total X-ray attenuation for the same materials. The curves for most biological materials lie in the regions bounded by the curves in the two figures.

The X-ray attenuation coefficient can thus be divided into a contribution due to Compton scattering and a contribution due to photoelectric absorption. Each of these contributions is the product of a material-dependent factor and an energy-dependent fac-

Dr Ir J. J. H. Coumans, formerly with Philips GmbH Forschungslaboratorium Hamburg, Hamburg, West Germany, is now with the Medical Systems Division, Philips NPB, Best.

tor. The energy-dependent factors differ for Compton scattering and photoelectric absorption but they are known: they are functions in which the microscopic collision cross-sections occur. We see that the material-dependent factors in the total X-ray attenuation coefficient are 'weighted' by the energy-dependent factors, so that changing the energy also changes the attenuation coefficient. This means that the contrast in an X-ray image can be altered by changing the energy. Later in this article it will be shown that the material-dependent factors that correspond to a particular ray path in the object can be calculated from *two* X-ray exposures at different energies. This is done by 'splitting off' the — known — energy-dependent factors in the total attenuation coefficient. In this calculation the material-dependent factors for Compton scattering and photoelectric absorption are the two unknowns in two equations, which in principle can therefore be solved.

It was already known in the twenties that the contrast between materials could be increased or reduced

by varying the energy of the X-rays [1]. The ideal would be to work with monoenergetic X-radiation, i.e. radiation of one wavelength, or 'colour' [2]. The problem is that the X-radiation from the usual source, an X-ray tube, includes radiation at different wavelengths. The spectrum of the radiation from an X-ray tube is a continuous (Bremsstrahlung) spectrum with a minimum wavelength λ_m given by

$$\lambda_m = hc/eV_m,$$

where h is Planck's constant, c the velocity of light, e the electronic charge and V_m the voltage on the X-ray tube. Superimposed on this continuous spectrum are peaks due to the characteristic radiation from the anode material. It is possible to obtain monoenergetic X-radiation by filtering, e.g. with a crystal monochromator. However, filtering considerably reduces the intensity of the radiation, making exposure times much too long for medical use. Monoenergetic X-radiation of sufficient intensity can be obtained with a synchrotron and a monochromator [3], but a synchrotron is large and expensive. The non-availability of practical monoenergetic X-ray sources means that it is necessary to resort to polyenergetic X-radiation for dual-energy X-ray diagnostics.

Ziedses des Plantes was able to give bone tissue extra contrast by photographically 'subtracting' one radiograph from another: one was made with hard X-radiation and the other with soft X-radiation [4]. In his subtraction method he combined these radiographs by using two film cassettes one above the other, separated by a copper plate that acted as a radiation filter. The photographic subtraction technique is cumbersome, however, and is rarely used now. In modern computed tomography different detectors with unequal spectral sensitivities are sometimes used for this [5]. The difficulty then is that twice as many detectors, with the associated electronics, are required; this makes the method expensive. Two successive scans can also be made with the X-ray tube at different voltages [6], but this more than doubles the scan time and therefore increases the risk of artefacts due to movement of the object.

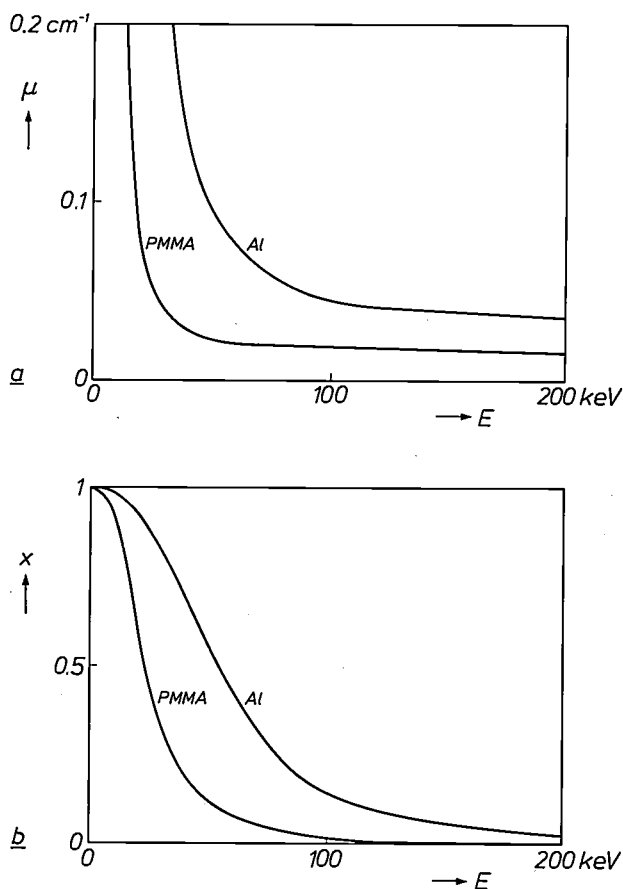


Fig. 1. *a*) The X-ray attenuation coefficient μ as a function of the energy E of the X-radiation for polymethyl methacrylate (PMMA) and aluminium (Al). ($E = hc/\lambda$, where λ is the X-ray wavelength, c the velocity of light and h Planck's constant.) *b*) The ratio x of the photoelectric absorption to the total X-ray attenuation as a function of X-ray energy for both materials.

- [1] R. Glocker and W. Frohnmayer, Über die röntgenspektroskopische Bestimmung des Gewichtsanteiles eines Elementes in Gemengen und Verbindungen, *Ann. Phys.* **76**, 369-395, 1925.
- [2] W. J. Oosterkamp, Monochromatic X-rays for medical fluoroscopy and radiography?, *Medicamundi* **7**, 68-77, 1961.
- [3] B. Vinocur, High-tech physics advance noninvasive angiography, *Diagnostic Imaging*, February 1985, pp. 109-110.
- [4] B. G. Ziedses des Plantes, *Subtraktion*, Thieme, Stuttgart 1961.
- [5] R. A. Brooks and G. Di Chiro, Split-detector computed tomography: a preliminary report, *Radiology* **126**, 255-257, 1978.
- [6] A. Macovski, R. E. Alvarez, J. L.-H. Chan, J. P. Stonestrom and L. M. Zatz, Energy dependent reconstruction in X-ray computerized tomography, *Comput. Biol. & Med.* **6**, 325-336, 1976.

To overcome these disadvantages we have modified a computer tomograph (a Philips Tomoscan 300 CT scanner) [7], see *fig. 2*, so that scans can be made at different X-ray energies without the occurrence of movement artefacts [8]. (The operation of a CT scanner will be dealt with at the end of the article.) The improvement was made by modifying the high-voltage generator to apply, every 14 ms, a high-voltage pulse followed by a low-voltage pulse. The pulse pairs are generated at a frequency equal to half that of the voltage pulses normally used for the CT scanner. Far less modification of the CT scanner is required than if different detectors were used; the modification is also suitable for the later types of CT scanner, the Tomoscan 310 and 350.

In modern dual-energy X-ray diagnostics computational methods are used to derive the attenuation coefficients for the individual pixels from the ratio of measured X-ray intensities with an object in the beam and without. The material-dependent factors corresponding to the photoelectric absorption and the Compton scattering can then be identified from these coefficients. These factors can then be converted into quantities such as the atomic number and the electron density for each pixel, so that in principle a quantitative analysis of tissue is now possible. It will be clear that these methods of calculation can be effectively combined with the digital image-reconstruction methods used in computed tomography.

We have developed a new method in which the X-ray images are recalculated to produce monoenergetic images for a wide energy range. After the actual X-ray CT scan the radiologist can select the notional X-ray energy that gives the greatest possible contrast between the tissues of interest. Images can then be studied at different X-ray energies without having to subject the patient to repeated exposures.

As the polyenergetic X-radiation travels through the object the mean wavelength is reduced owing to the energy-dependent attenuation of the rays. This hardening of the X-ray beams makes a special calibration technique necessary. The CT scanner is therefore regularly calibrated with objects in which aluminium simulates bone tissue and polymethyl methacrylate simulates soft tissue.

In the next section the way in which the X-ray attenuation coefficient can be split into separate contributions due to photoelectric absorption and Compton scattering will be explained. The representation of a material as a vector in a coordinate system will then be discussed. This will be followed by an account of the calibration method and the modifications to the Tomoscan 300. In the final section the applications of dual-energy X-ray diagnostics in CT scanning (com-



Fig. 2. The Philips CT scanner Tomoscan 300, which is outwardly similar to the later types Tomoscan 310 and 350. Only the scanner and patient table are shown here; the complete equipment is shown in *fig. 5a*.

puted tomography), CR scanning (computed radiography) and DVI (digital vascular imaging) will be discussed.

Theory

Splitting the X-ray attenuation coefficient

As we have just noted the X-ray attenuation coefficient μ (in cm^{-1}), which is a function of the energy of the X-ray quanta, can be split into separate contributions, one due to the Compton scattering and the other due to the photoelectric absorption. Each contribution is the product of a material-dependent factor and an energy-dependent factor. We thus obtain the function:

$$\mu(E) = a_c f_c(E) + a_p f_p(E), \quad (1)$$

where the subscripts c and p relate to Compton scattering and photoelectric absorption, and E represents the energy of the X-ray quanta.

It is found from equation (1) and *fig. 1b* that the energy of the X-radiation can be selected in such a way that either the photoelectric absorption or the attenuation due to Compton scattering predominates. The contrast between two tissues in an X-ray image can therefore be altered by varying the factors $f_c(E)$ and $f_p(E)$ in eq. (1). Since in principle these factors are known, it is sufficient to make two X-ray exposures at different energies. The unknown material-dependent factors a_c and a_p can then be found by solving two simultaneous equations.

An element can be characterized by its atomic number Z and electron density ρ (in cm^{-3}). A biological material can be assigned an effective atomic number

Z_{eff} and an effective electron density ρ_{eff} . Both these quantities then give the same material-dependent factors for a biological material as those for an element with atomic number $Z = Z_{\text{eff}}$ and electron density $\rho = \rho_{\text{eff}}$.

The electron density is the product of the atomic number and the atomic density N , the number of atoms per unit volume: $\rho = NZ$. It can be shown that the electron density is proportional to the factor a_c in equation (1) and that the atomic number is proportional to $(a_p/a_c)^{0.3}$. The two material-dependent energy-independent factors a_c and a_p can therefore be used to analyse biological tissue quantitatively.

It can be shown that the electron density is proportional to a_c and the atomic number is proportional to $(a_p/a_c)^{0.3}$ as follows. For a given element the term $a_c f_c(E)$ in (1) can also be written as $N\sigma_c$, where σ_c is the microscopic collision cross-section (in cm^2) for Compton scattering. This collision cross-section can be calculated for a given element and a given X-ray energy E from equation [9]

$$\sigma_c = 2\pi r_0^2 Z f_{\text{KN}} \left(\frac{E}{mc^2} \right).$$

In this expression Z represents the atomic number, $r_0 = 2.818 \times 10^{-13}$ cm is the classical radius of the electron, f_{KN} is the Klein-Nishina function, and $mc^2 = 510.975$ keV is the ground-state energy of the electron. We can now derive expressions for the factors a_c and $f_c(E)$ in (1):

$$a_c = 2\pi r_0^2 NZ \quad (2)$$

and

$$f_c = f_{\text{KN}} \left(\frac{E}{mc^2} \right). \quad (3)$$

The term $a_p f_p(E)$ in (1) can be written in a similar way as $N\sigma_p$, where σ_p is the microscopic collision cross-section for photoelectric absorption. This collision cross-section can be calculated from the expression

$$\sigma_p = C_p Z^n E^{-m},$$

where C_p is a constant (it is not dimensionless), and n and m represent material-dependent exponents [10]. For oxygen $C_p = 21 \times 10^{-24}$, $n = 4.6$ and $m = 3.2$. (For most biological materials a good approximation for m is 3.0.) We now have the following expressions for the factors a_p and $f_p(E)$ in (1):

$$a_p = NC_p Z^n \quad (4)$$

and

$$f_p(E) = E^{-m}. \quad (5)$$

An expression for the effective electron density of a biological material can be derived from (2):

$$\rho_{\text{eff}} = k_1 a_c,$$

where k_1 is a constant. Dividing equation (2) by equation (4) gives an expression for the effective atomic number:

$$Z_{\text{eff}} = k_2 \left(\frac{a_p}{a_c} \right)^{1/n},$$

where k_2 is a constant and the exponent $1/n$ is equal to $1/(n-1) \approx 0.3$.

For any given material the quantities $\mu(E)$, $f_c(E)$ and $f_p(E)$ in equation (1) are known: $\mu(E)$ is published in handbooks and $f_c(E)$ and $f_p(E)$ are known functions of the X-ray energy. It is therefore possible to calculate the material-dependent factors a_c and a_p by taking the minimum of the sum of the squares of the relative deviations

$$\varepsilon = \frac{\mu(E) - a_c f_c(E) - a_p f_p(E)}{\mu(E)} \quad (6)$$

for a number of different energy values. In this way we have calculated the factors a_c and a_p for the materials aluminium, polymethyl methacrylate and water in the energy range from 30 to 100 keV. Fig. 3 gives the deviation ε for these materials as a function of energy. From 30 to 150 keV the deviation is less than 0.5%. This shows that the model corresponding to equation (1) gives a good approximation to reality. In principle this only applies to materials whose atomic number is less than 50. In addition, the materials in the range of energies quoted should not have a K absorption edge (a sudden change in the absorption coefficient due to an energy transition of a K electron). Biological materials satisfy these conditions.

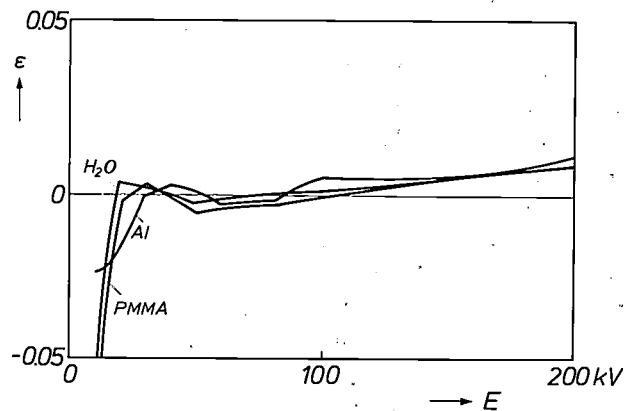


Fig. 3. The relative deviation ε (eq. 6) as a function of X-ray energy for polymethyl methacrylate (PMMA), water (H_2O) and aluminium (Al). The quantity ε is the deviation of the model that splits the X-ray attenuation due to Compton scattering and to combined photoelectric absorption and Rayleigh scattering into an energy-dependent factor and a material-dependent factor.

[7] F. W. Zonneveld, Computed tomography, Philips Medical Systems Division, Best 1983.

[8] F. W. Zonneveld, A new method for in vivo energy-selective CT imaging, Proc. 15th Int. Congr. of Radiology, Vol. Technics and Physics, Brussels 1981, pp. 280-289; W. R. Brody, D. M. Cassel, F. G. Sommer, L. A. Lehmann, A. Macovski, R. E. Alvarez, N. J. Pelc, S. J. Riederer and A. L. Hall, Dual-energy projection radiography: initial clinical experience, Am. J. Roentgenol. 137, 201-205, 1981; J. J. H. Coumans, Doppel-Energie Computer-Tomographie und -Radiographie, Thesis, Braunschweig 1983.

[9] O. Klein and Y. Nishina, Über die Streuung von Strahlung durch freie Elektronen nach der neuen relativistischen Quantendynamik von Dirac, Z. Phys. 52, 853-868, 1929.

[10] E. C. McCullough, Photon attenuation in computed tomography, Med. Phys. 2, 307-320, 1975.

Characterization of a material by a vector

For simplicity we shall assume here that our X-radiation is monoenergetic. As the radiation passes through the object the intensity I_i in front of the object falls to the intensity I_o behind the object. The relation between the two is given by

$$I_o = I_i e^{-M}, \tag{7}$$

where the attenuation exponent M is given by

$$M = \int_{s_i}^{s_o} \mu ds. \tag{8}$$

Here the material-dependent, and hence in general position-dependent, attenuation coefficient μ given by eq. (1) is integrated with respect to the coordinate of position s between the limits s_i and s_o for the incidence and emergence of the radiation. If the signals from an X-ray detector with and without an object in the beam are compared the natural logarithm of the ratio of the signals is $-M$ (eq. 7). The quantity $T = -M$ is called the logarithmic decrement. A large number of values for T , for different paths for the X-radiation through the object, must finally produce a reconstruction of a particular part of the object.

With the aid of (1) we can write equation (8) as:

$$M = A_c f_c(E) + A_p f_p(E), \tag{9}$$

where the material-dependent factors A_c and A_p are given by:

$$A_c = \int_{s_i}^{s_o} a_c ds, \tag{10}$$

$$A_p = \int_{s_i}^{s_o} a_p ds. \tag{11}$$

If the X-radiation passes through one kind of material, these factors are not only characteristic of that material but are also proportional to its thickness.

For a given thickness d_m we can characterize a material m — or a combination of a number of materials — by a vector m in a rectangular coordinate system in which normalized factors $A'_{c,m}$ and $A'_{p,m}$ are plotted along the two axes; see fig. 4a. The normalization consists in comparing the factors $a_{c,m}$ and $a_{p,m}$ for the material with the factors a_{c,H_2O} and a_{p,H_2O} for water. The components of the vector are then given by:

$$m = (A'_{c,m}, A'_{p,m}) = \left(\frac{a_{c,m}}{a_{c,H_2O}} d_m, \frac{a_{p,m}}{a_{p,H_2O}} d_m \right). \tag{12}$$

If the X-rays pass through an object consisting entirely of water with a layer thickness d_{H_2O} , the attenuation exponent given by (9) can be written for water as:

$$M_{H_2O} = a_{c,H_2O} d_{H_2O} f_c(E) + a_{p,H_2O} d_{H_2O} f_p(E). \tag{13}$$

With variable thickness d_{H_2O} , different values of M_{H_2O}

in a $(d_{H_2O} r_{c,E}, d_{H_2O} r_{p,E})$ -plane that we make coincident with the $(A'_{c,m}, A'_{p,m})$ -plane correspond to vectors whose end-points lie on a straight line with the directional vector

$$r = (r_{c,E}, r_{p,E}) = \{a_{c,H_2O} f_c(E), a_{p,H_2O} f_p(E)\}. \tag{14}$$

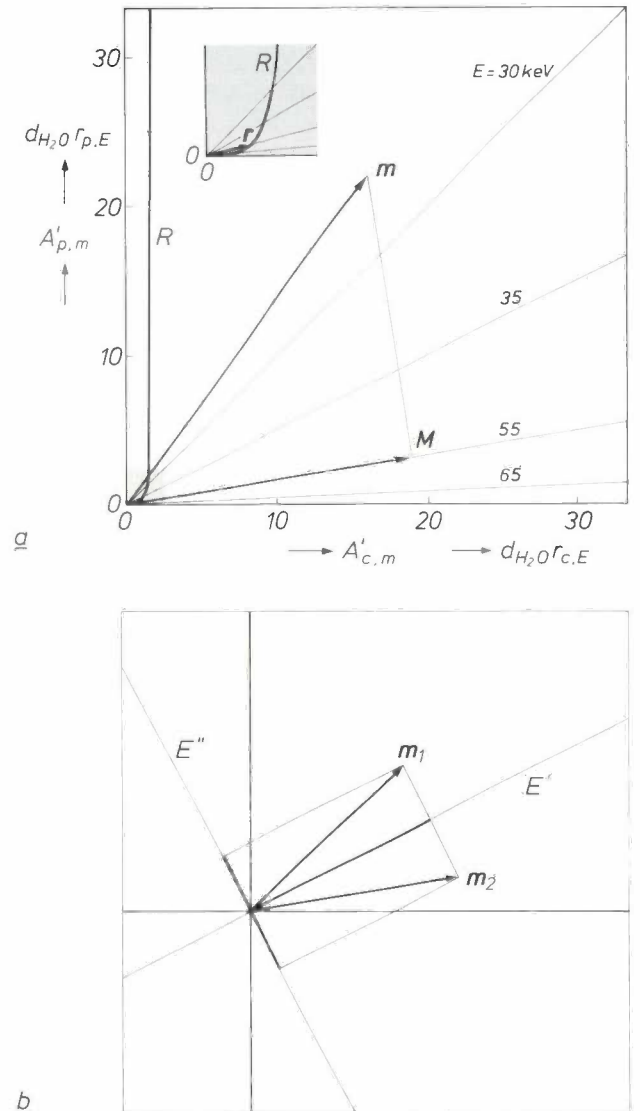


Fig. 4. a) Characterization of a material by a vector m with components $A'_{c,m}$ and $A'_{p,m}$ as given by equation (12). The components $A'_{c,m}$ and $A'_{p,m}$ are the energy-independent contributions to the attenuation exponent due to Compton scattering, and due to photoelectric absorption. The contributions are dependent on material and thickness, and are normalized with respect to water. R curve traced out by the end-points of vectors r with components $r_{c,E}$ and $r_{p,E}$ as given by equation (14). (See also the enlarged detail.) These vectors determine the direction of lines through the origin for the vectorial energy-dependent attenuation exponent of water with layer thickness d_{H_2O} as given by equation (13). Each line corresponds to a constant value of the X-ray energy E . The vectorial energy- and material-dependent attenuation exponent M , which is determined by the choice of a notional X-ray energy after the exposure, is found by projecting the vector m on to a line for the attenuation exponent of water at this X-ray energy. b) For two adjacent picture elements (pixels) with material vectors m_1 and m_2 the X-ray energy E' gives no contrast and E'' gives maximum contrast. The line for E' is perpendicular to the line that connects the end-points of the vectors; the line for E'' is perpendicular to the line for E' .

When E tends to infinity, r tends to take up the direction of the horizontal axis and becomes infinitely small (Compton scattering only); when E tends to zero, r tends to take up the direction of the vertical axis and becomes infinitely large (photoelectric absorption only). The end-points of the vectors r lie on a curve, R in fig. 4a. The figure also shows a number of lines for the attenuation exponent of water at constant energy; their direction follows from that of the directional vector given by (14).

The energy-dependent and material-dependent attenuation exponent M given by (9) can be displayed as a vector in the combined $(d_{H_2O}r_{c,E}, d_{H_2O}r_{p,E})$ - and $(A'_{c,m}, A'_{p,m})$ -plane. This vector is shown as M in fig. 4a. The length of the vector M is equal to the scalar product of the vectors m and r given by (12) and (14):

$$|M| = m \cdot r = a_{c,m}d_m f_c(E) + a_{p,m}d_m f_p(E).$$

The attenuation exponent for a given radiant energy (notional or not) can thus be found by projecting the material vector m given by (12) on to the line of the attenuation exponent of water for this energy.

Fig. 4b shows how certain contrasts can be selectively enhanced or removed by choosing an appropriate X-ray energy. The vectors m_1 and m_2 relate to two materials of a particular thickness. If we choose an energy E' , corresponding to a line perpendicular to the line that connects the end-points of m_1 and m_2 , the attenuation exponents are equal and so therefore are the logarithmic decrements. The reconstructed pixels then show no contrast. (For the same magnitude of m_1 and m_2 , as in fig. 4b, the line for E' corresponds to the bisector of the angle between the two vectors.) If we choose an energy E'' , corresponding to a line perpendicular to that of E' , the contrast between the reconstructed pixels is at a maximum.

It is possible in principle to choose an arbitrary notional energy for the X-radiation after an actual exposure by determining the factors A_c and A_p from two different monoenergetic measurements of the logarithmic decrement. From this the normalized factors $A'_{c,m}$ and $A'_{p,m}$ can be obtained, giving the direction and magnitude of the vector m . The vector M is obtained from the projection of m on to the line relating to the desired energy. As noted above, monoenergetic radiation sources are not available for routine X-ray diagnostics. As we shall now see, this problem can be overcome by means of calibration.

The calibration method

It was pointed out earlier that the change in the shape of the X-ray spectrum, as the radiation penetrates deeper into the material, complicates the choice of calibration method. The mean wavelength of the

spectrum is gradually reduced because soft radiation is attenuated more than hard radiation.

This hardening of the X-radiation can be described quantitatively as the change in the effective energy E_{eff} . The effective energy of polyenergetic X-radiation is defined as the energy of monoenergetic radiation which, in travelling a given distance in water, yields the same logarithmic decrement as the polyenergetic radiation does in travelling the same distance.

The calibration that has generally been used in computed tomography until now gives coefficients c_1 , c_2 and c_3 of a third-degree equation for the product of material thickness d_m and attenuation coefficient μ , with the measured logarithmic decrement T as independent variable:

$$\mu d_m = c_1 T + c_2 T^2 + c_3 T^3.$$

This calibration method, however, takes no account of the increase in the effective energy and hence of the change in the factors $f_c(E)$ and $f_p(E)$ in (1). The result of the calibration therefore contains a systematic error.

The calibration method that we use is not based on the attenuation coefficient, which is energy-dependent, but on the factors A_c and A_p , which are independent of energy. In this method we use objects made of layers of aluminium and polymethyl methacrylate — materials that are comparable with bone and soft tissue in terms of X-ray attenuation, as noted earlier. Using published tabulated data [11] we can calculate the factors A_p and A_c for the various combinations of layer thicknesses d_t and d_b in the objects from the relations

$$A_c = a_{c,t}d_t + a_{c,b}d_b,$$

and

$$A_p = a_{p,t}d_t + a_{p,b}d_b.$$

The subscript t relates to simulated soft tissue, and the subscript b to bone.

Two polyenergetic X-ray pencil beams, generated at different tube voltages, are used for measuring the logarithmic decrements T_h at high effective energy and T_l at low effective energy for the various calibration objects. From the measured T_h and T_l and the calculated A_c and A_p the method of least squares can be used to calculate two series of nine coefficients $c_{1,0}$ to $c_{3,3}$ and $p_{1,0}$ to $p_{3,3}$, which are defined by the relations

$$A_c = \sum_{j=1}^3 \sum_{k=0}^j c_{j,k} T_l^{j-k} T_h^k,$$

$$A_p = \sum_{j=1}^3 \sum_{k=0}^j p_{j,k} T_l^{j-k} T_h^k.$$

[11] J. H. Hubbell, Photon cross sections, attenuation coefficients and energy absorption coefficients from 10 keV to 100 GeV, National Standard Reference Data Series NSRDS-NBS-29, National Bureau of Standards, Washington, DC, 1969.

With the calibration coefficients calculated in this way logarithmic decrements of real biological materials measured in the same arrangement can be recalculated to give energy-independent factors A_c and A_p . These can then be used for reconstructing X-ray images in which the contrast is due to Compton scattering alone or photoelectric absorption alone. When the material-dependent factors are weighted by the energy-dependent factors, as in fig. 4a, images are obtained at any optional value of the effective energy. This notional variation of the X-ray energy can be used, as noted earlier, to enhance or reduce contrasts between tissues. We shall see that the contrast between soft tissue and bone can in fact be eliminated.

Applications

Computed tomography

Fig. 5a shows a complete Philips CT scanner. The heart of the equipment is shown in fig. 5b and c: the yoke with the X-ray source and the detector array. The source generates a 'fan' of rays over an angle of 43.2° ; the fan includes the complete object. The X-ray source is a metal/ceramic tube with rotating anode^[12]. Each of the 288 detectors in the Tomoscan 300 measures the intensity of a pencil beam after it has passed through the object. (The later types of Tomoscan, types 310 and 350, have 576 detectors, twice as many as the Tomoscan 300.) During a scan lasting 4.2 s the yoke rotates through an angle of 360° around the object, and a pulse of radiation is generated every 7 ms, so there are 600 pulses. (An even better signal-to-noise ratio can be obtained if the number of pulses during one rotation is doubled, and hence the radiation dose and the duration of the scan.) The array of detectors is contained in a common enclosure which is filled with the inert gas xenon. The individual detectors are formed by using the electrodes to subdivide the enclosure. This is achieved by mounting the electrodes radially with respect to the focus of the X-ray tube. Two adjacent electrodes form the side walls of the ionization chamber of one detector and also act as a Soller slit diaphragm for suppressing scattered radiation. In normal operation, with a fixed high voltage on the X-ray tube, the Tomoscan 300 obtains 600×288 values of the logarithmic decrement; the number in the Tomoscan 310 and 350 is 600×576 . These values are derived from the detector signals of scans with and without an object. The system computer uses a reconstruction algorithm to calculate, from the logarithmic decrements, values for the attenuation coefficient for the pixels of the object to be constructed. This gives a matrix of 256×256 numbers, which are converted into grey levels for the video pic-

ture that appears on the display screen of the operator's console.

As stated earlier, the object of our investigation was to modify the CT scanner in such a way that the values of the logarithmic decrement could be obtained at two different X-ray source voltages and therefore at two effective energy levels of the X-radiation. This can be done in different ways. Fig. 6a shows for each of the possible procedures the mean time τ between detector signals at high and low X-ray energy. If two

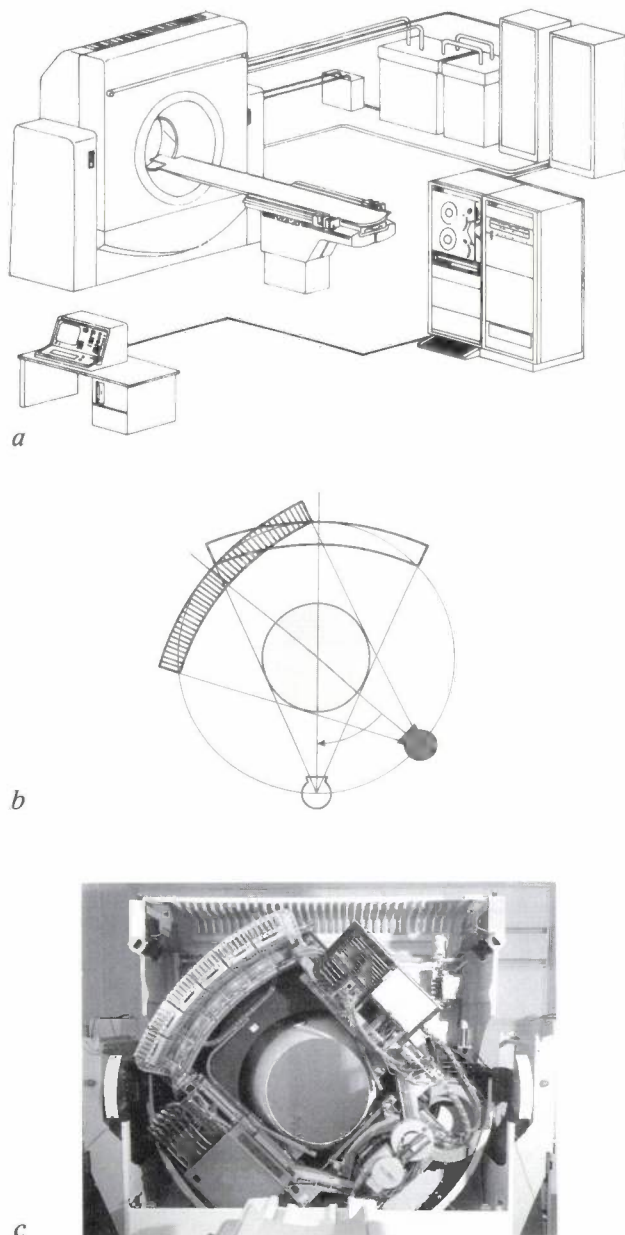


Fig. 5. a) The complete Philips CT scanner. The operating console is shown at the lower left, the power-supply units are on the right at the back, and the system computer at the lower right. b) The heart of the machine: the rotary yoke with the X-ray source and the detector array. The object is shown in light grey. c) Photograph of the yoke of the Tomoscan 300. The X-ray tube is at the lower right.

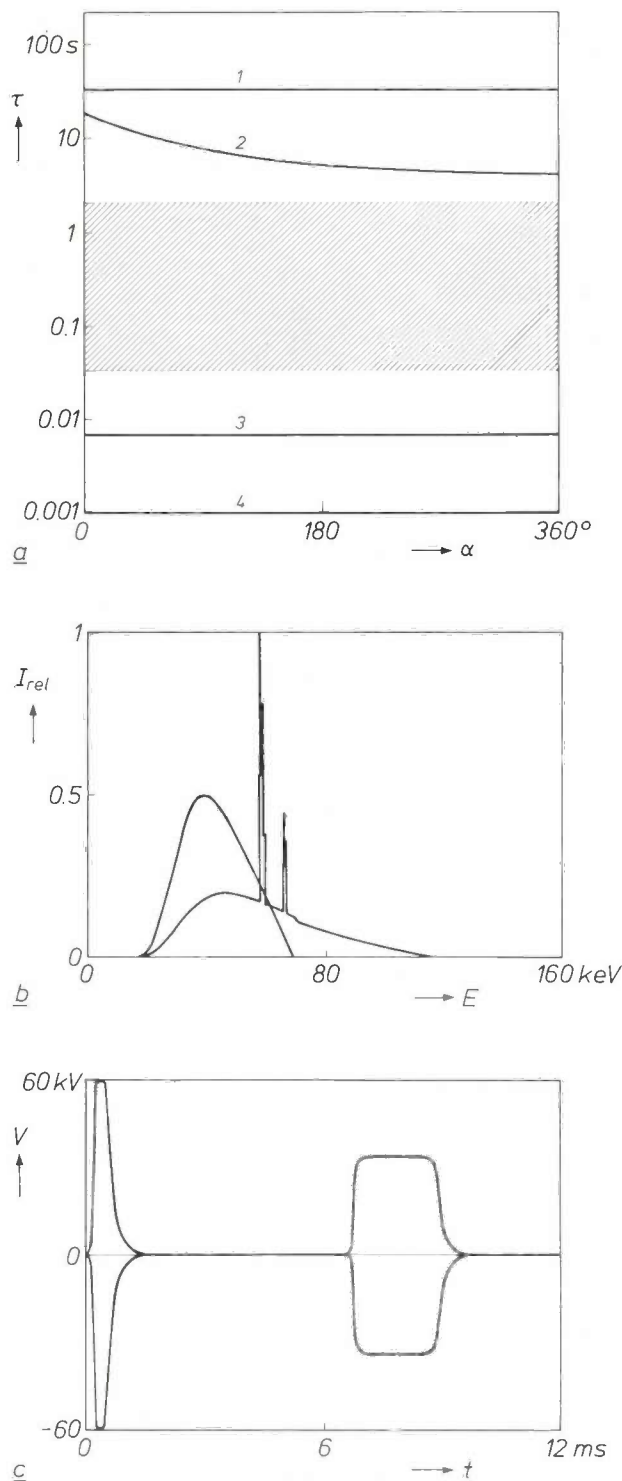


Fig. 6. a) The average time τ between detector signals of a CT scanner at high and low X-ray energy as a function of the angle of rotation α of the yoke; see fig. 5b and c. The possible procedures are: 1 two scans, one with high energy after another with low energy, with the same direction of rotation; 2 as 1, but with opposite directions of rotation; 3 one scan with alternating radiation pulses of high-energy and low-energy radiation; 4 one scan with duplicated radiation detectors of different sensitivity. The characteristic times for movements of the patient or organs in the patient come within the hatched area. b) Radiation spectra, the relative intensity I_{rel} as a function of X-ray energy E , corresponding to the alternating radiation pulses in our procedure 3. The tube voltages are 70 and 120 kV. c) Oscillogram of the voltage pulses applied to the X-ray tube. V voltage. t time.

successive scans are made at different energies, this time is longer than the characteristic times of movements of the patient (or of organs in the patient). These times correspond to the hatched area in the figure. If dual detectors are used, each with a different sensitivity to certain ranges for the radiant energy, then τ is equal to zero. However, operating with dual detectors requires extensive modification of the scanner. We therefore adopted a procedure in which, every 14 ms, an X-ray pulse is generated at 70 kV and a pulse at 120 kV tube voltage. The two radiation spectra are shown in fig. 6b, and the oscillogram of the voltage pulses is given in fig. 6c. The location of line 3 in fig. 6a makes it clear that this procedure involves no risk of movement artefacts.

Fig. 7 shows how the modification of the CT scanner allows the contrast in the X-ray image to be varied. Fig. 7a shows images in which the contrasts are due entirely to Compton scattering or entirely to photoelectric absorption. Fig. 7b shows synthesized monoenergetic images obtained with effective energies of 25 to 125 keV. The object is an AAPM (American Association of Physicists in Medicine) phantom. It consists of a polymethyl-methacrylate container filled with water and surrounded by a concentric ring of polytetrafluorethylene. Inside the container there are cylindrical inserts of different types of plastic. The X-ray attenuations of the materials of the model are very similar to those of bone and tissues in the cranium. The figure shows that certain contrasts in the 25-keV image completely disappear at high energy; on the other hand, other contrasts are enhanced at high energy. The photoelectric image and the low-energy images are 'noisy' because these images are formed from a smaller number of X-ray quanta.

Fig. 8 shows that this method can be used for measuring the bone mineral content of a vertebra, so that calcium loss and the effect of administering certain drugs can be determined. Our method is simpler than bone densitometry, previously the standard method. Dual-energy scanning can eliminate systematic errors in measurements of bone-calcium content, introduced for example by fatty tissue.

Computed radiography

Computed radiography (CR scanning) is an application of the CT scanner in which the yoke with tube and detector array is kept stationary while the patient table is moved along a straight line at right angles to the detectors. The image obtained in this way with the Philips scanners is called a 'scanogram' [13]. It is pro-

[12] W. Hartl, D. Peter and K. Reiber, A metal/ceramic diagnostic X-ray tube, Philips Tech. Rev. 41, 126-134, 1983/84.

[13] F. W. Zonneveld, The scanogram; technique and applications, Medicamundi 25, 25-28, 1980.

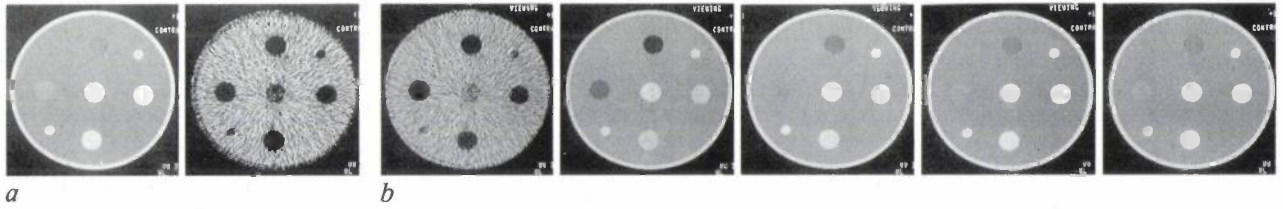


Fig. 7. Varying the contrast in CT images (computed tomography) of the AAPM phantom, which simulates the X-ray attenuation in the cranium. *a*) X-ray images with contrasts due entirely to Compton scattering (left) and entirely to photoelectric absorption (right). *b*) Synthesized monoenergetic X-ray images at 25, 50, 75, 100 and 125 keV.

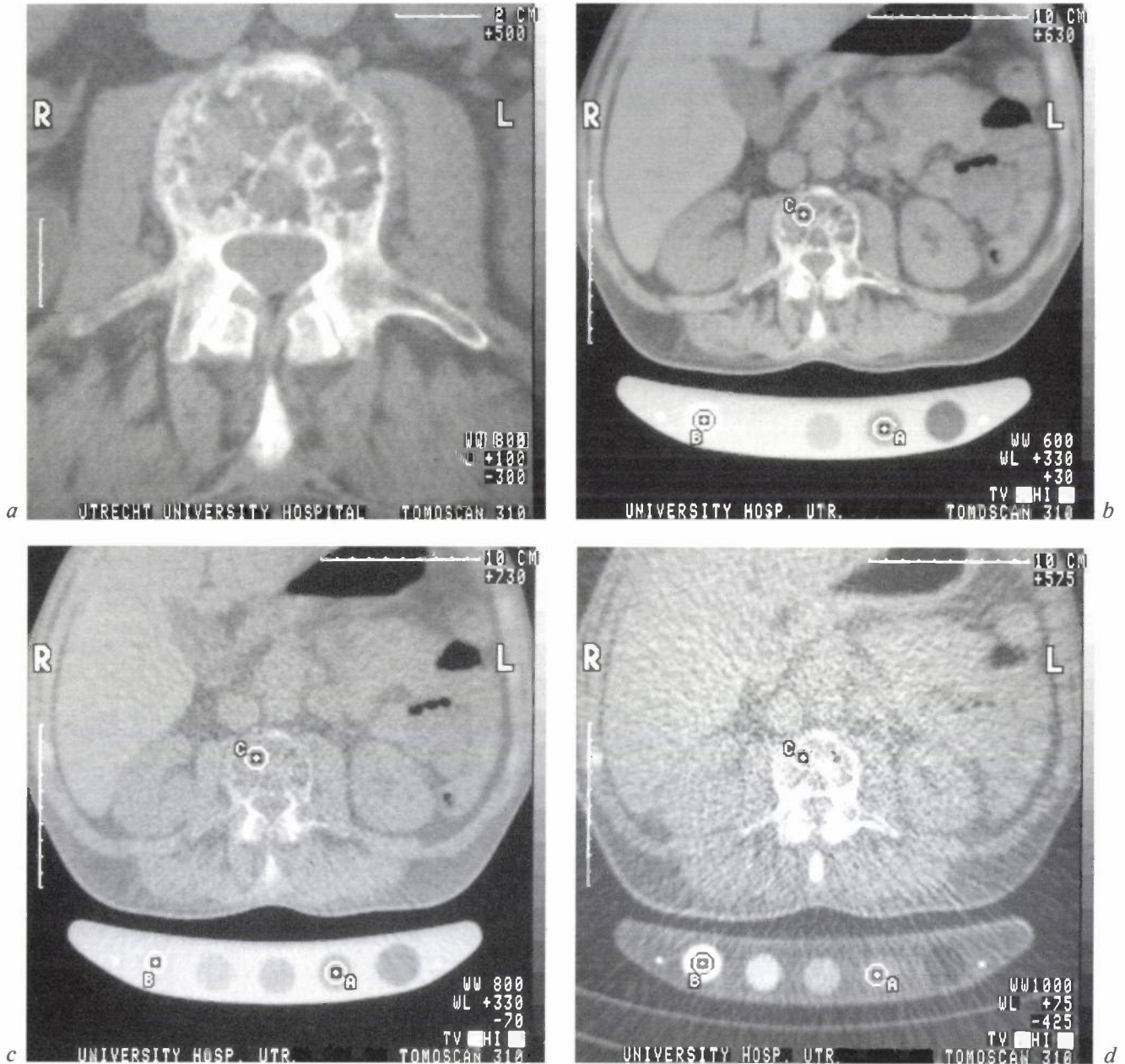


Fig. 8. Measurement of the mineral content of the bone in a vertebra (L3, the third lumbar vertebra from the top) with the modified Philips CT scanner. *a*) CT scan of the vertebra alone, to determine the position where the bone mineral content should be measured. *b*) Synthesized monoenergetic X-ray image at 75 keV. *c*) Position where the bone mineral content is measured. *A* water channel in a calibration phantom in the patient table. *B* channel containing a K_2HPO_4 solution at a concentration of 200 g/dm^3 , which has an attenuation comparable to that of bone mineral. Because of the

high fat content of the vertebra, calculations based on this exposure indicate an erroneous negative bone mineral content. *d*) as (*c*), but for photoelectric absorption. From these images the material-dependent factors due to Compton scattering and photoelectric absorption can be calculated for the pixels *A*, *B* and *C*. These factors give a positive bone mineral content for the point *C* in the vertebra. The measured bone mineral content gives an impression of the calcium loss, in this case for a patient suffering from Kahler's disease.

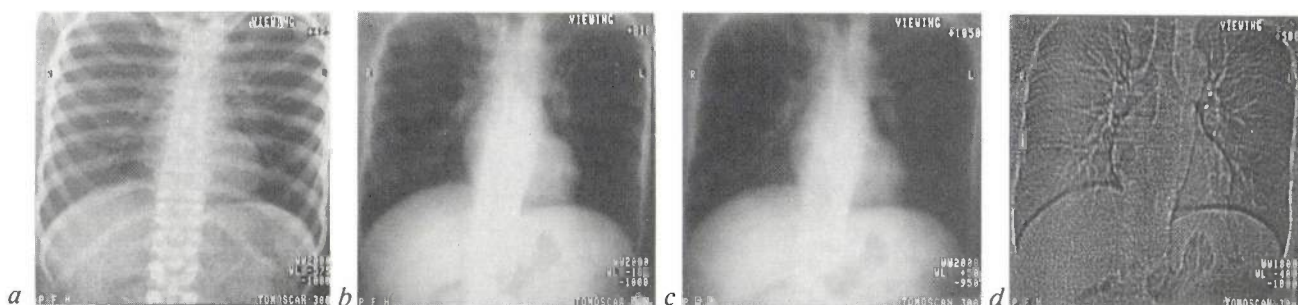


Fig. 9. Synthesized monoenergetic images of a CR (computed radiography) thorax scan at *a*) 10 keV, *b*) 50 keV and *c*) 120 keV, also made with the modified Philips CT scanner. In the image obtained at 120 keV the contrast between bone and surrounding tissue is almost zero, so that the lungs can be observed without the ribs. *d*) Example of a digital image-processing technique, edge enhancement, applied to the thorax exposure at 120 keV. This improves the visibility of the blood vessels.

duced in the following way. During the movement of the patient an X-ray pulse is generated every time the patient is displaced by a distance equal to the detector pitch. The logarithmic decrements of the detector signals with and without an object are processed to obtain an image that is comparable with that of a conventional radiograph. In this method, however, the digital values obtained for each pixel are very suitable for a variety of image-processing techniques. The scanogram, which was originally introduced just for positioning the patient correctly for CT scanning, has thus become a new medical aid with its own diagnostic potential. The principle of dual-energy image processing can also be applied here, by alternately applying high-voltage and low-voltage pulses to the X-ray tube.

Fig. 9 shows how the contrast of bone and tissue can be reduced almost to zero by changing the effective energy. The images are synthesized radiographs of the thorax, and were obtained at effective energies of 10, 50 and 120 keV by varying the contributions from Compton scattering and photoelectric absorption (*9a*, *b* and *c*). At high energy there is hardly any contrast between the ribs and the surrounding tissue, so that the image shows lung tissue alone.

The image of the lungs can be further improved by employing another digital image-processing technique, known as edge enhancement or 'unsharp masking'. This is one of the methods of manipulating the spatial frequencies in the image, called spatial filtering^[14]; it is one of the standard image-processing techniques offered by the Philips CT scanners. An 'unsharp mask' is generated from the original image by replacing the grey level for each pixel by the mean value of the grey levels of say the 5×5 pixels with the original pixel at their centre. The difference between the original and the unsharp mask is then added to the original with a weighting factor. The higher spatial frequencies in the image are then enhanced, as can be seen in *fig. 9d*,

where details such as the branching of the blood-vessels in the lungs are clearly visible.

DVI

The combination of X-ray images obtained at two energy levels has also been found useful in diagnostic systems in which video signals are processed digitally^[15]. Philips equipment for digital vascular imaging (DVI) is an example of such a system. In DVI, which is also known as DSA (Digital Subtraction Angiography), the Ziedses des Plantes subtraction method is applied to video signals of X-ray images with a contrast medium and without. *Fig. 10a* shows a photograph of X-ray equipment to which DVI equipment has been added; *fig. 10b* is a block diagram of a DVI system. Together with an X-ray stand, a complete system consists of a rotary-anode X-ray tube, an X-ray image intensifier, a TV camera tube that supplies the video signals, a high-voltage generator, electronics for the signal conversions and for processing and storing digital signals, and a magnetic disc memory (a Winchester disc).

The procedure in DVI diagnostics is as follows. First of all a radiograph is made, and after logarithmic amplification and analog-to-digital conversion, it is stored as a mask in the memory *RAM1*. Next a contrast medium is injected into a vein and exposures are then made at a maximum of 3 per second. The successive radiographs are temporarily stored in the memory *RAM2*. The memories *RAM1* and *RAM2* cannot contain more than the digital information from one image, so the previous image with the contrast medium in *RAM2* is always erased and replaced by a new image. Immediately after an exposure has

^[14] A. Hoyer and M. Schlindwein, Digital image enhancement, Philips Tech. Rev. 38, 298-309, 1978/79.

^[15] C. A. Mistretta *et al.*, Digital vascular imaging, Medicamundi 26, 1-10, 1981; L. A. J. Verhoeven, Digital subtraction angiography, Thesis, Delft 1985.

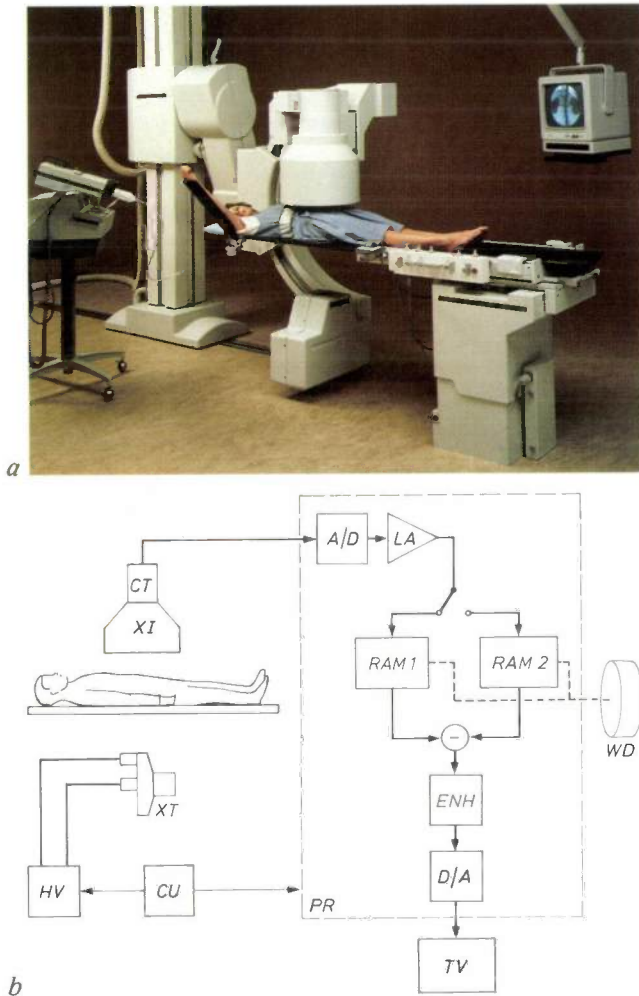


Fig. 10. *a)* Photograph of Philips X-ray diagnostic equipment with an image intensifier and a TV camera tube, with the addition of digital vascular imaging (DVI) equipment. *b)* Block diagram of a DVI system. *XI* image intensifier. *CT* camera tube. *PR* signal-processing equipment. *A/D* analog-to-digital converter. *LA* logarithmic amplifier. *RAM1* and *RAM2* semiconductor memories, each for one image; the contents of memory *RAM1* can be subtracted from the contents of memory *RAM2*. *ENH* digital signal enhancement. *D/A* digital-to-analog converter. *TV* display screen on operating console. *HV* high-voltage generator. *XT* rotating-anode X-ray tube. *CU* control electronics. *WD* Winchester disc.

been made with contrast medium, the image stored in *RAM1* is subtracted from the new image in *RAM2*. The static anatomical background is suppressed in the resultant subtraction. The radiologist can observe the successive results of subtractions on the TV monitor and can therefore estimate the flow of the contrast medium in the vascular system. All the images are stored on the Winchester disc, so that they can be reproduced later.

DVI has been of great value in the diagnosis of vascular disorders. However, when this technique is used, movement artefacts have to be taken into account. One kind of movement artefact, due to bowel gas, can lead to a false diagnosis of vascular stenosis. But when the dual-energy technique is used the radiologist can prevent such errors, by selecting a notional X-ray energy at which the contrast between gas and water is virtually zero (see fig. 4). The X-ray images with contrast medium and without must then each be derived from two images made at different energies spaced by about 0.1 s.

Another possibility worth looking at more closely is the use of DVI equipment in the same way as a CT scanner is used for computed radiography. This can be done because the closed-circuit television of the DVI system applies the same kind of digital information. The addition of the dual-energy technique then opens up new uses for DVI equipment, e.g. in the diagnosis of lesions in the abdomen, thorax and cranium. The calibration method described earlier cannot however be used. One reason for this is that scattered radiation is more of a problem with an X-ray image intensifier. This application of DVI therefore only gives qualitative information and not quantitative information for tissue analysis.

Finally, *fig. 11a* and *b* shows how the dual-energy technique can be used to reduce the contrast between

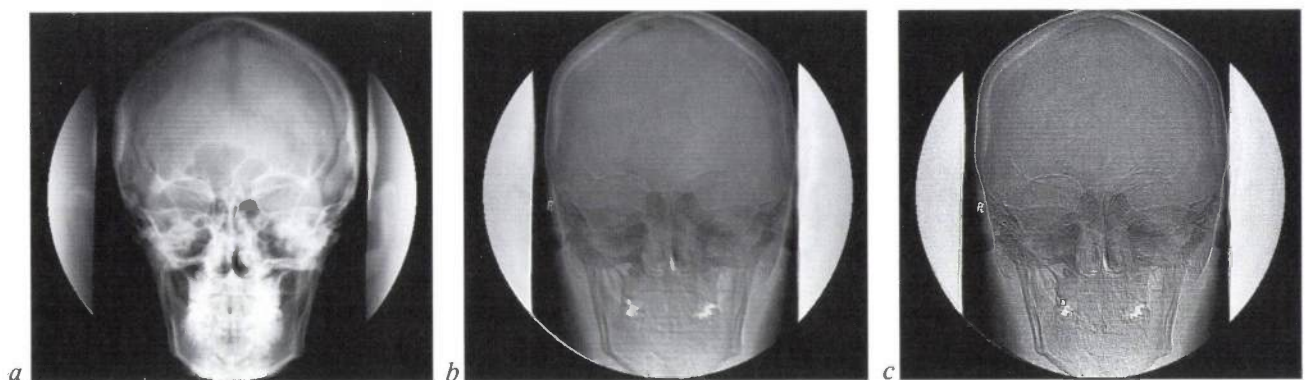


Fig. 11. *a)* Cranial image made with DVI equipment at a tube voltage of 70 kV. *b)* Weighted combination of exposures at 70 kV and 120 kV of the same cranium. The images show that by choosing the appropriate energy-dependent weighting factors the contrast between brain tissue and surrounding bone structures can be reduced to zero, so that the paranasal sinuses can be observed more clearly. *c)* The same exposure, but with edge enhancement. Details of the paranasal sinuses are now clearer still.

brain tissue and surrounding bone structures in a cranial exposure made with DVI equipment. As a result, details in the paranasal sinuses can be studied more closely, especially when the unsharp-masking technique is used at the same time (see fig. 11c).

Summary. The X-ray attenuation coefficient of biological materials can be split into separate contributions due to Compton scattering and photoelectric absorption. The contributions are each the product of a known energy-dependent factor and an unknown material-dependent factor. If two X-ray exposures are made at different energies the material-dependent factors due to Compton scattering and to photoelectric absorption can be determined. This enables X-ray images entirely due to Compton scattering or to photoelectric absorption to be calculated. These images can be weighted by the energy-dependent factors and combined to give monoenergetic X-ray images. The contrasts between tissues can then be varied by

varying the notional X-ray energy. A calibration procedure is necessary because the polyenergetic X-radiation becomes harder in the object. This procedure provides calibration coefficients for the material-dependent factors. A Philips CT scanner has been modified to supply alternate high-voltage and low-voltage pulses to the X-ray tube. The electron density and the atomic number can be derived from the material-dependent factors for each pixel. The electron densities and the atomic numbers of tissues can be used for quantitative analysis. The dual-energy technique can also be used in conjunction with Philips DVI (Digital Vascular Imaging) equipment.

varying the notional X-ray energy. A calibration procedure is necessary because the polyenergetic X-radiation becomes harder in the object. This procedure provides calibration coefficients for the material-dependent factors. A Philips CT scanner has been modified to supply alternate high-voltage and low-voltage pulses to the X-ray tube. The electron density and the atomic number can be derived from the material-dependent factors for each pixel. The electron densities and the atomic numbers of tissues can be used for quantitative analysis. The dual-energy technique can also be used in conjunction with Philips DVI (Digital Vascular Imaging) equipment.

Optical transmission in the 1.55- μm window



The photograph shows test equipment for measurements on the propagation of optical signals in a single-mode optical fibre 123 km in length (the stacked coils on the left). This fibre, a product of the Philips Glass-Fibre Works in Eindhoven, has an extremely effective transmission window in the near infrared ($\lambda = 1.55 \mu\text{m}$). This means that the attenuation of the signals may be no more than 0.25 dB per kilometre of cable, making optical communication possible over distances up to about 120 km without regeneration. The quality of the signal transmission can be assessed from an 'eye pattern', shown here on the oscilloscope screen (on the right). The eye pattern is formed by periodically displaying the pulses of the output signal one over the other. The 'eye' should be wide open, sharply outlined and should not oscillate (no 'winking'). In the case illustrated here the transmission quality is so good that the mean detection error in a signal consisting of a billion (10^9) bits is only two bits. This bit error rate (BER) is measured with a data gen-

erator, the white panel at the lower right, and the error detector just above it (it is reading a measured value of 2×10^{-9}). The small white panel is a digital power meter, for determining the detected power. The meter reading is -50.04 dB with respect to a reference level of 1 mW; this reading corresponds to a detected power of 10 nW. The grey column at the centre contains the system modules with the laser transmitter (above) and the radiation detector (below), with the supporting electronics. In the laser transmitter there is a special diode laser, designed at Philips Research Laboratories. The transmission rate of this communication system, developed by AT&T and Philips Telecommunications^[1], is 34 million bits per second. The system is particularly attractive for island regions with many submarine cables, since there will often be no need for expensive repeaters.

[1] A. Wismeijer, Long distance single-mode fibre transmission, Philips Telecommun. Rev. 43, 43-49, 1985.

Scientific publications

These publications are contributed by staff of laboratories and plants that form part of or cooperate with enterprises of the Philips group of companies, particularly by staff of the research laboratories mentioned below. The publications are listed alphabetically by journal title.

Philips GmbH Forschungslaboratorium Aachen, Weißhausstraße, 5100 Aachen, Germany	A
Philips Research Laboratory, Brussels, 2 avenue Van Becelaere, 1170 Brussels, Belgium	B
Philips Natuurkundig Laboratorium, Postbus 80 000, 5600 JA Eindhoven, The Netherlands	E
Philips GmbH Forschungslaboratorium Hamburg, Vogt-Kölln-Straße 30, 2000 Hamburg 54, Germany	H
Laboratoires d'Electronique et de Physique Appliquée, 3 avenue Descartes, 94450 Limeil-Brévannes, France	L
Philips Laboratories, N.A.P.C., 345 Scarborough Road, Briarcliff Manor, N.Y. 10510, U.S.A.	N
Philips Research Laboratories, Cross Oak Lane, Redhill, Surrey RH1 5HA, England	R
Philips Research Laboratories, Sunnyvale P.O. Box 9052, Sunnyvale, CA 94086, U.S.A.	S

O. Chantelou, M. le Quéau & I. Rak- hodai (<i>La Radiotechnique, Suresnes</i>) L	Réduction de la diaphotie en PAL et en SECAM	Acta Electron. 26	149-161	1984
D. W. Parker & L. J. van de Polder R, E	Display standards for extended definition compo- nent television systems	Acta Electron. 26	163-167	1984
S. L. Tan & R. N. Jackson E, R	Flexible coding and decoding for extended television	Acta Electron. 26	169-173	1984
J.-P. Arragon L	L'embrouillage du signal vidéo fréquence; applica- tion à la norme MAC	Acta Electron. 26	183-198	1984
M. le Quéau L	Méthodes numériques de démodulation de fréquence appliquées aux signaux de télévision	Acta Electron. 26	199-207	1984
M. Haghiri, J.-P. Kernin, J.-M. Kirichdjian, J.-J. Lhuillier & C. Rémus L	Réduction de débit d'images de télévision	Acta Electron. 26	209-239	1984
A. J. Fox R	Acoustooptic figure of merit for single crystal ger- manium at 10.6- μ m wavelength	Appl. Opt. 24	2040-2041	1985
P. H. Joosten, P. Heller, H. J. P. Nabben, H. A. M. van Hal, T. J. A. Popma & J. Haisma E	Optical thin layers of MgF ₂ produced by decomposi- tion of organic magnesium-fluoro compounds	Appl. Opt. 24	2674-2678	1985
J. Haisma, J. H. T. Pasman, J. M. M. Pasmans & P. van der Werf E	Wide-spectrum tint-free reflection reduction of view- ing screens	Appl. Opt. 24	2679-2686	1985
J. Khurgin & W. K. Zwicker N	High efficiency nanosecond miniature solid-state laser	Appl. Opt. 24	3565-3569	1985
P. H. Woerlee, G. A. M. Hurkx, W. J. M. J. Josquin & J. F. C. M. Verhoeven E	Novel method of producing ultrasmall platinum sili- cide gate electrodes	Appl. Phys. Lett. 47	700-702	1985
K. H. Nicholas & R. A. Ford R	Ghost proximity correction in an electron image projector	Appl. Phys. Lett. 47	1227-1228	1985
J. Hasker & N. C. J. van Hijningen E	Cathode and scaling properties related to the shape of current-voltage characteristics	Appl. Surf. Sci. 24	318-329	1985
J. Hasker & H. J. H. Stoffelen E	'Alternative' Auger analysis reveals important pro- perties of M-type and scandate cathodes	Appl. Surf. Sci. 24	330-339	1985
P. M. van Dooren & M. Verhaegen (<i>Katholieke Univ. Leuven, Heverlee</i>) B	On the use of unitary state-space transformations	Contemp. Math. 47	447-463	1985
P. Piret B	Word correction by means of convolutional codes	Discrete Math. 56	239-243	1985

- | | | | | | |
|--|------|---|--|-----------|------|
| N. D. Young & M. J. Hight | R | Automated Hall effect profiler for electrical characterisation of semiconductors | Electron. Lett. 21 | 1044-1046 | 1985 |
| A. F. Dadds | R | Miranda — a mobile ESM laboratory | IEE Proc. F 132 | 280-282 | 1985 |
| P. D. White, M. K. Gurcan & R. J. G. MacNamee | R | 900 MHz digital cordless telephone | IEE Proc. F 132 | 425-432 | 1985 |
| C. A. Fisher, J. M. Shannon, D. H. Paxman & J. A. G. Slatter | R | The performance of high-voltage field relieved Schottky barrier diodes | IEE Proc. I 132 | 257-260 | 1985 |
| J. B. H. Peek | E | Communications aspects of the Compact Disc digital audio system | IEEE Commun. Mag. 23 (No. 2) | 7-15 | 1985 |
| D. Lenstra (<i>Delft Univ. Technol.</i>), B. H. Verbeek & A. J. den Boef | E | Coherence collapse in single-mode semiconductor lasers due to optical feedback | IEEE J. QE-21 | 674-679 | 1985 |
| P. I. Kuindersma, A. Valster & W. Baks | E | 1.3 μm buried heterojunction laser diodes under high electrical stress: leakage currents and aging behavior | IEEE J. QE-21 | 726-736 | 1985 |
| R. Cuppens, C. D. Hartgring, J. F. Verwey, H. L. Peek, F. A. H. Vollebregt, E. G. M. Devens & I. A. Sens | E | An EEPROM for microprocessors and custom logic | IEEE J. SC-20 | 603-608 | 1985 |
| J. B. Hughes, N. C. Bird & R. S. Sojin | R | A receiver IC for a 1 + 1 digital subscriber loop | IEEE J. SC-20 | 671-678 | 1985 |
| F. P. J. M. Welten, A. Delaruelle, F. J. van Wijk, J. L. van Meerbergen, J. Schmid*, K. Rinner* (<i>* Tekade, Nürnberg</i>), K. J. E. van Eerdewijk & J. H. Wittek (<i>Valvo, Hamburg</i>) | E | A 2- μm CMOS 10-MHz microprogrammable signal processing core with an on-chip multiport memory bank | IEEE J. SC-20 | 754-760 | 1985 |
| R. Woudsma & J. M. Noteboom | E | The modular design of clock-generator circuits in a CMOS building-block system | IEEE J. SC-20 | 770-774 | 1985 |
| R. Eising (<i>Signaal, Hengelo</i>) | | Polynomial matrices and feedback | IEEE Trans. AC-30 | 1022-1025 | 1985 |
| P. Delsarte, Y. V. Genin & Y. G. Kamp | B | A generalization of the Levinson algorithm for Hermitian Toeplitz matrices with any rank profile | IEEE Trans. ASSP-33 | 964-971 | 1985 |
| M. Davio & C. Ronse | B | Insertion networks | IEEE Trans. C-34 | 565-570 | 1985 |
| V. Belevitch | B | Discrete frequency passivity conditions for n -ports | IEEE Trans. CAS-32 | 404-405 | 1985 |
| B. Dickinson (<i>Princeton Univ.</i>), P. Delsarte, Y. Genin & Y. Kamp | B | Minimal realizations of pseudo-positive and pseudo-bounded rational matrices | IEEE Trans. CAS-32 | 603-605 | 1985 |
| A. G. Tangena & G. A. M. Hurkx | E | Calculations of mechanical stresses in electrical contact situations | IEEE Trans. CHMT-8 | 13-20 | 1985 |
| P. A. Gough & J. A. Slatter | R | A model for the GTO thyristor during switch-off | IEEE Trans. ED-31 | 1796-1803 | 1984 |
| S. Makram-Ebeid & P. Minondo | E, L | The roles of the surface and bulk of the semi-insulating substrate in low-frequency anomalies of GaAs integrated circuits | IEEE Trans. ED-32 | 632-642 | 1985 |
| P. Piret | B | Binary codes for compound channels | IEEE Trans. IT-31 | 436-440 | 1985 |
| C. Tsironis | L | Highly stable dielectric resonator FET oscillators | IEEE Trans. MTT-33 | 310-314 | 1985 |
| F. A. Staas | E | On-line data reduction of the Doppler-difference autocorrelation function | Int. Proc. Conf. on Laser anemometry — advances and application, Manchester 1985 | 343-350 | 1985 |
| J. E. Knowles | R | Magnetic properties of individual acicular particles | Introduction to magnetic recording, R. M. White (ed.), IEEE Press, New York | 83-88 | 1985 |
| P. F. Fewster | R | Alignment of double-crystal diffractometers | J. Appl. Crystallogr. 18 | 334-338 | 1985 |
| C. Schiller | L | Precise orientation of semiconductor surfaces by the back-reflection Laue technique | J. Appl. Crystallogr. 18 | 373 | 1985 |
| P. A. Breddels & H. A. van Sprang | E | An analytical expression for the optical threshold in highly twisted nematic systems with nonzero tilt angles at the boundaries | J. Appl. Phys. 58 | 2162-2166 | 1985 |

- | | | | | | |
|--|---|--|------------------------------|---------------|------|
| P. Blood | R | Measurement of optical absorption in epitaxial semiconductor layers by a photovoltage method | J. Appl. Phys. 58 | 2288-2295 | 1985 |
| S. Hasegawa (<i>Kanazawa Univ., Kanazawa</i>) & P. C. Zalm | E | Formation and bonding structure of silicon nitride by 20-keV N ⁺ ion implantation | J. Appl. Phys. 58 | 2539-2543 | 1985 |
| A. A. van Gorkum & M. H. L. M. van den Broek | E | Spot reduction in electron guns using a selective pre-focusing lens | J. Appl. Phys. 58 | 2902-2908 | 1985 |
| P. M. J. Marée*, R. I. J. Olthof*, J. W. M. Frenken*, J. F. van der Veen* (*FOM, Amsterdam), C. W. T. Bulle-Lieuwma, M. P. A. Vieggers & P. C. Zalm | E | Silicon strained layers grown on GaP(001) by molecular beam epitaxy | J. Appl. Phys. 58 | 3097-3103 | 1985 |
| J. W. D. Martens & W. F. Godlieb | E | Magneto-optical properties of 100-keV Ne ⁺ -implanted epitaxial Y ₃ Fe ₅ O ₁₂ thin films | J. Appl. Phys. 58 | 3180-3184 | 1985 |
| A. H. van Ommen & R. A. M. Wolters | E | Influence of P and As implantation of the formation of MoSi ₂ | J. Appl. Phys. 58 | 4043-4048 | 1985 |
| J. Petruzello, T. F. McGee, M. H. Frommer, V. Rumennik, P. A. Walters & C. J. Chou | N | Transmission electron microscopy and Auger electron spectroscopy of silicon-on-insulator structures prepared by high-dose implantation of nitrogen | J. Appl. Phys. 58 | 4605-4613 | 1985 |
| K. A. Schouhamer Immink & J. J. M. Braat | E | Experiments toward an erasable Compact Disc digital audio system | J. Audio Eng. Soc. 32 | 531-538 | 1984 |
| J. C. Tranchart, B. Latorre, C. Foucher & Y. le Gouge | L | LPE growth of Hg _{1-x} Cd _x Te on Cd _{1-y} Zn _y Te substrates | J. Cryst. Growth 72 | 468-473 | 1985 |
| S. Colak, B. J. Fitzpatrick & R. N. Bhargava | N | Electron beam pumped II-VI lasers | J. Cryst. Growth 72 | 504-511 | 1985 |
| P. F. Bordui, S. P. Herko & G. Kosdecky | N | Computer-controlled crystal growth of KDP from aqueous solution | J. Cryst. Growth 72 | 756-758 | 1985 |
| M. W. M. Graef, B. J. H. Leunissen & H. H. C. de Moor (<i>Univ. Nijmegen</i>) | E | Antimony, arsenic, phosphorus, and boron auto-doping in silicon epitaxy | J. Electrochem. Soc. 132 | 1942-1954 | 1985 |
| P. Schobinger-Papamantellos (<i>ETH, Zürich</i>) & K. H. J. Buschow | E | Incommensurate magnetic structure of ErGe studied by neutron diffraction and magnetic measurements | J. Less-Common Met. 111 | 117-124 | 1985 |
| P. Schobinger-Papamantellos (<i>ETH, Zürich</i>) & K. H. J. Buschow | E | Ferromagnetism of NdGe and PrGe studied by neutron diffraction and magnetic measurements | J. Less-Common Met. 111 | 125-138 | 1985 |
| H. M. van Noort & K. H. J. Buschow | E | On the site preference of 3d atoms in compounds of the R ₂ (Co _{1-x} Fe _x) ₁₄ B type | J. Less-Common Met. 113 | L9-L12 | 1985 |
| J. P. Woerdman*, J. Schlejen*, J. Korving*, M. C. van Hemert* (*Univ. Leiden), J. J. de Groot (<i>Philips Lighting Div., Eindhoven</i>) & R. P. M. van Hal | E | Analysis of satellite and undulation structure in the spectrum of Na + Hg continuum emission | J. Phys. B 18 | 4205-4221 | 1985 |
| H. Zijlstra | E | Application of permanent magnets in electromechanical power converters; the impact of Nd-Fe-B magnets | J. Physique 46 (Colloque C6) | C6/3-C6/8 | 1985 |
| S. Sinnema*, J. J. M. Franse* (*Univ. Amsterdam), R. J. Radwanski (<i>Acad. Mining & Metallurgy, Cracow</i>), K. H. J. Buschow & D. B. de Mooij | E | Magnetic measurements on R ₂ Fe ₁₄ B and R ₂ Co ₁₄ B compounds in high fields | J. Physique 46 (Colloque C6) | C6/301-C6/304 | 1985 |
| M. Brouha, G. W. Turk & A. J. C. van der Borst | E | Soft magnetic properties of CoFeBSi amorphous ribbon improved by pulse annealing | J. Physique 46 (Colloque C6) | C6/413-C6/416 | 1985 |
| A. G. Dirks & J. J. van den Broek | E | Metastable solid solutions in vapor deposited Cu-Cr, Cu-Mo, and Cu-W thin films | J. Vac. Sci. & Technol. A 3 | 2618-2622 | 1985 |
| G. Duggan | R | A critical review of heterojunction band offsets | J. Vac. Sci. & Technol. B 3 | 1224-1230 | 1985 |
| J. Dieleman, F. H. M. Sanders, A. W. Kolfshoten, P. C. Zalm, A. E. de Vries* & A. Haring* (*FOM, Amsterdam) | E | Studies on the mechanism of chemical sputtering of silicon by simultaneous exposure to Cl ₂ and low-energy Ar ⁺ ions | J. Vac. Sci. & Technol. B 3 | 1384-1392 | 1985 |
| G. W. 't Hooft, M. R. Leys & F. Roozeboom | E | Low interface recombination velocity in GaAs-(Al,Ga)As double heterostructures grown by metal organic vapour phase epitaxy | Jap. J. Appl. Phys. 24 | L761-L763 | 1985 |

- | | | | | |
|---|---|--|----------------|--------------|
| A. E. T. Kuiper, F. H. P. M. Habraken (<i>Univ. Utrecht</i>) & J. T. Chen <i>E, S</i> | Hydrogenation during thermal nitridation of SiO ₂ | Mater. Res. Soc. Symp. Proc. 48 | 387-394 | 1985 |
| F. H. P. M. Habraken (<i>Univ. Utrecht</i>) & A. E. T. Kuiper <i>E</i> | Growth and composition of LPCVD silicon oxynitride films | Mater. Res. Soc. Symp. Proc. 48 | 395-401 | 1985 |
| J. Robertson (<i>Central Electric. Res. Labs, Leatherhead</i>) & M. J. Powell <i>R</i> | Defect states in silicon nitride | Mater. Res. Soc. Symp. Proc. 49 | 215-222 | 1985 |
| M. H. L. M. van den Broek <i>E</i> | Simulation of 3D electron beams with a fitting technique | Optik 71 | 27-30 | 1985 |
| A. A. van Gorkum <i>E</i> | The cup model for the cathode lens in triode electron guns | Optik 71 | 93-104 | 1985 |
| C. Ronse <i>B</i> | A simple proof of Rosenfeld's characterization of digital straight line segments | Pattern Recognition Lett. 3 | 323-326 | 1985 |
| H. Zijlstra <i>E</i> | Permanent magnet systems for NMR tomography | Philips J. Res. 40 | 259-288 | 1985 |
| G. F. M. Beenker, T. A. C. M. Claassen & P. W. C. Hermens <i>E</i> | Binary sequences with a maximally flat amplitude spectrum
Erratum | Philips J. Res. 40 | 289-304
399 | 1985
1985 |
| K. H. J. Buschow <i>E</i> | Rare earth based Invar alloys | Philips J. Res. 40 | 305-312 | 1985 |
| K. H. J. Buschow, D. B. de Mooij, T. T. M. Palstra*, G. J. Nieuwenhuys* & J. A. Mydosh* (<i>* Univ. Leiden</i>) <i>E</i> | Crystal structure and magnetic properties of several equiatomic ternary U compounds | Philips J. Res. 40 | 313-322 | 1985 |
| F. C. van den Heuvel & Q. H. F. Vreken <i>E</i> | Striations of the convective type and feedback in low-pressure mercury/noble-gas discharges | Phys. Fluids 28 | 3034-3039 | 1985 |
| R. Houdré*, C. Hermann*, G. Lampel* (<i>* Ecole Polytech., Palaiseau</i>), P. M. Frijlink & A. C. Gossard (<i>AT&T Bell Labs, Murray Hill, NJ</i>) <i>L</i> | Photoemission from a superlattice and a single quantum well | Phys. Rev. Lett. 55 | 734-737 | 1985 |
| J. M. Woodcock, J. J. Harris & J. M. Shannon <i>R</i> | Monolithic hot electron transistors in GaAs with high current gain | Physica 134B | 111-115 | 1985 |
| R. Woltjer, J. Mooren, J. Wolter (<i>Eindhoven Univ. Technol.</i>), J.-P. André & G. Weimann (<i>Forschungsinst. Deutschen Bundespost, Darmstadt</i>) <i>E, L</i> | Four-terminal quantum Hall and Shubnikov-De Haas measurements with pulsed electron fields | Physica 134B | 352-356 | 1985 |
| T. Krol & W. J. van Gils <i>E</i> | The input/output architecture of the (4,2) concept fault-tolerant computer | Proc. Ann. Int. Symp. on Fault-tolerant computing (FTCS 15), Ann Arbor, MI, 1985 | 254-259 | 1985 |
| R. S. Soin, J. B. Hughes & N. C. Bird <i>R</i> | A novel approach to the time domain simulation of switched capacitor systems | Proc. Eur. Conf. on Circuit theory and design, Prague 1985 | 713-716 | 1985 |
| M. Rocchi <i>L</i> | N-Off GaAs digital MESFET IC's | Proc. GaAs IC Seminar, London 1985 | 7 pp. | 1985 |
| P. Dautriche, B. Y. Lao (<i>Magnavox, Torrance, CA</i>), C. Villalon, V. Pauker, M. Bostelmann & M. Binet <i>L</i> | GaAs monolithic circuits for TV tuners | Proc. GaAs IC Symp., Monterey, CA, 1985 | 166-168 | 1985 |
| L. J. van de Polder, D. W. Parker & J. Roos <i>E, R</i> | Evolution of television receivers from analog to digital | Proc. IEEE 73 | 599-612 | 1985 |
| P. K. Bachmann, D. Leers, H. Wehr, F. Weirich, D. Wiechert, J. A. van Steenwijk, D. L. A. Tjaden & E. Wehrhahn (<i>Philips Kommun. Ind., Nürnberg</i>) <i>A, E</i> | PCVD DFSM-fibres: performance, limitations, design optimization | Proc. IOOC-ECOC, Venezia 1985 | 197-200 | 1985 |
| P. J. Severin & A. P. Severijns <i>E</i> | Passive components for multimode fibre-optic networks | Proc. IOOC-ECOC, Venezia 1985 | 453-456 | 1985 |
| G. D. Khoe & A. H. Dieleman <i>E</i> | TTOSS, a subscriber network for direct detection and coherent systems | Proc. IOOC-ECOC, Venezia 1985 | 479-482 | 1985 |
| C. M. G. Jochem & J. W. C. van der Light <i>E</i> | High-speed bubble-free coating of optical fibres on a short drawing tower | Proc. IOOC-ECOC, Venezia 1985 | 515-518 | 1985 |

- | | | | | | |
|--|---|---|---|-----------|------|
| D. J. Broer & G. N. Mol | E | Fast curing, low-modulus coatings for high strength optical fibres | Proc. IOOC-ECOC, Venezia 1985 | 523-526 | 1985 |
| J. P. André, J. P. Chané, J. L. Gentner, C. Mallet-Mouko, B. G. Martin, G. M. Martin, E. Menu & J. N. Patillon | L | Low dark current and low capacitance InGaAs PIN photodiode grown by MOVPE | Proc. IOOC-ECOC, Venezia 1985 | 541-544 | 1985 |
| G. D. Khoe & A. Valster | E | Coupling of laser diodes and side emitting LEDs to flat dispersion quadruple clad monomode fibres at 1300 and 1530 nm | Proc. IOOC-ECOC, Venezia 1985 | 641-644 | 1985 |
| C. A. M. de Vries & H. T. Arends | E | The influence of argon in fluorocarbon RF discharges for dry etching | Proc. ISPC-7, Eindhoven 1985 | 1019-1024 | 1985 |
| H. Baumgart & F. Philipp (<i>Max Planck Inst., Stuttgart</i>) | N | Low angle grain boundaries in zone-melting grown silicon films | Proc. Microscopy of Semiconductor Materials Conf., Oxford 1985 | 89-92 | 1985 |
| M. Lemonier, J. C. Richard, C. Cavailler*, A. Mens* & G. Raze* (<i>* Centre d'Etudes de Limeil-Valenton, Villeneuve-Saint-Georges</i>) | L | Lecture d'images de caméras á balayage de fente picosecondes par D.T.C. | Proc. SPIE 491 | 706-712 | 1985 |
| B. L. Michielsen | E | A new approach to electromagnetic shielding | Proc. Symp. & Tech. Exhibit. on Electromagnetic compatibility, Zürich 1985 | 509-514 | 1985 |
| F. M. Klaassen | E | Compact MOSFET modelling | Process & device modeling, W. L. Engl (ed.), Elsevier Science, Amsterdam | 393-412 | 1986 |
| H. C. de Graaff | E | Compact bipolar transistor modelling | Process & device modeling, W. L. Engl (ed.), Elsevier Science, Amsterdam | 431-432 | 1986 |
| P. M. L. O. Scholte*, M. Tegze*, F. van der Woude* (<i>* Univ. Groningen</i>), K. H. J. Buschow & I. Vincze* (<i>* Central Res. Inst. Phys., Budapest</i>) | E | Mössbauer spectroscopy on amorphous Fe_xZr_{100-x} ($20 < x < 90$) alloys | Rapidly quenched metals, S. Steeb & H. Warlimont (eds), Elsevier Science, Amsterdam | 541-544 | 1985 |
| G. Duggan, H. I. Ralph & R. J. Elliot (<i>Dept Theor. Phys., Oxford</i>) | R | Interface recombination in p-type GaAs-(AlGa)As quantum well heterostructures | Solid State Commun. 56 | 17-20 | 1985 |
| F. Berz | R | The Bethe condition for thermionic emission near an absorbing boundary | Solid-State Electron. 28 | 1007-1013 | 1985 |
| P. W. J. M. Boumans & J. J. A. M. Vrakking | E | Spectral interferences in inductively coupled plasma atomic emission spectrometry — I. A theoretical and experimental study of the effect of spectral bandwidth on selectivity, limits of determination, limits of detection and detection power | Spectrochim. Acta 40B | 1085-1105 | 1985 |
| P. W. J. M. Boumans & J. J. A. M. Vrakking | E | Spectral interferences in inductively coupled plasma atomic emission spectrometry — II. An experimental study of the effect of spectral bandwidth on the inaccuracy in net signals originating from wavelength positioning errors in a slew-scan spectrometer | Spectrochim. Acta 40B | 1107-1125 | 1985 |
| P. W. J. M. Boumans & J. J. A. M. Vrakking | E | Spectral interferences in inductively coupled plasma atomic emission spectrometry — III. An assessment of OH band interferences using the ratio of the limit of determination and the limit of detection as a rational criterion | Spectrochim. Acta 40B | 1423-1435 | 1985 |
| P. W. J. M. Boumans & J. J. A. M. Vrakking | E | Detection limits in inductively coupled plasma atomic emission spectrometry: an approach to the breakdown of the ratios of detection limits reported for different equipments | Spectrochim. Acta 40B | 1437-1446 | 1985 |
| P. N. T. van Velzen & M. C. Raas | E | An IETS study of the silylation of plasma aluminium oxide with four trimethylsilylamines and hexamethyldisiloxane | Surf. Sci. 161 | L605-L613 | 1985 |

J. J. Harris	R	III-V microwave devices	The technology and physics of molecular beam epitaxy, E. H. C. Parker (ed.), Plenum, New York	425-465	1985
A. J. M. Kaizer	E	On the design of broadband electro-dynamical loudspeakers and multiway loudspeaker systems	Thesis, Eindhoven	84 pp.	1986
H. J. G. Draaisma (<i>Eindhoven Univ. Technol.</i>), H. M. van Noort & F. J. A. den Broeder	E	Magnetic, microstructural and Mössbauer studies of Cu/Fe composition-modulated thin films	Thin Solid Films 126	117-121	1985
J. W. Smits & F. J. A. den Broeder	E	Magnetic and structural properties of ion-beam-sputtered thin films of $(\text{Co}_{90}\text{Cr}_{10})_{100-x}\text{TM}_x$ where TM denotes vanadium, niobium, molybdenum or tantalum	Thin Solid Films 127	1-8	1985
W. A. P. Claassen (<i>Philips Elcoma Div., Nijmegen</i>), W. G. J. N. Valkenburg, W. M. van de Wijgert & M. F. C. Willemsen	E	On the relation between deposition conditions and (mechanical) stress in plasma silicon nitride layers	Thin Solid Films 129	239-247	1985
J. J. van den Broek, A. G. Dirks & P. E. Wierenga	E, S	The composition dependence of internal stress, ultramicrohardness and electrical resistivity of binary alloy films containing silver, aluminium, gold, cobalt, copper, iron or nickel	Thin Solid Films 130	95-101	1985
B. A. J. Jacobs	E	Thin film requirements for optical recording	Vacuum 35	445-446	1985
E. D. Roberts	R	Resists used in plasma processing	Vacuum 35	479-483	1985
G. F. Weston	R	Pumping systems	Vacuum 35	493-497	1985
J. E. Curran & D. J. McCulloch	R	Reactive ion etching of GaAs and related materials for electro-optic and other devices	Vacuum 35	504-506	1985

Contents of Electronic Components & Applications 7, No. 2, 1986

- R. Volgers: Astable multivibrators using HCMOS ICs (pp. 66-72)
- J. Exalto: Crystal oscillators using HCMOS ICs (pp. 73-76)
- Automatic placement machine for hybrid-circuit assembly (pp. 77-80)
- M. Collet: MOS-XY, interline and frame-transfer sensors compared (pp. 81-88)
- J. Magill: Controller IC contends with multiple protocols (pp. 89-94)
- A. Jonas & D. Onck: Alloy bonding for power semiconductors (pp. 95-105)
- S. Baliga: VMEbus interface ICs for simpler asynchronous systems (pp. 106-111)
- C. Hamelin: Manually testing the a.c. characteristics of ECL ICs (pp. 112-115)
- A. Dolstra: Indoor unit for satellite-ready tv (pp. 116-118)

Contents of Electronic Components & Applications 7, No. 3

- H. Molko: HCMOS low-power ICs that set the standard (pp. 130-143)
- J. Exalto: HCMOS Schmitt-trigger applications (pp. 144-150)
- R. Volgers: Using 74HCT HCMOS to replace LSTTL and drive transmission lines (pp. 151-162)
- J. Exalto & H. Kloen: Protection of HCMOS logic ICs in the automotive environment (pp. 163-169)
- H. Kloen: Modifying LSTTL test programs to test HCMOS logic ICs (pp. 170-178)
- R. Croes: Battery backup of HCMOS logic ICs (pp. 179-186)
- R. Croes & P. Hendriks: Standardizing latch-up immunity tests for HCMOS logic ICs (pp. 187-197)

Anniversary Issue

Introduction

For fifty years the editors of this journal have tried to do justice to Philips research and its practical applications with representative and readable articles. Every article is an attempt to explain the essence of an investigation more clearly than is usual in publications in professional journals, but without the simplifications so often unavoidable in popular writing.

Our objectives remain unchanged. But the circumstances and the work are very different from what they were in the early days. This is clearly demonstrated by some reminiscences that Ir S. Gradstein, then Editor-in-chief, made when this journal celebrated its 25th anniversary: 'This is how it was done: the editorial committee [in those days this was the Laboratory Management] came along with suitable subjects that the editors could work on. [...] Every Saturday at 11 o'clock the editorial committee met the editors to discuss the articles that had been written — and which they had read — during the week. It really is a story from the good old days — think of it, a management that reads everything that you have written!' So in the early days, the management clearly contributed to the design of every article, and they even selected all the subjects.

Now 50 years have passed. Research has become much more complex, often with interplay between very divergent disciplines, spread over a number of laboratories at home and abroad, and very often it is hard to foresee all the practical consequences of the results. The articles are therefore more and more frequently selected after taking specialist opinion from advisers in research and in the Product Divisions. Because of increasing specialization, the actual editing of the articles becomes an ever greater challenge.

For this Anniversary Issue we have in a way made things easy for ourselves by choosing articles of a less specialized nature, written by authors with wide experience in a broad field. Starting from the different product sectors of Philips, we have compiled a selection from developments and achievements that have appealed to the imagination of a wide readership. This issue contains articles about television, IC technology, fluorescent lamps (with the SL and PL* lamps as the latest devices), medical systems (with the application of magnetic resonance as a recent highlight) and the 'electronification' of telephony. Then there is an article about glass and there are short articles on electric motors in small domestic equipment and about the Philishave. The subjects of all these articles do not just have a history, they have a future too.*

Besides a few evocative photographs we have included two instalments of our feature 'Fifty years ago'; we think they are appropriate to the nature of this Anniversary. This is also true of the first contribution: some personal and sometimes nostalgic reflections from Prof. H. B. G. Casimir, who was a member of the Board of Management and Director of Philips Research for many years, and has always shown a great interest in our journal.

This Anniversary Issue should again emphasize that Philips is a versatile company with many interfaces with society. We like to think that the broad scientific research on which all this is based has been reflected for half a century in Philips Technical Review, and we shall continue to build on this tradition in the future.

The Editors



In the thirties Philips Research Laboratories was located in the Kastanjelaan in Eindhoven. The Laboratories then had a staff of no more than a few hundred. The growth in the research was accommodated a few times by rebuilding and extension, but in the fifties it became essential to find a new site outside the town. The eventual result was the building of the Waalre complex.

The Waalre complex of Philips Research Laboratories was officially inaugurated in 1963, and many further buildings have been added since then. In the foreground is the extension for the new IC centre. The Laboratories now have a staff of some 2300. Philips also have long-established research laboratories in West Germany, Britain, France, Belgium and the United States; the total number of staff of all these laboratories is comparable with that at the Waalre laboratories.



Marginal notes for an anniversary

When the first issue of Philips Technical Review appeared in 1936 I was with the University of Leiden. I was struck by the clear and fascinating way in which technical products and working methods were explained, along with their scientific background, and probably I was one of the first external private subscribers. The journal was particularly useful to me because during that year I had exchanged the function of Assistant in Theoretical Physics for that of Senior Assistant at the Kamerlingh Onnes Laboratory, which meant not only that I had to start experimental work myself, but also that I had to take decisions about technical matters. I have since found out that the style of the Review was largely due to Dr Oosterhuis, who thus established a tradition that has continued to the present day. He was soon to be assisted by Ir G. Heller — a victim of the German occupation, sadly — and Ir S. Gradstein, who was later to be Editor-in-chief until his retirement in 1970.

The Review continues to be a reflection of the working methods and results of the Philips laboratories. Attention is also paid to special events. I shall give a few examples. In 1963 an international symposium was held from 25th to 27th September, celebrating simultaneously the 50th anniversary of the Philips Research Laboratories in Eindhoven and the inauguration of the first tall building on the new site at Waalre. A special issue of the Review was published to mark the occasion (Vol. 24, No. 11/12).

In 1966 the Philips company celebrated its 75th anniversary, and to mark this event Ir Gradstein and I compiled an 'Anthology' of articles that had appeared between 1950 and 1966. I still think this is an impressive collection. In the introduction to this book I also tried to formulate the fundamental tenets of the Review.

'From its early beginnings in 1936 the Philips Technical Review has tried to steer a middle course between two extremes and to establish a level of treatment that does not require expert knowledge and great mathematical skill on the readers' part, although it may require a good deal of concentration and real interest. It is our firm belief that it is possible to describe at this level the essential features of our work and our results, even though the work itself could never have been done without application of more sophisticated methods.'

In 1972 I retired and on that occasion the editors once again put together a special issue and also invited me to write a contribution myself.

And now it is the turn of the Review itself. It is celebrating its fifty years of existence and publishing an anniversary issue. The editors have asked me to write a brief introduction to it, and I appreciate this greatly. Today I am no longer familiar with recent developments, so I shall not try to introduce the various contributions to this anniversary issue separately. They do not need it: they speak plainly enough for themselves. But they do bring me to a few general considerations, which I would like to use to draw attention to some differences between the present situation and the one I used to know intimately in earlier days.

The first thing that strikes me is that experimental techniques have become much more sophisticated with the passing years. In former years the art of experimentation at Philips Research Laboratories was not at too high a level in this respect. Experimenters worked with verve and imagination, certainly, but there was no great respect for high accuracy or for high sensitivity, and hence the observation of very small effects. Nor was much attention paid to the creation of extreme conditions — such as high magnetic fields, high pressures, low temperatures, very high vacuum, extremely pure materials — which now play such an essential role. An exception was the work on high-voltage generators; I shall return to this later.

Modern thermionic devices — I think for example of Plumbicon tubes and other camera tubes and of various image intensifiers — make great demands on vacuum technology and the mastery of materials. Mechanical and optical precision and materials control are essential in the fabrication of microcircuits. Experimenters are therefore forced to refine their methods, and this in turn leads to a refinement of the products, which in turn again may be useful to the experimenters — and so on. Electronic automation also makes it possible to obtain and process a much larger number of measurement results than formerly. It hardly needs to be said that the impact of mathematics has been enormously increased by the computer. A significant new feature is the use of computer models for carrying out experiments. These do not make all the real experiments superfluous, of course, but supplement them and in some cases completely replace them.

I am pleased to find out that the contribution of research in the creation of new products has certainly not diminished, and the contents of this anniversary issue lead one to expect that this will remain so in the

future. However, I do have the impression that fundamental research occupies a supporting function here and is less of a driving force than it used to be. Here is a single example. A knowledge of gas discharges and of the existence of fluorescence was sufficient for the creation of the first fluorescent lamps. Fundamental knowledge brought us to a new product. The 'perfecting' discussed by A. J. Jack and Q. H. F. Vrehan required many experiments and calculations, but broke no new ground in fundamental physics. This sort of thing often happened earlier, too. Röntgen's discovery became the start of the manufacture of X-ray tubes and equipment; the perfecting of the tubes did not depend on new fundamental discoveries. And the late Dr Van Alphen, who was responsible for optics at Philips Research Laboratories, sometimes used to complain that although geometrical optics was a nice subject, there was really nothing more to it than Snell's law of refraction. But once again, my impression is that what I called the driving force has become less significant. Research at Philips today is almost entirely concerned with phenomena and theories whose main features are at least twenty years old and generally much older. Very little relationship can be found between recent pure fundamental work at the frontiers of science and the Philips interests.

Were things different formerly? Yes, I think so. When Holst and Oosterhuis started work on gas discharges, Bohr's ideas about stationary states and their confirmation by the experiments of Franck and Hertz were still at the centre of interest. In the late twenties it became possible to work out the properties of the solid state with the aid of the new quantum mechanics. During the thirties solid-state research was taken up at Philips Research Laboratories. The year 1932 was an 'Annus Mirabilis' for nuclear physics: discovery of the neutron, the positive electron and heavy water; production of nuclear reactions by bombardment with accelerated protons. From then on nuclear physics made great strides in many places and the Philips laboratories contributed too, both through their own experiments and by building high-voltage generators, including a generator to replace the original generator of Cockcroft and Walton. During the occupation a clandestine start was made on the construction of a cyclotron and after the war a number of high-voltage installations and a number of cyclotrons were designed and delivered. Gradually, however, Philips moved away from this work, and the next phase in pure physics, high-energy physics, dealing with particles and fields, drew no response from the Philips laboratories. Whether a proton is built up from

quarks, and if so how, how they are held together, whether it is possible to arrive at a universal theory for all force fields via a mathematical formalism in ten dimensions — all these questions have no significance for Philips at present, and I do not think that this will change in the next twenty or thirty years.

However, there is no point in deploring this situation. It is now just impossible for a single organization to cover the whole range of physics with all its existing and potential applications; and the fields of work chosen by Philips are already so extensive, and offer room for so much innovation, that it would be ill-advised to try to include fields that are entirely new and as yet extremely speculative. And the selected fields are completely within the compass of the 'ordinary' quantum mechanics and quantum electrodynamics (with classical mechanics and electrodynamics as the boundaries). We should all the same try to take advantage of the generally superior knowledge in the fields of measurement technology, data processing and construction of equipment that exists at the great centres such as CERN. The supply of components and equipment can also help, and is important in my opinion even if it provides little profit. This is also true for work in the field of astronomy.

Fortunately fundamental pure research does exist that falls within the range indicated above, and the Philips laboratories are indeed active and competent in these fields. Such work may be less fundamental than particle physics or relativistic cosmology, but it can nevertheless provide some surprising results, some of which can lead to new technical implementation. The detailed study of the quantum Hall effect is a striking recent example.

In the present issue the emphasis is on the technical function. Perhaps this is as it should be in a technical journal, but it would please me greatly if Philips Technical Review were ever to find a suitable opportunity to take a fundamental scientific principle as a starting point and devote an issue to results of research that excel through elegance or profundity, regardless of technical usefulness. Perhaps this is something for the 75th anniversary of Philips Research Laboratories or the centenary of the Philips Company. With a bit of luck I might just be able to see this happen.

H. B. G. Casimir

Prof. Dr H. B. G. Casimir was formerly a member of the Board of Management of N.V. Philips' Gloeilampenfabrieken and headed scientific research in the Philips group of companies worldwide.

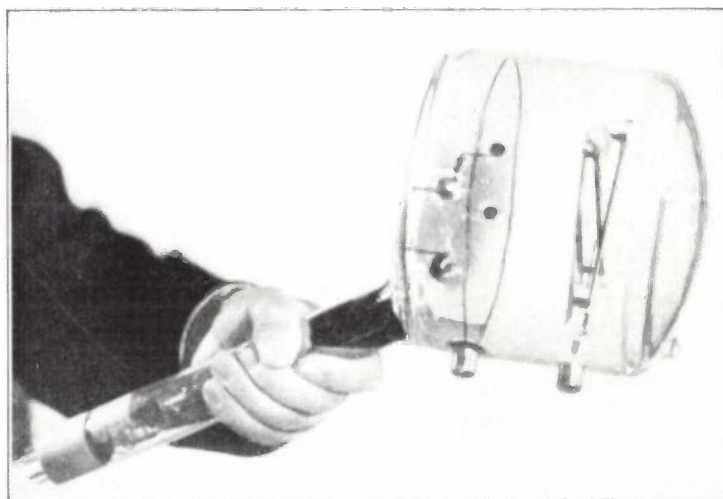
Looking back at distant vision: television technology from 1936 to 1986

K. Teer

Introduction

Television is a fascinating subject with a history rich in interest. A history whose aspects include the clearly technical, the programmes, the broadcasting system and the sociological. Here we shall look at some of that history, concentrating on:

casting controllers and ministers for the media — not forgetting the involvement of thousands of millions of viewers. This article is not therefore an all-embracing historical account, but a selective retrospective view.



a



b

Fig. 1. *a*) V. K. Zworykin's iconoscope; this is the image-sensing device in which the photographic shutter principle of mechanical scanning was first replaced by an electronic 'switch' — an electron beam originating from a thermionic cathode (lower left) — which connects the individual elements on a photosensitive plate (on the right in the large glass envelope) in sequence to the rest of the television system. *b*) 90-line picture obtained with an iconoscope; higher numbers of lines were soon used, considerably improving the picture quality.

- some of the time: the last 50 years,
- some of the aspects: the technical side, and
- some of the events: solving the essential problems.

This means that we shall look at the essential posing of the problem and the fundamentals of the approach, with the accent strongly on the first stages in the evolution of the technology (invention and feasibility model). In consequence talented development, manufacturing ability, entrepreneurial qualities and industrial vision — all equally necessary in making television a success — will hardly be mentioned. Because of the limitation to the technical, the same is true for the talent of performers, programme makers, broad-

The three basic problems of television

A brief reflection on the television problem, with the technology of radio and the cinema in mind, soon brings the conclusion that there are three vital steps: image acquisition (or 'image pickup'), transmission, and display. Let us look at these in turn.

Image acquisition

In the acquisition of an image the two-dimensional time-dependent entity of the image has to be translated into an electrical signal that is by its very nature one-dimensional. Just over 100 years ago P. Nipkow proposed a mechanical scanning method combined with the photoelectric effect as the answer. The scanning converts the image into a series of picture elements

Dr Ir K. Teer was a Director of Philips Research Laboratories, Eindhoven, before his retirement.

— or 'pixels' in today's terminology. During the scan of each element the reflected or transmitted light is measured from the photoelectric effect produced in a photocell.

In the iconoscope, invented by V. K. Zworykin in 1923, the scanning system was liberated from mechanical rigidity and inertia by using an electron beam to scan a photoelectric plate on which the image was projected in its entirety (*fig. 1*). It was very important here that the photoelectric effect remained continuously active at each element, and not — as in the Nipkow disc — just during the short time while an element was being scanned ^[1]. The condition for correct operation of this principle is that the elements on the photoelectric plate should be well insulated from one another electrically.

Scanning a photosensitive plate whose operation depends on photoemission with an electron beam is a complex charge-compensation process, as regards electron paths, secondary emission and re-entry of emitted electrons. This means that there can be many departures from the theoretical ideal; however, it also means that many more electron mechanisms can be devised for improving the operation of the entire process. An example of this is the use of an extra secondary emission, as introduced in the successors ^[2] to the iconoscope — the image iconoscope ^[3] and the image orthicon (first described in 1939 and 1946 respectively). In both of these the photosensitive plate (the 'photocathode') is not scanned directly, but is projected by electron optics on to a second target; the secondary emission arising here gives an intensified charge pattern that is available for scanning.

An alternative to photoemission as a basis for signal formation is photoconductivity. This was first introduced by RCA in 1950, to eliminate the complexity of the secondary intensification and scanning with high-velocity electrons. Higher sensitivity made the use of secondary emission unnecessary. Also, a considerably simpler charge-compensation process could be used at the scanning location.

However, the difficulties now transferred themselves to the special peculiarities of the photoconducting layer, which made it rather difficult to obtain the desired image quality. When these difficulties had been overcome, at Philips Research Laboratories, for photoconducting layers based on lead oxide — instead of the antimony sulphide used by RCA ^[4] — the result was a small and simple camera tube, the Plumbicon (*figs 2 and 3*) ^[5]. This was free of spurious effects (such as shadow images, smearing, dazzle and saturation) and it had a reproducible linear light/signal characteristic and a very high sensitivity. These features are of essential importance in television-camera technology,

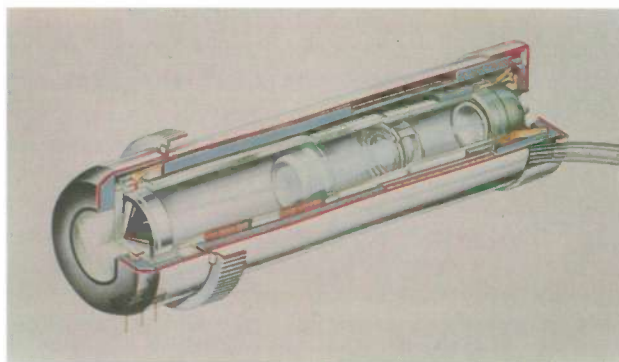


Fig. 2. Television camera tubes are still being continuously improved today: this cut-away view shows a modern Plumbicon tube (type XQ 4187). An electron beam scans a charge pattern (on the left). The diagonal of this pattern is only 1.1 cm. The total length of the tube is 7.8 cm.



Fig. 3. While the dimensions of television camera tubes diminished, the characteristics improved. Here in the top row we have, from left to right, an iconoscope, an image iconoscope and an image orthicon. Below there is a great variety of camera tubes: first a row of four vidicons, then a row of five Plumbicon tubes and finally another row of four vidicons.

and especially in colour-television image acquisition, which will be mentioned later in this article.

Transmission

The transmission of television signals as ordinary broadcast signals or by cable is not essentially different from the transmission of audio signals, apart from a considerable quantitative difference. A television signal, with several hundred lines in each picture and several tens of pictures per second requires about a thousand times as much bandwidth as an audio signal — megahertz, not kilohertz. The obvious thing was to use amplitude modulation for the transmission, with the bandwidth of one sideband limited as far as possible (*fig. 4*).

In addition the principle of interlacing (fig. 5) was introduced, which reduces the bandwidth required by a factor of about 2. When this principle is applied the 25 pictures (or frames) that are acquired and displayed per second (in the European system) are transmitted in the form of 50 half-pictures or 'fields', with alternate scans containing only the odd lines or only the even lines. The viewer is perceptually strongly inclined to interpret two successive half-pictures of $312\frac{1}{2}$ lines (in the European system) as a complete picture of 625 lines. Because of the interlacing the picture flicker is reduced to an acceptable level to the viewer, although parasitic visual effects are not completely absent. The amount of information transmitted per second is of course only a half compared with the situation of 50 complete scans of the picture per second.

Precisely because this intervention really gives the viewer less than his due, it is a rather frustrating thought that in another sense much more is transmitted than he really needs. This is because the picture content usually shows so many fragments that are strongly correlated in place and time that there may well seem to be frequent repetition of what has already been transmitted and hence an unheard-of wastage of transmission capacity.

Unfortunately it is not simple to improve the situation by using a more efficient procedure, although a difference of a factor of 100 in the amount of information transmitted and actually required can be made acceptable. The problem has received a lot of attention through the years [6], and although more efficient methods have been proposed they have not as yet led to genuine applications.

The high bandwidth of video signals compels the use of a correspondingly high carrier frequency (higher than 40 MHz) with the modulation. At these frequencies electromagnetic waves are propagated in a straight line in the Earth's atmosphere, so that a transmitter cannot reach much further than the horizon. This means that for a coverage area of any size a large number of relay transmitters soon become necessary. Moreover, this means that for television the competitive position of cable compared with broadcasting is stronger than in radio.

Important qualitative differences between audio and video signals are the nature and the measure of the permissible distortion. For audio signals the frequency content ('the spectrum') is the first essential, for video it is the signal waveform.

It was a while before anyone realized sufficiently that the old touchstone for system quality, the frequency characteristic, ought to be traded in for the step-function response [7], that nonlinearity could be

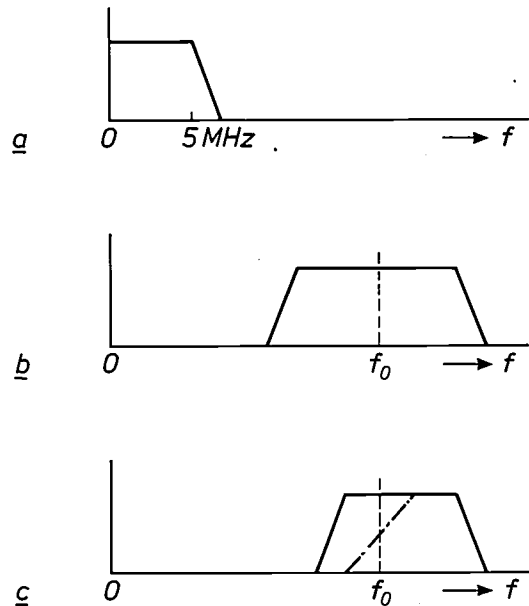


Fig. 4. a) The frequency spectrum of a television signal extends from zero to several megahertz. b) In the most well-known form of amplitude modulation ('double-sideband modulation') of a carrier of frequency f_0 the bandwidth required is doubled. c) To manage with a smaller bandwidth, without requiring too complicated a receiver, one sideband of the television signal is fully transmitted and the other is only partially transmitted. A filter in the receiver in front of the actual detector converts this into a true 'vestigial-sideband-modulated' signal (chain-dotted line) [2].

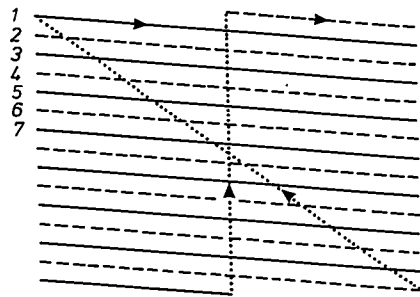


Fig. 5. In an interlaced scan all the odd lines (shown continuous) and then all the even lines (shown dashed) are scanned in turn. This gives two *fields* (or *rasters*), which combine to form one *picture* (or *frame*).

- [1] J. van der Mark, An experimental television transmitter and receiver, Philips Tech. Rev. 1, 16-21, 1936.
- [2] F. Kerkhof and W. Werner, Television, Meulenhoff, Amsterdam 1952; D. G. Fink (ed.), Television engineering handbook, McGraw-Hill, New York 1957.
- [3] P. Schagen, H. Bruining and J. C. Francken, The image iconoscope, a camera tube for television, Philips Tech. Rev. 13, 119-133, 1951/52.
- [4] P. K. Weimer, S. V. Fogue and R. R. Goodrich, The vidicon — photoconductive camera tube, RCA Rev. 12, 306-313, 1951.
- [5] E. F. de Haan, A. van der Drift and P. P. M. Schampers, The 'Plumbicon', a new television camera tube, Philips Tech. Rev. 25, 133-151, 1963/64.
- [6] K. Teer, Some investigations on redundancy and possible bandwidth compression in television transmission, Thesis, Delft 1959. Also published in: Philips Res. Rep. 14, 501-556, 1959 and 15, 30-96, 1960.
- [7] J. Haantjes, Judging an amplifier by means of the transient characteristic, Philips Tech. Rev. 6, 193-201, 1941.

treated more tolerantly in video transmission and that group delay needed much more careful attention.

The transmitted video information only has any significance for the viewer, of course, if the periodicity and phase of the image scan are in step at transmitter and receiver. For this reason signals also have to be transmitted to indicate the end of each line and each picture. This is done by adding easily detectable 'synchronization' pulses to the video information. A constant reference level for the picture brightness (the 'black level') is also transmitted to set the receiver so that pixels at zero brightness do indeed radiate no light (fig. 6).

Because of the enormous difference in the video and sound bandwidths, the television sound signals run the danger of ending up in some neglected corner — but certainly not in an unnecessary corner, since much picture material is completely incomprehensible without the associated sound. The sound channel is generally provided by an extra frequency-modulated carrier at a fixed frequency spacing from the vision carrier.

So far the number of lines has always been stated in terms of a few hundred. Regular transmissions of such signals, with 405 lines, started in the United Kingdom in 1936. In the United States, after many experiments with 343 and 441 lines, the official standard was set at 525 lines in 1941. Only after World War II was the number of lines settled in continental Europe, where most countries had fallen in with the proposal of 625 lines. In France and in a few other places, however, a standard of 819 lines had been chosen [8]. Regular television broadcasts started in the Netherlands in 1951.

Colour television has brought about a somewhat greater standardization in Europe in the sense that when it was introduced the United Kingdom and France also went over to 625 lines.

The choice of the picture frequency has so far led to an obvious dichotomy, based on the frequency of the existing electricity supply mains (30 pictures per second in the United States and Japan, 25 pictures per second in Europe).

Display

Just as in the acquisition of the image, in its display the mechanical solutions were soon replaced by electronic ones with an electron beam and a luminescent screen.

The 'Braunsche Röhre' (later called a cathode-ray tube, now usually a picture tube) had been known since 1897, but it required some improvement. Dimensions, shape, cathode, phosphors, electron optics, deflection and high-voltage circuits: all were subjects for

study in their combined context. Only the very oldest television tubes ('kinescopes') still contained the original green luminescent phosphor. This was very rapidly replaced by phosphor combinations that gave white light and had already been described in patents from

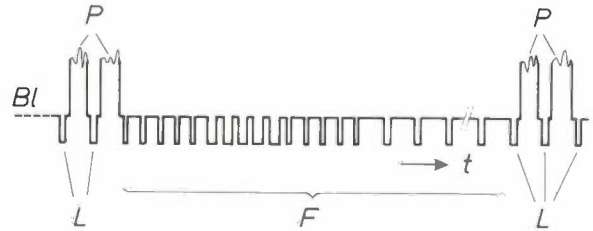


Fig. 6. In a television signal the actual picture information P is alternated with other important information. Between every two lines there is a clear pulse L for line synchronization. The transition from one field to the next is signalled by a fairly complicated pulse pattern F (the picture information is omitted here). The black level Bl is briefly inserted between every two lines.

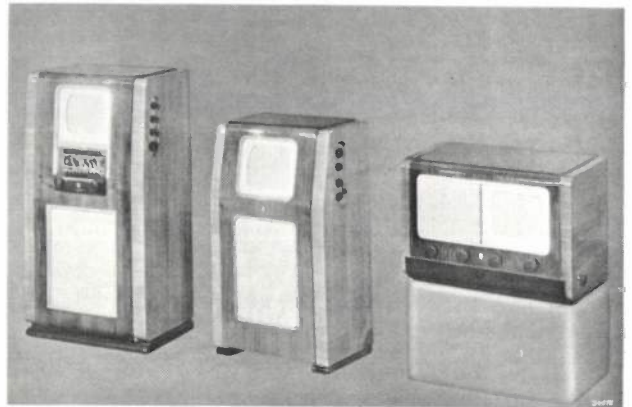


Fig. 7. Television receivers from the late thirties; left: console model with built-in radio; centre: console model for television only; right: table model.

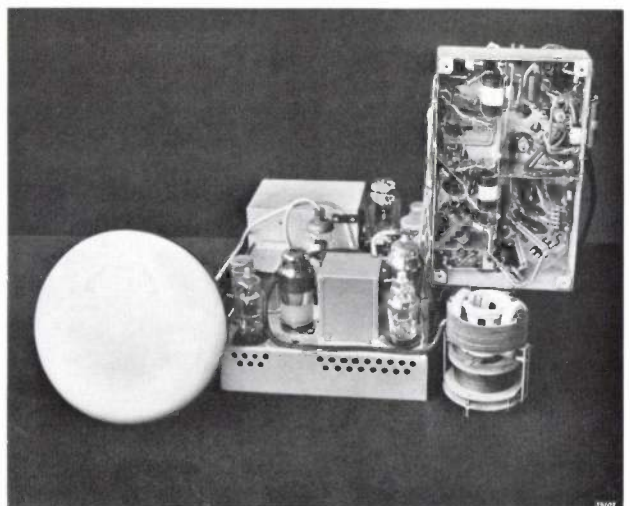


Fig. 8. The electrical components of the receiver of fig. 7 (centre). The screen of the cathode-ray tube is shown on the left. At the centre is a chassis with power-supply circuits (the 'high-tension supply') and the timebase generators. At the top right — in the vertical plane — is the chassis with the amplifier stages for picture, sound and synchronization signals. Below this is the system of coils for focusing and deflecting the electron beam in the cathode-ray tube.

the early twenties. The usual screen dimension in 1936 was 10 inches (*figs 7 and 8*). Philips were the first to bring in the 21-inch screen, in 1954.

Nor has there been any lack of attempts to obtain picture display by methods other than the picture tube. Much of the drive to obtain 'flatter' devices arose because of the inconvenient dimension perpendicular to the screen — the length of the tube. In recent years a few versions in which a flatter construction^[9] has been obtained by folding the electron beam (*fig. 9*) have appeared on the market. In addition new possibilities for display panels of small format have been found on the basis of liquid-crystal technology^[10].

A well-known extension of the potential applications of the cathode-ray tube is optical projection, which in addition to larger dimensions can also provide a different relation between picture size and cabinet depth (*fig. 10*). But as yet no real attack has been made on the position occupied by the conventional direct-vision picture tube.

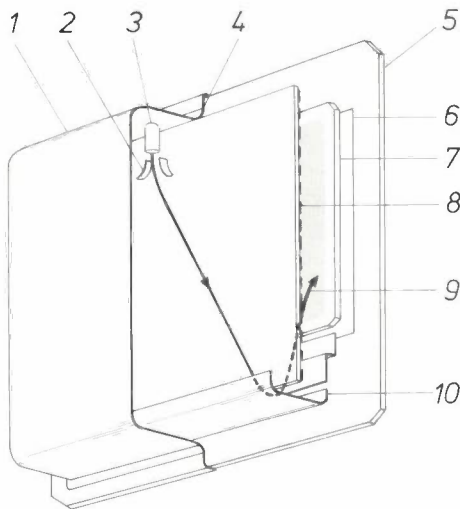


Fig. 9. A flat display tube developed by Philips, seen obliquely from the rear. The electron gun directs its beam downwards; the electrons are then deflected upwards round a metal screening plate and accelerated towards the screen. The total thickness of the tube is less than 7.5 cm and the picture diagonal is about 30 cm. 1 metal can; 2 line-deflection plates; 3 electron gun; 4 vacuum seal; 5 window; 6 phosphor screen; 7 electron multiplier; 8 frame-deflection plates; 9 electron beam; 10 deflection lens.

[8] W. Werner, The different television standards, considered from the point of view of receiver design, *Philips Tech. Rev.* 16, 195-200, 1954/55.

In 1985 the international recommendations for television systems with numbers of lines other than 525 or 625 were withdrawn. In practice this means the end of such systems.

[9] J. R. Mansell *et al.*, The metal-dynode multiplier: a new component in CRT design, *Displays* 4, 135-139, 1983.

[10] T. S. Perry, Pocket TVs are inching ahead, *IEEE Spectrum* 22, No. 7 (July), 54, 1985;

C. M. Apt, Perfecting the picture, *ibid.*, 60-66;

S. Morozumi, K. Oguchi and H. Ohshima, Latest developments in liquid crystal television displays, *Opt. Eng.* 23, 241-246, 1984.

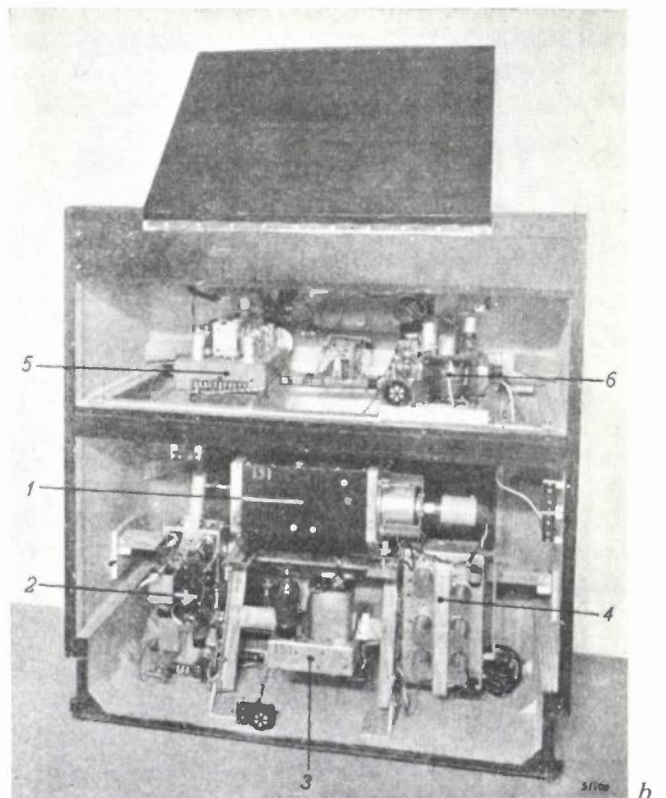


Fig. 10. Monochrome projection-television receiver dating from the late forties. *a*) The projection screen is raised above the console, which contains the television projector and also a radio. The screen can be folded away into the console. *b*) A view of the interior: 1 optical unit; 2 beam-deflection unit; 3 high-voltage generator (25 kV); 4 television receiver (picture and sound); 5 radio receiver; 6 rectifier. (See also *fig. 16*.)

Extension of the possibilities

With the three basic functions described a television broadcasting system can be set up that is suitable for the provision of most forms of visual information. There are however two important extras that, while not absolutely necessary, have been found to be particularly desirable. These are the recording of television signals and the addition of colour to the picture. The first serves to separate the instant at which a picture manifests itself from the instant of transmission or reception of that picture, so that there is a huge potential increase in the picture information available for transfer via television. The second extra serves of course to give a further and better approach to the impression of reality.

First of all we shall look at colour television, where, as in the foregoing, the triple basic problem of image acquisition, transmission and display again confronts us.

The measurement of colour information

The question of identification of a pixel by chrominance and luminance [11] is described in colour theory. There it is stated that practically all impressions of light can be obtained by the superposition of three well-chosen monochromatic component pictures in red, green and blue, and that a unique transformation exists from any arbitrary light impression that we wish to characterize to this triple-monochromatic imitation.

For colour television this means that three sub-pictures P_R , P_G and P_B should be derived from any given picture P via three colour filters (fig. 11), transmitted, reconstituted at the receiver and united to form a single picture, which will then resemble P as closely as possible [12].

There is another solution, which results in a simpler design and is based on the 'inertia' inherent in visual perception. This is to form the sub-pictures P_R , P_G and P_B in succession instead of simultaneously, by successively introducing — sufficiently rapidly — the three colour filters for a single camera tube into an ordinary monochrome arrangement.

This sequential principle can also be followed for transmission of the video information and reconstitution at the receiver, of course. The high picture rate then introduces an extra bandwidth problem, however. The sequential reproduction of the sub-pictures at the receiving end also entails problems, since the picture format desired there leads to bulky mechanical structures with rotating discs.

The first colour demonstrations [13] of the sequential system were given in 1940 by the American broadcasting organization CBS. The pressure that was exerted by CBS in favour of this approach was so great that the Federal Communications Commission (the FCC) in-

duced (rather prematurely) a sequential standard for the United States in 1950. This standard comprised a sequence of 24 pictures of 405 lines per second, broken down into 144 ($= 2 \times 3 \times 24$) fields by interlacing ($2 \times$) and colour sequencing ($3 \times$).

The transmission problem in colour television

The sequential system did not catch on in the end because it contained an incipient weakness relating to both product policy and television technology.

In product policy a gradual introduction of colour television was a hindrance, because existing sets made to the monochrome standard could do nothing with the colour transmission and the colour receivers could do nothing with the existing monochrome transmissions.

As television technology it was an inadequate concept because no use was made of some of the basic essentials of television transmission and perception. These notions were discovered and developed between 1949 and 1952 by the American companies RCA and Hazeltine (sitting with others on the National Television System Committee, the NTSC [13]). Let us look at four of them here [11]:

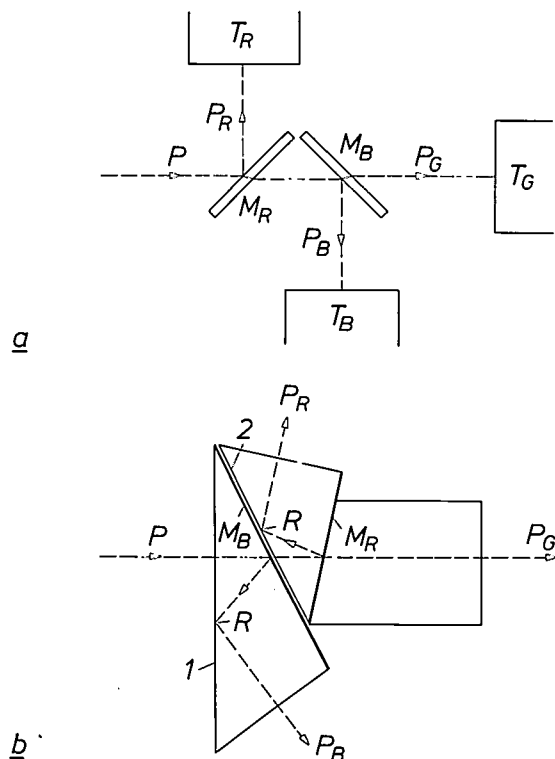


Fig. 11. a) Three sub-pictures P_R , P_G and P_B are derived by means of two half-silvered, colour-separating mirrors M_R and M_B from a colour picture P . With suitably set-up camera tubes T_R , T_G and T_B three television signals can be derived from this arrangement. b) By making use of a prismatic device with reflecting layers M_R and M_B a robust and compact system is produced; at the surfaces 1 and 2 there is a glass/air interface to give two total internal reflections R .

- In the first place there is the perceptual effect that with correct display of the luminance at standard sharpness, lower sharpness requirements can be set for filling in the colour.
- In the second place it was found that a high-frequency disturbance in the picture that occurs in opposite phase in successive lines and pictures can be tolerated to a high degree.
- A third important fact is that the eye is much more sensitive to errors of hue (yellow or orange) than to colour-saturation errors (bright yellow or light yellow).
- Fourthly, it was found that viewers object more to an incorrect colour than to a complete lack of colour.

All this has led to a system in which the basic signal is a luminance signal (similar in general terms to the conventional monochrome signal). Within the same bandwidth a subcarrier is added that has opposite phase in successive lines and pictures, and is modulated in quadrature by two colour-information signals of limited bandwidth (1 to 1.5 MHz); see *fig. 12*. In the receiver the colour information is recovered by synchronous detection because a suppressed carrier is used and because both amplitude and phase have to be determined.

The luminance signal Y is obtained from a linear combination of the three component signals R , G and B corresponding to red, green and blue ($Y = \alpha R + \beta G + \gamma B$). For modulating the chrominance subcarrier two 'colour-difference signals' were used ($Y - R$ and $Y - B$), which indicate, when correctly normalized, how much each pixel differs from a pure monochrome pixel.

The form of modulation chosen leads in the first instance to a low mean value of the subcarrier and in addition makes the amplitude more or less proportional to the colour saturation (a monochrome picture corresponds to a carrier amplitude of zero), while the phase is a measure of the hue.

Such a system was officially sanctioned in the United States under the name NTSC by the FCC in December 1953, and the sequential system was abandoned; Japan also chose the NTSC system. In Europe other systems were adopted, which can be seen however as modifications of the NTSC system: the SECAM system in France (1958) and in the East-European countries, and the PAL system in the other countries^{[14][15]}. Regular colour transmissions started in the United States in 1954, in Japan in 1960 and in Europe in 1967.

The display of colour pictures

The all-electronic compatible simultaneous-colour system described above requires simultaneous display of the colour components, of course. The 'single-tube solution' that was produced for this in 1950 was the shadow-mask tube from RCA, in which the three

colour components were presented next to one another *for each pixel* (*fig. 13*). A shadow mask just in front of the phosphor screen of the cathode-ray tube gives a pattern of dots as a shadow image of the scanning electron beam. The tube contains three electron guns so that three such dot patterns are formed on the phosphor screen. The phosphor surface is minutely divided into red, green and blue phosphor dots, accurately positioned with respect to the three dot patterns.

This idea — which has of course followed a long road of improvement in reproducibility, stability of alignment, format and tube shape — has so far remained the dominant one in colour television reproduction. In 1971 the 26-inch screen with 110° deflection was put on the market by Philips and RCA as an important milestone in this development.

Naturally there were many attempts to find alternatives during and after the long development of the shadow-mask principle. The index-tube principle^[14] should just be mentioned here, since it was extensively tested in laboratory versions and is applied, though only on a very modest scale. Most important, it again illustrates the possible choice in colour television between a simultaneous procedure and a sequential one.

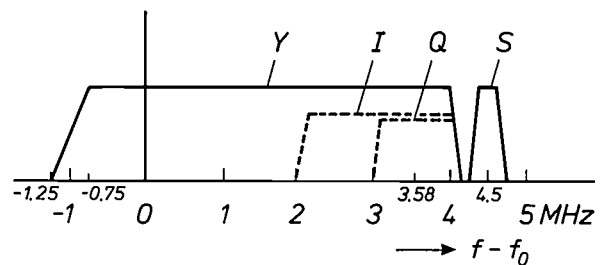


Fig. 12. Frequency spectrum of a colour television signal modulated by the vestigial-sideband method in the NTSC system. All the frequencies are related to the carrier frequency f_0 . The colour information takes the form of two colour-difference signals I and Q that modulate a subcarrier at 3.58 MHz. (Q has a smaller bandwidth than I .) For completeness the position of the sound information S in the spectrum is also shown: it has its own subcarrier at 4.5 MHz.

- [11] F. W. de Vrijer, Fundamentals of colour television, Philips Tech. Rev. 19, 86-97, 1957/58.
- [12] P. M. van Alphen, Applications of the interference of light in thin films, Philips Tech. Rev. 19, 59-67, 1957/58; H. de Lang and G. Bouwhuis, Colour separation in colour-television cameras, Philips Tech. Rev. 24, 263-271, 1962/63.
- [13] D. G. Fink, Perspectives on television: the role played by the two NTSC's in preparing television service for the American public, Proc. IEEE 64, 1322-1331, 1976.
- [14] J. Davidse, Transmission and decoding in colour television, Thesis, Eindhoven 1964. Also published in: Philips Res. Rep. 19, 112-194 and 195-280, 1964.
- [15] F. W. de Vrijer, Colour television transmission systems, Philips Tech. Rev. 27, 33-45, 1966/67; D. H. Pritchard and J. J. Gibson, Worldwide color television standards — similarities and differences, SMPTE J. 89, 111-120, 1980.



Fig. 13. *a*) In a shadow-mask tube a colour television image is generated by the combined action of three electron beams, a mask with a very large number of tiny holes and a picture tube coated on the inside with accurately positioned red, green and blue phosphor dots. The electron beams scan the entire screen 25 or 30 times a second under the control of a number of deflection coils on the neck of the tube. *b*) There is continuing refinement and improvement of the shadow-mask tube: the aim is to make the screen as flat and rectangular as possible with the minimum overall tube length. The type 45AX 'flat square tube' shown here also has an extremely thin neck (29.1 mm); this means that less energy is required for the deflection of the electron beam.

In the index tube the principle used is essentially pixel-sequential. Here again the pixels consist of three adjacent red, green and blue segments, but now these are excited by a *single* electron beam *sequentially*. Special measures are taken to link the actual target point of the electron beam on the phosphor screen directly to the modulation of the electron beam, so that the beam can be rapidly modulated by the correct red, green and blue information. This type of picture tube is available on the market for very small formats.

Recording television signals

In the late forties there was rapidly growing interest in recording audio signals on magnetic tape. Naturally enough, this prompted a search for comparable schemes for recording television signals. Film only gave an unsatisfactory solution to the problem, and it was not really compatible with electronics.

However, such ambitions ran into two problems: the very much larger bandwidth of television signals compared with audio signals, and the much greater importance in television of the very low frequencies and the d.c. component (the mean luminance or chrominance in a picture is essential information). Linear extrapolation of audio recording would require

colossal tape speeds, and with the conventional methods used in audio recording, which take no account of frequencies from zero to about 50 Hz, the low frequencies would be lost.

Elegant solutions were found for both problems. The high tape/head speed was obtained by using rotating heads against a slowly moving tape, to scan the tape in parallel tracks. The problem of the low frequencies was solved by using a form of frequency modulation, which ensured optimum processing for the vitally important low frequencies from the video signal. Both principles were first applied by the Ampex company and demonstrated in 1956. The rotating-head principle was put into practice in a head-wheel with four heads in a plane perpendicular to the direction of tape transport. The tape was curved through 90° in the lateral direction to lie against the wheel. Some professional recording equipment is still made to this design today (*fig. 14a*).

For popular use in the home a cheaper mechanical approach had to be found. The answer was the helical scan, in which the axis of the head-wheel is almost perpendicular to the direction of tape transport (*fig. 14b*). The tape is wound round the head-wheel in a helix through 360° or 180°, and the wheel has one head or

two heads respectively. The 'dwell time' for one rotating head corresponds to a complete field scan. This principle was developed at Philips Research Laboratories in the fifties^[16], and resulted in the first home video recorder (type EL 3400) in 1964, for monochrome signals only.

It is also worth mentioning that the high frequencies and the high tape/head speed that are at stake in video recording set requirements for the write and read heads that are quite different from those of audio recording. Drawing on their traditional expertise in magnetic materials, Philips came up with a very adequate solution: the use of ferrite as a basic material and glass as a filler material for the gap^[17]. This gave a wear-resistant, dimensionally constant material, which could handle the entire video spectrum.

New problems and answers

With the solution of all the basic problems like the ones considered in the previous sections, television technology had grown to a definitive, adult and worldwide attainment. This did not mean, however, that technological ambition was less keen. Indeed, its very persistence meant that technical problems of a fundamental nature were again encountered. Three problems in particular made their presence felt: widening the dissemination of television, improving the picture quality and increasing the autonomy of the viewer in relation to the video programme.

Before we go more deeply into these subjects, it should perhaps be mentioned that the developments that follow would be virtually inconceivable without

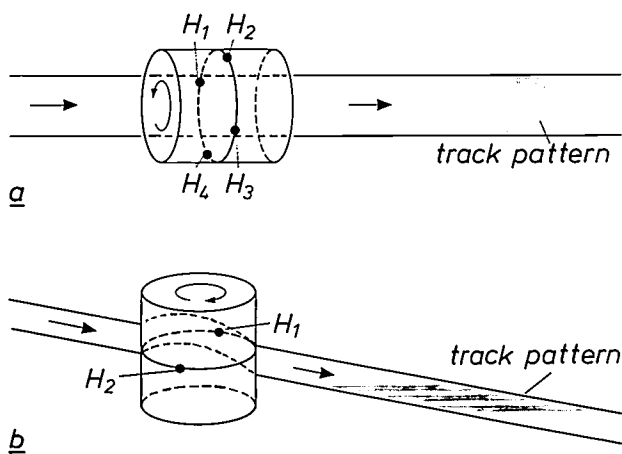


Fig. 14. *a*) The first practical method for recording television signals on magnetic tape made use of a rotating head-wheel whose axis is parallel to the direction of movement of the tape. The wheel contains four heads H_1 - H_4 that are used in turn. This produces a track pattern almost at right angles to the length of the tape. *b*) In the helical-scan recording method the track pattern is almost parallel to the length of the tape.

the transistor and the integrated circuit (the 'IC'). However, since the entire history of electronics from 1960 has been so universally and fundamentally decided by semiconductor technology, any further discussion of this here would probably be inequitable and superfluous.

Widening the dissemination

The line-of-sight propagation at the carrier frequencies generally used by television transmitters requires the highest possible location for the transmitting antennas to obtain the maximum coverage. Here, of course, space technology offers possibilities that cannot be equalled by any terrestrial antenna mast^[18].

The first use of terrestrial satellites for the transmission of — stationary — images was in 1960 (via Echo, actually a simple reflecting balloon). The first transatlantic link for television signals with an 'active' satellite was obtained in the Telstar project in 1962-1963.

The most elegant solution, however, was offered by geostationary satellites, which stand still above the equator at a height of 36 000 km (22 500 miles) with respect to any point on Earth. The first such satellite was launched in 1963 in the SYCNOM project. The systematic use of geostationary satellites for international telecommunication took shape in the founding of the Intelsat organization in 1965. More than 100 countries are now members.

All these examples relate to the use of satellites as an intermediate link for further dissemination. The direct link between satellite and viewing population, now possible through the direct-broadcasting satellite (fig. 15), dates from 1984^[18].

We do not belittle the telecommunication engineer if we maintain that this development is fundamentally based on contributions from space technology in propulsion, launching, orbit control and attitude control. Their existence enabled a new form of communication to come about without fundamental extensions to existing telecommunication technology.

The alternative to broadcasting, cable television, also contains no technology of a fundamental nature that requires special attention within the scope of this article. An exception must however be made for the recent transition from electrical transmission to op-

^[16] F. T. Backers and J. H. Wessels, An experimental apparatus for recording television signals on magnetic tape, Philips Tech. Rev. 24, 81-83, 1962/63.

^[17] S. Duinker, Durable high-resolution ferrite transducer heads employing bonding glass spacers, Philips Res. Rep. 15, 342-367, 1960.

^[18] W. L. Pritchard, The history and future of commercial satellite communications, IEEE Commun. Mag. 22, No. 5, 22-37, 1984.

tical transmission^[19] in the cable network. The arrival of the solid-state laser and the optical fibre are extremely important leaps in technological progress, in which the product of bandwidth and repeater spacing has undergone a fundamental change. They

networks provides sufficient reason for mentioning the subject here.

The first theoretical treatment of optical transmission was presented by K. C. Kao and G. A. Hockham^[20] in 1966. In 1970 F. P. Kapron, D. B. Keck



Photograph: MBB-ERNO, Munich

Fig. 15. In the Franco-German TV-SAT/TDF-1 project two geostationary satellites will be launched shortly. They are intended for direct broadcasting of radio and television programmes on a frequency of about 12 GHz. A dish antenna with a cross-section of only 60 to 90 cm will give satisfactory reception. The height of the satellite is 7 m and the width — including the deployed solar panels — is about 20 m. The launch weight of the satellite is 2050 kg. The German satellite is to be launched first. It has five transmitting channels; four of them will be used. A single television signal or a combination of 16 stereo-radio signals with 'compact-disc' quality can be transmitted on each channel. The transmitting and receiving zone for this German satellite are shown in the figure.

have introduced a new era for digital transmission and especially for the idea of integrating new and existing communication services. The effect of this is not so much a wider dissemination of television, but a completely new place for this dissemination in the total pattern of technical communication. Although experimental systems and operational long-distance links exist, there are as yet no operating networks carrying a combination of speech, music, text, data and image traffic for the public, but the prospect of such

and R. D. Maurer succeeded in producing an optical fibre with an attenuation of less than 20 dB/km and in the same year at the Bell laboratories continuous operation of the semiconductor laser at room temperature was achieved^[21].

A look back to that year 1970 makes us realize — with the present bandwidths in the GHz range and distances without amplifiers between 100 and 200 km — what enormous progress has been attained in optical fibres and lasers in a relatively short time.

Towards higher picture quality

Television technology is in large measure based on the peculiarities of our visual perception. By making continuous pictures discrete in place and time, by limiting the amount of data per unit area and per unit time, by accepting a minimum viewing distance and by tolerating parasitic effects with rapidly alternating polarity it was possible to remain within a certain transmission-channel capacity and to complete the transition from monochrome to colour television without making existing equipment unusable.

In the seventies the technical television world began to wonder whether an improvement in the perceived images was perhaps desirable and how this might be achieved. A first parameter in the rather vague concept of 'picture quality' that came up for further consideration was the picture size. Since the introduction of television the picture format had steadily increased, but had nevertheless reached a certain phase of stabilization at 26 inches, because price and weight seemed to preclude even larger dimensions. In the seventies, nevertheless, a further extrapolation received experimental attention. In addition, the principle of projection television, in which difficulties bear a completely different relationship to the increase in the picture size, was brought in once again (*fig. 16*). When all the available optical, electron-optical, electronic and phosphor technology was put to work this concept gained considerably in strength. Modest numbers have now come on to the market, some for home users.

Another aspect of picture quality is the presence or absence of spurious visual effects ('artefacts'). Although it was maintained earlier that these effects were not observable at a prescribed viewing distance because of visual tolerance, this is in general only a half-truth and for specific picture fragments it is quite untrue. (Everyone has seen this kind of effect in the cinema — in the classic example spoked wheels seem to rotate in the wrong direction.) Large-area flicker (especially with the European 25-Hz standard), line structure, line crawl and interference patterns (cross-colour and cross-luminance) are indeed noticeable in special situations, certainly when the viewer has become acquainted with the quality of pictures in which these imperfections have been virtually eliminated. There are three different methods — not independent of one another — of trying to clean up the picture in the broadcast system.

The first method is by linear extrapolation: greater information transfer with more lines (for example 1250 lines per picture instead of 625) and better resolution per line.

The second method is the separation of signal components that interfere with one another by trans-



Fig. 16. Modern projection-television set. It contains three separate 7-inch high-resolution cathode-ray tubes, which each reproduce a sub-picture in one of the basic colours red, green and blue. The three sub-pictures are projected on the screen under electronic control to give exact registration. The actual screen is rectangular and flat with a diagonal of 37 inches (about 94 cm). Below the screen there is a drawer (shown open) containing various controls for vision and sound. The set can also be operated with remote control.

mitting those components sequentially instead of simultaneously. In the MAC system (Multiplexed Analog Components) with its many variations luminance, chrominance and sound are transmitted in succession, in synchronism with the line period [22]; see *fig. 17*.

The third method is that of the ingenious processing of signals in the receiver, in which an apparently improved standard arises that has for example a quasi-heightened field frequency through the generation of extra fields, or an increased number of lines because the information from successive field scans is added together. The annoying interference effects can also be eliminated by combination of fields or lines since

[19] M. I. Schwartz, Optical fiber transmission — from conception to prominence in 20 years, *IEEE Commun. Mag.* 22, No. 5, 38-48, 1984.

[20] K. C. Kao and G. A. Hockham, Dielectric-fibre surface waveguides for optical frequencies, *Proc. IEE* 113, 1151-1158, 1966.

[21] I. Hayashi, M. B. Panish, P. W. Foy and S. Sumski, Junction lasers which operate continuously at room temperature, *Appl. Phys. Lett.* 17, 109-111, 1970.

[22] L. J. van de Polder, D. W. Parker and J. Roos, Evolution of television receivers from analog to digital, *Proc. IEEE* 73, 599-612, 1985.

these effects, as noted earlier, are deliberately alternated in polarity with fixed periodicities.

The third method mainly relates to the provisions in the receiver. The processing mentioned clearly implies the presence of signal memories that enable signal components to be combined during a period of at least one line period, or more usually during one or more field periods. Such signal processing can in practice only be performed digitally. This makes the receiver in part a digital signal-processing machine [23].

The second method, sequential transmission, requires another transmitter, of course, and a completely different receiver arrangement as well. This is because the time sequence in which the transmission is made has to be restored to the original pattern again. The signals have to be made simultaneously available by expansion of the time scale. This also requires provisions for storing signals temporarily, and reading them out again in another time regime — and hence digitization (or signal sampling, at the very least). Sequential transmission in the MAC system was first proposed in Britain in 1981 [24].

The direct method of setting the standard at twice the number of lines has been promulgated very insistently by Japanese institutions, NHK in particular, since the early seventies. Here, however, no kind of compatibility whatsoever with existing practice can be identified. Moreover, the quadrupling of the bandwidth required causes great problems with the electronics and the transmission methods. It makes the

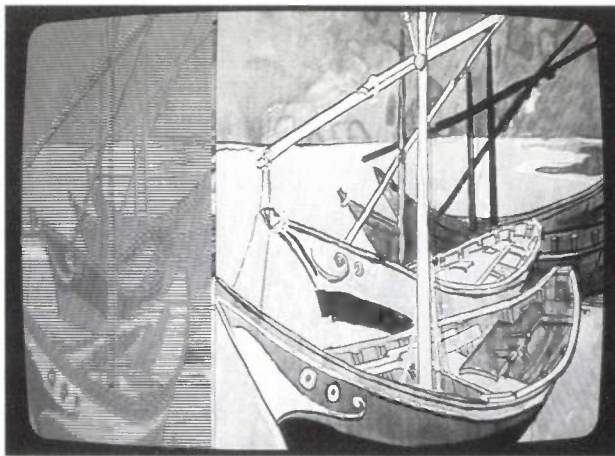


Fig. 17. Picture obtained when a 'MAC' signal is reproduced without special decoding, as if it was an ordinary television signal. In every line period a small part is first used to transmit the colour information, and the rest is used for the luminance information. Since there are two colour-difference signals (U and V), U -information and V -information alternate from line to line. A colour picture of very high quality can be obtained with a MAC decoder, because all the various undesirable interactions between colour and luminance information are intrinsically avoided with this system. (The line-flyback periods are used for sound transmission; this is not visible here, of course.)

demand for ways of reducing bandwidth particularly topical. As has been argued previously, 'natural' pictures contain sufficient correlation for bandwidth reduction to be supported by arguments from information theory. However, the difficult fact remains that solutions of that type do again lead in the direction of concessions to (new) vision-deceptive phenomena. Furthermore, the processing required is of such a complexity that the usual reassurance that the price of the electronics is bound to fall provides insufficient basis for confidence.

Television programme under viewer control

The video recorder was developed in the early seventies into a mechanical equipment that permitted the use of cassettes. This video cassette recorder was first put on the market by Philips in 1972 as the VCR system, to be followed later by the V2000 system. The enormous advances that the video cassette recorder has made since the late seventies received much of their impetus from the Sony and Matsushita companies, who reduced the tape usage so much that a complete film could be recorded without a break on a cassette. Besides the possibility of shifting broadcast television programmes in time, the video cassette recorder naturally offered from the start the possibility of prerecorded cassettes (with programmes selected and purchased by the viewer).

The video cassette, the analogue of the audio cassette, found a competitor in 1972 — the video disc (fig. 18), the analogue of the gramophone record. While no further fundamental technologies can be named in relation to the video cassette recorder, at least three significant technical measures used in the video-disc system should be mentioned [25]. In the first place there is the application of geometrical structures of similar dimensions to the wavelength of light as the carrier of the information to be detected optically. In the second place there is the application of the laser in large-volume consumer electronics and in the third place there is the accurate following of the information track by dual imaging of the information-reading light ray within the same optical system. This is used not only as the read optics but also as the alignment optics.

When the video disc was launched as a commercial product in the mid-seventies there were two versions: one with a mechanical 'pickup' — rather like an extrapolation of the traditional gramophone record (RCA, JVC) — and the other with the optical readout mentioned above (Philips). Philips were the first in the field (1976). As yet the video disc has obtained a less firm footing in the home than the video cassette. The optical version, however, is making steady progress

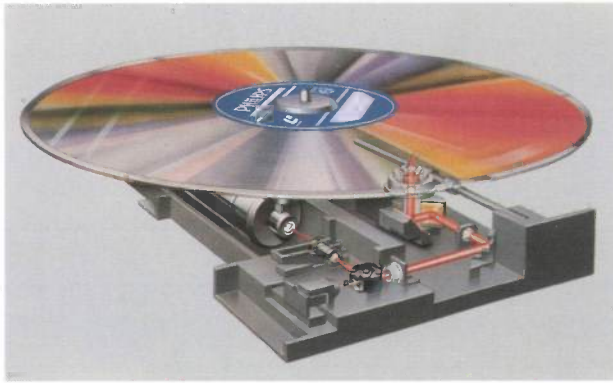


Fig. 18. The information on the LaserVision disc is read out with the aid of a light beam (shown red here) originating from a laser (horizontal cylinder, half-hidden below the disc). A system of lenses and moveable mirrors focuses the light beam on to the disc, where it is reflected to a greater or lesser degree. The reflected light then travels the same path in the reverse direction and arrives at a photosensitive detector (left foreground). This provides an electrical signal suitable for further processing.

in professional applications for education and instruction.

The freedom of the television viewer only becomes complete when he not only has effective autonomy over the pattern of the broadcast programmes and can procure programmes of his own choice, but can also produce his own programme material: the video camera plus portable recorder enables him to do this. For a good design two quite separate kinds of technical achievement are necessary: miniaturization of the video cassette recorder and miniaturization of the television camera, so that they can be combined to make a single unit of the same size as an amateur film camera (the 'camcorder').

A great deal could be said about the miniaturization of the recorder, but only little of a truly fundamental nature. The miniaturization of the television camera proceeds via two notable stages. The first is the replacement of the bulky 'three-tube' arrangement — used for many years in studio cameras — by a single tube^[26]; see fig. 19. This can be done by making do with a sequential succession of pixels measured separately for red, green and blue. A fine transparent coloured strip filter mounted on the light-sensitive surface of the single camera tube can achieve this. In essence this pixel-sequential approach is the converse situation to the index tube mentioned earlier, and as in that case the great thing is to detect at any precise instant which of the three basic colours the scan is working on. This problem can be solved by careful measurement of the cyclic components in the output signal of the tube, referenced to the deflection of the scanning electron beam. There are a number of sophisticated methods for this; for example the colour strips

for the different basic colours can be applied at different spacings, and therefore at different spatial 'frequencies'.

The second important stage in the miniaturization of the camera is the replacement of the camera tube by an 'image sensor'^[27]^[28]; see fig. 20. An image sensor is a photosensitive integrated circuit of some tens of square millimetres containing an array of many separate photoconducting elements. These are interconnected in such a way that the information about the illumination of each can be transferred to the edge of the chip via the other elements. This charge-transfer principle had been proposed long before, in the mid-sixties, in the operation of the bucket-brigade delay line^[29] (Philips, 1965) and of the charge-coupled device^[30] (Bell, 1970). The transfer in the image sensor takes place periodically and in relatively very short time intervals (5-500 μ s). This transfer puts the infor-



Fig. 19. Single-tube video camera for amateur use.

- ^[23] M. J. J. C. Annegarn, A. H. H. J. Nillesen and J. G. Raven, Digital signal processing in television receivers, *Philips Tech. Rev.* **42**, 183-200, 1986.
- ^[24] K. Lucas and M. D. Windram, Direct television broadcasts by satellite: desirability of a new transmission standard, IBA report 116/81, Independent Broadcasting Authority, Winchester 1981.
- ^[25] See for example the articles on these subjects that were published in *Philips Tech. Rev.* **33**, 177-193, 1973.
- ^[26] P. K. Weimer *et al.*, A developmental tricolor vidicon having a multiple-electrode target, *IRE Trans.* **ED-7**, 147-153, 1960.
- ^[27] H. Heyns, H. L. Peek and J. G. van Santen, Image sensor with resistive electrodes, *Philips Tech. Rev.* **37**, 303-311, 1977.
- ^[28] A. J. P. Theuwissen and C. H. L. Weijtens, The accordion imager, a new solid-state image sensor, to be published in *Philips Tech. Rev.* **43**, 1-8, 1986 (preprint available).
- ^[29] F. L. J. Sangster and K. Teer, Bucket-brigade electronics — new possibilities for delay, time-axis conversion and scanning, *IEEE J. SC-4*, 131-136, 1969.
- ^[30] W. S. Boyle and G. E. Smith, Charge coupled semiconductor devices, *Bell Syst. Tech. J.* **49**, 587-593, 1970.



Fig. 20. A comparison of an image iconoscope with a modern semiconductor image sensor gives a good impression of the dramatic reduction in size in 50 years of television-camera technology.

mation from the pixels temporarily into a memory that is read out later in such a way that the visual information appears in the correct sequence and at the correct rate. This memory is in fact a second integrated circuit, which is combined with the photosensitive sensor on a single chip.

The question of three sensor devices or one for colour detection is just the same here as in the camera tube, of course. For the 'home camera' a single sensor device with a colour-strip filter is used (at present with 600 pixels per line^[31]).

It is immediately obvious that the image sensor takes up far less space than the camera tube. The principle was first proposed at Philips (in 1966)^[32]. The first operating sensor dates from 1971. The devices first came on the market a few years later. Cameras with image sensor for amateur use appeared in the early eighties. The 'camcorder' combination with image sensor in one unit has recently become commercially available.

Television technology in another role

After this three-part review of the leading technical problems encountered in television, it is time for a final word about television technology in another role.

Traditionally television presents instruction and amusement taken from 'natural' material. Since the late sixties, however, television broadcasting and the television set have started to be used as a graphic information system. The words 'teletext', 'viewdata'

and 'home computer' are key words in this context. In relation to television technology the home computer has very few new fundamental aspects, and on the other hand it is still at such an early stage of use that further discussion here is inappropriate. A brief word should however be said about teletext^[22], since it depends on an addition to the existing system — in fact a relatively small modification to the now classical television signal and television receiver. The system was originally proposed and developed by British researchers.

The dead times that arise in the scan during the fly-back from the bottom right of the picture to the top left are used in teletext for transmitting coded lines of graphic information. This information is added to the television signal proper at the transmitting end at the correct instants. Adding together the lines of coded information from a number of fields (typically 12) produces reading matter that occupies one entire picture (one 'page'), see fig. 21. A certain number of pages (often several hundred) are transmitted in succession in a continuously repeated sequence. At the receiver a command can be given to select one page from this sequence. The corresponding information is then identified, separated from the television signal proper, collected in a memory that can contain the information for one page and decoded into a readable picture of 24 lines of 40 characters. There is a waiting time that depends on the position of the page in the sequence at the instant of command and on the length of the sequence. The average waiting time is 12 seconds for every 100 pages in the sequences. Adding to the receiver an electronic memory that can contain all the pages simultaneously will obviously eliminate the waiting time.

In another graphic information system, viewdata (or in general, videotex^[22]), a telephone connection and a television receiver are used. The characters from which the pictures are composed are generated in circuits much like those found in teletext, but otherwise this system has little resemblance to conventional television technology. Text can obviously be sent in both directions on the telephone line and can be imaged on the television screen with the aid of a page-sized electronic memory. The bandwidth of a telephone line is considerably less than that of a television transmitter, so that the information transfer takes place much more slowly (one page takes 4 seconds). On the other

[31] M. J. H. van de Steeg *et al.*, A frame-transfer CCD color imager with vertical antiblooming, IEEE Trans. ED-32, 1430-1438, 1985.

[32] Dutch patent application No. 6805 706, 23rd April 1968 and the corresponding United States patent No. 3621283, applied for on 17th April 1969 (inventors: K. Teer and F. L. J. Sangster).



Fig. 21. Two random examples of teletext pages. Simple diagrams can be shown as well as written information.

hand the user can send signals himself and can therefore reach the page file himself, so that his selection process is free from the cyclical presentation of teletext with the associated waiting time and limited content.

As we noted, home computers, teletext and videotex are the precursors of a kind of use of television technology that departs from the original intentions. An intrinsic feature here is the action of the viewer. As compared with the classic television situation, he originates more initiatives, intentions and impulses to obtain information in a more personal and business-oriented approach. In doing so he comes into greater contact with the system, not only literally, but mentally as well. This means that the man/machine interface is of growing importance — a concept that has

many aspects that we still know very little about. So once again we seem to stand at the start of an era, certain only of surprises, blessings and disappointments.

Summary. A retrospective look at the growth of television technology shows a number of successive phases, rather like ever-growing concentric circles. The first phase was that of the elementary problems of image acquisition, transmission, and display in monochrome. In the second phase these problems recurred, but now for colour pictures, and the idea of recording television signals also arose. In the next phase the central features were an extension of the methods of distribution (including the use of satellites), improvement in the picture quality and individual control of the acquisition and recording of video signals. Finally, television can be seen as a constituent element in a number of applications (teletext, videotex, home computer) that would have been inconceivable in the early days. This article gives a general picture of the developments in television in the last fifty years. The accent is strongly on the first stages in the evolution of the technology — invention and feasibility model.

The history of the Philishave

E. W. Tietjens

The original rotary-shaving principle

An article that appeared in Philips Technical Review in 1939 tells how it all began ^[1]. The rotary-shaving principle it described has meanwhile become rather more familiar. Fast-rotating cutters are combined with openings that trap the bristles of the beard and point in all directions, so that the system does not require accurate shaving movements. This was a very promising approach, as can be seen from the success of the Philishave as a product since 1950 ^[2]. Was the choice of this principle based on intuition or science?

The original point of departure was the rotation of cutters at a high speed, 5 to 6 m/s. Because of this rotation the cutting velocity can remain constant. This is not so in shaving systems using vibrating cutters. The high speed of rotation guarantees effective cutting action. In the first type of Philishave, the 'Staalbaard' (Dutch for 'steel beard'), see *fig. 1*, it was even assumed that relatively blunt cutters would still cut sufficiently well. The choice of material did not therefore depend entirely on its hardness. Bronze cutters were therefore used at first, because of their good running characteristics. The material of the cutters is in fact the only thing that was later modified; in other respects the principle used in the first Philishave is essentially the same today.

The original Philishave had a cutter wheel with three 'blades'. The shaver-head assembly was based on a statically determined design — with exactly the right number of support points for the cutter wheel, so that there were no special requirements for flatness of head or cutter. To enhance the cutting capacity the number of blades per cutter was soon increased to six. These six-blade heads, which did have a tight tolerance for flatness, were produced for many years.

Improving bristle capture

Dry shaving can be considered as a statistical process. At each pass of the shaver over the beard, some of the bristles are captured in a slot and some are not. Only the bristles that have been captured can be shaved off. So, however effective the cutters, better shaving can only be achieved by increasing the probability of capturing the bristles. One way of doing this

E. W. Tietjens is with the Domestic Appliances and Personal Care Division, Philips NPB, Drachten.



Fig. 1. The 'Staalbaard', the type 7733 Philishave brought out in 1947.



Fig. 2. The 'Eitje' (little egg), the type 7743 Philishave produced between 1951 and 1957.

would be to increase the number of shaver heads (see *fig. 2*), and another way would be to use more slots per head. To obtain more slots it was first necessary to increase the outer diameter of the shaver head. *Fig. 3* shows that the first head was 17 mm in diameter and had 48 slots. In 1962 a Philishave was introduced that had cutter heads of 22.5 mm diameter and 74 slots. At the same time Philishaves continued to be produced with 19.5-mm cutter heads and 60 slots.

In 1970 we managed to put 90 slots into this 19.5-mm shaver head. This was a great improvement. But

the improvements were not entirely due to the increase in the number of slots. The techniques used for polishing the heads and grinding and lapping the cutters were also undergoing continuous improvement, and the number of heads was increased to three. The triple-head shaver (*fig. 4*) is the one that has become most widely known.

A new principle

Empirical investigations to determine the proper dimensions of lamella and slot have continued for many years. Much progress has been made, but, as might be expected, it diminishes with the years, certainly when the advances are compared with the effort. There is a law of diminishing returns.













A	B	C	D	E	F
17	17	19,5	19,5	22,5	22,5
					
48 slots	48 slots	60 slots	60 slots	74 slots	74 slots
					
1939 1940	1940 1947	1947 1955	1955 1962	1959 1962	1962

Fig. 3. The shaver heads from 1939 to 1962.

The trade-off between smoothness and skin damage

We have seen that a shaver head has slots that have to capture the bristles. The metal 'lamellae' between the slots act both as cutting edges and prevent contact between skin and cutter.

It would be ideal if the skin pressed into the slot occupied a distance exactly equal to the thickness of a lamella. The bristle would then be snipped off very short and there would be no damage to the skin. Thinner lamellae and more deeply polished slots give a smoother shave, but also cause more skin irritation. Minor variations in the geometry very quickly affect the trade-off between smoothness and skin damage. Very close tolerances are therefore specified for the thickness of the lamellae, the radius of their rounded edges and the width of the slots.

There is still the great difficulty that there are marked variations in the distance that the skin protrudes into the slots, since the skin differs considerably from one person to another. This implies that a particular dimensioning of the slots and lamellae, however close the tolerances, can produce quite different results for different people. For this reason some types of Philishave have been given adjustable shaver heads, so that the pressure of the lamellae on the skin can be altered to suit the user.



Fig. 4. The triple-head HP 1335 Electronic shaver, now in production.

[1] A. Horowitz, A. van Dam and W. H. van der Mei, The dry shaving apparatus 'PhiliShave', Philips Tech. Rev. 4, 350-354, 1939.
 [2] Philishave is a trademark of Philips Export B.V.

Attempts have therefore been made to find new ways of manipulating the trade-off mentioned above, towards a smoother shave. The successful outcome is a device referred to in the Philips shaver laboratory as the 'retraction cutter'. Users know this as the 'lift-blade shaving system'.

The development of the new principle began in 1974. A thin and very light second cutter blade, the

way be affected by the experiment, the series of pictures lasted in all only 0.15 s. Ensuring that the series of exposures coincided with the actual cutting of a bristle therefore called for extreme accuracy.

The first shavers with a lift blade came on to the market in 1980. Experience has shown that these appliances do in fact produce a significantly smoother shave.

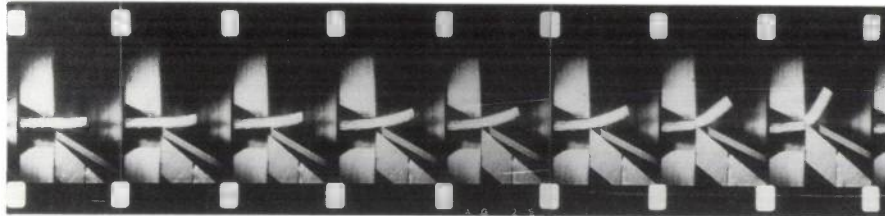


Fig. 5. Superfast moving pictures demonstrating the retraction mechanism on a 10:1 scale model of skin and bristle.

'lift blade', is mounted against the oblique front edge of each main cutter blade. As soon as the lift blade touches a bristle, it is lifted by the horizontal component of the cutting force. The bristle is then carried along a little way by the lift blade, so that it is pulled away from the skin. Then the main cutter blade snips it off; see *fig. 5*.

In the practical design, see *fig. 6*, this process takes place in 0.04 millisecond. The lift blade forms part of a mass-spring system, which must be carefully dimensioned because the resulting accelerations may reach $80\,000\text{ m/s}^2$. During the development it was not at all clear whether the skin would be able to follow the bristle: not only are there elastic and plastic components of the forces in the skin; viscous components also have to be considered.

In fact the skin does follow the bristle, so that the bristle follows the lift blade, as has been shown by super-high-speed moving pictures taken *'in vivo'*. This could also be seen from scanning electron micrographs of severed bristles, which clearly showed the notches made by the lift blade; see *fig. 7*. These micrographs are also used to determine the height of the 'bristle lift' produced by the lift blade.

A special technique had to be developed for the super-high-speed moving pictures. The short process time requires a frequency of 32 000 frames per second. The exposure time per frame is about 0.01 ms, which means that, with the double magnification of the imaging system, a great deal of light is required. The heat generated from this would burn hair and skin. But since it is essential that hair and skin should in no

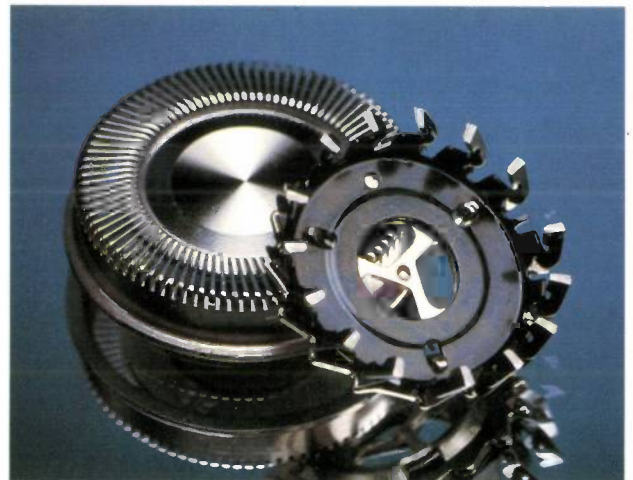


Fig. 6. The shaver-head assembly with lift-blade cutter.

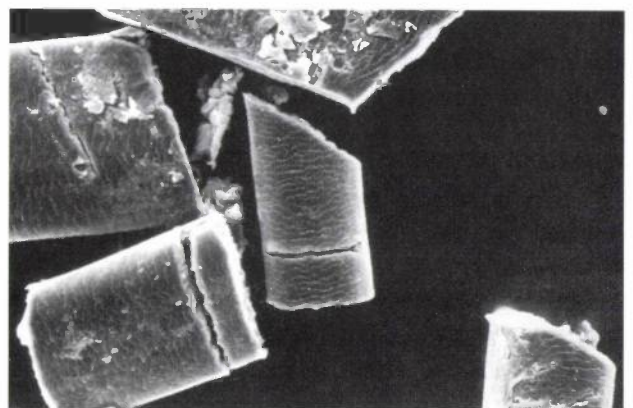


Fig. 7. 'Snipped-off' bristles. The distance between the notch made by the precursor blade and the end of the bristle is the length by which the bristles are pulled up. This takes place against the direction of the 'scales' on the hair.

General aspects

The market success of shavers does not depend entirely on the shave they give. Today's user is more demanding in matters of personal comfort. Better styling, lower weight, smaller dimensions, independence from the mains supply, quiet operation are all factors that are playing an increasingly important part in the development of a dry shaver. As can be seen from the cut-away view of a twin-head shaver from the fifties, shown in fig. 2, almost all of the space inside this mains-powered appliance is taken up by the motor. It is clear that the shape of this appliance is largely dictated by the components it has to accommodate.

Battery-powered shavers were also introduced — later versions with rechargeable batteries — and these were fitted with permanent-magnet (PM) motors. Better magnetic materials and improved design led to a gradual reduction in the size of the motors.

New winding techniques enable PM motors to be used at higher voltages, e.g. 50 V. With modern electronics and pulse-width modulation of the supply, these motors can also be used in mains appliances. Internal electronic control can keep the speed constant even with different mains voltages and varying loads. PM motors are quieter, and are much smaller, so that the motor only occupies a small part of the space available in the housing, as can be seen in fig. 8. Shaver head, drive and motor together form a relatively compact unit. This gives designers greater freedom with the styling of the appliance.

The rechargeable shavers are based on the low-voltage version of the PM motor. Formerly the batteries for these appliances had to be charged via 50-Hz transformers. Nowadays switched power supplies are used because they only require a very small transformer. Recharging can be completed in an hour, and if the batteries are run down, the appliance can be operated from the mains. Two LEDs on the casing flash a warning when the batteries are nearly run down.

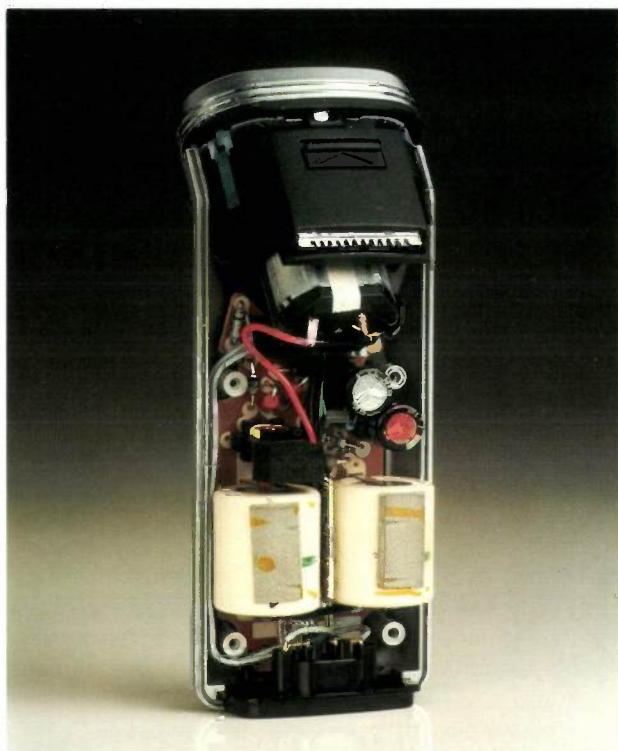


Fig. 8. Interior view of the HP 1335 shaver shown in fig. 4.

So is the success of the Philishave based on intuition or science? This could be agreed either way — and at length. What we do know is that some 50 years of Philishave history have taught us that a *combination* of intuition and scientific research generally give the most successful development.

Summary. The principle of the Philishave has not changed since 1939: it still has the rotating cutter. Bristle capture has however been improved by increasing the number of heads and the number of slots per head. Improved control of the geometry has also provided a better trade-off between a smooth shave and skin damage. The recent introduction of the retraction cutter gives an even better shave.

Glass — outline of a development

A. Kats

In the industrial development of our company, as outlined in this Anniversary issue for a number of fields during the last half century, glass has often played an important role. In the creation of new products it has been necessary time and again to have new compositions of glass. There has been a constantly recurring need for new manufacturing methods to allow the continued economic production of these products. Consequently the industrial development of our company has also been reflected in changing forms of organization in the Glass Division — now known as the Main Supply Group, Glass.

The outline given below of the various changes that have taken place is divided into three periods, which will be dealt with in three separate sections:

- The period from 1916 to 1950, in which the main emphasis of Philips products was on 'light and sound'.
- The period from 1950 to 1975, in which the main emphasis moved towards picture tubes and industrial applications.
- The period from 1975 up to today, in which the main emphasis has moved to products for information systems and office automation. In the section dealing with this period we shall also attempt to assess the role that glass is likely to play in the future.

The years 1916-1950; products for 'light and sound'

Our young company was in peril of an early demise in the war years 1914-1918 when the supply of incandescent lamp bulbs from Austria-Hungary and Germany showed serious signs of drying up. Anton and Gerard Philips therefore decided that the company should have its own glassworks, and this was duly opened in January 1916. In the first ten years this establishment grew into a large-scale labour-intensive business in which the lamp bulbs were 'mouth-blown' and the glass tube for stems (flares) and exhaust tubing was drawn by hand. In 1926 the glassworks produced a hundred million electric lamp bulbs with a work force of 2000, which included 600 glassblowers and 300 tapping-off operators.

The diversification into glass products soon became significant. In about 1920 Philips started manufactur-

ing what were then called wireless valves, for radio receivers (or 'wireless sets'). They were indeed shaped just like lamps. Later this activity extended to include the manufacture of the receivers, which included the valves that had meanwhile been developed as components. The manufacture of valves — still primarily based on the familiar trinity of 'glass, vacuum and filaments' — was still quite compatible with lamp-manufacturing technology.

In the early twenties a demand arose for X-ray tubes, for which new types of glass were developed. But diversification was continuing in the lamp sector as well, since a need had arisen for glass for high-power incandescent lamps. The type of glass required had to have a high softening temperature and be able to withstand severe temperature shocks. A borosilicate glass was used for this application. Since this glass has a low thermal expansion coefficient, tungsten wire had to be used for the lamp lead-throughs. The same type of glass was later used for the envelopes of X-ray tubes.

The company also became involved in the development of radio transmitting equipment, initially to meet the demand from radio amateurs for transmitting valves and rectifiers and finally for building complete transmitter installations. Since low dielectric losses are important for transmitting valves, special glasses were developed, suitable for tungsten or molybdenum lead-through wires.

This diversification of glass products and types of glass called for new raw materials, melting methods and shaping techniques: glass technology moved into the production line. In the twenties, thirties and forties mouth-blowing and manual drawing of glass reached a level of craftsmanship high enough for the company to produce large numbers of prototype envelopes and tubes. In the late thirties the first picture-tube envelopes were mouth-blown for Philips Research Laboratories, to be followed later by the manual drawing of the first fluorescent lamps.

After 1920 the rapidly increasing demand for glass left the glassworks no option but to mechanize the blowing and drawing operations. To do this it was necessary to change from batch melting in pots to continuous melting in furnaces. This was a gradual process that went through a number of phases and fin-

Dr Ir A. Kats was with the Main Supply Group, Glass, Philips NPB, Eindhoven, before his retirement.

ally resulted in the present type of tank furnace, consisting of a melting end connected to a working end from which the glass flows through one or more feeders to the glass-forming machines.

In the United States glass tubing was already being mechanically drawn in about 1920 by the Danner process, in which a stream of hot glass flows on to a rotating ceramic mandrel (*figs 1 and 2*). But the licence fees for this process were so expensive that Philips decided to develop their own process: in the Philips horizontal drawing machine a continuous stream of glass flows *into* a hollow rotating ceramic cylinder.

Until 1950 the Philips horizontal drawing machine was used for making stems and exhaust tubes for incandescent lamps and glass tubing for thermionic valves. The situation changed, however, when the fluorescent lamp appeared. This required long thin envelopes with very tight tolerances for the diameter and the wall thickness. These requirements are more easily met with the Danner process, because the thermal conditions can be carefully controlled while the hot glass is being drawn from the ceramic mandrel through the mandrel oven; this is virtually impossible in the Philips process. Meanwhile the patents on the Danner process had expired, so it was decided to

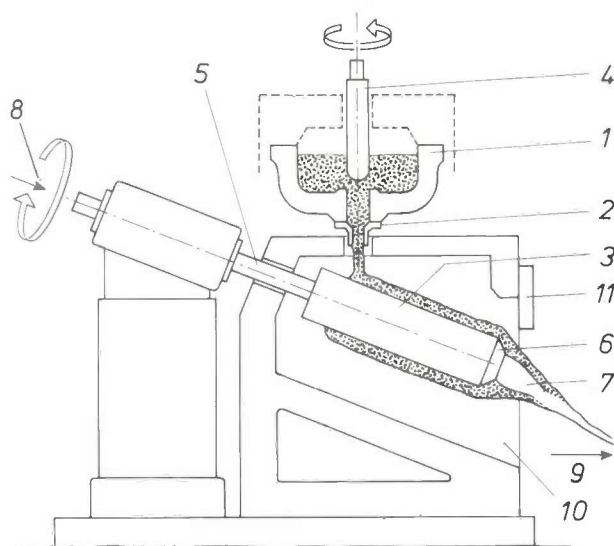


Fig. 1. Schematic arrangement of the Danner process. The molten glass flows from the feeder 1 through the orifice 2 to the mandrel 3. The rate of flow of the glass is controlled by a regulating pin 4. Rotation of the pin has a homogenizing effect on the glass. The ceramic mandrel is driven by a hollow metal shaft 5. Behind the nose 6 glass flowing from the mandrel forms an 'onion' 7. Air is blown into the hollow metal shaft (8). The rate of flow of the glass, the temperature of the 'onion', the pressure of the air in the mandrel and the speed of the drawing machine 9 determine the dimensions of the tubing. High dimensional accuracy is achieved if the glass flowing on the mandrel does not vary greatly in temperature. The temperature in the mandrel oven 10 is controlled by the gas burners projecting through the wall of the oven, and the shutter 11.

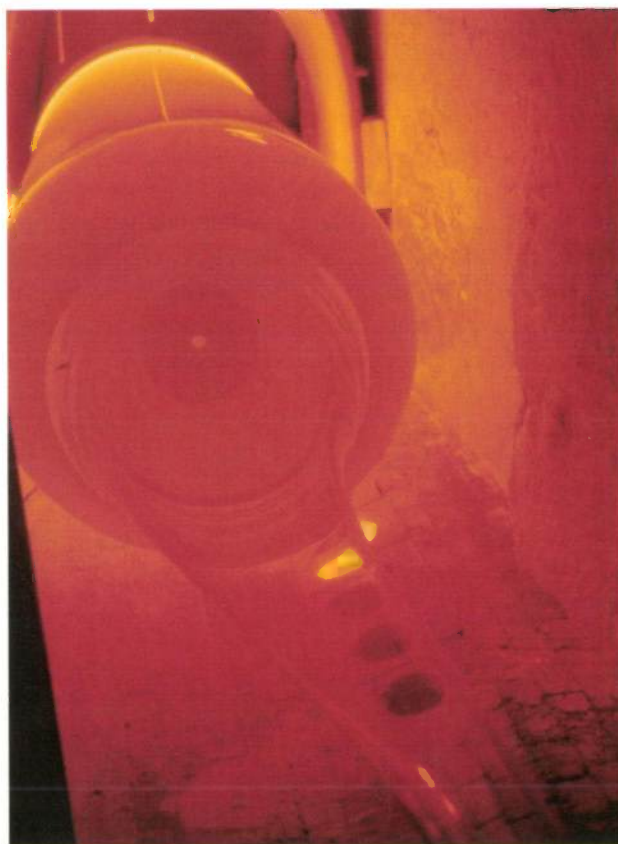


Fig. 2. Front view of the ceramic mandrel with the 'onion' and glass flowing from it.

introduce this process in our glassworks as well, first for the manufacture of fluorescent-lamp envelopes and later for making stems and exhaust tubing.

The mechanization of bulb blowing also took place in a number of phases. In 1930 the 4-head bulb-blowing machine was put into operation, on which each bulb is moulded at four stations at a rate of 375 bulbs per hour. The bulb quality obtained was very good, but the machine was not very suitable for higher rates and also required a great deal of maintenance. In the second phase an 8-head rotating bulb-blowing machine or carousel was therefore developed [1], which could turn out 1500 bulbs per hour. In the third phase further optimization of this machine led to the 16-head machine, whose hourly output was raised to 4500 standard 60-mm bulbs (*fig. 3*).

With the further growth of the European market for incandescent lamp bulbs even this machine proved to be too slow, and in 1968 the ribbon process was introduced (*fig. 4*). This process has since been optimized yet again and is capable of producing 80 000 bulbs per hour. Such a high production capacity per machine means that a single factory is sufficient for meeting the entire West European demand for electric lamp bulbs.

[1] See P. van Zonneveld, Philips Tech. Rev. 22, 320-336, 1960/61.

In the factories outside Europe the carousel has long been standard. In countries with a growing lamp industry, however, a need soon arose for a machine that had a greater capacity than the standard carousel, though not nearly as high as that of the ribbon machine. In the early seventies the Glass Division therefore developed the 'Karibo' machine, which is a cross between the carousel and the ribbon machine, and has a capacity of 7000 bulbs per hour. This machine has meanwhile been installed in countries such as Japan, Mexico, Brazil, Argentina and Spain.

In this article it is not possible to deal at length with all the new products of the company in which manual and mechanical glass-production methods played an important part in this period. One exception will be made, however, for the low-pressure sodium lamp.

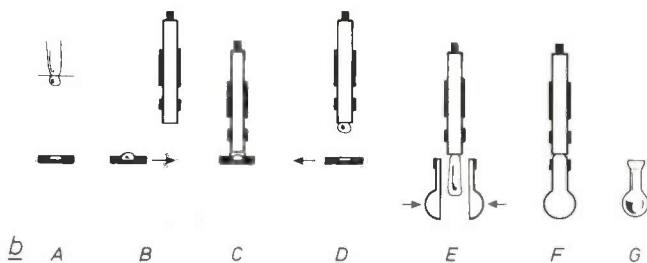
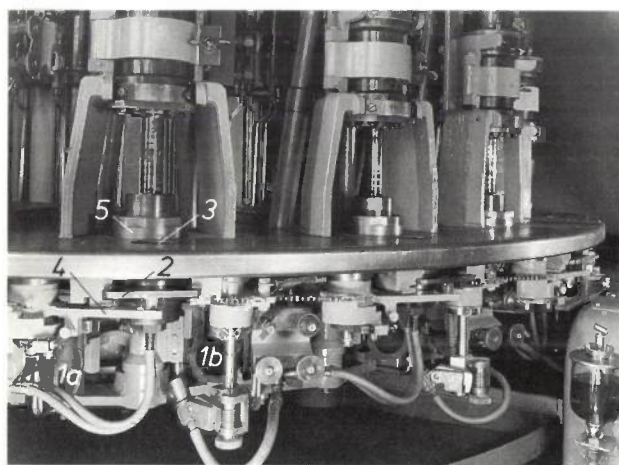


Fig. 3. *a*) View of part of the 16-head carousel bulb-blowing machine. Note in particular the following parts: two matching halves of the blow-mould *1a* and *1b*, the 'gobcatcher' *2*, the hole *3* in the orifice plate, the lever *4* and the moulding and puffing head *5*. *b*) Diagram showing stages (A-G) in the manufacture of the glass bulb. *A*) Shears sever a 'gob' from a glass rod. *B*) The gob is collected in the gobcatcher *2*, consisting of a plunger cup and a slide that can move in a radial groove in the orifice plate, which rotates continuously under the puffing heads. The tray containing the gob is then slid inwards by the lever *4*. *C*) The plunger presses the glass into jaws mounted around the edge of the plunger. *D*) The moulding and puffing head returns to its initial position, with the glass 'biscuit' in the jaws, and the empty gobcatcher moves radially outwards again. *E*) The moulding and puffing head descends until it abuts against the tapered edge of a ring on the orifice plate. The puffing head now rotates with the orifice plate and the glass begins to sag, forming a 'parison'. This process is accelerated by blowing a few puffs of air into the parison from the puffing head. The two halves of the mould *1a* and *1b* close around the parison (*F*). *G*) After the mould has opened again, the moulded bulb is ejected from the jaws.

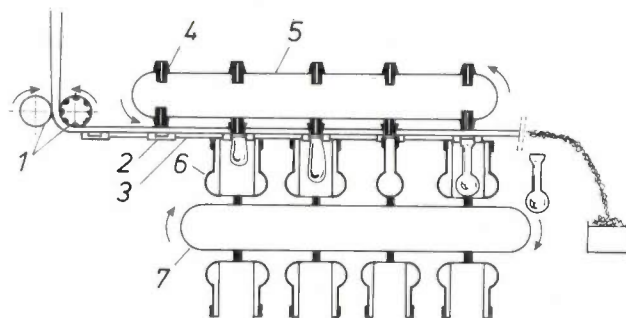


Fig. 4. Diagram of the ribbon machine. A continuous stream of glass from the furnace passes between two water-cooled rollers *1*, which produce a ribbon from it. The right-hand roller has circular 'cut-outs', so that the ribbon contains regularly spaced protrusions. When the protrusions are exactly above the holes *2* in the metal conveyor belt *3*, the blowheads *4* have also arrived at exactly the right position. The blowheads are mounted on an endless belt *5*. The glass now begins to sag between the still open halves of the mould tongues *6*, which travel with the ribbon on an endless belt *7*. A few puffs of air are blown into the sagging parison, the mould tongues close and the bulb is blown. After the two halves of the mould have opened again, the bulbs are allowed to cool a little and are finally 'tapped off' from the ribbon.

The main contribution from the Glass Division to this product was the provision of an inner bulb that is not discoloured by sodium during the discharge and does not absorb argon. For a long time it was difficult to meet these two requirements. Borate glass, which is resistant to sodium and does not absorb argon, has too small a transitional range near the softening point for the lamp to be formed easily in the traditional manner. The problem was finally solved by means of a soda-lime glass that was coated inside with a layer of borate glass about 80 μm thick. In the drawing process developed for this application the free-flowing molten borate glass is transferred in accurately defined quantities from a small platinum glass furnace into the orifice of the furnace from which the soda-lime glass is drawn. With carefully designed glass compositions the borate glass spreads uniformly over the soda-lime glass.

As a result of the developments outlined above for glass technology and production machines a Glass Development Centre was set up in 1957. This is a laboratory that also has its own pilot production plant. Since its inception the laboratory has been a continuous source of innovation in products and processes.

The years 1950-1975; picture tubes and industrial applications

Monochrome television

Monochrome picture tubes for television were first produced in quantity at Philips in about 1950. In the United States television-tube production had already made great headway, led by RCA. The first tubes had

a glass screen sealed to a metal cone. In 1949 American tube manufacturers changed to a glass cone, because it was cheaper and because it enabled glass manufacturers to respond more rapidly to developments of new types. Philips followed the same line.

It soon became clear that the television market had an enormous growth potential. Our company therefore wanted to have a free hand in type development, supplies and prices of the principal components, especially the glass components. Efforts were made at first to set up joint production with the major glass suppliers in the United States. An argument in favour of that approach was that one of these firms held the basic patent for sealing the screen to the cone. The arrangement was not successful, however, and Philips therefore decided in 1950 to build its own pressed-glass plant, which began operations in 1954.

In these years Philips was confronted with a situation resembling that in the years of World War I, when difficulties with the supplies of electric lamp bulbs put the expansion of the company in jeopardy. Because of the strong demand for glass components for television, it looked as if a monopoly in supplies was imminent. Philips therefore acted swiftly to expand its television-glass plants, and by 1960 five television-glass furnaces were already in operation.

It is worth mentioning here the development of the cone presses. In the early period the cones, which were still of the 70° type, were made of pressed glass. At about that time, however, Corning Glass invented the spinning process for making cones (a centrifugal process) and went over to this process, with their licences. Since Philips was unable to obtain a licence for this technique, it was obliged to continue with the pressing process. In later years the cones became less deep, a trend that was stimulated by other developments in picture tubes at Philips. The angle first went to 90°, then 110°. Since it is easier to press a flatter workpiece accurately than to spin it, spinning became less of an advantage and Philips found themselves in a favourable position again. Through the years the Glass Division has steadily perfected the cone-pressing process and has maintained its leading position for many years.

Colour television

In the period 1960-65 preparations were made to manufacture glass components for colour television. It was clear that this would require very considerable changes in production, since it would be necessary to take into account:

- other types of glass for both screen and cone;
- tighter tolerances for the surface and the edge of the screen;

- the necessity to seal pins into the glass, by r.f. heating, for attaching the metal shadow mask.

The first point referred to the need for a glass with a higher softening temperature than that of the glass used for monochrome television, which would also have to be of appreciably better optical-quality. The other two points meant that a high-precision machine would have to be developed for inserting the pins and performing measurements.

The international recognition that Philips had gained in the meantime for its technical results in the production of glass for monochrome television smoothed the way to a 'know-how' contract with Owens-Illinois, a leading American glass manufacturer. Starting up the manufacture of glass components for colour television was consequently a less hectic affair than it had been for monochrome television.

Philips also had a considerable influence on the composition of television glass. Other glass manufacturers had long used raw materials containing fluorine to speed up the melting of the glass. There are three reasons why Philips did not do this:

- there was a risk of cathode poisoning by fluorine released in the tube; this could shorten the life of the tube;
 - the emission of fluorine compounds from glass furnaces could eventually pollute the environment;
 - fluorine also reduces the life of the pressing tools.
- The Glass Division therefore developed types of fluorine-free glass that gave very similar melting behaviour to fluorine glass.

Another problem was the discoloration of the screen glass by electron bombardment, especially at the high tube voltages (30-40 kV) used for colour television. Philips discovered that this effect could be suppressed by adding CeO₂ to the screen glass. Both developments were adopted by nearly all the manufacturers throughout the world.

All this meant that by about 1972 'Philips Glass' had become one of the world's biggest manufacturers of pressed glass for television tubes (*fig. 5*) and this made an important indirect contribution to the company's profits on television products.

PAL delay line

In the PAL system for colour television receivers a glass ultrasonic delay line is used. Glass delay lines had already been in use for some time in radar applications. The lines were large and expensive, however, and made of high-grade quartz glass, which had to be used with a thermostat, since the propagation velocity of acoustic waves in quartz glass is highly temperature-dependent.



Fig. 5. Screens for colour picture tubes being pressed in the television pressed-glass works at Aachen, West Germany.

Philips developed a small inexpensive glass delay line for the PAL system; it had the following characteristics [2]:

- the propagation velocity of the shear waves used is low (so the dimensions can be small);
- the temperature coefficient of the propagation velocity is virtually zero (so a thermostat is unnecessary);
- the glass is highly stable, so that the delay does not vary with time;
- the attenuation is low.

Glass delay lines of this type are still used internationally in PAL/SECAM colour television receivers, and they were also used even more extensively later in video recorders.

Prismatic colour-separation systems

The Philips colour television camera has become widely known through its use of the 'Plumbicon' tube, which has outstanding colour sensitivity, especially to red. To exploit this feature to the full, the optics department of the Glass Division supplied an exit window of borosilicate glass of very good surface quality, in combination with an anti-halo window, i.e. a window that has a dark layer at the edges to absorb scattered light and an evaporated anti-reflection coating

on the 'scene' side. For the camera itself a prismatic colour-separation system was developed which was optimized to match the colour-sensitivity of the 'Plumbicon' tube. This system reflects the green and red components of the signal from two faces of the prism, while the complementary component of the light (the blue signal) passes straight through. The reflection mirrors for the green and red signals each consist of a set of vacuum-evaporated thin films, and the entire system meets extremely tight tolerances for the permitted wavelength range, even after long use.

The quality reputation that Philips won in these years for colour television was partly due to this new product.

Reed relay

Another professional product that was highly important for Philips from 1965 to 1980 was the reed relay. These relays have contacts mounted on 'reeds' sealed into a length of narrow glass tubing and are actuated by a low electric current. Before the digitization of telephone exchanges these relays were widely used to replace the slow mechanical relays. The large orders from Saudi Arabia were very largely due to the quality of the reed relays.

The Glass Division's contribution to this product was the manufacture of the glass tube in which the reed switches were sealed with metal lead-throughs. The relays were required to switch on and off reliably millions of times. This means that during the sealing process there must be no oxidation or contamination of the metal strips by vapour products of the glass. To meet this requirement a low-softening-point glass was developed that produces a minimum of vapour products. This glass is green, since ferrous iron is dissolved in it during melting, and this makes it possible to melt the glass tubes at the lead-throughs by infra-red radiation from a halogen lamp. It is therefore unnecessary to use a gas flame, which could contaminate the metal strips.

Quartz glass

Quartz-glass tubing has always been an important envelope material for high-power lamps, such as high-pressure mercury-discharge lamps, metal-halide and halogen lamps. Its advantageous properties are a high softening temperature, above 1200 °C, and high resistance to chemical attack and temperature shock.

Through the years the requirements placed on quartz glass in regard to the gases dissolved in it as well as bubbles and other inclusions have become increasingly stringent. The dimensional specifications have also become stricter. In specifying purity it was customary in the sixties to think in terms of parts per

million, but today we have moved into the parts-per-billion range, e.g. for Cu and Fe and for hydroxyl groups. To meet these requirements the Glass Division introduced a number of innovations:

- to replace the rock crystal formerly used as the raw material, which was too expensive and not constant in purity, a process was developed for the purification of certain kinds of quartz sand;
- a new type of electrically heated furnace was developed, in which the material of the furnace is almost unaffected by continuous operation at temperatures higher than 2000 °C, so that there is very little contamination of the glass.

Also introduced were:

- a melting process in which the bubble content of the glass produced is reduced to virtually zero, and
- a drawing process controlled by photosensitive sensors, giving the glass tubing exceptionally high dimensional accuracy.

These innovations were followed by methods for controlled doping of the glass. An important example of this is the '321' glass, specially manufactured for halogen lamps for vehicles. The addition to this glass of controlled amounts (a few hundreds of parts per million) of BaO, Al₂O₃ and K₂O results in a large reduction in softening temperature: 950 °C against 1250 °C for pure quartz glass. This has considerable advantages for automobile lamp manufacture. A softening temperature as low as this is acceptable for automobile lamps, since the wall temperature of a lamp does not exceed 700 °C, and on the other hand the low softening temperature means that the processing rate on the lamp machines can be substantially higher. Also, the quality of the pinch of the molybdenum-tape lead-through of the lamp benefits from the improved softening behaviour of the glass.

Fibre-optic plate

This review of the period 1950-1975 will conclude with a brief mention of the fibre-optic plate, which was developed in about 1965 for application in X-ray image intensifiers and in the camera tubes associated with them [3].

The vacuum-tight plate is composed of millions of square fibres with a pitch of about 10 µm. The fibres consist of a core with a high refractive index ($n_D \approx 1.80$) and a cladding with a low refractive index ($n_D \approx 1.50$). Each fibre acts as a 'light pipe' which conducts an image through the plate via the core without distortion. Light conduction via the cladding and

fibre deformation caused by manufacturing errors can give rise to light scattering. At regular distances in the plate there are therefore opaque fibres, called EMA fibres (Extra Mural Absorption), which eliminate the scattered light.

The manufacture of fibre-optic plates takes place in a number of discrete stages. Each intermediate product is carefully inspected for quality, so that the final result is a high-grade end-product.

Through the manufacture of this product, whose quality is unrivalled throughout the world, our company was also able to gain the know-how required for the production of glass fibres for optical communications, which will be dealt with in the next section.

The years 1975-2000; information systems and office automation; the near future

In the seventies, Japanese competitors strengthened their position considerably by building very large manufacturing units in which production was based on a quality principle carried to very great lengths. In this way they were able to achieve high yields and hence low prices. To restore its competitive power, the Philips group adopted the same principles. Pressed-glass activities, for example, were concentrated at a few locations in Europe, South America and the Far East, and the quality principle was also introduced in the Glass Division. In this context, 'quality' is development and production with the minimum of errors and defects.

The making and processing of glass, because of its historical evolution, has always been an integral and strongly interactive process. This implies that all the processing stages, such as batch preparation, melting, pressing, grinding and polishing have to progress smoothly one from the other, so that all the stages interact. This conflicts with the quality principle, in which each stage — after quality control — should lead to a fault-free intermediate product, with a perfect end-product at the end of the chain. In attempts to approximate as closely as possible to this principle, the glass-development departments made a thorough study of all the processing stages and fixed all the parameters that determine each process. In this way they gradually introduced a situation in which the final manufacture is divided into discrete stages, which must each be accurately controllable. This approach soon gave a higher production yield and products of improved quality.

Two recent developments in which this approach has proved successful will now be discussed: the manufacture of quartz-glass fibres for telecommunication and the manufacture of aspheric lenses.

[2] See F. Th. Backers, Philips Tech. Rev. 29, 243-251, 1968; A. J. Zijlstra and C. M. van der Burgt, Ultrasonics 5, 29-38, 1967.

[3] See B. van der Eijk and W. Kühn, Philips Tech. Rev. 41, 137-148, 1983/84.

Optical fibres for telecommunication

There are three main requirements that an optical fibre has to satisfy^[4]:

- the fibre must behave as a waveguide, with no lateral escape of light pulses;
- the attenuation due to absorption and scatter must be as low as possible;
- the dispersion must be as small as possible.

The first requirement is met by constructing a quartz-glass fibre from a core with a high refractive index and a cladding of low refractive index, in the same way as for fibres in a fibre-optic plate. The second requirement is met by using high-purity raw materials for the quartz-glass and by ensuring that no contaminants, such as Fe, Cu and hydroxyl groups, are introduced during manufacture.

As regards the third requirement, low dispersion, a distinction has to be made between colour dispersion and mode dispersion. Colour dispersion is important because the light from the source will have a finite spectral width. In the case of light from a GaAs laser (a multifrequency laser), which has a spectral width of about 2 nm, transit-time differences of 0.1 ns can occur between the spectral components over a distance of 1 km. It would be better to work with a laser that emits at exactly one wavelength (a single-fre-

quency laser), e.g. at 1300 nm or 1550 nm, where the attenuation in the quartz-glass fibre is at a minimum (0.4 dB/km at 1300 nm, 0.2 dB/km at 1550 nm). In practice, however, a single-frequency laser is virtually impossible to make.

Mode dispersion can be avoided by making the fibre core so small that only one mode is transmitted. Another method of eliminating mode dispersion is to use a fibre with an almost parabolic variation of the refractive index across the core (graded-index fibre). This eliminates transit-time differences between the different modes.

For the manufacture of graded-index fibres Philips have developed a method that is applied in three phases. The first phase is based on the PCVD process (Plasma-activated Chemical Vapour Deposition)^[5], fig. 6. In this process the quartz glass is separated out in layers from a gaseous mixture of SiCl₄, GeCl₄, C₂F₆ and O₂ by means of a reciprocating plasma. The reactions are very efficient. Since there is a direct transfer of energy into the gas mixture, there is no thermal inertia and the very thin layers can be formed very rapidly. The theoretically required refractive-index profile can be accurately approximated by using a process computer to program the gas composition

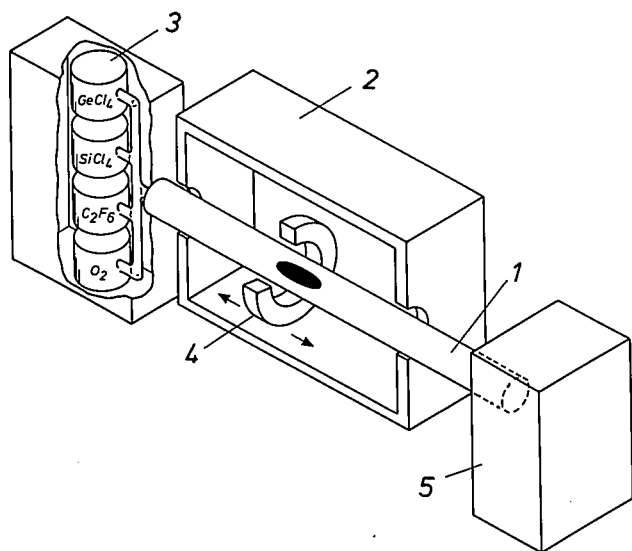
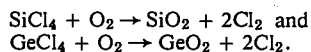


Fig. 6. Diagram of a PCVD arrangement used in the manufacture of optical fibres. A silica tube (1) enclosed by a furnace (2) carries a gaseous mixture (3), consisting of GeCl₄, SiCl₄, C₂F₆ and O₂. The quantities of these constituents are controlled by a process computer. A non-isothermal microwave plasma is generated in a cavity resonator (4), which moves rapidly backwards and forwards along the tube. 5 pumping section. The plasma activates the following reactions:



A complex reaction also takes place between C₂F₆ and O₂, with the production of fluorine, which opposes the formation of OH groups and thus prevents the occurrence of unwanted optical absorption in the glass at 1370, 950 and 725 nm.

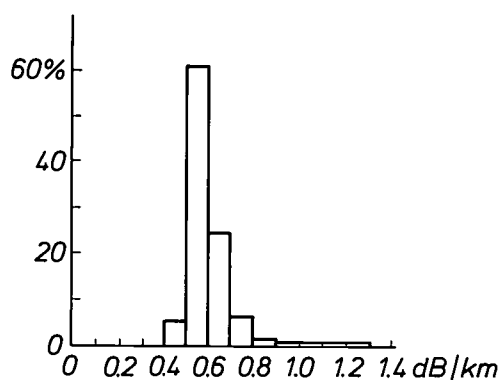


Fig. 7. Distribution of the attenuation coefficient at 1300 nm of a batch of 1600-km multimode fibres^[6], made by the PCVD method.

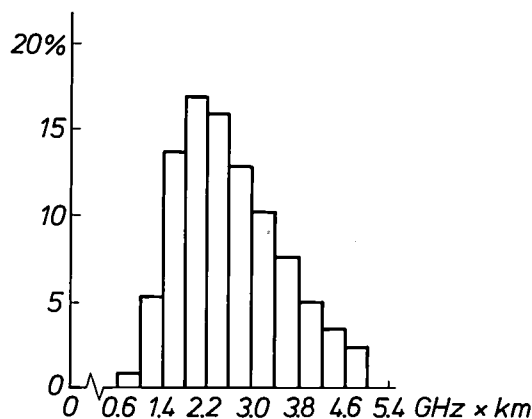


Fig. 8. Bandwidth distribution of the same fibres as in fig. 7^[6]. The bandwidth refers to a 1-km fibre.

as a function of time. In this way, some 1000 layers, each about 2 μm thick, can be formed. The rate of deposition in production is at present 1 g/min. It has already been shown, however, that rates of 2.5 g/min are possible.

The preform thus obtained is reduced in a following stage to a rod by passing an H_2/O_2 burner along the rotating tube a number of times. The tube then closes up by natural contraction. In the last stage of this process the small cavity that may still be present is etched with C_2F_6 . This has the effect of removing the surface layer, from which much of the GeO_2 has evaporated because of the high temperature. If this is not done, a central dip in germanium concentration forms in the fibre, to the detriment of the bandwidth.

In the final phase the rod is drawn at 4 m/s to form a fibre that passes through a vessel containing UV-curing lacquer, which forms a 60- μm coating around the fibre. This is necessary because the freshly drawn glass surface is very sensitive to damage or corrosion, which would make the strength of the fibre insufficient for cabling.

The advantage of the PCVD process is that the manufacturing takes place in discrete stages that can each be perfectly optimized, so that a high production yield and very high quality are obtained. Compared with other processes, the PCVD process occupies an unrivalled position throughout the world (figs 7 and 8).

In recent years various pilot projects have been carried out. The rapid progress that has been made in optical-fibre technology can be seen from the system specifications listed in Table I. In the future single-mode fibres will occupy an important position in the market since they will lead the way to data-bit densities in the Gbit/s range. It is already clear that this will require fibres with a cladding consisting of layers of different composition. Here again, the advantages of the PCVD process will keep Philips in the lead for quality internationally.

Table I. Data relating to pilot projects with optical-fibre cable.

Project	Year	Distance in km	Regeneration distance km	Number of fibres	System capacity Mbit/s	Wave-length of laser nm	Cable attenuation dB/km	Fibre attenuation dB/km
Berlin I	1978	4.3	4.3	6	34	850	6	5.5
Geldrop, in-house	1979	16	8	6	140	850	4.5	4.0
Nürnberg/Schwabach	1981	12.3	6	2	34	850	4.5	4
Helmond/Eindhoven	1982	10.1	9	6	140	850	4.5	4
Berlin III	1982	9	9	4	140	1300	1.5	1.3
Hamburg/Hannover, Bigfern I	1983/84	36	18	60	140	1300	1.0	0.8
Berlin IV	1984	18	18	4 (single-mode)	140	1300	0.55	0.5
Hannover/Münster, Bigfern II	1985	70	20	60	140	1300	1.0	0.8
PTI, in-house	1985	100	100	(single-mode)	34	1550	—	0.3
Breda/Belgian frontier	1985	26.7	26.7	6 (single-mode)	140	1300	0.5	0.4
TKD-Nürnberg, in-house	1985	37	37	(single-mode)	565	1300	0.55	—

Aspheric lenses

The light pen in optical recording and playback systems such as Compact Disc, LaserVision and the DOR system has to keep the light beam constantly focused on the pits in the disc that carry the information. The optical system for the light pen must therefore be of high quality and there must be no aberrations such as spherical aberration or coma. These aberrations can be eliminated by the conventional correction lenses, but these make the light pen very heavy and lessen the playback sensitivity of the player. Moreover, aligning the lens system is time-consuming.

In the current Compact Disc player a different system has been adopted, which does not have these disadvantages; it consists in the use of an aspheric objective lens, which makes two correction lenses unnecessary^[7]. It is of considerable interest here that Philips

[4] See P. Geittner, D. Küppers and H. Lydtin, Appl. Phys. Lett. 28, 645-646, 1976;

K. Mouthaan, Philips Tech. Rev. 36, 178-181, 1976; P. Bachmann, Pure & Appl. Chem. 57, 1299-1310, 1985.

[5] See D. Küppers, J. Koenings and H. Wilson, J. Electrochem. Soc. 123, 1079-1083, 1976;

H. M. J. M. van Ass, P. Geittner, R. G. Gossink, D. Küppers and P. J. W. Severin, Philips Tech. Rev. 36, 182-189, 1976; J. W. Versluis and J. G. J. Peelen, Philips Telecommun. Rev. 37, 215-230, 1979.

[6] See P. Matthijse, Proc. SPIE 584 (to appear shortly).

[7] See J. J. M. Braat, T. G. Gijsbers, J. Haisma, W. Mesman, J. M. Oomen and J. C. Wijn, Philips Tech. Rev. 41, 285-303, 1983/84.

have developed a method, based on the replication technique [8], for high-yield industrial production of these aspheric lenses.

First a preform, a 'body', is made in the conventional way. The body is spherical and approximates the aspheric surface as closely as possible (*fig. 9*). On the side of the body that must be made aspheric a drop of high-grade UV-curing lacquer is applied. This is pressed against the body with a precision mould, so that the lacquer takes up the aspheric contour of the mould. Finally, the lacquer is cured by passing UV radiation through the mould.

The mould must of course have an extremely accurate aspheric contour [7]. This can be produced with the COLATH high-precision lathe, another Philips invention [9].

The manufacturing process is automated, with the aid of servomotors and sophisticated positioning techniques. The quality of the moulds, bodies and end-products is monitored in stages with special measuring equipment.

Glass in the future

The glass for electronic components will have to meet increasingly strict tolerances in the future. This means that the homogeneity of the glass and the shaping methods will also have to be improved.

The pressure to divide up the glass-production process into discrete subprocesses will increase, because this is the only way of achieving the required high quality and high production yield. This will make production more flexible and give good prospects of type diversification.

A first step in this direction has been taken by the introduction of the pelletization process, in which the raw materials for the glass are homogeneously mixed in the form of pellets and subjected to continuous 'on-line' quality control during production. This ensures that the glass furnaces are supplied with pellets of accurately defined composition and size. After the furnace has been adapted to the specific melting properties of such pellets, a highly homogeneous glass melt of constant quality is obtained.

The next step will be the introduction of the pre-forming technique — the preliminary preparation of a discrete portion of glass that must meet strict specifications for surface quality, contour and weight. After final processing (pressing, blowing, drawing, densification) an end-product is obtained with high precision and high yield.

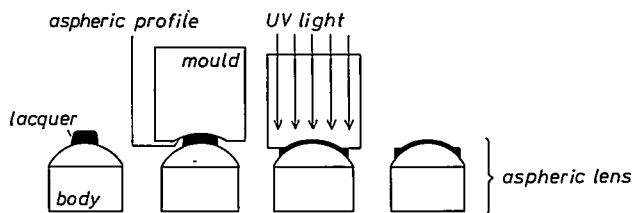


Fig. 9. Main process stages in the replication method.

In fact the techniques used for making optical fibres and aspheric lenses are already based on this principle. In the next ten years these methods will also have a profound influence on the manufacture of pressed-glass components for television.

The future will also see the growing use of glass, in the form of quartz glass or glass-ceramic with very low thermal expansion, in components of precision machines. The machining techniques for such glass parts already exist. For such applications the high density of glass and its high resistance to corrosion will be of overriding importance.

Another important future development will be the use in new products of high-grade plastics in combination with glass. As we saw, aspheric lenses and optical fibres have led the way here.

Finally, in the years ahead the opposite situation will also arise; we shall see new low-melting-point glasses with shaping temperatures between 200 and 300 °C which will take over some of the applications of plastics. At these low temperatures it will be possible to shape glass with techniques similar to those now used for plastics, such as injection moulding and extrusion. Like conventional glass products, these products will be characterized by high density and high resistance to ageing and corrosion.

[8] See J. M. Zwiers and G. C. M. Dortant, *Appl. Opt.* 24, 4483-4488, 1985.

[9] See T. G. Gijsbers, *Philips Tech. Rev.* 39, 229-244, 1980.

Summary. The evolution of the Philips glass activities is described, from the building of the first glassworks in 1916 up to the present day, and some indication is given of likely developments in the near future. The article deals with three periods, in which the corporate emphasis shifted from 'light and sound' (1916-1950) to picture tubes and industrial applications (1950-1975) and finally to information systems and office automation (1975 to today and the near future). A historical outline is given of the development of new types of glass needed for the manufacture of various products, and of the continual changes in manufacturing methods necessary for continued economic manufacture of these products. All of these developments have also affected the organization of the Glass Division.

Welding lead-through wires

Glass lead-throughs are found in many Philips products. They consist of metal pins sealed into glass for the purpose of establishing an electrical contact. When the lead-throughs take the form of wires, the piece of wire contained in the wall must form an air-tight seal to the glass. The average thermal expansion coefficient of the wire should be locally approximately equal to that of the glass, and in addition there should be good adhesion between the glass and the metal. The ends of the wire have to meet other requirements, so that a lead-through wire usually consists of two or three distinct parts that are welded together. The part inside the glass is often a copper-clad wire, a special type of wire that has a nickel-iron core and a copper sleeve; to provide good adhesion, the sleeve is coated with a thin layer of borax ($\text{Na}_2\text{B}_4\text{O}_7$). Wire of a special alloy may also be used. The photograph shows four types of lead-through wire. Going from left to right, the techniques used for welding the separate parts are of increasingly recent date. The lower end of each wire would be outside the device.

The first set of lead-through wires is meant for filament assemblies in fluorescent lamps. The welds were made by a reducing gas flame on a machine that produces 9000 lead-through wires an hour. The welding technique dates from the early days of incandescent-lamp manufacture. A welding bead is formed and the wires are discoloured by oxidation.

The resistance welds of the second set of lead-through wires, which are used in the manufacture of semiconductor diodes, have hardly any welding bead and there is less discolouration of the wire. Resistance welds are made by pressing the two parts together and connecting the ends to a current source. The machine that cuts, positions and welds the parts of the wire produces 30 000 lead-through wires an hour. For each diode two lead-through wires are sealed into a glass encapsulation with the diode crystal between the thicker ends of the wires.

The third set of lead-through wires is for mounting in high-pressure gas-discharge lamps. The wires are produced by percussion welding in a machine that turns out 7500 wires an hour. In this welding process a flame arc is first formed between the ends of the wire, and then the white-hot and partly molten ends are



pressed together. The appearance of the welds leaves something to be desired, but their quality is satisfactory.

The lead-through wires at the extreme right are made from two almost identical pieces of FeNiCr wire. The wires are sealed fifteen at a time into sintered glass to form the connection for an electron gun in a colour-television picture tube. The lead-through wire must be made in two parts because there is a slight probability of air leaking through minute channels in the wire or along grooves at the surface. (Such channels or grooves may occasionally be formed in the wire-production process.) The parts are welded by a laser on a machine that produces 30 000 lead-through wires an hour. As can be seen, laser welding produces neat-looking joints. It is also reliable and causes much less tool wear, so that the percentage of rejects is smaller and the machines require less maintenance. In the long run this method is therefore likely to replace conventional welding methods for many more products.

From transistor to IC: a long road?

J. C. van Vessel

Introduction

Electronic components fulfil a central function in industry today. They are the basic ingredients for the construction of electronic circuits. In turn, electronic circuits can be combined to form complete electronic systems. And these, today, are of great importance in industry as well as in daily life.

The influence of electronics here — at home and at work — has become very strong in the last ten years and is still increasing so rapidly that we must now think in terms of an approaching 'electronic era', in which these continuing developments will have a profound effect on all aspects of the world about us.

Closer examination soon shows that these far-reaching effects mostly arise from the revolutionary developments that we have seen in electronic components. The pace has been set by the astonishing progress in the technical performance of the components, combined with huge reductions in their dimensions and a plunge in the 'price per function'. This is a clear example of 'technological push'.

However, this technological leap forward has mainly occurred in a single sector of the components industry: the new semiconductor devices that appeared in about 1950: first of all diodes and transistors made from germanium, and later from silicon, and finally integrated circuits made from silicon — the silicon chip. In addition there are devices made from gallium arsenide and other combinations of trivalent and pentavalent elements, which will become of considerable importance in the next ten years.

With all these developments, several of the existing components, such as vacuum tubes [*] gradually became obsolescent. Others, such as resistors and capacitors, underwent considerable changes. Events in the semiconductor component sector, however, have moved so swiftly that the development of the other components, and the methods of mounting them to form a single piece of equipment, have not kept pace. Changes in methods of assembly are not easily introduced anyway, since new international standards have

to be agreed for circuit boards and automatic placement machines. Such changes are also very expensive.

New developments in the external shape of all components and the methods of combining them to form electronic systems will therefore have at least as much effect on the advance of electronics in the next ten years as the progress made in the semiconductor devices themselves.

Further decrease in prices as well as improvements in performance for the devices can be predicted fairly accurately from known data, but the future trends for system assembly and the styling of the 'other components' are far from certain. Although some trends can be discerned, the development of new international standards will still take time. This is unfortunate, for as the prices of semiconductor devices continue to fall, their packaging and system assembly could cost more than it takes to produce that 'miracle of the twentieth century', the chip itself.

A review of electronic components

Electronic components can be divided into two main groups: *active* components and *passive* components. A general picture is given in *Table I*. The active components may in turn be divided into solid-state devices (semiconductors) and vacuum or gas-filled devices. A completely separate group of active components are the devices with screens, generally referred to as displays. These are an indispensable means of communication between the increasingly automated world of electronics and man. There has consequently been a marked increase in the use of these displays — and it will continue. So far the vacuum and gas-filled devices have been well in the lead, although the solid-state devices are steadily advancing and here again show the advantages of being small and requiring little energy.

Of course, all the devices listed in *Table I* have undergone many developments and changes in the last fifty years. However, because the solid-state devices have set the pace, this article will concentrate on them,

[*] Or 'valves', but the author prefers the American term! *Ed.*

Dr J. C. van Vessel was a Director of the Philips Elcoma Division, Eindhoven, before his retirement, and is now an Industrial Management Consultant.

describing the developments and the motivations behind them, and giving some predictions for the future.

Early factors in the development of solid-state devices

The transistor was invented in December 1947, and first came on the market in 1953 (fig. 1). But the frequency range and maximum power of these first devices were very much inferior to those of the existing vacuum tubes. And they were expensive. Nevertheless, even then they had two advantages over tubes: they were much smaller, and only required a hundredth of the power. These were essential features for the computers then being developed, and at the same time they opened up a large new market for portable battery-operated receivers and appliances. W. Shockley, Nobel prize winner and joint inventor of the transistor, used to illustrate this progress by likening the handling of a small signal by a vacuum tube to using a train of sixty wagons to carry just a single packet of butter.

This is so because in a valve the electrons have to be released from an incandescent cathode and then attracted to the anode by a potential of 200-300 V. In a semiconductor two kinds of charge carrier, holes and electrons, are always present and a potential of a few volts is more than enough to cause them to cross a p-n junction (the characteristic element of a semiconductor device). Since, however, the movement of charge carriers through a solid is due mainly to diffusion (because of the internal field) and to a far lesser extent to the applied external field, the frequency behaviour is very largely determined by the distance they have to travel from one p-n junction to the other (this is the base thickness of the transistor). Since every p-n junction also has its own internal capacitance, which is

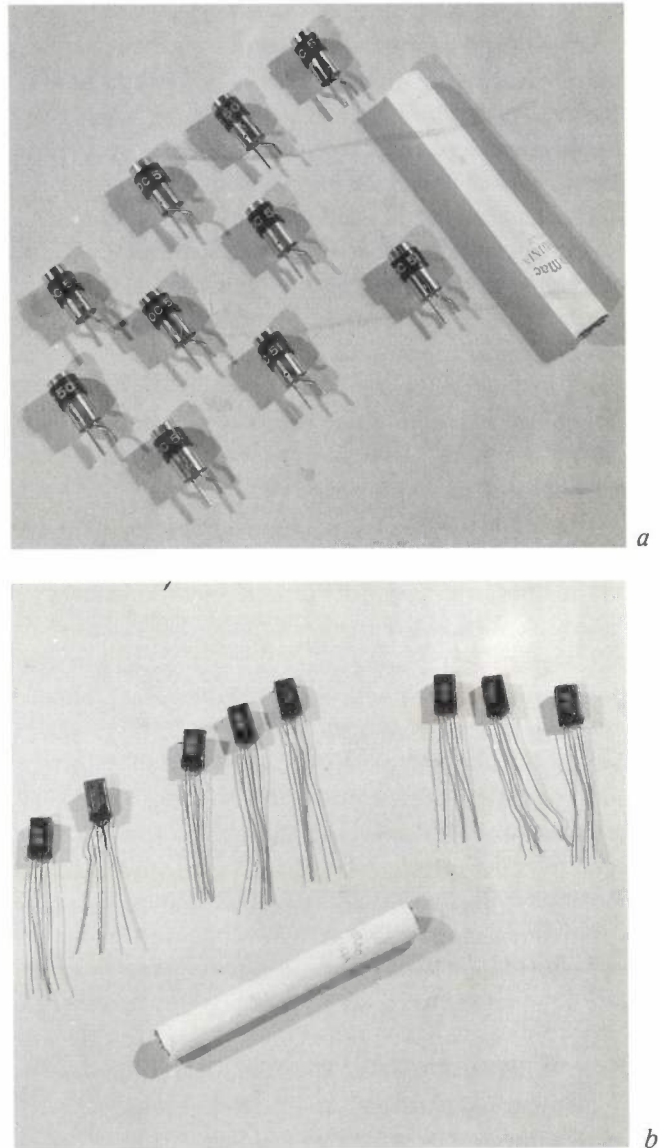


Fig. 1. The first commercial Philips transistors came on the market in 1953/54, a) point-contact transistors OC 50/51, b) germanium junction transistors OC 10/11/12.

Table 1. Existing electronic components.

Active elements		Passive elements
Vacuum or gas-filled	Solid-state devices	
Transmitting tubes	Diodes	Resistors (linear and nonlinear) Capacitors Inductors Magnetic materials Connectors Switches
Receiving tubes	Rectifiers	
Camera tubes	Transistors	
Image intensifiers	Thyristors	
X-ray tubes	Triacs	
	Integrated circuits	
	Displays	
Picture tubes	Liquid crystals	
Oscilloscope tubes	Light-emitting diodes	
Plasma panels		
Vacuum-fluorescent panels		

proportional to its area and sets limitations at higher frequencies, it is important to use small emitter and collector areas in high-speed transistors. In view of these considerations, smaller and better-controlled dimensions were therefore the primary objectives in the further technical development of the transistor.

The first methods used for making p-n junctions gave very unreliable results. The formation of the junctions in a point-contact transistor is shown in *fig. 2*. The p-n junctions in a junction transistor were often made at first by the alloy method, illustrated in *figs 3* and *4*. Because of the poor reproducibility, assiduous efforts were made to devise methods of producing p-type or n-type regions in the semiconductor material in a more controlled way.

The replacement of the alloy method by the diffusion method gave an appreciable improvement. Initially a combined method was used, with considerable success, and this led to the 'pushed out base' — or p.o.b. transistor^[1] (*fig. 5*), but the method of diffusion from the gas phase soon became predominant. This method gave readily reproducible layer thicknesses and dopant concentrations — but unfortunately over the entire semiconductor area. The collector-base junction had to be adjusted to the right size later by local etching. The resultant geometry led to the name 'mesa' transistor (*fig. 6*).

This local etching was a clumsy method, however, and efforts were therefore made to find a material that could be used to cover the semiconductor surface selectively before the diffusion. Silicon dioxide was ideal. Where the oxide covered the surface, no foreign elements could enter the semiconductor material; they did so, however, where there was an aperture. The entire surface of the transistor remained smooth — the 'planar' transistor was born (*fig. 7a*). This important discovery led to the changeover from germanium to silicon as the semiconductor material. Silicon could easily be coated with a dense and uniform oxide layer by oxidation. Apertures with accurately defined dimensions could then be etched in the layer by photolithography. Transistors with this planar structure gave problems, however, with the interconnections: the step in the metallization was found to be a weak spot. The answer was found in a method in which 'thick' oxide layers were recessed in the silicon. This is the method known as the LOCOS technique^[2]; see *fig. 7b*. Thus after the techniques of controlling the dopant concentration and the depth of penetration had been mastered, it was now possible to control the surface dimension as well. These discoveries of the late fifties and early sixties paved the way towards the colossal developments of the next twenty-five years, whose end is not yet in sight.

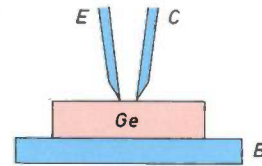


Fig. 2. Point-contact transistor. *Ge* germanium crystal. *E* emitter contact, *C* collector contact, *B* base contact. Thin phosphor-bronze springs (collector) and tungsten (emitter) were pressed against the germanium. The germanium was locally melted by a current pulse, and recrystallization resulted in a type of p-n junction.

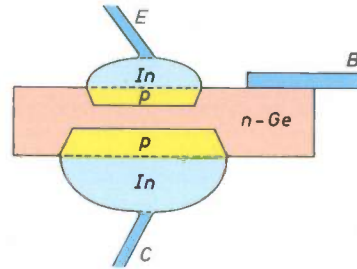


Fig. 3. Germanium junction transistor made by the alloy method. In applying each of the p-n junctions an indium bead or pellet was melted with the germanium, resulting in a recrystallized p-type region after cooling. The problem with this pnp alloy transistor was accurate control of the distance between the two p-type regions (the base width).

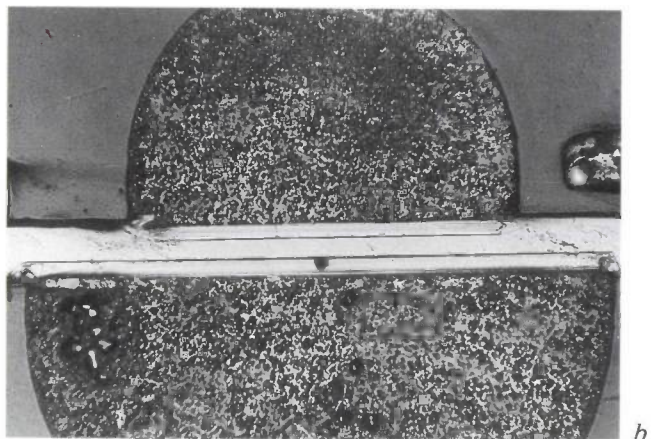
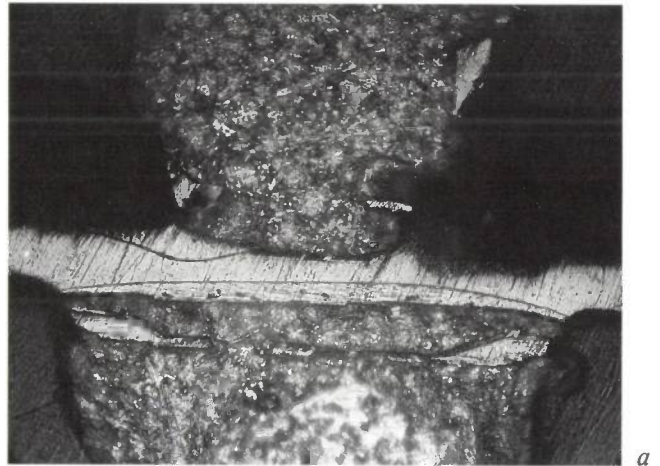


Fig. 4. Photographs illustrating the originally poor reproducibility (*a*) of the alloy method, and the improvement achieved (*b*) in later years.

Furthermore, silicon was a material that was more abundant than germanium and could operate at much higher temperatures because of its greater band gap. Initially, however, it was more difficult to purify the material and to grow single crystals, but these problems were solved soon after 1960. Today there are no

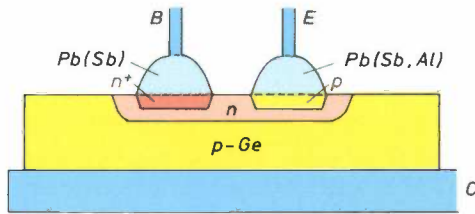


Fig. 5. Pushed-out base or p.o.b. transistor, which takes its name from the manufacturing process. Two lead pellets containing a small amount of antimony are alloyed at 780 °C on a p-type germanium wafer. At this temperature the antimony diffuses into the germanium, producing an n-type layer that functions as the base. Since one of the pellets also contains aluminium, a p-type region forms under this pellet when it cools, producing the emitter. The substrate, which functions as the collector contact, also acts as a heat sink.

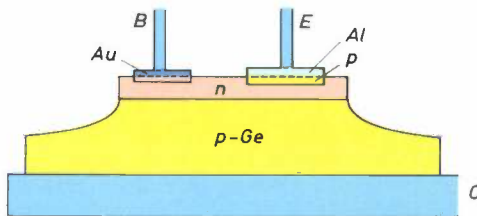


Fig. 6. Germanium pnp-mesa transistor with diffused base (n-type), vacuum-deposited base contact (of gold, Au) and vacuum-evaporated emitter (of Al). The p-n junction between collector and base is etched away as far as possible to minimize its capacitance. This gives a 'mesa' structure.

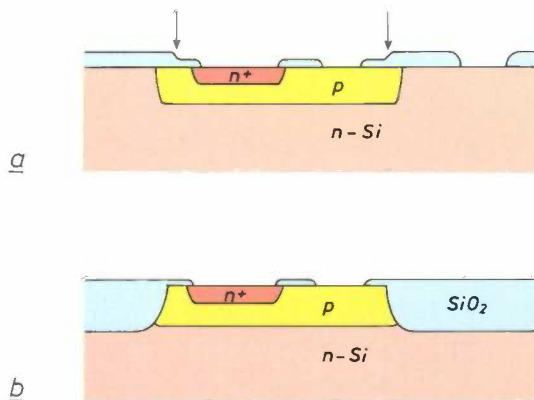


Fig. 7. *a)* Planar transistor. The steps in the SiO₂ (see arrows) are produced in the second oxidation, which serves as a preparation for the n⁺ diffusion. The application of external contacts (metal emitter and base contacts, not shown) gave rise to weak spots. *b)* Local oxidation of silicon or LOCOS technique. To avoid large steps in the metallization, the oxide is recessed in the silicon during the first oxidation. After the p-type diffusion the second oxidation takes place. A further advantage of the recessed SiO₂ is that it provides lateral isolation of the (p-type) base at the same time. This permits substantially higher packing densities in integrated circuits.

difficulties in producing silicon single crystals a metre long with a diameter of 15 cm, and if necessary even 20 cm.

New stimuli for the silicon transistor

The new 'planar' transistors of the early sixties had a greatly improved maximum operating frequency, could handle more power and could be manufactured more reproducibly than the earlier germanium devices. At the start, however, they had one disadvantage: they were expensive. This was due to a combination of two facts: at the time it was only possible to make moderately perfect silicon single crystals with a diameter not much more than three to four centimetres, and the process itself required expensive optical and mechanical equipment of extremely high precision, in a production process that consisted of a very large number of stages. The added value for labour on the original material, a silicon wafer, was consequently many times higher than the cost of the material itself, and mainly determined the prime cost. Since further technological developments only resulted in even more complicated processes and equipment, there was only one way left to make the silicon transistor cheaper: that was to increase the size of the silicon wafers and to reduce the dimensions of the transistor at the same time.

With the photolithographic methods in use it was fairly easy to reduce the dimensions, and the costs of processing a wafer did not rise significantly when the diameter was increased. This meant that many more transistors could be made at the same time on one slice for the same costs, so that the price fell dramatically and has continued to do so ever since. Indeed, prices have fallen so much that today the price of a discrete silicon transistor for small signals is no longer determined by the price of the silicon chip itself with the transistor diffused inside it, but almost entirely by the costs of packaging, testing and marking. In addition, it is becoming more difficult to fit the actual transistor element into a macrosystem, e.g. in the form of a circuit board with other large components.

This point will be dealt with later in this article when we look at integrated circuits, though it will be

[1] P. J. W. Jochems, The alloy-diffusion technique for manufacturing high-frequency transistors, Philips Tech. Rev. 24, 231-239, 1962/63;

P. J. W. Jochems and E. Kooi, Metallurgical aspects of the alloy-diffusion method in transistor technology, Philips Tech. Rev. 28, 246-250, 1967.

[2] J. A. Appels, E. Kooi, M. M. Paffen, J. J. H. Schatorjé and W. H. C. G. Verkuylen, Local oxidation of silicon and its application in semiconductor-device technology, Philips Res. Rep. 25, 118-132, 1970;

J. A. Appels and M. M. Paffen, Local oxidation of silicon; new technological aspects, Philips Res. Rep. 26, 157-165, 1971.

encountered in a somewhat different form. Finding ways of minimizing this discrepancy can thus become the key to further reductions in the prices of electronic circuits and systems.

It should be noted, however, that the story is rather different for semiconductor devices with high current ratings, such as power transistors, thyristors, triacs and power rectifiers. The size of the chip in these is primarily determined by the power to be handled and making the chip smaller is hardly possible. The encapsulation still accounts for much of the costs, however.

Let us now return to the optical process of reducing the dimensions of the transistor. It soon appeared that this method would enable transistors to be made that were much smaller than the smallest piece of silicon that could be sawn from a silicon wafer and processed; see *fig. 8*. In other words, a number of transistors could easily be accommodated on even the tiniest silicon chip. It seemed a good idea to try and do this and to interconnect the transistors where necessary via a vacuum-evaporated metal layer. When diffused resistors and capacitors were added (the capacitors were reverse-biased p-n junctions) the result was a little piece of electronic circuitry: the 'integrated circuit' — the IC — had been created.

The available technology imposed many limitations, however, and like the first transistors the first ICs were imperfect and expensive. But because of these technical limitations a new strategy once again emerged, and this has brought us to the point where we are today. And it will still have a great deal more to offer in the future. This will be the subject of the next section.

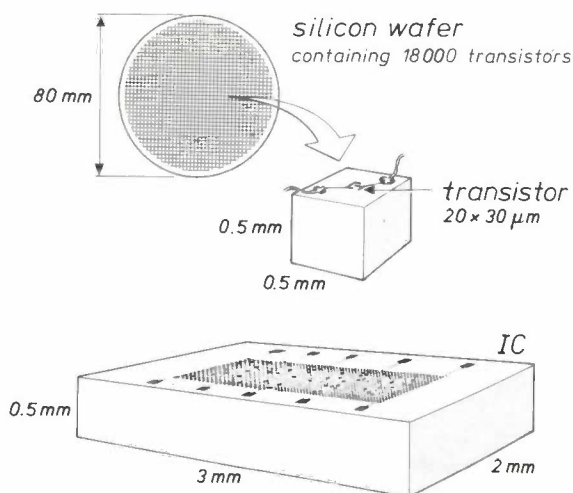


Fig. 8. Progress of the technology in the early sixties: from a single transistor sawn from a silicon crystal to an integrated circuit in silicon. To avoid breakages during manufacture, the silicon slice has a minimum thickness of 0.5 mm. The pieces that can be sawn from this for an individual transistor cannot be much smaller than 0.5 mm x 0.5 mm, i.e. small cubes. The transistor itself is frequently no larger than 20 μm x 30 μm.

The evolution of the integrated circuit

The manufacture of integrated circuits provided many problems, especially at the start.

- The characteristics of the diffused transistors showed a considerable spread from wafer to wafer and batch to batch.
- Large resistors and capacitors are difficult to make. They take up a lot of room and this makes them expensive. (This is still true today.)
- Increasing complexity and larger chip areas led to low yields, caused on the one hand by microscopic faults such as pinholes in the silicon oxide, and on the other by defects in the silicon crystal lattice.

This was a particular cause of problems in the manufacture of analog circuits, where the relation between input and output signal is extremely important. Digital circuits, whose main function is to recognize a 0 or a 1, were less critical and therefore easier to make. The great majority of ICs made in the first half of the sixties therefore consisted of simple logic elements, such as single or double gates and flip-flops. The transistors in the IC were double-diffused npn junction transistors, which were vertically diffused into the silicon. This technology is called 'bipolar', because the operation of the transistor depends on *two* charge carriers of opposite sign, electrons and holes (*fig. 9*).

In about 1965, however, the bipolar technology received a serious competitor in the form of the field-effect transistor (the FET). Many variations of this exist, but the most successful was the metal oxide-semiconductor field-effect transistor or MOSFET, later abbreviated to MOS transistor (see *fig. 10*). The MOS transistor was also referred to as 'unipolar', because the acting carrier was always a single species of charge carrier, either the negative electron (NMOS) or the positive hole (PMOS). The combination of both types of transistor on one silicon chip then gave a 'complementary' MOS circuit (CMOS).

The MOS transistors, which were positioned laterally in the surface, originally had a much simpler structure than the bipolar transistors, and therefore fewer process stages were required (which made them cheaper). Thus they also gave a higher yield (which made them even cheaper still). The only trouble was that the earlier versions were very much slower than their bipolar competitors, so that the bipolar devices remained in use for fast digital circuits — and of course for all the analog circuits, for which the MOS transistor was unsuitable.

The great breakthrough with the ICs built up from PMOS transistors, which were originally rather slow, came in about 1970, when a 1000-bit DRAM (Dynamic Random-Access Memory) was made. With the sub-

sequent adoption of the faster NMOS process and the continued miniaturization of the storage cells these memory products became steadily cheaper and better. The spectacular fall in price per storage bit by a factor of ten every five years caused the bit price to drop from one dollar cent in 1970 to about a thousandth of a dollar cent in 1985. The result was that the MOS memory technology became the driving force behind the development of integrated circuits, and the MOS memory market the fastest growing one. It has meanwhile become possible to accommodate a memory of a million bits on a single silicon chip, and the four-million-bit chip has already been announced.

And still the reduction of dimensions continues. The limit is set on the one hand by the wavelength of the radiation used in the lithographic process and on the other by the electrical and physical effects that occur on miniaturization. Whereas today in manufacture the smallest dimension in the new ICs is about

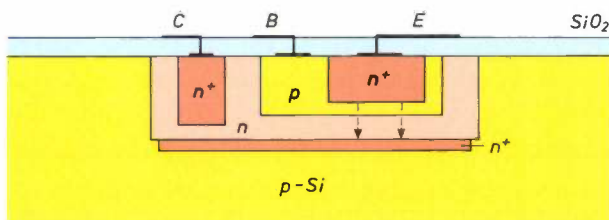


Fig. 9. Bipolar npn transistor. The current, consisting of both holes and electrons, flows vertically (arrows) from emitter to collector. The collector series resistance is kept small by a buried n⁺ layer in the substrate (p-Si) and an n⁺ contact diffused under the collector metallization.

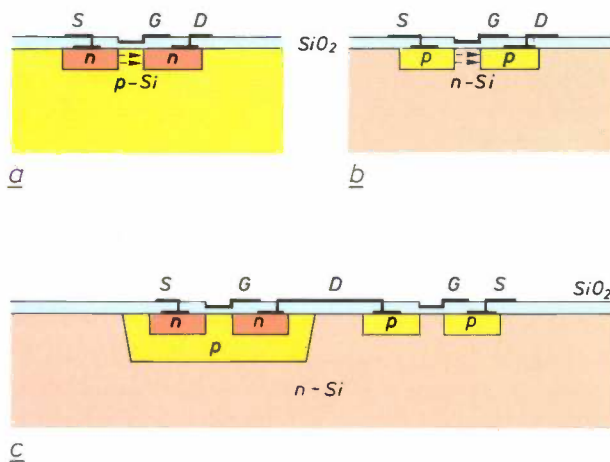


Fig. 10. a) NMOS transistor. The current, consisting of electrons, flows along the surface (arrows) from the source S to the drain D. G gate. b) PMOS transistor. The current, consisting of holes, flows from S to D. c) A CMOS circuit is a combination of NMOS and PMOS transistors in a single substrate. Here the circuit under (a) is completely contained in the n-substrate of (b), with the aid of a p-type well that has been locally pre-diffused.

There are other possibilities: the circuit of (b) can be completely contained in the substrate of (a), with the n-type well locally diffused beforehand, or (a) and (b) side by side in a neutral substrate, again with locally pre-diffused p-type and n-type wells. In all variants it is important that the gate region should be narrow and its oxide thin.

Table II. IC technologies and signal-processing techniques. The suitability of an IC technology for a particular device is not only dictated by the 'state of the art'; the devices themselves are also subject to developments: logic circuits become faster, memories become larger. It should not necessarily be assumed that the evaluations in the last two columns will still be the same in 1987.

IC technology	Signal-processing technique	Digital	
		Logic	Memories
Bipolar	++	+	+
NMOS, PMOS	-	+	+
CMOS	+	++	++

1.2 μm, the lower limit in the future could fall to about 0.3 μm. At the same time the MOS technology used is moving from NMOS to CMOS, since one of the advantages of CMOS is that less heat is generated.

A great stimulus to the creation of the digital memory market came with the development of the first integrated microprocessor in 1971/72. It appeared first as a 4-bit device, and today there are already 32-bit versions in use. Thus the combination of ever cheaper and better memories and processors has opened the way to what we now know as the 'digital era'.

Further competition between MOS and bipolar techniques

From the above it can be seen how the enormous growth that has taken place has helped the MOS technology to develop faster than the bipolar technology, although bipolar technology has not stood still. Through the continued reduction of dimensions, the MOS products have also become faster and are now approaching the speed of the bipolar devices, while in addition their power requirements are on average lower. This is a very important point at high packing densities, because of heat dissipation.

Today's world does not, however, consist of digital products alone: in the analog sector the position of the bipolar technology is still quite strong. Table II shows possible combinations of technologies and signal-processing techniques.

Apart from their position in the analog market, bipolar ICs will continue to play an important role in fast processors and high-speed memories. Their speed will of course also increase with decreasing circuit dimensions, while newer switching techniques such as integrated injection logic [3] and integrated Schottky logic [4], usually referred to as I²L and ISL, provide

[3] C. M. Hart and A. Slob, Integrated injection logic — a new approach to LSI, Proc. ISSCC 72, Philadelphia 1972, pp. 92, 93 and 219.

[4] J. Lohstroh, ISL, a fast and dense low-power logic, made in a standard Schottky process, IEEE J. SC-14, 585-590, 1979.

better packing density and lower dissipation. Bipolar circuits will remain faster than MOS for a while, but meanwhile field-effect transistors integrated on gallium arsenide are being made that can offer higher speeds because of greater electron mobility. These devices are already beginning to pose a threat to the fast bipolar versions. The GaAs technology is still relatively difficult and the material is expensive — but this is of course something we have seen before in the history of solid-state devices. Much can happen in the coming years.

Now let us return to the MOS ICs. Although PMOS has little more to offer now, NMOS has not yet completely yielded to CMOS. But in the end and in most cases CMOS will win, since it is virtually impossible for NMOS or PMOS to penetrate the analog field, whereas CMOS certainly can.

A more direct threat to the analog bipolar devices comes not so much from analog MOS circuits but from digital MOS circuits. The low prime cost of these circuits makes it interesting to convert analog signals to digital, process them digitally and then convert them back to analog. Such methods are becoming increasingly popular in audio, video and communication systems. Digital sound recordings or digital telephone networks are already in common use today. This is the future — or perhaps it is already here.

Important aspects for future electronic devices and circuits

In a nutshell, after tubes were superseded by transistors, the integrated circuit became the 'driving force' in the entire electronics field, for the following reasons:

- the smallest transistor today, on an IC, occupies a millionth of the area of the first germanium transistor made in 1953;
- it uses a millionth of the energy, and
- it is about a million times cheaper;
- the miniaturization that has brought all this about is still continuing and will not reach its smallest limits until about 1995;
- these techniques for 1995 are already in use in the laboratory, so we can make fairly accurate predictions about developments, devices, prices and performances.

But will these factors continue to determine the development of electronic functions and equipment and will they continue to be the driving forces? Or will other factors gradually come into play?

Two new factors are clearly beginning to emerge.

Major fields of applications for ICs, such as information technology, will continue to grow, but a large

number of other new fields, in which there is often a need for special modifications or completely new products, still lie fallow. In the years ahead these new fields will have to be opened up by close cooperation between IC developers and prospective users. This will require a great deal of application-specific work, since the market for 'application-specific ICs', or ASICs as they are called, is large and will account for much of the further growth in the IC market. In some cases, indeed, a manufacturer of electronic equipment will just have to have ASICs if he is to remain ahead. The world-wide demand for application-specific products, therefore, is now growing by leaps and bounds.

From the history of semiconductor devices we have already seen that the cost of manufacturing the actual semiconductor chip is gradually falling so far that the costs of testing, packaging and mounting are becoming disproportionately high in comparison. In the very large chips of the near future there is another problem to be faced: because of the great complexity of the integrated functions there will often be scores of tiny connection points on the silicon chip, one or two tenths of a millimetre apart. Mounting in an encapsulation on a fanned-out metal grid, with a distance of 2.54 mm between the pins, gives an end-product with a chip area of about ten square centimetres, which takes up an unnecessarily large part of a multi-layer panel. This costs money. Considerable efforts are now being made to bring the external connections of an IC much closer together, giving it a much smaller area. The IC is then soldered to the surface of the circuit board, which possesses a fine network of conductors and now has no holes. All the other components are then fitted in beside the IC by means of contacts on the underside. This technology, known as surface mounting, reduces the area of the board to a sixth, and the costs of mounting can be reduced by 30 to 40%.

The Philips approach

In view of the importance of the two points mentioned above (ASICs and surface mounting of semiconductors and other devices) it is interesting to see how quickly these problems have been recognized and tackled throughout Philips.

In early 1971 Philips established a design group to serve users within the organization. The group assists its customers in designing specific ICs, and, if necessary making the ICs and testing them. This ASIC group is in fact an extension of a group that had been set up some years earlier in the Research Laboratories, but it operates on a more industrial basis. For years, therefore, knowledge in depth has been present and available concerning the development, in cooperation

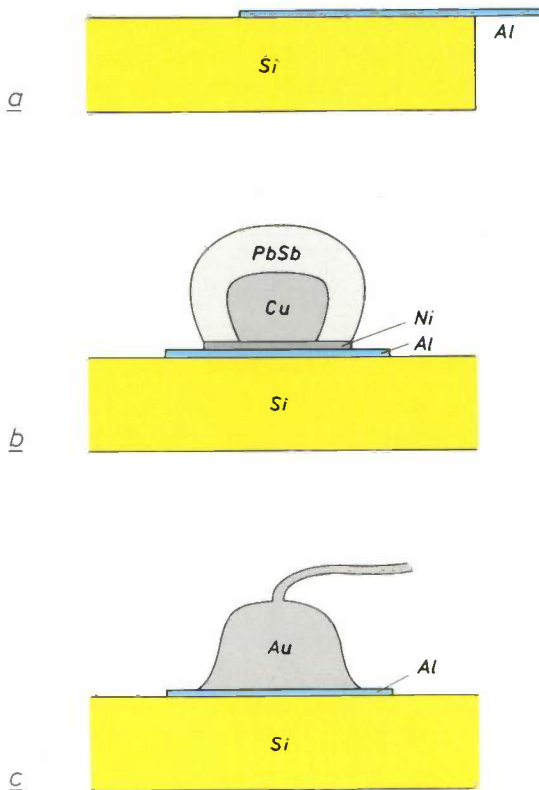


Fig. 11. *a)* Beam-lead bonding. Small fingers of aluminium, or gold, project over the edge of the Si chip and form part of the metallization pattern on the chip at that point. *b)* Solder bonds. Beads of solder (e.g. of a lead-antimony alloy) containing a hard metal core (e.g. of copper) are applied to the connection points of the aluminium metallization pattern. The metal core maintains the distance between the crystal and the ceramic substrate. A film of say nickel between the bead and the aluminium pattern improves adhesion and prevents diffusion into the interior. *c)* Gold-wire bonding. By heating under pressure, sometimes in combination with ultrasonic vibration, thin gold wires can be bonded directly to the bonding pads of the aluminium on the chip. At the end of the wire a bead is melted (ball bond). Various methods exist; for instance, aluminium wires may also be used.

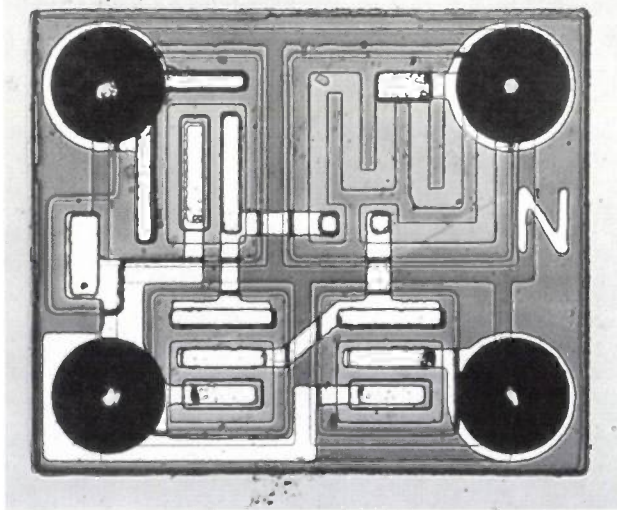


Fig. 12. The first IC put on the market by Philips in 1965, the OM 200, was designed for use in extremely small hearing aids. With dimensions of 0.75 mm × 0.75 mm, it consisted of three transistors and two resistors. The model shown, in a special version for direct mounting, has ball bonds at the ends of the connectors.

with users, of the most diverse products in all the available technologies. It should be noted here that it is not always so easy for the IC designer and manufacturer to learn to think in terms of the user — nor indeed is it easy for the user to learn to think about the optimum use of existing technology for his own design.

In encapsulation and methods of assembly Philips have always been very much in the forefront. However, the first ideas about new IC-interconnection techniques came from the USA. It was Bell Telephone that introduced the idea of beam leads, tiny metal strips that extend the metallization and run over the edge of the chip. Beam leads made it possible to fix the chip to a substrate while at the same time providing the electrical connections. IBM provided the chip with hard-core beads of solder to fix the chip to a ceramic substrate and make contact. Both versions were extensively tested by Philips, and 1967 saw the first pilot assembly of ICs with 'ball bonds' or 'solder bumps', for mounting on a polyimide foil with a metallization pattern (later announced by General Electric as 'tape bonding'). The various systems are shown in *fig. 11*, together with the method most widely used today, gold-wire bonding. *Fig. 12* shows an IC with ball bonds.

When an IC is mounted with bonding beads or beam leads, however, it cannot readily dissipate its heat and the silicon surface is difficult to protect from atmospheric attack. The SOT 23 mini-encapsulations developed by Philips in 1966 for transistors and the SOT 43 for ICs did not have these problems. Originally developed for mounting in hybrid integrated circuits, they initially had only limited success.

In recent years, however, the market for 'SO transistors' and 'SO ICs' has been growing enormously. (SO stands for 'Small Outline'. SO components are usually mounted directly on the surface of the board.) In addition to the various Philips SO encapsulations (*fig. 13*), which have become an international standard, all kinds of variations have been developed. It is estimated that in a few years time these mini-encapsulations for surface mounting will constitute a very large part of the total world production. All this arose from the switch to surface mounting, a method which very closely resembles the earlier method of mounting in hybrid integrated circuits. Because of the long period between invention and mass use, most people have forgotten that the 'small outline' products were first developed and put on the market by Philips.

Philips have also played a leading role for many years in the development of a totally new concept, consisting of components (active and passive), mounting boards to match, and complex robots for putting them all together. It is of course essential to arrive at international standards in this field, but once

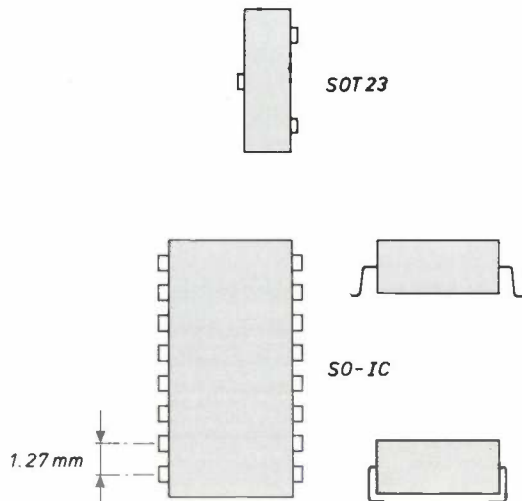
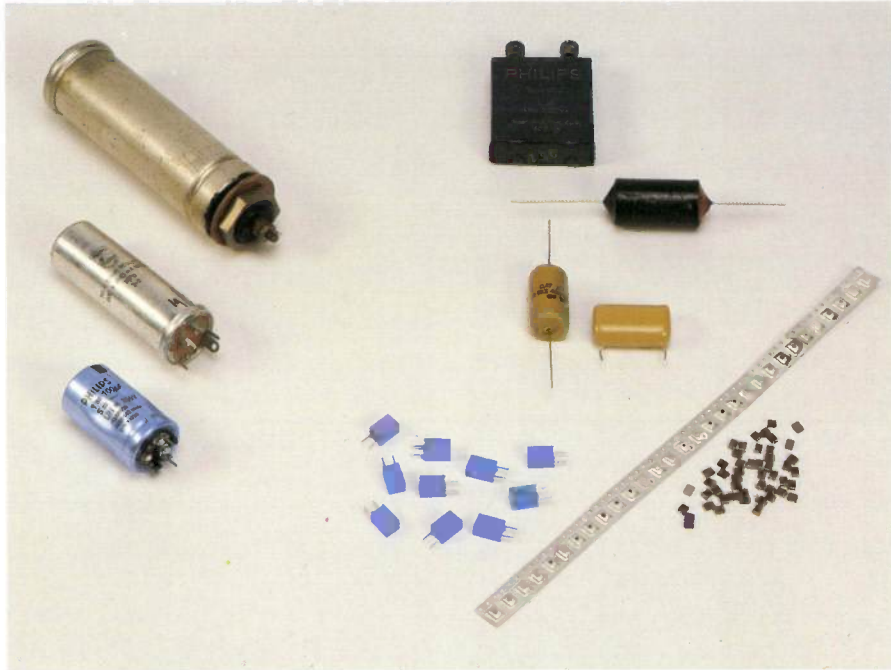


Fig. 13. 'Small outline' encapsulations, suitable for surface mounting. The SOT 23 was the world's first small-outline transistor encapsulation to be made in quantity production. The oldest small outline IC encapsulation — the SOT 43, not shown here — had connection points around it. It was later replaced by encapsulations with the connectors at two ends, with half the pitch of the existing standard IC encapsulation (1.27 instead of 2.54 mm). The contact pins usually project from the body (S form), but can also be used bent inwards (J form); see side view.

this has been achieved, we can again look forward to a period of strong growth in electronic circuits and systems — systems in which, as noted at the beginning of this article, the components must continue to be the driving force that they always have been. But we must never forget that in the last resort it is the function that counts, and not the component.

Samenvatting. The near-explosive development of electronic semiconductor components is outlined with reference to point-contact, junction, p.o.b., mesa and planar transistors and the advent of ICs, with discussion of the relative merits of bipolar and MOS techniques. The trend towards still more and smaller, hence cheaper, elements per chip will continue; the demand for application-specific ICs will increase. The future shape of other components — e.g. capacitors and resistors, which have not developed so rapidly — is more difficult to predict, however, because there are no international standards as yet. The same applies to the methods of assembly of all the components to form systems. Efforts are being made to arrive at international standards for encapsulation and for surface-mounting methods, since the relative costs of testing, packaging and mounting continue to increase in comparison with the cost of the actual components.

Miniaturization of capacitors



On the left are three electrolytic capacitors, designed for use in power supplies. In these familiar capacitors the dielectric consists of a thin layer of oxide on aluminium foil in an electrolyte. The upper one is a liquid capacitor with a capacitance of $25 \mu\text{F}$ at 330 V; this dates from about 1934. In the second capacitor the electrolyte is impregnated in paper. This one dates from 1952 and has a capacitance of $2 \times 50 \mu\text{F}$ at 400 V. The lowest one is a modern electrolytic capacitor; $100 \mu\text{F}$ at 385 V. It is clear that the dimensions have been reduced considerably. This has been achieved mainly by increasing the electrode area with the aid of special etching techniques.

The capacitors in the right-hand part of the photograph were mostly designed for use in electronic circuits. The upper one is a foil capacitor, $1 \mu\text{F}$ at 250 V, made in 1926. The internal construction is of rolled-up paper with a coating of tin. The second one is made from thin metal foil and paper. It dates from 1936 and has a capacitance of $0.1 \mu\text{F}$ at 400 V. The two buff capacitors were made in 1970 and differ in the configuration of their connecting leads. Their cap-

acitances are $0.47 \mu\text{F}$ and $1 \mu\text{F}$ (on the right). The dielectric of these capacitors consists of plastic film; the electrodes are applied to the dielectric by evaporation in vacuum. The capacitors at the bottom in the blue encapsulation — modern ones — were made in the same way, but the film is much thinner: $1.5 \mu\text{m}$. Their capacitance is $1 \mu\text{F}$ at 63 V.

The ceramic multilayer capacitors, lower right, have a completely different construction. They consist of a ceramic body with a large number of embedded electrode layers with a spacing of about $16 \mu\text{m}$. They also have a capacitance of $1 \mu\text{F}$ and are designed as SMDs (Surface-Mounted Devices). They have no leads and are bonded directly to the circuit board with adhesive; the electrical contact to the copper connector pads is formed later in a solder bath. The strip of the same capacitors is intended for automated mounting, for example with Philips modular chip-mounting (MCM) machines. The dimensions of these capacitors, $4.5 \text{ mm} \times 3.3 \text{ mm} \times 1.6 \text{ mm}$, indicate a reduction in volume of about 1700 times compared with the $1\text{-}\mu\text{F}$ foil capacitor from 1926.

Electric motors in small domestic appliances

R. H. Dijken

Introduction

After Oersted's discovery in 1820 that a force acts on an electric current in a magnetic field, the search was on for machines that could use this principle for converting electric power into mechanical power. The first machine that could be called a 'rotary electric motor' is probably Barlow's wheel, dating from 1831^[1], illustrated in *fig. 1*. The first practical rotary electric motors appeared in about 1870, and were used for driving water pumps in mines, for traction and other applications. These motors were rated at relatively high powers, typically 5 kW or more. Other types of electric motor gradually emerged, with increasing efficiency, longer life and lower prime cost.

The first 'small' electric motors were designed in about 1920. They were series-commutator motors used in vacuum cleaners. Later other types of small electric motor appeared, such as the d.c. commutator motor with permanent magnet stator, the single-phase induction motor and the single-phase synchronous motor with permanent-magnet rotor.

The early sixties marked the emergence of a fast-growing market for electrical domestic appliances in Western Europe. In that same period the Philips group, which was already producing electric shavers, embarked on the production of a wide variety of electrical domestic appliances, most of them containing an electric motor.

In the following we shall first consider the differences between large and small electric motors, with reference to laws of scaling. We shall then look at some of the leading developments in small electric motors. Finally we shall consider their applications in Philips products: series motors in vacuum cleaners and shavers, single-phase synchronous motors with permanent-magnet rotors in hair trimmers, citrus presses, knife sharpeners, can openers and vibratory shaving appliances, and d.c. commutator motors with permanent-magnet stator in rotary-action shavers.

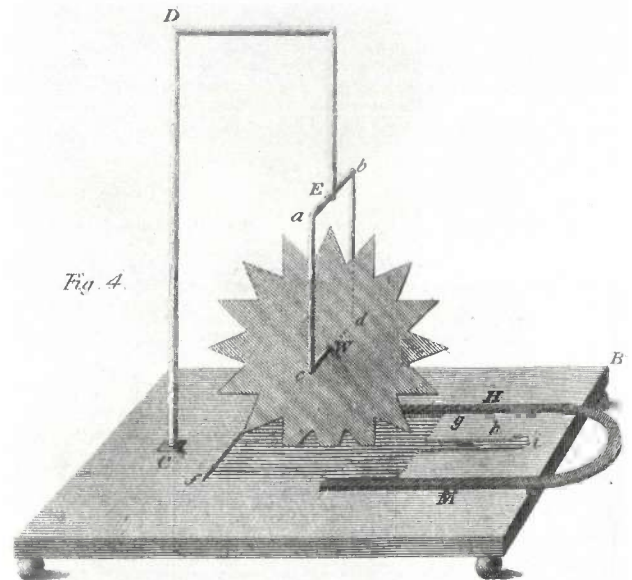


Fig. 1. Barlow's wheel. The teeth of the wheel *W* dip into mercury between the poles of a horseshoe magnet *HM*. When current flows the wheel turns.

Differences between large and small electric motors

The power P of an electric motor with a wound rotor can be expressed in terms of the current density j in the rotor windings, the air-gap flux density (or induction) B , the speed of rotation n and the rotor diameter d ^[2]:

$$P \propto j B n d^4. \quad (1)$$

The copper loss P_{Cu} in the rotor is related to j and d by:

$$P_{Cu} \propto j^2 d^3. \quad (2)$$

From (1) and (2) we have:

$$\frac{P_{Cu}}{P} \propto \frac{j}{B n d}. \quad (3)$$

If d is reduced while the values of j , B and n remain

Dr Ir R. H. Dijken is with the Domestic Appliances and Personal Care Division, Philips NPB, Groningen.

unchanged, the ratio P_{Cu}/P increases. This means that the efficiency of a small motor becomes lower and its torque-speed characteristic less steep^[3]. One consequence of this for the designer is that the current density j must be reduced as the size of the motor is diminished.

Apart from many other differences between 'large' and 'small' electric motors, there is a difference connected with the cooling. The heat generated in the rotor has to flow from the interior before it can be dissipated from the surface. The resulting temperature difference between the interior and the surface of the rotor is approximately proportional to d^2 . For a rotor diameter smaller than about 10 cm this temperature difference remains small compared with the permissible rise in the temperature of the rotor. At larger rotor diameters the interior of the rotor could become dangerously hot. There are therefore two cooling problems with the large electric motor, one relating to heat transfer from inside the rotor to the surface, and the other relating to heat dissipation from the rotor surface. The small electric motor only has to contend with the second cooling problem.

These critical factors (and many others) indicate that the line of demarcation between large and small electric motors corresponds roughly to a rotor diameter of 10 cm and a power of 1000 W.

Developments

We shall now consider some innovations in technology and materials that have largely determined the pattern of development of small electric motors in Philips domestic appliances from 1960 to the present day.

Insulation of the windings

The rotor and stator windings have to be electrically insulated from the laminated cores. The quality of the insulation must be high. In 1960 the insulation was provided by paper strips, stars and formers, as shown on the left in *fig. 2*, and these were gradually replaced by plastic. Nowadays, separate plastic insulators are used, and these are attached to the laminated core. In some cases the laminated cores are placed in a mould and surrounded by plastic injected in the mould. Plastics provide better insulation, reduce the number of components required and facilitate mechanical assembly. An example of plastic insulation in a shaver rotor is shown on the right in *fig. 2*. This rotor has three lobes, each with a winding around it. If paper insulation were used, the turns of the winding would receive little support, and the coils would therefore have to be impregnated. The injection-moulded plastic

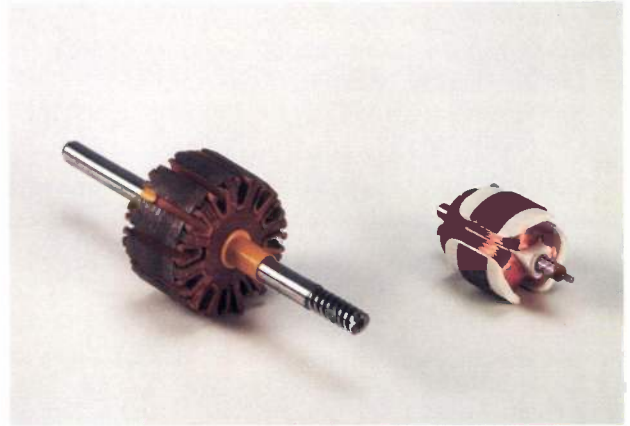


Fig. 2. The rotor of a series motor for a hand mixer is shown on the left. The laminated core is insulated with paper and plastic. On the right is the rotor of a series motor for a Philishave. The injection-moulded plastic around the core acts as a triple former for the windings.

around the rotor core produces a 'former', so that impregnation is not required.

Permanent-magnet materials

Scaling laws show that the stator windings of a commutator motor become heavier, larger and more expensive in relation to the total weight, volume and cost of the motor as the dimensions are scaled down. If the supply is d.c., there is much to be said for using permanent-magnet stators. Before 1960 the only suitable magnets were those made of steel alloys such as Ticonal. Although these materials have a high remanent flux density, about 1 T (tesla), they have two great disadvantages: their resistivity is low and they are easily demagnetized. The gaps between the rotor lobes make the reluctance of the magnetic circuit dependent on the position of the rotor, so that the flux from the magnet varies periodically as the rotor rotates. This sets up fairly large eddy currents in the magnet, and these adversely affect the efficiency of the motor. Since the magnet is easily demagnetized — and for other reasons — its volume must be relatively large, and this makes the motor heavy, bulky and expensive.

In about 1960 the sintered anisotropic iron oxide Ferroxdure became available. Although its remanent flux density is much smaller than that of Ticonal, about 0.35 T, Ferroxdure has such a high resistivity that the eddy currents are negligible. Other advantages are that its density is low, it is difficult to demagnetize and it is relatively inexpensive. All these advantages

[1] B. Bowers, The early history of the electric motor, Philips Tech. Rev. 35, 77-95, 1975.

[2] R. H. Dijken, Similarity relations for small electric motors, Proc. Symp. on Electrical machines for special purposes, Bologna 1981, pp. 439-447.

[3] R. H. Dijken, Optimization of small AC series commutator motors, Thesis, Eindhoven 1971.

account for a total annual world production of more than 500 million small commutator motors with magnets of Ferroxdure or similar materials.

The commutator

After 1960 there was a relatively marked increase in the number of d.c. commutator motors for supply voltages lower than 6 V. At these low voltages graphite brushes are not satisfactory: they have a voltage drop of a few volts and the high pressure of the brushes gives high friction. Brushes of copper graphite or silver graphite have a much smaller voltage drop, but they cause just as much friction as graphite brushes. Brushes and commutators both made of a noble-metal alloy provided the solution. The low brush pressure gives low friction, and the contact resistance between brushes and commutator is virtually negligible.

Examples of the evolution of some types of motor

The a.c. series motor in vacuum cleaners

A vacuum cleaner runs off the a.c. mains. The motor has to deliver a mechanical power of between 400 and 800 W at a speed of about 20 000 revolutions per minute. The high speed is necessary to obtain a pressure reduction of about 0.2 bar with a compressor of minimum dimensions.

A comparison of series motors used in vacuum cleaners made in 1960 and 1985 shows that plastic has widely replaced paper as insulating material in the rotor and that the turns of the rotor are now welded to the commutator, not soldered. A considerable difference, hardly visible externally, is that the motor dimensions have now been optimized.

The optimized motor of 1985 has thicker rotor lobes, the ratio of the height of the rotor core to its diameter is smaller, and the flux density in the magnetic circuit is lower. For the same power and speed the weight, volume and cost of the laminations and the windings of both rotor and stator have been almost halved^[3]. Fig. 3 shows the laminations of the rotor and stator of the 1960 motor and the optimized motor of 1985. The decrease in core cross-sectional area is clear. The decrease in the height of the core is about 30%.

The series motor in shavers

Until a few years ago all mains-powered Philishaves were fitted with a series motor, which is suitable for a.c. or d.c. operation. (In a.c. operation both magnetic field and current in the rotor windings change polarity periodically, so that the torque maintains direction.) Before 1960 the motor was only suitable for 110 V and a resistor in the plug had to be switched

into the circuit for operation at 220 V. The motor was later made suitable for 110 and 220 V by adding a tap to the stator winding. (At 110 V only some of the turns on the stator winding are used.) At both voltages the motor delivers about 3 W at about 12 000 revolutions per minute.

A comparison of these series motors for shavers made in 1960 and 1985 reveals a number of other differences; see fig. 4. The use of plastics has considerably simplified the design, as can also be seen on the right in fig. 2. Even though the regulations concerning the suppression of radio interference have become much stricter through the years, fewer components are now necessary for interference suppression. This has been achieved by designing the motor in such a way that it generates less r.f. interference. Metal plates near the commutator and the brushes, for instance, screen off much of the r.f. radiation energy.

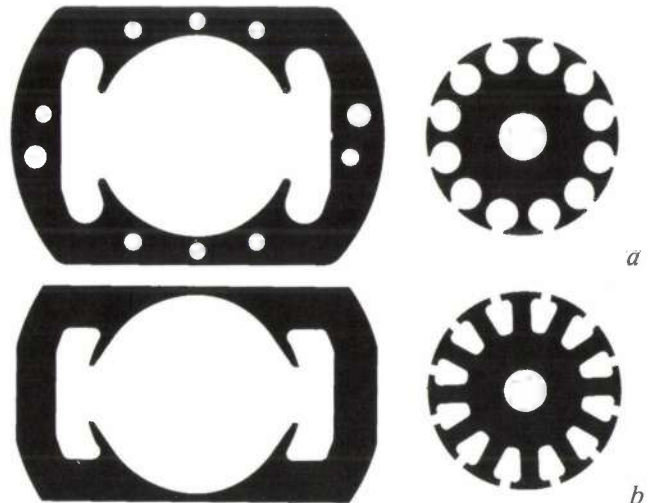


Fig. 3. a) Laminations of a stator and rotor (right) of an a.c. series motor for vacuum cleaners before optimization of the motor design. b) As (a), after optimization.



Fig. 4. A series motor for a 1960 Philishave (left), and for a 1985 Philishave (right).

The brush springs are designed to function as r.f. chokes, and the stator windings are dimensioned to resonate with their own stray capacitance as parallel LC circuits, presenting a high impedance at critical interference frequencies.

The single-phase synchronous motor with permanent-magnet rotor

Although the principle of this motor has long been known, some practical problems prevented its appli-

dynamic instability problem was found for this type of motor as well^[4]. A final, and as yet unsolved, problem is that after switching on, it remains to be seen which way the motor starts to rotate. The motor can therefore only be used for applications where this does not matter. The Philips single-phase synchronous motor with permanent-magnet rotor has so far been used in vibrator shavers, hair-trimmers, citrus-presses, knife-sharpeners, shoe-polishers, can-openers, cork-screws and ice-cream makers; *fig. 5*.



Fig. 5. A single-phase synchronous motor with permanent-magnet rotor and some Philips products in which this motor is used: two knife-sharpeners (left), a hair-trimmer (centre) and two citrus-presses (right).

cation. The magnet material used has to have a relatively high coercive force. Ferroxdure provided the answer to this problem in about 1960. A second problem was that the motor can only rotate at a speed that corresponds exactly to the frequency of the a.c. mains. As soon as the appliance is switched on, the rotor must therefore rotate synchronously within one mains period of switching on. The solution was found by giving the rotor the correct moment of inertia and shaping the stator poles so that the rotor has a defined magnetic preferential position when it is stationary.

A third problem is that of dynamic instability. This refers to a periodic speed variation that can become so great that the rotor 'falls out of step' with the alternating stator field. In large electric machines the dynamic-instability problem is solved by fitting an induction cage. Scaling laws show that this does not help for small single-phase synchronous motors. Nevertheless, after years of research, a solution to the

The d.c. commutator motor with permanent-magnet stator

In about 1960 mains-powered Philishaves operating with batteries or rechargeable nickel-cadmium cells became available as well as the mains-operated versions. The natural choice of the motor for the shavers operating with batteries or cells was the d.c. commutator motor with permanent-magnet stator. In recent years this motor has started to supersede the series motor in mains-operated Philishaves. The d.c. supply it requires is derived from the a.c. mains by an electronic circuit.

To get the maximum number of shaves from a battery or a rechargeable NiCd cell, the motor must have

^[4] H. Schemmann, Stability of small single-phase synchronous motors, Philips Tech. Rev. 33, 235-243, 1973; H. Schemmann, Theoretische und experimentelle Untersuchungen über das dynamische Verhalten eines einphasen-Synchronmotors mit dauermagnetischem Läufer, Thesis, Eindhoven 1971, also published as Philips Res. Rep. Suppl. 1971, No. 5 (in German).

the highest possible efficiency. High efficiency is therefore the key feature of the design. Since 1960 the efficiency of the motor has gradually been increased from about 25% to about 65%. Three developments made this possible. The first is the use of better magnet materials. Ticonal was still being used in 1960. As

a copper commutator, first by pieces of phosphor-bronze on a noble-metal commutator and later by noble-metal fingers on a noble-metal commutator; see fig. 6, right. The contact resistance between brushes and commutator and the brush-friction losses are virtually zero with the noble-metal combination.

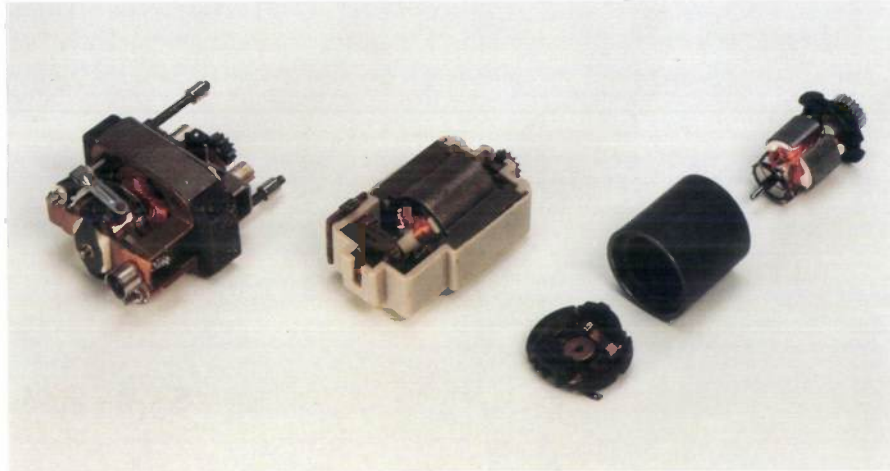


Fig. 6. Different versions of a d.c. commutator motor with permanent-magnet stator. A 1960 design with two Ticonal blocks (left). A later design with two Ferroxdure magnets (not visible) with steel 'pole-arcs' (centre). A design dating from the seventies with a Ferroxdure ring, later replaced by two Ferroxdure segments (right). (The motor is shown dismantled: the plate with noble-metal fingers is in the foreground, the magnet in the centre and the rotor in the background.)

can be seen on the left in *fig. 6*, Ticonal magnets were cast as blocks, which were fitted to the soft-iron stator. Ferroxdure gave a great improvement in efficiency. The motor shown centrally in *fig. 6* had Ferroxdure blocks and steel 'pole-arcs' to conduct the flux through the rotor. Although there were some eddy current losses in these pole-arcs, they were less than in the motor with Ticonal. The technology of making Ferroxdure in complex shapes was still advancing, and in about 1970 the blocks were replaced by rings, shown on the right in *fig. 6*. These rings consist of a plastic filled with anisotropic Ferroxdure powder. This arrangement virtually eliminated the eddy-current losses. Later on the ring was replaced by two segments.

The second development that improved the efficiency was the replacement of the carbon brushes on

Finally, further improvement in efficiency was obtained by optimizing the design of the motor^[5]. The ratio of lobe width to rotor diameter and the ratio of the height to the diameter of the rotor core played a particularly important part in this optimization.

[5] R. H. Dijken, Designing a small DC motor, Philips Tech. Rev. 35, 96-103, 1975.

Summary. In addition to optimization via theoretical considerations, developments since 1960 in small electric motors used in Philips domestic appliances include: improved insulation of the windings, better permanent-magnet materials, lower friction and lower contact resistance between brushes and commutator. These developments are illustrated by the evolution of the a.c. series motor in vacuum cleaners, the series motor in Philishaves, the single-phase synchronous motor with permanent-magnet rotor in various domestic appliances, and the d.c. commutator motor with permanent-magnet stator in shavers for mains and battery operation.

Philips Technical Review 50 years ago

APRIL 1936 THE V. R. 18 TRANSMITTING AND RECEIVING EQUIPMENT

By C. ROMEYN.

With the progressing development of commercial flying, the need for some means of intercommunication between an aircraft in flight and the airport very soon became apparent, and the first passenger and commercial airplanes, although still very small, were already equipped with wireless apparatus. With the steady and radical improvements in technical methods and apparatus during the last ten years both flying and wireless technology have made rapid strides. The importance of wireless intercommunication during flight has progressively increased and at the present day it is impossible to conceive of a passenger or commercial aircraft being without wireless apparatus. Reports of weather conditions along the aircraft route, landing instructions, direction-finding signals, etc., have become indispensable to the pilot.

It is the task of the wireless industry to provide suitable apparatus capable of meeting the special requirements for use in modern aircraft. That an aircraft radio equipment in many respects must differ fundamentally from a permanent and stationary ground equipment is obvious. In the present article the V. R. 18 aircraft transmitting-receiving equipment designed by Philips is described. This equipment has been specially evolved to meet the various requirements for use aboard aircraft, yet in its design attention has, moreover, been given to certain specialised needs considering the application of this equipment for the Douglas air liners operating on the Netherlands East Indies route of the K.L.M. air services.

Intercommunication between aircraft and airport is nowadays performed almost exclusively by telegraphic means. In this connection it is interesting to review briefly the historical development of the methods employed. During the early years of flying intercommunication with aircraft was carried out solely by means of the telephone. This instrument alone could be used at that time, since the pilot who had to operate the wireless apparatus already had both hands fully occupied in controlling the flight of the machine and it was thus impossible for him to work a Morse key. The disadvantages of using telephony became,

however, steadily more apparent. In the first place, to cover the same range a telephone transmitter has to have a greater power than a telegraph transmitter; yet the most serious drawback of telephony is that it requires a wider frequency band, since, owing to modulation, an additional side band is transmitted at both sides of the carrier-wave frequency. In view of the increasing number of transmitting stations, which were concentrated in a comparatively small geographical area, the few frequency bands available were soon taken up. The only practical means for avoiding intensive mutual interference of stations was to adopt the telegraphic method of intercommunication. This made it necessary to provide a wireless operator for each aircraft in addition to the pilot. This addition to the crew would, however, have become necessary for other reasons, even without changing over from the telephone to the Morse key. The greater demands made on the pilot by the more complex problems associated with navigation (flying at night and through fog) were already making the care of the telephone an onerous additional responsibility, while on the other hand wireless intercommunication for the self-same reason, viz, the much-increased number of reports required for safe navigation, itself demanded closer attention. Moreover, it had become practicable to carry a special operator, as larger aircraft were being built in which more room was provided in the pilot's cabin.

Intercommunication between aircraft and airports is thus at the present time almost exclusively based on telegraphy. By international agreement the wave-lengths of 600, 944, 918 and 932 m have been allocated for wireless aircraft transmitters, of which the 600-m wave-length is only allowed for transoceanic flights.

Installation of Equipment

The transmitter with the associated converter is accommodated in a corner of the luggage cabin. It is suspended by shock-absorbing cables and is thus adequately protected against jolts and vibration. The receiver is set up on spring rubber supports in front of the operator's seat (fig. 6), together with the control box, on which are

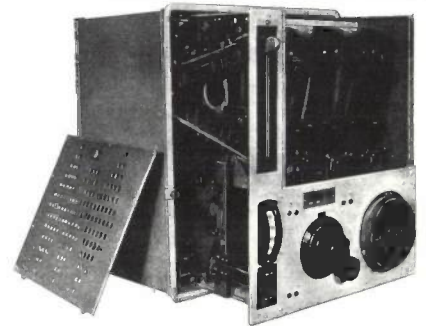


Fig. 5. V.Z. 18 transmitter with chassis drawn out and front wall removed. The housing and chassis are made of duralumin.

arranged, among other items, the Morse keys, various switches and the aerial ammeter. For night flying, dial illumination is provided, being capable of regulation and so placed that it does not interfere with the pilot's field of vision.

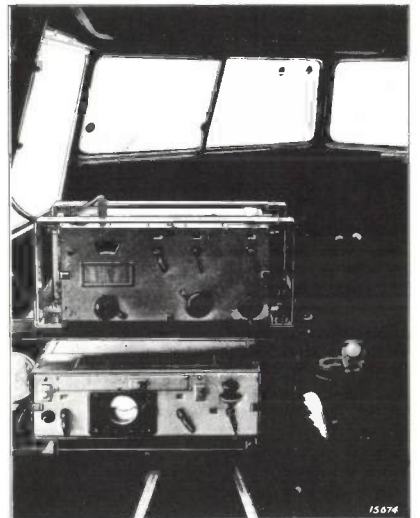


Fig. 6. Installation of the receiver (above) and the control box (below) in front of the wireless operator in the pilot's cabin of a Douglas air liner.

JULY 1936

IRRADIATION OF PLANTS WITH NEON LIGHT

By J. W. M. ROODENBURG and G. ZECHER.

After decades of abortive experiments in the Netherlands and elsewhere on the artificial irradiation of plants, an appreciable measure of success has recently been achieved in this direction. That light is one of the principal factors in the growth of plants has been realised for many years, and the idea has long been entertained of attempting

to influence the growth and development of plants by irradiation with artificial light. But only with the technical development of the requisite sources of light has a fundamental investigation of this problem been made possible and enabled the market grower and amateur horticulturist to employ irradiation methods on a practical scale.



Fig. 3. Star of Bethlehem (*Campanula isophylla*). Picture taken on February 5, 1934. Left: Irradiated with neon light, 600 lux, each night from 10 p.m. to 6 a.m. from November 2, 1933, to January 25, 1934. Right: plants non-irradiated.

The life and growth of plants are intimately connected with certain chemical processes. One of the chief of these is the assimilation of carbon dioxide, in the course of which the plants absorb carbon dioxide from the air and the carbohydrates from the water of which plants are principally built up. Carbon dioxide assimilation takes place only when a light stimulus is provided, the light being absorbed by the green colouring matter of the leaves, viz, chlorophyll. If the light available for the plant drops below a specific level, e.g. during the short days of winter, growth is practically static, even though all other conditions for their growth are adequately met, as for instance by placing in heated and moist greenhouses and by the addition of suitable fertilisers.

By augmenting the natural light with an auxiliary source of illumination, it has now been possible to promote the growth of plants even during the darkest winter months.

Carbon dioxide assimilation is most active in red light, which is absorbed to a high degree by chlorophyll. Hence, in providing auxiliary irradiation for plants, it is essential to utilise a source of light containing a sufficient concentration of red rays. At an early date it was therefore proposed to employ neon light for this purpose.

Progress in fluorescent lamps

A. G. Jack and Q. H. F. Vrehan

Introduction

Fluorescent lamps play an important part in present-day lighting technology. Their high efficiency, good colour rendering and long life make them particularly attractive for a range of applications [1]. The lamps derive their name from the phenomenon of fluorescence, i.e. the transformation of absorbed ultraviolet radiation into visible light by a suitable substance, a phosphor. Although fluorescence had been known for a long time, it was only in the thirties that all the ideas and discoveries necessary for the fluorescent lamps known today were brought together.

A fluorescent lamp consists of a glass vessel, usually of tubular shape, coated on the inside with a phosphor powder. The vessel contains a mixture of one or more noble gases (neon, argon, krypton) at a pressure of about 400 Pa and a small amount of mercury vapour. To operate the lamp a gas discharge is maintained in it, most commonly with the help of two electrodes at the ends of the tube, see *fig. 1*. In the discharge mercury atoms are excited to emit ultraviolet radiation. In the phosphor layer this radiation is transformed into visible light.

For an efficient light production both the generation of ultraviolet in the discharge and the subsequent fluorescence of the phosphor must be highly efficient. The phosphor moreover plays a key role in determining the colour and colour rendering of the lamp. The life of the lamps is mainly determined by the electrodes.

Phosphorescence, the property of 'shining in the dark' after exposure to light, was recorded more than a thousand years ago when it was noted that an oriental painting of a grazing bull continued to glow after dark. By about 1650 it had been deduced that the wavelength of the phosphorescent light was independent of that of the exciting light. This proved that the phenomenon was not simply due to the storage of light in a substance. In 1853 George Stokes published a law, later named after him, which states that the

wavelength for fluorescent radiation is greater than that of the stimulating radiation.

In the beginning of the eighteenth century Hawksbee produced a glow discharge by electrostatically charging the outside of a glass globe from which air had been evacuated. The first phosphor-coated discharge tube was put together by Antoine Becquerel in the eighteen fifties. He painted natural fluorescent powders on the inside of Georges Claude's neon tube. However, these experiments did not yield commercial products. The breakthrough in the nineteen-thirties was the combining of thermionic cathodes with the mercury-noble gas discharge and fluorescent pigments to give a low-voltage lamp of nearly double the efficiency of previous sources.

The final steps in this evolution are well recorded in the early volumes of Philips Technical Review. In 1936 there appeared an article by J. W. M. Roodenburg and G. Zecher [2] describing the irradiation of plants with neon light. The neon discharges have a long life due to the use of thermionic cathodes. Previously cold iron cathodes had been used and the resulting intense ion bombardment (electrode fall typically 300 V) limited the life to only a few hours. Only two years later W. Uytendhoeven and G. Zecher [3] described a low-pressure mercury discharge where the wall is coated with a phosphor such as a zinc beryllium silicate with a manganese activator. By then fluorescent lamps were already being used in commercial premises. P. Schouwstra and G. Zecher [4] describe one of the

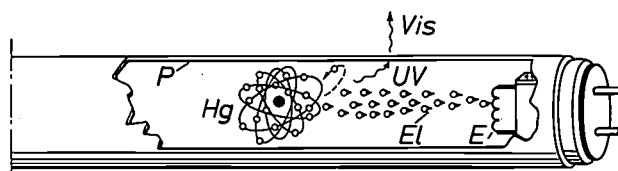


Fig. 1. Schematic representation of the main features of a fluorescent lamp. Electrons *El* in a gas discharge between two electrodes bring mercury atoms into an excited state. *E* electrode; *Hg* mercury atom. On returning to the ground state the mercury atoms emit ultraviolet radiation *UV*. This is transformed into visible light *Vis* by a phosphor coating *P* on the inside of the tube wall.

Dr A. G. Jack is with the Philips Lighting Division, Eindhoven; Dr Q. H. F. Vrehan is with Philips Research Laboratories, Eindhoven.

first installations, in the 'HEMA' department store in Amsterdam, as shown in *fig. 2*. The system luminous efficacy was about 30 lm/W, a dramatic improvement on the 12 to 13 lm/W of incandescent lamps. The lamp life amounted to about 2000 hours.

In the nearly fifty years since these early beginnings a continuing development effort has led to major improvements in luminous efficacy, colour rendering, life, compactness, etc. More recent trends are electronic power supplies that not only give a better efficacy of individual units, but also allow energy management to be introduced, and compact lamps for both the business and the home environment.

In this article we will describe some of these innovations and the associated scientific work. First we deal with the understanding of the gas discharge as it has evolved over the years, followed by a description of

occupies a dominant place in artificial lighting. It has been estimated that, excluding China and the USSR for which reliable data are not available, about 70% of all artificial light is generated by fluorescent lamps [6].

The gas discharge

General description

The basis of all fluorescent lamps is the low-pressure mercury-noble-gas discharge. In such a discharge most of the electrical power is dissipated in the 'positive column', and most of the radiation is produced there as well. The unavoidable dissipation in the regions near the electrodes represents a loss that has to be minimized.

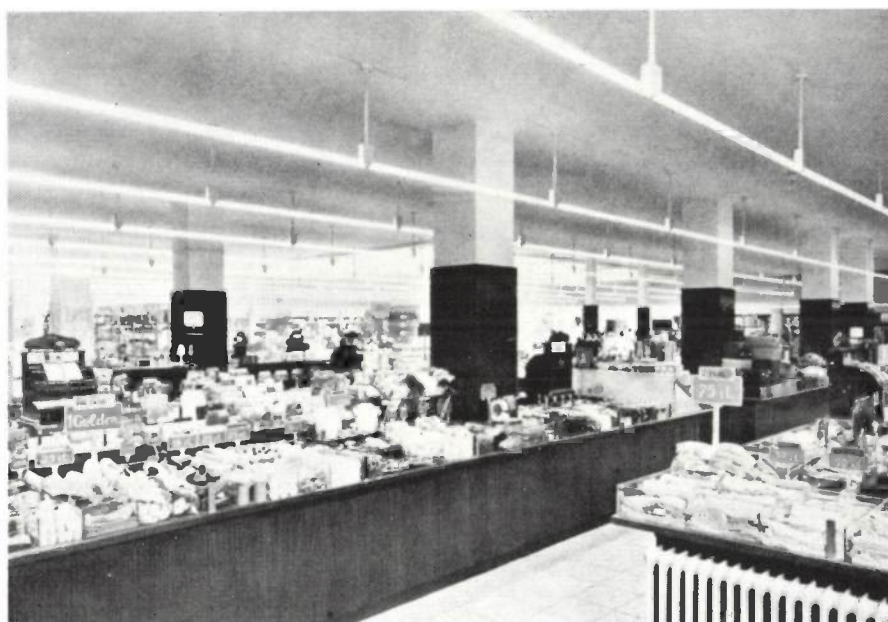


Fig. 2. Photograph made in 1939 in a department store (HEMA) in Amsterdam, showing an installation of a series of fluorescent lamps.

the significance of some new materials, mainly in the field of phosphors. Next, new products based on these developments are considered as well as some aspects of electronics. Finally, a speculative outlook is formulated.

To round off this introduction we give some commercial information. In 1939 the cost of a fluorescent lamp was 58 guilders and that of the control gear was 125 guilders. In the almost five decades since then the nominal prices (in guilders) have become considerably lower. In view of the enormous inflation in this period the real prices have fallen even more. Naturally, this sharp reduction in price is closely related to a momentous growth of the market. Fluorescent lighting now

- [1] Many details about fluorescent lamps can be found in the following review articles and books:
 J. F. Waymouth, *Electric discharge lamps*, M.I.T. Press, Cambridge, MA, 1971;
 W. Elenbaas, *Light sources*, Philips Technical Library, 1972;
 J. Polman, H. van Tongeren and T. G. Verbeek, *Low-pressure gas discharges*, Philips Tech. Rev. **35**, 321-330, 1975;
 A. G. Jack and L. E. Vrenken, *Fluorescent lamps and low pressure sodium lamps*, IEE Proc. A **127**, 149-157, 1980;
 M. A. Cayless and A. M. Marsden (eds), *Lamps and lighting*, 3rd edition, Arnold, London 1983.
- [2] J. W. M. Roodenburg and G. Zecher, *Irradiation of plants with neon light*, Philips Tech. Rev. **1**, 193-199, 1936.
- [3] W. Uytterhoeven and G. Zecher, *Low-pressure mercury discharge within a luminescent tube*, Philips Tech. Rev. **3**, 272-278, 1938.
- [4] P. Schouwstra and G. Zecher, *Tubular luminescence lamps*, Philips Tech. Rev. **4**, 337-341, 1939.
- [5] M. Koedam, *Materials vital to the lighting industry*, *Lighting Design & Appl.* **15**, No. 1 (January), 18-27, 1985.

In the positive column electrons and ions are present as well as neutral particles. However, at the relatively low densities prevailing in the plasma, collisions are not sufficiently frequent to establish thermal equilibrium between the various particles. In the applied electric field the average kinetic energy of the electrons can be as high as 1.5 eV, corresponding to an electron temperature of about 17 000 K. The ions and neutral particles, on the other hand, are not heated much above room temperature, with an average energy around 0.03 eV (about 350 K). The most energetic electrons, with an energy of about 5 eV or more, can raise the mercury atoms to excited states and even ionize them. The ionization processes compensate for the loss of ions and electrons that occurs by recombination at the wall, and thus maintain the discharge. The excited mercury radiates mainly via its two resonance lines, thus producing ultraviolet radiation at 254 nm and to a lesser extent 185 nm. With increasing mercury pressure the output at first increases, due to the increased number of excited mercury atoms, but then it decreases. This latter effect is due to the important phenomenon of 'radiation imprisonment': a photon at the resonance frequency is absorbed and re-emitted many times before it finally reaches the phosphor layer on the wall. At each absorption/re-emission event there is a finite possibility that the energy is released via a non-radiative process. Thus, for obtaining an efficient discharge without too much radiation trapping, the choice of the mercury vapour pressure is limited. In practice a value in the range of 0.1 to 2.5 Pa is necessary.

The noble gas is added to reduce the electron mean free path between collisions. For pure mercury at a few tenths of a Pa it is of the order of 1 to 10 mm, while the tube radius is typically 10 mm. Thus electrons and ions can quickly reach the wall and recombine there, with the loss of both the ionization energy and the electron kinetic energy. Moreover, excited mercury atoms can also give up their energy at the wall. These wall losses can be greatly diminished by adding a suitable buffer gas. It is chosen so that electrons have only elastic collisions with its atoms, i.e. without excitation or ionization taking place. A good choice is argon, but mixtures with neon or krypton are also used. With increasing noble-gas pressure the particle diffusion to the wall decreases, and thus the wall losses. However, the electrons undergo more elastic collisions with the noble-gas atoms. As a result the gas is heated and the electrons suffer an energy loss known as the volume loss. Because of their opposite pressure dependence there is a noble-gas pressure, typically between 10 and 250 Pa, for which the sum of wall and volume losses is a minimum. In actual lamps

a noble-gas pressure a little in excess of this range (e.g. 400 Pa) is often chosen in order to realize a sufficiently long electrode life.

Today the discharge is essentially the same as 50 years ago. However, significant progress has been made in the quantitative understanding of its rather complex dependence upon various parameters. It is now known, for example, how the electron temperature and thus the electrical and radiative properties can be modified by changing the noble-gas composition, the discharge tube cross-section or by the use of a special recombination structure^[6]. Such knowledge has been of paramount importance for the development of compact lamps.

Modelling and diagnostics

Detailed numerical modelling of gas discharges has been pursued vigorously in the past thirty years. Both the availability of large computers and the need for optimizing gas discharges for lasers have stimulated this trend. For the mercury noble-gas discharge fairly detailed descriptions have been given in the fifties and the early sixties^[7]. Within Philips several refinements have been added. For the radiation transport on the 254-nm line Lorentz broadening has been taken into account in the theory. A more realistic electron energy distribution function takes account of the depletion of high-energy electrons due to the excitation processes^[8]. Molecular ion formation has been recognized as an important ionization process^[9]. Very recently an improved description of radiation transport on the 185-nm line has been formulated^[10].

It is the aim of the models to enable the calculation of the electric field, the electron (and ion) density, and the production of radiation and heat for given values of the mercury-vapour and noble-gas pressure, the tube diameter and the discharge current. At present the required quantities can be obtained with high accuracy (better than 10%) for a wide range of parameter values. With that level of performance the models can be used to advantage as a tool in lamp development. When applied carefully they help to reduce the number of experiments required for design optimization. Moreover, a good knowledge of the homogeneous stationary discharge is extremely useful for the study of more complex phenomena such as mercury transport through cataphoresis and striation-type inhomogeneities in the light distribution over the lamp.

In a discharge the charged particles, ions and electrons, are accelerated in the electric field and thus pick up energy and momentum, which are subsequently transferred to the neutral particles in collisions. The transfer is very efficient for the ions and as a result the ions are not heated much above the temperature of

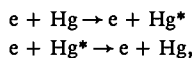
the noble gas. On the other hand it is rather inefficient for the electrons which, as a result, heat up to such high temperatures that they can raise the mercury atoms from the ground state to some excited state, or even ionize them. Little excitation of the noble-gas atoms can occur, however, since too much energy is required for that process.

The mercury atom has an infinite number of excited states. Only a small number of these reaches a significant population and has to be accounted for in the models. A simplified energy-level diagram is presented in fig. 3. The following levels are indicated:

- The ground state 6^1S_0 .
- The excited state 6^3P_1 . The transition from this state to the ground state gives emission of ultraviolet radiation at 254 nm. It is the most important atomic transition in fluorescent lamps: nearly 60% of the electrical power input is transformed into 254-nm radiation, which is then transformed into visible light by the phosphor layer.
- The metastable states 6^3P_0 and 6^3P_2 . Atoms in these states cannot decay to the ground state by radiation. However, they act as energy buffers, which can come into the 6^3P_1 state or transfer their energy to the electrons. Alternatively, they may diffuse to the wall and release their energy there.
- The excited state 6^1P_1 . The transition from this state to the ground state gives emission at 185 nm. This radiation contributes between 10 and 30% of the total ultraviolet output.
- The excited state 7^3S_1 . The transitions from this state to the $6P$ states lead to visible-emission peaks.
- The ground states of the mercury ions Hg^+ and Hg_2^+ . Although only a small percentage of the atoms are ionized, it is the electrons produced in the ionizations that sustain the discharge and provide the electrical conductivity.

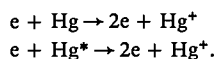
The most important processes that have to be considered are the following:

- Elastic collisions. The electrons collide with the heavy particles and transfer kinetic energy: the gas is heated.
- Electron impact excitation and de-excitation. In the collisions the atoms go to states of higher or lower energy, while the electrons lose or gain that same amount of energy:

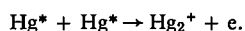


where Hg and Hg^* represent ground-state and excited state mercury atoms.

- Electron impact ionization:



- Associative ionization. Two excited Hg atoms combine to form a molecular ion plus an electron:



- Emission and absorption of ultraviolet and visible radiation.
- Diffusion of particles to the wall, where electrons and ions recombine and mercury atoms in excited states return to the ground state.

These processes must obey certain continuity equations which, for the case of a stationary discharge, take the form of conservation laws. The conservation of particles requires that, for example, the rate at which ions and electrons are generated by electron impact and associative ionization must equal the rate at which they are lost by volume recombination or diffusion to the wall. Energy conserva-

tion implies that the electrons pick up energy from the electric field at the same rate as they lose it by collisions with the heavy particles or by recombinations at the wall.

To calculate the rates for the various processes one must know the relevant cross-sections. Many cross-sections are known with good accuracy from detailed atomic collision studies or spectroscopic measurements. For others, such as associative ionization, the data are still rather poor. For the electron-impact processes the rates depend strongly on the electron-energy distribution. Its determination forms a major problem. To limit the complexity of the calculations some simplifying approximations are usually made. Thus it is often assumed that the distribution is Maxwellian, to be characterized by a single parameter, the electron temperature. In such an approach the tendency is to overestimate the density of the high-energy electrons, which are responsible for the excitation processes. Better results are obtained with L. Vriens's 'two-electron-group' model [8], describing the distribution with two temperatures, for low-energy and high-energy electrons.

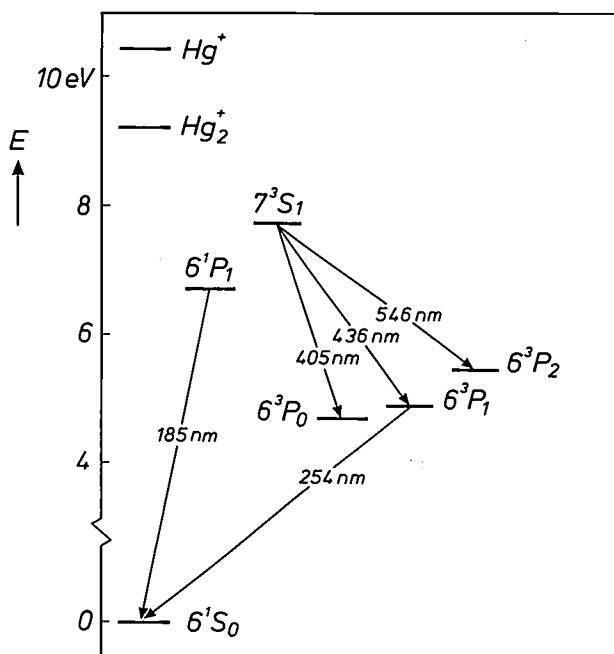


Fig. 3. Energy levels of the states of a mercury atom that are most significant in fluorescent lamps, and of the ground states of the mercury ions Hg^+ and Hg_2^+ . The only radiative transitions to the atomic ground state that are of significance here are those from the 6^1P_1 and 6^3P_1 states; they give ultraviolet radiation at 185 and 254 nm respectively. The transitions shown between excited states give visible emission lines.

- [6] J. Hasker, A new concept for fluorescent lamps, *J. Illum. Eng. Soc.* 6, 29-34, 1976.
- [7] C. Kenty, Production of 2537 radiation and the role of metastable atoms in an argon-mercury discharge, *J. Appl. Phys.* 21, 1309-1318, 1950; J. F. Waymouth and F. Bitter, Analysis of the plasma of fluorescent lamps, *J. Appl. Phys.* 27, 122-131, 1956; M. A. Cayless, Theory of the positive column in mercury rare-gas discharges, *Br. J. Appl. Phys.* 14, 863-869, 1963.
- [8] The energy balance of electrons in the gas discharge has been described by L. Vriens, *J. Appl. Phys.* 44, 3980-3989, 1973, and by L. Vriens and F. A. S. Lighthart, *Philips Res. Rep.* 32, 1-7, 1977.
- [9] The ionization processes in the gas discharge have been described by L. Vriens, R. A. J. Keijser and F. A. S. Lighthart, *J. Appl. Phys.* 49, 3807-3813, 1978.
- [10] H. A. Post, Excitation and radiative decay of the 184.9 nm Hg resonance line in low-pressure mercury noble-gas discharges, Thesis, Eindhoven 1985.

To indicate how the insights gained from the modeling can be put into practice, we consider the development of compact lamps. As explained later on, a reduction in size must preferably be obtained by an increased electric field at a constant current. With an unmodified gas filling this implies an increased input of power and a decreased number of electrons per unit length. Consequently the average electron energy increases and so does the ionization rate. To restore the particle balance the recombination rate must be increased as well. This can be realized by introducing a recombination structure^[6] or by using a narrower tube. In both cases electrons and ions diffuse more easily to the region of recombination. Another approach is to try to adapt the noble-gas composition.

Diagnostic measurements are essential to build up an understanding of the discharge and to check the validity of the models. Preferably those quantities should be measured that play a primary role in the models. Early work carried out within Philips involved measurements of electron densities and temperatures with Langmuir-probe techniques, and also absolute radiation measurements^[11]. More recently, laser diagnostics have been applied for determining excited-state densities, imprisonment times of resonant photons, excitation cross-sections and oscillator strengths^[12]. The laser diagnostics of the low-pressure mercury-noble-gas discharge will shortly be reviewed in this journal^[13]. A comparison of measured densities of mercury atoms in the 6^1P_1 state with those calculated from the models is presented in *fig. 4*. The calculated values depend strongly on the effective radiative lifetime of atoms in this state. The good agreement between theory and experiment shown here has only been obtained with a recent, greatly improved, treatment of the radiation imprisonment at the 185-nm resonance line^[10].

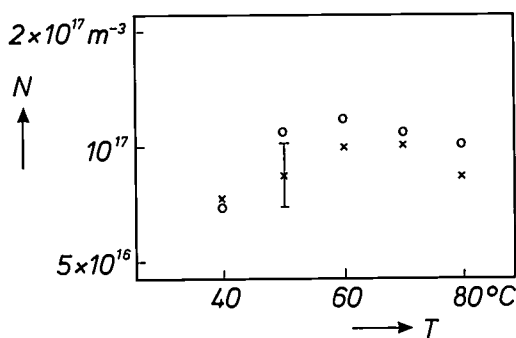


Fig. 4. Comparison between calculated (O) and measured (x) densities N of mercury atoms in the 6^1P_1 state, as a function of the wall temperature T of a discharge tube. The tube has a diameter of 15 mm, the discharge current is 500 mA and the noble gas used is argon at a pressure of 400 Pa. Within the experimental error of about 20% (denoted by a vertical bar) the measured densities agree well with the calculated values.

Materials

Throughout the history of electrical light sources the discovery and development of new materials has led to significant advances in their performance. This is especially true for fluorescent lamps; indeed most of the major steps forward have been made possible by the availability of new or improved materials. Examples are new phosphors, amalgams for the control of the mercury vapour pressure and emitter material for electrodes.

As already mentioned in the introduction, early fluorescent lamps used phosphors based on zinc beryllium silicates. These compounds were later found to be a serious health hazard. In 1948 the safe halophosphate phosphors were first used in fluorescent lamps and they have been further developed and perfected in the following decades. A typical emission spectrum of a fluorescent lamp with a halophosphate phosphor is shown in *fig. 5*. The spectrum consists of the phosphor-emission bands and the visible mercury lines generated directly by the gas discharge.

The next major breakthrough came in the nineteen-seventies. Theoretical studies showed that, by limiting the visible radiation to specific narrow bands, it is possible to obtain a high luminous efficacy together with a high colour-rendering index^[14]. Such results require a proper choice of the wavelengths and the intensity ratios of three narrow spectral bands. The correlated colour temperature can also be chosen over a wide range by varying the balance between the emission bands. Phosphors with the necessary narrow emission bands have been developed, thus transforming the theoretical predictions into working lamps^[15]. A typical emission spectrum of such a fluorescent lamp is given in *fig. 6*. It shows the narrow emission bands from the three phosphors in the lamp, together with the visible mercury lines.

These new phosphors also have another advantage. Compared with the standard halophosphates they can withstand a higher ultraviolet radiation intensity. This leads to an improved lamp maintenance and makes possible a drastic further miniaturization of fluorescent lamps as described in the following section.

Until recently special De Luxe lamps with excellent colour-rendering characteristics had a fairly low luminous efficacy. However, it has been discovered that the efficacy can be increased considerably, while maintaining the colour rendering, by combining five different emission bands rather than the above three bands^[16]. In order to generate such a spectrum as shown in *fig. 7* three newly developed phosphors were necessary as well as two standard calcium halophosphate phosphors. It has also been found that two of the phosphors can generate double emission bands so

that the necessary five emission bands can be obtained with a blend of three phosphors.

For standard fluorescent lamps the temperature of the discharge-tube wall is such that the optimum mercury vapour pressure (0.9 Pa) for efficient radiation generation is realized. However, if the wall loading is increased, as is possible with the new phosphors, then the discharge tube is almost always too hot and extra

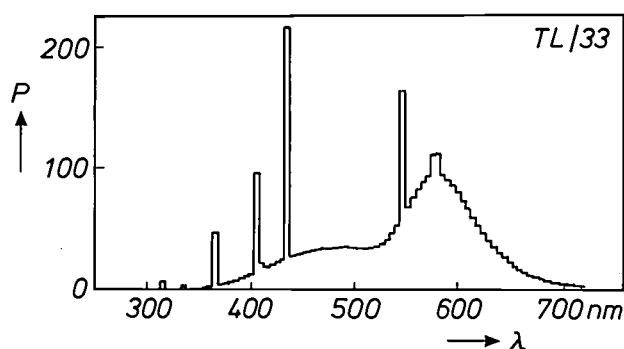


Fig. 5. Spectral distribution of a standard fluorescent lamp (36 W, colour 33) with a halophosphate as phosphor. The normalized spectral power P is plotted as a function of the wavelength λ ; P is the power emitted in a wavelength range of 5 nm for a total luminous flux of 10^6 lm. The spectrum contains broad phosphor-emission bands, with some visible mercury lines.

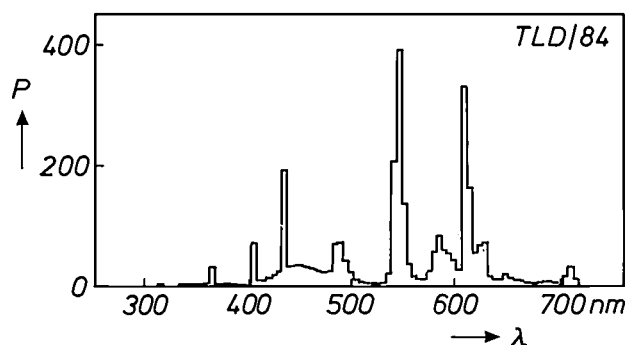


Fig. 6. Spectral distribution of a fluorescent lamp with an increased colour rendering (36 W, colour 84). The three phosphors in the lamp give narrow emission bands.

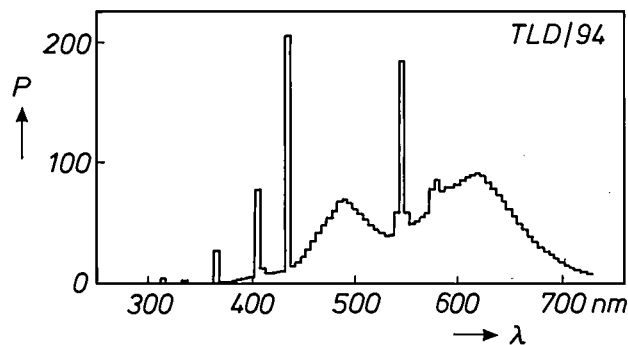


Fig. 7. Spectral distribution of an efficient De Luxe lamp (36 W, colour 94). The lamp contains two halophosphate phosphors with broad emission bands and three new phosphors with narrow emission bands.

measures have to be taken to maintain the optimum vapour pressure. This can take the form of a lower-temperature appendix which controls the mercury vapour pressure but in certain situations such a measure is not possible.

Another possibility is the use of an amalgam which at the operating temperatures is both in the solid phase, with only little mercury, and in the liquid phase, with a relatively high mercury content^[17]. At higher temperatures the mercury in the liquid is diluted by the partial melting of the solid. This counteracts the more intense evaporation from the liquid, so that the mercury vapour pressure above an amalgam is less dependent on temperature than it is above pure mercury. Fig. 8 shows, as a function of temperature, the mercury vapour pressure above pure mercury and above various compositions of a suitable amalgam, namely In-Bi-Hg^[18]. The mercury vapour pressure for which the lamp luminous flux is at least 90% of its maximum value is also indicated. From this figure it is seen that with an amalgam not only is a higher wall temperature possible but that the temperature range within which the lamp operates close to its optimum is significantly increased. When the lamp is initially switched on at room temperature the presence of an amalgam results in a lower initial mercury vapour pressure and hence a lower luminous flux than would have been the case with pure mercury. Thus an auxiliary amalgam is often necessary to generate a sufficiently high mercury vapour pressure immediately after ignition. Amalgams are applied in compact fluorescent lamps in which the discharge tube is integrated with the control gear to form a single unit.

In a fluorescent lamp the electrodes almost always consist of double or triple coiled helices. These are

- [11] Probe measurements of particle densities and electron mobilities have been carried out by W. Verwey, see Philips Res. Rep. Suppl. 1961, No. 2, and absolute radiation measurements by M. Koedam, A. A. Kruithof and J. Riemens, see Physica 29, 565-584, 1963.
- [12] Effective demonstrations of the utility of laser diagnostics have been given by H. A. Post, J. Phys. B 17, 3193-3208, 1984 and by P. van de Weijer and R. M. M. Cremers, J. Appl. Phys. 53, 1401-1408, 1982 and 57, 672-677, 1985.
- [13] P. van de Weijer and R. M. M. Cremers, Laser diagnostics for low-pressure mercury discharges, to be published in Philips Tech. Rev. 43, No. 3.
- [14] M. Koedam and J. J. Opstelten, Measurement and computer-aided optimization of spectral power distributions, Lighting Res. & Technol. 3, 205-210, 1971; W. A. Thornton, Luminosity and color-rendering capability of white light, J. Opt. Soc. Am. 61, 1155-1163, 1971.
- [15] J. M. P. J. Verstegen, D. Radielović and L. E. Vrenken, A new generation de luxe fluorescent lamps, J. Illum. Eng. Soc. 4, 90-98, 1975.
- [16] This result was presented by J. T. C. van Kemenade, E. G. Berns and R. C. Peters, 20th Session of the CIE, Vol. 1, Amsterdam 1983, pp. D702/1-D702/4.
- [17] The use of amalgams for reducing the temperature dependence has been described by (for example) K. Eckhardt and B. Kühn, Lichttechnik 22, 389-393, 1970.
- [18] J. Bloem, A Bouwknegt and G. A. Wesselink, Amalgams for fluorescent lamps, Philips Tech. Rev. 38, 83-88, 1978/79.

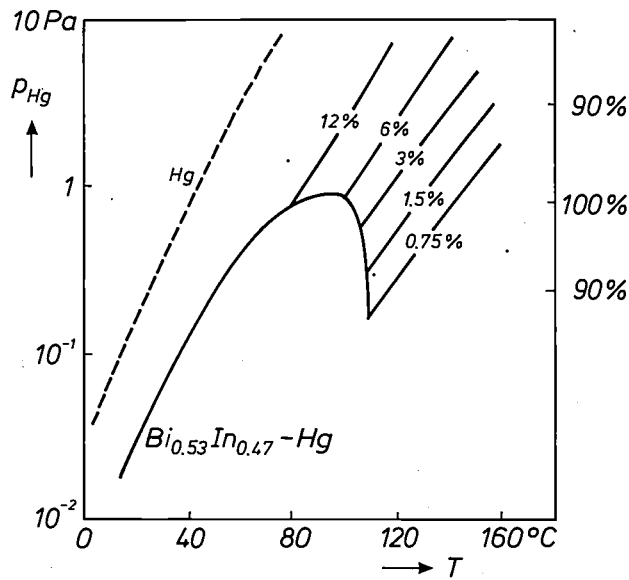


Fig. 8. Mercury vapour pressure p_{Hg} above the amalgam $\text{Bi}_{0.53}\text{In}_{0.47}\text{-Hg}$ for five different mercury contents and above pure mercury, as a function of temperature. The mercury vapour pressure at which the relative luminous flux of a fluorescent lamp is at a maximum is shown at the right, and also the pressures at which it reaches 90% of the maximum value. The pressure above the amalgams is considerably lower than that above pure mercury and varies much less with temperature. For the amalgams there is a relatively wide temperature range within which the vapour pressure differs very little from the optimum value.

coated with an emitter material usually consisting of a mixture of the oxides of barium, calcium and strontium. Gradual improvements to the structure and processing of the electrodes have led to the present long life performance. More detailed information can be found in various articles [19].

New fluorescent lamps

Thin lamps with narrow emission bands

Until the mid-seventies the 'standard' fluorescent lamp (type 'TL') was one with an external diameter of 38 mm and coated on the inside with a halophosphate phosphor. The 40-W version (1.2 m long) of such a lamp had typically a luminous efficacy of 80 lm/W and a general colour-rendering index of 67 (100 is ideal). With the introduction of phosphors with three narrow emission bands it was possible to improve both of these lamp characteristics. However, other changes were also possible.

As already noted, these new phosphors are capable of withstanding high ultraviolet radiation levels. Thus it became attractive to decrease the tube diameter to 26 mm. The increase in the lamp voltage due to the smaller lamp diameter can be compensated by replacing the usual neon-argon mixture with a krypton-argon or krypton-neon one, thus leading to a more efficient discharge. This lamp is mechanically and

electrically interchangeable with existing 38-mm diameter lamps in glow-switch starter circuits. The input power for the 1.2 m long version has been reduced from 40 W to 36 W, i.e. the increase in efficiency has been used to decrease the lamp power rather than to increase the luminous flux. In *Table I* the old 'standard' lamp and the new slimmer three-emission-band lamp are compared.

These thinner lamps have a further advantage. In existing luminaires designed for the 38-mm lamp, the 26-mm lamp leads to an improvement of the optical luminaire efficiency by, on average, about 5%. This is due to the fact that the thinner lamp gets less in the way of its own light.

New De Luxe lamps

The discovery and development of suitable phosphors with narrow emission bands has also resulted in a new generation of De Luxe lamps. By applying the phosphor blend mentioned with five emission bands, lamps are obtained which have a high luminous efficacy in addition to the required colour rendering. The new phosphors can also be used in narrow (26-mm diameter) lamps since they have much improved maintenance characteristics compared with the older phosphors. In *Table II* the properties of such a lamp are compared with those of two older types of De Luxe lamps with a diameter of 38 mm. The luminous efficacy of the new lamp is about 25% and 45% higher, while the general colour-rendering index does not deviate much. This lamp is also mechanically and electrically interchangeable with its predecessors in glow-switch starter circuits.

Table I. Characteristics of a standard fluorescent lamp and a new thinner lamp with three phosphors giving narrow emission bands. The data apply to 1.2-m lamps.

Lamp type	Diameter (mm)	Emission spectrum	Power (W)	Luminous efficacy (lm/W)	General colour-rendering index
TL/33	38	fig. 5	40	80	67
TLD/84	26	fig. 6	36	96	85

Table II. Characteristics of two old types of De Luxe lamp and a new thinner one with a special phosphor blend giving five emission bands (fig. 7). The lamps are 1.2 m long and the colour temperature is about 4000 K.

Lamp type	Diameter (mm)	Power (W)	Luminous efficacy (lm/W)	General colour-rendering index
TL/34	38	40	53	87
TL/37	38	40	45	96
TLD/94	26	36	65	93

Compact fluorescent lamps

Fluorescent lamps, which are very efficient light sources, are very widely used, but until a few years ago they were little used in the domestic environment. During the last decade there has been an increasing interest in energy-efficient light sources but fluorescent lamps were often found to be too large for domestic applications. However, the development of new phosphors, as described above, has made miniaturization of fluorescent lamps possible.

In order to realize a compact lamp it is necessary to increase the power dissipation per unit length of the discharge while at the same time retaining the efficiency of the discharge as much as possible. Increased dissipation can be obtained by either increasing the discharge current or by increasing the discharge electric field.

A viable solution is not normally realized when the discharge current is increased. Due to the discharge characteristics an increase in the current leads to a relatively smaller increase in the power dissipated and to a decrease in the radiation efficiency. However the electrode losses are proportional to the discharge current and the losses in the control gear are often more than proportional to the discharge current. All this leads to a relatively small increase in the light output at the expense of a relatively large increase in the system power.

The other alternative is an increase in the electric field. This can be realized by a reduction of the discharge-tube diameter, the application of a special recombination structure^[6] or the use of neon or helium or both as the buffer gas. Of course, various combinations of these options are also possible. The various alternatives have been investigated extensively^[20]. Fig. 9 shows some experimental and theoretical results. Here the discharge-column efficacy is plotted as a function of the electric field for a given discharge current. It is seen that, for a specified electric field, the discharge efficiency is almost independent of the measure which is used, provided that a proper optimization has been carried out.

In making a final selection other aspects must be taken into consideration. If neon or helium is used then the electrode life may be shorter, while there are technological problems associated with a recombination structure. A reduction of the tube diameter is often the most acceptable solution.

As can be seen from fig. 9 the higher the electric field, and thus the shorter the lamp, the lower the luminous efficacy. For a specified luminous flux there are optimum values for the tube length and diameter. For domestic areas where a luminous flux per lamp in the range 600 to 1200 lm is commonly required, an

optimum solution is often a discharge tube typically 300 to 500 mm long and with an internal tube diameter of about 10 mm. In order to realize a still more compact lamp various further size-reducing measures can be applied. Some configurations used at the present time are:

- A discharge arrangement in the form of two or four parallel tubes with external control gear^[20]. This modification, known as the PL* lamp, is shown in fig. 10.
- A 'square' discharge arrangement again with external control gear^[21].
- A doubly folded discharge tube with integrated control gear^[20]. This modification, known as the SL* lamp, is shown in fig. 11.

In these compact lamps with a high wall loading the discharge tube is almost always too hot, so that extra measures have to be taken to maintain the optimum vapour pressure. One alternative is to create a lower-temperature region, as has been done for PL* lamps (fig. 10). The bridge connecting the two discharge tubes is located some way from the tube ends. In this way there is no power dissipation at the ends which thus act as a low-temperature appendix. However, if the complete discharge tube is integrated with the control gear to form a single unit, as in the SL* lamp (fig. 11), then it is extremely difficult, if not impossible,

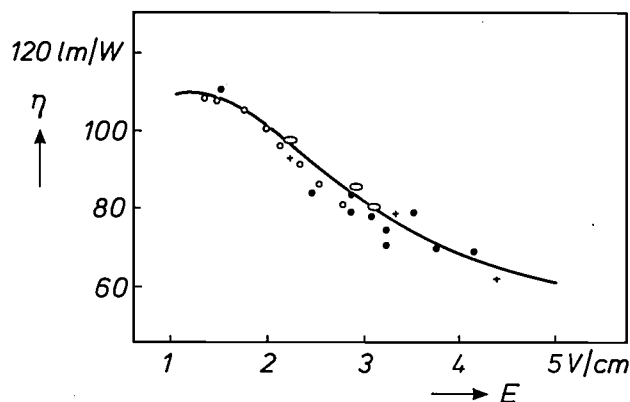


Fig. 9. Efficacy η of the discharge column as a function of its electric field E , for different discharge tubes at a discharge current of 200 mA. The variation of η with E was determined experimentally by variations of the tube diameter (O) and noble-gas composition (●) or by using different elliptical cross-sections (◻) and recombination structures (+). The line shown is the relation found from model calculations fitted to the experimental data at $E = 1.8$ V/cm. The experimental decrease in efficacy agrees well with the calculations and does not depend on the way in which the field increase is obtained.

^[19] See for example A. Bouwknecht, H. Nienhuis, D. J. Schipper and P. A.W. Tielemans, *Electrodes in discharge lamps*, Philips Tech. Rev. 35, 356-359, 1975.

^[20] A. Bouwknecht, *Compact fluorescent lamps*, J. Illum. Eng. Soc. 11, 204-212, 1982.

^[21] This modification has been described by A. H. Willoughby and B. H. Cannell, *Thorn Lighting J.* 24, 2, 1982.

to create the necessary cool area. In such a case an amalgam system is used in order to maintain the proper mercury vapour pressure.

The PL* and SL* lamps shown here are increasingly applied to replace incandescent lamps in locations

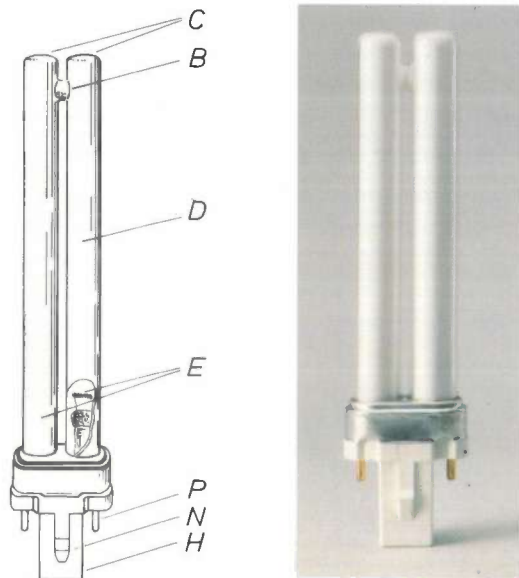


Fig. 10. Diagram and photograph of a PL* lamp consisting of two parallel 'half' discharge tubes *D*, only a few millimetres apart, and connected by a small bridge *B* containing the discharge. The top of the lamp contains cold areas *C* preventing the mercury vapour pressure from becoming too high. At the bottom are the electrodes *E*, a two-pin electrical connection *P*, a retention notch *N* and the housing *H* for starter and capacitor, which are integrated with the discharge tube and mounted in the lamp cap.

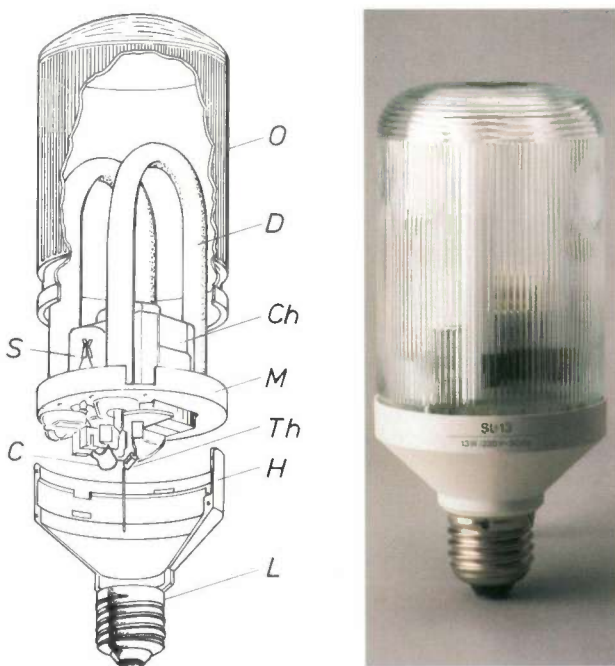


Fig. 11. Exploded view and photograph of an SL* lamp. Ballast, starter and the folded discharge tube *D* are integrated in a single unit. *O* outer bulb. *Ch* choke. *S* starter. *M* mounting plate. *Th* thermal cut-out. *C* capacitor. *H* housing. The lamp cap *L* is the same as in conventional incandescent lamps, so that the same fitting can be used.

such as homes, hotels, museums and theatres. They have about the same luminous flux and colour rendering, but require much less energy (a factor of more than four) and have about five times the life. Application of PL* lamps with their special flat configuration and low heat production offers new opportunities for miniaturization of the luminaire design. A particular feature of SL* lamps is that they have the same lamp caps as conventional incandescent lamps, allowing SL* lamps to be used in existing luminaires.

High-frequency operation of fluorescent lamps

It has been known for a considerable time that high-frequency operation as opposed to 50- or 60-Hz operation of fluorescent lamps leads to improvements in the lamp luminous efficacy [22]. In general the changes in the radiation efficiency of the positive column are not all that great as the supply frequency is increased. Numerical modelling of a.c. discharges shows a very slightly decreasing column efficiency from d.c. to about 500 Hz and then an increase to slightly above the d.c. value at some tens of kHz [23]. The main improvement of high-frequency operation is due to the decrease in the voltage fall near the electrodes.

Although high-frequency operation of fluorescent lamps has been applied on a small scale for special applications for some considerable time, it is only very recently that much larger-scale application has become both technically and economically feasible. The combination of new phosphors and high-frequency operation has resulted in lamps with a luminous efficacy of 100 lm/W combined with a very good colour rendering. Fig. 12 shows the power balance determined for such a lamp [24]. From this power balance it is seen that a major loss occurs on the conversion of ultraviolet to visible radiation. Since each ultraviolet photon absorbed in the phosphor produces only one visible photon, a power conversion loss of more than 50% occurs for ultraviolet radiation at 254 nm.

High-frequency operation of fluorescent lamps not only increases the efficacy, it also offers new and far-reaching possibilities for energy management. If electronic control gear rather than conventional magnetic control gear is used for fluorescent lamps, then it is relatively easy to add extra control functions. For example the level of artificial lighting can be adjusted to complement the amount of daylight that enters via the window. Another possibility is to detect the presence of occupants in a given area and to switch off or dim the lighting shortly after their departure. It is also possible to integrate the lighting control with a com-

puter which manages the total environment in a building. These are only some of the energy-management possibilities which could be realized with electronic control gear for fluorescent lamps.

efficiency: nearly every ultraviolet photon yields one visible photon. However, the energy efficiency is limited because an ultraviolet photon has two to three times the energy of a visible photon. Phosphors that

power consumption 32 W				
in discharge 29.7 W				loss at electrodes 2.3 W
near UV 0.2 W	visible emission 1.1 W	UV radiation 20.6 W		loss in discharge 7.8 W
phosphor				
		visible emission 8.1 W	heat 12.5 W	
near UV 0.2 W	total visible emission 9.2 W		total heat 22.6 W	

Fig. 12. Power balance of a high-frequency fluorescent lamp of 32 W with a luminous efficacy of 100 lm/W.

Outlook

Almost fifty years ago the first fluorescent lamps were introduced on to the market. Since then fluorescent lighting has developed into the preferred system for many applications, generating far more artificial light than all other sources combined. The major quality indicators have improved significantly. Luminous efficacy has increased three- to fourfold, life expectancy by a factor of five or more, while colour rendering and maintenance have also improved enormously. Where do we go from here?

Two recent trends have already been mentioned above. Electronic power supplies, with their advantage of higher system efficiency and the possibility of energy management, will gradually replace the conventional ballasts and starters in certain applications. In this field the lighting business will profit from the rapid progress being made in the semiconductor industry. Compact fluorescent lamps, with their inherent advantages of high efficiency and long life (hence low replacement costs) will find increased application both in professional and in domestic areas.

An important question is whether a significant further increase of luminous efficacy may be expected. The transformation of electrical energy into ultraviolet radiation already takes place at high efficiency in the discharge, and no great advances are possible there. The fluorescence process has a high quantum

would efficiently convert one ultraviolet photon into two visible photons could once more revolutionize the fluorescent-lamp field. No such phosphors are at present in sight, but since nothing in nature seems to prohibit their existence, another fifty years might suffice to make this engineer's dream come true.

[22] Light systems with high-frequency fluorescent lamps have been described by (for example) J. H. Campbell, *Illum. Eng.* 55, 247-256, 1960.

[23] Calculations on the effect of the supply frequency have been described by P. C. Drop and J. Polman, *J. Phys. D* 5, 562-568, 1972.

[24] The power balance of a fluorescent lamp with new phosphors and high-frequency operation has been reported by J. W. F. Dorleijn and A. G. Jack, *J. Illum. Eng. Soc.* 15, 75-84, 1985.

Summary. In fluorescent lamps, mercury atoms in a noble-gas environment are excited by a gas discharge to emit ultraviolet radiation, which is converted into visible light by a phosphor layer. Since the first applications, almost fifty years ago, there have been many significant improvements of the lamp performance. Insights gained from extensive investigations on the processes in the gas discharge have permitted important improvements of the lamp geometry and gas composition. Both a high luminous efficacy and an excellent colour rendering are obtained with a suitable combination of narrow-band-emitting phosphors. The temperature dependence of the mercury vapour pressure can be reduced by using an amalgam instead of pure mercury. Long lives can be obtained with good design and appropriate processing of the electrodes. In addition to the steady improvements in standard tubular lamps ('TL') with an external diameter of 38 mm and a typical length of 1.2 m, there have been some revolutionary developments in recent years. These include a drastic reduction of the diameter (e.g. to 26 mm) and the introduction of compact lamps (PL* and SL*) and high-frequency operation for a further increase in efficacy and better energy management.

Medical systems in the last half century

C. Kramer and P. J. M. Botden

Prelude

Like many activities of Philips, those of the Medical Systems Division (MSD) stemmed originally from the manufacture of incandescent lamps. In this case there happened to be some radiologists in the Netherlands during World War I who were no longer able to get their 'röntgen lamps' as they were then called, repaired

the foundation of an independent and prosperous business. In 1927 the shares of C. H. F. Müller were acquired by Philips.

The period up to 1936 saw substantial further developments of the X-ray tube. The most important one was the incorporation of the tube in a shield, a neat

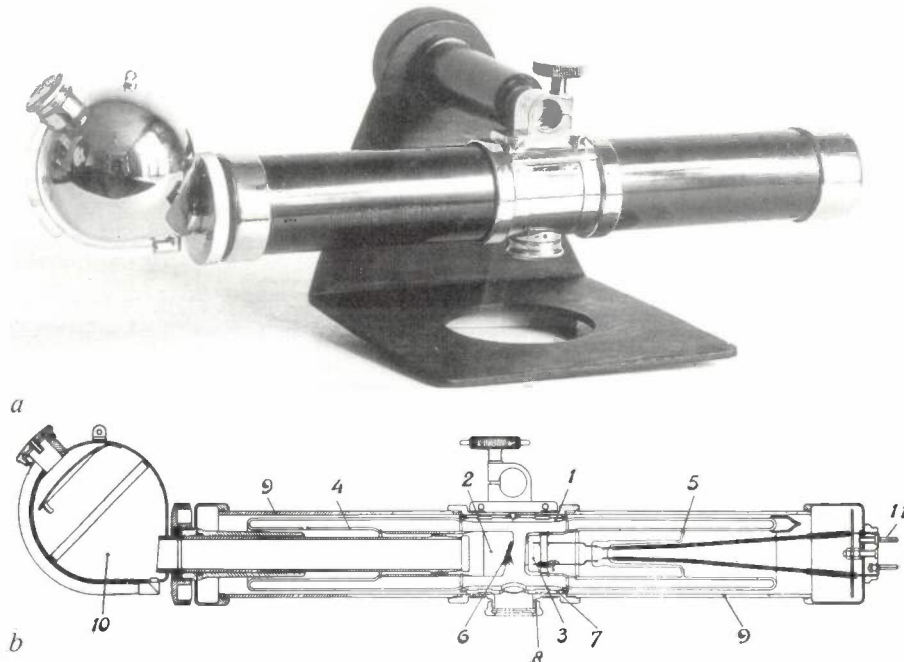


Fig. 1. The Philips Metalix, the first X-ray tube with radiation protection (1924). *a*) The Metalix tube, mounted on a Philite holder. *b*) Cross-section of the tube. 1 ferrochromium envelope. 2 anode. 3 cathode. 4 glass connection between anode and envelope. 5 glass connection between cathode and envelope. 6 tungsten target with line focus. 7 lead shield for radiation protection. 8 window. 9 Philite cylinders. 10 water cooler. 11 pin for filament-current connection.

in Germany. They therefore applied to Philips to see whether anything could be done to help. The answer appears to have been in the affirmative, and an X-ray business grew up which was the first diversification of the Philips incandescent-lamp operations.

Before that time, in 1896, the glass-blowing plant of C. H. F. Müller had already embarked on the manufacture of 'röntgen lamps' in Hamburg. This led to

Ir C. Kramer is with the Philips Medical Systems Division, Best; Drs P. J. M. Botden was with this Division before his retirement.

form of protection from radiation (*fig. 1*). This invention, the work of A. Bouwers, was of great significance because in the early history of X-ray diagnostics many radiologists had fallen victim to the then mysterious radiation sickness. Other advances of that time were the application of a directly heated cathode, invented by W. D. Coolidge, and cooling of the tube, first with water and later with oil. The introduction of the rotating anode^[1], also by Bouwers, dates back to this period.

1936-1946

In this period a great deal of work was done on the further development of the rotating-anode tube (fig. 2). This has the great advantage of allowing a considerably higher current to be applied to a small focus during short exposures, resulting in sharper images. W. J. Oosterkamp developed the theoretical principles for this tube [2] while many others worked on the practical implications [3]. Also developed at that time were the power-supply units necessary to provide the greatly increased peak power at the high voltage for short periods [4].

The examination of patients was speeded up by the introduction of universal tables and stands for X-ray diagnosis (fig. 3). These made it possible to position a patient in the required orientation for fluoroscopy and radiography.

X-radiation now began to show its value in therapy, and special equipment was developed for this.

Further developments in X-ray work were temporarily halted by the outbreak of World War II. The X-ray-tube factory in Eindhoven was bombed in 1942 and the damage was difficult to repair in war time (fig. 4). Further work was also made virtually impossible by the lack of vital materials such as tungsten.

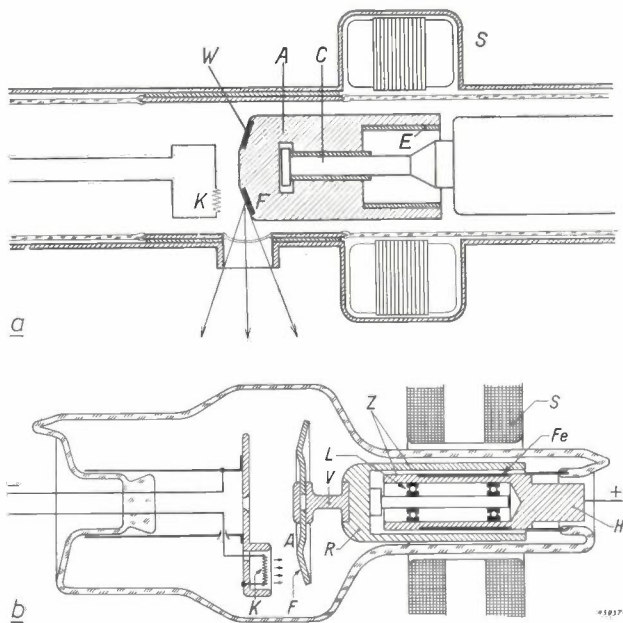


Fig. 2. X-ray tubes with rotating anode. *a*) The version originally developed by A. Bouwers, which was based on the conventional design for a stationary anode: a copper block containing a tungsten target. The block rotated on bearings (not shown) which were initially grease-lubricated. The anode was driven by a rotating magnetic field generated by a stator outside the tube. *b*) A later version, in which the anode consists of a solid tungsten disc that rotates on ball-bearings. Lead lubrication is used, because it does not degrade the vacuum — a problem with the original grease lubrication. The basic design remained the same for years, although the use of better materials and a higher speed of anode rotation permitted operation at higher power. The resulting higher temperature of the bearings required the use of silver to provide the lubrication.

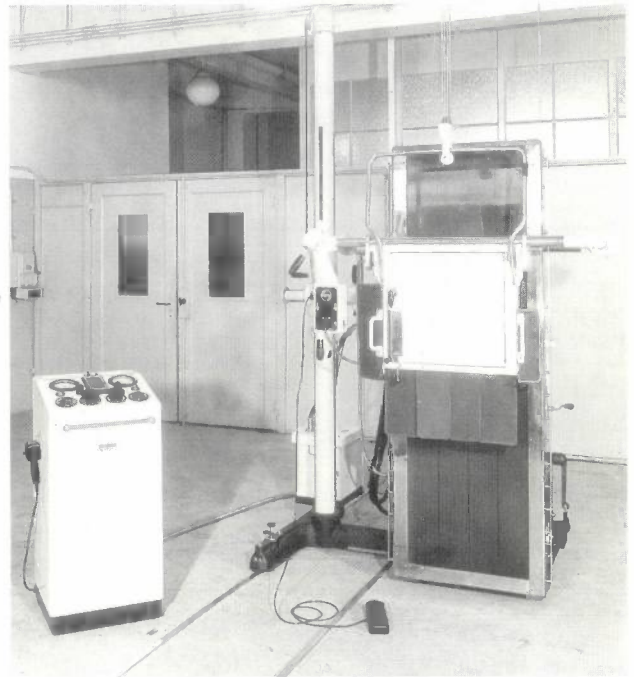


Fig. 3. The Standardoscoop II, the first manually tilting patient table with a retractable fluoroscopic screen, balanced by ceiling suspension. If a film cassette changer had to be used at the same time, the fluoroscopic screen and changer were fixed to their own balanced suspension, so that rapid interchange was possible.



Fig. 4. The results of the bombing in 1942. The assembly shop for X-ray tubes and rectifier valves was completely destroyed.

- [1] A. Bouwers, Een röntgenbuis met draaiende antikathode, *Physica — Ned. T. Natuurk.* 10, 125-134, 1930; also published in English in: X-ray research and development; a selection of the publications of the Philips X-ray Research Laboratories from 1923-1937, Philips, Eindhoven 1937, pp. 111-119.
- [2] W. J. Oosterkamp, *Philips Res. Rep.* 3, 49-59, 161-173 and 303-317, 1948.
- [3] J. H. van der Tuuk, *Philips Tech. Rev.* 3, 292-298, 1938 and 8, 33-41, 1946.
- [4] H. A. G. Hazeu and J. M. Ledebor, *Philips Tech. Rev.* 6, 12-20, 1941.

1946-1956

After the war the X-ray division, like all the other divisions of Philips, began the process of reconstruction and set about developing new X-ray products. The major trend in these years was the further specialization of equipment. An example was the Symmetrix stand [6], which enabled the radiologist to position the patient in any required orientation between upright and upside down (*fig. 5*). Because of the low luminance of the images obtained on the fluoroscopic screen at that time, fluoroscopy still had to be done in the dark. This period also saw the development of a new generation of power-supply units.

For mass X-rays for tuberculosis (then still highly relevant) a camera with a mirror-optical system was developed that produced an image of the X-ray screen on a small-format film [6]. An equipment was developed specially for dentists, the Oralix [7], in which X-ray tube and generator were combined in a highly compact unit.

Activities in this period were expanded by the acquisition of the French firm Massiot. The most interesting product of the firm was the Polytome, a device that made it possible to take radiographs in which one specific 'layer' in the patient was in sharp focus. This apparatus was based on an invention made in the twenties by B. G. Ziedses des Plantes, later a Professor of Radiology at Amsterdam.

The most significant event in this period, however, was the development of the X-ray image intensifier [8]. The much brighter image this produced made it unnecessary for the first time to examine a patient in a darkened room (*fig. 6*). The image intensifier was in fact an earlier invention due to M. C. Teves *et al.* in 1924, but at that time the idea was not capable of industrial implementation. This situation did not change until after World War II, when the technology developed for infrared night-viewing devices became available. After Westinghouse in the United States had brought out the first image intensifier, Philips was the first large X-ray firm to do so in Europe.

1956-1966

The development of the image intensifier did more than liberating the radiologist from darkness. It was soon realized that the brighter image on the output screen could be photographed so that rapid pictures could be made of smaller formats than true size (first 70 mm, later 100 and 105 mm).

The next step was to connect a television camera tube to the image intensifier. A breakthrough here was the invention at this period of the Plumbicon tube [9]. This enabled the radiologist to view the

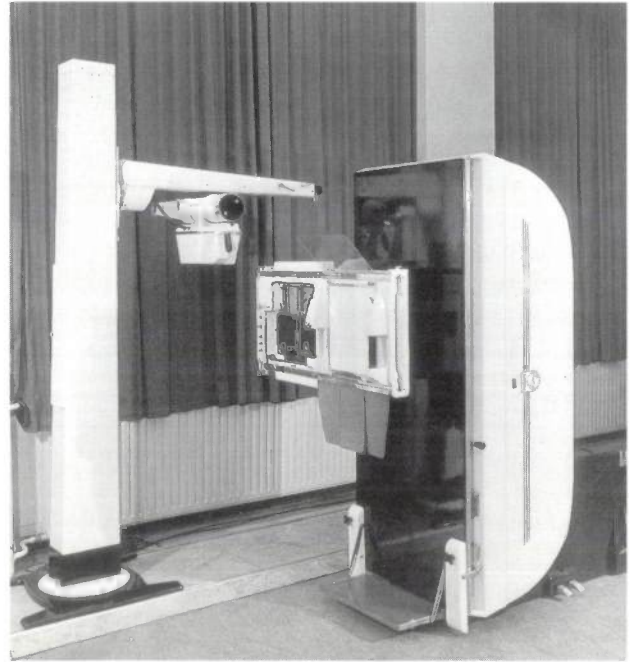


Fig. 5. The Symmetrix, the first X-ray equipment on which the patient could be examined upside down (the '90° Trendelenburg position'). The X-ray tube is mounted under the table. With a second tube, mounted on a travelling column, the same equipment could be used for radiography with the Potter-Bucky diaphragm. In a later version the table-top was made axially and laterally adjustable. Although the medical advantages of this freedom of movement were at first not so evident, it has since become an indispensable feature of diagnostic examinations.



Fig. 6. The Alfax, an X-ray image intensifier with a diameter of 9 inches, equipped with double mirror optics and a cine camera. During fluoroscopy two observers (e.g. radiologist and surgeon) could examine the image at the same time and film it when required.

fluoroscopic image on a monitor screen set up anywhere in the room, instead of from the output screen of the image-intensifier tube, which still had to be situated close to the X-ray beam. The image could now also be viewed by several people at the same

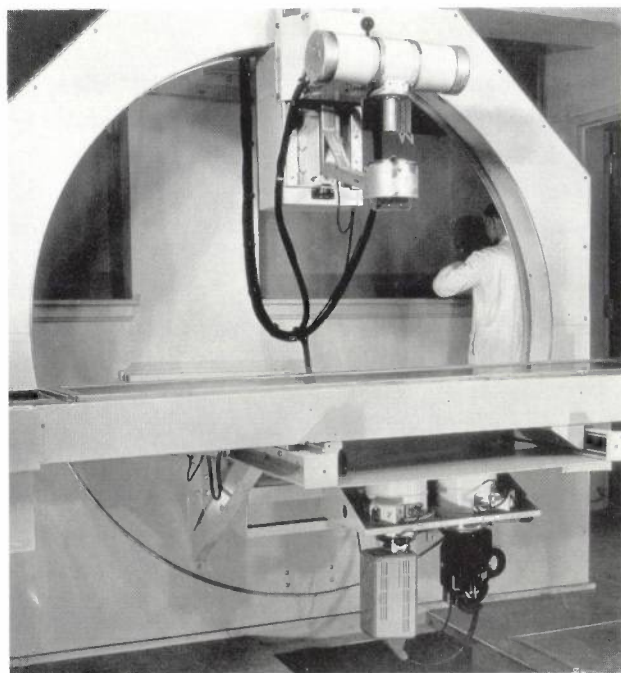


Fig. 7. The ring stand, the first remote-controlled X-ray table. The use of a vidicon television camera permitted remote viewing of the fluoroscopic picture, and small-format cine films could be taken at any required moment.



Fig. 8. A cobalt irradiation machine. The radioactive cobalt source is contained in a heavy shield, situated above the patient. The size of the irradiated area can be adjusted by means of remotely controlled shutters. The organ to be irradiated is moved into the centre of the beam. The cobalt source can rotate around the patient.

time, which was of particular importance in cardiovascular diagnostics.

With the advances in television technology it now made sense to build diagnostic equipment that could be remotely controlled by the radiologist from outside the examination room (fig. 7).

Another important application of the image intensifier was cinefluorography — taking cine films of the output screen. Attempts had already been made to take cine pictures of the fluoroscopic screen, but the

low luminance made this virtually impossible unless very high radiation doses were administered. The much brighter image of the image intensifier, however, could be filmed very readily^[10]. In combination with the technique developed earlier of introducing a catheter directly into the heart or the coronary arteries, for the selective injection of a contrast medium, detailed X-ray examination of the heart now became possible. In the development of this selective examination of the coronary arteries by Dr Mason Sones, a cardiologist associated with the Cleveland Clinics, Philips equipment played a major role.

The capability of the X-ray division was widened in this period by unifying the Philips and C. H. F. Müller programmes to form a single product range.

This decade also marked the beginning of various new activities not specifically concerned with X-rays. The first moves were made into nuclear medicine with a simple gamma camera, into ultrasound diagnostics with elementary equipment and into thermography^[11]. Irradiation equipment for radiotherapy was built that contained radioactive cobalt (fig. 8).

1966-1976

Following the introduction of the image-intensifier technique and the developments associated with it, the emphasis in X-ray work was mainly on further specialization. The programme was no longer limited to simple systems for making routine radiographs (Bucky tables^[12]) but was extended to include more complicated systems for abdominal and intestinal examinations, with versions for local operation and for remote control. In addition a whole range of specialized tables were developed, e.g. for surgery (the 'C-arc table'), for cardiovascular examinations, for cranial radiography and urology. This specialization was also reflected in the generators, for example in the Optimus generator for cardiovascular diagnosis.

Apart from the functional specialization in X-ray equipment there were also drastic changes in X-ray technology. Whereas at the beginning of this period

[6] J. J. C. Hardenberg and H. W. Dumbrill, Philips Tech. Rev. 17, 112-120, 1955/56.

[6] W. Hondius Boldingh, Philips Tech. Rev. 13, 269-281, 1951/52.

[7] J. Fransen, Philips Tech. Rev. 10, 221-230, 1948.

[8] M. C. Teves and T. Tol, Philips Tech. Rev. 14, 33-43, 1952/53. The application of the X-ray image intensifier was the subject of a series of six articles in this journal; see Philips Tech. Rev. 17, 69-97, 1955/56.

[9] E. F. de Haan, Philips Tech. Rev. 24, 57-58, 1962/63; E. F. de Haan, A. van der Drift and P. P. M. Schampers, Philips Tech. Rev. 25, 133-151, 1963/64.

[10] J. Feddema, Philips Tech. Rev. 17, 88-93, 1955/56.

[11] M. Jatteau, Philips Tech. Rev. 30, 278-289, 1969.

[12] See W. J. Oosterkamp, Eliminating scattered radiation in medical X-ray photographs, Philips Tech. Rev. 8, 183-192, 1946.

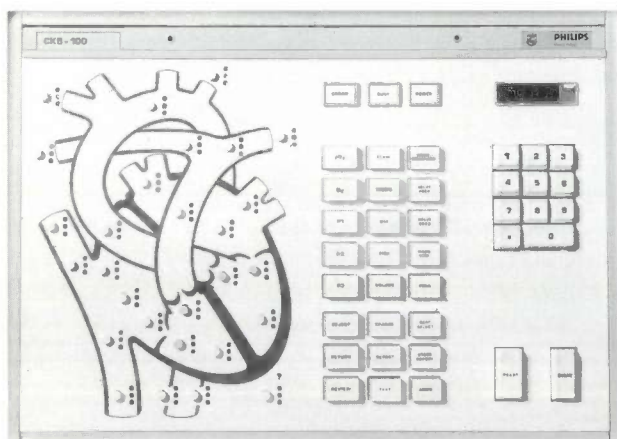


Fig. 9. Cardiological keyboard of the automated catheterization system. This system was used with a special cardiological X-ray system. During an examination one or more catheters with pressure or temperature transducers were introduced into the heart. The cardiologist could enter the position of these transducers from the keyboard, for further processing of the data in association with the resultant X-ray images.

nearly all the tables and generators were controlled by relays, at the end of the period most equipment included digital logic systems.

The Division also pushed ahead with activities, already started in the previous decade, concerned with other imaging techniques depending on radioactive isotopes and ultrasound. For the gamma camera a marked improvement in image quality and count rate was achieved by the use of a larger number of photomultipliers and digital image-processing techniques, which were then adopted by MSD as first in the field. The two-level 'black-and-white' images previously used with ultrasound were superseded by grey-level images, which had much greater diagnostic value. Our position in this field was substantially strengthened by the acquisition of the Californian company Rohe.

In radiotherapy the further development of the cobalt irradiator was accompanied by the advent of the linear accelerator as a source of both photons (gamma radiation) and electrons. A start was even made on an equipment for neutron irradiation, based on a deuterium-tritium nuclear reaction in a sealed-off tube [13]. For accurately planning irradiation with the cobalt generator and with the linear accelerator, a system was developed in which the irradiation is simulated beforehand by calculating the dose distribution.

The diversification of MSD, as the division came to be called in this period, was not however confined to imaging and therapy equipment. A Medical Electronics group was formed, which developed and manufactured a wide range of products. The most important one was the patient-monitoring equipment for use in intensive-care departments and equipment for physiological measurements, especially on the heart

(fig. 9). The group also made electronic respiratory equipment and defibrillators (for cardiac resuscitation by applying electrical pulses).

A range of products for medical data processing was also introduced, chiefly by C. H. F. Müller. This led to a pilot project for the automation of administrative tasks in hospitals, as well as to programmes for the automation of clinical laboratories, the management of hospital dispensaries, centres for population surveys and finally for the radiology department itself.

In 1972 the invention of the computerized tomograph, now better known as the CT scanner [14], came upon the radiological world as something of a surprise. This invention made it possible to obtain cross-sections of the human body with an unprecedented contrast by processing X-ray absorption data with a fast computer. This invention was first introduced by a complete outsider in the X-ray field, the British company EMI, and led in a very short time to a completely new situation in medical imaging techniques.

1976-1986

These developments forced the established X-ray firms to bring out their own computerized tomographic equipment very quickly. An initial product, the Tomoscan 200, was developed and manufactured by our company at Shelton in the USA. To keep abreast of the rapid advances in this field and the new 'generations' that were quickly following each other, a CT scanner was developed at the same time in the Netherlands: the Tomoscan 300. Further work on this led to the marketing of two greatly improved versions of

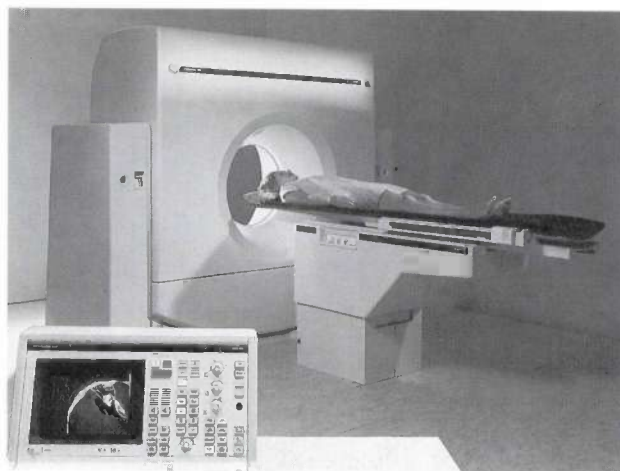


Fig. 10. The Tomoscan T 350. The patient is placed on the table and moved inside the scanner. During examination an X-ray tube rotates around the patient; at the same time a large number of detectors at the other end move around the patient. A computer calculates a cross-sectional image from the detector signals; the image can be examined on a screen.

this scanner, the Tomoscan 310 and later the 350^[15] (fig. 10).

This development, as well as other innovations that required a great deal of effort, obliged MSD to limit its product range so that staff and finance could be deployed to deal with all new activities at an adequate level. It was therefore decided to transfer the medical-electronics activities to Honeywell Medical Electronics, first in the form of a joint venture, later followed by MSD's complete withdrawal from this business. The MSD activities for the eighties were therefore defined as 'Systems for medical image diagnosis and radiation therapy'.

Along with the development of the CT scanner, work continued on the development of new X-ray systems, in which the use of microprocessors played an increasingly important part. This led to the marketing of computer-controlled generators, new remote-control stands and a new generation of examination equipment for cardiovascular diagnostics.

In image intensifiers and television technology, the leading feature was the development of a very large image intensifier (14 inches in diameter) in a completely new technology, with the large glass envelope largely replaced by metal. At the same time the image quality was considerably improved by refinements of the electron-optics and improvements in the method of manufacturing the input screen. Improved television cameras were also introduced, using twice the number of lines per frame for applications requiring a very high resolution. This development was based on a Plumbicon tube in which the sensitive area had been increased by a factor of two (fig. 11).

The use of television, particularly for angiography (examination of blood vessels), was given a new dimension by exploiting the potential of digital image processing. In digital subtraction angiography^[16] a series of X-ray pictures are made in rapid succession with an image intensifier and television monitor, digitized and stored in an image memory. Shortly before the first pictures are taken, the patient is injected with a contrast medium. Subtracting the image made before the contrast medium arrived, from an image obtained when the contrast medium was present gives an image that in principle only contains the contrast medium — so that the vascular system becomes visible (fig. 12). These images provide important diagnostic

^[13] O. Reifenschweiler and K. Nienhuis described this principle 24 years ago in Philips Tech. Rev. 23, 325-337, 1961/62.

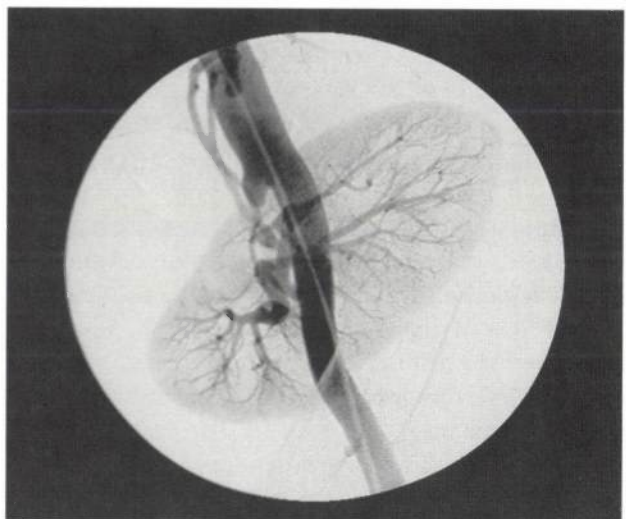
^[14] G. N. Hounsfield, Computerized transverse axial scanning (tomography): Part 1. Description of system, Br. J. Radiol. 46, 1016-1022, 1973.

^[15] F. W. Zonneveld, Computed tomography; possibilities and impossibilities of an anatomical-medical imaging technique, Acta Morphol. Neerl.-Scand. 23, 201-220, 1985.

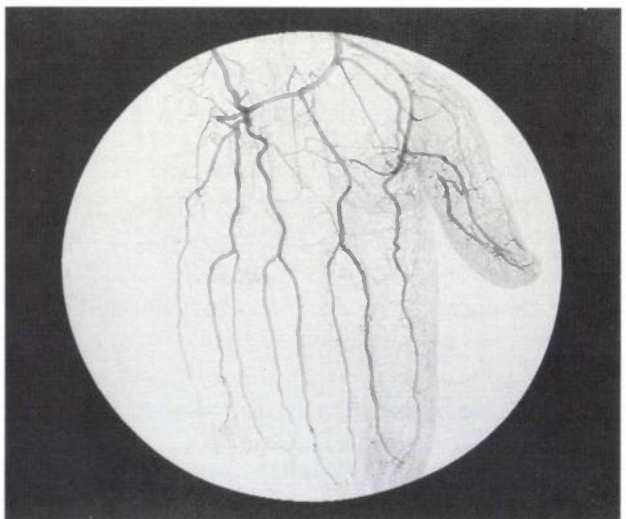
^[16] R. A. Kruger *et al.*, A digital video image processor for real-time X-ray subtraction imaging, Opt. Eng. 17, 652-657, 1978.



Fig. 11. 1-inch and 2-inch Plumbicon tubes. The Plumbicon tube replaced the vidicon and solved the problem of excessive inertia. Enlargement of the photosensitive area enabled the number of lines in the frame to be doubled, thus greatly increasing the picture definition. This was turned to great advantage in digital imaging techniques.



a



b

Fig. 12. a) Digital subtraction angiogram of a kidney after injection of a diluted contrast medium into the pelvic artery. b) Digital subtraction angiogram of a hand after injection of a diluted contrast medium into the main artery of the arm.

information about the vascular system, without any need to insert a catheter into veins or arteries^[17]. Philips was the first on the market with this technique, called digital vascular imaging. It is a digital version of the technique published years before, in 1964^[18], in which analog television signals stored on a magnetic wheel were subtracted. At the time, however, this technique did not produce acceptable results.

In these ten years the division pursued its activities in nuclear medicine and ultrasound diagnostics. Here again the computer played an important part. In nuclear medicine this had in fact begun earlier: the small amount of information contained in an image from a gamma camera made computer processing of the image both relatively simple and at the same time highly desirable. In ultrasound diagnostics the application of digital image storage gave an enormous improvement in image quality, making it possible for the first time to obtain ultrasound images with reasonably high contrast. As a consequence the market for ultrasound equipment expanded dramatically. This led to the decision to concentrate all our ultrasound activities at Santa Ana, California, to provide more room for new activities at Best, in the Netherlands.

In radiotherapy the cobalt source has been gradually replaced by the linear accelerator. This makes it possible to work with harder gamma rays so as to obtain a better dose distribution in the patient; electron irradiation is also possible with this equipment. A further advantage of a linear accelerator is that the radiation can be switched on and off easily. Complicated irradiation programmes can therefore be carried out, with even more accurate dose distribution. These features, and the availability of true cross-sectional images, the result of computerized tomography, again led to even more advanced methods for setting up an irradiation programme.

In the later seventies a new medical imaging technique appeared, based on work at a number of universities. This is now known as nuclear magnetic resonance (NMR) or latterly as plain MR^[19]. The work was undoubtedly stimulated by the success of the CT scanner. At an early stage it had been decided to build a prototype^[20] in a joint project between MSD and Philips Research Laboratories. The object was to gain a deeper technical understanding of the possible medical applications. This Proton machine, a system with a 0.15-tesla resistive magnet, was used for examining many patients at Best.

Since radiologists were showing very keen interest in this method, it was decided to move into product development. The new products, unlike the Proton machine, mainly used superconducting magnets of 0.5 and 1.5 tesla (Gyrosan S5 and Gyrosan S15, see

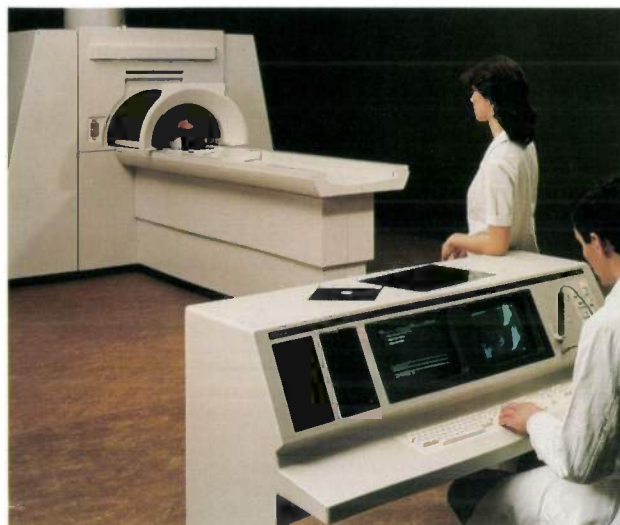


Fig. 13. The Gyrosan. The patient is introduced into the constant field of a very strong, superconducting magnet. Hydrogen nuclei in the tissue are set into resonance by means of a radio-frequency magnetic field; the resonant frequency is proportional to the strength of the constant field. By systematically making small variations in the constant field and at the same time detecting the resultant resonances, an image of the distribution of the hydrogen nuclei in the patient can be obtained. This image can then be displayed rather as in the CT scanner. The image thus obtained provides an extremely useful supplement to conventional radiographs.

fig. 13). This increase in field-strength was prompted by the need for better image quality and also by the wish to be prepared for spectroscopic applications.

The last extension of the activities of MSD that we must mention is the Picture Archiving and Communication System, or PACS^[21]. As can be seen from the foregoing, medical images are increasingly available in digital form rather than on film. These images can therefore be filed on digital optical memory discs (DOR, or Digital Optical Recording). The improved access to these stored records is expected to lead to wider use of earlier examination results, and hence to more accurate diagnosis. The stored images can be conveyed to and from the files and between individual

[17] L. A. J. Verhoeven, Digital subtraction angiography, Thesis, Delft 1985.

[18] W. J. Oosterkamp, Th. G. Schut and A. Druppers, Röntgenbeeldsubtractie met behulp van een magnetisch beeldgeheugen, Ned. T. Geneesk. 108, 2051-2054, 1964.

See also W. J. Oosterkamp, A. P. M. van 't Hof and W. J. L. Scheren, Philips Tech. Rev. 27, 228-230, 1966/67.

[19] R. Damadian, Tumor detection by nuclear magnetic resonance, Science 171, 1151-1153, 1971;

P. C. Lauterbur, Image formation by induced local interactions: examples employing nuclear magnetic resonance, Nature 242, 190-191, 1973.

[20] P. R. Locher, Proton NMR tomography, Philips Tech. Rev. 41, 73-86, 1983/84.

[21] D. Meyer-Ebrecht, D. Böhring, R. Grewer, K.-J. Mönnich, J. Schmidt and Th. Wendler, Hierarchical approach to distributed picture information systems, Proc. SPIE 318, 112-116, 1982;

J. Holzkamp, R. Heu and J. Tiemann, Erste Erfahrungen mit einem elektronischen Bildarchiv, Röntgenstrahlen No. 53, 42-45, 1985.

imaging equipments by a computer network. Universal image-analysis stations can also be built for analysing images independently of the method used to make them. The development of systems for PACS is now well under way and the first products have already been announced.

In view of the growing need to store all medical images in digital form, it is essential to have a good method of making large-format X-ray images in electronically legible form, without the intervention of film. Such methods are now becoming available, in various versions. They will enable PACS to be widely introduced in practice, and, through the application of digital image processing, they will greatly increase the diagnostic value of the images without any increase of the X-ray dose.

Developments after 1986

The developments of the last ten years will undoubtedly continue to be of vital importance to MSD in the near future. For example, digitized television signals, obtained from an image intensifier/camera combination, will be used for cardiac investigations, and will eventually supersede cinefluorography and cineradiography. Interesting technological developments can also be expected in classical X-ray diagnostic systems.

The major events are to be expected in the new areas, of course. Magnetic-resonance equipment requires further development for the full imaging potential of the method to become available to the user in a simple

form. Magnetic resonance combined with spectroscopy can also be used for performing chemical examinations on patients, so that detailed investigations of metabolic processes in the patient can be made without the need for laboratory analyses of body fluids. Research in this field, although still in its early stages, looks promising.

Finally, the further development of electronic image storage and transmission, which in fact is still in its infancy, will require a great deal of attention in the years ahead.

Summary. The Philips activities in the field of medical systems began with the repair of X-ray tubes, which could no longer be sent abroad to the manufacturers during World War I. As a result, Philips soon embarked upon its own development and production of X-ray tubes, power-supply generators, and equipment for patient support and diagnosis. Typical contributions included the rotating anode, which permitted a considerable increase in power and the first ideas on an X-ray image intensifier, which greatly increased the range of capabilities of the radiologist and also reduced very considerably the dose of radiation administered to the patient. The activities in medical electronics grew strongly at first, but are not now pursued, so that Philips can concentrate on systems for medical image diagnosis and radiation therapy. Developments in this area include the gamma camera and the use of ultrasound. Equipment for radiotherapy includes, apart from the well-established X-ray tubes, equipment using radioactive cobalt, linear electron accelerators and a sealed-off neutron tube. The combination of image intensifier with television techniques not only gave the radiologist much more freedom but also led to digitization of the X-ray image. Digitization made it possible to use computer techniques for image processing, which led to computerized tomography (the CT scanner) and to digital vascular imaging, and also to automated storage of X-ray images. One of the latest and very promising imaging techniques (MR) makes use of nuclear magnetic resonance.

Philips Technical Review 50 years ago

MAY 1936

OPTICAL TELEPHONY

By J. W. L. KÖHLER

Introduction

The term optical telephony has been applied to the method of telephonic intercommunication by means of light rays, and is thus an extension of the principle of the ordinary signalling lamp by means of which telegraphic signals are transmitted. In the latter method an incandescent lamp fitted with a reflector is provided as a transmitter at each of the two points of intercommunication and by means of these a parallel beam of light is transmitted to the opposite receiving point. Each lamp is connected in circuit with a Morse key and, with the aid of the two beams of light employed, Morse signals can be transmitted and thus a channel of intercommunication established.

This system of telegraphic intercommunication occasions a considerable loss of time which in many cases has proved a serious obstacle to its use. This difficulty has been avoided in optical telephony, where the intensity of a beam of light is also varied periodically, not by Morse signals but by the speech frequencies which are used for intensity modulation. Reception is therefore not possible with the naked eye as with Morse signals, but requires the use of a photo-sensitive cell with an amplifier and telephone.

Practical Results.

The efficiency and reliability of intercommunication depend inter alia on the wave-length of the light used, since the photo-electric cell has a different sensitivity for different wave-lengths, whilst more-

over atmospheric absorption may also vary for different wave-lengths. Standard caesium photo-electric cells have a maximum sensitivity in the infra-red region of the spectrum, but also respond to visible light. Red light is less dispersed by air than violet light; nevertheless the intensity still decreases considerably if, in place of white light, dark red or even infra-red light is used by introducing a filter. The range of transmission is then reduced by at least 30 per cent.

With the apparatus built in the laboratory, satisfactory inter-communication was maintained over a distance of 4.5 km with white light and over 3 km with red light. The transmitting and receiving mirrors were each 130 mm in diameter. It should be mentioned in this connection that the range of transmission is proportional to the diameter of each of the reflectors. The data given here apply for good visibility, but it is quite possible to maintain intercommunication over a medium distance also through fog when once established, although to set up the required channel of communication is very difficult under these circumstances.

Compared with other methods of intercommunication, optical telephony has the disadvantages of being dependent on atmospheric conditions and of offering only a restricted range of transmission. On the other hand it has certain advantages; thus, compared with signalling lamps, messages can be transmitted with much greater speed, which applies in fact as regards all methods of telegraphic trans-

Summary. In the apparatus for optical telephony described in this article, a modulated ray of light is generated by feeding an incandescent lamp simultaneously with a direct current and with an alternating current from a microphone amplifier. The characteristics of this lamp are discussed. The range of transmission of this method is limited by the noise interference produced at the receiving apparatus. The means for suppressing this interference as far as possible are outlined. The apparatus described has a transmission range of 4.5 km when using white light and of 3 km with red light.

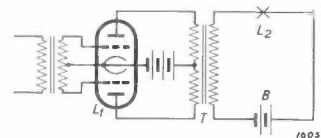


Fig. 4. Modulation of the incandescent lamp. The lamp L_2 is fed from the battery B . This circuit contains the secondary winding of the output transformer T of the transmitting amplifier. L_1 is the power valve of the amplifier, viz. Philips KDD 1 valve.

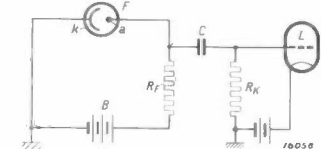


Fig. 5. Connection of photo-electric cell with receiving amplifier. The battery B furnishes the voltage for the photo-electric cell F . The alternating currents, which are produced by variable illumination of the cell, generate an alternating voltage at the resistance R_1 . This voltage is passed through the condenser C and the resistance R_k to the grid of the input valve L of the amplifier.

mission. In regard to short-wave spark telegraphy there is, moreover, the added advantage of secrecy. Owing to the extremely small dispersion of the ray it is impossible to detect the position of the transmitter during the day, even when using white light; messages therefore cannot be tapped. For the same reasons intercommunication is also proof against malicious interference.

A NEW METAL RECTIFYING VALVE WITH MERCURY CATHODE

By J. G. W. MULDER.

For the rectification of high powers, rectifying valves with a mercury cathode¹⁾ are particularly suitable, owing inter alia to their ability to withstand overloading. The development of these rectifying valves has resulted in the production of two main types, the glass valve and the metal valve.

Where high powers have to be rectified the main difficulty in the design of rectifying valves, as in many other branches of electrical technology, has been the dissipation of the heat generated. This problem is dealt with by introducing a system of artificial cooling, a current of water being the most efficient. Water cooling is most suitably carried out with a metal valve body and has led to the construction of mercury cathode rectifiers with iron jackets for currents above 1000 amps, which are equipped with a water-cooling system and a high-vacuum pump. The latter was essential in this class of rectifier, as hydrogen ions present in the water diffuse through the iron walls. But the need for high-vacuum pumps in order to employ water cooling had many disabilities, since the presence of the pump, in spite of the use of automatic regulating devices, called for more careful supervision of these rectifiers than was required with sealed rectifier valves.

For this and other reasons metal rectifier valves were not constructed for currents below 1000 amps. In the glass valves which were used for these ratings, the dimensions had to be very large in order to provide for the necessary dissipation of the heat generated. But there is naturally an upper limit in dimensions to which glass bulbs can be manufactured. So that if with the maximum practical dimensions the valve was still unable to dissipate all the heat generated, it became imperative to adopt more intensive air cooling.

At the Philips Works a new type of metal single-phase rectifying valve with mercury cathode has now been evolved which, like glass valves, is used in a sealed condition. In this valve which is intended for a power range at present catered for by glass mercury-cathode rectifying valves (and even for still higher powers) the same advantages are offered as by the iron types rated for high powers, while the pump necessary in the latter has been dispensed with in the new rectifiers.

The valve shown in fig. 2 is rated for a medium current of 75 amps and a peak current of 500 amps. Like other mercury-cathode rectifying valves this valve can without trouble carry heavy overloads for short periods.

The efficiency depends on the rectified power. The total losses in the valve at full load are 1150 watts, including the consumption for auxiliary

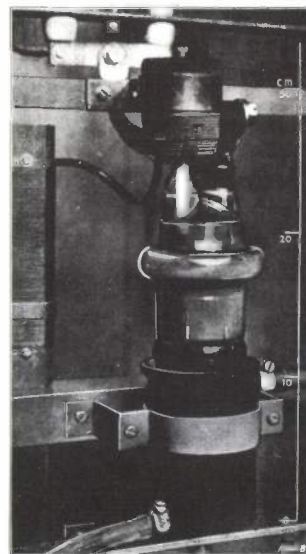


Fig. 2. Construction of the single-phase metal rectifying valve shown diagrammatically in fig. 2.

ignition. The efficiency at 220 volts and 75 amps is therefore 93 per cent and at 120 volts and 75 amps 88 per cent.

Regarding the life of these valves no numerical data can yet be furnished, as up to the present not a single one of the valves (which have been under test for more than a year) has failed. The life therefore amounts in any case to many thousands of hours.

¹⁾ This term appears to us more suitable than that in common use hitherto, viz. "mercury rectifying valve", as thermionic rectifying valves nowadays also frequently contain an atmosphere of mercury vapour.

Half a century of 'electronification' in telephony systems

J. F. Brouwer

The vast progress in electronics in countless fields of application has led to striking results. It is certainly no mere chance that the thermionic valve (or electron tube) was first used for wireless telegraphy. The inventor of the diode (Sir J. A. Fleming) and the inventor of the triode (Lee De Forest) were closely involved in this branch of electrical telecommunication, which was then in its infancy.

Later, the cross-fertilization between electronics and telecommunication led to wireless transmission of speech and music in radio communication and radio broadcasting, two related fields that gave rise to great growth and expansion in the electronics industry.

This article is mainly concerned with another form of cross-fertilization: between electronics and line-dependent telephony systems. Without electronics it would not have been possible to span the Earth with underground and submarine cables for telephone transmission. Modern digital telephone exchanges controlled by special telephony computers would also be inconceivable without the use of the most advanced electronic components and modules.

An interesting aspect here is the long time it has taken to introduce electronics into the most important telephony functions. Although the first electronic telephone repeaters were in use before World War I, it is only in the last fifteen years that electronics has really penetrated into the heart of the telephone exchange. Because of the great complexity of the switching operations and the reliability already achieved with electromechanical systems, electronics had not previously had much to offer here — and there was also the question of price.

In this article transmission systems will be considered first, then switching systems and the review concludes with a look at the near future. Much space has intentionally been given over to developments at Philips, although the treatment must necessarily be incomplete in range and detail.

Ir J. F. Brouwer was a Director of Philips' Telecommunicatie Industrie B.V., Hilversum, and of the former Philips Telecommunication and Defence Systems Division, before his retirement.

TELEPHONE TRANSMISSION SYSTEMS

Background

Not long after the invention of the triode by Lee De Forest in 1906, electronics entered the world of telephony in the form of repeaters. As long ago as 25 January 1915 the first transcontinental telephone circuit came into operation in America: a route some 5000 km long with overhead copper wires fixed to poles, incorporating repeaters at three points^[1].



Fig. 1. At first, telephone connections were almost always made with overhead lines. Because there were so many wires, the result was not always particularly attractive. The picture shows a street scene in one of the larger cities in the United States in the early days of telephony (about 1880).

^[1] More than 1000 tons of copper wire were used in the link; the number of repeaters was later increased to eight. See M. D. Fagen (ed.), *A history of engineering and science in the Bell System; the early years (1875-1925)*, Bell Telephone Laboratories 1975, p. 262.

With the rapid growth in telephone traffic, however, it very soon became necessary to use underground cables, first for the urban networks and subsequently for the other circuits as well. This resulted in less interference from induction, fewer interruptions and less maintenance but — inevitably — also in a lower signal strength at the end of the line. Although the intrinsically higher attenuation of telephone cables could be significantly reduced by artificially increasing their self-inductance — as demonstrated by Pupin and Krarup — it could never achieve such low values as those attainable with the overhead systems using

over the same pair of wires. The only fundamentally correct solution to this problem was the four-wire circuit (*fig. 2*). Connections of this type were desirable because of their low overall attenuation, but they were also expensive, so that the telephone companies wanted to use them for more than one telephone call at a time. The most appropriate principle for this was carrier telephony, a form of frequency-division multiplexing (FDM); see *fig. 3*. Such systems were first used in expensive submarine cable links and long overhead routes, then later in both coaxial and multi-wire (symmetrical) underground cables as well.

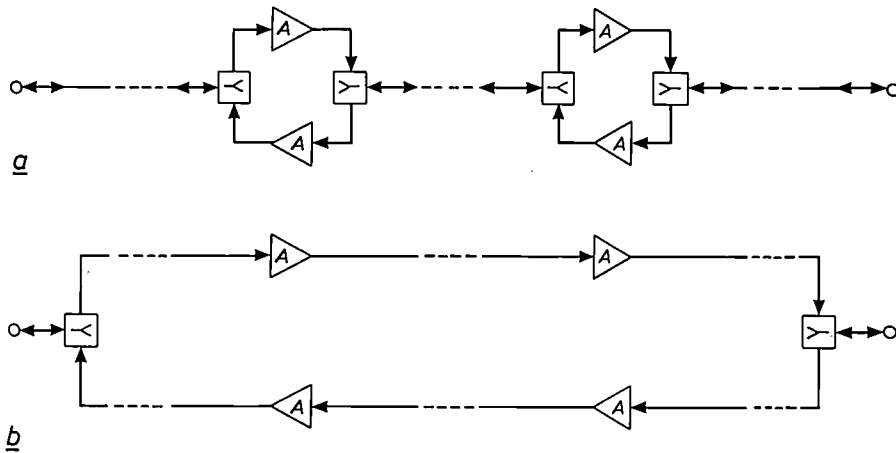


Fig. 2. *a*) In two-wire circuits both telephone signals for each telephone call are transmitted over only one pair of wires. The signals from the two directions are only separated, amplified and recombined at repeaters (A), if installed. Separation and recombination take place in 'hybrids' (>). *b*) In a four-wire circuit hybrids are only found at the two ends; two wires are available for the signals in both the go and return paths for the entire length of the circuit. (N.B. one continuous line in this diagram represents two wires.)

wires a few millimetres thick (overhead lines, *fig. 1*). After 1920, therefore, an ever-increasing number of low-frequency ('voice-frequency') repeaters were used on both international and long-distance national trunk circuits. Typical distances between repeaters were 100 to 200 km, depending on the diameters of the wires used in the cables. For the time being, however, overhead lines continued to be used for very long circuits.

It was soon found that transmission circuits incorporating repeaters had to be very carefully dimensioned. Excessive gain could lead to oscillation or 'singing' (negative feedback had not yet been invented); too many repeaters connected in cascade caused echo effects, and the longer the line the more annoying these became. Excessive differences in signal strength in neighbouring pairs of wires led to unacceptable interference between one channel and another (crosstalk). Many of these problems were caused by the use of the traditional two-wire circuits in which telephone signals were transmitted in two directions

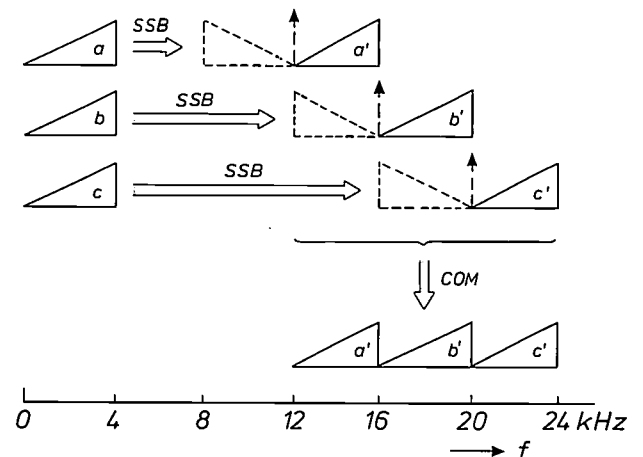


Fig. 3. Carrier telephony is based on frequency-division multiplexing; a number of telephone signals are displaced to different positions on the frequency scale by single-sideband modulation with a suppressed carrier (SSB). They are then combined (COM) into a single multiplexed signal. An arbitrarily chosen example is shown here for three signals (*a*, *b* and *c*), each with a bandwidth of 4 kHz, which produce a single multiplexed signal (*a'b'c'*) extending from 12 to 24 kHz.

The year 1936 was marked by extensive pioneering activities in this field: the first coaxial routes were laid from New York to Philadelphia and from Berlin to Leipzig. In the Netherlands, the Dutch PTT Administration brought its own 12-channel symmetrical cable system into use between Groningen and Leeuwarden. Extending for 60 km, this route was one of the first object lessons for the small Philips Transmission Group of those days. It was to be almost fifty years before it would receive an order for the longest digital coaxial link in the world (see page 366), which, incidentally, made use of a principle now also nearly half a century old: Reeves's pulse-code modulation (PCM), dating from 1938.

Transmission activities in Philips — the start

After it was set up at the start of the thirties, the activities of the Transmission Group at Philips were initially confined to voice-frequency amplifiers and Pupin coils. The company offered fertile soil for this: knowledge in the field of thermionic valves was available (the pentode patent and the negative-feedback patent), and use could also be made of research results in the field of magnetic materials. Even before World War II a 17-channel carrier system was developed for which the first export order was obtained in 1938 (from Sydney to Maitland, in Australia).

After World War II the transmission activities were continued at Philips Telecommunicatie Industrie in Hilversum. Development and production centres in this field also gradually grew up in Philips plants in other countries. Now let us look at what has happened in Philips since those times, particularly as regards analog, digital and optical transmission systems for telephony.

Analog transmission systems

Even during the war, Philips had been working on a 48-channel carrier system^[2], which went into production in 1947. A significant reduction in size as compared with the earlier 12- and 17-channel systems was made possible by using Ferroxcube^[3] as the core material for inductors and transformers, semiconductor cells for modulators and an improved type of valve.

The great increase in telephone traffic, which was much stimulated by the progressive automation of long-distance networks, resulted in turn in a growing demand for transmission equipment. In particular, improvements in line-amplifier techniques showed that the various transmission lines could be used for considerably higher frequencies than had been expected

Table I. Internationally recommended hierarchy of carrier systems for telephony.

	Number of channels	Basic frequency position (kHz)
Group	12	60-108
Supergroup	60	312-552
Mastergroup	300	812-2044
Supermastergroup	900	8516-12 388

when they were purchased. Such an increase in bandwidth can be seen in the symmetrical carrier cable, in which the number of channels was extended to 120 in about 1962.

Since not every type of cable had the same transmission capacity, and the number of channels required varied very widely from connection to connection, the need arose for carrier systems with varying channel capacities. This led to international agreements about a hierarchy of carrier systems: in a number of successive modulator stages twelve channels are first combined or 'multiplexed' (fig. 3) to form a 'group' with a fixed basic position on the frequency scale. Next, five groups are multiplexed to form one supergroup, etc. (Table I). When the highest required level in the hierarchy has been reached, the signal is converted by a final modulation operation from its basic frequency position to the frequency position ultimately required on the cable. Through the years, Philips have developed a virtually complete hierarchy of analog transmission systems for use on overhead lines, cables and microwave links. The modular structure meant that, for example, the same channel and group modulation equipment was used in a 120-channel system as in a system for 10 800 channels.

More refined design techniques, space-saving construction methods, the automation of production processes and the selection of the most suitable components led to new generations of equipment with improved characteristics^[4]. A good example of this is to be found in the 'channel unit' (fig. 4). Transistorization (1959) made the main contribution to reducing dissipation; a significant gain in space was mainly achieved by a virtually continuous reduction in the size of the passive filter components, which account for more than 50% of the total number of components (fig. 5).

Widening the frequency band used on symmetrical and coaxial cables meant that ever-smaller intervals

^[2] G. H. Bast, D. Goedhart and J. F. Schouten, A 48-channel carrier telephone system, Philips Tech. Rev. 9, 161-170, 1947/48 and 10, 353-362, 1948/49.

^[3] J. L. Snoek, Non-metallic magnetic material for high frequencies, Philips Tech. Rev. 8, 353-360, 1946.

^[4] A. van Dedem, 8TR 400: a new generation of channel equipment, Philips Telecommun. Rev. 31, 156-157, 1973.

were required between repeaters, because cable attenuation increases at higher frequencies (*Table II*). In the 48-channel system with symmetrical cables valve amplifiers were used, spaced at about 25 km. They were housed in above-ground repeater stations equipped with reliable power supplies fed by the local electricity mains. The 120-channel system, which was used on the same cables, required considerably shorter distances

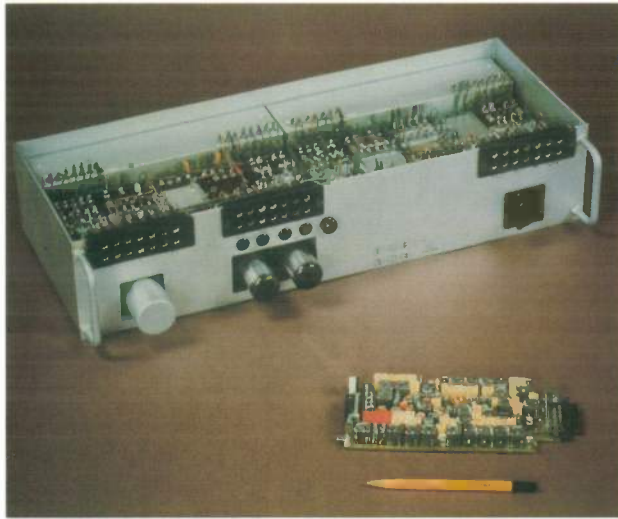


Fig. 4. The channel unit, which is required for each separate transmission channel in the formation of a group in carrier systems, underwent substantial improvements between 1947 (background) and 1975 (foreground). The number of channels in each equipment bay rose from 12 to 600; the dissipation in each channel fell from 12 W to less than 0.1 W, while both technical performance and reliability were significantly increased.

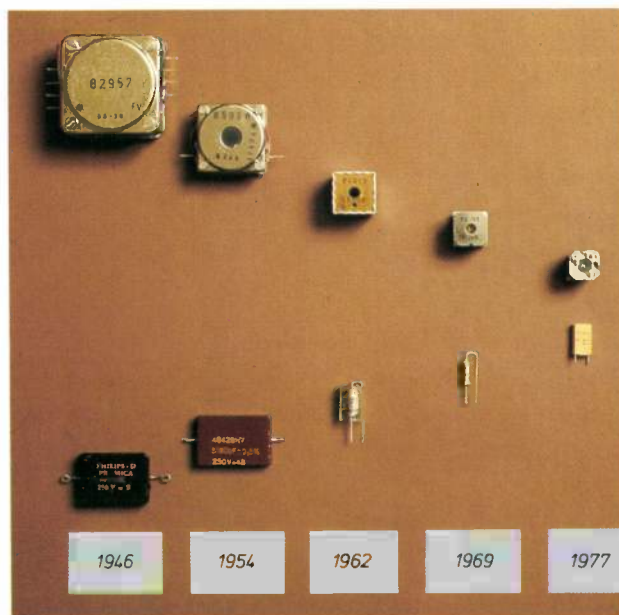


Fig. 5. The inductors (top) and capacitors (bottom) used in filters for telephone transmission equipment have diminished in size through the years, mainly because of improvements in the magnetic and dielectric materials and perfection of the winding technique.

Table II. Analog transmission systems for carrier telephony. (With a 'standard' coaxial cable the diameters of the inner and outer conductors are 2.6 mm and 9.5 mm, respectively. The corresponding values for a 'mini' coaxial cable are 1.2 mm and 4.4 mm, and for a 'micro' coaxial cable — see Table III — 0.7 mm and 2.9 mm.)

Highest frequency (MHz)	Number of channels	Repeater spacing (km)		
		Symmetrical carrier cable	Coaxial cable	
			Standard	Mini
0.2	48	25	—	—
0.5	120	8	—	—
<hr/>				
4	900	—	9	4
6	1200	—	8	3
12	2700	—	4.5	2
18	3600	—	4.5	2
60	10 800	—	1.5	—

between repeaters. Here semiconductor technology came into its own, because the power required for transistor amplifiers is so low that they could be fed via the cable wires by a low-current d.c. supply. This resulted in a significant saving in costs, since the repeaters could now be installed in an underground housing (repeater case).

Philips was one of the first companies to use transistor amplifiers for coaxial cables as well [5]. On long coaxial circuits it is often necessary to compensate for an attenuation of many tens of thousands of decibels, while as a result of seasonal variations in ground temperature the nominal cable attenuation varies by some hundreds of decibels (every 100 dB means a power variation of a factor of 10^{10}). The large number of repeaters in cascade puts a premium on reliability. A solution has been found for this by not incorporating any 'regulation' in most of the repeaters. They can therefore be constructed with the smallest possible number of components. The mean time between failures, or MTBF, of these repeaters is about 1000 years. In addition, in a small number of regulated underground repeaters a patented control system matches the gain to the varying cable attenuation by sending a control command from the terminal stations via the coaxial conductors. The overall attenuation of the total link can thus be kept constant to within about 1.5 dB [6].

Digital transmission systems

Digital transmission systems use pulse-code modulation and operate on the time-division-multiplex principle. A number of low-frequency telephone signals are sampled every 125 μ s; each signal amplitude found is converted into an 8-bit code word by a non-linear analog-to-digital converter. On the transmission line, one code word in succession from each

channel is now transmitted at high speed in each interval of 125 μ s. At a transmission rate of say 2 Mbit/s, 30 channels can be processed. Digital systems require a considerably larger bandwidth than analog systems with the same number of channels, but they are relatively immune to impulse noise and interference originating from other circuits. In addition, the digital signal can be restored to its original pure form (i.e. it can be regenerated) relatively simply in intermediate repeaters. The regenerated signal will of course contain a bit error that cannot be immediately recognized if a bit is excessively mutilated as a result of poor conditions on the transmission path.

Pulse-code-modulation systems have been widely used in short-haul transmission links with voice-frequency cables where the use of carrier equipment would have been economically inappropriate because of the short distance. As these digital systems became cheaper, they found their way into other types of links, which had previously been the domain of analog systems. Besides being cheaper, they were — of course — also more suitable for transmitting digital information (telegraphy and data traffic) with permissible rates of up to 64 kbit/s per channel. For economic reasons, a need arose for digital systems with more channels for longer distances. The digital system hierarchy, as laid down by the international organizations CEPT and CCITT, comprises systems of 2 to 565 Mbit/s with 30 to 7680 channels (*Table III*). In the future this hierarchy will certainly be extended to the giga-bit/s range for optical digital systems.

Higher-order digital transmission systems consist of multiplexers (in which a number of lower-order bit streams in the hierarchy are converted into a bit stream of the next higher order) and digital line equipment. This is always specific to a particular type of cable and therefore different for, say, coaxial cables and optical-fibre cables.

The first PCM system developed by Philips was delivered in 1968; it was a 24-channel system and was rapidly followed by a 2-Mbit/s system with 30 channels complying with a new European standard introduced by CEPT. In both systems, standard circuits



Fig. 6. This standard repeater case intended for underground use is not only suitable as a housing for analog repeaters (18 MHz and 60 MHz) and digital repeaters (34 Mbit/s, 140 Mbit/s and 565 Mbit/s), but also as a housing for optical repeaters.

(ICs) were used for the digital functions and discrete components for the analog functions. For economic reasons, the coder/decoder in which the analog-to-digital conversion takes place was still common to all channels.

In younger generations of the 30-channel system low-power Schottky circuits and custom-designed ICs are mainly used for the coder/decoder, constituting an individual unit for each channel. (At present the coder/decoder is combined with the associated filters to form a single IC.) The regenerators also contain a number of custom-built bipolar ICs for the analog functions.

Digital systems have of course benefited more than analog systems from the reduction in volume and dissipation provided by modern IC technology. This has also led to a decrease in the number of individual components, which has improved the reliability.

In addition to analog transmission on the channels already in use, the multiple coaxial cable ('multi-tube cable') permits digital transmission on previously unused 'tubes'. It was therefore a great advantage if the (analog) underground repeater cases were also suitable for housing digital regenerators (*fig. 6*). However, this introduced two extra requirements for the design of these regenerators. They had to permit the same spacing between repeaters and they had to be no larger than the corresponding analog repeaters. To meet these requirements, Philips designed 140-Mbit/s and 565-Mbit/s regenerators with special custom-designed ICs and hybrid circuits^[7]. A number of orders were received for major projects, testifying to the

Table III. Digital telephone-transmission systems.

Transmission capacity (Mbit/s)	Number of channels	Repeater spacing (km)			
		Low-frequency cable	Coaxial cable		
			Standard	Mini	Micro
2	30	2	—	—	—
8	120	2	—	—	4
34	480	—	—	4	2
140	1920	—	4.5	2	—
565	7680	—	1.5	—	—

[6] J. F. Lansu, Transistorized line equipment with 4, 6 and 12 Mc/s frequency bands for coaxial cables, Philips Telecommun. Rev. 26, 53-61, 1966.

[6] H. L. Bakker, The 60 MHz coaxial transmission system 8TR 341, Philips Telecommun. Rev. 30, 103-112, 1971/72.

[7] A. M. Giacometti and Ph. Uythoven, The 565 Mb/s 8TR640 system: equalisation design and performance analysis, Philips Telecommun. Rev. 41, 175-192, 1983.

great advantages that could be achieved with these regenerators in digital long-distance systems.

The long-distance connection between Sacramento and Chicago was the longest 140-Mbit/s link in the world when it was commissioned in December 1982. It was constructed with Philips equipment, and is 3750 km in length with underground regenerators at a spacing of about 3 km.

Optical transmission systems

Making use of its own research results in optical-fibre production and welding techniques, systems studies and optical components such as lasers, avalanche photodiodes and connectors, Philips constructed an experimental optical 140-Mbit/s system as long ago as 1979 that was almost entirely based on components available within the company. After an experimental system operating under normal conditions had been set up between Eindhoven and Geldrop in 1980, an ambitious development programme was started. The objective was the early completion of a series of optical-transmission systems for a complete digital system hierarchy (*fig. 7*). Recently (April 1986) the first international optical-fibre communications link in Europe was officially commissioned: Breda in the Netherlands and Herentals, 60 km away in Belgium, are now linked by a cable of twelve optical fibres, each with a transmission capacity of 1920 telephone channels (140 Mbit/s).

The wavelength of 850 nm originally used permitted repeaters to be spaced at intervals of 10 km to 20 km, representing a significant economic advantage as compared with coaxial cables. There was, however, one complication: optical fibres are non-conducting and electrical power for the regenerators cannot be supplied via these fibres. Even longer regenerator sec-



Fig. 7. Receiving equipment for a 565-Mbit/s optical-transmission system.

Table IV. Optical transmission systems.

Type of fibre	Wavelength (nm)	Attenuation (dB/km)	Typical repeater spacing (km)
Graded-index	850	2.7	15-20
	1300	0.6	45-60
Step-index (single-mode)	1300	0.5	50-70
	1500	0.2	100-140

tions were therefore necessary if underground regenerators in the links between surface regenerator stations were eventually to be entirely eliminated. In the past few years much study has consequently been devoted to the use of other wavelengths (1300 nm and 1500 nm) and to the employment of single-mode optical fibres with significantly lower optical attenuation. *Table IV* gives a general indication of the distances that can be bridged with the various types of system under operating conditions without intermediate regeneration^{[8][9]}. Further improvements in the optical components and in optical-fibre technology will certainly result in further increases in these values in the future.

TELEPHONE SWITCHING SYSTEMS

Background

Two years after the invention of the first practical telephone by Alexander Graham Bell, the first public telephone network came into use in New Haven in 1878^[10], rapidly followed by other similar networks both in the USA and elsewhere. All these networks were manually operated in 'central offices' or 'exchanges' (*fig. 8*), but an experimental automatic exchange had already come into operation by 1892. An improved version of this 'step-by-step' system, also called the Strowger system (after its inventor), rapidly spread throughout both America and Europe where it was manufactured under licence.

Nevertheless, there was some initial hesitation about introducing automation into large urban networks. There were doubts about the user-friendliness of a self-service system in which subscribers had to select the long local telephone numbers themselves. The larger exchanges, which came into operation shortly before and just after World War I, were therefore generally equipped for semi-automatic traffic, with the operator — and not the subscriber — selecting the number requested verbally by the caller.

Experience with fully automatic exchanges was so good, however, that operators began to disappear from local exchanges in the twenties.

By 1936 some 50% of the total number of subscriber lines — estimated at 35 million worldwide —

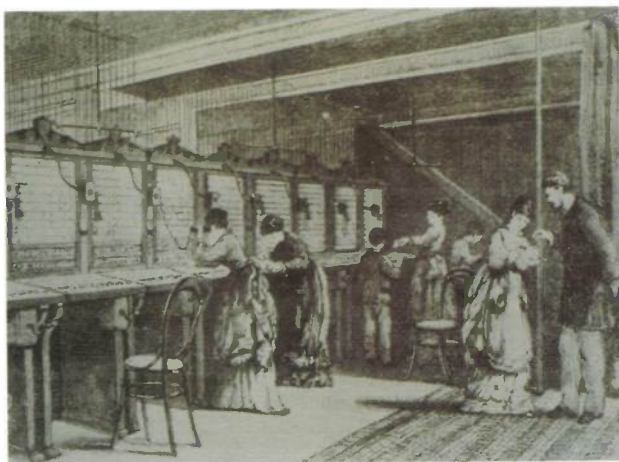


Fig. 8. One of the oldest types of manual exchange (about 1880).



Fig. 9. An ordinary telephone exchange half a century ago (manual exchange, 1936).

were connected to automatic exchanges^[11]. This high percentage, however, was mainly achieved as a result of the automation of the large urban networks. Most smaller towns and virtually all rural areas still had to make do with manual operation (*fig. 9*). Trunk calls, particularly over longer distances, were also usually handled by the operator, so that long waiting times were frequently inevitable.

As to future developments, half a century ago more extensive automation of the national telephone network was the top priority: in some smaller countries (Switzerland and the Netherlands) plans already existed for the complete automation of all local networks^[12]. Apart from this, there was little indication of other major changes. Although there were many reasons for seeking systems that required less maintenance, took up less space and were cheaper to produce, a further evolution of the electromechanical modules looked more promising than using electronic switching devices such as valves.

Nevertheless, attempts were already under way to achieve more practical electronic components. The telephone selector, with its dozens of outputs, inspired many designs of complex valves with similar facilities. Even before World War II there were studies of the usefulness of semiconductor elements — and these ultimately led to the invention of the transistor. There were also innovations in system concepts half a century ago: the first pulse-code modulation patent (1938) not only opened up new paths for digital transmission systems but also offered prospects for digital switching systems based on time-division multiplex.

Many years were to pass, however, before new technologies and system concepts could be adapted for practical application in commercial telephone exchanges. Meanwhile the electromechanical exchange had the field to itself.

Some basic concepts

In a telephone exchange a distinction can be made between the switching network and the control system. In a switching network a connecting path is set up by the exchange for every telephone call between a particular input and the output required for the call. It is generally composed of a number of successive switching stages in the form of telephone selectors (*fig. 10*), each with one input and several outputs or — more generally — in the form of switching matrices (*fig. 11*), in which each of the M inputs can be connected to each of the N outputs by means of crosspoints. The crosspoint may be a mechanical contact (selector or crossbar switch) or an electronic switching element (diode or transistor).

The control system's task is to set up the required connection in the switching network on the basis of information received from the subscriber, monitor it and terminate it again at the end of the call. In a manual system, these tasks are performed by a telephone operator. Automatic exchanges contain control units that receive the information dialled by the subscriber making the call and process this into control instructions for the stages in the switching network. In addition, the control system handles the exchange of information with the subscriber (engaged or busy tone, ringing tone, dialling tone, etc.) and with other exchanges involved in setting up the connection.

Telephone exchanges can be divided into two groups: local (or subscriber) exchanges and trunk (or transit) exchanges. Local exchanges have both subscriber lines and trunk lines connected to them, while trunk exchanges only have trunk lines connected to them (*fig. 12*).

[8] N. A. Buijs and A. J. M. Dingjan, Optical fibre systems: towards long distances, Philips Telecommun. Rev. 41, 165-173, 1983.

[9] J. Drupsteen, A high-capacity 565 Mb/s optical system bridges long distances, Philips Telecommun. Rev. 43, 31-42, 1985.

[10] A relatively high number, in view of the fact that after 1000 circulars had been distributed only one subscriber replied; see [1], p. 477.

[11] R. J. Chapuis, 100 years of telephone switching: Part I, North-Holland, Amsterdam 1982.

[12] This was completed in 1959 (Switzerland) and 1962 (the Netherlands). See for example: J. H. Schuilenga, J. D. Tours, J. G. Visser and J. Bruggeman (eds), Honderd jaar telefoon, Dutch Post Office, The Hague 1981.

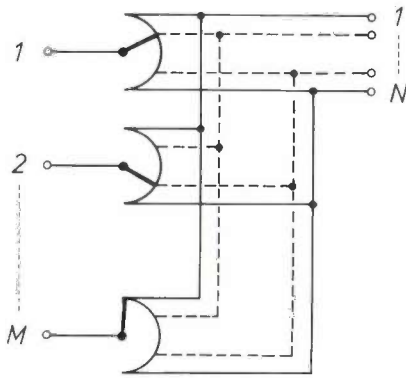


Fig. 10. Switching stage consisting of M individual telephone selectors with N outputs. Each selector represents an electromechanically operated N -position switch. The corresponding outputs of the selectors are interconnected.

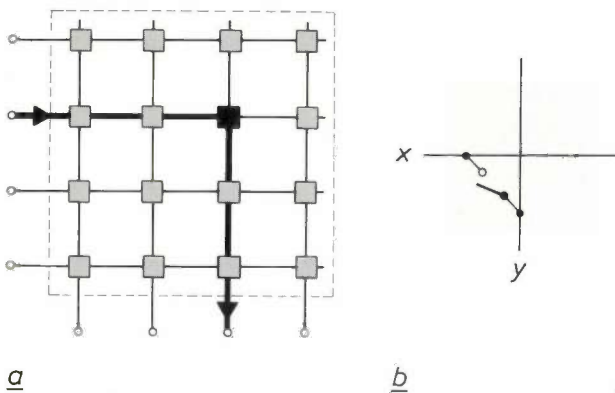


Fig. 11. a) Analog switching matrix with 4 inputs and 4 outputs. A conducting crosspoint is indicated by a black square and a non-conducting crosspoint by a grey square. b) More detailed representation of a crosspoint in a switching matrix. When the switch is closed a connection is made between the horizontal and vertical conductors x and y .

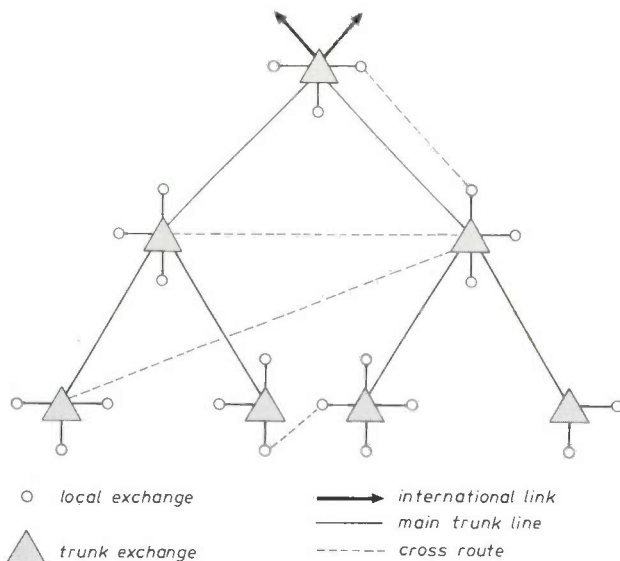


Fig. 12. Hypothetical example of a hierarchically structured telephone network with local and trunk exchanges.

Automatic telephony in Philips — the beginning

Philips, who are mainly known as a lighting and electronics company, were not active in automatic telephony until the end of World War II. This situation was changed by its participation in the reconstruction work in the Netherlands of repairing the many telephone exchanges that had been destroyed or damaged during hostilities. The next step was to start production of a pre-war 'two-motion selector' system that was widely used in the Dutch network and which, at that time, could not be supplied in sufficient quantities from abroad. After this, the company rapidly developed their own system (the 'UR system') on the basis of the latest electromechanical modules [13].

This new activity in switching techniques fitted in well with existing Philips activities in radio communications and carrier transmission. Together, the three fields constituted the new scene of operations for its subsidiary Nederlandsche Seintoestellen Fabriek, which became Philips' Telecommunicatie Industrie in 1947.

The electrification of the switching network

In most exchanges designed for switching analog telephone signals, the path set up for every call in the switching network and maintained for the duration of the call is an individual one, which is physically different from all the other paths in existence at the same time (fig. 13). These are analog space-division exchanges, and differ in many respects from their most modern counterparts: digital time-division exchanges.

In analog exchanges the switches or crosspoints in the switching network must meet the following requirements:

- they must be switchable from a very-low-resistance state to a very-high-resistance state and vice versa;
- they must not be affected by the relatively high voltages and currents that occur on conventional subscriber lines, e.g. when ringing the subscriber or as a

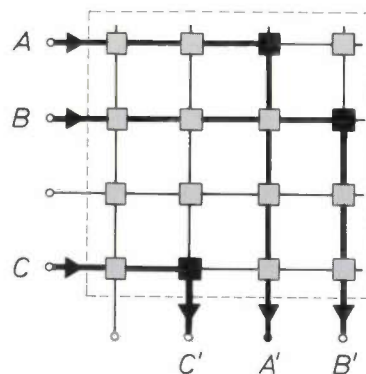


Fig. 13. Switching matrix (4x4) with three simultaneous and physically separate speech paths A-A', B-B' and C-C'.

result of induction from external electromagnetic fields (electric traction, lightning, high-voltage lines):

- the switching rate must be high enough;
- the resistance in both states must be reasonably stable and must not be affected by factors such as climatic conditions or mechanical vibration, which can lead to contact noise.

Electromagnetic switches

The electromechanical contacts of the old 'step-by-step' systems satisfied all the above requirements reasonably well except the last one: the step-by-step lifting and rotation of the moving part of the selector mechanism caused vibration that led to contact noise in selectors already in position. Nor could dirty and worn contacts ever be completely avoided, and correcting these faults required frequent maintenance.

One of the methods adopted to avoid the sharp jerky movements in the more modern one-dimensional selector systems was to connect the rotating part of the selector to a central continuously driven shaft and disconnect it only after the selector had reached the required position. With a careful choice of contact materials a significant reduction in maintenance could be achieved for selectors of this type.

The first Philips (two-wire) telephone exchange (type UR 49 of 1955) was of this kind. It was suitable for use both as a local and as a trunk exchange and remained in production — with appropriate modifications — until 1980. In that year, 1.3 million subscribers were connected to these exchanges in the Netherlands alone.

Good contact quality was also achieved with crossbar switches. These have a switching matrix consisting of contacts and a set of horizontal and vertical bars for activating the contacts. By rotating one of the horizontal bars and one of the vertical bars through a small angle, the contact located at the imaginary crosspoint of the two bars is activated. It remains in this state for as long as one of the bars retains its angular displacement; the other bar is released to permit the selection of the next crosspoint.

Electronic crosspoints

In the fifties and sixties the crossbar matrix served as a model for all kinds of switching matrices with electronic crosspoints. For example, at a fairly early date the cold-cathode tube was used in a number of experimental exchanges (by Philips^[14] and others). Because of a number of disadvantages, however, this turned out to be not very practicable: the high ignition voltage was a disadvantage and the relatively high resistance in the conducting state gave excessively high attenuation for speech signals.

In the later evaluation of semiconductor matrices attention was mainly concentrated on the pnpn transistor, which can be switched not only as a diode but also as a transistor. Using electronic crosspoints of this type Philips installed complete experimental exchanges for 1000 subscribers in 1967 in Utrecht (the Netherlands) and Aarhus (Denmark).

Although pnpn crosspoints permitted a very high switching rate, this was little help in analog exchanges. The resistance in the conducting state reached lower values than with cold-cathode tubes, but it was nevertheless between 10 and 20 times higher than the resistance of electromechanical contacts. Since in addition the permissible currents and voltages were limited, one of the other requirements mentioned above was not satisfied either, so that fairly expensive protective circuits were necessary for each subscriber line. When modern analog exchanges with electronic control were developed in the seventies, the electronic crosspoint was still not very attractive for technical and economic reasons. In this generation of exchanges electromechanical switches were therefore still predominant (mini-reed relays and mini-crossbar switches were often used); hence the name 'semi-electronic exchanges'.

Reed relays

The modern version of the reed contact — the principle had already been known in 1936 — consists of two strips or 'reeds' of a material that conducts electrically and can be magnetized. This assembly is sealed into a gas-filled glass tube and the reeds are positioned so that a small contact aperture is created between them, giving a compact contact system that is completely protected from unwanted external influences (*fig. 14*). The contact is energized by an external magnetic field.

From 1973 onwards, Philips has marketed the very successful PRX system, which is based on mini-reed relays^[15]. It soon became widely used in public networks, at first in the Netherlands. Large numbers of local and trunk exchanges were produced (and still are), sometimes in the form of ready-made, mobile 'container' exchanges (*fig. 15*). These were used in systems like the ones supplied for the 'telecommunications order of the century', for the modernization of the telephone network in Saudi Arabia, which represented a total value of some billions of dollars.

^[13] J. M. Unk, A high-speed uniselector for automatic telephone exchanges, Philips Tech. Rev. 18, 349-357, 1956/57.

^[14] J. Domburg and W. Six, A cold cathode gas-discharge tube as a switching element in automatic telephony, Philips Tech. Rev. 15, 265-280, 1953/54.

^[15] T. M. Schuringa, Reed switches for telephony switching, Philips Telecommun. Rev. 27, 105-123, 1967/68.

Switching matrices for digital exchanges

Switching networks for digital telephone exchanges have to meet completely different requirements from those in analog exchanges. In the first place, they handle digital signals, which are regenerated at the input and output of the exchange. If analog subscriber lines are connected to the exchange, analog-to-digital conversion takes place at the periphery of the exchange. All the problems relating to the provision of power for subscriber calls, ringing voltage and surge protection must therefore be solved there and not in the switching network.

In the second place, the digital signal for each call is not switched separately, but a large number of calls are switched in time-division multiplex: this means that the switching network establishes the required

connection from input to output very briefly for each call in succession and that this cycle is repeated periodically.

Since the internationally agreed sampling rate in pulse-code modulation for telephony is 8 kHz, the switching network must connect *each* call very briefly 8000 times a second (*fig. 16*). In modern digital exchanges, where some 256 calls are presented to each input of the switching matrix in time-division multiplex, the crosspoints therefore have to be activated over two million times a second. High switching rates such as this can of course only be achieved by using electronic devices.

The electronification of the control system

Relay control

In the simplest type of control the exchange reacts as soon as each digit dialled by the subscriber is received. Each switching stage is therefore provided with relay circuits that immediately convert the incoming signalling pulses into control pulses. These *direct* systems (like type UR 49 when used as a local exchange) are very suitable for use in straightforward network configurations.

Indirect systems make use of common control devices, often called registers, which are only needed while a connection is being made. The register receives the information dialled by the subscriber and analyses the digits selected so as to determine the connection that must be set up by the switching network. The switching stages are then activated. Because of their greater 'intelligence', indirect systems can handle more complex routing rules than direct systems. In 1967 Philips put an indirect system of this type on the market for use as a trunk exchange. In this 'UV system' both two-wire and four-wire through-connections were possible. The selector stages and the relays were basically still the same as those of the older UR system, but now electronic circuits were introduced for a number of functions in the control system. This related not only to the main functions of the registers, but also to an auxiliary device (the 'number analyser') that was consulted by the register, e.g. to analyse the dialled information for the purpose of routing and billing. Here electronics offered the advantage of speed, so that expensive common equipment capacity was utilized for shorter periods at a time. However, the combined use of relays and electronic circuits also required special attention, to prevent the electronics from reacting to very brief interruptions of a control signal caused by 'bouncing' contacts, or from adverse effects such as radio-frequency interference from the relay circuits.



Fig. 14. Mini-reed contact from a Philips reed relay. The magnetic 'reeds' can clearly be seen in the hermetically sealed glass encapsulation. To operate the contact, a coil is required, to produce a magnetic field; one coil is often used to operate more than one contact simultaneously.



Fig. 15. Because automatic telephone exchanges have become much smaller, it is possible to use ready-made mobile 'container' exchanges for certain applications. This container is being shipped from the Netherlands to Saudi Arabia.

Electronic control

In about 1960 Philips were already developing experimental exchanges with full electronic control. Discrete semiconductor components were used in the logic modules, while ferrite cores were used as memory elements. The logical functions, however, were still incorporated in the wiring and not — or only partly — in memories [16].

Although it had been demonstrated that exchanges such as this operated effectively under normal conditions they offered few specific advantages over existing electromechanical exchanges. They were, however, an excellent training school for the designers of a new generation of computer-controlled systems using 'processor control' or 'stored-program control (SPC)'.

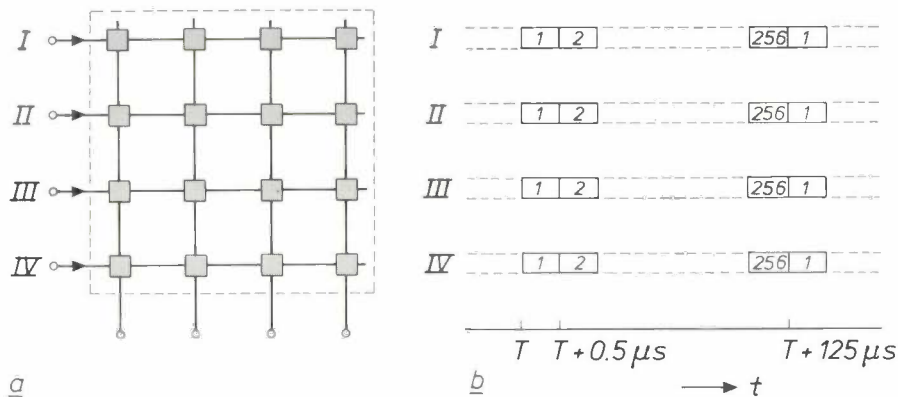


Fig. 16. a) Space-division matrix (4×4) for four time-division-multiplexed digital signals (I to IV). b) Time frame for digital signals I to IV . Each signal consists of a time multiplex of 256 telephone signals. The switching matrix operates as follows: at time T the crosspoints make the connections required for signals $I-1$ to $IV-1$; at time $T + 0.5 \mu s$ they do the same for signals $I-2$ to $IV-2$, etc. From time $T + 125 \mu s$ onwards the entire cycle is repeated.

Processor control

The idea of using one or more computers to control a telephone exchange was a fairly obvious one. The use of computers, consisting of relays, was therefore investigated even before 1950. Fast electronic computers became available in the sixties and were soon used in all kinds of fields (particularly in numerical record-keeping and other routine calculations), where they were mainly used for batch processing. Telephone exchanges, in which between 100 and 10 000 calls have to be handled simultaneously in real time, called for a different solution, however.

There were also considerable differences in the requirements relating to reliability. In batch processing, the supply of services can be interrupted in a relatively flexible way for maintenance to be carried out, and certain tasks can be repeated or postponed. Telephone exchanges often have to meet the requirement that the total duration of complete failure should not be more

than two hours in forty years (the average life of an exchange).

The first program-controlled exchanges appeared on the market shortly before 1970. They generally included computers or processors specially designed for optimum performance of the telephony process. The instruction sets were adapted to the specific needs of telephony and an extensive range of communication facilities was provided. Because of the very strict requirements for reliability, extra measures had to be taken to increase the reliability of both software and hardware.

For example, the Philips program-controlled PRX system [17] mentioned above is provided with dual processors. Such a pair of processors operates in the

'hot standby' mode, in which the standby processor receives all the information about the running of the process to keep it fully informed so that it can take over immediately in the event of a switchover. In addition, the circuits in this system are mainly TTL-type integrated circuits, in which the probability of failure is substantially reduced by the consistent use of hermetically sealed encapsulations, aluminium bonding wires and derating (i.e. remaining well within the specifications) by avoiding high equipment temperatures. In addition, the decline to be expected in particular characteristics because of ageing is taken into account in the design of the electronic circuits.

An important feature of program-controlled exchanges is their great flexibility. The software can be

[16] W. Smit, Electronic telephone exchanges in field trials, Philips Telecommun. Rev. 27, 55-72, 1967/68.

[17] Special issue 'PRX', Philips Telecommun. Rev. 31, 45-112, 1973.

altered relatively easily. One of the things this offers the network management is the possibility of remote control via data links from a central maintenance or control centre. In principle, the exchanges themselves can be unattended: any changes in the number of subscribers and the routing and billing data can be made from the control centre.

The flexibility of program-controlled exchanges also makes it easy to introduce new forms of amenities for subscribers, such as temporary transfer of incoming calls to another subscriber's number, temporarily disabling a connection for incoming traffic or outgoing traffic (to particular destinations), abbrevi-



Fig. 17. Two suites of racks from the extremely modern digital processor-controlled 5ESS-PRX telephone-switching system. Here 'electronification' is complete: both the switching network and the control system consist of electronic rather than electromechanical components. (5ESS is a trademark of AT&T Technologies Inc.)

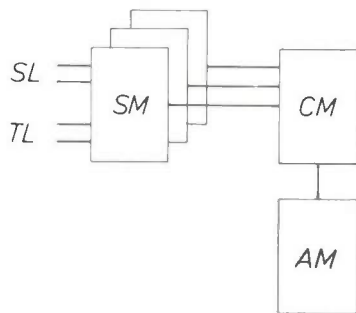


Fig. 18. Schematic representation of the architecture of the 5ESS-PRX digital switching system. The most important components are the switching modules *SM*, which are relatively autonomous, the communication module *CM* and the administrative module *AM*. The administrative module performs a large number of centralized functions. The communication module connects the switching modules both with each other and with the administrative module. The subscriber lines *SL* are connected to the switching modules, as are any trunk lines to other exchanges *TL*.

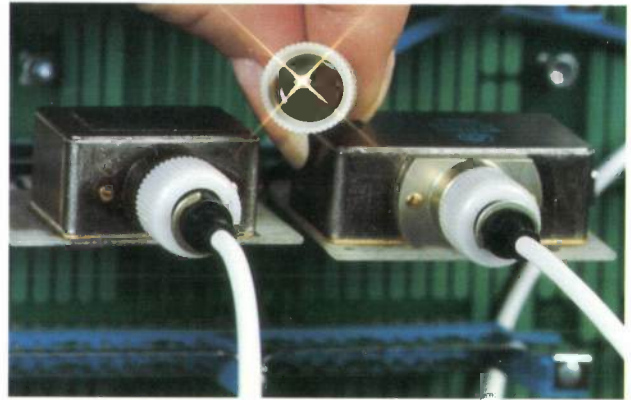


Fig. 19. In the 5ESS-PRX switching system 32-Mbit/s optical-fibre links are used for carrying information between the most important modules. A total of 256 telephony signals, with all the related information for functions such as control and error protection, can be transmitted (apparently) simultaneously over each optical fibre.

ated dialling, and so on. It is the network management, of course, who decide whether such amenities should be introduced, and when.

Control of digital exchanges

The first digital telephone exchanges appeared in about 1975. Because of the high cost of processors and memories they had centralized control, just like the semi-electronic analog exchanges mentioned earlier. As a result of the vigorous developments in semiconductor technology and the related reduction in costs, however, a second generation of digital exchanges soon emerged. These were arranged to have 'distributed control', in which processors at more than one location cooperate closely with one another. This can be illustrated with the aid of the 5ESS-PRX system^[18] (fig. 17) from AT&T and Philips Telecommunications, a company formed in 1984. This system is based on the distribution of 'intelligence' over a large number of relatively autonomous switching modules (fig. 18). Each switching module has its own 32-bit microprocessor and can set up connections independently between all the digital or analog subscriber lines and trunk lines connected to it. Traffic with other switching modules and the exchange of messages with the administrative module are effected via the communication module using a double 32-Mbit/s optical-fibre link (fig. 19). In the communication module, a space-division switching network establishes the required connection between two switching modules for each individual call in time-division.

The administrative module not only performs all the centralized switching functions, such as setting up the connection in the communication module, but also stores data for routing, billing, costing and traffic metering. In addition, the administrative module has

monitoring devices, diagnostic programs and facilities for communication with operating and maintenance staff. On the other hand, some 95% of the call-processing operations are handled by the switching modules. The 32-Mbit/s optical-fibre links enable the switching modules to be installed at distances of up to 50 km from the communication module. Even greater distances can be bridged by using internationally standardized digital transmission systems. Traffic handling within any switching module continues normally even if an interruption occurs in the link with the communication module. In view of the reliability required all common equipment is duplicated.

THE FUTURE: INTEGRATION OF SERVICES

The oldest kind of electrical communication — telegraphy — is in fact based on a form of digital transmission. The era of analog communication only started with the introduction of the telephone. Until now both types of communication have existed side by side: telegraphy and telex alongside telephony.

The emergence of communication with computers and between computers (data communication) has resulted in a sharp increase in the need for facilities for transmission of digital information. By using special equipment (data modems) information of this type can be transferred via the analog telephone network. However, there are some restrictions. The bandwidth of analog telephony channels clearly limits the capacity for transmitting digital information. In addition, data transmission and to some extent text transmission set their own special requirements for making the connection and for the transmission quality. Consequently, side by side with the analog telephone network and the digital telex network, special data networks have emerged — frequently based on packet-switched transmission — with their own digital exchanges and subscriber connections.

Now that increasing use is being made of digital transmission and switching devices in the telephone network as well, it is obvious that for both economical and practical reasons the aim should be to achieve a single universal digital communications network. In addition to telephony, this Integrated Services Digital Network (ISDN) will also permit the communication of text, data, graphics and images in many forms. This will have to take place in a gradual process of development, extending over a period of perhaps twenty or thirty years. First of all an Integrated Digital Network (IDN) will be set up which will still mainly be

used for telephony, followed by a narrow-band ISDN for digital communication services with rates of up to 64 kbit/s. At a later stage it will be possible to add services with transmission rates of up to 2 Mbit/s (e.g. for video conferences) and this development will finally culminate in a wideband ISDN, with the possibility of high-quality video communication.

Modern digital telephone exchanges already contain a number of functions that permit the flexible introduction of new services^[19]. Here the existing resources are used as far as possible; for example, the narrow-band ISDN will be using the existing analog subscriber lines. International standardization provides for a category of digital subscriber connections with an effective transmission capacity of 144 kbit/s. Advanced signal processing methods will permit most analog subscriber lines to be adapted for this purpose^[20].

In the information society of tomorrow the ISDN will undoubtedly be just as indispensable as the telephone network is today. Electronic and opto-electronic modules will play an increasingly important part in the creation of the necessary equipment. If the stage is ever reached where integrated optics or bio-chip technology supplants electronics from transmission and switching systems, it will mark the end of a particularly fascinating era in telecommunications — and possibly herald the start of an even more fascinating age.

[18] Special issue 'SESS-PRX', Philips Telecommun. Rev. 42, 109-184, 1984;

SESS is a trademark of AT&T Technologies Inc.

[19] W. Lemstra and H. van der Veer, ISDN capabilities of the SESS-PRX, Trends Telecommun. 1, 41-54, 1985.

[20] K. J. Wouda, An implementation of a 144 kbit/s transmission system for two-wire loops, Trends Telecommun. 1, 55-66, 1985.

Summary. When the telephone was invented more than hundred years ago, nothing of what we now know as 'electronics' was in existence. It was only much later, mainly in the last half-century, that the gradual development took place that can be described as the 'electronification' of telephony systems. Present-day analog transmission systems would not have been possible without revolutionary new system concepts and this is also true for digital and optical transmission systems — but all of them would have been quite impossible without electronics. Until recently, electromechanical components have been able to hold their own in the switching network; it is only in the digital exchange that the advantages of electronic crosspoints have become so significant. In particular, the advent of processor control with special telephony computers has led to complete electronification in the control sections of the switching systems. In the twenty or thirty years ahead electronic technology will enable the telephone network and other existing networks (e.g. for telex and data) to merge into one universal digital communications network with common transmission and switching facilities. This Integrated Services Digital Network (ISDN) will offer subscribers a multitude of services, both existing and new.

Scientific publications

These publications are contributed by staff of laboratories and plants that form part of or cooperate with enterprises of the Philips group of companies, particularly by staff of the research laboratories mentioned below. The publications are listed alphabetically by journal title.

Philips GmbH Forschungslaboratorium Aachen, Weißhausstraße, 5100 Aachen, Germany	A
Philips Research Laboratory, Brussels, 2 avenue Van Becelaere, 1170 Brussels, Belgium	B
Philips Natuurkundig Laboratorium, Postbus 80 000, 5600 JA Eindhoven, The Netherlands	E
Philips GmbH Forschungslaboratorium Hamburg, Vogt-Kölln-Straße 30, 2000 Hamburg 54, Germany	H
Laboratoires d'Electronique et de Physique Appliquée, 3 avenue Descartes, 94450 Limeil-Brévannes, France	L
Philips Laboratories, N.A.P.C., 345 Scarborough Road, Briarcliff Manor, N.Y. 10510, U.S.A.	N
Philips Research Laboratories, Cross Oak Lane, Redhill, Surrey RH1 5HA, England	R
Philips Research Laboratories, Sunnyvale P.O. Box 9052, Sunnyvale, CA 94086, U.S.A.	S

C. A. M. Mulder & J. G. van Lierop E	Preparation, densification and characterization of autoclave dried SiO ₂ gels	Aerogels, J. Fricke (ed.), Springer, Berlin	68-75	1985
D. C. L. Vangheluwe (<i>Philips Centre for Manuf. Technol., Eindhoven</i>)	Exact calculation of the spring constant in the buckling of optical fibers	Appl. Opt. 23	2045-2046	1984
B. Aldefeld & H. Richter H	Semiautomatic three-dimensional interpretation of line drawings	Comput. & Graphics 8	371-380	1984
P. A. Devijver B	Cluster analysis by mixture identification	Data analysis in astronomy, V. Di Gesu <i>et al.</i> (eds), Plenum, New York	29-44	1985
C. M. G. Jochem & J. W. C. van der Ligt E	Method for cooling and bubble-free coating of optical fibres at high drawing rates	Electron. Lett. 21	786-787	1985
A. Valster, L. J. Meuleman, P. I. Kuindersma & T. van Dongen E	Improved high-frequency response of InGaAsP double-channel buried-heterostructure lasers	Electron. Lett. 22	16-18	1986
P. Haaker, E. Klotz, R. Koppe, R. Linde & D. G. Mathey (<i>Univ. Hospital Eppendorf, Hamburg</i>) H	First clinical results with digital flashing tomosynthesis in coronary angiography	Eur. Heart J. 6	913-920	1985
A. R. Calderbank (<i>AT&T Bell Labs, Murray Hill, NJ</i>) & J. M. Goethals B	On a pair of dual subschemes of the Hamming scheme $Hn(q)$	Eur. J. Comb. 6	133-147	1985
J. N. Sandoe, J. R. Hughes & J. A. G. Slatter R	Characterisation and modelling of SIPOS on silicon high-voltage devices	IEE Proc. I 132	281-284	1985
S. Moridi & H. Sari L	Analysis of four decision-feedback carrier recovery loops in the presence of intersymbol interference	IEEE Trans. COM-33	543-550	1985
M. Hartmann, K. Witter & P. Willich H	Temperature dependence of anisotropy constant and saturation magnetization of amorphous GdFeM (M = Ge, Si, Sn, Bi, Au) alloys	IEEE Trans. MAG-21	2044-2046	1985
M. H. Kuhn, W. Menhardt & I. C. Carlsen H	Real-time interactive NMR image synthesis	IEEE Trans. MI-4	160-164	1985
M. L. Verheijke, J. Hanssen, H. Jaspers, L. Steuten & P. Wijnen E	Neutron activation analysis for the modern electronics industry	Instrumentelle multi-elementanalyse, B. Sansoni (ed.), VCH Verlag, Weinheim	603-606	1985
J. F. Verwey & D. R. Wolters E	Breakdown fields in thin oxide layers	Insulating films on semiconductors, J. J. Simonne & J. Buxo (eds), Elsevier Science, Amsterdam	125-132	1986

- | | | | | |
|---|---|--|-------------------|------|
| D. R. Wolters & J. J. van der Schoot
E | Breakdown by charge injection | Insulating films on semiconductors, J. J. Simonne & J. Buxo (eds), Elsevier Science, Amsterdam | 145-149 | 1986 |
| H. L. Peek & J. F. Verwey
E | The influence of arsenic S-D implantations on thin oxides | Insulating films on semiconductors, J. J. Simonne & J. Buxo (eds), Elsevier Science, Amsterdam | 199-202 | 1986 |
| J. N. Sandoe & J. R. Hughes
R | Properties of the SIPOS-silicon interface | Insulating films on semiconductors, J. J. Simonne & J. Buxo (eds), Elsevier Science, Amsterdam | 217-220 | 1986 |
| P. Hansen & K. Witter
H | Growth-induced uniaxial anisotropy of bismuth-substituted iron-garnet films | J. Appl. Phys. 58 | 454-459 | 1985 |
| C. Colinet*, A. Pasturel* (* Lab. Thermodyn. & Physico-Chimie Metallurgiques, St. Martin d'Hères) & K. H. J. Buschow
E | Molar enthalpies of formation of LnAl ₂ compounds | J. Chem. Thermodyn. 17 | 1133-1139 | 1985 |
| B. Pichaud*, N. Burle-Durbec*, F. Minari* (* Univ. Aix-Marseille III, Marseille) & M. Duseaux
L | Study of dislocations in highly In doped GaAs crystals grown by liquid encapsulation Czochralski technique | J. Cryst. Growth 71 | 648-654 | 1985 |
| J. van de Ven (Univ. Nijmegen), J. E. A. M. van den Meerakker & J. J. Kelly
E | The mechanism of GaAs etching in CrO ₃ -HF solutions. I. Experimental results | J. Electrochem. Soc. 132 | 3020-3026 | 1985 |
| J. J. Kelly, J. van de Ven (Univ. Nijmegen) & J. E. A. M. van den Meerakker
E | The mechanism of GaAs etching in CrO ₃ -HF solutions. II. Model and discussion | J. Electrochem. Soc. 132 | 3026-3033 | 1985 |
| A. van Eenbergen & E. Bruninx
E | On the intrinsic resolution of the LHS-10 electron spectrometer | J. Electron Spectrosc. & Relat. Phenom. 37 | 265-268 | 1985 |
| H. M. van Noort, D. B. de Mooij & K. H. J. Buschow
E | ⁵⁷ Fe Mössbauer investigation of ternary compounds of the R ₂ Fe ₁₄ B type | J. Less-Common Met. 115 | 155-165 | 1986 |
| M. Brouha, A. J. C. van der Borst, G. W. Turk & C. H. M. Witmer
E | High frequency magnetic properties of sputtered thin films | J. Magn. & Magn. Mater. 54-57 | 1665-1666 | 1986 |
| E. Bruninx, A. F. P. M. van Eenbergen, P. van der Werf & J. Haisma
E | X-ray photoelectron spectroscopy of hafnium nitride | J. Mater. Sci. 21 | 541-546 | 1986 |
| J. Robertson (Central Electr. Res. Labs, Leatherhead) & M. J. Powell
R | Defect model of charge transfer doping at a-SiN _x :H/a-Si:H interfaces | J. Non-Cryst. Solids 77 & 78 | 1007-1010 | 1985 |
| C. van Berkel & M. J. Powell
R | The photosensitivity of amorphous silicon thin film transistors | J. Non-Cryst. Solids 77 & 78 | 1393-1396 | 1985 |
| J. F. Goldenberg & T. S. McKechnie
N | Diffraction analysis of bulk diffusers for projection-screen applications | J. Opt. Soc. Am. A 2 | 2337-2348 | 1985 |
| H. Heitmann, M. Hartmann, M. Rosenkranz & H. J. Tolle
H | Amorphous rare earth-transition metal films for magneto-optical storage | J. Physique 46 (Colloque C6) | C6/9-
C6/18 | 1985 |
| R. Grössinger*, X. H. Sun*, R. Eibler*, K. H. J. Buschow & H. R. Kirchmayr* (* Tech. Univ. Vienna)
E | The temperature dependence of the anisotropy field in R ₂ Fe ₁₄ B compounds (R = Y, La, Ce, Pr, Nd, Gd, Ho, Lu) | J. Physique 46 (Colloque C6) | C6/221-
C6/224 | 1985 |
| C. A. M. Mulder, Th. P. M. Meeuwssen & G. E. Thomas
E | Analysis of the reduction of hydrogen-induced infrared loss increases in fluorine-doped PCVD silica fibre preforms | J. Physique 46 (Colloque C8) | C8/591-
C8/595 | 1985 |
| S. M. Marcus (Inst. Perception Res., Eindhoven) & U. H. Frauenfelder (Max Planck Inst., Nijmegen) | Word recognition — uniqueness or deviation? A theoretical note | Lang. & Cognitive Process. 1 | 163-169 | 1985 |
| E. H. L. Aarts, F. M. J. de Bont, J. H. A. Habers & P. J. M. van Laarhoven
E | A parallel statistical cooling algorithm | Lect. Notes Comput. Sci., Vol. 210, B. Monien & G. Vidal-Naquet (eds), Springer, Berlin | 87-97 | 1986 |

K. M. Lüdeke, P. Röschmann & R. Tischler	H	Susceptibility artefacts in NMR imaging	Magn. Resonance Imaging 3	329-343	1985
G. M. Loiacono & J. C. Jacco	N	Thermal characterization of KClO ₃ , KBrO ₃ , and KIO ₃	Mater. Lett. 4	27-29	1985
K. H. Nicholas, R. A. Ford & R. W. Wilks	R	Proximity corrections for electron image projection	Microelectron. Eng. 3	77-84	1985
F. A. Vollenbroek, W. P. M. Nijssen, H. J. J. Kroon & B. Yilmaz	E	High resolution optical lithography by formation of a built on mask (B.O.M.)	Microelectron. Eng. 3	245-252	1985
R. L. Bronnes & R. C. Sweet	N	Metallography of a novel Stirling engine heat receptor	Microstruct. Sci., Vol. 12, D. Northwood <i>et al.</i> (eds), Am. Soc. Met., Metals Park, OH	571-576	1985
P. A. Devijver	B	Probabilistic labeling in a hidden second order Markov mesh	Pattern recognition in practice II, E. S. Gelsema & L. N. Kanal (eds), Elsevier Science, Amsterdam	113-123	1986
P. A. Devijver	B	Baum's forward-backward algorithm revisited	Pattern Recognition Lett. 3	369-373	1985
A. J. E. M. Janssen	E	On the eigenvalues of an infinite Jacobi matrix	Philips J. Res. 40	323-351	1985
J. A. Geurst	E	Two-fluid hydrodynamics of bubbly liquid/vapour mixture including phase change	Philips J. Res. 40	352-374	1985
P. Houdy, E. Ziegler (<i>MST Argonne Nat. Lab., Argonne, IL</i>) & L. Névoit (<i>I.O.T.A., Orsay</i>)	L	Application of sputtering to the realization of amorphous ultra-thin layers (10 Å) stacks: advantages of in situ ellipsometry control system	Philips J. Res. 40	375-398	1985
G. Harding, J. Kosanetzky & U. Neitzel (<i>CHF Müller Röntgenwerk, Hamburg</i>)	H	Elastic scatter computed tomography	Phys. Med. & Biol. 30	183-186	1985
M. R. Simpson, P. A. Gough, F. I. Hshieh & V. Rumennik	N	Analysis of the lateral insulate gate transistor	Proc. IEDM-85, Washington, DC, 1985	740-743	1985
P. M. L. O. Scholte*, M. Tegze*, F. van der Woude* (<i>* Univ. Groningen</i>), K. H. J. Buschow & I. Vincze* (<i>* Central Res. Inst. Phys., Budapest</i>)	E	The influence of the conduction electrons on the EFG in amorphous intermetallic alloys	Proc. Int. Conf. on the Applications of the Mössbauer effect, Leuven 1985	4 pp.	1985
J. J. P. Bruines, R. P. M. van Hal, H. M. J. Boots & J. Wolter	E	Pulsed-laser melting of amorphous silicon on glass: time-resolved reflectivity measurements	Proc. MRS Conf., Strasbourg 1985	525-529	1985
T. S. te Velde & A. T. A. Zegers-van Duynhoven	E	The electroscopic fluid display	Proc. SID 26	167-170	1985
M. J. Powell	R	Amorphous-silicon thin-film transistors: performance and material properties	Proc. SID 26	191-196	1985
N. M. Marinovic & G. Eichmann (<i>City Univ. New York</i>)	N	Feature extraction and pattern classification in space-spatial frequency domain	Proc. SPIE 579	19-26	1985
M. Erman & N. Vodjdani	L	Optique intégré sur substrat semiconducteur: quelques résultats obtenus au LEP	Rev. de l'ISEP, No. spécial: les perspectives d'avenir de l'opto-électronique	9-10	1985
M. G. Collet	E	Solid state image sensors	Solid state devices 1985, P. Balk & O. G. Folberth (eds), Elsevier Science, Amsterdam	183-200	1986
H. J. Cornelissen	E	Laser spectroscopy in low-pressure sodium-neon discharges	Thesis, Eindhoven	89 pp.	1986
G. J. van Gorp & F. J. du Chatenier	E	Measurement of thermomigration in thin metal films	Thin Solid Films 131	155-162	1985
F. H. M. Sanders & J. Dieleman	E	Plasma etching damage: theory and practice	Vide/Couches Minces 40 (Suppl. to No. 229)	45-61	1985

Recent United States Patents

Abstracts from patents that describe inventions from the following research laboratories, which form part of or cooperate with the Philips group of companies:

Philips GmbH Forschungslaboratorium Aachen, Weißhausstraße, 5100 Aachen, Germany	A
Philips Research Laboratory Brussels, 2 avenue Van Becelaere, 1170 Brussels, Belgium	B
Philips Natuurkundig Laboratorium, Postbus 80 000, 5600 JA Eindhoven, The Netherlands	E
Philips GmbH Forschungslaboratorium Hamburg, Vogt-Kölln-Straße 30, 2000 Hamburg 54, Germany	H
Laboratoires d'Electronique et de Physique Appliquée, 3 avenue Descartes, 94450 Limeil-Brévannes, France	L
Philips Laboratories, N.A.P.C., 345 Scarborough Road, Briarcliff Manor, N.Y. 10510, U.S.A.	N
Philips Research Laboratories, Cross Oak Lane, Redhill, Surrey RH1 5HA, England	R
Philips Research Laboratories Sunnyvale, P.O. Box 9052, Sunnyvale, CA 94086, U.S.A.	S

4 517 525

Balancing compensation in differential amplifiers with a single-ended drive

E. C. Dijkmans E
R. J. van de Plassche

A differential amplifier with single-ended drive includes a balancing capacitor coupled between the base of a transistor connected to the signal input and the common point of the two emitters of transistors, which form a differential pair. The capacitance value of the capacitor is substantially equal to the capacitance value of the stray capacitance of the collector-substrate junction of a transistor which forms a current source. This provides a symmetry of the capacitances between the input and the common point and between the common point and ground via the transistor, which forms the current source. This results in an improved balance in the output signals at the output terminals and a flat frequency response of the differential amplifier for higher frequencies.

4 547 801

Tunable Fabry-Perot interferometer and X-ray display device having such an interferometer

J. Haisma E
C. L. Adema
J. M. M. Pasmans
J. H. Walters

In a tunable Fabry-Perot interferometer, the supports for two parallel mirrors consist of bundles of optical fibers with the mirrors being provided on the ends of the fibers. This structure may be used advantageously in an X-ray display device wherein the structure is located between the display screen on which the visible X-ray image is displayed and a television camera tube. By using the Fabry-Perot interferometer as a light attenuator in such a device, problems where the camera tube is overridden when making an X-ray record can be prevented by causing the reflection coefficient of the mirrors in the visible range of the spectrum to be 99% or more. Also, the half width of the transmission wavelength pass-band of the Fabry-Perot interferometer can be made less than 50 nm.

4 537 506

Atomizer for atomic absorption spectroscopy

B. Lersmacher A, R
M. P. Wassall
P. J. Connor

The atomizer of the present invention serves for generating free atoms and an atomic cloud by heating a sample for analysis. The device includes a preferably tubular cuvette for receiving the sample, and the cuvette consists either of a basic body of carbon, which is enveloped by a pyrolytic graphite layer, or only of pyrolytic graphite layers. An electric supply unit for Joule heating the cuvette is in contact with the cuvette by contact members. In order to achieve a radial temperature distribution in the cuvette such that the inner wall of the cuvette is at an essentially higher temperature than the outer wall of the cuvette, the contact surfaces of the cuvette and the contact surfaces of the contact members contact each other in such a manner that the electric current applied during operation of the atomizer preferably flows through the inner wall of the cuvette.

4 547 902

Radio receiver comprising a frequency-locked loop with audio frequency feedback, and a muting circuit

W. G. Kasperkovitz E

Radio-receiver having a frequency-locked loop which comprises a tunable voltage-controlled oscillator, a mixer stage, a filtering element, as well as a frequency-voltage converter which is connected to the tunable voltage-controlled oscillator. Several stable tunings are possible for each transmitter. An unambiguous selection is made from these stable tunings of a tuning to a desired station by muting the radio receiver in the other stable tuning frequency ranges. To this end the radio receiver according to the invention comprises a muting circuit as well as a control circuit for the muting circuit. A further frequency-voltage converter comprising an all-pass frequency-dependent 180° phase shifting network, a phase detector and a limiter detects a tuning error. By adjusting the muting circuit of the radio receiver to the quiescent condition only in the desired tuning range and by activating it outside this range, a suppression of interstation noise is obtained.



4 548 129

Coffee maker

W. L. N. van der Sluys

J. Pastoor

J. C. M. Roelofs

The invention relates to a coffee maker comprising a water reservoir, a filter device and a flow heater for heating water from the water reservoir for delivery to the filter device. A problem associated with coffee makers is the deposit of scale in the flow heater. It is proposed to provide a coffee maker with means for adding a small amount of coffee extract to the water before it enters the flow heater. Coffee extract naturally contains phosphoric-acid-like compounds which inhibit the crystal growth of metal salts in the water. Preferably, coffee extract is fed continuously from the filter device to the water reservoir.

E

4 549 145

Switching amplifier

R. J. van de Plassche

E

A switching amplifier is described which is intended in particular for sample-and-hold circuits. The switching amplifier has an output stage of the npn-npn-type comprising two output transistors in series. The output is connected to the emitter of a first one of the two output transistors and to the collector of the second output transistor, a diode being arranged between the output and this collector. The output can be switched off by switching the voltage on the base of the first transistor and the voltage on the point between the diode and the collector of the second transistor relative to the output voltage, a third transistor ensuring that in this situation the collector current of the second transistor can be drained when said diode is turned off, so that initially said second transistor can remain conductive.

4 549 288

Apparatus for enhancing the playback signal in an optical data recording system

A. Y. Chan

N

Optical data recording apparatus which enhances a playback signal by comparing the lengths of the lands on a recording medium with the lengths of the pits on it and changes the playback signal to represent equality between such lengths.

4 551 269

Non-linear resistor and method of manufacturing the same

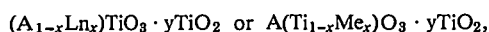
D. Hennings

A. Schnell

H. Schreinemacher

A

A non-linear resistor having an operational field strength which optionally is formed as a VDR or as an NTC-resistor having a ceramic sintered body on the basis of a polycrystalline alkaline earth metal titanate doped with a small quantity of a metal oxide so as to produce an n-type conductivity, in which the sintered body comprises at its grain boundaries insulating layers formed by re-oxidation of the sintered body and consists of an alkaline earth metal titanate having a Perovskite structure of the general formula



wherein: A = alkaline earth metal; Ln = rare earth metal; Me = metal having a valency of 5 or more; $0.0005 < x <$ solubility limit in the Perovskite phase; $y = 0.001$ to 0.02 . The sintered body becomes adjustable in its non-linear resistance variation by selection of the re-oxidation temperature and of the re-oxidation duration in such manner that an initially present NTC-characteristic gradually is observable only at ever increasing temperatures and changes into a VDR-characteristic in the range of the operating temperature of the resistor.

4 552 020

Apparatus for the scanning of objects by means of ultrasound echography

M. J. Auphan

L

An apparatus for the scanning of objects by means of ultrasound echography, comprising a mosaic of ultrasound transducers which is connected to a transmitter stage and a receiver stage for the reception and processing of the ultrasound echos corresponding to the obstacles encountered by the transmitted signals in their direction of propagation, and also comprising a display stage. The transducers of the mosaic are grouped in 2^n subwindows in which a non-corrected echogram of an area of the objects scanned is formed. The receiver stage comprises a device for determining correction delays to be applied to delay devices, said device comprising $2^n - 1$ intercorrelation circuits which operate on the basis of n successive divide-by-two operations of the aperture of the mosaic.

4 552 301

Method of bonding ceramic components together or to metallic components

M. R. Liehr

W. Nolting

R. U. D. Kobs

R. U. Orłowski

H

The invention relates to a method for the force-coupled and vacuum-tight bonding of components of ceramic material together or to metallic components by means of thermocompression while using a soldering material in the form of an AlMgZn alloy provided between the components to be bonded prior to the thermocompression process. The soldering material used consists preferably of an aluminium-zinc-magnesium alloy having 95% by weight of Al, 4% by weight of Zn and 1% by weight of Mg.

4 553 234

Method and system of transmitting digital information in a transmission ring

J. R. Brandsma

A. A. M. L. Bruekers

J. L. W. Kessels

E

The invention relates to a broad-band, time-division multiplex, token-passing, ring local area network, with which both circuit-switched and packet-switched traffic, namely data, text, picture and speech traffic can be supported. The invention has for its object to provide a method of transmitting digital information in a ring having a comparatively high transmission capacity with which rapid access to the common ring transmission means can be obtained, without however high requirements being imposed on the processing speed of the stations. According to the invention this is in principle achieved by means of a method which guarantees that per time-division multiplex frame only one time slot, which is known to the station, needs to be accessed.

4 553 250

Signal transmission system

S. F. Bryant

R

A signal transmission system comprises a transmitter, a receiver and a transmission link in which the signal to be transmitted is pulse code modulated. The transmission link comprises a plurality of channels (0-7), one for each bit of the pulse code modulated signal. The quality of each channel is monitored and the bits of the pulse code modulated signal are applied to the channels such that the most significant bits of the pulse code modulated signal are allocated to the channels having the lowest level of interfering signal.

4 553 266

RF circuit arrangement

R. N. Bates

P. M. Ballard

R

An RF circuit with at least one RF transmission line including a strip conductor and a ground plane on an insulating substrate and having two diodes respectively dc-connected to two portions of the ground plane. The two portions are mutually dc-isolated by a slot to enable the diodes to be biased. The substrate is mounted in a housing of conductive material, and the two portions of the ground plane are mutually RF-coupled via the conductive material. One of the portions is electrically-connected to an adjacent housing member and the other portion is separated therefrom by a thin insulating layer. The slot inhibits coupling of RF energy out of the circuit into the slot, suitably being very narrow, e.g. 20 μm , so as to form a further transmission line with a very low characteristic impedance and also to have a high attenuation along its length for operation at mm-wavelengths.

4 554 030

Method of manufacturing a semiconductor device by means of a molecular beam technique

J. Haisma

P. K. Larsen

T. de Jong

J. F. van der Veen

W. A. S. Douma

F. W. Saris

E

A monocrystalline layer of one semiconductor material is grown onto a surface of a monocrystalline semiconductor body by means of molecular beam epitaxy. During such growth, the semiconductor body is kept at such a low temperature that a non-monocrystalline layer is obtained. The non-monocrystalline layer is then converted by a heat treatment into a monocrystalline form. Accordingly, an abrupt junction between the two semiconductor materials is obtained.

4 554 471

Electric motor having a U-shaped stator iron

L. Bertram

H. Schemmann

J. de Boer

H

The invention relates to an electric motor having a U-shaped stator iron such as a series-, split-pole- or single-phase synchronous motor. Between the free shank ends of the stator, pole shoes are formed and on the shanks, induction coils are provided. The shanks of the stator iron in the area between the pole shoes and the coils are bent with respect to the central plane of the stator iron in such manner that the shaft of the rotor with the central plane of the stator iron encloses an angle differing from the perpendicular to the central plane.

4 554 503

Current stabilizing circuit arrangement

W. G. Kasperkovitz

E

A current stabilizing arrangement includes a first circuit having a series arrangement of a first resistor, a second resistor, and the collector-emitter path of a first transistor having its base connected to a point between the first and second resistors. A second circuit includes the collector-emitter path of a second transistor whose base is coupled to the collector of the first transistor. By providing a third resistor in the first circuit, in series with the first and second resistors and connected between the base of the second transistor and the collector of the first transistor, improved current stabilization with variations in supply voltage is obtained.

4 554 564

Semiconductor device and method of manufacturing same, as well as a pick-up device and a display device having such a semiconductor device

G. G. P. van Gorkom

A. M. E. Hoeberechts

E

The invention relates to a method for displaying a pattern on a resist using electron lithography. In particular, a cathode device having a matrix of semiconductor cathodes generates an electron beam which exposes a resist layer. The electron beam is generated by applying control signals to selected ones of the matrix of cathodes to cause electron emission therefrom.

4 555 374

Method of manufacturing a disc resonator

P. Roschmann

H

A method is described for adjusting the temperature coefficient of the ferrimagnetic resonant frequency in gallium or aluminium substituted YIG disc resonators. At the compensation temperature, T_0 , the temperature coefficient of the resonant frequency, f_r , in a given frequency range is approximately zero. Where this range lies, depends, inter alia, on the substitution value. By annealing the discs, T_0 can be moved into the desired temperature range. When the manufactured disc has a compensation temperature above the desired temperature range, annealing must be carried out at approximately 850 to 1400 °C. When the manufactured disc has a compensation temperature below the desired temperature range, annealing is performed at approximately 400 to 850 °C.

4 555 460

Mask for the formation of patterns in lacquer layers by means of X-ray lithography and method of manufacturing same

M. Harms

A. Bruns

H. Lüthje

B. Matthiessen

H

In a mask for X-ray lithography, in which a pattern of a layer corresponding to the structure to be manufactured and consisting of a material opaque to visible light is applied to a thin diaphragm of a material transparent to X-ray radiation, an adjustment with visible radiation, such as laser light, is made possible using a diaphragm consisting of a material opaque to visible light and using adjustment windows of a material transparent to the visible light of the spectrum through the diaphragm.

4 555 631

Apparatus for transmitting signals between two relatively rotatable parts

G. Martens

H

An optical transmission system arrangement for transmitting data between two relatively rotatable parts. A hollow cylinder with a mirror-coated inner surface onto which the light is incident at the smallest possible grazing angle and is frequently reflected. The light is coupled in and out through a coupling section in the hollow cylinder, at which the light is incident onto the inner surface. The system achieves a comparatively low damping because the reflecting power at small angles of incidence is comparatively high.

4 555 673

Differential amplifier with rail-to-rail input capability and controlled transconductance

J. H. Huijsing

R. J. van de Plassche

E

A differential amplifier operable between a pair of supply voltages that define a rail-to-rail supply range contains a pair of differential portions that together provide representative signal amplification

across the supply range, although neither differential portion individually does so. A current control regulates operating currents for the differential portions in such a way that the amplifier transconductance can be controlled in a desired manner as the common-mode part of the amplifier input signal varies across the supply range. The transconductance is typically controlled to be largely constant. A summing circuit selectively combines internal currents from the differential portions to generate at least one output signal representative of the input signal.

4 555 676

Dual-section amplifier arrangement having a protection circuit

R. J. van de Plassche E
E. C. Dijkmans

An amplifier arrangement includes a first section and a second section. The second section has an output transistor which is protected by a protection circuit. The protection circuit acts on the input of the second section in order to obtain a higher gain in the protection loop. In order to preclude instabilities, the protection circuit has a falling frequency response with a flat portion in view of the frequency compensation of the second section.

4 555 729

System for transmitting television picture information using an error-protection code

L. M. H. E. Driessen E

An error protection code which acts on subpictures together constituting a television picture for the transmission of data for reconstructing the television picture at the receiving end. First each subpicture is transformed by Hadamard functions. Of the coefficients thus formed, a number of most significant coefficient bits which are associated with low frequency transformation functions are protected against a bit error. Moreover, a comparatively small number of coefficient bits within said number are protected against an additional bit error.

4 555 797

Hybrid loudspeaker system for converting digital signals to acoustic signals

J. A. M. Nieuwendijk E
W. D. A. M. van Gijssel
G. B. J. Sanders
J. M. van Nieuwland

In a loudspeaker system for converting an n -bit digitized electric signal into an acoustic signal a plurality of p sections of a digital loudspeaker are driven directly by the p most significant bits of the n -bit digitized electric signal. The loudspeaker comprises at least one additional section $p + 1$. This $(p + 1)^{\text{th}}$ section receives a signal from a digital-to-analog converter, the input signal of the digital-to-analog converter comprising at least the $n - p$ least significant bits. In a different embodiment the digital-to-analog converter receives all the n bits of the digitized electric signal as the input signal. At least the p sections which correspond to the p most significant bits are provided with means for producing a signal which is a measure of the sum of their instantaneous drive signals and for applying the said signal to a signal combination unit arranged in the line from the output of the digital-to-analog converter to the $(p + 1)^{\text{th}}$ section. By means of this correction circuit the distortion in the loudspeaker system can be reduced substantially.

4 555 810

Distribution system for a local area network

G. D. Khoe E
J. H. C. van Heuven

A distribution system for a local area network has a distribution unit which is coupled to a plurality of subscribers' premises via optical transmission links. Each subscriber is provided with a terminal

unit having an input coupled to an optical transmission link. The terminal unit has a plurality of outputs which are connected to optical wall sockets. Opto-electrical converters are provided at each socket. Each terminal unit has a power splitter and a distribution box. The distribution box has a plurality of inputs, a larger number of optical outputs, and a plurality of links between the inputs and outputs.

4 556 796

Infrared radiation detector

M. Renals R

An infrared radiation detector comprises two differentially connected pyroelectric detector elements in parallel-opposition. The detector elements are formed in a single body of pyroelectric material having two adjacent pairs of overlapping electrodes on opposite major surfaces of the body. The two detector elements are poled in the same direction. To electrically connect the top electrodes of each pair to the bottom electrodes of the other pair, each electrode is provided with an L-shaped extension. Each extension is arranged such that at an edge of the body the extension of the top electrode of one pair overlaps the extension of the bottom electrode of the other pair. The overlapping extensions can be electrically connected together by conductive epoxy or by conductive clips on the edge of the body.

4 556 967

Record carrier having an optically readable information structure comprised of information areas of two different phase depths

J. J. M. Braat E

A record carrier is described which has an optically readable information structure in which information areas of adjacent information track portions have different phase depths, and an apparatus for reading said record carrier. By a suitable choice of the phase depths and by an electronic phase shift of the signals supplied by the read detectors, cross-talk between adjacent tracks can substantially be eliminated.

4 557 564

Movable scanning unit for an optical recording or playback apparatus

G. E. van Rosmalen E

An electro-optical device for reading an information disc comprises an optical system which is movable relative to the disc by at least one electro-magnetic actuator. The optical system is supported by elongated members whose length is great relative to their thickness and which are pretensioned in the longitudinal direction by magnets which cooperate with each other via an air gap, enabling the use of very flexible supporting elements, for example guys which have a low resistance to bending and a very low mass.

4 558 448

Semiconductor laser with end zones for reducing non-radiating recombination

J. A. de Poorter E
P. J. de Waard
R. P. Tijburg
G. L. Dinghs

A semiconductor laser having mirror faces serving as resonators, in which the active laser region includes end zones adjoining the mirror faces which have implanted ions, preferably protons, with associated crystal damage. The end zones have a length which is at least equal to the diffusion length of the recombining charge carriers in the end zones. As a result of the high recombination rate in the end zones substantially no non-radiating recombination occurs at the mirror faces, so that mirror erosion is avoided.

4 559 280

Metallized rare earth garnet and metal seal to same

R. L. Bronnes
J. K. McKinlay
R. C. Sweet
W. K. Zwicker

N

A reliable garnet to metal hermetic seal is obtained by metallizing the garnet with successive sputtered layers of tantalum or titanium, molybdenum or tungsten and nickel, followed by soldering or brazing the metallized garnet to a metal member.

4 559 467

Ion-generator for producing an air flow

F. K. Beckmann
H. Dötsch
D. Gossel

H

An ion-generator for producing an air flow includes a plurality of rectangularly shaped plate electrodes spaced from one another and respectively lying in planes parallel to the direction of the air flow, such plate electrodes extending perpendicularly to the direction of the air flow, the edge of each plate electrode facing upstream being rounded. There is a plurality of rows of needle electrodes disposed upstream of the plate electrodes and extending perpendicularly to the direction of the air flow, such rows of needle electrodes being respectively associated with and oriented towards the gaps between the plate electrodes, the tips of all the needle electrodes being disposed in a plane perpendicular to the direction of the air flow. There is an electrically conductive rod-shaped support for each row of needle electrodes, such rod-shaped supports being arranged parallel to the rounded edges of the plate electrodes. An electrically insulating material covers each rod-shaped support and its associated row of needle electrodes except for the tip of each needle electrode. The plate electrodes are connected to one terminal of a high-voltage dc source; and the rod-shaped supports are connected to the other terminal of such dc source.

4 559 469

Green emitting phosphor and cathode-ray tube provided with such a phosphor

T. Welker
K. Carl
W. Czarnojan

A

A green emitting phosphor for heavily loaded cathode-ray tubes comprises a mixture of a deep-green and a yellowish-green emitting phosphor. Mixtures of $Zn_2SiO_4:Mn$ and at least one phosphor from the group comprising $Y_2SiO_5:Tb$; $X_2O_2S:Tb$; $ES:Ce$ and $XOZ:Tb$, where $X = Y, La, Gd, Lu$; $E = Ca, Sr, Ba$; and $Z = Cl, Br, I, F$; satisfy the EBU specification.

4 559 612

Sorting device for data words

H. Vrieling

E

An integrated sorting device for data words comprises a bidirectional bus to which are connected the address input of a memory, a command register for memory clear, sorting criterion and pointer reset signals, a multiplexer and an address counter. In a write mode of operation, data words arriving on the bus address the memory and representations thereof, e.g. binary 1s, are stored therein. Briefly before each such storage operation, the same memory location is read and any representation already stored therein is used to trigger a flip-flop to indicate that an overflow condition exists. During a read operation, the address counter addresses the successive memory addresses under the control of an oscillator. When a filled memory location is reached, a further flip-flop causes the counter to stop and a 'ready' signal is outputted. The counter resumes counting when the relevant memory location has been read completely. The multiplexer feeds the overflow signal and a read termination signal derived from the address counter to the bus.

4 559 635

Auto-adaptive amplitude-equalizing arrangement for digital radio links

H. Sari

L

An auto-adaptive amplitude-equalizing arrangement for digital radio links having an intermediate-frequency signal input, a transversal filter and a circuit for the control of the filter. The transversal filter comprises a delay circuit providing, with respect to the intermediate-frequency signal input, a delay T equal to $(2k - 1)/4F_c$, where k is a positive integer and F_c the center frequency of the intermediate-frequency signal, a first and a second multiplication circuit whose inputs are respectively connected to the output of the delay circuit and to the intermediate-frequency signal input, and an adder connected to the outputs of the multiplication circuits. The first multiplication circuit may be an analog amplifier whose gain is controlled by the control circuit, or may comprise a fixed-gain amplifier and a digitally controlled attenuator, the control inputs of the attenuator being connected to the count outputs of an up/down-counter, which is controlled by a zero comparator connected to the output of the control circuit.

4 559 703

Process for silver plating rotary contact assemblies

D. F. Gagas

N

A process for silver plating a rotary switch contact assembly wherein a brass metal plate and a plastic rotor retainer are first formed, force-fitted together and then silver-plated as an assembly.

4 560 836

Four-wire communication line circuit and conference network comprising such circuits

A. W. M. van den Enden

E

J. F. P. van Mil

A four-wire communication line circuit for two or more two-wire subscriber lines, comprising a pair of amplifiers respectively connected in the line pairs of the four-wire line for each direction of transmission and a transmission direction detection circuit connected to each line pair. The detection circuit generates a control signal from the voltage signals transmitted on the line pairs, and which is dependent on the direction in which the net energy of such voltage signals is transmitted over the two-wire subscriber lines. The control signal is applied to control circuitry which switches the gain factors of the line amplifiers between a high and a low value, as determined by the direction of net energy transmission. When used in a conference network, the four-wire communication line circuit includes circuitry for establishing a higher threshold level at which the amplifier gain factors will be switched to a high level for transmission than the threshold level at which they are switched to a high value for reception.

4 560 898

Colour picture display tube

A. G. Knapp

R

J. R. Mansell

A deflection colour selection system for a single beam channel plate display tube includes, within an envelope, a laminated dynode channel plate electron multiplier having channels whose exit apertures are aligned in columns. An apertured extractor electrode is mounted on and electrically insulated from an output face of an electron multiplier, the apertures in the extractor electrode being aligned with respective channels. A luminescent screen spaced from the extractor electrode includes patterns of phosphor elements (R, G, B) adapted to luminesce in different colours. A current multiplied electron beam exiting from an aperture in the extractor electrode is deflected onto an associated pattern of phosphor elements by pairs of first and second deflector electrodes insulated electrically from each other and from the extractor electrodes, the first and second deflector electrodes being disposed as pairs between each column of apertures in the extractor electrode. All of the first electrodes are interconnected as are all of the second electrodes. This electrode arrangement enables good resolution and electrical correction of misalignment errors between the electron multiplier and the screen.

4 560 908

High-frequency oscillator-inverter ballast circuit for discharge lamps

*E. H. Stupp
M. W. Fellows
W. G. Steneck*

N

A current fed high frequency oscillator-inverter ballast circuit includes a parallel resonant tank circuit for driving a pair of series connected discharge lamps via a series ballast capacitor. A regenerative power supply switches on when a fluctuating main dc supply voltage drops below a given level thereby providing a constant level auxiliary dc supply voltage to the oscillator inverter to maintain oscillation and lamp operation. When the main dc supply voltage exceeds said given level, the regenerative power supply switches out. The oscillation frequency is f_2 during operation of the main supply and automatically switches to a frequency f_1 when the regenerative power supply takes over. The frequency shift is automatic during each half cycle of a 60 Hz ac supply and is in a direction so as to maintain lamp current relatively constant. A novel high frequency leakage transformer may be provided to couple the high frequency inverter to the discharge lamp load to provide both a current limiting (ballast) action and automatic control of the lamp heater current to maintain high efficiency operation.

4 560 963

Analog RC active filter

R. Sharpe

R

An RC active filter device which is implemented with integrated circuit technology. Each RC filter element of the device has a distributed series resistance and a distributed shunt capacitance. The series resistance is formed by a strip of resistive material which overlies a resistive plate (or substrate) with an intervening insulating layer to form the shunt capacitance. The filter device can be designed to have a pass-band ripple response which is not affected by variation in nominal absolute resistance and capacitance values resulting from process spreads. These variations only stretch or compress the filter response along the frequency axis. The filter device comprises three RC filter elements and an operational amplifier determine a low pass band, while the input filter element prevents high frequency components outside the low pass band being leaked directly to the filter device output.

4 561 005

Solid-state infrared radiation imaging devices having a radiation-sensitive portion with a superlattice structure

J. M. Shannon

R

An infrared radiation imaging device comprises a semiconductor body, for example of silicon, having a radiation-sensitive portion in which charge-carriers are generated on absorption of infrared radiation. The semiconductor body also includes a signal-processing portion in which the charge-carriers are collected in a charge-transfer shift register, for example a surface-channel or buried-channel CCD. An electrical signal representative of the detected radiation is produced at an output of the shift register. At least the radiation-sensitive portion is depleted of free charge-carriers in the absence of the radiation. The semiconductor material of the signal-processing portion has an energy band gap (E_g) which is greater than the quantum energy of the detected infrared radiation. The radiation-sensitive portion is of the same semiconductor material as the signal-processing portion but comprises a plurality of alternating n-type and p-type layers. These layers form an energy band bending superlattice structure locally in the body with a reduced effective band gap (E_g'). The n-type and p-type layers have a doping concentration and thickness such that the superlattice structure can be depleted through its thickness without producing breakdown. The charge-carriers are generated in the superlattice structure by transitions across the effective band gap (E_g') between the conduction and valence bands of the semiconductor material of the radiation-sensitive portion.

4 561 081

Opto-electronic apparatus for inscribing and/or reading recording tracks by means of a radiation beam

*P. J. M. Janssen
G. E. van Rosmalen*

E

An opto-electronic apparatus for inscribing and/or reading recording tracks on a record carrier by means of a radiation beam comprises an objective mounted in an objective holder. The objective holder is supported in a frame by bearing arrangement for movement in accordance with a number of desired degrees of freedom and the apparatus includes electromagnetic actuator means for driving the objective holder in accordance with the desired directions of movement. The bearing arrangement of the objective holder on the frame comprises electromagnetic bearing means for counteracting movements in accordance with at least one undesired degree of freedom. An objective-position measuring device supplies a positional error signal which represents the deviation of the objective holder in accordance with the undesired degree of freedom relative to the frame and which is utilized by a levitation control circuit which counteracts movement of the objective holder relative to the frame in accordance with the undesired degree of freedom by means of electromagnetic levitation forces.

4 561 173

Method of manufacturing a wiring system

T. S. te Velde

E

A self-registering method of manufacturing an air(vacuum)-insulated crossing multilayer wiring system of large density is disclosed. Between the lowermost and uppermost wiring layers an intermediate layer is provided in which recesses are formed between the intermediate layer and the lowermost wiring layer. By means of said recesses the intermediate layer can be removed entirely at the area of the crossings during the etching process, while elsewhere portions of the intermediate layer remain as supporting parts or as connecting members.

4 561 259

Method of operating a bimodal heat pump and heat pump for use of this method

W. L. N. van der Sluys

E

A method of operating a bimodal heat pump is provided, such heat pump operating in a first mode as an absorption heat pump and in a second mode as a device for indirectly heating a heat-transport medium. This procedure comprises in the first mode heating by heat exchange a generator containing a solution of a working medium in a solvent to separate a part of the dissolved working medium in the gaseous state from the solvent, passing the separated gaseous working medium to a condenser for liquefaction by the giving up of thermal energy to the heat-transport medium, thereafter expanding and evaporating the liquefied working medium in an evaporator by the taking up of thermal energy from the environment, passing the evaporated working medium to an absorber for solution in the solvent while giving up thermal energy to the heat-transport medium, and passing another part of the working medium-solvent solution from the absorber to the generator. The procedure also comprises in the second mode indirectly heating by heat exchange all the heat-transport medium in a heat boiler separate from the generator. The procedure further comprises, in switching over from the first mode to the second mode, discontinuing the heating of the generator, discontinuing the pumping of the working medium-solvent solution between the absorber and the generator, and diverting all the heat-transport medium to and through the heat boiler for indirect heating by heat exchange therein. In addition, the procedure comprises, in switching back from the second mode to the first mode, restarting the heating of the generator and the pumping of the working medium-solvent solution, and discontinuing passing the heat-transport medium through the heat boiler.

4 562 567

Apparatus for controlling the write beam in an optical data recording system

E. J. Frankfort N
G. C. Kenney
R. McFarlane

Apparatus for recording data by means of a beam of radiation on a recording medium which upon exposure to the beam undergoes optically detectable changes in the form of pits, which apparatus includes means for reducing the beam intensity as a result of pit initiation thereby forming more accurate pits.

4 562 587

X-ray tube having a rotary anode

J. Gerkema E
A. K. Niessen
J. B. Pelzer

An X-ray tube having a rotary anode which is accommodated in a vacuum-tight housing so as to be rotatable by means of at least one spirally grooved bearing. The mutually cooperating surfaces of the bearing consist essentially of Mo or of an alloy of Mo and W and are effectively wetted by a Ga-alloy serving as a bearing lubricant. In order to extend the life of the X-ray tube, 1 to 4% by weight of Ag and/or Cu are added to the Ga-alloy, as a result of which the formation of crystalline compounds is inhibited.

4 562 591

Digital dynamic range converter

E. F. Stikvoort E

A digital dynamic range converter of the forward control type for varying the dynamic range of a digital audio signal constituted by a sequence of audio signal samples. Each audio signal sample is multiplied by a control signal sample which is delivered by a digital control signal generator. This control signal generator has applied to it unipolar signal samples which are derived via a transmission channel from the audio signal samples. In order to cause this dynamic range converter to respond rapidly to abrupt variations in the audio signal and to render it moreover universally usable, the control signal generator is provided with a digital peak-value detector which converts the sequence of unipolar signal samples into a sequence of peak-value samples. The latter are applied to a digital non-linear amplitude transformation circuit which has an adjustable amplitude transmission characteristic curve determined by adjustment quantities. It delivers the transformation samples which are preferably converted in a digital low-pass filter into the control signal samples which are applied to the multiplier device.

4 562 955

Air-conditioner

H. Hörster A
K. Klinkenberg

An air-conditioner comprises an air-to-air heat exchanger; a fresh air supply duct, a fresh air by-pass duct, a used air exhaust duct, and a used air by-pass duct, the fresh air supply duct and the used air exhaust duct being respectively connected to the air-to-air heat exchanger, the fresh air supply duct having a part in common with the used air by-pass duct, and the used air exhaust duct having a part in common with the fresh air by-pass duct. Included are a condenser provided in the common part of the fresh air supply duct, and an evaporator provided in the common part of the used air exhaust duct, the condenser and the evaporator being parts of a heat pump. A blower is provided in the common part of the fresh air supply duct and is connected to the used air by-pass duct, and a separate blower is provided in the common part of the used air exhaust duct and is connected to the fresh air by-pass duct. A first three-way valve is arranged in the used air exhaust duct in front of the air-to-air heat exchanger, and a second three-way valve is arranged in the fresh air supply duct behind the air-to-air heat exchanger viewed in the direction of fresh air supply for switching the air conditioner into first, second and third modes wherein the air conditioner functions as a heat pump, a heat pump and a fresh air supplier, and a fresh air supplier, respectively.

4 563 752

Series/parallel/series shift register memory comprising redundant parallel-connected storage registers, and display apparatus comprising a picture memory thus organized

M. J. M. Pelgrom E
A. Slob
H. A. Harwig
J. W. Slotboom

A series/parallel/series shift register memory comprises a substrate on which there are provided storage positions for multivalent data elements. There is provided a redundancy generator for generating one or more redundant code elements on the basis of a group of data elements, said redundant code elements being applied to the series input of the shift register memory later than the associated data elements. The code elements are conducted through parallel-connected storage registers which are shorter than those used for the associated data elements, so that a redundancy reducer receives the redundant code elements from a series output before the associated data elements appear on this series output. The reduction of the storage registers, expressed in periods of the shift drive, can be performed in different ways from a technological point of view.

4 564 866

Optical printer

A. Comberg A

The invention relates to an optical printer in which light signals emitted by an information-controlled light source are applied to a photosensitive record carrier via a mirror system and a circular-to-linear converter which consists of optical fibers. In order to improve the optical coupling between the light source and the record carrier and hence the printing quality, the mirror system comprises a conical mirror which opens in the direction of the circular-to-linear converter and which enables the light beam to be axially coupled into the circularly arranged ends of the optical fibers at the entrance of the circular-to-linear converter.

4 566 020

Hot-electron and hot-hole transistors having silicide contacts

J. M. Shannon R

A unipolar hot-electron or hot-hole transistor has its base region and/or collection region electrically contacted and extended to the semiconductor body surface by a metal-silicide region which extends through a silicon surface region belonging to either the transistor emitter or the emitter-base barrier. The metal-silicide region forms an isolating Schottky barrier with an adjacent semiconductor portion. Preferably, the surface region is divided into separate first and second portions by the base-contacting metal-silicide region, with the emitter-base barrier and base-collector barrier terminating at one or more sides in this metal-silicide region. The isolating Schottky barriers are good quality unipolar diodes, thus avoiding minority charge carrier storage effects in these unipolar transistors, while the metal-silicide region can form good ohmic contacts to highly-conductive base and collector regions which typically comprise a high-doped semiconductor layer or a metal-silicide layer.

4 566 076

Method of attenuating a digital signal and device for carrying out said method

A. C. A. M. van der Steen E

In the method of attenuating or amplifying digital signal values as described herein the desired modification is realized in two steps. A coarse attenuation or amplification in steps of 6 dB is effected by shifting the digital word to be modified into a shift register, after which fine amplification is realized by adding the word, which is attenuated by shifting it a number of times, to the word thus shifted. Furthermore, a device for carrying out said method is described, in which the signal processing section only comprises one shift register and an adding circuit, the additional shift being achieved by means

of the wiring between the said shift register and the adder circuit, so that no further signal-processing registers are required for carrying out the said cumulative addition.

4 566 112

Tomosynthesis apparatus

R. Linde

E. Klotz

H

A tomosynthesis apparatus for the formation of layer images of a body. The apparatus has a large number of radiation source positions which are situated in one radiation source plane. The radiation from the sources is stopped by a diaphragm device so that the radiation beams passing through the diaphragm apertures irradiate a common superposition zone and are incident on a detector surface which is arranged behind the superposition zone. The diaphragm apertures are shaped so that in the detector plane the edge of the radiation beam of each radiation source is at least locally tangent to the edge of a cylinder which is centrally projected onto the detector surface by the radiation source and which is situated within the superposition zone. The axis of the cylinder extends at least approximately perpendicular to the radiation source plane.

4 566 120

Loudspeaker system and loudspeaker for use in a loudspeaker system for converting an n-bit digitized electric signal into an acoustic signal

J. A. M. Nieuwendijk

F. J. op de Beek

G. B. J. Sanders

W. D. A. M. van Gijssel

J. M. van Nieuwland

E

A loudspeaker system for converting an n-bit digitized electric signal into an acoustic signal comprises an electrodynamic loudspeaker with n voice-coil sections which cooperate with a magnet system. The loudspeaker system further comprises means for short-circuiting a voice-coil section if the value of the bit corresponding to the voice-coil section is such that the relevant voice-coil section is not driven.

4 566 177

Formation of electromigration resistant aluminium alloy conductors

E. P. G. T. van de Ven

J. M. Townner

S

Electromigration resistance of aluminium alloy conductors in semiconductor devices is found to significantly increase by rapidly annealing the conductors by employing an annealing cycle with a peak temperature of 520-580 °C and a cycle time of about 5 to 30 seconds such as is developed by high intensity CW lamps.

4 566 756

Projection screen

W. A. L. Heijnemans

E

A projection screen comprises a single plate of a transparent material. The diffusion in the horizontal direction is provided by filamentary particles which are oriented substantially in one direction in the plate material. Both surfaces of the plate are then capable of performing different functions, yielding a projection screen with an optimally uniform brightness distribution, minimal colour faults and maximum contrast.

4 566 936

Method of trimming precision resistors

S. L. Bowlin

N

A method for trimming precision resistors which includes forming a helical groove in a conductive film coating on a cylindrical core. Final trimming includes forming discrete circular depressions in the film coating by using a pulsed laser. This method enables the manufacture of precision resistors having a tolerance of 0.25% or better.

4 567.386

Integrated logic circuit incorporating fast sample control

N. F. Benschop

E

A MOS integrated logic circuit is described which comprises a plurality of groups of combinatory logic elements. These groups form a cascade in that a data output of a preceding group is directly coupled to a data input of a next group within the cascade. During successive clock pulse phases the groups of combinatory logic elements are sampled in the sequence in which they are arranged in the cascade. Charging means provide the charge to be sampled, either by means of a precharge clock phase, or by virtue of being pull-up means.

4 567 399

Cathode ray tube with spherical aberration correction means

A. A. van Gorkum

E

A curved, electrically-conductive foil or gauze member is provided in a second cylindrical accelerating electrode of an electron gun for a cathode ray tube. The curvature of the foil or gauze member initially decreases with distance from the longitudinal axis of the electrode, thereby modifying the shape of the field produced by the electrode and minimizing spherical aberration. The curvature preferably varies according to a zero order Bessel function. Spherical aberration can be made negative by adjusting the relative positions of the member and nearby ends of the second and an adjacent first cylindrical accelerating electrode.

4 567 426

Current stabilizer with starting circuit

R. J. van de Plassche

P. J. M. Sijbers

E

Two current circuits are between two common terminals ($+V_B$ and $-V_B$). The ratio between the currents in the two current circuits is defined by a first current-dividing circuit, and the absolute values of these currents are defined by means of a second current-dividing circuit, in particular a resistor in this second current-dividing circuit. In order to ensure that the current-stabilizing assumes the proper state upon activation, a first current-supply circuit is coupled to the input of the second current-dividing circuit, which current-supply circuit comprises the series arrangement of a resistor and a transistor arranged as a diode, and a second current-supply circuit is coupled to the output of the current-dividing circuit, which second current-supply circuit includes a transistor whose base is connected in common with that of the transistor of the first current-supply circuit.

4 567 484

Doppler radar measuring apparatus

W. Schiltz

B. Schiek

H

Range-dependent sensitivity of an RF doppler radar apparatus is reduced to prevent false alarms when small objects move in close proximity to the apparatus' antenna. The sensitivity is reduced by periodically FM-modulating the transmitted RF signal at a frequency corresponding to a wavelength which is at least four times the operating range of the apparatus. The reflection of the transmitted signal is mixed with the transmitted signal to produce a difference frequency signal which is sampled at instants of maximum amplitude.

4 567 508

Two-channel compatible television transmission system for wide picture formats

M. G. Hulyer

R

A television transmission system for the simultaneous transmission of television signals, depicting the same scene, for standard and wide picture formats of, respectively, a standard aspect ratio and a wider standard aspect ratio. The television signal for the scene having 1249 lines per field is divided to produce a first television signal of 625 lines per field representing the wide picture format where

adjacent lines of a field are derived from alternate lines of the scene television signal and a second television signal also of 625 lines per field representing the standard picture format where adjacent lines of a field are derived from the intervening lines of the scene television signal. The first and second television signals may be received together for the provision of a wide screen television display and the invention has the advantage that the second television signal may be received alone by currently manufactured television receivers for reproduction of a display of standard aspect ratio.

4 567 518

System for decoding and displaying encoded television pictures

L. M. H. E. Driessen

E

An error protection code which acts on subpictures for the transmission of television picture information. First the picture is subpicture-wise transformed by means of transformation functions, for example, Hadamard functions. Of the coefficients thus formed, a number of most significant coefficient bits which are associated with low frequency transformation functions are protected against a bit error. Moreover, a comparatively small number of coefficient bits within said number are protected against an additional bit error.

4 567 520

Television circuit arrangement for determining in a video signal frame periods comprising two field periods

L. J. van de Polder

E

A television circuit arrangement for determining in a video signal, frame periods comprising two field periods when a picture signal repeated in cycles of two successive field periods and with a possible change of picture content therebetween is present. Signal sources, such as, for example, cine-film television converters and 'field skip' signal storage- and display devices, supply such a signal. It may be required for signal processing operations improving the picture quality during display, to use the cycles as frame periods. For this purpose, the circuit arrangement is provided with a switching circuit, a first and a second signal integration circuit which can be reset and are alternately operative every other field period, and a succeeding signal comparison circuit for supplying a voltage determining the frame period.

4 567 522

Line synchronizing circuit for a picture display device

M. V. C. Stroomer

E

F. M. Boekhorst

A line synchronizing circuit for a picture display device comprising a voltage-controlled oscillator for generating a signal whose frequency is higher than the line frequency, a frequency dividing circuit for dividing the frequency of the oscillator signals and a phase comparison stage for generating a control voltage in dependence on the phase deviation between the signals applied thereto, more specifically a received line synchronizing signal and a locally generated reference signal. The elements of the line phase control loop, are part of an integrated circuit which functions as a frequency synthesizing circuit. The reference-frequency dividing circuit incorporated in the integrated circuit is programmed to operate with a constant divisor.

4 567 605

X-ray analysis apparatus comprising a four-crystal monochromator

W. J. Bartels

E

In order to achieve high resolution in X-ray analysis, a monochromator comprising four crystals which are pair-wise positioned in parallel orientation is used with the two pairs being positioned in an offset anti-parallel orientation. An X-radiation source may be arranged in the immediate vicinity of the first crystal pair in order to achieve a high beam intensity. Each of the crystal pairs is preferably cut so as to form a U-shape from a single block of a monocrystalline material which is relatively free from dislocations. Germanium is a monocrystalline material of preferred use.

4 567 644

Methods of making triple diffused ISL structure

D. F. Allison

S

An ISL structure is fabricated by a process in which impurities are introduced into a semiconductor substrate of first type conductivity (p) to form major and minor portions of a first region of opposite second type conductivity (n). The minor portion has a lower net impurity concentration than the major portion and extends to a considerably lesser depth. An impurity is introduced into the major and minor portions to form a second region of first type conductivity. An impurity is introduced into the second region to form a third region of second type conductivity spaced laterally apart from the minor portion. Metallization is then performed to create at least one Schottky rectifying contact with the major portion and ohmic contacts with the substrate and second and third regions.

4 567 736

Absorption heat pump

W. L. N. van der Sluys

E

J. Pastoor

J. C. M. Roelofs

An absorption heat pump comprising a heat-mass-exchanger which is arranged in an absorber and has a metal pipe to which a metal fin is secured. The metal fin consists of a number of interconnected lamellae which are helically wound around the pipe, while adjacent lamellae of successive turns overlap each other in part, viewed in the circumferential direction of the pipe. The finned pipe yields a comparatively strong heat-mass transfer in the absorber.

4 568 140

Optical element comprising a transparent substrate and an antireflection coating for the near-infrared region of wavelengths

P. van der Werf

E

J. Haisma

An optical element comprises a transparent substrate. An antireflection coating is provided on the substrate for reducing reflections of wavelengths from approximately 700 nm to approximately 1700 nm. The coating comprises a plurality of stacked, uniform layers with refractive indices which decrease toward the top of the stack. A base coating is arranged between the layer stack and the substrate. The effective refractive index at the top of the base coating is at least 2.5, and the base coating is a graded index layer.

4 568 853

Electron multiplier structure

J.-P. Boutot

L

An electron multiplier structure comprising an electron multiplier section with one or more microchannel plates and a dynode stage having secondary electron emission. This structure makes it possible to obtain an amplification which is higher than the amplification obtainable with only the electron multiplier section while maintaining the instantaneously obtained characteristics and special resolving power associated therewith.

4 568 890

Microwave oscillator injection locked at its fundamental frequency for producing a harmonic frequency output

R. N. Bates

R

A microwave oscillator suitable for millimeter wavelengths comprises a Gunn diode coupled to a waveguide by a resonant-cap structure. The diode generates microwave energy both at a fundamental frequency f_0 which is below the cut-off frequency of the waveguide and at a second harmonic frequency $2f_0$ above cut-off. To control the generation of microwave energy at $2f_0$, energy at f_0 is coupled into the waveguide from an adjacent further waveguide above its cut-off, by means of an electric probe extending close to the cap.

The probe may couple in a locking signal at or close to the free-running value of f_0 from another oscillator having better noise performance and electronic tuning, thereby locking $2f_0$ to twice the frequency of the locking signal, or alternatively may couple to a varactor-tuned cavity resonant at f_0 .

4 568 906

Sensor having a magnetic field-sensitive element with accurately defined weight and thickness dimensions in the nanometer range

J. de Wilde

E

W. G. M. van den Hoek

A sensor suitable for measuring magnetic field gradients spanning very small regions has a magnetic field-sensitive element with a very accurately defined height and thickness (even into the nanometer range) which is perpendicular to the surface of a substrate so that the substrate surface may be used in aligning the element.

4 568 993

Magnetic head

D. Stoppels

E

P. F. Bongers

J. P. M. Damen

E. G. Visser

Magnetic head for a magnetic recording and playback apparatus includes a core of a Mn-Zn-ferrous ferrite having a very high saturation magnetization. The Mn-Zn-ferrous ferrite has a composition (not counting optional substitutions) according to the formula $Mn_aZn_bFe_c^{11}Fe_e^{11}O_4$ with $0 < a \leq 0.55$, $0.06 \leq b \leq 0.4$, $0.25 \leq c \leq 0.9$, ($a + b + c = 1$). The result is that the magnetic head may be used in combination with magnetic tapes having a very high coercive force up to 104 kA/m (1300 Oersted) and may be used for transducing signals having a frequency of a few MHz.

4 569 072

Clock-controlled filtering arrangement

A. H. M. van Roermund

E

A clock-controlled filtering arrangement for suppressing a number of interference frequencies related to a clock frequency, which comprises a time-discrete comb filter included in a negative feedback loop for a selective negative feedback of the said interference frequencies, which time-discrete comb filter is connected to an output of a clock generator for controlling the frequency location of the pass ranges of the comb filter. In order to avoid on the one hand the introduction of quantizing noise and the use of additional circuits, such as A/D and D/A converters, and on the other hand the occurrence of error cumulation while maintaining an adequate interference suppression, the time-discrete comb filter is of the switched capacitor N-path filter type.

4 569 121

Method of fabricating a programmable read-only memory cell incorporating an antifuse utilizing deposition of amorphous semiconductor layer

S. C. P. Lim

S

D. F. Ridley

S. A. Raza

G. W. Conner

In fabricating a PROM cell, an electrical isolation mechanism is formed in a semiconductive body to separate islands of an upper zone of first type conductivity (n) in the body. A semiconductor impurity is introduced into one of the islands to produce a region of opposite type conductivity (p) that forms a pn junction laterally bounded by the island's side boundaries. A highly resistive amorphous semiconductive layer which is irreversibly switchable to a low resistive state is deposited above the region in such a manner as to be electrically coupled to the region. A path of first type conductivity extending from the pn junction through another of the islands to its upper surface is created in the body to complete the basic cell.

4 596 806

Method and device for manufacturing an information carrier of a synthetic material having a laminated structure

P. L. Holster

E

A method and a device for manufacturing an information carrier of synthetic material having a laminated structure, in which a transparent carrier is provided away from the mould with a resin layer and is then brought to a position opposite a mould with its resin layer facing the mould, after which the carrier is pressed against the mould progressively from a boundary surface of the carrier by means of one or more rollers and at least the part of the carrier located directly behind the roller or rollers is exposed for curing the resin layer, the carrier with the cured resin layer being subsequently removed from the mould and further transported.

4 570 036

Digital duplex communication system

N. S. Virdee

R

A digital duplex communication system for data signals having a power-versus-frequency spectrum having two side bands located one each side of a symbol frequency, the system comprising a transmitter/receiver which includes an echo canceller. The received signal is sampled at a multiple of the bit rate and has in each symbol period a first time during which data is valid (true eye) and a second time during which data is invalid (false eye). The receiver includes circuitry to decode the data from the sample signal during the true eye. The echo canceller is designed to be operative only during the sampling instant in the true eye and at one of the zero crossing instants in each bit period. This enables the storage capacity of a look-up table type echo canceller to be reduced and the processing speed of a transversal filter type echo canceller to be reduced.

4 570 063

Device for the optical scanning of a document

J. H. de Bie

E

A. J. J. Franken

The device comprises a transducer with photoelectric elements and a coupling member which comprises an entrance face which is to be aimed at the document and an exit face which is optically coupled to the transducer. The coupling member comprises a number of light conductors having first ends which are arranged in at least one straight line in the entrance face and second ends which are situated in arbitrary positions in the exit face. The relation between the positions of the first ends in the entrance face and the positions of the second ends in the exit face is stored in a memory. The photosensitive surface of the transducer may have an arbitrary length/width ratio and the light conductors may extend rather arbitrarily through the coupling member so that the cost of the device may be comparatively low.

4 570 125

FSK demodulator with concurrent carrier and clock synchronization

R. W. Gibson

R

A data demodulator for digital signals in which the times of the zero crossings in hard limited signals in the orthogonal outputs of a direct demodulation receiver are used to recover the carrier and clock signals.

4 571 276

Method for strengthening terminations on reduction fired multilayer capacitors

J. R. Akse

N

The strength of end terminations on multilayer capacitors employing base metal electrodes is increased by heating the terminations, subsequent to firing in a reducing atmosphere, in an atmosphere in which the oxygen partial pressure is at least equal to that of air for a period of at least 15 minutes at a temperature in the range of from 375 to 600 °C.

4 571 526

Low-pressure discharge lamp with cooled internal ballast

G. A. Wesselink

E

A compact screw-base discharge lamp having an electrical stabilization ballast which occupies a central position in the lamp. The discharge vessel surrounds the ballast. To dissipate the heat generated by the ballast during operation to the environment of the lamp, a thin-walled heat sink of a heat-conductive material is provided between the ballast and the discharge vessel, and bears on the ballast. This body has a collar which extends to the exterior of the lamp.

4 571 604

Method of and device for the electrophotographic printing of information

U. Schiebel

A

A method of electrophotographic printing of electrically stored information by means of a cathode ray tube. The tube is controlled so that each time only one picture line of the information on the display screen is activated several times in succession. Thus, the transport movement of the record carrier is continuous. The optical system provided between the cathode ray tube and the record carrier may be constructed to be rigid, so that on the record carrier there is formed an image whose individual pixels represent a small line which consists of several overlapping dots. The necessary brightness is achieved by using a cathode ray tube having a wide display screen on which the picture lines to be transferred to the record carrier are displayed with a 1:1 ratio. Furthermore, the display screen is provided with a coarse-grained phosphor of the zinc sulfide type which has a high light yield. Moreover, the line frequency of the cathode beam is increased beyond the customary value in order to counteract phosphor saturation.

4 571 616

Device for displaying three-dimensional images

J. Haisma

E

G. Bouwhuis

In a device for displaying three-dimensional pictures, N (with $N = 2, 3, 4, \dots$) recorded images corresponding to differential spatial observation positions are displayed on one or more intermediate display screens. The device comprises a viewing screen having lens elements via which corresponding picture segments of the recorded images are displayed. An optical coupling having a plurality of light conductors exists between the viewing screen and the intermediate display screen(s). The light conductors unambiguously associate groups of N corresponding picture segments with lens elements of the viewing screen. By means of the device, three-dimensional pictures can be observed without further auxiliary means for the viewer.

4 571 625

Television camera with a solid-state pick-up device

A. J. J. Boudewijns

E

A television camera has a solid-state pick-up device having pick-up elements arranged in rows and columns, wherein a charge transfer can be effected in the columns by means of control electrodes and an associated control circuit. To have the pick-up device generate a single or multiple interlace picture signal without specific measures being required due to the structure of the pick-up elements, the control circuit supplies during at least one field scanning period out of a number of field periods forming a picture period, a charge transfer signal for effecting a single charge transfer between all the consecutive pick-up elements in each column of pick-up elements.

4 571 637

Device for optically scanning a document

M. L. G. Thoone

E

Optical scanning device having linear opto-electronic transducers which are substantially aligned with spaces between adjacent transducers. With each transducer is associated an individual imaging

system for imaging a narrow strip of the document on the transducer. Each transducer is displaceable with the aid of adjustment means with respect to the associated imaging system. As a result the transducers can be adjusted so that the narrow strips adjoin each other and are aligned. Together they cover a narrow elongate part of the document. In this manner, a comparatively large document can be scanned with a high resolving power by means of comparatively simple and hence inexpensive transducers and imaging systems.

4 571 664

Solid electrolyte capacitor for surface mounting

W. J. Hyland

N

A solid electrolyte chip capacitor having a conductive cathode coating, a coated and plated conformal cathode termination and an anode termination clip providing a thin-walled conformal construction with opposed termination connections on a base for surface mounting.

4 573 005

Current source arrangement having a precision current-mirror circuit

R. J. van de Plassche

S

In a digital-to-analog converter a plurality of binary weighted currents are generated, which currents must be in an accurate current ratio relative to each other. By means of a coupling network which is controlled by a control circuit, a plurality of currents from said digital-to-analog converter can be coupled to a precision current-mirror circuit in accordance with a cyclic pattern, this allowing deviations in the ratios of the currents from the digital-to-analog converter to be detected by detection means which control correction means by means of which the currents from the digital-to-analog converter are corrected so as to reduce the detected deviations.

4 573 034

Method of encoding n -bit information words into m -bit code words, apparatus for carrying out said method, method of decoding m -bit code words into n -bit information words, and apparatus for carrying out said method

K. A. Schouhamer Immink

E

A method of encoding n -bit information words into m -bit code words and the other way round is described, which code words have a specific disparity d and a digital sum value which is limited to values p and q . In order to enable encoding and decoding without the use of an extensive look-up table, use is made of a series of numbers which is a modified version of numbers in conformity with the Newton binomial. By means of this modified series, the n -bit information words, which are arranged in conformity with their binary weights, are mapped lexicographically and unambiguously onto code words with said limitations, and the other way round.

4 573 047

Binary selector stage and a selector and selector system comprising such selector stages

C. J. Koomen

E

Contemporary communication networks, telephony exchanges in particular, are frequently provided with a central control. A consequence thereof is that they are very complex. The invention provides a communication network having a high degree of distributed control and processing by providing a binary selector stage from which selectors and selector systems may be assembled to form the entire network. The selector stage comprises an identification circuit for identifying destination addresses applied by its input and which are associated with the service area of the selector stage. An indicator circuit determines from a list-of-free-outputs circuits to which free output the destination address, which is identified by and transferred to a first output, must be conveyed. Non-identified destination addresses are transferred to a second output, to which output a further selector stage can be connected.

4 573 066

Breakdown voltage increasing device with multiple floating annular guard rings of decreasing lateral width

K. R. Whight

R

In order to increase the breakdown voltage of a reverse-biased p-n junction of a semiconductor device, at least three annular regions which extend around the active device region are located within the spread of a depletion layer from the junction. At least one inner annular region is wider than outer annular regions, and this increased width of the inner region or regions reduces peak electrostatic fields found to occur at the bottom outer corners of the active device region and inner annular regions. The spacing of the annular regions increases with remoteness from the active device region, although at least two inner annular regions may have the same spacing as that of the innermost annular region from the active device region. A group of annular regions may have the same width as each other in the group.

4 573 169

Communication system for bi-phase transmission of data and having sinusoidal low pass frequency response

P. J. van Gerwen

E

W. A. M. Snijders

A data communication system for transmission of bi-phase signals modulated by data symbols and in which the signals are filtered in accordance with a frequency response which approximates zero at 0 Hz and at exceeding frequency $3/(2T)$ Hz and which has an approximately sinusoidal variation between those frequencies, T being the symbol interval. This filter characteristic minimizes inter-symbol interference and improves the signal-to-noise ratio. The requisite filtering may be provided in the receiver or in part in the receiver and in part in the transmitter of the communication system.

4 573 330

Absorption heat pump comprising an integrated generator and rectifier

W. L. N. van der Stuyts

E

J. Pastoor

J. C. M. Roelofs

An absorption heat pump comprising a generator which is provided with a condensation pipe comprising a lower generating section and an adjoining upper rectifying section. The upper section is filled with a thermally insulating gas which separates the generating section from the rectifying section. Thus, a simple construction is obtained, in which the rectifier is integrated in the generator.

4 573 769

Projection lens system

J. A. Clarke

R

A lens system is provided which is suitable for back-projecting an enlarged image of a TV cathode-ray tube (CRT). To achieve a compact cabinet design for such a projection television set, a short projection throw and a wider projection angle are required, together with a wide aperture for a bright projected picture and with a definition sufficient to resolve 625 line television pictures. The lens system comprises a concave CRT face plate and only two lens elements, each of positive power and each having one aspheric surface, the powers of the elements being chosen so that $0.4K < K_1 < 0.60K$ and $0.75K < K_2 < 1.05K$, where K_1 is the power of the element remote from the object surface, K_2 is the power of the element adjacent the object surface and K is the total power of the projection lens system.

4 574 216

Cathode-ray tube and semiconductor device for use in such a cathode-ray tube

A. M. E. Hoeberechts

E

G. G. P. van Gorkom

A semiconductor cathode is provided with deflection electrodes, with which a dipole field can be generated. As a result of this, electrons released at the surface of the semiconductor cathode leave the surface at a certain angle. For use inter alia in camera tubes, display tubes, such an inclined beam can be aligned without any problems. Positive ions which are released inter alia from residual gases and are accelerated in the direction of the cathode impinge on the cathode at an acute angle. As a result of this, the active part of the cathode is substantially not attacked by said positive ions, so that degradation is prevented.

4 574 257

Crystal resonator oscillator having circuitry for suppressing undesired crystals harmonics

W. G. Kasperkovitz

E

H. W. van Rumpft

Oscillator circuit comprising an amplifier arrangement being connected to a reference level an output and an input thereof being coupled via a single signal-carrying terminal to a resonant network which is connected to the same reference level as the amplifier arrangement, the resonant network comprising a crystal resonator. A stable oscillation at a higher order crystal resonant frequency is provided by means of an LC network which selects said higher order crystal resonant frequency and a resistor connected in parallel across the crystal resonator, which prevents parasitic oscillations at the resonant frequency determined by the components of the LC network and the case or holder capacitance of the crystal resonator.

4 574 270

Analog-to-digital current converter

R. J. van de Plassche

S

An analog-to-digital current converter comprises n series-connected stages which each provide one bit of the Gray code. For this purpose each stage m derives a difference current from the input current (i_{ijm}), which is the output current ($i_{o/m-1}$) of the preceding stage, and a reference current ($I/2^{m-1}$) from a source. This difference current flows to the output of the stage m ($i_{o/m}$) either via a diode or via a current mirror circuit depending on its direction. Conduction of the diode or of the current-mirror circuit is used for the bit indication. This results in a very fast analog-to-digital converter with few components and a high accuracy and resolution.

4 574 300

High-definition colour television transmission system

M. G. Hulyer

R

A high definition television transmission system in which a wide band interlaced television signal having 1249 lines per field is divided to provide first and second interlaced television signals each having 625 lines per field and consequently reduced bandwidth. Adjacent lines of the first television signal have their low frequency information (0.3 MHz) derived from alternate lines in the wide band signal while the corresponding information for adjacent lines in the second television signal is derived from the intervening lines in the wide band signal. The high frequency information (3.5.5 or 6 MHz) for the lines of both the first and second television signals is derived from the average of the corresponding information in adjacent lines of the wide band signal. The first television signal also contains a colour subcarrier which is modulated by the average of the colour information in adjacent lines of the wide band signal. The two television signals may be jointly received for the provision of a high definition display but the invention has the distinct advantage that the first television signal may be received alone by currently manufactured television receivers for reproduction of a display of a quality which is currently acceptable.